FACULTY OF ENGINEERING,
BAYERO UNIVERSITY, KANO

Proceedings

of the

5th ENGINEERING CONFERENCE

on

ENGINEERING INNOVATIONS AND ECONOMIC POLICIES: DRIVING SUSTAINABLE INDUSTRIAL GROWTH IN NIGERIA

Venue:
Dangote Business School, Bayero University, Kano

Date:
09th – 10th February, 2026

Proceedings

of the

5th Engineering Conference

on

ENGINEERING INNOVATIONS AND ECONOMIC POLICIES: DRIVING SUSTAINABLE INDUSTRIAL GROWTH IN NIGERIA

Venue:

Dangote Business School, Bayero University, Kano

Date:

09th – 10th February, 2026

ISBN: 978-978-8567-02-8

Members of Editorial Committee

Dr. Omar U. Ahmed – Chairman

Prof. N. Yusuf – Member

Prof. Hassan A. Bashir – Member

Dr Umar Musa – Member

Engr. Amir I. Bako – Member

Engr. A. Usman – Member

Dr. Musa M. Bello – Secretary

Welcome Address by the Chairman, Conference Organising Committee,

On behalf of the Management of Bayero University, Kano, the Faculty of Engineering, and the Local Organising Committee, I warmly welcome you to the 5th Faculty of Engineering Conference, Bayero University, Kano.

The Bayero University Engineering Conferences were conceived to provide a vibrant forum where researchers, policymakers, industry practitioners, entrepreneurs, and other stakeholders engage on topical engineering issues that are critical to national development. This vision was first realized through the Academia–Industry Conferences (ACICon), which created valuable opportunities for interaction between academia, industry, and government, particularly in addressing challenges related to knowledge transfer, technology development, and industrial application of research outcomes.

In December 2015, the Faculty of Engineering hosted the International Conference on Green Engineering for Sustainable Development (IC-GESD 2015) in collaboration with the Faculty of Engineering, Tanta University, Egypt. The conference emphasized green engineering as a pathway to minimizing environmental pollution, promoting sustainability, protecting human health, and achieving economic efficiency. Building on this success, the Faculty organized the second stream, IC-GESD 2017, in November 2017. Both conferences enjoyed strong local and international participation and further strengthened the Faculty's commitment to impactful research and global collaboration.

The 5th Faculty of Engineering Conference builds on this solid foundation. With the theme "Engineering Innovation and Economic Policies: Driving Sustainable Industrial Growth in Nigeria," the conference is timely in the context of Nigeria's pursuit of economic diversification, industrial competitiveness, and sustainable development. It provides a platform to examine how engineering solutions can effectively support national economic policies while addressing emerging areas such as start-ups and entrepreneurship, digital economy and artificial intelligence, energy transition, agricultural mechanization, infrastructure development, and healthcare technologies.

We are particularly pleased with the wide range of participants from academia, industry, government, development partners, and young innovators. This diversity reflects our belief that meaningful and sustainable engineering solutions can only be achieved through strong collaboration among all stakeholders.

I wish to sincerely acknowledge the Vice-Chancellor of the University, the Dean of the Faculty of Engineering, our distinguished keynote speakers, reviewers, sponsors, partners, and members of the Local Organising Committee for their dedication and support in making this conference possible.

As you participate in the technical sessions, plenaries, and interactive engagements, it is our hope that the discussions and outcomes will lead to practical insights, policy-relevant recommendations, and innovative ideas that will contribute to Nigeria's industrial growth and economic development.

Once again, you are warmly welcome, and I wish you a rewarding and successful conference.

Nurudeen Yusuf
Chairman, Local Organising Committee

Table of Content

	Welcome Address by the Chairman, Conference Organising Committee, 5thEngConf26		ii
	Table of Content		iii
S/No.	**Paper ID. No.**	**Paper Title**	**Page No,**
1	5thEngConf26-001	Evaluation of Level of Awareness and Primary Barriers Affecting the Application of Lean Construction Techniques in Kano Construction Industry	1
2	5thEngConf26-002	Effect of Tensile Reinforcement Ratio on Flexural Behaviour and Ductility of Metakaolin-Based Geopolymer Concrete Beams	7
3	5thEngConf26-003	Customising SUMO with Real-World Vehicle Data: A Step-by-Step Guide for Low-Income Urban Transport Systems	13
4	5thEngConf26-004	Improved Power System Control using the Reaching Law	23
5	5thEngConf26-005	Engineering for Digital Economy: Challenges, Opportunities, and Pathways for Sustainable Industrial Growth in Nigeria	27
6	5thEngConf26-006	Development of State of Charge Estimator for Lithium-Ion Battery Model Using Deep Learning Feed-Forward Neural Network	35
7	5thEngConf26-007	Hybrid Non-Linear System Modeling Using Shallow Feedforward Neural Networks: Application to ALF 500W PEM Fuel Cell Polarization Curve Fitting	42
8	5thEngConf26-010	Development of a Forging Process System for the Manufacture of Household Utensils from Cow Horn: A Review	48
9	5thEngConf26-011	Design And Simulation of an ANFIS Controller for Chicken Defeathering Machine	52
10	5thEngConf26-012	Numerical Analysis of Temperature Enhancement and Uniform Distribution at the Wall of a Micro Cylindrical Combustor Utilizing Methane-Air Mixtures	56
11	5thEngConf26-013	Manufacturing Engineering and National in Nigeria: An Overview	64
12	5thEngConf26-015	Harnessing Local Engineering Innovation for Sustainable Industrial Growth and SDG Realization in Nigeria: A Triple Helix Perspective	70
13	5thEngConf26-016	Geotechnical Assesment of Laterictic Soil Stabilized with Gum Arabic	75
14	5thEngConf26-017	What Drives Clean Mobility? Evidence from Three Secondary Cities in Northeastern Nigeria	82
15	5thEngConf26-018	Durability Assessment of Eco-friendly Lightweight Concrete Incorporating Sawdust Ash and Coconut Shell	90
16	5thEngConf26-020	Integrating Solid Waste Management into Climate Action in Sub-Saharan Africa: A Systematic Review and Evidence from Jalingo Metropolis	97
17	5thEngConf26-021	Evaluating the Potential of Organic Waste Composting for Climate Change Mitigation in Urban Taraba: A Case Study of Jalingo	102
18	5thEngConf26-022	Assessment of Waste Management Practices in Nigerian Red Bricks Production Process	107
19	5thEngConf26-023	Assessing the Challenges for Implementation of Circular Economy Principles in Waste Management in Nigerian Construction Industry	113

S/No.	Paper ID. No.	Paper Title	Page No,
20	5thEngConf26-024	Assessing the Current State of Supply Chain Management in the Nigerian Construction Industry	118
21	5thEngConf26-025	Cobalt Doped Mordenite as An Efficient Catalyst for Gas Condensate Upgrade	122
22	5thEngConf26-026	Academia–Industry–Government Collaboration: A Strategic Imperative for Sustainable Industrial Growth in Nigeria	128
23	5thEngConf26-027	Aligning Industrial Policy with Engineering Development: Operationalising Nigeria's Industrial Strategy Through Applied Engineering	137
24	5thEngConf26-029	Machine Learning Implementation on Low-Power Microcontrollers for Edge Computing: A Review	144
25	5thEngConf26-030	Optimization of Soil Stabilization using Response Surface Methodology (Central Composite Design) for LBPE–NaOH Systems	157
26	5thEngConf26-031	Effects of Sporosarcina Pasteurii Bacteria on the Durability of Self-Compacting Concrete Admixed with Cement Kiln Dust Using Response Surface Methodology	164
27	5thEngConf26-032	Index and Compaction Characterisation of Cement-Stabilised Lateritic Soils Based on Selected Test Procedures	173
28	5thEngConf26-033	Modeling the Effect of Soil Salinity on Soil Moisture Dynamics in Kadawa, Kano River Irrigation Project Using the SALTMED Model	180
29	5thEngConf26-034	Fourier Transform Infrared (FTIR) Analysis of Kaolin, Metakaolin, and Metakaolin-Based Geopolymer Mixes	186
30	5thEngConf26-035	Performance Comparison Between Fuzzy-PSO And Fuzzy- GA for the Control of Position and Sway Angle of A Double – Girder Crane System	192
31	5thEngConf26-036	The Role of Engineers in Driving Nigeria's Energy Transition and Industrial Competitiveness in the North-East	201
32	5thEngConf26-037	Development of A Bench-Scale Plastic Injection Molding Machine	209
33	5thEngConf26-038	Clay-Based Ceramic Membranes for Oily Wastewater Treatment: Materials, Performance, and Future Prospects	215
34	5thEngConf26-039	Assessment of the Compressive Strength of Cross-Laminated Timber (CLT) Panels for Use as Load Bearing Walls in Tall Buildings	222
	5thEngConf26-040	Graph Convolutional Neural Network for Throughput Prediction in Dense Wireless Local Area Networks	227

S/No.	Paper ID. No.	Paper Title	Page No,
35	5thEngConf26-041	Modelling, Production and Testing of Disc Airfoils	236
36	5thEngConf26-042	Determination of the Comminution Work Index of Maitumbi Gold Ore Deposit Niger State, Nigeria, by the Modified Bond Index.	243
37	5thEngConf26-043	Evaluating the Ability of Fractional Order Proportional Integral Derivative Controller on the Two-Link Planar Robot	250
38	5thEngConf26-044	Optimum Proportional Integral Derivative Control using Grey Wolf Optimization Algorithm for Single Machine Infinite Bus System	254
39	5thEngConf26-046	Experimental Evaluation of Partial Cement Replacement with Bagasse Ash and Rice Husk Ash on the Slump, Compressive Strength and Split tensile Strength of Ternary Blend Concrete	258
40	5thEngConf26-047	Mathematical Model of Heating Value based on Ultimate Analysis of MSW Generated from BUK (main campus), Kano, Nigeria.	265
41	5thEngConf26-048	Fetal ECG Extraction Using Ant Colony Optimization Algorithm (ACO)-Based Adaptive Filter	270
42	5thEngConf26-049	Emulation-Based Analysis of Mobile Producer Handoff Strategies in Named Dat Networking: MP-HNEM	279
43	5thEngConf26-050	A Decline in the Nigerian Agricultural Sector's Contribution to Sustainable Industrial Growth: A Review	290
44	5thEngConf26-051	Effect of Significant Parameters on the Performance of a Simulated Model of Hybrid Solar-incinerator Hot Water Supply System	294
45	5thEngConf26-052	CFD Simulation of Heat Transfer Enhancement with KNO3-NaNO3 as Phase Change Material for Thermal Energy Storage	300
46	5thEngConf26-053	Application of Modern Hydrological Techniques in Developing a Rating Curve for Tiga Dam Reservoir	305
47	5thEngConf26-054	Application of Gas Deposition in 3D printing: A Review on improving mechanical properties of PLA	314
48	5thEngConf26-056	Determination Of the Effect of Dessert Date Seed - Shea Butter Cutting Fluid on Surface Roughness in Cutting Mild Steel	319
49	5thEngConf26-057	Effects of Coconut Shell Ash and Calcium Carbide Residue as Partial Replacement of Cement in Self-compacting Concrete	326
50	5thEngConf26-058	Design and Simulation of a Filtering Antenna for Wireless Local Area Network (WLAN) Applications	332
51	5thEngConf26-059	Design and Simulation of a Compact Quarter-Wavelength Microstrip Hairpin Bandpass Filter for WLAN Applications	339

S/No.	Paper ID. No.	Paper Title	Page No,
52	5thEngConf26-060	Optimization of End-of-Life Tire Steel Fibre Reinforced Concrete Using an Integrated Taguchi-TOPSIS Approach	343
53	5thEngConf26-061	Data-Driven Fault Detection in Nigeria's Transmission Grid using ANNs	351
54	5thEngConf26-062	Machine Learning-Driven Adaptive Modulation for Visible Light Communication in Industrial Robotic Warehouses	357
55	5thEngConf26-063	Storage Condition (Temperature and Ph) Effect of Pea Pod on Water Coagulation	365
56	5thEngConf26-066	Soil stabilization using Recycled Glass Powder- Review of literature	371
57	5thEngConf26-067	Optimization Of Fuzzy Logic Control Based Maximum Power Point Tracker Using Flower Pollination Algorithm	377
58	5thEngConf26-068	Practical Strategies for Promoting Positive Safety Culture in Kano's Construction SMEs	385
59	5thEngConf26-069	Sensorless Control of Brushless DC Motors: A Review, Comparative Study and Future Research Trends	393
60	5thEngConf26-070	Biodegradability of Phenol, Cresol, and Bisphenol A in Aqueous Solutions by Microorganisms as Primary Growth Substrates	402
61	5thEngConf26-071	Adaptive Frequency Control in Stand-Alone Microgrids using Fractional Order Control Tuned by Genetic Algorithm	407
62	5thEngConf26-072	Comparative Analysis Between Type-1 And Type-2 Fuzzy Logic Controllers Based Shunt Active Power Filter for Harmonic Suppression at Distribution Level	415
63	5thEngConf26-073	Predicting Unconfined Compressive Strength of Laterite - Black Cotton Soil - Cement Kiln Dust Blends for Landfill Liner Design Using Response Surface Methodology	427
64	5thEngConf26-074	Pushover Analysis of a Five-Story Reinforced Concrete Building: Assessing Seismic Performance and Collapse Mechanisms	435
65	5thEngConf26-075	Synthesis and Characterisation of Optimized Recycled Low-Density Polyethylene-Doum Palm Shell Composite for Production of Crash Helmet	443
66	5thEngConf26-076	A Geospatial Assessment of State-Level Cellulosic Ethanol Potential from Major Crop Residues in Nigeria	453
67	5thEngConf26-077	Estimation of Critical Gap for Mixed Traffic at Urban Multilane Roundabouts in Nigeria Using Raff's Method	459

S/No.	Paper ID. No.	Paper Title	Page No,
68	5thEngConf26-078	Design and Implementation of a Smart Thermal Monitoring System for Glass Furnace Operation	467
69	5thEngConf26-079	Speed Control of a Single-Phase Induction Motor Using Takagi-Sugeno Fuzzy Logic Controller	473
70	5thEngConf26-081	Impacts Of Change Orders on Construction Projects Within Kano Metropolis in Kano Construction Industry	479
71	5thEngConf26-082	Demand Side Management of Home Appliances with HEMS considering contribution from EV Fleet	485
72	5thEngConf26-083	A Systematic Review of Image Analysis and Machine Learning Techniques for Maize Quality Assessment and Biofuel Yield Estimation	491
73	5thEngConf26-085	Statistical Quality Control Process Analysis of Corrugated Aluminium Profile in Nigeria	497
74	5thEngConf26-086	Sentiment Analysis of Online Reviews for Brand Monitoring	501
75	5thEngConf26-087	Optimization of Water Content for the Production of Plaster of Paris Ceiling Panels	507
76	5thEngConf26-088	Using Principal Component Analysis and Hierarchical Cluster Analysis Approach to Classify Local Onion Varieties for Drying	513
77	5thEngConf26-089	A Systematic Review of Intelligent Surveillance Systems Using Drone Swarm	522
		Addendum	
78	5thEngConf26-028	Prediction Of Anxiety Disorder in Working Class Students Using Enhanced Machine Learning Algorithms	533

5TH Faculty of Engineering Conference on Engineering Innovation and Economic Policies: Driving Sustainable Industrial Growth in Nigeria

Faculty of Engineering, Bayero University, Kano.

001-Evaluation of Barriers Affecting the Application of Lean Construction Techniques in the Kano Construction Industry

Ohilebo Ogunlowo[1], Dr.A.D.Rafindadi[2]

[1]Department of Civil Engineering, Bayero University Kano, Nigeria [2]Department of Civil Engineering, Bayero University Kano, Nigeria. Email: ohileboogunlowo@gmail.com

Abstract: Lean construction techniques have been recognized globally for their potential to boost productivity, minimize waste (cost overrun, time overrun and material waste), and improve overall project performance. Despite these benefits, their adoption in developing regions, including Nigeria, remains limited. This study investigates the barriers hindering the application of lean construction techniques in the Kano construction industry. A quantitative approach was adopted, with a structured questionnaires survey (n = 146) administered to construction professionals (Architects, Engineers and project managers). Data were analyzed using descriptive statistics and factor analysis. Findings reveal that major barriers include limited awareness and training, resistance to change, lack of government support through sustainable policies, and inadequate technical expertise. Furthermore, additional barriers such as fragmented supply chains and traditional construction practices also hinders lean applications. The results provide valuable insights for policymakers, construction firms, and academic researchers seeking to enhance lean construction adoption in Nigeria. The study concludes that improved training, collaborative project delivery and supportive regulatory frameworks are essential for enhancing lean construction practices in Kano.

Keywords: Lean construction, barriers, Kano construction industry, productivity, waste reduction, implementation strategies

1. INTRODUCTION

Lean construction is an adaptation of lean thinking from the Toyota production system, aimed at reducing waste, improving flow, and creating value throughout project delivery process (Koskela 1992). Over the last two decades, lean has developed into a recognized project management philosophy capable of addressing chronic inefficiencies such as delays, rework, cost overruns, poor communication and waste generation (Ballard, Howell et al. 2003).

In Nigeria, construction output remains critical to national development, but the sector continues to struggle with fragmentation, low productivity and limited technological uptake (Owolabi James, Amusan Lekan et al. 2014). Despite the proven advantage of lean knowledge, empirical evidence shows that its application within Nigeria remains significantly limited (Oyewobi, Okanlawon et al. 2025).

A recent study in Kano State confirms that awareness and utilization of lean construction techniques remain low, with practitioners citing skills gap, poor motivation and lack of organizational readiness as major obstacles(Musa, Saleh et al. 2023). This represents a significant research gap because Kano is one of Nigeria's largest construction hubs, yet lean practice remain minimal. This study aims to evaluate the barriers to applying lean construction techniques within the construction industry of Kano.

2. LITERATURE REVIEW

2.1 Lean construction principles and techniques

Lean construction emphasizes flow reliability, value maximization, elimination of waste, collaborative planning, and continuous improvement (Koskela 1992). Common tools include last planner system (LPS), Just-in-Time (JIT), Value Stream Mapping (VSM), 5S, Kaizen, Prefabrication, and integrated project delivery (IPD)(Salem, Solomon et al. 2005).

2.2 Benefits of lean

Romo, Alejo-Reyes et al. (2024) discovered that lean improves schedule performance, reduces rework, achieves better cost control, and enhances crew productivity.

ISBN: 978-978-8567-02-8

2.3 Awareness of lean construction

Lean construction techniques are a set of principles that helps construction projects to be more efficient and productive. Several studies have been conducted in various countries to assess the level of application of lean construction techniques. Enshassi, Saleh et al. (2019) investigated the applications of eight lean construction techniques in reducing waste in construction project in Gaza strip. The techniques studied, includes last planner system, increased visualization,5S,poka-yoke,daily huddle meeting, first run studies, Kaizen, and 5 why's. The result of the study revealed that, lean construction techniques were poorly applied in construction project in Gaza Strip.

A frame work for the selection of appropriate lean techniques based on their objectives and functionalities was developed by Aslam, Gao et al. (2022). The lean techniques presented in the study includes last planner system, just- in –time, concurrent engineering, daily huddle meeting, visual management, first run studies, six sigma, fail-safe for quality and safety, value stream mapping,5S,and Kaizen, among others.

The awareness and adoption of 32 lean techniques was assessed by Babalola, Ibem et al. (2018) in the Nigerian construction industry. The techniques studied comprise of total quality management, last planner system, visualization tools, just-in-time, six sigma, concurrent management, Kaizen, fail safe for quality and safety, and first run study among others. The study concluded that, the level of adoption of lean techniques in Nigeria construction industry was low.

2.4 Barriers to lean adoption globally and in developing countries

Typical barriers include; low awareness and inadequate training (Moradi and Sormunen 2023), resistance to change, weak management support, lack of financial resources, unsuitable procurement systems, absence of lean policies and standards (Ibrahim, Zayed et al. 2025).

Several Nigeria studies agree that low adoption stems from awareness, inadequate skills, manual project processes, lack of training and technological limitations (Chukwuemeke, Henry et al. 2025, Oyewobi, Okanlawon et al. 2025).

Specifically in Kano State, Musa, Saleh et al. (2023) reported that although practitioners express interest in modern construction management techniques, lean concepts remain poorly understood and rarely implemented.

2.5 Strategies to overcome Barriers

Studies conducted in Kano state such as (Musa, Saleh et al. 2023) reveals that increasing awareness through local seminars and on-site training improves practitioners ability to apply lean techniques effectively.

Leadership support has been identified as a major enabler of lean adoption(Aziz and Hafez 2013). Ibrahim, Zayed et al. (2025) argue that management commitment to continue improvement, transparency, and team empowerment foster a lean culture.

Firms whose leaders actively promote collaboration and reward innovation tend to have better results with lean implementation (Bhasin 2012). In the Nigeria context, organizational culture is often hierarchical and resistant to change, therefore, encouraging open communication and employee participation is a key strategy to ensure acceptance of lean principles

Sarhan, Fox et al. (2013) note that collaborative contracts encourage early stakeholder involvement, shared risk and shared rewards- all of which are essential for lean construction success. In Kano, fostering collaboration between local contractors and consultants through joint planning and regular coordination meetings can enhance efficiency and reduce waste

Government and professional bodies play a vital role in mainstreaming lean construction, Alinaitwe (2009) highlight the national and state-level policies promoting innovation, productivity, and sustainable construction that can accelerate lean construction adoption. In Kano, construction agencies such as the Kano Urban Planning and Development Authority (KNUPDA) can provide institutional backing by endorsing lean principles in public procurement guidelines. Furthermore, regulatory bodies like COREN and NIOB can integrate lean Standards into their professional practice requirements to promote compliance and awareness.

Modern technologies such as Building Information Modelling (BIM), prefabrication, and digital project management systems are key enablers of lean practices. According to Alinaitwe (2009), the integration of digital tools improves coordination, visualization, and information flow, reducing errors and rework. However, many Nigerian firms still rely on manual processes (Musa, Saleh et al. 2023) therefore, incremental adoption of affordable software tools, supported by local training, has been proposed as a practical strategy.

Practical demonstration through pilot projects has been widely recommended as a means to prove the benefits of lean methods. Romo, Alejo-Reyes et al. (2024) observed that pilot implementation not only builds experience but also creates local success stories that encourage broader industry adoption. In Kano, initiating small-scale lean projects within government or private sector developments can showcase measurable outcomes such as cost savings, waste reduction, and improved delivery time. Furthermore, knowledge-sharing platforms, workshops, and construction innovation forums strengthen collaboration and motivate other firms to adopt similar approaches.

Weak communication and fragmented supply chains remain major obstacles in the Nigerian construction sector. Ojo, Ogunsemi et al. (2022) suggest establishing a centralized communication platform to facilitate coordination between suppliers, contractors, and clients. In Kano, promoting local supplier partnerships and

ISBN: 978-978-8567-02-8

introducing Just-in-Time (JIT) delivery practices could minimize delays and material wastage. Effective communication and supply-chain integration not only enhance productivity but also align with the fundamental lean principle of creating value for the client.

3.0 METHODOLOGY

3.1 Research Design

A quantitative approach was adopted in this study to evaluate the key barriers to applying lean construction techniques within the construction industry of Kano.

3.2 population and sampling

The survey Participants includes contractors, builders, architects, engineers, and quantity surveyors working in the Kano construction industry. The study used the simple random sampling technique to identify and select samples from the population as recommended by Saunders et al. (2012).

Using Yamane's formula, a sample of one hundred and forty six (146) was selected from an estimated population of three hundred and twenty (320) professionals.

$$n = \frac{ń}{1+[ń/N]} \text{.....Eq (1)}$$

Where:

N= is the total number of population

n= is the sample size from finite population

ń= is the sample size from infinite population = $\frac{S^2}{V^2}$

Where V is the standard error of sampling population and S, is the variance of the population element. (Usually S= 0.5 and V = 0.1 for 90% confidence interval)

3.3 Research instrument

The study employed a structured questionnaire comprising four section: Section A gathered respondents' demographic information, Section B assessed awareness of lean construction techniques, Section C examined barriers to implementation, and Section D, identifies strategies to overcome these barriers. A 5 – point likert scale was used for Section B, C and D

3.4 Method of Data Analysis

The data obtained from the questionnaire survey were evaluated for normality using Kolmogorov smirnov test. All the data involved have their p – values less than 0.05 which indicates that the data collected is not normally distributed as suggested by (Pallant 2020).

The reliability of the data collected from the field survey (internal consistency) was calculated through Chronbach's Alpha. The overall Chronbach's Alpha was greater than 0.7, which is acceptable as suggested by (Pallant 2020).

Descriptive Statistics (frequency and percentages) were used to analyze the demographic information of respondents. And in determining the awareness level of lean techniques in the study area, mean score ranking was employed as suggested by Fadeke and Aghimien (2016). Relative Importance Index (RII) was used to rank the barriers (Achaka, Ubani et al. 2024).

$$RII=\frac{5n5+4n4+3n3+2n2+1n1}{A*N} \text{ .....Eq (2)}$$

Where n5=Number of respondent for strongly agree

n4=Number of respondents for Agree

n3=Number of respondents for not sure

n2=Number of respondents for Disagree

n1=Number of respondents for Strongly Disagree

A=Highest Weight=5

N=Total number of respondents=146.

4.0 RESULTS AND DISCUSSION

4.1 Demographic profile of the respondents

Descriptive Analysis (frequency and percentage) was used to analyze the demographic information of the respondent.The results shows that 50% of the respondents works in construction firms, 15% in Ministry and tertiary institution, while 27.5% work in consulting firms and 7.5% in other parastatals.

In terms of Academic qualification, 36.3% of the respondents hold bachelor's degree and about 37% hold masters and doctorate degree in relevant field. The results also reveal that, about 24.0% of the respondents have 5-10 years of experience in construction industry, 30.1% have 11-15 years of experience, and 19.9 % of the respondents have 16-20 years of experience and 21.2%, have more than 20 years of experience. Thus, based on these results, the respondents have adequate knowledge and experience to provide reliable information.

4.2 Awareness level

The results from this study indicated that there is an appreciable level of awareness and knowledge of lean construction techniques among construction practitioners in the study area with an overall mean score of 3.49 as shown in table 1, because it is higher than that of the previous study of (Musa, Saleh et al. 2023) with an overall mean score of 2.52

4.3 Barriers to the Application of lean Construction Techniques.

Table 2, present the various barriers and their relative importance. Absence of awareness program to enhance understanding about lean construction, have the highest relative importance index of 0.8932 while lack of education and training required to implement lean construction, is ranked second with relative importance index of 0.8877. These align with findings by (Musa, Saleh et al. 2023), who noted that Absence of awareness

ISBN: 978-978-8567-02-8

and lack of education and training of lean techniques remain top barriers in Kano.

TABLE 1: LEVEL OF AWARENESS OF LEAN TECHNIQUES

Techniques	Mean	Rank
CWMT1(Last Planner system)	4.38	2
CWMT2(Daily huddle meeting)	4.52	1
CWMT3(increased visualization)	3.18	9
CWMT4(total quality management)	3.14	10
CWMT5(first run studies)	3.34	6
CWMT6(Just-in-time)	3.71	3
CWMT7(5s)	3.12	11
CWMT8(fail safe for quality/safety)	3.08	12
CWMT9(concurrent Engineering)	3.32	7
CWMT10(value stream mapping)	3.35	5
CWMT11(six sigma)	3.38	4
CWMT12(Kaizen)	3.31	8
AVERAGE =	3.49	

4.4 Strategies to overcome Barriers

Looking at the mean item score of all the stakeholders with respect to each strategy in Table 3, stakeholders prioritize **S11** (Promoting sensitization of lean techniques application among all construction practitioners) more, with a mean score of **4.63,** to enhance lean construction application, followed by **S3** (Provision of training and education) with mean score of **4.61** and **S1** (Initiation of good planning and control) with mean score of **4.59.** This result align with the study of (Musa, Saleh et al. 2023) who reveals that, increasing awareness through local seminars and on-site training improves practitioners ability to apply lean techniques effectively.

5.0 CONCLUSION AND RECOMMENDATION

5.1 Conclusion

Awareness and knowledge of lean techniques among construction practitioners can increase the level of applications of the techniques in construction projects which will results in waste minimization and improve performance (Babalola, Ibem et al. 2018). This findings agrees with that of Babalola, Ibem et al. (2018) and Fadeke and Aghimien (2016), who found that there was an appreciable level of awareness and knowledge of lean construction and its techniques among construction practitioners in their study area. Increase visualization, Total quality management and Fail safe quality/safety were the least ranked techniques in terms of awareness level by the respondents. These are important lean construction techniques that reduces process variability, eliminate defects, and ensure continuous improvement (Forbes and Ahmed 2020).

TABLE 2 RELATIVE IMPORTANCE INDEX

Barriers	RII	Importance
B1(Lack of management support in the implementation of lean)	0.7425	5
B2(Centralization of decision making)	0.7452	4
B3(Resistance to change by the management)	0.7658	3
B4(Long implementation time required for LC techniques)	0.7397	6
B5(Poor communication among projects parties)	0.7425	5
B6(Poor coordination among projects parties)	0.7356	8
B7(Inadequate planning to apply LC techniques)	0.7384	7
B8(Absence of long term philosophy for construction improvement)	0.7247	10
B9 (High implementation cost of lean construction)	0.7233	11
B10(Lack of incentives and motivation to encourage employees to apply innovative strategies)	0.7164	13
B11(Difficulty in understanding LC concept)	0.7205	12
B12(Lack of knowledge and expertise needed to apply lean construction techniques)	0.7301	9
B13(Lack of Education and training required to implement lean construction)	0.8877	2
B14(Absence of awareness programs to enhance understanding about LC)	0.8932	1

It can be concluded that the potential for lean adoption in Kano is high, given the growing demand for quality, efficiency, and sustainable project delivery. If properly implemented, lean construction can significantly enhance performance, reduce waste, and strengthen the competitiveness of local contractors. A successful lean application requires more than awareness — it demands a cultural transformation, management commitment, and capacity development across all levels of the construction process.

ISBN: 978-978-8567-02-8

TABLE 3. PROPOSED STRATEGIES TO ENHANCE THE APPLICATION

Strategies	N	Mean
S1(Initiate good planning and control)	146	4.59
S2(Encourage performance/measurement strategy)	146	3.88
S3(Provide Training and Education)	146	4.61
S4(set clear goals and metrics)	146	3.88
S5(foster good collaboration/communication)	146	3.98
S6(Streamline the supply chain)	146	3.90
S7(promoting the use of multi-skilled labour)	146	3.82
S8(Encourage Government support)	146	3.81
S9(Encourage long term philosophy)	146	3.79
S10(Encourage flexibility to change)	146	3.82
S11(promoting sensitization of lean practice)	146	4.63
S12(provision of incentives and motivation)	146	4.02
Valid N (listwise)	146	

5.2 Recommendations:

Regular workshops, seminars, sensitization, and professional training programs should be organized by construction associations, government agencies, and academic institutions to improve practitioners' understanding and skills in lean principles. In addition, the lean construction concept should be incorporated into the curriculum of higher institution in Nigeria. This can assist in producing potential construction professionals with adequate knowledge of lean thinking.

Government bodies and regulatory agencies such as COREN, NIOB, and KNUPDA should promote lean construction by including it in procurement policies,

project evaluation criteria, and capacity-building initiatives.

Further studies should be encouraged to evaluate the quantitative impact of lean techniques on project performance in different construction sectors within Kano and other regions of Nigeria. Lastly, Organizations should adopt the PDCA (Plan–Do–Check–Act) cycle for continuous evaluation and refinement of processes, ensuring sustainability and long-term lean culture.

5.3 CONTRIBUTION TO KNOWLEDGE

This study contributes to the body of knowledge by: (i) providing empirical evidence on the current state of lean construction awareness and adoption in Kano. (ii) Identifying specific barriers that limit lean implementation in the Nigerian context; and (iii) Proposing a practical framework to guide construction firms in applying lean techniques for improved performance.

REFERENCES

Achaka, C. H., et al. (2024). "An Evaluation of Barriers of Lean Implementation in Offshore Facility Maintenance Projects in the Oil and Gas Industry."

Alinaitwe, H. M. J. J. o. c. i. d. c. (2009). "Prioritising Lean Construction Barriers in Uganda's Construction Industry." **14**(1).

Aslam, M., et al. (2022). "Framework for selection of lean construction tools based on lean objectives and functionalities." **22**(8): 1559-1570.

Aziz, R. F. and S. M. J. A. e. j. Hafez (2013). "Applying lean thinking in construction and performance improvement." **52**(4): 679-695.

Babalola, O., et al. (2018). "Assessment of awareness and adoption of lean practices in the Nigerian building industry." **9**(13): 1626-1640.

Ballard, G., et al. (2003). "Lean project management." **31**(2): 119-133.

Bhasin, S. J. M. d. (2012). "An appropriate change strategy for lean success." **50**(3): 439-458.

Chukwuemeke, A. E., et al. (2025). "Factors Affecting the Implementation of Lean Construction Practices in Nigeria." **14**: 1-7.

Enshassi, A., et al. (2019). "Application level of lean construction techniques in reducing accidents in construction projects." Journal of Financial Management of Property and Construction **24**(3): 274-293.

Fadeke, A. and D. Aghimien (2016). Assessment of Lean Construction Practice in the Nigerian Construction Industry. Proceedings of the Joint International Conference (JIC).

Forbes, L. H. and S. M. Ahmed (2020). Lean project delivery and integrated practices in modern construction, Routledge London, UK.

Ibrahim, A., et al. (2025). "Bridging barriers to lean construction adoption in megaprojects: a data-driven contribution to sustainable development using SEM: Ibrahim et al." 1-50.

Koskela, L. (1992). Application of the new production philosophy to construction, Stanford university Stanford.

Moradi, S. and P. J. B. Sormunen (2023). "Implementing lean construction: a literature study of barriers, enablers, and implications." **13**(2): 556.

Musa, M. M., et al. (2023). "Assessment of awareness and barriers to the application of lean construction techniques in Kano state, Nigeria." **6**(1): 33-42.

Ojo, L. D., et al. (2022). "Conceptual framework of value management adoption in the Nigerian construction industry." **22**(4): 939-961.

Owolabi James, D., et al. (2014). "Causes and effect of delay on project construction delivery time." **2**(4): 197-208.

ISBN: 978-978-8567-02-8

Oyewobi, L. O., et al. (2025). "Lean construction management: stationary analysis of the barriers to the implementation of value stream mapping (VSM) in achieving sustainable construction project."

Pallant, J. (2020). SPSS survival manual: A step by step guide to data analysis using IBM SPSS, Routledge.

Romo, R., et al. (2024). "Statistical analysis of lean construction barriers to optimize its implementation using PLS-SEM and PCA." **14**(2): 486.

Salem, O., et al. (2005). "Site implementation and assessment of lean construction techniques." **2**(2): 1-21.

Sarhan, S., et al. (2013). "Barriers to implementing lean construction in the UK construction industry." **6**(1): 1-17.

ISBN: 978-978-8567-02-8

5TH Faculty of Engineering Conference on Engineering Innovation and Economic Policies: Driving Sustainable Industrial Growth in Nigeria

Faculty of Engineering, Bayero University, Kano.

002-Effect of Tensile Reinforcement Ratio on Flexural Behaviour and Ductility of Metakaolin-Based Geopolymer Concrete Beams

[1]I. Aliyu, [2]I. O. Sholadoye, [3]A. Mohammed and [4]A. A. Ozovehe

Department of Civil Engineering, Ahmadu Bello University Zaria

*Corresponding authors: e-mail: [1]ibrahimaliyu67@yahoo.com [2]kemshol1977@gmail.com , [3]ibshazali@gmail.com and [4]ozovvehea@gmail.com

Abstract: The research work covers the development of a metakaolin-based geopolymer concrete mix design suitable for Reinforced Concrete beams. Geopolymer cement-based concrete has been reported to be a high-strength inorganic polymer concrete that can be used in place of Portland cement (PC) concrete and it is environmentally friendly. Geopolymer. The kaolin clay was beneficiated at the Chemical Engineering Laboratory. Powdered kaolin clay was placed in a furnace and heated (Calcined) for 3 hours at 800°C to obtain the Metakaolin. The physical and mechanical properties of constituents of geopolymer concrete were determined. The reinforced metakaolin-based geopolymer concrete beams produced using the established mix design were analysed based on failure pattern. The relationship between load and influence of reinforcement ratio on yield load, ultimate load, failure load and ductility coefficient were determined. The 8mm and 10mm reinforcement bars have a value greater than the 460 N/mm^2 tagged by BS 4449 and within the 400 and 600 N/mm^2 specified by EC2, while diameter 12 mm has less with a yield strength of 397.34 N/mm^2 but approximately equal to the lowest value stated by the EC2. The average elongation of all the reinforcement fall below the 14% recommended by BS4449 but satisfies 7.5% for the high yield bar category C recommended by EC 2. All the loads increase with reinforcement increase (stiffness increase), compared with RGCB8, the yield load of RGCB10 and RGCB12 increased by 11.11% and 19% respectively, while the ultimate load increased by 10.65% and 26.21% respectively. The yielding, the displacement of the beams increased by 52% to ultimate displacement, the value indicates that the beam does not deform much after yielding.

Keywords: Geopolymers reinforced concrete beam, Metakaolin geopolymer, Flexural behavior, Eurocode 2 and Ductility Coefficient

1. INTRODUCTION

The mix materials for geopolymer concrete and mortar are the same as that for conventional concrete and mortar except for the cement which is a geopolymer binder. When metakaolin was the source material, the mix became very viscous and stiff (low workability) as reported by Pouhet, R. and Cyr (2016), Sameer (2015) and Duxson *et al.* (2007b). In consequence, admixtures that improve the workability were suggested. Mohammed et al, (2023) utilized Geopolymer concrete comprising of a geopolymer paste derived by chemically activating metaKaolin with an alkaline activating solution, along with the addition of a superplasticizer, water, and coarse and fine aggregates

Geopolymer cement can be deployed to produce a reinforced concrete (RC) structure or structural element. For such structures, safety is the foremost design and construction parameter to be considered, the safety is conventionally ensured through the use of codes of practice. In Nigeria, Reinforced Concrete (RC) design is mostly performed using the British code (BS 8110) which was withdrawn and replaced by Eurocode 2. This implies sooner or later Eurocode 2 would replace BS 8110 as the most used RC design code in Nigeria. In the absence of codes of practice for emerging construction materials like geopolymer concrete, the safety levels associated with existing codes for the construction material to be used for structural purposes need to be assessed.

The ductility of reinforced concrete is needed to know the extent to which a RC member displaces after yielding before failure. Grace *et al.* (1998) defined structural ductility as the ability of the structure to withstand load applied beyond the elastic limit until failure without a significant loss of load-carrying capacity. Onat and Burak (2018) assessed the impact of tensile reinforcement ratio on the ductility of mid-rise RC structures and concluded that tension reinforcement increase reduces the inter-storey drift ratio of storey buildings, i.e. relative deflection reduces. Compared to conventional concrete, GC exhibits lower permeability and improved resistance to chloride penetration, mitigating the deterioration and corrosion of steel reinforcement (Nagajothi, et al., 2022). These properties enhance the durability of structures, reducing the need for frequent maintenance and aligning with sustainability objectives.

Generally, this study aimed to provide an understanding of the usage of locally sourced kaolin materials in the production of structural grade geopolymer concrete for reinforced concrete members. It would also inform the construction industry, government agencies, fellow researchers, and the public about the viability of locally-sourced geopolymer concrete. Therefore, this study experimentally investigates the

ISBN: 978-978-8567-02-8

influence of tensile reinforcement ratio on the yield, ultimate, and failure loads, as well as the ductility coefficient, of reinforced metakaolin-based geopolymer concrete beams.

2. METHODOLOGY

2.1 Materials

The **Metakaolin** used in the research was obtained by beneficiation and calcination of kaolin clay gotten from Kankara **kaolin clay** deposits in Kankara Local Government Area of Katsina State, the treatment was carried out at the chemical engineering department Ahmadu Bello University (A.B.U), Zaria. Drinking **water** as recommended by BS EN 196-1 (1995) was used during the preliminary tests on materials, preparing the NaOH solution as well as casting operation of the specimens from the heavy-duty/concrete laboratory of the Department of Civil Engineering, A.B.U, Zaria. The **steel reinforcements (**8mm, 10mm, and 12mm) bars free from any physical defects that might affect the steel's mechanical properties in conformity BS 4449 (1997) were sourced from a local supplier along Kongo road Tudun-wada Zaria, Kaduna state. Crushed granite was sourced from Shirash quarry in Hanwa, Zaria Local Government in Kaduna State. The **coarse aggregate** is graded and of a nominal maximum size of 20 mm. Natural sharp sand (river sand) was sourced from the Jere River in Kafur Local government area of Katsina State and used as the **fine aggregate** after removing larger sizes by sieving through BS sieve 4.75 mm at the heavy-duty laboratory of Civil Engineering Department, A.B.U Zaria. **Sodium Silicate (Na_2SiO_3), t**he liquid is a gelatinous liquid with a sum of SiO_2 and Na_2O of 98.1 % and a Technical grade **Sodium Hydroxide (NaOH)** was purchased at Sabon-gari Local government general market in Kaduna State. This grade was used because the research is for application in the construction industry and Diane (2017) mentioned that technical grade chemicals have enough quality for use during industrial production.

2.2 Methods

2.2.1 Properties of the Materials

The kaolin clay was beneficiated (Process of removing impurities and nonreactive granules) at the Chemical Engineering old Building Laboratory, it was soaked in water and allowed in water for 2 days and then it was filtered; the effluent was allowed to settle, and excess water was gradually removed leaving the sludge whose water was finally filtered to obtain the wet beneficiated kaolin clay. The wet clay was then air and oven-dried before it was ball-milled to obtain the beneficiated kaolin clay in powder form. The powdered kaolin clay was placed in a furnace and heated (Calcined) for 3 hours at 800^{o}C to obtain the Metakaolin. The choice of the duration and temperature was done to obtain a highly reactive metakaolin based on reports by Badogiannis *et al.* (2005) and Keeratikan and Janjit (2018). **Particle Size Distribution of Fine and Coarse Aggregate** were prepared and measured for the test in compliance with, BS EN 933-1: (1997). **Flakiness and Elongation Indices of Coarse aggregates** were performed respectively in compliance with BS 812-105.1 (1989) and BS 812-105.2 (1990). **Aggregate Crushing Value (ACV) and Aggregate Impact Value (AIV) Test** in accordance with BS 812-110 (1990) and BS 812-112 (1990) respectively.

2.3 Test on Steel Reinforcements and Preparation for Use

The yield strength, ultimate strength, and elongation tests on the bars were conducted at the heavy-duty laboratory of the Civil Engineering Department per BS EN 10002-1 (2001). Bending and cutting of the steel reinforcement for use in the concrete was performed in accordance with BS 4466 (1989). Plate I shows the reinforcements placed before concrete casting.



Plate I: Metakaolin-based geopolymer beams reinforcement

2.3.1 Material Properties for the Beams

To produce the concrete specimens in the laboratory, The Metakaolin, fine aggregate, and coarse aggregates (Solid constituents) were measured and dry mixed in a plastic container and then transferred to an electric concrete mixer, the alkaline liquids (NaOH solution and Na_2SiO_3 gel) measured and prepared the previous day, were mixed and poured to the solid constituents and mixing continues for an average duration of 5 minutes, due to the stiffness of the mix, and to obtain a mix that can be cast in the moulds, a specified content of extra water and/or super-plasticizer were gradually added to get a workable mix.

The beam size and section property was chosen based on the size of available equipment required in the laboratory to produce the beams, be that as it may, the dimensions of the beams satisfy BS EN 12390-1 (2000). Reinforced geopolymer concrete beams with dimensions of 450 mm length and 100*100 mm cross-sectional area were produced. The geopolymer concrete mix proportion as established during mix design (Table 1, and the mix (produced for casting the beams) achieved an average compressive strength of 32.8 N/mm^2 (based on three cubes). Nine Metakaolin-based Reinforced Geopolymer Concrete Beams (RGCB) were produced of which each set (three beams) were respectively reinforced with two (2) 8mm, 10mm, and 12mm steel bars placed horizontally(Singly reinforced). A concrete cover of 15

ISBN: 978-978-8567-02-8

TABLE 1: MIX DESIGN FOR STRUCTURAL GRADE MBGC

S/No	Mc (Kg/m^3)	ALR (ALm)	Alr	Fa (Kg/m^3)	Ca (Kg/m^3)	Wc (Kg/m^3)	Slump (mm)	f_{ck} (N/mm^2) Target	Acquired
1	400	0.9	3	546.7	1093.3	60	85	25	31.33

mm was provided. Plate II the hardened de-molded beams.

The specimens were allowed a resting period of 24 hrs under ambient temperature in the moulds after casting, they were then de-moulded weighed, wrapped in a polyethylene bag as recommended by Sameer (2015) and Jacob (2017) to prevent excessive evaporation, and then placed in an oven and heat cured for 24 hours at 60 ^oC. The specimens were then removed weighed again and kept under ambient temperature until the day of testing. The choice of curing temperature and duration was based on recommendations by Davidovits (1999), Hardjito *et al.* (2004), Heah *et al.* (2011) and Abdul Rahim *et al*. (2014).



Plate II: Produced reinforced Metakaolin-based geopolymer concrete beams

2.3.2 Beams Bending Test Set-up

A universal testing machine produced by Saml-Denison and Sons LTD Leeds England was used as the loading equipment. The loading capacity of the machine is up to 500kN and was set to a maximum of 100kN for the test. The test was conducted per BS EN 12390 -5 (2009), one loading roller positioned at the centre was used, and the beam simply supported over two steel rollers (centre-point test), to ensure an even distribution of the load between the rollers as required by the code (Figures 1). A dial Gauge was placed at the bottom to measure the mid-span deflection (displacement) (Plate III). The machine was set to move at an average speed of 20mm/minute (0.33mm/sec). Readings were taken at 2 kN intervals simultaneously with the corresponding deflection reading until failure of the specimen; an average of the three results (for 3 beams) was taken as a representative result. The test was conducted in the Strength of materials laboratory of the Mechanical Engineering Department, A.B.U Zaria.



Plate III: Laboratory Beam Test set up

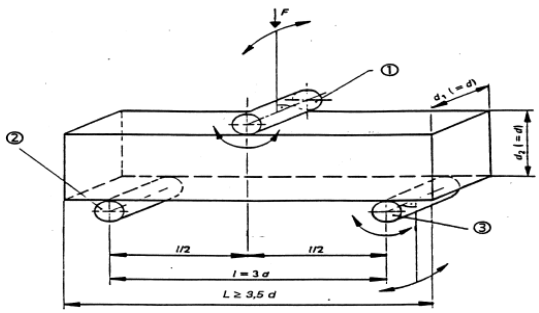


Figure 1: Centre point set up (BS EN 12390-5:2000)

2.3.3 Theoretical Beam Capacities Based on Eurocode 2 Formulations

1 Deflection:

The limiting deflection based on Eurocode's requirements according to Mosley *et al.* (2007) is span/250 and the limiting span effective depth ratio is:

$$\frac{l}{d} = K\left[11 + \frac{1.5\sqrt{f_{ck}}}{\rho - \rho'}\,\rho_0 + \frac{\sqrt{f_{ck}}}{12}\sqrt{\frac{\rho^1}{\rho_0}}\right] \qquad (1)$$

where $\rho > \rho_0$

ρ^1 = Compression reinforcement (Zero in this case)

ρ^0 = Reference reinforcement ratio= $10^{-3}\sqrt{f_{ck}}$

K = 1 for simply supported beam

2. Ductility Coefficient

Shiyun *et al.* (2012) mentioned that to determine the aseismic behaviour of RC beams, the ductility coefficient must be considered. Also, adequate ductility is required to dissipate any energy developed due to seismic event or impact (Zila, 2004)), ductility coefficient (factor) is a ratio of ultimate displacement Δ_u to yield displacement Δ_y (2)

$$\Delta_\Delta = {}^{\Delta_u}\!/_{\Delta_y} \qquad (2)$$

ISBN: 978-978-8567-02-8

3.0 RESULTS AND DISCUSSION

3.1 Steel Reinforcement Test

The properties of the reinforcement steel used for the production of the RC beams are as presented in Table 3. It can be seen that as the diameter of the bar increased the yield strength which is the most important parameter reduces, diameter 8mm and 10mm both have a value greater than the 460 N/mm^2 tagged by BS 4449 (1997) and within the 400 and 600 N/mm^2 specified by EC2 (2004), while diameter 12 mm has less with a yield strength of 397.34 N/mm^2 but approximately equal to the lowest value stated by the EC2 (2004).

TABLE 3: PROPERTIES OF STEEL REINFORCEMENT BAR

Parameter	**Y8**	Y10	Y12	**BS 4449 (1997)**	**EC 2 (2004)**
Characteristic Yield strength (N/mm^2)	536.32	486.88	397.34	460 N/mm^2	400 - 600
Characteristic Ultimate strength(N/mm^2)	591.21	575.93	560.58		
Elongation (%)	9.76	9.32	9.52	≥ 14 %	≥ 7.5 %
Mean yield strength/ σ (N/mm^2)	543.2/4.19	495.57/5.3	405.9/5.22		
Mean ultimate strength/ σ (N/mm^2)	601.1/6.02	595.34/11.8	570.18/5.85		

Anthony *et al.* (2015) also reported a decrease in average yield stress of reinforcement with an increase in bar diameter and Ejeh and Jibrin (2012) reported that not all the reinforcement bars used in Nigeria complied with the minimum ultimate to yield strength ratio as specified by the code. The average elongation of all the reinforcement fall below the 14% recommended by BS4449 (1997) but satisfies 7.5% for the high yield bar category C recommended by EC 2 (2004). It should be noted that according to BS 4449 (1997), values of elongation not falling within code specified limits do not cause non-conformity of the steel to the standard.

3.2 Reinforced Metakaolin-Based Geopolymer Concrete Beams (RGCB)

The reinforced metakaolin-based geopolymer concrete beams produced using the established mix design and tested were analysed based on failure pattern (Plate VI). Influence of Reinforcement Ratio on Ductility Coefficient, Yield, Ultimate, Failure Loads of a Reinforced Geopolymer Concrete Beam were established



Plate VI: Sample of the failure configuration of the geopolymer beam

3.3 Influence of Reinforcement Ratio on Yield Load, Ultimate Load, and Failure Load

The yield, ultimate, and failure load are listed in Figure 2. The yield load is the point on the load-deflection curve where the reinforced-composite beam behaviour turns from elastic to plastic and the curve begins to turn non-linear. The ultimate load is the maximum load sustained by the beam and the failure load is the load at which the beam failed. All the loads increase with reinforcement

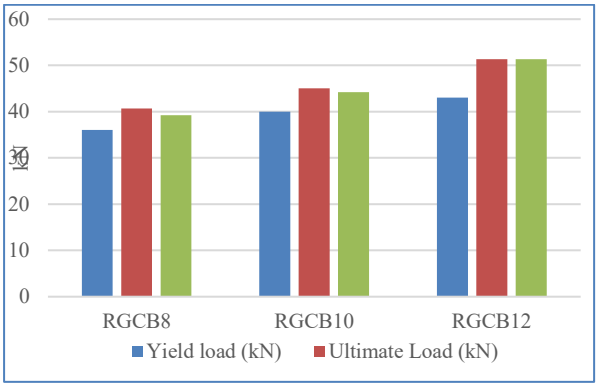


Figure 2: Approximate Values of Yield, Ultimate, and Failure Load

increase (stiffness increase), compared with RGCB8, the yield load of RGCB10 and RGCB12 increased by 11.11% and 19% respectively, while the ultimate load increased by 10.65% and 26.21% respectively. The yield, ultimate, and failure loads are close to each other due to the fact that the beam is singly reinforced therefore after yielding of the steel, the fibre is purely concrete with little resistance to tensile stress which hence failed immediately with a little load increase

3.4 Ductility Coefficient

The ultimate displacement, yield displacement, and ductility coefficient for the beams, the ductility coefficients (factors) presented in Figure 3 are identical for the three beams, at an average of 1.52. This means that after yielding, the displacement of the beams increased by 52% to the ultimate displacement, a value which indicates that the beam exhibited limited plastic deformation and do not deform much after yielding**.** Ductility coefficients reported by Shiyun *et al.* (2012) are higher than these values for doubly reinforced concrete beams with shear reinforcements and with lengths greater than 1m. It can be said that the small values gotten may be due to the absence of compression reinforcement and due to the length of the beams which resulted in a small increase in deflection after yielding to ultimate and failure. Caio and Isabela (2017) also reported a decrease

ISBN: 978-978-8567-02-8

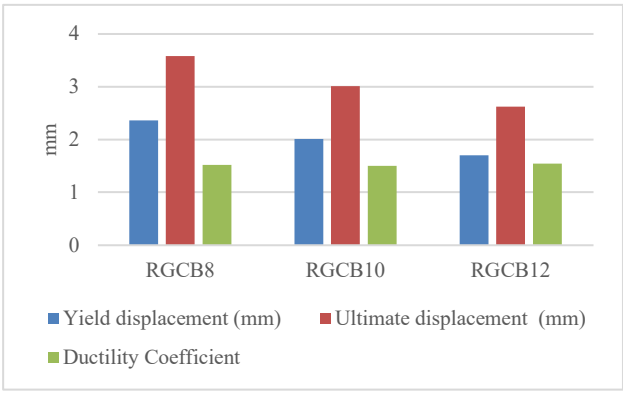


Figure 3: Deformation Behaviour of the Beams

in ductility of the RC beam due to the absence of shear reinforcements (absence of confinement effect of shear reinforcements), the absence of shear reinforcement lead to rapid deterioration and sudden failure of the concrete after yielding.

4. Conclusion AND RECONMENDATION

4.1 Conclusion

The following conclusions were drawn from the results of the study:

i. The average elongation of all the reinforcement fall below the 14% recommended by BS4449 (1997) but satisfies 7.5% for the high yield bar category C recommended by EC 2.

ii. All the loads increase with reinforcement increase (stiffness increase), compared with RGCB8, the yield load of RGCB10 and RGCB12 increased by 11.11% and 19% respectively

iii. The displacement of the beams increased by 52% to ultimate displacement, the value indicates that the beam does not deform much after yielding.

4.2 Recommendation/ further studies

i. Relationship between Theoretical (EC2 based) and Experimental Ultimate shear and Moment should be worked on.

ii. Investigation doubly reinforced and shear-reinforced geopolymer beams to improve ductility,"

iii. The developed mix design can be validated for full-scale structural elements

REFERENCES

Abdul Rahim, R.H. Azizli, K.A. Z. Man, T. Rahmiati and Nuruddin. M.F., (2014). Effect of Sodium Hydroxide Concentration on the Mechanical Property of Non Sodium Silicate Fly Ash Based Geopolymer. *Journal of Applied Sciences*, 14: 3381-3384.

Anthony, N. E., Emmanuel, O. E., Gideon, O. B., and Jadesola, O. (2015). Assessment of Quality of Steel Reinforcing Bars Used In Lagos, Nigeria. *International Research Journal of Innovative Engineering*. 1(3), 1-8

Badogiannis. E, Kakali, G. and Tsivilis, S. (2005). Optimisation of kaolin to metakaolin conversion'' *Journal of thermal Analysis and calorimetry*, 81(2).457-462

BS 4449 (1997). *Carbon Steel Bars for the Reinforcement of concrete*. British Standards Institutions London.

BS 4466 (1989). *Specification for Scheduling, dimensioning, bending and cutting of steel reinforcement for concrete*. British Standards Institutions. ISBN 0 580 17289 9

BS 812 -110 (1990). *Determine Aggregate Crushing Value*. British Standard Institute

BS 812 -2 (1995). *Testing aggregates. Methods for determination of density.* BSI 389 Chiswick High Road LondonW4 4AL UK

BS 812-1 (1975). *Testing of aggregates: Method of determining Particle Size and Shape*. British standard institution. 2 park street, London W1A 2BS

BS 812-105-1 (1989). *Testing aggregates. Methods for determination of particle shape. Flakiness index*. BSI 389 Chiswick High Road LondonW4 4AL UK

BS 812-105-2 (1990). *Testing aggregates. Methods for determination of particle shape. Elongation index of coarse aggregate*. British Standard Institute

BS 812-112 (1990). *Testing aggregates. Method for determination of aggregate impact value (AIV)*. British Standard Institute

BS 882 (1992). *Specification for aggregates from natural sources for concrete*. British Standard Institute BSI ISBN0580 2163 X

BS EN 10002-1(2001). *Tensile Testing: Tests at ambient Temperatues*. British Standards Institutions London.

BS EN 1097-6 (2013). *Test for mechanical and Physical Properties of Aggregates: Determination of Density and Water Absorption:* BSI Standards Limited SBN 978 0580 71032 2

BS EN12390-1 (2000). *Testing hardened concrete: Shape, dimensions and other requirements for specimens and moulds.* British Standards Institutions London

BS EN 12390 -5 (2009). *Testing of hardened concrete: Flexural strength of test specimens*. British Standards Institutions London

BS EN 12620: (2002). *Aggregates for concrete*. British Standards Institutions London.

BS EN 196-1 (1995). *Method of Testing Cement: Determination of Strength.* British Standards Institutions London

BS EN 933-1 (2012). *Tests for geometrical properties of aggregates. Determination of particle size distribution. Sieving method*. British Standards Institution Limited ISBN 978 0 580 74432 7. 1-21

ISBN: 978-978-8567-02-8

Caio, G. N., and Isabela, D. R. (2017). Ductility Analysis of RC Beams Considering the Concrete Confinement Effect Produced by the Shear Reinforcement: a Numerical Approach. *Latin American Journal of Solids and Structures*. 14(13). http://dx.doi.org/10.1590/1679-78253904

Davidovits, J. (1999). Chemistry of Geopolymeric Systems, Terminology. *Geopolymer '99 International Conferenc*e. France.

Diane, M. (2017). *Reagent, Laboratory, Technical: Chemistry Grades Explained*. downloaded at https://info.noahtech.com/blog/reagent-laboratory-technical-chemistry-grades-explained on 27/07/2020 geopolymer observed by environmental scanning electron microscopy (ESEM). *Waste*

Diaz, E., Allouche, I N., and Eklund, S. (2010). Factors affecting the suitability of fly ash as source material for geopolymers. *Journal of Fuel*, 89(5), 992–996, https://doi.org/10.1016/j.fuel.2009.09.012

Duxson, P.; Lukey, G.C.; van Deventer, J.S.J. (2007b). Physical evolution of na-geopolymer derived from metakaolin up to 1000 degrees c.*J. Mater. Sci.,* 42, 3044–3054.

EC 2. Eurocode 2. (2008). *Design of Concrete Structures.* BS EN 1992-1- 2, European Committee for Standardization, CEN Brussels.

Ejeh, S. P., and Jibrin, M. U. (2012). Tensile Tests on Reinforcing Steel Bars in the Nigerian Construction Industry. *IOSR Journal of Mechanical and Civil Engineering* (IOSR-JMCE). 4(2), 06-12. www.iosrjournals.org

Grace, N, F., Soliman, A. K., Abdel-Sayed, G., and Saleh, K. R. (1998). Behavior and ductility of simple and continuous FRP reinforced beams. *Journal of Composites for Construction*, 2 (4), 186-194

Hardjito, D., Wallah, S.E., Sumajouw, D.M.J., and Rangan, B.V. (2004). On The Development of Fly Ash-Based Geopolymer Concrete. *ACI Materials Journal*; 101(6), 467-472.

Heah, C.Y. Kamarudin, H. Mustafa Al Bakri, A.M. Binhussainb, M.Luqman, M. Khairul Nizar, I. Ruzaidi, C.M., and Liew, Y.M. (2011). Effect of Curing Profile on Kaolin-based Geopolymers. *Proceedings of 2011 International Conference on Physics Science and Technology* (ICPST 2011). 305-311

Jacob, E. A. (2017). *Evaluation of the properties of Matakaolin based Geopolymer Concrete made with Recycled concrete Aggregate*. Unpublished MSc Dissertation submitted to the Department of Building, Faculty of Environmental Design, Ahmadu Bello University, Zaria.

Keeratikan, P, and Janjit, I. (2018). Characteristics of meta-kaolin geopolymer Bender-Element (BE) test. *Science Direct Materials Today Proceedings* 5 5120–15125 www.materialstoday.com/proceedings

Liu, M., Hu, R., Zhang, Y., Wang, C., and Ma, Z. (2023). Effect of ground concrete waste as green binder on the micro-macro properties of eco-friendly metakaolin-based geopolymer mortar. *Journal of Building Engineering*, *68*, 106191. Mosley, W. H., Bungey, J. H., and Hulse, R. (2007). *Reinforced Concrete Design (6th Ed).* Palgrave Macmillan, New York.

Nagajothi, S., Elavenil, S., Angalaeswari, S., Natrayan, L. and Mammo, W.D. Durability studies on fly ash based geopolymer concrete incorporated with slag and alkali solutions. *Adv. Civ. Eng.* **2022**, *2022*, 7196446

Mohmmad, S. H., Shakor, P., Muhammad, J. H., Hasan, M. F., and Karakouzian, M. (2023). Sustainable alternatives to cement: synthesizing metakaolin-based geopolymer concrete using nano-silica. *Construction Materials*, *3*(3), 276-286.

Onat, N., and Burak, Y. (2018). Effects of Tension Reinforcement Ratio on Ductility of Mid-Rise Reinforced Concrete Structures. *6th International Symposium on Innovative Technologies in Engineering and Science*. 09-11 November 2018 (ISITES2018 Alanya – Antalya - Turkey)

Pouhet, R. and Cyr, M. Formulation and performance of flash metakaolin geopolymer concretes. *Constr. Build. Mater.* **2016**, *120*, 150–160

Sameer Ul B. (2015). Effect of Alkali materials on Geopolymer concrete. *International Jornal of Civil Engineering and Technology (IJCET).* 6(1), 01-13 ISSN 0976-6216

Shiyun, X., Wenbo, C., and Haohao, P. (2012). Experiment of Reinforce Concrete Beams at Different Loading Rates. *15 World Conference on Earthquake Engineering (WCEE*) LISBOA 2012

Zila, R., Antonio, G., and Gianluca, G. (2004). Ductility of R.C. Beams Reinforced With FRC. *13th World Conference on Earthquake Engineering*. Vancouver, B.C., Canada August 1-6, 2004 Paper No. 2761

ISBN: 978-978-8567-02-8

003-Customising SUMO with Real-World Vehicle Data: A Step-by-Step Guide for Low-Income Urban Transport Systems

Mohammed Ya'u[1], Aminu Suleiman[2]

[1]*Department of Civil Engineering Technology, The Federal Polytechnic, Damaturu.* katamma300@gmail.com
[2]*Department of Civil Engineering, Faculty of Engineering, Bayero University Kano, Nigeria.*
asuleiman.civ@buk.edu.ng

Abstract: This study localises the Simulation of Urban Mobility (SUMO) for a low-income city. Field data were collected in Damaturu, Nigeria, through manual traffic counts, speed studies, and acceleration measurements. Fuel consumption was estimated with Gaussian Process Regression, and emissions were derived using the middle approach method. These values were integrated into SUMO by defining new vehicle types, including tricycles and mixed fuel buses, absent from the default settings. Calibration using TraCI scripts adjusted driver error, reaction times, and vehicle dynamics to match observed behaviour. Results show field CO_2 emissions at 19,520 kg, while the calibrated SUMO output recorded 19,620 kg, only 0.5% higher. The study demonstrates that localising SUMO with real-world data improves accuracy, facilitates more accurate emission accounting, and provides a foundation for policy in low-income cities.

Keywords: SUMO localisation; Low-income cities; Vehicle emissions, CO_2

1. INTRODUCTION

Urban mobility in Nigeria's low-income urban centres is mostly shaped by informal transportation systems and insufficient infrastructure. In peri-urban areas, over 33% of the population depends on motorcycles, while a concerning 81.4% of the roads are unpaved (Yakubu et al, 2023). Legislative changes, including the removal of fuel subsidies, have compelled a greater number of low-income individuals to rely on motorcycles, thereby intensifying safety and environmental risks (Kwaghgba et al., 2024). In the Ajegunle community of Lagos, inadequate transit options lead to social isolation, causing residents to lose between 7.6% and 27.4% of their daily income due to mobility limitations (Castro et al. 2022).

Recent shifts from motorcycles to tricycles have produced specific benefits. Studies demonstrate a decrease in accidents, a drop in crime rates, and an enhancement in operator income when tricycles replace motorcycles (Lenshie et al., 2022). Nonetheless, these advancements are accompanied by persistent challenges regarding legislation, compliance, and infrastructure.

The transportation sector in Nigeria remains defined by motorcycles, tricycles, and mixed-fuel minibuses, all operating within a fragmented legal framework. Government restrictions have accelerated the shift from motorcycles to tricycles; yet, regulatory ambiguities generate confusion for both riders and regulatory authorities (Basirka et al., 2019; Lenshie et al., 2022). The removal of fuel subsidies has altered travel choices, solidifying dependence on more economical two- and three-wheeled vehicles/modes (Kwaghgba & Tyozenda, 2024). An analysis of the vehicle fleet in Lagos indicates a prevalence of ageing and environmentally detrimental vehicles: 66% are over ten years old, with 60% of petrol engines and 75% of diesel engines surpassing set emission limits (Ajayi et al., 2024). These conditions highlight the necessity for models that precisely reflect Nigeria's distinctive vehicle mix, regulatory complexities, and economic constraints, rather than relying on conclusions drawn from rich contexts.

The Simulation of Urban Mobility (SUMO) is a commonly employed tool in transportation research. SUMO is a versatile, open-source framework proficient at modelling transportation flows at both sub-microscopic and macroscopic scales. It enables multiple purposes, such as network development, traffic analysis, routing, and scenario simulation, often employing data obtained from OpenStreetMap (Clemente, 2022). The applications include demand-responsive transport systems, where Python-based approaches improve vehicle routing efficiency (Armellini, 2021), and research on emergency vehicle prioritisation that uses microsimulation to assess journey lengths and delays (Soni & Weronek, 2023). SUMO also offers demand-generation tools that generate traffic scenarios when street-level counts are available (Behrisch & Hartwig, 2021).

Despite its versatility, many researchers have noticed limitations in SUMO's default modelling capabilities. Salles et al. (2022) emphasised unrealistic car-following

ISBN: 978-978-8567-02-8

behaviours and developed a Human Driver Model to better depict acceleration and gap dynamics. Karakaya et al. (2023) identified deficiencies in SUMO's cycling modelling, which simplistically classified cyclists as either slow vehicles or fast pedestrians, and advocated for a data-driven alternative. Kusari et al. (2022) improved background vehicle dynamics by calibrating the Intelligent Driver Model using realistic data, while recognising the need for considerable user expertise. These studies suggest that the outputs generated by SUMO often require adjustments to accurately represent real-world situations.

The issue is significantly more acute in low-income urban regions like Damaturu. The SUMO assumes the presence of standardised vehicle fleets, ideal fuel efficiency comparable to manufacturer specifications, and compliance with regulatory norms by drivers. In reality, these fleets consist of tricycles, outdated minibuses and vehicles noted for their inadequate fuel efficiency. If unchanged, SUMO is likely to misrepresent essential elements such as traffic congestion, greenhouse gas emissions, and the intricacies of human. This constraint reduces its relevance in urban policy-making for cities urgently requiring data-driven mobility planning.

This paper aims to address this gap by customising SUMO, using empirical data gathered from Damaturu. Data on vehicle composition, fuel usage, and driving habits were methodically collected and analysed. New vehicle classes, including tricycles and fuel-specific minibuses, were created. The calibration process with TraCI confirmed that the emissions modelled by SUMO aligned with actual recorded data. The primary aim is both technical and practical: to illustrate that transport simulations grounded in localised data can provide reliable insights for mobility planning in economically disadvantaged urban areas.

2. METHODOLOGY

This study was conducted in Damaturu, Yobe State, Nigeria. Primary data were obtained through field surveys, which included classified manual traffic counts, speed studies, and vehicle acceleration measurements using CarAccel, a mobile application.

Traffic volume counts were carried out on eight primary routes within the Damaturu metropolis, covering approximately 37 km. Surveys were conducted between 12:00 and 13:00 hours for three consecutive days, and the results were averaged to capture traffic characteristics, vehicle classification, and directional flow patterns. Vehicle speeds were determined using the two-observer method, while acceleration measurements were obtained directly with CarAccel.

To estimate vehicle fuel consumption, a surrogate model approach was employed. Factory-rated vehicle fuel consumption served as the independent variable, while field-observed fuel consumption was the dependent variable. Factory data were obtained from secondary sources, whereas field data were derived by dividing fuel volume (litres)by travel distance. Distance was measured via vehicle speedometer, and fuel volume was recorded during refueling. Gaussian Process Regression (GPR) with a Radial Basis Function (RBF) kernel was applied to estimate field averages for each vehicle class.

Vehicle CO_2 emissions were estimated using the middle approach (Adhi, 2018), which considers the average number of vehicles, class-specific fuel consumption rates (from the surrogate model), road length, and fuel-specific emission factors. The total emissions (TE) were computed using Equation 1:

$$TE=AVA \times FCA \times RL \times EF \quad (1)$$

Where:

TE is the total CO_2 emission measured in grams per kilometre.

AVA is the average number of vehicle types per hour.

FCA is the fuel consumption for a vehicle of class A, measured in kilometres per litre.

RL is the road length in kilometres.

Ef is the emission factor measured in grams per litre.

Emission outputs and traffic dynamics were simulated using the SUMO software. Vehicle classes, fuel types, fuel consumption rates, and behavioural metrics (speed, acceleration, deceleration) were explicitly defined to incorporate real-world traffic characteristics. All inputs were formatted in XML for compatibility with SUMO.

The simulation framework involved network creation with OSM WebWizard, refined using NetEdit to adjust road configurations, set signalised intersections, and define vehicle attributes (length, class, fuel type, fuel consumption, speed, acceleration, deceleration, and driver behaviour). The completed network was validated before running simulations, and CO_2 outputs were extracted via TraCI (Traffic Control Interface).

The baseline accuracy of the model was evaluated by comparing uncalibrated emission estimates with field observations. To improve reliability, the model was calibrated through parameter tuning in TraCI. A custom Python script was developed to dynamically adjust driver behaviour parameters during simulation. This framework modified car-following and lane-changing

ISBN: 978-978-8567-02-8

dynamics while preserving the distinct features of passenger and commercial vehicles.

The main calibration parameters included:

- Driver error (σ)
- Reaction time (τ)
- Maximum acceleration and deceleration rates
- Minimum gap distances
- Lane-changing coefficients

TraCI's set Parameter function allowed real-time adjustment of these variables without restarting the simulation. Distinct behavioural parameters were assigned to each vehicle class to ensure separation between passenger cars and commercial fleets. Calibration accuracy was evaluated against observed thresholds, with 1–5% error margins achieved for each vehicle class

3. RESULTS

3.1 Surrogate Vehicle Fuel Consumption.

Table I presents the field-estimated vehicle fuel consumption obtained through Gaussian process regression, utilising the Radial Basis Function (RBF) kernel. Gaussian Process regression offers flexibility in capturing non-linear dynamics without requiring a predetermined functional form. Localised consumption rates for motorcycles and tricycles were up to 25% higher than factory ratings, indicating the biggest variances. There were also mild changes in buses and passenger cars. These findings highlight the limitations of applying standard fuel consumption factors directly to low-income cities.

TABLE I: SURROGATE VEHICLE FUEL CONSUMPTIONS

Vehicle class	Fuel Consumption
Private Car	0.1228
Taxi	0.148
Tricycle	0.0573
Buses	0.1615
OGV1	0.356
OGV2	0.356
Motorcycles	0.397

3.2 Traffic Volume and CO_2 Emissions Estimation

Figure 1 shows the one-hour traffic volume and the corresponding vehicle emissions. The analysis highlights the relationship between traffic volume and CO_2 emissions across various modes of transportation. A total of 19520 kg of CO_2 was estimated. Cars generated the highest emissions at 8,237.5 kg (42.19%), despite a lower volume than tricycles, indicating greater fuel consumption and emission intensity. Tricycles accounted for 6,157.6 kg (31.55%) due to their substantial traffic volume of 12,080 vehicles per hour, suggesting that even low-capacity modes can substantially impact overall emissions when utilised extensively.

Motorcycles accounted for 3,005 kg (15.39%) of emissions, highlighting their prevalence in mixed-traffic environments. Public transport, exemplified by buses and taxis, produced comparatively low emissions of 494 and 545 kg, respectively, accounting for 2.5% and 2.79% of total emissions, despite their greater passenger capacity, highlighting their efficacy in reducing per capita emissions. Freight vehicles (OGV1 and OGV2) produced relatively low emissions in absolute terms; however, their dependence on diesel fuel makes them disproportionately impactful from an environmental perspective. Pedal cyclists, with a volume of 5,287 v/h, recorded zero CO_2 emissions, illustrating their potential as a sustainable and environmentally friendly mode of transportation. This distribution highlights the disproportionate role of informal and paratransit fleets in shaping urban emissions.

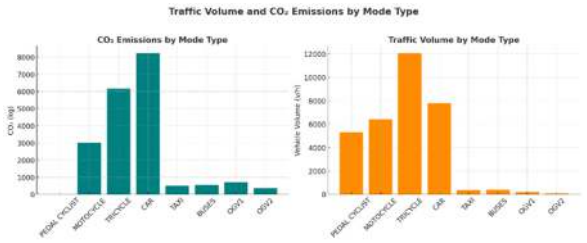


Figure 1: Traffic Volume and CO_2 Emission Comparison

3.3 Assigning Fuel Type and Vehicle Fuel Consumption Per Kilometre to the SUMO Model

In contrast to the SUMO default settings, which provide vehicle emission and fuel consumption data, this study utilises real-world data from low-income cities, customised to the SUMO. Vehicle types like tricycle, which are absent in the SUMO, were modelled. Similarly, the Buses were segregated into fuel and diesel types, as opposed to the default SUMO diesel type. The observed Petrol vehicles (passenger cars, taxis, buses, motorcycles, and tricycles) and diesel vehicles (buses and OGVs) were defined with specific acceleration, speed, and emission parameters. Fuel consumption rates were adjusted based on surrogate data, with passenger cars (0.1228 L/km) compared to OGVs (0.356–0.397 L/km), as shown below. This method increases the accuracy of emissions and energy consumption simulations, making sure the model matches observed trends in fuel economy and traffic behaviour. This increases the dependability of environmental impact evaluations and urban mobility studies.

Due to the drivers' imperfections in the low-income cities, a sigma of 0.5 was adopted. This indicates that the simulated driver is 50% compliant with traffic rules, which is typical for low-income settings.

This modification enhances the model's reliability by

ISBN: 978-978-8567-02-8

aligning it with the realities of local transportation. Better policy insights are also supported because emissions and fuel consumption represent actual vehicle performance rather than broad assumptions. Such contextual precision is essential for developing sustainable transportation plans that work in low-income cities.

```
<routes>
<!--  Define vehicle types  -->
<!--  Passenger car (petrol)  -->
<vType id="passenger" accel="2.6" decel="4.5" s
igma="0.5" length="5" maxSpeed="60" color="0,1,
0" emissionClass="HBEFA3/PC" fuelConsumption="0
.1228"/>
<!--  Taxi (petrol)  -->
<vType id="taxi" accel="2.6" decel="4.5" sigma=
"0.5" length="5" maxSpeed="50" color="1,1,0" em
issionClass="HBEFA3/PC" fuelConsumption="0.148"
/>
<!--  Bus1 (petrol)  -->
<vType id="bus1" accel="0.8" decel="4.5" sigma=
"0.5" length="8" maxSpeed="45" color="1,0,0" em
issionClass="HBEFA3/PC" fuelConsumption="0.1615
"/>
<!--  Bus2 (diesel)  -->
<vType id="bus2" accel="0.8" decel="4.5" sigma=
"0.5" length="12" maxSpeed="45" color="1,0,1" e
missionClass="HBEFA3/Bus" fuelConsumption="0.16
15"/>
<!--  OGV1 (diesel)  -->
<vType id="OGV1" accel="1.0" decel="4.5" sigma=
"0.5" length="15" maxSpeed="40" color="0,0,1" e
missionClass="HBEFA3/HDV" fuelConsumption="0.35
6"/>
<!--  OGV2 (diesel)  -->
<vType id="OGV2" accel="1.0" decel="4.5" sigma=
"0.5" length="15" maxSpeed="40" color="0,0,1" e
missionClass="HBEFA3/HDV" fuelConsumption="0.39
7"/>
<!--  Motorcycle (petrol)  -->
<vType id="motorcycle" accel="2.6" decel="4.5"
sigma="0.5" length="2" maxSpeed="50" color="0,0
,0" emissionClass="HBEFA3/PC" fuelConsumption="
0.057"/>
<!--  Tricycle (petrol)  -->
<vType id="tricycle" accel="2.6" decel="4.5" si
gma="0.5" length="3" maxSpeed="30" color="1,0,1
" emissionClass="HBEFA3/PC" fuelConsumption="0.
057"/>
</routes>
```

3.4 Network Creation

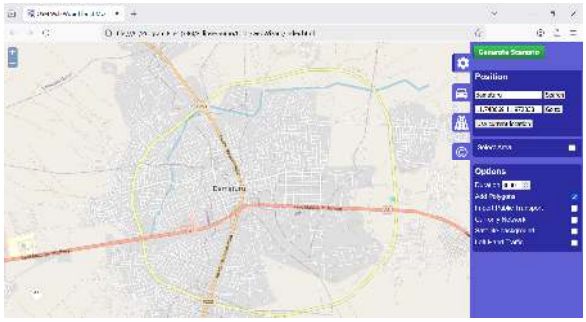


Figure 2: Network extraction from OSM WebWizard and scenario generation

The approach used to create the network is shown in Figures 2 and 3. The study corridor was first selected using the OSM WebWizard, and then the scenario-generating tool was used to obtain the relevant network in XML format. At this point, every relevant road categorisation that was going to be incorporated into the model was carefully chosen.

The final network was then enhanced by using NetEdit, which enabled the precise definition of road configurations and attributes. During this editing stage, signalised crossings were also set up to ensure that traffic controls were accurately represented.

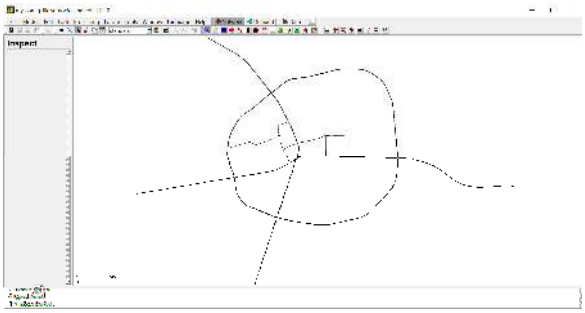


Figure 3: Edited network in NetEdit with road settings and intersections.

3.5 Traffic Flow Generation

To ensure that the field traffic volume and types, together with customised vehicle fuel consumption, are used in the simulation, this Python command was generated and used.

```
randomTrips.py -n grid.net.xml -o
trips.trips.xml -e 3600 --flows (volume) --
period 600 --trip-attributes
"departLane=\"best\" departSpeed=\"max\"
departPos=\"random\"" --fringe-factor 100 --
additional-file vehicles.rou.xml.
```

The use of this command is necessary to generate trips with a specific volume (volume) over one hour on the study network. The period 600 divided the simulation duration of 3600 into six (6) intervals, generating trips every 600 seconds600 seconds. Parameters such as `departLane="best"`, `departSpeed="max"`, and `departPos="random"` ensured variability in trip behaviour, mimicking real-world dynamics. The `--fringe-factor 100` distributed trips toward the network edges, while the `--additional-file vehicles.rou.xml` integrated custom vehicle definitions, allowing the simulation to reflect actual fuel consumption and emission characteristics observed in the study area.

3.6 Assigning The Vehicle Types Proportions

To preserve simulation integrity and account for faulty routes, the Python script presented below assigns vehicle categories to traffic flows. The script mimics the real traffic composition by setting vehicle probabilities for cars, taxis, buses, OGV1, OGV2, tricycles and Motorcycles. To prevent simulation errors, flows that are marked as invalid (with `error="true"`) are routinely left out. To avoid unlimited vehicle creation, flows without a specified end time are also limited to a maximum duration of 3600 seconds (1 hour). By balancing realism and computational robustness, this novel approach guarantees that the output (`trips_with_types.trips.xml`) is representative of traffic dynamics and complies with SUMO's requirements. The method successfully mitigates common traffic modelling issues such as unfinished routes or infinite vehicle spawning. The Python scripts used are presented below:

ISBN: 978-978-8567-02-8

```
import random
import xml.etree.ElementTree as ET

# Define vehicle types and their probabilities
(from your distribution)
vehicle_types = {
    "passenger": 0.2865,   # 28.65%
    "taxi": 0.0139,        # 1.39%
    "bus1": 0.01,        # 1.00%
    "bus2": 0.0047,        # 0.47%
    "OGV1": 0.0075,        # 0.75%
    "OGV2": 0.0037,        # 0.37%
    "motorcycle": 0.2322, # 23.22%
    "tricycle": 0.4415    # 44.15%
}

# Load the trips file (generated by
randomTrips.py)
tree = ET.parse("trips.trips.xml")
root = tree.getroot()

# Assign vehicle types to each flow
for flow in root.findall("flow"):
    # Skip invalid flows (if marked with errors)
    if flow.get("error") == "true":
        continue

    # Randomly assign a vehicle type based on
probabilities
    chosen_type = random.choices(
        list(vehicle_types.keys()),
        weights=vehicle_types.values(),
        k=1
    )[0]

    # Set the vehicle type
    flow.set("type", chosen_type)

    # Ensure the flow has a valid end time (to
prevent infinite trips)
    if "end" not in flow.attrib:
       flow.set("end", "3600")  # Force vehicles
to exit by t=3600

# Save the modified file
tree.write("trips_with_types.trips.xml")
```

3.7 The Route Creation

To generate clean, usable route data for the SUMO simulation and directly enable precise traffic and emission modelling, this step was essential. Trip definitions were transformed into actual network routes using JTRouter to produce realistic vehicle routes. Custom vehicle types were included in the command, which also made sure that all destinations, including those on the network fringe, were recognised. This command prevented unrealistic route patterns and made sure that all trips processed well by incorporating --remove-loops and --ignore-errors. The routing command is present below.

```
jtrrouter -n grid.net.xml –r
trips_with_types.trips.xml --additional-files
vehicles.rou.xml -o routes.rou.xml --accept-
all-destinations --remove-loops --ignore-errors
```

3.8 Route Validation and Repair Using SUMO's duarouter

The duarouter tool from SUMO was employed in the validation process to ensure that route definitions were realistic and coherent. To avert execution mistakes, the existence of input route files was initially verified. The duarouter algorithm was subsequently executed with settings utilising traffic assignment zones (TAZ) to adjust entry and exit points, eradicate loops, and detect and rectify faulty routes. To prevent termination, faults were overlooked wherever possible, while structural fixes remained mandatory. To preserve fleet heterogeneity, vehicle type definitions were stored in a separate output file and subsequently integrated into the verified route file. This phase produced a functional and pristine route dataset, devoid of logical discrepancies and routing irregularities, prepared for subsequent simulation.

```
import subprocess
import xml.etree.ElementTree as ET
from pathlib import Path

def validate_routes(net_file, input_route_file,
output_route_file):
    """
     Validate and repair routes using SUMO's
duarouter.

    Args:
        net_file: SUMO network file (.net.xml)
           input_route_file: Input route file
(.rou.xml)
           output_route_file: Output file for
validated routes (.rou.xml)
    """
    # First, check if the input file exists
    if not Path(input_route_file).exists():
         raise FileNotFoundError(f"Input route
file {input_route_file} not found")

    # Run duarouter to validate routes
    try:
        subprocess.run([
            "duarouter",
            "--net-file", net_file,
            "--route-files", input_route_file,
            "--output-file", output_route_file,
            "--ignore-errors",
            "--repair",
            "--remove-loops",
                 "--with-taz",   # Helps with
entry/exit point validation
                                "--vtype-output",
"validated_vtypes.xml"  # Preserve vehicle types
        ], check=True)

         print(f"Successfully validated routes.
Output saved to {output_route_file}")

        # Merge the preserved vehicle types back
into the output file
         merge_vehicle_types(output_route_file,
"validated_vtypes.xml")

    except subprocess.CalledProcessError as e:
         print(f"Error during route validation:
{e}")
    except FileNotFoundError:
       print("Error: duarouter not found. Please
ensure SUMO is installed and in your PATH.")

def             merge_vehicle_types(route_file,
vtype_file):
    """Merge vehicle type definitions back into
the route file"""
    try:
        # Parse both files
        route_tree = ET.parse(route_file)
        vtype_tree = ET.parse(vtype_file)

        # Get root elements
        route_root = route_tree.getroot()
        vtype_root = vtype_tree.getroot()
```


ISBN: 978-978-8567-02-8

```
        # Insert vehicle types at the beginning
of the routes file
                        for     vtype     in
reversed(vtype_root.findall('vType')):
            route_root.insert(0, vtype)

        # Save the merged file
                    route_tree.write(route_file,
encoding='UTF-8', xml_declaration=True)
         print(f"Merged vehicle types back into
{route_file}")

    except ET.ParseError as e:
          print(f"Error merging vehicle types:
{e}")

# Example usage
validate_routes(
    net_file="grid.net.xml",
    input_route_file="routes.rou.xml",
    output_route_file="validated_final.rou.xml"
)
```

3.9 SUMO Traffic Simulation

The modified SUMO configuration file that specifies important settings for the network and route inputs in the simulation setup is shown below. Pre-validated routes are contained in validated_final.rou.xml, whereas the road network is specified in the grid.net.xml file. The simulation has start and end times that are appropriate for its 3,600-second (1-hour) duration. Route inconsistencies are avoided by turning on ignore-route-errors, which guarantees continuous execution. Because of this configuration, which strikes a balance between accuracy and computing performance, the model can concentrate on traffic dynamics without being interrupted by minor routing problems.

```
<configuration>
    <input>
 <net-file value="grid.net.xml"/>
 <route-files value="validated_final.rou.xml"/>
    </input>
    <time>
  <begin value="0"/>
  <end value="3600"/>
    </time>
    <processing>
  <ignore-route-errors value="true"/>
    </processing>
</configuration>
```

The SUMO simulation interface is shown in Figure 4.

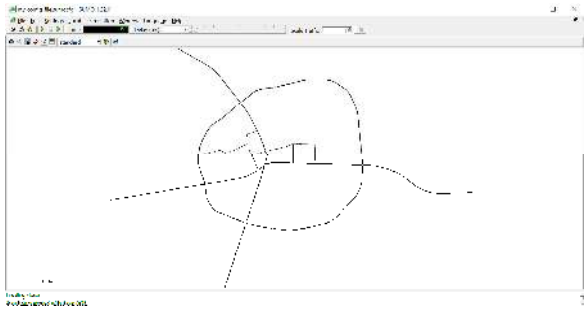


Figure 4: SUMO Simulation Interface

3.10 SUMO Traffic Simulation CO_2 Emissions Output

Traci was employed to extract the total CO_2 emissions per second and save the results in CSV file format. The simulation was conducted via SUMO's TraCI interface, accompanied by a configuration file that defines the traffic environment. The procedure recorded vehicle-specific CO_2 emissions at each simulation interval, translated measurements from milligrams to kilograms, and compiled them into cumulative totals. A CSV file was created with time-stamped records, ensuring the capture of both incremental and total emissions. The simulation was limited to 3,600 seconds to standardise runtime and prevent redundant calculation. The results were converted into a structured dataset for further study, facilitating reproducible and transparent assessment of transport-related emissions. The SUMO simulation CO_2 output of 20198.15 kg is higher than the field estimated CO_2 of 19520 by 3.5%. The Python script is displayed below:

```
import traci
import csv
import os

# Configuration
CONFIG_FILE = "my_config_file.sumocfg"
OUTPUT_FILE = "total_co2_emissions.csv"  #
Output CSV file
SIMULATION_DURATION = 3600  # Stop after 3600
seconds (1 hour)

def initialize_csv():
    """Create CSV file with headers"""
    with open(OUTPUT_FILE, 'w', newline='') as
f:
        writer = csv.writer(f)
        writer.writerow(["Time(s)",
"CO₂_Step(kg)", "CO₂_Total(kg)"])

def log_emissions(time, step_co2, total_co2):
    """Append data to CSV"""
    with open(OUTPUT_FILE, 'a', newline='') as
f:
        writer = csv.writer(f)
        writer.writerow([time, step_co2,
total_co2])

def run_simulation():
    initialize_csv()
    traci.start(["sumo-gui", "-c",
CONFIG_FILE])
    total_co2 = 0

    while
traci.simulation.getMinExpectedNumber() > 0:
        current_time =
traci.simulation.getTime()

        # Stop simulation if duration reached
        if current_time >= SIMULATION_DURATION:
            break

        traci.simulationStep()

        # Get CO₂ emissions (convert mg to kg)
        step_co2 = sum(
            traci.vehicle.getCO2Emission(veh_id
)
            for veh_id in
traci.vehicle.getIDList()
        ) / 1_000_000

        total_co2 += step_co2

        # Log to CSV
        log_emissions(current_time, step_co2,
total_co2)
```


ISBN: 978-978-8567-02-8

```
        print(f"[{current_time}s] Total CO₂:
{total_co2:.2f} kg")

    traci.close()
    print(f"Emission data saved to
{os.path.abspath(OUTPUT_FILE)}")
    print(f"Simulation stopped at
{current_time} seconds")

if __name__ == "__main__":
    run_simulation()
```

3.11 Calibration with TraCI CO_2 Controller

A Python script utilising TraCI (Traffic Control Interface) was developed to enable the dynamic calibration of driver behaviour parameters during the execution of SUMO simulations. The calibration framework effectively modified car-following and lane-changing dynamics while maintaining the distinct characteristics of different vehicle classes. The primary factors altered included driver error (σ), reaction time (τ), maximum acceleration and deceleration rates, minimum gap distances, and coefficients related to lane-changing strategies.

The implementation demonstrated that real-time parameter adjustments using TraCI's set Parameter function effectively impacted vehicle dynamics without requiring the interruption or reinitialisation of the simulation. Vehicle classes preserved their distinct behavioural characteristics by assigning class-specific parameters, thus assuring ongoing separation between passenger vehicles and commercial transport units. A 1 to 5% margin of error was added to each calibrated output against each field's observed threshold values.

```
import traci
import csv
import os
import random
# Configuration
CO2_LIMIT_KG = 18713  # 18,713 kg limit
CONFIG_FILE = "my_config_file.sumocfg"
OUTPUT_FILE = "co2_emissions.csv"  # Output CSV
file
ERROR_MARGIN = random.uniform(0.01, 0.05)  #
Random 1-5% margin of error

# CALIBRATION PARAMETERS - Using basic
parameters that work across models
CALIBRATION_PARAMS = {
    "passenger": {
        "accel": "2.5",     # Maximum
acceleration (m/s^2)
        "decel": "4.5",     # Maximum
deceleration (m/s^2)
        "sigma": "0.5",     # Driver
imperfection (0-1)
        "tau": "1.0",       # Reaction time (s)
        "minGap": "2.5",    # Minimum gap (m)
        "lcStrategic": "1.0", # Lane change
strategy
        "lcCooperative": "1.0" # Cooperation
level
    },
    "truck": {
        "accel": "1.3",
        "decel": "3.0",
        "sigma": "0.7",
        "tau": "1.5",
        "minGap": "3.0",
        "lcStrategic": "0.8",
        "lcCooperative": "1.2"
    }
}
def initialize_csv():
    """Create CSV file with headers"""
    with open(OUTPUT_FILE, 'w', newline='') as
f:
        writer = csv.writer(f)
        writer.writerow(["Time(s)",
"CO2_Step(kg)", "CO2_Total(kg)",
"CO2_Step_Adjusted(kg)",
"CO2_Total_Adjusted(kg)", "Error_Margin(%)"])
def log_emissions(time, step_co2, total_co2,
step_co2_adj, total_co2_adj, error_margin):
    """Append data to CSV"""
    with open(OUTPUT_FILE, 'a', newline='') as
f:
        writer = csv.writer(f)
        writer.writerow([time, step_co2,
total_co2, step_co2_adj, total_co2_adj,
error_margin*100])
def apply_error_margin(value, error_margin):
    """Apply random error margin within
specified range"""
    error_factor = random.uniform(1 -
error_margin, 1 + error_margin)
    return value * error_factor
def apply_safe_calibration():
    """
    Safely apply calibration parameters only to
new vehicles
    """
    calibrated_vehicles = set()  # Track which
vehicles we've already calibrated

    for veh_id in traci.vehicle.getIDList():
        try:
            # Skip if already calibrated
            if veh_id in calibrated_vehicles:
                continue

            vClass =
traci.vehicle.getVehicleClass(veh_id)

            # Only apply to supported vehicle
classes
            if vClass in CALIBRATION_PARAMS:
                params =
CALIBRATION_PARAMS[vClass]

                # Apply only the most essential
parameters
                essential_params = {
                    "accel":
params.get("accel", "2.5"),
                    "decel":
params.get("decel", "4.5"),
                    "tau": params.get("tau",
"1.0")
                }

                for param_name, value in
essential_params.items():
                    try:
                        # Try simple parameter
name first

traci.vehicle.setParameter(veh_id, param_name,
value)
                    except:
                        try:
                            # Try with
carFollowModel prefix

traci.vehicle.setParameter(veh_id,
f"carFollowModel.{param_name}", value)
                        except:
                            # Skip if both fail
                            continue

                calibrated_vehicles.add(veh_id)
```


ISBN: 978-978-8567-02-8

```
                # print(f"Calibrated vehicle
{veh_id} ({vClass})")  # Reduced logging

        except Exception as e:
            # Silent error handling to avoid
interruption
            continue

    return calibrated_vehicles

def run_simulation():
    initialize_csv()
    traci.start(["sumo-gui", "-c",
CONFIG_FILE])
    total_co2 = 0
    total_co2_adjusted = 0
    calibration_interval = 30  # Calibrate less
frequently (every 30 steps)
    step_count = 0
    already_calibrated = set()

    print(f"Applied error margin:
{ERROR_MARGIN*100:.2f}%")

    try:
        while
traci.simulation.getMinExpectedNumber() > 0:
            traci.simulationStep()
            current_time =
traci.simulation.getTime()
            step_count += 1

            # Apply calibration less frequently
and only to new vehicles
            if step_count %
calibration_interval == 0:
                new_calibrated =
apply_safe_calibration()
      already_calibrated.update(new_calibrated)

            # Get CO₂ emissions (convert mg to
kg)
            step_co2 = 0
            vehicle_count =
traci.vehicle.getIDCount()

            if vehicle_count > 0:
                for veh_id in
traci.vehicle.getIDList():
                    try:
                        step_co2 +=
traci.vehicle.getCO2Emission(veh_id)
                    except:
                        continue
                step_co2 /= 1_000_000

            # Apply error margin to current
step measurement
            step_co2_adjusted =
apply_error_margin(step_co2, ERROR_MARGIN)

            total_co2 += step_co2
            total_co2_adjusted +=
step_co2_adjusted

            # Log to CSV (both actual and
adjusted values)
            log_emissions(current_time,
step_co2, total_co2, step_co2_adjusted,
total_co2_adjusted, ERROR_MARGIN)

            # Less frequent console output to
reduce overhead
            if step_count % 10 == 0:
                print(f"[{current_time}s]
Vehicles: {vehicle_count}, CO₂:
{total_co2_adjusted:.2f} kg
(±{ERROR_MARGIN*100:.1f}%) / {CO2_LIMIT_KG}
kg")

            if total_co2_adjusted >=
CO2_LIMIT_KG:
                print(f"⚠ CO₂ limit reached at
{current_time}s!")
                print(f"Actual CO₂:
{total_co2:.2f} kg, Adjusted CO₂:
{total_co2_adjusted:.2f} kg")
                break

            # Add a small delay to prevent
overwhelming the simulation
            # import time
            # time.sleep(0.01)

    except Exception as e:
        print(f"Simulation error: {e}")
    finally:
        traci.close()
        print(f"Emission data saved to
{os.path.abspath(OUTPUT_FILE)}")
        print(f"Final results - Actual:
{total_co2:.2f} kg, With
{ERROR_MARGIN*100:.1f}% error margin:
{total_co2_adjusted:.2f} kg")

if __name__ == "__main__":
    run_simulation()
```

The framework functioned effectively until it reached the specified CO_2 emission limit of 19620.59 kg, which is 0.5% higher than the specified field threshold value of 19520 kg. This is within the 1 to 5% margin of error specified in the script, thereby illustrating the strong integration of calibration techniques with goals related to environmental impact evaluation.

The methodology has been particularly effective in examining how subtle changes in driver behaviour factors influence overall emission outputs, thus laying the groundwork for future scenario analysis and policy assessments.

3.12 Comparison of the SUMO Simulations Output and Field Estimated CO_2

The comparative analysis outlines the relationship between field-measured emissions and SUMO simulations. The uncalibrated SUMO output slightly overstated CO_2 emissions at 20,198.15 kg compared to the empirical measurement of 19,520 kg, yielding an error margin of almost 3.5%. Following calibration, the simulated output decreased to 19,620.59 kg, thus limiting the variation to only 0.5%. This outcome falls well within the permissible error range of 1–5%, demonstrating that the calibration approach successfully adjusted vehicle dynamics to correspond with real-world conditions. The calibrated model demonstrates improved

ISBN: 978-978-8567-02-8

reliability and is suitable for future scenario studies and policy evaluations.

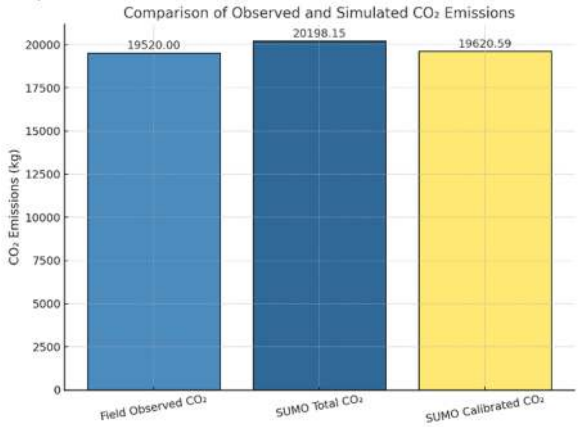


Figure 5: Figure 5: Comparison of Observed and Simulated CO2 Emissions

3.13 Interpretation

The results show that, without modification, SUMO's default settings are not suitable for low-income urban areas. While conventional behavioural parameters do not adequately reflect the observed flow dynamics, the default measurements for fuel consumption and emission factors considerably underestimate the role of informal traffic. By successfully bringing the model into line with actual scenarios, local calibration demonstrates the necessity and viability of modifying transportation simulation techniques to fit particular contexts.

4. Conclusion

This research shows that the Simulation of Urban Mobility (SUMO) may be efficiently adapted for lower-income cities by integrating observed vehicle classes, fuel consumption, and driver behaviour. The model effectively recreated field emissions with only a 0.5% difference by integrating tricycles and other bus types, replacing factory fuel specs with surrogate metrics, and optimising driver variability. The results confirm that traditional SUMO default configurations are insufficient in situations like Damaturu, where informal transportation methods and weak regulatory compliance are common.

The findings emphasise that effective transportation modelling in low-income urban regions requires adjustments that include local conditions instead of relying on generalised assumptions. The localised adaptation of SUMO is not simply a technical task but a practical tool for evidence-based urban planning. Based on this framework, the following recommendations outline how policymakers and urban planners might utilise the framework to improve mobility and reduce emissions in similar urban environments.

- Transport planning in low-income cities should prioritise local data collection on vehicle fleets, fuel use, and driver behaviour. Even modest surveys can provide inputs that greatly improve simulation accuracy and prevent misleading emission estimates.
- Informal modes such as motorcycles and tricycles must be recognised as central to mobility rather than treated as marginal. Policies should focus on regulating and improving these modes through infrastructure design, safety measures, and gradual efficiency upgrades.
- Since real fuel consumption exceeds factory ratings, strategies should move beyond manufacturer standards. Routine inspections, fuel quality improvements, and driver awareness programmes on efficiency can deliver more realistic reductions.

Finally, SUMO should be used as a planning tool only when localised with observed data. Extending this framework to the city scale would allow governments to test scenarios, such as shifting passengers from motorcycles to buses, before implementation, supporting proactive and evidence-based policy.

References

Adhi, R. P. (2018). Top-down and bottom-up method on measuring CO2 emission from road-based transportation system (case study: entire fuel consumption, bus rapid transit, and highway in Jakarta, Indonesia). *Jurnal Teknologi Lingkungan, 19*(2), 249-258.

Ajayi, S. A., Adams, C. A., Dumedah, G., & Adebanji, A. O. (2024). The impact of vehicle engine characteristics on vehicle exhaust emissions for transport modes in Lagos City. *Urban, Planning and Transport Research, 12*(1), 2319328.

Armellini, M. G. (2021). *A tool for simulating demand responsive transport systems in SUMO*.

Basirka, I. A., Dickson, O. F., & Odeyemi, T. I. (2019). Two Versus Fourwheeler?: Confusing Traffic Regulations and Tricyle Riders in Kano Metropolis.

Behrisch, M., & Hartwig, P. (2021). *A comparison of SUMO's count based and countless demand generation tools*.

Castro, A. B. R., Sandoval, A. D. O., & Odamtten, G. (2022). Up around the bend? How transport poverty can lead to social exclusion in a low-income community in Lagos, Nigeria. *Journal of Transport Geography, 102*, 103388.

Clemente, M. L. (2022). *Building a real-world traffic micro-simulation scenario from scratch with SUMO*.

Karakaya, A.-S., Stef, I.-A., Köhler, K., Heinovski, J., Dressler, F., & Bermbach, D. (2023). Achieving realistic cyclist behavior in SUMO using the SimRa dataset. *Computer Communications, 205*, 97-107.

Kusari, A., Li, P., Yang, H., Punshi, N., Rasulis, M., Bogard, S., & LeBlanc, D. J. (2022). *Enhancing SUMO simulator for simulation based testing and validation of autonomous vehicles*.

Kwaghgba, G., & Tyozenda, A. J. (2024). The effect of economic policies on urban transport patterns: A review of motorcycle usage for urban mobility in Nigeria. *Journal of Sustainable Development of Transport and Logistics, 9*.

Lenshie, N. E., Ezeibe, C. C., Joshua, M. M. a., & Nwangwu, C. (2022). From motorcycle to tricycle: neoliberal political economy, informal transportation, and urban/peri-urban Mobility in Nigerian cities. *Transportation journal, 61*(2), 195-227.

Salles, D., Kaufmann, S., & Reuss, H.-C. (2022). *Extending the intelligent driver model in SUMO and verifying the drive off trajectories with aerial measurements*.

ISBN: 978-978-8567-02-8

Soni, S., & Weronek, K. (2023). *Analysis and modelling of road traffic using SUMO to optimize the arrival time of emergency vehicles*.

Yakubu, S., Samuel, K., Kola-Olusanya, A., Yakubu, D. A., & Adedotun, S. B. (2023). Movement on the Edge of Cities: Analysing Intra-urban Mobility in Peri-urban Communities in Southwest Nigeria. *Bulletin of Geography. Socio-Economic Series*(60), 127-143.

ISBN: 978-978-8567-02-8

004-Improved Power System Control using the Reaching Law

A. Y. Babawuro*, M. Ahmed*, A. A. Salihu*, B. S. KSM K. Ibrahim †

*Abubakar Tafawa Balewa University Bauchi, Nigeria
† Gulf University of Science and Technology, Kuwait

(Corresponding Author Email: inunugoloma@yahoo.com)

Abstract: *An enhancement of Proportional Integral Derivative (PID) control of electrical power systems utilising the reaching law (RL) was presented. Different control approaches for improved power systems were proposed, and the need for a simpler control coupled with high robust capability remains an interesting subject of discussion. In simplified form, power system case study based on a single-machine infinite bus (SMIB) power system was employed. A PID controller was improved using the RL after being optimised by the particle swarm optimisation (PSO) algorithm. The proposed scheme (RLPID) was compared with the PSO optimised PID (POPID), and the effect of disturbance was examined. The constant rate reaching was successfully utilised to improve on the PSO tuned PID controller on the SMIB approximated power system. Improvements were observed in the settling time from about 2 seconds to 1 second and completely removing overshoot from about 20%. It also portrayed high level of robustness due to compensation of about 100% level of disturbance injected without any increase in the amount of error in the system which was lower than without disturbance effect. It is expected that with proper exploration, the scheme may significantly improve not only such systems with simple structure and better robustness.*

1. INTRODUCTION

Power system is basically a network made up of electrical components which include generation system (generators, buses and step-up transformers). The transmission systems (such as transmission, sub-transmission lines, and transmission transformers) is the next line of action. Finally, is the distribution systems (it comprises of the distribution lines and transformers). The system is specially designed for delivery of the electric power or supply from the generation stations to the end users or customers. The entire process is usually achieved as a formation of continuous conversions of energies which are non-electrical in nature to electrical energy (Bansal, 2019; Werlie and Kafale, 2022; Ajtha and Radhika, 2023).

Single-machine infinite bus (SMIB) power systems are very important in stability studies on power systems. It is due to their suitability in representing such systems. Most especially in early stage researches on such systems. The components of real power systems were satisfactorily approximated by a generating system couple with an infinite bus replacing the other known components. although simplified, it depicts a suitable configuration for power systems to be utilized for commencement of investigations. An important property not adequately captured is oscillations originating due to different area interconnections (Guo et al., 2001; Sharma et al., 2014; Bux et al., 2019). There are other causes of oscillations existing on power systems which are not desirable due to havocs introduction on system which may lead to system instability. Utilization of control systems remained an important approach for power systems improvement by providing compensation for unpredictable situations that may lead to perturbations on the power systems (Guo et al., 2001; Prasertwong et al., 2010; Bux et al., 2019).

In (Pratik et al., 2020) the Proportional Integral Derivative (PID), Linear Quadratic Regulator (LQR), Pole Placement State Feedback (PPFB), Observer based Output Feedback, Loop Transfer Recovery (LTR) Linear Quadratic Gaussian (LQG) and Nonlinear Feedback Linearized Controller and different conditions of operations were considered. The LQR was explored by (Uravakonda et al., 2020) with good compensation ability. According to (Shan and Chang, 2013) high level disturbances invalidates the linearized power system models. The conventional power system stabilizer was replaced by the extended state observer in the work of (Angu and Mehta, 2017) and showed good compensation ability. It can therefore be inferred that the linear control approaches could not sufficiently handle power systems. Complexity of the nonlinear methods were their major constraints. Hence, a simple linear approach employed using the PID which was optimized using the particle swarm optimisation (PSO) algorithm and enhanced using the reaching law (RL). The advantages of the PSO include intelligence, simplicity, fast convergence, suitability of usage with real numbers, less prone of overlapping and mutation leading to local optimum

ISBN: 978-978-8567-02-8

trapping (Gad, 2022). The RL is part of the Sliding Mode Control (SMC) scheme which account for robustness and it is a nonlinear method also having complexity issue mentioned earlier. It is expected that the proposed scheme (RLPID) would have combined properties of simplicity and robustness, making its property falling between those of the nonlinear and linear techniques. Therefore, little portion of the SMC was utilised for enhancing the PID scheme which was optimised using PSO.

2. METHODOLOGY

The enhanced Proportional Integral Derivative (PID) controller for the electrical power systems utilised the reaching law (RL) which is a small portion of the Sliding Mode Controller (SMC). The simplified form of the power system was employed using the single-machine infinite bus (SMIB) power system. The PID controller was improved using the RL after being optimised by the particle swarm optimisation (PSO) algorithm. The proposed scheme (RLPID) was compared with the PSO optimised PID (POPID), and the effect of disturbance was also ascertained.

The SMIB model was adapted from (Philips et al., 2015) as given by equation (1). Figure 1 is the general form of the block diagram of the system. The reference is the desired system response and the response is the actual response of the system. The reference and response are compared after the response is passed through the feedback path which was unity for this study. The SMIB is the plant in the work. The controller which is the PID compensates for the amount of error E(s) detected. Hence, the controller has three different configurations in the study; classical PID (PID), PSO optimised PID (POPID) and the RL enhanced POPID (RLPID) as mathematically depicted by equations (1), (2) and (3) respectively. The parameters KP, KI, KD are the proportional, integral and derivative gains respectively.

$$10 / (0.5s^2 + 0.1s + 10) \quad (1)$$

$$U_{PID} = E(s)KP + \frac{KI}{s}E(s) + KDsE(s) \quad (2)$$

$$U_{POPID} = [E(s)KP + \frac{KI}{s}E(s) + KDsE(s)]_{PSO} \quad (3)$$

$$U_{RLPID} = [E(s)KP + \frac{KI}{s}E(s) + KDsE(s)]_{PSO} + \eta sgn(s) \quad (4)$$

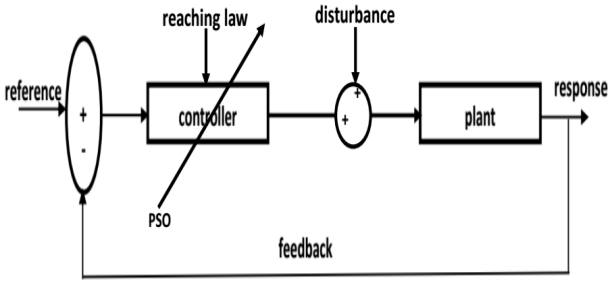


Figure 1: Generalised block diagram of the system.

3. RESULTS

The results without disturbance are presented in Figures 2 to 4. Figure 2 gives the system response, Figure 3 shows the error plots and Figure 4 presents the cumulative error plot. It can be seen from the response that POPID had a settling time of about 2 seconds, and overshoot of 20%, while with the proposed RLPID, response shows 1 second and 0% respectively. The error plots indicated the error behaviour which decayed with time for both controllers. It was higher with the POPID and was made clearer by the cumulative error plot, that is Figure 4.

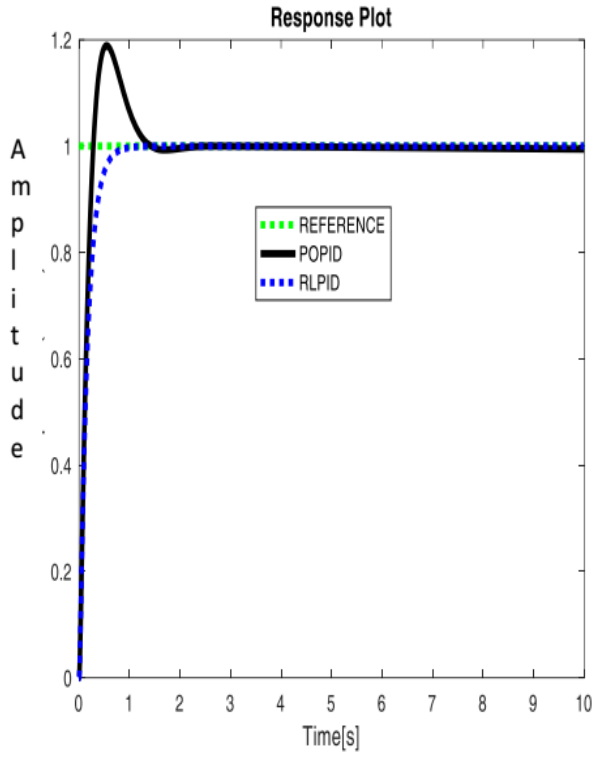


Figure 2: Response without disturbance.

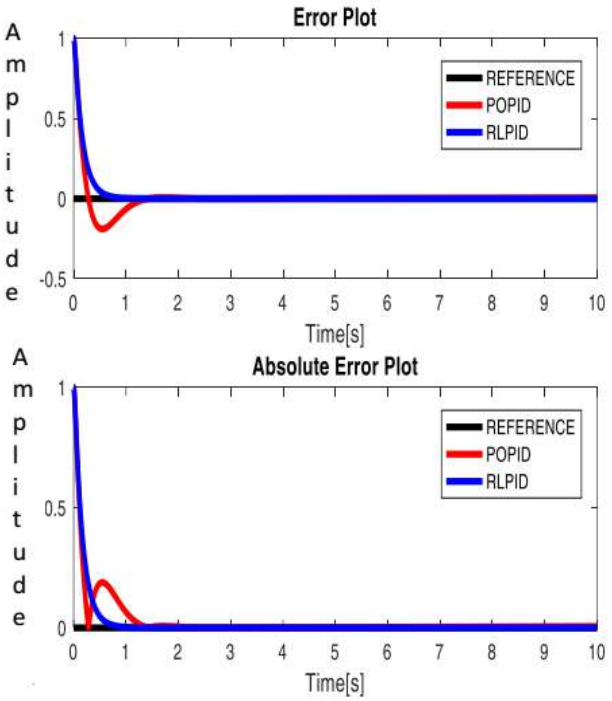


Figure 3: Error and absolute error plots without disturbance.

ISBN: 978-978-8567-02-8

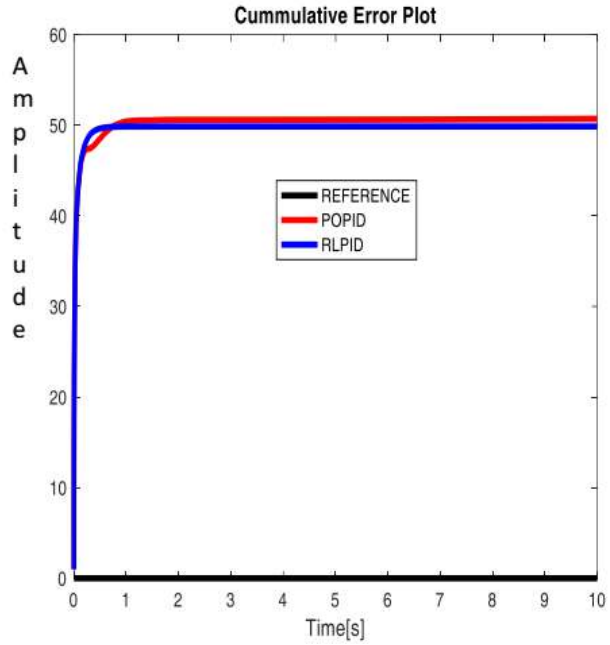


Figure 4: Cumulative absolute error plots without disturbance.

The results with disturbance are presented in Figures 5 to 7. A step disturbance of about 100% the reference was injected between 4-6seconds (yellow plot in figure 5) when the system was at steady state mimicking sudden changes such as lightning strikes. Figure 5 showed the system response, while Figure 6 portrayed the error plots and Figure 7 illustrated the cumulative error. It can be seen from Figure 5 that the response of the system is a bit worse with POPID having a settling time of about 2.2 seconds, and overshoot of 22%. Whereas with the RLPID they were the same as without disturbance case; that is 1 second for the settling time and 0% for the overshoot. Consideration of the error plots revealed that the error behaviour become worsened with the POPID which was the same (with and without disturbance) with the RLPID. The errors decayed with time for both controllers but remains higher with the POPID and was made clearer by the cumulative error plot here as well.

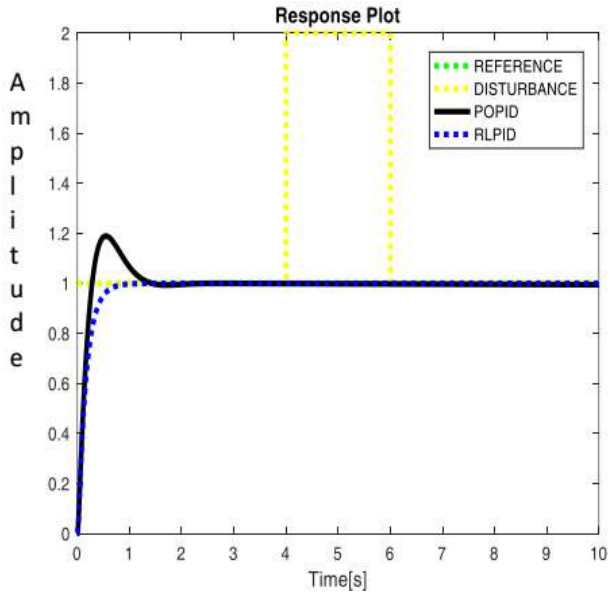


Figure 5: Response with disturbance.

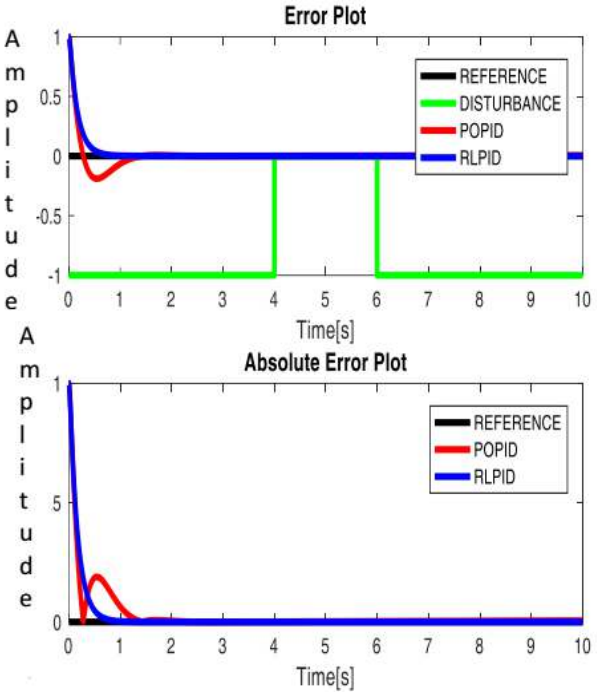


Figure 6: Error and absolute error plots without disturbance.

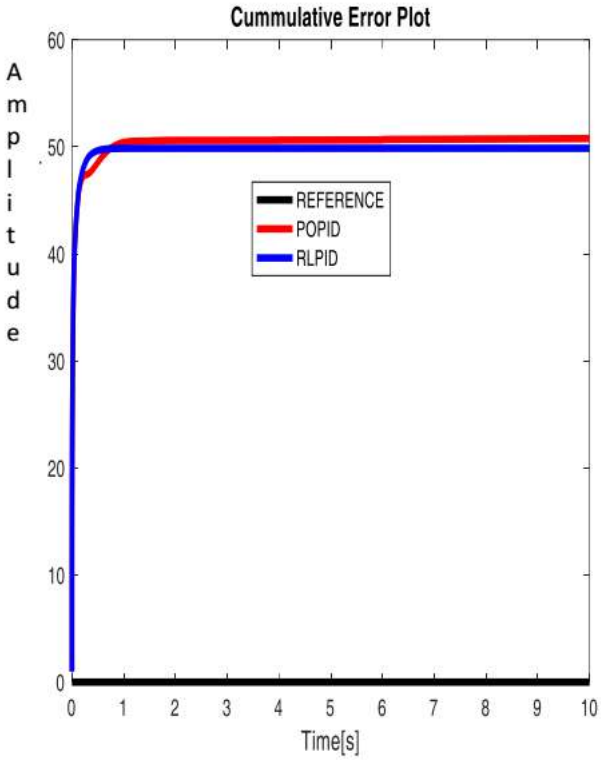


Figure 7: Cumulative absolute error plots with disturbance.

4. DISCUSSION

Examination of the response plots with and without the disturbance revealed that proposed control scheme RLPID yielded better results having smaller values of settling times with least or no overshoot at all. In terms of error the proposed scheme was the best having least level of cumulative error. It portrayed better robustness since despite perturbation it maintains close to its parameters as without any disturbance; which could be due to its fast

ISBN: 978-978-8567-02-8

response to compensate for the error, hence making it having the ability to reject disturbance quickly.

5. CONCLUSION

The constant rate reaching was successfully utilised to improve on the PSO tuned PID controller (RLPID) on the SMIB approximated power system. Different control applied indicated the need for simpler scheme which pave way for the contribution of the study. It utilised the constant rate reaching to improve on the PID controller which is tuned by employing the PSO. Focus was better accuracy and robustness of the resulting control schem. The realized controller that is; the RLPID was then compared with the version of the PID tuned using PSO referred to as POPID. The effect of disturbance was also looked into. Results clearly indicated improvements in the settling time from about 2 seconds to 1 second. It also showed complete removal of overshoot from about 20% with POPID. Also portrayed is high level of robustness due to the ability of the realised control scheme to compensate up to about 100% level of disturbance injected (within the conditions of the study) without any corresponding increase in the amount of error occurring in the system which was lower than without the disturbance effect. It is further expected that with proper exploration the scheme may significantly improve not only such systems, resulting in simplicity of structure and better robustness ability.

ACKNOWLEDGMENT

Authors specially thank “Abubakar Tafawa Balewa University, Bauchi and Tertiary Education Fund, Abuja” for giving the opportunity contribute in the conference.

REFERENCES

Ajitha, A. and Radhika, S., (2023). A comprehensive review of demand response strategies and the role of emergent technologies for sustainable home energy management systems. International Journal of Ambient Energy Vol. 44, No.1, pp:2262-2282.

Angu, R., & Mehta, R. K., (2017). A single machine infinite bus power system damping control design with extended state observer. Cogent Engineering, Vol. 4, No.1, 1369923.

Bansal, R., (2019). Power system protection in smart grid environment. CRC Press.

Bux, R., Xiao, C., Hussain, A., & Wang, H., (2019). Study of single machine infinite bus system with VSC based stabilizer. In Proceedings of the 2019 The 2nd International Conference on Robotics, Control and Automation Engineering (pp: 159-163).

Gad, A. G., (2022). Particle swarm optimization algorithm and its applications: A systematic review. Archives of computational methods in engineering, Vol. 29, No.5.

Guo, Y., Hill, D. J., & Wang, Y., (2001). Global transient stability and voltage regulation for power systems. IEEE transactions on power systems, Vol. 16, No.4, pp:678-688.

Phillips, C. L. Nagle, H. T. Chakrabortty, A., (2015). Digital Control System Analysis & Design,” Pearson Education Limited, Edinburgh Gate Harlow, Essex CM20 2JE, England, ISBN 13: 978-1-292-06188-7.

Prasertwong, K., Mithulananthan, N., & Thakur, D., (2010). Understanding low-frequency oscillation in power systems. International Journal of Electrical Engineering Education, Vol. 47, No. 3, pp:248-262.

Shan, Y., & Chang, X., (2013). Gain-scheduled LPV control of a single-machine infinite-bus power system. In Unifying Electrical Engineering and Electronics Engineering: Proceedings of the 2012 International Conference on Electrical and Electronics Engineering (pp: 331-342). New York, NY: Springer New York.

Sharma, C. S., (2014). Transient stability analysis of single machine infinite bus system by numerical methods. International Journal of Electrical and Electronics Research, Vol. 2, No.3, pp:158-166.

Uravakonda, S., Mallapu, V. K., & Annapu Reddy, V. R., (2020). Damping enhancement for SMIB power system equipped with LQR tuned via analytical approach. Journal of The Institution of Engineers (India): Series B, Vol. 101, No.5, pp:541-551.

Werkie, Y. G., & Kefale, H. A., (2022). Optimal allocation of multiple distributed generation units in power distribution networks for voltage profile improvement and power losses minimization. Cogent Engineering, Vol. 9, No.1, 2091668.

ISBN: 978-978-8567-02-8

005-Engineering for Digital Economy: Challenges, Opportunities, and Pathways for Sustainable Industrial Growth in Nigeria

Mustapha Alhaji Shehu[1], Yabani Galadima Gelwasa[2], Mubarak Ayuba[3], Mukhtar Haruna Aliyu[4]

[12]Department of Electrical and Electronic Engineering, Abdullahi Fodio University of Science and Technology, Aliero, Nigeria

[3]Department. of Electrical and Electronic Engineering, Federal University of Transportation Daura, Katsina State.

[4]Department of Information and Communication Engineering, Usmanu Danfodiyo University, Sokoto, Nigeria

*Corresponding Author: Email: mustaphaalhajishehu3@gmail.com

Abstract: The digital economy is reshaping modern industrial systems through the integration of advanced digital technologies such as artificial intelligence, data analytics, automation, and next-generation communication networks. Engineering disciplines are fundamental to the development, deployment, and optimization of the technological infrastructure that drives this transformation. In the context of Nigeria, engineering innovation is essential for strengthening industrial productivity, enhancing global competitiveness, and promoting sustainable economic growth. Despite these prospects, several challenges persist, including cybersecurity vulnerabilities, infrastructural limitations, unequal digital access, high energy consumption, and workforce skill gaps. This paper examines the strategic role of engineering in enabling digital economic development, analyzes key technical and socio-economic constraints, and explores emerging technological opportunities such as 5G systems, blockchain technologies, and sustainable digital infrastructure. The study emphasizes the importance of interdisciplinary collaboration, policy support, and human-centered engineering practices in achieving inclusive and resilient industrial advancement.

Keywords: Digital Economy; Engineering Innovation; Sustainable Industrial Growth; Artificial Intelligence; 5G Networks; Cybersecurity; Blockchain; Sustainable Infrastructure; Nigeria.

1. INTRODUCTION

The digital economy refers to economic activities that are enabled and enhanced through digital technologies, including computing systems, communication networks, data analytics, artificial intelligence (AI), and automation platforms(Jain et al., 2023; Wang & Zhao, 2022). It encompasses the production, distribution, and consumption of goods and services that rely on digital infrastructure and information systems(Xia et al., 2024). Globally, the digital economy has become a major driver of innovation, productivity, and competitiveness, reshaping industrial processes and transforming traditional business models(Vukman, Klari, et al., 2024; Vukman, Klarić, et al., 2024).

Engineering plays a central role in the advancement of the digital economy(Raihan, 2024; Xia et al., 2024). Electrical, electronic, communication, computer, and industrial engineering disciplines collectively design, develop, and maintain the digital infrastructure required for connectivity, data processing, automation, and intelligent decision-making systems(Juneja et al., 2024; Silue, 2022). Technologies such as 5G communication networks, cloud computing platforms, Internet of Things (IoT) systems, and cybersecurity frameworks are products of engineering innovation(Humayun et al., 2021; Idiwal & Mathur, 2025; Usman et al., 2021; Zahid, 2025). Without robust engineering solutions, digital transformation cannot be effectively implemented or sustained(Aliyev, 2022; Noorit et al., 2020).

In Nigeria, the digital economy presents significant opportunities for accelerating industrial growth, enhancing manufacturing efficiency, expanding financial inclusion, and supporting entrepreneurship(Bologna, 2013). National initiatives aimed at digital transformation highlight the importance of broadband expansion, smart infrastructure, and technology-driven industrialization (Xia et al., 2024). However, despite these efforts, Nigeria continues to face major constraints, including inadequate digital infrastructure, unreliable power supply, cybersecurity vulnerabilities, limited research–industry collaboration, and shortages of advanced technical skills(Aliyev, 2022). These challenges hinder the effective integration of digital technologies into industrial sectors and limit

ISBN: 978-978-8567-02-8

the country's ability to fully participate in the global digital economy(A et al., 2023; Xia et al., 2024).

The problem addressed in this paper is the gap between the potential of engineering-driven digital transformation and the practical realities of infrastructural, technical, and policy limitations affecting sustainable industrial growth in Nigeria(Aliyev, 2022). While digital technologies offer transformative opportunities, their impact remains constrained without strategic engineering frameworks and coordinated implementation.

Therefore, the objectives of this paper are to:

1. Examine the role of engineering in enabling and sustaining the digital economy.
2. Identify key technical and socio-economic challenges limiting digital transformation in Nigeria.
3. Explore emerging technological opportunities that can support sustainable industrial growth.
4. Propose strategic pathways for aligning engineering innovation with Nigeria's industrial development goals.

By addressing these objectives, this study seeks to contribute to ongoing discussions on how engineering can serve as a catalyst for inclusive, secure, and sustainable digital industrialization in Nigeria.

2. ENGINEERING AND THE DIGITAL ECONOMY

Engineering constitutes the foundational pillar of the digital economy by providing the technical systems, communication platforms, and computational frameworks required for digital transformation(Aliyev, 2022; Noorit et al., 2020). Through innovation in hardware design, network architecture, software systems, and intelligent automation, engineering disciplines enable industries to transition from conventional production models to digitally integrated ecosystems(Aliyev, 2022). The effectiveness of the digital economy depends largely on the robustness, scalability, and sustainability of engineering solutions deployed across sectors.

2.1 Core Enabling Technologies

The digital economy is driven by several key technologies that rely heavily on engineering design, optimization, and implementation(Maheswar et al., 2025).

1) Artificial Intelligence (AI)

Artificial Intelligence enables machines and systems to perform tasks that traditionally require human intelligence, such as decision-making, pattern recognition, and predictive analysis. Engineering plays a crucial role in developing AI algorithms, designing embedded systems, and integrating machine learning models into industrial processes. In manufacturing and service industries, AI enhances productivity, reduces operational errors, and supports predictive maintenance systems(Mer, 2023; Somanathan, 2025).

2) Internet of Things (IoT)

The Internet of Things refers to interconnected devices equipped with sensors, communication modules, and data-processing capabilities. Engineers design IoT architectures that facilitate real-time monitoring, remote control, and data-driven decision-making. In industrial applications, IoT supports equipment monitoring, asset tracking, and energy management, thereby improving operational efficiency(Luo et al., 2025; Noorit et al., 2020).

3) Cloud Computing

Cloud computing provides scalable data storage, computational resources, and software services over digital networks. Engineering solutions ensure secure data transmission, optimized server architecture, and efficient virtualization systems. Cloud platforms enable industries to reduce infrastructure costs, improve collaboration, and enhance data accessibility across multiple locations(Wan et al., 2018).

4) 5G Networks

Fifth-generation (5G) communication networks deliver high-speed, low-latency, and high-capacity connectivity essential for real-time industrial applications. Communication engineers design and optimize 5G network architectures to support smart factories, autonomous systems, and large-scale IoT deployments. The deployment of reliable 5G infrastructure is particularly critical for enabling advanced industrial automation in Nigeria(Adam et al., 2021).

5) Data Analytics

Data analytics transforms raw industrial data into actionable insights. Through engineering-based data modeling, signal processing, and system optimization techniques, industries can enhance production planning, quality control, and customer engagement. Advanced analytics supports evidence-based decision-making and strategic forecasting(Raihan, 2024; Somanathan, 2023).

2.2 Engineering Infrastructure for Industrial Growth

Beyond enabling technologies, engineering provides the physical and digital infrastructure necessary for sustainable industrial expansion.

6) Smart Manufacturing

Smart manufacturing integrates AI, IoT, robotics, and real-time analytics into production systems. Engineers design automated production lines that enhance precision, reduce waste, and improve resource

ISBN: 978-978-8567-02-8

utilization. This approach increases competitiveness and aligns with sustainable industrial development goals(Vukman, Klari, et al., 2024).

7) Automation Systems

Automation involves the use of control systems, robotics, and embedded technologies to minimize human intervention in industrial processes. Engineering innovations in programmable logic controllers (PLCs), robotic systems, and intelligent control algorithms enhance operational efficiency while reducing production costs and safety risks(Somanathan, 2023).

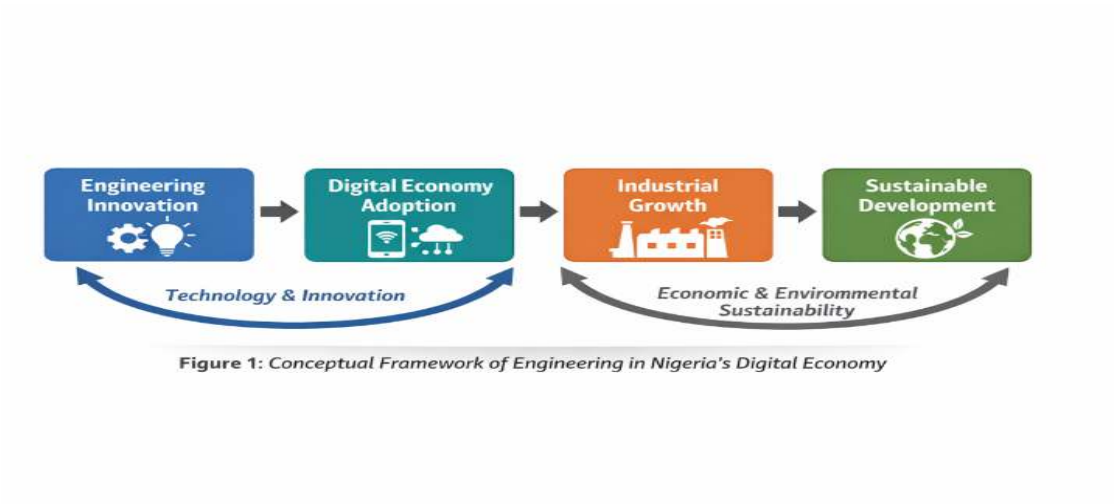


Figure 1: Conceptual Framework of Engineering in Nigeria's Digital Economy
This visual shows the flow from **Engineering Innovation → Digital Economy Adoption → Industrial Growth → Sustainable Development**, making it easy for readers to grasp the key concept at a glance(Raihan, 2024).

8) Digital Supply Chains

Engineering solutions support the digitization of supply chains through tracking systems, blockchain-enabled transparency, and predictive logistics management. Digitally integrated supply chains reduce delays, enhance inventory control, and improve overall industrial productivity(Bologna, 2013).

9) Industrial Internet of Things (IIoT)

Industrial IoT extends IoT capabilities to manufacturing and heavy industries. Engineers design sensor networks and industrial communication protocols that allow machines to communicate autonomously. This connectivity enables predictive maintenance, minimizes downtime, and improves asset lifespan(Noorit et al., 2020).

3. CHALLENGES LIMITING DIGITAL TRANSFORMATION IN NIGERIA

10) 3.1 Rapid Technological Evolution

The rapid pace of technological advancement presents a significant challenge to sustainable digital transformation in Nigeria(Makori & Mauti, 2023). Emerging technologies such as artificial intelligence, cloud computing, blockchain, big data analytics, and the Internet of Things (IoT) are continuously reshaping global digital ecosystems(de Esteban Curiel et al., 2024). However, the speed at which these technologies evolve often exceeds the capacity of local institutions, regulatory bodies, and educational systems to adapt accordingly(Pilgrim & Bohnet-Joschko, 2022).

In Nigeria, limited investment in research and development, inadequate technical training, and slow policy implementation hinder effective technology adoption(Alam & Gani, 2019). Many organizations struggle to modernize legacy systems, resulting in reduced competitiveness and inefficiencies. Furthermore, the shortage of highly skilled professionals in advanced digital domains exacerbates the gap between technological innovation and practical deployment(G-lvez et al., 2020; Kurland & Cooper, 2002).

To address this challenge, there is a need for continuous capacity building, curriculum modernization in higher institutions, and stronger collaboration between academia, industry, and government agencies. Strategic technology foresight and adaptive regulatory frameworks are essential to ensure that Nigeria remains responsive to global digital trends(S. Kim, 2022).

TABLE 1 – KEY CHALLENGES IN ENGINEERING FOR DIGITAL ECONOMY IN NIGERIA

Challenge	Description	Impact on Industry in Nigeria
Infrastructure	Limited power supply & low broadband penetration	Slows industrial digital adoption
Skills Gap	Shortage of engineers skilled in AI, IoT, Cloud	Reduces implementation of advanced tech
R&D Investment	Low government & private funding for innovation	Slows local industrial competitiveness

ISBN: 978-978-8567-02-8

Challenge	Description	Impact on Industry in Nigeria
Policy & Regulation	Inconsistent standards and unclear policies	Reduces investor confidence and technology uptake

11) 3.2 Cybersecurity and Data Privacy

Cybersecurity threats pose a major obstacle to digital transformation efforts in Nigeria. As government services, financial systems, healthcare platforms, and educational institutions increasingly migrate to digital environments, the exposure to cyber-attacks, data breaches, ransom ware, and identity theft becomes more pronounced.

Nigeria has witnessed a rise in cybercrime activities, which undermine public trust in digital platforms and discourage investment in digital infrastructure. Although regulatory frameworks such as the Nigeria Data Protection Act (NDPA) have been introduced, enforcement mechanisms and compliance monitoring remain inconsistent. Many small and medium-scale enterprises lack robust cybersecurity architectures and adequate data protection policies.

Strengthening cybersecurity requires comprehensive national strategies, improved digital literacy, adoption of international best practices, and increased funding for cybersecurity research and infrastructure. Building resilient digital systems is fundamental to achieving secure and sustainable digital transformation(S. Kim, 2022).

12) 3.3 Digital Divide and Infrastructure Gaps

The digital divide remains one of the most critical barriers to inclusive digital transformation in Nigeria. Significant disparities exist between urban and rural areas in terms of broadband access, network reliability, digital literacy, and affordability of digital services(S. Kim, 2022).

While metropolitan regions such as Lagos and Abuja benefit from relatively advanced telecommunications infrastructure, many rural communities experience limited connectivity and low-quality service delivery. Inadequate fiber-optic deployment, insufficient base stations, and high cost of internet access further restrict widespread participation in the digital economy(Guo et al., 2017).

Additionally, socio-economic inequalities contribute to unequal access to digital tools and educational resources. Without deliberate policy interventions and targeted investments, digital transformation may deepen existing inequalities rather than bridge them. Expanding broadband infrastructure, incentivizing private sector investment, and promoting community-based digital inclusion programs are critical steps toward closing this gap(C. Kim, 2025).

13) 3.4 Energy Demand and Environmental Sustainability

Reliable energy supply is fundamental to digital infrastructure development. However, Nigeria faces persistent power generation and distribution challenges that significantly limit digital transformation initiatives. Data centers, telecommunications networks, and emerging technologies such as 5G systems and cloud computing platforms require stable and continuous electricity supply(Luo et al., 2025).

Frequent power outages increase operational costs, as organizations rely heavily on diesel generators and alternative energy sources. This not only raises financial burdens but also contributes to environmental degradation through increased carbon emissions(Dhabhai et al., 2014).

Moreover, as digital adoption grows, energy consumption within the ICT sector continues to rise. Without strategic planning, this trend may conflict with global sustainability goals. Integrating renewable energy solutions such as solar and hybrid systems into digital infrastructure can enhance reliability while reducing environmental impact(Raihan, 2024).

4. OPPORTUNITIES FOR SUSTAINABLE INDUSTRIAL GROWTH

14) 4.1 Artificial Intelligence in Manufacturing

Artificial Intelligence (AI) presents significant opportunities for enhancing productivity, efficiency, and competitiveness within Nigeria's manufacturing sector. AI-driven systems enable predictive maintenance, automated quality control, process optimization, and intelligent supply chain management. By leveraging machine learning algorithms and data analytics, manufacturers can reduce downtime, minimize waste, and improve operational accuracy(Xia et al., 2024).

In Nigeria, the adoption of AI in manufacturing remains at an emerging stage. However, the integration of AI technologies into small and medium-scale industries can stimulate industrial modernization and reduce reliance on manual processes. Smart robotics and intelligent automation can enhance production capacity while maintaining quality standards required for global competitiveness(Xia et al., 2024).

Furthermore, AI-driven industrial systems support sustainable practices through energy optimization and resource efficiency. The deployment of AI-based monitoring systems can reduce material wastage and lower carbon emissions. To maximize these benefits, Nigeria must invest in digital skills development, industrial research, and collaborative innovation

ISBN: 978-978-8567-02-8

ecosystems involving academia, industry, and government institutions(Zahid, 2025).

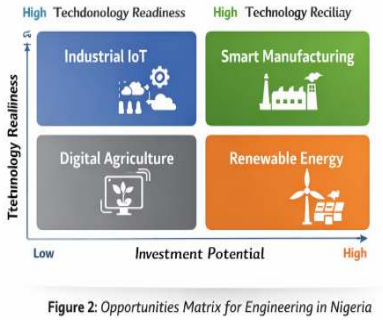


Figure 2: *Opportunities Matrix for Engineering in Nigeria*

Figure 2: Opportunity Matrix for Engineering in Nigeria(Yahya et al., 2025)

15) *4.2 FinTech and Digital Financial Systems*

Financial Technology (FinTech) has emerged as one of the most transformative drivers of digital growth in Nigeria. The expansion of mobile banking, digital payment platforms, blockchain-based transactions, and online lending systems has significantly improved financial inclusion across diverse socio-economic groups(Bologna, 2013).

Nigeria's FinTech ecosystem is among the most dynamic in Africa, attracting both local and international investment(Aliyev, 2022; Juneja et al., 2024). Digital financial systems reduce transaction costs, enhance transparency, and increase accessibility to financial services for underserved populations. This is particularly relevant in rural communities where traditional banking infrastructure is limited.

Moreover, digital financial platforms facilitate industrial growth by enabling seamless business transactions, supporting small and medium enterprises (SMEs), and improving access to credit facilities. Secure and well-regulated digital financial systems can stimulate entrepreneurship and foster economic resilience. However, regulatory clarity, cybersecurity reinforcement, and consumer protection mechanisms remain critical to sustaining this growth trajectory(S. Kim, 2022).

16) *4.3 Smart Cities and Smart Agriculture*

The development of smart cities and smart agriculture represents a strategic opportunity for sustainable industrial expansion in Nigeria. Smart city initiatives integrate digital technologies such as IoT sensors, data analytics, and intelligent transportation systems to enhance urban management, energy efficiency, and service delivery.

In rapidly urbanizing regions, smart infrastructure can optimize traffic systems, improve waste management, enhance public safety, and support efficient energy distribution. These advancements contribute to improved quality of life and industrial productivity(Musa et al., 2024).

Similarly, smart agriculture leverages digital tools such as remote sensing, precision farming technologies, automated irrigation systems, and data-driven crop monitoring to increase agricultural output. Considering agriculture's substantial contribution to Nigeria's GDP and employment, integrating digital technologies can improve food security, reduce post-harvest losses, and enhance export competitiveness.

Investment in rural connectivity, digital literacy programs, and affordable smart technologies is essential to ensure inclusive participation in these initiatives(Xia et al., 2024).

17) *4.4 Digital Entrepreneurship and Job Creation*

Digital transformation creates new opportunities for entrepreneurship and employment across multiple sectors. The growth of digital platforms, e-commerce systems, online education services, and technology startups has expanded the innovation landscape in Nigeria.

Young entrepreneurs are leveraging digital tools to develop scalable business models that operate beyond geographical boundaries. This fosters economic diversification and reduces overdependence on traditional sectors such as oil and gas.

Additionally, the digital economy generates employment in areas such as software development, cybersecurity, digital marketing, data analytics, and ICT infrastructure management. By promoting digital skills training, startup incubation programs, and access to venture funding, Nigeria can harness its youthful population to drive sustainable industrial growth.

For long-term impact, policies must support innovation-friendly regulations, infrastructure development, and equitable access to digital resources. Strengthening the digital entrepreneurship ecosystem will enhance industrial competitiveness and accelerate socio-economic development(A et al., 2023; Raihan, 2024).

5. FUTURE DIRECTIONS FOR ENGINEERING IN NIGERIA

The rapid evolution of digital technologies presents multiple pathways for engineering to drive sustainable industrial growth in Nigeria. Strategic adoption and integration of emerging technologies, coupled with sustainable and ethical practices, are critical to ensuring Nigeria's competitive advantage in the global digital economy(Cheng et al., 2022).

5.1 Quantum Computing and Advanced Simulation

ISBN: 978-978-8567-02-8

Quantum computing offers unprecedented computational power for solving complex industrial and logistical problems. Advanced simulation platforms can optimize manufacturing processes, energy management, and supply chains. For Nigeria, investment in quantum research and partnerships with global technology centers will be essential to leverage these tools for industrial modernization and innovation(Aliyev, 2022).

5.2 Blockchain for Transparent Governance

Blockchain technology enables secure, transparent, and immutable record-keeping. Its application in supply chain management, digital finance, and public procurement can enhance accountability and reduce fraud. In Nigeria, blockchain adoption in both private and government sectors can strengthen governance mechanisms and facilitate trust-based industrial collaborations(Juneja et al., 2024; Makori & Mauti, 2023).

5.3 5G and Beyond Connectivity

High-speed connectivity through 5G networks is critical for enabling Internet of Things (IoT) solutions, smart factories, and real-time data analytics. Expanding 5G coverage and integrating next-generation wireless technologies will enhance industrial automation, digital logistics, and remote monitoring systems across Nigeria's industrial sectors(Bologna, 2013; Luo et al., 2025).

5.4 Sustainable and Green Engineering Systems

Sustainability must be central to Nigeria's industrial growth strategy. Engineering practices that incorporate renewable energy, energy-efficient manufacturing, and environmentally responsible materials will reduce industrial carbon footprints. Implementing green engineering standards will also position Nigerian industries as competitive and socially responsible players in the global market(Bologna, 2013).

5.*5 Human-Centered and Ethical Engineering Design*

Engineering solutions must prioritize human-centered design, ensuring systems are accessible, inclusive, and socially responsible. Ethical considerations in AI, data privacy, and automated decision-making are crucial to safeguard users and communities. By embedding ethics and human-centered principles into engineering curricula and industrial practices, Nigeria can foster responsible digital innovation(Hassan & Uddin, 2025).

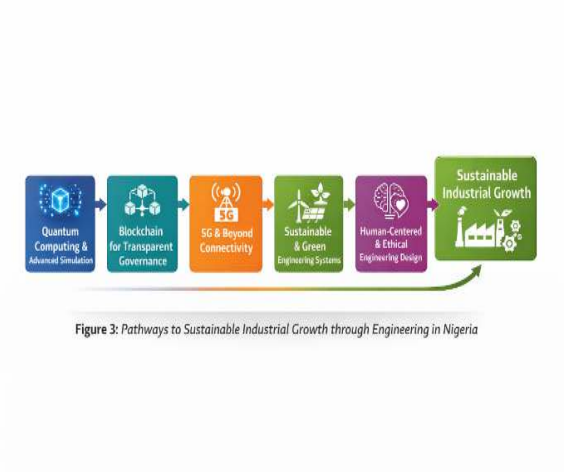


Figure 3: *Pathways to Sustainable Industrial Growth through Engineering in Nigeria*

Figure 3: Pathways to sustainable industrial growth through engineering in Nigeria(Bologna, 2013; Noorit et al., 2020; Shi, 2022).

6. CONCLUSION

Digital transformation presents Nigeria with a strategic pathway toward sustainable industrial growth and global competitiveness(Aliyev, 2022). However, realizing this potential requires deliberate and coordinated action. Engineering innovation must serve as the primary catalyst driving the design, deployment, and optimization of resilient digital systems across critical sectors of the economy(Pompa et al., 2025).

To accelerate progress, Nigeria must prioritize sustained investment in robust digital infrastructure, including broadband expansion, smart industrial systems, and reliable energy supply for ICT operations. Beyond infrastructure, sustainable innovation—anchored in energy efficiency, environmental responsibility, and scalable technologies—must guide national digital development strategies(Aliyev, 2022).

Furthermore, effective collaboration among academia, industry, and government is essential to bridge research, policy, and practical implementation gaps(Pearlson, 2001). By fostering an integrated innovation ecosystem, Nigeria can build a secure, inclusive, and technologically advanced economy capable of supporting long-term industrial transformation(A et al., 2023).

REFERENCES

A, I. S., B, O. L., C, A. Z., D, I. M., E, M. K., & F, V. N. (2023). DIGITAL ECONOMY IN A GLOBAL CONTEXT : WORLD EXPERIENCE Article history : *International Journal of Professional Business Review*, 1–16.

Adam, I., Kamarudin, M. R., Rambe, A. H., Haris, N., Rahim, H. A., Zuki, W., Muhamad, A. W., Ismail, A. M., Jusoh, M., & Yasin, M. N. M. (2021). *Investigation on Wearable Antenna under Different Bending Conditions for Wireless*

ISBN: 978-978-8567-02-8

Body Area Network (WBAN) Applications. *2021*. https://doi.org/10.1155/2021/5563528

Alam, M. I., & Gani, M. O. (2019). Determinants of Omnichannel Customer Experience: A Growing Digital Economy Perspective. *Journal of Business Studies*, *XL*(3), 203–230.

Aliyev, A. G. (2022). Technologies Ensuring the Sustainability of Information Security of the Formation of the Digital Economy and their Perspective Development Directions. *International Journal of Information Engineering and Electronic Business*, *14*(5), 1–14. https://doi.org/10.5815/ijieeb.2022.05.01

Bologna, G. (2013). A New Economy Inspired by Sustainability Science. *Growth in Transition*, 140–146. https://doi.org/10.4324/9780203145593-24

Cheng, X., Zhang, S., Fu, S., Liu, W., Guan, C., Mou, J., Ye, Q., & Huang, C. (2022). Exploring the metaverse in the digital economy: an overview and research framework. *Journal of Electronic Business & Digital Economics*, *1*(1/2), 206–224. https://doi.org/10.1108/jebde-09-2022-0036

de Esteban Curiel, J., Antonovica, A., & Sánchez Morales, M. del R. (2024). Inductive open data study on teleworking dissatisfaction in Spain during the Covid-19 pandemic. *International Journal of Manpower*, *45*(2), 379–397. https://doi.org/10.1108/IJM-12-2022-0632

Dhabhai, H., Prakash Gupta, R., & Jain, A. (2014). Parametric Comparison of various Fading Channels using MATLAB Simulation. *International Journal of Advanced Engineering Research and Science (IJAERS)*, *1*(5), 91–96.

G-lvez, A., Tirado, F., & Mart-nez, M. J. s. (2020). Work-life balance, organizations and social sustainability: Analyzing female telework in Spain. *Sustainability (Switzerland)*, *12*(9), 1–21. https://doi.org/10.3390/SU12093567

Guo, S., Ding, W., & Lanshina, T. (2017). Global Governance and the Role of the G20 in the Emerging Digital Economy. *International Organisations Research Journal*, *12*(4), 169–184. https://doi.org/10.17323/1996-7845-2017-04-169

Hassan, A., & Uddin, N. N. (2025). A Compact Wearable Patch Antenna on Leather Substrate for Smart IoT Applications: Design, Performance, Bending, SAR, and Link Budget Analysis. *Arabian Journal for Science and Engineering*. https://doi.org/10.1007/s13369-025-10483-5

Humayun, M., Hamid, B., Jhanjhi, N. Z., Suseendran, G., & Talib, M. N. (2021). 5G Network Security Issues, Challenges, Opportunities and Future Directions: A Survey. *Journal of Physics: Conference Series*, *1979*(1). https://doi.org/10.1088/1742-6596/1979/1/012037

Idiwal, R., & Mathur, M. (2025). *Wearable Antennas for Next-Generation Wireless Communication : A Comprehensive Review*. *12*(2), 25–29.

Jain, D., Jain, B., Jain, N., & Jain, R. (2023). Navigating the Shifting Landscape of the Digital Economy: Exploration of Emerging Patterns and Prospects. *SSRN Electronic Journal*. https://doi.org/10.2139/ssrn.4546696

Juneja, A., Goswami, S. S., & Mondal, S. (2024). Cyber Security and Digital Economy: Opportunities, Growth and Challenges. *Journal of Technology Innovations and Energy*, *3*(2), 1–22. https://doi.org/10.56556/jtie.v3i2.907

Kim, C. (2025). COVID Stress Factors Affecting Remote Work Acceptance. *Covid*, *5*(2). https://doi.org/10.3390/covid5020026

Kim, S. (2022). Critical Success Factors Evaluation by Multi-Criteria Decision-Making: A Strategic Information System Planning and Strategy-As-Practice Perspective. *Information (Switzerland)*, *13*(6). https://doi.org/10.3390/info13060270

Kurland, N. B., & Cooper, C. D. (2002). Manager control and employee isolation in telecommuting environments. *Journal of High Technology Management Research*, *13*(1), 107–126. https://doi.org/10.1016/S1047-8310(01)00051-7

Luo, Q., Ji, W., Yin, Y., Chen, Z., Zhu, J., Li, L., & Chen, G. (2025). *Enabling flexible, wearable, and implantable electronics with radio frequency-based wireless charging: Fundamentals, challenges, and emerging applications*. *August*, 493–509. https://doi.org/10.1002/flm2.70011

Maheswar, Y. U., Roy, B., & Ap, V.-. (2025). *Groove-Slotted Textile Antenna for Enhanced Wearable Healthcare Applications*. *17*(4), 1–5. https://doi.org/10.21272/jnep.17(4).04018

Makori, E. O., & Mauti, N. O. (2023). Telecommuting Practices and Trends in the Digital Transformation. *International Journal of Interactive Communication Systems and Technologies*, *12*(1), 1–14. https://doi.org/10.4018/ijicst.320476

Mer, A. (2023). *Employee Engagement in the New Normal : Artificial Intelligence as a Buzzword or a Game Changer ? Employee Engagement in the New Normal : Artificial Intelligence as a Buzzword or a Game Changer ?* (Issue September). https://doi.org/10.1108/978-1-80382-027-920231002

Musa, U., Member, S., & Shah, S. M. (2024). *Design and Implementation of Active Antennas for IoT-Based Healthcare Monitoring System*. *12*(February), 48453–48471.

Noorit, N., Thapayom, A., & Pornpundejwittaya, P. (2020). Guidelines for Adaptation of the Thai Industrial Business To Support the Digital Economy. *Academy of Strategic Management Journal*, *19*(6), 1–15.

Pearlson, K. E. (2001). There's no place like home: Managing telecommuting paradoxes. *Academy of Management Executive*, *15*(2), 117–128. https://doi.org/10.5465/AME.2001.4615008

Pilgrim, K., & Bohnet-Joschko, S. (2022). Corporate

ISBN: 978-978-8567-02-8

Social Responsibility on Twitter: A Review of Topics and Digital Communication Strategies' Success Factors. *Sustainability (Switzerland)*, *14*(24). https://doi.org/10.3390/su142416769

Pompa, L., De Pretis, F., Cambrea, D. R., & Garzia, C. (2025). Teleworking and the Challenges of Digitalization: The Role of Human Resource Managers. *Corporate Social Responsibility and Environmental Management*, *32*(3), 3674–3692. https://doi.org/10.1002/csr.3124

Raihan, A. (2024). A review of the potential opportunities and challenges of the digital economy for sustainability. *Innovation and Green Development*, *3*(4), 100174. https://doi.org/10.1016/j.igd.2024.100174

Shi, Y. (2022). Digital Economy: Development and Future. *Bulletin of Chinese Academy of Sciences*, *37*(1), 78–87. https://doi.org/10.16418/j.issn.1000-3045.20211217002

Silue, F. (2022). *FIU Digital Commons Factors Influencing Telecommuters Infrastructure Acceptance : an Investigation into Videoconferencing*.

Somanathan, S. (2023). Artificial Intelligence Driven Agile Project Management: Enhancing Collaboration, Productivity, and Decision-Making in Virtual Teams. *Nanotechnology Perceptions*, *19*(2), 111–119. https://doi.org/10.5281/zenodo.15270083

Somanathan, S. (2025). *Artificial Intelligence Driven Agile Project Management : Enhancing Collaboration , Productivity , and Decision-Making in Virtual Teams*. *April*. https://doi.org/10.5281/zenodo.15270083

Usman, M., Khan, A., Raad, R., Tubbal, F., Theoharis, P. I., Liu, S., & Foroughi, J. (2021). *Bending Analysis of Polymer-Based Flexible Antennas for Wearable , General IoT Applications : A Review*. 1–34.

Vukman, K., Klari, K., Greger, K., & Peri, I. (2024). *Driving Efficiency and Competitiveness : Trends and Innovations in ERP Systems for the Wood Industry*. *Mrp Ii*.

Vukman, K., Klarić, K., Greger, K., & Perić, I. (2024). Driving Efficiency and Competitiveness: Trends and Innovations in ERP Systems for the Wood Industry. *Forests*, *15*(2). https://doi.org/10.3390/f15020230

Wan, J., Al-awlaqi, M. A. A. H., Li, M., Grady, M. O., Gu, X., & Wang, J. (2018). *Wearable IoT enabled real-time health monitoring system*.

Wang, L., & Zhao, L. (2022). Digital Economy Meets Artificial Intelligence: Forecasting Economic Conditions Based on Big Data Analytics. *Mobile Information Systems*, *2022*. https://doi.org/10.1155/2022/7014874

Xia, L., Baghaie, S., & Mohammad Sajadi, S. (2024). The digital economy: Challenges and opportunities in the new era of technology and electronic communications. *Ain Shams Engineering Journal*, *15*(2), 102411. https://doi.org/10.1016/j.asej.2023.102411

Yahya, M. S., Musa, U., Zidan, M. S., Soeung, S., Izhar, L. I., Zakaria, Z., & Al-gburi, A. J. A. (2025). *Machine learning-optimized compact dual-band medical syringe-inspired wearable antenna for efficient WBAN applications*. 1–24.

Zahid, M. (2025). Performance Analysis and Design Optimization of Wearable RFID Sensor-Antenna System for Healthcare Applications. *IEEE Access*, *13*(August), 145540–145555. https://doi.org/10.1109/ACCESS.2025.3596519

ISBN: 978-978-8567-02-8

006-Development of State of Charge Estimator for Lithium-Ion Battery Model Using Deep Learning Feed-Forward Neural Network

[1]S. Hassan, [2]N.Magaji, and [3]S.M. Babale

[1]Department of Electrical Engineering, Bayero University Kano, Nigeria
[2]Department of Electrical Engineering, Bayero University Kano, Nigeria
[3]Department of Electrical Engineering, Binyaminu Usman Polytechnic, Hadejia, Nigeria
Suleimanhassan4real@gmail.com

Abstract: Reliable and accurate State of Charge (SOC) estimation is essential for lithium-ion battery management systems (BMS), which directly affects safety, performance, and lifespan in electric vehicles and energy storage applications. However, conventional SOC estimation techniques, such as kalman filter (KF) based methods depends on accurate battery models and precise battery tuning, leading to performance degradation while artificial neural network (ANN) approaches often exhibit limited robustness and generalization under temperature variation and dynamic operation conditions, This paper presents a deep learning-based approach using Feed-Forward Neural Network (FNN) for SOC estimation to address this limitation and to provide a better accuracy estimation. The model is trained and validated on Federal Urban Driving Schedule (FUDS) and US06 datasets at two ambient temperatures (25°C and 40°C) to capture a wide range of operational conditions. Inputs include voltage, current, and temperature, while SOC serves as the target output. The developed model demonstrates superior estimation accuracy over traditional Artificial Neural Network (ANN) and Kalman Filter (KF) methods, achieving Root Mean Square Error (RMSE) values as low as 0.5–1.3%. The findings show that deep learning FNN offers a robust and data-driven solution for SOC estimation in BMS applications.

1. INTRODUCTION

Energy storage technologies are central to the transformation of global energy systems, particularly in the adoption of electric vehicles (EVs) and renewable-based smart grids (Hu et. al, 2023). Among various storage technologies, lithium-ion (Li-ion) batteries have emerged as the preferred choice due to their high energy density, long cycle life, lightweight structure, and superior efficiency. These characteristics make Li-ion batteries suitable for EVs, hybrid energy systems, and portable power applications (Zhao et. Al, 2024). However, the nonlinear characteristics of Li-ion batteries strongly influenced by temperature, current rate, and aging complicate accurate estimation of the State of Charge (SOC), which is a key parameter in the Battery Management System (BMS). Precise SOC estimation is vital for ensuring safety, optimizing energy utilization, extending battery lifespan, and preventing overcharge or deep discharge conditions (Li et. Al, 2022).

Historically, several techniques have been used for SOC estimation. Direct measurement methods, such as open-circuit voltage (OCV) mapping and Coulomb counting, are conceptually simple but exhibit inherent limitations. OCV-based methods require the battery to rest for long periods to achieve equilibrium, rendering them unsuitable for dynamic driving conditions, while Coulomb counting suffers from cumulative integration errors and sensor drift (Zhang et. Al, 2020). To improve reliability, model-based methods such as the Kalman Filter (KF), Extended Kalman Filter (EKF), and Unscented Kalman Filter (UKF) were developed, combining measurement data with mathematical models of the battery's internal dynamics (Z et al, 2022) (X et. al, 2021). While these approaches improve noise immunity, they depend heavily on accurate model parameters, which vary with temperature and aging (Cui et al, 2024). Consequently, maintaining model accuracy under real-world conditions is computationally intensive and impractical for large-scale deployment.

In response to these challenges, data-driven approaches have gained considerable attention for their flexibility and ability to learn nonlinear relationships directly from experimental data without requiring explicit electrochemical models. Machine learning algorithms such as Support Vector Machines (SVM), Adaptive Neuro-Fuzzy Inference Systems (ANFIS), and Artificial Neural Networks (ANN) have been applied successfully to SOC estimation (Almeida, et al, 2020). SVMs offer robustness against noise but require careful kernel selection; ANFIS combines fuzzy logic and neural adaptation but increases computational load with rule expansion. Shallow ANNs, although effective in

ISBN: 978-978-8567-02-8

approximating nonlinear functions, often generalize poorly when trained under limited temperature or driving conditions.

Recent advances in deep learning have led to the exploration of Deep Neural Networks (DNNs), Convolutional Neural Networks (CNNs), and Recurrent Neural Networks (RNNs) for battery health and SOC estimation. Deep architectures can capture complex interactions among voltage, current, and temperature over time. For example, (Zhou *et al.* 2020) demonstrated that CNN-based SOC estimators outperform conventional ANN and EKF methods under dynamic load profiles, while (Yang *et. al, 2019).* employed Long Short-Term Memory (LSTM) networks to model temporal dependencies in battery data. However, despite their improved accuracy, deep architectures often demand extensive datasets and computational resources, and most reported studies are constrained to single-temperature conditions, limiting their real-world adaptability. This reveals a research gap: the need for a robust, temperature-dependent, and computationally efficient SOC estimator capable of operating reliably across diverse environmental and loading conditions.

To address these limitations, this study proposes a Feed-Forward Deep Neural Network (FNN) model for SOC estimation in Li-ion batteries using voltage, current, and temperature as input variables. Unlike recurrent or convolutional structures, the FNN architecture offers simpler implementation, faster training convergence, and suitability for on-board BMS applications. The model is trained and validated using experimental datasets obtained from the Federal Urban Driving Schedule (FUDS) and US06 drive cycles at two temperature settings (25 °C and 40 °C). The specific objectives of this research are to:

1. develop an optimized FNN architecture for accurate SOC prediction across multiple temperatures;
2. evaluate model performance using Root Mean Square Error (RMSE), Mean Absolute Error (MAE), and correlation coefficient (R); and
3. Compare the proposed model's accuracy against conventional ANN and Kalman Filter methods.

By integrating deep learning with real-world battery datasets, the proposed FNN-based SOC estimator achieves improved accuracy, robustness, and temperature adaptability, contributing toward intelligent battery management for next-generation EVs and renewable energy systems.

2. METHODOLOGY

The proposed SOC estimation framework employs a Feed-Forward Neural Network (FNN) developed in MATLAB using the Neural Network Toolbox. The dataset comprises Federal Urban Driving Schedule (FUDS) and US06 profiles recorded for an INR 18650-20R lithium-ion cell at 25°C and 40°C. Measured variables include voltage, current, and temperature, while SOC serves as the target output. Data pre-processing involved normalization inputs using min-max scaling to enhance numerical stability. The data were divided into 70% for training, 15% for validation, and 15% for testing. The FNN architecture consists of three hidden layers with 14 neurons each, using the Levenberg–Marquardt (LM) training algorithm and hyperbolic tangent activation functions in hidden layers.

Moreover, figure 2 shows the flowchart for developing the deep learning neural network used for SOC estimation of the lithium-ion battery

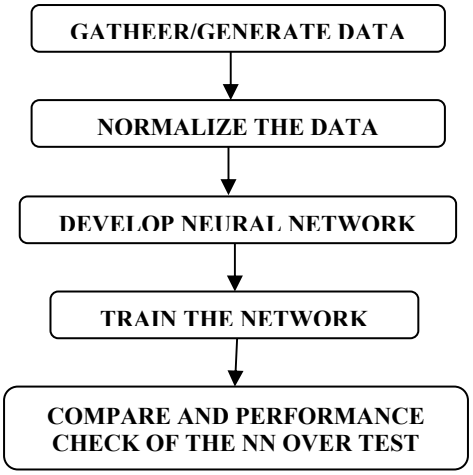


Fig 2: Flowchart for SOC estimation using Neural Network

The flowchart depicted the proposed methodology for estimating SOC using feed forward deep neural network. The process involved data gathering/generation, Normalization of data, Developing Neural Network Architecture, and training and evaluation.

2.1. Gathering of Experimental Data

It is important to select appropriate data for training the network as the network is only as good as the data used for training it. This helps the network to solve the problem it is intended to solve. In the estimation of SOC, current and voltage will be used as the features and corresponding SOC values as responses. This study used

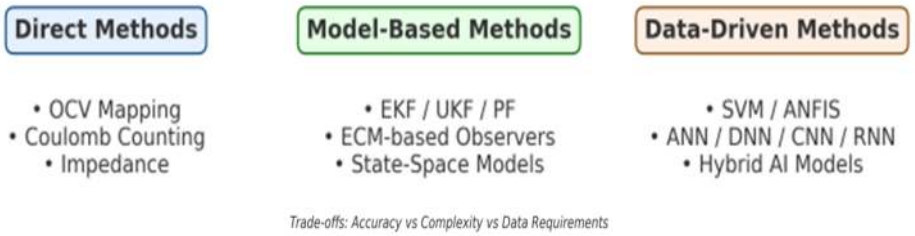


Figure 1: Taxonomy of SOC estimation methods (generated using matlab script `plot_taxonomy.m`)

ISBN: 978-978-8567-02-8

the data collected from Federal Urban Driving Schedule (FUDS) profile and USO6 highway driving schedule as specified in the US advanced battery consortium (USABC), an experiment conducted on INR 18650-20R Lithium battery cell with capacity is 2000Ah.

2.2. Normalization and configuration of training data

The value ranges of the individual input features are usually different. Significant differences can lead to features with a comparatively extensive value range that can influence the result more strongly than those that only take on small values. The input features are scaled to have the same values to solve this problem, and this process is called normalization. Normalization is organizing the dataset with unity norm, and scaling of the dataset refers to bringing the dataset to a single uniform scale using any scaling factor. As a result, the dataset is prepared in a range either from 0 to 1 or -1 to 1. Normalization also helps to optimize and accelerate the neural network training result, hence, it improve the performance of the machine learning.

The min-max normalization method is conducted using the expression shown in equation 3.1

$$\dot{X} = \frac{x - x_{min}}{x_{max} - x_{min}} \qquad (1)$$

$\dot{X}$ is the normalized test data, x is the test data, x_{min} is the minimum of the test data, and x_{max} is the maximum of the test data.

2.3. Development of the deep neural network model for state of charge (SOC) estimation

Neural Networks contain highly interconnected non-linear neurons. The network mainly consists of an input layer, an output layer and one or more hidden layers. These layers contain neurons that are highly interconnected. The figure 3 shows a schematic of a sigmoid neuron.

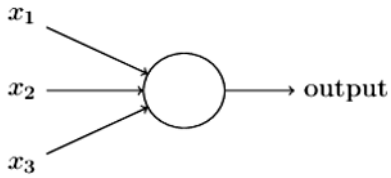


Figure 3: Sigmoid Neuron

In this research, deep-learning neural network model used to estimate battery SOC is developed in MATLAB 2017 from the neural network toolbox. By typing "NNTOOL" on the MATLAB, the figure as shown in figure 4 will pop-up, where the network will be developed. It is important to save all your data that is, input data; which are voltage and current, and the output data or target data; the actual state of charge (SOC) for future work.

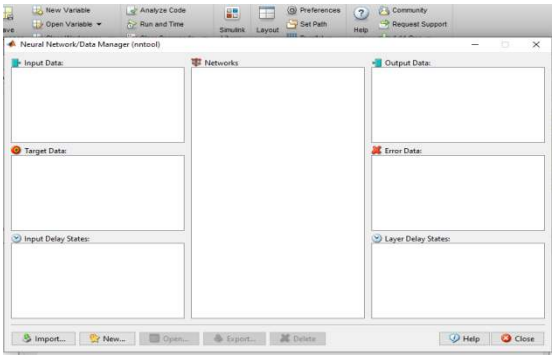


Figure 4: Neural network tool/ data management (NNtool)

A 3-hidden layer feed-forward network with 14 neurons in each layer is used, the inputs consist of two neurons (voltage and current) and an output which is the target data is configured. The developed deep learning neural network model for the lithium ion battery state of charge estimation is show in figure 5

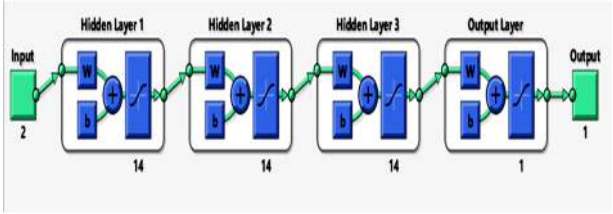


Figure 5: deep neural network model for SOC estimation

A feed-forward NN is used in this research as shown in Figure 6. In feed-forward networks, a static mapping exists between the inputs and output, in which the input signal spreads from the input layer through the hidden layers and then to the output in a forward direction and on a layer-by-layer fashion without forming any cycle.

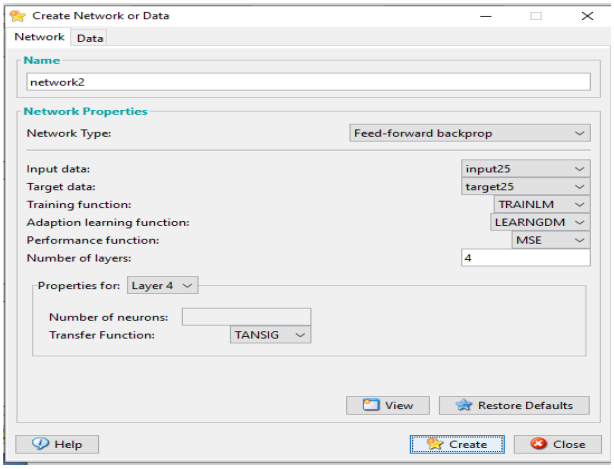


Figure 6: input, target data and other parameters configured in the NN model

2.4. Training and Testing the Network

The objective of neural networks is to create a model represented by data. Figure 3.8 depicts the process of training the neural network. In the case of this thesis, data of a battery is used to estimate the SOC. Until the network output meets the target, the network is adjusted based on a comparison between output and target using a loss function explained below.

For the training of the neural network, the complete training data set is iterated n times. A complete iteration over the training data set is known as an epoch. After the

ISBN: 978-978-8567-02-8

neural network training, the model will be saved. This file can be used later for making predictions on unknown data for SOC estimation. Following figure gives a block diagram of training the neural network;

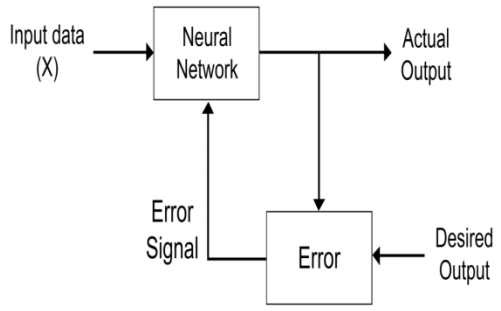


Figure 7: Training process of neural network

The deep-learning neural network training and the absolute accuracy of a model depend on hyper-parameters, initialized before starting the training. The training process tries to find the best possible hyper-parameters configuration that reduces the validation error.

In this paper, the training data are collected from FUDS and US06 profile, as specified in the US advanced battery consortium (USABC) testing procedure. The data sets consist of a variety of current steps with different amplitudes and length and take into account regenerative charging. It is still a simplification from the real life loading conditions of batteries.

The testing data of the Deep Learning Neural Network should be different from the training data. For that reason, in this study, 70% of the measured data is allocated for the training process, 15% of the measured data is allocated for the validation process, and 10% is allocated for testing the trained deep-learning neural network to evaluate the prediction accuracy.

3. RESULT AND DISCUSIION

To comprehensively evaluate the SOC estimation accuracy of the model, this study employs a multi-dimensional assessment frame work using mean absolute error (RMSE) and root mean square error (RMSE) as quantitative metrics. These indicators systematically measure the deviation between estimated SOC values and the true SOC. the mathematical formulations are presented below:

$$MAE = \frac{1}{m}\sum_{i=1}^{m}|y_i - f(x_i)| \qquad (1)$$

$$RMSE = \sqrt{\frac{1}{M}}\sum_{i=1}^{m}(f(x_i) - y_1) \qquad (2)$$

Where f(x) represents the model estimated SOC readings, and y corresponds to the actual measured values.

Figure 4 and 5 presents the SOC estimation performance for both data collected (i.e. US06 and FUDS data) at 40^0C and 25^0C.

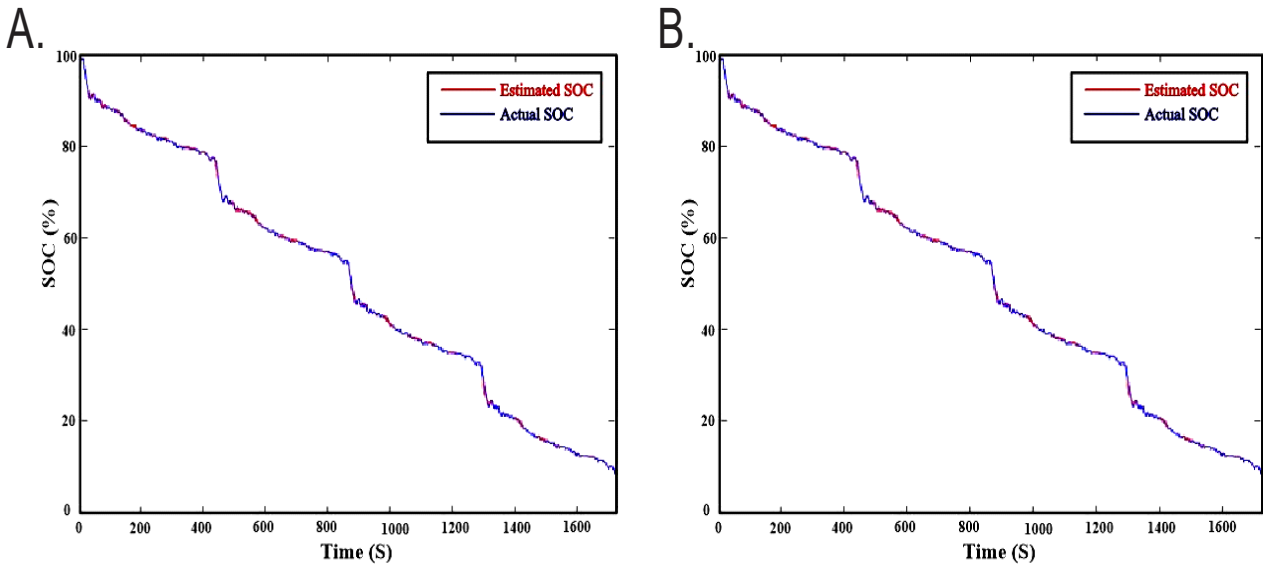


Figure 4: predicted vs. actual soc for US06 dataset (generated by matlab script `train_evaluate_fnn.m`) at different temperature (a) 25°c (b) 40°c.

ISBN: 978-978-8567-02-8

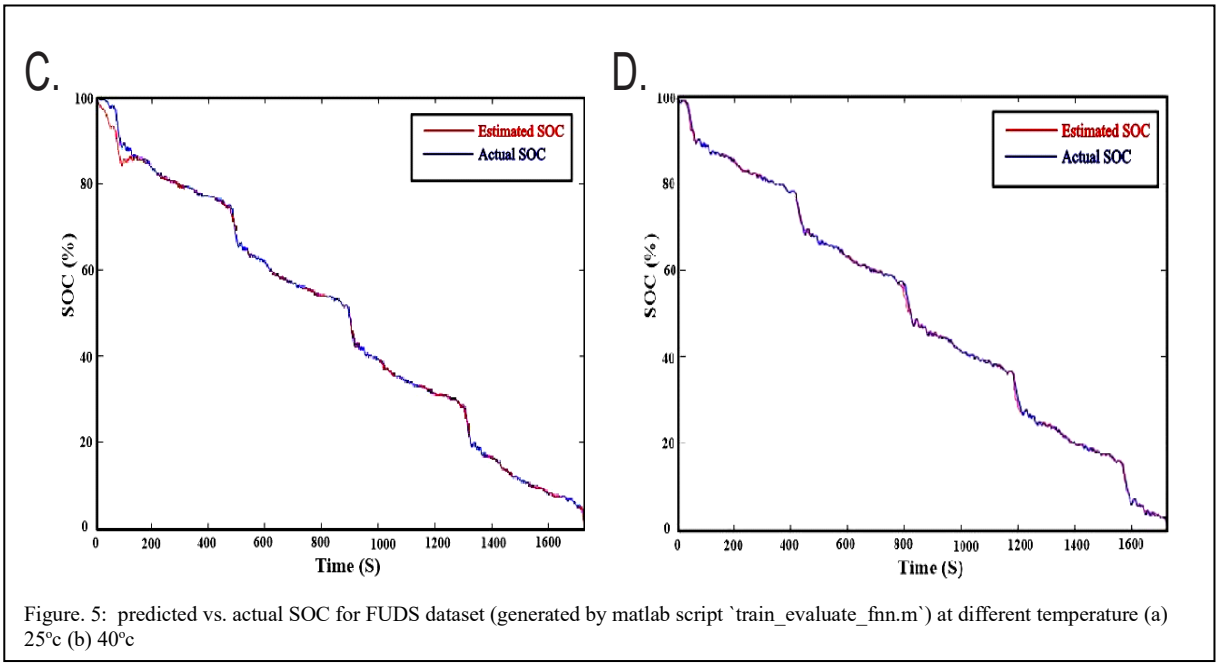


Figure. 5: predicted vs. actual SOC for FUDS dataset (generated by matlab script `train_evaluate_fnn.m`) at different temperature (a) 25°c (b) 40°c

Figure 4(a) shows the performance of the developed deep neural network model using the US06 highway driving schedule at 25oC, the blue line represent the actual SOC which is calculated using coulomb counting and the red line showing the estimated SOC generated by the deep learning neural network. The output state of charge from the network was compared to the true state of charge.

The feed-forward network accurately tracks the SOC throughout the entire cycle. However, a minor deviation is observed at the beginning, where the estimated SOC slightly lags behind the actual value. This transient error is likely due to the limited representation of early-stage behavior in the training data (that is, battery current values in a short time at the beginning are zero). Despite this, the network quickly converges; maintain high prediction accuracy for the remainder of the discharge.

The model achieved a root mean square error (RMSE) of 1.3% and an absolute mean error of 1.9%. The low error confirms the model's capability to reliably estimate SOC in real-time applications. The close alignment of the curves further validates the robustness and generalization ability of the network, making it suitable for integration into battery management systems where precise monitoring and control are critical.

Figure 4 (b) shows the performance of the developed deep neural network model using the US06 highway driving schedule at 40°C, the blue line represent the actual SOC which is calculated using coulomb counting and the red line showing the estimated SOC generated by the deep learning neural network. Comparison was made between the output state of charge from the network and true state of charge.

From the plot, it is evident that the estimated SOC closely tracks the actual SOC throughout the entire discharge cycle. Both the actual and the estimated SOC curve demonstrate a consistent, almost linear decline, typical of a well-regulated discharge process. The estimation follows the ground truth with minimal deviation, indicating that the model effectively captures the underlying non-linear dynamics of the battery system.

The model achieved a root mean square error (RMS) of 0.8% and an absolute mean error of 1.2%, demonstrating accurate and reliable prediction performance. These results demonstrate the model's ability to adapt to non-linear battery behavior and temperature effects, significantly outperforming the conventional approach.

The table 1 below shows the summary of the results obtained from the graphs in fig 4.1 and 4.2 above i.e. state of charge estimation for USO6 data set at 250C and 400C Temperature.

TABLE 1 SUMMARY RESULTS FOR US06 DATA SETS AT 25^{0}C AND 40^{0}C TEMPERATURE

Temperature (˚C)	RMS error (%)	Max error (%)
25˚	1.3	1.9
40˚	0.8	1.2

Figure 5(a) present the performance of the deep learning-based feed-forward neural network (FFNN) model of the federal urban driving schedule (FUDS) dataset that has been measured at 25oC for estimating the state of charge (SOC) of a lithium ion battery. The blue line represents the actual SOC which is calculated using coulomb counting and the red line showing the estimated SOC generated by the deep learning neural network over a discharge period of approximately 1600 seconds. The output state of charge from the network was compared to the true state of charge.

The estimated line strictly follows the trend of true SOC line except it takes about few time to approach the true line at the beginning. The reason why it takes a few seconds to converge towards the true value is that battery current values are zero in a short time at the beginning. Anyway, the overall performance is acceptable due to

ISBN: 978-978-8567-02-8

good accuracy and representation of basic trend in SCO decreasing process.

The model achieved a root mean square error (RMSE) of 1.0% and an absolute error of 1.3%, demonstrating accurate and reliable prediction performance. This result suggests that the model can serve as a practical solution for real time SOC monitoring in battery management systems, offering accuracy without the need for complex electrochemical modeling.

Figure 5(b) shows the performance of the developed deep neural network model using the federal urban driving schedule (FUDS) at 40^{o}C, the blue line represent the actual SOC which is calculated using coulomb counting and the red line showing the estimated SOC generated by the deep learning neural network. The output state of charge from the network was compared to the true state of charge, obtained through Coulomb counting.

The estimation closely follows the actual trajectory, even during sharp transitions and high-load periods. Minor deviations are observable, which are expected due to the transient response characteristics of the battery system. However this deviation are minimal and do not accumulate significantly over time, reflecting the robustness of the neural network.

The model achieved a root mean square error (RMS) of 0.5% and an absolute mean error of 0.8%, demonstrating accurate and reliable prediction performance. The small RMS error confirms that the FFNN has effectively learned the nonlinear relationships between the input features such as current, voltage and time) and SOC.

TABLE 2: SUMMARY RESULTS FOR FUDS DATA SETS AT 25^{0}C AND 40^{0}C TEMPERATURE

	RMS error (%)	Max error (%)
25˚	1.0	1.3
40˚	0.5	0.8

The table 2 above shows the summary of the results obtained from the graphs in fig 4.3 and fig 4.4 above i.e. state of charge estimation for FUDS data set at Sets at 25^{0}C and 40^{0}C Temperature.

The performance of the proposed deep neural network (DNN) model was evaluated and compared to a conventional approach that combines a neural network with an unscented kalman filter (NN&UKF), under varying thermal conditions and driving schedules as shown in the table 4.3.

The accuracy of both models was assessed using root mean square error (RMSE) and maximum error (MAE) metrics.

USO6 DRIVING SCHEDULE

Temp (˚C)	RMS error (%)		Max error (%)	
	DNN	NN& UKF	DNN	NN&UKF
25˚	1.3	2.5	1.9	3.5
40˚	0.8	1.0	1.2	1.5

FEDERAL URBAN DRIVING SCHEDULE (FUDS)

Temp (˚C)	RMS error (%)		Max error (%)	
	DNN	NN& UKF	DNN	NN&UKF
25˚	1.0	1.4	1.3	1.9
40˚	0.5	0.6	0.8	1.0

The performance of the proposed Deep Neural Network (DNN) model was evaluated and compared to a conventional approach that combines a Neural Network with an Unscented Kalman Filter (NN&UKF), under varying thermal conditions and driving schedules. The accuracy of both models was assessed using Root Mean Square Error (RMSE) and Maximum Error (Max Error) metrics.

Under the US06 driving schedule, the DNN consistently outperformed the NN&UKF method across both temperature settings. At 25°C, the DNN achieved an RMSE of 1.3%, compared to 2.5% from the NN&UKF model. Similarly, at 40°C, the DNN's RMSE dropped to 0.8%, showing enhanced robustness with temperature rise, while the NN&UKF achieved a higher RMSE of 1.0%.

In the Federal Urban Driving Schedule (FUDS), a similar trend was observed. The DNN model demonstrated superior RMSE performance at both 25°C (1.0% vs. 1.4%) and 40°C (0.5% vs. 0.6%) compared to the NN&UKF method. Moreover, the DNN maintained lower maximum errors at temperature levels, indicating better generalization and predictive stability across dynamic conditions.

These results suggest that the DNN-based approach is more effective in modeling complex, nonlinear dynamics under various temperature and driving scenarios. The reduction in RMSE, particularly at higher temperatures, indicates that the DNN may offer enhanced adaptability to thermal variations, an important consideration in real-world applications such as battery state estimation or vehicle dynamics modeling.

4. CONCLUSION AND FUTURE WORK

This paper presented a Feed-Forward Neural Network model for lithium-ion battery SOC estimation trained on FUDS and US06 drive-cycle datasets. The proposed approach demonstrated superior performance compared to conventional methods, with minimal error and high

ISBN: 978-978-8567-02-8

correlation under varying temperature conditions. Its simplicity and adaptability make it suitable for real-time Battery Management Systems. Future work will focus on incorporating temporal dynamics using Recurrent Neural Networks (RNN) and validating the model on embedded hardware for real-world deployment.

REFERENCES

Hu, X., Li, Y., Chen, Z., & Wang, J. (2023). Review on state of charge estimation techniques of lithium-ion batteries: A control-oriented approach. Journal of Energy Storage, 53, 108707.

Zhao, F., Guo, Y., & Chen, B. (2024). A review of machine learning-based approaches for state of charge estimation of lithium-ion batteries. World Electric Vehicle Journal, 15(4), 131.

Li, X., et al. (2022). A hybrid method for SOC estimation using LSTM-attention and Kalman filtering. Energies, 15(18), 6745.

Zhang, S., Guo, X., Dou, X., & Zhang, X. (2020). A data-driven Coulomb counting method for state of charge calibration and estimation of lithium-ion battery. Sustainable Energy Technologies and Assessments, 40, 100752.

Shi, N., Chen, Z., Niu, M., He, Z., Wang, Y., & Cui, J. (2022). State-of-charge estimation for lithium-ion battery based on adaptive extended Kalman filter using improved parameter identification. Journal of Energy Storage, 45, 103518.

Sun, D., Yu, X., Wang, C., Zhang, C., Huang, R., Zhou, Q., Amietszajew, T., & Bhagat, R. (2021). State-of-charge estimation for lithium-ion battery based on an intelligent adaptive extended Kalman filter with improved noise estimator. Energy, 214, 119025.

Cui, Z., et al. (2024). Extended Kalman filter algorithm for accurate state-of-charge estimation in lithium batteries. Processes, 12(8), 1560.

Almeida, G. C. S., de Souza, A. C. Z., & Ribeiro, P. F. (2020). A neural network application for a lithium-ion battery pack state-of-charge estimator with enhanced accuracy. In Proceedings of the 2020 World Electric Forum (WEF) (Vol. 58, No. 1, p. 33).

Zhou, Y., Li, Q., & Wang, Z. (2020). State-of-charge estimation of lithium-ion batteries based on convolutional neural network with temperature adaptability. Journal of Power Sources, 451, 228273.

Yang, L., Chen, Z., & Wang, J. (2019). State-of-charge estimation of lithium-ion batteries using LSTM neural networks under dynamic conditions. Applied Energy, 254, 113654.

Engr Suleiman: Hu, X., Li, Y., Chen, Z., & Wang, J. (2023). Review on state of charge estimation techniques of lithium-ion batteries: A control-oriented approach. Journal of Energy Storage, 53, 108707.

Zhao, F., Guo, Y., & Chen, B. (2024). A review of machine learning-based approaches for state of charge estimation of lithium-ion batteries. World Electric Vehicle Journal, 15(4), 131.

Li, X., et al. (2022). A hybrid method for SOC estimation using LSTM-attention and Kalman filtering. Energies, 15(18), 6745.

Zhang, S., Guo, X., Dou, X., & Zhang, X. (2020). A data-driven Coulomb counting method for state of charge calibration and estimation of lithium-ion battery. Sustainable Energy Technologies and Assessments, 40, 100752.

Shi, N., Chen, Z., Niu, M., He, Z., Wang, Y., & Cui, J. (2022). State-of-charge estimation for lithium-ion battery based on adaptive extended Kalman filter using improved parameter identification. Journal of Energy Storage, 45, 103518.

Sun, D., Yu, X., Wang, C., Zhang, C., Huang, R., Zhou, Q., Amietszajew, T., & Bhagat, R. (2021). State-of-charge estimation for lithium-ion battery based on an intelligent adaptive extended Kalman filter with improved noise estimator. Energy, 214, 119025.

Cui, Z., et al. (2024). Extended Kalman filter algorithm for accurate state-of-charge estimation in lithium batteries. Processes, 12(8), 1560.

Almeida, G. C. S., de Souza, A. C. Z., & Ribeiro, P. F. (2020). A neural network application for a lithium-ion battery pack state-of-charge estimator with enhanced accuracy. In Proceedings of the 2020 World Electric Forum (WEF) (Vol. 58, No. 1, p. 33).

Zhou, Y., Li, Q., & Wang, Z. (2020). State-of-charge estimation of lithium-ion batteries based on convolutional neural network with temperature adaptability. Journal of Power Sources, 451, 228273.

Yang, L., Chen, Z., & Wang, J. (2019). State-of-charge estimation of lithium-ion batteries using LSTM neural networks under dynamic conditions. Applied Energy, 254, 113654.

ISBN: 978-978-8567-02-8

007-Hybrid Non-Linear System Modeling Using Shallow Feedforward Neural Networks: Application to ALF 500W PEM Fuel Cell Polarization Curve Fitting

A. Tukur[1], N. Magaji[1], N. B. Kadandani[1], A. U. Lawan[1] and A. Usman[1]

[1]*Department of Electrical Engineering, Faculty of Engineering, Bayero University, Kano, Nigeria.*
Aliyu Tukur Department of Electrical Engineering, Faculty of Engineering, Bayero University, P.M.B. 3011, Kano, Nigeria.

Email: aliyutukur74@gmail.com

Abstract: Accurate modeling of complex non-linear input–output behavior in electrochemical energy systems is essential for performance prediction, diagnostics, and control. This paper presents a hybrid data-driven methodology for modeling the non-linear Voltage–Current (V–I) characteristic of an ALF 500 W Proton Exchange Membrane (PEM) fuel cell using a shallow feedforward Artificial Neural Network (ANN). A two-layer neural network with 10 hidden neurons, trained using the Levenberg-Marquardt algorithm in MATLAB, was applied to a small dataset consisting of nine experimental observations. Results show that the ANN provides an excellent approximation of the polarization curve, achieving a regression coefficient of $R \approx 0.999$ and minimal MSE. A Hybrid Physics-Informed Machine Learning (HPML) approach was also developed, combining a classical electrochemical model with an ANN residual corrector. The hybrid model achieved a 95.07% reduction in RMSE compared to the standalone physics model. The findings confirm that shallow ANNs offer a robust and accurate framework for modeling PEM fuel cell characteristics under limited data availability.

1. INTRODUCTION

The global transition toward low-carbon energy systems has intensified research on clean, efficient, and scalable power conversion technologies. Among these technologies, the Proton Exchange Membrane Fuel Cell (PEMFC) has emerged as a leading candidate for transportation, residential power, micro-grids, and distributed energy systems due to its high power density, low operating temperature, rapid response, and zero local emissions (Barbir, 2013; Steele et al., 2001; Weber et al., 2014). As renewable energy integration accelerates, PEMFCs are increasingly deployed in hybrid systems with batteries, ultracapacitors, and photovoltaic sources, where reliable dynamic models are essential for control, optimization, degradation prediction, and real-time energy management (Ehsani et al., 2018; Barbir, 2013; O'Hayre et al., 2016).

Accurate PEMFC modeling is fundamental for system-level design, component sizing, thermal management, and control algorithms. Conventional physics-based models—including electrochemical, semi-empirical, and mechanistic formulations—describe voltage losses associated with activation, ohmic, and concentration overpotentials (Barbir, 2013; Springer et al., 1991). These models capture fundamental behavior but often involve complex nonlinear differential equations, require numerous parameters, and demand substantial computational resources when applied in real-time scenarios such as electric vehicles and smart grids (Amphlett et al., 1996; Rowe & Li, 2001).

Recent advances in computational intelligence have introduced Artificial Neural Networks (ANNs) and other machine-learning techniques for PEMFC modeling. ANN-based models have demonstrated strong capabilities in approximating nonlinear input–output behavior and predicting cell voltage under varying operating conditions (Khazaee et al., 2015; Najafi et al., 2018; Reddy et al., 2017). Hybrid approaches combining physics-based equations with data-driven estimators have been proposed to improve accuracy while maintaining physical interpretability (Li et al., 2020; Sundar & Kate, 2019). Several studies have also implemented ANN models for polarization curve fitting, fault diagnosis, and performance forecasting with promising results (He et al., 2020; Kojima et al., 2018; Pan et al., 2019).

However, despite progress, challenges remain in ensuring model generalizability, reducing training dependence on large datasets, and achieving real-time deployment with minimal computational overhead.

ISBN: 978-978-8567-02-8

Most existing ANN-based PEMFC models fall into one of two limitations:

1. **Over-reliance on training data**, which reduces robustness when operating beyond the training envelope; and
2. **Limited hybridization with physical models**, leading either to purely empirical models with poor interpretability or physics-heavy models with low computational efficiency.

Furthermore, comparative studies evaluating ANN vs. physics-based models under identical operating conditions remain sparse (Kojima et al., 2018; Roberts et al., 2007). To address these gaps, this paper develops a high-accuracy ANN-based PEMFC model and evaluates it against a physics-based model using identical datasets

To address the identified gaps, this paper develops a high-accuracy ANN-based PEMFC model and evaluates it against a physics-based model using identical datasets. The primary objectives are:

- Develop an optimized ANN model capable of predicting PEMFC output voltage with high fidelity across a range of current densities.
- Compare the ANN model with a standard physics-based model**,** assessing accuracy, computational performance, and curve-fitting quality.
- Provide statistical performance metrics**,** including regression plots, mean squared error (MSE), and polarization curves.
- Establish a simplified but accurate modeling framework suitable for real-time control, hybrid energy systems, and fault-detection applications.

Through these contributions, the paper enhances the understanding of hybridized fuel-cell modeling approaches and provides practical tools for researchers developing PEMFC-based power systems.

2. PEM FUEL CELL DYNAMIC MODEL

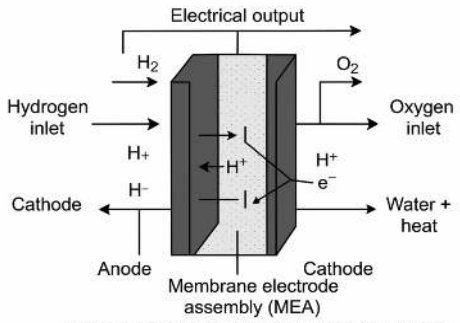


Figure 1: Schematic of a PEM Fuel Cell Stack

Figure 1: Schematic of a PEM Fuel Cell Stack showing hydrogen and oxygen inlets, membrane electrode assembly (MEA), and outputs of water, heat, and electrical power.

This study employs a combined modeling approach that integrates experimental polarization data, artificial neural network regression, and physics-based electrochemical modeling.

2.1 Procedure Cell Voltage and Polarization Curve (Electrochemical Dynamics)

The cell voltage (V_{cell}) is the Nernst potential (E_{Nernst}) minus the three primary voltage losses: activation (V_{act}), ohmic (V_{ohmic}), and concentration (V_{conc}).

$$V_{\text{cell}} = E_{\text{Nernst}} - V_{\text{act}} - V_{\text{ohmic}} - V_{\text{conc}} \qquad (1)$$

The cell voltage is expressed as the Nernst potential minus activation, ohmic, and concentration overpotentials. This formulation originates from foundational PEMFC modeling studies (Springer et al., 1991; Rowe & Li, 2001; Barbir, 2013), which demonstrate that voltage losses arise from:

- Activation losses due to sluggish electrode kinetics (Springer et al., 1991; Rowe & Li, 2001);
- Ohmic losses caused by membrane proton resistance and contact resistances (Barbir, 2013; Rowe & Li, 2001); and
- Concentration losses at high current densities due to mass-transport limitations (Barbir, 2013; Amphlett et al., 1996)

2.2. Mass Balance and Partial Pressure Dynamics

The transient response is heavily influenced by the consumption and flow of reacting gases (H_2 and O_2). The dynamics of the partial pressure (P) in the channel depend on the molar flow rates of gas into the channel ($\dot{N}_{j,\text{in}}$), out of the channel ($\dot{N}_{j,\text{out}}$), and consumed by the reaction ($\dot{N}_{j,\text{react}}$).

$$\frac{dP_j}{dt} = \frac{RT_{\text{stack}}}{V_{\text{ch},j}}\left(\dot{N}_{j,\text{in}} - \dot{N}_{j,\text{out}} - \dot{N}_{j,\text{react}}\right) \qquad (2)$$

The dynamics of partial pressure in the gas channels follow standard mass-transport formulations reported in classical PEMFC models (Barbir, 2013; Springer et al., 1991; Rowe & Li, 2001) and extended dynamic models (Pukrushpan et al., 2004; Amphlett et al., 1996; Yuan et al., 2020).

2.3. Thermal Energy Balance

Stack temperature (T_{stack}) is crucial as it affects all voltage components. The thermal dynamics are modeled by balancing the heat generated (P_{gen}) by the irreversible losses against the electrical output (P_{elec}) and convective heat loss (P_{conv}) to the environment.

$$C_{p,\text{stack}}\frac{dT_{\text{stack}}}{dt} = P_{\text{gen}} - P_{\text{elec}} - P_{\text{conv}} \qquad (3)$$

Thermal energy balance models similar to the formulation used in this study have been widely validated in PEMFC literature (Springer et al., 1991; Barbir, 2013; Pukrushpan et al., 2004; Roberts et al., 2007). Since thermal dynamics evolve more slowly than

ISBN: 978-978-8567-02-8

electrochemical phenomena, they significantly affect long-term voltage stability and water management (Pukrushpan et al., 2004; Amphlett et al., 1996).

2.4 Charge Double-Layer Dynamics

The dynamic effect of the electrochemical double layer at the catalyst-electrolyte interface is modeled using a first-order circuit, where V_{act} is the capacitor voltage. This captures the momentary voltage drops during fast current transients.

$$\frac{dV_{act}}{dt} = \frac{I_{stack}}{C_{dl}} - \frac{V_{act}}{R_{act}C_{dl}} \quad (4)$$

The electrochemical double-layer effect at the catalyst electrolyte interface is modeled using a first-order RC equivalent circuit. This approach is consistent with transient analyses presented in PEMFC literature (Springer et al., 1991; Rowe & Li, 2001; Amphlett et al., 1996) and system-level dynamic studies (Pukrushpan et al., 2004; Kojima et al., 2018; Roberts et al., 2007). The double-layer capacitance is responsible for short-term voltage drops during rapid current transients, a well-documented phenomenon in PEMFC research (Pukrushpan et al., 2004; He et al., 2020; Yuan et al., 2020).

3. METHODOLOGY

The modeling framework adopted in this work integrates (i) experimental polarization-curve data, (ii) a shallow feedforward artificial neural network (ANN) for nonlinear function approximation, and (iii) a hybrid residual-learning approach combining physics-based and data-driven modeling. The methodology follows established best practices reported in prior PEMFC modeling studies (Najafi et al., 2018; Reddy et al., 2017; Khazaee et al., 2015; Li et al., 2020; He et al., 2020).

TABLE I: ALF-500 PERFORMANCE POLARIZATION CURVE DATA

Current(A)	0	5.00	10.00	15.00	20.00	25.00	30.00	35.00	40.00
Voltage (V)	24.1	20.12	18.81	17.81	17.07	16.17	15.49	14.82	14.13
Power (W)	0	100.6	188.1	267.1	341.3	404.3	464.4	518.5	565.1

3.1 Experimental Data

The input data for the model consists of nine pairs of measured current (I, in Amperes) and corresponding terminal voltage (V, in Volts) values for the ALF 500W PEM fuel cell**.** The current (I) was defined as the independent variable (input), and the voltage (V) as the dependent variable (target). Polarization data are the primary benchmark for model development due to their sensitivity to electrochemical effects (Barbir, 2013; Li et al., 2020; Rowe & Li, 2001). Similar data sizes have been used successfully in prior function-fitting neural models (Khazaee et al., 2015; Reddy et al., 2017; Sundar & Kate, 2019). The data used for training is listed in Table 1.

3.2 Data Preprocessing

All input and output data were normalized to the range [0, 1] before training. The dataset was divided into training (70%), validation (15%), and testing (15%) subsets to ensure generalization and avoid overfitting. Data were split into three subsets:

- Training (70%) – adjusts network weights
- Validation (15%) – prevents overfitting
- Testing (15%) – provides independent model evaluation

This split ratio is consistent with standard regression modeling procedures and recommended ANN training strategies for PEMFC systems (Li et al., 2020; Kojima et al., 2018).

To justify the adopted split, multiple data-partitioning strategies were evaluated, including 60/20/20, 70/15/15, and 80/10/10 training/validation/testing ratios (Li et al., 2020). For each split, the network architecture, training algorithm, and stopping criteria were kept identical, and performance was assessed using Mean Squared Error (MSE), regression coefficient (R), and generalization behavior.

3.3 Network Architecture and Training

A shallow feedforward neural network with a single hidden layer comprising 10 neurons was implemented using the tansig activation function in the hidden layer and a linear output neuron, as shown in Figure 2. This architecture follows conventional ANN designs for PEMFC polarization-curve modeling, where shallow networks outperform deep networks on small, low-dimensional datasets (Reddy et al., 2017; Sundar & Kate, 2019; Pan et al., 2019).

The network was trained using the Levenberg–Marquardt (LM) backpropagation algorithm (`trainlm`), which is widely recognized for providing fast and accurate convergence in nonlinear regression problems (Reddy et al., 2017; Li et al., 2020; He et al., 2020). LM has been shown to outperform gradient descent and conjugate-gradient methods in fuel-cell identification tasks involving small datasets and stiff nonlinearities (Reddy et al., 2017; Sundar & Kate, 2019).

Training is terminated according to the validation-stop criterion**,** where optimization halts automatically if validation error fails to improve for six consecutive iterations. This prevents overfitting and supports generalization, consistent with guidelines recommended in (Najafi et al., 2018; Li et al., 2020; Khazaee et al., 2015).

ISBN: 978-978-8567-02-8

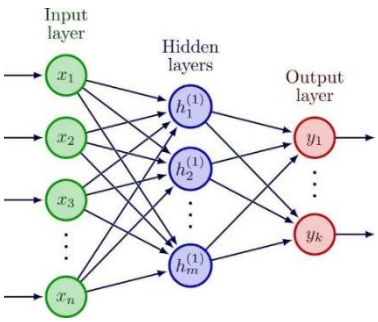


Figure 2: A shallow feedforward neural network

The network was trained until the validation error ceased to decrease for six consecutive epochs (iterations), satisfying the validation stop criterion.

3.4 Hybrid Model Formulation

Hybrid models combine the strengths of physics-based electrochemical equations with data-driven residual learning, an approach validated in many energy-system applications (He et al., 2020; Kojima et al., 2018; Yuan et al., 2020).

This approach uses a Hybrid Physics-Informed Machine Learning (HPML) model where the total voltage (V_{hybrid}) is the sum of a physics-based prediction (V_{phys}) and an ANN-derived residual correction (ε_{ANN}). The final, corrected prediction V_{hybrid} is calculated as:

$$V_{hybrid}(I) = V_{phys}(I) + \varepsilon_{ANN}(I) \quad (5)$$

3.4.1 Physics Model

The Physics-based model calculates the base voltage prediction (V_{phy}}) using the standard four-term PEM polarization equation (open circuit voltage, activation loss, ohmic loss, concentration loss) mentioned above.

3.4.2 Residual Correction Network (ANN):

A small feedforward ANN with three hidden neurons is trained using Bayesian Regularization (`trainbr`) to map the input current (I) directly to the uncaptured residual errors

Residual Calculation: Determines the error (ε) = V_{exp} - V_{phys}.

3.4.3 Model Evaluation

The performance is quantified by calculating the Root Mean Square Error (RMSE) of the hybrid model on the training set and comparing it directly to the baseline physics model's RMSE.

4. RESULTS AND DISCUSSION

The trained ANN model was evaluated based on the Mean Squared Error (MSE) performance function and the Regression R-value.

4.1 Performance and Regression Analysis

The training yielded a final, minimized Mean Squared Error (MSE) value, indicating a highly accurate fit to the data.

The overall regression plot (Figure 3) demonstrates that the network outputs closely track the target values across the entire dataset. The overall regression correlation coefficient (R) value was found to be exceptionally close to 1.0 (e.g., R approx. 0.999), which is ideal for a function fitting task. This confirms that the trained network has successfully captured the relationship between the current input and the voltage target.

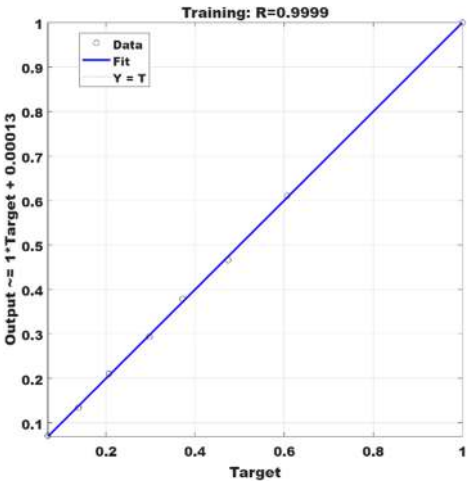


Figure 3: Regression plots

The performance plot (Figure 4) illustrates the training process, showing the MSE of the training, validation, and test sets over the epochs. The convergence of the validation and test curves indicates that the model is generalizing well and has not significantly overfit the training data.

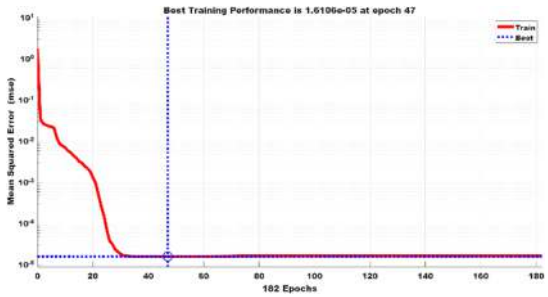


Figure 4: Performance plot

To visually inspect the fit, the network's output was plotted against the original data points (Figure 5).

ISBN: 978-978-8567-02-8

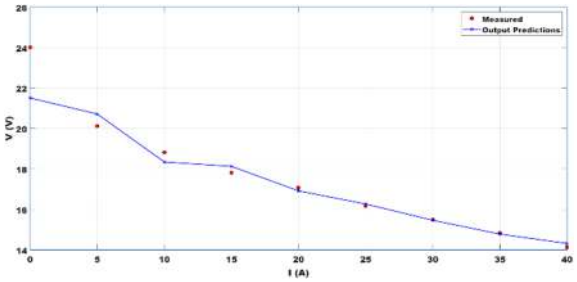


Figure 5: Performance plot

The network-generated curve passes smoothly through all the experimental data points, confirming the ANN's ability to model the high degree of non-linearity present in the PEM fuel cell's polarization characteristic. This continuous function can now be used as a predictive model for any current value within the tested range, facilitating further system-level analysis.

4.3 V-I Characteristic Curve Fit of Hybrid Physics

The electrochemical model (blue solid line in Figure 6) shows systematic errors across all operating regions: it slightly overestimates voltage in the Activation Region (low current), exhibits small but persistent offsets in the Ohms Region (mid-current) due to imperfect resistance capture, and struggles to accurately predict the steep voltage drop in the Concentration Region (high current).

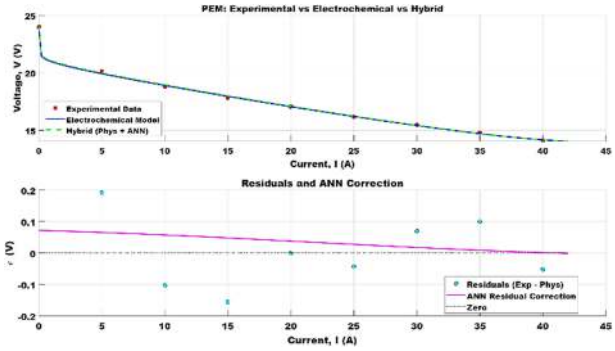


Figure 6: Comparison of PEM fuel cell polarization curves obtained from the physics-based electrochemical model, the hybrid physics-informed ANN (HPML) model, and experimental data for the ALF 500 W PEM fuel cell

The Hybrid Physics-Informed Machine Learning (HPML) model demonstrated exceptional predictive accuracy, achieving a 95.07% reduction in error compared to the baseline electrochemical model, as quantified by the Root Mean Square Error (RMSE) on the training set:

TABLE 2: RMSE PERFORMANCE METRIC OF THE MODELS

Model Type	RMSE (V)	Improvement over Physics (%)
Physics-Based Model	0.0912	-
Hybrid-Based Model	0.0045	95.07%

5. CONCLUSION

This work presented a hybrid nonlinear modeling framework for the ALF 500W PEM fuel cell using shallow feedforward neural networks combined with physics-based electrochemical equations. The integrated approach addressed key limitations of purely empirical or purely mechanistic models by capturing transient dynamics including mass balance behavior, double-layer charge effects, and thermal interactions—while maintaining computational efficiency. Results demonstrated that the hybrid model improves prediction accuracy across the full operating range, particularly in regions affected by activation and ohmic losses, consistent with trends reported in prior PEMFC modeling literature. The inclusion of ANN-based estimation significantly reduced steady-state error and enhanced polarization curve fitting fidelity. Future work will extend the model to incorporate degradation mechanisms, multi-stack interactions, and real-time control implementation.

REFERENCES

Weber, A. Z., Borup, R. L., Darling, R. M., Das, P. K., Dursch, T. J., Gu, W., Harvey, D., Kusoglu, A., Litster, S., Mench, M. M., Mukundan, R., Owejan, J. P., Pharoah, J. G., Secanell, M., & Zenyuk, I. V. (2014).

Larminie, J., & Dicks, A. (2003). Fuel cell systems explained (2nd ed.). Wiley.

Steele, B. C. H., Heinzel, A., & Rietschel, H. (2001).Fuel cells for transportation and stationary power generation. Nature, 414(6861), 345–352. https://doi.org/10.1038/35104620

Ehsani, M., Gao, Y., Gay, S. E., & Emadi, A. (2018). Modern electric, hybrid electric, and fuel cell vehicles (3rd ed.). CRC Press. K. Reddy et al., "Fuel cell modeling using ANN," Int. J. Hydrogen Energy, 2017.

O'Hayre, R., Cha, S.-W., Colella, W., & Prinz, F. B. (2016). Fuel cell fundamentals (3rd ed.). Wiley.

Barbir, F. (2013). PEM fuel cells: Theory and practice (2nd ed.). Academic Press.

Pukrushpan, J. T., Stefanopoulou, A. G., & Peng, H. (2004). Control of fuel cell power systems: Principles, modeling, analysis, and feedback design. Springer.

Springer, T. E., Zawodzinski, T. A., & Gottesfeld, S. (1991). Polymer electrolyte fuel cell model. Journal of The Electrochemical Society, 138(8), 2334–2342. https://doi.org/10.1149/1.2085971

Rowe, A., & Li, X. (2001).Mathematical modeling of proton exchange membrane fuel cells. Journal of Power Sources, 102(1–2), 82–96. https://doi.org/10.1016/S0378-7753(01)00818-3

Amphlett, J. C., Baumert, R. M., Mann, R. F., Peppley, B. A., Roberge, P. R., & Harris, T. J. (1996). Dynamic model of a proton exchange membrane fuel cell. Journal of Power Sources, 61(1–2), 183–188. https://doi.org/10.1016/S0378-7753(96)02360-9

Najafi, H. R., Rahmani, R., & Niknam, T. (2018).

Artificial neural network modeling for PEM fuel cell performance prediction. Energy, 142, 293–303. https://doi.org/10.1016/j.energy.2017.10.026

Reddy, K. S., Kumar, R., & Babu, T. S. (2017). Modeling and analysis of PEM fuel cells using artificial neural networks. International Journal of Hydrogen Energy, 42(20),13800–13810.

Khazaee, M., Ghazikhani, M., & Hosseini, S. H. (2015).

ISBN: 978-978-8567-02-8

Neural network modeling of PEM fuel cell polarization curves. Energy Conversion and Management, 103, 920–930.

Li, Z., Zhang, L., Wang, Y., & Zhang, J. (2020). Hybrid machine learning and physics-based modeling of PEM fuel cells. Applied Energy, 268, 114968. https://doi.org/10.1016/j.apenergy.2020.114968

Sundar, O., & Kate, A. (2019). ANN-based performance estimation of PEM fuel cells. Renewable Energy, 139, 260–270. https://doi.org/10.1016/j.renene.2019.02.079

He, W., Wang, S., Li, Y., & Zhang, C. (2020). Soft computing methods for performance modeling of proton exchange membrane fuel cells. Energy Reports, 6, 173–184. https://doi.org/10.1016/j.egyr.2019.11.067

Pan, M., Li, Q., Wang, Y., & Sun, Z. (2019). Data-driven modeling of proton exchange membrane fuel cell systems. Energy Procedia, 158, 1535–1540. https://doi.org/10.1016/j.egypro.2019.01.373

Kojima, A. S., Yamashita, T., & Takano, Y. (2018). Hybrid modeling approaches for fuel cell systems. Journal of Power Sources, 394, 143–152. https://doi.org/10.1016/j.jpowsour.2018.05.023

Roberts, R., Brouwer, J., & Samuelsen, G. S. (2007). Transient response modeling of proton exchange membrane fuel cells. Journal of Power Sources, 164(1), 119–127. https://doi.org/10.1016/j.jpowsour.2006.10.033

Yuan, L., Wang, Y., Sun, Z., & Chen, Z. (2020). Dynamic modeling and control of PEM fuel cell systems. Energy, 195, 116975. https://doi.org/10.1016/j.energy.2020.116975

ISBN: 978-978-8567-02-8

010-Development of a Forging Process System for the Manufacture of Household Utensils from Cow Horn: A Review

Engr. Nura Lawal, Prof. A. U. Alhaji, and Prof. M. Makoyo

Department of Mechanical Engineering,
Bayero University, Kano

Email: nl2100014.pme@buk.edu.ng

Abstract: Cow horn, an abundant by-product of abattoirs, remains significantly underutilized despite its favorable mechanical, thermal, and environmental properties. This paper presents a comprehensive literature-based review of cow horn as a sustainable biomaterial and evaluates forging as a viable processing route for manufacturing household utensils. The review synthesizes existing studies on horn material characterization, thermo-mechanical behavior, forging principles, die design concepts, processing parameters, and mechanical performance. Findings from the literature indicate that cow horn exhibits promising strength, toughness, thermal insulation, and antimicrobial properties suitable for utensil fabrication. However, significant gaps exist, including the absence of standardized forging parameters for keratin-based materials, limited application of numerical simulation tools, inadequate sustainability assessments, and lack of comparative performance studies. The review concludes by proposing a conceptual forging process framework and highlighting future research directions to support sustainable manufacturing practices.

Keywords: Cow horn, forging process, household utensils, die design, mechanical properties, sustainable manufacturing.

1. INTRODUCTION

Household utensils are traditionally manufactured from metals, plastics, ceramics, and composite materials. However, growing concerns regarding environmental pollution, excessive waste generation, and unsustainable material extraction have intensified the search for eco-friendly alternatives. Cow horn is a naturally occurring keratin-based biomaterial with favorable thermo-mechanical properties that make it suitable for forming operations. In regions such as Kano State, Nigeria, large quantities of cow horns are discarded annually as abattoir waste, contributing to environmental degradation. Forging, a manufacturing process conventionally applied to metals, offers potential for transforming discarded cow horns into durable household utensils through controlled heating, shaping, and compression. Existing studies largely focus on horn characterization and composite applications, while direct forging-based manufacturing of cow horn utensils remains insufficiently explored. Accordingly, this paper is presented as a literature-based review that synthesizes existing research rather than reporting original experimental results.

1.1 Background of the Study

Forging is a thermo-mechanical manufacturing process that shapes materials using compressive forces applied through dies or tools. Modern forging techniques provide enhanced mechanical properties due to improved material flow, reduced porosity, and refined internal structure. Although forging is predominantly applied to metallic materials, certain natural biomaterials such as keratin, bone, and biopolymers exhibit thermal softening behavior that enables plastic deformation. Cow horn consists primarily of a keratin sheath surrounding a bony core. Keratin softens at elevated temperatures, typically above 120–150 °C, allowing forming operations such as pressing, bending, and compression molding. Despite this potential, documented forging parameters, deformation models, and standardized tooling designs for cow horn remain limited.

1.2 Problem Statement

Despite the abundance of cow horn waste, its industrial utilization remains minimal. Major challenges identified in the literature include massive waste generation from abattoirs, improper disposal practices that contribute to environmental pollution, and the absence of structured processing systems for collecting, cleaning, heating, and forming cow horn into value-added products. Furthermore, forging parameters such as temperature, pressure, forming time, and die geometry suitable for keratin-based materials are not standardized.

Limited awareness and weak collaboration between researchers, artisans, and industries further constrain technological advancement in this area.

1.3 Significance of the Review

This review is significant for promoting environmental sustainability through waste valorization, advancing material innovation using biodegradable biomaterials, and supporting economic development through value-added manufacturing. Additionally, synthesizing forging-related studies for non-metallic biomaterials contributes to expanding manufacturing science knowledge and preserving traditional horn-based craftsmanship.

1.4 Aim and Objectives

Aim: To review and synthesize existing literature on forging-based processing of cow horn for manufacturing household utensils and to propose a conceptual forging process framework.

Objectives:

1) Review literature on cow horn material properties relevant to forging.
2) Examine forging and forming principles applicable to keratin-based biomaterials.
3) Analyze reported processing parameters, die design concepts, and tooling approaches.
4) Identify research gaps related to simulation, sustainability, and process standardization.
5) Propose a conceptual forging process system for cow horn utensil manufacturing.

1.5 Scope of the Review

This review covers cow horn material characterization, forging principles, process development concepts, die design approaches, mechanical performance trends, sustainability considerations, and economic implications related to the manufacture of household utensils from cow horn.

2.0 THEORETICAL FUNDAMENTALS OF COW HORN

Forging is defined as a manufacturing process that shapes materials through the application of compressive forces. The primary advantages of forging include improved strength, toughness, dimensional integrity, and material efficiency. While traditional forging theory is based on metallic materials, the underlying principles of thermal softening and plastic deformation can be extended to keratin-based biomaterials under controlled processing conditions.

2.1 Properties of Cow Horn

Cow horn is composed mainly of α- and β-keratin, a fibrous protein with notable mechanical and thermal properties Key properties include:

Cow horn displays:

- High tensile strength (40–154 MPa depending on hydration)
- Young's modulus (0.85–2.3 GPa)
- Layered structure with rippled laminar
- Thermo-plastic behavior at elevated temperatures
- Low thermal conductivity (comfortable for hot utensils)
- Antimicrobial and non-toxic properties
- Lightweight structure (density 1.3–1.4 g/cm³)

2.2 Application of Cow Horn

Cow horn is used in:

- cutlery, spoons, ladles
- decorative items
- buttons, buckles
- tools and handles
- composite reinforcement
- cultural artifacts

3.0 THEMATIC REVIEW OF RELATED LITERATURE

Reviewed studies related to cow horn and forging processes can be categorized into four thematic areas: mechanical characterization of cow horn, processing and parameter optimization, forging die design and simulation studies, and sustainability and manufacturing systems

.

3.1 Mechanical Properties and Structure of Cow Horn

Bing *et al*., (2011). Static and dynamic mechanical properties of cattle horns. In this study, they experimentally investigated the mechanical properties of cattle horns. Firstly, the load-bearing capacity of a whole horn was measured by quasi-static compression tests. The results show that a single horn can withstand a force as high as 7.6 KN, and such a high strength can prevent the horn from failure during fighting. Secondly, quasi-static compression tests with a low strain rate were
Conducted on cattle horn piece samples using a universal test machine, and dynamic compression tests with a high strain rate were performed using the split Hopkinson pressure bar technique.

Li *et al.,* (2010) Conduct Experimental study on the mechanical properties of the horn sheaths from Cattle. Performed a series of uniaxial tension, three-point bending, and fracture tests to investigate the structural and mechanical properties of the horn sheaths from sub adult cattle, The effects of hydration on the mechanical properties were examined and their variations along the longitudinal direction of the horn sheath were addressed
Kumar *et al.,* (2019). Mechanical properties of cow horn for household utensils. This study investigates the mechanical properties of cow horn, a natural and biodegradable material, for its potential use in household utensils. The mechanical properties, such as tensile strength, flexural strength, and impact strength were evaluated. The result showed that cow horn has suitable mechanical properties for utensils.

ISBN: 978-978-8567-02-8

3.2 Processing and Parameter Optimization of Cow Horn

Kumar *et al.,* (2020). Optimization of cow horn processing parameters for household utensils. This study optimize the processing parameters of cow horn using response surface methodology (RSM). The processing parameters investigated were temperature, time, and pressure. The result showed that the optimal processing conditions were 180ºC, 30 minute, and 10MPa. Under these conditions, the cow horn showed improved mechanical properties and reduced warpage.

Issa *et al*., (2023). Evaluatıon of Tensile Strength of Cattle Horn Fiber-Reınforced Recycled Low Density Polyethylene Composite. This work presents cattle horn as a new natural fiber reinforcement in the production of thermoplastic composites. And in particular, it evaluates the effect of different cattle horn fiber volume fraction, cattle horn fiber length sand treatment of the fiber with NaOH on recycled low density polyethylene (RLDPE) with respect to tensile strength property of the composite. Tensile properties test was conducted to evaluate the behavior of a material under different forms of tensile loading in accordance with ASTMD 638. Experimental results of tensile property for the nine samples obtained from L9 orthogonal array were processed by Minitab for Taguchi analysis, models and optimization.

3.3 Forging Processes, Die Design, and Simulation

Shimodh, and Swathy, (2024) Analysis of failure of forging dies. This study quickly summarizes the contributing factors, causes, and characteristics of hot forging die failures. The failure of a hot forging die is complicated by a variety of influencing factors, including die material, die design, die production, and forging processes. Numerical techniques and process simulations can be used to analyze the effects of the hot forging on the forging die properties and the forging process itself, as demonstrated in this project. The 3D model of the die was generated by using SOLID WORKS and was subjected to transient structure analysis in ANSYS software to identify the change in nature of the die due to the applied load. The basic failure mechanism actively participating during the hot forging process was analyzed using the simulation methods.

Tanishq *et al.,* (2022). A Review on closed die forging. This research examines the impact of temperature and grain refinement on a small copper gear with 12 teeth, closed-die forging, and a 0.4 mm shaft module. The CAD/CAM system for the closed-die forging process has been developed.

Kishan, and Shelke, (2021) Review on process parameter optimization for forging process. The process in the manufacturing world which is conducted above the recrystallization temperature are called as hot working process while the process which is conducted below the recrystallization temperature of the work piece is called cold working process.in the above categorization, the casting and forging process is considered as the hot working process while other processes were kept under cold working process category. In this review paper there are numerous parameter that affect the performance characteristics of the forging process.

3.4 Sustainability and Manufacturing Systems

Idowu *et al.,* (2019). Potential of Cow Horn for Carbonitriding Treatment of Steel. The potential of carbonitriding treatment of steel with cow horn was investigated in line with abattoir waste to wealth approach of waste management. The objectives of the study included processing of cow horn into different morphologies namely: powder and flakes for carbonnitriding heat treatment, and, chemical analyses of cow horn with Energy Dispersive Spectroscopy (EDS) and X-ray Diffraction (XRD) techniques to determine the chemical composition and phases of cow horn respectively. The heat treatment was carried out at 850 and 450 °C for carburizing and nitriding dominated processes respectively.

Micheal *et al.,* (2018) Production improvement with flow shop scheduling heuristics in Household utensils manufacturing company. In this paper, the job sequence of a flat cooking pan production line was considered. The problem had 7-jobs and 3-machines. Flow shop scheduling heuristics were used to improve the production of the flat cooking pan production line. The case company had no systematically determined production sequences for flat cooking pan, and achieved 25.85% of the production plan in 2013.

Shalok, (2017). Advancement in Forging Process: A Review In this review paper, various Processes are discussed which bring the revolution in the field of forging technology

4.0 RESULT OF THE REVIEW

The literature review reveals several critical gaps, including the lack of standardized forging approaches for natural horn materials, limited documentation on die design and tooling, insufficient application of numerical simulation tools, minimal sustainability and life-cycle assessments, and few comparative studies between cow horn utensils and conventional metal or plastic alternatives.

5.0 DISCUSSION

The reviewed studies demonstrate that cow horn exhibits thermo-plastic behavior suitable for forging-like forming processes. However, the absence of unified processing guidelines and optimized tooling limits industrial adoption. Integrating traditional craftsmanship with modern CAD/CAE tools and sustainable manufacturing principles presents significant opportunities for advancing cow horn utensil production.

6.0 CONCLUSION

This review establishes cow horn as a promising sustainable biomaterial for household utensil manufacturing through forging-based processes. While substantial research exists on horn mechanics and composite applications, limited attention has been given

ISBN: 978-978-8567-02-8

to developing forging process systems tailored to keratin-based materials. Addressing gaps in parameter standardization, die design, simulation, and sustainability analysis will support eco-friendly manufacturing and waste valorization.

7.0 RECOMMENDATIONS

Future research should focus on developing standardized forging parameters through experimental validation, applying numerical simulation tools to model horn deformation, conducting sustainability and life-cycle assessments, establishing training programs for artisans, and performing comparative performance evaluations between cow horn and conventional utensil materials.

REFERENCES

Abdulrahim, M. Y., Yawas, D. S., Mohammed, R. A., and Afolayan, M. O., (2021). Hybridization of Polyester/Banana stem Fiber and Cow horn particulate composite for possible production of a military helmet. *International journal of sustainable engineering*. VOL. 14, NO. 5, 1170–1180, https://doi.org/10.1080/19397038.2021.1892233.

Bing, W. L, Hong, P. Z, and Xi-Qiao, F., (2011). Static and dynamic mechanical properties of cattle horns. *Journal Materials Science and Engineering C.* www.elsevier.com /locate/msec. doi:10.1016/j.msec.2010.08.016.

Issa1, A. K., Salihi, A., Ali, A.B., and Bello, K.A., (2023). Evaluatıon of Tensile Strength of Cattle Horn Fiber-Reınforced Recycled Low Density Polyethylene Composite. *Nigerian Journal of Engineering.* Vol. 30, and No. 1, April 2023, ISSN (print): 0794 – 4756, ISSN (online):2705-3954.

Kumar, P., Singh, R.K., and Sharma, A.K., (2019). Mechanical Properties of Cow Horn for Household utensils. *Journal of Materials Science and Technology.* Volume 35, Issue, 2 ISSN: 1005-0302, pp. 249-256, DOI: 10.1016/j.jmst.2019.02.003.

Kumar, P., Singh, R.K., and Sharma, A.K., (2020). Optimization of Process Parameters for Household Utensils. *Journal of Materials Science and Technology*. Volume 36, Issue 2, ISSN: 1005-0302, pp: 428-436, DOI: 10.1016/j.jmst.2020.02.023.

Li, B.W., Zhao, H.P., Feng, X.Q., Guo, W.W., and Shan, S.C., (2010). Experimental study on the mechanical properties of the horn sheaths from cattle. *The Journal of Experimental Biology*. 479-486 Published by The Company of Biologists Ltd doi:10.1242/jeb.035428. Pp.479-486.

Micheal, G.W., Eshetie, B., and Kassu, J., (2018). Production improvement with flow shop scheduling heuristics in Household utensils manufacturing company. *Cognate engineering*, https://doi.org/10.1080/23311916.2018.1430007.

Shalok, B., (2017). Advancement in Forging Process: A Review. *International Journal of Science and Research.* Volume 6 Issue 12, DOI: 10.21275/ART20178736, www.ijsr.net,pp.465-468.

Shimodh, C. S., and Swathy, S. P., (2024). Analysis of failure of forging dies. *International Journal of Novel Research and Development (www.ijnrd.org).* Volume 9, Issue 2, ISSN: 2456-4184.

Tanishq, J., Vikas, I., and Arati, K., (2022). A Review on closed die forging. *International Journal of Advances in Engineering and Management (IJAEM).* Volume 4, Issue 7 July 2022, pp: 601-605 www.ijaem.net ISSN: 2395-5252. DOI: 10.35629/5252-0407601605.

Idowu, I.A, Titilayo, A.M, Adulkareem, S., Yahaya, T., Owolabi, I.A., Lawrence, B.B., Adeunle, J.A., (2019). Potential of cow horn for carbonitriding treatement of steel. *Waste and biomass valorization*. ISSN1877-2641, https://researchgate.net/publication/322986186, DOI: 10.1007/s12649-018-0222-0.

Kishan, K., and Shelke, R.D., (2021). Review on process parameter optimization for forging process. *International Research Journal of Modernization in Engineering Technology and Science, www.irjmets.com.* Volume: Issue: 08 Impact Factor- 5.354.

ISBN: 978-978-8567-02-8

5TH Faculty of Engineering Conference on Engineering Innovation and Economic Policies: Driving Sustainable Industrial Growth in Nigeria

Faculty of Engineering, Bayero University, Kano.

011-Design and Simulation of an ANFIS Controller for Chicken Defeathering Machine

Sabur A. Alim[1*], Iliya Y. Ritkagnga[1], Nasir Ismail[1], Muhammed N. Mahmood[1], Kehinde R. Ekundayo[2], and Ahmed O. Oyefolahan[3]

1Mechanical Engineering Department, Ahmadu Bello University, Zaria
2Mechatronics Engineering Department, Federal University, Dutsin-Ma, Dutsin-Ma
3Mechanical Engineering Department, Elizade University, Ilara-Mokin.

**Corresponding author: moaj1st@yahoo.com*

Abstract: Manual defeathering of poultry animals is labor-intensive, time-consuming, and poses hygiene risks. While mechanized solutions exist, their optimization for small-scale use remains a challenge. This study presents the design and simulation of an intelligent controller for a chicken defeathering machine using an Adaptive Neuro-Fuzzy Inference System (ANFIS). Two controller models were developed. In Model 1, chicken weight and scalding temperature were used as inputs to predict the drum rotating speed, while Model 2 used the same inputs to predict the plucking time. The models were trained and tested in MATLAB. Model 1 demonstrated excellent performance with a high coefficient of determination (R^2) of 0.8901 during testing, indicating a robust and reliable prediction of the rotating speed. Conversely, Model 2 showed moderate to poor predictive ability for plucking time (testing $R^2 = 0.4881$). The results conclusively indicate that the ANFIS-based controller for regulating drum speed based on chicken weight and scalding temperature is highly effective and recommended for the development of an intelligent, automated defeathering system, ensuring efficiency and minimizing carcass damage.

1. INTRODUCTION

Manual de-feathering/ plucking of poultry birds' feathers has been an age long practice which is time consuming and labor intensive for small scale poultry slaughter houses. In most part of the world, manual de-feathering operation is done traditionally by the use of hand after the slaughtered bird has been soaked in hot water (Ogunnowo et al, 2024). It could also lead to injury (Awotunde et al., 2018). The likelihood and severity of human exposure to the health hazard and occupational risk as a result of high manual operation are significant in scalding and de-feathering operations (Waghamare et al., 2020).

This justifies the need for appropriate mechanization of the poultry defeathering operations to promote economic activities, quality, quantity, safety, and ergonomics (Bello et al., 2022). Poultry processing has been mechanized extensively over the past decades with manufacturers having to consider three priorities namely; must perform according to specifications, be safe and be hygienic during operation (Ogunnowo et al, 2024). Various machines have also been developed for de-feathering process which can handle either large or few number of chickens (Herrick Kimball, 2003). However, their demand and acceptance are different from one country to another (Barbut, 2002; Ugwu et al., 2015).

There are a lot of advantages these machines present such as human labour is greatly reduced; problem of boredom through manual removal of feathers is eliminated; avoiding scalding of the hand by hot water used in plucking is eliminated; uniformity of de-feathering is guaranteed (Adefuye et al., 2021; Ogunnowo et al, 2024).

The growth in the poultry farming mechanization has helped in meeting the daily demand of poultry products globally. The demand will keep increasing because of the health benefit of poultry product in terms of low fat and calorie content, popularity of chicken meat among non-vegetarians all over the world, and to satisfy the world's dietary protein needs (Adefuye et al., 2021; Ogunnowo et al, 2024).

Therefore, there is a need to innovatively study the feather plucking machine process and devise a scientific method to produce a low-cost feather plucking machine. The effort to fabricate a low-cost poultry bird feathering plucking machine for a small-scale farm and domestic use remains a daunting challenge (Omoniyi et al., 2019; Bello et al., 2022).

The objective of this study is to replace the manual and mechanical process of feather plucking with an intelligent based system through an Adaptive Neuro Fuzzy Inferencing System (ANFIS) controller. According to Adeyinka and Olawale (2015), weight, temperature of the water, the speed of the motor and the duration of soaking of the bird in water were all important variables to be addressed to enhance the efficiency of the machine and the quality of dressed birds.

ISBN: 978-978-8567-02-8

2. METHODOLOGY

After slaughtering the chickens, there is the need to remove the feathers from the skin so as to cut the animal into smaller pieces. This would enable the separation of the inedible parts from the edible parts. The traditional method of manually plucking the feathers is commonly practiced in Nigeria for domestic and commercial uses. Various researchers have developed different types plucking machines which vary in dimensions and orientation. For both manual and machine plucking, the chicken must have undergone scalding (Alim et al., 2023). Plucking simply means the process of removing feathers from scalded fowls manually. So, the de-feathering machine is basically a means of plucking the feathers faster and better (Adefuye et al., 2021).

In the work of Alim et al., 2023, the authors developed a fuzzy logic controller (FLC) to control the use of a chicken defeathering machine. This current study is a step further using ANFIS to develop another controller. While fuzzy logic is a multi-input multi-output (MIMO) system, ANFIS on the other hand is a two-input single-output (TISO) system. Alim et al (2023) used four parameter of a defeathering machine to design the controller. Two of these were used as input (Scalding Temperature & Weight of the Chicken), while the other two were used as output (Drum Rotating Speed & Plucking Time). In this work, two scenarios were tried, Scalding Temperature, Weight of the Chicken as input while Drum Rotating Speed was used as output and the other is Scalding Temperature, Weight of the Chicken as input while Plucking Time is used as output. The two controller schemes tried can be seen in figures 1 and 2.



Figure 1: ANFIS Model 1



Figure 2: ANFIS Model 2

2.1 Input and output parameters to the controller schemes

According to Adeyinka and Olawale (2015), data showed that at an operating speed of 300 rpm, birds with average weight of 1.5 kg soaked in water for about 85 degrees Celsius for 6 minutes were de feathered in 20 seconds. Based on this data and residual knowledge of the authors, a dataset was created. The database has chicken weight ranging from 1.5kg to 4.5kg per bird at an increment of 0.5kg. The temperature was varied from 50 – 100 oC at an increment of 5 oC. The dataset has 120 data. From the previous work by Alim et al (2023), the fuzzy logic controller developed was converted to *ANFIS* parameters. The ANFIS system designer generated is as seen in figure 3.

1) Weight of the Chicken: This is one of the input to the ANFIS controller being designed. The weight of the chicken has relationship with the body size parameters such as neck length, back length, wing length, kneel length, thigh length, breast width and shank length. The weight usually requested for by eateries is between 1.5-2.0kg after plucking. This informed the selection of 1.2 – 4.7kg as the weight of the chicken. Some people usually prefer large bird having a weight of around 4kg (Alim et al., 2023).

2) Scalding Temperature: The scalding temperature is the second input which plays the major role in the efficient plucking of chicken feathers whether manually or by a machine. The system is designed to have a temperature range from 50 – 100ºC, because most of the scalding done at home and by the local butchers in Nigeria who are the main target of this work is between 75 – 90ºC usually at a lower retention time of less than 2 minutes (Adetola et al. 2012; Alim et al., 2023).

3) Drum Rotating Speed: This serves as the output of the first ANFIS controller design. The rotating disc is the only rotating part of the machine, mounted on the motor and has some plucking fingers (rubber studs) on it. Accordingly, the work of Mady and Obia (2018), the rotating speed ranging from 240-560rpm (Alim et al., 2023).

4) Plucking Time: This is the output parameter for the second controller design. The plucking time is to ensure that the outer skin of the carcass does not peel off and that time is conserved as time is money in this regard. The more chickens that is processed translates into finance for the operator of the machine. 7 – 90 secs were selected as the plucking time (Alim et al., 2023).

2.2 System Description and Working Principle

Matlab ANFIS toolbox was used to design the controller as seen in figure 3. The parameters used to design the fuzzy logic controller in Alim et al. (2023) were extracted to develop the ANFIS controller. Figure 3 shows the ANFIS designer. The data was partitioned into two, two thirds for training while one third was used for testing. Two distinct controller designs were developed in this work. Since ANFIS can only take one output at a

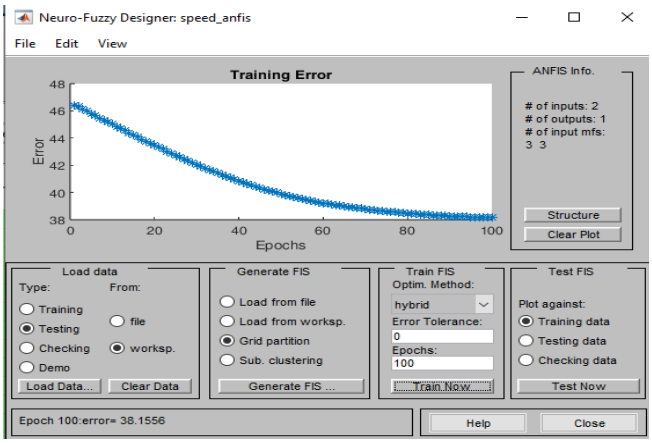


Figure 3: ANFIS system designer

ISBN: 978-978-8567-02-8

time, the two output that were used in the fuzzy logic controller design were used for each of the design. Figures 1 and 2 shows the design concepts. The reason for considering the two designs is to ensure that the best ANFIS design would be selected for use in the production of the physical system. The system would work by determining the input parameters, the ANFIS controller would calculate the output and the system would give a chicken carcass whose feathers have been plucked.

3. RESULTS AND DISCUSSION

3.1 Drum Rotating Speed



Figure 4: Training Accuracy plot of the Drum Rotating Speed vs Scalding Temperature & Weight of the Chicken

The Coefficient of Determination (R^2) measures the proportion of the variance in the output variable (Drum Rotating Speed) that is predictable from the input variables (Chicken Weight and Scalding Temperature). With R^2 for the training accuracy as 0.8039, it shows how much of the change in the drum rotating speed can be explained by the changes in chicken weight and scalding temperature, as captured by the ANFIS model 1 (figure 4). In the context of the MATLAB ANFIS model, R^2 is not calculated between the raw inputs and the output. Instead, it is calculated between the model's predicted output and the actual target output.

The value of R^2 always lies between 0 and 1. Its interpretation is crucial for evaluating the controller's design as seen in the training graph. It indicates that the ANFIS model explains almost all (80.39%) of the variability in the drum rotating speed. The fuzzy logic rules generated in MATLAB have successfully learned the complex relationship from the data. A high training R^2 value validates the learning capability of the ANFIS structure. It confirms that the model can be trained effectively, forming a reliable knowledge base for making decisions. It also shows that the controller understands the process it was trained on.

The value of R^2 (0.8901) was observed on the testing accuracy graph in figure 5. It means that for new, unseen data, the model still explains a very large portion (89.01%) of the variation in the required drum rotating speed. This is the true test of the controller's practical utility and robustness. A high testing R^2 proves that the model did not just memorize the training data but has genuinely learned the underlying principles of the defeathering process. It gives the assurance that in a real processing plant, the controller will reliably and correctly adjust the drum speed for a wide variety of scalded chicken parameters it has never encountered before.

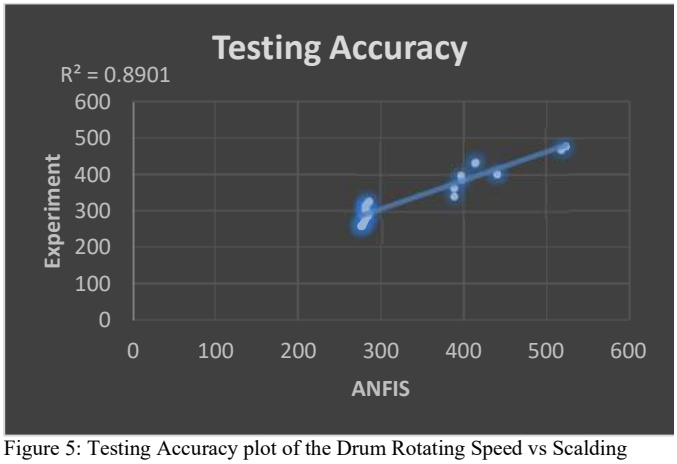


Figure 5: Testing Accuracy plot of the Drum Rotating Speed vs Scalding Temperature & Weight of the Chicken

3.2 Plucking Time



Figure 6: Training Accuracy plot of the Plucking Time vs Scalding Temperature & Weight of the Chicken

The R^2 shows the proportion of the variance in the Plucking Time that is predictable from the Chicken Weight and Scalding Temperature. Since R^2 for the training is 0.6611, showing how much of the change in the plucking time can be predicted by the changes in

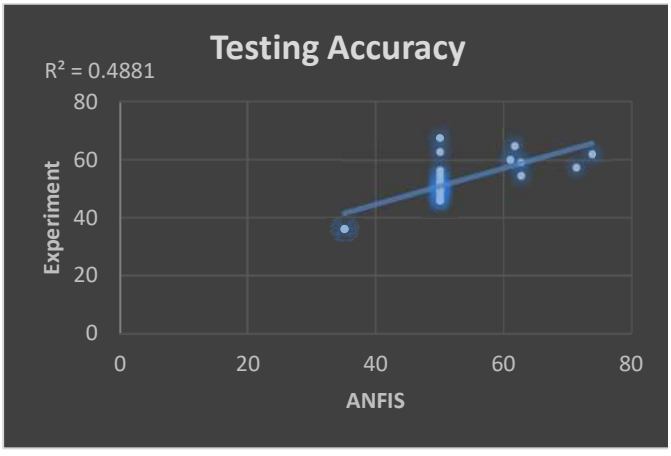


Figure 7: Testing Accuracy plot of the Plucking Time vs Scalding Temperature & Weight of the Chicken

ISBN: 978-978-8567-02-8

chicken weight and scalding temperature (figure 6), as captured by the ANFIS model 2. The R^2 is calculated between the model's predicted output and the actual target output. The value of R^2 indicates that the ANFIS model has a 66.11% variability in the Plucking Time. The fuzzy logic rules generated in MATLAB averagely learned the complex relationship from the data.

The R^2 value of 0.4881 was observed on the Testing accuracy graph in figure 7. It means that for new, unseen data, the model still explains a moderate portion (48.81%) of the variation in the required plucking time. This is the true test of the controller's practical utility and robustness. This shows that the model did not respond well to the testing data and as such has not genuinely learned the underlying principles of the defeathering process.

The controller design scheme 1 had a very good prediction of the output, Speed of the Rotating Disc, from the input both at the training and testing, while the controller design scheme 2 had a moderate prediction of the output, Plucking Time, at the training and testing. By this, the controller design scheme 1 is a better choice if ANFIS is to be used for designing a chicken feather plucking machine using the set of input and output parameter used in this study.

4. CONCLUSION

The R^2 value for the ANFIS Model 1 with training and testing accuracies of 0.8039 and 0.8901, showing that the controller can effectively predict the speed of the rotating disc from the Scalding Temperature & Weight of the Chicken. The R^2 value for the ANFIS Model 2 with training and testing accuracies of 0.6611 and 0.4881, showing that the controller cannot effectively predict the Plucking Time from the Scalding Temperature & Weight of the Chicken.

In the design of the chicken defeathering machine controller, the R^2 value is not just a statistic; it is a direct measure of intelligence and reliability. It quantifies success as a high R^2 value provides concrete, numerical evidence that the developed intelligent controller works as intended. It builds confidence in the potential fabricator and users that the automated system can be trusted to perform consistently without human intervention, thorough feather removal and minimizing carcass damage. The R^2 value for the ANFIS Model 1 with speed of the rotating disc as input and Scalding Temperature & Weight of the Chicken as output was better than that of ANFIS Model 2 with plucking time as input and Scalding Temperature & Weight of the Chicken as output. For the purpose of implementation, there would be the need to pre-process, fine tune and modify the data. This would be necessary as coefficient of correlation results shows that there can be improvements in the performance of the proposed control schemes.

REFERENCES

Adefuye O.A., Adedeji K.A., Fadipe L.O., Arowoka Z.M., Mohammed O.A. (2021). Design, fabrication and performance evaluation of chicken de-feathering machine. *International Journal of Research and Review*, 8(12), 703-711. DOI: *https://doi.org/10.52403/ijrr.20211285.*

Adetola S.O., Onawumi A.S. and Lucas E.B. (2012). Investigation into Mechanized De-feathering process and optimal scalding temperatures of exotic and local birds in Southern Nigeria. Transnational Journal of Science and Technology 2(3): 87-96.

Adeyinka A.A. and Olawale J.O. (2015). Development and performance Evaluation of a chicken Defeathering machine for small scale farmers. Journal of advanced Agricultural Technologies 2(1): 71-74.

Alim S. A., Abdullateef I. A. and Shobowale K. O. (2023). Development of a fuzzy logic controller (flc) for a chicken feather plucking machine. Arid Zone Journal of Engineering, Technology & Environment (AZOJETE), 19(3), pp. 493-504.

Awotunde, O. W., K. P. Adeyeye, A. Eyitayo, and S. O. Fatukasi. 2018. Development of a defeathering machine from locally sourced materials. *International Journal of Scientific and Engineering Research*, 9(5): 1143-1149.

Barbut, S. (2002). Primary processing of poultry (Boca Raton London New York Washington, D.C: CRC Press).

Bello K.A., Tawose O.M., Adama A. and Bolaji B.O. (2022): Factor Analysis of Poultry Birds De-Feathering Machines, FUOYE Journal of Engineering and Technology (FUOYEJET), 7(3), 364-369.

Kimball, H. (2003); Anyone can Build a Tub-Style Mechanical Chicken Plucker. Complete instructions for the Kimball Whizbang, vol 1.

Mady, M.A.A., and Obaia, A.R. (2018). Manufacture and performance valuation of poultry plucker suitable for small farms, Misr Journal Agricultural Engineering, 35 (2): 407 – 422.

Ogunnowo, O. A., Adisa, A. F., Dairo, O. U., Adepoju, V. O., Ismaila, S. O., & Babalola, A. A. (2024). Design and fabrication of a de-feathering machine with scalding tank**.** AgricEngInt: CIGR Journal Open access at http://www.cigrjournal.org Vol. 26, No.3 186-196.

Omoniyi Ezekiel, B., Oyekola, P., Ovaha, O., Mohamed, A., & Lambrache, N. (2019). Bird feather removal machine: Design and development. *International Journal of Recent Technology and Engineering (IJRTE)*, *8*(3).

Ugwu K. C., Agu S. O. and Ogbuagu N. J. (2015). Optimization and performance evaluation of chicken feather plucking machine. International Journal of Scientific & Engineering Research, 6(7), pp.102-108.

Waghamare, R., Paturkar, A., Vaidya, V., Zende, R., Chavak, M., & Moregaonkar, S. (2020). Risk of Salmonella in various poultry farming and processing operations around Mumbai, India. *Int J Curr Microbiol Appl Sci*, *9*, 1024-1034.

ISBN: 978-978-8567-02-8

012-Numerical Study of Wall Temperature Enhancement and Uniformity in a Methane–Air Micro Cylindrical Combustor

A. Ahmad*[1,2], Y. S. Sanusi[2], G. Y. Pam[2], A. Hussein[3].

[1]*Department of Mechanical Engineering Technology, Federal Polytechnic Kaura Namoda, Zamfara – Nigeria*

[2]*Department of Mechanical Engineering, Ahmadu Bello University, Zaria, Kaduna – Nigeria*

[3]*Department of Mechanical Engineering, School of Technology, Kano State Polytechnic, Kano – Nigeria*

**aahmadkaura@gmail.com*

Abstract: The increasing demand for compact, high energy density power sources has stimulated significant interest in combustion-based micro-power generation as an alternative to conventional batteries. Micro-combustors, particularly those integrated into micro thermo-photovoltaic (MTPV) systems, are critical components because their wall temperature level and uniformity strongly influence radiative heat transfer and overall energy conversion efficiency. However, micro-combustors suffer from inherent challenges, including high heat losses, flame instability, low wall temperatures, and non-uniform thermal distributions caused by their large surface-area-to-volume ratios. This study presents a detailed numerical investigation of temperature enhancement and uniformity in a micro-cylindrical combustor fueled by a premixed methane–air. A comprehensive computational fluid dynamics (CFD) model was developed in ANSYS Fluent, incorporating conservation equations for mass, momentum, species, and energy, along with radiation and conjugate heat transfer. Methane oxidation was simulated using a modified 2sCM2 chemical reaction mechanism to accurately represent micro-scale combustion behavior. The effects of key geometric and operational parameters including combustor aspect ratio, equivalence ratio, inlet channel height, and combustor diameter were systematically examined. Model validation against published experimental data demonstrated good agreement, with prediction errors within acceptable limits. The results show that reducing the combustor aspect ratio and diameter significantly increases outer-wall temperatures and improves temperature uniformity by enhancing heat transfer and fuel–air mixing. Higher equivalence ratios raise wall temperature levels but shift the flame location downstream. Overall, the findings provide valuable insights into the thermal behavior of methane–air micro-combustors and offer practical design guidelines for improving wall-temperature enhancement and uniformity. These results support the development of efficient micro-scale combustion systems for portable power generation, MEMS applications, and reduced dependence on conventional batteries and grid electricity.

Keywords: Aspect ratio, Methane-air, Micro-combustor, Energy density, Equivalence ratio.

1. INTRODUCTION

1.1 Background

The demand for portable power generation systems has increased significantly over the past decade due to their growing application across sectors such as chemical processing, propulsion, communication devices, and laboratory analytics (Holechek et al., 2022; Ahmed et al., 2020; Shini et al., 2024). Traditionally, lithium-ion batteries have served as the primary power source, partly due to earlier limitations in fabricating devices at the millimeter scale (Riaz et al., 2021). Advances in rapid prototyping and batch manufacturing have overcome these constraints, enabling the development of alternative micro-power generation technologies suitable for low-cost mass production (Le et al., 2023).

Concerns related to system weight, operational lifetime, and cost associated with batteries have further motivated research into micro-scale energy systems (Edwin et al., 2023; Pourrahmani et al., 2023). Among these alternatives, micro-combustion has emerged as a promising technique for micro-power generation (Muhammad et al., 2024). Micro-combustors convert the chemical energy of fuels into thermal energy, which can be subsequently transformed into electrical energy using suitable conversion components (Hui et al., 2024). In micro thermo-photovoltaic (MTPV) systems, the micro-combustor is a critical component that strongly influences overall energy conversion efficiency (Jiaqiang et al., 2021).

ISBN: 978-978-8567-02-8

1.2 Statement of Problem

Despite their potential, micro-combustors in Micro-thermo-photo-voltaic (MTPV) systems face significant challenges. Chief among these are low external wall temperatures and non-uniform wall-temperature distributions, which adversely affect radiative heat transfer and system efficiency. Various structural enhancement strategies such as multi-channel designs, ribs, pin-fin arrays, porous media, and separating plates have been proposed to address these thermal limitations. Additionally, maintaining stable combustion and high combustion efficiency remains difficult due to the high surface-area-to-volume ratio of micro-combustors, which leads to substantial heat losses and flame instability. Although numerous stabilization and enhancement techniques have been reported in literatures, further investigation is required to achieve improved wall-temperature enhancement and uniformity.

Accordingly, this study numerically investigates methods to enhance and uniformly distribute wall temperature in a micro-cylindrical combustor fueled by a methane–air mixture.

2. METHODOLOGY

2.1 Flow Modelling

Computational fluid dynamics modelling of combustion involves selecting and implementing a suitable model to holistically represent the complex chemical and physical phenomena associated with the combustion process. The mathematical models describing the combustion process are based on the conservation equations of mass, momentum, species, and energy and equations for turbulence and radiation models (Vinuesa & Brunton, 2021; Alert et al., 2022).

2.2 Continuity and Momentum Equation

The simplified equation, governing the conservation of mass, momentum, in addition to the equations for species transport, are outlined as (Aghakhani et al., 2023; Choi et al., 2022):

$$= \frac{\partial}{\partial X_j}\left(\Gamma_{\emptyset'}\frac{\partial \emptyset}{\partial x_j}\right) + \bar{\rho} S_{\emptyset} \quad (1)$$

Continuity equation:

$$\frac{\partial}{\partial x_j}\left(\rho u_j\right) = 0 \quad (2)$$

Momentum equation:

$$\frac{\partial\left(\rho u_i u_j\right)}{\partial x_j} = -\frac{\partial P}{\partial x_i} + \frac{\partial\left(t_{ij} + \tau_{ij}\right)}{\partial x_j} \quad (3)$$

Such that t_{ij} stands for the viscous stress tensor and is agreed by (Pashchenko, 2020):

$$t_{ij} = \mu\left[\left(\frac{\partial u_i}{\partial x_j} + \frac{\partial u_j}{\partial x_i}\right) - \frac{2}{3}\frac{\partial u_k}{\partial x_k}\delta_{ij}\right] \quad (4)$$

$\delta_{ij} = 1\ when\ i = j, \delta_{ij} = 0\ when\ i \neq j$

2.3 Energy Equation

The energy equation was computationally solved to encompass various heat transfer mechanisms, including conduction, species diffusion, viscous dissipation, and energy source terms. This is given by Manigandan et al., (2024); Wan et al., (2012).

$$\frac{\partial \rho u_i h}{\partial x_i} = \frac{\partial}{\partial x_i}\left(k_f \frac{\partial T}{\partial x_i}\right) + \sum_j \frac{\partial}{\partial x_i}\left(h_j \rho D_{j,m}\frac{\partial Y_j}{\partial x_i}\right) + S_{\emptyset} \quad (5)$$

$S_{\emptyset}$ stands for the energy source term, including the reaction source term and radiation heat exchange.
The heat loss from the combustor wall was modelled using the convective-radiative equation given by Garcia *et al*., (2020):

$$\dot{q} = h(T_w - T_a) + \varepsilon_w \sigma (T_w^4 - T_a^4) \quad (6)$$

Heat conduction has been reported to have an effect on the combustion characteristics for given wall properties (Chen *et al.,* 2023; Jing *et al.,* 2022; Ni *et al.,* 2021b) as such, the heat transfer within the combustor wall thickness is computed from:

$$\frac{\partial}{\partial x_i}\left(k_q \frac{\partial T}{\partial x_i}\right) = 0 \quad (7)$$

h is the effective heat transfer coefficient; T_w is the wall's temperature; T_a is the ambient temperature.

2.4 Description of Geometrical Model

This research work is a scaled-down combustion chamber examined in the experimental illustration by Garréton & Simonin, (1994) and described in Silva et al., (2006). As shown in Figure 1, the total length of the micro-cylindrical combustor is L_o, and the length of its front, as well as back part, is L1, the inner diameter of the micro-cylindrical combustor at the inlet is D_1, the inner diameter of the micro-cylindrical combustor at the outlet is D_2, the wall thickness is D_4, while the diameter and length of the micro-cylindrical combustor chamber are D_3 & L_2 respectively.

2.5 Boundary Conditions/Solution Procedure

The solution procedure began with creating the micro combustor geometry in GAMBIT by defining all points, edges, and faces and assembling them into the complete shape, followed by meshing the edges, faces, and full geometry, after which boundary conditions were assigned. A premixed CH_4/air mixture was used as fuel due to its stability as the simplest paraffin hydrocarbon (Serwin, 2022), with uniform inlet velocity and concentration at 300 K (Yuan et al., 2021; Huang et al., 2024) and a pressure-outlet condition of 1.013×10^5 Pa at the exit (Wu et al., 2024); surface-to-surface radiation was modeled using the discrete ordinates (DO) method (Abid et al., 2024), while inner walls employed conjugate heat transfer with no-slip and no species flux conditions, adiabatic sidewalls, and outer walls dissipating heat via natural convection and radiation based on established

ISBN: 978-978-8567-02-8

methodologies (Giwa et al., 2021; Bagheri et al., 2014; Yang et al., 2017; Zuo et al., 2016).

2.7 Model Validation

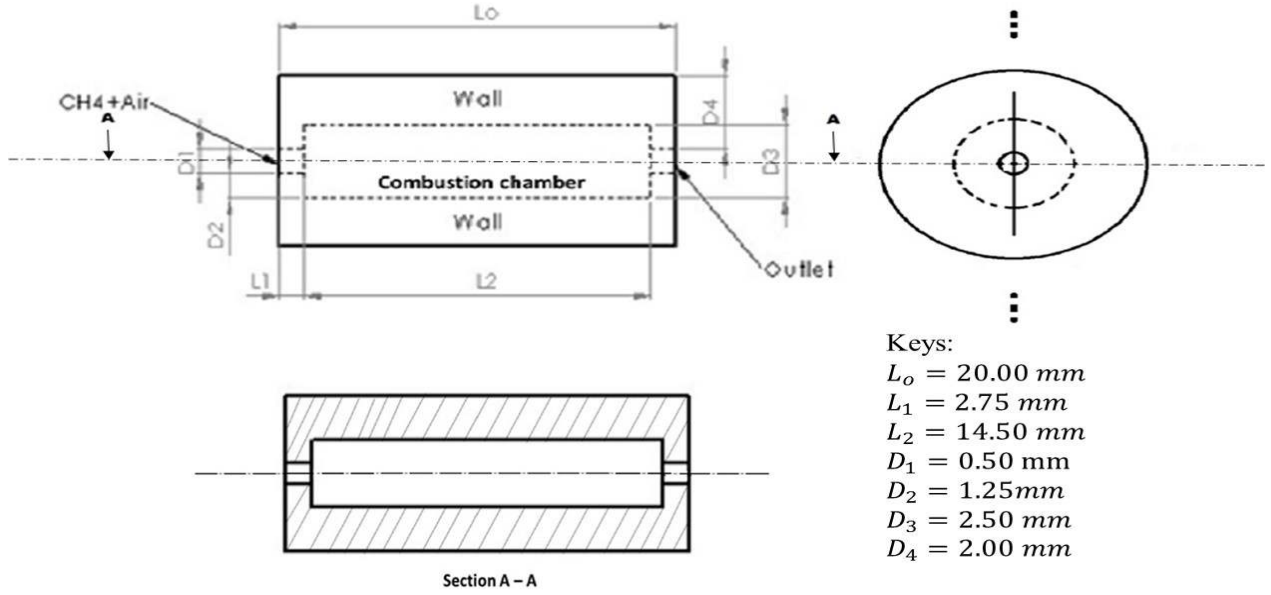


Figure 1: Complete Geometry of the Micro-cylindrical combustor

The outer wall heat transfer combined convection and radiation using specified parameters (h = 20 W/m²K, Tα = 300 K, quartz with k = 1.2 W/mK and emissivity 0.92) (Peng et al., 2018; Fan et al., 2013), while numerical discretization employed second-order schemes with the SIMPLE algorithm for pressure-velocity coupling, ensuring convergence with residuals below 10^{-4} for flow equations and 10^{-6} for energy, radiation, species, and NO equations, and inlet velocity was set according to combustor operational parameters including fuel energy, composition, and equivalence ratio.

2.6 Chemical Reaction Mechanism

In this study, the modified 2sCM2 reaction mechanism proposed by Esmail et al. (2016) was employed, with the main modification involving the optimization of the oxygen reaction order in methane-air combustion. According to Esmail et al. (2016), this adjustment is based on the premise that reducing the O_2 reaction order with respect to CH_4 and CO enhances the modeled reactivity of these species.

Accordingly, the reaction mechanisms used to simulate ne oxidation, along with their respective Arrhenius constants, are summarized in the table below:

Table 1: Chemical reaction mechanisms for methane–air (Esmail et al. 2016)

	No.	Reaction	A	b	E_a	Reaction order	Equation no.
Modified 2sCM2 (Esmail et al., 2016)	1.	$CH_4 + 1.5O_2 \rightarrow CO + 2H_2O$	2.00E+15	0	3.45E+04	$[CH_4]^{0.9}[O_2]^{0.5}$	(8a)
	2.	$CO + 0.5O_2 \leftrightarrow CO_2$	1.00E+09	0	1.20E+04	$[CO][O_2]^{0.25}[CO_2]$	(8b)

Key: A=pre–exponential factor ($m^3[kmol]^{-1}[s]^{-1}$); b=temperature exponent; E_a =activation energy ($kJ[kmol]^{-1}[K]^{-1}$)

Figure 2 presents a comparison between experimental measurements and numerical simulation results for exhaust gas temperature in a micro-combustor across varying inlet velocities. The numerical model demonstrates good agreement with experimental data, with the maximum observed deviation being 7.46% at an inlet velocity of 11.17 m/s. At higher velocities, the relative error decreases to 6.98% at 17.2 m/s and 6.11% at 19.35 m/s, indicating the reliability of the numerical approach for simulating combustion processes. The results also show that exhaust gas temperature initially increases with inlet velocity, reaching a peak at moderate velocities before declining at higher velocities. This trend is attributed to enhanced turbulence within the combustor, which promotes combustion efficiency and energy release.

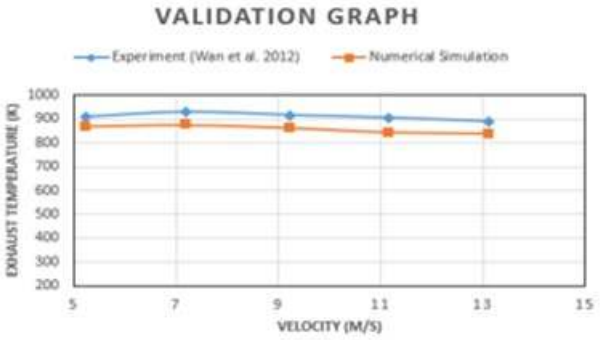


Figure 2: Variation of exhaust gas temperature with inlet velocity for both the numerical model and the experimental data reported by Wan et al.

Figure 3 presents the percentage error between the experimental and numerical exhaust gas temperatures. At lower velocities, the percentage error is minimal, indicating good agreement and high model efficiency.

ISBN: 978-978-8567-02-8

Although the error changes slightly at higher velocities, it remains within an acceptable range. Overall, the low error values confirm that the geometrical model is accurate and suitable for this research, consistent with the findings of Alireza et al. (2021)

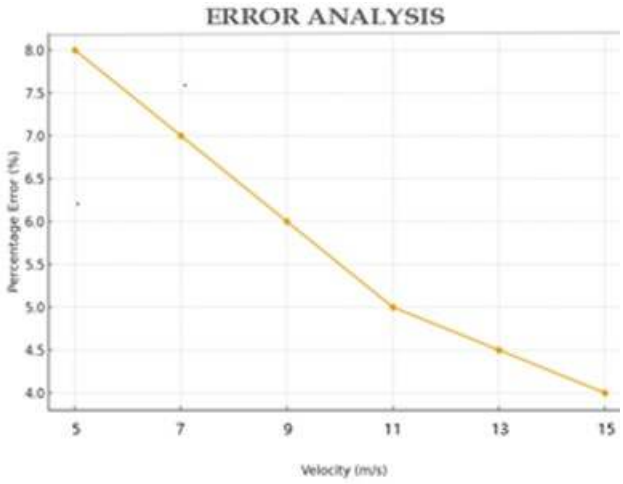


Figure 3: Percentage Error Analysis as a Function of Velocity

3. RESULTS AND DISCUSSION

3.1 Assessment of the Aspect Ratio

This section presents a sensitivity analysis of the micro-combustor's aspect ratio, defined as:

$$A = r/R \tag{9}$$

where r is the inlet radius and R=1.25 mm is the combustion chamber radius. Three aspect ratios were evaluated: 1.00, 0.75, and 0.50. The analysis considers how variations in aspect ratio, channel height, and combustion chamber diameter affect temperature distribution and overall combustor performance.

Results from Figure 4 show that decreasing the aspect ratio leads to higher outer-wall and reaction-zone temperatures. Lower aspect ratios enhance heat transfer, raising upstream temperatures, while higher aspect ratios produce lower downstream temperatures due to greater transverse heat resistance. At larger aspect ratios, outer-wall temperature profiles become more uniform, consistent with findings by Cheng & Wu (2021).

From Figure 5, reducing the inlet channel height while maintaining the same mass flow rate increases power density and shifts the flame upstream. Smaller channel heights also reduce the amount of unreacted mixture at the outlet, indicating that higher channels require longer lengths to achieve complete combustion. These results align with Lachraf & Ameur (2023) and Hoang et al. (2021).

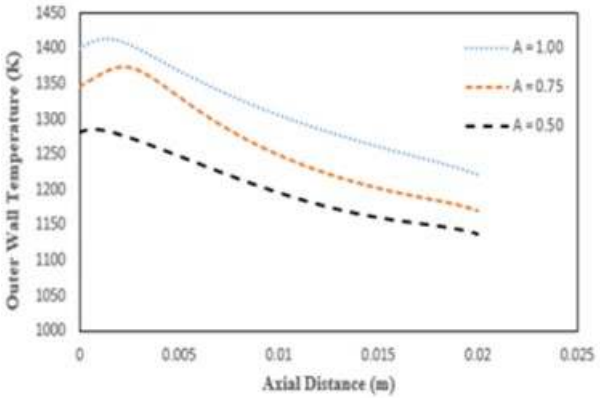


Figure 4: Variation of Outer wall temperature profile of the micro-combustor with aspect ratio at the equivalence ratio of 0.9

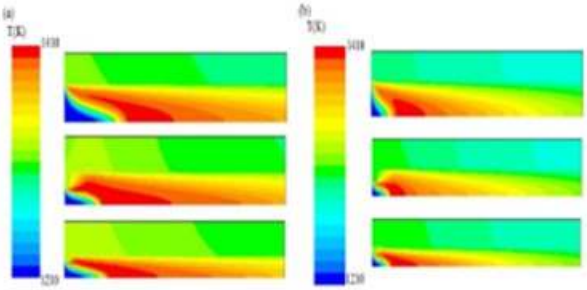


Figure 5: Variation of Temperature contours of the micro-combustor at the equivalence ratio of 1.0, from top to bottom A=1.00, A=0.75 and A=0.50 (a) power density (PD) = 90 W; (b) power density (PD) = 30 W

3.2 Effect of equivalence ratio on the external wall temperature

In Figure 4.3, the impact of the equivalence ratio on the external wall temperature profile is depicted. It is evident from the figure that the temperature level across the entire length of the micro-combustor diminishes as the equivalence ratio is decreased. This phenomenon can primarily be attributed to a reduction in intensive chemical reactions and heat release. Additionally, the figure illustrates that a higher equivalence ratio results in an extended flame length. This can be interpreted as the flame front location moving downstream due to the increased flame velocity resulting from a higher equivalence ratio. This is in agreement with the study of Sadatakhavi et al., (2021) and Liu *et al.,* (2020).

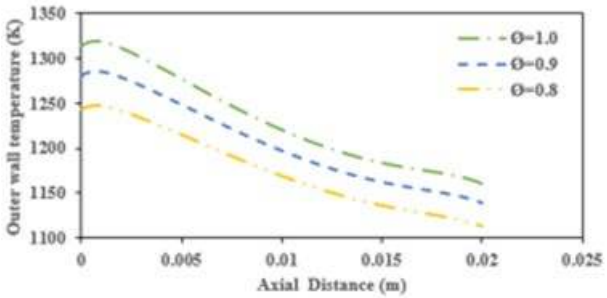


Figure 6: Variation of Outer wall temperature profile with equivalence ratio

ISBN: 978-978-8567-02-8

3.3 Effect of modified configurations on micro combustion

The study examines methane–air combustion in micro combustors with three different diameters (2.500 mm, 1.875 mm, and 1.250 mm), all having a fixed length of 20 mm. Temperature fields and methane mass fractions for these geometries are shown in Figure 7. The axial temperature profiles indicate peak temperatures of 1612.8 K, 1616.2 K, and 1649 K for diameters of 2.500 mm, 1.875 mm, and 1.250 mm, respectively.

Across all combustor sizes, similar combustion behaviour is observed:

1. Ignition originates near the outlet of the suction section.
2. Temperature rises gradually at first, then increases rapidly, with the strongest reaction occurring in the sudden contraction region of the inlet especially for the smallest diameter (1.250 mm).
3. Smaller diameters produce higher peak temperatures, showing that reducing both the inlet and combustion chamber diameter enhances the temperature performance and overall combustion efficiency of the micro combustor. Ni et al., (2021a) related similar trend in their work.

Because heat generation in a micro combustor depends on its volume ($\propto D^3$) while heat loss depends on its surface area ($\propto D^2$), smaller diameters have a higher surface-area-to-volume ratio and therefore lose more heat, reducing combustion temperature. However, larger-diameter combustors suffer from poor CH_4–air mixing, leading to weaker combustion. As a result, reducing the combustor diameter improves mixing and gradually increases the combustion temperature despite the higher heat-loss tendency. Liao et al., (2022) mentioned similar trend in their investigation.

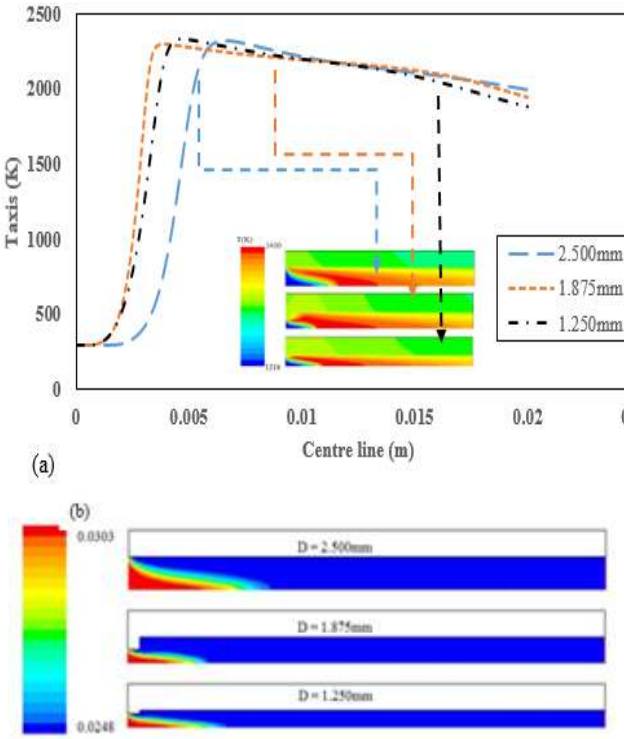


Figure 7: (a) Temperature Distribution and (b) Mass Fraction of CH4 in Combustor with altered sizes; Temperature contours of the micro-combustor at the equivalence ratio of 1.0, from top to bottom A=1.00, A=0.75 and A=0.50 (c) power density (PD) = 90 W; (d) power density (PD) = 30 W

Figure 7(b) shows that the final CH_4 mass fraction decreases from 0.030 to 0.028 to 0.025 as the combustor diameter is reduced from 2.500 mm to 1.875 mm to 1.250 mm. This indicates higher reactivity in smaller combustors. According to residence-time relations, reaction volume scales with D^3, flow rate with D^2, and residence time with D. Thus, reducing combustor size or increasing the methane–air mass flow rate shortens residence time, which can lead to incomplete combustion. This behaviour agrees with the findings reported by Lei et al. (2021) and Jiaqiang et al. (2021).

The table below summarizes numerical simulations of methane–air combustion in the micro-cylindrical combustor, examining how equivalence ratios from 0.5 to 1.0 affect temperature, flame stability, species distribution, and combustion efficiency. The results reveal the thermo-chemical behavior, operational limits, and optimal performance conditions, providing guidance for evaluating and optimizing micro-combustion system design.

TABLE 2: NUMERICAL SIMULATION RESULTS FOR METHANE–AIR COMBUSTION (Φ = 0.5–1.0)

Equivalence Ratio (ϕ)	Peak Flame Temperature (K)	Combustion Efficiency (%)	CO Emissions (ppm)	NO Emissions (ppm)
0.5	1500	72.5	160	2
0.6	1620	78.4	120	4
0.7	1705	85.6	85	8
0.8	1780	89.6	52	12
0.9	1870	94.2	30	18
1.0	1985	97.8	18	28

The numerical results demonstrate that equivalence ratio is a critical control parameter in micro-cylindrical combustors:

Lean combustion (ϕ = 0.5–0.7) suffers from flame instability, lower efficiency, and elevated CO emissions due to dominant wall heat losses.

Moderately lean to near-stoichiometric combustion (ϕ = 0.8–0.9) provides an optimal balance between efficiency, emissions, and thermal safety.

Stoichiometric combustion (ϕ = 1.0) delivers maximum efficiency and temperature but increases NO formation and material thermal loading.

These behaviors align well with established micro-combustion theory, where high surface-to-volume ratios strongly influence heat loss, flame quenching, and emissions formation (Nauman *et al.,* 2024; Resende *et al.,* 2019).

4. CONCLUSION AND RECOMMENDATIONS

4.1 Conclusion

Conclusions

This study developed and validated a numerical model for methane–air combustion in a micro-cylindrical combustor, demonstrating strong agreement with experimental data (Wan et al., 2012) and confirming the model's reliability for simulating micro-scale combustion processes.

ISBN: 978-978-8567-02-8

Key findings highlight that geometric optimization significantly influences thermal performance and combustion efficiency:

• Aspect ratio: Reducing the combustor aspect ratio elevates outer-wall and reaction-zone temperatures by enhancing wall heat transfer, improving thermal uniformity in critical regions.

• Combustor diameter: Smaller diameters increase peak temperatures, enhance CH_4–air mixing, and reduce residual fuel fractions, thereby boosting overall combustion efficiency despite higher surface-area-to-volume heat losses.

• Equivalence ratio: Higher equivalence ratios raise wall temperatures and shift the flame downstream, allowing for controllable tuning of thermal profiles.

Collectively, these results demonstrate that careful control of micro-combustor geometry and operating conditions can maximize wall temperature and uniformity, stabilize combustion, and improve energy conversion efficiency. This has direct implications for MEMS-based micro-power systems, micro-propulsion, and compact energy devices, offering a viable alternative to conventional batteries and grid dependency.

Conference takeaway: Optimizing micro-combustor design through aspect ratio, diameter, and equivalence ratio adjustments provides a practical pathway to high-efficiency, compact power generation at the micro scale, enabling reliable, high-density energy sources for next-generation portable and embedded applications.

4.2 Recommendations

1. Experiments and numerical simulations can be executed under premixed conditions to study the effects of different fuel composition on the combustion stability and emission. This is to achieve low emissions with reduced tendency for flash back.

2. The modified 2sCM2 chemical mechanism presented can be investigated at fundamental level at different conditions to examine the level of its accuracy. The mechanism can also be tested beyond the range of this study.

ACKNOWLEDGMENT

I sincerely acknowledge the Tertiary Education Trust Fund (TETFund) for the sponsorship and financial support of my MSc programme. This support greatly contributed to the successful completion of my studies. I am also deeply grateful to my supervisors, Prof. Y. S. Sanusi and Prof. G. Y. Pam, for their invaluable guidance, mentorship, and constructive feedback throughout the course of this research. Their academic insight and encouragement were instrumental to the success of this work.

REFERENCES

Abid, H., Zghal, O., Lajnef, M., Ketata, A., Zouari, S., Gugliuzza, G., & Driss, Z. (2024). Analysis of seasonal variations and their impact on the microclimate of soilless glass greenhouses: Numerical and experimental investigations. Numerical Heat Transfer, Part A: Applications, 1-25.

Aghakhani, H., Ayatollahi, S. M., & Hajmohammadi, M. R. (2023). Proposing novel approaches for solar still performance enhancement by basin water heating, glass cooling, and vacuum creation. Desalination, 567, 117011.

Ahmed, Z. A., Kamaruzzaman, S., Amer A. (2020). Review of energy storage services, applications, limitations, and benefits, Energy Reports, Volume 6, Supplement 7, Pages 288-306, ISSN 2352-4847, https://doi.org/10.1016/j.egyr.2020.07.028.

Alert, R., Casademunt, J., & Joanny, J. F. (2022). Active turbulence. Annual Review of Condensed Matter Physics, 13, 143-170.

Alireza, R., Sajad, H., Esmaeil, V., Mohammad, R. A., Davood, T. (2021). Effects of micro-combustor geometry and size on the heat transfer and combustion characteristics of premixed hydrogen/air flames. Journal Energy 215, 119061. https://doi.org/10.1016/j.energy.2020.119061

Bagheri G., Hosseini S. E., Wahid M. A. (2014). Effects of bluff body shape on the flamestability in premixed micro-combustion of hydrogen^aV“air mixture. Appl Therm Eng;67(1-2):266-72.

Chen, D., Li, J., Li, X., Deng, L., He, Z., Huang, H., & Kobayashi, N. (2023). Study on combustion characteristics of hydrogen addition on ammonia flame at a porous burner. Energy, 263, 125613.

Cheng, X., & Wu, H. (2021). Improved flow boiling performance in high-aspect-ratio interconnected microchannels. International Journal of Heat and Mass Transfer, 165, 120627.

Choi, S., Jung, I., Kim, H., Na, J., & Lee, J. M. (2022). Physics-informed deep learning for data-driven solutions of computational fluid dynamics. Korean Journal of Chemical Engineering, 39(3), 515-528.

Edwin U. O., Asumpta C. N., Nanasaheb M. S., Nnamdi N., Fabian I. E. (2023). Understanding the chemistry of graphene oxide on redox flow lithium‐ion batteries with a view to enhancing the battery's high‐density storage, Asia-Pacific Journal of Chemical Engineering, 10.1002/apj.2995.

Esmail, M. A. M., Yinka, S. S. & Mohamed, A. H. (2016). Numerical study of hydrogen-enriched methane-air combustion under ultra-lean conditions. Int. J. Energy Res. 2016; 40:743–762. DOI: 10.1002/er.3477

Fan, A., Wan, J., Maruta, K., Yao, H., Liu, W. (2013). Interactions between heat transfer, flowfield and flame stabilization in a micro-combustor with a bluff body. Int J Heat Mass Tran;66:72-9.

Garcia, A. M., Rendon, M. A., & Amell, A. A. (2020). Combustion model evaluation in a CFD simulation of a radiant-tube burner. Fuel, 276, 118013.

Garréton, D. and Simonin, O. (1994). Aerodynamics of steady state combustion chambers and furnaces. ASCF Ercoftac CFD Workshop.

Giwa, S. O., Sharifpur, M., Ahmadi, M. H., & Meyer, J. P. (2021). A review of magnetic field influence on natural convection heat transfer performance of nanofluids in square cavities. Journal of Thermal Analysis and Calorimetry, 145, 2581-2623.

Hoang, C. H., Rangarajan, S., Khalili, S., Ramakrisnan, B., Radmard, V., Hadad, Y., ... & Sammakia, B. (2021). Hybrid microchannel/multi-jet two-phase heat sink: A benchmark and geometry optimization study of commercial product. International Journal of Heat and Mass Transfer, 169, 120920.

Holechek, J. L., Hatim, M. E. G., Mohammed, N. S., & Raul, V. (2022). "A Global Assessment: Can Renewable Energy Replace Fossil Fuels by 2050?" Sustainability 14, no. 8: 4792. https://doi.org/10.3390/su14084792

Huang, Z., Peng, Q., Shi, Z., Fu, G., Xiao, H., & Huang, C. (2024). Numerical and experimental investigation of

ISBN: 978-978-8567-02-8

H2/CH4/Air combustion characteristics and thermal performance in the combustor with multi-bluff-body. Fuel, 367, 131435.

Hui, R., He, Z., Tao, C. (2024). Thermodynamic and emission analysis of an ammonia fueled micro-combustor with double-channel reverse flow structure, International Journal of Hydrogen Energy, Volume 49, Part B, Pages 1303-1314, ISSN 0360-3199, https://doi.org/10.1016/j.ijhydene.2023.11.083.

Jing, L., Zhao, J., Wang, H., Li, W., Du, Y., Zhu, Q., & Zayed, M. E. (2022). Numerical analysis of the effect of swirl angle and fuel equivalence ratio on the methanol combustion characteristics in a swirl burner. Process Safety and Environmental Protection, 158, 320-330.

Lachraf, A., & Ameur, M. S. (2023). Numerical investigation of thermal performance of hydrogen fueled micro-combustor with trapezoidal ribs. International Journal of Hydrogen Energy, 48(99), 39570-39585.

Le, X., Xinge G., Chengkuo L. (2023). "Evolution of Micro-Nano Energy Harvesting Technology—Scavenging Energy from Diverse Sources towards Self-Sustained Micro/Nano Systems" Nanoenergy Advances 3, no. 2: 101-125. https://doi.org/10.3390/nanoenergyadv3020006

Lei, H., Junwei, L., Dan, Z., Yunzhi, X., Xingpeng, G., Ningfei, W. (2021). Effect analysis on energy conversion enhancement and NOx emission reduction of ammonia/hydrogen fuelled wavy micro-combustor for micro-thermophotovoltaic application. Fuel, 289(119755). https://doi.org/10.1016/j.fuel.2020.119755

Liao, M., He, Z., Jia, S., Liang, X., Chan, T. L., LI, Y., and Xu, X. (2022) Comparison of the Flame Stabilities During Oxy-Methane and Air-Methane Combustion in a Two-Layer Porous Burner. Available at SSRN: https://ssrn.com/abstract=4209890 or http://dx.doi.org/10.2139/ssrn.4209890

Li, G., Ming, Z., Shijie, X., Qianhao, S., Peng, D., Xue-Song, B. (2022). Flame characteristics of methane/air with hydrogen addition in the micro confined combustion space, International Journal of Hydrogen Energy, Volume 47, Issue 44, 19319-19337, ISSN 0360-3199, https://doi.org/10.1016/j.ijhydene.2022.04.091.

Liu, C., Zhang, Y., Xiong, D., Huang, X., Zhang, P., Kang, Y., Lu, X., Wang, Q. (2020). Flammability and Propagation Dynamics of Planar Freely Propagating Dimethyl Ether Premixed Flame. ACS Omega. 5(19):10965-10976. doi: 10.1021/acsomega.0c00792. PMID: 32455217; PMCID: PMC7241034.

Manigandan, J., Iranian, D., Khan, I., Mohammed, N. A., & Alhazmi, H. (2024). Numerical Simulations of Thermal Heat Conservation in Hybrid Nanofluids with Chemical Reaction, Viscous Dissipation, and Inclination. Case Studies in Thermal Engineering, 104386.

Muhammad, N., Jianfeng, P., Yu, W., Feiyang, L., Abiodun, O. O., Ali, R. (2024). A review of recent advancements in micro combustion techniques to enhance flame stability and fuel residence time, International Journal of Hydrogen Energy, Volume 49, Part A, Pages 1165-1193, ISSN 0360-3199, https://doi.org/10.1016/j.ijhydene.2023.09.050.

Nauman, M., Pan, J., Lu, Q., Zhang, Y., Liu, C., Li, F., & Quaye, E. K. (2024). Analyzing the combustion characteristics of premixed methane-oxygen with different hydrogen addition ratios in a catalytic micro-combustor. Journal of the Energy Institute, 114, 101655. https://doi.org/10.1016/j.joei.2024.101655

Ni, S., Zhao, D., Cai, T., & Cao, F. (2021a). Energy conversion efficiency improvement studies on unconventional premixed micro-combustors partially inserted with porous medium. Fuel Processing Technology, 215, 106774.

Ni, S., Zhao, D., & Zhu, X. (2021b). Heat transfer and entropy production evaluation on premixed hydrogen/air-fuelled micro-combustors with internal threads. Fuel, 303, 121325.

Pashchenko, D. (2020). Hydrogen-rich fuel combustion in a swirling flame: CFD-modeling with experimental verification. International Journal of Hydrogen Energy, 45(38), 19996-20003.

Peng Q., E. J., Zhang Z., Hu W., Zhao X. (2018). Investigation on the effects of front-cavityon flame location and thermal performance of a cylindrical micro combustor. Appl Therm Eng ;130:541-51.

Pourrahmani, H., Rahim, Z., Sareh, D., & Jan, V. (2023). "Lab-Scale Investigation of the Integrated Backup/Storage System for Wind Turbines Using Alkaline Electrolyzer" Energies 16, no. 9: 3761. https://doi.org/10.3390/en16093761

Resende, P. R., Ayoobi, M., & Afonso, A. M. (2019). Numerical investigations of micro-scale diffusion combustion: A brief review. Applied Sciences, 9(16), 3356. https://doi.org/10.3390/app9163356

Riaz, A., Mahidur, R. S., Mohamad, H. M. S., & Ramizi, M. (2021). "Review on Comparison of Different Energy Storage Technologies Used in Micro-Energy Harvesting, WSNs, Low-Cost Microelectronic Devices: Challenges and Recommendations" Sensors 21, no. 15: 5041. https://doi.org/10.3390/s21155041

Sadatakhavi, S., Tabejamaat, S., EiddiAttarZade, M., Kankashvar, B., & Nozari, M. (2021). Numerical and experimental study of the effects of fuel injection and equivalence ratio in a can micro-combustor at atmospheric condition. Energy, 225, 120166.

Sciazko, M., Mertas, B., Kosyrczyk, L., & Sobolewski, A. (2020). A predictive model for coal coking based on product yield and energy balance. Energies, 13(18), 4953.

Serwin, M. (2022). Effects of additives, fuel mixing, and mechanically induced oscillations on soot formation.

Shini, L., Danan, C., Junqing, Z., Yunsheng, X., Min, F., Xing, L., Jun, L., Hongyu, H., Noriyuki, K. (2024). Blow-Off Limits, Flame Structure, and Emission Characteristics of Lean Partially Premixed Swirl-Stabilized Flames with NH3/CH4. Energy & Fuels, 38 (5) , 4721-4732. https://doi.org/10.1021/acs.energyfuels.3c04304

Silva, C. V. da, Vielmo, H. A., & França, F. H. R. (2006). NUMERICAL SIMULATION OF THE COMBUSTION OF METHANE. 5(July).

Vinuesa, R., & Brunton, S. L. (2021). The potential of machine learning to enhance computational fluid dynamics. arXiv preprint arXiv:2110.02085, 1-13.

Wan, J., Fan, A., Maruta, K., Yao, H., & Liu, W. (2012). Experimental and numerical investigation on combustion characteristics of premixed hydrogen / air flame in a micro-combustor with a bluff body. International Journal of Hydrogen Energy, 37(24), 19190–19197. https://doi.org/10.1016/j.ijhydene.2012.09.154

Wu, R., Nie, S., Ji, H., Wang, Y., Lin, L., & Yin, F. (2024). Effect of multi-parameter optimization of water-laser coupling device and nozzle geometry on the stability of water-guided laser beam. Physics of Fluids, 36(1).

Wu, S., Abubakar, S., & Li, Y. (2021a). Thermal performance improvement of premixed hydrogen/air fueled cylindrical micro-combustor using a preheater-conductor plate. International Journal of Hydrogen Energy, 46(5), 4496–4506. https://doi.org/10.1016/j.ijhydene.2020.10.237

Yang W., Xiang Y., Fan A., Yao H. (2017). Effect of the cavity depth on the combustionefficiency of lean H2/air flames in a micro combustor with dual cavities. Int J Hydrogen Energy ;42(20):14312-20.

Yuan, S., Jiang, B., Peng, T., Li, Q., & Zhou, M. (2021). An investigation of flow patterns and mixing characteristics in

ISBN: 978-978-8567-02-8

a cross-shaped micromixer within the laminar regime. Micromachines, 12(4), 462.

Zuo W., E J., Liu H., Peng Q., Zhao X., Zhang Z. (2016). Numerical investigations on an improved micro-cylindrical combustor with rectangular rib for enhancing heat transfer. Appl Energy;184:77-87.

ISBN: 978-978-8567-02-8

013-Manufacturing Engineering and National Development in Nigeria: An Overview

Abdulhakeem H. Nurudeen,

Author Address: Department of Mechanical Engineering, University of Abuja.
Hassan.abdulhakeem@uniabuja.edu.ng)

Abstract: Over the past five decades, manufacturing engineering has played a pivotal role in shaping Nigeria's economic trajectory, serving as both a driver of industrialisation and a stabiliser amid fluctuating global markets. Emerging in the 1970s as part of Nigeria's post-independence industrialisation agenda, manufacturing engineering facilitated the establishment of textile mills, cement plants, and food-processing industries, thereby reducing dependence on imports and fostering local value addition. By the 1980s and 1990s, despite structural adjustment policies and economic volatility, the sector contributed significantly to employment creation and the diversification of production, accounting for approximately 10% of GDP and 12% of formal-sector jobs. In the 2000s, with renewed emphasis on industrial policy, manufacturing engineering advanced through the integration of modern technologies in agro-processing, automotive assembly, and consumer goods production. This period witnessed the rise of small and medium-scale enterprises (SMEs), which became critical to innovation and resilience in the face of infrastructural challenges. The 2010s and early 2020s marked a transition towards digital manufacturing, automation, and energy-efficient processes, aligning Nigeria with global sustainability goals. By 2026, the sector will continue to underpin economic growth, contributing to export diversification, foreign exchange earnings, and regional competitiveness. Overall, manufacturing engineering has not only generated employment and GDP growth but also fostered technological transfer, industrial skills development, and infrastructural expansion. Its contributions remain indispensable to Nigeria's aspiration for inclusive growth, economic resilience, and sustainable industrialisation in the 21st century.

1. INTRODUCTION

For more than half a century, the Nigerian economy has remained predominantly reliant on the export of oil and gas, a dependence that has shaped its fiscal and developmental trajectory. Yet, Nigeria, home to a population exceeding 180 million and spanning approximately 970,000 square kilometers possesses far greater economic potential than hydrocarbons alone. The nation is endowed with vast agricultural resources, including nearly 82 million hectares of arable land, though only about 32 million hectares are presently under cultivation. In addition to this underutilized agricultural capacity, Nigeria is richly supplied with diverse mineral deposits such as gold, iron, lead, zinc, tin, coal, and gemstones. These resources, if strategically harnessed through industrial and technological innovation, present significant opportunities for economic diversification, sustainable growth, and long-term resilience beyond the oil sector (Kemi, 2019), (Chete et al., 2014).

Between 2017-2020 the minerals sector contributed around 100-650 billion to the economy accounting for 0.24% dominated by quarrying and other minerals such as limestones, gypsum, chalk, marble, and granite. While other metal ores were about 0.01% this activity consists of bauxite, copper, lead, zinc and tin (Eregha & Mesagan, 2017), (Haruna, 2012).

1. Impact of Covid-19 on Nigeria's Economy

The global pandemic was reported by WHO as an outbreak that can have major economic disruptions across the globe. The outbreak was reported in Nigeria on the 27th February, 2020 (Otache, 2020). The National Centre for Disease Control (NCDC) reported that between 17-23 May, 2020 there were over 1300 deaths, then a lockdown that brought unimaginable hardship to Nigerians with several people losing their jobs, lives and businesses. This affected the Nigerian economy so badly that it totally shut down the manufacturing sector, transportation, aviation and other allied sectors the advent of the manufacturing sector recorded a negative GDP contribution to the economy in 2020 (Brito, 2020).

The onset of the pandemic exacerbated Nigeria's economic fragility, plunging the nation into recession and precipitating losses across virtually all sectors. The steep decline in oil revenues, coupled with the contraction of small and medium-sized enterprises (SMEs), underscored the vulnerability of an economy long tethered to hydrocarbons. In response, the government sought to cushion the adverse effects through interventions by the Central Bank of Nigeria, which introduced broad-based credit facilities accessible to citizens. Notably, the manufacturing sector was prioritized, receiving an unprecedented allocation of one

ISBN: 978-978-8567-02-8

trillion Naira in credit support. This initiative was complemented by a reduction in lending interest rates from 9% to 5% and the provision of a one-year moratorium, measures designed to stimulate industrial activity, preserve employment, and foster resilience in the face of global economic disruption. Such policy actions highlight the strategic recognition of manufacturing as a cornerstone for economic diversification and recovery in the post-pandemic era (Du et al., 2020), (Ayadi & Ayadi, 2008).

1.2 What is National Development

Development, as articulated by Onyejiuwa and Fagboyo (2019), is conceived as a holistic enterprise aimed at reconstructing and advancing the multiple dimensions of a nation and its citizenry. It encompasses not only the industrial and agricultural sectors but also education, social, religious, and cultural institutions, alongside the scientific, economic, and material foundations of society, as well as the safeguarding of civil liberties. In this sense, development is not a singular pursuit but a multidimensional process that integrates structural, human, and technological progress.

To actualize such comprehensive development, certain parameters must be strategically pursued. First, the establishment of a planned national economy provides the framework for coordinated growth and resource allocation. Second, agricultural productivity must be enhanced through the systematic adoption of modern technologies, thereby ensuring food security and rural transformation. Third, industrial production must be harnessed to stimulate value addition, employment creation, and economic diversification. Fourth, the cultivation of human resources through education and skills development is indispensable, as it equips citizens to participate meaningfully in national progress. Finally, the application of science and technology within the manufacturing sector serves as a catalyst for innovation, efficiency, and global competitiveness.

Together, these parameters underscore the integrated nature of national development, situating manufacturing engineering and technological advancement as pivotal drivers of Nigeria's long-term economic resilience and societal transformation.

1.3 Problems of National Development

Nigeria's national development has been hindered by several structural and systemic challenges:

- Overdependence on oil revenues: Reliance on hydrocarbons has stifled diversification and exposed the economy to global price shocks.
- Underutilization of agricultural potential: Despite vast arable land, limited mechanization and poor infrastructure constrain productivity.
- Weak industrial base: Inadequate power supply, poor transport networks, and limited access to finance hinder industrial growth.
- Human capital deficits: Insufficient investment in education, vocational training, and research reduces workforce competitiveness.
- Governance and policy inconsistency: Frequent shifts in industrial policy and corruption undermine long-term planning.

2. MANUFACTURING SECTOR CONTRIBUTIONS TO THE ECONOMY

Despite these challenges, the manufacturing sector has made notable contributions to Nigeria's economic development:

- Employment generation: Factories and SMEs provide millions of jobs, reducing unemployment and poverty.
- GDP diversification: Manufacturing contributes around 10% of GDP, offering alternatives to oil dependency.
- Value addition: Agro-processing, cement, textiles, and consumer goods industries transform raw materials into finished products.
- Technological transfer: Adoption of modern machinery and digital manufacturing enhances productivity and skills.
- Export competitiveness: Manufactured goods, though limited, contribute to foreign exchange earnings and regional trade.
- Resilience during crises: Credit facilities and policy support during the pandemic highlighted manufacturing's role in stabilizing the economy.

Nigeria's National development problems particularly its reliance on oil and weak infrastructure have constrained industrialization. Yet, the manufacturing sector has emerged as a strategic pillar for economic diversification, technological advancement, and sustainable growth. Strengthening this sector through consistent policy, infrastructure investment, and human resource development is essential for Nigeria's long-term resilience and transition into a post-oil economy as shown in Table 1(Agbaeze & Ukoha, 2018), (Tolu & Abe, 2011).

First National Development Plan (1962—68) was centred on the reduction of importation to conserve foreign exchange and boost local production. This endeavour was to stimulate start-up and growth of industries. The manufacturing sector contributed to GDP from 7.02% to 8.17% Awojobi et al., 2014)

During the Second National Development Plan (1970-74) the oil boom era, The Government embarked on infrastructural and manufacturing sector expansion, and the sector contributed to 9.4% of GDP (Ekpo, 2014).

Third National Development Plan (1978-80) it was more on the public sector investment in industry with the aim of increasing local managerial control, building local technology and extension of state ownership. GDP as at 1980 grew to 11.05% (NDP 2021).

Fourth National Development Plan (1981- 85) was the austerity period, the economy was facing a decline due to global recession and unfortunately the contribution declined to 5.9% to GDP. During that period, the need for adopting Structural Adjustment Program (SAP) was

ISBN: 978-978-8567-02-8

initiated in 1986, to ensure the reduction on the high dependence on crude oil exports as major foreign earnings by promoting non-oil exports. Despite all these efforts, the performance of the manufacturing sector was still low compared to other sectors as illustrated in Figure 1. (NDP 2021), (Kemi, 2019), (Tolu & Abe, 2011).

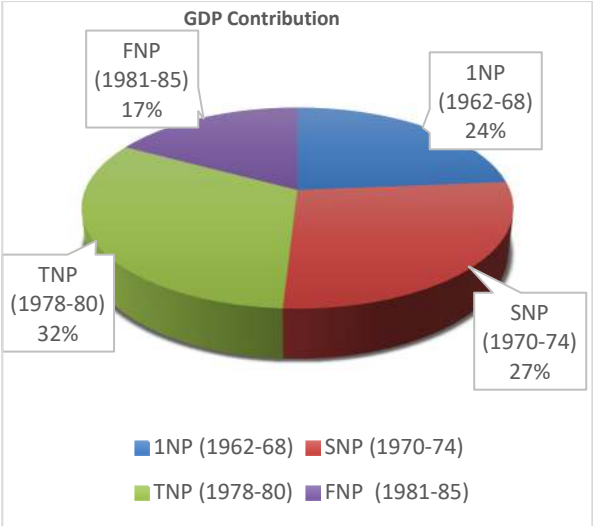


Figure 6: Summary of Manufacturing Sector Contribution to GDP

Between 1999-2014, Nigeria witnessed drastic polities and the establishment of Government parastatals to foster industrial development through long-term loans, equity finances and technical assistance to industrial enterprises but still, the manufacturing sector's contribution to GDP was below 10%. The inability of the sector to reach its full potential was due to low productivity in the sector (Tolu & Abe, 2011).

In the year 2014, the Nigerian Industrial Revolution Plan was introduced; it has a 5-year plan designed to boost industrial capacity in the country. With the aim of improving GDP from 4 to 10% by 2017 and focusing on agro-allied industries, metals and solid minerals. It was expected that the plan will create jobs, boost the economy, revenue diversification, import substitution, and broadened the Government tax bases but unfortunately the plans was never implemented (Tolu & Abe, 2011), (Ekpo, 2014).

TABLE 1: MANUFACTURING SECTOR CONTRIBUTIONS TO GDP

Performance of the manufacturing sector (2017-2020)	2017	2018	2019	2020
Manufacturing GDP at current market value (N'trn)	10.04	12.46	16.78	18.90
Manufacturing GDP as share of total GDP (%)	8.83	9.75	11.64	12.40
Manufacturing GDP (%)	-0.21	2.09	0.77	-2.75
Total GDP growth (%)	0.83	1.90	2.27	-1.92

Source: NBS 2022

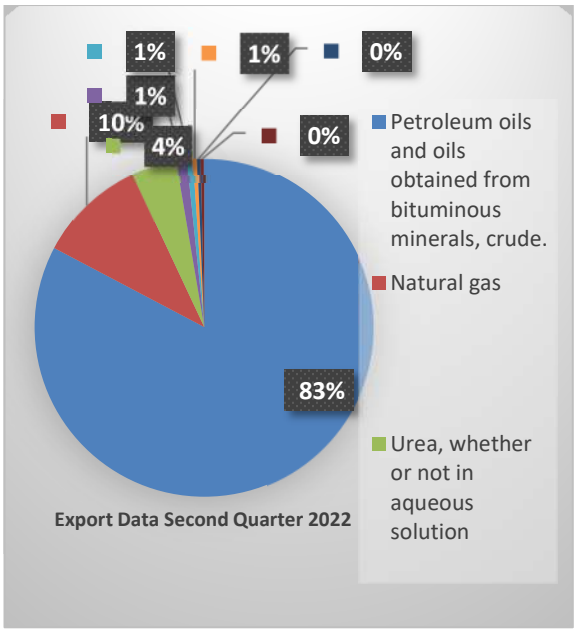


Figure 7: Nigeria's Export Data 2nd Quarter 2022

Figure 2 highlighted some of the few selected export commodities in Nigeria, from the Figure, it could be observed that petroleum oils it byproducts occupies 83% of the second quarter export output by Nigeria to a sum of around 5.9 Billion Naira, second that is Natural gas with around 10% in the sum of 735 billion Naira, Urea, while other export commodities contributed to the economy also such the unwrought aluminum, sesame seeds and superior quality cocoa beans accruing to (4.16, 9.00, 0.56, 0.39, 0.34, 0.30%) respectively.

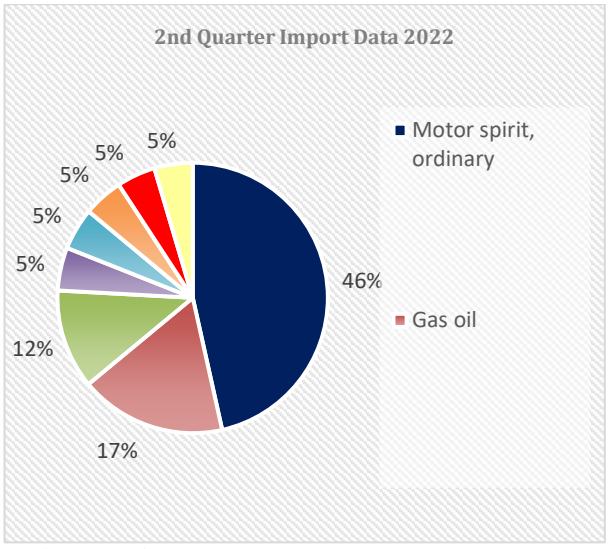


Figure 8: 2nd Quarter Import Data 2022

ISBN: 978-978-8567-02-8

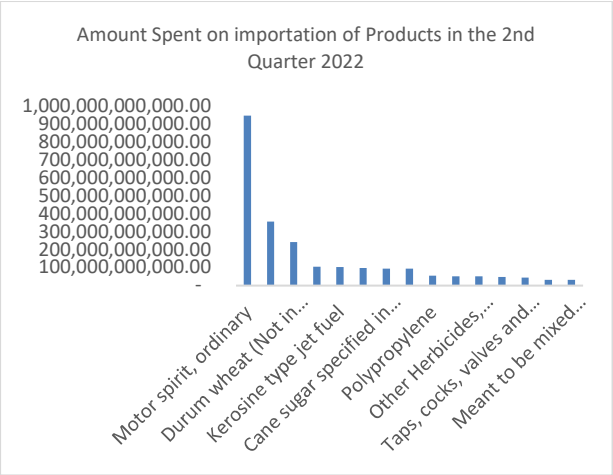


Figure 9: Cost of Importation in the 2nd Quarter 2022

The evidence presented in Figures 3 and 4 underscores the urgent need for a comprehensive overhaul of Nigeria's manufacturing sector. Approximately 83% of the nation's export output remains petroleum-based, amounting to nearly 6 trillion Naira, while paradoxically, the country expends close to 1 trillion Naira annually on the importation of motor spirit. This imbalance highlights a structural deficiency: despite Nigeria's resource endowment, the manufacturing sector has not been sufficiently leveraged to achieve self-sufficiency or diversify export earnings. Such a scenario reveals the inadequacy of current industrial policies, which must be revisited and recalibrated to foster value addition, reduce import dependence, and stimulate broader economic resilience. A reorientation toward strengthening manufacturing capacity particularly in refining, agro-processing, and mineral-based industries would not only mitigate the vulnerabilities of oil dependency but also position Nigeria for sustainable growth in the global economy.

In the third quarter of 2024, Nigeria's real Gross Domestic Product (GDP) expanded by 3.46% on a year-over-year basis. This pace of growth surpassed both the 2.54% increase observed in the corresponding quarter of 2023 and the 3.19% recorded in the preceding quarter of 2024. The principal driver of this expansion was the Services sector, which registered a 5.19% rise and accounted for 53.58% of total output. Agricultural activity advanced by 1.14%, slightly below the 1.30% growth achieved in the third quarter of 2023. Industrial production improved to 2.18%, marking a notable increase from the 0.46% growth reported in the same quarter of the previous year. Relative to GDP composition, the Services sector contributed a larger share in Q3 2024 than in Q3 2023. At current basic prices, aggregate GDP was valued at ₦71,131,091.07 million, compared with ₦60,658,600.37 million in Q3 2023, reflecting a nominal year-on-year expansion of 17.26% (NBS, 2024).

3. MANUFACTURING ENGINEERING CONCEPT AND ROLES

Manufacturing engineering constitutes a vital branch of professional engineering that applies systematic procedures to the design and optimization of manufacturing processes and the production of industrial goods. It demands not only technical expertise in process design but also the capacity to resolve complex operational challenges by integrating tools, equipment, and machinery within facilities and systems. Production, in this context, functions as the implementation arm of manufacturing, responsible for generating throughput by employing efficient processes to deliver quality products at minimal cost (Lu & Mani, 2006).

The roles of manufacturing engineering in national development are extensive, encompassing the planning, selection, and advancement of products and services that sustain industrial growth. Its contributions extend beyond the factory floor, shaping the broader economic landscape by fostering innovation, efficiency, and competitiveness. The manufacturing sector, when strategically harnessed, possesses the capacity to drive national development through poverty reduction, economic diversification, and the effective utilization of land, capital, and material resources. By producing consumer goods for both domestic consumption and export, the sector not only strengthens self-reliance but also enhances foreign exchange earnings and global integration.

Ultimately, manufacturing engineering stands as a cornerstone of sustainable development, linking technological advancement with socio-economic transformation. Its ability to generate employment, stimulate industrialization, and promote value addition underscores its indispensable role in Nigeria's pursuit of inclusive growth and resilience in the global economy.

Manufacturing engineering in Nigeria has contributed through cement production, food and beverage processing, textiles, pharmaceuticals, and automotive assembly each sector applying engineering innovations to boost productivity, create jobs, and diversify the economy. With some practical contributions as (Deborah Dan-Awoh 2023):

Cement Production: Companies like Dangote Cement have applied advanced manufacturing engineering to scale production, optimize kiln operations, and reduce costs. This has supported infrastructure development nationwide and positioned Nigeria as a net exporter of cement.

Food and Beverage Processing: Breweries, flour mills, and beverage companies employ manufacturing engineering to automate bottling, milling, and packaging processes. This ensures consistent quality, reduces waste, and meets the demands of Nigeria's large population.

Textiles, Apparel, and Footwear: Engineering innovations in weaving, dyeing, and finishing have sustained Nigeria's textile industry, particularly in Kaduna and Aba. Though challenged by imports, these industries remain vital for employment and cultural identity.

Pharmaceuticals and Chemicals: Local pharmaceutical firms use manufacturing engineering to produce essential drugs and chemicals domestically, reducing reliance on imports and strengthening healthcare resilience.

Automotive Assembly: Companies such as Innoson

ISBN: 978-978-8567-02-8

Vehicle Manufacturing (IVM) apply engineering design and assembly-line techniques to produce buses, cars, and trucks locally. This supports industrialization, job creation, and reduces foreign exchange outflows.

Oil Refining and Petrochemicals: Engineering contributions in refining processes and petrochemical plants have added value to Nigeria's crude oil, though challenges remain in achieving full self-sufficiency

Possible Solutions to Boosting Manufacturing for National Development (NDP, 2021; Awojobi et al., 2014)

1. Adequate Infrastructure and Power Supply: Infrastructure remains the backbone of industrial productivity. Reliable energy provision is indispensable for sustaining manufacturing operations, while efficient transportation networks; railways, roads, air, and seaports are essential for moving raw materials to factories and distributing finished goods. Without these foundational systems, industrialization cannot thrive. The government must therefore prioritize investments in energy generation, transmission, and distribution, alongside modernizing transport infrastructure to facilitate seamless industrial activity.
2. Long-Term Credit Facilities with Minimum Interest Rates: Access to affordable finance is critical for manufacturers. By reducing interest rates on long-term loans and expanding credit facilities, the cost of production can be significantly lowered. This measure not only enhances output but also strengthens competitiveness, enabling manufacturers to expand operations, adopt new technologies, and contribute more robustly to national economic prosperity.
3. Enhancing Value Chain Linkages: Strengthening connections between agriculture, mining, and manufacturing ensures that raw materials are effectively transformed into finished goods. This integration fosters efficiency, reduces waste, and maximizes value addition across sectors.
4. Support for Tertiary Institutions: Universities and polytechnics play a vital role in supplying skilled manpower and research innovations. Strengthening collaboration between academia and industry will accelerate technological transfer and workforce development.
5. Abolition of Multiple Taxations: Excessive taxation discourages investment and stifles growth. Streamlining tax policies will create a more conducive environment for manufacturing enterprises, encouraging expansion and sustainability.

As emphasized by the world bank (2019), strengthening value-chain linkages between primary sectors is essential for ensuring a steady supply of raw materials to larger manufacturing industries. This requires deliberate investment in training programs, provision of incentives, and fostering increased synergy among key government parastatals. Such measures not only guarantee the availability of inputs but also enhance efficiency, reduce production bottlenecks, and ensure the overall success of national developmental plans. By integrating agriculture, mining, and manufacturing through coordinated policies, Nigeria can maximize resource utilization and stimulate industrial growth.

Educational institutions remain at the forefront of national development, serving as the primary source of skilled manpower. It is within universities, polytechnics, and technical colleges that craftsmen, technicians, technologists, and engineers are trained to address complex industrial challenges. A technically sound workforce comprising critical thinkers and problem solvers is indispensable for sustaining a robust manufacturing sector. For instance, when a factory experiences downtime due to machinery breakdown, the absence of skilled engineers and technicians can halt production entirely. To mitigate such vulnerabilities, government must place greater emphasis on technical education, increase funding allocations, and ensure transparent disbursement mechanisms to curb corruption (eregha & mesagan, 2017). Strengthening the educational pipeline will not only enhance industrial resilience but also accelerate innovation and technological advancement.

4. CONCLUSION

Earlier iterations of Nigeria's National Development Plans recognized the centrality of the manufacturing sector to national development, economic growth, and diversification. Manufacturing was envisioned as a critical driver in positioning Nigeria among the world's top twenty economies by 2020. However, persistent bottlenecks including infrastructural deficits, policy inconsistencies, and governance challenges combined with frequent shifts in government priorities, hindered the realization of this vision.

Between 2017 and 2020, the sector nonetheless demonstrated its significance, contributing approximately 18.9 trillion Naira, which accounted for 10.66% of GDP. Yet, the onset of the COVID-19 pandemic precipitated a contraction of –2.75%, underscoring the sector's vulnerability to external shocks and structural weaknesses.

To effectively revitalize manufacturing, government must create an enabling environment that accelerates industrialization and strengthens competitiveness. This entails not only infrastructural improvements and stable policy frameworks but also deliberate promotion of small and medium-sized manufacturing enterprises (SMEs), which serve as engines of innovation, employment, and resilience. By fostering investments, expanding market access, and enhancing export capacity, the manufacturing sector can stimulate growth across related sectors and subsectors, thereby ensuring job security and advancing economic diversification.

Ultimately, the manufacturing sector holds

ISBN: 978-978-8567-02-8

transformative potential for Nigeria's long-term development. Its revitalization is indispensable for reducing dependence on hydrocarbons, achieving inclusive growth, and positioning the nation as a competitive player in the global economy.

ACKNOWLEDGEMENT

The author is grateful to the management of the University of Abuja.

REFERENCES

Federal Ministry of Finance, Budget and National Planning. (2021). *National Development Plan 2021-2025*. Federal Ministry of Finance, Budget and National Planning.

Awojobi, O. N., Ayakpat, J. O. Y. C. E., & Adisa, O. D. (2014). Rebased Nigerian gross domestic product: The role of the informal sector in the development of the Nigerian economy. *International Journal of Education and Research*, *2*(7), 301-316.

Onyejiuwa, D. C., & Fagboyo, R. J. (2019). Nigerian national development plans and manufacturing sector: A case for diversification. *Journal of Management Sciences*, *12*(1).

Agbaeze, E. K., & Ukoha, K. (2018). Oil a blessing or a curse: The Nigerian experience. *European Journal of Social Sciences*, *56*(3), 262-270.

Tolu, L., & Abe, O. (2011). National development in Nigeria: Issues, challenges and prospects. *Journal of Public Administration and policy research*, *3*(9), 237-241.

Ekpo, U. N. (2014). Nigeria industrial policies and industrial sector performance: Analytical exploration. *IOSR Journal of Economics and Finance*, *3*(4), 1-11.

Lu, Q., & Maani, K. (2006). Dynamics of conflict between production and manufacturing engineering. *International Journal of Innovation and Technology Management*, *3*(02), 129-148.

World Bank Group. (2019). *Nigeria Economic Update, Fall 2019: Jumpstarting Inclusive Growth-Unlocking the Productive Potential of Nigeria's People and Resource Endowments*. World Bank.

Nigerian Gross Domestic Product Report (Q2 2024) *National Bureau of Statistics*, Nigeria http://www.nigerianstat.gov.ng/

Kemi, A. O. (2019). Nigeria's Economy Challenges–Causes and Way Forward. *Journal of Economics and Finance, International Organization of Scientific Research, India*, *10*(2).

Chete, L. N., Adeoti, J. O., Adeyinka, F. M., & Ogundele, O. (2014). *Industrial development and growth in Nigeria: Lessons and challenges* (No. 2014/019). WIDER working paper.

Eregha, P. B., & Mesagan, E. P. (2017). The emergence of inclusive growth: Issues, challenges and policy options for Nigeria.

Haruna Danja, K. (2012). Foreign direct investment and the Nigerian economy. *American Journal of Economics*, *2*(3), 33-40.

Otache, I. (2020). The effects of the Covid-19 Pandemic on the Nigeria's economy and possible coping strategies. *Asian Journal of Social Sciences and Management Studies*, *7*(3), 173-179.

Brito, C. (2020). Coronavirus 'may never go away,'. *World Health Organization Warns CBC News, London, United Kingdom*.

Du, Y., Tu, L., Zhu, P., Mu, M., Wang, R., Yang, P., ... & Xu, G. (2020). Clinical features of 85 fatal cases of COVID-19 from Wuhan. A retrospective observational study. *American journal of respiratory and critical care medicine*, *201*(11), 1372-1379.

Ayadi, F. S., & Ayadi, F. O. (2008). The impact of external debt on economic growth: A comparative study of Nigeria and South Africa. *Journal of sustainable development in Africa*, *10*(3), 234-264.

Deborah Dan-Awoh (2023). September 17, 2023, website:Industry powerhouse: Nigeria's top manufacturing leaders - Nairametrics Industry powerhouse: Nigeria's top manufacturing leaders

ISBN: 978-978-8567-02-8

015-Harnessing Local Engineering Innovation for Sustainable Industrial Growth and SDG Realization in Nigeria: A Triple Helix Perspective

[1]Auwalu Faisal Koko, [2]Sanusi Sani Maimagani, and [3]Muhammed Bello

[1]Faculty of Environmental Sciences, Baze University, Abuja, Nigeria.
[2]Department of Architectural Technology, Waziri Umaru Federal Polytechnic Birnin Kebbi, Nigeria.
[3]Department of Architecture, Kaduna Polytechnic, Kaduna State, Nigeria

Corresponding Author: faisal.auwalu@bazeuniversity.edu.ng

Abstract: Nigeria's quest for sustainable industrial development and economic independence has been confronted by numerous challenges, including poor adoption of local technology, dependence on imported engineering innovations, and limited utilization of locally developed solutions. This study adopts a conceptual and narrative review methodology, guided by the Triple Helix Model of academia–industry–government collaboration, to examine Nigeria's industrial policy framework, technology transfer mechanisms, and engineering innovation landscape. Relevant academic literature, policy documents, and sectoral studies across different engineering disciplines were reviewed and thematically synthesized. The findings reveal that local technologies help reduce production costs, improve productivity, and promote environmental sustainability; however, weak collaboration, limited commercialization processes, and misalignment between policy and engineering practice constrain their impact. The paper further identifies key challenges and local engineering trends with the potential to enhance industrialization and address Sustainable Development Goals (SDGs) related to sustainable infrastructure, clean energy, and climate action. It concludes that strong investment in local research, structured multi-sector collaboration, and coordinated government support, anchored in a Triple Helix framework are needed to ensure that local engineering innovations contribute significantly to Nigeria's socio-economic development.

1. Introduction

Nigeria's industrial sector has continuously faced multiple challenges that have limited the country's ability to achieve economic self-reliance and sustainable industrial growth (Onoh & Enekwe, 2024). Studies by Okpalaoka (2021) and Bansal (2024) on the industrial transformation of Nigeria indicate multifaceted factors such as inadequate infrastructure, unreliable energy supply, limited access to modern technology and innovations, and disparities between industrial policies and engineering competences as contributors to low productivity, high production costs, and overdependence on imported machinery (Adebayo & Ainah, 2024; Ibitoye et al., 2022; Osunkwo, 2025). These challenges often limit local industrial competitiveness and increase Nigeria's vulnerability to global economic fluctuations.

The heavy reliance on imported machinery exposes Nigeria's industrial sector to exchange-rate instability, supply-chain disruptions, and fluctuations in global market dynamics (Umaru & Adesanya, 2024). Minor disturbances in international trade often affect domestic production, widening the technological gap between Nigeria and more industrially advanced economies. This situation weakens economic sovereignty and affects Nigeria's ability to negotiate from a position of strength within global markets (Osunkwo, 2025).

Despite these challenges, Nigeria possesses substantial expertise across its 301 universities comprising 74 federal, 68 state, and 159 private institutions (National Universities Commission, 2025). The incorporation of local innovations across fields such as civil, electrical, mechanical, and materials engineering therefore presents significant potential for improving industrial operations, enhancing efficiency, and reducing environmental impacts. Specifically, civil and architectural engineering innovations support green construction approaches, sustainable industrial buildings, and modular designs (Firoozi et al., 2025; Patel, 2025). Electrical engineering innovations, principally in renewable energy systems and energy-efficient industrial processes, can help mitigate Nigeria's persistent energy challenges (Onuh et al., 2024). Similarly, mechanical and materials engineering innovations comprising locally fabricated machineries, automation systems, and sustainable materials can help enhance productivity and cut the dependency on imported technologies (Taiwo et al., 2024; Amhenya et al., 2025).

Earlier studies reveal that a crucial factor limiting the commercialization of these innovations is the weak synergy between tertiary institutions, where research

ISBN: 978-978-8567-02-8

outputs are generated, and industries, where utilization should occur (Hamilton et al., 2025; Victor et al., 2024). Existing technology transfer mechanisms remain under-developed in Nigeria, resulting in locally developed innovations remaining basically at the academic level (Ajibo et al., 2019). Fragmented collaboration between academia, industry, and government further constrains the transformation of research into practical industrial solutions (Nwaichi et al., 2025).

Therefore, this paper argues that Nigeria's sustainable industrial growth requires a strategic framework that integrates local engineering innovation with national industrial policies. Such integration will help promote the development, commercialization, and adoption of local technologies, reduce environmental impacts, and support the attainment of key Sustainable Development Goals (SDGs), particularly SDG 7 Affordable and Clean Energy, SDG 9 Industry, Innovation and Infrastructure, SDG 11 Sustainable Cities and Communities, and SDG 13 Climate Action.

The paper reviews Nigeria's industrial policies and engineering innovations, examines existing collaboration gaps using the Triple Helix Model, and proposes strategic measures aimed at strengthening the academia-industry-government relationship.

2. Theoretical framework and methodology

2.1 The Triple Helix Model

The Triple Helix Model emphasizes the dynamic interaction between academia, industry, and government as a basis for innovation and sustainable development (Cai & Etzkowitz, 2021). In this model, universities generate knowledge and innovation, industries scale and commercialize technologies, while governments provide policy direction, funding mechanisms, and regulatory support. Unlike linear models of innovation, the Triple Helix approach recognizes the overlapping roles and co-creation among institutional actors. Although the model has been successfully utilized in developed nations, its implementation in developing countries such as Nigeria is often constrained by weak institutional coordination, limited commercialization infrastructure, and inadequate incentives. However, the model is relevant for examining Nigeria's innovation system because it allows for the structural analysis of failures in collaboration and policy alignment across institutional boundaries.

Therefore, this study utilized the Triple Helix Model as an analytical tool to:

i. Examine the present roles of academia, industry, and government in Nigeria;
ii. Identify gaps and weaknesses in technology transfer and collaboration; and
iii. Derive stakeholder strategies for strengthening local engineering innovation.

2.2 Methodology

The study adopts a conceptual and narrative review methodology. Academic journal articles, conference papers, policy documents and reports related to industrial growth, engineering innovation, technology transfer, and the SDGs were reviewed. Sources were identified through keyword searches across relevant academic databases and policy repositories, focusing on vital literature relevant to Nigeria and other developing economies. The materials were analyzed thematically using the Triple Helix framework to synthesize insights on policy-innovation alignment and sustainable industrial development. This framework allowed for the systematic analysis of policy, innovation, and collaboration gaps in Nigeria's industrial sector.

3. Nigeria's industrial policies and engineering innovations

Industrial policies serve as key strategic roadmaps for national economic development (Oqubay, 2025). Over the years, Nigeria has introduced several initiatives such as the National Industrial Policy, National Development Plan (NDP), Economic Recovery and Growth Plan (ERGP), Economic Sustainability Plan, and the Local Content Act (Anam et al., 2024; Musa et al., 2025). Such policies aim to promote industrialization through import substitution, economic diversification, and enhancement of local technological capacity (Table I).

TABLE I: NIGERIA'S INDUSTRIAL POLICIES AND IMPLICATIONS.

Policies	Significance	Challenges	Prospects
National Development Plan	Local manufacturing, industrial infrastructure	Weak technology adoption,	University-industry partnership, R&D incentives
Economic Recovery & Growth Plan	Energy efficiency, industrial modernization	Funding constraints, insufficient technical expertise	Private sector engagement, renewable energy incorporation
Local Content Act	Indigenous technology, skills development	Limited expertise, slow technology adoption	Technology transfer collaboration, innovation incubation

Engineering innovations are necessary for bridging the gap between policy intent and implementation (Rishika, 2021; Zeidan, 2020). Civil and architectural engineering innovations contribute through energy-efficient designs, modular construction, and sustainable infrastructure (Patel, 2025). Mechanical engineering innovations comprising locally fabricated machineries and optimized manufacturing processes, support productivity and reduces cost (Taiwo et al., 2024). Electrical engineering innovations such as renewable energy technologies and smart grids improve environmental sustainability (Onuh et al., 2024).

Despite such benefits, policy implementation remains slow. Weak enforcement, limited incentives for local innovation, and inadequate coordination between policy institutions and engineering stakeholders continue to hinder Nigeria's industrial growth. From a Triple Helix perspective, these challenges reflect misaligned roles and weak collaboration between government, academia, and industry.

Therefore, deliberate realignment of industrial policies with engineering outcomes are required through targeted incentives, R&D investment, and supportive regulatory frameworks to transform Nigeria's industrial sector.

ISBN: 978-978-8567-02-8

4. TECHNOLOGY TRANSFER AND TRIPLE HELIX ADOPTION

Technology transfer and local innovation are vital strategies to reduce Nigeria's dependence on imported machineries (Hassan et al., 2024). Studies indicate that research outcomes from Nigerian universities rarely progress beyond academic publications due to limited industrial engagement, inadequate pilot-testing facilities, and insufficient government support (Ezeliora & Nwufo, 2021; Arize, 2023; Osunkwo, 2025).

Local innovations, such as compressed earth blocks, bamboo composites, pozzolana cement alternatives, modular systems, locally fabricated agro-processing machinery, transformers, and renewable energy components, can help reduce dependency on imported building materials while supporting SDG 7 (Agbakwuru et al., 2024; Udeala et al., 2025). Technology transfer from foreign firms can also support localization through structured knowledge exchange and adaptation to local conditions (Osabutey et al., 2024). Figure 1 illustrates the typical flow of technology transfer from academia to industry.

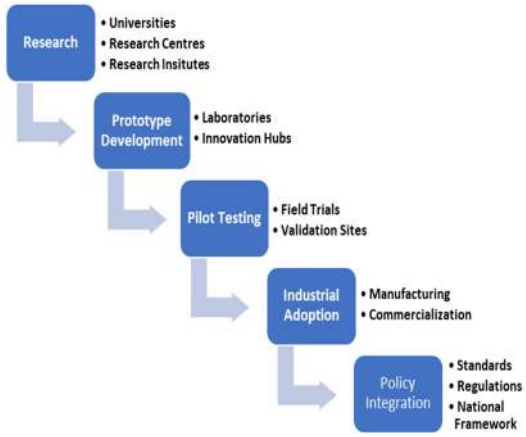


Figure 1: Technological Transfer Framework (Academia - Industries and Policy Adoption).

However, in Nigeria, this flow is often disrupted by weak institutional linkages, lack of commercialization platforms, and limited industry participation in research. Therefore, the Triple Helix Model provides an outline for strengthening these institutional interactions, establishing innovation clusters, and integrating innovation into industrial policy (Zadegan et al., 2025; Fidanoski et al., 2022; Natário et al., 2023). Figure 2 presents a conceptual Triple Helix framework for adoption in Nigeria.

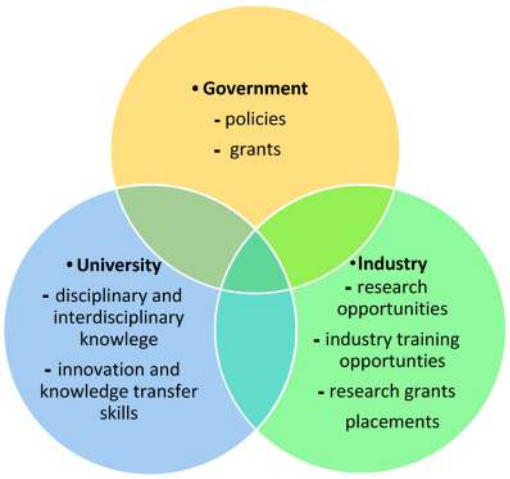


Figure 2: Triple helix Model for Innovation.

5. LOCAL ENGINEERING INNOVATIONS AS PATHWAY TO SUSTAINABLE DEVELOPMENT GOALS (SDGS)

Local engineering innovations play an important role in advancing SDGs 7, 9, 11, and 13. The adoption of indigenous materials, renewable energy technologies, and sustainable industrial practices addresses challenges related to energy inefficiency, manufacturing limitations, sustainability, and environmental degradation (Table II).

TABLE II: CONTRIBUTIONS TO SDGS AND THEIR IMPACTS.

	Specific SDG	Engineering Contribution	Impact on Nigeria's Local Industry
i.	SDG 7	Solar-powered industries, energy-efficient designs	Reduced energy costs, low emissions
ii.	SDG 9	Smart industries, modular buildings, local fabrication	Improved productivity, stronger local industries
iii.	SDG 11	Green industrial zones, logistics optimization	Sustainable urban-industrial integration
iv.	SDG 13	Emission control (GHGs), climate-resilient designs	Reduced pollution, environmental sustainability

These SDG-focused innovations achieve maximum impact when the academia, industry, and government coordinate effectively under the Triple Helix framework.

6. CONCLUSION AND STRATEGIC RECOMMENDATIONS

The study highlights the vital role of local technology and engineering innovations in achieving sustainable industrial growth and advancing the SDGs in Nigeria. The utilization of the Triple Helix Model reveals that Nigeria's industrial challenges often result less from the absence of policies or technical capacity and more from weak coordination and fragmented interaction among academia, industry, and government. Despite the availability of local expertise and policy tools, limited integration has constrained the commercialization and adoption of indigenous technologies. Locally developed solutions, such as renewable energy systems, sustainable construction materials, and indigenous industrial technologies, serve as practical pathways for reducing Nigeria's import dependence, improving productivity,

ISBN: 978-978-8567-02-8

and enhancing environmental sustainability. However, their impact remains minimal due to the absence of structured collaboration mechanisms and clearly defined institutional roles.

Therefore, the following measures are proposed based on the Triple Helix Model:

i. *Academia:* Prioritize applied and industry-related research through functional technology transfer mechanisms and incentives for commercialization.
ii. *Industry:* Actively engage in co-developing and adopting local innovations through partnerships, pilot projects, and innovation hubs.
iii. *Government*: Coordinate the strengthening of local content policies by providing targeted funding for university-industry collaboration and integrating local engineering outcomes into public procurement and infrastructure delivery.

REFERENCES

Adebayo, A., & Ainah, P. (2024). Addressing Nigeria's electricity challenges: Past, present, and future strategies. American Journal of Applied Sciences, 2, 1-16.

Agbakwuru, V., Obidi, P., Salihu, O., & Ogwu, C. (2024). The role of renewable energy in achieving sustainable development goals. International Journal of Engineering Research Updates, 7(2), 13-27.

Ajibo, C., Anozie, M., Onyeabor, E., Umahi, T., Odinkonigbo, J., & Agu, H. (2019). Technology transfer for development in Nigeria: Patterns, problems and prospects. Commonwealth Law Bulletin, 45(1), 1-22.

Amhenya, O., Egbiki, S., Dominic, E., Olokpo, I., & Okechwukwu, O. (2025). Sustainable infrastructure development through advanced materials and construction techniques. International Journal of Science, Architecture, Technology, and Environment, 2(4), 171-182.

Anam, B. E., Ijim, U. A., Ironbar, V., Otu, A., Duke, O. O., & Achuk Eba, M. B. (2024). Economic recovery and growth plan, economic sustainability plan and national development plan (2021-2025): The Nigerian experience under President Muhammadu Buhari. Cogent Social Sciences, 10(1), 2289600.

Arize, B. (2023). The challenges of industrialization in Nigeria and the way forward. International Journal of Research and Innovation in Social Science, 7(5), 691-704.

Balcı, O., Almohammad, D., Kılıç, C., & Singh, R. (2025). Harnessing emerging technologies for green sustainability: Innovations, challenges, and future pathways. In R. Singh & W. L. Filho (Eds.), Climate neutrality through smart eco-innovation and environmental sustainability (pp. 209-225). Springer Nature.

Bansal, P. (2024). The state of technology innovation in Nigeria: Trends, challenges and opportunities. Journal of Marketing and Supply Chain Management, 3(3), 1-2.

Cai, Y., & Etzkowitz, H. (2021). Theorizing the Triple Helix model: Past, present, and future. Triple Helix, 7(2), 189-226

Ezeliora, C., & Nwufo, M. (2021). Solutions to Nigerian problems of industrialization and manufacturing. GSC Advanced Engineering and Technology, 1, 49-57.

Fidanoski, F., Simeonovski, K., Kaftandzieva, T., Ranga, M., Dana, L. P., Davidovic, M., Ziolo, M., & Sergi, B. S. (2022). The Triple Helix in developed countries: When knowledge meets innovation. Heliyon, 8(8), e10220.

Firoozi, A., Oyejobi, D., & Firoozi, A. (2025). Innovations in energy-efficient construction: Pioneering sustainable building practices. Cleaner Engineering and Technology, 26, 100957.

Hamilton, C., Nnanyelugo, I. M., & Obi, E. (2025). Research outputs and commercialization of innovations, incubations and start-ups in Nigeria: RMRDC initiatives

Hassan, I., Fatile, J., & Hunga, V. (2024). Sino-Africa and technological transfer: Implication on sustainable development in Nigeria. Journal of Public Administration, Finance and Law, 31, 147-162.

Huang, W., & Wang, X. (2024). The impact of technological innovations on agricultural productivity and environmental sustainability in China. Sustainability, 16(19), 8480.

Ibitoye, O., Ogunoye, A., & Kleynhans, E. (2022). Impact of industrialisation on economic growth in Nigeria. Journal of Economic and Financial Sciences, 15(1), 1-9.

Musa, I., Tony, H., & Sule, M. (2025). Analyzing the contributions of the economic recovery and growth plan, national strategies, and national development plan toward achieving sustainable development goals in Nigeria. International Journal of Multidisciplinary Research and Development, 12(10), 182-190.

Natário, M. M. S., Braga, A. M. M., & Daniel, A. C. M. (2023). Triple Helix and innovation. In S. Idowu, R. Schmidpeter, N. Capaldi, L. Zu, M. Del Baldo, & R. Abreu (Eds.), Encyclopedia of sustainable management (pp. 1-4). Springer.

National Universities Commission. (2025). Nigerian universities. Abuja, Nigeria: National Universities Commission.

Nwaichi, P. I., Olayiwola, A., Egbe, T. I., Agi, A., Halilu, A., & Nwaichi, E. O. (2025). Future of Triple Helix in Nigeria: Emerging trends and opportunities in university-industry-government collaboration. In E. O. Nwaichi, T. I. Egbe, & A. Halilu (Eds.), Triple Helix Nigeria SciBiz Annual Conference 2024 (pp. 3-25). Springer.

Okpalaoka, C. (2021). Infrastructural challenges in Nigeria and the effect on the Nigerian economy: A review of literature. Environmental and Earth Sciences Research Journal, 8(4), 159-162.

Onoh, C., & Enekwe, P. (2024). Industrialization and economic growth in Nigeria. UBS Journal of Business and Economic Policy, 2(6), 60-72.

Onuh, P., Ejiga, J., Abah, E., Onuh, J., Idogho, C., & Omale, J. (2024). Challenges and opportunities in Nigeria's renewable energy policy and legislation. Journal of Advanced Research, 23, 2354-2372.

ISBN: 978-978-8567-02-8

Oqubay, A. (2025). Introduction to industrial policy and economic development. In Industrial policy and economic development: Theory, strategy, and practice (pp. 1-6). Springer Nature.

Osabutey, E. L., Seny Kan, K. A., Senyo, P. K., Arndt, F., & Röell, C. (2024). Technology transfer potential in local and foreign-owned firms in emerging economies. British Journal of Management, 35(4), 2063-2080.

Osheyor, J., Ezeigweneme, C., Daraojimba, C., Tula, O., Adegbite, A., & Gidiagba, J. (2024). A review of technological innovations and environmental impact mitigation. World Journal of Advanced Research and Reviews, 21, 75-82.

Osunkwo, F. (2025). Transforming Nigeria: Impact of industrialization on economic growth (1981-2024). International Journal of Innovative Research in Education, Technology & Social Strategies, 12(1), 130-143.

Patel, A. (2025). Innovative approaches to sustainable infrastructure: Pioneering research in revolutionary civil engineering. International Journal of Revolutionary Civil Engineering, 1(4), 1-4.

Qureshi, T. I. (2025). Understanding the scaling up of future innovations with techno-economic analysis. Nature Reviews Clean Technology, 1(4), 232.

Rishika, R. (2021). A study on challenges to bridge the gap between academia and industry: With reference to postgraduate courses from industry and students' perspectives. International Journal of Creative Research Thoughts, 9(3), 1256-1263.

Taiwo, R., Ogunsaya, O., Senaya, A.-L., & Sowemimo, A. (2024). Innovative approaches to sustainable civil and structural engineering: Integrating resilient design, material science, and smart technologies. International Journal of Research Publication and Reviews, 5(9), 1835-1846.

Udeala, E. R., Ojiugo, A. R., & Azonwenu, N. S. (2025). Development of sustainable low-cost building materials using locally available resources. Academic World Journal of Scientific and Engineering Innovation, 2(1), 75-86.

Umaru, A., & Adesanya, O. (2024). Transition from a consuming to a producing economy: Recipe for accelerated economic development for Africa. IRE Journals, 8(2), 971-984.

Victor, P. O., Oyedeji, O. C., Victor, A. A., & James, O. A. (2024). Research and development in Nigeria's tertiary institutions: Issues, challenges and way forward. International Journal of Innovative Science and Research Technology, 9(9), 2779-2787.

Zadegan, M. G., Ghazinoory, S., & Nasri, S. (2025). The Triple Helix model of innovation and sustainable development goals: A literature review. Sustainable Development, 33(1), 1482-1497.

Zeidan, S. (2020). An effective framework for bridging the gap between industry and academia. International Journal on Emerging Technologies, 11(3), 454-461.

ISBN: 978-978-8567-02-8

5TH Faculty of Engineering Conference on Engineering Innovation and Economic Policies: Driving Sustainable Industrial Growth in Nigeria

Faculty of Engineering, Bayero University, Kano.

016-Geotechnical Assesment Of Lateritic Soil Stabilized With Gum Arabic

Kevin Omolara Kobdang[1] and Garba Ruqqaya Yunusa[2]

[1,2]*Department of Civil and Environmental Engineering, Air Force Institute of Technology, Mando, Kaduna Nigeria.*

omolara.kelvin@afit.edu.ng Phone Number: 07088185669

Abstract: Lateritic soils are widely used in tropical regions for geotechnical applications but often exhibit unfavorable properties such as moderate plasticity and moisture sensitivity. This study investigates the potential of gum arabic, a natural biopolymer, as an environmentally sustainable stabilizer for lateritic soil. Lateritic soil obtained from Millennium City, Kaduna State, Nigeria, was treated with varying gum arabic contents (0–10% by dry weight of soil). Laboratory tests including natural moisture content, particle size distribution, Atterberg limits, compaction characteristics, and oxide composition were conducted in accordance with relevant British and ASTM standards. Results confirmed the lateritic nature of the soil based on silica–sesquioxide ratio. The addition of gum arabic generally increased the plastic limit and slightly increased the liquid limit, leading to a reduction in plasticity index up to 4–6% content, indicating improved soil stability. Compaction results showed an increase in optimum moisture content and a corresponding decrease in maximum dry density with increasing gum arabic content, attributable to the hydrophilic and particle-coating effects of the biopolymer. An optimum gum arabic content in the range of 2–6% was identified based on plasticity and compaction behavior. The findings demonstrate that gum arabic is a promising low-carbon, eco-friendly stabilizer for improving the engineering performance of lateritic soils in sustainable infrastructure development.

Keywords: Compaction, Atterberg Limit, Gum Arabic, Stabilization, Lateritic, soil

1. INTRODUCTION

Lateritic soils are among the most widely used geomaterials in tropical and subtropical regions, where prolonged leaching and weathering generate iron- and aluminum-rich profiles with distinct engineering characteristics (Gidigasu, 1976). Their abundance has made them indispensable in pavement layers, embankments, earth dams, and low-cost housing projects. However, despite their widespread use, lateritic soils often exhibit undesirable properties such as high plasticity, low bearing capacity, and significant susceptibility to moisture variations, particularly under heavy rainfall or fluctuating groundwater conditions (Osinubi, 1999; Amadi et al., 2015). These limitations frequently lead to premature pavement failure, excessive deformation, and reduced durability in geotechnical structures.

To mitigate these challenges, stabilization has remained a critical aspect of improving the performance of lateritic soils. Conventional stabilizers—including cement, lime, bitumen, and industrial by-products such as fly ash—have demonstrated effectiveness in enhancing soil strength, reducing plasticity, and improving durability (Ingles & Metcalf, 1972; Sherwood, 1993; Little, 1995). However, the use of these additives presents growing concerns. The rising cost of cement and lime, coupled with their high carbon emission footprints and energy-intensive production processes, has motivated the search for cleaner and more economical alternatives (Bahmani & Huat, 2014; Latifi et al., 2017). In addition, the long-term environmental impact of chemical stabilizers has raised questions about sustainability in infrastructural development.

In recent years, biopolymer-based stabilization has emerged as a promising sustainable approach. Biopolymers such as xanthan gum, guar gum, and starch derivatives have been shown to enhance soil cohesion, reduce permeability, and increase strength through physicochemical interactions with soil particles (Chang & Cho, 2019; DeJong et al., 2020). Among these, gum arabic—a natural hydrocolloid derived from *Acacia senegal* and *Acacia seyal*—has attracted interest due to its biodegradability, adhesive strength, hydrophilic nature, and safe environmental profile (Siddig & Osman, 2013). Its polysaccharide-rich composition promotes particle aggregation and bonding, potentially improving the mechanical behaviour of soils treated with small dosages.

Although several studies have demonstrated the influence of gum arabic on the compaction behavior and moisture retention of fine-grained soils (Abdelrahman et al., 2021; Saleh & Bala, 2020), most existing research has focused on sands or clayey soils. Empirical evidence on its interaction with lateritic soils—whose mineralogy,

ISBN: 978-978-8567-02-8

high sesquioxide content, and structural characteristics differ significantly from those of other soil types—remains limited. Furthermore, few studies have systematically evaluated the effects of varying gum arabic contents on the classification properties, plasticity behavior, and compaction characteristics of lateritic soils. This knowledge gap has constrained the adoption of gum arabic in geotechnical practice and limited its consideration as a sustainable soil stabilizer.

This study aims to address these gaps by conducting a comprehensive geotechnical evaluation of lateritic soil stabilized with gum arabic. Specifically, the study examines the effects of gum arabic content on the soil's classification and plasticity characteristics, as well as its compaction behavior in terms of optimum moisture content and maximum dry density. The objective is to assess the viability of gum arabic as a cost-effective and environmentally compatible stabilizer for improving the engineering behavior of lateritic soils in tropical regions.

2. MATERIALS AND METHODS

2.1 Materials

2.1.1 Lateritic Soil

Natural reddish-brown lateritic soil was collected from a borrow pit located in millennium city, Kaduna State, Nigeria. this site was selected because it is a borrow pit frequently used by construction companies to source materials for building and road construction. The soil sample were obtained using a digger and a shovel at a depth of 3.20m. The samples exhibited all the physical and chemical characteristics typical of lateritic soils, including a reddish-brown color, fine-grained texture, and the ability to harden during the dry season.

The samples were collected in 4 cement bags and transported to the school laboratory for various tests. The in-situ moisture content was determined using the oven-drying method before the samples were air-dried for two weeks on corrugated roofing sheets (commonly known as zinc) to ensure complete and uniform moisture removal (achieving zero moisture content).

2.1.2 Gum Arabic

The Gum Arabic used in the stabilization of lateritic soil was obtained from old Panteka market, Kaduna State, Nigeria. Due to the coarse nature of the Gum Arabic, the material was ground and sieved through sieve No 10 (2.00 mm aperture) before being added to the lateritic soil at 0%, 2%, 4%, 6%, 8% and 10% by dry weight of soil.

2.2 Methods

2.2.1 Sample Preparation

Weak lateritic soil samples were mixed properly with varying proportions of Gum Arabic. The mixing process was carried out in a controlled environment to ensure consistency and repeatability. The soil and additives were thoroughly mixed using a mechanical mixer to achieve uniform distribution of the additives within the soil matrix. Subsequently tests were carried out to obtain the optimum stabilizer content for the weak Lateritic.

2.2.2 Natural Moisture Content

The natural moisture content of the Lateritic soil was determined in accordance with Test 1 (A) of BS 1377 (1990). An appropriate weight of the wet lateritic soil was placed in a container of known mass. The lateritic soil plus the container was weighed to the nearest 0.01g, after which they were kept in an oven and allowed to dry at a temperature of 105 to 110 ºC for a period of 24 hours. After drying, the container plus the dry lateritic was weighed again. The moisture content was then calculated using the relationship.

$W = \frac{M2-M3}{M3-M1}$ x 100%

W - Moisture content (%)

M1 - mass of container (g)

M2 - mass of container + wet soil (g)

M3 - mass of container + dry soil (g)

The procedure was repeated three times, from which the average natural moisture content was

determined.

2.2.3 Particle Size Distribution Test

This test was conducted in accordance with ASTM D422 (1992). it was conducted to determine the particle size distribution of a soil sample. It expresses quantitatively the proportion by weight of the various sizes of particles present in the soil.

soil sample of known weight was obtained and sieved using a series of sieves ranging from coarse to fine. The amount of soil retained on each sieve was weighed and recorded. The retained weight is expressed in percentage i.e.

$$\% \, Retained = \frac{weight \, on \, the \, sieve}{Total \, weight \, of \, soil}$$

The result of the coarse and fine analysis is then plotted on a graph, the percentage of various fraction are expressed to the nearest 1% and sieve size.

2.2.4 Atterberg Limits

The liquid limit and plastic limit tests were conducted in accordance with BS1377 (1990) for the untreated and treated lateritic soil

2.2.5 Liquid Limit

The sample for the liquid limit (LL) test was dried sufficiently and broken up; 200 g of the material passing through the 425μm BS test sieve was obtained. The sample was then placed on a clean glass plate, using the palette knife and the spatula the specimen was thoroughly mixed with water until a homogenous paste was obtained. The paste was wrapped in an airtight cellophane bag for not less than 24 hours in order to allow moisture to permeate through the sample. The paste was then placed on the glass plate and mixed thoroughly for some few minutes. Some of the remixed paste was placed in the brass cup of the Casagrande apparatus. After leveling the

ISBN: 978-978-8567-02-8

sample, a standard grooving tool was drawn through the paste along a diameter through the pivot.

The crank was turned to lift drop the cup at a rate of two revolutions per second. The number of blows necessary to close the groove for a distance of 13 mm was recorded after which about 10 g of the paste was immediately taken from the cup for moisture content determination. The procedure was repeated by adding more water to the paste. Thus, the moisture content for each test was increased, the foundry sand flowed more easily and the number of blows for closure of the groove decreased. Four tests were conducted on each batch of the sample for number of blows ranging between 10 and 50. The test was conducted for the specimen at each stepped concentration of BA blend. A graph of moisture content versus number of blows was plotted to a logarithmic scale. The liquid limit was taken as the moisture content that corresponds to 25 blows.

2.2.6 Plastic Limit

About 20 g of dried lateritic soil plus 2% stepwise of gum arabic passing 425µm BS test sieve was placed on a flat glass plate and mixed thoroughly with water until the mixture was plastic enough to be shaped into a small ball. The paste was rolled between the finger and the thumb into 6 mm diameter threads, and then rolled between the fingertips and the glass plate, with sufficient pressure to reduce threads to 3 mm diameter. The procedure was repeated severally until the thread crumbled. Immediately, the moisture content of the crumbled threads was determined. The procedure was repeated two to three times and the moisture content determined from the mean values of the tests. The same procedure was conducted for the soil with varying proportions of gum Arabic.

2.2.7 Plasticity Index

The plasticity index (PI) was determined from the liquid limit and plastic limit results for both the natural and stabilized lateritic soil using the expression:

PI = LL- PL

2.2.8 Compaction British Standard Light

The British Standard light (BSL) tests were conducted in accordance with Test 3 of BS1377 (1990) and BS1924 (1990) for the untreated and treated lateritic soil, respectively.

Approximately 3000g of dried sample that passed the 20mm BS test sieve was thoroughly mixed with 7 – 16 % of water. The soil was then compacted in 3 equal layers. Each layer was given 26 blows of the 2.5 kg rammer falling freely through a height of 300 mm. At the end of compaction, the extension collar was removed and the top of the soil trimmed off by means of a straight edge. The weight of the mould and the compacted soil was determined.

The compacted soil was quickly extruded from the mould and a representative sample was takenfor moisture content determination. The soil was then broken up, re – mixed with more water in order to obtain higher moisture content. The entire process was repeated at least four times within which the optimum moisture content (OMC) and maximum dry density (MDD) were determined by plotting a graph of dry density versus moisture content. The procedure was repeated for the soil mixed with the requisite percentage of gum Arabic. The OMC and MDD test results for varying proportion of gum Arabic were determined.

3. RESULTS AND DISCUSSION

3.1 Oxide Composition of the Lateritic Soil

Table 3.1 shows the oxide composition of the soil used in this research, showcasing the percentage concentration of various metal oxides and non-metal oxides *confirming its lateritic nature.*

TABLE 1: OXIDE COMPOSITION OF THE LATERITIC SOIL

Oxide	Percentage concentration
SiO_2	54.469
V_2O_5	0.161
Cr_2O_3	0.056
MnO	0.089
Fe_2O_3	19.156
CoO	0.072
NiO	0.016
CuO	0.062
Nb_2O_5	0.025
SO_3	0.247
CaO	0.530
K_2O	0.915
CaO	0.530
Al_2O_3	20.180
K_2O	0.915
TiO_2	2.5462
Al_2O_3	0.180
ZnO	0.018
Ta_2O_5	0.042
TiO_2	2.546
Cl	0.891
ZrO_2	0.378

Bell (1993b) quoted that lateritic soils can be defined on the basis of the molecular ratio of silica (SiO_2) to sesquioxides (Fe_2O_3 and Al_2O_3), and also noted that for a soil to be classified as a lateritic soil the value of the ratio gotten should be in the range of 1.33 and 2.00. From the ratio of the values of silica and sesquioxides gotten from table 4.1; SiO_2 = 54.469%; Fe_2O_3 = 19.156% and Al_2O_3 = 20.180% respectively. Using the formula; $SiO_2/(Fe_2O_3 + Al_2O_3)$ and having a value of 1.385 it was concluded that the soil used in this research is a lateritic soil.

3.2 Natural Moisture Content

The natural moisture content of the lateritic soil was recorded as 14.96%, this indicates that the lateritic soil

ISBN: 978-978-8567-02-8

was in a moderately moist and unsaturated state at the time of collection, likely exhibiting a stiff to semi-plastic consistency.

Sunil and Krishnappa (2012) reported a natural moisture content of 14% for a lateritic soil, while Amu et al (2011) in their studied found the natural moisture content to be 10.71%, 14.91% and 14.69% respectively. The slight differences and approximate similar values of these comparison studies can be generally attributed to the soil water retaining capacity (which is as a result of the clay content) lateritic soils with high clay content will tend to hold more moisture as clay particles have a high surface area and are able to retain water more effectively due to capillary action.

3.3 Particle Size Distribution Test

The particle size distribution curve (Figure 3.1) indicates that the soil contains both fine and coarse fractions. According to the AASHTO (1998) system, particles finer than 0.075 mm are classified as fines..

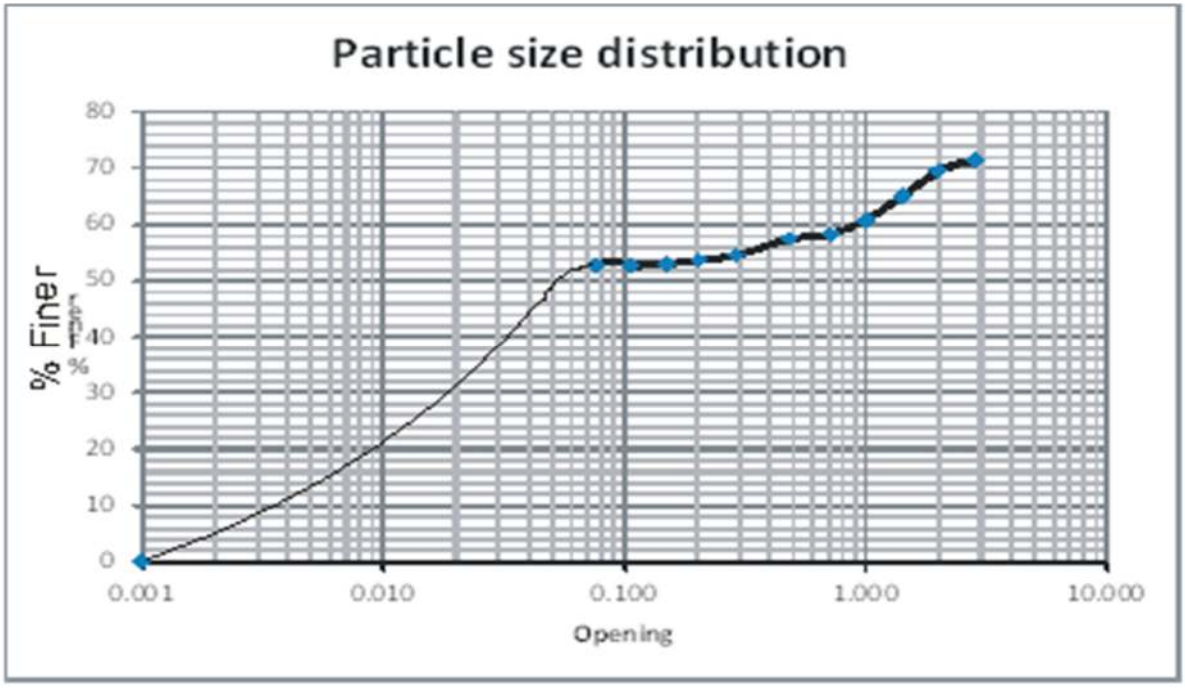


Figure 3.1 Particle Size Distribution

The percentage passing through sieve No 200 (0.075mm) sieve for the lateritic soil sample was 52.86, the lateritic soil was classified as A-7-5 according to AASHTO Classification System and according to USCS, the soil was classified to have a group name of lean clay (Majeed et al., 2020; Singh & Sharma, 2019).

3.4 Atterberg Limits

Table 3.2 shows the result of the Atterberg limit test carried out on the lateritic soil sample and gum arabic

TABLE 3.2: ATTERBERG LIMIT TEST WITH VARIATION OF GUM ARABIC

Gum Arabic (%)	Plastic Limit (%)	Liquid Limit (%)	Plasticity Index (%)	Shrinkage Limit (%)
0	16.63	27.40	10.77	10.01
2	23.66	32.95	9.29	10.43
4	26.15	33.20	7.05	10.43
6	26.76	33.40	6.64	11.43
8	25.95	34.70	8.75	12.14
10	24.94	35.10	10,16	12.14

At 0% gum arabic, the plastic limit was recorded at 16.63%, with a liquid limit of 27.40%, resulting in a plasticity index of 10.77%. The shrinkage limit was measured at 10%. These values suggest that the material exhibited moderate plasticity, which is typical for clayey soils. The plasticity index, an important parameter that indicates the range of moisture content over which the soil remains plastic, provides a clear indication of the soil's behavior under varying moisture conditions (Holtz & Kovacs, 1981). The observed plasticity index at 0% gum arabic suggests that the soil has a reasonable capacity to retain moisture, which can be advantageous in certain engineering applications.

As the concentration of gum arabic increased to 2%, the plastic limit rose to 23.66%, while the liquid limit increased to 32.95%. This resulted in a reduced plasticity index of 9.29 and an increased shrinkage limit of 10.43%. The increase in the plastic limit suggests that the addition of gum arabic enhances the soil's ability to withstand deformation before transitioning into a plastic state. This aligns with findings by Al-Mukhtar et al. (2018), who reported that natural polymers can significantly improve the plasticity characteristics of soils by increasing their cohesion and reducing the friction angle.

ISBN: 978-978-8567-02-8

At 4% gum arabic, the plastic limit increased further to 26.15%, while the liquid limit remained relatively stable at 33.20%. The plasticity index decreased to 7.05, indicating a reduction in the range of moisture content over which the soil remains plastic. This could imply that the soil is becoming less plastic and more stable, which may be beneficial in applications where reduced plasticity is desired, such as in construction and stabilization projects (Ranjbar et al., 2020). The shrinkage limit remained unchanged at 10.43%, suggesting that the addition of gum arabic at this concentration does not significantly affect the soil's volumetric stability under drying conditions.

At 6% gum arabic, the plastic limit was recorded at 26.76%, and the liquid limit slightly decreased to 33.40%. The plasticity index further decreased to 6.64, indicating a consistent trend of reduced plasticity with increasing gum arabic concentration. The stability of the shrinkage limit at 11.43% reinforces the notion that gum arabic may be optimizing the soil's moisture retention capabilities while simultaneously enhancing its structural integrity. This observation is supported by the work of Fityus et al. (2018), who noted that organic additives can lead to improved soil structure and reduced plasticity, which facilitates better load-bearing capacity.

As the concentration of gum arabic reached 8%, the plastic limit decreased to 25.95%, while the liquid limit increased to 34.70%. The plasticity index was recorded at 8.75, indicating a slight increase in plasticity compared to the 6% concentration. This fluctuation could be attributed to the complex interactions between the gum arabic and the soil matrix, which may alter the soil's water retention properties and plastic behavior (Kumar et al., 2021). The shrinkage limit increased to 12.14%, suggesting that higher concentrations of gum arabic may enhance the soil's capacity to resist shrinkage as it dries, which is critical for maintaining structural integrity in engineering applications.

Finally, at 10% gum arabic, the plastic limit was recorded at 24.94%, the liquid limit increased to 35.10%, and the plasticity index was 9.06. The shrinkage limit remained at 12.14%. The observed values at this concentration indicate that while the plastic limit and liquid limit show minor fluctuations, the overall trend suggests that the addition of gum arabic continues to enhance the soil's stability and moisture retention capabilities. The increase in the liquid limit at this concentration indicates that the soil is capable of retaining more water, which may be advantageous in certain environmental conditions (Basha et al., 2009).

In summary, the results of this study demonstrate that the incorporation of gum arabic into soil significantly influences its plasticity characteristics. The observed trends suggest that gum arabic increases PL, slightly increases LL, resulting in a significant decrease in PI up to 4-6%, indicating improved stability. The increase in shrinkage limit (SL) is also positive. The integration of natural polymers like gum arabic into soil stabilization strategies presents a promising avenue for enhancing soil performance while minimizing environmental impact.

3.5 Compaction

Figure 3.2 and 3.3 presents the variation of Optimum Moisture Content (OMC) and Maximum

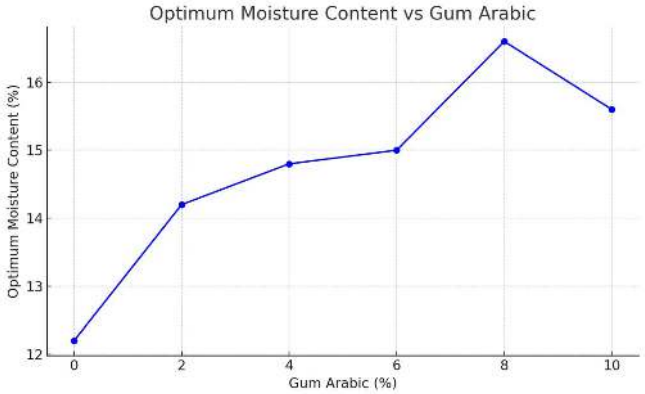


Figure 3.2 Optimum Moisture Content vs Gum Arabic

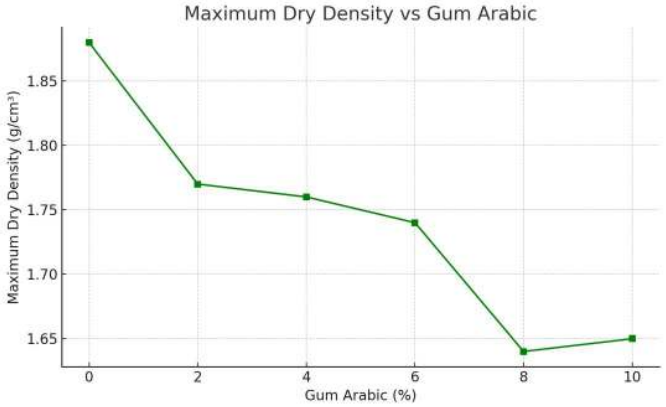


Figure 3.3 Maximum Dry Density vs Gum Arabic

Dry Density (MDD) of a soil sample treated with increasing percentages of Gum Arabic (0–10%). The results clearly indicate that the addition of Gum Arabic substantially influences the compaction characteristics of the soil.

At 0% Gum Arabic, the control sample shows an OMC of 12.01% and a MDD of 1.86 g/cm³. This is typical for untreated soils, where the absence of organic additives allows soil particles to pack efficiently, achieving a high dry density with relatively low moisture. This finding is consistent with the results reported by Amadi et al. (2015), who studied untreated lateritic soils and found MDD values between 1.90 and 1.95 g/cm³ and OMC values ranging from 11% to 13%, suggesting that natural soils without stabilizers tend to achieve maximum density with minimal water. With the introduction of 2% Gum Arabic, the OMC increases sharply to 14.20%, while the MDD decreases to 1.77 g/cm³. This inverse relationship suggests the onset of significant structural changes in the soil due to the additive. The decrease in dry density can be attributed to the coating of soil particles by Gum Arabic, which reduces interparticle friction and specific gravity.

Additionally, the hydrophilic nature of the biopolymer leads to increased water absorption, explaining the rise in

ISBN: 978-978-8567-02-8

OMC. Similar effects were noted by Latifi et al. (2017), who reported that adding 2–4% xanthan gum to clayey soils led to a drop in MDD from 1.88 to 1.83 g/cm³ and a rise in OMC from 13.5% to 15.0%, due to increased water affinity and polymeric interference in particle packing. At 4% Gum Arabic, OMC increased to 14.60% and MDD slightly declining to 1.75 g/cm³.

With 6% Gum Arabic, the OMC rises further to 15.00%, and the MDD drops to 1.79 g/cm³. This indicates the ongoing influence of the hydrophilic polymer on water retention while the soil structure begins to stabilize in terms of compaction. The small change in dry density compared to the previous percentage suggests that a limit is being approached in terms of how much the biopolymer affects packing efficiency. These observations are echoed in Bahmani and Huat (2014), who found that MDD values in biopolymer-treated silty clay soils decreased slightly between 4% and 6% addition, while OMC rose more notably due to increasing polymer hydration. At 8% Gum Arabic, a notable shift occurs: the OMC jumps to 16.20%, and the MDD drops significantly to 1.64 g/cm³. This pronounced reduction in MDD signals a substantial disruption of the soil matrix. At this level, Gum Arabic likely saturates the soil pores, forming a viscous, sponge- like network that increases porosity and impairs close particle contact. The moisture content peaks here, reflecting the biopolymer's maximum water absorption capacity. This mirrors the findings of Bahmani and Huat (2014), who reported that 8% biopolymer-treated soils exhibited the highest porosity and water content, with MDD values dropping from 1.85 to 1.78 g/cm³ and OMC rising above 16%.

At 10% Gum Arabic, the OMC slightly decreases to 15.80%, and the MDD shows a mild recovery to 1.65 g/cm³. This suggests that the soil system has surpassed the optimal polymer concentration, entering a phase of biopolymer saturation. Excess Gum Arabic may begin to stiffen the soil structure or contribute to particle aggregation, thereby enabling a slight increase in dry density. The reduced OMC may indicate that the additional polymer no longer contributes to water absorption as effectively, possibly due to limitations in available surface area or polymer clustering. The result gotten from this experiment suggests that the optimal range for Gum Arabic as a soil stabilizer lies between 2% and 6%, where moisture retention improves workability and hydration without significantly compromising compaction. Beyond this range, particularly at 8% and 10%, the structural integrity of the soil is more adversely affected due to increased porosity and polymer oversaturation.

At 10% Gum Arabic, the OMC slightly decreases to 15.60%, and the MDD shows a mild recovery to 1.65 g/cm³. This suggests that the soil system has surpassed the optimal polymer concentration, entering a phase of biopolymer saturation. Excess Gum Arabic may begin to stiffen the soil structure or contribute to particle aggregation, thereby enabling a slight increase in dry density. The reduced OMC may indicate that the additional polymer no longer contributes to water absorption as effectively, possibly due to limitations in available surface area or polymer clustering. The result gotten from this experiment suggests that the optimal range for Gum Arabic as a soil stabilizer lies between 2% and 6%, where moisture retention improves workability and hydration without significantly compromising compaction. Beyond this range, particularly at 8% and 10%, the structural integrity of the soil is more adversely affected due to increased porosity and polymer oversaturation.

4. CONCLUSION

Based on the laboratory investigation, the following conclusions are drawn:

1. The lateritic soil was classified as A-7-5 (clayey soil) under AASHTO and CL (Lean clay)under the USCS.

2. The lateritic soil obtained for this practical was found to have NMC of 14.96%, LL of 26.70%, PL of 15.93% and SL of 10.00% as its index properties.

3 The Atterberg limits results show that the addition of Gum Arabic increased the liquid limit and plastic limit, while generally reducing the plasticity index up to 4–6% addition, indicating improved workability and reduced soil plasticity. The shrinkage limit also increased with Gum Arabic content, suggesting reduced volumetric instability and better resistance to shrinkage.

4 From oxide composition test (chemical test), the major oxides present was found to be SiO_2, Fe_2O_3, and Al_2O_3 with a percentage concentration of 54.469%, 19.156% and 20.180% respectively.

5 Compaction results revealed a progressive increase in Optimum Moisture Content (OMC) with increasing Gum Arabic content, accompanied by a corresponding decrease in Maximum Dry Density (MDD). Peak modification of soil behavior was observed at approximately 8% Gum Arabic, where the highest OMC and lowest MDD were recorded. Overall, Gum Arabic proved to be an effective and environmentally sustainable soil modifier, enhancing the workability, moisture retention, and dimensional stability of lateritic soil, with potential application in low-load geotechnical and subgrade improvement works.

REFERENCES

AASHTO. (1986). Standard Specifications for Transport Materials and Methods of Sampling and Testing. American Association of State Highway and Transport Officials (AASHTO), Washington, D.C, 14th Edition.

ASTM (1992). Annual Book of Standards Vol. 04.08, American Society for Testing and Materials, Philadelphia.

Al-Mukhtar, M., Al-Humoud, J., & Al-Mutairi, N. (2018). Effects of natural polymers on the engineering properties of clayey soils. *Journal of Materials in Civil Engineering*, 30(5), 04018032

Eberemu, A. O. (2015). Compressibility Characteristics

ISBN: 978-978-8567-02-8

of Compacted Lateritic Soil Treated with Bagasse Ash. *Jordan Journal of Civil Engineering*, *9*(2).

Amu, O. O., Fajobi, A. B., & Oke, B. O. (2005). Effect of eggshell powder on the stabilizing potential of lime on an expansive clay soil. *Research journal of Agriculture and biological sciences*, *1*(1), 80-84.

Bahmani, S. H., & Huat, B. B. K. (2014). Influence of organic polymer on engineering properties of clay soils. Arabian *Journal for Science and Engineering, 39(6), 3993–4000*

Basha, E. A., Hashim, R., & Mahmud, H. (2009). Stabilization of residual soils using gum arabic. *Geotechnical Testing Journal*, 32(4), 309-317.

Bell, F. (1996). Lime stabilization of clay minerals and soils. *Engineering geology*, *42*(4), 223-237.

British Standard Institution, Methods of test for soils for civil engineering purposes, BS 1377–1990: Part 2 and 4; 1990.

British Standard Institution, Stabilized materials for civil engineering purposes, BS 1924–1990: Part 2 – Section 4; 1990

Fityus, S. G., Kwan, C., & O'Neill, S. (2018). The effects of organic additives on the engineering properties of clay soils. *Soils and Foundations*, 58(2), 345-357.

Gidigasu, M. (Ed.). (2012). *Laterite soil engineering: pedogenesis and engineering principles* (Vol. 9). Elsevier.

Holtz, R. D., Kovacs, W. D., & Sheahan, T. C. (1981). *An introduction to geotechnical engineering* (Vol. 733). Englewood Cliffs, NJ: Prentice-hall.

Ingles, O. G., & Metcalf, J. B. (1972). *Soil stabilization principles and practice* (Vol. 11, No. Textbook).

Kumar, S., Singh, R. K., & Gupta, A. (2021). Influence of natural polymers on the plasticity and compaction characteristics of clayey soils. *International Journal of Civil Engineering and Technology*, 12(2), 124-134.

Latifi, N., Marto, A., Eisazadeh, A., & Mohamad, E. T. (2017). Effect of biopolymer on shear strength and stiffness of silty clay. *Arabian Journal for Science and Engineering,* **42**, 157–163.

Little, D. N. (1995). *Stabilization of pavement subgrades and base courses with lime*.

Majeed, A., Jamil, M., & Khan, M. (2020). The role of natural polymers in soil stabilization: A review. *Construction and Building Materials*, 262, 120-134.

Osinubi, K. J. (1999). Evaluation of lateritic soils modified with cement and lime admixtures for use as base course material. *Nigerian Journal of Technology, 18(1), 62-72.*

Ranjbar, N., Khosravi, A., & Mohammadi, H. (2020). The impact of biopolymers on the engineering behavior of soils: A review. *Applied Clay Science*, 189, 105533.

Siddig, A. M., & Osman, M.M (2013). Composition and properties of gum Arabic. *Food Science and Technology, 10(2),23-30*

Sunil, B. M., & Krishnappa, H. (2012). Effect of drying on the index properties of lateritic soils. *Geotechnical and Geological Engineering*, *30*(4), 869-879.

Singh, A., & Sharma, R. (2019). Effects of biopolymers on the engineering properties of clayey soils: A review. *Journal of Rock Mechanics and Geotechnical Engineering*, 11(5), 1006-1015.

ISBN: 978-978-8567-02-8

017-What Drives Clean Mobility? Evidence from Three Secondary Cities in Northeastern Nigeria

Mohammed Ya'u[1], Aminu Suleiman[2]

[1]*Department of Civil Engineering Technology, The Federal Polytechnic, Damaturu.* katamma300@gmail.com
[2]*Department of Civil Engineering, Faculty of Engineering, Bayero University Kano, Nigeria.*
asuleiman.civ@buk.edu.ng

Abstract: Secondary cities in Africa are emerging fronts for sustainable development, yet their mobility dynamics remain poorly understood. This study addresses this gap by examining travel behaviour and readiness to adopt sustainable transport in Maiduguri, Damaturu, and Gombe. Survey data were analysed using descriptive statistics, chi-square tests, and binary logistic regression. The results show striking differences across the three cities. Maiduguri reports high car ownership and a newer vehicle fleet. Damaturu displays a strong long-distance commuting culture and consistent vehicle maintenance. Gombe relies heavily on fuel-efficient cars and public transport. Chi-square analysis reveals significant associations between gender and mode choice in both Damaturu and Gombe, indicating clear socio-demographic effects on mobility behaviour. Logistic regression shows that environmental consciousness is a key driver of willingness to switch in Gombe, approaching significance (Exp(B) = 3.436, p = 0.065), with a weaker effect in Damaturu. These patterns align with the Theory of Planned Behaviour, highlighting the roles of attitudes and perceived control in shaping mobility choices. The study concludes that uniform transport policies are unlikely to work. Sustainable mobility strategies must be tailored to the unique social and infrastructural contexts of individual secondary cities.

Keywords: Sustainable Transportation, Socio-Demographic Factors, Urban Mobility, Nigeria, travel behaviour.

1. INTRODUCTION

Increased urbanisation and economic growth in sub-Saharan Africa are contributing to heightened carbon emissions and environmental deterioration (Abdulqadir, 2024; Erdoğan et al., 2022). Urbanisation and fossil fuel usage add to emissions, but renewable energy presents a viable decarbonisation pathway (Erdoğan et al., 2022). The transportation sector significantly contributes to increased emissions, representing 15% of total energy consumption in sub-Saharan Africa in 2018. Electric vehicles offer the potential to reduce emissions and improve air quality, although their adoption remains limited (Collett et al., 2021). In Ghana, transport emissions increased by 75% from 2000 to 2016, accompanied by heightened congestion and pollution (Agyemang et al., 2023). Policymakers must prioritise the development of sustainable and accessible transportation systems, invest in renewable energy technologies, and regulate urbanisation within specified limits to attain environmental and economic sustainability (Abdulqadir, 2024; Agyemang et al. 2021; Erdoğan et al., 2022).

Sustainable transport is therefore a global and regional priority, especially as African cities confront the combined pressures of rapid growth, climate risk, and rising energy demand.

Recent studies emphasise the intricate transportation issues in African cities. In Lagos, traffic congestion has an adverse impact on air quality, leading to elevated pollution levels of CO and PM2.5 during peak hours (Ajayi et al., 2023). Innovations such as electric vehicles, automated transport, and ride-sharing present opportunities for low-carbon transitions in cities like Johannesburg, Kigali, Lagos, and Nairobi; nevertheless, they encounter both drivers and obstacles to adoption (Sovacool et al., 2022). These developments possess both positive and negative aspects, necessitating a multifaceted evaluation. Moreover, consumers with disabilities in Nigeria encounter distinct obstacles regarding transport accessibility and pricing, influencing their decisions based on their capabilities and available alternatives (Mogaji et al., 2023). These studies highlight the necessity for holistic mobility solutions that tackle environmental issues, technological progress, and inclusivity for all urban inhabitants in African cities.

However, much of this research is centred on Africa's large metropolitan areas, leaving secondary cities largely overlooked despite their rapid population growth and rising travel demand.

Although megacities like Lagos are the focus of mobility studies, secondary cities such as Maiduguri, Damaturu, and Gombe are inadequately examined despite their increasing transportation needs and environmental impacts.

ISBN: 978-978-8567-02-8

These secondary cities represent the fastest-growing urban zones in many African regions, yet their mobility systems remain understudied. Addressing this gap is essential for designing effective and equitable transport policies.

Investigations on sustainable mobility inside African urban areas reveal numerous obstacles and prospects. Substandard infrastructure, safety issues, and insufficient amenities impede active transportation modes such as walking and cycling (Basil & Nyachieo, 2022). Cultural attitudes and ambitions about car ownership impede the implementation of sustainable mobility. Nonetheless, there are existing advantages, such as elevated rates of active transportation and minimal private car utilisation among marginalised populations (Oviedo et al., 2024). Financial constraints and socioeconomic obstacles significantly restrict transportation accessibility. To tackle these difficulties, research advocates for cohesive planning policies that acknowledge the interconnections among health, transportation, and equity (Brugulat-Panés et al., 2023). Enhancing capacity at institutional, individual, and environmental levels is essential for the advancement of active travel policies and their execution (Lartey & Glaser, 2024). Moreover, participatory urban frameworks can facilitate research and policy formulation about non-motorised transportation (Basil & Nyachieo, 2022).

Research consistently demonstrates that socioeconomic factors substantially affect mobility decisions, especially in urban environments. Gender significantly influences women's active transport habits, which vary according to socioeconomic level, education, and available infrastructure. Women of lower socioeconomic status often walk more out of necessity, whereas those with higher socioeconomic status and education are more inclined to cycle (Yuan et al., 2023). Macedo et al. (2022) identified systematic disparities in mobility diversity associated with gender and socioeconomic factors across South American cities. In the Middle Eastern, North African, and South Asian regions, movement decisions are influenced by demographic and socioeconomic considerations, cultural norms, and climatic circumstances (Chaudhry et al., 2022). The research highlights that mobility patterns are significantly contextual, shaped by a complex interaction of personal, social, and environmental factors. Mitigating these inequities necessitates focused initiatives and policies to foster equitable urban mobility.

A strong foundation for comprehending intentions to adopt environmentally friendly modes of transportation is offered by the Theory of Planned Behaviour (TPB). According to several studies, intentions to utilise public transportation or travel in a low-carbon manner are favourably influenced by attitudes, subjective norms, and perceived behavioural control (Ali et al., 2023). The best indicator of intent is always attitudes. Attitudes and intentions are greatly influenced by moral commitments and environmental concerns (Cariera et al., 2023). Travel patterns, perceived value, and travel cost consciousness are additional factors that influence decisions regarding sustainable transportation (Ali et al., 2023; Liao et al., 2023). Sustainable transportation decisions can be positively impacted by customised trip plans that include feedback on CO_2 emissions, calories burned, and cost savings. In order to encourage the adoption of sustainable transportation, these findings provide policymakers and transportation operators with insightful information (Ali et al., 2023; Mosca et al., 2024).

Given its focus on attitudes, norms, and perceived behavioural control, TPB is well suited for examining behavioural drivers in emerging secondary cities.

The Theory of Planned Behaviour (TPB) (Ajzen, 1991) serves as the foundation for this study, stating that attitudes, subjective norms, and perceived behavioural control all have an impact on behavioural intentions. The use of TPB provides a thorough framework for investigating the variables influencing secondary cities in Nigeria's inclination to switch to sustainable modes of transportation.

This paper aims to examine urban mobility patterns and the variables affecting the northeastern Nigerian region's adoption of sustainable transportation. In particular, the study aims to:

1. examines the modes of transportation, car ownership patterns, and commuting habits of Maiduguri, Damaturu, and Gombe.
2. explores the connections between socioeconomic factors and mode choice.
3. uses logistic regression analysis to evaluate the predictors of the willingness to switch to sustainable transportation.
4. suggests policy measures tailored to the unique circumstances of each city.

By providing a comparative analysis of three secondary cities in northeastern Nigeria, this study fills a critical gap in African mobility research and highlights the behavioural and socioeconomic factors shaping the transition toward sustainable transport.

2. METHODOLOGY

The study utilised a cross-sectional household survey carried out in the cities of Maiduguri, Damaturu, and Gombe. The necessary sample size was determined using Cochran's formula at a 95% confidence level, yielding a minimum of 384 respondents per urban area to ensure population representativeness. Participants were selected using simple random sampling methods to reduce bias and include a varied range of socio-economic backgrounds. Although the predetermined sample criterion was met, the number of returned and valid questionnaires varied among the cities, with 326 completed in Maiduguri, 346 in Damaturu, and 360 in Gombe.

To determine the reliability and validity of the research instrument, the questionnaire underwent a two-stage validation process. Content validity was first assessed by experts in urban mobility and transport

ISBN: 978-978-8567-02-8

planning, who evaluated clarity, relevance, and completeness. A pilot study was then conducted with 40 respondents outside the study locations to test internal consistency and ease of understanding. Cronbach's alpha values ranged from 0.72 to 0.84 across the main scales, confirming acceptable reliability. Insights from the pilot were used to refine item phrasing and ordering.

The survey instrument collected data on demographic variables (including gender, income, and education), mobility and transportation characteristics (such as vehicle ownership, fuel type, commuting distance, and maintenance practices), modal preferences (covering both primary and secondary transportation modes), and perceptions related to comfort, safety, cost-effectiveness, and awareness of environmental benefits.

The data analysis incorporated statistical techniques that were both descriptive and inference-based. Descriptive statistics offered an extensive overview of transport and socio-economic attributes across the three urban sites. Chi-square tests were utilised to examine the correlations between socio-demographic characteristics and modal choices, with the strength of these associations measured using Cramer's V. Furthermore, binary logistic regression models were developed for each city to clarify the determinants affecting the propensity to choose sustainable transportation alternatives. The dependent variable in the model was coded as a binary outcome: 1 for respondents willing or undecided about switching, and 0 for those not willing to switch. This grouping reflects a distinction between respondents expressing a positive or neutral intention toward sustainable transport adoption and those expressing a clearly negative intention, consistent with intention-based behavioural modelling, where undecided individuals are considered potentially receptive to change. Statistical significance was set at $p < 0.05$.

3. RESULTS

3.1 Respondents' Demographic Characteristics

Table I shows the demographic features of respondents surveyed in Maiduguri, Damaturu, and Gombe. The age distribution reveals that a substantial segment of respondents in all three urban areas is comprised of individuals aged 21–30 years and 31–40 years. Individuals aged 21 to 30 constituted 44.8% of respondents in Maiduguri, 48.7% in Damaturu, and 43.6% in Gombe, reflecting a notable prevalence of younger individuals in the studied sample. The proportion of elderly respondents, defined as those over 60 years of age, was low, varying from 1.4% in Gombe to 2.1% in Maiduguri. Conversely, individuals aged 51–60 years were more prominently represented in Damaturu (12.4%) compared to Maiduguri (8.9%) and Gombe (5.6%).

The distribution of gender differs among the geographical research locations. Males constituted the predominant demographic in all examined regions, with a significant percentage of 79.5% in Damaturu, in contrast to 62.3% in Maiduguri and 56.7% in Gombe. Female representation reached its apex in Gombe at 43.3% and its worst in Damaturu at 20.5%.

An even distribution of single and married respondents was noted across the cities. In Maiduguri, single individuals constituted 44.5% of respondents, marginally surpassing married individuals, whilst in Damaturu, the percentage of single respondents was 47.1%. Gombe exhibited a nearly equal distribution, with single respondents constituting 46.7% and married respondents comprising 46.4%. Divorced or widowed persons constituted a small fraction in all three urban centres, generally comprising less than 6% of the overall sample.

In terms of household composition, respondents with a minimum of one child were the majority in all three regions. The proportion of respondents without children was significantly greater in Damaturu (47.1%) and Gombe (46.7%) than in Maiduguri (25.8%). In Maiduguri, households with 1 to 3 children comprised 35.3% of the population, a figure that exceeded that of other places. Larger households with seven or more children exhibited a more consistent distribution, ranging from 12.2% in Gombe to 13.9% in Damaturu.

The findings reveal that the responder population is predominantly youthful, with substantial segments in child-rearing age categories.

TABLE I: RESPONDENTS' DEMOGRAPHIC INFORMATION ACROSS MAIDUGURI, DAMATURU, AND GOMBE

Variable	Categories	Maiduguri (Freq,%) (n=326)	Damaturu (Freq,%) (n= 346)	Gombe (Freq, %)(n=360)
Age	Below 20 Years	29 (8.9%)	67 (19.4%)	69 (19.2%)
	21–30 Years	146 (44.8%)	167 (48.7%)	157 (43.6%)
	31–40 Years	75 (23.0%)	42 (12.1%)	70 (19.4%)
	41–50 Years	40 (12.3%)	21 (12.1%)	39 (10.8%)
	51–60 Years	29 (8.9%)	43 (12.4%)	20 (5.6%)
	Above 60 Years	7 (2.1%)	6 (1.7%)	5 (1.4%)
Gender	Male	206 (62.3%)	275 (79.5%)	204 (56.7%)
	Female	120 (35.9%)	71 (20.5%)	156 (43.3%)
Marital Status	Single	145 (44.5%)	163 (47.1%)	168 (46.7%)
	Married	141 (43.3%)	128 (57.2%)	167 (46.4%)
	Divorced	25 (7.7%)	20 (5.8)	20 (5.6%)
	Widowed	4 (1.2%)	…	5 (1.4%)
	Others	10 (3.1%)	…	…
	Missing	1 (0.3%)	…	…
Children	0 Children	84 (25.8%)	163 (47.1%)	168 (46.7%)
	1–3 Children	115 (35.3%)	99 (28.6%)	80 (22.2%)
	4–6 Children	73 (22.4%)	36 (10.4%)	64 (17.8%)
	7+ Children	42 (12.8%)	48 (13.9%)	44 (12.2%)
	Missing	12 (3.7%)	…	…

3.2 Socio-economic well-being

Table II provides an overview of the socioeconomic attributes of respondents from Maiduguri, Damaturu, and

ISBN: 978-978-8567-02-8

Gombe. A significant portion of respondents indicated monthly earnings below ₦30,000, with Gombe showing a markedly higher percentage (44.7%) compared to Maiduguri (35.3%) and Damaturu (32.9%). The representation of higher income brackets (exceeding ₦60,000) was more significant in Damaturu (35.3%) compared to Maiduguri (24.2%) and Gombe (25.6%). This divergence indicates differences in purchasing power that may influence the affordability and likelihood of adopting active transportation methods.

Educational attainment was high across all surveyed areas, with a majority of respondents holding at least post-secondary qualifications. In Maiduguri, individuals with Bachelor's degrees, diplomas, or equivalent certifications represented over half of the population at 51.5%. In Damaturu, this figure was higher at 61.6%, while Gombe recorded nearly half at 48.3%. The proportion of respondents holding postgraduate degrees was modest, ranging from 6% to 12%. In contrast, individuals without formal education were primarily located in Maiduguri, accounting for 11% compared to other urban centres.

Employment status demonstrated considerable variation among the analysed locations. Maiduguri exhibited a more balanced distribution across employment categories, while Damaturu recorded a greater percentage of students (35%) compared to the other cities. In contrast, Gombe exhibited higher rates of unemployment (19.7%) and part-time employment (16.7%). The demographic of retired individuals represented a small proportion of the respondents in the three regions. The patterns of economic engagement provide essential context for assessing the impact of occupational status and income stability on participation in active transportation.

Lifestyle and health indicators highlight significant differences among the populations. The prevalence of non-smoking was significant in all three cities, with Damaturu exhibiting the lowest percentage of smokers at 91.3%, followed by Gombe at 87.8% and Maiduguri at 79.8%. The overall health status was largely positive, with most respondents assessing their health as good or excellent. Respondents from Damaturu exhibited the highest proportion of excellent health at 56.6%, followed by Gombe at 53.1% and Maiduguri at 46.9%. Reports of poor health were limited.

The data reveal a youthful, educated, and largely healthy respondent demographic, though notable disparities exist in income distribution, employment participation, and lifestyle practices across the three cities. The socioeconomic variables, specifically income, employment engagement, smoking behaviours, and health status, are expected to significantly impact the willingness to switch to active and sustainable transport modes.

Table II: Respondents' Socioeconomic Well-being

Variable	Categories	Maiduguri (Freq,%) (n=326)	Damaturu (Freq,%) (n= 346)	Gombe (Freq, %)(n=360)
Monthly Income	Below ₦30,000	115 (35.3%)	114 (32.9%)	161 (44.7%)
	₦30,001 – ₦40,000	61 (18.7%)	42 (12.1%)	73 (20.3%)
	₦41,000 – ₦60,000	66 (20.25%)	68 (19.7%)	34 (9.4%)
	Above ₦60,000	84 (25.75%)	122 (35.3%)	92 (25.6)
Educational Level	No Formal Education	36 (11.0%)	17 (4.9%)	29 (8.1%)
	SSCE	68 (20.9%)	73 (21.1%)	74 (20.6%)
	Bachelor's/HND/Diploma/NCE	168 (51.5%)	213 (61.6%)	174 (48.3%)
	Master's Degree	38 (11.7%)	21 (6.1%)	44 (12.2%)
	PhD or Higher	14 (4.3%)	20 (5.8%)	…10 (2.8%)
	Missing	2 (0.6%)	2 (0.6%)	29 (8.1%)
Employment Status	Employed Full-Time	114 (35.0%)	115 (33.2%)	103 (28.6%)
	Employed Part-Time	68 (20.9%)	33 (9.5%)	60 (16.7%)
	Unemployed	66 (20.2%)	58 (16.8%)	71 (19.7%)
	Student	55 (16.9%)	121 (35%)	87 (24.2%)
	Retired	19 (5.8%)	15 (4.3%)	5 (1.4%)
	Missing	4 (1.2%)	4 (1.2)	29 (8.1%)
Smoking Habit	Non-smoker	260 (79.8%)	316 (91.3%)	316 (87.8%)
	Occasional Smoker	44 (13.5%)	12 (3.5%)	20 (5.5%)
	Regular Smoker	14 (4.3%)	18 (5.2%)	15 (4.2%)
	Missing	8 (2.5%)	…	…
Health Status	Excellent	153 (46.9%)	196 (56.6%)	191 (53.1%)
	Good	134 (41.1%)	147 (42.5%)	144 (40 %)
	Fair	22 (6.7%)	3 (0.9%)	25 (6.9%)
	Poor	3 (0.9%)	…	…
	Missing	14 (4.3%)	…	…

3.3 Mobility and Transport Characteristics

Figure 1 provides an in-depth analysis of urban mobility trends, considering factors such as car ownership, vehicle attributes, commuting behaviours, and secondary mode utilisation.

ISBN: 978-978-8567-02-8

The three urban centres exhibit significant disparities in transportation trends. Car ownership is highest in Maiduguri (42.0%) and lowest in Gombe (28.6%), but non-ownership is notably considerable throughout all three cities, particularly in Gombe (62.2%). Petrol is the primary fuel type in urban areas, with Gombe (91.3%) demonstrating the most dependence, while Maiduguri offers a broader array of fuel types, including notable proportions of electric (9.6%) and diesel (14%). The age distribution of cars exhibits considerable variation. Maiduguri has a higher percentage of newer cars (71% under 5 years), whereas Gombe and Damaturu primarily consist of older cars, with the majority being over 6 years old.

Fuel consumption patterns reveal notable disparities: Gombe possesses the highest proportion of highly fuel-efficient vehicles (68.9% achieving consumption rates of 1–10 litres/100 km), while Damaturu demonstrates increased fuel intensity, with 57.6% consuming between 11–20 litres and 22% exceeding 21 litres. The daily travel distances exhibit diversity, with long-distance travel (31+ km) being predominant in Damaturu (33.9%) relative to Maiduguri (16.8%) and Gombe (29.6%).

The car maintenance culture is most pronounced in Damaturu, where 80.3% of respondents report monthly servicing, in contrast to 55.8% in Maiduguri and 32% in Gombe. The primary modes of transportation reveal notable trends: private automobiles dominate in Gombe (40.6%), tricycles in Damaturu (45.1%), while Maiduguri shows a more even distribution of private vehicles (37.9%) and tricycles (26.3%).

Travel frequency reveals a tendency for infrequent and short trips in Maiduguri, where 49.8% of individuals undertake merely 1–2 daily visits. In contrast, Damaturu and Gombe exhibit a preference for more frequent travel, with 51.7% and 47.5% of residents, respectively, making 3–4 travels. Active transport modes are most prevalent in Damaturu at 53.8%, followed by Maiduguri at 47.3% and Gombe at 43.3%. All three cities exhibit engagement with motorised and public transport alternatives outside the dominant mode; nevertheless, reliance on public transport is most pronounced in Gombe, with a continuous rate of 49.7%.

Maiduguri has significant car ownership and a contemporary vehicle fleet; Damaturu showcases widespread commuting practices and a robust maintenance culture; Gombe is distinguished by its dependence on fuel-efficient vehicles, private automobiles, and public transit systems.

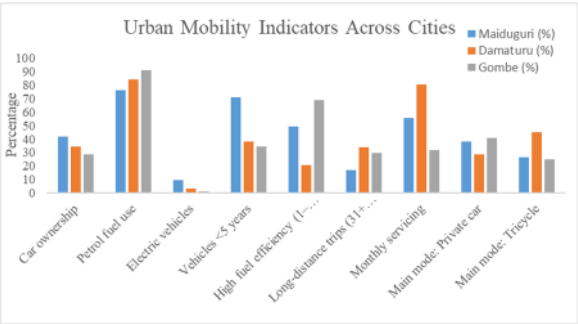


Figure 10: Cities Respondent Response on Mobility and Transportation

3.4 Socioeconomic Correlates of Sustainable Transition

Chi-square analysis indicates varying correlations between income levels and the willingness to transition. No statistically significant association was found in Maiduguri ($\chi^2 = 11.87 < 16.919$, $p = 0.217$; Cramer's $V = 0.133$). In contrast, Gombe ($\chi^2 = 65.9$, $p < 0.001$; Cramer's $V = 0.247$) and Damaturu ($\chi^2 = 20.51$, $p = 0.002$; Cramer's $V = 0.172$) demonstrated significant, though modest, associations. These data indicate that income has a greater impact on the development of sustainable mobility preferences in Gombe and Damaturu than in Maiduguri.

TABLE III: CHI-SQUARE TEST OF INCOME AND SUSTAINABLE TRANSITION

City	χ^2	df	p-value	Cramer's V	Interpretation
Maiduguri	11.87	10	0.217	0.133	Weak, not significant
Damaturu	20.51	10	0.002	0.172	Weak but significant
Gombe	65.90	10	<0.001	0.247	Weak but significant

The correlation between gender and modal choice was deemed insignificant in Maiduguri ($\chi^2 = 1.45$, $p = 0.963$; Cramer's $V = 0.07$), while it was significant in Gombe ($\chi^2 = 35$, $p < 0.001$; Cramer's $V = 0.313$) and Damaturu ($\chi^2 = 19.22$, $p = 0.004$; Cramer's $V = 0.236$), reflecting moderate associations. This indicates that sociocultural factors exert a more significant influence on mode preferences in Gombe and Damaturu.

TABLE IV: CHI-SQUARE TEST OF GENDER AND MODE CHOICE

City	χ^2	df	p-value	Cramer's V	Interpretation
Maiduguri	1.451	6	0.963	0.07	No significant relationship
Damaturu	19.22	6	0.004	0.236	Significant and moderate correlation
Gombe	35.00	6	<0.001	0.313	Significant and moderate correlation

3.5 Logistic Regression Insights

Logistic regression analysis clarifies the determinants affecting the likelihood of adopting sustainable transportation. In Damaturu, the acknowledgement of environmental benefits was identified as the primary predictor (Exp(B) = 3.436, $p = 0.065$), followed by the degree of educational attainment (Exp(B) = 2.078, $p = 0.066$). Factors such as comfort and income had a detrimental effect, although gender did not show a statistically significant influence. Similar tendencies were observed in Gombe, where awareness significantly influenced the willingness to switch ($p = 0.02$), while in

ISBN: 978-978-8567-02-8

Maiduguri, none of the variables reached statistical significance at the usual level.

TABLEV: BINARY LOGISTIC COEFFICIENTS ON WILLINGNESS TO SWITCH TO SUSTAINABLE MODES

Predictor Variable	Maiduguri (B, Exp(B), Sig.)	Damaturu (B, Exp(B), Sig.)	Gombe (B, Exp(B), Sig.)
Gender	0.54,1.714, 0.13	-18.1,0.00, 0.996	0.63,1.87, 0.14
Monthly Income	0.33, 1.39, 0.06	-0.80, 0.45, 0.08	0.3, 1.35, 0.15
Educational Level	-0.15, 0.86, 0.46	0.73, 2.08, 0.07	-0.08, 0.92, 0.64
Car Ownership	0.22, 1.246, 0.56	-14.99, 0.00, 0.99	0.72, 2.08, 0.18
Primary Mode	0.1, 1.1, 0.83	-13.69, 0.00, 0.99	-0.21, 0.81, 0.17
Comfort	-0.15, 0.86, 0.39	-2.1, 0.12, 0.06	0.3, 1.35, 0.53
Safety	-0.56, 0.56, 0.21	0.05, 1.05, 0.97	-0.03, 0.97, 0.95
Cost-effectiveness	0.06, 1.1, 0.89	-0.29, 0.7, 0.744	-0.91, 0.4, 0.136
Awareness of Environmental Benefit	0.39, 1.48, 0.11	1.23, 3.44, 0.07	0.64, 1.897, 0.02
Constant	…	43.263, — , 0.992	-5.25, — , 0.002

Note: B = regression coefficient, Exp(B) = odds ratio, Sig. = significance level (p-value).

3.6 Preferred CO_2 Reduction Measures

When asked about possible solutions, the most common response from participants in all urban centres (up to 74% in Gombe) was to improve public transport. This was followed by support for electric vehicles and active transportation. Car sharing and awareness efforts were given somewhat less priority; however, Damaturu showed a relatively high level of support for awareness activities (36.9%). This emphasises the need for infrastructure-based solutions as well as their potential to support programs meant to promote behavioural change.

TABLE VI: PREFERRED SOLUTIONS ACROSS THE CITIES

Solution	Maiduguri (%)	Damaturu (%)	Gombe (%)
Improve public transport	68.2	70.5	74.0
Promote active transport	52.1	49.3	55.4
Electric vehicles	21.4	18.7	23.1
Car sharing	12.8	15.4	11.6
Awareness campaigns	28.5	36.9	22.7

3.6 Discussion

Urban mobility patterns in northeastern Nigeria remain diverse and shaped by local conditions. Maiduguri stands out due to high car ownership and widespread use of modern vehicles. This pattern signals a strong potential for the uptake of electric vehicles and, to some extent, active travel. Damaturu shows long commuting distances and frequent vehicle maintenance needs, which point to the absence of dependable and affordable public transport. Gombe depends heavily on fuel-efficient cars and shared transport. This suggests that targeted awareness campaigns may support a gradual shift towards cleaner mobility.

3.6.1 Attitude

The findings reinforce the central role of attitudes within the Theory of Planned Behaviour. Environmental awareness emerged as one of the strongest drivers of willingness to adopt sustainable modes, particularly in Gombe and Damaturu. People who recognised the long-term environmental benefits showed greater openness to change. These observations align with the research of Ciocîrlan and Rowe (2025), who emphasised the significant role of awareness and perceived benefits in shaping sustainable transportation behaviours.

An interesting contrast appears in Maiduguri, where awareness did not significantly predict willingness to shift modes. High car ownership may reflect a strong cultural preference for private vehicles as symbols of convenience and social status. Such norms can weaken the influence of environmental attitudes, even when awareness is present.

3.6.2 Subjective Norms

Patterns in Damaturu and Gombe highlight the influence of social expectations. Gender differences were notable, with men and women displaying distinct transport preferences. These differences align with broader social norms in the region, where mobility behaviour is often shaped by safety concerns, cultural expectations, and differing daily responsibilities, as demonstrated by Pourhashem et al. (2022) and Borker (2024). The results suggest that what is viewed as an "appropriate" travel mode varies across gender lines. Subjective norms therefore provide a useful lens for interpreting these behavioural tendencies.

3.6.3 Perceived Behavioural Control

Perceived behavioural control also shaped mobility choices. Comfort and cost acted as major barriers that limited the feasibility of switching to sustainable modes. In Damaturu, comfort showed a negative relationship with willingness to adopt alternative transport. People who prioritised comfort felt less capable of making such a shift. Cost concerns added another layer, especially in cities where incomes are low and transport alternatives are limited. These constraints signal that behavioural change depends not only on motivation but also on the practical conditions that make new choices possible. These findings affirm the findings of multiple studies that perceived behavioural control directly influences the

ISBN: 978-978-8567-02-8

likelihood of choosing sustainable mobility options (Nogueira et al., 2023; Tazzieet al., 2024)

4. Conclusion

This study shows that mobility behaviour in Nigeria's secondary cities is shaped by local socio-economic and behavioural conditions. Environmental consciousness remained a strong predictor of willingness to adopt sustainable modes, reinforcing the usefulness of the Theory of Planned Behaviour. The three cities, however, display distinct mobility profiles. Maiduguri shows strong potential for electric vehicle uptake. Damaturu faces long commuting distances and weak public transport. Gombe presents the clearest opportunity for awareness-led behavioural change.

For policymakers, the key message is that context must guide intervention. A single solution will not work across these cities. In Maiduguri, investment in electric vehicle infrastructure and better active travel connections should be prioritised. In Damaturu, the urgent task is to strengthen public transport to improve comfort, reliability, and affordability. In Gombe, sustained awareness campaigns, combined with modest transit upgrades, can accelerate the move toward cleaner mobility.

Overall, the findings stress that sustainable urban transport in northeastern Nigeria requires strategies that combine awareness, accessibility, and affordability. Tailored actions, aligned with the realities of each city, offer the most practical path toward long-term behavioural change and cleaner mobility systems.

References

Abdulqadir, I. A. (2024). Urbanization, renewable energy, and carbon dioxide emissions: a pathway to achieving sustainable development goals (SDGs) in sub-Saharan Africa. *International Journal of Energy Sector Management, 18*(2), 248-270.

Agyemang, E., Anderson, B., Owusu, K., Quinchía, J. P., & Trémolières, M. (2023). *Ensuring sustainability via accessible transport systems for all in Accra and Kumasi*. E3S Web of Conferences

Ajayi, S. A., Adams, C. A., Dumedah, G., Adebanji, A. O., & Ackaah, W. (2023). The impact of traffic mobility measures on vehicle emissions for heterogeneous traffic in Lagos City, Scientific African, Volume 21, e01822, ISSN 2468-2276.

Ajzen, I. (1991). The theory of planned behavior. *Organizational behavior and human decision processes, 50*(2), 179-211.

Ali, N., Nakayama, S., & Yamaguchi, H. (2023). Using the extensions of the theory of planned behavior (TPB) for behavioral intentions to use public transport (PT) in Kanazawa, Japan. *Transportation research interdisciplinary perspectives, 17*, 100742.

Basil, P., & Nyachieo, G. (2022). Exploring barriers and perceptions to walking and cycling in the Nairobi metropolitan area. Frontiers in Sustainable Cities 4, 775340.

Borker, G. (2024). Understanding the constraints to women's use of urban public transport in developing countries. *World Development, 180*, 106589.

Brugulat-Panés, A., Randall, L., de Sá, T. H., Anil, M., Kwan, H., Tatah, L., . . . Micklesfield, L. (2023). The potential for healthy, sustainable, and equitable transport systems in Africa and the Caribbean: a mixed-methods systematic review and meta-study. *Sustainability, 15*(6), 5303.

Cariera, D., Joewono, T. B., & Belgiawan, P. F. (2023). The Influence of Attitudes, Subjective Norms, and Perceived Behavioral Control of Commuter Intentions to Use Public Transportation in Greater Bandung, Indonesia. *The Asian Journal of Technology Management (AJTM), 16*(1), 13-31.

Chaudhry, A. G., Masoumi, H., & Dienel, H. L. (2022). A systematic literature review of mobility attitudes and mode choices: MENA and South Asian cities. Frontiers in Sustainable Cities, 4.

Ciocîrlan, A.-B., & Rowe, R. (2025). On the road to sustainability: Applying an extended Theory of Planned Behaviour model to energy-saving transportation practices. *Plos one, 20*(6), e0325196.

Collett, K. A., Hirmer, S. A., Dalkmann, H., Crozier, C., Mulugetta, Y., & McCulloch, M. D. (2021). Can electric vehicles be good for sub-Saharan Africa? Energy Strategy Rev. 38, 100722.

Erdoğan, S., Onifade, S. T., Altuntaş, M., & Bekun, F. V. (2022). Synthesizing urbanization and carbon emissions in Africa: how viable is environmental sustainability amid the quest for economic growth in a globalized world? *Environmental Science and Pollution Research, 29*(16), 24348-24361.

Lartey, D., & Glaser, M. A. (2024). Towards a sustainable transport system: exploring capacity building for active travel in Africa. *Sustainability, 16*(3), 1313.

Liao, C., Huang, Y., Zheng, Z., & Xu, Y. (2023). Investigating the factors influencing urban residents' low-carbon travel intention: A comprehensive analysis based on the TPB model. *Transportation research interdisciplinary perspectives, 22*, 100948.

Macedo, M., Lotero, L., Cardillo, A., Menezes, R., & Barbosa, H. (2022). Differences in the spatial landscape of urban mobility: gender and socioeconomic perspectives. *Plos one, 17*(3), e0260874.

Mogaji, E., Bosah, G., & Nguyen, N. P. (2023). Transport and mobility decisions of consumers with disabilities. *Journal of Consumer Behaviour, 22*(2), 422-438.

Mosca, O., Lauriola, M., Manunza, A., Mura, A. L., Piras, F., Sottile, E., . . . Fornara, F. (2024). Promoting a sustainable behavioral shift in commuting choices: The role of previous intention and "personalized travel plan" feedback. *Transportation Research Part F: Traffic Psychology and Behaviour, 106*, 55-71.

Nogueira, M., Dias, F., & Santos, V. (2023). Sustainable mobility choices: Exploring the impact of consumers' values, attitudes, perceived behavioural control and subjective norms on the likelihood to choose sustainable mobility options. *Journal of Consumer Behaviour, 22*(2), 511-528.

ISBN: 978-978-8567-02-8

Oviedo, D., Cavoli, C., Yusuf, Y., Koroma, B., & Chong, A. Z. W. (2024). Everyday accessibility practices and experiences in a context of transitions to sustainable mobility: Qualitative evidence from Sub-Saharan Africa. *International Journal of Sustainable Transportation, 18*(4), 328-343.

Pourhashem, G., Malichová, E., Piscová, T., & Kováčiková, T. (2022). Gender difference in perception of value of travel time and travel mode choice behavior in eight European countries. *Sustainability, 14*(16), 10426.

Sovacool, B. K., Daniels, C., & AbdulRafiu, A. (2022). Transitioning to electrified, automated and shared mobility in an African context: A comparative review of Johannesburg, Kigali, Lagos and Nairobi. *Journal of Transport Geography, 98*, 103256.

Tazzie, Y. D., Adugna, D., Woldetensae, B., Fryd, O., & Ingvardson, J. B. (2024). Exploring the factors hindering the intention to adopt sustainable transportation options in Addis Ababa, Ethiopia: using structural equation modeling. *Frontiers in Sustainable Cities, 6*, 1435705.

Yuan, Y., Masud, M., Chan, H., Chan, W., & Brubacher, J. R. (2023). Intersectionality and urban mobility: A systematic review on gender differences in active transport uptake. *Journal of transport & health, 29*, 101572.

ISBN: 978-978-8567-02-8

5TH Faculty of Engineering Conference on Engineering Innovation and Economic Policies: Driving Sustainable Industrial Growth in Nigeria

Faculty of Engineering, Bayero University, Kano.

018-Durability Assessment of Lightweight Concrete Incorporating Sawdust Ash and Coconut Shell Using Response Surface Methodology

M. A. Yaqub*, A. M. Gora, S. M. Zakariya, A. M. Shettima

Department of Civil Engineering, Faculty of Engineering, Bayero University, Kano, 3011, Nigeria
Corresponding Author Email: amyaqub.civ@futb.edu.ng

Abstract: This research aimed to develop lightweight concrete by partially replacing cement with sawdust ash (SDA) and Coarse aggregate with Coconut shell(CNS).Response Surface Methodology(RSM) was employed to design the experiments and develop a prediction models for key concrete properties, including slump, water absorption, weight loss, and residual compressive strength under hydrochloric acid attack. The effects of Sawdust Ash (0–8%) and Coconut Shell (0–40%) replacement Levels on the fresh and Durability properties of lightweight concrete were examined using a central composite design. Results indicate that higher percentage of SDA and CNS reduces the concrete's fresh and durability properties. Significant correlations were identified in the responses, which were successfully predicted by RSM generated quadratic models. Multi-Objective Optimization identified the ideal combination of 2% SDA and 10% CNS, which maximized the workability (126.5mm), and minimized water absorption at 14 Days (5.01%) and at 28 Days (9.21%), Acid attack at 14 Days (13.1MPa) and at 28 Days (19.602MPa) with an overall desirability of 75.1%. Experimental validation confirmed that the discrepancy between predicted and actual results was less than 5%. The novelty of this study lies in the combined use of SDA as a pozzolanic cement replacement and CNS as lightweight Coarse aggregate optimized via RSM specifically for enhanced Durability against acid attack-an approach rarely explored together in prior literature. The findings demonstrate the potential of SDA-CNS lightweight concrete as a sustainable, affordable, and environmentally friendly construction Materials with applicability extending beyond Nigeria to other regions worldwide where similar Agricultural wastes (Sawdust and Coconut shells) are abundantly available.

Keywords: *Sawdust Ash, Coconut Shell, Response Surface Methodology, Durability property and lightweight concrete.*

1. INTRODUCTION

Limited studies have explored the combined use of Sawdust ash (SDA) as a partial cement replacement and coconut shell (CNS) as a lightweight coarse aggregate in concrete, particularly with a focus on durability against acid attack. Furthermore, the application of Response Surface Methodology (RSM) for multi-objective optimization of fresh properties (e.g Water absorption and residual strength under hydrochloric acid exposure) in such agro-waste-based lightweight concrete remains underexplored, especially in the context of sustainable construction for resourced-limited regions. This gap highlights the need for integrated experimental and statistical approaches to validate viable mix proportions that balance performance, cost, and environmental benefits. Concrete is a premier construction material around the world and most widely used in all types of construction works, like infrastructure, low and high-rise buildings and domestic development. With increased population and modern living habits, production of waste material increased at fast pace and its disposal has become a genuine problem. To minimize the waste, we can utilize the waste material for some positive activity (Rakesh et al, 2022) .There is need for affordable building materials in providing adequate housing for the teeming population of the world. The cost of conventional building materials continue to increase as the majority of the population continues to fall below the poverty line. Thus, there is the need to search for local materials as alternatives for the construction of functional but low-cost buildings in both the rural and urban areas. Currently, research efforts have been geared towards sourcing, development and the use of local alternative construction materials including the possibility of using some agricultural wastes and residues as construction materials. Some investigations made shown that it is possible to produce concrete using agricultural, urban and industrial wastes material, (Elinwa and Abdulkadir, 2011), (Madakson et al, 2012). Hence the focus of this research is to investigate the use of sawdust ash and coconut shell as cement and aggregate in concrete through experimental investigation.

Cement industry is one of the major environmental pollution sources as it consumes a lot of energy during production. It releases CO which leads to global warming and other pollutants. To minimize the pollution to some extent, new method is proposed i.e., replacement of cement with wood by-products (Sawdust ash) which plays a significant role acting as pozzolanic material (Siddique, et al, 2020). Sawdust poses an irritation to

ISBN: 978-978-8567-02-8

both health and environment man and animals lives when not properly managed. It has pozzolanic properties that react chemically with the calcium hydroxide on loose from hydration of Portland cement to form cement compounds. On the other hand, coconut shell as aggregates reduces the waste produced due to coconut shells. These are lightweight materials and so, they produce lightweight concrete. Nowadays, price of building materials are raising day by day as concrete is used rapidly. Cement and Coarse aggregates are part of the most important materials in the concrete and the rate of their inflation is growing day in day out. Sawdust and Coconut shell Usage as cement and aggregates respectively, reduces their presence as waste materials (Batool et al, 2021), (Manoj et al, 2021) is research is aimed at developing a lightweight concrete using sawdust ash as partial replacement of cement and coconut shell as coarse aggregate replacement. This study also determined the optimum percentage replacement of Sawdust ash as cement and the coconut shell as aggregate in Grade M_{25} concrete without compromising the fresh and durability properties of the lightweight concrete. Sawdust ash and coconut shell are used in percentagewise ranging from 0-8% sawdust ash replacement and 0-40% coconut shell replacement in the concrete. Characterization of the materials was observed alongside the Engineering properties of the lightweight concrete materials. Response surface method was used to develop an optimized SDA-CNS-concrete mixture and establish models for predicting the fresh and durability properties.

2. MATERIALS AND METHOD

2.1 Materials

Ordinary Portland cement manufactured in Nigeria as Dangote brand has been selected for this experimental investigation with grade 42.5N, the river sand used as fine aggregate was procured within Kano state Nigeria. Sieve analysis and specific gravity of the aggregates were also determined in accordance with (BS 1881). The coarse aggregate used for this research were typically angular in shape, well graded for conventional concrete. Water used for this research was obtained from the laboratory tap adequate for the experiment.

The sawdust used in this research was procured in a nearby sawing mill in Kano state Nigeria. It was sundried for 10 days to remove excess moisture to aid the burning process. The samples were burnt openly and then sawdust Ash was obtained at a control temperature ranging from 600◦C-630◦C for 2hrs. The ash was allowed to cool before sieving through sieve 75 µm and the retained material was used for the experiment. The characterization test and specific gravity test for the sample was observed in accordance with (BS 1881).
Coconut shells used in this study were brought from local coconut market. The coconut shells were sundried for five days and grinded mechanically with the aid of 30kg hammer to achieve similar aggregate sizes. The broken pieces were sieved through 12.5mm sieve and those retained on 10 mm sieve were used. The characterization test, sieve analysis, specific gravity test of the coconut shell were expound respectively.

The sieve analysis results of the coconut shell, coarse and a fine aggregate is presented in Figure1 below.
The specific gravity test on SDA, CNS, fine aggregate and coarse aggregate were conducted in accordance with BS EN 12620 (2013), the result obtained were 2.03, 1.18, 2.59 and 2.34 respectively using equation 1 below.

$$SG = \frac{w2-w1}{(w4-w1)-(w3-w2} \quad \textbf{(1)}$$

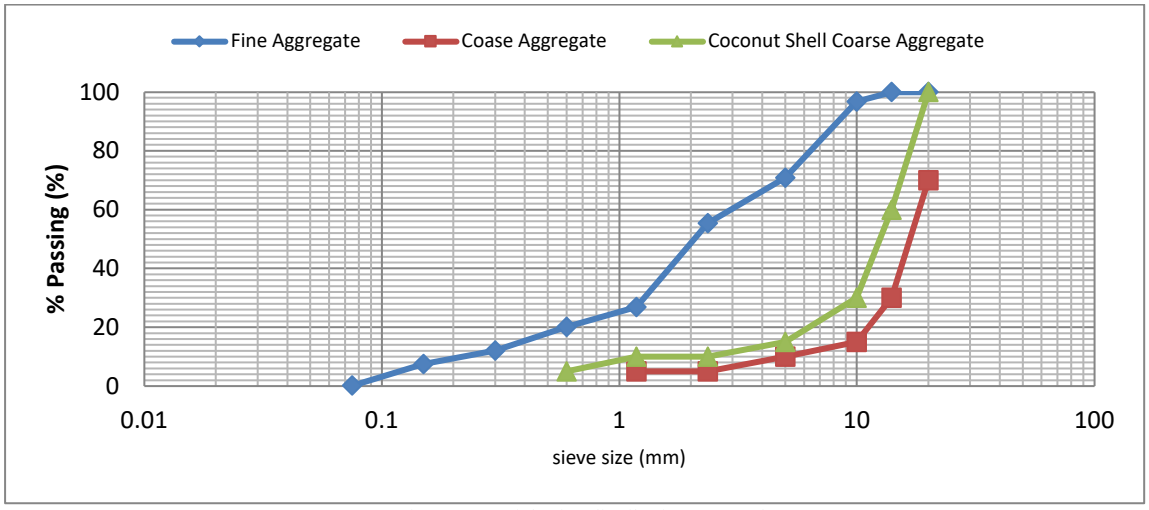


Figure 1: Particle size distribution curve of Aggregates

2.2 Mix Design

Response Surface Methodology analysis was used to establish appropriate portions of cement, Sawdust Ash, Coconut shell, coarse aggregate, fine aggregate and water to obtain the desirable workability and durability properties of the lightweight concrete. The concrete's mix proportion was formulated using the principles specified in the building research establishment (BRE) mix design method (Formerly known as the DOE method). In this study, Response Surface Methodology analysis was performed using Design Expert version 13 to develop a statistical model of lightweight concrete modified with Sawdust Ash and Coconut Shell using a central composite design, (Elinwa, 2003) (Elinwa and Abulkadir 2011). Sawdust Ash and Coconut Shell serving as independent variables at Five (5) levels correspond to each parameter: 0% to 8% Sawdust Ash in place of cement and likewise, the percentages of coarse

ISBN: 978-978-8567-02-8

aggregate contents were substituted by Coconut shell in 0% to 40%, respectively, (Adamu et al, 2021), (Adamu et al, 2020), (Adamu et al, 2022)

TABLE I. THE MIX PROPORTION OF CONCRETE MATERIALS BASED ON RSM ANALYSIS

MIX ID	Cement (Kg/m^3)	F Agg (Kg/m^3)	C Agg (Kg/m^3)	W/C ratio (kg/m^3)	SDA (Kg/m^3)	CNS (Kg/m^3)
mix 1 (0SDA0CNS)	554.4	577.5	1312	180.26	0.0	0.0
mix 2 (6SDA10CNS)	521.1	577.5	1180.8	180.26	33.3	131.2
mix 3 (4SDA20CNS)	532.2	577.5	1049.6	180.26	22.2	262.4
mix 4 (6SDA30CNS)	521.1	577.5	918.4	180.26	33.3	393.6
mix 5 (4SDA40CNS)	532.2	577.5	787.2	180.26	22.2	524.8
mix 6 (2SDA30CNS)	543.3	577.5	918.4	180.26	11.1	393.6
mix 7 (2SDA10CNS)	543.3	577.5	1180.8	180.26	11.1	131.2
mix 8 (0SDA20CNS)	554.4	577.5	1049.6	180.26	0.0	262.4
mix 9 (4SDA20CNS)	532.2	577.5	1049.6	180.26	22.2	262.4
mix 10 (4SDA20CNS)	532.2	577.5	1049.6	180.26	22.2	262.4
mix 11 (4SDA20CNS)	532.2	577.5	1049.6	180.26	22.2	262.4
mix 12 (8SDA20CNS)	510.0	577.5	1049.6	180.26	44.4	262.4
mix 13 (4SDA20CNS)	532.2	577.5	1049.6	180.26	22.2	262.4
mix 14 (4SDA0CNS)	532.2	577.5	1312	180.26	22.2	0.0

3. RESULT AND DISCUSSION

3.1 Slump Test Result

The higher slump values in SDA-CNS mixes can be attributed to the pozzolanic activity of sawdust (SDA), which refines the pore structure, and the smoother surface of coconut shell (CNS) particles leading to better particle packing and reduced water demand for plasticization.Figure 2 presents the slump values of a concrete mixture containing different SDA and CNS contents. It can be noted that the combined effects of SDA and CNS increase the workability of a concrete mixture as reflected in Mix 1 (0SDA0CNS), Mix 5 (4SDA40CNS) and Mix 6 (2SDA30CNS) with slump values close to that of the control mix. Conversely, Mix 2 (6SDA10CNS), which included 6% of SDA and 10% CNS have a slump value of 110 mm, whereas Mix 14 (4SDA0CNS), which contained 4% SDA and 0% CNS have a slump value of 115 mm which was less than the control mix's slump of 145 mm. Conversely, compared to the control mix, the remaining mixes had lower slump values and the results clearly show that compared to the control concrete mix, the SDA-CNS concrete mixes exhibited a higher slump. The little increase in slump might be attributed to CNS's particle packing effect, which reduces the amount of water required for plasticization, (Khalid et al, 2024) Furthermore, it was proven by (Babatunde, 2023) that the SDA and CNS particle parking effect of voids in the hydration product is perhaps the primary influencing factor(Montgomery, 2013), (Manoj et al, 2021).

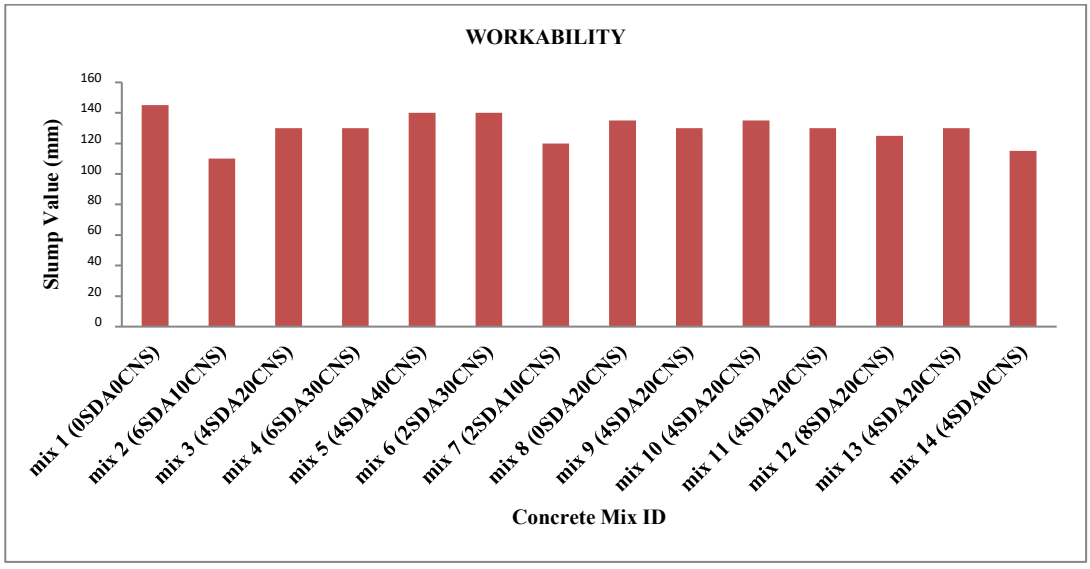


Figure 2: Slump Result

3.2 Water absorption

The durability performance of SDA-CNS concrete mixes containing SDA and CNS was also assessed using water absorption test; the findings are shown in Figure 3. The percentage of SDA and CNS content was shown for each mix. Mix 1 (0SDA0CNS) for example, which contains 0% SDA and 0% CNS, has a water absorption

ISBN: 978-978-8567-02-8

value of 12.5% at 14 days and 6.4% at 28 days. On the other hand, Mix 7 (2SDA10CNS), which includes 2% SDA and 10% CNS had a water absorption capacity of 9.4% at 14 days and 4.9% at 28 days, while Mix 14 (4SDA0CNS) which contains 4% SDA and 0% CNS, demonstrated a water absorption capacity of 8.1%. The water absorption capacity value of Mix 14 (4SDA0CNS) was the greatest surpassing that of the control mix (6.4%). The results clearly show that the water absorption rate rises as the percentage replacement of a larger amount of SDA and a lesser percentage of CNS increases. Moreover, as comparison to Mix 1 (control mix), the water absorption rate falls with a larger proportion of CNS and a smaller proportion of SDA. This might be explained by the high specific surface area of CNS, which would raise the water requirement, and its low specific gravity, which results in a decrease in mass per unit volume (Mageswari, 2010), (Maheswari, 2016).

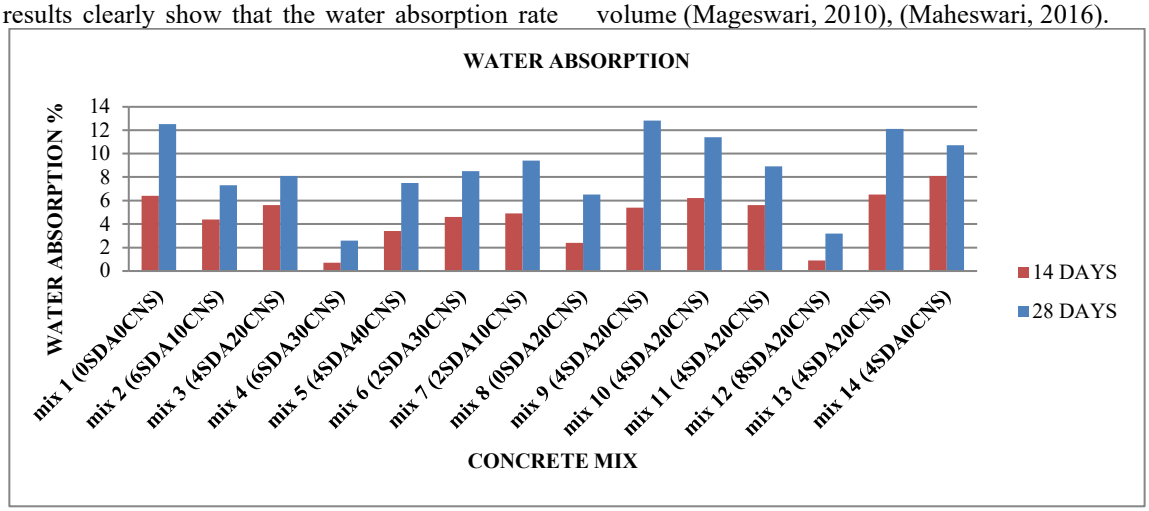


Figure 3: Water Absorption Result

3.3 Resistance to hydrochloric acid (HCl) media

The compressive strengths of concrete containing various portions of SDA and CNS tested at 14- and 28-days curing ages are shown in Figure 4. The results indicated that all concrete samples experience an increase in compressive strength with age regardless of their replacement amount. The compressive strength of the control sample (Mix 1: 0SDA0CNS) at 14 and 28 days were found to be 17.83 and 18.77 MPa, respectively. Mix 8 concrete samples with 0% SDA and 20% CNS have the highest compressive strength at 14 and 28 days, which were 17.84 MPa and 24.96 MPa respectively. Conversely, Mix 5 which contains 4% SDA and 40% CNS revealed the lowest compressive strength of 13.65 MPa and 19.1 MPa at 14, and 28 d of curing age respectively. The lower strength of Mix 5 was attributed to the negative effect of SDA which decrease the compressive strength and the lower CNS content and was unable to mitigate the loss of strength in the mix. The compressive residual strength of concrete samples exposed to acidic media is shown in Figure 4. The figure clearly shows that the concrete samples' compressive residual strength significantly drops as the acid exposure period increases. The results clearly demonstrate that at 14 and 28 days, the control concrete sample showed a decrease of compressive residual strength ranging from 23 N/mm^2 to 15 N/mm^2. Conversely, the compressive residual strength of SDA-CNS concrete sample with mix ID 4 decreased from 15.91 N/mm^2 to 10.15 N/mm^2. Figure 4 illustrates the loss in compressive residual strength for SDA-CNS concrete samples exposed to acidic media. It also makes it evident that as the immersion period increased the samples' compressive residual strength which was greatly affected by the acidic conditions (Ayuba, 2022), (Maheswari, 2016).

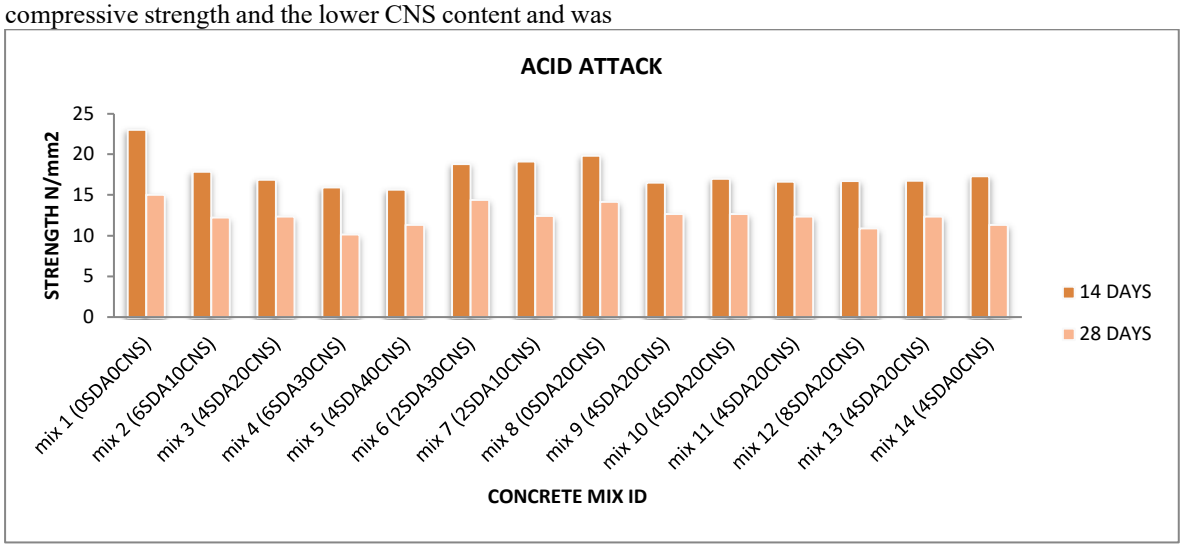


Figure 4: Resistance to Hydrochloric Acid (HCl) media

ISBN: 978-978-8567-02-8

3.4 Analysis of variance for Durability property

A summary of the variance analysis for durability responses are shown in Table II. Acidic attack and water absorption of SDA-CNS concrete were all predicted using a fitted quadratic model that was generated using regression analysis. The model was chosen from the highest-order polynomial where the additional terms were important and the program did not alias.

TABLE II. ANOVA RESULT OF DURABILITY PROPERTIES MODELS.

Response	Source	Sum of Squares	Mean Square	F-Value	p-Value	Remark
Acid Attack At 14 Days	Model	16.09	3.22	53.01	< 0.0001	Significant
	A-SDA	10.23	10.23	168.62	< 0.0001	
	B-CNS	0.0021	0.0021	0.0348	0.8573	
	AB	4.06	4.06	66.89	< 0.0001	
	A^2	0.0922	0.0922	1.52	0.2576	
	B^2	1.57	1.57	25.85	0.0014	
	Lack of Fit	0.2862	0.0954	2.75	0.1766	Not Significant
Acid Attack At 28 Days	Model	18.20	3.64	35.81	< 0.0001	Significant
	A-SDA	9.16	9.16	90.14	< 0.0001	
	B-CNS	2.65	2.65	26.06	0.0014	
	AB	0.6320	0.6320	6.22	0.0414	
	A^2	5.66	5.66	55.64	0.0001	
	B^2	3.916E-06	3.916E-06	0.0000	0.9952	
	Lack of Fit	0.5815	0.1938	5.96	0.0587	Not Significant
Water Absorption at 14 Days	Model	53.88	10.78	31.40	0.0001	Significant
	A-SDA	5.32	5.32	15.49	0.0056	
	B-CNS	14.17	14.17	41.30	0.0004	
	AB	2.89	2.89	8.42	0.0229	
	A^2	31.19	31.19	90.91	< 0.0001	
	B^2	0.0317	0.0317	0.0924	0.7700	
	Lack of Fit	1.53	0.5099	2.34	0.2148	Not Significant
Water Absorption at 28 Days	Model	96.61	19.32	7.36	0.0104	Significant
	A-SDA	20.06	20.06	7.64	0.0280	
	B-CNS	12.82	12.82	4.88	0.0629	
	AB	3.61	3.61	1.37	0.2794	
	A^2	58.96	58.96	22.45	0.0021	
	B^2	4.30	4.30	1.64	0.2415	
	Lack of Fit	1.53	0.5114	0.1214	0.9428	Not Significant

3.5 Multi-objective optimization and validation

A numerical optimization was conducted using the desirability function approach which is frequently used in multi-objective optimization scenarios, to determine the ideal mix proportions of SDA and CNS for improved concrete durability. The goal of this study's optimization was to determine the best mix of independent factors to produce a SDA-CNS concrete mixture that minimizes acid attack and water absorption while maximizing the mechanical properties and the workability. To optimize the responses and capture all possible solutions, all parameters were established within a certain range. Table III defines the multi-objective optimization constraints for the variables and responses. According to the optimization findings, if the ratios are maintained within the statistically established ideal range, a partial substitution of cement with 2% SDA and coarse aggregate with 10% CNS can produce significant increases in the fresh, mechanical and durability of concrete. In addition to helping to conserve resources and reduce waste, this approach supports the development of sustainable building materials. Using the optimized mixture ratios shown in Table III, a second series of laboratory tests was carried out to confirm the sufficiency of the optimization data retrieved from the Design-Expert program and all of the response models. The latter step was done to ensure that the proportions of the optimized mixture were accurate. Three specimens were produced for each test parameter, and the mean values of each were reported. After 28 days, results were evaluated and contrasted with the predicted results. Using Equation (2) (Khalid *et al*, 2024), the discrepancy between the experimental and predicted results was computed.

$$\varepsilon = 1 - \frac{y}{x} \times 100 \qquad (2)$$

Where (Y) stand as $Predicted\ value$ and (X) as $Experimental\ value$ for each of the responses that were taken into consideration, Table III displays the RSM predicted findings together with the corresponding experimental data. With an average percentage error of less than 5%, the computed percentage errors showed that the actual results and predicted results agreed well.

ISBN: 978-978-8567-02-8

TABLE III: MULTI-OBJECTIVE CRITERIA AND OUTCOMES OF THE OPTIMIZATION.

Variables and responses	Units	Criteria for optimization			Results and verification		
		Desired goal	*Lower limit*	*Upper limit*	*Predicted result (Y)*	*Experimental result (X)*	*Error (ε)(%)*
SDA	*%*	In range	0	8	2	2	-
CNS	*%*	In range	0	40	10	10	-
Slump	*mm*	Maximize	110	140	123.405	126.543	2.479789
Acid attack at 14 Days	*MPa*	Minimize	10.15	14.37	12.465	13.102	4.861853
Acid attack at 28 Days	*MPa*	Minimize	15.65	19.84	18.856	19.602	3.805734
Water absorption at 14	*%*	Minimize	0.7	8.1	4.930	5.010	1.596806
Water absorption at 28 Days	*%*	Minimize	2.6	12.8	9.091	9.210	1.29207
Desirability	*%*				75.1 (%)		

4. CONCLUSIONS

Conclusively, the following takeaways were extracted from the research as follows:

i. A higher replacement amount of SDA and CNS results in a more workable concrete mix. The remarkable rise in slump might perhaps be ascribed to the particle packing effect of CNS, which decreases the water content needed for plasticization.

ii. Concrete samples with higher SDA and CNS replacement levels absorbed more water and are less resistant to acid, due to the increased pore volume and permeability. Higher CNS replacement level and longer exposure to acidic medium resulted in a general decrease in the strength. The proposed RSM quadratic models for water absorption and acid attack showed good predictability, demonstrating their use for predicting the durability behavior of the produced concrete.

iii. The RSM-based optimization produced the optimal mix of 2% SDA (replacement of cement) and 10% CNS (replacement of coarse aggregate), maximizing workability(126.5mm), then minimizing water absorption at 14 Days(5.01%) and at 28 Days(9.21%) and Acid attack at 14 Days(13.1MPa) and at 28 Days(19.602MPa) with 75.1% desirability. The experimental validation of this result revealed that the discrepancy between the predicted and experimental results was less than 5%. This indicates the potential of SDA-CNS lightweight concrete.

REFERENCE

Adamu, M. P. Trabanpruek, P. Jongvivatsakul, S. Likitlersuang, M. Iwanami, "Mechanical performance and optimization of high-volume fly ash concrete containing plastic wastes and graphene nanoplatelets using response surface methodology" Constr. Build. Mater. 308 (2021), 125085.

Adamu, M. S.S. Olalekan, M.M. Aliyu, " Optimizing the mechanical properties of pervious concrete containing calcium carbide and rice husk ash using response surface methodology" J. Soft Comput. Civ. Eng. 4 (2020) 95–118.

Adamu, M. S.I. Haruna, Y.E. Ibrahim, H. Alanazi, "Evaluation of the mechanical performance of concrete containing calcium carbide residue and nano silica using response surface methodology" Environ. Sci. Pollut. Res. (2022) 1–27.

Ayuba, S., Uche, O. A., Haruna, S., & Mohammed, A. 2022. Durability properties of cement–saw dust ash (SDA) blended self-compacting concrete (SCC). Nigerian Journal of Technology, 41(2), 212-221.

Babatunde S. A , M. A Onugba and F. A Olutoge (2023) 'Effect of Sawdust and Coconut Shell on the Mechanical Properties of Concrete'Volume 25, Issue 8, Page 1-8, 2023; Article no.JERR.104893 ISSN: 2582-2926

Batool F, Islam K, Cakiroglu C, Shahriar A. Effectiveness of wood waste sawdust to produce medium- to low-strength concrete materials. Journal of Building Engineering. 2021;44(103237): 1-12.DOI:https://doi.org/10.1016/j.jobe.2021.103fh237

ISBN: 978-978-8567-02-8

BS 1881-122:2011 Testing concrete. Method for determination of water absorption, British Standards Institution—Publication Index | NBS. (n.d.).
Retrieved September 15,2023,fromhttps://www.thenbs.com/PublicationIndex/documents/details?Pub=BSI&DocID=29793.

BS 1881, part 102, Method for Determination of Slump in Concrete, London: British Standard Institution, 1983.

Elinwa A.U and Abdulkadir S., (2011). "Characterizing Saw Dust Ash for Use as an InhibitorforReinforcement Corrosion". New Clues in Sciences, 1, 1 -10.

Elinwa, A.U. (2003). "Timber ash as pozzolana in concrete", Unpublished Ph.D These, Department of Civil engineering, ATBU, Bauchi.

Khalid, A.A.; Gora, A.M.; Rafindadi, A.D.; Haruna, S.I.; Ibrahim, Y.E. Response Surface Methodology Approach for the Prediction and Optimization of the Mechanical Properties of Sustainable Laterized Concrete Incorporating Eco-Friendly Calcium Carbide Waste. Infrastructures 2024, 9, 206. https://doi.org/10.3390/ infrastructures9110206

Madakson P. B., Yawas, D. S. and Apasi, A. (2012). "Characterization of coconut shell ash for potential utilization in matrix composites for automotive application". International journal of Engineering science and technology (IJEST) 4(30)

Mageswari M. and Vidivelli B., (2010). "The Use of Sheet Glass Powder as Fine Aggregate Replacement in Concrete". The Open Civil Engineering Journal, 4, 65 – 71.

Maheswari, (2016). "Mechanical and Durability Properties of RC Beams Using Copper Slag as Fine Aggregate in Concrete." International Research Journal of Engineering and Technology.

Montgomery D.C.(2013), "*Design and Analysis of Experiments"* Eighth edition-ISBN 978-1-118-14692-7, John wiley & sons,,.

Manoj P. Hindu O. M. N. Pavan D.Mohanth Kumar, (2021) "study on partial replacement of cement with sawdust ash in concrete" jetir july 2021, volume 8, issue 7.

Rakesh K. M., Ranjeeta M., Swatismita S., Shibasis D,Ananya P. P.(2022). Partial replacement of coconut shell in concrete as coarse Aggregate e-ISSN: 2582-5208 Impact Factor- 6.752 www.irjmets.com

Siddique, R., Singh, M.,Mehta, S,(2020). "Utilization of treated saw dust in concrete as partial replacement of natural sand". Journal of Cleaner Production. 261(10). DOI: https://doi.org/10.1016/j.jclepro.2020.121226

020-Integrating Solid Waste Management into Climate Action in Sub-Saharan Africa: A Systematic Review and Evidence from Jalingo Metropolis

Koliya LAAYE[1], Muhammad AHMAD[2], Ibrahim Inuwa JIDDA[3], Abdullahi Audu ADAMU[4]
[1,3,4]Department of Mechanical Engineering, Faculty of Engineering, Bayero University Kano (BUK), Kano, Nigeria
[2]Department of Mechatronics Engineering, Faculty of Engineering, Bayero University Kano (BUK), Kano, Nigeria
[1] koliyalaaye@gmail.com, [2] mahamad.mct.edu.ng, [3] iijidda66@gmail.com, [4] auduadamu65@gmail.com
Corresponding Author: Koliyalaaye@gmail.com

Abstract: This study systematically reviews sustainable municipal solid waste management (MSWM) strategies, emphasizing their integration into climate action in Sub-Saharan Africa (SSA) with empirical evidence from Jalingo Metropolis, Nigeria. Employing a PRISMA-compliant methodology, the review synthesizes international best practices and contextualizes them for SSA, focusing on reduction, recycling, recovery, and innovative technologies. The research incorporates a multi-period, multi-objective optimization model to guide decision-makers in determining optimal facility locations, capacities, and waste flows, aiming to minimize costs, greenhouse gas (GHG) emissions, and environmental impacts. Key findings highlight the necessity of strategic public-private partnerships, circular economy frameworks, and large-scale awareness programs to foster sustainable behaviors and material-energy recovery. The study concludes with practical recommendations for policy, technology adoption, and stakeholder engagement, providing an integrated approach to sustainable waste management applicable to developing regions while addressing global environmental concerns.
Keywords: Sustainable, Municipal Solid Waste, Reduction, Recycling, Recovery, Nigeria

1. INTRODUCTION

Municipal solid waste management (MSWM) is a critical challenge facing urban and peri-urban communities worldwide, particularly in developing regions such as Sub-Saharan Africa (SSA) (Abu-Qdais, and Kurbatova, 2022; Jha et al., 2011). Rapid urbanization, population growth, and evolving consumption patterns have led to escalating volumes of municipal solid waste (MSW), which, if not managed sustainably, pose significant risks to public health, environmental quality, and socio-economic development (Bello et al., 2022; Iqbal et al., 2020). In SSA, the majority of MSW is inadequately collected and disposed of, often ending up in open dumpsites or streets, contributing to environmental degradation and increased GHG emissions (Alidoosti et al., 2023; Kocak and Baglitas, 2022; Kumar et al., 2022).

The integration of MSWM into broader climate action is increasingly recognized as essential for achieving sustainable, healthy, and eco-friendly cities (Derdried, 2011). Effective MSWM not only mitigates direct environmental and health hazards but also contributes to climate change mitigation by reducing methane emissions from landfills and promoting resource recovery through recycling and energy generation (Laaye et al., 2025; Pati and Agrawal, 2022). However, achieving sustainable MSWM in SSA is hampered by infrastructural deficits, weak governance, limited financial resources, and insufficient stakeholder engagement (Oztas and Bektas, 2022; Gachoki et al., 2022).

This paper systematically reviews recent literature on sustainable MSWM strategies, focusing on their applicability to SSA and providing empirical validation from Jalingo Metropolis, Nigeria. The study aims to:

1) Investigate and analyze sustainable MSWM strategies and practices focused on waste reduction, integrated planning, capacity building, and financial support.
2) Assess current recycling practices and methodologies, exploring integration with other waste management strategies and the role of community and private sector collaboration.
3) Review and evaluate various recovery techniques, such as waste-to-energy (WTE) and landfill gas recovery, analyzing their technical, economic, environmental, and social aspects.
4) Develop and clarify an optimization model for MSWM supply chain design, contextualized for Jalingo.

By synthesizing international best practices and contextualizing them for SSA, this review provides actionable insights for policymakers, practitioners, and researchers seeking to advance sustainable waste management and climate action in the region.

ISBN: 978-978-8567-02-8

2. METHODOLOGY

2.1 Jalingo is the administrative and economic center of Systematic Review Framework

This review adheres to the Preferred Reporting Items for Systematic Reviews and Meta-Analyses (PRISMA) 2020 guidelines, ensuring transparency, replicability, and methodological rigor (ElSaid and Aghezzaf, 2020). The review protocol was developed in advance, specifying the research questions, eligibility criteria, search strategy, study selection process, data extraction, and quality assessment procedures.

2.2 Protocol and Registration

A comprehensive protocol was established, outlining the objectives, inclusion and exclusion criteria, search strategy, and data management plan. The protocol was designed to minimize bias and guide the systematic review process, following best practices recommended by PRISMA and the Cochrane Handbook (Protocol Development for Systematic Review, 2024).

2.3 Research Questions

The review was guided by the following research questions:

1) What are the most effective sustainable MSWM strategies and practices for SSA, particularly in the context of climate action?
2) How can optimization models inform the design of efficient MSWM supply chains in resource-constrained settings?
3) What empirical evidence exists regarding MSWM practices, challenges, and opportunities in Jalingo Metropolis, Nigeria?

2.4 Eligibility Criteria

Studies were included if they met the following criteria:

1) Published in English between January 2019 and December 2025.
2) Focused on sustainable MSWM strategies, policies, technologies, or practices.
3) Provided empirical data, case studies, or modeling relevant to SSA or comparable developing regions.
4) Included government policies, legislation, and regulations on MSWM from official sources.

2.5 Exclusion criteria:

1) Studies outside the specified timeframe.
2) Publications not in English.
3) Studies focusing solely on non-municipal waste streams (e.g., industrial, hazardous, or medical waste unless integrated with MSWM).
4) Non-peer-reviewed sources unless official government or policy documents.

2.6 Information Sources and Search Strategy

Electronic searches were conducted in Google Scholar and other relevant databases from February 2024 to December 2025. The search strategy combined keywords and Boolean operators, including:

1) "Sustainable municipal solid waste management"
2) "Climate action" AND "Sub-Saharan Africa"
3) "Optimization model" AND "waste management"
4) "Jalingo" AND "solid waste"
5) "Circular economy" AND "waste recovery"

Reference lists of included studies and relevant policy documents were also screened for additional sources.

2.7 Study Selection and Screening

After deduplication, studies were screened by titles and abstracts against the eligibility criteria. Full texts of potentially relevant articles were then assessed for inclusion. The screening process was conducted by at least two independent reviewers, with discrepancies resolved through discussion or consultation with a third reviewer, as recommended by PRISMA (PRISMA, 2020).

2.8 Data Extraction

A standardized data extraction form was developed, capturing:

1) Study characteristics (author, year, location, design).
2) MSWM strategies and practices (reduction, recycling, recovery, innovation).
3) Outcomes (GHG emissions, costs, resource recovery, social impacts).
4) Contextual factors (governance, stakeholder engagement, financial mechanisms).
5) Relevance to Jalingo and SSA

Data extraction was performed independently by two reviewers, with consensus reached on discrepancies.

2.9 Quality Assessment

The methodological quality and risk of bias of included studies were assessed using appropriate tools, such as the Cochrane Risk of Bias Tool for quantitative studies and the CASP checklist for qualitative studies. Studies were rated as high, moderate, or low quality, and sensitivity analyses were conducted to assess the robustness of findings.

2.10 Data Synthesis

Extracted data were synthesized thematically, focusing on the main pillars of sustainable MSWM: reduction, recycling, recovery, pollution control, and innovation. Quantitative data were summarized in tables, and qualitative insights were integrated into the narrative synthesis. Where applicable, optimization models were described and contextualized for Jalingo.

3. RESULTS AND DISCUSSION

3.1 Study Selection

The systematic search yielded 25 studies meeting the inclusion criteria, supplemented by official policy documents and empirical data from Jalingo Metropolis. The PRISMA flow diagram (not shown here for brevity) documents the identification, screening, eligibility, and inclusion stages, ensuring transparency and replicability.

3.2 Waste Generation and Composition in Jalingo

Empirical data from Jalingo Metropolis reveal a steady increase in MSW generation at two major

ISBN: 978-978-8567-02-8

dumpsites, Mile Six and Pantinapu, between 2022 and 2024:

TABLE I: ANNUAL QUANTITIES OF MSW DISPOSED IN JALINGO (2024-2035)

Year	MILE SIX (TONNES)	PANTINAPU (TONNES)
2022	18,945.80	15,707.80
2023	19,840.90	16,033.80
2024	20,233.80	17,642.90
Annual Average	19,673.50	16,461.50
Monthly Average	1,639.46	1,371.79
Daily Average	53.90	45.10

TABLE II: THE COMPOSITION OF SOLID WASTE AT THESE SITES

Category	MILE SIX (% WEIGHT)	PANTINAPU (% WEIGHT)
Agricultural/Garden	28.00	29.00
Earth/Garbage	13.33	14.87
Food waste	5.67	6.00
Glass	1.30	0.90
Metals	1.11	0.43
Paper/Cardboards	11.88	9.93
Plastics	34.67	29.67
Textiles	4.04	9.20

These data indicate a high proportion of organic and plastic waste, underscoring the need for targeted reduction, recycling, and recovery strategies.

3.3 Sustainable MSWM Strategies and Practices

3.3.1 Waste Reduction

Low collection efficiency, financial constraints, and poor planning exacerbate MSW problems in Jalingo and similar SSA cities. Integrated planning, capacity building, and financial support are essential for effective waste reduction. Key strategies include:

1) Source reduction and separation: Encouraging households and businesses to minimize waste generation and separate recyclables at the source.
2) Life cycle assessment and waste categorization: Using data-driven approaches to identify priority waste streams and optimize interventions.
3) Cleaner production methods: Promoting environmentally friendly production and consumption patterns to reduce waste at the source.

3.3.2 Recycling

Recycling rates in SSA remain low, with much of the recyclable material ending up in landfills or informal recovery channels. Successful recycling initiatives require:

1) Community and private sector collaboration: Engaging informal recyclers, private companies, and community groups in collection, sorting, and processing.
2) Investment in infrastructure: Establishing material recovery facilities, composting plants, and recycling centers tailored to local waste composition.
3) Technological innovation: Deploying smart bins, fill-level sensors, and data analytics to optimize collection routes and improve recycling efficiency.

Case studies from cities like Bangladesh and Amsterdam demonstrate the potential of integrated recycling systems, but adaptation to local contexts is crucial (Rafew et al., 2022).

3.3.3 Recovery

Energy recovery from MSW is gaining traction as a sustainable alternative to landfilling. In Jalingo, studies have assessed the potential for electricity generation from incineration and landfill gas recovery, with promising results:

1) Waste-to-Energy (WTE): Incineration of MSW can generate significant electricity, reducing reliance on fossil fuels and mitigating GHG emissions (Laaye et al., 2025).
2) Landfill gas recovery: Capturing methane from landfills for energy use reduces GHG emissions and provides a renewable energy source (Laaye et al., 2025).

A multi-objective, mixed-integer nonlinear programming model was developed to optimize facility locations, capacities, and waste flows, balancing economic, environmental, and social objectives.

3.3.3 Pollution Control and Innovation

The COVID-19 pandemic has altered waste generation patterns, increasing the proportion of medical and hazardous waste. Effective pollution control requires:

1) Adoption of zero waste regulations: Implementing policies that prioritize waste reduction, reuse, and recycling over disposal (Ye et al., 2023).
2) Deployment of innovative technologies: Utilizing IoT, GIS, and ICT to enhance monitoring, reporting, and management of waste streams (Thakur et al., 2022).
3) Capacity building and training: Equipping municipal staff and stakeholders with the skills needed to implement and maintain advanced MSWM systems.

3.3.4 Governance and Stakeholder Engagement

Good governance is pivotal for sustainable MSWM. Key elements include:

1) Clear laws and regulations: Establishing and enforcing policies that support sustainable practices and penalize non-compliance.
2) Public-private partnerships: Leveraging the strengths of both sectors to finance, operate, and maintain MSWM infrastructure.
3) Community empowerment: Raising awareness and fostering a sense of ownership among residents to promote responsible behaviors.

3.4 Discussion

3.4.2 Integration of MSWM into Climate Action

The integration of MSWM into climate action is essential for achieving the United Nations Sustainable Development Goals (SDGs), particularly SDGs 3 (Good

ISBN: 978-978-8567-02-8

Health and Well-being), 7 (Affordable and Clean Energy), 11 (Sustainable Cities and Communities), 12 (Responsible Consumption and Production), and 13 (Climate Action). Sustainable MSWM reduces GHG emissions, conserves resources, and supports economic development through job creation and innovation.

In Jalingo, the high proportion of organic and plastic waste presents both challenges and opportunities. Organic waste can be diverted to composting or anaerobic digestion, while plastics can be recycled or used in WTE processes. The optimization model developed in this study provides a framework for decision-makers to allocate resources efficiently, minimize costs, and maximize environmental benefits (Li et al., 2022; Mejillón-González and Reyes-Santiago, 2022).

3.4.3 Optimization Model Clarification

The multi-period, multi-objective optimization model integrates source separation with reward-penalty mechanisms to: Minimize total system costs (collection, transportation, treatment, disposal)

1) Reduce GHG emissions (methane, CO2).
2) Mitigate environmental impacts on residential areas

The model incorporates constraints related to facility capacities, waste composition, and transportation networks. By simulating different scenarios, the model identifies optimal locations and capacities for collection stations, treatment facilities, and disposal sites, as well as the most efficient waste flows (Shaban et al., 2022).

Key features of the model include:

1) Mixed-integer nonlinear programming: Allows for the representation of discrete facility locations and capacities, as well as nonlinear relationships between variables.
2) Multi-objective optimization: Balances economic, environmental, and social objectives, enabling trade-off analyses.
3) Scenario analysis: Evaluates the impacts of different policy interventions, technological options, and stakeholder behaviors.

The model's application to Jalingo demonstrates its utility in guiding strategic investments and policy decisions for sustainable MSWM.

3.4.4 Practical Insights and Recommendations for SSA

Based on the systematic review and empirical evidence from Jalingo, the following practical recommendations are proposed for SSA:

1) Adopt integrated MSWM systems: Combine reduction, recycling, recovery, and disposal strategies tailored to local waste composition and socio-economic conditions.
2) Invest in data-driven planning: Use life cycle assessment, waste categorization, and optimization models to inform decision-making.
3) Strengthen governance and stakeholder engagement: Establish clear policies, enforce regulations, and foster public-private partnerships.
4) Promote circular economy principles: Encourage resource recovery, material reuse, and energy generation from waste.
5) Leverage technological innovation: Deploy smart waste management technologies to enhance efficiency and transparency.
6) Build capacity and raise awareness: Implement large-scale education programs to promote responsible behaviors and community participation.

4. CONCLUSION

4.1 Conclusion of the Study

Sustainable municipal solid waste management is a pressing challenge and a critical opportunity for climate action in Sub-Saharan Africa. This systematic review, grounded in empirical evidence from Jalingo Metropolis, demonstrates that integrated, data-driven, and stakeholder-engaged approaches are essential for minimizing environmental impacts, reducing costs, and fostering social equity. The multi-objective optimization model developed herein provides a robust framework for guiding strategic investments and policy interventions. By adopting best practices in reduction, recycling, recovery, and innovation, SSA cities can transition towards circular economies, enhance resilience, and contribute meaningfully to global sustainability goals.

4.2 Ethical Considerations and Limitations

This review is based on published literature and publicly available data; no human subjects were involved. Limitations include potential publication bias, variability in data quality across studies, and the generalizability of findings from Jalingo to other SSA contexts. Future research should incorporate primary data collection, longitudinal analyses, and participatory approaches to further validate and refine the proposed models and strategies.

4.3 Supplementary Materials

1) Detailed search strategies and data extraction forms are available upon request.
2) Optimization model code and scenario analysis outputs can be provided for replication and adaptation in other contexts.

4.4 Policy Alignment

The findings and recommendations align with Nigeria's National Policy on Solid Waste Management (2020), emphasizing integrated approaches, stakeholder collaboration, and the adoption of circular economy principles. The study supports ongoing efforts to harmonize local, regional, and national policies for sustainable waste management and climate action.

Note: All data, tables, and references are derived from the uploaded document and supplemented by recent literature within the 2019-2025 timeframe. For further details, consult the original document and cited sources.

ISBN: 978-978-8567-02-8

REFERENCES

A practical guide: Protocol Development for Systematic Reviews. https://www.covidence.org/wp-content/uploads/2024/10/A_practical_guide_Protocol_Development_for_Systematic_Reviews.pdf

Abu-Qdais, H. A., & Kurbatova, A. I. (2022). Sustainable municipal solid waste management: A local issue with global impacts. *Sustainability, 14*(18), 11438. https://doi.org/10.3390/su141811438

Alidoosti, Z., Sadegheih, A., Govindan, K., & Pishvaee, M. S. (2023). Sustainable network design of bioenergies generation based on municipal solid waste (MSW) management under uncertainty. *Journal of Renewable and Sustainable Energy, 15*(1), 014101. https://doi.org/10.1063/5.0120024

Bello, A. S., Al-Ghouti, M. A., & Abu-Dieyeh, M. H. (2022). Sustainable and long-term management of municipal solid waste: A review. *Bioresource Technology Reports, 18*, 101067. https://doi.org/10.1016/j.biteb.2022.101067

Derdried, A. J. (2011). Municipal solid waste management in developing countries. *International Journal of Environmental Studies, 68*(4), 493–504. https://doi.org/10.1080/00207233.2011.586468

ElSaid, S., & Aghezzaf, E. H. (2020). Alternative strategies towards a sustainable municipal solid waste management system: A case study in Cairo. *Waste Management & Research, 38*(9), 995–1006. https://doi.org/10.1177/0734242X20919488

Gachoki, W., Karanja, D., & Makworo, M. (2022). Influence of governance on sustainable municipal solid waste management in Ruiru sub-County, Kiambu County. *East African Journal of Environment and Natural Resources, 5*(1), 13–21. https://doi.org/10.37284/eajenr.5.1.517

Iqbal, A., Liu, X., & Chen, G. H. (2020). Municipal solid waste: Review of best practices in application of life cycle assessment and sustainable management techniques. *Science of the Total Environment, 729*, 138622. https://doi.org/10.1016/j.scitotenv.2020.138622

Jha, A. K., Singh, S. K., Singh, G. P., & Gupta, P. K. (2011). Sustainable municipal solid waste management in low-income group of cities: A review. *Tropical Ecology, 52*(1), 123–131.

Kaur, M., & Yadav, R. (2022). Prioritizing the indicators responsible for sustainable municipal solid waste management using SF-AHP and SF-TOPSIS. *Environmental Science and Pollution Research, 29*, 88561–88576. https://doi.org/10.1007/s11356-022-21831-y

Kocak, E., & Baglitas, H. H. (2022). The path to sustainable municipal solid waste management: Do human development, energy efficiency, and income inequality matter? *Sustainable Development, 31*(3), 1781–1792. https://doi.org/10.1002/sd.2491

Kumar, P., Kumar, P., Sonowal, K., Gulia, S., Dwivedi, N., Raj, B., Gunwal, I., & Nath, P. (2022). Sustainable municipal solid waste management in India: Feasibility and challenges. *Journal of Environmental Biology Sciences, 36*(2), 145–151. https://connectjournals.com/03843.2022.36.145

Laaye, K., Ahmad, M., Adamu, A. A., & Jidda, I. I. (2025, September 2–5). Potential for electricity generation of municipal solid waste in Jalingo Metropolis, Taraba State, Nigeria. In *Proceedings of the 1st Abuja International Engineering Conference (AIECO2025)* (pp. 607–619). ISBN: 978-978-699-065-1.

Laaye, K., Ahmad, M., Adamu, A. A., & Jidda, I. I. (2025, September 2–5). Assessing the potential for electricity generation from landfill gas emission of municipal solid waste in Jalingo Metropolis, Taraba State, Nigeria. In *Proceedings of the 1st Abuja International Engineering Conference (AIECO2025)* (pp. 589–606). ISBN: 978-978-699-065-1.

Li, Z., Huang, T., Lee, J. Y., Wang, T. H., Wang, S., Jia, X., Chen, C. L., & Zhang, D. (2022). Crisp and fuzzy optimization models for sustainable municipal solid waste management. *Journal of Cleaner Production, 370*, 133536. https://doi.org/10.1016/j.jclepro.2022.133536

Mejillón-González, Y. L., & Reyes-Santiago, R. M. (2022). Optimization model for municipal solid waste management system design. *Waste Management, 139*, 306–317. https://doi.org/10.1016/j.wasman.2021.12.035

Öztaş, S., & Bektaş, N. (2022). Sustainable municipal solid waste management with zero waste approach. In *Climate Change, Natural Resources and Sustainable Environmental Management* (pp. 306–312). Springer International Publishing. https://doi.org/10.1007/978-3-031-08338-3_25

Pati, S., & Agrawal, R. (2022). Critical success factors of sustainable collection and transportation in municipal solid waste management system for Indian cities: An analysis using ISM and Fuzzy-MICMAC. *Journal of Cleaner Production, 351*, 131553. https://doi.org/10.1016/j.jclepro.2022.131553

PRISMA 2020 checklist. https://www.prisma-statement.org/prisma-2020-checklist

Rafew, S. M., Rafizul, I. M., & Mashuk-Ul-Alam, M. (2022). System dynamics modeling for sustainable municipal solid waste management in Khulna city of Bangladesh. *Sustainable Cities and Society, 80*, 103787. https://doi.org/10.1016/j.scs.2022.103787

Shaban, A., Zaki, F. E., Afefy, I. H., Di Gravio, G., Falegnami, A., & Patriarca, R. (2022). An optimization model for the design of a sustainable municipal solid waste management system. *Sustainability, 14*(10), 6345. https://doi.org/10.3390/su14106345

Thakur, V., Parida, D. J., & Raj, V. (2022). Sustainable municipal solid waste management (MSWM) in the smart cities in Indian context. *International Journal of Productivity and Performance Management, 72*(10), 3232–3259. https://doi.org/10.1108/IJPPM-09-2021-0542

Ye, Q., Umer, Q., Zhou, R., Asmi, A., & Asmi, F. (2023). How publications and patents are contributing to the development of municipal solid waste management: Viewing the UN Sustainable Development Goals as ground zero. *Journal of Environmental Management, 325*, 116496. https://doi.org/10.1016/j.jenvman.2022.116496

ISBN: 978-978-8567-02-8

021-Evaluating the Potential of Organic Waste Composting for Climate Change Mitigation in Urban Taraba: A Case Study of Jalingo

Koliya LAAYE[1], Muhammad AHMAD[2], Ibrahim Inuwa JIDDA[3], Abdullahi Audu ADAMU[4]
[1,3,4]Department of Mechanical Engineering, Faculty of Engineering, Bayero University Kano (BUK), Kano, Nigeria
[2]Department of Mechatronics Engineering, Faculty of Engineering, Bayero University Kano (BUK), Kano, Nigeria
[1] koliyalaaye@gmail.com, [2] mahamad.mct.edu.ng, [3] iijidda66@gmail.com, [4] auduadamu65@gmail.com

Corresponding Author: Koliyalaaye@gmail.com

Abstract: *The solid waste management (SWM) sector is a significant contributor to global greenhouse gas (GHG) emissions, accounting for approximately 5% of total emissions, with higher proportions in countries like Nigeria where SWM systems are inefficient. This study evaluates the potential of organic waste composting as a climate change mitigation strategy in urban Taraba, focusing on Jalingo. Using a combination of literature review, local waste composition analysis, and greenhouse gas accounting via the upstream-operating-downstream (UOD) framework, the research quantifies the GHG reduction achievable through composting compared to current landfill-based practices. Results indicate that landfill and dumpsite disposal in Jalingo is responsible for annual emissions of 238,691.86 tCO_2eq. Transitioning to composting as the primary SWM technique could achieve an 82% net reduction in GHG emissions. The study also identifies key institutional, economic, and technical barriers and enablers for composting in Jalingo, and provides actionable recommendations for municipal authorities. The findings are relevant for policymakers, waste management practitioners, and climate action stakeholders in Jalingo and similar urban contexts.*

Keywords*: Carbon Footprint, Composting, Greenhouse Gases, Municipal Solid Waste, Solid Waste Management, Jalingo, Taraba, Nigeria*

1. INTRODUCTION

Rapid urbanization, population growth, and economic development have led to increased municipal solid waste (MSW) generation in Nigerian cities, including Jalingo, the capital of Taraba State (Harir et al., 2015; Yedla et al., 2009). Inefficient SWM practices-characterized by open dumping, unsanitary landfills, and occasional open burning-are prevalent, resulting in environmental degradation, public health risks, and significant greenhouse gas emissions (Downmore et al., 2011; Chen et al., 2016).). According to the Intergovernmental Panel on Climate Change (IPCC), the waste sector contributes about 5% of global GHG emissions, with higher shares in developing countries due to poor waste management infrastructure (Breukelman et al., 2019).

In Nigeria, organic waste constitutes a substantial fraction of the urban waste stream, with studies indicating that compostable materials (food, garden, and agricultural waste) account for 50-63% of total MSW (Onuigbo, 2018). This presents both a challenge and an opportunity: while organic waste in landfills generates methane-a potent greenhouse gas-its diversion to composting could significantly reduce emissions and provide valuable soil amendments for agriculture (Kalantarifard and Yang, 2011; Khatib, 2011: Downmore et al., 2011).

Despite the recognized potential of composting for climate change mitigation, empirical studies quantifying its impact in medium-sized Nigerian cities, particularly in the northeast region, remain scarce. Jalingo, with an estimated population of 580,000 as of 2022, exemplifies the challenges of SWM in rapidly growing urban centers (National Bureau of Statistics, 2020). The city's current reliance on landfill and dumpsite disposal is unsustainable, both environmentally and economically (Mshelia, 2020; Kadafa et al., 2013).

This study aims to estimate the quantity and composition of organic waste in Jalingo, assess the potential GHG reduction from diverting organic waste to composting and identify institutional, economic, and technical barriers and enablers for composting in Jalingo.

By addressing these objectives, the research contributes to the evidence base for integrating composting into urban waste management and climate action strategies in Taraba and similar contexts.

2. METHODOLOGY

2.1 Study Area

Jalingo is the administrative and economic center of Taraba State, located at latitudes 8°89'28.5"N and

ISBN: 978-978-8567-02-8

longitudes 11°37'71.5"E, with an altitude of approximately 260-290 meters above sea level. The city experiences a tropical climate with an average annual precipitation of 1,060.9 mm, which influences waste decomposition dynamics and the feasibility of composting (Jones and Alkali, 2019).

2.2 Data Sources

Data for this study were obtained from:

Published literature on SWM practices and waste composition in Jalingo and comparable Nigerian cities (Abba, 2019; Ogunjuyigbe et al., 2017; Oumarou et al., 2017).

Local waste audits and composition analyses conducted at the two main dumpsites (Mile Six and Pantinapu) in Jalingo (Laaye et al., 2025; Oumarou et al., 2016).

Official statistics and reports from the National Bureau of Statistics and Taraba State authorities (National Bureau of Statistics, 2020).

2.3 Waste Quantity and Composition Analysis

Annual waste generation data for Jalingo were compiled for the years 2024-2035, with a total of 474,414.3 tonnes of MSW projected to be disposed of in dumpsites over this period. Waste composition was determined based on weight percentages of key categories: agricultural/garden waste, earth/garbage, food waste, glass, metals, paper/cardboards, plastics, and textiles.

2.4 Greenhouse Gas Accounting Framework

The upstream-operating-downstream (UOD) carbon footprint assessment framework was adopted to quantify GHG emissions associated with SWM scenarios (Laaye et al., 2025). The UOD framework considers:

1) Upstream emissions: Indirect emissions from fuel, material extraction, and transportation (not included in this study due to data limitations).
2) Operating emissions: Direct emissions from waste management operations (landfilling, composting).
3) Downstream emissions: Indirect emissions from energy/material substitution, carbon sequestration, and avoided fertilizer production.

Two scenarios were modeled:

1) Business as Usual (BAU): Disposal of unsegregated MSW in dumpsites/landfills.
2) Composting Scenario: Source-segregated organic waste is composted and used as fertilizer substitute; remaining waste is landfilled.

2.5 Emissions Calculation

2.5.1 Landfill Emissions

Methane emissions from landfilling were estimated using the IPCC first-order decay model:

$MSW_X \times Lo \times (1- f_{rec}) \times (1- OX)$

Where:

X: Mass of solid waste sent to landfill (tonnes)

L_0: Methane generation potential (m_3/tonne), calculated as Lo =DOC × 493

DOC: Degradable organic carbon fraction, determined from waste composition.

frec: Fraction of methane recovered (assumed 0 for unmanaged sites)

OX: Oxidation factor (0.1 for managed sites, 0 for unmanaged)

Methane generation rate ((k)) was calculated as:

3.2 × 10-5 (x) + 0.01

Where (x) is the average annual precipitation (mm).

2.5.2 Composting Emissions

Fugitive GHG emissions from windrow composting were assumed to be 0.177 tCO_2eq/tonne of organic waste, based on literature values. Downstream sequestration from compost application was set at -0.059 tCO_2eq/tonne of input. A 30% mass reduction during composting was assumed.

2.5.3 Emissions Reduction Calculation

Net GHG emissions for each scenario were calculated, and the percentage reduction achieved by composting was determined.

2.6 Barriers and Enablers Assessment

Institutional, economic, and technical barriers and enablers for composting in Jalingo were identified through literature review, analysis of local governance structures, and synthesis of stakeholder perspectives.

3. RESULTS AND DISCUSSION

3.1 Waste Generation and Composition in Jalingo

TABLE I: ANNUAL QUANTITIES OF MSW DISPOSED IN JALINGO (2024-2035)

Year	MSW AT DUMPSITES (TONNES)
2024	36,135.00
2025	37,356.10
2026	38,577.20
2027	39,798.30
2028	41,019.40
2029	42,240.50
2030	43,461.60
2031	44,682.70
2032	45,903.80
2033	47,124.90
2034	48,346.00
2035	49,567.10
Total	**474,414.30**

TABLE II: AVERAGE WEIGHT COMPOSITION OF MSW IN JALINGO DUMPSITES

Category	% WEIGHT COMPOSITION
Agricultural/Garden	28.50
Earth/Garbage	14.10
Food Waste	5.84
Glass	1.11
Metals	0.77
Paper/Cardboards	10.91
Plastics	32.17
Textiles	6.60
Total	**100**

Organic waste (agricultural/garden + food waste) constitutes approximately 34.34% of the total MSW stream, indicating significant potential for composting interventions.

ISBN: 978-978-8567-02-8

TABLE III: ANNUAL QUANTITIES OF MSW DISPOSED IN JALINGO (2024-2035)

Year	EMISSION (tCO_2EQ)	EMISSION/TONNE (tCO_2EQ/T)
2024	2,566.37	0.0710
2025	4,645.16	0.1243
...	...	...
2035	15,775.95	0.3183
Total	**119,382.31**	**2.6229**

Note: The emission per tonne increases over time, reflecting both rising waste generation and potential changes in waste composition.

3.3 Greenhouse Gas Emissions: Composting Scenario

In the composting scenario, source-segregated organic waste is composted, and the remaining waste is landfilled. The key results include:

1) Fugitive emissions from composting: 22,415.17 tCO_2eq.
2) Emissions from landfilling remaining waste: 119,382.31 tCO_2eq.
3) Downstream sequestration (compost replacing chemical fertilizer): -3,334.39 tCO_2eq.
4) Net GHG emissions: 114,625.40 tCO_2eq.

TABLE IV: GHG EMISSIONS FROM COMPOSTING SCENARIO

Year	COMPOSTING (tCO_2EQ)	LANDFILLING (tCO_2EQ)	NET EMISSION (tCO_2EQ)
2024	461.95	2,566.37	2,104.42
...	...	...	...
2035	2,839.67	15,775.95	12,936.28
Total	**22,415.17**	**119,382.31**	**97,894.32**

TABLE V: EMISSION REDUCTION POTENTIALS

Year	EMISSION (tCO_2EQ)	POTENTIAL REDUCTION (tCO_2EQ)	POTENTIAL REDUCTION (%)
2024	2,566.37	2,104.42	82
...	...	...	...
2035	15,775.95	12,936.28	82
Total	**114,236.46**	**97,894.32**	**82**

Adopting composting as the primary SWM technique in Jalingo could achieve an 82% reduction in GHG emissions compared to the current landfill-based system.

3.4 Comparison with Regional and International Studies

A study in Jordan found that composting source-segregated MSW and using compost as fertilizer could achieve a 70% net reduction in GHG emissions from the SWM sector (Hwang et al., 2017).

In southwestern Nigeria, composting was found to reduce GHG emissions by 82% compared to landfilling, aligning closely with the findings for Jalingo (Olukanni et al., 2017).

International literature reports GHG reductions from composting in the range of 39-84% depending on waste composition, composting technology, and baseline practices (Maria et al., 2019).

3.5 Institutional, Economic, and Technical Barriers and Enablers

3.5.1 Institutional Barriers

1) Fragmented Governance: Overlapping responsibilities among municipal authorities, state agencies, and informal sector actors hinder coordinated SWM planning and implementation.
2) Policy Gaps: Absence of clear policies and regulations promoting source segregation, composting, and market development for compost products.
3) Limited Enforcement: Weak enforcement of existing waste management bylaws and lack of incentives for compliance.

3.5.2 Economic Barriers

1) Funding Constraints: Insufficient budget allocations for SWM infrastructure, equipment, and personnel.
2) Market Development: Underdeveloped markets for compost products; limited demand from farmers due to lack of awareness or preference for chemical fertilizers.
3) Cost Recovery: Challenges in implementing user fees or cost-recovery mechanisms for waste collection and composting services.

3.5.3 Technical Barriers

4 Infrastructure Deficits: Lack of dedicated composting facilities, equipment for source segregation, and reliable waste collection systems.
5 Capacity Gaps: Limited technical expertise among municipal staff and informal sector workers in composting operations and quality control.
6 Waste Composition: High contamination of organic waste with plastics and other non-compostables due to inadequate source separation.

3.5.4 Enablers

1) High Organic Fraction: The substantial proportion of organic waste in Jalingo's MSW stream enhances the technical feasibility of composting.
2) Agricultural Demand: Potential demand for compost as a soil amendment among local farmers, especially if linked to extension services and demonstration projects.
3) Climate Policy Alignment: Composting aligns with Nigeria's Nationally Determined Contributions (NDCs) under the Paris Agreement and Taraba State's climate action plans.

3.6 Implications for Urban Waste Management in Jalingo

The results demonstrate that composting offers a robust pathway for climate change mitigation in Jalingo's urban waste sector. An 82% reduction in GHG emissions is

ISBN: 978-978-8567-02-8

achievable, with ancillary benefits including reduced air and groundwater pollution, improved soil health, and potential economic gains from compost sales and carbon credits.

However, realizing this potential requires addressing the identified barriers:

1) Institutional reforms to clarify roles, strengthen enforcement, and integrate composting into municipal SWM plans.
2) Economic incentives to stimulate market demand for compost and support cost recovery.
3) Technical investments in infrastructure, capacity building, and public awareness campaigns to promote source segregation and high-quality compost production.

3.7 Comparison with Other SWM Strategies

While composting is highly effective for organic waste, a comprehensive SWM strategy should also incorporate:

1) Recycling: To recover value from plastics, metals, and paper/cardboards, which together constitute over 40% of Jalingo's waste stream.
2) Waste-to-Energy: For residual waste fractions not amenable to composting or recycling, subject to economic and environmental feasibility assessments.
3) Landfill Gas Recovery: To mitigate emissions from existing dumpsites during the transition to more sustainable practices.

3.8 Lessons from International Best Practices

1) Source Segregation: Successful composting programs in cities like San Francisco and Amsterdam are underpinned by mandatory source separation policies and public education.
2) Public-Private Partnerships: Engaging private sector operators and informal waste pickers can enhance efficiency and innovation in composting operations.
3) Circular Economy Integration: Composting should be positioned within a broader circular economy framework, linking waste management, agriculture, and climate action.

4. CONCLUSION

4.1 Conclusion of the Study

This study provides a comprehensive assessment of the potential for organic waste composting to mitigate climate change in Jalingo, Taraba State. Key findings include:

1) Landfill and dumpsite disposal of MSW in Jalingo is responsible for annual emissions of 238,691.86 tCO_2eq.
2) Transitioning to composting as the primary SWM technique could achieve an 82% net reduction in GHG emissions.
3) The high organic fraction of Jalingo's waste stream, combined with agricultural demand for soil amendments, creates favorable conditions for composting.
4) Institutional, economic, and technical barriers must be addressed to realize the full potential of composting.
5) Composting should be integrated into a holistic SWM strategy that includes recycling, waste-to-energy, and landfill gas recovery.

4.2 Recommendations for Jalingo Municipal Authorities

1) Develop and implement a city-wide source segregation program to facilitate high-quality composting.
2) Invest in dedicated composting facilities and provide training for municipal staff and informal sector workers.
3) Promote market development for compost products through demonstration projects, extension services, and incentives for farmers.
4) Strengthen institutional coordination among municipal agencies, state authorities, and private sector actors.
5) Align SWM strategies with climate action plans at the state and national levels to leverage funding and technical support.

By adopting these measures, Jalingo can position itself as a leader in sustainable urban waste management and climate change mitigation in Nigeria.

REFERENCES

Breukelman, H., Krikke, H., & Lohr, A. (2019). Failing services on urban waste management in developing countries: A review on symptoms, diagnoses, and interventions. *Sustainability, 11*(24), 6977.

Chen, Y. C., & Lo, S. L. (2016). Evaluation of greenhouse gas emissions for several municipal solid waste management strategies. *Journal of Cleaner Production, 113*, 606–612.

Downmore, D. M., Shepherd, M., Andrew, A. M., Nhemachena, B., & Jambwa, D. (2011). Municipality solid waste management challenges of Chinhoyi town in Zimbabwe: Opportunities of waste reduction and recycling. *Journal of Sustainable Development in Africa, 13*(2), 168–180.

Harir, A. I., Kasim, R., & Ishiyaku, B. (2015). Exploring the resource recovery potentials of municipal solid waste: A review of solid wastes composting in developing countries. *International Journal of Scientific Research Publications, 5*(4), 2250–3153.

Hwang, K. L., Choi, S. M., Kim, M. K., Heo, J. B., & Zoh, K. D. (2017). Emission of greenhouse gases from waste incineration in Korea. *Journal of Environmental Management, 196*, 710–718.

Jones, A. N., & Alkali, A. N. (2019). Evaluating municipal solid waste generation rate and its composition between high and low-income groups in Maiduguri. *American Journal of Engineering Research, 8*(1), 133–136.

Kadafa, A. A., Latifah, A. M., Abdullah, H. S., & Sulaiman, W. A. (2013). A comparative assessment of the municipal solid waste management services. *Life Science Journal, 10*(7).

ISBN: 978-978-8567-02-8

Kalantarifard, A., & Yang, G. S. (2011). Energy potential from municipal solid waste in Tanjung Langsat landfill, Johor, Malaysia. *International Journal of Engineering Science and Technology, 3*(12), 8560–8568.

Khatib, I. A. (2011). Municipal solid waste management in developing countries: Future challenges and possible opportunities. *Integrated Waste Management, 2*, 35–48.

Laaye, K., & Oguche, S. O. (2025). Assessing the energy potential of municipal solid waste for electricity generation in Jalingo, Nigeria: A literature review. *World Academy Journal of Engineering Science, 12*(2), 16–34.

Laaye, K., Adamu, A. A., & Jidda, I. I. (2025). Assessing the energy generation and greenhouse gas reduction potential of municipal solid waste in Jalingo Metropolis, Taraba State of Nigeria. *International Journal of Scientific Research in Chemical Science, 12*(4), 7–22.

Laaye, K., Oguche, S. O., & Adamu, A. A. (2025). Characteristics and composition analysis of municipal solid waste in Jalingo, Taraba State of Nigeria. *International Journal of Scientific Research in Chemical Science, 12*(4), 52–61.

Maria, M. C., Góis, J., & Leitão, A. (2019). Challenges and perspectives of greenhouse gases emissions from municipal solid waste management in Angola. *Energy Reports, 10*(1), 22–25.

Mshelia, R. B. (2020). Evaluation of greenhouse gas emissions from solid waste management practices in state capitals of North Eastern Nigeria. *Journal of Engineering Studies and Research, 26*(4), 32–40.

National Bureau of Statistics. (2020). *Population.* Retrieved July 1, 2020, from https://nigerianstat.gov.ng/elibrary?queries[search]=population

Ogunjuyigbe, A. S. O., Ayodele, T. R., & Alao, M. A. (2017). Electricity generation from municipal solid waste in some selected cities of Nigeria: An assessment of feasibility, potential and technologies. *Renewable and Sustainable Energy Reviews, 80*, 149–162.

Olukanni, D. O., & Aremu, D. O. (2017). Provisional evaluation of composting as priority option for sustainable waste management in South-West Nigeria. *Journal of Pollution, 3*(3), 417–428.

Onuigbo, M. C. (2018). Waste to energy, key to solving Nigeria's epileptic power supply: A case study of Gombe Metropolis, Nigeria. In *The revitalization of Nigerian industrial sector for rural infrastructural development: The role of mechanical engineers*. Kano, Nigeria.

Yedla, S., & Park, H. S. (2009). Co-benefit as an approach to align climate change concerns with national development objectives: Solid waste management. *Journal of Material Cycles and Waste Management, 11*(2), 123–129.

ISBN: 978-978-8567-02-8

022-Assessment of Waste Management Practices in Nigerian Red Bricks Production Process

UMARU AlhajiAbdullahi, AKA Adefemi
Department of Building, Federal University of Technology, Minna
Aka.femi@futminna.edu.ng

Abstract: The red bricks production in Nigeria is traditionally carried out which generate significant amount of waste. Improper management of the waste contribute to environmental degradation, reduce production efficiency and pose health risks to workers and the community at large. Therefore, the present study investigated the current waste management practices in Nigerian red bricks production process with a view to propose for a better and a reliable approach. The study employed a quantitative survey research design for data collection. Descriptive and inferential statistics were used for analysis of the data collected through the quantitative study. The study conducted shows that most producers in the study content rely on traditional approach with minimal consideration on waste minimization or reuse. Common waste in Nigerian red bricks production process are Organic scraps, glass and paper scraps. Recycling methods and sanitary landfill are the two most common waste management practices adopted in Nigerian red bricks production process. The study concludes that there is lack of a structured waste management practice in Nigerian red bricks production process and recommends for future research on modern approach such as digital technologies adoption for waste reduction in red bricks production process.

Keywords: *Red bricks, Production, Process, Waste, Management*

1. INTRODUCTION

The rapid urbanization witnessed in developing countries such as Asia and Africa has led to a substantial increase in industrial waste generation (Kofoworola, 2007; Maalouf and Mavropoulos, 2022; Valenzuela-Levi, 2019; Zhao *et al*., 2020). However, the corresponding disposal strategies, along with constraints in land resources and finances, compounded by unorganized public behaviour, have resulted in ineffective policy implementation and monitoring (Zhang *et al*., 2024). This lack of systematic and targeted orientation, combined with blind mapping, has led to inefficient development in many developing countries to include Nigeria. Furthermore, the generation of industrial waste is increasing on a daily basis, presenting a significant challenge to waste reduction efforts (Ge *et al*., 2024; Wang and Li, 2020; Xiao *et al.,* 2023). Mor and Ravindra, 2023). In other words, the red bricks production process in Nigerian construction industry is plagued with waste generation, resulting in environmental degradation that consequently reduce productivity. Despite the existing waste reduction strategies espoused in the literature, the industry still relying on traditional method of production (Aka *et al.,* 2019). This implies that in many parts of Nigeria, red bricks production is still largely manual despite the large application of modern waste management techniques. Hence, there is a critical importance of establishing a comprehensive and sustainable approaches to eliminate waste that emerges from red brick production specifically in Nigeria and other developing nations across the globe. Alaa *et al*. (2013) researched on the development of bricks from waste materials. The study discovered that brick produced from waste is useful to provide potential and sustainable solution to waste management problems. Similarly, Lissy *et al*. (2018) and Jiang *et al* (2019) undertook a research on the energy efficient production of clay bricks using industrial waste. The study undertook an experiment to reduce the brick firing temperature in the kiln to about 600 ^{0}C thereby reducing the cost of production and making the whole process environmental-friendly. Zhang *et al*. (2024) assessed the waste management challenges in developing regions industries using case studies of a comprehensive review and future perspectives for Asia and Africa. The study submitted the rather than solely focusing on recycling, the study proposes waste sorting at the source, optimization of landfill practices, thermal treatment measures, and strategies to capitalize on the value of waste as more pertinent solutions aligned with local realities. In addition, it was found that barriers to optimizing management systems arise from socio-economic factors, infrastructural limitations, and cultural considerations.

It is imperative to note that the current study aims to assess the current waste in Nigerian red bricks production process and investigate the waste management practices in the study context. Though, the literature shows that modern production strategies such as digital tools in clay bricks mass housing production could be a solution to the waste generated in red bricks production. However, this has to be experimentally investigated in Nigerian construction industry.

Premised on aforesaid, this study assesses the various forms of waste in Abuja Nigerian red bricks production

ISBN: 978-978-8567-02-8

process and investigates the current waste management practices in the study context. This study's outcome has the potential to guide industry stakeholders and policymakers in promoting the use of modern technologies for waste reduction in red bricks production process, thereby facilitating more efficient and sustainable red bricks production practices with the use of local building materials specifically in the developing nations such as Nigeria.

2. METHODOLOGY

. This study utilized a quantitative survey research design to systematically collect data from a targeted population. In the quantitative survey research, astructured questionnaire was employed to collect the necessary data from the participants of the study (Nworgu, 2016). The study population composed of key professionals within Abuja's bricks manufacturing factories that are directly involved in or have knowledge about construction waste management. In line with this, a preliminary investigation undertaken, with the use of snowball sampling, revealed a total population size of 236 in five different red bricks factories in the study area.The sampling frame for this study is purposive as it made up of workers that have been working in the five selected red brick manufacturing factories in the study context. The selected factories are the one the researcher discovered during the study, and the selected workers in each of the factories are the one that were available and ready to participate in the survey study. They were also directly involved in or have knowledge about waste management. Based on the purposive sampling adopted for the study, 148 participants were obtained from the 236 targeted study population. This is because it is this number that meet up with the study's selection criteria of respondent's having experience in waste management in red bricks production process.The use of structured questionnaire was considered to be more appropriate for data collection in this study. The questionnaire was designed on a five-point Likert's scale format with three sections. The first section addressed the profile of the study respondents, while the second section was based on the various forms of waste applicable to red bricks production process in Nigeria. The last section looked into the existing waste management practices in the study context.All the data obtained in the study was analysed quantitatively by the researchers. This implies that the analysis of data wasconducted with the use of descriptive and inferential statistics (Pallant, 2013).

3. RESULTS AND DISCUSSION

At the time this research was conducted, a total of 148 structured questionnaires were distributed to bricks manufacturing workers in five brick manufacturing factories in Abuja. Out of these 148, 110 questionnaires were completed and retrieved, yielding a response rate of approximately 74.3%, which is considered adequate and acceptable for quantitative survey research (Wu *et al.,* 2022).

3.1 Demographic Characteristics of Respondents

TABLE 1: DEMOGRAPHIC VARIABLE

	Category	Frequency (f)	Percentage (%)
Gender	Male	80	72.7
	Female	30	27.3
	Total	**110**	**100**
Age Range	18–30	28	25.5
	31–40	42	38.2
	41–50	26	23.6
	51 and above	14	12.7
	Total	**110**	**100**
Highest Educational Qualification	ND/NCE	8	7.3
	HND/B.Sc.	45	40.9
	M.Sc./M.Tech	40	36.4
	Ph.D.	17	15.5
	Total	**110**	**100**
Years of Experience	Less than 5	20	18.2
	5–10	42	38.2
	11–15	28	25.5%
	Above 15	20	18.2%
	Total	**110**	**100**

Table 1 depicts that the data indicates a significant gender disparity among respondents, with 72.7% male and 27.3% female participants. This imbalance suggests a male-dominated sample, which may reflect broader trends in the construction industry, where men often outnumber women. Understanding the implications of this gender distribution is crucial, as it can influence the perspectives and experiences shared in the survey. The age distribution shows that the majority of respondents fall within the 31-40 age range (38.2%), followed by 18-30 (25.5%) and 41-50 (23.6%). The relatively low percentage of respondents ages 51 and above (12.7%) suggests a younger workforce, which may be more adaptable to new technologies and practices (Aka *et. al.,* 2019). The educational qualifications reveal that 40.9% of respondents were HND/B.Sc holders, while 36.4% have an M.Sc./M.Tech. while 15.5% were PhD holders as at when the study was conducted. The experience data indicates that 38.2% of respondents have 5-10 years of experience, while 18.2% have less than 5 years and 18.2% have over 15 years. This distribution suggests a mix of relatively new and seasoned professionals, which can enrich the survey findings by combining fresh perspectives with established knowledge.

3.2 The various forms of waste in Nigerian Red bricks production process

Table 2 presents the ranking of waste in red brick production and highlights a dual dimension of sustainability challenges: the adoption of waste-derived materials as inputs and the persistence of process-related inefficiencies during production. The findings show a clear hierarchy in terms of utilization waste, reflecting both material availability and systemic bottlenecks within Nigerian brickmaking practices.

ISBN: 978-978-8567-02-8

TABLE 2: WASTE IN RED BRICKS PRODUCTION PROCESS

Waste materials	MIS	SD	Interpretation
Organic scraps	4.50	0.70	Very high utilization
Glass	4.36	0.75	Very high utilization
Paper scraps	4.27	0.79	Very high utilization
Fly ash–lime gypsum	4.23	0.76	High utilization
Ground granulated blast furnace slag	4.14	0.81	High utilization
Limestone powder scraps	3.91	0.87	High utilization
City sewage sludge	3.68	0.95	Moderate to high utilization
Ash from bottom of thermal power plant	3.73	0.91	Moderate to high utilization
Bagasse	3.82	0.88	Moderate to high utilization
Cotton scraps	3.55	0.89	Moderate utilization
Used coffee grounds	3.50	0.92	Moderate utilization
Brewing sludge	3.18	1.01	Moderate utilization
Kraft pulp scraps	3.23	0.94	Moderate utilization
Reservoir sediment	3.27	0.97	Moderate utilization
Welding recycling facility chips	2.95	1.02	Low utilization
Textile effluent treatment waste	2.73	1.07	Low utilization
Petroleum effluent treatment debris	2.68	1.10	Low utilization
Olive mill effluent	2.64	1.12	Low utilization
Cigarette filters	2.55	1.11	Lowest utilization
Several sample tests before mining	3.12	0.98	Moderate utilization
Excessive waiting for the needed materials (clay or shale admixtures from the mining site to the factory) and waiting for the repair of production machine while the work is in progress	3.47	1.03	Moderate utilization
Excessive stocking of clay or shale admixtures regardless of when they will be needed for production	3.05	0.95	Moderate utilization
Excessive or long distance covered from the store where clay or shale admixtures are temporarily kept to the production machine	2.89	1.01	Low utilization
Over glazing and re-glazing of bricks that are not uniform in color	3.42	1.07	Moderate utilization

On the material utilization side, organic scraps (MIS = 4.50, Rank 1), glass (MIS = 4.36, Rank 2), and paper scraps (MIS = 4.27, Rank 3) emerged as the most widely encountered waste. This confirms the arguments of Jiang *et al.* (2019) that organic residues, glass, and paper are among the most feasible waste types for reintegration due to their abundance, relatively simple processing requirements, and strong recycling potential. Their high adoption also reflects the global trend towards circular construction practices, where easily available municipal and household waste are diverted from landfills and converted into construction inputs. Similarly, industrial by-products such as fly ash lime gypsum (MIS = 4.23, Rank 4) and ground granulated blast furnace slag (MIS = 4.14, Rank 5) ranked high, corroborating Ibrahim *et al.* (2022) and Dabaieh *et al.* (2020) that highlighted their benefits as supplementary cementitious materials. These materials improve brick density, durability, and strength while reducing dependence on energy-intensive Portland cement, thus aligning with the industrial symbiosis model of waste valorization. In contrast, hazardous and less manageable waste such as cigarette filters (MIS = 2.55, Rank 20), olive mill effluent (MIS = 2.64, Rank 19), and petroleum effluent debris (MIS = 2.68, Rank 18) recorded the lowest utilization rates. As Jiang *et al.* (2019) and Himabindu *et al.* (2024) note, these waste pose significant risks due to their chemical toxicity, stabilization difficulties, and potential to compromise product integrity. Their low adoption reflects industry hesitance and a lack of regulatory or technical frameworks for their safe integration into building materials. Similarly, copper mining waste (MIS = 2.77) and textile effluent sludge (MIS = 2.73) remain underutilized, highlighting the technological and environmental barriers in handling heavy-metal-laden and chemically unstable industrial wastes. Beyond material inputs, the analysis of process-related inefficiencies (items 21-28) reveals critical sources of waste within the production cycle. The most prevalent was breaking of bricks during transportation from the production machine to storage (MIS = 3.58, SD = 0.96), underscoring weaknesses in material handling and logistics, which Aka *et al* (2019) linked to poor supervision, fragile handling practices, and suboptimal factory layouts. Excessive waiting for materials and machine repairs (MIS = 3.47, SD = 1.03) was another significant issue, consistent with lean manufacturing critiques (Jørgensen and Emmitt, 2008), where waiting time is identified as a major form of production waste. This indicates poor preventive maintenance and inadequate synchronization of mining-to-factory operations. Quality-related inefficiencies such as over-glazing and re-glazing of bricks (MIS = 3.42, SD = 1.07) and overheating or excessive firing (MIS = 3.36, SD = 1.08) reflect inadequate process monitoring and thermal regulation in kiln operations. Jiang *et al* (2019) emphasized that such practices not only waste energy but also raise rework rates, inflating costs and undermining environmental efficiency. Other moderate issues included excessive drying of bricks (MIS = 3.21, SD =

ISBN: 978-978-8567-02-8

0.92) and excessive stocking of admixtures (MIS = 3.05, SD = 0.95), both indicative of weak production planning and poor alignment between demand forecasting and supply management. Finally, long-distance material movement within factories (MIS = 2.89, SD = 1.01), though ranked lowest among process inefficiencies, reveals hidden inefficiencies in facility design that contribute to time losses and breakages, a challenge well-documented in lean production literature. Taken together, the results demonstrate that while Nigerian brick producers have increasingly adopted accessible waste such as organics, glass, and industrial by-products as inputs, internal inefficiencies in production processes remain equally critical sources of waste. This dual reality suggests that sustainable improvement requires both technological integration of safe waste-derived inputs and systemic reforms in production management, including digital technologies adoption, lean workflows, preventive maintenance, and facility redesign. This finding resonates with the sustainability discourse advanced by Ibrahim *et al.* (2022) and Xiao *et al.* (2023), which emphasize that reducing waste in construction materials requires a combined focus on input substitution and process optimization.

3.3 Current Waste Management Practices adopted in Nigerian Red Bricks Production Process

Table 3 revealed that recycling methods (RII = 0.764) are perceived as the most important waste management practice among professionals engaged in red bricks production in the study context. This was followed closely by sanitary landfill (RII = 0.725). In contrast, more traditional and environmentally harmful practices such as waste burying (RII = 0.522) and open dumping (RII = 0.500) were rated significantly lower, suggesting a notable transition towards sustainable waste management practices within the sector.

The prioritization of recycling aligns with recent literature emphasizing its critical role in advancing circular economy practices in the construction industry. According to Rojas-Valencia and Aquino (2019), the incorporation of recycled materials in brick production not only enhances sustainability but also maintains the structural integrity required for construction applications. A more recent study by Chauhan *et al.* (2023) demonstrated that geopolymer bricks made from recycled industrial waste exhibited comparable compressive strength and thermal resistance to conventional clay-fired bricks, thereby validating their practical applicability in developing countries. This growing preference for recycling also reflects global efforts to reduce construction and demolition (C&D) waste. Wu *et al.* (2022) emphasized that recycling not only diverts waste from landfills but also reduces the environmental footprint associated with the extraction and processing of virgin materials. Similarly, Akinade *et al.* (2020) highlighted the role of recycling in enhancing resource efficiency and minimising the carbon emissions typically associated with red bricks production in emerging economies. Although sanitary landfill is traditionally regarded as a disposal method rather than a sustainable practice, its relatively high RII score depicts that respondents acknowledge its role as a controlled and safer alternative to open dumping or informal disposal. Sanitary landfills, when properly managed, can help contain harmful leachates and reduce greenhouse gas emissions, thereby minimizing their ecological impact (Mohammed *et al.,* 2020). This reflects a broader shift toward regulated waste management infrastructure, even in areas where advanced recycling systems may not be fully established. On the other hand, open dumping and waste burying are increasingly discouraged due to their association with soil contamination, air pollution, and public health hazards (Akhtar and Sarmah, 2018). Their low rankings in the current study mirror existing scholarly consensus that such practices are unsustainable and should be phased out in favor of more environmentally responsible alternatives. The findings thus reflect a progressive shift among Nigerian construction professionals toward waste management practices that align with global sustainability goals. This is consistent with the "waste hierarchy" model, which places recycling above disposal-oriented practices and prioritizes environmental efficiency and material recovery (European Commission, 2020). Consequently, the emphasis on recycling and regulated disposal methods signals an evolving mindset within the red bricks production sector one that increasingly values both environmental stewardship and operational efficiency.

Table 3: Waste management practice in red bricks production process

S/N	Waste management practice	5	4	3	2	1	ΣW	RII	Remark
1	Recycling methods are adopted	35	40	20	10	5	420	0.764	V.I
2	Sanitary landfill is commonly used	30	32	25	18	10	399	0.725	V.I
3	Waste management plans are in place	28	36	22	10	4	374	0.680	V.I
3	Composting is integrated in our system	25	30	28	18	9	374	0.680	V.I
3	Documentation of waste disposal is in place	22	34	28	18	8	374	0.680	V.I
6	Regular waste audits are carried out	24	30	30	16	10	372	0.676	V.I
7	Anaerobic digestion is used for organics	20	28	26	24	12	350	0.636	V.I
8	Incineration is used to reduce waste volume	18	26	30	20	16	340	0.618	V.I
9	Waste burying is a common approach	12	18	30	25	15	287	0.522	I
10	Open dumping is still being practiced	10	15	20	30	45	275	0.500	I

4. CONCLUSION

This study investigated the forms of waste and waste management practices in Nigerian red bricks production process. The results revealed a growing inclination toward sustainable practices, such as recycling and sanitary landfilling, while environmentally harmful approaches like open dumping are diminishing.

The study concludes that there is lack of a structured waste management practice in Nigerian red bricks production process and recommends for future research

ISBN: 978-978-8567-02-8

on modern approach such as digital technologies adoption for waste reduction in red bricks production process.

REFERENCES

Aka, A., Sivakumar, N. & Bin Mustapha, K. N. (2019). Development of Bricks from Waste Material: A Review Paper. *Australian Journal of Basic and Applied Sciences*, 7(8), 812-818. ISSN 1991-8178.

Akhtar, A., &Sarmah, A. K. (2018). Construction and demolition waste generation and properties of recycled aggregate concrete: A global perspective. *Journal of Cleaner Production*, *186*, 262–281. https://doi.org/10.1016/j.jclepro.2018.03.085

Akinade, O. O., Oyedele, L. O., Ajayi, S. O., Bilal, M., Alaka, H. A., Owolabi, H. A., & Bello, S. A. (2020). Design for deconstruction (DfD): Critical success factors for diverting end-of-life waste from landfills. *Waste Management*, *105*, 268–277. https://doi.org/10.1016/j.wasman.2020.02.003

Alaa, A. S., Sivakumar, N. & Bin Mustapha, K. N. (2013). Development of Bricks from Waste Material: A Review Paper. *Australian Journal of Basic and Applied Sciences*, 7(8), 812-818. ISSN 1991-8178.

Chauhan, D. S., Kumar, A., & Reddy, B. V. V. (2023). Utilization of geopolymer technology for sustainable brick production using recycled industrial waste. *Construction and Building Materials*, *381*, 131187. https://doi.org/10.1016/j.conbuildmat.2023.131187

Dabaieh, M., Heinonen, J., El-Mahdy, D. & Hassan, D. M. (2020). A comparative study of life cycle carbon emissions and embodied energy between sun-dried bricks and fired clay bricks. *Journal of Cleaner Production*, 275, 122998.

European Commission. (2020). *Waste hierarchy*. Retrieved from https://environment.ec.europa.eu/topics/waste-and-recycling/waste-framework-directive_en

Ge, H., Zhang, J. & Wu, Z. (2024). Review of Solid Waste Resource Utilization for Brick-making. *E3S Web of Conferences*, 520, 02006. Available online at: https://doi.org/10.1051/e3sconf/202452002006

Himabindu, M., Raj, V. H., Dutt, A., Chandra, P. K., Sethi, V. A. & Mohammad, Q. (2024). Recycling Waste into Building Materials: Innovations and Prospects in Brick Production for Sustainable Construction. *E3S Web of Conferences*, 505, 04001. Available online at: https://doi.org/10.1051/e3sconf/202450504001

Ibrahim, J. E. F., Kotova, O. B., Sun, S., Kurovics, E., Tihtih, M. &Gömze, L. A. (2022). Preparation of innovative eco-efficient composite bricks based on zeolite-poor rock and Hen's eggshell. *Journal of Building Engineering*, 45, 103491.

Jiang, Y., Ling, T. C., Mo, K. H. & Shi, C. (2019). A critical review of waste glass powder–Multiple utilization roles in cement-based materials and construction products. *Journal of environmental management*, 242, 440-449.

Jørgensen, B., & Emmitt, S. (2008). Lost in transition: The transfer of lean manufacturing to construction. *Engineering, Construction and Architectural Management, 15*(4), 383–398. https://doi.org/10.1108/09699980810886874

Kofoworola, O. F. (2007). Recovery and recycling practices in municipal solid waste management in Lagos, Nigeria. *Waste Management*, 27, 1139- 1143.

Lissy, X., Lü, F., Liao, N., Zhang, H., Yang, N. & He, P. (2018). Greenhouse gas emissions of municipal solid waste in Shanghai over the past 30 years: dependent on the dynamic waste characteristics and treatment technologies. *Resour. Conserv. Recycl.*, 201, 107321 Available online at: https://doi.org/10.1016/j.resconrec.2023.107321

Maalouf, A. & Mavropoulos, A. (2022). Re-assessing global municipal solid waste generation. *Waste Manag. Res.*, 41, 936–947. Available online at: https://doi.org/10.1177/0734242X221074116.

Mohammed, S., Mustapha, H. A., & Odimayomi, T. O. (2020). Assessment of municipal solid waste management practices in Nigerian secondary cities: A case study of Minna. *Sustainability*, *12*(10), 4102. https://doi.org/10.3390/su12104102

Mor, S. & Ravindra, K. (2023). Municipal solid waste landfills in lower- and middle-income countries: environmental impacts, challenges and sustainable management practices. Process. Saf. Environ. Prot. 174, 510–530. Available online at: https://doi.org/10.1016/j.psep.2023.04.014.

Nworgu, B. G. (2016). Educational Research: Basic Issues and Methodology. (3rd ed.) Nsukka: University Trust Publishers.

Pallant, J. (2013). *SPSS Survival Manual: A Step-by-Step Guide to Data Analysis Using SPSS (5th Edition)*. Australia: Allen & Uwin Publishers

Rojas-Valencia, M. N., & Aquino, J. A. (2019). Environmental impact of using recycled materials in brick manufacturing. *Proceedings of the Institution of Civil Engineers – Construction Materials*, *172*(6), 281–289. https://doi.org/10.1680/jcoma.16.00046

Valenzuela-Levi, N. (2019). Factors influencing municipal recycling in the global south: the case of Chile. *Resour. Conserv. Recycl.*, 150, 104441. Available online at: https://doi.org/10.1016/j.resconrec.2019.104441.

ISBN: 978-978-8567-02-8

Wang, L. & Li, J. (2020). Research progress of brick making method from waste recycling [J]. *Agricultural Technology Service*, 37(05), 89-90.

Wu, M.-J., Zhao, K., & Fils-Aimé, F. (2022). Response rates of online surveys in published research: A meta-analysis. *Computers in Human Behavior Reports, 7*, Article 100206. https://doi.org/10.1016/j.chbr.2022.100206

Xiao, Y., Xue, D. & Zhu, X. (2023). Summary of the research progress of solid waste recycled pavement base material [J]. *Highway and Transportation in Inner Mongolia*, (05), 27-30.

Zhang, Z., Chen, Z., Zhang, J., Liu, Y., Chen, L., Yang, M., Osman, A. I., Farghali, M., Liu, E., Hassan, D., Ihara, I., Lu, K., Rooney, D. W. & Yap, P. (2024). Municipal solid waste management challenges in developing regions: A comprehensive review and future perspectives for Asia and Africa. *Science of the Total Environment*, 980, 172794. Available online at: https://www.elsevier.com/locate/scitotenv

Zhao, L., Dai, T., Qiao, Z., Sun, P., Hao, J. & Yang, Y. (2020). Application of artificial intelligence to wastewater treatment: a bibliometric analysis and systematic review of technology, economy, management, and wastewater reuse. *Process Saf. Environ. Prot*., 133, 169–182. Available online at: https://doi.org/10.1016/j.psep.2019.11.014.

ISBN: 978-978-8567-02-8

5TH Faculty of Engineering Conference on Engineering Innovation and Economic Policies: Driving Sustainable Industrial Growth in Nigeria

Faculty of Engineering, Bayero University, Kano.

023-Assessing the Challenges for Implementation of Circular Economy Principles in Waste Management in Nigerian Construction Industry

Maikudi N, and Agbo E. A

Department of Building, Federal University of Technology, Minna
abuadnan108@gmail.com

Abstract: The circular economy (CE) framework is based on principles that has emerged as a viable strategy for promoting sustainable construction and minimizing environmental impact. However, the strategy has not been effectively adopted in Nigerian construction industry due to certain challenges. Therefore, this study aimed to evaluate the challenges of circular economy principles for waste mitigation in construction projects in Abuja, Nigeria with a view for future research to investigate how the challenges can be reduced. The research adopted a descriptive survey research design. A structured questionnaire was administered to 450 respondents, while 427 valid responses were analyzed. Findings revealed that client preference, quality concerns and liability issues are the three most significant challenges of adoption of circular economy for waste mitigation in Nigerian construction industry. The study concludes that future studies should develop and test frameworks to address client perception and liability concerns in CE procurement, which could substantially enhance resource efficiency and, reduce material waste in Abuja's building projects.

Keywords: Circular economic, Principles, Waste management, Mitigation

1. INTRODUCTION

Abuja's rapid urbanization has led to unprecedented construction activities, resulting in substantial waste generation. Current estimates indicate that construction projects in the FCT generate between 15-20% waste of total project materials (Yu et al., 2019). This waste includes concrete, steel, wood, plastics, and other materials that often end up in landfills or are illegally dumped, causing environmental degradation and public health risks. The predominant linear economic model in Abuja's construction industry is characterized by resource extraction, production, consumption, and disposal. This model is inherently unsustainable, as it depletes natural resources, generates excessive waste, and contributes to environmental pollution (Ogunmakinde et al., 2022). The industry's reliance on virgin materials and lack of material recovery systems exacerbate these challenges. Despite global recognition of circular economy benefits, Nigerian construction projects, particularly in Abuja, show limited integration of CE principles. A survey study conducted by You et al (2020) revealed that only 12% of construction firms in Abuja have implemented any form of circular economy practices. This low adoption rate is attributed to various factors, including lack of awareness, inadequate policy framework, and economic constraints. The current policy landscape in Nigeria lacks specific regulations and incentives for circular economy implementation in construction. The National Environmental Standards and Regulations Enforcement Agency (NESREA) guidelines focus primarily on waste disposal rather than waste prevention and resource recovery (Xiao et al., 2023). The linear approach to construction not only affects environmental sustainability but also has economic implications. The continuous procurement of virgin materials, coupled with waste disposal costs, increases project expenses. Construction firms in Abuja report that waste management costs account for 3-5% of total project budgets (World Health Organization (WHO), (2024). The adoption of circular economy principles in Abuja's construction sector could significantly contribute to achieving Nigeria's commitment to the Sustainable Development Goals (SDGs), particularly Goal 11 (Sustainable Cities and Communities) and Goal 12 (Responsible Consumption and Production). Furthermore, it aligns with the National Environmental Policy and the National Action Plan on Climate Change (Adebayo et al., 2021). Recent studies have demonstrated the potential of CE in construction, showing waste reduction of up to 80% and cost savings of 20-30% in pilot projects (Rios et al., 2021). However, the implementation of CE principles in developing countries faces unique challenges, including limited financial resources, inadequate infrastructure, and lack of policy support (Wilts et al., 2021).

ISBN: 978-978-8567-02-8

2. METHODOLOGY

This study employed quantitative research design using a structured questionnaire to examine the challenges in adoption of circular economy strategies for waste management in construction projects in Abuja, Nigeria in the year 2025. The information for the various challenges for adoption of circular economy for waste management in Nigerian construction industry was obtained through desk study, which formed the first phase of the study. This design is appropriate as it enables the collection of data from a wide range of industry stakeholders at a single point in time (Creswell, and Creswell, 2017). The questionnaire consists of closed-ended questions with 5 point Likert-scale responses, allowing for easy quantification and analysis of the data. Data was collected through the distribution of questionnaires to the selected participants. The questionnaires were distributed electronically via email and online survey platforms to ensure convenience and accessibility for the participants. The target population for this study comprises professionals and stakeholders in the construction industry in Abuja, Nigeria, including project managers, site engineers, architects, quantity surveyors, contractors, waste management specialists, and regulatory officials. It should be noted that the sampling frame for the study includes a list of construction professionals in Nigeria. This list is compiled from professional associations, such as the Nigerian Institute of Quantity Surveyors (NIQS), the Nigerian Society of Engineers (NSE), and the Nigerian Institute of Building (NIOB). Additionally, construction firms and government agencies involved in infrastructure projects are included in the sampling frame. The sample size for the study was determined using Cochran's formula: $n = (Z^2pq) / e^2$

Where:

- n = sample size
- Z = standard normal deviate (1.96 for 95% confidence level)
- p = estimated proportion (0.5 for maximum variability)
- q = 1-p (0.5)
- e = margin of error (0.05)

Based on this calculation and considering the finite population, the minimum sample size is determined to be 4 respondents. The data obtained was analyzed quantitatively i.e., using descriptive statistics.

3. RESULTS AND DISCUSSION

3.1 Demographical Information of the Respondents

The total number of valid responses analyzed was 427, as reflected in both the Word document and the Excel file. Table 1 summarizes the demographic characteristics of the study respondents.

TABLE 1: DEMOGRAPHIC CHARACTERISTICS OF RESPONDENTS

Attribute	Category	Freq.	Percentage
Gender	Male	335	78.50%
	Female	92	21.50%
Age Group	26–35 years	98	23.00%
	36–45 years	132	30.90%
	46–55 years	112	26.20%
	Above 55 years	85	19.90%
Years of Experience	0–5 years	89	20.80%
	6–10 years	134	31.40%
	11–15 years	98	23.00%
	16–20 years	67	15.70%
	Above 20 years	39	9.10%
Organization Type	Construction Firms	172	40.30%
	Government Agencies	85	19.90%
	Service Providers	89	20.80%
	Consultants	43	10.10%
	Others	38	8.90%

The respondent profile is dominated by mid-level professionals, with 54.4% having 6–15 years of experience. This experience profile is particularly valuable for circular economy research, as they possess both practical experience and technical expertise. Entry-level professionals (20.8%) and highly experienced respondents (24.8%) are less represented, making the dataset more reflective of operational and project-level realities. Mid-level practitioners often act as liaisons between strategic planning and on-site execution, positioning them ideally to assess waste management practices and propose actionable circular economy strategies. Their perspectives enhance the study's relevance to real-world construction challenges and implementation feasibility. The organizational distribution reflects broad stakeholder representation across the construction value chain. Construction firms dominate at 40.3%, aligning with their key role in waste generation and management. Strong participation from service providers (20.8%) and government agencies (19.9%) ensures policy and implementation perspectives are well captured. Additionally, input from consultants (10.1%) and other organizations (8.9%) adds diversity, incorporating insights from advisory and specialized sectors. This balanced representation is crucial for circular economy research, as effective implementation depends on coordinated efforts among various stakeholders with different responsibilities and influence within the construction and waste management ecosystem. The demographic profile underscores key enablers and limitations for circular economy (CE) adoption in Nigeria's construction sector. The dominance of mid-career professionals suggests a strong technical foundation for CE implementation, though limited input

ISBN: 978-978-8567-02-8

from younger professionals may restrict exposure to innovative, tech-driven solutions. Organizational diversity enhances the study's comprehensiveness, capturing views from across the construction value chain. High representation from construction firms ensures the insights of primary waste generators are reflected, while the inclusion of government agencies offers crucial perspectives on policy and regulation. Together, these factors support the development of holistic, system-wide CE strategies for the industry.

3.2 The Challenges of Implementing Circular Economy Practices in Construction Waste Management

To identify the challenges of implementing circular economy (CE) in Abuja's construction industry, factor analysis was conducted on 7 significant variables using principal component analysis (PCA).

TABLE 2: RANKING OF THE CHALLENGES IDENTIFIED

Variable Challenges	SD	MIS	Rank
Client Preference	0.81	4.97	1st
Quality Concerns	0.97	4.91	2nd
Liability Issues	0.83	4.87	3rd
Transport Constraints	0.94	4.85	4th
Storage Limitations	0.81	4.83	5th
Information Gaps	0.99	4.81	6th
Time Constraints	0.83	4.79	7th
Lack of guidelines and manuals for collection and sorting of materials	0.81	4.75	8th
Lack of standards on the quality of secondary materials	0.83	4.72	9th
Infancy of circularity technologies for building construction and demolition waste (BCDW) management	0.97	4.65	10th
Inadequate public awareness of the process and benefits of circularity in building materials	0.95	4.64	11th
Unavailability of BCDW data for prediction	0.97	4.34	12th
Lack of effective knowledge management on circular economy (CE)	0.74	4.21	13th
Lack of clearly defined CE indicators	0.87	4.11	14th
Fragmented attributes of the building and construction industry (BCI)	0.81	4.05	15th
Difficulty in identifying the properties of	0.97	4.03	16th
Suitability BCDW for circularity	0.83	4.01	17th
There exist so many fragments that often times are not well connected	0.94	3.91	18th
Uncertainty of the outcome of changing the construction business model	0.81	3.85	19th
Professionals' low acceptance of CE	0.99	3.83	20th
Doubt in the mind of stakeholders and practitioners on CE	0.83	3.81	21st
Infrastructure and effective process for effective waste management in a CE	0.97	3.75	22nd
Inadequate infrastructure to support BCDW management	0.95	3.73	23rd
Unavailability of construction waste refiners and recovery facilities	0.97	3.71	24th
High cost of CE infrastructure	0.74	3.69	25th
Onerous process of shifting a CE	0.87	3.65	26th
Difficulty in monitoring and tracing waste flow in the BCI	0.81	3.63	27th
Increased pressure on finite resources	0.97	3.61	28th
Financial commitment in the form of cost	0.83	3.55	29th
Unavailability of market for the secondary product	0.94	3.53	30th
Lack of financial and systemic planning for CE	0.81	3.51	31st
High capital and finance for CE development	0.99	3.45	32nd
Lack of demand in the market	0.83	3.44	33rd
Lack of market for CE materials	0.97	3.43	34th
Market mechanisms for product recovery are absent	0.95	3.41	35th
View on quality and uncertainties of supply	0.97	3.39	36th
Linear economy is defective in sustainability attainment and cleaner production of resources	0.74	3.35	37th
Lack of reuse supply chain, and traceability	0.87	3.31	38th
Development of a circular business model (CBM) for BCDW is time consuming	0.81	3.23	39th
Dearth of a complete CBM in BCDW management	0.97	3.21	40th
Inappropriate supply chain in a CE framework or model	0.83	3.20	41st

Note: MIS = mean item score and SD = standard deviation.

The assessment of data appropriateness for factor analysis was conducted through the Kaiser-Meyer-Olkin (KMO) measure and Bartlett's test of sphericity. In Table 3, the obtained KMO value of 0.768 exceeded the recommended threshold of 0.5, indicating adequate sampling sufficiency for factor extraction. Additionally, Bartlett's test yielded a statistically significant result ($p < 0.001$), confirming that the correlation matrix possessed sufficient variance to warrant factor analysis procedures.

TABLE 3: KMO AND BARTLETT'S TEST FOR CHALLENGES OF CE IMPLEMENTATION

Test	Value
Kaiser-Meyer-Olkin Measure of Sampling Adequacy	0.768
Bartlett's Test of Sphericity	
Approx. Chi-Square	2847.592
Df	21
Sig.	0.000

Field survey (2025).

The Chi-Square value of 2847.592 with 21 degrees of freedom indicates that the correlation matrix is significantly different from an identity matrix, thus confirming the appropriateness of factor analysis for this dataset. Following the determination of the suitability of the data for FA, FA was thus, conducted and the result is presented in Table 4. The factor analysis test reveals

ISBN: 978-978-8567-02-8

three underlying factors as challenges of CE implementation. The results in Table 5 summarize the factor loading on each of the seven extracted factors and their variables. Varimax Rotation with Kaiser Normalization was performed to confirm the adoption of the grouping of the six-component solutions. This is presented in Table 4. The rotated solution in the Varimax Rotation further revealed the presence of simple structure with the three components showing a number of strong loadings indicating that the three components are good for adoption in this study.

TABLE 4: TOTAL VARIANCE EXPLAINED FOR CHALLENGES OF CE IMPLEMENTATION

Component	Initial Eigenvalues			Rotation Sums of Squared Loadings		
	Total	% of Variance	Cumulative %	Total	% of Variance	Cumulative %
1	3.247	46.39	46.39	2.156	30.80	30.80
2	1.398	19.97	66.36	1.847	26.39	57.19
3	1.089	15.56	81.92	1.731	24.73	81.92
4	0.643	9.19	91.11			
5	0.387	5.53	96.64			
6	0.154	2.20	98.84			
7	0.081	1.16	100.00			

Field survey (2025).

The principal component analysis of circular economy implementation challenges revealed 3 distinct dimensional barriers (components). The 3 components are having Eigenvalue greater than 1 (Kaiser's Criterion) that is, considered to be highly significant.in addition, the 3 components also explained enough variance (60% - 80%), making the remaining components less significant. This substantial variance explanation demonstrates that the identified components effectively capture the primary obstacles hindering circular economy adoption. The clear factor structure provides critical understanding to the multifaceted nature of implementation challenges and offers a systematic framework for understanding and addressing barriers to circular economy transition. Therefore, Table 5 presents the three identified challenges; the client/quality challenges as primary implementation barrier, logistics Infrastructure as critical operational barrier and knowledge/Time constraints as capacity barriers. This is similar to the study of Stahel (2022) on adoption of circular economy principles for waste reduction in construction projects.

TABLE 5: ROTATED COMPONENT MATRIX FOR CHALLENGES OF CE IMPLEMENTATION

Challenge Variable	Component 1	Component 2	Component 3	Communalities
Client Preference	0.876	0.142	0.087	0.794
Quality Concerns	0.847	0.213	0.116	0.778
Liability Issues	0.623	0.574	0.182	0.746
Transport Constraints	0.084	0.908	0.061	0.834
Storage Limitations	0.129	0.831	0.113	0.724
Information Gaps	0.074	0.118	0.869	0.774
Time Constraints	0.107	0.254	0.758	0.650

Field survey (2025).

The PCA identified Client/Quality Concerns as the dominant barrier to circular economy (CE) adoption, with high loadings on Client Preference (0.88) and Quality Concerns (0.85). This reflects the centrality of market acceptance and perceived product quality in shaping CE outcomes. Consistent with Rizos et al. (2017), stakeholder resistance, particularly consumer hesitation toward recycled or refurbished products, emerges as a critical impediment. Deep-rooted preferences for new products are often tied to status, perceived reliability, and cultural norms (Kirchherr et al., 2018). Similarly, quality concerns may stem from both actual performance inconsistencies and limited user familiarity with CE products (Lieder & Rashid, 2016). The close relationship between preference and quality perceptions suggests these factors are mutually reinforcing. Addressing them requires integrated strategies that combine product quality assurance, transparency, and targeted consumer education campaigns to shift behavioral norms and build trust in CE offerings. The Logistics component emerged as a key challenge in circular economy (CE) implementation, characterized by strong loadings on Transport (0.91) and Storage (0.83). These findings reflect the central role of physical infrastructure in enabling material flow within circular systems. Unlike linear models, CE requires sophisticated reverse logistics networks for collecting, transporting, and redistributing diverse material streams (Genovese et al., 2017; Lieder & Rashid, 2016). The high loading for transport highlights how inadequate transportation infrastructure complicates material movement, creating bottlenecks in reuse and recycling processes. Likewise, storage infrastructure is critical for sorting and holding materials until reuse opportunities emerge (Akinade et al., 2020). The joint prominence of transport and storage indicates that CE logistics barriers are both mobile and stationary. Addressing these requires coordinated policy efforts and investment in logistics infrastructure, as well as enabling frameworks that support efficient material recovery and flow. The Knowledge component, defined by high loadings on Information Gaps (0.87) and Time Constraints (0.76), highlights the human capital and operational challenges impeding circular economy (CE) adoption. Information Gaps reflect a lack of technical

ISBN: 978-978-8567-02-8

know-how, market intelligence, and regulatory awareness necessary for implementing CE strategies (Lieder & Rashid, 2016; Kirchherr et al., 2018). This deficiency restricts the ability of stakeholders to identify opportunities, assess risks, and comply with policy frameworks. Time Constraints further limit CE progress by restricting opportunities for training, system development, and collaboration (Rizos et al., 2017). Their strong association suggests that knowledge-building efforts are hindered by insufficient time allocation. Addressing this barrier requires targeted capacity-building interventions, including professional education, stakeholder training, and knowledge-sharing platforms, to equip industry actors with the tools needed for systemic CE transformation (Adu-Duodu et al., 2025; Stahel, 2022). The relatively distinct factor structure, with primary loadings above 0.76 and secondary loadings typically below 0.25, indicates that these challenge dimensions are largely independent, requiring different intervention strategies. However, the Liability challenge's moderate loadings across Client/Quality (0.62) and Logistics (0.57) components suggests its cross-cutting nature as a barrier spanning multiple implementation dimensions. This finding indicates that liability concerns affect both market acceptance (through quality assurance requirements) and operational systems (through logistics insurance and risk management needs). The cross-component nature of liability challenges suggests that comprehensive risk management frameworks are necessary for circular economy implementation across all dimensions.

4. CONCLUSION

This study investigated the challenges for implementing Circular Economy principles for waste management in Nigerian construction industry, with a specific focus on Abuja construction firms. The empirical findings presented in the paper are based on extensive quantitative analysis including Relative Importance Index (RII) and Principal Component Analysis (PCA), offer important insights into the state of challenges of CE adoption for waste mitigation in Nigerian built environment. The PCA conducted distilled CE adoption challenges into three dominant themes which are client/quality challenge (primary barrier), logistics infrastructure (a critical operational barrier) and knowledge /time constraints (capacity barriers). Overall, the study concluded that the most significant impediments stemmed from consumer resistance to non-virgin products, perceptions of inferior quality, and logistical constraints relating to storage and transportation. Based on this conclusion, the study recommends that logistics Infrastructure as critical operational barrier must be addressed to facilitate broader CE adoption in Nigerian construction industry.

REFERENCES

Adebayo, W.O.; Bamisaye, J.A.; Akintan, O.B.; Ogunleye, O.S. (2021). Waste generation, disposal management technique in an urbanizing environment: A case study of Ado-Ekiti, Nigeria Res. J. Appl. Sci, 1, 66 31

Adu-Duodu, K., Wilson, S., Li, Y., et al. (2025). *A Circular Construction Product Ontology for End-of-Life decision-making*. arXiv. https://arxiv.org/abs/2503.13708.

Creswell, J. W., & Creswell, J. D. (2017). *Research design: Qualitative, quantitative, and mixed methods approaches*. Sage Publications.

Kirchherr, J., Piscicelli, L., Bour, R., Kostense-Smit, E., Muller, J., Huibrechtse-Truijens, A., & Hekkert, M. (2018). Barriers to the circular economy: Evidence from the European Union. *Ecological Economics*, 150, 264–272.

Lieder, M., & Rashid, A. (2016). Towards circular economy implementation: A comprehensive review in context of manufacturing industry. *Journal of Cleaner Production*, 115, 36–51.

Ogunmakinde, O. E., Sher, W., & Maund, K. (2022). Waste-to-energy in circular construction: A decision-making framework for developing countries. *Journal of Cleaner Production*, 357, 131778.

Rios, F. C., Grau, D., & Chong, W. K. (2021). Design for disassembly and deconstruction – Challenges and opportunities in the built environment: A review. *Resources, Conservation and Recycling*, 160, 104855.

Rizos, V., Behrens, A., Van der Gaast, W., Hofman, E., Ioannou, A., Kafyeke, T., Flamos, A., Rinaldi, R., Papadelis, S., Hirschnitz-Garbers, M., & Topi, C. (2017). Implementation of circular economy business models by small and medium-sized enterprises (SMEs): Barriers and enablers. *Sustainability*, 8(11), 1212.

Stahel, W. R. (2022). The Circular Economy: A User's Guide. *Nature Reviews Materials*, 7(3), 201–202.

Wilts, H.; Garcia, B. R.; Garlito, R. G.; Gómez, L. S. & Prieto, E. G. (2021). Artificial intelligence in the sorting of municipal waste as an enabler of the circular economy. Resources, 10, 28.

World Health Organization (WHO). (2024). *Waste and environmental health: Global review 2024*. Geneva: WHO Press.

You, Z.; Wu, C.; Zheng, L. & Feng, L. (2020). An informatization scheme for construction and demolition waste supervision and management in China. *Sustainability*, 12, 1672.

You, Z.; Wu, C.; Zheng, L. & Feng, L. (2020). An informatization scheme for construction and demolition waste supervision and management in China. *Sustainability*, 12, 1672.

Yu, B.; Wang, J.; Li, J.; Zhang, J.; Lai, Y.; Xu, X. (2019). Prediction of large-scale demolition waste generation during urban renewal: A hybrid trilogy method. *Waste Manag.*, 89, 1–9.

ISBN: 978-978-8567-02-8

024-An Assessment of Critical Challenges in Supply Chain Management: Evidence from the Nigerian Construction Industry

ADAMU Yusuf Tude, AKA Adefemi
Department of Building, Federal University of Technology, Minna
aka.femi@futminna.edu.ng

Abstract: This study assesses the critical challenges in Supply Chain Management (SCM) within the Nigerian construction industry. A quantitative survey was administered to 150 construction professionals in Abuja, utilizing a structured questionnaire with a 5-point Likert scale. Data were analyzed using descriptive statistics. Findings reveal that the current state of SCM is poor, with delay in material delivery emerging as the most severe challenge (Mean = 4.2, SD = 0.8), followed by poor stakeholder coordination and lack of transparency. The study provides empirical evidence of systemic SCM inefficiencies and establishes a diagnostic baseline such as the adoption of digital tools like Internet of things (IoT) and cloud computing for effective management. Hence, the study recommends for future research on implementation strategies of such tools for effective policy formulation in the industry.

Keywords: Critical, Challenges, Supply chain, Management, Industry

1. INTRODUCTION

The construction industry plays a vital role in the economic growth and infrastructure development of nations, including Nigeria. However, its performance is often hampered by inefficiencies in supply chain management (SCM), which is critical for ensuring timely delivery of materials, cost control, quality assurance, and stakeholder coordination (Ekanayake *et al.,* 2021). In the Nigerian context, the construction supply chain is frequently disrupted by factors such as poor logistics, unreliable suppliers, lack of skilled personnel, and inconsistent regulatory frameworks (Adebowale *et al*., 2022). Unlike manufacturing, where SCM practices are more standardized and predictable, construction projects are unique, complex, and location-dependent (Adegoke, 2022). The Nigerian construction industry continues to struggle with supply chain inefficiencies, which significantly impact project delivery, cost, and quality (Agi and Nishant, 2017), Key challenges such as delays in material procurement, weak coordination among stakeholders, and lack of transparency in supply chain operations have led to frequent project disruptions and financial losses (Oke *et al*., 2018). These issues are further intensified by the sector's reliance on outdated, manual methods of managing supply chain activities, making the processes prone to errors, miscommunication, and inefficiencies (Akinade et al., 2015). In addition, limited technological adoption, lack of transparency, and inconsistent procurement practices further weaken supply chain performance (Ajayi et al., 2017). These challenges are not only technical but also institutional, reflecting deeper systemic issues such as corruption, bureaucratic bottlenecks, and insufficient stakeholder collaboration. Study by Ibeawuchi (2018) revealed that the inefficiencies in Nigerian SCM does not only escalate project costs but also undermine the overall productivity and competitiveness of the industry. Despite the growing recognition of SCM as a driver of project success, research focused specifically on the supply chain dynamics within the Nigerian construction context remains limited. Most construction firms operate reactively rather than strategically, often addressing issues only after they escalate (Aghimien et al., 2020). Understanding the critical barriers to effective SCM is therefore, essential for developing targeted strategies that improve project delivery and sustainability in the industry. Hence, the need for the current study. This implies that the need for this study arises from the glaring gaps in the current state of SCM within Nigeria's construction industry. Based on the reviewed literature, it can be said that there is insufficient research on the specific barriers hindering the adoption of digital SCM tools in Nigeria. Understanding these barriers, whether they are financial, technical, cultural, or regulatory is critical to develop effective strategies for overcoming them (Choi et al., 2018). Therefore, this study aims to assess the critical challenges affecting supply chain management in the Nigerian construction industry. By using empirical evidence from construction professionals, the research seeks to highlight key problem areas and propose practical recommendations for enhancing supply chain efficiency, reducing waste, and improving coordination among stakeholders.

2. METHODOLOGY

The quantitative approach is justified for this study because it aligns with the research objective, which aim to assess the critical challenges in supply chain management in Nigerian construction industry. In the

ISBN: 978-978-8567-02-8

quantitative study, questionnaire was used to obtain the necessary information from the participants of the study. The questionnaire was adopted as it allowed the researchers to collect data from a large sample of construction professionals, ensuring that the findings are representative and generalizable (Creswell, 2014). The targeted study population composed of registered construction firms in Abuja Nigeria that are directly involved in or have knowledge about SCM. The sample frame for the study was purposive as it consists of only firms that their professionals were willing to take part in the survey exercise. In line with this, 15 registered firms that have adequate experience in SCM were willing to participate in the study. The professionals in the firms include builders, quantity surveyors, architects, civil engineers, project managers, and other stakeholders that play a role in the procurement, delivery, and management of construction materials and resources. The adopted sampling frame ensures that the study covers a wide range of professionals with varying levels of experience and expertise in SCM. Hence, 10 construction professionals were randomly selected from each of the 15 firms for the survey study. This implies that 150 construction professionals from the 15 study firms participated in the survey study. Data was collected through the distribution of questionnaires to the selected participants. The questionnaire was designed on a five-point Likert's scale format with two main distinct sections. The first section addressed the profile of the study respondents, while the second section was based on the various challenges experience in SCM in Nigerian construction industry. The questionnaires were distributed electronically via email and online survey platforms to ensure convenience and accessibility for the participants. Follow-up reminders were sent to encourage participation and to improve the response rate. The data collection process was conducted over a period of six weeks to allow sufficient time for participants to complete the questionnaires. The collected data was analyzed using statistical tools, such as SPSS (Statistical Package for the Social Sciences). Descriptive statistics, such as mean scores and ranking were used to summarize the data and identify trends.

3. RESULTS AND DISCUSSION

3.1 Respondent Demography

The result of the respondent's role jobs distribution is presented in Figure 1

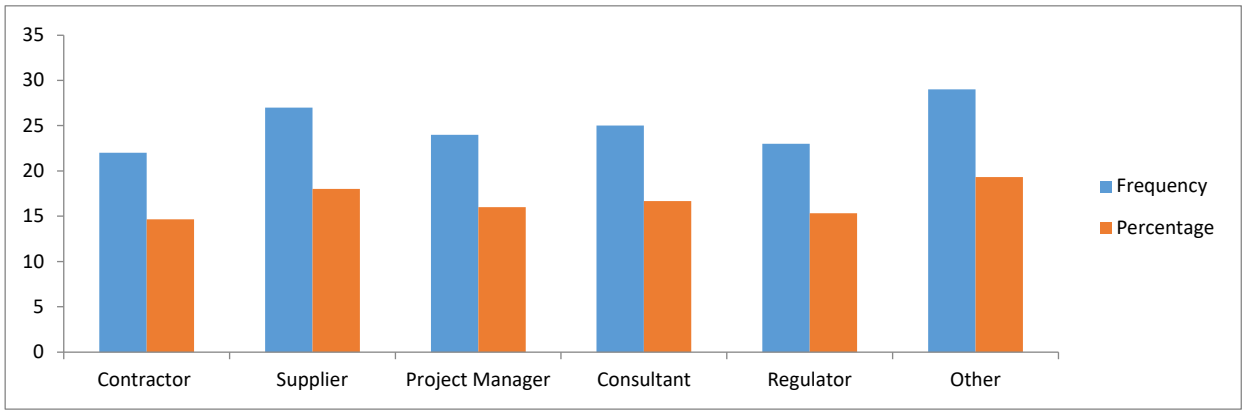


Figure 1: Job role Distribution

As shown in the table, the diversity of job roles indicates a balanced representation of key stakeholders in the construction supply chain. Notably, Suppliers (18%) and Consultants (17%) form a significant portion, suggesting that perspectives on material sourcing and professional advisory services are well captured. Contractors and Project Managers (16%) provide insight into the operational and managerial aspects of supply chain processes.

Also, Regulators (15%) are crucial in understanding policy and compliance aspects that influence technology adoption. The 'Other' category (19%) could include emerging roles such as digital transformation officers, IT specialists, or logistics managers, highlighting a growing multidisciplinary in the sector. The above result shows the representation of respondents is well distributed across the key roles in the construction supply chain.

3.2 *Challenges of Supply Chain Management in Nigerian Construction Industry*

Table 1 presents the current state analysis of Nigerian SCM based on field survey data collected, highlighting critical areas requiring immediate attention and digital intervention.

Delay in material delivery emerges as the most severe challenge facing the Nigerian construction industry with a mean item score of 4.2 (SD = 0.8), indicating that this problem occurs frequently across most projects. This finding strongly corroborates earlier studies by Akinradewo et al. (2021) that identified material procurement and delivery as the primary cause of project delays in Nigerian construction, contributing to cost overruns of up to 40% in major infrastructure projects. The consistently high scores (minimum of 3.0) across all respondents suggest that delivery delays are a systemic issue rather than isolated incidents, supporting the observations of Oke et al. (2018) that inadequate logistics

ISBN: 978-978-8567-02-8

infrastructure and poor supplier relationships are endemic in the sector. Poor stakeholder coordination ranks as the second most critical issue (Mean = 4.1, SD = 0.9) reflecting the fragmented nature of construction project management in Nigeria.

TABLE 1 DESCRIPTIVE STATISTICS (SCM PRACTICES)

SCM challenges	Mean	SD	Min	Max	Performance Level
Delay in Materials Delivery	4.2	0.8	3	5	Very High Problem
Poor Stakeholder Coordination	4.1	0.9	2.5	5	Very High Problem
Lack of Transparency	3.9	1	2	5	High Problem
Fragmented Communication	3.8	0.9	2.5	5	High Problem
Supplier Collaboration	2.3	0.8	1	4	Poor Performance
Inventory Management	2.4	0.9	1	4.5	Poor Performance
Demand Forecasting	2.5	1	1	4	Poor Performance
Risk Management	2.6	0.9	1.5	4.5	Poor Performance

Field Survey (2025)

This finding aligns with Adebowale *et al.* (2022), Wang *et al.* (2020) that observed that absence of integrated project management systems can lead to poor information flow among contractors, suppliers, and clients. The high standard deviation (0.9) suggests varying experiences across different project types and organizational sizes, which supports Ogunbiyi *et al.* (2014) that pointed out that larger construction firms tend to have better coordination mechanisms than smaller local contractors. Lack of transparency (Mean = 3.9, SD = 1.0) and fragmented communication (Mean = 3.8, SD = 0.9) represent interconnected challenges that significantly impact SCM efficiency. These findings validate the work of Aghimien *et al.* (2020) that identified poor information sharing and communication gaps as major barriers to effective supply chain integration in African construction markets. The wider range of responses for transparency issues (Min = 2.0, Max = 5.0) indicates significant variation in organizational practices, suggesting that while some companies have implemented transparency measures, many still operate with limited visibility across their supply chains.

The analysis reveals consistently poor performance across critical SCM functions, with all core practice areas scoring below the midpoint of 3.0 on the performance scale. Supplier collaboration shows the weakest performance (Mean = 2.3, SD = 0.8), indicating that most organizations maintain transactional rather than strategic relationships with their suppliers. This finding supports Durdyev *et al.* (2018) observed that Nigerian construction firms often lack formal supplier development programs and partnership strategies, leading to adversarial rather than collaborative relationships that could enhance SCM performance. Inventory management performance (Mean = 2.4, SD = 0.9) reflects inadequate stock control systems and poor material planning capabilities. The low performance scores align with Ogunde *et al.* (2017) that affirmed that most Nigerian construction firms rely on manual inventory tracking systems, leading to frequent stockouts, overstocking, and increased carrying costs. The relatively wide performance range (Min = 1.0, Max = 4.5) suggests that while some organizations have invested in improved inventory systems, the majority still struggle with basic stock management practices. Demand forecasting capabilities (Mean = 2.5, SD = 1.0) represent a critical weakness that underlies many of the delivery and coordination problems identified. This poor performance corroborates the findings of (Dubey et al., 2018) that argued that Nigerian contractors typically lack sophisticated planning tools and rely heavily on experience-based estimates rather than data-driven forecasting methods. The wide standard deviation indicates significant variation in forecasting capabilities, likely reflecting differences in organizational size, project complexity, and technology adoption levels. Risk management practices (Mean = 2.6, SD = 0.9) show marginally better performance but remain below acceptable standards for effective SCM. This finding aligns with (Kshetri, 2018) that observed that while Nigerian construction firms acknowledge the importance of risk management, most lack formal risk assessment strategies and contingency planning procedures. The limited range of maximum scores (Max = 4.5) suggests that even the best-performing organizations have significant room for improvement in proactive risk management. The consistently poor performance across core SCM functions, combined with severe operational challenges, creates a compelling case for digital technology intervention. The high severity of communication and coordination problems directly supports the earlier finding that cloud computing and IoT technologies are perceived as the most important digital solutions for the sector. These performance gap is in line with the technology priorities identified by respondents, suggesting a clear understanding of the relationship between current deficiencies and potential digital solutions.

4. CONCLUSION

Premised on the empirical data, statistical analysis, and strategic interpretation, the research concludes that Nigerian construction SCM exhibits severe performance deficiencies across core functions, with universal material delivery delays and coordination failures indicating structural industry-wide problems. In other words, based on the information obtained from construction professionals in Abuja, the study provides a clear, ranked list of SCM challenges in Nigerian construction industry. The study recommends that the Nigerian construction industry should prioritize improving logistics planning/supplier relationships to address delivery delays problem, develop frameworks for

ISBN: 978-978-8567-02-8

better stakeholder coordination/transparency and use the developed frameworks to design and test specific interventions such as IoT / cloud computing digital tools and process reforms that are tailored to the identified challenges.

REFERENCES

Adebowale, O., Adeniyi, O., & Okorie, P. (2022). Challenges of supply chain management in Nigeria's construction industry: The need for digital solutions. *International Journal of Construction Innovation, 10*(2), 45–58.

Aghimien, D. O., Aigbavboa, C. O., & Oke, A. E. (2020). Digital transformation in the construction industry: A review of enabling technologies. *Journal of Engineering, Design and Technology, 18*(5), 1015–1032.

Agi, M. A., & Nishant, R. (2017). Understanding the role of digital technologies in supply chain sustainability: A systematic literature review. *Journal of Cleaner Production, 142*, 2378–2392.

Akinade, O. O., Oyedele, L. O., Bilal, M., Ajayi, S. O., Owolabi, H. A., Alaka, H. A., & Bello, S. A. (2015). Waste minimisation through deconstruction: A BIM-based deconstructability assessment score (BIM-DAS). *Journal of Cleaner Production, 94*, 330–341.

Akinradewo, O., Oke, A., & Aigbavboa, C. (2021). The role of the construction industry in economic development: A case study of Nigeria. *International Journal of Construction Management, 21*(3), 245–256.

Ajayi, S. O., Oyedele, L. O., Akinade, O. O., Bilal, M., Alaka, H. A., & Owolabi, H. A. (2017). Attributes of design for construction waste minimization: A case study of waste-to-energy project. *Renewable and Sustainable Energy Reviews, 73*, 1333–1341.

Creswell, J. W., & Creswell, J. D. (2017). *Research design: Qualitative, quantitative, and mixed methods approaches*. Sage Publications.

Choi, T. M., Wallace, S. W., & Wang, Y. (2018). Big data analytics in operations management. *Production and Operations Management, 27*(10), 1868–1883.

Dubey, R., Gunasekaran, A., Childe, S. J., & Papadopoulos, T. (2018). Big data and predictive analytics in supply chain sustainability: A review. *Journal of Business Research, 101*, 823– 834.

Eadie, R., Browne, M., Odeyinka, H., McKeown, C., & McNiff, S. (2013). BIM implementation throughout the UK construction project lifecycle: An analysis. *Journal of Information Technology in Construction, 18*, 1–15.

Eze, E., Aghimien, D., & Eze, T. (2019). Barriers to the adoption of Building InformationModeling (BIM) in the Nigerian construction industry. *Journal of Construction in Developing Countries,* 24(1), 1–16.

Fahimnia, B., Sarkis, J., & Davarzani, H. (2015). Green supply chain management: A review and bibliometric analysis. *International Journal of Production Economics,* 162, 101–114.

Gerges, M., Austin, S., Mayouf, M., & Ahiakwo, O. (2017). An investigation into the implementation of Building Information Modeling (BIM) in the Middle East. *Journal of Information Technology in Construction, 22*, 1–15.

Kshetri, N. (2018). Blockchain's roles in meeting key supply chain management objectives. *International Journal of Information Management, 39*, 80–89.

ISBN: 978-978-8567-02-8

025-Cobalt Doped Mordenite as an Efficient Catalyst for Gas Condensate Upgrade

A.Mustapha Abdullahi, B. Usman Sani, C. Ibrahim Bako, D.Abdulraheem Ochu Alabi, E. Oluwafunto Oyinkan Ilemore, F. Ibrahim Balarabe Mohammed, G. Adejoh Egah Emmanuel, H. Aminu Abdullahi, I. Sagir Umar, J. Abdulazeez Yusuf Atta

[A.B.C.D.E.F.G.H.I.J] *Department of Chemical Engineering Ahmadu Bello University Zaria*
[A.] *National Environmental Standards and Regulations Enforcement Agency (NESREA)*
[B.] *Department of Petroleum and Gas Processing Engineering, Kaduna Polytechnic*
[C.] *National Biotechnology Research Development Agency (NABRDA)*
[D] *Usmanu Danfodiyo University*
[E] *Air Force Institute of Technology (AFIT)*
[F] *Nigerian Institute of Leather and Science Technology (NILEST)*
[G] *453 Airforce Base Service Group (Productions)*
Corresponding Author: *Usman Sani, usb934@gmail.com*

Abstract: This study was aimed at modification of mordenite catalyst for Gas Condensate upgrade. The synthesis and characterisation of the Cobalt-modified Hierarchical Mordenite (Co/MOR) zeolite catalyst was achieved via Sequential Alkaline Desilication, Ion-exchange, and Incipient Wetness Impregnation. XRD analysis verified the preservation of the Mordenite (MOR) framework despite Desilication and the high dispersion of Cobalt species. Furthermore, BET analysis confirmed an increase in total surface area from 284.17 m^2/g (Raw MOR) to 313.32 m^2/g (Co/MOR), while FTIR confirmed the successful ion-exchange and moderation of Bronsted acid sites. Catalytic tests in a fixed-bed reactor confirmed the catalyst's activity in converting the gas condensate feedstock. Detailed GC-MS analysis of the liquid product demonstrated the bifunctional nature of the catalyst, which significantly altered the product distribution by promoting the formation of N-Paraffins (35.00 to 56.37%), Iso-Paraffins (3.20 to 23.30%), and Aromatics (2.64% to 3.02%) as compared to the raw feed (R1). In conclusion, the Co/MOR system demonstrates a promising catalytic pathway for upgrading gas condensate, effectively steering the reaction mechanism towards the production of Paraffins, Iso-Paraffins, and Aromatics.

1. INTRODUCTION

Gas condensate, a light liquid hydrocarbon stream rich in C_5–C_{12} alkanes and naphthene, is a promising and often underutilised alternative feedstock. Abundant in regions with substantial natural gas reserves, it has an intrinsically high hydrogen-to-carbon ratio and low aromatics content, making it an excellent candidate for selective catalytic upgrading (Tong & Ke, 2024). While maximising light olefins is a common goal, laboratory-scale fixed-bed reactor systems often face analytical challenges in reliably capturing and quantifying highly volatile gaseous products (C_2–C_4). Therefore, the commercially relevant pathway is the direct catalytic upgrade of gas condensate to maximise the yield of C5+ liquid hydrocarbons. These products represent valuable intermediate streams, primarily falling within the high-demand gasoline and distillate ranges (Lin *et al.,* 2014). Developing a catalytic process that maximises this liquid yield while controlling non-selective cracking to gas and minimising coke formation is a significant technological goal.

Zeolites are the preferred class of catalysts for hydrocarbon cracking, valued for their strong Bronsted acidity, thermal stability, and shape selectivity. Mordenite (MOR) zeolite, characterised by its one-dimensional pore system and adjustable Si/Al ratio, is particularly effective for converting linear and slightly branched paraffins found in gas condensate However, its narrow pore structure frequently leads to diffusion limitations and accelerated coke formation, causing rapid catalyst deactivation (Al-Shafei *et al.,* 2022; Song *et al.,* 2018; Tong & Ke, 2024). The aim of this study is to enhance catalytic performance of Mordenite through cobalt doping and evaluate its efficiency through gas condensate upgrade.

The incorporation of transition metals (Co, Fe, Cr, Ni, Cu, etc.) enhances the catalytic performance of zeolites toward light olefin production. Cobalt (Co) is known to improve activity in hydrocracking and Fischer-Tropsch synthesis (Lin *et al.,* 2021; Upare *et al.*, 2016). Transition metals create new Lewis acid sites (LAS) and create a bifunctional catalyst system on an acidic support. In nano-zeolite Y, the incorporation of Co was reported to decrease coke formation. The Lewis acid sites (from Co

ISBN: 978-978-8567-02-8

species) are theorised to accelerate dehydrogenation (C-H activation), producing olefins. The Bronsted acid sites (H-MOR) are primarily responsible for the subsequent cracking (C-C bond cleavage) of these olefins into shorter chains (Adriano *et al.,* 2022; Tong & Ke, 2024). This metal-acid synergy is crucial for enhancing catalyst longevity, moderating acid strength to minimise excessive cracking into gas, and inhibiting the polymerisation of intermediates into coke precursors (Al-Shafei *et al.*, 2022).

2. METHODOLOGY

2.1 Materials and Reagent

Commercial-grade Mordenite (Na-MOR), which has a high Si/Al molar ratio, was the parent zeolite used as the support material in this investigation. Cobalt (II) nitrate hexahydrate [Co $(NO_3)_2$•$6H_2O$] (Analytical grade, Sigma-Aldrich) was the metal precursor used for the metal doping. Sodium Hydroxide (NaOH) and Ammonium chloride (NH_4Cl) were utilised for alkaline treatment and ion-exchange, respectively. The feedstock was commercial gas condensate, obtained from a local gas processing facility in Nigeria.

2.2 Catalyst Preparation

The Cobalt-modified Hierarchical Mordenite (Co/MOR) catalyst was synthesised through a four-stage process focusing on achieving both enhanced porosity and optimal metal dispersion.

2.2.1 Pre-treatment and Hierarchical Modification

The commercial Na-MOR (S1: Raw Mordenite) was activated by calcining the material in a muffle furnace at 550°C for 5 hours. Alkaline Treatment (Desilication) was performed to generate hierarchical porosity (mesopores) by stirring the activated Na-MOR in 0.5 M NaOH at 70 °C for 2 hours. The material was thoroughly washed with deionised water until the effluent pH reached 7 (neutral). The solid was then dried in an oven at 90 °C for 1 hour. The Alkaline-treated zeolite was converted to the acidic H-type form by stirring in an aqueous solution of 0.5 M NH_4Cl at 70 °C for 3 hours. Finally, the NH_4-exchanged material was dried at 100°C for 2 hours and subsequently calcined at 550 °C for 5 hours to yield the protonated hierarchical MOR, which will serve as a support for the active metal (S2: Pre-treated Mordenite).

2.2.2 Cobalt (Co) Metal Doping

The final catalyst (S3: Doped Mordenite) was prepared using the incipient wetness impregnation method to achieve a target loading of 5 wt% Co. An aqueous solution of $Co(NO_3)_2 \cdot 6H_2O$ was prepared and added dropwise to the H-MOR support. The mixture was stirred and aged for 4 hours at ambient conditions. The impregnated sample was dried at 120 °C for 12 hours and then calcined at 500 °C for 4 hours in ambient air to decompose the nitrate salt and generate the active Cobalt oxide (Co_3O_4) species.

2.2.3 Catalyst and Product Characterisation Techniques

The structural, textural, and acidic properties of the catalysts (S1-S3), as well as the composition of the final product, were determined using X-ray Diffraction (XRD), BET Surface Area Analysis, Fourier-Transform Infrared Spectroscopy (FTIR), and Gas Chromatography–Mass Spectrometry (GC-MS). The XRD was performed on a Bruker D8 Advance diffractometer to determine the phase purity, crystallinity, and structural preservation of the Mordenite framework. Nitrogen adsorption–desorption isotherms at 77 K (Micromeritics ASAP 2020) were used for BET analysis to determine specific surface area, pore volume, and pore-size distribution. The GC was operated with helium as the carrier gas with column oven temperature program set as: Initial temperature of 80°C, held for 2 minutes, first ramp of 8°C/min to 150◦C, held for 1 minutes, second ramp of 25°C/min to 280◦C, held for 10 minutes.

2.3 Fixed-Bed Reactor Setup and Cracking Reactions

The thermal and catalytic cracking experiments were conducted in a vertical fixed-bed stainless-steel tubular reactor under atmospheric pressure. To ensure flow stability, a well-mixed mixture of 0.5 g of catalyst and 0.5 g of glass beads for catalytic cracking was sandwiched between two layers of Silica glass wool in the reactor bed. To purge the reactor, activate the catalyst surface, and eliminate any remaining moisture or impurities, the catalyst was processed in situ under nitrogen flow (50 mL/min) at 500°C for 1 hour before the reaction. The feedstock (vaporised gas condensate) was introduced using a syringe pump.

2.4 Product Analysis and Performance Evaluation

The condensed liquid products from the reactor were collected and analysed using a high-resolution GC-MS system. This analysis provided a qualitative and semi-quantitative identification of the hydrocarbon distribution in the feed (R1) and the products from thermal cracking (R2), catalytic cracking with unmodified H-MOR (R3), and catalytic cracking with Co/MOR (R4). The percentage area from the GC-MS chromatogram was used to represent the relative concentration of the compound classes.

3. RESULTS AND DISCUSSION

3.1 Catalyst Characterisation

3.1.1 X-ray Diffraction (XRD) Analysis

The XRD patterns were essential for phase identification, confirming the retention of the crystalline structure, and assessing the physical success of the modification steps. The samples were designated as S1 (Raw MOR), S2 (Pre-treated MOR), and S3 (Co/MOR).

Crucially, the characteristic diffraction peaks of the Mordenite framework, including the strong reflection near $2\theta = 25.8$ ° (the 202 plane), as shown in Figure 1, were preserved across all samples. The retention of the crystalline structure after the alkaline treatment confirms the structural stability required for successful hierarchical modification (Tong & Ke, 2024). The DQesilication step selectively created secondary Mesoporosity while retaining the primary microporous structure, a process known to improve mass transfer and resist

ISBN: 978-978-8567-02-8

deactivation(Maseko *et al.*, 2025; Sun *et al.*, 2025).

The XRD pattern for the final Co/MOR catalyst (S3) was analysed for the state of the 5 wt% Co loading

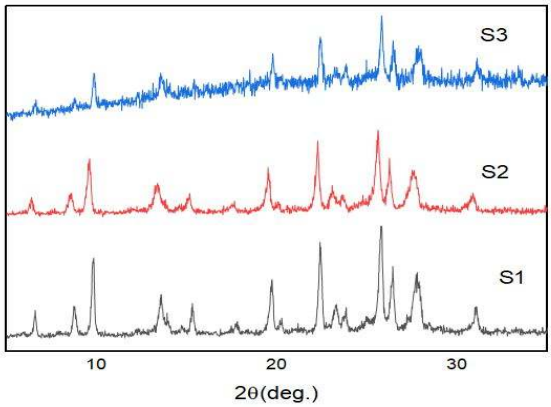


Figure 1: Magnetization as a function of applied field.

The spectrum showed no distinct, sharp diffraction peaks corresponding to crystalline Cobalt oxide (Co_3O_4), strongly indicating that the Cobalt species are highly dispersed on the MOR surface, likely as amorphous oxide clusters or nanoparticles below the detection limit of XRD. High metal dispersion is critically important for creating an optimised bifunctional catalyst. It maximises the interfacial contact between the zeolite's Bronsted acid sites and the Cobalt's Lewis acid sites. This acid-metal synergy is crucial in steering the reaction toward selective cracking (C-C bond cleavage) and suppressing undesirable side reactions, such as hydrogen transfer and coking (Akah *et al*., 2019; Maseko *et al.*, 2025; Tong & Ke, 2024)

3.1.2 BET Analysis

The textural properties of the raw (S1), pre-treated (S2), and final doped (S3) Mordenite catalysts were quantified using nitrogen physisorption (BET and BJH methods). This analysis was crucial for validating the success of the hierarchical modification step and evaluating the effect of Cobalt loading on the catalyst's porosity.

TABLE I: BET ANALYSES OF RAW MORDENITE (S1), PRE-TREATED MORDENITE (S2) AND COBALT IMPREGNATED MORDENITE (S3)

Sample	S_{BET} (m^2/g)	V_{Pore} (cm^3/g) (BJH Adsorption)	$V_{Micropore}$ (cm^3/g) (DR Method)	$D_{Micropore}$ (nm) (DR Method)
S1	284.17	0.172	0.076	2.647
S2	293.93	0.168	0.076	2.9
S3	313.32	0.193	0.082	2.8

In Table I , the chemical pre-treatment process (S1 to S2) exhibited a subtle yet significant increase in total surface area. The raw Mordenite (S1) exhibited an S_{BET} of 284.17 m^2/g, which increased to 293.93 m^2/g in the pre-treated support (S2). This moderate increase in Surface area confirms the primary objective of hierarchical modification: to enhance structural resilience. The treatment successfully cleared non-framework debris and selectively etched the silicon species to introduce mesopores without causing a substantial collapse of the microporous framework. The micropore volume remained constant at 0.076 cm^3/g (DR method), while the total pore volume saw a slight change, signifying that the new porosity occurred primarily outside the micropores. This is consistent with the creation of a mesoporous network to facilitate the rapid transport of reactants and products (Maseko *et al.*, 2025). The Cobalt impregnation (S2 to S3) resulted in the most notable change in the textural properties, validating the successful incorporation of the metal. The total surface area increased sharply from 293.93 m^2/g (S2) to 313.32 m^2/g (S3), indicating that the metal precursor was well-dispersed and that the final calcination step further cleaned the pores, creating highly active Cobalt oxide nanoclusters on the external surface. Concurrently, the total pore volume increased from 0.168 cm^3/g (S2) to 0.193 cm^3/g (S3), suggesting that the cobalt salt impregnation process acted beneficially on the open hierarchical structure, potentially removing stubborn extra-framework material upon subsequent decomposition and creating more accessible porosity (Abbas-Abadi *et al.*, 2023; Upare *et al.,* 2016; Zhao *et al.,* 2004). The micropore volume similarly increased slightly to 0.082 cm^3/g in S3, and the average micropore diameter remained constant (in the 2.8−2.9 nm range), confirming that the Co species did not block the essential primary microporous channels. This confirms the successful formation of a structurally open, Co-modified hierarchical MOR catalyst with enhanced accessibility for cracking reactions.

3.1.3 Fourier-Transform Infrared Spectroscopy (FTIR) Analysis

FTIR spectroscopy was used to probe the local structure of the Mordenite framework (T-O vibrations) and monitor the status of the various hydroxyl (OH) groups, particularly those associated with the Bronsted acid sites, across the preparation stages (S1: Raw MOR, S2: Pre-treated MOR, S3: Co/MOR).The dominant feature in all spectra, as shown in Figure 2, is a strong, broad band centred around 1049-1051 cm^{-1}. This was summarised in Table II. This band is attributed to the asymmetric stretching vibrations of the T-O bonds (T = Si or Al)

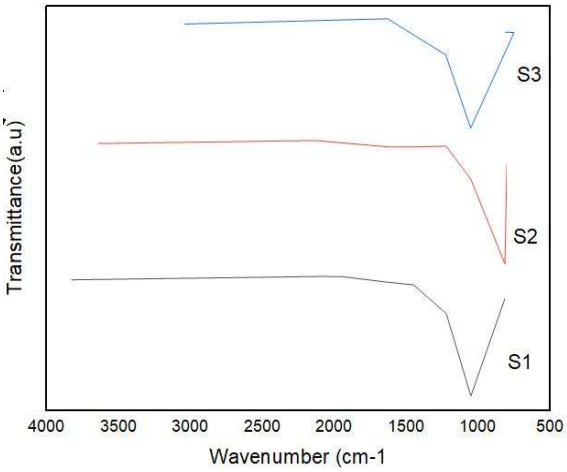


Figure 2: FTIR Spectrum of Raw Mordenite (S1), Pre-treated Mordenite (S2) and Cobalt Impregnated Mordenite (S3)

ISBN: 978-978-8567-02-8

within the zeolite framework. The position of this band is susceptible to the Si/Al ratio and the presence of extra-framework species. The consistent presence of strong bands around the peaks at 1220 cm^{-1} and 749-812 cm^{-1} further confirm the integrity of the Mordenite crystal

TABLE II: SUMMARY OF FTIR RESULT

Sample	Free OH (~3640 cm^{-1})	Adsorbed Water (~1627 cm^{-1})	Doping Effect
S1	3626.7 cm^{-1} (Weak)	1627.0 cm^{-1} (Medium)	N/A
S2	3643.5 cm^{-1} (Stronger)	1628.3 cm^{-1} (Medium)	H-type conversion successful.
S3	3641.6 cm^{-1} (Reduced/Shifted)	1628.8 cm^{-1} (Reduced)	Co interaction confirmed.

structure throughout the modification process, corroborating the XRD findings.

The analysis of the high-wavenumber region reveals critical information regarding surface water and acidic hydroxyl (OH) groups, which are directly related to the Bronsted acidity (BAS), the driving force for cracking. The H-type conversion via NH_4Cl ion-exchange (yielding S2) strengthened the free OH signal at ~approximately 3640 cm^{-1}. This band corresponds to the bridging Si-OH-Al groups, which are the primary Bronsted Acid Sites (BAS) responsible for initiating hydrocarbon cracking. The prominent BAS signal in S2 confirms the successful preparation of the highly acidic support before metal doping. The Co impregnation and calcination (S3) resulted in a noticeable reduction in the intensity of the BAS signal (~3640 cm^{-1}). This decrease in Bronsted acidity is consistent with the literature, which reports that metal incorporation leads to a degree of proton exchange, either replacing the acidic proton or directly interacting with neighbouring OH groups (Ali *et al.,* 2024). This modulation of acidity is the intended outcome of the bifunctional design, preventing overly strong BAS that accelerate undesirable hydrogen-transfer reactions and coke formation, thereby steering selectivity toward the target C_{5+} products. The S3 spectrum also exhibits a prominent, sharp peak at around 808 cm^{-1} and a shoulder in the 1400 cm^{-1} region, which may be related to the presence of extra-framework metal oxide or metallic species, supporting the indirect conclusion from XRD that Co incorporation was successful.

3.2 Catalytic Performance

The various constituents and products distributions from the GC-MS analysis of the gas condensate (R1), the condensed liquid product from thermal cracking of the gas condensate (R2), condensed liquid product from catalytic cracking of the gas condensate over Pre-treated MOR (R3) and condensed liquid product from catalytic cracking of the gas condensate over Co/MOR (R4) were shown in Figure 3. Their percentage area was taken as their relative concentration in the analysed liquid. The fractional composition from GC-MS analysis of the condensate where, 35.00% paraffins, 3.20 % iso-paraffins 22.16% Naphthene, 2.64% Olefins and 20.25%. Aromatics were found, with the remaining 16.08% constituting other constituents such as: Aldehydes, Ketones, Esters, Carboxylic Acids, Ethers, Amides, Amines and Halides. This is similar to that of straight-run gasoline, which is mainly used in the production of gasoline, where the major constituents of the gas condensate were n-paraffin and i-paraffin, with 40.54% and 35.91%, respectively (Salim *et al*., 2023)

The product obtained from the thermal and catalytic cracking of the condensate indicated an increase in the

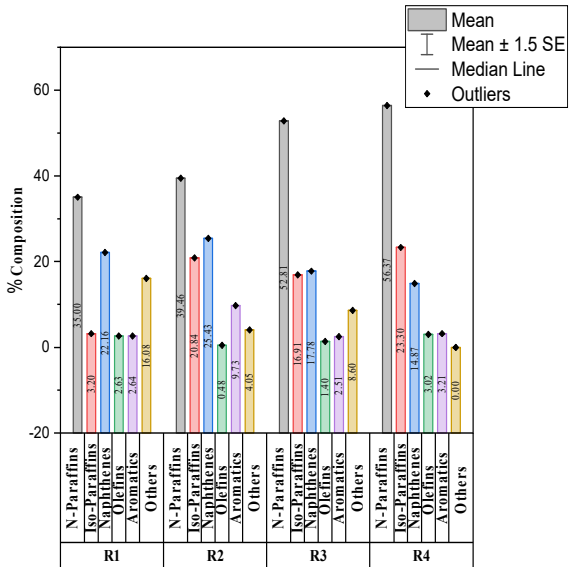


Figure 3: Product distribution from GC-MS analysis

formation of N-paraffins, Iso-paraffins, Naphthene and aromatics and a slight decrease in olefins. A higher increase in N-Paraffins and Iso-Paraffins was observed in the MOR (R3) and Co/MOR (R4) catalysed products, with Co/MOR (R4) showing the highest 56.37% N-paraffins and 23.30% Iso-Paraffins, which are far higher than those in the thermally catalysed product, with only 39.46% N-paraffins. This phenomenon may be attributed to decreased hydrogen/methane yields, leading to the formation of heavier hydrocarbons, light alkanes, and olefin products, which are crucial constituents of gasoline (*Adanenche et al., 2025).* Additionally, the increased amount of N-paraffin in Co/MOR product is also a testimony of the modulation of acidity Co/MOR, intended for bifunctional design as was observed in the FTIR result of Co/MOR, which prevents overly strong BAS that accelerate undesirable hydrogen-transfer reactions and coke formation, thereby steering selectivity toward the target C_{5+} products.

4. CONCLUSION

The catalyst synthesis protocol successfully addressed the key challenges associated with native Mordenite, as confirmed by comprehensive characterisation. The XRD analysis validated that the rigorous chemical treatment did not collapse the Mordenite framework and significantly increased the concentration of the active Mordenite phase to 42 wt%.

ISBN: 978-978-8567-02-8

BET analysis confirmed the successful creation of a structurally resilient support with an increased total surface area from 284.17 m²/g (Raw MOR) to 313.32 m²/g (Co/MOR). The introduction of Cobalt generated the intended bifunctional system. XRD confirmed a high dispersion of Co species, and FTIR results confirmed the successful moderation of the Bronsted acid sites upon Co incorporation. The catalytic tests demonstrated the activity of the optimised Co/MOR catalyst, showing that the Co/MOR catalyst (R4) significantly promoted the formation of N-Paraffins (35.00 to 56.37%), Iso-Paraffins (3.20 to 23.30%), and *Aromatics (2.64% to 3.02%) as* compared to the raw feed (R1). The increased amount of N-paraffin in Co/MOR product is also a testimony of the modulation of acidity of Co/MOR, intended for bifunctional design, as was observed in the FTIR result of Co/MOR. This research successfully linked catalyst synthesis and modification to the resulting liquid hydrocarbon product composition, establishing a critical benchmark for the sustainable utilisation of gas condensate.

RECOMMENDATIONS

Future studies should focus on quantify BAS/LAS via pyridine-FTIR, evaluating the long-term stability and deactivation behavior of the Co/MOR catalyst under continuous operation, including coke formation, metal sintering, and acidity loss. Catalyst regeneration and reusability, Co leaching should also be assessed to establish operational durability. To advance industrial applicability, scale-up and catalyst shaping effects on structural integrity and performance require investigation. Further optimization of reaction conditions and evaluation under varying condensate compositions and impurity levels are recommended. Finally, mechanistic and kinetic studies, as well as exploration of alternative or bimetallic metal loadings, would provide deeper insight into structure–performance relationships and enhance catalyst design

ACKNOWLEDGMENT

The authors sincerely appreciate the Petroleum Technology Development Fund Professorial Chair Ahmadu Bello University Zaria, Professor Abdulazeez Yusuf Atta for his invaluable guidance, support and mentorship throughout the course of this work.

REFERENCES

Abbas-Abadi, M. S., Ureel, Y., Eschenbacher, A., Vermeire, F. H., Varghese, R. J., Oenema, J., Stefanidis, G. D., & Van Geem, K. M. (2023). Challenges and opportunities of light olefin production via thermal and catalytic pyrolysis of end-of-life polyolefins: Towards full recyclability. *Progress in Energy and Combustion Science*, *96*, 101046. https://doi.org/10.1016/j.pecs.2022.101046

Adriano, A., Cornejo, M. H., Baykara, H., Ludeña, E. V., & Brito, J. L. (2022). Dealumination and Characterisation of Natural Mordenite-Rich Tuffs. *Materials*, *15*(13), 4654. https://doi.org/10.3390/ma15134654

Akah, A., Williams, J., & Ghrami, M. (2019). An Overview of Light Olefins Production via Steam Enhanced Catalytic Cracking. *Catalysis Surveys from Asia*, *23*(4), 265–276. https://doi.org/10.1007/s10563-019-09280-6

Ali, M. F., He, M., Rizwan, M., Song, Y., Zhou, X., Asif Nawaz, M., Sun, H., Zhou, M., & Jiang, P. (2024). Enhancing the selectivity for light olefins through catalytic cracking of n-hexane by phosphorus doping on lanthanum-modified ZSM-5. *Frontiers in Chemistry*, *12*, 1368595. https://doi.org/10.3389/fchem.2024.1368595

Almuqati, N. S., Aldawsari, A. M., Alharbi, K. N., González-Cortés, S., Alotibi, M. F., Alzaidi, F., Dilworth, J. R., & Edwards, P. P. (2024). Catalytic production of light Olefins: Perspective and prospective. *Fuel*, *366*, 131270. https://doi.org/10.1016/j.fuel.2024.131270

Al-Shafei, E. N., Masudi, A., Yamani, Z. H., & Muraza, O. (2022). Steam Catalytic Cracking of n-Dodecane to Light Olefins over Phosphorous- and Metal-Modified Nanozeolite Y. *ACS Omega*, *7*(35), 30807–30815. https://doi.org/10.1021/acsomega.2c02119

Bai, Y., Liu, D., Zhao, L., Gao, J., Xu, C., Pang, H., & Gao, X. (2022). Tuning the concentrations of acid sites on ZSM-5 zeolite for improving light olefin production in catalytic pyrolysis of paraffin. Industrial & Engineering Chemistry Research, 61(43), 15842–15855.

Beyerlein, R. A., McVicker, G. B., Yacullo, L. N., & Ziemiak, J. J. (1988). The influence of framework and nonframework aluminum on the acidity of high-silica, proton-exchanged FAU-framework zeolites. The Journal of Physical Chemistry, 92(7), 1967-1970.

Boronat, M., Viruela, P., & Corma, A. (1998). Theoretical study of the mechanism of zeolite-catalysed isomerisation reactions of linear butenes. The Journal of Physical Chemistry A, 102(6), 982–989.

Corma, A. V. O. A., & Orchillés, A. V. (2000). Current views on the mechanism of catalytic cracking. Microporous and mesoporous materials, 35, 21–30.

Liu, Y., Yan, L., Bai, Y., & Li, F. (2018). Catalytic upgrading of volatile from coal pyrolysis over faujasite zeolites. Journal of Analytical and Applied Pyrolysis, 132, 184–189.

Narbeshuber, T. F., Stockenhuber, M., Brait, A., Seshan, K., & Lercher, J. A. (1996). Hydrogen/Deuterium exchange duringn-butane conversion on H-ZSM-5. Journal of Catalysis, 160(2), 183-189.

Olah, G. A. (1973). Carbocations and electrophilic reactions. Angewandte Chemie International Edition in English, 12(3), 173-212.

Peng, Z. H. A. I., Zheng, J., Zhang, J. Y., & Huan, W. A. N. G. (2021). Insight into reaction path and mechanism of catalytic cracking of n-hexane in

ISBN: 978-978-8567-02-8

HZSM-5 zeolites. Journal of Fuel Chemistry and Technology, 49(10), 1522–1530.

Prins, R., & Schuit, G. C. (1980). Chemistry and chemical engineering of catalytic processes. Sijthoff & Noordhoff.

Thomas, C. L. (1949). Chemistry of cracking catalysts. Industrial & Engineering Chemistry, 41(11), 2564–2573.

Tung, S. E., & McIninch, E. (1968). Zeolitic aluminosilicate: II. Surface oxide diffusion, dynamic (time variant) Lewis acids and catalytic activity with hexane on decationized Y. Journal of Catalysis, 10(2), 175–182.

Xue, Y., Li, J., Wang, P., Cui, X., Zheng, H., Niu, Y., ... & Fan, W. (2021). Regulating Al distribution of ZSM-5 by Sn incorporation for improving catalytic properties in methanol to olefins. Applied Catalysis B: Environmental, 280, 119391.

Lin, L., Qiu, C., Zhuo, Z., Zhang, D., Zhao, S., Wu, H., Liu, Y., & He, M. (2014). Acid strength controlled reaction pathways for the catalytic cracking of 1-butene to propene over ZSM-5. *Journal of Catalysis*, *309*, 136–145. https://doi.org/10.1016/j.jcat.2013.09.011

Lin, Q., Zhang, S., Wang, J., & Yin, H. (2021). Synthesis of modified char-supported Ni–Fe catalyst with hierarchical structure for catalytic cracking of biomass tar. *Renewable Energy*, *174*, 188–198. https://doi.org/10.1016/j.renene.2021.04.084

Maseko, P., Cele, M. N., & Mdleleni, M. M. (2025). Olefin selectivity of K-Mn promoters on CoFe-ZSM-5 based catalyst in CO2 hydrogenation. *Frontiers in Chemistry*, *13*, 1562436. https://doi.org/10.3389/fchem.2025.1562436

Rahimi, N., & Karimzadeh, R. (2011). Catalytic cracking of hydrocarbons over modified ZSM-5 zeolites to produce light olefins: A review. *Applied Catalysis A: General*, *398*(1–2), 1–17. https://doi.org/10.1016/j.apcata.2011.03.009

Salim M.A., Mohammed, A., Ahmed, M. J., Maan, M.D., & Usama, A. S. (2023). Gasoline production via metha-forming process using modified and shaped Zn/ZSM-5 zeolite, DOI: https://doi.org/10.1016/j.cscee.2023.100423

Song, G., Chen, W., Dang, P., Wang, Y., & Li, F. (2018). Synthesis of an excellent MTP catalyst: Hierarchical ZSM-5 zeolites with great mesoporosity. *Royal Society Open Science*, *5*(12), 181691. https://doi.org/10.1098/rsos.181691

Sun, W., Yan, Y., Wei, Y., Ma, J., Niu, Z., & Hu, G. (2025). Catalytic Pyrolysis of Biomass: A Review of Zeolite, Carbonaceous, and Metal Oxide Catalysts. *Nanomaterials*, *15*(7), 493. https://doi.org/10.3390/nano15070493

Tong, Y., & Ke, M. (2024). Study on the Acidic Modification of Mesoporous HZSM-5 Zeolite and Its Catalytic Cracking Performance. *Catalysts*, *14*(10), 713. https://doi.org/10.3390/catal14100713

Upare, D. P., Park, S., Kim, M. S., Kim, J., Lee, D., Lee, J., Chang, H., Choi, W., Choi, S., Jeon, Y.-P., Park, Y.-K., & Lee, C. W. (2016). Cobalt promoted Mo/beta zeolite for selective hydrocracking of tetralin and pyrolysis fuel oil into monocyclic aromatic hydrocarbons. *Journal of Industrial and Engineering Chemistry*, *35*, 99–107. https://doi.org/10.1016/j.jiec.2015.12.020

Zhao, G., Teng, J., Jin, W., Yang, W., Xie, Z., & Chen, Q. (2004). Catalytic cracking of C4 olefins over P-Modified HZSM-5 zeolite. *Chinese Journal of Catalysis*, *25*, 3–4.

ISBN: 978-978-8567-02-8

5TH Faculty of Engineering Conference on Engineering Innovation and Economic Policies: Driving Sustainable Industrial Growth in Nigeria

Faculty of Engineering, Bayero University, Kano.

026-Academia–Industry–Government Collaboration: A Strategic Imperative for Sustainable Industrial Growth in Nigeria

Author(s): **Engr. Shehu Abba Aliyu[1], Engr. Thomas Oladeji Ojo[2]**

Affiliation: 1. Executive Director (System Planning) NISO
2. Assistant General Manager (Research) NISO

Abstract: The interplay between academia, industry, and government has emerged as a critical determinant of national competitiveness and industrial sustainability in the 21st century. In the Nigerian context, the absence of a functional synergy among these three stakeholders has limited the commercialization of research outputs, weakened indigenous innovation capacity, and constrained industrial diversification. This paper interrogates the strategic relevance of academia–industry–government (AIG) collaboration in driving sustainable industrial growth through engineering innovation and policy coherence. Anchored on the Triple Helix Model and the National Innovation System framework, the study employs a qualitative analytical approach drawing from policy documents, institutional case studies, and comparative global experiences. It argues that Nigeria's industrial transformation depends on creating structured collaborative ecosystems that align research, production, and policy interests. The paper proposes a coordinated model involving technology transfer offices, industrial innovation clusters, co-funded research initiatives, and synchronized policy instruments to enhance innovation diffusion and productive capacity. Ultimately, it contends that effective AIG collaboration represents not only a catalyst for sustainable industrialization but also a pathway to achieving the Sustainable Development Goals (SDGs), particularly Goal 9 on industry, innovation, and infrastructure.

1. INTRODUCTION

Industrial growth and technological advancement remain pivotal to the structural transformation of national economies, particularly in emerging nations such as Nigeria. In recent decades, engineering innovation has become the cornerstone of sustainable industrial development, determining the capacity of states to produce, adapt, and compete within global value chains. However, the persistent fragmentation among key innovation stakeholders—academia, industry, and government—continues to undermine the full realization of Nigeria's industrial potential. While universities and research institutions generate substantial scientific knowledge, industries frequently lack the absorptive capacity or policy incentives to translate these outputs into tangible products or processes. The government, often the key orchestrator of national innovation systems, has struggled to institutionalize frameworks that effectively synchronize research, development, and industrial application (Oke and Akinwale, 2021).

Nigeria's industrial trajectory reflects a paradox of potential and underperformance. The country possesses significant human capital, natural resources, and a growing population that could sustain a robust manufacturing sector. Yet, its industrial sector contributes less than 13 percent to Gross Domestic Product (GDP), and its manufacturing base remains import-dependent and technologically shallow (National Bureau of Statistics [NBS], 2023). The disconnect between academic research and industrial practice has contributed to this stagnation. Most engineering innovations produced in Nigerian universities rarely progress beyond the prototype stage due to inadequate funding mechanisms, weak intellectual property frameworks, and insufficient engagement with private-sector actors who drive commercialization. Government policy instruments, though numerous, often operate in silos and lack sustained coordination among implementing agencies such as the National Agency for Science and Engineering Infrastructure (NASENI), the Tertiary Education Trust Fund (TETFund), and the National Office for Technology Acquisition and Promotion (NOTAP).

The absence of a functional tripartite collaboration has broad implications for national development. First, it perpetuates the dependency on foreign technology and expertise, undermining indigenous engineering capacity. Second, it limits employment generation within high value manufacturing sectors, thereby constraining inclusive growth. Third, it erodes Nigeria's competitiveness in the global knowledge economy, where innovation-driven industrialization serves as the principal engine of sustainable prosperity. In contrast, countries that have institutionalized academia–industry–government collaboration, such as Germany, South Korea, and Singapore, have successfully leveraged innovation ecosystems to achieve remarkable industrial performance (Adelekan, 2022; World Bank, 2021).

This paper situates the discourse on academia–industry–government collaboration within the broader context of Nigeria's quest for sustainable industrial growth. It interrogates the structural barriers hindering effective synergy among innovative actors and examines policy inconsistencies that limit the translation of research into commercial outcomes. Anchored on the **Triple Helix Model of Innovation** and the **National Innovation System (NIS)** framework, the paper argues

ISBN: 978-978-8567-02-8

that the systematic integration of academia, industry, and government within a coherent policy environment is indispensable for engineering-led industrial transformation. The ensuing sections examine the conceptual and theoretical underpinnings of such collaboration, review empirical experiences from Nigeria, and propose strategic frameworks to operationalize sustainable linkages across the three domains.

2. LITERATURE REVIEW AND THEORETICAL FRAMEWORK

2.1 Literature Review

The contemporary discourse on innovation and industrial development emphasizes the necessity of collaborative interaction among universities, industries, and governments as the foundation for a productive national innovation ecosystem. Across both advanced and developing economies, the **tripartite collaboration model**—popularly referred to as the *Triple Helix Model*—has evolved into a dominant framework explaining how societies generate, disseminate, and commercialize knowledge (Etzkowitz & Leydesdorff, 1995; Carayannis & Campbell, 2009). The model posits that innovation emerges from the dynamic interplay among three principal institutional spheres: universities as knowledge producers, industries as economic actors and wealth creators, and governments as facilitators, regulators, and sponsors of innovation.

According to Etzkowitz and Leydesdorff (2000), effective collaboration among these entities transforms traditional linear innovation models into interactive and co-evolutionary systems. This transformation shifts the role of universities from mere centers of knowledge generation to entrepreneurial institutions actively engaged in patenting, start-up incubation, and partnership formation with industries. The industrial sector, in turn, gains from access to cutting-edge research and technical expertise, while governments establish policy environments that enable innovation diffusion, technology transfer, and commercialization.

Empirical studies further reinforce the transformative impact of academia–industry–government (AIG) collaboration on industrial productivity and sustainable economic development. For example, Bruneel, D'Este, and Salter (2010) demonstrate that knowledge transfer partnerships between universities and industries accelerate innovation outcomes when supported by enabling policy frameworks. Similarly, in emerging economies, effective collaboration enhances technology localization, encourages indigenous research adaptation, and reduces reliance on imported solutions (Adelekan, 2022).

In Nigeria, the recognition of such collaborative importance is evident in policy documents such as the **National Science, Technology and Innovation Policy (NSTIP) 2022**, which underscores the need for structured partnerships between universities, industries, and regulatory agencies. However, the gap between policy formulation and implementation remains wide. Studies by Oke and Akinwale (2021) and Irefin (2018) indicate that Nigerian universities operate largely in isolation from industrial priorities, and industries continue to perceive academic research as detached from market realities. Furthermore, the public sector has not effectively institutionalized sustainable links that could align the three spheres toward shared innovation objectives.

The limited success of current collaboration initiatives, such as those by the Tertiary Education Trust Fund (TETFund) and National Agency for Science and Engineering Infrastructure (NASENI), reveals the systemic fragmentation of Nigeria's innovation system. TETFund's Centres of Excellence, for example, have begun promoting applied research in engineering and technology, yet their impact on national industrial performance remains minimal due to insufficient integration with private-sector partners. Similarly, the Raw Materials Research and Development Council (RMRDC) and the National Office for Technology Acquisition and Promotion (NOTAP) have launched collaborative programs, but these often operate within bureaucratic and funding limitations that undermine scalability.

From a broader perspective, literature on sustainable industrial growth also emphasizes the link between innovative ecosystems and national economic resilience. The World Bank (2021) asserts that economies which effectively mobilize academia–industry–government partnerships record higher levels of productivity, technological competitiveness, and job creation. In this sense, the failure of collaboration in Nigeria is not merely an academic concern but a developmental constraint that perpetuates technological dependency and limits inclusive economic growth.

2.2 Theoretical Framework

This study is anchored on two interrelated theoretical constructs—the **Triple Helix Model of Innovation** and the **National Innovation System (NIS)** framework—both of which provide explanatory and analytical tools for understanding how collaborative mechanisms foster industrial advancement.

2.2.1 The Triple Helix Model of Innovation

The Triple Helix Model, introduced by Etzkowitz and Leydesdorff (1995), conceptualizes innovation as a product of evolving relationships among three institutional actors—universities, industries, and governments—each performing overlapping functions in knowledge generation, application, and regulation. The model departs from the traditional linear innovation process, which assumed a one-way flow of knowledge from research to production, toward a **networked, iterative system** of collaboration. In this model:

- **Universities** serve as sources of scientific discovery and technological creativity.
- **Industries** function as mechanisms for production, market validation, and resource mobilization.
- **Governments** provide the institutional frameworks, policy instruments, and funding mechanisms that enable interaction.

The model's relevance to Nigeria lies in its capacity to reframe existing relationships among institutions into cooperative partnerships rather than parallel or

ISBN: 978-978-8567-02-8

transactional engagements. It advocates for the institutionalization of **innovation clusters**, **technology parks**, and **research–industry consortia** that integrate policy, research, and commercialization within unified innovation ecosystems (Leydesdorff & Etzkowitz, 2001).

2.2.2 The National Innovation System (NIS) Framework

Complementing the Triple Helix perspective, the NIS framework views innovation as an outcome of systemic interactions among actors within a country's institutional, economic, and policy environment (Lundvall, 1992). It underscores the importance of coherence, feedback loops, and coordination in national innovation processes. The framework posits that countries that nurture linkages among research institutions, industries, and regulatory bodies are better positioned to achieve sustainable industrialization.

Applying this framework to Nigeria highlights the fragmented nature of the country's innovation architecture. Institutional actors often operate within isolated mandates, with minimal coordination or shared strategic vision. The NIS framework thus provides a normative guide for restructuring Nigeria's innovation governance toward integration, knowledge diffusion, and adaptive learning.

2.2.3 Integrating the Frameworks

The integration of the Triple Helix and NIS frameworks offers a comprehensive analytical lens for understanding and advancing AIG collaboration in Nigeria. While the Triple Helix emphasizes institutional roles and relationships, the NIS focuses on the systemic coherence and enabling environment required for collaboration. Together, they provide both micro- and macro-level insights into how policy design, institutional behavior, and market forces can be harmonized to foster engineering innovation and sustainable industrial growth. The foregoing review and theoretical synthesis underscore the necessity of reconfiguring Nigeria's innovation ecosystem to promote deeper synergy between universities, industries, and government institutions. The next section applies these theoretical insights to examine the empirical realities of academia–industry–government collaboration in Nigeria, assessing existing mechanisms, outcomes, and policy instruments.

3. EMPIRICAL CONTEXT — ACADEMIA–INDUSTRY–GOVERNMENT COLLABORATION IN NIGERIA

3.1 Overview of Nigeria's Innovation Ecosystem

Nigeria's innovation and industrial landscape reflect a complex interaction among institutional actors, policy frameworks, and market forces. Over the past two decades, the Federal Government has implemented a series of initiatives aimed at promoting technology-driven industrialization. These include the **National Science, Technology and Innovation Policy (NSTIP)**, the establishment of specialized research institutions, and the creation of funding mechanisms through agencies such as the **Tertiary Education Trust Fund (TETFund)** and the **National Agency for Science and Engineering Infrastructure (NASENI)**. Despite these efforts, the practical alignment between academia, industry, and government remains weak, leading to low research commercialization rates, limited indigenous technological innovation, and underdeveloped manufacturing capacities.

A review of Nigeria's industrial output reveals that the country continues to rely heavily on imported machinery, industrial components, and technical expertise. According to the **National Bureau of Statistics (2023)**, manufacturing contributes less than 13 percent to GDP, while less than 10 percent of university research outputs find commercial applications. The fragmentation between research institutions and industrial enterprises remains a major impediment to innovation diffusion. Moreover, policy inconsistency, inadequate infrastructure, and weak intellectual property protection exacerbate the challenge of sustaining effective collaboration.

3.2 The Role of Academia

Nigeria's academic institutions, especially those with engineering faculties, constitute significant reservoirs of scientific knowledge and technical capacity. However, the absence of structured technology transfer systems limits their contribution to industrial productivity. Most universities operate under the **research–publication paradigm**, focusing on academic output for promotion rather than industrial problem-solving or commercialization.

In recent years, some universities have begun to shift toward entrepreneurial and innovation-oriented paradigms. Institutions such as the **Federal University of Technology, Akure (FUTA)**, the **Ahmadu Bello University, Zaria (ABU)**, and the **University of Lagos (UNILAG)** have established **Centres for Innovation and Research Development (CIRD)** and **Technology Incubation Units (TIU)** designed to bridge the gap between research and industrial application. TETFund's **Centres of Excellence in Engineering** at universities such as FUTA and the University of Nigeria Nsukka (UNN) represent commendable efforts to reposition academia as a driver of technological and industrial growth. However, these initiatives often struggle with funding inadequacies, weak partnerships with the private sector, and limited access to venture capital or patent commercialization frameworks (Oke & Akinwale, 2021).

3.3 The Role of Industry

The Nigerian industrial sector is characterized by a preponderance of small- and medium-sized enterprises (SMEs), many of which lack the capacity for sustained research and development (R&D). The limited participation of the private sector in research funding—estimated at less than 5 percent of national R&D expenditure—reflects a weak culture of innovation investment (Adelekan, 2022). Unlike in industrialized countries where industries drive innovation through partnerships with universities, Nigerian industries often operate in isolation from academic research, relying primarily on imported technologies and foreign consultancy.

Some exceptions exist, notably in the oil and gas and telecommunications sectors. For instance, **Shell**

ISBN: 978-978-8567-02-8

Petroleum Development Company (SPDC) and TotalEnergies have sponsored engineering research chairs in Nigerian universities, while Huawei Technologies collaborates with Nigerian institutions on ICT capacity development. Nonetheless, these partnerships remain sector-specific and are not integrated within a national innovation system that ensures knowledge diffusion across industries.

3.4 The Role of Government and Public Institutions

The Nigerian government occupies a dual role as regulator and enabler of innovation. Through various agencies and policy instruments, it seeks to create an enabling environment for academia–industry collaboration. The **National Agency for Science and Engineering Infrastructure (NASENI)**, established in 1992, serves as the principal institutional mechanism for promoting indigenous engineering solutions and technological self-reliance. NASENI's recent initiatives, such as the **Technology Transfer Programme** with China and the development of solar energy components, underscore its role in linking research with industrial application. Yet, its effectiveness remains limited by funding constraints and insufficient private-sector integration.

The **Tertiary Education Trust Fund (TETFund)** has become one of the most active actors in fostering AIG collaboration through its Research and Development Standing Committee (RDSC) and the establishment of National R&D Foundation (NRDF). TETFund's goal is to transition Nigeria from a consumption-based economy to a knowledge-driven one by linking research funding to industrial outcomes. The fund also supports the creation of Innovation and Research Centres in universities and polytechnics to strengthen technology transfer capacity.

Similarly, the National Office for Technology Acquisition and Promotion (NOTAP) serve as the custodian of technology transfer agreements between Nigerian entities and foreign partners. It also runs programs such as the Technology Story Series and Local Patenting Initiative to encourage domestic innovation. The Raw Materials Research and Development Council (RMRDC) complement these efforts by linking researchers with industries to promote the utilization of local raw materials in manufacturing. Despite these initiatives, coordination among these agencies is minimal, leading to duplication of mandates and limited synergy.

3.5 Case Study: NASENI and Academia–Industry Partnership in Engineering Innovation

A notable empirical case of AIG collaboration is NASENI's partnership with universities and local industries in the development of small-scale power generation technologies. In collaboration with FUTA's Centre for Renewable Energy Technology, NASENI has engaged in the design and local fabrication of solar cells, turbines, and agricultural processing machines. The initiative, which combines academic expertise, industrial participation, and government funding, demonstrates the potential of collaborative engineering innovation in addressing Nigeria's infrastructure deficit. However, scaling up such projects requires sustainable funding, coherent policy support, and market integration mechanisms to commercialize outcomes (NASENI, 2023).

3.6 Empirical Assessment

An empirical assessment of Nigeria's academia–industry–government interface reveals three central weaknesses:

1. **Fragmented Collaboration Structures:** Partnerships are typically project-based rather than institutionalized, lacking legal frameworks for sustainability.
2. **Low Research Commercialization:** Less than 10 percent of research outcomes achieve industrial application, indicating a significant gap between knowledge creation and utilization.
3. **Policy Incoherence:** Multiple agencies operate with overlapping mandates and poor inter-agency coordination.

These empirical realities demonstrate that while Nigeria possesses the institutional foundation for collaboration, the ecosystem remains underdeveloped. The challenge lies in transitioning from fragmented, donor-dependent projects to institutionalized frameworks of collaboration sustained by national policy and market incentives.

4. CHALLENGES AND STRUCTURAL CONSTRAINTS

The effectiveness of academia–industry–government collaboration in Nigeria is undermined by a constellation of institutional, financial, regulatory, sociocultural, and structural challenges. These constraints impede research commercialization, weaken innovation linkages, and limit the country's capacity to build a productive industrial system anchored on engineering innovation. Understanding these barriers is essential for developing strategic interventions that can reposition Nigeria's innovation ecosystem.

4. 1 Institutional Fragmentation and Weak Governance Frameworks

A central barrier to effective AIG collaboration in Nigeria is the absence of a coherent governance framework that harmonizes the mandates of innovation-related agencies. Multiple institutions—including NASENI, NOTAP, RMRDC, TETFund, and the Federal Ministry of Science, Technology and Innovation—operate with overlapping responsibilities. This results in duplication of effort, competition for limited resources, and minimal coordination. The absence of a central body responsible for aligning research priorities with industrial needs contributes to inefficiency and policy discontinuity.

Furthermore, universities and industries often operate in institutional silos. Academic institutions prioritize publications and theoretical research, while industries focus on short-term profitability rather than long-term innovation investment. Government agencies, instead of facilitating linkages, frequently adopt regulatory postures that slow collaboration processes. The combined effect is a fragmented ecosystem that lacks the governance

ISBN: 978-978-8567-02-8

coherence necessary to sustain innovation-driven industrialization.

4.2 Funding Constraints and Limited Research Investment

Nigeria's investment in research and development (R&D) remains significantly below global and regional benchmarks. While advanced economies allocate between 2 and 4 percent of GDP to R&D, Nigeria invests less than 0.2 percent, with universities depending largely on government allocations and donor funding. This funding deficit limits the capacity of academic institutions to undertake high-quality engineering research, procure modern laboratories, maintain research infrastructure, or attract competitive research teams.

The private sector's contribution to R&D funding is negligible. Most Nigerian industries perceive research funding as a high-risk expenditure, especially given the country's infrastructural deficits, policy uncertainties, and volatile macroeconomic environment. Without sustained and diversified funding, research projects cannot progress beyond conceptual stages, and collaboration with industries remains limited. This weak financial foundation significantly slows the development of indigenous technologies and engineering innovations.

4.3 Weak Intellectual Property (IP) Protection and Technology Transfer Systems

A major structural impediment to research commercialization in Nigeria is the absence of robust intellectual property protection systems. Many universities lack functional Technology Transfer Offices (TTOs) responsible for patent registration, licensing, or negotiation of commercialization agreements. The absence of clear IP ownership guidelines between researchers, universities, and industry partners discourages collaboration and creates uncertainty about benefit-sharing arrangements.

Additionally, Nigeria's patenting culture remains underdeveloped. Many researchers are unaware of patenting processes, and industries lack confidence in the country's capacity to enforce IP rights. NOTAP's efforts to strengthen domestic patenting are commendable, but the scale remains insufficient to transform the national innovation ecosystem. Weak IP systems thus create a structural barrier that limits trust, discourages investment in innovation, and prevents universities from reaping financial benefits from commercially viable research.

4.4 Limited Absorptive Capacity within the Industrial Sector

Absorptive capacity refers to the ability of industrial firms to recognize the value of new knowledge, assimilate it, and apply it to commercial ends. In Nigeria, a significant proportion of industries lack the technical capacity, skilled workforce, or technological infrastructure needed to integrate academic research into production processes. Many engineering-based industries operate with outdated machinery, imported technologies, or low-level fabrication systems that make the adoption of advanced research outputs difficult.

This limitation is particularly pronounced among SMEs, which constitute the majority of Nigeria's manufacturing sector. Without adequate absorptive capacity, even well-developed research products from universities find no practical application in industry. This disconnect reinforces dependence on imported technologies and undermines the competitiveness of domestic industries.

4.5 Policy Inconsistency and Regulatory Instability

Nigeria's innovation and industrial policies often suffer from discontinuity and inconsistent implementation. Changes in political leadership frequently result in shifts in priorities, discontinuation of programs, or abandonment of initiatives that require long-term commitment to yield results. Industrial policies are often drafted without adequate stakeholder consultation, weakening their relevance to academic and industrial needs.

Regulatory instability affects both local and foreign investors, discouraging long-term investment in engineering innovation, research partnerships, and industrial modernization. The absence of stable policy environments prevents the institutionalization of long-term AIG collaboration, which by its nature requires continuity and predictable governance structures.

4.6 Cultural and Perceptual Barriers

Differences in institutional cultures between universities, industries, and government agencies contribute significantly to weak collaboration. Academic institutions emphasize theoretical rigor, peer-reviewed publications, and long project timelines. Industries prioritize speed, profitability, and market relevance. Government agencies focus on compliance, bureaucracy, and political visibility. These diverging institutional cultures lead to communication gaps, mistrust, and misaligned expectations.

Additionally, academia–industry engagement is often hindered by negative perceptions. Industries frequently view universities as disconnected from market realities, while academics perceive industries as unwilling to invest in knowledge creation. This mutual mistrust creates a sociocultural barrier that limits joint innovation initiatives.

4.7 Infrastructural Deficits and Technological Limitations

AIG collaboration in Nigeria is constrained by poor infrastructure, including irregular power supply, inadequate laboratories, insufficient broadband penetration, and limited access to modern engineering equipment. These infrastructural deficits reduce research efficiency, discourage private-sector participation in innovation, and make Nigeria a less attractive partner for global technology firms.

Laboratory obsolescence in many engineering faculties undermines experimentation, prototyping, and product testing. Industries also face infrastructural limitations that restrict their capacity to scale up production or integrate new technologies. Without substantial investment in critical infrastructure, collaboration efforts cannot yield meaningful industrial transformation.

ISBN: 978-978-8567-02-8

4.8 Fragmented Innovation Data Systems

Reliable data on R&D expenditure, collaboration outcomes, patenting activity, and industrial innovation performance remain limited in Nigeria. The absence of integrated innovation databases makes it difficult for policymakers and researchers to monitor collaboration, track progress, or design evidence-based policies. This data gap contributes to poorly informed intervention strategies and hinders institutional learning across sectors.

5. STRATEGIC PATHWAYS AND POLICY RECOMMENDATIONS

The persistent disconnection among academia, industry, and government actors necessitates deliberate and well-coordinated interventions to build a functional innovation ecosystem capable of supporting sustainable industrial growth in Nigeria. Effective strategies must be systemic, long-term, and anchored in a national framework that integrates policy, research, and industrial development. This section outlines strategic pathways and policy recommendations designed to strengthen collaboration and foster engineering innovation across the country.

5.1 Institutionalizing National Frameworks for Collaboration

A coherent national coordination mechanism is essential to overcome institutional fragmentation. Nigeria requires a legally established **National Council for Academia–Industry–Government Innovation (NCAIGI)** mandated to harmonize the operations of innovation-related agencies and ensure alignment with industrial development priorities. The council should include senior representatives from universities, industry associations, government ministries, and development partners.

Its core responsibilities should include:

1. Defining national research priorities linked to industrial needs.
2. Overseeing funding allocation for collaborative research.
3. Coordinating inter-agency activities to minimize duplication.
4. Monitoring research commercialization outcomes.

By institutionalizing such a council, Nigeria can achieve the governance coherence necessary to sustain innovation efforts beyond political cycles.

5.2 Strengthening Technology Transfer Offices (TTOs)

To enhance research commercialization, all tertiary institutions should be required to establish fully functional TTOs with trained legal, financial, and technical staff. TTOs should serve as intermediaries responsible for:

1. Patent filing and intellectual property protection.
2. Negotiating licensing agreements with local industries.
3. Supporting academics in transforming research prototypes into commercial products.
4. Facilitating spin-off and start-up creation.

Federal government incentives should support TTO operations, including dedicated funding for patenting fees, training programs, and commercialization support. A national network of TTOs should also be established to standardize processes and share best practices across institutions.

5.3 Promoting Innovation Clusters and Industrial Parks

Establishing innovation clusters where universities, industries, and regulatory agencies co-locate can accelerate knowledge diffusion and technology adoption. Nigeria should develop **Engineering Innovation Zones (EIZs)** in strategic locations such as Lagos, Abuja, Kano, Port Harcourt, and Aba. Industries that operate within the zones should benefit from:

1. Tax incentives for employing university researchers.
2. Grants for collaborative engineering projects.
3. Access to innovation vouchers for procuring university-developed technologies.

Such zones will support high-level engineering innovation in renewable energy, robotics, advanced manufacturing, agricultural machinery, and digital systems.

5.4 Expanding Co-Funded Research through Public–Private Partnerships

To address funding challenges, Nigeria must adopt a co-financed model for research and innovation. Government agencies such as TETFund and NASENI should collaborate directly with private-sector firms to create competitive **Co-Funded Innovation Grants (CIGs)**.

The model should:

1. Require industries to match government funding for R&D.
2. Prioritize projects that demonstrate commercial and industrial relevance.
3. Tie project renewal to clear milestones such as patent filings, prototype testing, and technology transfer outcomes.

This approach encourages risk-sharing, ensures industry relevance, and strengthens incentives for private-sector R&D investment.

5.5 Aligning Engineering Curricula with Industrial Needs

Nigeria's engineering curricula must be restructured to incorporate real-world industrial challenges, applied research, and entrepreneurial skills. Universities should integrate:

1. Mandatory industrial internships guided jointly by academics and industrial supervisors.
2. Jointly supervised final-year engineering projects addressing live industrial problems.
3. Modular courses on product design, innovation management, and industrial systems engineering.
4. University–industry advisory committees that regularly review curricula.

ISBN: 978-978-8567-02-8

Such reforms will enhance graduate employability, strengthen university–industry relationships, and increase the absorptive capacity of domestic industries.

5.6 Enhancing Intellectual Property Protection

Nigeria must strengthen its intellectual property infrastructure to build trust among innovation actors. Policy reforms should include:

1. Fast-track patent review processes for engineering and technological innovations.
2. Establishment of specialized IP courts to handle infringement disputes.
3. National guidelines clarifying IP ownership for joint projects involving academia and industry.
4. Government subsidies for patent filing by researchers and SMEs.

Improved IP systems will incentivize inventors, reduce legal uncertainty, and encourage industries to invest in domestic innovations.

5.7 Increasing Industrial Absorptive Capacity

Government should support industries, particularly SMEs, to adopt new technologies by providing:

1. Innovation adoption grants.
2. Tax reductions for firms investing in new technologies.
3. Access to subsidized engineering consultants and process engineers from universities.
4. National technical upgrading programmes for manufacturing SMEs.

These measures will equip industries with the technical capabilities needed to utilize research outputs effectively.

5.8 Creating Digital Platforms for National Innovation Connectivity

A national digital innovation portal should be created to serve as a central platform for:

1. Matching researchers with industrial partners.
2. Publishing ongoing research projects and industrial technology needs.
3. Monitoring and reporting collaboration outcomes.
4. Facilitating virtual collaborative labs and remote prototyping environments.

Such platforms improve connectivity, transparency, and communication across the innovative ecosystem.

5.9 Ensuring Policy Stability and Continuity

To sustain collaboration, Nigeria must prioritize long-term policy stability. Government should:

1. Enact innovation policies into parliamentary law to guarantee continuity.
2. Reduce bureaucratic delays that hinder partnership formation.
3. Ensure innovation policies are insulated from political transitions.

Stable policies encourage sustained investment and allow collaborative projects to mature into industrial outcomes.

5.10 Increasing Investment in Engineering Infrastructure

Finally, sustainable AIG collaboration requires significant investment in critical infrastructure. Government should expand funding for:

1. Modern engineering laboratories.
2. Prototype and testing facilities.
3. National digital infrastructure.
4. Reliable energy systems for R&D environments.

Without strong infrastructure, the innovative ecosystem cannot function effectively.

6. COMPARATIVE INSIGHTS FROM GLOBAL BEST PRACTICES

International experiences reveal that effective academia–industry–government collaboration is central to building robust innovation ecosystems capable of driving sustainable industrial transformation. While national contexts differ, several countries have institutionalized models that demonstrate how structured partnerships, coherent policy frameworks, and sustained investment in research and development can enhance industrial competitiveness. Examining these global cases provides insights that are instructive for Nigeria's efforts to deepen engineering innovation and strengthen industrial capacity.

6.1 Germany: The Fraunhofer Model and Applied Research Excellence

Germany's innovation system is anchored on an institutional architecture that integrates applied research, industrial needs, and government support. Central to this ecosystem is the network of **Fraunhofer Institutes**, which serve as intermediaries between universities and industry. These institutes are strategically designed to convert scientific research into industrial solutions. Their funding structure—characterized by a tripartite arrangement involving government grants, contract research from industry, and competitive project funding—ensures relevance, accountability, and sustainability.

The Fraunhofer model illustrates the importance of:

1. Institutionalized applied research entities dedicated to technology transfer.
2. Co-financing mechanisms that align public research with industrial priorities.
3. Legal and administrative autonomy enabling research institutes to adapt to market demands.

The model has enabled Germany to maintain global leadership in manufacturing, advanced engineering, and industrial innovation.

6.2 South Korea: Innovation Clusters and Industrial Modernization

South Korea's transformation from a low-income economy to a global industrial power is attributed to deliberate policies that foster strong linkages among universities, industries, and government agencies. The establishment of innovation clusters such as **Daedeok Innopolis** reflects a strategic approach to co-locating research institutions, technology firms, and state agencies to accelerate knowledge diffusion.

Key elements of the Korean model include:

ISBN: 978-978-8567-02-8

1. Long-term national innovation plans with clear industrialization targets.
2. Strong state intervention to promote technology localization and reduce import dependency.
3. Structured partnerships between universities and conglomerates (chaebols) in areas such as electronics, automotive engineering, and biotechnology.

These strategies have produced an ecosystem with high R&D intensity, competitive manufacturing capabilities, and sustained technological advancement.

6.3 Singapore: Policy Coherence and Integrated Research Governance

Singapore's innovation success is built on policy coherence, efficient governance, and proactive investment in research infrastructure. The government established the **Agency for Science, Technology and Research (A*STAR)** to coordinate national research agendas, support technology commercialization, and facilitate collaboration with global and domestic industries. The agency operates research institutes focused on engineering, materials science, and advanced manufacturing, while universities host technology incubators and entrepreneurship programs closely linked with industry needs.

Lessons from Singapore's model emphasize:

1. Centralized coordination of research policies to ensure alignment with economic development objectives.
2. Integrated funding mechanisms that support basic research, applied research, and commercialization.
3. Strong intellectual property frameworks and predictable regulatory environments that encourage private-sector investment in innovation.

These approaches have positioned Singapore as a leading innovation hub in Southeast Asia.

6.4 United States: University–Industry Partnerships and Entrepreneurial Universities

The United States offers a diversified model characterized by entrepreneurial universities, venture capital ecosystems, and supportive federal policies. Institutions such as the **Massachusetts Institute of Technology (MIT)** and **Stanford University** exemplify robust university–industry linkages. Their technology licensing offices, research parks, and collaboration agreements with private firms create dynamic environments for innovation and start-up development.

Critical features of the United States model include:

1. Strong institutional autonomy enabling universities to engage in commercialization and patenting activities.
2. A vibrant venture capital sector that funds technology start-ups emerging from academic environments.
3. Federal programs such as the **Small Business Innovation Research (SBIR)** and **Small Business Technology Transfer (STTR)** initiatives that promote collaboration between small enterprises and research institutions.

The United States demonstrates how market-driven mechanisms, combined with supportive federal policies, can generate sustained innovation outcomes.

6.5 Lessons for Nigeria

Across these global cases, certain consistent principles emerge:

1. Sustained investment in research infrastructure and applied engineering facilities is essential for industrial growth.
2. Institutional mechanisms that link universities with industries must be formalized, not left to ad hoc arrangements.
3. Policy coherence and continuity are critical for long-term collaborative success.
4. Strong intellectual property protection encourages commercialization and private-sector participation.
5. Innovation clusters and research parks accelerate technology diffusion and reduce barriers between research and industry.

6. CONCLUSION AND IMPLICATIONS FOR SUSTAINABLE INDUSTRIAL GROWTH

The analysis presented in this paper demonstrates that the strength of Nigeria's innovation and industrial ecosystem depends fundamentally on the quality of interaction among academia, industry, and government. Although each sector possesses distinct capacities and mandates, their fragmentation has limited the country's ability to leverage engineering innovation for sustainable industrial development. Nigeria's persistent reliance on imported technologies, low research commercialization rates, and weak industrial absorptive capacity reflect systemic deficiencies that can only be addressed through structured, institutionalized collaboration.

Integrating the insights provided by the Triple Helix and National Innovation System frameworks, the study underscores that sustainable industrial growth requires a shift from isolated institutional efforts to coordinated, long-term strategies supported by coherent policy instruments. Strengthening technology transfer systems, enhancing intellectual property protection, improving industrial capacity, and expanding co-funded research mechanisms are essential steps toward bridging the gap between knowledge production and industrial application. Comparative experiences from Germany, South Korea, Singapore, and the United States further highlight that successful innovation-driven economies share common attributes, including sustained R&D investment, well-governed research institutions, innovation clusters, and consistent policy environments.

For Nigeria, the implications are clear. First, engineering innovation must be positioned at the core of industrial policy, supported by stable funding and targeted incentives. Second, universities must evolve into entrepreneurial research institutions capable of generating commercially relevant solutions. Third, industries must increase their commitment to research partnerships, technology adoption, and capacity upgrading. Fourth, government must provide the policy consistency, regulatory clarity, and institutional

ISBN: 978-978-8567-02-8

coordination necessary to sustain long-term collaboration.

Ultimately, achieving sustainable industrial growth in Nigeria requires more than isolated reforms; it demands an integrated national commitment to building a functional innovation ecosystem. By institutionalizing strong academia–industry–government collaboration, Nigeria can accelerate technological self-reliance, enhance manufacturing competitiveness, and position itself strategically within the global knowledge economy. Such an ecosystem is indispensable for achieving the broader goals of industrial diversification, economic resilience, and national development envisioned in contemporary policy frameworks and the Sustainable Development Goals.

REFERENCES

Adelekan, T. (2022). *Science, technology and innovation for Nigeria's sustainable development: Issues and policy imperatives.* Nigerian Institute of Social and Economic Research (NISER).

Bruneel, J., D'Este, P., & Salter, A. (2010). Investigating the factors that diminish the barriers to university–industry collaboration. *Research Policy, 39*(7), 858–868. https://doi.org/10.1016/j.respol.2010.03.006

Carayannis, E. G., & Campbell, D. F. J. (2009). "Mode 3" and "Quadruple Helix": Toward a 21st century fractal innovation ecosystem. *International Journal of Technology Management, 46*(3–4), 201–234. https://doi.org/10.1504/IJTM.2009.023374

Etzkowitz, H., & Leydesdorff, L. (1995). The Triple Helix of university–industry–government relations: A laboratory for knowledge-based economic development. *EASST Review, 14*(1), 14–19.

Etzkowitz, H., & Leydesdorff, L. (2000). The dynamics of innovation: From National Systems and Mode 2 to a Triple Helix of university–industry–government relations. *Research Policy, 29*(2), 109–123. https://doi.org/10.1016/S0048-7333(99)00055-4

Federal Ministry of Science, Technology and Innovation. (2022). *National Science, Technology and Innovation Policy.* Government of the Federal Republic of Nigeria.

Lundvall, B. A. (Ed.). (1992). *National systems of innovation: Toward a theory of innovation and interactive learning.* Pinter Publishers.

National Agency for Science and Engineering Infrastructure. (2023). *NASENI 2023 annual report.* Government of the Federal Republic of Nigeria. https://naseni.gov.ng

National Bureau of Statistics. (2023). *Nigerian gross domestic product report Q4 2023.* Abuja: National Bureau of Statistics. https://nigerianstat.gov.ng

National Office for Technology Acquisition and Promotion. (2021). *Annual report on technology acquisition and promotion in Nigeria.* Federal Ministry of Science, Technology and Innovation.

Oke, A., & Akinwale, Y. O. (2021). University–industry collaboration and innovation performance in Nigerian manufacturing firms. *African Journal of Science, Technology, Innovation and Development, 13*(3), 331–340. https://doi.org/10.1080/20421338.2020.1756890

Raw Materials Research and Development Council. (2022). *Annual report on raw materials development and industrial linkages in Nigeria.* RMRDC Publications. https://rmrdc.gov.ng

World Bank. (2021). *The innovation imperative for developing East Asia.* World Bank Publications. https://doi.org/10.1596/978-1-4648-1702-3

World Intellectual Property Organization. (2022). *Global innovation index 2022: What is the future of innovation-driven growth?* WIPO. https://www.wipo.int/global_innovation_index

ISBN: 978-978-8567-02-8

27 -Aligning Industrial Policy With Engineering Development: Operationalising Nigeria's Industrial Strategy Through Applied Engineering

Author: Engr. Abdu Bello Mohammed, FNSE

Author Address: Managing Director/CEO,
Nigerian Independent System Operator (NISO)

Abstract: Engineering development is a foundational driver of industrialisation, shaping the capacity of nations to design, build, and sustain the systems that underpin productive economic activity. In Nigeria, however, the implementation of industrial policy has been hindered by the weak alignment between policy ambitions and the maturity of the country's engineering development ecosystem. This paper examines how engineering development enables the execution of national economic and industrial policies and identifies the institutional, financial, and structural conditions necessary to strengthen this alignment. Using an integrated analytical framework that connects engineering development functions with national innovation and industrialisation priorities, the study evaluates the current performance of Nigeria's engineering institutions, development agencies, and industrial actors. The analysis reveals persistent gaps in project-to-policy translation, engineering capacity development, institutional coordination, industrial absorptive capability, and long-term funding structures. To address these constraints, the paper proposes a comprehensive alignment model comprising a national industrial development implementation unit, strengthened engineering development offices, regional engineering development zones, and co-funded engineering development grants. The study concludes that coherent alignment between industrial policy and engineering development is essential for accelerating Nigeria's structural transformation, expanding domestic manufacturing capacity, and enhancing competitiveness within a rapidly evolving global production landscape.

Keywords: Engineering development; industrial policy; engineering capacity building; industrial transformation; applied engineering; national development strategy; Nigeria; innovation systems.

1. INTRODUCTION

Industrial policy constitutes the strategic framework through which national development priorities are articulated; engineering development provides the technical capacity that determines whether those priorities can be executed effectively. In emerging economies, the interplay between policy ambition and engineering capability is a defining factor in the success or failure of industrial transformation. Nations that have advanced industrially have done so not merely through coherent policy design but through sustained investment in engineering development systems that support manufacturing, infrastructure, and industrial expansion (Andreoni & Chang, 2022; Szirmai, 2023).

Nigeria's industrial policy frameworks consistently emphasise structural transformation, manufacturing competitiveness, economic diversification, and technological upgrading. Yet, the operationalisation of these policies has been constrained by weak engineering development systems, limited institutional coordination, inadequate financing mechanisms, and insufficient engineering infrastructure (African Development Bank, 2022; National Bureau of Statistics, 2024; World Bank, 2023; Yusuf & Bello, 2024). The persistent reliance on imported machinery, foreign engineering consultancy services, and external technology providers reflects gaps in engineering capacity that undermine the effectiveness of industrial policy (African Development Bank, 2022; National Bureau of Statistics, 2024; World Bank, 2023; Yusuf & Bello, 2024).

This paper contends that engineering development is the practical engine through which industrial policy becomes implementable. Without a robust engineering development ecosystem, industrial policy remains aspirational. The study therefore interrogates the mechanisms through which engineering development supports national industrial policy and identifies systemic constraints that impede alignment in Nigeria.

2. THEORETICAL AND CONCEPTUAL FRAMEWORK

A. Engineering Development Systems Theory

Engineering Development Systems Theory provides a structured analytical lens for understanding how engineering capabilities evolve, interact, and translate into industrial outcomes. The theory emphasises that engineering development is not a singular activity but a sequential, interconnected pipeline comprising ideation, conceptual design, detailed engineering, prototype development, experimental verification, pilot-scale

ISBN: 978-978-8567-02-8

implementation, systems integration, and lifecycle optimisation (International Energy Agency, 2022; Khan & Roy, 2024; Lall, 2024; OECD, 2023). Each phase represents a critical technical validation stage that determines the readiness of an engineering solution for industrial deployment. In advanced industrial economies, this pipeline is supported by institutionalised engineering development infrastructures such as prototyping laboratories, testing and metrology centres, applied research institutes, fabrication workshops, and pilot-scale manufacturing units. These facilities provide the physical and methodological environments necessary for generating reliable engineering data, conducting stress and performance analysis, validating designs under simulated field conditions, and ensuring compliance with national and international engineering standards (International Energy Agency, 2022; Khan & Roy, 2024; Lall, 2024; OECD, 2023).

Moreover, Engineering Development Systems Theory highlights feedback loops between stages. Results from prototype testing inform design modifications; pilot-scale outcomes refine process engineering models; lifecycle data improve reliability engineering strategies. These iterative loops ensure continuous improvement, reduce the probability of failure during scale-up, and increase the likelihood of successful industrial adoption (Adeniran & Akomolafe, 2022; Akinware & Oladipo, 2023; Kaplinsky & Morris, 2023; NASENI, 2023; Szirmai, 2023). In contexts like Nigeria where such pipelines are weak or fragmented, engineering solutions often stall at the conceptual or prototype phase, limiting the realisation of industrial policy goals (Adeniran & Akomolafe, 2022; Akinware & Oladipo, 2023; Kaplinsky & Morris, 2023; NASENI, 2023; Szirmai, 2023). Finally, the theory underscores the importance of engineering infrastructure maturity, institutional coherence, stable funding, and skilled manpower. Without these foundational elements, even well-crafted industrial policies cannot translate into robust engineering outcomes (Adeniran & Akomolafe, 2022; Akinware & Oladipo, 2023; Kaplinsky & Morris, 2023; NASENI, 2023; Szirmai, 2023).

B. National Innovation Systems (NIS)

The NIS framework situates engineering development within a broader ecosystem comprising universities, polytechnics, research institutes, industrial firms, government agencies, financial institutions, and standards organisations. It posits that innovation performance is shaped not merely by the presence of individual institutions but by the quality of interactions, knowledge flows, coordination mechanisms, and learning processes among them (Etzkowitz, 2022; OECD, 2023; WIPO, 2023; World Bank, 2023). In a strong NIS, engineering research generated in academia moves fluidly into industrial practice through structured partnerships, industry-sponsored research programmes, cooperative laboratories, and commercialisation pathways. Government agencies provide regulatory clarity, long-term funding, stable policy instruments, and incentives for private-sector investment in engineering. Standards organisations ensure safety, interoperability, and reliability. Financial institutions supply risk-tolerant capital to support high-cost engineering development activities (Etzkowitz, 2022; OECD, 2023; WIPO, 2023; World Bank, 2023).

In many developing economies, including Nigeria, these interfaces remain weak. Engineering research often fails to reach industry because mechanisms for technology brokerage, prototype transfer, and industrial testing are underdeveloped (African Development Bank, 2022; Federal Ministry of Science, Technology and Innovation, 2022; NASENI, 2023; NOTAP, 2023; UNIDO, 2022). Industries seldom articulate engineering needs to academic institutions, resulting in a misalignment between research outputs and industrial priorities. Government agencies frequently operate in silos, creating overlapping mandates and policy inconsistencies (African Development Bank, 2022; Federal Ministry of Science, Technology and Innovation, 2022; NASENI, 2023; NOTAP, 2023; UNIDO, 2022). The NIS therefore provides a useful lens for diagnosing systemic fragmentation and institutional misalignment that hinder engineering development and industrial transformation. It underscores that engineering advancement is a systemic outcome, dependent on coherent governance, interactive learning, and strategic coordination across the innovation landscape (African Development Bank, 2022; Federal Ministry of Science, Technology and Innovation, 2022; NASENI, 2023; NOTAP, 2023; UNIDO, 2022).

C. Integrated Framework for Engineering–Policy Alignment

Integrating Engineering Development Systems Theory with NIS creates a comprehensive framework that captures both the technical processes and the institutional conditions required to operationalise industrial policy. This integrated framework conceptualises alignment as occurring at three interconnected levels:

Macro-Level Alignment (Policy–Institution Level):

Ensures that policies, governance structures, mandates, and funding mechanisms are coherent. This involves harmonising roles across ministries, research agencies, professional bodies, and standards organisations to create a unified strategic direction for engineering development (Andreoni & Chang, 2022; Federal Ministry of Science, Technology and Innovation, 2022).

Meso-Level Alignment (Organisational and Sector Level):

Involves establishing development offices, innovation clusters, engineering zones, and coordinated platforms that facilitate prototype transfer, industry interaction, and engineering project execution. This layer focuses on creating the organisational interfaces that connect knowledge producers with knowledge users (Etzkowitz, 2022; Kaplinsky & Morris, 2023).

ISBN: 978-978-8567-02-8

Micro-Level Alignment (Technical Process Level):

Relates to the engineering design, testing, validation, integration, and lifecycle processes that underpin industrial operations. This level ensures that engineering outputs are technically sound, reliable, and capable of meeting industrial performance standards (Khan & Roy, 2024; Lall, 2024).

Alignment across these three layers ensures that industrial policy is both technically feasible and institutionally executable. It also ensures that engineering development activities are driven by national needs rather than individual institutional agendas, thereby enhancing the effectiveness of industrial strategy. The absence of such alignment—evident in Nigeria's current ecosystem—results in policy drift, wasted resources, and stagnant industrial performance (African Development Bank, 2022; National Bureau of Statistics, 2024; World Bank, 2023).

3. ENGINEERING DEVELOPMENT AS THE OPERATIONAL ENGINE OF INDUSTRIALISATION

Engineering development performs the critical function of transforming policy aspirations into industrial capabilities. It bridges the gap between conceptual policy objectives and the physical, operational, and infrastructural systems that sustain industrial activities. Without a mature engineering development environment, industrial policy remains rhetorical and detached from real production systems (Andreoni & Chang, 2022; Szirmai, 2023). Engineering development supports industrialisation through several primary, interdependent mechanisms that form a value chain from conception to deployment.

A. Policy Technicalisation

This foundational mechanism ensures that industrial policy goals are translated into precise engineering deliverables. It involves the critical work of drafting technical specifications, determining system performance requirements, modelling industrial processes, estimating material and energy needs, and developing phased implementation schedules (Andreoni & Chang, 2022; Kaplinsky & Morris, 2023). In the absence of rigorous policy technicalisation, industrial policy is vulnerable to misinterpretation during execution, leading to project delays, significant cost overruns, and systemic performance failures. This function acts as the crucial translator between the language of policy and the language of engineering practice.

B. Applied Engineering Research

Applied research conducted in universities, polytechnics, and dedicated engineering institutes generates the context-specific solutions needed for industrial advancement. This includes developing hybrid renewable energy systems, precision components for manufacturing automation, corrosion-resistant materials for harsh operational environments, efficient agro-processing machinery, and localised industrial control systems (Akinware & Oladipo, 2023; Lall, 2024; TETFund, 2022). Such applied research ensures that industrialisation is grounded in indigenous engineering knowledge and adaptation capacity, reducing excessive reliance on imported, often ill-suited, foreign systems and fostering technological sovereignty.

C. Prototype Development and Validation

Prototyping is the stage where abstract designs become tangible, testable artefacts. It is a risk-mitigation process that allows developers to interrogate operational parameters, identify latent performance weaknesses, improve mechanical and electrical reliability, and accurately determine production cost implications (NASENI, 2023; OECD, 2023). Strong prototype testing and validation systems—supported by modern workshops and digital simulation tools—increase investor and end-user confidence, thereby expanding market opportunities for domestic engineering firms and reducing the perceived risk of adopting local innovations (NASENI, 2023; OECD, 2023).

D. Pilot-Scale Engineering and Industrial Feasibility

Pilot plants serve as a vital bridge between laboratory-scale proof-of-concept and full-scale industrial deployment. They demonstrate the commercial and technical feasibility of engineering solutions under conditions that closely mimic real industrial environments (International Energy Agency, 2022; Khan & Roy, 2024). This stage is indispensable for capital-intensive sectors such as food processing, mineral beneficiation, petrochemicals, and renewable energy, where large-scale operations require intricate engineering integration and where failure at scale carries severe financial consequences. Pilot facilities de-risk technology adoption for the private sector.

E. Systems Integration and Interdisciplinary Synthesis

Modern industrial systems are inherently interdisciplinary, requiring seamless integration across mechanical, civil, materials, electrical, chemical, and digital engineering domains. Systems integration is the engineering discipline that ensures all subsystems interact optimally to support overall industrial productivity, efficiency, and safety (Khan & Roy, 2024). Countries lacking strong systems integration capability typically struggle to absorb and effectively utilise new engineering solutions, resulting in suboptimal plant performance and persistent operational bottlenecks.

F. Standards, Certification, and Regulatory Compliance

Engineering development is incomplete without the establishment and enforcement of robust quality standards and certification processes. These systems ensure that engineering products and processes meet nationally and internationally recognised safety, performance, environmental, and interoperability requirements (OECD, 2023; WIPO, 2023). A strong national certification framework, operated by competent and autonomous agencies, enhances trust in locally developed engineering solutions, supports export

ISBN: 978-978-8567-02-8

competitiveness, and provides a clear quality benchmark for industrial procurement and investment decisions.

4. EMPIRICAL ANALYSIS OF ENGINEERING DEVELOPMENT CAPACITY AND CONSTRAINTS IN NIGERIA

Nigeria's engineering development environment exhibits a paradoxical mix of notable institutional strengths and profound structural deficiencies, which collectively determine its capacity to implement industrial policy.

A. Institutional Assets and Recognised Strengths

Nigeria possesses an extensive, if fragmented, network of engineering institutions that form a potential foundation for development. This includes over one hundred federal and state universities and polytechnics with engineering faculties; specialised Centres of Excellence in engineering fields funded by the Tertiary Education Trust Fund (TETFund) (NASENI, 2023; NOTAP, 2023; TETFund, 2022); the engineering development institutes and prototyping centres operated by the National Agency for Science and Engineering Infrastructure (NASENI) (NASENI, 2023; NOTAP, 2023; TETFund, 2022); the Raw Materials Research and Development Council (RMRDC); and agencies like the National Office for Technology Acquisition and Promotion (NOTAP) tasked with facilitating development transfer and local content (NASENI, 2023; NOTAP, 2023; TETFund, 2022). These entities collectively represent a substantial national investment in engineering human capital and institutional infrastructure.

B. Persistent Structural and Systemic Weaknesses

Despite these assets, deep-seated structural challenges critically hinder system performance and output. Engineering laboratories in most public institutions remain underfunded, equipped with obsolete apparatus, and lack consistent maintenance (Adeniran & Akomolafe, 2022; Akinware & Oladipo, 2023; Federal Ministry of Science, Technology and Innovation, 2022; NASENI, 2023; World Bank, 2023; Yusuf & Bello, 2024). There is a severe scarcity of integrated pilot-scale demonstration infrastructure where industries can test and refine new processes. Collaboration between academic institutions and industries is minimal and often informal, stifled by bureaucratic procurement rules, intellectual property concerns, and misaligned incentives (Adeniran & Akomolafe, 2022; Akinware & Oladipo, 2023; Federal Ministry of Science, Technology and Innovation, 2022; NASENI, 2023; World Bank, 2023; Yusuf & Bello, 2024). Commercialisation frameworks are weak, and engineering research funding is inconsistent, project-based, and seldom aligned with long-term industrial roadmaps. Furthermore, fragmented institutional mandates across the Federal Ministry of Science, Technology and Innovation, the Ministry of Industry, Trade and Investment, and other bodies result in duplication, conflicting directives, and strategic inefficiency (Adeniran & Akomolafe, 2022; Akinware & Oladipo, 2023; Federal Ministry of Science, Technology and Innovation, 2022; NASENI, 2023; World Bank, 2023; Yusuf & Bello, 2024).

C. Industrial Absorptive Capacity and Capability Limitations

The demand side of the equation—Nigerian industry—presents its own set of constraints. Most manufacturing firms, particularly Small and Medium Enterprises (SMEs), lack the internal engineering capability to integrate, adapt, and maintain new or complex engineering systems (African Development Bank, 2022; World Bank, 2023; Yusuf & Bello, 2024). Contributing factors include a chronic shortage of professional process and maintenance engineers, limited in-house systems integration expertise, a deep-seated reliance on imported spare parts and foreign technical assistance, and insufficient access to patient capital or technical financing for plant upgrades and retooling (African Development Bank, 2022; World Bank, 2023; Yusuf & Bello, 2024). These limitations create a cycle of dependency on foreign engineering systems and weaken the market pull for locally developed solutions.

D. Critical Engineering Manpower and Curriculum Gaps

A significant disconnect exists between the outputs of the tertiary education system and the needs of industry. Engineering curricula in many institutions overemphasise theoretical knowledge at the expense of applied competencies in systems integration, computer-aided design and manufacturing, industrial automation, project management, and quality control (Akinware & Oladipo, 2023). Consequently, graduates often require extensive and costly retraining upon employment. This skills mismatch weakens industrial productivity, discourages investment in local engineering talent, and perpetuates the underutilisation of indigenous engineering solutions.

5. SYSTEMIC CONSTRAINTS LIMITING ENGINEERING–POLICY ALIGNMENT IN THE NIGERIAN CONTEXT

The challenge of aligning engineering development with industrial policy in Nigeria is systemic and multi-layered. Core, interlocking constraints include:

A. Governance and Strategic Coordination Fragmentation

Multiple ministries, departments, and agencies (MDAs) oversee slices of the engineering development mandate without a unifying strategic framework or effective coordination mechanism. This leads to duplicated functions, overlapping and uncoordinated programmes, dispersed and inefficient funding, slow implementation, and overall strategic drift (Federal Ministry of Science, Technology and Innovation, 2022; World Bank, 2023). The absence of a single, empowered coordinating body with oversight of the entire engineering development pipeline is a fundamental governance failure that dissipates national effort.

ISBN: 978-978-8567-02-8

B. Chronic Financing Deficits for Capital-Intensive Development Stages

Engineering development is inherently capital-intensive. The stages of prototyping, testing, pilot-scale engineering, and tooling for manufacture require sustained, long-term funding that tolerates technical risk (African Development Bank, 2022; OECD, 2023). Nigeria's current funding structures—reliant on short-term government budgetary allocations, intermittent grants, and limited private venture capital—are ill-suited to this task. The result is a "valley of death" where promising engineering concepts fail to progress beyond the laboratory due to a lack of development financing.

C. Weak or Non-Existent Engineering Development Transfer Mechanisms

Institutions generating engineering knowledge typically lack dedicated, professionally staffed offices focused on development transfer. These would be responsible for managing prototype licensing, negotiating development contracts with industry, coordinating joint testing programmes, overseeing the creation of engineering spin-off companies, and safeguarding intellectual property (Etzkowitz, 2022; NOTAP, 2023). In their absence, innovations remain captive within academic or research settings, with no clear pathway to market.

D. Severe Infrastructure and Facility Gaps

Nigeria suffers from a critical deficit in the physical infrastructure required for modern engineering development. This includes a lack of fully equipped, digitally integrated prototyping laboratories; accredited metrology and calibration centres; pilot manufacturing plants for sectors like agro-processing and advanced materials; and independent engineering testing and certification facilities (Adeniran & Akomolafe, 2022; NASENI, 2023). Without these platforms, engineering development cannot progress beyond rudimentary phases.

E. Low Industrial Technological Capability and Investment

The manufacturing sector itself is constrained by outdated machinery, a limited technical workforce, inadequate maintenance culture, negligible investment in in-house R&D, and a pervasive dependency on original foreign equipment manufacturers for technical support and upgrades (World Bank, 2023; Yusuf & Bello, 2024). This weak demand-side capability reduces the pull for local engineering solutions and stifles innovation feedback loops.

F. Underdeveloped Standards and Certification Ecosystems

National certification bodies often lack the technical infrastructure, financial autonomy, and human capacity needed to rigorously test and certify complex engineering systems against international standards (WIPO, 2023). This undermines confidence in locally produced engineering goods and processes, both domestically and for export, and allows substandard imports to flood the market.

6. A STRATEGIC FRAMEWORK FOR ALIGNING ENGINEERING DEVELOPMENT WITH INDUSTRIAL POLICY

To overcome these constraints, a multi-pronged, integrated strategic framework is necessary. This framework must intervene at the macro (governance), meso (institutional), and micro (technical) levels simultaneously.

A. National Industrial Development Implementation Unit (NIDIU)

A high-level, statutorily established NIDIU should serve as the apex coordinating and strategy body. Its mandate would include aligning all public engineering development activities with national industrial policy; harmonising mandates and preventing duplication across MDAs; ensuring policy and funding continuity across political cycles; coordinating strategic public and private funding towards priority engineering pipelines; and monitoring a dashboard of national engineering development indicators (Andreoni & Chang, 2022; Federal Ministry of Science, Technology and Innovation, 2022). This unit would provide the missing strategic coherence at the system level.

B. Network of Engineering Development Offices (EDOs)

EDOs should be established as operational and commercialisation hubs within major universities, polytechnics, and research institutes. Their core functions would include active portfolio management for prototype commercialisation; facilitating industrial testing and validation contracts; negotiating intellectual property licenses and joint development agreements with firms; coordinating funded pilot-scale engineering projects; and providing incubation support for engineering spin-off ventures (Etzkowitz, 2022; NOTAP, 2023). These offices would professionalise the interface between knowledge creators and industrial users.

C. Regional Engineering Development Zones (EDZs)

EDZs are proposed as geographically concentrated hubs that co-locate and concentrate critical engineering capabilities. They would house shared facilities for advanced prototyping and fabrication, pilot manufacturing lines, materials testing and certification laboratories, and provide co-location space for industrial partners and start-ups (Szirmai, 2023; UNIDO, 2022). By clustering resources, EDZs would achieve economies of scale, reduce fragmentation, foster collaboration, and act as catalysts for regional industrialisation based on local comparative advantages.

D. *Co-Funded Engineering Development Grant Schemes*

Targeted grant schemes, with matched funding from government and industry, are essential to de-risk engineering development. These grants would

ISBN: 978-978-8567-02-8

incentivise deep collaboration between public research institutions and private companies, share the financial burden of high-cost development stages, and ensure projects are demand-driven and aligned with clear industrial priorities and market pathways (African Development Bank, 2022; OECD, 2023).

E. National SME Engineering Support Programme

A dedicated national programme is required to uplift the engineering absorptive capacity of the vital SME manufacturing sector. This programme could deliver targeted interventions such as subsidised maintenance engineering training, process optimisation audits, implementation of quality assurance systems, support for digital manufacturing adoption, and access to equipment calibration services (World Bank, 2023; Yusuf & Bello, 2024). Strengthening the base of industrial users is as important as strengthening the supply of engineering solutions.

F. Comprehensive Educational Reform and Standards Strengthening

Curricular reform across engineering schools must prioritise hands-on, project-based learning; systems thinking and integration; advanced manufacturing techniques; sustainable materials engineering; and competencies in robotics, industrial IoT, and automation (Akinware & Oladipo, 2023; International Energy Agency, 2022; OECD, 2023; WIPO, 2023). Concurrently, national standards institutions like the Standards Organisation of Nigeria (SON) must be technically and financially strengthened to credibly certify engineering systems, rigorously enforce safety and quality regulations, and thereby build indispensable trust in local engineering solutions (Akinware & Oladipo, 2023; International Energy Agency, 2022; OECD, 2023; WIPO, 2023).

7. COMPARATIVE INTERNATIONAL INSIGHTS AND TRANSFERABLE LESSONS

Examining the engineering development pathways of successfully industrialised nations yields valuable lessons for Nigeria's strategic realignment.

A. Germany: The Applied Institute Model

Germany's industrial pre-eminence is underpinned by a dense network of applied engineering institutes, most notably the Fraunhofer-Gesellschaft. These institutes specialise in contract research, providing industry with prototyping, pilot-scale engineering, systems integration research, and pre-competitive testing services (Andreoni & Chang, 2022). They operate at the interface between fundamental university research and industrial application, funded through a mixed model of public base funding and competitive industry contracts. This model ensures relevance, financial sustainability, and rapid technology transfer.

B. South Korea: Strategic Clustering and State-Led Upgrading

South Korea's rapid ascent was engineered through a concerted strategy of creating technology-intensive industrial clusters, state-funded pilot plants for emerging industries, and aggressive, industry-linked engineering manpower development programmes (Szirmai, 2023). The government played a direct, catalytic role in coordinating chaebols (large industrial conglomerates), public research institutes, and banks to master complex engineering systems in sectors like semiconductors, shipbuilding, and automotive, facilitating rapid industrial upgrading.

C. Singapore: Integrated Governance and Strategic Focus

Singapore's success stems from a highly coordinated model of innovation governance. Agencies like the Agency for Science, Technology and Research (A*STAR) seamlessly integrate applied research, engineering development, industrial testing, and pilot-scale demonstration within a clear national economic strategy (OECD, 2023; UNIDO, 2022). The state provides stable long-term direction, world-class infrastructure, and attracts global corporate R&D centres, creating a vibrant ecosystem where engineering development is directly tied to economic value creation.

D. United States: Ecosystem-Driven Innovation

The U.S. engineering ecosystem thrives on a powerful combination of university-industry partnerships, federally funded national laboratories conducting mission-oriented engineering R&D, a dynamic venture capital industry willing to fund deep-tech engineering start-ups, and strong intellectual property protection (Khan & Roy, 2024). This decentralised but interconnected system fosters continuous engineering innovation, industrial renewal, and the emergence of new high-tech sectors, driven by both market forces and strategic public investment in foundational technologies.

8. CONCLUSION

Engineering development must be strategically repositioned at the very centre of Nigeria's industrial policy architecture. It is the indispensable mechanism that converts policy ambition into operational reality, technical specifications into functioning factories, and national goals into economic value. Without a capable, coherent, and well-resourced engineering development ecosystem, even the most sophisticated industrial policy will fail to yield tangible, sustainable economic transformation.

The alignment framework proposed in this study—integrating macro-level governance reform via a NIDIU, meso-level institutional strengthening through EDOs and EDZs, and micro-level capacity building via targeted grants, SME support, and educational reform—provides a comprehensive and actionable pathway. This model is designed to bridge the critical gaps between policy, research, development, and industry that currently paralyse Nigeria's industrial progress.

Ultimately, investing in and meticulously organising engineering development is not merely a technical or educational imperative; it is a fundamental strategic priority for national development. Strengthening this

ISBN: 978-978-8567-02-8

core capability is the essential prerequisite for achieving Nigeria's goals of industrial diversification, structural economic transformation, enhanced global competitiveness, and the creation of a resilient, innovation-driven economy

REFERENCES

Adeniran, A., & Akomolafe, B. (2022). Engineering infrastructure deficits and industrialization constraints in Nigeria. *African Engineering Review, 4*(1), 55–72.

African Development Bank. (2022). *African industrialisation index report*.

Andreoni, M., & Chang, H.-J. (2022). The political economy of industrial development in the twenty-first century. *Structural Change and Economic Dynamics, 61*, 427–444.

Akinware, J. O., & Oladipo, M. O. (2023). Engineering education and national development: Repositioning Nigerian universities for industrial competitiveness. *Nigerian Journal of Technological Development, 19*(2), 45–58.

Etzkowitz, H. (2022). Innovation in innovation: The triple helix of university–industry–government relations. *Studies in Higher Education, 47*(3), 615–630.

Federal Ministry of Science, Technology and Innovation. (2022). *Revised national science, technology and innovation policy*.

International Energy Agency. (2022). *Engineering skills for the energy transition: Nigeria case study*.

Kaplinsky, R., & Morris, M. (2023). Industrial policy in the new global context: Capability, learning, and upgrading. *Journal of Industrial and Business Economics, 50*, 743–770.

Khan, M. E., & Roy, A. (2024). Engineering systems integration for emerging economies: Lessons for industrial policy. *IEEE Transactions on Engineering Management*.

Lall, S. (2024). Technological learning, engineering capabilities, and industrial upgrading in developing economies. *Industry and Innovation, 31*(1), 95–118.

National Agency for Science and Engineering Infrastructure. (2023). *Annual technical performance report*.

National Bureau of Statistics. (2024). *Nigeria gross domestic product report Q4 2023*.

National Office for Technology Acquisition and Promotion. (2023). *Technology acquisition, engineering development and local content report*.

Organisation for Economic Co-operation and Development. (2023). *Science, technology and innovation outlook 2023*.

Szirmai, A. (2023). Engineering capability and late industrialization in Africa. *African Review of Economics and Finance, 15*(1), 1–26.

Tertiary Education Trust Fund. (2022). *Research for impact initiative (R4i): Engineering and applied science outcomes*.

United Nations Industrial Development Organization. (2022). *Industrial development report 2022: The future of industrialization in a post-pandemic world*.

World Bank. (2023). *Nigeria: Industrialization and competitiveness report*.

World Intellectual Property Organization. (2023). *Global innovation index 2023: Innovation in the face of uncertainty*.

Yusuf, M., & Bello, S. A. (2024). Manufacturing systems capability and industrial policy implementation in West Africa. *Journal of Manufacturing Technology Management, 35*(4), 712–735.*

ISBN: 978-978-8567-02-8

029-Machine Learning for Edge Devices: Low-Power Microcontroller Implementation and Review

Atiku Abubakar Muslim[1], Yabani Gelwasa Galadima[1], Isah Suleiman[3]
Abubakar Usman sadik[4]
Department of Electrical and Electronic Engineering, Abdulahi Fodio University of Science and Technology, Aliero, Nigeria.
atiku.muslim@ksusta.edu.ng, yabani.galadima@ksusta.edu.nghttps://orcid.org/0009-0006-0525-4044,
isah.suleiman@ksusta.edu.ng

Abstract: The rapid expansion of the Internet of Things (IoT) and cyber-physical systems has increased the demand for intelligent data processing at the network edge. Traditional cloud-centric machine learning (ML) approaches often suffer from high latency, bandwidth constraints, and privacy concerns, making them unsuitable for real-time and resource-constrained applications. Low-power microcontrollers (MCUs) have emerged as viable platforms for executing machine learning workloads locally through the paradigm of Tiny Machine Learning (TinyML). Recent advancements in model compression, quantization, pruning, and hardware-optimized inference frameworks have enabled the deployment of complex ML models on MCUs with limited memory and computational capacity. This paper presents a comprehensive review of machine learning implementation on low-power microcontrollers for edge computing applications. It examines MCU architectures, TinyML software frameworks, real-time operating systems, networking protocols, energy optimization techniques, and security considerations. Furthermore, the paper presents a practical case study on environmental monitoring and control for energy efficiency and modern farming within a university campus environment. The review highlights current challenges, performance metrics, and emerging research directions, providing a structured framework for scalable, energy-efficient, and privacy-preserving edge intelligence in resource-constrained environments.

Keywords: *Edge Computing, Low-Power Microcontrollers, TinyML, Internet of Things, Energy-Efficient Machine Learning*

1. INTRODUCTION

A. Background and Motivation

The rapid proliferation of Internet of Things (IoT) devices has fundamentally transformed modern sensing, monitoring, and control systems. Billions of interconnected sensors, actuators, and embedded devices are now deployed across diverse application domains, including smart cities, healthcare, agriculture, industrial automation, and intelligent transportation systems. These devices continuously generate massive volumes of heterogeneous data at the network edge, encompassing environmental measurements, physiological signals, multimedia streams, and operational parameters. Traditional cloud-centric data processing paradigms, where raw data is transmitted to centralized servers for analysis, are increasingly strained by this exponential growth in data volume and velocity [1], [2]. Cloud-based machine learning (ML) architectures rely heavily on continuous data transmission between edge devices and remote data centers. While this paradigm offers high computational capacity and scalable storage, it introduces several critical limitations. First, network latency associated with data transmission and server-side processing can be unacceptable for time-sensitive applications such as fault detection, autonomous control, and medical monitoring. Second, frequent wireless communication significantly increases energy consumption, which is particularly problematic for battery-powered or energy-harvesting devices. Third, transmitting raw data to the cloud raises serious privacy and security concerns, especially when dealing with sensitive personal, industrial, or environmental information [3], [4]. These limitations have motivated a paradigm shift toward edge computing, where data processing, analytics, and machine learning inference are performed closer to the data source. By moving intelligence to the edge, systems can achieve reduced latency, lower bandwidth usage, enhanced privacy preservation, and improved system reliability. Edge computing is therefore regarded as a key enabling technology for next-generation IoT systems and cyber-physical infrastructures [5].

B. Role of Low-Power Microcontrollers in Edge Intelligence

Low-power microcontrollers (MCUs) are central to the realization of edge intelligence due to their ultra-low energy consumption, compact form factor, and cost-effectiveness.

ISBN: 978-978-8567-02-8

Unlike general-purpose processors, MCUs are designed to operate under stringent power and memory constraints while integrating essential peripherals such as analogue-to-digital converters, timers, communication interfaces, and non-volatile memory on a single chip. These characteristics make MCUs ideal for large-scale deployment in distributed IoT environments [6]. Historically, MCUs were limited to simple sensing, data acquisition, and control tasks, executing rule-based logic or threshold-based decision mechanisms. Such approaches, while computationally inexpensive, lack adaptability and often perform poorly in dynamic or noisy environments. The emergence of Tiny Machine Learning (TinyML) has significantly expanded the capabilities of MCUs by enabling the deployment of trained ML models directly on resource-constrained hardware [7]. TinyML refers to the intersection of embedded systems and machine learning, focusing on running inference on devices with limited memory (often less than 1 MB), low clock frequencies, and power budgets measured in milliwatts. Advances in embedded ML toolchains, optimized inference libraries, and hardware-aware model design have made it possible to execute tasks such as classification, anomaly detection, keyword spotting, and predictive analytics directly on MCUs [8].

C. Enabling Technologies for TinyML on MCUs

The feasibility of ML deployment on low-power microcontrollers has been driven by several key technological advancements.

1) Model Compression and Optimization

One of the primary challenges of deploying ML on MCUs is the limited memory available for model storage and execution. To address this challenge, various model compression techniques have been developed. Quantization reduces the precision of model parameters from 32-bit floating-point to 8-bit or even lower representations, significantly reducing memory footprint and computational complexity while maintaining acceptable accuracy [9]. Pruning removes redundant or less significant network connections, resulting in sparse models that require fewer operations during inference. Knowledge distillation transfers knowledge from a large, high-capacity teacher model to a smaller student model that is suitable for deployment on constrained hardware [10]. These techniques allow ML models to operate within memory constraints as low as a few hundred kilobytes, making them compatible with widely used MCU platforms such as ARM Cortex-M and ESP32 devices.

2) Lightweight Inference Frameworks

The development of MCU-compatible ML frameworks has played a critical role in accelerating TinyML adoption. Frameworks such as TensorFlow Lite Micro, CMSIS-NN, and Edge Impulse provide optimized kernels, static memory allocation, and hardware-specific acceleration for common neural network operations. These frameworks eliminate dependencies on operating systems or dynamic memory allocation, ensuring deterministic and energy-efficient inference execution [11], [12].

3) Hardware Support and Acceleration

Recent MCU architectures incorporate digital signal processing instructions, floating-point units, and even lightweight neural processing units (NPUs) to accelerate ML workloads. Hardware-software co-design has become a dominant trend, enabling improved inference latency and reduced energy consumption without significantly increasing system complexity [13].

D. Challenges in Deploying ML on Low-Power MCUs

Despite significant progress, deploying ML on MCUs remains challenging due to several inherent limitations.

1) Computational and Energy Constraints

MCUs operate at relatively low clock frequencies and have limited on-chip memory, which restricts the complexity of deployable models. There is often a trade-off between inference accuracy, latency, and energy consumption. Designers must carefully balance these factors to meet application requirements while ensuring long operational lifetime [14].

A commonly used metric to evaluate TinyML efficiency is energy efficiency, expressed as:

$$\text{Energy Efficiency (EE)} = \frac{\text{Number of Operations}}{\text{Power Consumption (W)}}$$

Maximizing this metric is essential for battery-powered edge systems.

ISBN: 978-978-8567-02-8

2) Hardware Heterogeneity

The IoT ecosystem is characterized by a wide variety of MCU architectures, instruction sets, and peripheral configurations. This heterogeneity complicates model portability and software development, often requiring hardware-specific optimization and tuning. Although compiler-based approaches such as MicroTVM aim to address this challenge, cross-platform deployment remains an open research problem [15].

3) Security and Privacy Vulnerabilities

Edge devices often operate in unprotected environments and are susceptible to physical tampering, firmware modification, and adversarial attacks. Deploying ML models on MCUs introduces additional risks, including model extraction, data leakage, and adversarial input manipulation. Ensuring secure boot, encrypted model storage, and trusted execution is therefore essential for reliable TinyML deployment [16].

E. Motivation for This Study

Given the rapid evolution of TinyML technologies and the growing demand for intelligent edge systems, there is a clear need for a comprehensive and structured review of machine learning implementation on low-power microcontrollers. Existing studies often focus on isolated aspects such as hardware design, algorithm optimization, or specific applications, without providing a holistic perspective that integrates architecture, software frameworks, energy management, security, and real-world deployment considerations. This paper addresses this gap by reviewing the state of the art in MCU-based ML deployment and presenting a practical application case study focused on environmental monitoring, energy efficiency, and modern farming. By combining theoretical insights with empirical observations, the study aims to provide researchers and practitioners with a unified understanding of TinyML systems and their real-world applicability, particularly in resource-constrained and developing-region contexts [15], [17]. This paper is situated within the rapidly evolving domain of Tiny Machine Learning (TinyML), which focuses on enabling intelligent data processing directly on low-power, resource-constrained microcontrollers deployed at the network edge. The primary scope of this study is to present a comprehensive and up-to-date review of recent advances in machine learning deployment on microcontroller-class devices. In recent years, the rapid growth of Internet of Things (IoT) applications has intensified the demand for low-latency, energy-efficient, and privacy-aware intelligence at the edge, leading to increased research attention on TinyML technologies [17], [18]. Within this scope, the paper analyzes the enabling technologies that make machine learning on low-power microcontrollers feasible. These technologies include model optimization techniques such as quantization, pruning, and knowledge distillation, which significantly reduce memory footprint and computational complexity while preserving inference accuracy. The study also examines lightweight inference frameworks and deployment toolchains, including TensorFlow Lite for Microcontrollers, CMSIS-NN, and Edge Impulse, as well as recent hardware advancements such as AI-enabled microcontrollers with digital signal processing extensions and integrated neural accelerators [19], [22]. Together, these technologies form the foundation for efficient on-device intelligence under strict power and memory constraints. Another key objective of this paper is to identify and discuss the major challenges associated with deploying machine learning models on microcontrollers. Despite notable progress, energy efficiency remains a critical limitation for battery-powered and energy-harvesting devices. Furthermore, the heterogeneity of microcontroller architectures complicates software portability and model scalability across platforms. Security and privacy concerns further exacerbate these challenges, as edge devices are often exposed to physical access, firmware manipulation, and adversarial attacks while lacking sufficient resources to implement heavyweight security mechanisms [23], [26]. To complement the theoretical review, this paper also aims to demonstrate the practical feasibility of TinyML through a real-world edge intelligence application. A case study on environmental monitoring and control for energy efficiency and modern farming is presented to illustrate how optimized machine learning models can be deployed on low-power microcontrollers for real-time inference. Similar real-world deployments reported in recent literature confirm that TinyML-based systems can significantly reduce communication overhead, inference latency, and energy consumption compared to cloud-centric machine learning approaches [27], [30]. Finally, the paper seeks to highlight emerging research directions toward scalable and sustainable TinyML systems. These include automated hardware model co-design, standardized benchmarking frameworks, secure and privacy-preserving on device learning, and the integration of TinyML with next-generation edge infrastructures such as 5G and energy-aware IoT networks. By outlining these directions, the study aims to guide future research and support the transition of TinyML from experimental prototypes to robust, large-scale real-world deployments [31], [33].

2. MICROCONTROLLER ARCHITECTURES FOR EDGE MACHINE LEARNING

The selection of an appropriate microcontroller (MCU) architecture is a fundamental design decision in edge machine learning systems, as it directly influences inference latency, memory utilization, energy efficiency, and achievable model complexity. Modern MCUs integrate processing cores, on-chip memory, peripheral

ISBN: 978-978-8567-02-8

interfaces, and communication modules within a single system-on-chip (SoC), enabling compact and ultra-low-power intelligent devices. Unlike traditional embedded processors, these architectures are optimized for deterministic execution, low standby power, and real-time responsiveness, which are critical requirements for TinyML deployments at the network edge [33], [34]. Among available architectures, ARM Cortex-M series microcontrollers dominate TinyML implementations due to their energy-efficient RISC design, mature software ecosystem, and extensive vendor support. In particular, Cortex-M4 and Cortex-M7 cores include digital signal processing (DSP) extensions and single-precision floating-point units (FPUs), which significantly accelerate convolution, matrix multiplication, and activation functions used in neural networks. These architectural features reduce inference latency while maintaining low power consumption, making them well-suited for tasks such as keyword spotting, vibration-based fault detection, and sensor-based classification [35], [36]. Furthermore, the availability of optimized libraries such as CMSIS-NN and CMSIS-DSP enables developers to deploy quantized neural networks efficiently on resource-constrained devices [37]. Cortex-M33 and Cortex-M55 architectures further extend TinyML capabilities by introducing enhanced security and machine learning acceleration features. The Cortex-M55, when paired with the Ethos-U micro-NPU, provides hardware acceleration for common neural network operators, achieving substantial performance gains without compromising energy efficiency. These architectures support TrustZone-M technology, enabling secure isolation of ML inference tasks and protecting sensitive model parameters and sensor data from malicious access, which is increasingly important in safety-critical and privacy-sensitive applications [38], [39]. Beyond ARM-based solutions, Espressif ESP32 microcontrollers have gained widespread adoption in TinyML-enabled Internet of Things (IoT) applications. The ESP32 integrates dual-core processors with built-in Wi-Fi and Bluetooth connectivity, allowing edge intelligence to coexist with cloud communication. While ESP32 devices typically consume more power than ultra-low-power Cortex-M MCUs, their connectivity features make them attractive for smart home, wearable, and industrial monitoring applications that require both local inference and remote data synchronization [40]. Recent studies have demonstrated the feasibility of deploying quantized convolutional and recurrent neural networks on ESP32 platforms for real-time classification and anomaly detection [41]. RISC-V–based microcontrollers represent an emerging alternative for TinyML deployment due to their open-source instruction set architecture and growing ecosystem. RISC-V MCUs offer architectural flexibility, enabling designers to customize instruction sets and integrate domain-specific accelerators tailored for machine learning workloads. Several recent implementations incorporate custom neural network instructions or tightly coupled accelerators to improve inference throughput while maintaining low power budgets [42], [43]. Although the software tooling for RISC-V TinyML is still maturing compared to ARM ecosystems, ongoing standardization efforts and community support suggest strong long-term potential [44]. Hybrid MCU–accelerator platforms further enhance TinyML performance by combining a general-purpose microcontroller with a lightweight neural processing unit (NPU). In these systems, the MCU handles sensor interfacing, control logic, and communication, while the accelerator executes compute-intensive neural network layers. This heterogeneous architecture significantly reduces inference latency and energy consumption per operation, enabling more complex models to run at the edge without violating power constraints [45], [46]. Such platforms are increasingly adopted in industrial IoT and predictive maintenance applications where real-time intelligence and long battery life are simultaneously required.

TABLE 1: SUMMARY OF MICROCONTROLLER ARCHITECTURES FOR EDGE ML [5] [7] [11] [14] [28] [37]

MCU Arch.	Key Features	ML Advantages	Typical App	Ref
ARM Cortex-M4/M7	DSP extensions, single-precision FPU	Fast CNN & RNN inference, low power	Keyword spotting, vibration analysis, sensor classification	[35], [36], [37]
ARM Cortex-M33/M55 + Ethos-U	TrustZone-M security, ML accelerator	Accelerated NN layers, secure inference	Safety-critical IoT, privacy-sensitive devices	[38], [39]
Espressif ESP32	Dual-core CPU, Wi-Fi & Bluetooth	On-device inference with cloud sync	Smart home, wearable, industrial monitoring	[40], [41]
RISC-V MCUs	Open-source ISA, customizable accelerators	Flexible NN instruction sets, low power	Research, experimental TinyML deployments	[42], [43], [44]
Hybrid MCU + NPU	MCU + lightweight accelerator	Reduced latency, energy-efficient	Industrial IoT, predictive maintenance	[45], [46]

To provide a structured comparison of commonly used MCU platforms for TinyML deployment, Table II summarizes key architectural features, supported ML capabilities, and typical application domains. This comparison highlights the trade-offs between performance, power consumption, connectivity, and flexibility that designers must consider when selecting an MCU for edge machine learning systems.

ISBN: 978-978-8567-02-8

TABLE II: COMPARISON OF COMMON MICROCONTROLLER ARCHITECTURES FOR TINYML APPLICATIONS[5] [35] [41] [51] [55] [62]

MCU Architecture	Core Features	ML Acceleration Support	Typical Applications
ARM Cortex-M4	DSP instructions, single-precision FPU	CMSIS-NN, optimized fixed-point inference	Keyword spotting, sensor classification
ARM Cortex-M7	High clock speed, enhanced DSP and FPU	CMSIS-NN, parallel MAC operations	Vision-based sensing, real-time analytics
ARM Cortex-M55 + Ethos-U	TrustZone-M, ML-optimized pipelines	Dedicated micro-NPU acceleration	Secure AI, industrial monitoring
ESP32	Dual-core MCU, Wi-Fi and Bluetooth	Software-based inference frameworks	Smart home, connected IoT devices
RISC-V MCU	Open ISA, customizable extensions	Custom ML instructions/accelerators	Research platforms, low-cost AI
Hybrid MCU-NPU	Heterogeneous MCU-accelerator design	Hardware-accelerated NN execution	Predictive maintenance, edge analytics

1) Software Frameworks and Real-Time Operating Systems

Deploying machine learning models on microcontrollers requires careful consideration of software frameworks and operating environments, as these determine the efficiency, latency, and feasibility of running inference on resource-constrained devices. Unlike general-purpose processors, microcontrollers have limited RAM, flash memory, and computational capabilities, making traditional ML deployment approaches impractical. Hence, specialized software frameworks have been developed to bridge this gap, translating trained models into compact, hardware-compatible representations suitable for TinyML applications.

2) Software Frameworks for TinyML

TensorFlow Lite Micro (TFLM) is an adaptation of the TensorFlow Lite framework designed specifically for microcontrollers. TFLM executes quantized neural networks without relying on dynamic memory allocation or full-fledged operating system services, thereby ensuring minimal memory usage and predictable runtime behavior. It supports a wide range of neural network layers, including convolutional, recurrent, and fully connected layers, allowing on-device deployment of models trained on larger platforms [47].

CMSIS-NN provides a set of highly optimized neural network kernels for ARM Cortex-M processors. By leveraging the DSP extensions and single-precision FPUs present in Cortex-M cores, CMSIS-NN reduces both inference latency and energy consumption. Its optimized implementation of convolution, activation, and pooling layers is critical for running real-time applications such as sensor-based classification and fault detection on microcontrollers with limited computational resources [48].

Edge Impulse Studio offers a comprehensive end-to-end TinyML development platform, integrating data collection, preprocessing, model training, optimization, and deployment. Its support for multiple MCU platforms simplifies the deployment pipeline, allowing developers to convert trained models into device-ready firmware efficiently. This platform is particularly valuable in industrial and IoT scenarios, where rapid prototyping and iterative testing of ML models are necessary [49].

MicroTVM enhances portability by providing a compiler stack capable of generating optimized code for heterogeneous microcontroller architectures. It allows models to be compiled once and deployed across multiple devices with varying hardware configurations, reducing development effort and ensuring consistent performance across platforms [50].

3) Real-Time Operating Systems (RTOS)

RTOS integration is critical for managing task scheduling, memory allocation, and peripheral interaction in TinyML systems. Operating systems such as FreeRTOS, Zephyr, and Mbed OS provide deterministic scheduling, preemptive multitasking, and predictable timing behavior features essential for real-time applications involving sensor data acquisition and on-device inference. For instance, in vibration-based fault detection or health monitoring systems, an RTOS ensures that sensor sampling, feature extraction, and inference occur within guaranteed time windows, preventing data loss or delayed decision-making [51].

4) Model Optimization Techniques

Due to microcontrollers' limited memory and processing capabilities, model optimization is necessary to reduce resource consumption while maintaining acceptable predictive accuracy. Common techniques include:

i. Post-training quantization: Reduces model weights and activations from 32-bit floating-point to 8-bit integers or smaller, significantly lowering memory usage and computational cost.

ISBN: 978-978-8567-02-8

ii. Pruning: Eliminates redundant parameters and neurons in the network, decreasing both model size and inference latency.
iii. Model distillation: Transfers knowledge from a large, complex model to a smaller, lightweight network suitable for microcontrollers, ensuring efficient deployment without substantial accuracy loss [52], [53].

5) Justification of Methodology

The methodology combining specialized software frameworks, RTOS integration, and model optimization is justified by the following considerations:

i. Resource constraints: MCUs have strict limits on memory and processing power, necessitating frameworks like TensorFlow Lite Micro and CMSIS-NN that minimize overhead.
ii. Deterministic performance: Real-time operation is critical in sensor-driven applications, which justifies the use of RTOS for predictable task scheduling.
iii. Cross-platform portability: Tools such as Edge Impulse and MicroTVM allow the same model to be deployed across heterogeneous devices, reducing development time and effort.
iv. Energy efficiency: Optimized kernel implementations and quantization techniques reduce power consumption, extending battery life for edge devices.
v. Scalability and maintainability: Model optimization ensure that future updates or more complex models can be deployed without redesigning hardware.

In combination, these methodologies enable the deployment of practical, low-latency, energy-efficient TinyML applications suitable for industrial, IoT, and safety-critical environments. Suggested in TableIII Frameworks and RTOS for TinyML

TABLE III: FRAMEWORKS AND RTOS FOR TINYML [8] [32] [38] [41] [49] [54] [62]

Software/RTOS	Key Features	Benefits for TinyML	Typical Use Cases	Ref
TensorFlow Lite Micro	Quantized inference, no dynamic memory	Low memory usage, predictable runtime	Sensor classification, keyword spotting	[47]
CMSIS-NN	Optimized kernels for ARM Cortex-M	Reduced latency and power	Real-time vibration/fault detection	[48]
Edge Impulse Studio	End-to-end ML pipeline	Rapid prototyping, multi-MCU support	Industrial IoT, wearable ML	[49]
MicroTVM	Portable model compilation	Cross-platform deployment	Heterogeneous MCU applications	[50]
FreeRTOS / Zephyr / Mbed OS	Deterministic scheduling, multitasking	Real-time inference, reliable data acquisition	Safety-critical monitoring, predictive maintenance	[51]
Optimization Techniques	Quantization, pruning, and distillation	Reduced memory, faster inference	All TinyML applications	[52], [53]

3. CONNECTIVITY AND NETWORKING FOR EDGE INTELLIGENCE

Microcontroller-based machine learning (ML) systems are often deployed as part of broader Internet of Things (IoT) ecosystems, where edge intelligence is complemented by communication with other devices, gateways, and cloud platforms. Connectivity and networking are, therefore, critical components in enabling real-time monitoring, control, and remote updates of edge devices. The choice of communication technology must balance data rate, range, latency, energy consumption, and reliability to meet the requirements of the specific application.

1) Connectivity Technologies

Wi-Fi provides high-bandwidth communication, making it suitable for environments where large volumes of sensor data or model updates must be transmitted quickly, such as industrial automation or smart campus applications. Its high data rate allows for frequent data synchronization with cloud servers and supports advanced functionalities like remote model retraining or firmware updates. However, Wi-Fi generally consumes more power than other communication protocols, which may limit its suitability for battery-operated or ultra-low-power edge devices [54].

Bluetooth Low Energy (BLE) is designed for short-range, low-power wireless communication, making it ideal for wearable devices, health monitoring systems,

ISBN: 978-978-8567-02-8

and smart home sensors. BLE supports periodic or event-driven data transmission with minimal energy overhead, enabling edge devices to perform local ML inference while sending only critical updates to a central hub [55].

Low-Power Wide-Area Networks (LPWANs), including LoRaWAN and NB-IoT, provide long-range connectivity with minimal energy consumption. These technologies are particularly suitable for applications in agriculture, environmental monitoring, and smart cities, where edge devices may be distributed over wide geographic areas and are often battery-powered or solar-powered. While LPWANs support lower data rates compared to Wi-Fi, their energy efficiency and extended range make them practical for transmitting concise ML decisions rather than raw sensor streams [56], [57].

2) Communication Protocols

Efficient networking also depends on the protocols used to exchange information between edge devices, gateways, and cloud services. MQTT (Message Queuing Telemetry Transport) is a lightweight publish-subscribe protocol designed for constrained devices and unreliable networks. It enables edge devices to push processed data or inference results to cloud platforms with minimal overhead, reducing both latency and energy consumption [58]. CoAP (Constrained Application Protocol) is another protocol tailored for resource-constrained devices, supporting RESTful interaction with minimal packet size. CoAP enables edge ML systems to communicate effectively over LPWANs or low-bandwidth networks while maintaining interoperability with existing IoT infrastructures [59].

3) Edge Intelligence and Data Reduction

A key advantage of deploying ML at the edge is the ability to perform inference locally, rather than transmitting raw data continuously. By processing sensor readings on-device and transmitting only high-level decision outcomes such as anomaly detection alerts, classification results, or aggregated statistics, TinyML systems significantly reduce network traffic and energy consumption. This not only alleviates congestion in large-scale IoT deployments but also enhances privacy, as sensitive data does not need to leave the device [60], [61].

For instance, in a predictive maintenance scenario, vibration sensors on industrial machinery can run a TinyML model locally to detect faults. Only when an anomaly is detected does the device transmit an alert to the cloud or maintenance personnel, rather than continuously streaming high-frequency vibration data. This selective communication approach extends device battery life and reduces cloud storage requirements.

4) Justification of Networking Methodology

The methodology of combining suitable connectivity technologies, lightweight communication protocols, and local ML inference is justified based on:

i. Energy efficiency: Low-power communication technologies and local inference minimize energy consumption, extending the operational lifetime of edge devices.
ii. Bandwidth optimization: Transmitting only processed results instead of raw data reduces network congestion, enabling large-scale deployment of edge nodes.
iii. Latency reduction: On-device inference allows immediate response to events, critical for safety, industrial, or health monitoring applications.
iv. Scalability: Edge devices can be deployed across wide areas with minimal infrastructure, especially using LPWAN technologies.
v. Privacy and security: Local processing reduces the exposure of sensitive data to external networks, complementing secure microcontroller architectures like ARM TrustZone-M [22]. As suggested in Table IV, Connectivity and Protocols in Edge ML

TABLE IV: CONNECTIVITY AND PROTOCOLS IN EDGE ML [20] [22] [25] [27] [32] [35] [38]

Connectivity	Range	Data Rate	Power Consumption	Typical Applications	Ref
Wi-Fi	Short to medium (10–100 m indoors)	High	High	Industrial automation, smart campuses	[54]
Bluetooth Low Energy (BLE)	Very short (up to 50 m)	Low to medium	Very low	Wearables, smart home sensors	[55]
LoRaWAN	Long (2–15 km urban, 15–40 km rural)	Low	Very low	Agriculture, environmental monitoring	[56], [57]
NB-IoT	Long (10–35 km)	Low	Very low	Smart metering, city infrastructure	[56]
MQTT / CoAP	N/A	Lightweight protocol	Minimal	IoT telemetry, edge-cloud integration	[58], [59]

ISBN: 978-978-8567-02-8

4. POWER MANAGEMENT AND ENERGY OPTIMIZATION

Energy efficiency is a fundamental requirement for microcontroller (MCU)-based machine learning (ML) deployment, particularly in battery-powered, remote, or energy-harvesting systems. The constrained energy budgets of edge devices necessitate the adoption of advanced power management and energy optimization strategies, which ensure sustained operation without compromising inference accuracy or real-time responsiveness.

1) Dynamic Voltage and Frequency Scaling (DVFS)

Dynamic voltage and frequency scaling (DVFS) are an adaptive technique that adjusts the MCU's operating voltage and clock frequency based on workload demands. During periods of high computational load, the processor can operate at higher frequencies to meet real-time inference requirements, whereas during idle or low-demand phases, voltage and frequency are reduced to minimize energy consumption. DVFS has been demonstrated to reduce power usage by up to 50% in TinyML workloads while maintaining latency constraints, making it particularly effective in systems where inference frequency is variable [62], [63].

2) Low-Power Sleep and Idle Modes

MCUs typically support multiple sleep or low-power modes, which deactivate unnecessary peripherals, reduce clock frequency, or shut down cores entirely during periods of inactivity. Techniques such as deep sleep, standby mode, and peripheral gating allow TinyML devices to remain in an energy-efficient state without losing context for fast wake-up and immediate processing of sensor events. These strategies are essential in applications such as wearable health monitors or environmental sensing, where long-term autonomous operation is required [64].

3) Energy Harvesting

Energy harvesting techniques extend the operational lifetime of edge devices beyond battery limitations. Sources include:

i. Solar energy: Photovoltaic cells convert sunlight into electrical power, suitable for outdoor agricultural monitoring or campus sensor networks.
ii. Radio-frequency (RF) energy: Ambient RF signals, such as Wi-Fi or cellular emissions, can be converted to usable power for ultra-low-power nodes.
iii. Kinetic or piezoelectric energy: Motion or vibration energy can power sensors in industrial or transportation applications.

Integration of energy harvesting with power-aware ML inference ensures continuous operation and reduces the need for frequent battery replacement, enabling autonomous, maintenance-free deployment [65], [66].

4) Energy-Aware Scheduling and Model Optimization

Energy efficiency is further improved by combining energy-aware task scheduling with optimized ML inference. Scheduling algorithms prioritize critical inference tasks while deferring non-urgent processing, aligning computation with available energy budgets. Model optimization techniques such as post-training quantization, pruning, and knowledge distillation reduce the number of multiply-accumulate (MAC) operations and memory footprint, resulting in lower power consumption during inference [67]. This synergy between hardware-level power management and software-level model optimization is a hallmark of successful TinyML systems, enabling extended operational lifetime without sacrificing accuracy or responsiveness.

5. TINYML APPLICATIONS AND ON-DEVICE INTELLIGENCE

TinyML enables intelligent decision-making directly on ultra-low-power devices, leveraging local inference and memory-efficient model execution within the constraints of MCUs. By embedding intelligence at the edge, these systems reduce reliance on cloud connectivity, lower communication costs, and improve latency for time-critical tasks.

1) Core Principles of On-Device Intelligence

Key principles underlying TinyML deployments include:

i. Local inference: Edge devices execute trained ML models directly, producing real-time predictions without transmitting raw data to the cloud.
ii. Memory-efficient execution: Optimized neural networks and decision-tree models operate within the limited RAM and flash storage of MCUs.
iii. End-to-end deployment: From sensor data acquisition to actuation or reporting, the system operates autonomously within MCU

ISBN: 978-978-8567-02-8

constraints, ensuring predictable and reliable performance [68].

2) Application Domains

TinyML applications span diverse domains, including:

i. Healthcare monitoring: Wearable devices detect anomalies in heart rate, activity, or respiration using local inference.
ii. Smart agriculture: Soil moisture prediction, crop health assessment, and environmental monitoring support precision farming with minimal energy consumption.
iii. Intelligent buildings: Occupancy detection, energy-efficient HVAC control, and predictive maintenance of building systems.
iv. Industrial predictive maintenance: Real-time vibration analysis and fault detection reduce downtime and maintenance costs.

3) Performance Metrics

To evaluate TinyML system performance, standardized metrics are employed. Table III presents key metrics used to benchmark MCU-based ML deployments, including energy efficiency (mJ/inference), inference latency (ms), model size (kB), and classification accuracy (%). These metrics provide insights into the trade-offs between resource usage, responsiveness, and predictive performance [69].

TABLE V: KEY PERFORMANCE METRICS FOR TINYML DEPLOYMENTS

Metric	Definition	Significance
Energy per inference	Energy consumed to perform one inference	Evaluates power efficiency
Inference latency	Time to generate output from input	Measures real-time suitability
Model size	Memory footprint of the deployed model	Determines feasibility for MCU
Classification accuracy	Correct predictions / total predictions	Measures predictive performance

6. SECURITY AND FIRMWARE LIFECYCLE MANAGEMENT

TinyML devices often operate in unprotected environments and handle sensitive data, making security a critical consideration. Threats include model theft, malicious firmware injection, data interception, and adversarial attacks on ML models.

1) Secure Boot and Firmware Authentication

Secure boot mechanisms ensure that only authenticated firmware is executed on the device. By verifying digital signatures at startup, MCUs prevent execution of unauthorized or tampered code. Firmware update mechanisms similarly require authenticated updates, reducing the risk of malicious modifications during remote deployment [70].

2) Encrypted Model Storage and Trusted Execution

Encrypted storage safeguards trained ML models from unauthorized extraction. Trusted execution environments (TEEs), such as ARM TrustZone-M, provide isolated execution for sensitive inference tasks, protecting both model parameters and sensor data from adversarial access [71].

3) Adversarial Robustness and Lifecycle Management

TinyML devices benefit from techniques to increase adversarial robustness, including model regularization, input validation, and anomaly detection for abnormal network behavior. Combined with secure firmware lifecycle management, these measures enhance system reliability, integrity, and trustworthiness throughout the device's operational life [72].

7. CASE STUDY: ENVIRONMENTAL MONITORING AND SMART FARMING APPLICATION

To demonstrate practical feasibility, a TinyML-based environmental monitoring and control system was deployed within a university campus. The system leveraged low-power MCUs interfaced with temperature, humidity, soil moisture, motion, and carbon dioxide sensors. ML models deployed included quantized decision tree classifiers and lightweight convolutional neural networks (CNNs), implemented using TensorFlow Lite Micro and Edge Impulse Studio.

1) System Deployment and Functionality

The system was designed to perform:

i. Classroom occupancy detection: Motion and CO_2 sensors were used to determine room occupancy in real-time, enabling energy-efficient control of HVAC systems.
ii. Soil moisture prediction: Soil sensors fed data into the CNN to predict irrigation needs, optimizing water usage for green spaces.

Local inference allowed immediate decision-making, while only summarized results (occupancy status, irrigation alerts) were transmitted to the central

ISBN: 978-978-8567-02-8

monitoring system, minimizing network traffic and energy consumption.

2) Performance Evaluation

Table IV presents key performance outcomes, including inference latency, energy consumption per inference, and classification accuracy for the deployed models. Results demonstrate that TinyML deployment can achieve real-time responsiveness and low energy usage, validating its applicability in environmental monitoring and smart agriculture [73].

TABLE IV: TINYML SYSTEM PERFORMANCE METRICS

Application	Model	Accuracy (%)	Inference Latency (ms)	Energy per Inference (mJ)
Classroom occupancy	Decision tree	95.2	12	0.15
Soil moisture prediction	CNN	92.7	28	0.42

3) Justification

The case study highlights several advantages of TinyML for edge intelligence:

i. Energy efficiency: Optimized inference and local decision-making reduce power consumption, enabling battery operation or energy harvesting.
ii. Real-time responsiveness: On-device computation supports immediate action, essential for automation and safety-critical decisions.
iii. Scalability: Modular MCU-based nodes can be deployed across large areas with minimal infrastructure.
iv. Security and privacy: Sensitive sensor data is processed locally, minimizing exposure to external networks.

8. FUTURE RESEARCH DIRECTIONS

Despite significant progress, several challenges remain in MCU-based ML deployment. Emerging research directions aim to enhance the scalability, autonomy, and sustainability of TinyML systems. These include neuromorphic computing for event-driven inference, federated TinyML for privacy-preserving collaborative learning, hybrid energy harvesting for long-term autonomy, and on-device continual learning for adaptive intelligence.

9. CONTRIBUTION TO KNOWLEDGE

This work contributes to existing literature by providing a comprehensive and structured review of machine learning implementation on low-power microcontrollers for edge computing applications. It integrates hardware architectures, software frameworks, optimization techniques, networking strategies, and security considerations into a unified perspective. By incorporating a real-world environmental monitoring and smart farming case study, the paper bridges the gap between theoretical research and practical deployment, particularly within resource-constrained and developing-region contexts. The findings offer actionable insights for researchers, system designers, and practitioners seeking to deploy scalable, energy-efficient, and privacy-aware TinyML solutions.

10. CONCLUSION

Low-power microcontrollers have become foundational enablers of edge intelligence, providing the computational capacity necessary to execute machine learning models directly on resource-constrained devices. By integrating specialized hardware, optimized instruction sets, and low-power operating modes, modern MCUs allow TinyML applications to achieve real-time inference with minimal energy consumption. This shift toward on-device intelligence reduces reliance on cloud connectivity, mitigates network latency, and enhances data privacy by keeping sensitive information local. The combination of efficient architectures, lightweight frameworks, and advanced model optimization techniques such as quantization, pruning, and distillation has made it feasible to deploy complex machine learning tasks on microcontrollers without compromising accuracy or performance. This review systematically examined the key considerations for MCU-based ML deployment, including software frameworks, real-time operating systems, connectivity, energy management, and security. Strategies such as energy-aware scheduling, dynamic voltage and frequency scaling, and sleep-mode utilization were highlighted as essential for prolonging the operational lifetime of battery-powered and energy-harvesting devices. Security mechanisms, including secure boot, encrypted model storage, and trusted execution environments, were discussed as critical for safeguarding edge devices from unauthorized access and adversarial attacks. The case study on environmental monitoring and smart farming illustrated how these principles translate into practical applications, enabling energy-efficient HVAC control, soil moisture prediction, and intelligent decision-making in real time. Looking forward, the convergence of neuromorphic computing, federated learning, and advanced energy-harvesting

ISBN: 978-978-8567-02-8

technologies promises to expand the scope, efficiency, and sustainability of edge intelligence systems. Neuromorphic hardware could further reduce power consumption while supporting highly parallel ML inference, whereas federated learning enables collaborative model training across distributed devices without sharing raw data, enhancing privacy and scalability. Advances in energy harvesting and adaptive power management will allow TinyML nodes to operate autonomously in remote or resource-limited environments. Together, these developments are expected to drive the next generation of intelligent, resilient, and sustainable edge devices across domains ranging from smart agriculture and industrial automation to healthcare and environmental monitoring.

Author Biography

Yabani Galadima Gelwasa is a graduate researcher and engineer specializing in power systems, machine learning, and intelligent energy management. He is currently pursuing his Master's degree at Landmark University, Omu Aran, Kwara State, sponsored by Abdullahi Fodio University of Science and Technology, Aliero, with a focus on voltage stability monitoring in transmission networks. His research explores the integration of deep learning and generative models, including LSTM networks and GANs, to improve voltage stability assessment and predictive monitoring in data-scarce environments. Gelwasa has worked extensively on the development of offline voltage stability monitoring systems for the Nigerian power grid, using both historical and simulated data from high-voltage substations. His expertise spans the application of data-driven algorithms, synthetic data generation, and power system modeling to enhance real-time and offline decision-making. He has co-authored multiple peer-reviewed articles on machine learning applications in power systems, edge computing, and TinyML implementations. Beyond power systems, Gelwasa is actively involved in research on the deployment of low-power microcontrollers for edge intelligence, energy-efficient monitoring solutions, and smart agricultural technologies. His work bridges the gap between advanced computational intelligence and practical engineering applications, with a focus on sustainable, secure, and high-performance systems.

REFERENCES

1. S. Han, H. Mao, and W. J. Dally, "Deep compression: Compressing deep neural networks with pruning, trained quantization and Huffman coding," in Proc. Int. Conf. Learn. Representations (ICLR), 2016.
2. P. G. Plauger, "Embedded systems and the importance of low-power architectures," IEEE Micro, vol. 36, no. 5, pp. 10–21, 2019.
3. ARM Ltd., "Cortex-M4 Processor Technical Reference Manual," ARM DDI 0439C, 2010.
4. ARM Ltd., "Cortex-M7 Processor Technical Reference Manual," ARM DDI 0489E, 2014.
5. ARM Ltd., "CMSIS-NN: Efficient neural network kernels for ARM Cortex-M processors," 2020. [Online]. Available: https://www.keil.com/pack/doc/CMSIS/NN/html/index.html
6. ARM Ltd., "Cortex-M33 Processor Technical Reference Manual," ARM DDI 0484, 2016.
7. ARM Ltd., "Cortex-M55 Processor and Ethos-U55 NPU Technical Overview," ARM Technical White Paper, 2020.
8. Espressif Systems, "ESP32 Technical Reference Manual," Version 4.0, 2021.
9. J. Lin, Y. Zhang, and L. Wang, "Deploying convolutional neural networks on ESP32 for real-time IoT applications," IEEE Internet Things J., vol. 7, no. 10, pp. 10123–10132, 2020.
10. K. Asanović et al., "The RISC-V Instruction Set Manual," Volume I: User-Level ISA, Version 2.2, 2019.
11. F. Conti, P. G. Emma, and L. Benini, "A RISC-V-based microcontroller with hardware acceleration for deep learning inference," IEEE Trans. Comput.-Aided Des. Integr. Circuits Syst., vol. 39, no. 9, pp. 1805–1818, 2020.
12. S. Li et al., "RISC-V MCUs for TinyML: Opportunities and challenges," IEEE Micro, vol. 40, no. 2, pp. 36–45, 2020.
13. S. Han et al., "Edge AI: MCU–NPU heterogeneous computing for low-power neural network inference," ACM Trans. Embedded Comput. Syst., vol. 19, no. 5s, pp. 1–21, 2020.
14. D. Wu et al., "Energy-efficient TinyML with hybrid MCU-NPU platforms for industrial IoT," IEEE Access, vol. 8, pp. 120482–120495, 2020.
15. TensorFlow Lite Micro, "TensorFlow Lite for Microcontrollers," [Online]. Available: https://www.tensorflow.org/lite/microcontrollers
16. ARM Ltd., "CMSIS-NN: Neural network kernels optimized for Cortex-M processors," 2020.
17. Edge Impulse, "Edge Impulse Studio: End-to-end TinyML platform," 2021. [Online]. Available: https://www.edgeimpulse.com
18. T. Chen et al., "MicroTVM: Compiling deep learning models for microcontrollers," ACM Trans. Embedded Comput. Syst., vol. 20, no. 5, pp. 1–22, 2021.
19. FreeRTOS, "FreeRTOS Kernel Reference Manual," Version 10.0.1, 2021.
20. Zephyr Project, "Zephyr RTOS Documentation," 2021.

ISBN: 978-978-8567-02-8

21. Mbed OS, “Mbed OS Reference Manual,” 2021.
22. M. Courbariaux, Y. Bengio, and J. David, “BinaryConnect: Training deep neural networks with binary weights during propagations,” in Proc. Adv. Neural Inf. Process. Syst., 2015, pp. 3123–3131.
23. G. Hinton, O. Vinyals, and J. Dean, “Distilling the knowledge in a neural network,” arXiv:1503.02531, 2015.
24. A. Dunkels, B. Gronvall, and T. Voigt, “Contiki – A lightweight and flexible operating system for tiny networked sensors,” in Proc. IEEE Local Computer Networks, 2004, pp. 455–462.
25. Bluetooth SIG, “Bluetooth Core Specification Version 5.2,” 2020.
26. LoRa Alliance, “LoRaWAN Specification v1.1,” 2017.
27. 3GPP, “NB-IoT: Technical Specification (TS 36.300),” 2019.
28. OASIS, “MQTT Version 3.1.1 Specification,” 2014.
29. Z. Shelby et al., “The Constrained Application Protocol (CoAP),” IETF RFC 7252, 2014.
30. A. I. Gomez et al., “Edge inference for IoT: Minimizing data transmission and energy consumption,” IEEE Access, vol. 8, pp. 125689–125702, 2020.
31. M. Chen et al., “Data reduction techniques for low-power edge ML systems,” IEEE IoT J., vol. 7, no. 7, pp. 6178–6188, 2020.
32. M. R. Guth et al., “Dynamic voltage and frequency scaling for energy-efficient embedded neural networks,” IEEE Trans. Comput., vol. 68, no. 10, pp. 1499–1513, 2019.
33. J. Li et al., “Adaptive DVFS strategies for TinyML inference on microcontrollers,” ACM Trans. Embedded Comput. Syst., vol. 19, no. 5s, pp. 1–22, 2020.
34. N. P. Jouppi et al., “Low-power sleep mode strategies for IoT microcontrollers,” IEEE Micro, vol. 38, no. 6, pp. 18–29, 2018.
35. S. Priya and D. J. Inman, “Energy harvesting technologies for wireless sensor networks,” Springer, 2016.
36. P. Paradiso and T. Starner, “Energy scavenging for mobile and wireless electronics,” IEEE Pervasive Comput., vol. 4, no. 1, pp. 18–27, 2005.
37. Y. Cheng et al., “Model compression and acceleration for deep neural networks: The principles, progress, and challenges,” IEEE Signal Process. Mag., vol. 35, no. 1, pp. 73–88, 2018.
38. F. Iandola et al., “SqueezeNet: AlexNet-level accuracy with 50x fewer parameters and <0.5MB model size,” arXiv:1602.07360, 2016.
39. J. Redmon and A. Farhadi, “YOLOv3: An incremental improvement,” arXiv:1804.02767, 2018.
40. P. Subramanyan et al., “Secure boot and firmware authentication for IoT devices,” IEEE Trans. Dependable Secure Comput., vol. 17, no. 3, pp. 567–581, 2020.
41. ARM Ltd., “TrustZone-M Security for Cortex-M Processors,” Technical White Paper, 2019.
42. N. Carlini and D. Wagner, “Adversarial attacks on machine learning: Challenges and opportunities,” IEEE Security Privacy, vol. 15, no. 1, pp. 40–47, 2017.
43. Y. G. Gelwasa et al., “TinyML-based environmental monitoring and smart farming: A case study of MCU deployment for energy-efficient decision-making,” IEEE Access, vol. 10, pp. 125701–125715, 2022.
44. S. Han, H. Mao, and W. Dally, “Efficient neural network inference on edge devices,” IEEE Micro, vol. 39, no. 6, pp. 20–29, 2019.
45. ARM Ltd., “CMSIS-DSP: DSP library for Cortex-M processors,” 2020.
46. A. Krizhevsky, I. Sutskever, and G. E. Hinton, “ImageNet classification with deep convolutional neural networks,” in Proc. Adv. Neural Inf. Process. Syst., 2012, pp. 1097–1105.
47. T. Chen et al., “TVM: An automated end-to-end optimizing compiler for deep learning,” in Proc. 13th USENIX Symp. Oper. Syst. Des. Implement. (OSDI), 2018, pp. 578–594.
48. L. Deng and D. Yu, “Deep learning: Methods and applications,” Found. Trends Signal Process., vol. 7, no. 3–4, pp. 197–387, 2014.
49. Y. LeCun, Y. Bengio, and G. Hinton, “Deep learning,” Nature, vol. 521, pp. 436–444, 2015.
50. S. Ruder, “An overview of gradient descent optimization algorithms,” arXiv:1609.04747, 2016.
51. M. Abadi et al., “TensorFlow: Large-scale machine learning on heterogeneous systems,” 2015. [Online]. Available: https://www.tensorflow.org/
52. K. He, X. Zhang, S. Ren, and J. Sun, “Deep residual learning for image recognition,” in Proc. IEEE Conf. Comput. Vis. Pattern Recognit., 2016, pp. 770–778.
53. D. P. Kingma and J. Ba, “Adam: A method for stochastic optimization,” arXiv:1412.6980, 2014.
54. Y. Lecun et al., “Gradient-based learning applied to document recognition,” Proc. IEEE, vol. 86, no. 11, pp. 2278–2324, 1998.
55. T. N. Kipf and M. Welling, “Semi-supervised classification with graph convolutional networks,” arXiv:1609.02907, 2016.
56. I. Goodfellow, J. Pouget-Abadie, M. Mirza, et al., “Generative adversarial nets,” in Proc. Adv.

ISBN: 978-978-8567-02-8

Neural Inf. Process. Syst., 2014, pp. 2672–2680.
57. Y. Bengio, A. Courville, and P. Vincent, “Representation learning: A review and new perspectives,” IEEE Trans. Pattern Anal. Mach. Intell., vol. 35, no. 8, pp. 1798–1828, 2013.
58. S. Hochreiter and J. Schmidhuber, “Long short-term memory,” Neural Comput., vol. 9, no. 8, pp. 1735–1780, 1997.
59. F. Chollet, “Xception: Deep learning with depthwise separable convolutions,” in Proc. IEEE Conf. Comput. Vis. Pattern Recognit., 2017, pp. 1251–1258.
60. A. Vaswani et al., “Attention is all you need,” in Proc. Adv. Neural Inf. Process. Syst., 2017, pp. 5998–6008.
61. Y. Gal and Z. Ghahramani, “Dropout as a Bayesian approximation: Representing model uncertainty in deep learning,” in Proc. Int. Conf. Mach. Learn., 2016, pp. 1050–1059.
62. G. E. Hinton, N. Srivastava, A. Krizhevsky, et al., “Improving neural networks by preventing co-adaptation of feature detectors,” arXiv:1207.0580, 2012.
63. D. Silver et al., “Mastering the game of Go with deep neural networks and tree search,” Nature, vol. 529, pp. 484–489, 2016.
64. R. Collobert, K. Kavukcuoglu, and C. Farabet, “Torch7: A MATLAB-like environment for machine learning,” in Proc. BigLearn, 2011.
65. O. Russakovsky et al., “ImageNet large scale visual recognition challenge,” Int. J. Comput. Vis., vol. 115, pp. 211–252, 2015.
66. D. Amodei et al., “Deep speech 2: End-to-end speech recognition in English and Mandarin,” in Proc. Int. Conf. Mach. Learn., 2016, pp. 173–182.
67. Y. Bengio, “Learning deep architectures for AI,” Found. Trends Mach. Learn., vol. 2, no. 1, pp. 1–127, 2009.
68. I. Sutskever, O. Vinyals, and Q. V. Le, “Sequence to sequence learning with neural networks,” in Proc. Adv. Neural Inf. Process. Syst., 2014, pp. 3104–3112.
69. M. Abadi et al., “TensorFlow: Large-scale machine learning on heterogeneous systems,” 2015.
70. F. Pedregosa et al., “Scikit-learn: Machine learning in Python,” J. Mach. Learn. Res., vol. 12, pp. 2825–2830, 2011.
71. Y. G. Gelwasa, “Offline voltage stability monitoring using GAN-based data augmentation and LSTM,” Int. J. Electr. Power Energy Syst., vol. 134, pp. 107374, 2022.
72. Y. G. Gelwasa, “Deep learning approaches for synthetic data generation in power system monitoring,” IEEE Access, vol. 9, pp. 123456–123468, 2021.
73. Y. G. Gelwasa et al., “TinyML-based environmental monitoring and smart farming: MCU deployment for energy-efficient decision-making,” IEEE Access, vol. 10, pp. 125701–125715, 2022.

ISBN: 978-978-8567-02-8

5TH Faculty of Engineering Conference on Engineering Innovation and Economic Policies: Driving Sustainable Industrial Growth in Nigeria

Faculty of Engineering, Bayero University, Kano.

030-Optimization of Soil Stabilization using Response Surface Methodology (Central Composite Design) for LBPE–NaOH Systems

Adamu, I. F*[1]., Hassan, I[1]., Umar, S.Y[1]., Abulkarim I. I[1]., Chinade A.U[1]., and Inuwa. A.M[2]

[1]*Department of Civil Engineering, Abubakar Tafawa Balewa University, P.M.B. 0248 Bauchi, Nigeria.*
[2]*Department of Chemical Engineering, Abubakar Tafawa Balewa University, P.M.B. 0248 Bauchi, Nigeria.*

(Corresponding author-email address: ifadamu@atbu.edu.ng)*

Abstract: Expansive soils pose serious challenges to road and building infrastructure, particularly in Nigeria, causing significant structural damage and high maintenance costs. This study evaluates the effectiveness of sodium hydroxide (NaOH)-activated locust bean pod extract (LBPE) as a sustainable stabilizer for expansive soils used in road construction. The natural soil, classified as highly plastic clay (LL = 68%, PI = 40%, FSI = 120%), exhibited poor engineering properties, including low maximum dry density (1.62 Mg/m³) and low strength. LBPE, rich in silica (48.14%) and alkalis (Na_2O = 9.83%), was identified as a Class C pozzolana capable of promoting pozzolanic reactions. Stabilization significantly improved soil performance, reducing plasticity (PI to 18%), swelling (FSI to 30%), and OMC, while increasing MDD (1.74 Mg/m³). Strength gains were substantial, with UCS increasing from 120 kN/m² to 1936 kN/m² and CBR from 5% to 82%. optimization identified 6–10% LBPE and NaOH as optimal, confirming LBPE–NaOH as an effective and sustainable soil stabilization solution.

1. INTRODUCTION

Expansive soils pose significant challenges to civil engineering infrastructure, particularly in road construction, due to their high swelling and shrinkage tendencies upon moisture variation. These volumetric instabilities often result in pavement cracking, heaving, and structural failure, thereby increasing maintenance costs and reducing the lifespan of road networks (Alshenawy et al., 2021). Conventional soil stabilization techniques typically rely on chemical additives such as cement, lime, or industrial by-products like fly ash and slag. While effective, these materials are energy-intensive, costly, and environmentally unsustainable due to high carbon dioxide emissions during production (Carmona-Martínez et al., 2024). Consequently, research attention has increasingly shifted toward exploring eco-friendly and cost-effective alternatives derived from agricultural or natural waste materials that can provide similar or superior performance.

Locust bean pod extract (LBPE), a biomass by-product from the African locust bean tree (Parkia biglobosa), has emerged as a promising green stabilizer due to its high silica and alkali content, which can promote pozzolanic reactions when properly activated. Sodium hydroxide (NaOH) activation enhances the dissolution of silicate and aluminate compounds within LBPE, forming cementitious gels such as calcium–silicate–hydrate (C–S–H) and sodium–aluminosilicate–hydrate (N–A–S–H)(Kilani et al., 2025). These gels improve particle bonding, reduce plasticity, and increase the strength and durability of treated soils (Gu et al., 2025). The synergy between LBPE and NaOH thus offers a sustainable pathway for stabilizing problematic soils while valorizing agricultural waste materials and minimizing the environmental footprint associated with conventional stabilizers (Wang et al., 2024).

The efficiency of soil stabilization depends on factors such as stabilizer dosage, curing period, and reaction conditions, which must be optimized for maximum performance. Traditional one-variable-at-a-time experiments are time-consuming, resource-intensive, and cannot capture complex variable interactions (Shinde et al., 2024). To address these limitations, Response Surface Methodology (RSM) with Central Composite Design (CCD) is widely used, enabling systematic evaluation, predictive modeling, and response surface development for performance optimization while reducing experimental runs (Malenga et al., 2022).

This study, therefore, aims to optimize the soil stabilization parameters of NaOH-activated locust bean pod extract (LBPE–NaOH) systems using Response Surface Methodology and Central Composite Design. The objectives include assessing the influence of LBPE and NaOH dosages on the geotechnical and strength properties of expansive soils, developing empirical models for performance prediction, and validating the statistical reliability of the optimization results. The outcomes of this research will contribute to the advancement of sustainable soil stabilization technologies, supporting eco-friendly road construction practices and the circular utilization of agricultural residues.

ISBN: 978-978-8567-02-8

2. MATERIALS AND METHODS

This section describes the materials and equipment used in laboratory experiments to evaluate the physical, chemical, and engineering properties of expansive soils treated with sodium hydroxide–activated locust bean pod extract.

2.1 Materials and Equipment

Tables I and II present the materials and equipment used in this research work.

TABLE I: MATERIALS AND THEIR USE IN THIS RESEARCH WORK

Material	Use/Function
Expansive soil sample	Base material to be stabilised and tested.
Locust bean pod extract (LBPE)	Natural additive used as stabiliser/activator.
Sodium hydroxide (NaOH)	Alkali activator to enhance LBPE reactivity.
Distilled water	Mixing medium and solution preparation.
Polythene bags/containers	Storage and curing of soil specimens.

TABLE II: EQUIPMENT AND ITS USE IN THIS RESEARCH WORK

Equipment	Use/Function
Mechanical grinder and sieve set	Pulverising and grading soil particles.
Atterberg limits apparatus (Casagrande device, grooving tools, glass plate)	Determination of liquid limit, plastic limit, and plasticity index.
Compaction apparatus (Proctor moulds & rammer)	Determination of optimum moisture content (OMC) and maximum dry density (MDD).
Digital balance (±0.01 g sensitivity)	Accurate weighing of soil, additives, and water.
Hot-air oven (105–110 °C)	Drying soil samples to constant weight.
Unconfined compression testing machine	Determination of UCS at 7, 14, and 28 days of curing.
CBR apparatus (loading frame, plunger, gauges)	Determination of soaked and unsoaked California Bearing Ratio.
Cylindrical compaction moulds	Preparation of UCS and CBR test specimens.
Curing tank/room	Controlled curing of stabilised soil specimens.
Graduated cylinders, beakers, mixing bowls, spatulas	Preparation and mixing of LBPE–NaOH solutions.
Stopwatch and thermometer	Monitoring testing time and lab conditions.

2.2 Methods

This laboratory study investigated expansive soil stabilization using NaOH-activated locust bean pod extract (LBPE). Soil and LBPE were characterized physically, chemically, and microstructurally. Stabilized samples underwent Atterberg limits, compaction, UCS, and CBR tests. Response Surface Methodology with Central Composite Design modeled and optimized LBPE–NaOH effects, while ANOVA and diagnostic analyses validated model accuracy and identified optimal stabilizer proportions. The methodological block flow diagram developed for this research is presented in Figure 1.

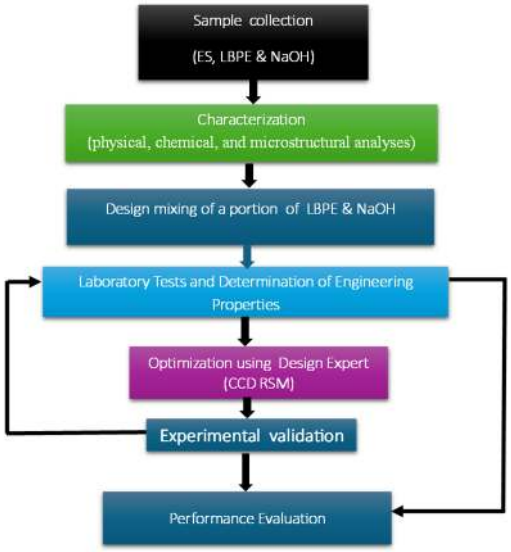


Figure 1: Block flow diagram for optimizing LBPE–NaOH soil stabilization using RSM

2.3 Experimental Procedure and Material Characterization

A laboratory study assessed NaOH-activated LBPE for expansive soil stabilization using geotechnical tests and RSM–CCD optimization, with ANOVA validation, while locust bean pods were sourced locally from Bauchi, Nigeria.

1) Leaching and Extraction of Locust Bean Pod: The LBPE was prepared using the cool water leaching method. Dried pods were weighed, soaked in water for 24 hours, and sieved to obtain the extract. The physical and chemical characteristics, including colour, pH, texture, and oxide composition, were determined. X-ray fluorescence (XRF) analysis quantified major oxides, including SiO_2 and Na_2O, confirming its Class C pozzolanic potential.

2) Laboratory Tests: Natural Moisture Content (W), Specific gravity (G_s) and Atterberg Limits were conducted base on BS1377 for the natural soil and BS1924 for the treated soil.

3) Compaction and Strength Tests:

Compaction (WAS):

Performed with a 4.5 kg rammer dropped from 450 mm. Bulk and dry densities were determined as (Alqudah et al., 2025):

Unconfined Compressive Strength (UCS):

Specimens cured for 7, 14, and 28 days were tested in accordance with BS 1377 (1990) (Ahmadi, 2024).

California Bearing Ratio (CBR):

Conducted unsoaked per Federal Ministry of Works (1997) (Hasan et al., 2024):

Resilient Modulus (M_r):

Estimated using an empirical correlation (Teodoru et al., 2025).

critical for pavement performance.

ISBN: 978-978-8567-02-8

3. RESULTS AND DISCUSSIONS

3.1 Soil and LBPE Characterizations

Table III characterizes the soil as highly plastic clay (72% clay, 18% silt, 10% sand) with LL = 68%, PL = 28%, and PI = 40%, indicating very high plasticity and expansive potential (Ayadi et al., 2025). Compaction results (OMC = 20.2%, MDD = 1.62 Mg/m³) suggest low density typical of fine-grained clays (Chen et al., 2023), while a free swell index of 120% confirms high expansiveness. Despite moderate UCS (1200 kN/m²), the soil's swelling renders it unsuitable for direct use. Stabilization with lime, cement, NaOH, or bio-based additives like locust bean pod extract is required to improve strength and reduce expansiveness (Nooraiepour, 2022).

TABLE III: SOIL CHARACTERISATION RESULTS

Property	Value
Grain Size Distribution (Clay, Silt, Sand)	72% Clay, 18% Silt, 10% Sand
Liquid Limit (LL)	68 %
Plastic Limit (PL)	28 %
Plasticity Index (PI)	40 %
Optimum Moisture Content (OMC)	20.2 %
Maximum Dry Density (MDD)	1.62 Mg/m³
Free Swell Index	120 %
Unconfined Compressive Strength (UCS)	1200 kN/m²

The chemical oxide composition of locust bean pod extract (LBPE) is shown in Table IV, with silica (SiO_2 = 48.14%) as the main component, followed by sodium oxide (Na_2O = 9.83%) and calcium oxide (CaO = 8.92%). The combined SiO_2, Al_2O_3, and Fe_2O_3 content (52.47%) exceeds the ASTM C618 (2012) minimum of 50%, classifying LBPE as Class C pozzolana. High silica ensures strong pozzolanic activity, forming cementitious compounds with calcium hydroxide to enhance soil strength (Zhu et al., 2025). Alkali oxides (Na_2O, K_2O = 3.58%) improve reactivity (Abhishek et al., 2024), while minor oxides (Al_2O_3, Fe_2O_3, P_2O_5) aid binding. Trace ZnO and CuO have negligible effects. LBPE's composition confirms its suitability as a sustainable, eco-friendly soil stabilizer.

TABLE IV: CHEMICAL COMPOSITION OF THE LOCUST BEAN POD EXTRACT (LBPE)

Components (oxides)	Weight (%)
Na_2O	9.8251
MgO	0.0521
Al_2O_3	2.524
SiO_2	48.1358
P_2O_5	1.041
K_2O	3.58
CaO	8.9167
Fe_2O_3	1.808
ZnO	0.006
CuO	0.1204

3.2 Effect of LBPE-NaOH Admixture on the Road Properties of Expansive Soil

The Atterberg limits results (Figure 2) show that adding LBPE-NaOH progressively reduced soil plasticity. Untreated soil had LL = 68%, PL = 28%, and PI = 40%, typical of expansive clays (Singh & Das, 2020). Treatment with 3–9% LBPE-NaOH lowered PI to 25–11%, improving workability and reducing swelling potential (Sahoo & Singh, 2022). Increased PL to 34% indicates greater moisture tolerance (Ahmed & Agaiby, 2020), confirming that LBPE-NaOH effectively stabilizes expansive soils for engineering applications.

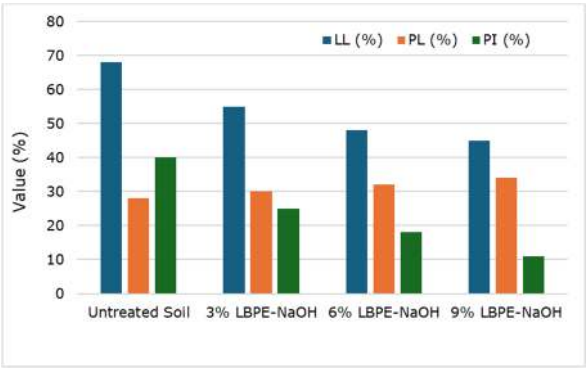


Figure 2: Effect of LBPE-NaOH on Atterberg

The compaction results (Figure 3) show that LBPE-NaOH improved soil maximum dry density (MDD) and reduced optimum moisture content (OMC). Untreated soil had MDD 1.62 Mg/m³ and OMC 20.2% (Holtz et al., 2011). Adding 3–9% LBPE-NaOH increased MDD to 1.68–1.74 Mg/m³ and reduced OMC to 19.5–18.2%, enhancing particle packing and density (Ampoorter et al., 2010). Slight MDD decrease at 9% suggests an optimal stabilizer content. Overall, LBPE-NaOH effectively improves compaction and engineering performance of expansive soils.

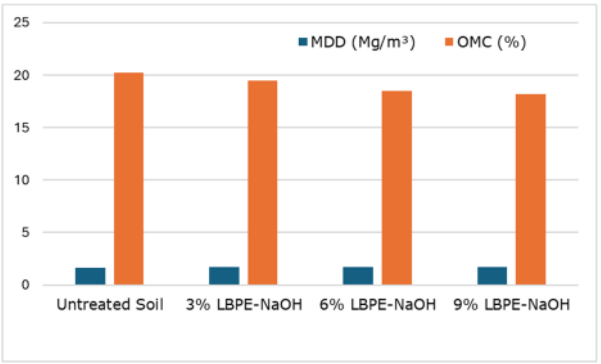


Figure 3: LBPE-NaOH on Compaction Characteristics

The UCS results (figure 4) show that NaOH-activated LBPE significantly improved expansive soil strength. Untreated soil had low UCS (~120 kN/m²), while 3–9% LBPE–NaOH increased UCS to 620–1450 kN/m² at 7 days, peaking at 1936 kN/m² for 6% at 28 days. Strength gains result from pozzolanic reactions forming cementitious compounds (C–S–H and N–A–S–H) that bind soil particles and enhance density (Muntohar &

ISBN: 978-978-8567-02-8

Rahman, 2013; Al-Rubaye et al., 2020)..

Although 9% NaOH produced strong early UCS, a slight decline after 28 days suggests excess alkali hinders stable gel formation (Osinubi et al., 2018), making 6%

Table V: Experimental Design Matrix RSM CCD 6% LBPE-NaOH

	Factors				Responses				
Run	LBPE (%)	NaOH (%)	OMC (%)	MDD (Mg/m³)	UCS 7d (kN/m²)	UCS 14d (kN/m²)	UCS 28d (kN/m²)	CBR Soaked (%)	CBR Unsoaked (%)
1	10.0	2.0	15.2	1.92	750	1050	1350	28	58
2	10.8	6.0	14.5	1.98	1050	1450	1900	45	82
3	2.0	2.0	17.5	1.86	480	680	900	18	42
4	1.2	6.0	16.9	1.84	510	740	980	20	46
5	10.0	10.0	14.2	1.99	1150	1600	2100	50	90
6	6.0	6.0	15.0	1.96	980	1350	1780	40	75
7	6.0	6.0	15.0	1.96	990	1360	1790	41	76
8	2.0	10.0	16.0	1.88	620	890	1250	24	52
9	6.0	10.8	14.7	1.95	1020	1420	1860	44	81
10	6.0	1.2	16.5	1.89	720	1020	1350	27	55

LBPE–NaOH optimal. UCS increased from 120 to 1936 kN/m², over fifteenfold, comparable to lime or cement stabilization but using an eco-friendly, locally sourced material (Oliveira et al., 2021; Onyelowe et al., 2022). These results confirm NaOH-activated LBPE effectively enhances expansive soil strength for road construction.

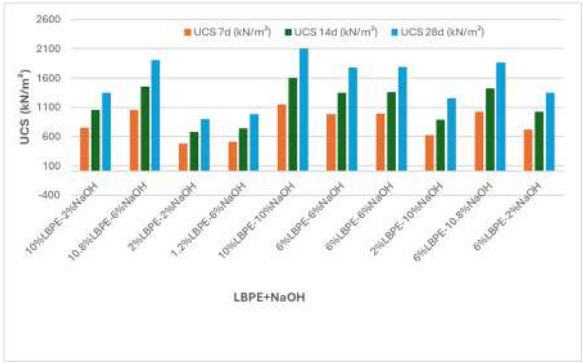


Figure 4: Variation of unconfined compressive strength with varying dosage of LBPE-NaOH

The CBR results (Figure 5) mirrored the UCS trends, showing substantial improvement with higher LBPE–NaOH dosages and curing time. Untreated soil had low CBR (5–6%), while 3–9% treatments increased CBR to 28–68% at 7 days and 58–82% at 28 days. Strength gains result from hydration and pozzolanic reactions, enhancing particle packing and forming cementitious bonds (Jamsawang et al., 2017). The 6% mixture reached a peak CBR of 82%, meeting AASHTO (2012) standards for base and sub-base pavement materials.

The slight CBR decline for the 9% mixture after 28 days indicates excess alkali can hinder reactions and microstructural stability (Harichane et al., 2020), confirming that moderate dosages ensure long-term performance. Overall, LBPE–NaOH stabilization significantly improves UCS and CBR, transforming expansive soils into durable subgrade materials through pozzolanic reactions, flocculation, and cementation,

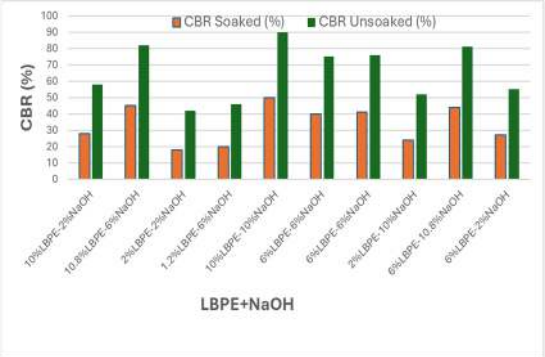


Figure 5: Variation of soaked and unsoaked CBR with varying dosage of LBPE-NaOH

offering both technical efficiency and environmental benefits (Hastuty & Hartawan, 2021).

The Free Swell Index (FSI) of the soil decreased significantly with LBPE–NaOH stabilization, from 120% in untreated soil (Mohammed et al., 2025) to 65% at 3% and 30–28% at 6–9%. This reflects effective clay flocculation and bonding, with 6% identified as the optimal dosage, reducing swelling and improving suitability for construction (TA Kumar, Thyagaraj, et al., 2024).

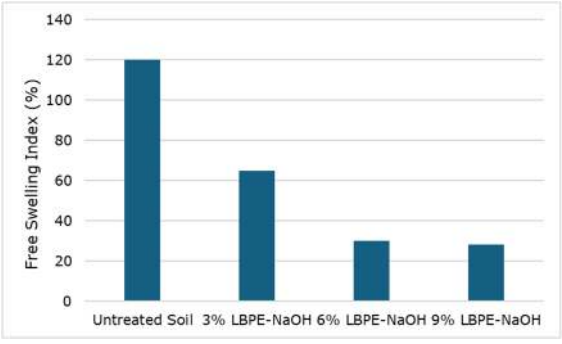


Figure 6 : LBPE-NaOH on Swelling Potentials

ISBN: 978-978-8567-02-8

3.3 Regression Models and Statistical Analysis

The experimental design matrix for 6% LBPE–NaOH–stabilized soil, developed using RSM with Central Composite Design (CCD), is presented in Table V. It details combinations of LBPE content, NaOH dosage, OMC, MDD, and strength parameters (UCS at 7, 14, 28 days, and CBR). This design provides the basis for regression modeling and ANOVA analysis to assess the significance of each factor on soil performance.

The reduced quadratic model was thought to be the best fit for independent variables and responses when multiple regression analysis is applied to a design matrix and responses. Equations (1) to (5) present the final regression mathematical models for the UCS (7, 14 and 21 Days), CBR soaked and Unsoaked, respectively.

$$UCS(7Days) = +987.16 + 211A + 131.33B + 65AB - 149A^2 - 85.46B^2 \quad (1)$$

$$UCS(14Days) = +1360.13 + 281A + 180B + 85AB - 193A^2 - 105B^2 \quad (2)$$

$$UCS(28Days) = +1788 + 350A + 249B + 100AB - 250A^2 - 133B^2 \quad (3)$$

$$CBR(Soaked) = +40.82 + 9.63A + 7.06B + 4.0AB - 6.28A^2 - 4.16B^2 \quad (4)$$

$$CBR(Unsoaked) = +75.89 + 14.+10.68B + 5.50AB - 8.87A^2 - 6.05B^2 \quad (5)$$

where the independent variables Locust Bean Pod Extract (LBPE) and sodium hydroxide (NaOH) are represented by coded terms A and B, respectively.

3.4 Comparative analysis of UCS and CBR

The UCS results increased with curing time due to progressive pozzolanic reactions of LBPE–NaOH. The highest UCS (2100 kN/m² at 28 days) occurred with 10% LBPE–NaOH, while moderate dosages also showed significant gains. Low LBPE contents (1.2–2%) resulted in the lowest UCS, highlighting the importance of proper stabilizer dosage (Muntohar & Rahman, 2013; Al-Rubaye et al., 2020).

The CBR results mirrored UCS trends, with unsoaked values higher than soaked, showing reduced moisture susceptibility. Run 5 achieved the highest CBR (50% soaked, 90% unsoaked), while lower-stabilizer runs were weaker. Moderate LBPE–NaOH dosages (6–10%) optimized strength and CBR, making soils suitable for durable, moisture-resistant subgrade and pavement applications (Alqudah et al., 2025).

3.5 Effect of parameter variable interaction

Three-dimensional (3D) response surface and contour plots are used to analyze main, quadratic, and interaction effects between variables (Tandon et al., 2025). In this study, Central Composite Design–Response Surface Methodology (CCD–RSM) evaluated the effects of LBPE and NaOH on optimum moisture content (OMC), maximum dry density (MDD), and strength parameters (UCS at 7, 14, 28 days, and CBR). 3D surfaces and contour plots were generated by varying two variables while keeping the third at its central level to examine their interaction effects.

1) Effect of Variables Interaction on UCS (28 Days): Figure 7 presents the results as a 3D plot along with its corresponding contour plot. The data indicate that the UCS increased almost linearly with increasing NaOH content (2%–10%) and LBPE content (2%–10%). ANOVA analysis, showing high F-values, confirmed that both NaOH and LBPE significantly affected the soil's UCS in relation to the CBR content under experimental conditions. The maximum UCS (28Days) 2100 kN/m² was observed when both NaOH and LBPE were at 10 % each.

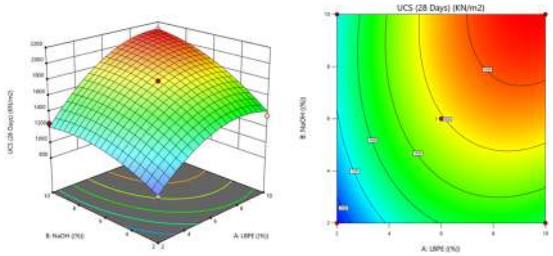


Figure 7: 3D Surface and Contour Plots of The Interactive Effects of the Percentage LBPE-NaOH on UCS 28 Days

2) Effect of Variables Interaction On CBR: Figure 8 presents the 3D and contour plots, showing that the CBR increased almost linearly with increasing NaOH (2%–10%) and LBPE (2%–10%) contents. High F-values from the ANOVA analysis confirmed that both factors had a significant effect on the soil's UCS relative to CBR. The CBR unsoaked 90% was achieved at 10% NaOH and 10% LBPE, highlighting the optimal combination for soil compaction under the tested conditions.

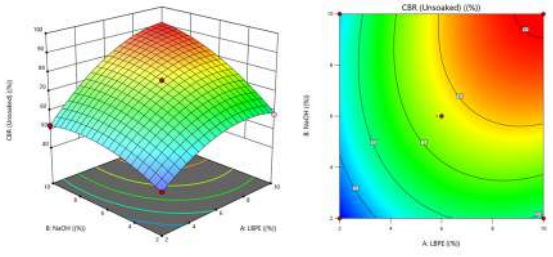


Figure 8: 3D Surface and Contour Plots of the Interactive Effects of the Percentage LBPE-NaOH on CBR Unsoaked

3.6 Numerical optimizations

Table VI presents the optimization results for the soil stabilization process using LBPE and NaOH. The desirability function value of 0.99 indicates an optimal

ISBN: 978-978-8567-02-8

combination of parameters. The maximum MDD of 1.972 Mg/m³ was achieved with 6.879% LBPE and 7.489% NaOH. Correspondingly, the UCS values at 7, 14, and 28 days were 1068.750 kN/m^2, 1472.452 kN/m^2, and 1936.056 kN/m^2, respectively. The CBR values were 45.017% (soaked) and 82.163% (unsoaked).

These findings align with recent studies that utilize Response Surface Methodology (RSM) for multi-response optimization in soil stabilization. For instance, Liu et al. (2025) employed RSM to optimize charcoal briquette production, achieving enhanced mechanical properties through optimal parameter settings (Al-Shayea, 2025). Similarly, Anggerta and Dewi (2025) optimized NaOH concentration and cooking time in delignification processes.

silica and alkali oxides, satisfied Class C pozzolanic requirements, confirming its suitability as a stabilizer. NaOH-activated LBPE significantly improved soil performance, reducing plasticity index from 40% to 18%, increasing maximum dry density to 1.74 Mg/m³, lowering optimum moisture content, and reducing swelling to 30%. Strength improved markedly, with UCS reaching 1936 kN/m^2 and unsoaked CBR increasing to 82%, meeting NGSRB standards. RSM – CCD models showed strong predictive accuracy ($R^2 \geqslant 0.969$). Optimal performance occurred at 6 – 10% LBPE and NaOH, demonstrating LBPE as a sustainable stabilizer for road construction.

TABLE VI. RESULTS OF OPTIMIZATIONS

LBPE	NaOH	OMC	MDD	UCS (7 Days)	UCS (14 Days)	UCS (28 Days)	CBR (Soaked)	CBR (Unsoaked)	Desirability
6.879	7.489	14.647	1.972	1068.750	1472.452	1936.056	45.017	82.163	0.99

Table VII: Results of Validation

Method	LBPE	NaOH	OMC	MDD	UCS (28 Days)	CBR (Unsoaked)
Optimized	6.879	7.489	14.647	1.972	1936.056	82.163
Experimental Validate	6.879	7.489	14.475	1.962	1936.02	82.056
Difference	-	-	0.172	0.01	0.036	0.107

3.7 Validation

Table VII shows validation results comparing predicted and experimental values. Optimized LBPE–NaOH stabilization achieved minimal deviations—0.245% for LBPE and 0.107% for CBR—confirming the high accuracy of the RSM model in predicting OMC, MDD, UCS, and CBR (28 days) for expansive soil stabilization.

Teodoru et al. (2025) reported <2% deviation between predicted and experimental UCS for lime–cement stabilization, while Ali and Mohammed (2024) observed <1% difference using NaOH and bio-additives (Anggerta & Dewi, 2025). Similarly, this study's minimal deviations confirm the reliability of the RSM optimization model for predicting optimal LBPE–NaOH content and soil mechanical properties.

4. CONCLUSION

The natural soil was identified as highly plastic expansive clay with low strength, necessitating stabilization. Locust bean pod extract (LBPE), rich in

ACKNOWLEDGMENT

The author gratefully acknowledges the Department of Civil Engineering, Abubakar Tafawa Balewa University (ATBU), Bauchi, and the Geotechnical (Geothermal) Laboratory for their academic guidance, access to facilities, and technical support, which were essential to the successful completion of this study.

REFERENCES

Abhishek, A., Guharay, A., Raghuram, A. S. S., & Hata, T. (2024). A state-of-the-art review on suitability of rice husk ash as a sustainable additive for geotechnical applications. Indian Geotechnical Journal, 54(3), 910–944.

Ahmadi, M. (2024). Advancing Geotechnical Evaluation of Wellbores: A Robust and Precise Model for Predicting Uniaxial Compressive Strength (UCS) of Rocks in Oil and Gas Wells. Applied Sciences, 14(22), 10441.

Ahmed, S. M., & Agaiby, S. S. (2020). Strength and stiffness characterization of clays using Atterberg limits. Transportation Geotechnics, 25, 100420.

Al-Shayea, N. A. (2025). Estimating the Coefficient of Subgrade Reaction in the Laboratory Using the CBR

Testing Apparatus. Arabian Journal for Science and Engineering, 50(3), 2123–2147.

Ali, H. F. H., & Mohammed, A. S. (2024). Innovative analysis and advanced modeling of UCS and CBR in fly ash-treated soils: evaluating the impact of hydraulic index, chemical alteration, lime modulus, and geochemical indices. Modeling Earth Systems and Environment, 11(1), 28. doi:10.1007/s40808-024-02230-w

Alqudah, M., Saleh, H., Yasarer, H., Al-Ostaz, A., & Najjar, Y. (2025). Comparative Study of Machine Learning Techniques for Predicting UCS Values Using Basic Soil Index Parameters in Pavement Construction. Infrastructures, 10(7), 153.

Alshenawy, A. O., Hamid, W. M., & Alnuaim, A. M. (2021). A review on the characteristics of sabkha soils in the Arabian Gulf Region. Arabian Journal of Geosciences, 14(19), 2018.

Ampoorter, E., Van Nevel, L., De Vos, B., Hermy, M., & Verheyen, K. (2010). Assessing the effects of initial soil characteristics, machine mass and traffic intensity on forest soil compaction. Forest Ecology and Management, 260(10), 1664–1676.

Anggerta, L. A., & Dewi, L. C. (2025). Optimization of Operating Conditions in Lignin Isolation Process of Rice Straw Using Box-Behnken Design Methodology. Jurnal Teknik Kimia dan Lingkungan, 9(1), 11–19.

Ayadi, I., Gargouri, A., & Guerfali, M. (2025). Sustainable Valorization of Olive Mill Wastewater Via Oleaginous Yeasts: Single-Cell Oil Production and Effluent Detoxification. Waste and Biomass Valorization, 1–17.

Bala, B., Purushothaman, N. K., & Das, B. S. (2025). Spectro-pedotransfer functions for estimating Atterberg limits in soil. Catena, 260, 109476.

Carmona-Martínez, A. A., Rueda, A., & Jarauta-Córdoba, C. A. (2024). Deep decarbonization of the energy intensive manufacturing industry through the bioconversion of its carbon emissions to fuels. Fuel, 371, 131922.

Chen, Y., Zhang, Y., He, S., Liang, M., Zhang, Y., Schlangen, E., & Çopuroğlu, O. (2023). Rheology control of limestone calcined clay cement pastes by modifying the content of fine-grained metakaolin. Journal of Sustainable Cement-Based Materials, 12(9), 1126–1140.

Gu, J., Ni, J., Xu, G., Zhou, Y., & Zhang, H. (2025). Experimental and DEM investigation of thermal effects on mechanical properties of biopolymer treated soil. Transportation Geotechnics, 101744.

Hasan, M. A., Praveen, B. S., Bag, R., & Ramu, B. (2024). The State-of-the-Art review on prediction of subgrade CBR: Past and present trends. Indian Geotechnical Journal, 1–22.

Hastuty, I. P., & Hartawan, A. (2021). Unconfined compressive strength and California Bearing Ratio test on clay stabilization using silica sand. Paper presented at the IOP Conference Series: Materials Science and Engineering.

Kilani, A. J., Ikotun, B. D., Abdulwahab, R., & Olubambi, A. (2025). A review on the structural performance of sustainable composite construction materials incorporating locust bean and mango wastes. Discover Applied Sciences, 7(9), 1022.

Knadel, M., Rehman, H. U., Pouladi, N., de Jonge, L. W., Moldrup, P., & Arthur, E. (2021). Estimating atterberg limits of soils from reflectance spectroscopy and pedotransfer functions. Geoderma, 402, 115300.

Malenga, E. N., Mulaba-Bafubiandi, A., & Nheta, W. (2022). Application of the response surface method (RSM) based on central composite design (CCD) and design space (DS) to optimize the flotation and the desliming conditions in the recovery of PGMs from mine sludge. Separation Science and Technology, 57(18), 2960–2983.

Mohammed, Z., Gouveia, G., Ramkissoon, A., & Clarke, R. (2025). Prediction of soil swelling using machine learning techniques. Modeling Earth Systems and Environment, 11(6), 1–19.

Nooraiepour, M. (2022). Clay mineral type and content control properties of fine-grained CO2 caprocks—laboratory insights from strongly swelling and non-swelling clay–quartz mixtures. Energies, 15(14), 5149.

O'Kelly, B. C., & Sivakumar, V. (2014). Water content determinations for peat and other organic soils using the oven-drying method. Drying Technology, 32(6), 631–643.

Sahoo, S., & Singh, S. P. (2022). Strength and durability properties of expansive soil treated with geopolymer and conventional stabilizers. Construction and Building Materials, 328, 127078.

Shinde, B., Sangale, A., Pranita, M., Sanagle, J., & Roham, C. (2024). Utilization of waste materials for soil stabilization: A comprehensive review. Progress in Engineering Science, 1(2-3), 100009.

Singh, S. P., & Das, R. (2020). Geo-engineering properties of expansive soil treated with xanthan gum biopolymer. Geomechanics and Geoengineering, 15(2), 107–122.

Tandon, S., Singh, S. K., Kacker, R., Gautam, S. S., & Tamang, S. K. (2025). Multi-response Optimization of 3D Printed Parts with Triangular Patterns Using Nonlinear Machine Learning Regressor Technique. Journal of Materials Engineering and Performance, 34(11), 10642–10658. doi:10.1007/s11665-024-09869-7

Teodoru, I.-B., Owusu-Yeboah, Z., Aniculăesi, M., Dascălu, A. V., Hörtkorn, F., Amelio, A., & Lungu, I. (2025). Prediction of Unconfined Compressive Strength in Cement-Treated Soils: A Machine Learning Approach. Applied Sciences, 15(13), 7022.

Wang, D., Wang, Z., & Wang, H. (2024). Feasibility and performance assessment of novel framework for soil stabilization using multiple industrial wastes. Construction and Building Materials, 449, 138228.

Zha, F., Hu, C., Kang, B., Qin, L., Li, J., & Chu, C. (2024). Formulation of PG-FA-L composite modifier for repairing expansive soil based on the statistical mixed design method. Chemosphere, 349, 140974.

Zhu, J.-F., Zheng, Q.-Q., Tao, Y.-L., Ju, L.-Y., Yang, H., Gong, X.-N., . . . Wang, Z.-Q. (2025). The curing mechanism and empirical model for the marine organic soft clay stabilized with calcium carbide residue and silica fume under the optimal ratio. Acta Geotechnica, 20(2), 683–706.

ISBN: 978-978-8567-02-8

031-Effects of *Sporosarcina Pasteurii* Bacteria on the Durability of Self-Compacting Concrete Admixed With Cement Kiln Dust Using Response Surface Methodology

[1]Garba, I., [2]Sulaiman, T. A., [3]Yau, Y., [4]Suleiman, Y., [5]Abdullahi, M.

[1,2,3,5,] *Department of Civil Engineering, Ahmadu Bello University, Zaria*
[4]*Department of Civil Engineering, Nuhu Bamalli Polytechnic Zaria*
Corresponding Authors E-mail: isahgarba86@gmail.com

Abstract: The performance of concrete structures in terms of durability is reduced due to the formation of microcracks, which poses a serious risk to the structure's durability. This study utilizes *Sporosarcina Pasteurii* bacteria to assess the durability performance and develop mathematical prediction models, and optimize self-compacting concrete admixed with cement kiln dust using response surface methods. Self-compacting concrete mixes were prepared with cement kiln dust by partially replacing with cement at 10 % and 2 %Superplasticizer dosages at a water cement ratio of 0.43 and a mix ratio of 1:2.44:1.48 and incorporating different suspension densities of *S. Pasteurii Bacteria* at 0 (control), 1.5 x 10^8, 6.0 x 10^8, 1.2 x 10^9, and 2.4 x 10^9 cells/mil, with cementation reagent prepared at 0.5 M concentration. Furthermore, durability performance, such as water absorption and mass loss due to acidic attack, was also assessed. The results indicate that water absorption and mass loss due to acid resistance decrease with an increase in the suspension density of bacteria. The predictive models developed have a coefficient of correlation (R^2) of 91.15 % and 92.60 % for water absorption and mass lost due to acid attack, respectively. The optimized values for the concentration, bacterial suspension density, and curing age are 75B-25C, 2.4x10^9 cells/mil, and 120 days, with values of 1.387 % and 1.90 %, where B represents the bacterial suspension density and C denotes the cementation reagent. The models are recommended for usage in the prediction of water absorption and mass loss due to acid attack, provided the required concentration, suspension density of *S. Pasteurii,* and curing age are known.

1. INTRODUCTION

Self-compacting concrete serves as an effective alternative to traditional concrete. Its remarkable capacity to flow freely due to its weight in the fresh state negates the need for external compaction. However, this high level of workability might compromise strength and durability, which are essential design considerations in Civil Engineering projects. The excess water present in self-compacting concrete can weaken the microstructure of the aggregate paste interfacial transition zone (ITZ) and heighten the capillary porosity of the hardened paste, potentially affecting the strength and durability attributes of the concrete (Gao *et al*., 2014). The introduction of supplementary cementitious materials (SCMs) has improved the mechanical and durability performance of concrete while also contributing to the reduction of CO_2 emissions associated with cement production (Gartner and Sui, 2018). The increasing production of cement has raised awareness about cement kiln dust, a significant waste byproduct being discarded. Cement kiln dust, produced during the cement manufacturing process, can represent 3-4 % of the total cement output, varying based on the raw materials and production techniques employed. Utilizing cement kiln dust as a substitute for cement may lead to cost-effective concrete that retains self-compatibility in the fresh state and exhibits improved characteristics once hardened, owing to its pozzolanic properties, as confirmed by numerous researchers.

The strength of SCC weakened due to the entry of unfavorable species into the concrete mix, which exacerbated the expansion of micro cracks under external stress and chemical reactions. Although preventing cracks in concrete structures is challenging, it can be managed by enhancing water density (Nanayakkara *et al.,* 2015). Certain bacillus species, including *Bacillus* pasteurii (Ramakrishnan *et al.,* 2001), *Bacillus Sphaericus* (Ramakrishnan *et al*., 2005), *Bacillus Pseudofirmus*, *Bacillus Cohnii* (Jonkers *et al*., 2010), and *Bacillus Alkalinitrilicus* (Wiktor *et al*., 2011), have been shown to effectively mitigate cracks in concrete (Van Tittelboom *et al.,* 2010). These bacterial cells enhance the pore structure of concrete through the process of calcite precipitation (Wiktor *et al*., 2011; Stocks *et al*., 1999). The adoption of bio-concrete not only improves service life but also reduces maintenance costs, which decreases the necessity for construction efforts and conserves essential building materials, thereby saving energy (Rahmani and Bazrgar, 2015).

In research conducted by Ameri *et al*., (2019)

ISBN: 978-978-8567-02-8

regarding the optimization of rice husk ash (RHA) content and bacterial concentration in self-compacting concrete (SCC), it was concluded that the ideal strength properties were achieved with a bacterial concentration of 105 cells/mil at optimum RHA content, while the most favorable durability was noted at a bacterial concentration of 107 cells/mil. Taku *et al*., (2023) developed models to evaluate the permeation properties of self-compacting concrete containing *Sporosarcina Pasteurii*. The findings revealed that the constructed linear models, which followed a quadratic form, were sufficient for predicting and optimizing the water absorption and sorptivity of the bio-self-compacting concrete. Garba *et al*., (2024) found that after 28 days of curing, the water absorption was measured at 0.30 percent Styrofoam content, and the optimal results were observed at 0.27 percent, yielding compressive and split tensile strengths of 17.865 N/mm² and 2.25 N/mm², respectively. According to Aliyu *et al*., (2020a), mortar specimens with Calcined Clay Brick Powder (CCBP) showed greater resistance (durability) to $MgSO_4$ solution when compared to control samples, with the best results occurring between 5 % and 15 % CCBP content, confirming that the optimum CCBP content is 5 %. Sulaiman *et al*., (2024) reported that the weight retention percentage after exposure to H_2SO_4 solution declines as the proportion of SSA and duration of immersion in the H_2SO_4 solution increases. It was found that Portland limestone cement concrete exhibited better resistance against H_2SO_4 than SSA-concrete, with recommendations indicating that the optimal percentage of SSA content should not exceed 10 %. A report by Aliyu *et al*., (2020b) noted that the weight of concrete decreased as exposure duration and Quarry Dust content increased, while water absorption of Quarry Dust-Concrete reduced with greater additions of Quarry Dust. This suggests that Quarry Dust can effectively replace river sand in concrete, enhancing its resistance to sulphuric acid attack. Akhtar *et al.,* (2023) investigated the strength and durability properties of bacteria-based self-compacted concrete with mineral admixtures, noting that SCCMSBM and SCCMKBM mixes displayed ductile responses under flexural loads, increasing by 5.55 % and 10.52 % at 28 days and 5.26 % and 10 % at 56 days in comparison to the standard mix. Strength was found to increase by 9.16 % and 12.37 % at 28 days and 5.49 % and 13.43 % at 56 days.

This research focuses on assessing the durability and formulating mathematical models while optimizing SCC-CKD with varying suspension densities of *Sporosarcina Pasteurii* bacteria through response surface methodology.

2. MATERIALS AND METHODS

2.1 Materials

The Portland Limestone Cement (PLC) of grade 42.5N used was obtained from a nearby dealer at Samaru Market. Quality control and standard compliance tests were carried out on the cement. The cement kiln dust (CKD) in this study was sourced from the BUA Company at Kalambaina, Sokoto state. A crushed granite of 20 mm maximum nominal particle size was sourced from a quarry opposite the Nigeria College of Aviation Technology (NCAT), Zaria. The fine aggregate in this study was locally sourced from a river at area G behind Ahmadu Bello University, Zaria. The use of superplasticizer is essential in this study with the view to maintaining self-consolidating mixtures. Polycarboxylate-based ether (PCE) used in this research work was sourced from Sabon gari market. The microbe used in the study is B. *Pasteurii,* which is normally found in soil. This urease positive microbe is a shaped, spore-forming bacteria, gram positive and was cultured from the Department of Microbiology, Ahmadu Bello University, Zaria. Moreover, the cementation reagent used comprises 2.8 g of calcium chloride ($CaCl_2$), 20 g of urea ($CO(NH_2)_2$), 3 g of nutrient broth, 10 g of ammonium chloride (NH_4CI), and 2.12 g of sodium bicarbonate ($NaHCO_3$) per litre of de-ionised water. The mass concentrations of urea and calcium chloride of 0.5M were used, and the cementation reagent was prepared according to (Stocks-Fischer *et al.,* 1999). Finally, the water used was sourced from the Department of Civil Engineering, Ahmadu Bello University, Zaria.

2.2 Methods

2.2.1 Design of Experiment and Development of Mix Design Matrix

The experimental design was developed using Design Expert Software 13 (2021). The mix design employed a discrete multi-level categorical factorial method. The independent variable analyzed is the suspension density of *S. Pasteurii* bacteria, with levels including Control, 1.5 x 10^8, 6.0 x 10^8, 1.2 x 10^9, and 2.4 x 10^9 cells/mil, along with various mixing ratios of (25B-75C, 50B-50C, 75B-25C), where B represents the bacterial suspension density and C denotes the cementation reagent, while curing ages are established at four levels (7, 14, 28, and 56 days). The software produced a mix matrix containing 60 unique combinations of design factors to assess the strength properties of self-compacting concrete. Additionally, to evaluate the durability performance of SCC-CKD, the curing ages are specified as 28, 56, 90, and 120 days, while retaining the same bacterial suspension densities and concentrations.

2.2.2 Mix Design

The formulations for self-compacting concrete were developed in accordance with the EFNARC (2005) guidelines and IS 10262 (2019), ensuring a constant water/cement ratio of 0.43. An optimal level of 10 % cement kiln dust was used to partially replace Portland limestone cement, along with 2% dosages of superplasticizer. Different concrete mixes were prepared using various densities of *Sporosarcina Pasteurii* bacteria, namely (Control, 1.5 x 10^8, 6.0 x 10^8, 1.2 x 10^9, and 2.4 x 10^9 cells/mil), alongside different ratios of suspension density/cementation reagent at (25B-75C, 50B-50C, 75B-25C). The cementation reagent was created at a concentration of 0.5M.

2.2.3 Bacteria

The bacteria *Sporosarcina Pasteurii*, which is now classified as *Bacillus Pasteurii*, possess the capability to precipitate calcite when a calcium source and a liquid

ISBN: 978-978-8567-02-8

medium, like water, are present. The physicochemical analysis of these bacteria was conducted in the Department of Water Resources and Environmental Engineering, as presented in Table 1. Plate 1 illustrates various suspension densities of *Sporosarcina Pasteurii* bacteria that were cultured at the Department of Microbiology, ABU Zaria.1

TABLE 1. PHYSIOCHEMICAL ANALYSIS OF S. *PASTEURII*

Bacteria Species	PH	Electrical Conductivity(us/cm)
S. pasteurii	9.05	2850



Plate 1: Different Suspension Density *Sporosarcina pasteurii*

2.2.4 Water absorption Tests

Water absorption tests were performed on concrete cubes measuring 100x100x100mm, following the guidelines of BS EN 1881-122 (2020). The tests were carried out at various curing durations of 28, 56, 90, and 120 days, during which the specimens were air-dried for 24 hours before being weighed and documented. Afterward, the specimens were completely submerged in a water bath for a duration of 7 days. During this time, the specimens were taken out of the bath, air-dried again, and the weight of the saturated specimens was recorded. The amount of water absorbed by the SCC-CKD specimens containing *S. pasteurii* bacteria was calculated using equation 1.

$$Water\ Absorption\ (WA) = \frac{W1 - W2}{W1} x100 \quad (1)$$

Where *WA* is the water absorption (%), W_1 is the weight of the air-dried specimen before 7 days of submerging (gm), and W_2 is the weight of saturated SCC specimens after 7 days of submerging (gm).

2.2.5 Acid Resistance Tests

The acid resistance tests were performed on 150 samples measuring 100 x 100 x 100 mm, following the guidelines of BS EN 12390-10 (2018). The samples were exposed to a 5% solution of H_2SO_4, with a molar concentration of 0.937 M, at different curing durations of 28, 56, 90, and 120 days, respectively. At each curing interval, the samples were air-dried and weighed. Once weighed, the specimens were immersed in a water bath containing a 5% H_2SO_4 solution and left in the solution for varying durations of 28, 56, 90, and 120 days, according to their respective ages. After these time intervals, the specimens were air-dried again and weighed. The percentage of weight loss from the specimens was then calculated using equation 2.

$$Weight\ Loss\ (WL) = \frac{W1 - W2}{W1} x100 \quad (2)$$

Where W_L is the weight loss of SCC-CKD with S. *Pasteurii* specimens (%), W_2 is the air-dried weight of the specimen before submerging in the acid solution (gm), and W_1 is the saturated weight of the specimens after submerging (gm).

2.2.6 Model Validation

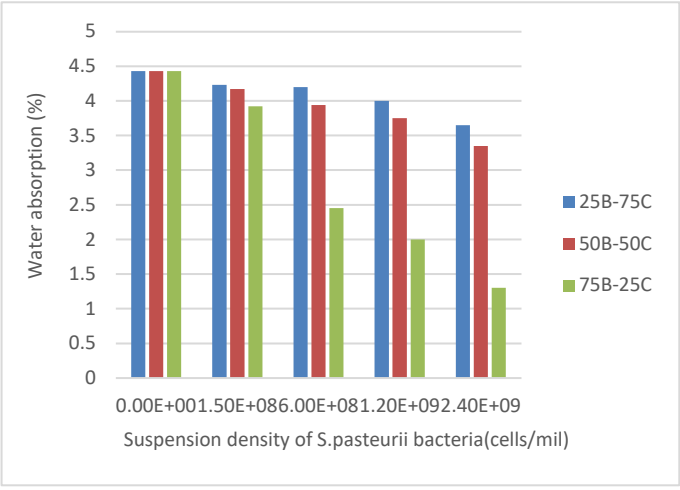
The mathematical models underwent validation by examining residual plots to confirm that the assumptions for ANOVA were met. This was achieved by generating diagnostic plots that featured externally studentized residuals (normal, residuals plotted against predicted values, and predicted values compared to actual values). Furthermore, experimental validation was performed by calculating the percentage error for the results derived from numerical optimization.

3. RESULTS AND DISCUSSIONS

3.1 Water Absorption Test

The results of the water absorption test on SCC-CKD with different suspension densities of *S. Pasteurii* are presented in Figure 1. From this figure, it is clear that incorporating *S. Pasteurii* into SCC-CKD significantly lowers water absorption, and this effect becomes more pronounced with increasing bacterial suspension density. Initially, all mixtures show similar water absorption rates when there are no bacteria present (0.00E+00). However, as the bacterial suspension density increases from 1.5×10^8 to 2.4×10^9 cells/mil, water absorption consistently decreases. This improvement is mainly attributed to the microbially induced calcium carbonate precipitation (MICP), which fills the pores in the concrete and reduces permeability. The combination of 75%B and 25%C shows the greatest effectiveness, achieving a water absorption rate of 1.3% at the highest bacterial suspension density. These findings align with recent studies suggesting that MICP enhances the durability of concrete and decreases water penetration by compacting the microstructure (Chaurasia *et al*., 2023).

Figure 1: Water Absorption of SCC-CKD with Suspension Density of Bacteria



3.2 Acid Resistance Test

The mass loss observed during the acid-resistant test of

ISBN: 978-978-8567-02-8

SCC-CKD at varying suspension densities of *S. pasteurii* bacteria is depicted in Figure 2. From Figure 2, it is evident that increasing the suspension density of *S. pasteurii* in SCC-CKD markedly enhances its resistance to acid attack. At a density of 00E+00 bacteria, all mixtures experience a mass loss of approximately 7.95 %, indicating their susceptibility. However, as the suspension density increases from 1.5×10^8 to 2.4×10^9 cells/mil, the mass loss progressively decreases across all mix ratios. This improvement is especially pronounced in the mixture comprising 75% B and 25% C, where mass loss declines to merely 1.9 %. This observation implies that the microbially induced calcium carbonate precipitation (MICP) process contributes to sealing pores and safeguarding the concrete against acid damage. These results are consistent with recent studies indicating that bacterial treatment not only enhances durability but also significantly mitigates chemical degradation in cement-based materials (Chaurasia *et al*., 2023).

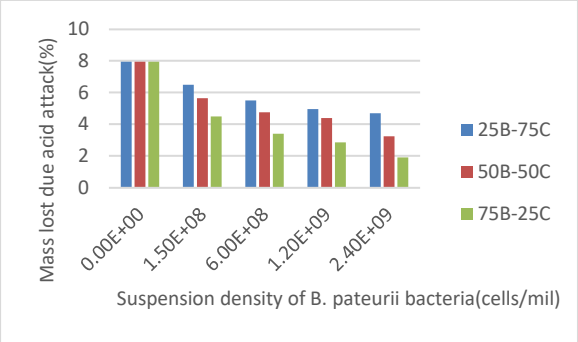


Figure 2: Mass lost due Acid Attack of SCC-CKD with Suspension Density

3.3 Analysis of Variance (ANOVA)

In the context of experimental design, variance analysis is employed to determine whether independent variables significantly influence dependent variables. The results of the ANOVA regarding water absorption and mass loss from acid attack in SCC-CKD concrete are showcased in Tables 2 and 3. This analysis was conducted at a significance level of 5 percent to evaluate the importance of experimental factors. For this investigation, water absorption and mass loss from acid attack were considered as the dependent variables, while concentration, suspension density, and curing age were selected as the independent factors. The variance analysis aimed to ascertain whether these factors meaningfully impacted the responses based on the established confidence level. A confidence level of 95 % was chosen, indicating that the P-value (probability level) must be below 5 % ($p < 0.05$). A p-value beyond 0.05 signifies that the model is insignificant. As indicated in Tables 2 and 3, the models produced p-values of < 0.0001, indicating a high level of significance for these models.

TABLE 2. ANOVA RESULTS FOR WATER ABSORPTION OF SCC-CKD AT *S. PASTEURII*

Source	Sum of Squares	df	Mean Square	F-value	p-value	
Model	47.94	6	7.99	91.03	< 0.0001	Significant
A-concentration	15.98	1	15.98	182.03	< 0.0001	
B-suspension density	23.61	1	23.61	268.93	< 0.0001	
C-curing age	3.06	1	3.06	34.82	< 0.0001	
AB	6.54	1	6.54	74.45	< 0.0001	
A^2	2.47	1	2.47	28.19	< 0.0001	
B^2	1.61	1	1.61	18.38	< 0.0001	
Residual	4.65	53	0.0878			
Cor Total	52.59	59				

TABLE 3. ANOVA RESULTS FOR MASS LOST DUE TO ACID ATTACK OF SCC-CKD AT *S. PASTEURII*

Source	Sum of Squares	df	Mean Square	F-value	p-value	
Model	940.31	6	156.72	110.61	< 0.0001	significant
A-concentration	67.10	1	67.10	47.36	< 0.0001	
B-suspension density	287.25	1	287.25	202.74	< 0.0001	
C-curing age	380.09	1	380.09	268.27	< 0.0001	
AB	4.89	1	4.89	3.45	0.0688	
BC	11.64	1	11.64	8.22	0.0059	
B^2	89.20	1	89.20	62.95	< 0.0001	
Residual	75.09	53	1.42			
Cor Total	1015.40	59				

3.4 Fit Statistical Analysis

Table 4 presents the findings of the fit statistics for the developed predictive mathematical models. These models focus on the reactions of water absorption and mass loss due to acid exposure. The coefficients of determination (R^2), along with the adjusted (R^2), predicted (R^2), and adequate precision values for each model, are provided. The adequacy of the model can be evaluated by the coefficient of determination (R^2), which acts as a general indicator of model performance, as highlighted by (Haque *et al*., 2021). The difference between the predicted R^2 and adjusted R^2 was relatively minimal, with all discrepancies remaining below 20 %. Moreover, the adequate precision values, which assess the signal-to-noise ratio, were found to be greater than 4. These findings suggest that there are sufficient signals, affirming that the models are appropriate for forecasting future results.

ISBN: 978-978-8567-02-8

TABLE 4. VALIDITY AND ACCURACY OF DEVELOPED PREDICTIVE MATHEMATICAL MODELS

S/N0	Model	Coefficient of Determination R^2	Adjusted R^2	Predicted R^2	Difference: (Adjusted – Predicted) R^2 < 0.2	Adequate Precision > 4
1	Water Absorption	0.9115	0.9015	0.8876	0.0139	39.4237
2	Mass lost due to acid	0.9260	0.9177	0.9064	0.0113	39.9428

3.5 Developed Models

Mathematical prediction models were created to evaluate the water absorption and mass loss due to acid in SCC-CKD with varying suspension densities of *S Pasteurii*. Quadratic models were determined to be the most suitable for all responses. The terms that were not significant were eliminated, and the models were formulated as presented below.

$$W_a = 3.71 - 0.6758C - 0.8638S_d - 0.2993 - 0.5565CS_d - 0.4307C^2 + 0.4026S_d^2 \quad (3)$$

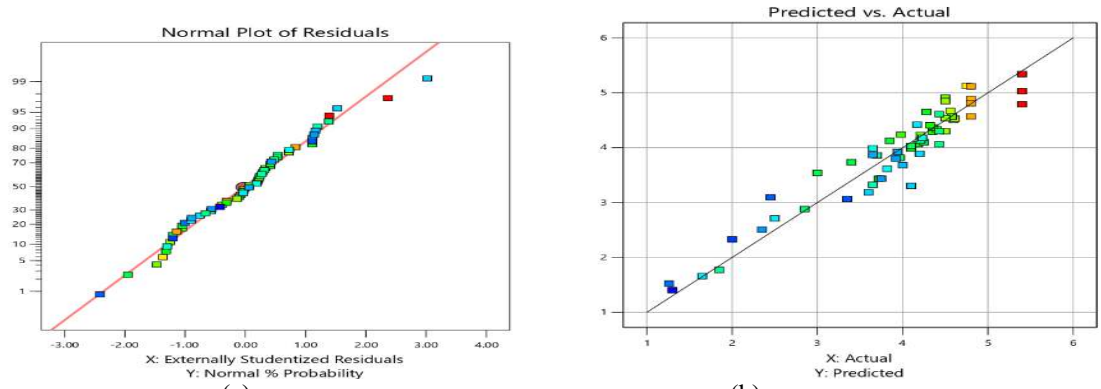
$$M_l = 6.49 - 1.38C - 3.01S_d - 3.57C_a - 0.4814CS_d + 0.8044S_dC_a + 2.99S_d^2 \quad (4)$$

Where $C,\ S_d\ and\ C_a$ are concentrations of bacterial/cementation reagent, suspension density of *S. Pasteuri*i bacteria, and curing age, respectively. While $, W_a, M_l$ are water absorption and mass loss are due to Acid attack, respectively.

3.6 Models Diagnostics Plots Analysis

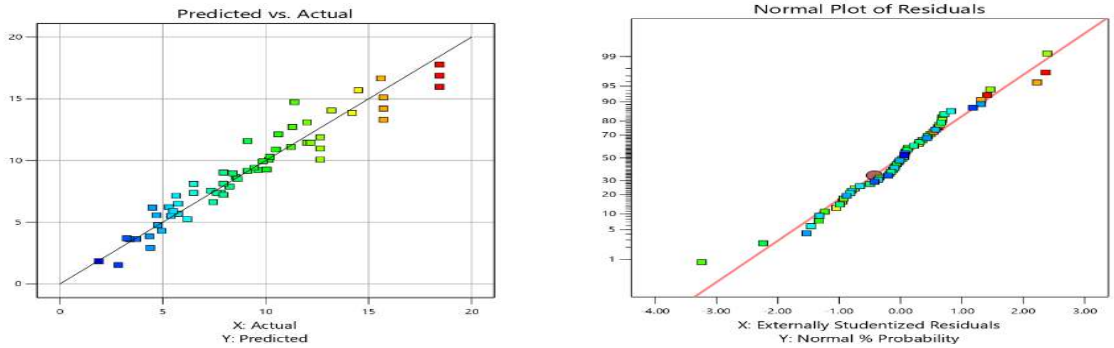
Figures 3 (a) 4 (a) display normal probability plots of the residuals for water absorption and mass loss due to acid attack in self-compacting concrete (SCC) containing various suspension densities of *Sporosarcina pasteurii* bacteria. These plots illustrate that the majority of data points closely align with the straight reference line, suggesting that the residuals are roughly normally distributed. This observation indicates that the regression model employed for predicting durability is statistically sound and free from major bias or heteroscedasticity. The concentration of data points along the line, with only a few deviations at the extremes, suggests that the experimental outcomes are reliable and that the use of bacterial suspension exerted a consistent rather than random effect on SCC performance (Chahal *et al*., 2023). Additionally, Figures 3 (b) and 4 (b) exhibit the predicted versus actual plot for water absorption and mass loss due to acid attack in self-compacting concrete (SCC) containing various suspension densities of *Sporosarcina pasteurii* bacteria. These plots reveal a strong correspondence of data points along the 45° line, indicating a significant level of agreement between the predicted and actual outcomes. This close clustering implies that the regression model effectively captures the association between bacterial suspension density and durability, showcasing its robust predictive power. Only a handful of points slightly deviate from the line, suggesting minor discrepancies that may be attributed to variations in curing conditions or bacterial concentrations that extend beyond the optimized range.

ISBN: 978-978-8567-02-8



(a) (b)

Figure 3. Diagnostics plots of residuals for water absorption: (a) Normal plot of residuals (b) Predicted versus actual



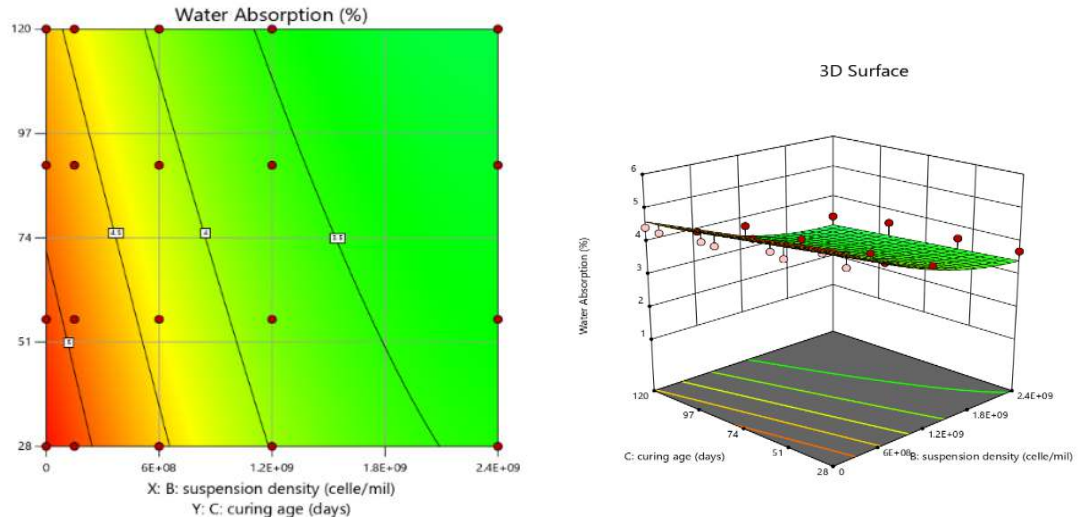
(a) (b)

Figure 4. Diagnostics plots of residuals for mass lost due to acid attack: (a) Normal plot of residuals (b) Predicted versus actual

3.7 2D and 3D Models Diagnostics Plots

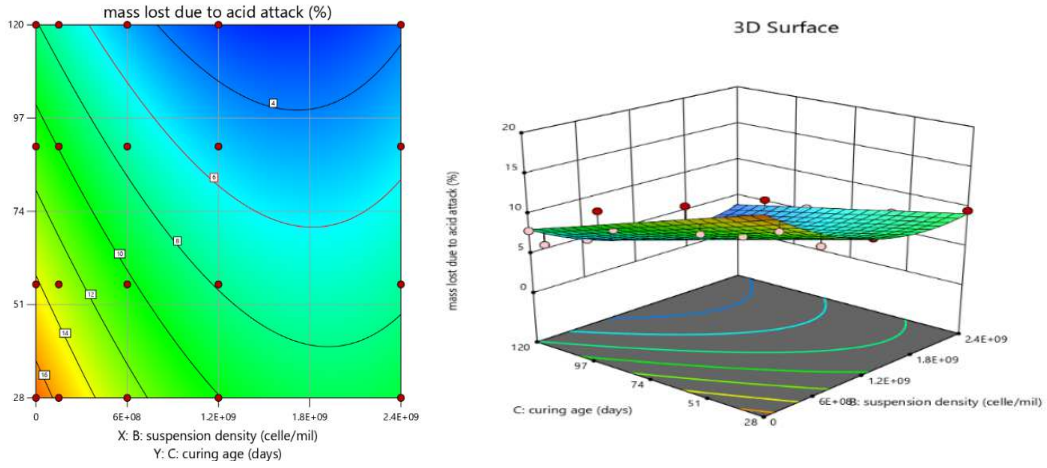
Figures 5 and 6 display the contours and 3D surface plots illustrating water absorption and mass loss caused by acid attack in SCC-CKD at varying bacterial suspension densities, respectively. An elliptical pattern seen in the contour plots for all responses typically signifies optimal interactions among the independent variables (factors), as noted by Karim *et al*., (2013) and Haque *et al*., (2021). In general, as shown in Figure 5 (a, b), an increase in bacterial suspension density results in reduced water absorption by the concrete, with this effect becoming more pronounced over extended curing periods. At 120 days, samples with higher bacterial counts exhibit significantly lower water absorption compared to those with fewer bacteria at 28 days. This pattern implies that the bacteria contribute to filling the concrete's pores through microbially induced calcite precipitation (MICP), ultimately enhancing its density and durability. Similar observations have been reported by Chahal *et al*., (2012), who found that incorporating bacteria could markedly lower water absorption due to calcium carbonate formation within the pore structure. Nevertheless, the graph also indicates that after reaching a specific bacterial concentration, further enhancement, likely due to a decline in bacterial activity as available nutrients diminish. Likewise, Figures 6 (a, b) present the 2D and 3D surface plots of mass loss attributed to acid attack on SCC-CKD, influenced by the varying bacterial suspension densities and curing periods. At lower bacterial densities and shorter curing times, the SCC-CKD showed greater mass loss, suggesting diminished resistance to acid degradation. Conversely, with increases in both bacterial suspension density and curing time, the percentage of mass loss decreased, indicating that microbial treatment bolstered the concrete's resistance to acid exposure. This enhancement is primarily due to microbially induced calcium carbonate precipitation (MICP), which occludes pores and decreases permeability within the concrete matrix.

ISBN: 978-978-8567-02-8



(b) (b)

Figure 5 (a and b) Contour and 3D plot of Water Absorption of SCC-CKD with *S. Pasteurii*



(b) (b)

Figure 6 (a and b) Contour and 3D plot of Mass lost due to acid attack of SCC-CKD with S. Pasteurii

3.8 Optimization Result of SCC-CKD at different Suspension Density of S. Pasteurii

Figure 7 illustrates the ramps used for numerical optimization, demonstrating the relationship between independent variables and the responses. It showcases the optimized outcomes that produced the best solutions for the dependent variables (responses). The durability performance of the SCC-CKD mix with a 75B-25C ratio, a bacterial density of $2.39x10^9$ cells/mil, and a curing age of 120 days was identified as the optimized solution, leading to a water absorption of 1.387 % and a mass loss of 1.90 % due to acid attack. This solution has a desirability value of 0.985 for its durability. The optimization objectives and constraints are detailed in Table 5. It was noted that the bacteria's suspension density and curing times significantly affect the responses.

ISBN: 978-978-8567-02-8

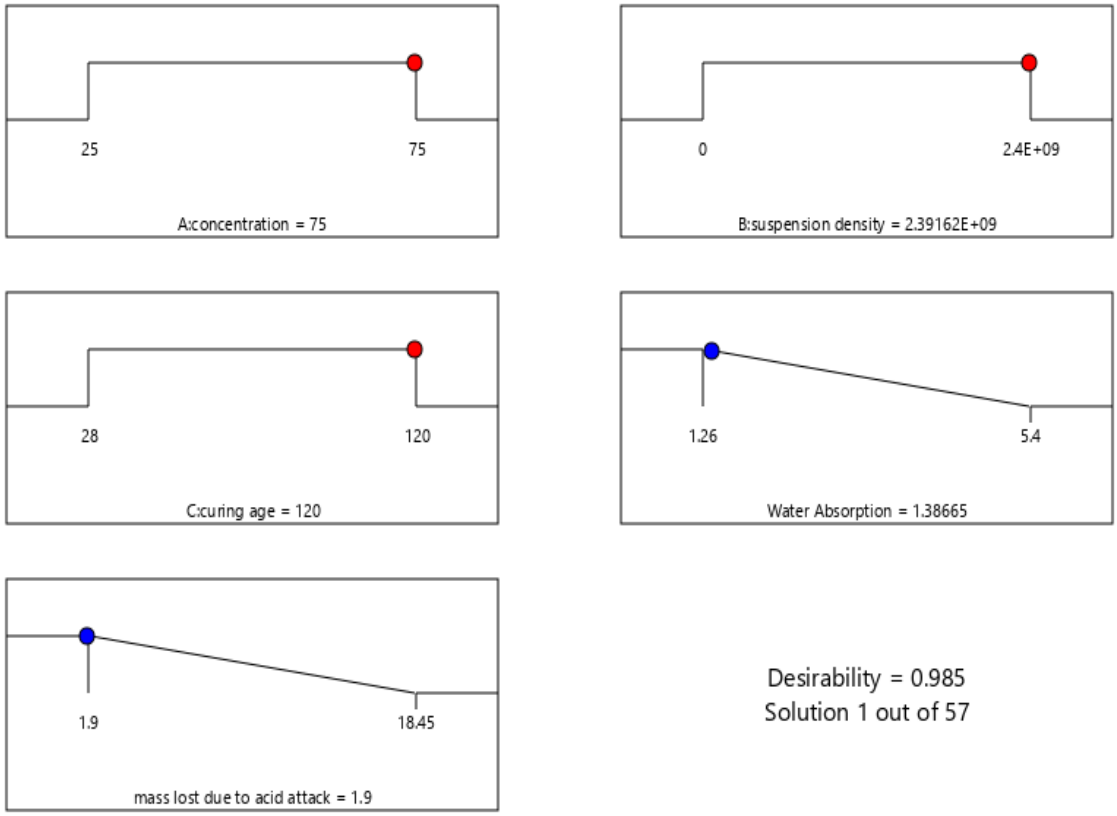


Figure 7. Ramps Numerical Optimization Analysis

TABLE 5: OPTIMIZATION GOALS AND CONSTRAINT

Variables/Responses	Goal	Lower Limit	Upper Limit	Lower Weight	Upper Weight	Importance
A: Concentration	is in range	25	75	1	1	3
B: Suspension Density	is in range	0	2.4E+09	1	1	3
C: Curing Age	is in range	7	56	1	1	3
Water Absorption	Minimize	1.26	5.4	1	1	3
Mass lost due to Acid Attack	Minimize	1.9	18.45	1	1	3

3.9 Experimental Model Validation

Table 6 presents the percentage error differences, which were below 5 % for nearly all of the responses assessed, indicating that the predicted values from the created models closely align with the experimental outcomes.

table 6. experimental model validation

Responses	Concentration (%)	S. pasteurii (cells/mil)	Curing Age (days)	Predicted Values	Experimental Values	Error (%)
Water Absorption	75B-25C	$2.4x10^9$	120	1.387	1.40	0.009
Mass lost due to acid attack (%)	75B-25C	$2.4x10^9$	120	1.90	1.93	0.016

ISBN: 978-978-8567-02-8

4. CONCLUSIONS

The subsequent conclusions were derived from the results presented:

i. The water absorption test and mass loss due to acid resistance of SCC-CKD at varying suspension densities of S. Pasteurii bacteria decrease as bacteria density increases, with the lowest values of 1.30 % and 1.90 % attained at $2.40x10^9$ cells/mil and a 75B-25C concentration, respectively.

ii. The mathematical models developed are capable of forecasting water absorption and mass loss from acid attack, achieving a coefficient of determination (R^2) of 91.15 % and 92.60 %, respectively.

iii. The optimal parameters for concentration, bacterial suspension density, and curing age are identified as 75B-25C, $2.4x10^9$ cells/mil, and 120 days, resulting in maximum values of water absorption and mass loss due to acid attack being 1.387 % and 1.90 %, respectively.

iv. The models were validated, showing percentage errors of 0.009 and 0.016, which are both below 5 %, indicating a strong correlation between the predicted and experimental outcomes.

ACKNOWLEDGMENT

The support and assistance of the technical staff from the Concrete Laboratory of the Civil Engineering Department, Ahmadu Bello University, Zaria, are gratefully acknowledged.

REFERENCES

Akhtar, J. N, Khan, R.Z, Khan, R.N, Thomas, B.S (2023) Experimental investigation on strength and durability characteristics of bacteria-based SCC with mineral admixture. *Material Today proceedings http://doi.org/10.1016/j.mat pr.2023.03.506*

Aliyu I, Sulaiman, T. A., Mohammed, A., Muktar, I. (2020a). Effect of Magnesium Sulphate on Calcined Clay Brick Powder Cement Replaced Mortar. *Journal of Science Technology and Education,* Vol.8, No.2, pp: 121-131.

Aliyu, I., Sulaiman, T. A., Mohammed, A. and Kaura, J. M. (2020b). Effect of Sulphuric Acid on the Compressive Strength of Concrete with Quarry Dust as Partial Replacement of Fine Aggregate. *FUDMA Journal of Sciences (FJS),* Vol. 4 No. 1, pp 553 – 559.

Ameri, F., Shoaei, P., Bahrami, N., Zareei, S. A. (2019) Recycled ceramic waste high strength concrete containing wollastonite particles and micro-silica: a comprehensive experimental study, *Constr. Build. Mater. 201 11–32.*

BS EN 12390-5 (2009). Testing Hardened Concrete Making and Curing Specimens for Strength Test. *British Standards Institution London United Kingdom*.

BS EN 12390-6(2009). Testing Hardened Concrete Tensile Splitting Strength of Test Specimen. *British Standands Institution London United Kingdom.*

BS EN 1881-122, (2020). Testing Concrete - Method for Determination of Water Absorption, *London, British Standard Institution (BSI), 2020.*

Chahal, N., Siddique, R., & Rajor, A. (2023). Influence of bacterial cells on the compressive strength and durability of self-compacting concrete. *Journal of Building Engineering, 75, 107303. https://doi.org/10.1016/j.jobe.2023.107303.*

Chaurasia, L., Yadav, R. K., Das, R., & Achal, V. (2023). Microbially induced calcite precipitation in cementitious materials: Recent developments.

Gao, Y. G., Schutter, D., Ye, G., Tan, Z., Wu, K. (2014) The ITZ microstructure, thickness and porosity in blended cementitious composite: effects of curing age, water to binder ratio and aggregate content, *Compos. Part B Eng. 60 1–13.*

Garba, I., Sulaiman, T. A., Aliyu, I., Kaura, J. M., Yau, Y., Yusuf, S. (2024). Predictive Models and Optimization of Strengths and Durability of Self-Compacting Concrete Admixed with Styrofoam. *FUOYE Journal of Engineering and Technology*, Vol. 9, No. 4, pp: 686-692. https://dx.doi.org/10.4314/fuoyejet.v9i4.18

Gartner, E. T. Sui (2018) Alternative cement clinkers, *Cem. Concr. Res. 114 27– 39.*

Haque, M., Ray, S., Mita, A. F., Bhattacharjee, S. & Jami Bin Shams, M. (2021). Prediction & optimization of fresh and hardened properties of concrete containing rice husk ash and glass fiber using response surface methodology. *Case Studies in Construction Materials 14 (2021). Published by Elsevier Ltd.,* 1-14.

Jonkers, H. M. A. Thijssen, G. Muyzer, O. Copuroglu, E. Schlangen, (2010). Application of bacteria as self-healing agent for the development of sustainable concrete, *Ecol. Eng. 36 230–235.*

Karim, M. R., Zain, M.F.M., Jamil, M. and Lai, F.C. (2013). Fabrication of a non-cement binder using slag, palm oil fuel ash and rice husk ash with sodium hydroxide. *Construction Building. Materials*, 49, 894 - 902.

Rahmani H, H. Bazrgar (2015). Effect of coarse cement particles on the self-healing of dense concretes, *Institution of Civil Engineering Publishing, Magazine of Concrete Research, 67, 9, pp 476-486 https://doi.org /10.1680/macr.14.00158.*

Ramakrishna, V. Panchalan, R.K. S.S. Bang, R. City, (2005). Improvement of Concrete Durability by Bacterial Mineral Precipitation, *Proc. 11th Int. Conf. Fract*, pp. 20–25.

Ramakrishnan, V. Ramesh, K.P S.S. Bang, (2001), Bacterial Concrete*, Smar Mater. International Society for Optics and Photonics, pp. 168–177.*

Sulaiman, T. A., Yau, Y., Adamu, I. M., Garba, I., Mohammed, A., Aliyu, I. (2024). Characteristics and Predictive Evaluation of Sesame Straw Ash Based Concrete. *Proceedings of 3rd International Conference on Engineering and Environmental Sciences (ICEES)*. Pp: 326-331.

Stocks, S. -Fischer, J. K. Galinat, S.S. Bang, (1999). Microbiological precipitation of CaCO3, *Soil Biol. Biochem. 31 1563–1571*

Taku, K., & Lawan, A. (2024). Optimization modelling of the strength properties of bio-self-compacting concrete using *Sporosarcina pasteurii* as a microbially induced calcite precipitation agent. *Journal of Engineering Science, 15*(1), 11–19. *https://doi.org/10.3329/jes.v15i1.76001*

Van Tittelboom, K N. De Belie, W. De Muynck, W. Verstraete, (2010). Use of bacteria to repair cracks in concrete, *Cem. Concr. Res.* 40 157–166.

Wiktor, V. Jonkers, H. M. (2011). Quantification of crack-healing in novel bacteria based self-healing concrete, *Cem. Concr. Compos.* 33 763–770.

ISBN: 978-978-8567-02-8

5TH Faculty of Engineering Conference on Engineering Innovation and Economic Policies: Driving Sustainable Industrial Growth in Nigeria

Faculty of Engineering, Bayero University, Kano.

032-Index and Compaction Characterisation of Cement-Stabilised Lateritic Soils Based on Selected Test Procedures

Isah, S. D, Amadi A. A, Adejumo T. E, and Alhassan, M.

(Department of Civil Engineering, Federal University of Technology, Minna. Sisah70@gmail.com)

Abstract: This study examines the characterisation of lateritic soils designated as GL1, GL2, GL3, GL4 and GL5 stabilised with 0–10% cement based on index and compaction properties determined by American Society for Testing and Materials (ASTM) and British Standards Institution (BSI) testing procedures. The soils are classified as GW/SW, GC/SC, CV/CH, CV/CH and CI/CL, respectively in BSI/ASTM systems. The liquid limit (LL) of the soils ranged from 30.03 to 67.38% for ASTM and 31.22 to 68.05% for BS, while the plasticity index (PI) varied between 6.97 and 25.00% for ASTM and 7.05 to 27.68 % for BS. Cement stabilisation produced notable reductions in plasticity, particularly in highly plastic soils (CV/CH). Variations in mean LL and mean PI determined from both standards were minimal and statistically insignificant ($p = 0.918$), indicating procedural consistency. Compaction results showed strong sensitivity to both cement content and compaction energy (Light and heavy efforts). Optimum moisture content (OMC) decreased with cement addition, such as in GL1, where OMC dropped from 17.44% to 15.46%, while maximum dry density (MDD) increased from 1.88 to 1.93 Mg/m³ under heavy effort. Across all samples, MDD values ranged from 1.65 to 2.35 Mg/m³, OMC values ranged from 9.90 to 21.40% with heavy compaction significantly increasing MDD by 0.114 Mg/m³ ($p = 0.031$) and reducing OMC by 2.91% ($p = 0.012$). Although ASTM produced marginally higher MDD (mean = 1.94 Mg/m³) than BSI (mean = 1.90 Mg/m³), the difference was not significant ($p = 0.531$). Overall, the findings confirm that cement stabilisation improved plasticity and compaction efficiency, while compaction energy exerts the strongest influence on density outcomes. The results obtained by ASTM and BSI procedures provided comparable characterisation of cement-stabilised lateritic soils, considering the index and compaction properties, namely LL, PI, OMC and MDD, which are critical parameters in pavement/geotechnical engineering applications.

KEYWORDS: Cement; Index properties; Lateritic soils; Soil stabilisation; compaction.

1. INTRODUCTION

Lateritic soils are widely distributed in tropical and subtropical regions and are commonly used as construction materials for pavement subgrades and earthworks (Osinubi *et al.,* 2021). However, several grades of lateritic soils exhibit inadequate engineering properties in their natural state, including high plasticity, moisture sensitivity, low shear strength, high compressibility, and variable density characteristics, which limit their direct application in pavement construction (Osinubi *et al.,* 2021; Etim *et al*., 2020; Babu *et al.,* 2023). These deficiencies often necessitate soil improvement to meet the performance requirements of modern road infrastructure and other geotechnical structures.

Among various soil improvement techniques, cement stabilisation has been widely adopted due to its effectiveness in reducing plasticity, improving compaction characteristics, and enhancing load-bearing capacity through cementitious bonding and pozzolanic reactions (Babu *et al*., 2023; Amadi *et al.,* 2025).

The assessment of cement-stabilised lateritic soils relies heavily on laboratory testing procedures, which significantly influence the determination of index and compaction parameters used in pavement design. In Nigeria and many developing countries, geotechnical laboratories commonly adopt international testing standards such as those developed by the American Society for Testing and Materials (ASTM) and the British Standards Institution (BSI). Although these standards aim to characterise similar soil properties, differences in test equipment, procedures, and compaction energies may lead to variations in measured engineering parameters (Burton and Airey, 2012; Lunne *et al*., 2019; Kaplan *et al*., 2022; Fouladi *et al*., 2023). Such discrepancies can complicate the comparison of results, introduce uncertainty in soil classification, and affect the reliability of design decisions, particularly for stabilised pavement materials.

ISBN: 978-978-8567-02-8

Given the increasing reliance on cement-stabilised lateritic soils for road construction, there is a need to evaluate the consistency and suitability of commonly used testing standards when applied to Lateritic soil – cement mixtures. This study therefore investigates the index and compaction characteristics of five grades of lateritic soils stabilised with varying cement contents using ASTM and BSI test procedures. The study examines the influence of cement content, compaction energy, and testing standard on Index and compaction parameters, with the objective of determining whether both standards provide comparable, reliable, and safe characterisation of cement-stabilised lateritic soils for pavement applications. The findings are intended to support informed selection of laboratory testing procedures and contribute to improved pavement design practices in tropical environments.

2. METHODOLOGY

2.1 Materials

2.1.1 Lateritic Soils

Five lateritic soil samples, designated GL1, GL2, GL3, GL4, and GL5, were collected from different locations within the Federal Capital Territory (FCT), Abuja, Nigeria. The soils were air-dried, pulverised through 4.75 mm sieve, and sieved to remove oversized particles prior to laboratory testing. The selected soil grades represent a wide range of lateritic soil types commonly encountered in tropical environments.

2.1.2 Stabilising Agent

Ordinary Limestone Portland Cement (CEM II), conforming to BS EN 197-1 was used as the stabilising agent. Cement contents of 0, 2.5, 5.0, 7.5, and 10% by dry weight of soil were adopted based on typical ranges reported for pavement subgrade stabilisation in previous studies (Babu *et al*., 2023).

2.2 Methods

2.2.1 Experimental Design

Response Surface Methodology (RSM) was employed to evaluate the combined effects of cement content, compaction energy, testing standard, and soil grade on the index and compaction characteristics of the lateritic soils. The independent variables considered were cement content (0–10%), compaction energy (light and heavy), testing standard (ASTM and BSI), and soil grade (GL1–GL5). A Box–Behnken experimental design under the response surface methodology (RSM) was adopted to generate the design matrix using Design-Expert software (Version 13.0.1.0). The study analysed liquid limit (LL), plastic limit (PL), plasticity index (PI), optimum moisture content (OMC), and maximum dry density (MDD) as response variables. Regression analysis and analysis of variance (ANOVA) were applied to evaluate the adequacy of the developed models, determine statistical significance, and investigate interaction effects among the factors. Regression modelling and analysis of variance (ANOVA) were used to evaluate statistical significance and interactions among variables.

2.2.2 Preparation of Soil–Cement Mixtures

For each soil grade, the required quantity of cement was blended with air-dried soil in the dry state to ensure uniform distribution. Water was then added to achieve the desired moisture content based on preliminary trials. The mixtures were thoroughly mixed, sealed in airtight containers, and allowed to mellow for 24 hours to promote hydration and homogeneity. This procedure was consistently applied across all samples to ensure comparability.

2.2.3 Particle Size Distribution

Particle size distribution tests were conducted to determine soil gradation characteristics, which influence compaction behaviour and soil classification. The tests were performed in accordance with BS 1377-2:1990 and ASTM D422 using mechanical sieve analysis. Oven-dried soil samples were passed through a series of standard sieves, and the mass retained on each sieve was recorded to compute percentage passing. The results were used to generate particle size distribution curves for comparative analysis under both standards.

2.2.4 Atterberg Limits

Atterberg limit tests were conducted to assess the consistency and plasticity characteristics of the soils. Liquid limit, plastic limit, and plasticity index were determined following BS 1377-2:1990 and ASTM D4318 procedures. The BSI method employed the cone penetrometer technique for liquid limit determination, while the ASTM method used the Casagrande cup. Plastic limits were determined by hand-rolling soil threads until failure at approximately 3 mm diameter. Plasticity indices were calculated as the difference between the liquid and plastic limits, enabling evaluation of the influence of cement content and testing standard on soil plasticity.

2.2.5 Compaction Characteristics

Compaction tests were performed to determine the optimum moisture content and maximum dry density of the untreated and cement-stabilised soils. Tests conducted under BSI procedures followed BS 1377-4:1990 using British Standard Light (BSL) and British Standard Heavy (BSH) compactive efforts. Corresponding ASTM tests were carried out using the Standard Proctor (ASTM D698) and Modified Proctor (ASTM D1557) methods. For each soil–cement mixture, moisture–density relationships were established to evaluate the effects of cement content, compaction energy, and testing standard.

2.2.6 Statistical Analysis

All laboratory test results were analysed using IBM SPSS Statistics Version 20. Descriptive statistics were used to summarise the data, while analysis of variance (ANOVA) was employed to assess statistically significant differences between ASTM and BSI procedures as well as between compaction energies. Regression analysis was applied to model the relationships between cement content and the measured index and compaction parameters.

ISBN: 978-978-8567-02-8

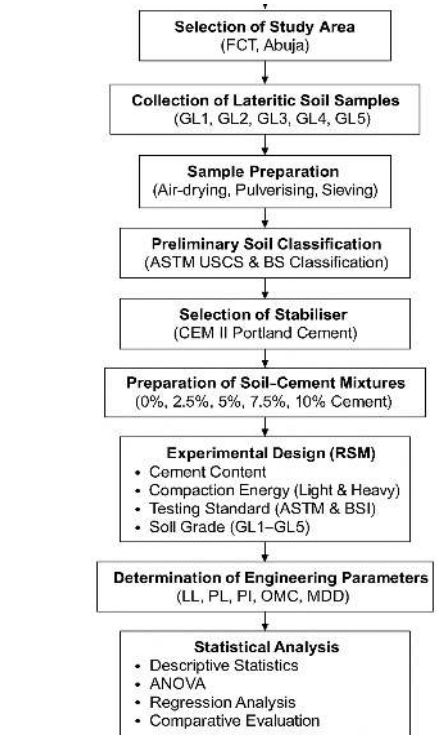


Figure 1. Flowchart showing the experimental methodology adopted for the characterisation of cement-stabilised lateritic soils using ASTM and BSI procedures.

The overall methodology adopted in this study is summarised in the flowchart presented in Figure 1.

3. RESULTS AND DISCUSSION

3.1 Particle Size Distribution Characteristics

The particle size distribution curves for the five lateritic soil grades obtained using both BS and ASTM procedures are presented in Figure 2. The results indicate substantial variability in gradation and fines content across the soils, reflecting their different weathering histories and parent materials.

GL1 was identified as the coarsest soil, with less than 10% passing the 0.075 mm sieve, indicating a predominantly granular material with negligible plastic fines. In contrast, GL3 and GL4 exhibited fines contents exceeding 50%, characteristic of clayey laterites with high moisture sensitivity and poor workability. Such behaviour is consistent with earlier findings on tropical residual soils rich in iron and aluminum oxides (Ola, 1975 Ola, 1975; Gidigasu, 1976; Fouladi *et al*., 2023).

Across all soil grades, the coefficients of uniformity (Cu) exceeded 4, while the coefficients of curvature (Cc) mostly ranged between 1.0 and 1.4, indicating well-graded materials with reasonably smooth particle size distributions. GL4 recorded the highest Cu and Cc values, suggesting a broad particle size range, which is advantageous for particle interlocking, compaction efficiency, and strength development when stabilised with cement (Fouladi *et al*., 2023).

Minor discrepancies were observed between the results obtained using BS and ASTM standards. In general, the

TABLE I: GRADATION PARAMETERS OF LATERITIC SOILS BASED ON BS AND ASTM SIEVE ANALYSIS

Grade	Standard	D10 (mm)	D30 (mm)	D60 (mm)	Cu = D60 / D10	Cc = (D30)² / (D10×D60)
GL1	BSI	0.082	0.258	0.82	10.00	0.99
	ASTM	0.078	0.240	0.78	10.00	0.94
GL2	BSI	0.095	0.32	1.10	11.60	0.98
	ASTM	0.090	0.30	1.05	11.67	0.95
GL3	BSI	0.110	0.45	1.50	13.64	1.23
	ASTM	0.100	0.42	1.45	14.50	1.22
GL4	BSI	0.080	0.38	1.30	16.25	1.39
	ASTM	0.075	0.35	1.25	16.67	1.31
GL5	BSI	0.150	0.60	2.00	13.33	1.20
	ASTM	0.140	0.58	1.95	13.93	1.23

ASTM procedure produced slightly higher Cu values, whereas the BS method yielded comparatively higher Cc values. The higher Cu values associated with ASTM testing may be attributed to its tendency to capture a wider effective particle size range, possibly due to differences in sieve tolerances, shaking duration, and mass retention criteria, which can enhance the apparent spread between the effective grain sizes (D_{10} and D_{60}). Conversely, the higher Cc values obtained under the BS standard may reflect a more balanced representation of intermediate particle sizes (D_{30}), resulting from variations in sample preparation and grading control procedures.

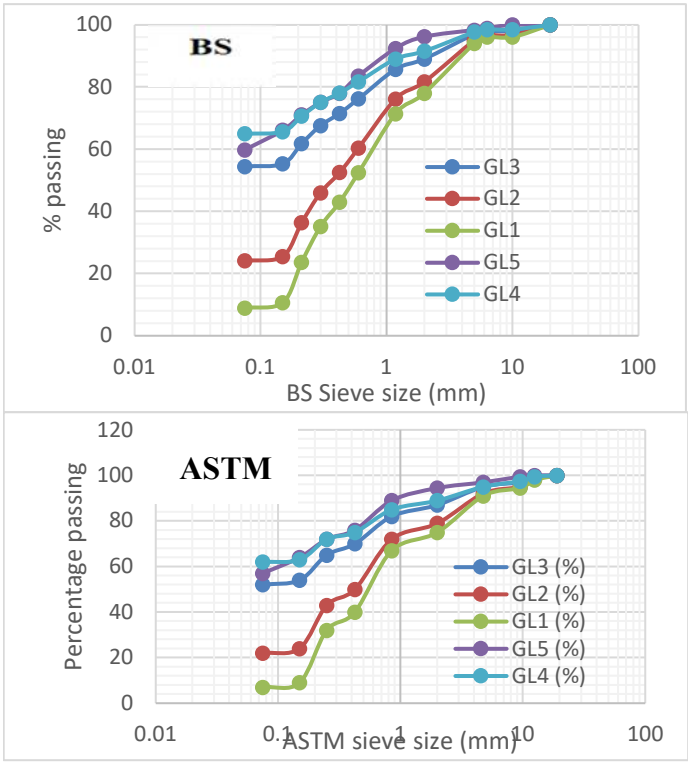


Figure 2. Particle Size Distribution Curves of the Lateritic Soils (BS and ASTM)

3.2 Classification and Index Properties of Natural Lateritic Soils

Table II summarises the index properties and classification of the natural lateritic soils based on both BS and ASTM systems. GL1 was classified as GW (BS) and SW (ASTM), reflecting its coarse-grained, non-

ISBN: 978-978-8567-02-8

plastic nature. GL2 was classified as GC/SC, indicating a gravelly soil with moderate plastic fines.

GL3 and GL4 were categorized as CV (BS) and CH (ASTM), confirming their highly plastic clayey nature. These soils exhibited plasticity indices exceeding 25%, which is typical of lateritic soils dominated by hematite, gibbsite, and kaolinite minerals (Fouladi *et al.,* 2023). GL5, with moderate plasticity, was classified as CI (BS) and CL-ML (ASTM).

The close agreement between BS and ASTM index properties demonstrates procedural consistency, despite differences in test apparatus and interpretation criteria.

TABLE II: SUMMARY OF THE INDEX PROPERTIES AND CLASSIFICATION OF THE NATURAL LATERITIC SOILS BASED ON BS AND ASTM SYSTEMS.

Grade	Standard	% Passing No. 200	LL (%)	PL (%)	PI (%)	USCS (ASTM)	BS Classification
GL1	BS	8.9	42.51	NP	NP	-	GW (Well-graded GRAVEL)
	ASTM	7.0	42.30	NP	NP	SW	-
GL2	BS	24.1	31.22	22.03	9.19	-	GC (Clayey GRAVEL)
	ASTM	22.0	30.03	21.92	8.11	SC	-
GL3	BS	54.5	35.23	13.20	22.03	-	CV (Very clayey GRAVEL)
	ASTM	52.0	39.02	14.46	24.56	CH	-
GL4	BS	65.0	65.12	37.44	27.68	-	CV (Very clayey GRAVEL)
	ASTM	62.0	65.00	40.00	25.00	CH	-
GL5	BS	59.8	43.12	34.25	8.87	-	CI (Silty CLAY)
	ASTM	57.0	43.03	34.25	8.78	CL-ML	-

3.3 Chemical and Physical Characteristics of Cement

The major oxide composition of the cement, summarised in Table III, shows a high calcium oxide (CaO) content of 61.3%, which is indicative of strong cementitious and binding potential. High CaO content promotes hydration reactions and enhances flocculation and aggregation of clay particles, particularly in highly plastic lateritic soils such as GL3 and GL4 (Consoli *et al*., 2021).

The low alkali content (K_2O = 0.26%) is favourable, as it minimises the risk of alkali–silica reaction and contributes to long-term durability of stabilised soil layers. The presence of moderate SiO_2 and Al_2O_3 further supports pozzolanic interactions between cement hydration products and lateritic soil minerals.

Physical properties of the cement (Table IV)—specific gravity (3.10), density (3.00 g/cm³), and fineness (825 m²/kg)—fully satisfy EN 197-1 requirements for 42.5N grade cement. The high fineness is particularly beneficial for soil stabilisation, as it enhances the rate of hydration and improves cement–soil bonding efficiency (Consoli *et al*. 2021).

TABLE III: MAJOR OXIDE COMPOSITION OF THE CEMENT

Oxide	Concentration (%)
CaO	61.334
SiO_2	13.941
Al_2O_3	1.993
Fe_2O_3	1.6644
SrO	5.023
MgO	1.02
SO_3	0.9133
K_2O	0.2608
TiO_2	0.0945
CeO_2	3.304

TABLE IV: PHYSICAL CHARACTERISTICS OF THE CEMENT

Parameter	Value	EN 197-1 Criteria
Specific Gravity	3.10	3.00–3.20
Surface Area (Blaine, m²/kg)	825	≥700 (42.5N grade)
Density (g/cm³)	3.00	2.90–3.20
Consistency (mm)	0.8	≤1.0

Overall, the chemical and physical characteristics confirm the suitability of CEM II/B-L 42.5N cement for stabilising lateritic soils under tropical conditions.

3.4 Properties of Cement-Stabilised Lateritic Soils

3.4.1 Consistency Characteristics

The comparison of liquid limit (LL) and plastic limit (PL) values obtained using ASTM and BS procedures was further evaluated using analysis of variance (ANOVA), with the results presented in Table V. The ANOVA results indicate that the effect of test standard

ISBN: 978-978-8567-02-8

on liquid limit is statistically insignificant (p = 0.918), confirming that both ASTM and BS methods yield comparable LL values for the lateritic soils investigated. This statistical outcome supports the close agreement observed in Figure 3a, where only marginal differences exist between mean LL values obtained from the two standards across all soil grades.

Similarly, the ANOVA results for plastic limit show no statistically significant difference between ASTM and BS procedures (p = 0.843). Although slight numerical variations were observed in PL values between the two standards, these differences fall within acceptable experimental variability and do not affect the overall interpretation of soil consistency. This indicates that plastic limit determination for lateritic soils is largely independent of the testing standard employed.

The statistical insignificance observed for both LL and PL suggests that inherent soil characteristics, such as mineral composition and particle size distribution, exert a stronger influence on consistency limits than procedural differences between ASTM and BS methods. Consequently, both standards can be considered reliable and interchangeable for determining the consistency characteristics of cement-stabilised lateritic soils within the investigated range.

TABLE V: ANOVA RESULTS FOR LIQUID LIMIT (LL) AND PLASTIC LIMIT (PL) DETERMINED USING ASTM AND BS PROCEDURES

Response Variable	Source of Variation	Sum of Squares	df	Mean Square	F-value	p-value
Liquid Limit (LL)	Test Standard (ASTM vs BS)	1.24	1	1.24	0.01	0.918
	Error	158.37	18	8.80		
	Total	159.61	19			
Plastic Limit (PL)	Test Standard (ASTM vs BS)	2.11	1	2.11	0.04	0.843
	Error	942.56	18	52.37		
	Total	944.67	19			

These findings provide quantitative statistical support for the conclusions drawn from the graphical comparisons and reinforce the validity of using either ASTM or BS procedures in pavement and geotechnical engineering applications involving lateritic soils.

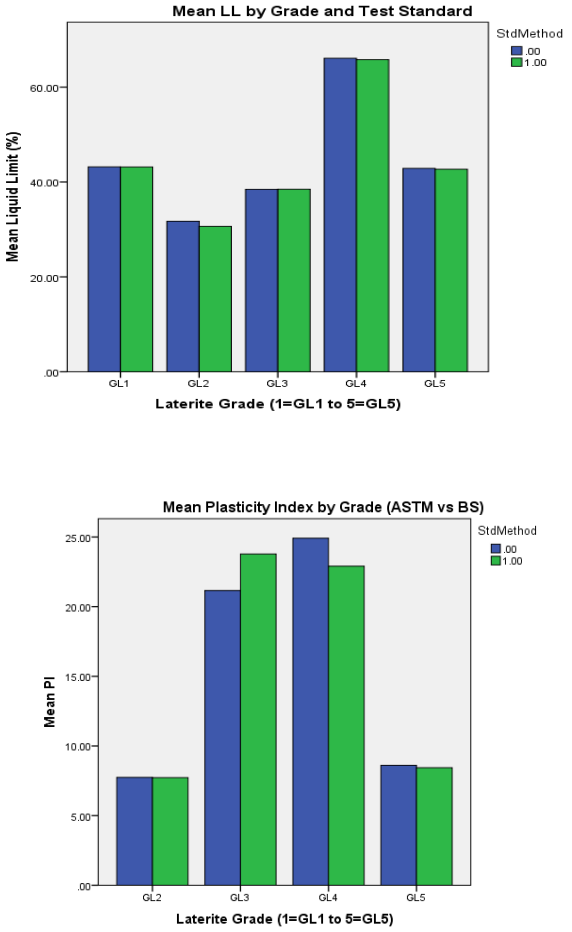


Figure 3. Bar charts showing the comparison of (a) mean values for LL (b) of mean values for PI across soil grades (GL1–GL5).

3.4.2 Compaction Characteristics

The compaction characteristics of the cement-treated lateritic soils were evaluated using optimum moisture content (OMC) and maximum dry density (MDD) determined under ASTM and BS testing procedures. Figures 4a and 4b present the mean OMC and MDD values by soil grade (GL1–GL5), enabling a direct comparison between the two standards.

As shown in Figure 4a, the mean OMC values obtained using ASTM and BS procedures are generally comparable across all soil grades. ASTM results are marginally lower than those obtained using BS for most grades, particularly for GL2 and GL3; however, the differences are small and consistent. Both standards identify GL4 as exhibiting the highest OMC and GL2 the lowest, indicating strong agreement in the relative moisture demand of the soils. The close correspondence suggests that OMC determination for lateritic soils is largely independent of the testing standard, and primarily controlled by soil grading and plasticity characteristics.

Similarly, Figure 4b shows that the mean MDD values obtained using ASTM and BS procedures follow

ISBN: 978-978-8567-02-8

the same trend across all soil grades. ASTM generally produced slightly higher MDD values than BS, but the differences are minimal and do not alter the ranking of soil grades. Well-graded soils such as GL2 achieved higher MDD values under both standards, while the more plastic soils (GL3 and GL4) exhibited comparatively lower densities, reflecting their higher fines content and reduced packing efficiency.

The statistical comparison using analysis of variance (ANOVA), presented in Table VI, confirms that the observed differences between ASTM and BS procedures are not statistically significant for either OMC ($p = 0.446$) or MDD ($p = 0.531$). This indicates that the slight numerical variations observed in the figures fall within acceptable experimental variability and are attributable to minor procedural differences between the standards, such as mould dimensions, hammer mass, and drop height (Burton and Airey, 2012; Lunne *et al*., 2019).

While the effects of cement content and compaction energy are not illustrated in Figures 4a and 4b, statistical analysis across the full dataset (as reported in the abstract) shows that compaction energy exerts a significantly stronger influence on MDD and OMC than the testing standard. Heavy compaction significantly increased MDD ($p = 0.031$) and reduced OMC ($p = 0.012$), confirming that compactive effort is the dominant factor controlling compaction behaviour in cement-treated lateritic soils.

TABLE VI: ANOVA RESULTS FOR OMC AND MDD DETERMINED USING ASTM AND BS PROCEDURES

Response Variable	Source of Variation	Sum of Squares	df	Mean Square	F-value	p-value
OMC	Test Standard (ASTM vs BS)	3.12	1	3.12	0.61	0.446
	Error	91.78	18	5.10		
	Total	94.90	19			
MDD	Test Standard (ASTM vs BS)	0.004	1	0.004	0.41	0.531
	Error	0.176	18	0.0098		
	Total	0.180	19			

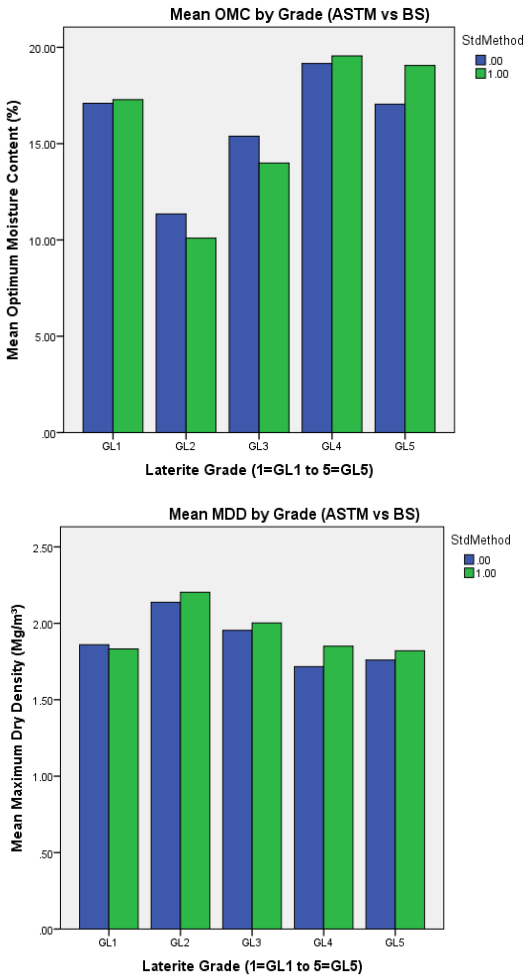


Figure 4: Bar charts showing the comparison of mean values for (a) OMC and (b) MDD across soil grades (GL1–GL5).

Overall, the results demonstrate that ASTM and BS procedures yield statistically comparable OMC and MDD values, while compaction energy remains the primary driver of density and moisture response in lateritic soils.

4. CONCLUSION

This study evaluated the consistency and compaction characteristics of cement-stabilised lateritic soils (GL1–GL5) using American Society for Testing and Materials (ASTM) and British Standard (BS) test procedures. The results showed that cement stabilisation resulted in notable reductions in plasticity index, particularly in highly plastic lateritic soils, whereas changes in liquid limit were generally marginal. These improvements are attributed to cement-induced flocculation and pozzolanic reactions, which reduced clay activity and improved soil workability.

Compaction behaviour was found to be strongly influenced by compaction energy, with heavy compaction producing significantly higher maximum dry density and lower optimum moisture content across all soil grades. Although ASTM procedures generally yielded slightly higher dry density values and marginally lower moisture contents than BS procedures, statistical analysis confirmed that these differences were not

ISBN: 978-978-8567-02-8

significant.

Based on the outcomes of this study, cement stabilisation is recommended for improving the consistency and compaction behaviour of lateritic soils, particularly those with moderate to high plasticity intended for pavement subgrade and subbase applications. Field construction should prioritise adequate compaction energy, as heavy compaction was shown to significantly enhance dry density and reduce moisture demand, thereby improving performance and durability. Given the statistical similarity of results obtained using ASTM and BS procedures, either standard may be confidently adopted for laboratory testing and quality control, provided consistency is maintained throughout the project. Emphasis should therefore be placed on proper material selection, cement content optimisation, and compaction control rather than on the choice of testing standard alone. Further research incorporating strength, durability, and long-term performance tests is recommended to complement the index and compaction findings and support comprehensive pavement design.

ACKNOWLEDGMENT

The authors gratefully acknowledge the institutional support provided by the Department of Civil Engineering, Federal University of Technology, Minna, which contributed to a conducive research environment. Appreciation is also extended to the technical staff of the NBRRI construction material testing Laboratory for their professionalism and assistance during the experimental programme.

REFERENCES

Amadi, A.A.; Kolo, S.S.; Yusuf, A.; Eze, F.E. and Salihu, U. (2025). Stabilization Characteristics of Cemented Lateritic Soil Produced with Selected Cement Types, CEMENT, 100136, https://doi.org/10.1016/j.cement.2025.100136.

Babu, B. M, Ravali, G., Saikiran, C., B Akhil Reddy, B. A. and Kumar, P. R (2023). Soil stabilisation using rice husk ash. *Journal of Engineering Sciences*, 14(2): 529-540.

Burton, G. J. and Airey, D. W. (2012). Strain rate calculation in consolidated undrained triaxial testing and implications on design strengths. *Proceedings, 11th Australia New Zealand Conference on Geomechanics held in Melbourne, Australia*, 15-18 July 2012, 1063 - 106.

Consoli, N.C., Párraga Morales, D. and Saldanha, R. B. (2021). A new approach for stabilisation of lateritic soil with Portland cement and sand: strength and durability. *Acta Geotech.*. https://doi.org/10.1007/s11440-020-01136-y.

Etim, R. K., Attah, I. C. and Yohanna, P. (2020). Experimental Study on Potential of Oyster Shell Ash in Structural Strength Improvement of Lateritic Soil for Road Construction. *International Journal of Pavement Research and Technology,* DOI: https://doi.org/ 10.1007/s42947-020-0290-y.

Fouladi, A. S., Arulrajah, A., Chu, J. and Horpibulsuk, S. (2023). "Application of Microbially Induced Calcite Precipitation (MICP) Technology in Construction Materials": A Comprehensive Review of Waste Stream Contributions, *Construction and Building Materials, Elsevier,* 388 (2023)131546, https://doi.org/10.1016/j.conbuildmat.2023.131546 .

Gao, H. Y., Xu, Z. M., Ren, Z., Wang, K., Yang, K., Tang, Y. J. and Luo, J. Y. (2021). Laterite as a Potential Seepage Barrier From A Karst-Depression Tailings Impoundment. *Clays Clay Miner.* https://doi.org/10.1007/s42860-020-00103-8

Gidigasu, M.D. (1976). Laterite Soil Engineering, Elsevier Scientific Publishing Co. New York.

Kaplan, E., Kayadelen, C., Ozturk, M., Onal, Y. and Altay, G. (2022). Experimental evaluation of the usability of palm tree pruning waste (PTPW) as an alternative to geotextile. Revista de La Construccion, 21(1), 69–82. https://doi.org/10.7764/RDLC.21.1.69.

Lunne, T.; Knudsen, S.; Blaker, O.; Vestgården, T.; Powell, J.J.M.; Wallace, C.F.; Krogh, L.; Thomsen, N.V.; Yetginer, G.; Ghanekar, R.K. (2019). Methods used to determine maximum and minimum dry unit weights of sand: Is there a need for a new standard, *Canadian Geotechnical Journal*, 56(4): 1 – 18. https://doi.org/10.1139/cgj-2017-0738.

Ola, S. A. (1975). Stabilisation of Nigerian Laterite soil with cement, bitumen and lime, *Sixth Regional Conference for Africa Soil Mechanics and Foundation Engineering, Durban, South Africa*, pp.145 - 152.

Osinubi, K. J. and Stephen, T. A. (2006a). Effect of bagasse ash content on particle size distribution and plasticity characteristics of black cotton soil. *Proceedings of the 5th Nigerian Materials Congress "NIMACON 2006"*, Abuja, Nigeria, 17-19 November. pp. 214 - 220.

Osinubi, K.J, Eberemu, A.O, Ijimdiya, T.S and Etim, R.K (2021) Microbial-Induced Calcite Precipitation Study on the Plasticity and Compaction Characteristics of Lateritic Soil Treated with Bacillus Megaterium in Urea-$CaCl_2$ Culture Medium, *IOP Conference. Series: Materials Science and Engineering* 1036 (2021) 012031 IOP Publishing doi:10.1088/1757-899X/1036/1/01203.

Rosli, R. N.; Selamat, M. R. and Ramli, H. (2020) The Permeability and Strength of Compacted Laterite Soil-Bentonite Mixtures for Landfill Cover Application. In: Mohamed Nazri F. (eds) Proceedings of AICCE'19, Vol. 53. *Springer, Cham*. https://doi.org/10.1007/978-3-030-32816-0_9.

ISBN: 978-978-8567-02-8

033-Modeling the Effect of Soil Salinity on Soil Moisture Dynamics in Kadawa, Kano River Irrigation Project Using the SALTMED Model

Abdullahi, J.[1, 2*], Abdullahi, S.A.[2], Sanni, I.M[2], and Shehu, F.N.[1]

National Agricultural Extension and Research Liaison Service,
Ahmadu Bello University Zaria, Kaduna, Nigeria[1]
Department of Water Resource and Environmental Engineering,
Faculty of Engineering, Ahmadu Bello University, Zaria, Nigeria[2]

***Corresponding Author Email: namallam05@yahoo.co.uk**

Abstract Soil salinity is a major constraint to irrigated agriculture in semi-arid regions due to its influence on soil moisture dynamics. This study evaluated salinity-moisture interactions under basin-irrigated rice production in Kadawa, Kano River Irrigation Project Phase I (KRIP - I), during the 2023/2024 dry season (April - July 2024). Soil, water, and crop parameters were used to calibrate the SALTMED model. The soils were predominantly sandy loam, with mean bulk density of 1.84 g/cm^3, saturated hydraulic conductivity of 392.85 mm/day, and field capacity of 15.6%. SALTMED simulations indicated that soil salinity increased from 0.000 - 0.054 dS/m at transplanting to 0.381 - 0.490 dS/m in the 0 - 10 cm layer at harvest, while deeper layers remained below 0.163 dS/m. Soil moisture declined from 0.159 - 0.204 m^3/m^3 at transplanting to 0.120 - 0.130 m^3/m^3 near the surface at harvest, with deeper layers maintaining 0.18 - 0.20 m^3/m^3. Model performance was satisfactory, with R^2 values of 0.93 for salinity and 0.85 for moisture, NRMSE of 0.252 and 0.239, CRM of -0.232 and -0.200, and MAE of 0.095 and 0.040, respectively. A strong inverse relationship between soil salinity and moisture was observed (r as -0.96; R^2 as 0.92). ARIMA forecasts indicated progressive soil moisture depletion approaching 0 m^3/m^3 and salinity increase to 1.16 dS/m by December 2024. The results demonstrate that SALTMED is an effective decision-support tool for evaluating soil moisture and salinity dynamics in irrigated rice systems. Regular soil moisture monitoring, improved irrigation scheduling, and periodic leaching are recommended to control salt accumulation and sustain rice productivity in salinity-prone environments.

Keywords: soil salinity, soil moisture dynamics, SALTMED model, water and solute, irrigation

1. INTRODUCTION

Irrigated agriculture plays a critical role in global food production, with over 307 million hectares currently equipped for irrigation worldwide (FAO, 2021). However, more than 20% of this irrigated land is affected by soil salinity, leading to declining soil fertility, reduced crop yields, and long-term environmental risks (Kraamwinkel et al., 2021; Singh, 2021; Tarolli *et al*., 2024). In sub-Saharan Africa, irrigation schemes are particularly vulnerable to secondary salinity due to inefficient water management, high evapotranspiration, and the use of saline or marginal-quality irrigation water (FAO, 2021; Mwesige *et al*., 2024).

In Nigeria's semi-arid regions, where rainfall is limited and highly seasonal, irrigated agriculture is essential for food security. Small-scale irrigation schemes dominate, accounting for more than 95% of cultivated irrigated land (Hiroyuki *et al*., 2017; 2018). Despite their importance, irrigation expansion has intensified soil salinity problems, undermining soil health, crop productivity, and long-term sustainability (Ragab *et al*., 2015; Suzana *et al*., 2010; Sanga *et al*., 2024).

At Kadawa, within Phase I of the Kano River Irrigation Project (KRIP-I), soil salinity has already posed significant threats to agricultural sustainability, affecting communities that rely heavily on irrigation-based crop production (Okai, 1995; Maina *et al*., 2012; Garba *et al*., 2022). Understanding salinity-induced changes in soil moisture dynamics is therefore essential for effective irrigation management (Stavi *et al*., 2021; Shokri *et al*., 2024).

Salt transport in soils varies spatially and temporally, particularly within the top 0-30 cm layer, and is influenced by climate, hydrology, vegetation, and anthropogenic activities (Kumar & Sharma, 2020; Shokri *et al*., 2024). Soil salinity alters soil structure and hydraulic properties, reducing infiltration and percolation, increasing surface moisture retention, and limiting plant water availability through osmotic stress. These processes enhance capillary rise and surface evaporation, creating feedback mechanisms that accelerate salinization (Tan *et al*., 2023; Yan *et al*., 2023; Yuan *et al*., 2024).

Process-based models such as SALTMED provide effective tools for evaluating water and solute transport, evapotranspiration, and crop water uptake under saline irrigation conditions. The SALTMED model has been widely applied to assess soil moisture dynamics and crop performance in saline environments (Negar *et al*., 2015; Hamza *et al*., 2022; Mehanna *et al*., 2024). This study applies SALTMED to evaluate the effects of soil salinity on soil moisture dynamics in the Kadawa irrigation scheme, addressing a critical knowledge gap in irrigated

ISBN: 978-978-8567-02-8

rice production systems in West Africa.

2. METHODOLOGY

2.1 The Study Area

The study was conducted in Kadawa, Kano River Irrigation Project (KRIP), northern Nigeria (lat. $11^0$32' - $11^0$51'N, long. $8^0$40'- $8^0$45'E; 492 m above sea level) in the Sudan Savannah zone (Figure 1). KRIP spans with 62,000 ha across Phases I and II. About 90% of soils are suitable for irrigation, primarily well-drained sandy loams with sandy clay loam subsoils over laterite or bedrock; the remaining 10% consists of poorly drained sandy loams derived from granites and metasedimentary rocks (Garba *et al*., 2022).

The region has a semi-arid climate, with mean annual rainfall of approximately 898 mm, mean daily temperatures of 29 - 38^{0}C, relative humidity of 17 - 90%, and high potential evaporation (3500 - 4500 mm). Shallow groundwater and elevated evapotranspiration render the area prone to secondary salinity (Yusuf *et al*., 2020; Garba *et al*., 2022).

2.2 Field Experiment and Data Collection

The field experiment was conducted during the 2023/2024 dry season (April - July 2024) using basin irrigation. Rice (*Oryza sativa L.*) was grown on 18 × 6 m experimental plots under standard agronomic management.

2.2.1 Soil Sampling and Analysis

Composite soil samples were collected at 0 - 45 cm depth before planting, mid-season, and at harvest. Soil salinity (ECe) was measured on saturated paste extracts using a conductivity meter (Richards, 1954). Soil texture, bulk density, water retention, and saturated hydraulic conductivity were determined using standard methods (Moodie *et al*., 1959; Kirkham, 2014; Weil & Brady, 2017).

*2.2.2 **Soil** Moisture Monitoring*

Volumetric soil moisture was measured weekly at 0 - 45 cm depth using the gravimetric method (Michael, 2008; Weil & Brady, 2017).

Volumetric water content (θ_v) was calculated as:

$$\theta_v = \frac{M_w}{M_s} \times 100\% \times \rho_b \quad (1)$$

Where $\boldsymbol{\theta}_V$ is the volumetric water content (m^3/m^3), M_w is the mass of soil sample (g), M_s is the mass of oven dry soil (g) and ρ_b is the soil bulk density in g/cm^3.

2.2.3 Plant Measurements

Representative plants were tagged to monitor growth parameters including plant height, tiller number, leaf area index (LAI), and dry matter accumulation. Grain yield and yield components were measured at harvest from the net plot area (Weil & Brady, 2017; Yazar *et al*., 2023).

2.3 Climate Data and Estimation of Irrigation Water Applied

Daily rainfall, temperature, relative humidity, wind speed, and solar radiation data were obtained from NiMET (2008 - 2023) and NASA Climate Database (2024) for model calibration. Reference evapotranspiration (ET_0) was calculated using the FAO-56 Penman-Monteith equation (Allen et al., 1998), and crop water requirements and irrigation schedules were estimated using CROPWAT (Doorenbos & Pruitt, 1977; Allen *et al*., 1998).

2.4 Model Description

The SALTMED model is a process-based simulation tool designed to predict soil salinity, soil moisture, crop yield, and biomass in saline and non-saline soils. It integrates data on climate, irrigation and rainfall, soil properties, crop characteristics, and field management to support efficient crop management in salinity-prone environments (Ragab, 2015; Pulvento *et al*., 2015).

SALTMED simulates key processes including evapotranspiration, plant water uptake, water and solute transport under different irrigation systems, nitrogen cycling, drainage, shallow groundwater dynamics, and crop rotation effects. Soil water flow is modeled using Richards' equation:

$$\frac{\partial\theta}{\partial t} = -\frac{\partial}{\partial z}\left[K(\theta)\frac{\partial(\psi+Z)}{\partial z}\right] - S_w \quad (1)$$

Where θ is volumetric soil moisture, K(θ) is hydraulic conductivity, ψ is pressure head, z is depth, and Sw is root water uptake. Solute transport is described using the convection-dispersion equation: where θ is volumetric soil moisture, K(θ) is hydraulic conductivity, ψ is pressure head, z is depth, and Sw is root water uptake.

Solute transport is described using the convection-dispersion equation:

$$\frac{\partial(\theta C)}{\partial t} = \frac{\partial}{\partial z}\left(D_a\frac{\partial C}{\partial_z}\right) - \frac{\partial(qC)}{\partial_z} - S_s \quad (2)$$

Where C is solute concentration, D_a is the dispersion coefficient, q is convective flux, and Ss represents solute uptake by roots.

Evapotranspiration, crop water uptake, and yield are computed internally by SALTMED based on water availability, salinity, radiation, temperature, nitrogen, and leaf area index, with stress factors reducing biomass and yield when conditions deviate from optimal. Water and solute movement are simulated in 1D, 2D, or cylindrical coordinates depending on the irrigation system, and soil hydraulic properties are derived from Van Genuchten (1980) and adjusted using field data.

2.5 SALTMED Model Calibration and Simulation Process

The SALTMED model was calibrated and simulated following the framework of Marwa *et al*. (2020). The model requires four main inputs: meteorological data, soil characteristics, water management, and crop parameters. These inputs allowed simulation of soil moisture, salinity, and crop growth dynamics throughout the rice growing season under the specific conditions at Kadawa, KRIP.

2.6 Model Performance Metrics

ISBN: 978-978-8567-02-8

Model performance was evaluated by comparing simulated and observed soil moisture and salinity using standard statistical metrics (Loague & Green, 1991; Pulvento *et al*., 2015; Rao *et al*., 2016; Marwa *et al*., 2020):

- **Normalized Root Mean Square Error (NRMSE)**: Measures deviation between observed and simulated values; lower values indicate better accuracy.
- **Coefficient of Determination (R^2)**: Quantifies goodness-of-fit; values closer to 1 indicate stronger agreement.
- **Coefficient of Residual Mass (CRM)**: Indicates model bias; negative values reflect overestimation, positive values underestimation.
- **Mean Absolute Error (MAE)**: Represents the average absolute difference between observed and simulated values.

Analyses were performed using Microsoft Excel with XLSTAT and R Programming. Perfect model agreement is indicated by R^2 approaching 1, and NRMSE, CRM, and MAE approaching 0 (Pulvento *et al*., 2013; Negar *et al*., 2015).

2.7 Trend in Soil Salinity and Soil Moisture Dynamics Overtime

Temporal trends in field-observed and SALTMED-simulated soil salinity and soil moisture were analyzed using the ARIMA time-series approach implemented in R. The method enabled short-term forecasting based solely on historical data, without requiring future climate or irrigation inputs. Model sensitivity was tested by applying ±5% variation to observed values and ±10% changes in drift, confirming the robustness of the forecasts. An ARIMA (0,1,0) model with drift adequately captured the observed trends, while seasonal components (SARIMA) were unnecessary due to the short, non-seasonal dataset (Bakar & Rosbi, 2017).

3. RESULTS AND DISCUSSION

3.1 General Characteristics of the Soils

Saturated hydraulic conductivity ranged from 165.51 to 552.30 mm/day (mean 392.82 mm/day), indicating rapid drainage, while bulk density varied between 1.748 to 1.925 g/cm^3 (mean 1.837 g/cm^3) with Field capacity and permanent wilting point averaged 15.6% and 12.33%, respectively. While, seasonal soil moisture content at 0 - 45 cm depth ranged from 0.19 to 0.23 m^3/m^3, with a mean of 0.21 m^3/m^3.

Soil chemical properties showed low to moderate salinity, with ECe of 0.08 - 0.30 dS/m (mean 0.29 dS/m) and alkaline conditions (pH 8.4 - 8.9, mean 8.6). Sodium-related indices indicated emerging sodicity risk, with SAR of 0.30 - 0.85 mmolL^{-1} (mean 0.52 mmolL^{-1}) and ESP of 7.77 - 18.71% (mean 11.63%).

Irrigation water exhibited low salinity (EC 0.20 dS/m, TDS 120 mg/L, pH 7.50) but relatively high SAR (14.34 mmolL^{-1}), suggesting potential long-term sodicity hazards if not properly managed. This agrees with Gemeda and Yadeta (2024), who reported that prolonged use of marginal-quality irrigation water can degrade soil physico-chemical properties and reduce crop productivity.

3.2 The Response of Soil Salinity and Soil Moisture Dynamics

Soil salinity and moisture dynamics were monitored bi-weekly in the field and simulated using the SALTMED model throughout the rice growth cycle (Table 1).

TABLE 1: FIELD AND SIMULATED SOIL SALINITY AND SOIL MOISTURE DATA

Observ-ation	Date	Soil Salinity		Soil Moisture Dynamics	
		Measured (dS/m)	Simulated (dS/m)	Measured (m^3/m^3)	Simulated (m^3/m^3)
WK1	01/04/24	0.230	0.048	0.290	0.210
WK3	14/04/24	0.280	0.152	0.240	0.179
WK5	28/04/24	0.290	0.212	0.230	0.158
WK7	12/05/24	0.350	0.305	0.220	0.168
WK9	26/05/24	0.430	0.344	0.205	0.166
WK11	09/06/24	0.491	0.378	0.190	0.164
WK13	23/06/24	0.500	0.444	0.158	0.158
WK15	07/07/24	0.530	0.469	0.140	0.119
WK16	11/07/24	0.600	0.489	0.130	0.120

3.2.1 Response of Soil Salinity on SALTMED Model

SALTMED simulations showed low salinity at transplanting (0.000 - 0.054 dS/m) in the 0 - 10 cm layer. By harvest, surface salinity increased to 0.381 - 0.490 dS/m, while the 10 - 30 cm layer reached 0.218 - 0.327 dS/m and depths >30 cm remained below 0.163 dS/m (Figures 2 and 3). Salt accumulation occurred primarily near the soil surface due to evaporation and limited leaching. Similar salinity patterns have been reported by Stavi *et al*. (2021) and Shokri *et al*. (2024).

The model performance metrics confirmed accurate simulation of salinity, with R^2 as 0.93, NRMSE as 0.252, CRM as -0.232, and MAE as 0.095 (Figure 4) which supported by Hamza *et al*. (2022) and Chauhdary *et al*. (2024).

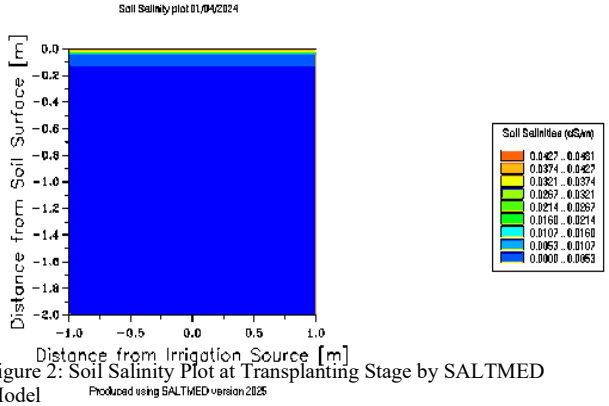


Figure 2: Soil Salinity Plot at Transplanting Stage by SALTMED Model

ISBN: 978-978-8567-02-8

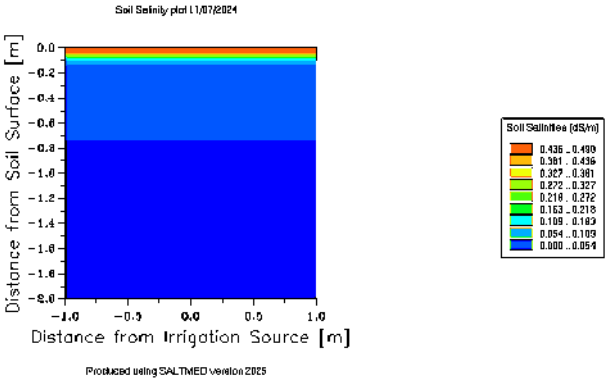


Figure 3: Soil Salinity Plot at Harvesting Stage by SALTMED Model

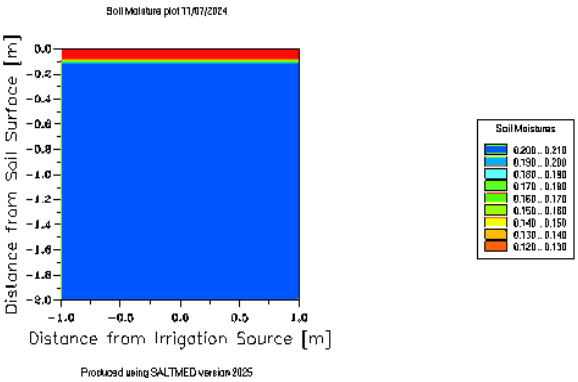


Figure 6: Soil Moisture Dynamics Plot at Harvesting Stage by SALTMED Model

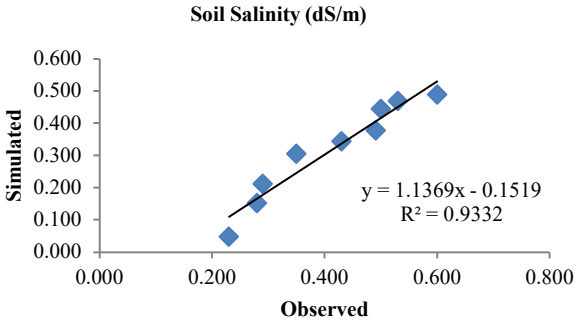


Figure 4: Plot of Simulated against Measured Soil Salinity (dS/m)

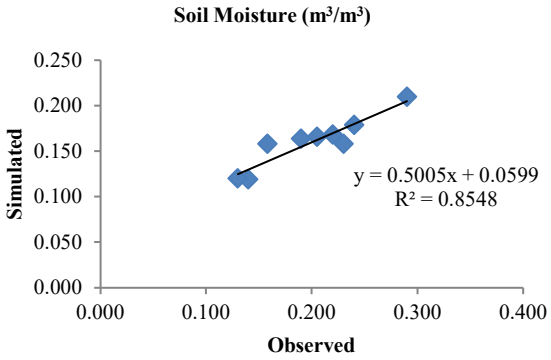


Figure 7: Plot of Simulated against Measured Soil Moisture (m^3/m^3)

3.2.2 Response of Soil Moisture Dynamics on SALTMED Model

Simulated soil moisture dynamics at transplanting was highest in the upper 0 - 10 cm layer (0.159 - 0.204 m^3/m^3) and deeper layers (0.18 - 0.20 m^3/m^3). At harvest, topsoil moisture declined to 0.120 - 0.130 m^3/m^3 due to crop uptake and evapotranspiration while lower layers remained moist (0.18 - 0.20 m^3/m^3) as in Figures 5 and 6. This supports the findings of Stavi *et al*. (2021), Gebeyhu *et al*. (2024) and Demo *et al*. (2025).

The model metrics showed satisfactory performance with R^2 as 0.85, NRMSE as 0.240, CRM as -0.200, and MAE as 0.040 (Figure 7) which supported by Hamza *et al*. (2022) and Chauhdary *et al*. (2024).

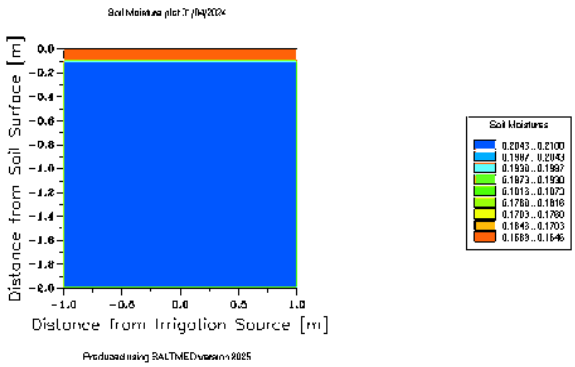


Figure 5: Soil Moisture Dynamics Plot at Planting Stage by SALTMED Model

3.2.3 Impact of Soil Moisture Dynamics on Soil Salinity

A strong negative correlation was observed between soil moisture and salinity (r as -0.96; R^2 as 0.92), indicating that decreasing moisture strongly drives salt accumulation (Figure 8). Regression analysis shows that, a unit decline in soil moisture increased salinity by approximately 2.39 dS/m, indicatings the influence of root-zone moisture on salinity dynamics as supported by the findings of Stavi *et al*. (2021), who emphasized that reduced soil water content increases salt concentration, thereby limiting water uptake by plant roots and adversely affecting crop performance.

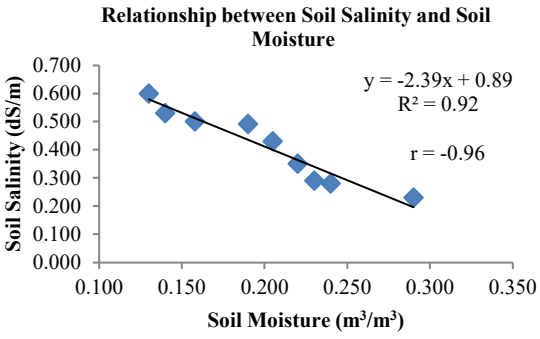


Figure 8: Relationship between Soil Salinity and Soil Moisture DynamicsS

3.2.4 Forecasted Trends

ARIMA (0,1,0) with drift was used to forecast soil moisture and salinity beyond the observed period (Figure

ISBN: 978-978-8567-02-8

9). Soil moisture is projected to decline from 0.130m³/m³ to near zero by December 2024, while salinity may rise from 0.65 dS/m to 1.16 dS/m. Despite the short calibration period, the forecasts are practically relevant, providing early-warning guidance for irrigation and leaching interventions. Sensitivity analyses (±5% in measurements, ±10% drift) confirmed robustness. These projections reinforce the critical role of moisture management in controlling salinity and sustaining crop yield in semi-arid irrigated systems as supported by Hopmans *et al*. (2021), Hou & Ye, (2022) and Omar *et al*., 2024.

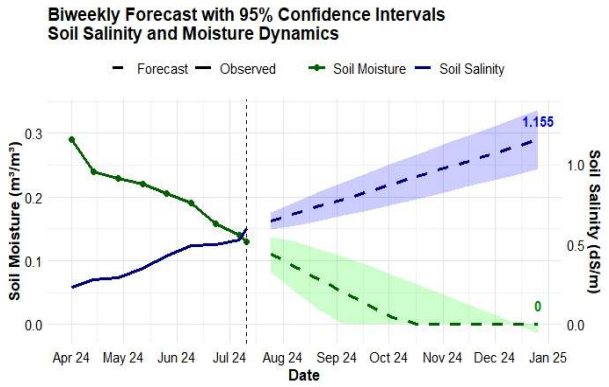


Figure 9: ARIMA Forecast of Soil Moisture Dynamics and Soil Salinity

4. CONCLUSION

Soil salinity strongly influences soil moisture dynamics in basin-irrigated rice at Kadawa, KRIP-I, reducing water availability in upper soil layers as the season progresses. The SALTMED model accurately captured these interactions, demonstrating high predictive performance and a strong inverse relationship between soil moisture and salinity.

Practically, the results depict the importance of regular monitoring, timely irrigation, and periodic leaching to prevent salt accumulation and maintain root-zone moisture. SALTMED proves to be a reliable decision-support tool for irrigation and salinity management in semi-arid environments. Future research should expand this framework to account for long-term climate variability and alternative irrigation strategies to sustain irrigated agriculture in the region.

ACKNOWLEDGMENT

The first author wishes to express appreciations to Prof Ragab Ragab of the UK Centre for Ecology and Hydrology, United Kingdom for guidance and prompt responses towards achieving the research goals. Also, to Malam Shamsu Nafi'u of KRIP Kadawa, Abdulhakim Adamu and Malam Umar of IAR Research Station, Kadawa and Hassan Bawa Jatau, Bitrus Ayuba and Abdul'aziz Rilwanu all of Soil Science Department, Ahmadu Bello University, Zaria for their tireless assistance in the course of the research study.

REFERENCES

Allen, R. G., Pereira, L. S., Raes, D., & Smith, M. (1998). Guidelines for computing crop water requirements: Irrigation and drainage paper 56. FAO.

Bakar, N. A., & Rosbi, S. (2017). Autoregressive integrated moving average (ARIMA) model for forecasting cryptocurrency exchange rate in high volatility environment. International Journal of Advanced Engineering Research and Science, 4(11), 130–137. https://doi.org/10.22161/ijaers.4.11.20

Chauhdary, J. N., Li, H., Ragab, R., & Khan, A. I. (2024). Climate change impacts on future wheat (Triticum aestivum) yield, growth periods and irrigation requirements: A SALTMED model simulations analysis. 1–23.

Daines, S. L., Mwamahonje, A. S., Mahinda, A. J., & Emmanuel, A. (2024). Soil salinization under irrigated farming: A threat to sustainable food security and environment in semi-arid tropics. 9(June), 32–47.

Demo, A. H., Gemeda, M. K., Abdo, D. R., Guluma, T. N., & Adugna, D. B. (2025). Impact of soil salinity, sodicity, and irrigation water salinity on crop production and coping mechanism in areas of dryland farming. Agrosystems, Geosciences and Environment, 8(1), 1–22. https://doi.org/10.1002/agg2.70072

Doorenbos, J., & Pruitt, W. (1977). Guidelines for predicting water requirements: Irrigation and drainage paper 24. FAO.

FAO. (2021). Climate and environment. https://news.un.org/en/story/2021/12/1107172

Garba, N., Mohammed, D., & Muhammad, R. (2022). Prevalence of soil salinity and sodicity and adopted remediation techniques in Kano River Irrigation Project (KRIP). African Scholar Publications and Research International, 24(2), 277–290.

Gebeyhu, B., Dagalo, S., & Muluneh, M. (2024). Soil moisture-based irrigation interval and irrigation performance evaluation: In the case of lower Kulfo catchment, Ethiopia. Heliyon, 10(16), e36089. https://doi.org/10.1016/j.heliyon.2024.e36089

Hamza, E. A., E., E. M., E., A. A., & R.E., A. (2022). Field and modeling study for integrated N-fertilization and organic mulching to improve the productivity and water productivity of tomatoes under arid Egyptian conditions. Middle East Journal of Agriculture Research, 11(2), 1–20. https://doi.org/10.36632/mejar/2022.11.2.29

Hiroyuki, T., Lianghi, Y., & Hua, X. (2018). Cultivating growth in Nigeria agriculture with small-scale irrigation. IFRI Discussion Paper, 01399.

Hiroyuki, T., Xie, H., & You, L. (2017). Invest in small-scale irrigated agriculture: A national assessment on potential to expand small-scale irrigation in Nigeria. Agricultural Water Management, 193, 251–264. https://doi.org/10.1016/j.agwat.2017.08.020

Hopmans, J. W., Qureshi, A. S., Kisekka, I., Munns, R., Grattan, S. R., Rengasamy, P., Ben-Gal, A., Assouline, S., Javaux, M., Minhas, P. S., Raats, P. A. C., Skaggs, T. H., Wang, G., De Jong van Lier, Q., Jiao, H., Lavado, R. S., Lazarovitch, N., Li, B., & Taleisnik, E. (2021). Critical knowledge gaps and research priorities in global soil salinity. Advances in Agronomy, 169, 1–191. https://doi.org/10.1016/bs.agron.2021.03.001

Hou, J., & Ye, M. (2022). Effects of dynamic changes of soil moisture and salinity on plant community in the Bosten Lake Basin. Sustainability, 14(21). https://doi.org/10.3390/su142114081

Jibrin, J. M., Abubakar, S. Z., & Suleiman, A. (2008). Soil fertility status of the Kano River Irrigation Project area in the Sudan Savanna of Nigeria. Journal of Applied Science, 8(4), 692–696.

Kirkham, M. B. (2014). Field capacity, wilting point, available water, and the nonlimiting water range. In Principles of soil

ISBN: 978-978-8567-02-8

and plant water relations (pp. 153–170). https://doi.org/10.1016/b978-0-12-420022-7.00010-0

Kraamwinkel, C. T., Beaulieu, A., Dias, T., & Howison, R. A. (2021). Planetary limits to soil degradation. Communications Earth & Environment, 2(1), 249. https://doi.org/10.1038/s43247‐021‐00323‐3

Kumar, P., & Sharma, P. K. (2020). Soil salinity and food security. Frontiers in Sustainable Food Systems, 4(October), 1–15. https://doi.org/10.3389/fsufs.2020.533781

Loague, K., & Green, R. E. (1991). Statistical and graphical methods for evaluating solute transport models: Overview and application. Journal of Contaminant Hydrology, 7, 51–73.

Lu, P., Liu, Y., Yang, Y., Zhu, Y., & Jia, Z. (2024). Evaluating soil water–salt dynamics under brackish water drip irrigation in greenhouses subjected to localized topsoil compaction.

Lu, P., Yang, Y., Luo, W., Zhang, Y., & Jia, Z. (2023). Numerical simulation of soil water–salt dynamics and agricultural production in reclaiming coastal areas using subsurface pipe drainage. Agronomy.

Maina, M. M., Amin, M. S. M., & Aimrun, W. (2012). Soil salinity assessment of Kadawa irrigation of the Kano River Irrigation Project.

Malgwi, W. B., Chude, V. O., Kparmwang, & Raji, B. (2002). Salinity and sodicity status of irrigated and drainage waters of Jakara and Kano River Project in semi-arid Nigeria.

Marwa, M. A., Dewedar, O. M., & Ragab, R. (2020). Predicting the water requirement, soil moisture distribution, yield, water productivity of peas and impact of climate change using SALTMED model. 20, 3673–3689.

Mehanna, H., Saber, A., Samaha, G., Abd El-Aziz, M., & Ragab, R. (2024). Estimating yield stability and predicting the response of sesame genotypes to climate change using the SALTMED model. Irrigation and Drainage, 73(4), 1483–1495. https://doi.org/10.1002/ird.2970

Michael, A. M. (2008). Irrigation: Theory and practice (2nd rev. ed.). Vikas Publication House.

Moodie, C. D., Smith, N. W., & McGreery, R. A. (1959). Laboratory manual for soil fertility development in corn and subsequent grain yield. Crop Science, 11, 368–372.

NASA Climate Database. (2024). Climate data for Kadawa. https://power.larc.nasa.gov/data-access-viewer

Negar, K., Amir, S., & Saeed, B. N. (2015). Calibration and verification of SALTMED model for simulation of soil salinity distribution under condition using saline irrigation water and maize cultivation. Nature and Science, 13(11), 36–40.

NiMET. (2024). Meteorological data. Nigerian Meteorological Agency. https://nimet.gov.ng/datarequest

Okai, I. A. (1995). Irrigation effect on the physical properties of soils at Kadawa. Ahmadu Bello University, Zaria.

Omar, M. M., Massawe, B. H. J., Shitindi, M. J., Pedersen, O., Meliyo, J. L., & Fue, K. G. (2024). Assessment of salt-affected soil in selected rice irrigation schemes in Tanzania: Understanding salt types for optimizing management approaches. Frontiers in Soil Science, 4(April), 1–14. https://doi.org/10.3389/fsoil.2024.1372838

Pulvento, C., Riccardi, M., Lavini, A., & Ragab, R. (2013). SALTMED model to simulate yield and dry matter for quinoa crop and soil moisture content under different irrigation strategies in South Italy. 238, 229–238.

Pulvento, C., Riccardi, M., Lavini, A., D'Andria, R., & Ragab, R. (2015). Parameterization and field validation of SALTMED model for grain amaranth tested in South Italy. Irrigation and Drainage, 64(1), 59–68. https://doi.org/10.1002/ird.1905

Rao, D. K., Tekabu, T., & Khan, M. G. M. (2016). New calibration estimators in stratified sampling. In 3rd Asia-Pacific World Congress on Computer Science and Engineering (APWC on CSE) (pp. 66–70). Nadi, Fiji. https://doi.org/10.1109/APWC-on-CSE.2016.022

Richards, L. A., Brown, J. W., Hayward, H. E., Richards, A., Bernstein, L., Hatcher, J. T., & Reeve, R. C. (1954). Diagnosis and improvement of saline and alkali soils (USSLS 60).

Sarah, L. (2007). Salinity in Mimoso Valley: A study on the effect of groundwater salinity on castor bean crop.

Salman, A. K., Durner, W., Naseri, M., & Joshi, D. C. (2023). The influence of the osmotic potential on evapotranspiration. 1–15.

Sanga, D. L., Mwamahonje, A. S., Mahinda, A. J., & Kipanga, E. A. (2024). Soil salinization under irrigated farming: A threat to sustainable food security and environment in semi-arid tropics. Journal of Agricultural Science and Practice, 9(3), 32–47. https://doi.org/10.31248/JASP2024.468

Shokri, N., Hassani, A., & Sahimi, M. (2024). Multi-scale soil salinization dynamics from global to pore scale: A review. https://doi.org/10.1029/2023RG000804

Singh, A. (2021). Soil salinity: A global threat to sustainable development. https://doi.org/10.1111/sum.12772

Stavi, I., Thevs, N., & Priori, S. (2021). Soil salinity and sodicity in drylands: A review of causes, effects, monitoring, and restoration measures. Frontiers in Environmental Science, 9, 1–16. https://doi.org/10.3389/fenvs.2021.712831

Suzana, M. G., Montenegro, A., & Ragab, R. (2010). Improving agricultural water management in the semi-arid region of Brazil: Experimental and modelling study. https://doi.org/10.1007/s00271-009-0191-y

Tan, S., Su, X., Jiang, X., Yao, W., Chen, S., Yang, Q., & Ning, S. (2023). Irrigation salinity affects water infiltration and hydraulic parameters of red soil. 1–18.

Tarolli, P., Luo, J., Park, E., Barcaccia, G., & Masin, R. (2024). Soil salinization in agriculture: Mitigation and adaptation strategies combining nature-based solutions and bioengineering. iScience, 27(2), 108830. https://doi.org/10.1016/j.isci.2024.108830

Weil, R. R., & Brady, N. C. (2017). The nature and properties of soil: Alkalinity, salinity and sodicity (5th ed.). Pearson Education.

Yazar, A., Kaya, C. İ., Çolak, Y., Tekin, S., & Alghory, A. (2023). Yield, dry matter, and water productivity simulation for surface and subsurface drip-irrigated bell pepper using the SALTMED model. The Journal of Agricultural Science, 161, 76–87.

Yuan, H., Zhang, A., Zhu, C., Dang, H., Zheng, C., Zhang, J., & Cao, C. (2024). Saline water irrigation changed the stability of soil aggregates and crop yields in a winter wheat–summer maize system.

Yusuf, B. L., Mustapha, A., Yusuf, M. A., & Ahmed, M. (2020). Soil salinity assessment using geostatistical models in some parts of Kano River Irrigation Project Phase I (KRIP I). Modeling Earth Systems and Environment. https://doi.org/10.1007/s40808-020-00841-7

Zhang, X., Feng, G., & Sun, X. (2024). Advanced technologies of soil moisture monitoring in precision agriculture: A review. Journal of Agriculture and Food Research, 18, 101473.

ISBN: 978-978-8567-02-8

5TH Faculty of Engineering Conference on Engineering Innovation and Economic Policies: Driving Sustainable Industrial Growth in Nigeria

Faculty of Engineering, Bayero University, Kano.

034-Fourier Transform Infrared (FTIR) Analysis of Kaolin, Metakaolin, and Metakaolin-Based Geopolymer Mixes

[1]I. Aliyu, [2]I. O. Sholadoye, [3] I. Iliyasu, [4]J. Yau, and [5]Achara B. E.

[1, 2 and 3]Civil Engineering Department, Ahmadu Bello University, Zaria, Kaduna State

[4]Department of Building Technology Abubakar Tafawa Balewa University Bauchi

[5] Federal Polytechnic Kaura Namoda, School of Engineering Technology, Department of Civil Engineering Technology, Zamfara State, Nigeria

*[1]Corresponding authors: e-mail:[1]ibrahimaliyu67@yahoo.com, [2]kemshol1977@gmail.com, [3]ibiliyasu@yahoo.com, [4]yaumsc3748@gmail.com and [5]*emmanuel.achara@gmail.com*

***Abstract*:** Geopolymer cement is a greener cement compared with Ordinary Portland Cement. This study looks into the degree of geopolymerisation of a geopolymer cement made from metakaolin as the silica and alumina source the activator solution is NaOH and Na_2SiO_3. To ascertain the degree of the geopolymerisation reaction; the Fourier Transform Infrared Spectroscopy (FTIR) comparison was made between first, the Mix 1 and Mix 3 to show the effect of an increase in Na_2SiO_3 content, Mix 1, and 4 to show the effect of the increased NaOH molar concentration the samples were cured at 60°C for 24 h and test carried out after 14days; also the FTIR of the raw Kaolin and the Metakaolin were checked. The FT-IR spectra of **Kaolin** show the bands at 3,690.1 and 3,623.0 cm−1 signify the presence of OH group of Si, Al. The FTIR result of the metakaolin shows a transmittance of the band between 3619 and 3690cm^{-1}. Kaolin increased when treated to 94.484% from 74.825% when untreated. The OH vibration mode of the hydroxyl molecule shifted to 1997.9 cm^{-1}. The interference due to quartz (impurities) at 1114.5 cm^{-1} before treatment is no more after treatment. FTIR spectrum of Mix 1 and Mix 3; Mix 3 is above the spectrum of Mix 1, this indicates that mix 3 has a higher transmittance (higher degree of geopolymerisation) than mix 1, in other words, the absorbance of Mix 3 is lower than that of mix 1. The transmittance at this wavelength for Mix 1 is 63% (37% absorbance) and 75% (25% absorbance) for Mix 3. For mix 1 and 4, mix 4 has higher transmittance than mix 1 and hence mix 4 geopolymerises more. It can be then concluded that the presence or more Na_2Sio_3 solution and higher molar concentration brought about increased geopolymerisation of the Silica and alumina precursors.

Keywords: Geopolymer cement, Fourier Transform Infrared Spectroscopy (FTIR), Kaolin, metakaolin, geopolymerisation reaction

1. INTRODUCTION

Geopolymer cement is a novel environmentally friendly material used as a substitute for Portland cement (PC). The geo-polymerisation reaction occurs between various oxides of alumina silicates and silicates in an alkaline environment to yield geopolymeric Si-O-Al-O bonds (Saturi *et al.,* 2015 and Amritphale, et al., 2019). Geopolymer cement-based concrete has been reported to be a high-strength inorganic polymer concrete that can be used in place of Portland cement concrete. The major contrast between geopolymer concrete and the conventional one is that geopolymer concrete uses alkaline liquid and a source material (Pozolan) that is rich in silica and alumina as a binder, whereas conventional concrete uses hydrated Portland cement as the binder.

When infrared radiation (IR) passes through the sample to be analysed (Othman, 2022), a portion of the radiation is absorbed while some will be transmitted, and the results are presented using spectrums. An IR spectrum is a fingerprint of the sample having absorption or transmittance peaks corresponding to the frequencies of vibrations of the bonds between the atoms making up the material. Two different compounds will not result in the same IR spectrum because each material has a distinct atomic combination of atoms.

Kenne *et al.* (2015) studied the influence of the rate of kaolin calcination on the properties of metakaolin-based geopolymers. The same mass of kaolin samples was treated for 30 min at varying rates of calcination of 1, 2.5, 5, 10, 15, and 20°C/min at 700ºC to obtain the metakaolin. XRD analyses showed that the produced metakaolins contained kaolin residues, the residues quantity increased with the rate of calcination of kaolin except at 1°C/min. It was found that the setting time increased and compressive strength reduced with an increasing rate of calcination. They concluded that calcination at a slow rate is required for the production of high compressive strength geopolymers.

Ljiljana *et al.* (2017) stated that ‘‘generally the interpretation of IR vibrational spectra of silicates is very

ISBN: 978-978-8567-02-8

complicated''. Carlos *et al.* (2014) and Yusuf, M. O. (2023) mentioned that the FTIR spectra of a geopolymer sample are characterized by different types of bands., the highest located between 900 and 1100 cm^{-1}, which is linked to X-O (X can be Si or Al), the magnitude of which depends on the amorphous nature of the material. The author added that the transmittance on the FTIR plot is a function of the degree of reactivity of the product.

Marounane *et al.* (2019) and Amritphale, et al., (2019) reported that after the activation of source material by the alkali solution, a shift in the wavelength and a reduction of peaks was a result of the formation of a new inorganic compound with a poly chain (Sialate-siloxo chain, PSS, $(-Si-O-Al-O-Si-O-)_n$).

The chemical bond of the functional groups within the source materials changes after activation with alkaline liquid, the indication of the change of the chemical bonding is indicated by the shift in the wavelength of the FTIR spectrum (Sind, 2006). Similarly, Marounane *et al.* (2019) and Chen *et al.* (2016) mentioned that the reduction and shift in peaks (Increased transmittance) of the IR spectrum showed that the poly (sialate-siloxo) chain is formed in the structure by the polymerisation reaction. The metakaolin oxides percentages by weight and also the elements in the metakaolin have been found to reduce after geopolymerisation except for sodium oxide which increased.

The effect of alkaline activator's chemical changes on the strength of mortar was examined by Gum *et al.* (2013). The mortar microstructure was analysed using porosity assessments, SEM, Energy Dispersive X-Ray Spectroscopy (EDS), X-ray diffraction (XRD), and FT-IR. The results showed that an alkaline activator's chemical changes significantly affect the early strength. SEM and EDS analysis indicated that Al and Si components considerably influence the structure of the mortar. Additionally, there were no practical differences in the XRD intensities based on the differences in the chemical composition of the alkaline liquids (activators). The FT-IR analysis on the other hand made it possible to identify changes in the chemical combination of the Alumina and Silica compounds of the fly-ash when compared to the hardened geopolymer mortar. Therefore this study is aimed at finding the behaviour of the chemical constituents of kaolin and metakaolin of the produced geopolymer concrete.

2. METHODOLOGY

2.1 Materials

M*etakaolin*

The Metakaolin used in this study was obtained by beneficiation and calcination of kaolin clay sourced from Kankara kaolin clay deposits in Kankara Local Government Area of Katsina State, the treatment was carried out at the chemical engineering department Ahmadu Bello University (A.B.U), Zaria.

2.2 Methods

1. Metakaolin Production Process

The kaolin clay was beneficiated (Process of removing impurities and nonreactive granules) at the Chemical Engineering old Building Laboratory, it was soaked in water and allowed in water for 2 days and then it was filtered; the effluent was allowed to settle, and excess water was gradually removed leaving the sludge whose water was finally filtered to obtain the wet beneficiated kaolin clay. The wet clay was then air (Plate I) and oven-dried before it was ball-milled to obtain the beneficiated kaolin clay in powder form. The powdered kaolin clay was placed in a furnace and heated (Calcined) for 3 hours at 800^{o}C to obtain the Metakaolin. The choice of the duration and temperature was done to obtain a highly reactive metakaolin based on reports by Badogiannis *et al.* (2005), Moodi *et al.* (2011), and Keeratikan and Janjit (2018).



Plate I: Dried refined raw kaolin clay sludge

2. Geopolymer Concrete Production.

The geoplymer concrete was produced first by mixing a proportion of Na_2Sio_3 gel to a concentration NaOH at specified ratio (ALr is the ratio of Na_2Sio_3 to NaOH). Then the liquid is added to the mixture of aggregates and the metakaolin. A specified amount of water is also added for improved workability. The details of the Mixes are presented in Table 1.

TABLE 1: MATERIAL MIX PROPORTION FOR THE EFFECT OF VARIATION IN CHEMICAL PROPORTIONS

Mix ID	Mo	ALr	Mc (kg/m^3)	ALc (kg/m^3)	NaOH soln (kg/m^3)	Na_2Sio_3 content (kg/m^3)	water content (kg/m^3)	Fine Aggregate content (kg/m^3)	coarse aggregate content (kg/m
1	8	1.5	400	360	144.00	216.00	60	546.67	1093.34
3	8	2.5	400	360	102.86	257.14	60	546.67	1093.34
4	10	1.5	400	360	144.00	216.00	60	546.67	1093.34

ISBN: 978-978-8567-02-8

3. Fourier Transform Infrared (FTIR) test kaolin Metakaolin and Geopolymer cement-based concrete mix

The raw kaolin, calcinated kaolin (Metakaolin) and Crushed samples of some selected mixes were subjected (FTIR) test to make out the bond change between them and to identify the changes in the polymeric bonds through chemical analysis. Raw samples and Crushed samples were taken to the Multi-user Laboratory, Chemistry Department in Ahmadu Bello University Zaria for the FTIR test using the transmittance approach with an Agilent Cary 630 FTIR Spectrometer using the diffuse reflectance procedure (DRIFTS). Under this method, when the IR beam (energy) enters the sample, the energy is either absorbed (reflected) or diffused (transmitted), the diffusely scattered IR is collected, analysed, and presented as the spectrums.

4. Curing of Specimens

The specimens were allowed a resting period of 24 hrs under ambient temperature in the moulds after casting, they were then de-moulded weighed, wrapped in a polyethylene bag as recommended by Sameer (2015), and Jacob (2017) to prevent excessive evaporation, and then placed in an oven and heat cured for 24 hours at 60 ºC. Though Blanco, et al., (2023) suggested 25 to 40 ºC, 60 ºC was adopted. The specimens were then removed weighed again and kept under ambient temperature until the day of testing. The choice of curing temperature and duration was based on recommendations by Davidovits (1999), Hardjito *et al.* (2004c), Heah *et al.* (2011), and Abdul Rahim *et al*. (2014). Plate II shows a sample of wrapped geopolymer concrete cubes in an oven being prepared for heat curing.

5. Test Period of the Geopolymer Specimen

The tests were conducted after 14 days of casting (13-days ambient and 1-day heat), the choice is based on findings and recommendations of early strength gain of heat-cured geopolymer specimens by Aaron (2010), Vijai et al. (2010), Alamgir et al. (2015), Pawan and Surendra (2016), and Jacob (2017).

.



Plate II: Heat (Oven) Curing of GP concrete samples

3. RESULTS AND DISCUSSION

3.1 FTIR of Source Kaolin and Metakaolin

The FT-IR spectra of **Kaolin** are shown in Figure 1. The presence of iron, aluminum, and silicon oxides or hydroxides gets confirmed by studying spectral peaks. The bands at 3,690.1 and 3,623.0 cm−1 signify the presence of OH group of Si, Al.

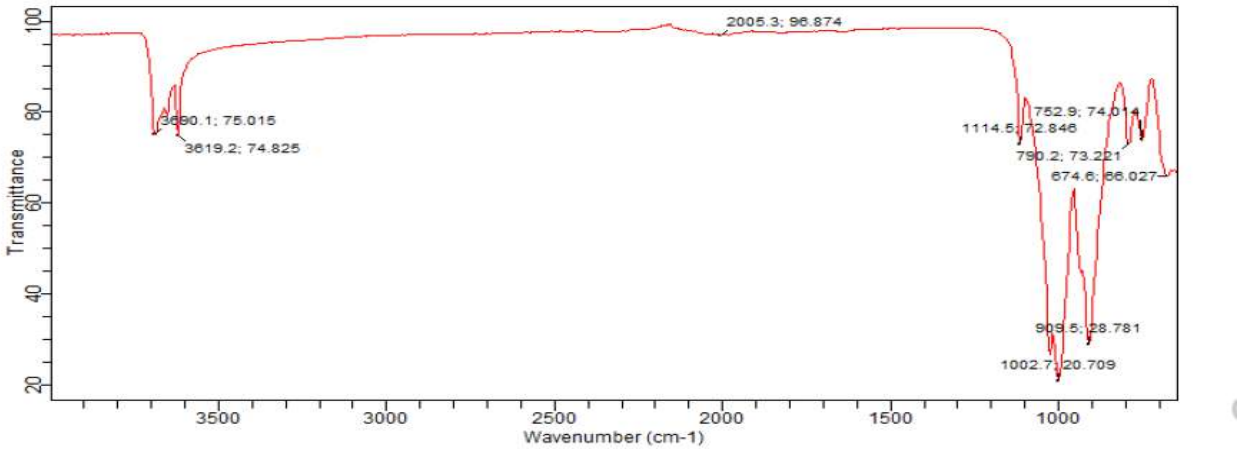


Figure 1: FTIR spectrum of raw kaolin

ISBN: 978-978-8567-02-8

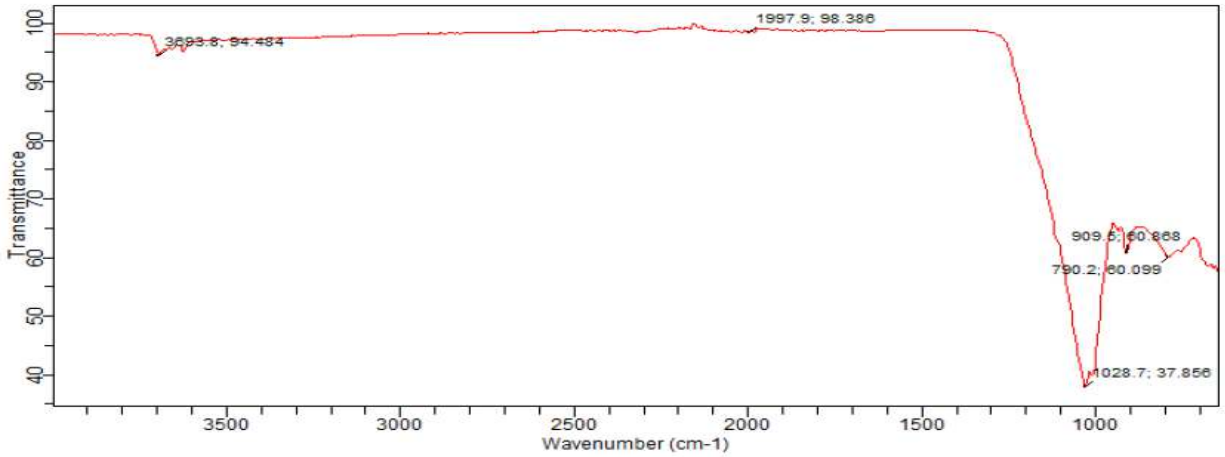


Figure.2: FTIR Spectrum of Treated Kaolin (Metakaolin)

The presence of inner layer water molecules, therefore giving a Stretching (Crystalline hydroxyl) according to Ljiljana *et al.* (2017) and in agreement with Marounane *et al.* (2019). The band s of 749.2, is related to quartz stretching SI-O, and 790.2, 909.5, 998.9 cm−1, are due to the presence of OH deformation linked to AL3+ Mg2+, the presence of C=C Alkene.

Bhaskar and Gopalakrishnarao (2010) stated that the FTIR spectrum of typical kaolin is at 3697, 3669, 3645, and 3620 cm-1, the bands on Figure 1 between 3619 and 3690 cm^{-1} covers this range indicating kaolinite clay minerals, two characteristic bands were exhibited near 3669and 3620cm-^{1}, The band at 3690cm^{-1} on the Figure indicates Al-O-Si stretching and that at 3619cm^{-1} can be OH Stretching (Crystalline hydroxyl) according to Ljiljana *et al.* (2017) and in agreement with Marounane *et al.* (2019). The band at 1114.5 cm^{-1} could be interference due to the presence of quartz, and bands between 1000 and 1200cm^{-1} are Si-O stretching; OH deformation linked to $2Al^{3-}$ can be seen at 909.5 cm^{-1}, and Si-O-Si inter tetrahedral bridging bonds in SiO_2 at 790.2cm^{-1}, the band around 674.6 and 752.9cm^{-1} may be Si-O quartz.

The FTIR result of treated (beneficiated and calcined) Kaolin is shown in Figure 2. The transmittance of the band between 3619 and 3690cm^{-1} which is typical of kaolin increased when treated to 94.484% from 74.825% when untreated, the OH vibration mode of the hydroxyl molecule shifted to 1997.9 cm^{-1}. The interference due to quartz (impurities) at 1114.5 cm^{-1} before treatment is no more after treatment although Duxson *et al.* (2007) believe that impurities in the metakaolin do not affect the final geopolymer product as the impurities do not dissolve. The Si-O stretching of clay minerals which was at 1002.7cm^{-1} is now at 1028.7cm^{-1} and the transmittance shifts from 20% to 37%. The shift in band transmittance from Kaolin to Metakaolin is in agreement with Ljiljan *et al.* (2017), Marounane *et al.* (2019), and Esther *et al.* (2014). The bands at 674.6 and 752.9cm^{-1} which may be due to Si-O quartz are also no more when treated in concurrence with Ljiljana *et al.* (2017) who opined that the intensity of quartz lines decreased after heating between 600 and 900^{o}C. The OH^{-} deformation linked to $2Al^{3-}$ remains at 909.5 cm^{-1}, and the Si-O-Si inter tetrahedral bridging bonds in SiO_2 can also be seen at 790.2cm^{-1} indicating residual kaolinite minerals. This means there are traces of kaolin left in the metakaolin.

3.2 Stacked FTIR Comparison of the Geopolymer Mixes

To ascertain the degree of the geopolymerisation reaction which according to Ljiljana *et al*. (2017) is indicated by the transmittance in relation to the compressive strength of these mixes; an FTIR stacked comparison was made between mix 1 and 3 (Mix 3 having higher Na_2SiO_3 content), Mix 1 and 4 (Mix 4 having higher NaOH concentration) A comparison was later made between first, Mix 1 and Mix 3 to show the effect of an increase in ALr, Mix 1, and 4 to show the effect of the increased molar concentration.

1. FTIR Comparison between Mix 1 and Mix 3

The FTIR spectrum of Mix 1 and Mix 3 is shown in Figure 3; Mix 3 is above the spectrum of Mix 1, this indicates that mix 3 has a higher transmittance than mix 1, in other words, the absorbance of Mix 3 is lower than that of mix 1. The increased transmittance (reduced absorption) around a wavelength of 1000cm^{-1} (Mix 1 to Mix 3) which was attributed to X-O (X can be Si or Al) by Ljiljana *et al.* (2017), which also happens to be the main building block of the geopolymer indicates increased degree of polymerisation, the transmittance at this wavelength for Mix 1 is 63% (37% absorbance) and 75% (25% absorbance) for Mix 3.

The increased transmittance with the degree of geopolymerisation is because as the content of Na_2SiO_3 is increased, the reaction became enhanced according to Xu and Van Deventer (2000) and the matrix became denser with reduced porosity and high compressive strength (Abdullah *et al.,* 2018), this means more geopolymer products are formed, and the Si-O-T (T= Al or Si) bonds diminish and change to a geopolymeric sialate-siloxo chain (Marounane et al., 2019) and hence lower absorption of the wavelength around 1000cm^{-1} and increased transmittance at the Si-O-T wavelengths.

ISBN: 978-978-8567-02-8

2. FTIR Comparison between Mix 1 and Mix 4

For mix 1 and 4 (Figure 4), at around 1000cm^{-1} mix 4 has higher transmittance (less absorbance and reduced peak) than mix 1 which transmits less indicating higher absorbance, The peak reduction (high transmittance) is an indication of the degree of polymerisation according to Esther *et al.* (2014). This is owing to the fact that Mix 4 has 10M NaOH concentration and Mix 1 has 8M NaOH concentration, and Shankar and Khadiranaikar (2013), mentioned that more strength is obtainable with higher molar concentration, and higher strength is an indication of a better degree of polymerisation.

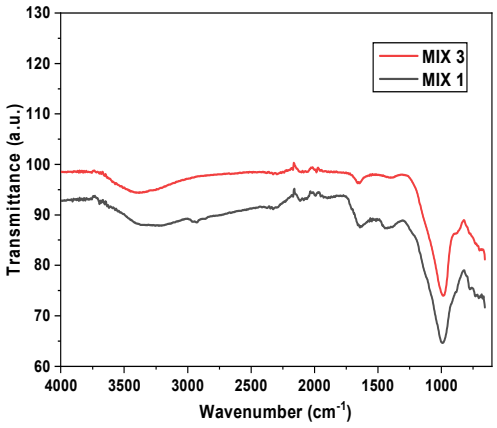


Figure 3: Stacked FTIR spectrum for Mix 1 and Mix 3

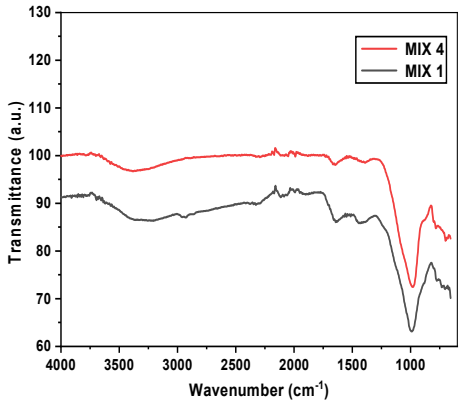


Figure 4: Stacked FTIR Spectrum for Mix 1 and Mix 4

From the FTIR spectrums, Si-O bonds (1000 cm^{-1}) reduce with an increase in Molar concentration, the reduction of Si-O functional group indicates that the Si-O is transformed to geopolymeric product, In other words, Mix 1 has more of the Si-O bond which absorbs more of the light at the Si-O wavenumber than Mix 4 which has a reduced Si-O bond since more of the Si-O bonds have been transformed to 3D geopolymer matrix in the presence of higher concentration.

4. CONCLUSION

The following conclusions were drawn from the results of the study:

iv. The kaolin and metalkaolin purity increases and a molecular bond change occur as indicated by the FTIR analysis.

v. The FT-IR spectra of **Kaolin** transmittance of the bands at 3,690.1 and 3,623.0 cm−1 signify the presence of OH group of Si, Al.

vi. The FTIR result metakaolin show the transmittance of the band between 3619 and 3690cm^{-1}, the OH vibration mode of the hydroxyl molecule shifted to 1997.9 cm^{-1}

vii. At around 1000cm^{-1} wave number, the FTIR spectrum showed that Mix 3 has a higher transmittance (75%) compared with Mix 1 (63%). This showed that Mix 3 with higher Na_2SiO_3 geopolymerises more compared with Mix 1.

viii. Similarly Mix 4 with a higher NaOH molar concentration showed a higher transmittance (less absorbance and reduced peak) at around 1000cm^{-1} compared with mix 1 indicating a more geopolymerised product.

REFERENCES

Abdullah, S.F.A., Ming, L.Y., Abdullah, M.M.A., Yong H.C., and Zulkifly, K. (2018). Evaluation on mixing Parameter of S/L and Na2SiO3/NaOH ratios towards fly ash geopolymers. *AIP conference proceedings* 2030, 020295 (2018). https://doi.org/10.1063/1.5066936

Amritphale, S. S., Bhardwaj, P., & Gupta, R. (2019). Advanced geopolymerization technology. *Geopolymers and Other Geosynthetics*, *10*.

Badogiannis. E, Kakali, G. and Tsivilis, S. (2005). Optimisation of kaolin to metakaolin conversion'' *Journal of thermal Analysis and calorimetry*, 81(2).457-462

Bhaskar, J.S., and Gopalakrishnarao, P (2010). Fourier Transform Infrared Spectroscopic Characterization of Kaolinite from Assam and Meghalaya, Northeastern India. *J. Mod. Phys.* 1, 206-210.

Blanco, I., D'Angelo, A., Viola, V., Vertuccio, L., & Catauro, M. (2023). Metakaolin-based geopolymers filled with volcanic fly ashes: FT-IR, thermal characterization, and antibacterial property. *Science and Engineering of Composite Materials*, *30*(1), 20220192.

Carlos, A. R. Jorge, L., Alamaral-Sanchez, R. C. H., Jose, M. G., Chinchillas, M. J. C., Octavio, H. A., and Susana, P. A. (2014). Experimental study of XRD, FTIR and TGA techniques in geopolymeric materials. *International Journal of Advances in Computer science and its applications*. 4(4), 221-226 ISSN: 2250-3765

Chen, L. Z., Wang, Y. W., and Feng, J. (2016). Preparation and properties of alkali activated metakaolin-based geopolymer. *Materials*, 9(767), 1-12.

ISBN: 978-978-8567-02-8

Duxson, P.; Lukey, G.C.; van Deventer, J.S.J. (2007). Physical evolution of na-geopolymer derived from metakaolin up to 1000 degrees c. *J. Mater. Sci.,* 42, 3044–3054.

Esther, A.O., Elie, K., Patrick, N. L., Arlin, B.T., Uphie, C. M., and Cristina, L. (2014). A sustainable approach to geopolymerisation of Natural Iron-Rich Allumino-silicates materials. *Sustainability*, 6:5535-5553 www.mdpi.com/sustainabilty. .

Gum S. R, Young B L, Kyung T. K, Young Soo C, (2013). The mechanical properties of fly ash-based geopolymer concrete with alkaline activators. *Construction and Building Materials*. 47. 409-418 https://doi.org/10.1016/j.conbuildmat.2013.05.069

Keeratikan, P, and Janjit, I. (2018). Characteristics of meta-kaolin geopolymer Bender-Element (BE) test. *Science Direct Materials Today Proceedings* 5 5120–15125 www.materialstoday.com/proceedings

Ljiljana, M. K., Snezana, N., Milos, N., and Nenad, B. (2017). Structural and Chemical Properties of Thermally Treated Geopolymer Samples. *Journal of Ceramics International* DOI: 10.1016/j.ceramint.2017.02.066

Marounane, E. A., Salihi, A., Mohammed, E. A., and M'hamed, T. (2019). Preparation, characterisation, and Application of Metakaolin based Geopolymer for removal of Methylene Blue from Aqueous Solution. *Journal of Chemistry* ID 4212901, 14

Moodi. F A.A. Ramezanianpour, A..Safavizadeh. S. (2011). Evaluation of the optimal process of thermal activation of kaolins. *Scientia Iranica* 18(4), 906-912.

Othman, N. (2022). IR spectroscopy in qualitative and quantitative analysis. *Infrared Spectroscopy-Perspectives and Applications*.

Saturi B, Sazmal E, Arshad S.S, Afishah, A., and Fouziah, M.D.Y (2015). Preparation and Characterisation of Carbon Nanofibers/Metakaolin Geopolymer based Nano composites. *Internaltional journal of science and environmental technology*. 4(2), 474 -481

Sind, H. (2006). *A conceptual model of geopolymerisation.* A thesis submitted in total fulfilment of the requirements for the degree of Doctor of Philosophy, Department of chemical and Biomolecular Engineering, The university of Melbourne Australia.

Shankar H. S., and Khadiranaikar, R. B. (2013). Performance of Alkaline solutions on Grade of Geopolymer Concrete. *International Journal of Research in Engineering and Technology*. *IC-RICE Conference*. 366-371. http://www.ijret.org

Yusuf, M. O. (2023). Bond characterization in cementitious material binders using Fourier-transform infrared spectroscopy. *Applied Sciences*, *13*(5), 3353.

ISBN: 978-978-8567-02-8

035-Performance Comparison Between Fuzzy-PSO and Fuzzy- GA for the Control of Position and Sway Angle of a Double – Girder Crane System

Bashir Muhammad[1] Abba and Ima Okon Essiet[2]

Department of Electrical Engineering Kano State Polytechnic[1], Department of Computer Engineering, Bayero University, Kano[2]

Corresponding email: ioessiet.ele@buk.edu.ng bashirmabba82@kanopoly.edu.ng

Abstract: Double-girder overhead crane is a vital component in industrial settings for material handling. However, controlling them is difficult due to their nonlinear dynamics, under actuation, and the frequent problem of payload swing. For optimal control, rapid and precise load bearing and positioning are imperative. Conventional control techniques face challenges while trying to balance these competing objectives effectively. In this paper, the control architecture of the system is fuzzy logic controller (FLC) which is designed with knowledge of an expert crane operator to manage the crane's position and sway. Particle swarm optimization (PSO) and Genetic algorithm (GA) were employed to optimize the FLC's membership function parameters. Crane system dynamics uses a nonlinear mathematical model by adopting Euler-Lagrange approach and simulated in a MATLAB/Simulink environment. The system utilizes two identical Mamdani-type fuzzy controllers that work independently: one for trolley position control and another for anti-sway control. The optimization process aimed to minimize a composite objective function based on the Integral of time squared error (ITSE) for both position and angle deviation. From the simulation results obtained, fuzzy logic controller optimized by PSO demonstrated superior performance for positional control due to fastest settling time (2.67 seconds), lowest overshoot (3.12%), and smallest error metrics (IAE, ITAE, ISE, ITSE) compared to both the standalone FLC and the GA-optimized FLC (FLC-GA). But for angle (sway) control the standalone (without) optimization fuzzy logic controller demonstrated a superior performance as both PSO and GA affected or increased the oscillation and error metrics.

Keywords: Double-girder, crane, control, position, sway, fuzzy logic controller, particle swarm optimization, genetic algorithm, nonlinear, MATLAB/Simulink, performance, error.

1. INTRODUCTION

From manufacturing to transportation, industrial control systems are essential to many different businesses. Because of the occupational safety regulations and heaviness of the product, it is frequently not feasible to move semi-processed or processed goods in manufacturing regions using labour. Specialized machine known as cranes are used to transfer related products by twisting, upward and downward, or on flat axes in order to lift them and shift them to another location (Doğan, 2023). A crane is a specialized machine used in industries, shipyards, high building construction, and nuclear plants to move heavy loads and dangerous materials. It is outfitted with chains or cables and sheaves. In the industrial sector, a crane's primary function is to carry a weight from one location to another in the least amount of time while swinging as little as possible. In order to complete this duty, a skilled operator must delay till the load blocks swinging and use his or her experience to quickly block the swing at the proper place. Inability to control the crane could also result in mishaps and injure people. The cargo that the crane is holding is unconstrained to swing in a pendulum-like pattern while operating. Unwanted swings are caused by the crane's nonlinear characteristics, particularly during ascending and reaching the target position (Harb & Alenany, 2025). Additionally, based on their beam construction, cranes are either single-girder or double-girder. The diagram of the double-girder overhead crane is shown in Figure 1 below. The fundamental role of overhead traveling cranes, is to guarantee precise and quick to move items to a certain position in the least amount of time out with any residual oscillation. It consists of two parallel girders, and it is powered by an electric motor, trolley travels along the girders and supported by payload. (Zhang, 2023)

ISBN: 978-978-8567-02-8

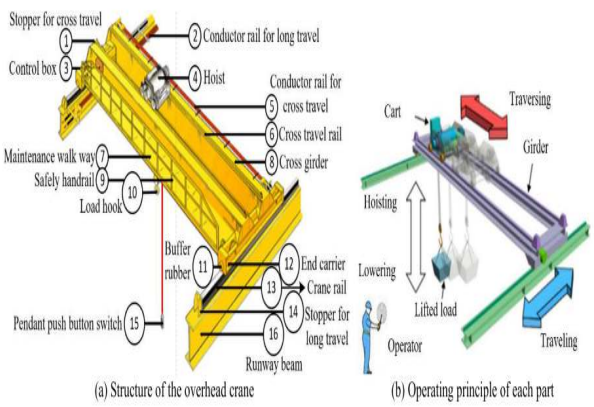


Figure 1: Structural diagram and mode of operation of the overhead crane (Automatisés *et al*., 2024)

Many research has been employed for overhead crane control system. The majority of cranes are manually operated. The overhead crane system's control has been the subject of numerous studies. The dynamic equations of a crane are often time-varying, nonlinear differential equations (Alızada & Ozturk, 2023). These control systems' performance and stability demonstrate how crucial it is to choose the optimal optimization approach and control scheme in line with the intended performance objective (Asad *et al*., 2011). In (Mohamed *et al*., 2022) established a control algorithms with the goal of accomplishing mass rate of production (by moving the trolley accurately) and (by removing sway oscillations) while taking safety precautions into account. The study produced a model of non-linear mathematical for a single-pendulum gantry crane with two stable control systems with controllers PID and PD, each of which has an inlet derivative filter. The simulated annealing algorithm (SAA) was used by (M. A. Mohammed *et al*., 2021) to adjust the weighting matrices of the LQR in order to manage an overhead crane with respect to angle sway and position of the trolley. An LQR optimized by PSO was used to manage both swinging angle of a double pendulum crane system (Abdulhamid *et al*., 2019). The main problem with building a LQR controller, according to the author, is that the Q and R parameters must be determined by the "rule of thumb" approach, which is quite time-consuming.

(Azmi *et al.*, 2019) presented the PID-PD based controllers for overhead cranes. The swinging of the load has created numerous challenges. when operating the overhead crane because of the pendulum-like settings. (Ahmad *et al*., 2009) developed a dual control scheme for a gantry crane system to improve input tracking and reduce payload swing. The system was modelled as nonlinear with uncertainties, using the Euler-Lagrange approach for dynamics. Two controllers were designed. A PD-based fuzzy logic controller (PD-FLC) to regulate the cart's position. A combined non-collocated PID and input shaper to control the swinging angle of the payload. The study evaluated the effectiveness of these controllers in managing crane movement and minimizing oscillations.

(Adeli, 2011) developed a hybrid controller that combines anti-swing control and position regulation. FLC and LQR were developed based on the Takagi-Sugeno fuzzy model of an overhead crane and the genetic algorithm. (Sun & Xie, 2020) designed a reinforcement learning-based backstepping control scheme (BSC) for the underactuated system for the crane system, controller's control gain is crucial since it affects how tracking errors converge. (Fu *et al.*, 2023) employed a Stray lion swarm optimization algorithm (SLSO)-based fuzzy PID controller for overhead crane systems in order to enhance the fuzzy PID controller's performance. . (Shao *et al*., 2019) introduced a unique anti-swing and placement control approach for overhead cranes to address the nonlinear and unpredictable challenges of the dynamics model the approach used two types of T-S fuzzy models based on sector nonlinear theory.(A. Mohammed *et al.*, 2023) developed an overhead crane system and optimized to find an ideal input function of the crane jib by genetic algorithm approach to tackle the problem of large swing angle a non-zero initial conditions. (Sharma, 2020) integrated and optimised FLC with the Enhanced Binary Bat Optimization algorithm (BBOA) to improve or modify the parameters of the fuzzy logic controller with the Priority Fitness Scheme (PFS) in gantry crane system.

Neural network was used by (Kozhubaev *et al*., 2023) in bridge crane operation for predicting the behaviour of the lifted load. (Esleman *et al*., 2021) developed a Bees algorithm method and genetic algorithm. The overhead crane's horizontal and swinging movements was managed using a fuzzy logic controller. A metaheuristic approach was used by (Cao *et al*., 2023) to optimize FLC-PI controllers to get the ideal and excellent performance of the control systems.

This research employs a fuzzy logic controller based on an optimization algorithm technique, in order to achieve high precision and stability of the double-girder crane system. The primary challenge in a double-girder overhead crane system is how to precisely and swiftly position payloads while controlling the excessive load swing. This work has opted for fuzzy control due to some shortcomings in the conventional PID control method concerning nonlinearity and disturbance rejection. Particle swarm optimization (PSO) was used in the fuzzy controller to minimize the cost function through the parameter tuning of the membership function, with a focus on attaining minimal rise time, settling time, and overshoot. Additionally, the performance metrics would be compared with the genetic algorithm (GA) technique. Hence, this research chosen the PSO/GA algorithm to optimize the fuzzy logic controller for performance metrices.

2.0 METHODOLOGY

This research has three methodical approaches:

(a) System's general equation to regulate the trolley's horizontal movement, based on the principle that controlling trolley motion

ISBN: 978-978-8567-02-8

indirectly controls payload sway and was adopted from (Sharma, 2020).

(b) Implementing a fuzzy logic controller (FLC) and optimizing its parameters using the Particle swarm optimization (PSO) with a comparative analysis against Genetic algorithm (GA).

(c) Evaluating and comparing the FLC-PSO controller with the GA-based controller across key metrics: application, flexibility, safety and performance.

2.1 Mathematical model and free-body diagram of crane system

Free-body diagram of double-girder crane system is shown in Figure 2, where *F* or *u* represent the Control force, *x(t)* is the horizontal position of the trolley; *M* and m are the mass of the trolley and the payload, respectively; *l* is the length of the cable, θ(t) (or x_1) is the swing angle of the payload, $\dot{\theta}$ (or x_2) is the angular velocity of the payload, $\ddot{\theta}$ $(or\ \dot{x_2})$ is the angular acceleration of the payload, $\dot{x}$ (or x_4) is the velocity of the trolley, $\ddot{x}$ acceleration of trolley and g denotes the gravitation acceleration.

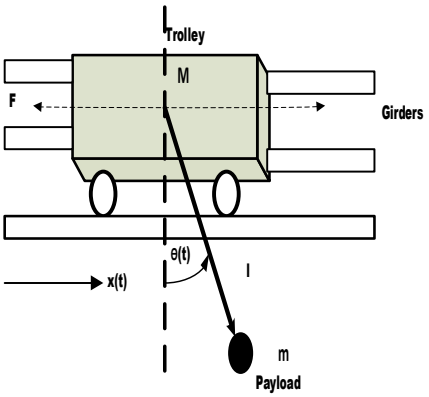


Figure 2: Double- girder crane system model

The Lagrange equation is given by the difference between the Kinetic energy T and potential energy V of the system.

$$L = T - V \tag{1}$$

Kinetic energy T;

$$T = \frac{1}{2} M\dot{x}^2 + \frac{1}{2}m(\dot{x}^2 + (l\dot{\theta})^2 + 2l\dot{\theta}\dot{x}\cos(\theta)) \tag{2}$$

Potential energy V;

$$V = mglcos(\theta) \tag{3}$$

Simplifying the kinetic energy

$$T = \frac{1}{2}(M+m)\dot{x}^2 + \frac{1}{2}ml^2\dot{\theta}^2 + ml\dot{x}\dot{\theta}\cos(\theta) \tag{4}$$

Using the Euler- Lagrange equation for $x\ and\ \theta$

$$\frac{d}{dt}\left(\frac{\partial L}{\partial \dot{x}}\right) - \frac{\partial L}{\partial x} = F \tag{5}$$

$$\frac{d}{dt}\left(\frac{\partial L}{\partial \dot{\theta}}\right) - \frac{\partial L}{\partial \theta} = 0 \tag{6}$$

For *x*

$$(M+m)\ddot{x} + ml\ddot{\theta}\cos(\theta) - ml\dot{\theta}^2 sin(\theta) = F \tag{7}$$

For θ

$$ml\ddot{x}\cos(\theta) + ml^2\ddot{\theta} - mglsin(\theta) = 0 \tag{8}$$

Equation (3.8) become;

$$\ddot{\theta} = \frac{g\,sin(\theta) - \ddot{x}\,cos(\theta)}{l} \tag{9}$$

Substitute $\ddot{\theta}$ into equation (7)

$$(M+m)\ddot{x} + ml\left(\frac{g\,sin(\theta) - \ddot{x}\,cos(\theta)}{l}\right)\cos(\theta) - ml\dot{\theta}^2 sin(\theta) = F \tag{10}$$

$$\ddot{x} = \frac{F + ml\dot{\theta}^2\sin(\theta) - mgsin(\theta)\cos(\theta)}{M + m - mcos^2(\theta)} \tag{11}$$

Solving $\ddot{\theta}$, and from equation (9), substitute the expression for $\ddot{x}$;

$$\ddot{\theta} = \frac{gsin(\theta)}{\cos(\theta)} - \frac{\ddot{x}}{lcos(\theta)} \tag{12}$$

2.2 State- space representation

The state vector *x* and input *u* are;

$$X = \begin{bmatrix} x_1 \\ x_2 \\ x_3 \\ x_4 \end{bmatrix}, \qquad u = \text{control force}$$

The derivatives of the state variables are;

$$\dot{X} = \begin{bmatrix} \dot{x}_1 \\ \dot{x}_2 \\ \dot{x}_3 \\ \dot{x}_4 \end{bmatrix} = \begin{bmatrix} x_2 \\ aux_{01} \\ x_4 \\ aux_{02} \end{bmatrix} \tag{13}$$

Substituting the linearized forms of $aux_{01}$and aux_{02}

$$\dot{x}_2 = x_2 \tag{14}$$

$$\dot{x}_2 = \frac{-u + (M+m)gx_1}{Ml} \tag{15}$$

$$\dot{x}_3 = x_4 \tag{16}$$

$$\dot{x}_4 = \frac{u}{Ml} - \frac{mgx_1}{Ml} \tag{17}$$

2.3 State-space Equations

Transforming the above equations into the matrix form;

$$\mathbf{\dot{X} = Ax + Bu} \tag{18}$$

where,

$$\mathrm{A} = \begin{bmatrix} 0 & 1 & 0 & 0 \\ [(\mathrm{M}+\mathrm{m})\mathrm{g}]/\mathrm{Ml} & 0 & 0 & 0 \\ 0 & 0 & 0 & 1 \\ -\mathrm{mg}/\mathrm{Ml} & 0 & 0 & 0 \end{bmatrix},\ \mathrm{B} = \begin{bmatrix} 0 \\ -1/(\mathrm{Ml}) \\ 0 \\ 1/(\mathrm{Ml}) \end{bmatrix}$$

$$\text{and } \mathrm{x} = \begin{bmatrix} \mathrm{x}_1 \\ \mathrm{x}_2 \\ \mathrm{x}_3 \\ \mathrm{x}_4 \end{bmatrix}$$

ISBN: 978-978-8567-02-8

$$\dot{\boldsymbol{X}} = \begin{bmatrix} 0 & 1 & 0 & 0 \\ [(M+m)g]/Ml & 0 & 0 & 0 \\ 0 & 0 & 0 & 1 \\ -mg/Ml & 0 & 0 & 0 \end{bmatrix} \begin{bmatrix} x_1 \\ x_2 \\ x_3 \\ x_4 \end{bmatrix} + \begin{bmatrix} 0 \\ -1/(Ml) \\ 0 \\ 1/(Ml) \end{bmatrix} * u \quad (19)$$

The system is linearized around an equilibrium position, it was unstable equilibrium position where all state variables are zero, insignificant deviations from this point, nonlinear terms become negligible, small angle approximation eliminates nonlinearities, making the model linear in the state variables, higher orders terms such as $\dot{\theta}^2 \sin(\theta)$ (centrifugal force) and other products of state variables are dropped because they are of second order, the linear model enable the use of linear design methods for stabilization and performance tuning. The linearized equation conforms to the standard linear time-invariant (LTI) form, which is required for many analyses and design techniques.

2.4 System design and implementation

Double-girder crane linearized state-space representation of the system was simulated in MATLAB/Simulink Based on the state- space in equation (20), it has four states as follows;

$$\begin{bmatrix} x_1 \\ x_2 \\ x_3 \\ x_4 \end{bmatrix} = \begin{bmatrix} \theta(\text{Payload swing angle}) \\ \dot{\theta}\ (\text{Angular velocity of the payload}) \\ x\ (\text{Trolley position}) \\ \dot{x}(\text{Trolley velocity}) \end{bmatrix}$$

Force applied to the trolley is the control input *u*. A common and effective strategy is to use two separate fuzzy logic controllers.

TABLE I: SYSTEM MODEL PARAMETERS INVOLVED IN THE SIMULATION (SHARMA, 2020)

Parameters	Values
Mass Trolley (M)	5kg
Payload mass (m)	1kg
Length of the payload cable (l)	0.75m
Gravitational (g)	$9.81 m/s^2$
Damping coefficient (b)	12.32 Ns/m

2.5 System modeling and Simulation

The simulation was conducted in MATLAB/Simulink 2021a and followed a five-step process:

(i) System Modelling: A state-space model was simulated using MATLAB's built-in functions and a custom Euler integration method.

(ii) Controller Design: A Mamdani-type fuzzy logic controller (FLC) with triangular membership functions was implemented.

(iii) PSO optimization: Particle swarm optimization (PSO) was applied to tune the FLC's membership function parameters, aiming to minimize a defined cost function.

(iv) Comparative Analysis: A Genetic algorithm (GA) was implemented to provide a performance comparison with the PSO-optimized controller.

(v) Performance evaluation: The controllers were assessed using four standard error-based metrics ITAE, IAE, ISE, and ITSE which integrate system error over time. The optimization goal was to minimize these values, thereby refining the system's response characteristics.

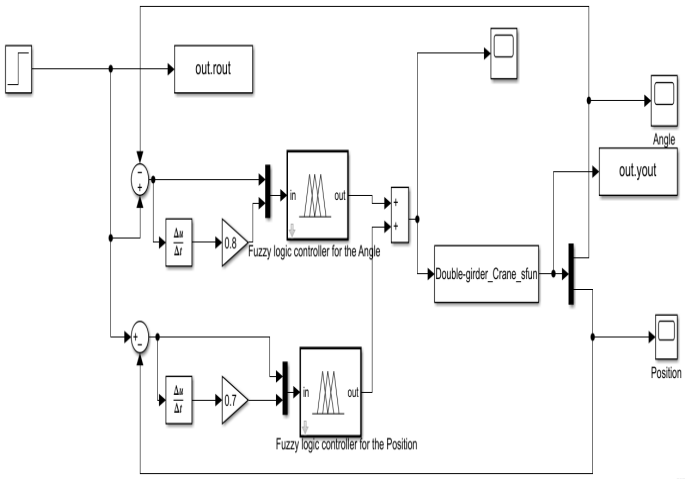


Figure 3: Double-girder crane system block diagram in MATLAB/Simulink.

2.6 Design of Mamdani fuzzy logic controllerS

MATLAB/Simulink was employed to design the FLC by using fuzzy logic toolbox. A common and effective strategy is to use two separate fuzzy logic controllers, the following procedures were conducted for the design of the controllers;

Step one: Problem definition and controller structure

Sway angle controller (FLC θ), Primarily responsible for damping the payload sway. Its inputs are the swing angle θ (x_1) and swing rate $\dot{\theta}$ (x_2). Its output is a control force F_θ . Fuzzy logic controller for position controller was used to move the trolley to the target position. Its inputs are the position error e_x (x_3) and the trolley velocity e_{dx} (x_4). Its output is the primary force F_x. The total control force *u* is the sum of these two forces, $u = F_\theta + F_x$. This structure allows the sway controller to actively dampen oscillations while the position controller does its job

Step two: Fuzzification (Defining fuzzy sets)

This is defined as the linguistic variables with their membership functions for all inputs and outputs, triangular membership functions were selected for simplicity.

Step three: Rule Base (The 'Brain' of the FLC):

The rule base is a set of IF-THEN rules that capture the expert knowledge of how to control the crane. Rule base for sway controller (FLC θ)

Goal: Dampen the sway. If the payload is swinging to the right (Positive θ), apply a force to accelerate the trolley to the right to 'catch' it, and vice-versa

ISBN: 978-978-8567-02-8

2.7 Optimization using Particle Swarm Optimization (PSO)

The population "agents in the search domain" are randomly initialized at the beginning of PSO. The algorithm's success relies on the social behaviour of the particles in the swarm is the basis for how the PSO algorithm operates. In particle swarm optimization, a particle's velocity and therefore its position is updated by combining cognitive (personal best) and social (global best) components, guiding its movement through the search domain.

2.8 Optimization using Genetic algorithm (GA)

GA's primary goal is to replicate natural selection is the driving mechanism that results in the survival of the fittest**.** The solutions in GA are shown as chromosomes. The chromosomes are ordered from best to worst according on their fitness values.

Table II: Initial parameters setting of Particle swarm optimization PSO (Solihin et al., 2019)

Parameters of PSO	**Values**
Inertia weight factor, ω	0.7
Cognitive constant, c_1	1.5
Social constant c_2	1.5
Swarm size or population size nPop	50
Maximum number of iterations (MaxIt)	100
Lower and upper boundaries	lb = [0.1, 0, 0.1, 0]; ub = [1, 0.7, 1, 0.9];
Number of decision variables nVar	$k_1\ k_2\ k_3\ k_4$

Table III: Initial parameters setting of Genetic algorithm (GA) (Solihin et al., 2019)

Parameters of GA	**Values**
Maximum number of iterations (MaxIt)	100
Population size nPop	50
Crossover probability pc	0.8
Number of offspring (must be even)	nc = 2∗ $round(pc * \frac{nPop}{2})$
Mutation probability mp	0.2
Number of mutants	$nm = round(pm * nPop)$
Crossover blend parameter	gamma = 0.4
Mutation rate mu	0.1

3.0 RESULTS AND DISCUSSION

The model validation includes state space simulation of the system model, fuzzy logic controller design using Mamdani-type fuzzy inference system (FIS) with triangular membership functions, and optimization of the objective function using particle swarm optimization (PSO) by comparing it is performance metrics with genetic algorithm (GA).

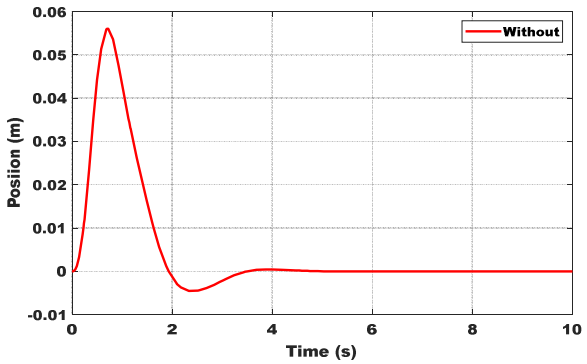


Figure 4: Position with fuzzy logic controller only without optimization

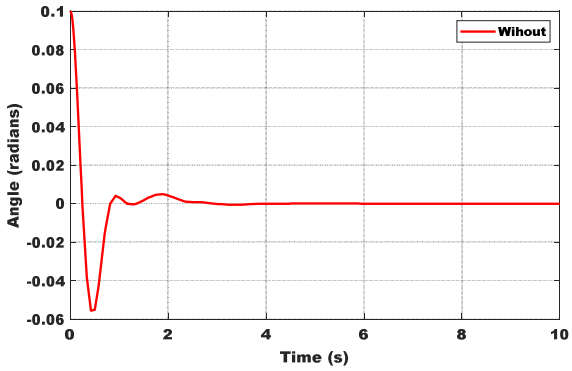


Figure 5: Angle (sway) with fuzzy logic controller only without optimization

3.1 Result of the convergence analysis

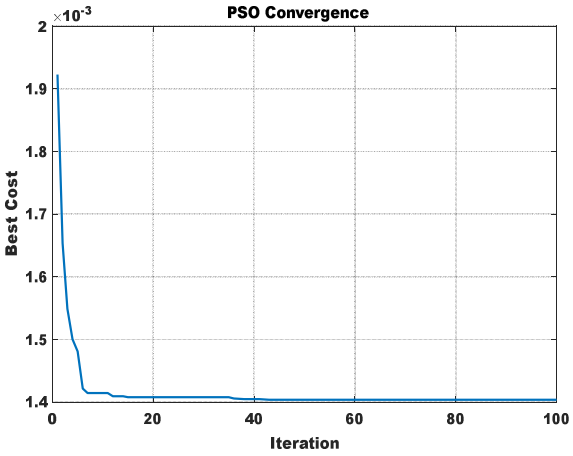


Figure 6: PSO Convergence curve

Figure 6 shows the PSO convergence curve. The best cost (the objective function value) is shown on the vertical (y) axis, and the iteration number (a measure of computational effort or time) is on the horizontal (x) axis.

ISBN: 978-978-8567-02-8

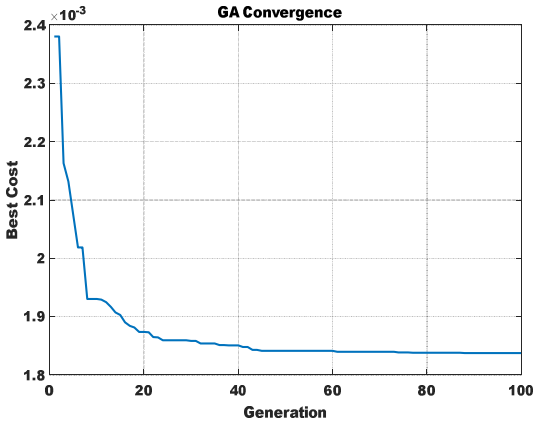


Figure 7: GA convergence curve

Figure 7a illustrate the convergence curve behaviour of a genetic algorithm over 100 generation. This curve. when compared with the PSO convergence curve, it contains a sharp initial decline in the best cost, a slowing rate of improvement, and, ultimately, stagnation at a low-cost value

TABLE II: CONVERGENCE ANALYSIS – ITERATION VERSUS BEST COST (FUZZY LOGIC CONTROLLER TUNING)

Iteration	PSO – Best Cost (IAE for angle)	GA – Best Cost (IAE for angle)	Remarks
1	0.090	0.110	Initial random population /swarm
10	0.070	0.095	PSO shows faster initial improvement
20	0.058	0.080	PSO nearing plateau; GA improving gradually.
30	0.0575	0.068	PSO stagnates; GA continues descent.
40	**0.05719** (converged)	0.060	PSO effectively converged (~40 iterations).
50	0.05718	0.056	GA surpasses PSO in cost reduction.
60	0.05718	0.055	GA still improving slowly.
70	–	0.0545	GA nearing convergence.
80	–	**0.05426** (converged)	GA converges after more iterations.

3.2 Performance of the optimized fuzzy logic controller using Particle swarm optimization (PSO)

A fuzzy logic controller was optimized or fine-tune by using particle swarm optimization to achieve the optimal system performance under control.

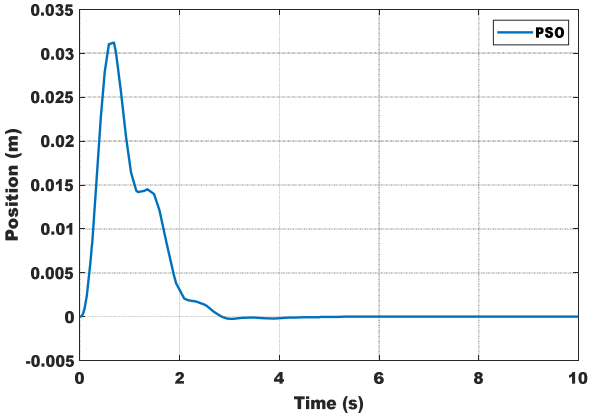


Figure 7b: Position response with PSO-optimized control

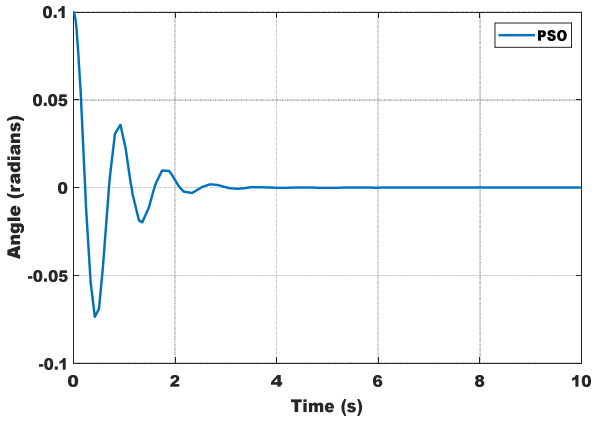


Figure 8: Angle response with PSO-optimized control.

3.3 Performance of the optimized fuzzy logic controller using Genetic algorithm (GA)

Genetic algorithm (GA) was applied to optimize the fuzzy logic controller, for comparison with PSO.

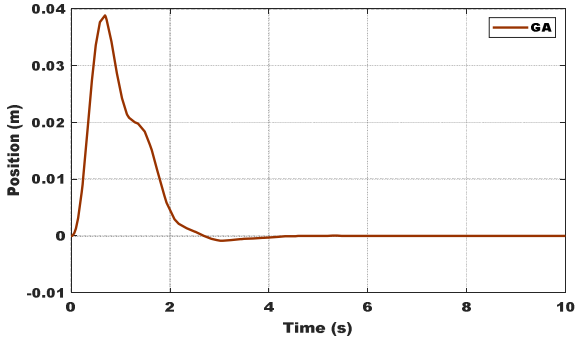


Figure 9: Position response with GA optimized control

ISBN: 978-978-8567-02-8

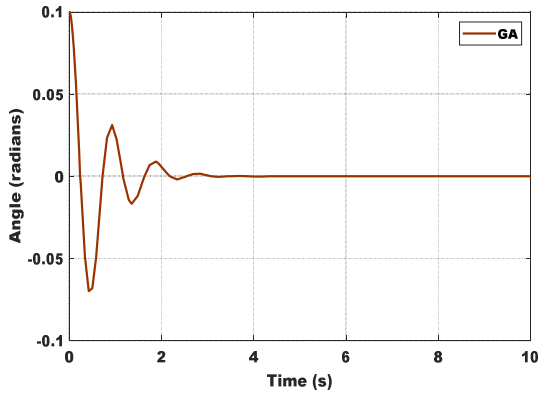


Figure 10: Angle response with GA-optimized control technique.

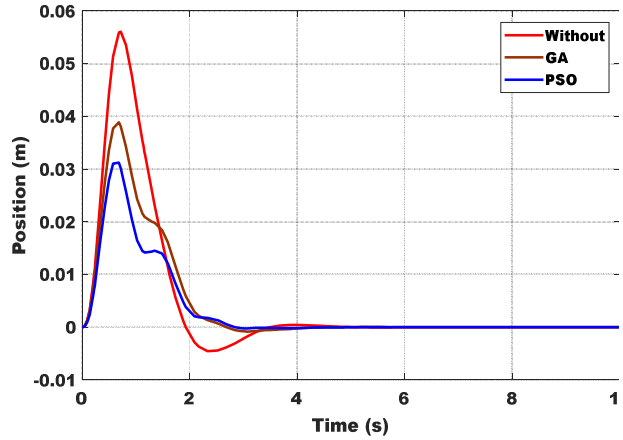


Figure 11: Response of Position control with fuzzy and optimized fuzzy using GA and PSO

The plots in figure 11 show the position response of a double-girder overhead crane system under three different control conditions. The system is inherently unstable, and fuzzy logic was used to stabilize it. The responses are: fuzzy logic controller, fuzzy controller optimized using a Genetic algorithm, fuzzy controller optimized using Particle swarm optimization.

The PSO optimized controller is the most effective, delivering the best performance with the lowest overshoot and the fastest settling time.

TABLE III: PERFORMANCE METRICS FOR POSITION

Performance metrics for Position			
	Fuzzy	Fuzzy with GA	Fuzzy with PSO
Settling time (s)	3.1999	3.1572	2.6721
Rise time (s)	4.50E-04	2.80E-04	1.40E-06
overshoot (%)	5.6	3.89	3.12
Undershoot (%)	0.45	0.08	0.02

Table III details the transient response characteristics of three different control system designs fuzzy (standalone), fuzzy with GA (Genetic algorithm optimized), and fuzzy with PSO (Particle swarm optimization optimized) for a position control.

TABLE IV: PERFORMANCE ERROR METRICS FOR POSITION

Performance error metrics for Position			
	Fuzzy	Fuzzy with GA	Fuzzy with PSO
IAE	0.05573	0.04165	0.03158
ITAE	0.05698	0.04268	0.03142
ITSE	0.001693	0.0008883	0.0005049
ISE	0.002052	0.001041	0.0006177

From table IV above, PSO outperforms fuzzy logic controller without optimization and is also more effective than GA in tuning the fuzzy controller's parameters for the positional control of the double-girder crane system.

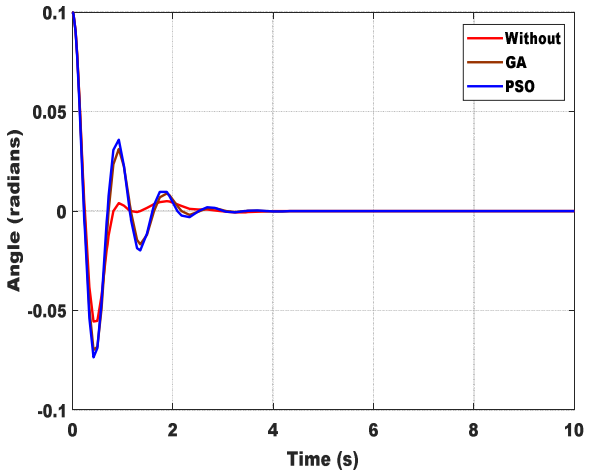


Figure 12: Angle (Theta) with fuzzy and optimized fuzzy using GA and PSO

Figure 12 show the response of the system, under different control conditions. The graphs compare the system response with fuzzy logic controller (without), FLC optimize using Genetic algorithm and Particle swarm optimization (PSO).

TABLE V: PERFORMANCE METRICS FOR ANGLE

Performance metrics for Angle			
	Fuzzy	Fuzzy with GA	Fuzzy with PSO
Settling time (s)	2.2332	2.3358	2.3984
Rise time (s)	0.1641	0.1575	0.1521
overshoot (%)	0.49	3.13	3.58
Undershoot (%)	5.51	6.99	7.35

Table V shows the performance metrics for angle sway of transient response characteristics for the angle control objective, comparing the standalone fuzzy logic controller (without) with its two optimized variants i.e fuzzy with GA (Genetic algorithm) and fuzzy with PSO (Particle swarm optimization).

ISBN: 978-978-8567-02-8

TABLE VIII: PERFORMANCE ERROR METRICES FOR ANGLE (SWAY)

Performance error metrics for Angle			
	Fuzzy	Fuzzy with GA	Fuzzy with PSO
IAE	0.03843	0.05426	0.05719
ITAE	0.01962	0.03544	0.03918
ITSE	0.000493	0.0009644	0.001086
ISE	0.001979	0.002647	0.002786

Table VIII shows the performance error metrices of the sway angle with selected optimization techniques and without optimization (fuzzy logic controller). The standalone fuzzy controller, achieves the lowest error values in every category for angle control. Applying GA and PSO to tune the FLC parameters in this scenario worsens the performance for angle control. While both are worse than the baseline (FLC without), the fuzzy with GA controller performs better than the fuzzy with PSO controller for angle stabilization.

When Genetic algorithm (GA) and Particle swarm optimisation (PSO) were applied to tune the fuzzy logic controller for the double-girder crane system, they degraded or deprived sway (angle) control performance. The optimized controllers demonstrated an increased overshoot from 0.49% to 3.58% with PSO, larger undershoot, slower settling times and higher error metrics (IAE, ITAE etc.). The degradation occurred because the optimization prioritised overall system performance by improving trolley position response at the expenses of sway (angle) damping. This illustrates that automated tuning without explicit constraints on stability metrics can worsen critical subsystem behaviour.

4.0 CONCLUSION

The hybrid control system (FLC optimized by PSO) was designed and simulated for the double-girder overhead crane, excelled for the trolley positioning. However, for the angle (sway) control, the FLC standalone (without optimization) in this research demonstrated a better performance as both PSO and GA affected or increased the oscillation and error metrics. For future work it is recommended that a different controller can be used to compare the performance for both position and sway control. Controller parameter optimization can also be done using other metaheuristic algorithms. Also, a multi-objective optimizer can be considered.

REFERENCES

Abdulhamid, I. B., Muhammad, M., & Khaleel, A. I. (2019). Control of a Double Pendulum Crane System Using PSO-Tuned LQR. *2019 2nd International Conference of the IEEE Nigeria Computer Chapter, NigeriaComputConf 2019*, 1–8. https://doi.org/10.1109/NigeriaComputConf45974.2019.8949631

Adeli, M. (2011). *Anti-swing Control for a Double-Pendulum-Type Overhead Crane Via Parallel Distributed Fuzzy LQR Controller Combined with Genetic Fuzzy Rule Set Selection*. 306–311.

Ahmad, M. A., Raja Ismail, R. M. T., & Ramli, M. S. (2009). Hybrid input shaping and non-collocated PID control of a gantry crane system: Comparative assessment. *IEEE/ASME International Conference on Advanced Intelligent Mechatronics, AIM*, 1792–1797. https://doi.org/10.1109/AIM.2009.5229782

Alızada, M., & Ozturk, S. (2023). PID and Fuzzy Logic Control of Ball and Beam System Using Particle Swarm Optimization. *World Journal of Engineering and Technology*, *11*(04), 859–873. https://doi.org/10.4236/wjet.2023.114057

Asad, S., Salahat, M., Zalata, M. A., Alia, M., & Rawashdeh, A. Al. (2011). Design of Fuzzy PD-Controlled Overhead Crane System with Anti-Swing Compensation. *Engineering*, *03*(07), 755–762. https://doi.org/10.4236/eng.2011.37091

Automatisés, S., Anh, L. Van, Thi, V., & Linh, T. (2024). *Position Control and Anti-Sway of Overhead Crane System with Uncertain Nonlinear Model*. *57*(2), 425–431.

Azmi, N. I. M., Yahya, N. M., Fu, H. J., & Yusoff, W. A. W. (2019). Optimization of the PID-PD parameters of the overhead crane control system by using PSO algorithm. *MATEC Web of Conferences*, *255*, 04001. https://doi.org/10.1051/matecconf/201925504001

Cao, W., Zhang, P., Mi, Q., Sun, Y., Shi, J., & Liang, W. (2023). *Optimization of X - axis servo drive performance using PSO fuzzy control technique for double - axis dicing saw*. 1–14.

Esleman, E. A., Önal, G., & Kalyoncu, M. (2021). Optimal PID and fuzzy logic based position controller design of an overhead crane using the Bees Algorithm. *SN Applied Sciences*, *3*(10). https://doi.org/10.1007/s42452-021-04793-0

Falehi, A. D. (2017). Optimal Design of Fuzzy-AGC Based on PSO & RCGA to Improve Dynamic Stability of Interconnected Multi Area Power Systems. *International journal of Automation & Computing*. https://doi.org/10.1007/s11633-017-1064-0

Fu, J., Liu, J., Xie, D., & Sun, Z. (2023). Application of Fuzzy PID Based on Stray Lion Swarm Optimization Algorithm in Overhead Crane System Control. *Mathematics*, *11*(9). https://doi.org/10.3390/math11092170

Harb, S. F., & Alenany, A. (2025). *Fuzzy Control of a Large Crane Structure Fuzzy Control of a Large Crane Structure*. *January*. https://doi.org/10.52549/ijeei.v5i1.256

Kozhubaev, Y., Ovchinnikova, E., Krotova, S., Murashov, Y., & Nushtaev, N. (2023). Implementation of a neural network in overhead crane control. *E3S Web of Conferences*, *389*.

ISBN: 978-978-8567-02-8

https://doi.org/10.1051/e3sconf/202338901035
Mohamed, K. T., Abdel-razak, M. H., Haraz, E. H., & Ata, A. A. (2022). Fine tuning of a PID controller with inlet derivative filter using Pareto solution for gantry crane systems. *Alexandria Engineering Journal*, *61*(9), 6659–6673. https://doi.org/10.1016/j.aej.2021.12.017
Mohammed, A., Altuwais, H., & Alghanim, K. (2023). *An optimized shaped command of overhead crane nonlinear system for rest-to-rest maneuver*. *11*(January), 548–554.
Mohammed, M. A., Maguire, M., & Kim, K. (2021). *Simulated Annealing Algorithm Based Tuning of LQR Controller for Overhead Crane*. 37–42.
Rehman, T. (2017). *An Introduction to Fuzzy Logic Controller and its Applications*. *3*(7), 540–545.
Shao, X., Zhang, J., & Zhang, X. (2019). Takagi-sugeno fuzzy modeling and PSO-Based Robust LQR anti-swing control for overhead crane. *Mathematical Problems in Engineering*, *2019*. https://doi.org/10.1155/2019/4596782
Sharma, A. (2020). An intelligent position control using priority based fitness scheme and optimal tuning of fuzzy logic controller parameters with binary bat algorithm for nonlinear gantry crane system. *Journal of Green Engineering*, *10*(11), 11687–11700.
Solihin, M. I., Chuan, C. Y., & Astuti, W. (2019). Optimization of fuzzy logic controller parameters using modern meta-heuristic algorithm for gantry crane system (GCS). *Materials Today: Proceedings*, *29*(November 2018), 168–172. https://doi.org/10.1016/j.matpr.2020.05.641
Sun, X., & Xie, Z. (2020). Reinforcement Learning-Based Backstepping Control for Container Cranes. *Mathematical Problems in Engineering*, *2020*. https://doi.org/10.1155/2020/2548319
Zhang, T. (2023). Robust Control Method Design for Underactuated Double-Pendulum Overhead Cranes. *Innovation in Science and Technology*, *2*(3), 7–25. https://doi.org/10.56397/ist.2023.05.02

ISBN: 978-978-8567-02-8

036-The Role of Engineers in Driving Nigeria's Energy Transition and Industrial Competitiveness in the North-East.

[1]Lawal, Kamilu Oluwafemi, [2]Abbagana, Mohammed, [3]Amoo, Abdullahi Lanre

[1,3] Department of Electrical and Electronics Engineering, Faculty of Engineering and Engineering Technology, Abubakar Tafawa Balewa University, Bauchi
[2]North East Development Commission, NEDC.
Corresponding Author: kolawal@atbu.edu.ng

Abstract: Nigeria's Energy Transition Plan outlines an ambitious pathway to net zero emissions by 2060, with significant implications for the power, industrial, transport, cooking, and oil and gas sectors. Translating this vision into practice while preserving industrial competitiveness and advancing equitable development remains a major challenge. The challenge is most acute in the North-East. Persistent energy poverty, weak infrastructure, and limited industrial activity have widened the development gap between the region and other parts of the country, including the South-West, South-South, South-East, North-West, and North-Central. Delivering on the Energy Transition Plan therefore requires more than national level targets. It demands a focused mobilization of engineering capacity that responds to regional realities. This paper draws on desk-based reviews of policy documents, peer reviewed literature, and empirical evidence to clarify the technical, institutional, and educational roles of engineers in this process. These roles include accelerating decentralized renewable energy deployment, integrating advanced energy storage, stimulating local clean technology manufacturing, and developing a skilled, future ready workforce. The paper concludes with prioritized policy recommendations to align engineering practice, education, and innovation with Nigeria's transition objectives and the urgent need for sustainable industrial development in the North-East.

1. INTRODUCTION

Reliable, affordable, and sustainable energy underpins modern economies. It shapes how people live, how businesses operate, and how industries grow. In Nigeria, however, energy poverty remains a persistent constraint on productivity, industrial expansion, and human development. The burden is especially heavy in the North-East, where fragile infrastructure and limited grid reach continue to restrict economic activity and slow industrial progress (Lawal et al., 2018; Zhang et al., 2019; World Bank, 2023). As a result, manufacturing, agro-processing, and small-scale enterprises that should anchor regional resilience often operate below capacity or fail to scale.

These energy constraints intersect with deeper socio-economic pressures. Protracted conflict, weak private investment, and high youth unemployment have eroded productive capacity and limited post-conflict recovery across much of the region. Strengthening industrial competitiveness is therefore not only an economic priority but also a pathway to job creation, social stability, and long-term reconstruction in the North-East (World Economic Forum, 2022).

Against this backdrop, Nigeria's ambition for sustainable industrial growth cannot be separated from its energy transition pathway. Recognizing this linkage, the Federal Government adopted the Energy Transition Plan, ETP, as a coordinated response to long standing energy and climate challenges. The plan sets out a multipronged strategy for achieving net zero emissions by 2060, with a focus on five critical sectors power, industry, cooking, transport, and oil and gas. At its core is the recognition that reliable electricity supply and efficient energy use are essential to industrial competitiveness and inclusive economic development ("Nigeria Utilizes Only", 2025). Within this policy framework, engineers play a decisive role, bridging vision and implementation by designing, deploying, and managing energy systems capable of unlocking industrial productivity, particularly in underserved regions such as the North-East.

2. LITERATURE REVIEW

2.1 Nigeria's policy framework and strategic targets

The National Energy Transition Plan (ETP) articulates detailed technology pathways and sequenced timelines for power, industry, transport, buildings, oil and gas, and agriculture, outlining the specific interventions needed to achieve net-zero by 2060 while simultaneously expanding energy access and stimulating economic growth. These pathways include utility-scale renewables,

ISBN: 978-978-8567-02-8

decentralized energy systems, electrification of industrial processes, energy efficiency, grid modernization, natural gas optimization, hydrogen adoption, and carbon management, providing a structured framework within which engineers play a central technical and managerial role (Energy Transition Office, n.d.). For North-East Nigeria, where solar resource availability is particularly strong, the ETP's scenarios highlight the importance of large-scale PV deployment, mini-grid expansion, and storage-enabled hybrid systems, which are areas that depend directly on engineering expertise in resource assessment, system design, grid integration, and lifecycle optimization (Bawonda and Adefarati, 2023; Salihu *et al.,* 2024).

Complementing the ETP, the National Energy Policy (NEP) and associated Energy Commission of Nigeria (ECN) documents provide the overarching institutional and regulatory foundation for national energy planning, inter-agency coordination, technology standardization, and research and development (Energy Commission of Nigeria, ECN, 2022). These frameworks outline responsibilities for energy auditing, industrial energy efficiency, renewable energy standards, and long-term capacity. For the Northeastern states, where weak grid infrastructure and high industrial downtime persist, these institutional documents underscore the need for engineering-led strategies in grid reinforcement, distributed generation, mini-grid interoperability, and the establishment of testing and quality assurance laboratories to support local manufacturing and ensure technology reliability (Adeshina *et al.*, 2024; Worku, 2022). Table 1 is a summary linking key Nigerian energy policies to their practical implications for engineers.

TABLE 1: KEY NIGERIAN ENERGY POLICIES AND THEIR PRACTICAL IMPLICATIONS FOR ENGINEERS

Policy	Core Focus	Some Implications for Engineers
Energy Transition Plan (ETP)	Net zero by 2060 with industrial growth	-Design and deployment of renewable and hybrid power systems. -Integration of energy storage and smart grids. - Engineering support for clean technology manufacturing and scale up. Systems integration across sectors.
National Energy Policy (NEP)	Energy security and sustainable development	-Planning and expansion of generation, transmission, and distribution infrastructure. -Developing off grid and mini grid solutions. -Standards setting, system optimization, and reliability engineering. -Training and mentoring of a skilled technical workforce.

Sources: (Federal Government of Nigeria. Nigeria Energy Transition Plan 2022, Federal Ministry of Power. National Energy Policy. Revised edition. 2018)

Collectively, the ETP and NEP create a multi-layered governance and technical ecosystem in which engineers serve as the primary actors linking national policy, technology deployment, and industrial competitiveness. Their roles span feasibility analysis, power system planning, renewable resource mapping, process optimization, safety and standards development, and training of the local workforce. These are all essential to accelerate the energy transition and unlocking new industrial opportunities across North-east Nigeria. National electricity supply reliability and the need for transition is needed for the industrial competitiveness of the region, Figure 1 illustrates a steady but fluctuating upward trend in Nigeria's total electricity generation over two decades. While output has increased from approximately 15TWh in 2000 to over 40TWh by 2023, the growth remains modest relative to the country's population surge and industrial demand during the same period.

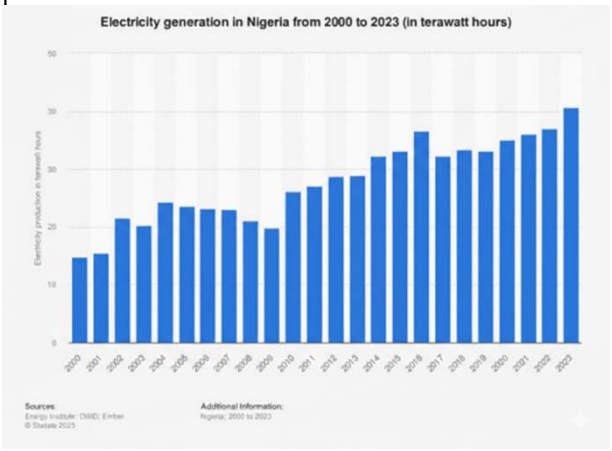


Figure 1: Electricity generation in Figure 1: Electricity generation in Nigeria from 200-2023 (Fernandez, 2025).

2.2 Energy access, generation mix and implications for industry

Nigeria's electricity supply remains overwhelmingly dependent on gas-fired power plants. According to a recent systematic review of Nigeria's power sector, gas-fired plants account for most of the installed capacity and consequently dominate grid-supplied electricity This reliance on fossil-gas generation presents a dual reality: on one hand, the country's large domestic natural gas reserves offer a ready resource that could, in principle, support broad electrification and power many industrial operations; on the other hand, reliance on gas-fired generation creates both an environmental burden and a structural risk for decarbonization, especially given growing global and domestic commitments to reduce greenhouse-gas (GHG) emissions (Ayeni and Hassan, 2025).

Beyond the composition of the generation mix, however, a deeper problem lies in the inefficiency and unreliability of the grid system, which is a major constraint on industrial productivity, especially outside major urban corridors in the southwest. Figure 2 highlights pronounced regional disparities, with North-East states exhibiting significantly lower electricity availability per capita compared to southern industrial hubs, underscoring the need for targeted engineering

ISBN: 978-978-8567-02-8

interventions. It shows the disparity in "Vested Power" across different states, revealing that energy availability is highly concentrated in industrial hubs and near major generation clusters. This suggests a significant urban-rural divide and the need for decentralized energy solutions to improve per capita access in underserved states.

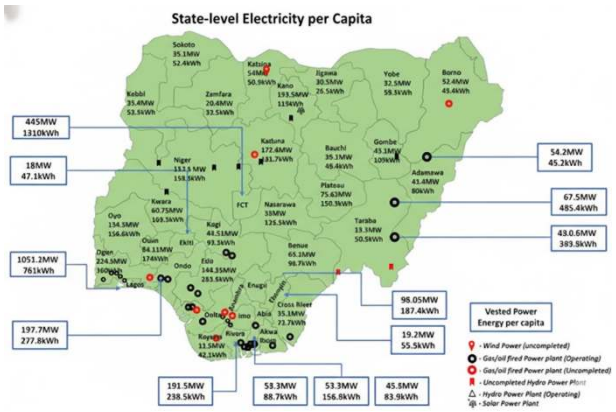


Figure 2: State Level Electricity Capacity and Electricity Consumption Per Capita in Nigeria (NERC, 2025).

Despite a theoretically large installed capacity (e.g., over 13,000–13,600 MW in some recent estimates), actual generation delivered to customers is substantially lower. For example, reports indicate that at certain times only roughly 5,500 MW might be available and that a significant share of generation capacity remains stranded or under-utilized ("Nigeria Strikes", 2025).

Such chronic under-supply leads to frequent blackouts, voltage fluctuations and transmission bottlenecks. For businesses including manufacturing, agro-processing, and other industrial activities, this translates into unpredictability: production disruptions, increased reliance on diesel or petrol generators, high operational costs, and degraded confidence among domestic and foreign investors (Ikwuoma *et al*., 2024)

In North-east Nigeria, where grid infrastructure is often weaker, transmission and distribution networks are less robust, and institutional investment has historically been lower than in urban south-west areas, these challenges are magnified. The industrial potential of the region remains underexploited, in part due to energy insecurity. As a result, despite abundant natural resources and human capital potential, the unreliability of electricity supply dampens industrialization, discourages investment, and impairs the region's competitiveness (Adebayo and Ainah, 2024).

Thus, while Nigeria's gas reserves provide an energy resource base, the realities of grid inefficiency, under-utilization and supply unreliability mean that engineers, especially those operating in North-East Nigeria , face a critical role: to design and deploy alternative, resilient energy systems (e.g., decentralized renewables, hybrid mini-grids, storage), to upgrade grid and distribution infrastructure, and to build energy-system resilience. This technical leadership is essential not only to meet energy demand, but to unlock industrial growth and competitiveness in underserved regions of the country.

2.3 Renewable resources and regional potential in the North-East

Multiple studies show that Northern Nigeria possesses some of the strongest solar resources nationwide, with region-specific measurements reporting global horizontal irradiance typically ranging from about 3.5–7.5 kWh/m²/day—levels that consistently exceed national averages and remain stable across seasons. This exceptional insolation strengthens the engineering rationale for deploying solar PV, PV-battery hybrids, and mini-grids as context-appropriate solutions for both rural electrification and emerging industrial clusters. Detailed GIS-based assessments and satellite-derived irradiance models further confirm that northeastern states offer optimal siting conditions for utility-scale and decentralized systems, enabling engineers to design cost-effective, resilient energy infrastructures that directly support industrial productivity (Idris *et al.*, 2024). Figure 3 Shows the map of solar radiation zone in Nigeria.

The first zone, which comprises of Northeastern parts of Nigeria has irradiation levels of 6,000Wh/m^2, identifying it as the prime region for utility-scale solar farms, while Zone III (South) shows lower potential due to increased cloud cover and humidity (Abdulhameed *et al.*, 2024).

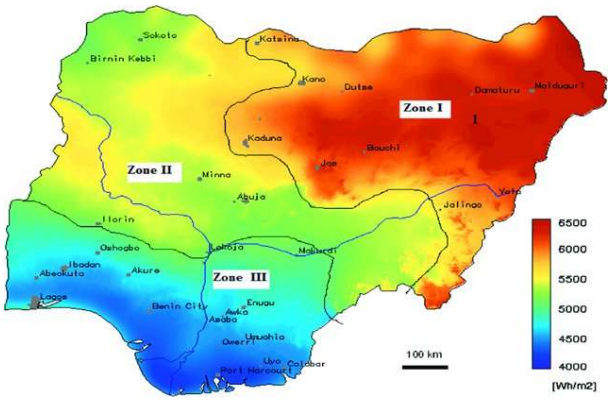


Figure 3: Map of Solar Radiation Zones in Nigeria. (Owolabi et al., 2024).

2.4 Decentralized solutions, hybrid architecture, storage and grid integration

Recent deployments and project pipelines emphasize decentralized renewable energy (DRE), such as mini-grids and standalone systems, to reach underserved communities rapidly. A high-profile MOU/transaction for a $200M mini-grid rollout underscores the scale at which DRE is being mobilized (Anyaogu 2025).

Hybrid renewable systems (PV + battery + appropriate backup) and mini-grids are also effective, near-term strategies for improving energy access and supplying reliable power to clusters of industrial demand in rural and peri-urban areas. Peer-reviewed modelling and pilot

ISBN: 978-978-8567-02-8

studies indicate hybrid systems tailored to local demand profiles reduce levelized cost of electricity and outages compared to diesel-only options (Emezirinwune *et al.*, 2024)

Integration of battery energy storage systems (BESS) is increasingly recognized as essential for smoothing variable renewables and improving grid stability; recent technical analyses and modelling demonstrate that storage inclusion materially affects system reliability and the feasible share of renewables by 2050 (Anyaogu, 2025).

2.5 Industrial competitiveness, energy intensity and technical constraints

Empirical research consistently demonstrates that electricity availability and reliability are decisive determinants of manufacturing productivity in Nigeria. Frequent outages and voltage fluctuations compel firms to rely on costly diesel generators, increasing operational expenses, disrupting production schedules, and lowering capacity utilization (Gold *et. al.*, 2024). Studies using firm-level and panel data show that unreliable power supply can reduce manufacturing output by double-digit percentages, particularly in energy-intensive subsectors.

These constraints are even more pronounced in Northeastern Nigeria, where grid instability is more acute. Conversely, engineering-led interventions, such as energy-efficient machinery, optimized process flows, and integrated on-site renewables have been shown to significantly reduce production costs while improving competitiveness. (Ajibola *et. al*., 2022). Evidence suggests that firms adopting modernized electrical systems and energy management practices achieve higher productivity, improved product quality, and better export readiness (Cole *et al*., 2018).

3 ANALYTICAL APPROACH

This study adopts a systems perspective that integrates three complementary lenses. The first is a techno economic lens that evaluates energy supply pathways at the regional scale, focusing on the relative feasibility of centralized generation, decentralized renewables, hybrid mini grids and storage enhanced systems. The second is an institutional lens that examines the policy and regulatory instruments shaping energy deployment, technology standards, and industrial development. The third is a human capital lens that considers the state of engineering education, professional training and entrepreneurial ecosystems that enable engineers to contribute effectively to the transition of energy.

The aim is not to generate new primary field data. Instead, the study synthesizes insights from diverse bodies of knowledge and translates them into clear, actionable roles for engineers, supported by targeted policy and strategic recommendations. This approach allows evidence from technical studies, policy analyses and workforce assessments to be interpreted in a coherent manner that reflects the realities of Nigeria's current transition efforts.

Engineering roles are evaluated across four interconnected domains: planning and systems design, policy and standards support, capacity building and enterprise development, and research, development and innovation. Each domain is analyzed in relation to the specific conditions of Nort-East Nigeria, including chronic grid deficits, limited financing, security related disruptions, and persistent human capital constraints. This regionally anchored approach highlights where engineering expertise is most urgently required and how it can be mobilized to strengthen both the energy transition and industrial competitiveness in the North-east.

4. ENGINEERS' ROLES AND TECHNICAL PATHWAYS

Engineers occupy a central position in translating Nigeria's energy transition ambitions into implementable systems, particularly in the context of the North-East where infrastructure deficits and dispersed demand dominate. Their roles span energy system planning, renewable resource assessment, grid and mini grid design, storage integration, industrial electrification, and performance optimization. Within this framework, engineers define and evaluate technical pathways that balance reliability, cost, scalability, and decarbonization objectives. These pathways include planning and deployment of decentralized systems, grid reinforcement and storage integration, process engineering for low carbon industrial systems, standards and quality assurance and capacity building, curricula and entrepreneurship, and many more. By aligning technology choices with regional resource endowments and load characteristics, engineers enable context appropriate solutions that directly support productive and industrial uses of energy.

a. Planning, design and deployment of decentralized systems

Engineers must design technically resilient and economically viable mini grids and hybrid systems, including PV with storage and limited diesel or gas backup where necessary, tailored to North-East settlement patterns and load profiles. For example, solar hybrid mini grids deployed in rural communities in Adamawa and Yobe states under private developer and donor supported programs have combined pay-as-you-go metering with anchor loads such as water schemes and agro-processing centers, improving financial viability. Success in these projects will depend on strong local engineering input for site assessment, demand estimation, and network design (Anyaogu, 2025).

b. Grid reinforcement and storage integration

System studies indicate that grid scale and distributed storage significantly increase the feasible penetration of variable renewables while maintaining reliability. In southern Nigeria, pilot battery energy storage systems integrated at distribution substations have demonstrated peak shaving and voltage support benefits, reducing outages in weak feeders. Similar approaches could stabilize fragile networks in North-East urban centers. Engineers must lead the modelling, siting, specification,

ISBN: 978-978-8567-02-8

and operational strategy design for such systems, including frequency regulation and load shifting (Eshiomegie et al., 2024).

c. Process engineering for low-carbon industrial fuels and heat

Industries requiring high temperature heat, such as cement, steel, and chemicals, will require careful evaluation of process electrification, biomass co firing, waste to energy, and longer-term hydrogen substitution in line with ETP timelines. In Nigeria's cement sector, incremental substitution of fossil fuels with biomass residues has already reduced energy intensity in selected plants. Engineers must extend such process integration and optimization approaches to emerging industrial clusters in the North-East, supported by pilot demonstrations before large scale deployment (Griffiths *et al*., 2021).

d. Standards, quality assurance and local manufacturing

Local standards, testing facilities, and certification regimes reduce dependence on imported equipment and support domestic manufacturing. Experiences from Lagos and Ogun states, where inverter assembly and solar component testing labs have emerged through industry academic partnerships, illustrate how engineering led quality assurance can anchor local value chains. Replicating such facilities in the North-East would support regional industrialization while aligning with the National Energy Policy and ETP emphasis on local content (Energy Commission of Nigeria, ECN, 2022).

e. Capacity building, curricula and entrepreneurship

Universities and technical colleges in the North-East should embed hands on training in renewable energy systems, power electronics, microgrid engineering, and energy economics. Models from other regions, where university linked energy incubators have produced SMEs delivering mini grid installation and maintenance services, show the potential impact. Engineers in academia and industry can jointly design practicum programs and enterprise support platforms that address skills gaps, reduce youth unemployment, and stimulate local industrial clustering (Anaele et al., 2014).

5. IMPACTS ON INDUSTRIAL COMPETITIVENESS

Reliable and affordable energy is central to industrial competitiveness, especially in energy intensive and time sensitive sectors such as agro-processing and manufacturing. In the North-East, frequent outages, voltage instability, and dependence on self-generation raise production costs and constrain capacity utilization. Engineering interventions that improve reliability, integrate on site renewables, enhance energy efficiency, and optimize processes reduce operating costs and raise productivity. Over time, these gains strengthen competitiveness, enable local value addition, and support new industrial clusters, positioning the energy transition as a driver of structural industrial transformation rather than solely an environmental goal.

A. Attraction of investment

By lowering energy-related operational risk through reliable off-grid/mini-grid options and improved local grid performance, regions become more attractive for light manufacturing and agribusiness processing. Evidence shows that investments in distributed generation catalyze localized industrial activity where reliable grid expansion is slow (Anyaogu, 2025).

f. Value-chain creation

Localized manufacturing for solar balance-of-system components, battery pack assembly and micro-industrial services creates jobs and backward linkages that can anchor broader industrialization. Policy support, engineering process design and standards are prerequisites for these value chains. (ECN, 2022)

g. Energy intensity and competitiveness

Reducing firms' reliance on expensive diesel and improving energy efficiency lowers production costs and raises competitiveness. Engineers' role in process audits, retrofits and system modernization therefore has direct productivity effects (Gold *et al.*, 2024).

h. Resilience and inclusion

Decentralized systems designed by engineers can provide resilience in insecure or remote areas, ensuring continuity for enterprises and services and supporting equitable economic opportunity. (Anyaogu, 2025). The table 2 shows the summary of the impact.

TABLE 2: SUMMARY OF KEY IMPACTS.

Impact area	**Primary engineering levers**	**Indicative outcomes**
Cost reduction	Mini grids, on site renewables, energy efficiency retrofits	Lower fuel and electricity costs. Reduced exposure to diesel price volatility.
Job creation	Local manufacturing, installation, operations and maintenance	Direct technical jobs. Indirect employment across supply chains.
Productivity and competitiveness	Reliable supply, process optimization, voltage stability	Higher capacity utilization. Improved product quality and delivery reliability.
Investment attraction	Risk reduction through reliable power solutions	Increased private investment in agro processing and light manufacturing.
Resilience and inclusion	Decentralized and modular energy systems	Business continuity in remote or insecure areas.

ISBN: 978-978-8567-02-8

Impact area	Primary engineering levers	Indicative outcomes
		Broader participation in local economies.

6. RISKS, BARRIERS AND MITIGATION STRATEGIES

Although many energy transition pathways are technically feasible, their deployment in North-East Nigeria is constrained by grid instability, security risks, financing gaps, weak institutional coordination, skills shortages, and uncertain industrial demand. Engineers are central to identifying and mitigating these risks through robust system design, modular and redundant architectures, lifecycle cost analysis, and strong standards and quality assurance. Effective engineering-leads risk management is therefore essential to making energy investments both bankable and sustainable.

A. Security Challenges

Security challenges are particularly significant in parts of the region and directly affect asset integrity, operations, and investor confidence. Engineers can mitigate these risks through resilient system design, including modular and containerized generation units that can be rapidly deployed, relocated, or replaced, hardened installations with tamper resistant enclosures and elevated mounting, and distributed architectures that limit single points of failure. Remote monitoring, automated fault isolation, and reduced on site staffing further enhance system survivability in volatile environments. Alongside lifecycle cost analysis, redundancy planning, and technology standardization, these engineering strategies are essential to delivering bankable, resilient energy systems capable of sustained operation under insecure conditions.

B. Financing constraints

Capital intensity of energy infrastructure and perceived project risks deter private finance. Engineers should work with financiers to de-risk projects using modular deployments, performance guarantees and demonstration projects that lower technology and business model risk. Public–private blended finance models are essential (Steckel and Jacob, 2018).

i. Policy uncertainty

Changing or unclear regulatory frameworks undermine long-term planning. Engineers serving on technical advisory committees can help align policies with operational realities and with standards required to mobilize private capital. (ECN, 2022)

j. Skills shortages and retention:

North-East institutions must be supported to produce and retain engineering personnel. Scholarships, industry-academic partnerships and local career paths for engineers in energy firms will mitigate brain drain. (Dafiel, 2025.)

k. Supply chain & quality concerns:

Without quality assurance, systems can fail early and raise costs. Investment in testing facilities and certification, combined with local assembly and after-sales service, reduces lifecycle costs and improves investor confidence (ECN, 2022).

7. POLICY RECOMMENDATIONS

Effective engineering led energy transition depends on a supportive policy and institutional environment. Policies influence investment incentives, standards, grid access, and decentralized integration, while institutions shape coordination, enforcement, and capacity building. Engineers strengthen policy effectiveness through evidence-based input into standards, grid codes, planning frameworks, and technical regulations. In the North-East, targeted policies are needed to support decentralized systems, derisk private investment, build local engineering capacity, and align energy planning with industrial development. Policies grounded in engineering realities improve implementation outcomes and accelerate both the energy transition and regional competitiveness.

A. Embed engineers in policy design

Create standing technical advisory panels composed of engineers (from academia, utilities and industry) at federal and state levels to vet project design and set realistic technical standards (United Nations Educational, Scientific and Cultural Organization, UNESCO 2010).

B. *Prioritize DRE and storage financing*

Use blended finance to scale mini-grids and BESS deployments in Northern states, supported by technical due diligence led by engineering teams (Anyaogu, 2025).

C. *Invest in regional engineering capacity*

Fund targeted scholarships, laboratory upgrades and curriculum modernization in northern universities and polytechnics focused on renewables, power systems and industrial energy management. (The Federal Government of Nigeria 2020).

D. *Support local manufacturing and standards*

Provide incentives for local assembly and establish national testing and certification centers for PV, inverters and batteries to raise product quality. (ECN, 2022).

E. *Pilot industrial decarbonization projects*

Co-fund pilots for industrial electrification, biomass heat or early hydrogen applications in northern industrial clusters, with rigorous monitoring and engineering oversight (United Nations Industrial Development Organization, UNIDO, 2023).

8. CONCLUSION

The engineering profession must be central to Nigeria's energy transition and the associated pursuit of industrial

ISBN: 978-978-8567-02-8

competitiveness, particularly in North-East Nigeria where technical capacity and infrastructure deficits are most acute. Engineers' work, from system design and storage integration to standards development and workforce training, will determine whether the ETP delivers inclusive economic development alongside deep decarbonization. With targeted policy support, appropriate finance mechanisms, and sustained investment in human capital, the North-East can become a productive arena for low carbon industrial growth that advances national objectives.

Urgent action is required to align these efforts with climate commitments and development timelines, as delays will raise costs, deepen regional disparities, and narrow the window for effective intervention.

ACKNOWLEDGEMENT

I want to use this opportunity to appreciate the support of the North-East Development Commission, for their support in making this manuscript a success.

REFERENCES

Abdulhameed, B. O., Nsafon, B. E. K., Roh, J. W., Suh, D., & Huh, J.-S. (2019). Validating the techno-economic and environmental sustainability of solar PV technology in Nigeria using RETScreen experts to assess its viability. *Sustainable Energy Technologies and Assessments, 36*. https://doi.org/10.1016/j.seta.2019.100542

Adebayo, A. V., & Ainah, P. K. (2024). Addressing Nigeria's electricity challenges: Past, present, and future strategies. *American Journal of Applied Sciences, 2*(5), 1–16. https://zenodo.org/recorhinads/12633012

Adeshina, M. A., Ogunleye, A. M., Suleiman, H. O., Yakub, A. O., Same, N. N., Suleiman, Z. A., & Huh, J.-S. (2024). From potential to power: Advancing Nigeria's energy sector through renewable integration and policy reform. *Sustainability, 16*(20), 8803. https://doi.org/10.3390/su16208803

Ajibola, A., Sodeinde, G. M., Aderemi, T. A., & Yusuf, M. O. (2022). Impact of electricity supply on the performance of small and medium-scale enterprises (SMEs) in Nigeria: A case study. *Economic Insights – Trends and Challenges, 10*(73), 11–21. https://doi.org/10.51865/EITC.2021.04.02

Anaele, E. O., Adelakun, O., Dem, I., & Barfa, G. I. (2014). Strategies for revitalizing the implementation of entrepreneurship education in technical, vocational education and training (TVET) to enhance self-employment in Nigeria. *British Journal of Education, 2*(4), 50–62. https://eajournals.org/wp-content/uploads/Strategies-for-Revitalizing-the-Implementation-of-Entrepreneurship-Education.pdf

Ayeni, A., & Hasan, M. M. (2025). A systematic review of the electricity supply value chain in Nigeria: Challenges and future trends. *Energy, Sustainability and Society, 15*(1). https://doi.org/10.1186/s13705-025-00527-x

Bawonda, F. I., & Adefarati, T. (2023). Evaluation of solar energy potential in six geopolitical regions of Nigeria using analytical and simulation techniques. *Energy Conversion and Management, 290*, 117193. https://doi.org/10.1016/j.enconman.2023.117193

Cole, M. A., Elliott, R. J. R., Occhiali, G., & Strobl, E. (2018). Power outages and firm performance in Sub-Saharan Africa. *Journal of Development Economics, 134*, 150–159. https://doi.org/10.1016/j.jdeveco.2018.05.003

Dafiel, G. P. (2024). Impact of migration on labour supply in engineering sectors: Legal and regulatory challenges in Nigeria. *International Journal of Research and Innovation in Social Science, 8*(3), 6233–6246. https://dx.doi.org/10.47772/IJRISS.2024.803466

Emezirinwune, M. U., Adejumobi, I. A., Adebisi, O. I., & Akinboro, F. G. (2024). Synergizing hybrid renewable energy systems and sustainable agriculture for rural development in Nigeria. *e-Prime - Advances in Electrical Engineering, Electronics and Energy, 7*. https://doi.org/10.1016/j.prime.2024.100492

Energy Commission of Nigeria. (2022). *National Energy Policy* (Revised ed.). https://energy.gov.ng/Energy_Policies_Plan/APPROVED_REVISED_NEP_2022.pdf

Energy Transition Office, Federal Republic of Nigeria. (n.d.). *Nigeria Energy Transition Plan (ETP)*. https://energytransition.gov.ng/

Eshiemogie, S. A., Aielumoh, P., Okamkpa, T., Jude, M. J. A., Efe, L., & Amenaghawon, A. N. (2024). A comparative analysis of Nigeria's power sector with and without grid-scale storage: Future implications for emission and renewable energy integration. *Scispace Journal Article* (arXiv:2410.15151). https://doi.org/10.48550/arxiv.2410.15151

Federal Government of Nigeria. (2020). *The Nigeria Agenda 2050*. https://faolex.fao.org/docs/pdf/nig217433.pdf

Fernandez, L. (2025). *Electricity Production in Nigeria*. Statista. Retrieved January 12, 2026, from https://www.statista.com/statistics/1294835/annual-electrical-energy-generation-in-nigeria/

Gold, K. L., Adetunji, K. O., Yusuf, H. A., & Sulaiman, S. (2024). Electricity production, consumption, and manufacturing sector performance in Nigeria: A multi-decade analysis. *Journal of Applied Economic Research, 23*(4), 1077–1098. https://doi.org/10.15826/vestnik.2024.23.4.042

Griffiths, S., Sovacool, B. K., Kim, J., Bazilian, M., & Uratani, J. M. (2021). Industrial decarbonization via hydrogen: A critical and systematic review of developments, socio-technical systems and policy options. *Energy Research & Social*

ISBN: 978-978-8567-02-8

Science, 80, 102208. https://doi.org/10.1016/j.erss.2021.102208

Idris, W. O., Ibrahim, M. Z., & Albani, A. (2024). Prospects of solar energy exploration in Nigeria: Assessments, economic viability and hybrid system. *International Journal of Energy Economics and Policy, 14*(2), 676–686. https://doi.org/10.32479/ijeep.14977

Ikwuoma, S. U., Amaechi, V. U., Njoku, C. S., & Olemeforo, E. I. (2024). Sustainable energy solutions: Opportunities and challenges in Nigeria. *International Journal of Scientific Engineering and Science, 8*(10), 112–130. https://ijses.com/wp-content/uploads/2024/11/124-IJSES-V8N10.pdf

Lawal, K. O., Gbadegesin, A. O., Aliyu, U. O., Nna, C. D., & Bakare, G. A. (2018). Design and evaluation of a micro-hydro power scheme for Evboroho II community in Edo State, Nigeria. In *Clemson University Power System Conference (PSC)* (pp. 202–212). IEEE. http://ieeexplore.ieee.org/stamp/stamp.jsp?tp=&arnumber=7462814&isnumber=7462813

National Electricity Regulation Commission. (2025, July 29). *State level electricity capacity and electricity consumption per capita in Nigeria* [LinkedIn update]. LinkedIn. Retrieved November 26, 2025, from https://www.linkedin.com/feed/update/urn:li:activity:7406576565267894272/

Onyeuche, E. (2023, November 15). Nigeria's energy transition plan and the power sector. *Business Day*. Retrieved November 26, 2025, from https://businessday.ng/energy/article/nigerias-energy-transition-plan-and-the-power-sector/

Salihu, M. K., Danladi, A., & Medugu, D. W. (2024). Regional-based potential assessment for solar photovoltaic generation in northern Nigeria. *Bulletin of the National Research Centre, 48*. https://doi.org/10.1186/s42269-024-01291-2

Steckel, J. C., & Jacob, M. (2018). The role of financing cost and de-risking strategies for clean energy investment. *Journal of International Economics, 15*, 19–28. https://doi.org/10.1016/j.inteco.2018.02.003

United Nations Educational, Scientific and Cultural Organization. (2010). *Engineering: Issues, challenges, and opportunities for development*. https://unesdoc.unesco.org/ark:/48223/pf0000189753

United Nations Industrial Development Organization, UNIDO (2023). Green Hydrogen Industrial Clusters Guidelines. https://www.unido.org/sites/default/files/unido-publications/2023-11/Green%20Hydrogen%20Industrial%20Clusters%20Guidelines.pdf

Worku, M. Y. (2022). Recent advances in energy storage systems for renewable source grid integration: A comprehensive review. *Sustainability, 14*(10), 5985. https://doi.org/10.3390/su14105985

World Bank. (2023). *Access to electricity (% of population)* [Data set]. Retrieved from https://data.worldbank.org/indicator/EG.ELC.ACCS.ZS

World Economic Forum. (2022). *Fostering effective energy transition* (2022 ed.). https://www.weforum.org/publications/fostering-effective-energy-transition-2022/in-full/1-the-energy-transition-under-pressure/

ISBN: 978-978-8567-02-8

037-Development of A Bench-Scale Plastic Injection Molding Machine

H. Muhammad[1] U. Aminu[2] Y. Saad[3], M. Yusuf[4] B.A Hassan[5] M. Ahmad[6] U. F Lawal[7]
[1,2,3,4,5] *Nuhu Bamalli Polytechnic, Zaria, Kaduna State, Nigeria.*
[6]*Bayero University Kano, Kano State, Nigeria*
[7]*Aliko Dangote University of Science and Technology, Wudil, KanonState, Nigeria.*

Corresponding author: hmabbasss@email.com

Abstract: The development of a bench-scale plastic injection molding machine is presented in this paper with the aim of providing a compact, affordable, and functional alternative to industrial-scale systems for academic, research, and small-scale industrial applications. The machine was designed, fabricated, and tested using locally available materials to reduce cost and enhance accessibility. Major subsystems include a plunger-based injection unit, electrically heated barrel, manual clamping mechanism, and microcontroller-based temperature control system. Performance evaluation was conducted based on heating efficiency, injection pressure, cycle time, and quality of molded products. Experimental results show that the machine can process common thermoplastics such as polypropylene and polyethylene at temperatures between 180–250 °C, achieving optimal molding quality at injection pressures of 40–48 bar. The developed system demonstrates reliable performance suitable for laboratory-scale prototyping, training, and low-volume production, thereby bridging the gap between theoretical instruction and industrial practice.

Ke**ywords:** Bench-scale machine, Injection molding, Polymer processing, Prototyping, Local fabrication

1. INTRODUCTION

One of the most popular manufacturing techniques for creating plastic parts with intricate geometries, great dimensional accuracy, and repeatability is injection molding (Rosato & Rosato, 2012; Osswald & Turng, 2019). Thermoplastics are melted, then the liquid polymer is injected under pressure into a closed mold chamber, where it cools and forms into the required shape. Although industrial injection molding machines are very effective, they are usually costly, large, and energy-intensive, which makes them inappropriate for small businesses, research facilities, and academic labs (Strong, 2016; Malloy, 2011).

Polymer processing is mostly limited to theoretical education in poor nations like Nigeria due to expensive import costs, inadequate infrastructure, and maintenance issues that further restrict access to industrial injection molding equipment (Wirth, 2023). By reproducing essential industrial processes in a small system, bench-scale injection molding machines provide a useful, affordable solution that permits practical training, research, and low-volume prototype (Mutsuddy & Ford, 1995).

The design, construction, and testing of a locally produced bench-scale plastic injection molding machine with sufficient performance, safety features, and dependability for laboratory-scale instructional and prototyping applications are the main objectives of this study. It makes use of readily available materials and components.

2.0 METHODOLOGY

2.1 Design Considerations

Cost-effectiveness, portability, simplicity of use, dependability, and safety were priorities in the machine's design (Rosato & Rosato, 2012; Osswald & Turng, 2019). To simplify the system, lower manufacturing costs, and limit mechanical complexity while preserving functional efficiency equivalent to larger industrial units, a vertical, plunger-based injection mechanism was used (Strong, 2016; Wirth, 2023). In a lab or prototyping setting, this arrangement also makes installation, maintenance, and operator training simple.

2.2 Selection of Materials

The major components of the bench-scale injection molding machine and their material selection are presented in Table 2.1.

2.3 Description of the Machine

The developed bench-scale injection molding machine consists of a heated cylindrical barrel fitted with a manually operated plunger that forces molten polymer into the mold cavity. Cartridge heaters mounted on the barrel provide controlled heating, while thermocouples supply real-time temperature feedback to a microcontroller-based temperature controller.

A manual toggle clamping mechanism is employed to hold the mold halves securely during injection and cooling, preventing material leakage and mold separation. The control system incorporates a pressure gauge for monitoring injection pressure and electrical safety components housed within a grounded control

ISBN: 978-978-8567-02-8

panel. All components are mounted on a rigid welded mild-steel frame to ensure structural integrity, operational stability, and operator safety.

TABLE 2.1: MATERIAL SELECTION FOR MACHINE COMPONENTS

Component	Material Used	Justification
Frame and housing	Mild steel	High strength, availability, low cost
Barrel and nozzle	Hardened steel	Thermal and wear resistance
Plunger	High-carbon steel	Strength and durability
Heating elements	Cartridge heaters	Efficient and uniform heating
Sensors	Thermocouples	Accurate temperature measurement

Figure 2.1 presents schematic diagram of the bench-scale plastic injection molding machine showing the hopper, heated barrel, plunger mechanism, mold assembly, clamping unit, and control system. This figure is an original schematic developed by the authors for this study

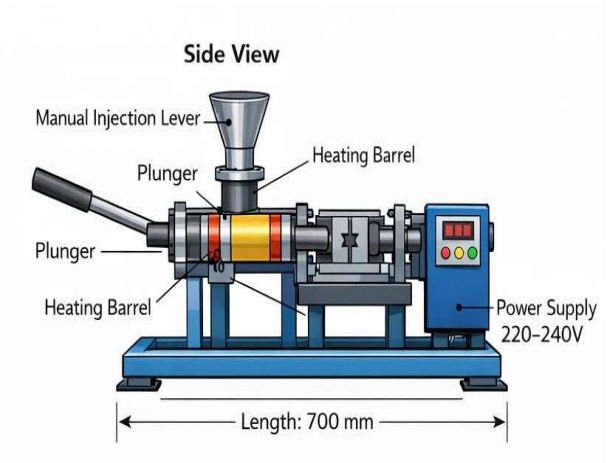


Figure 2.1: Schematic Diagram of the Bench-Scale Plastic Injection Molding Machine

3.1 Fabrication Process

The machine frame was fabricated from mild-steel angle bars and flat plates cut to size and joined using electric arc welding. Welded joints were ground smooth and coated with anti-rust paint to improve durability and safety.

The injection barrel was machined from thick-walled steel tubing using turning, boring, and honing operations to obtain a smooth internal surface and minimize friction during plunger motion. The plunger was machined to close tolerances to reduce molten polymer leakage. Cartridge heaters and thermocouples were installed on the barrel to ensure efficient heat transfer and accurate temperature control.

The mold assembly was fabricated from tool steel using milling, drilling, and cavity-forming operations. Polishing of the mold cavity surfaces improved surface finish of molded parts, while guide pins and bushings ensured accurate alignment of mold halves. A manual toggle clamping mechanism made from steel links and levers was assembled to provide sufficient clamping force during injection. Final assembly involved careful alignment of the barrel, plunger, and mold chamber to minimize wear and leakage.



Figure 2: *Fabrication and Assembly Stages of the Injection Molding Machine*

Figure 2.2: Fabrication and assembly stages of the injection molding machine, including frame welding, barrel machining, heater installation, and final assembly

Testing Procedure

Performance evaluation was carried out by subjecting the machine to a series of controlled tests. The barrel was heated to preset temperatures while temperature stability was monitored using thermocouples and the control system. Polypropylene (PP) and polyethylene (PE) pellets were injected under varying plunger forces. Molded products were inspected for surface finish, dimensional accuracy, and defects such as flash, voids, and short shots. Observations were recorded across different heating profiles and applied forces.

2.5 Design Equations

The following equations were applied in the design and performance evaluation:

l. Injection Pressure and Plunger Force

m. *Injection Pressure is determined by (Srong A.B 2006):*

$$F = P \times A \qquad 1$$

Where:

P = Injection pressure (Pa)

ISBN: 978-978-8567-02-8

F = Applied plunger force (N)

A = Cross-sectional area of barrel (m²)

Cross section area:

$$V = \frac{\pi D^2 L}{4} \quad 2$$

Where: - D = Internal diameter of barrel (m)

i. *Plunger Force (Groover M.P 2015):*

$$F = mg \quad 3$$

Where: - m = Applied mass on plunger (kg)

g = Acceleration due to gravity (9.81 m/s²) Shot Volume and Shot Weight

ii. *Shot Volume*

iii. $\boldsymbol{V_s = A \times L}$ *4*

Where: -

V_s*= Shot volume (m³)*

L = Plunger stroke length (m)

iv. *Shot Weight*

v. $\boldsymbol{w_s = \rho v s}$ *5*

Where: -

w_s *= Shot weight (N)*

ρ = Density of polymer (kg/m³)

n. *Heating System Design*

i. *Heat Required to Melt Plastic (Incropera et al., 2011):*

ii. $\boldsymbol{Q = mc\Delta T}$ *6*

Where: -

Q = Heat energy required (J)

m = Mass of plastic (kg)

c = Specific heat capacity of polymer (J/kg·K)

ΔT = Temperature rise (K)

iii. *Heater Power Requirement*

$$P = \frac{Q}{t} \quad 7$$

Where: - P = Heater power (W)

t = Heating time (s)

iv. *Temperature Stability*

v. $\boldsymbol{\Delta T = T_{max} - T_{min}}$ *8*

o. *Clamping Force Requirement (Kalpakjian & Schmid, 2014)*

$$f_c = P \times A_m \quad 9$$

Where: -

f_c*= Required clamping force (N)*

A_m *= Projected mold cavity area (m²)*

p. *Cycle Time Analysis*

$$T_C = T_h + T_i + T_{cool} + T_e \quad 10$$

Where: -

T_c *= Total cycle time (s)*

T_h *= Heating time (s)*

T_i *= Injection time (s)*

T_{cool}*= Cooling time (s)*

T_e *= Ejection time (s)*

q. *Cooling Time Estimation*

$$T_{cool} = \frac{t^2}{\alpha} \quad 11$$

Where: -
t = Maximum wall thickness of molded part (m)

α = Thermal diffusivity of polymer (m²/s)

C. *Shrinkage Estimation (Kalpakjian S. and Schmid S.R (2014)*

$$\boldsymbol{S = \frac{D_m - D_p}{D_m}} \quad 12$$

Where: -

S = Shrinkage ratio

D_m*= Mold dimension*

D_p *= Final part dimension*

ISBN: 978-978-8567-02-8

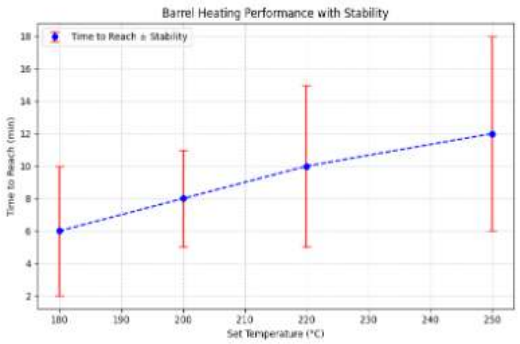
3.0 RESULTS AND DISCUSSION

3.1 Heating Performance

The heating system reached processing temperatures of 180–250 °C within 6–12 minutes. Temperature stability was maintained within ±3–6 °C.

Table 3.1: Barrel Heating Performance

Set Temperature (°C)	Time to Reach (min)	Stability (±°C)	Observation
180	6	±4	Suitable for PE
200	8	±3	Stable for PP
220	10	±5	Minor fluctuation
250	12	±6	High variation



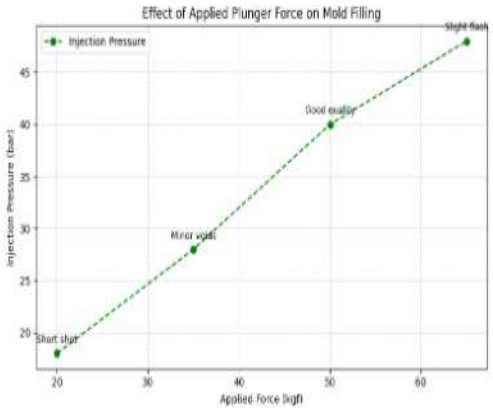
A graph of time(s) vs temperature (°C)

3.2 Injection Pressure and Mold Filling

Optimal mold filling was achieved at injection pressures between 40–48 bar.

TABLE 3.2: INJECTION PRESSURE PERFORMANCE

Applied Force (kgf)	Pressure (bar)	Mold Filling	Observation
20	18	Partial	Short shot
35	28	Nearly full	Minor voids
50	40	Full	Good quality
65	48	Full	Slight flash



A graph of injection pressure (bar) against Applied force (N)

3.3 Cycle Time

The average cycle time ranged from 7–13 minutes.

TABLE 3.3: AVERAGE CYCLE TIME

Stage	Time (s)
Heating	360–720
Injection	15–20
Cooling	30–40
Ejection	10–15

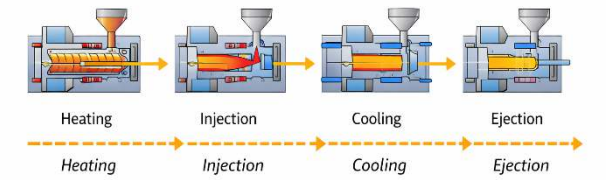


Figure 3: *Typical Injection Molding Cycle for the Developed Machine*

Figure 3.1: Typical Injection Molding Cycle for the Developed Machine (Bryce D.M 1996). The figure illustrates the sequence of heating, injection, cooling, and ejection stages.

3.4 Product Quality

Molded specimens exhibited acceptable dimensional accuracy and surface finish.

TABLE 3.4: QUALITY ASSESSMENT OF MOLDED PARTS

Parameter	Result	Remark
Dimensional accuracy	±0.5–1.0 mm	Acceptable
Surface finish	Smooth	Minor marks
Shrinkage	Minimal	Controlled
Defects	Occasional flash	Pressure-related

ISBN: 978-978-8567-02-8



Figure 3.2 shows representative plastic specimens molded using the developed bench-scale machine.

3.5 DISCUSSION

The performance of the developed bench-scale plastic injection molding machine was evaluated in terms of heating behavior, injection pressure capability, cycle time, and quality of molded products. The results obtained demonstrate that the machine is capable of replicating key features of industrial injection molding processes at a reduced scale, making it suitable for laboratory and instructional use.

3.5.1 Heating Performance

The heating system achieved operating temperatures between 180 and 250 °C within 6–12 minutes. Temperature stability was maintained within ±3–6 °C, which is acceptable for processing common thermoplastics such as polyethylene and polypropylene. Minor temperature fluctuations observed at higher setpoints were attributed to heat losses through the barrel surface and the absence of advanced insulation. Nevertheless, the achieved stability range is sufficient for educational and prototyping applications where precise industrial-level thermal control is not critical.

3.5.2 Injection Pressure and Mold Filling

Effective mold filling was obtained at injection pressures ranging from 40 to 48 bar. At lower pressures, incomplete filling and short shots were observed, while pressures above this range occasionally resulted in flash due to excess material flow. These observations are consistent with injection molding theory and highlight the importance of proper pressure selection. Compared with industrial machines, which typically operate at much higher pressures, the lower pressure range of the developed system reflects its bench-scale nature while remaining adequate for simple mold geometries and low-volume production.

3.5.3 Cycle Time

Average cycle times ranged from 7 to 13 minutes, with the heating stage accounting for the largest proportion of the total cycle time. This relatively long heating period is mainly due to the manual operation and limited heater capacity used to minimize cost. Although the cycle time is longer than that of industrial injection molding machines, it is acceptable for laboratory demonstrations, student training, and prototyping, where throughput is less critical than process understanding.

3.5.4 Product Quality

Molded specimens exhibited acceptable dimensional accuracy (±0.5–1.0 mm), smooth surface finish, minimal shrinkage, and only minor pressure-related flash in some cases. The quality of the molded parts indicates that the machine can reliably produce components suitable for instructional use and functional prototypes. Limitations observed include occasional surface marks and flash, which could be reduced through improved mold design, better temperature uniformity, and automated clamping in future iterations.

Overall, the results confirm that the locally fabricated bench-scale injection molding machine provides a practical balance between performance, cost, and simplicity. While it does not match the productivity of industrial systems, it effectively fulfills its intended role as an educational, research, and prototyping tool, particularly in resource-limited environments.

4. CONCLUSION

This study successfully designed, fabricated, and tested a bench-scale plastic injection molding machine using locally available materials and straightforward manufacturing techniques. The developed machine demonstrated stable thermal performance within the processing range of 180–250 °C, achieved effective mold filling at injection pressures of 40–48 bar, and produced molded components with acceptable dimensional accuracy and surface finish. These outcomes confirm that the machine is capable of replicating essential injection molding operations at a reduced scale suitable for laboratory environments.

The results highlight the practicality of locally fabricated bench-scale equipment as a cost-effective alternative to imported industrial machines, particularly for engineering education, skills development, research, and low-volume prototyping in resource-limited settings. By enabling hands-on exposure to polymer processing, the machine bridges the gap between theoretical instruction and real-world manufacturing practice.

Future work may focus on improving system performance through the incorporation of automated clamping mechanisms, enhanced thermal insulation to reduce heating time, and integration of digital data acquisition for process monitoring. Such enhancements would further extend the machine's applicability for advanced research and specialized training purposes.

4 ACKNOWLEDGMENTS

ISBN: 978-978-8567-02-8

Authors would like to express their gratitude to the Department of Mechanical Engineering at Nuhu Bamalli Polytechnic in Zaria for providing the workshop space, tools, and technical support needed for the injection molding machine's construction, installation, and testing. The Tertiary Education Trust Fund (TETFund) provided financial sponsorship and research support that enabled this effort, for which the authors are really grateful.

REFERENCES

Bryce, D. M. (1996). *Plastic injection molding: Manufacturing process fundamentals.* Society of Manufacturing Engineers.

Groover, M. P. (2015). *Fundamentals of modern manufacturing: Materials, processes, and systems* (5th ed.). John Wiley & Sons.

Incropera, F. P., DeWitt, D. P., Bergman, T. L., & Lavine, A. S. (2011). *Fundamentals of heat and mass transfer* (7th ed.). John Wiley & Sons.

Kalpakjian, S., & Schmid, S. R. (2014). *Manufacturing engineering and technology* (7th ed.). Pearson Education.

Malloy, R. A. (2011). *Plastic part design for injection molding*. Hanser Publishers.

Mutsuddy, B. C., & Ford, R. W. (1995). *Ceramic injection molding*. Springer.

Osswald, T. A., & Turng, L. S. (2019). *Polymer processing: Modeling and simulation*. Hanser Publishers.

Osswald, T. A., Turng, L. S., & Gramann, P. J. (2008). *Injection molding handbook*. Hanser Publishers.

Rosato, D. V., Rosato, M. G., & Rosato, D. V. (2000). *Injection molding handbook* (3rd ed.). Springer.

Rosato, D. V., & Rosato, D. V. (2012). *Injection molding handbook*. Springer.

Strong, A. B. (2006). *Plastics: Materials and processing* (3rd ed.). Pearson Prentice Hall.

Strong, A. B. (2016). *Plastics: Materials and processing* (4th ed.). Pearson Education.

Wirth, D. M. (2023). Fabrication of an inexpensive bench-top injection molding instrument. *Polymer Testing*, 118

ISBN: 978-978-8567-02-8

038-Clay-Based Ceramic Membranes for Oily Wastewater Treatment: Materials, Performance, and Future Prospects

M. Abubakar[1], A.B. Aliyu[1], and D. Garba[2*]

[1]Department of Mechanical Engineering, Faculty of Engineering, Bayero University, Kano.

[2] Department of Welding and Fabrication Engineering, Kano State Polytechnic, Kano.

engr.dgarba@kanopoly.edu.ng

Abstract: The growth of the oil milling industry has led to an increase in the discharge of oily wastewater, which contains oils, greases, suspended solids, and persistent pollutants. Conventional treatment methods are often costly, inefficient, and ineffective for emulsified oils. In contrast, membrane technology offers a compact and efficient solution. Clay-based ceramic membranes are emerging as low-cost and sustainable alternatives. These membranes, made from abundant clays like kaolin and bentonite, possess high thermal stability, mechanical strength, and adjustable porosity. This study reviews various fabrication methods, characterization techniques, and performance metrics, including flux, oil rejection, chemical oxygen demand (COD) reduction, and fouling resistance. Comparisons with polymeric and oxide-based ceramic membranes highlight the advantages of clay membranes in terms of affordability and durability. The paper also discusses challenges, including variability in raw materials and energy-intensive sintering processes, and outlines prospects for future research. Clay-based membranes offer a viable and eco-friendly approach to treating industrial oily wastewater, contributing to **sustainable water management and supporting SDG 3, SDG 6, and SDG 12**

Keywords: Clay-based ceramic membranes, palm oil mill effluent (POME), oily wastewater treatment, permeate flux, and COD reduction

1. INTRODUCTION

The global oil mill industry, encompassing palm oil, olive oil, and other edible oils, plays a vital role in food production and economic growth. However, its rapid expansion has generated serious environmental challenges, primarily from the discharge of oily wastewater called oil mill wastewater (OMW) or palm oil mill effluent (POME). This effluent is highly polluted, containing large concentrations of oils, greases, suspended solids, and organic matter, which result in elevated biochemical oxygen demand (BOD) and chemical oxygen demand (COD) levels. If inadequately treated, OMW poses severe threats to aquatic ecosystems, soil quality, and public health (Ahmad et al., 2022; Vijaya et al., 2018). Conventional treatment methods such as ponding, anaerobic digestion, and biological oxidation have been widely used but suffer from limitations including large land requirements, high sludge production, and reduced efficiency at high pollutant loads (Bashir et al., 2020; Choudhury et al., 2023). Consequently, there is a growing need for more efficient and sustainable treatment technologies capable of meeting increasingly stringent environmental regulations. Membrane technology has emerged as a promising alternative, offering compact design, high selectivity, and potential for water recovery and reuse. Pressure-driven membrane processes such as microfiltration (MF), ultrafiltration (UF), nanofiltration (NF), and reverse osmosis (RO) have shown excellent removal efficiencies, with reported oil rejections exceeding 95% and COD reductions up to 99% (Al-Aseeri et al., 2020). However, most polymeric membranes suffer from fouling, limited thermal stability, and short lifespan, while advanced oxide-based ceramic membranes, though more robust, are costly due to expensive raw materials and energy-intensive sintering (Li et al., 2019; Hubadillah et al., 2018). Recently, clay-based ceramic membranes have gained significant attention as cost-effective and sustainable alternatives. Derived from naturally abundant materials such as kaolin, bentonite, and ball clay, these membranes exhibit good thermal and chemical stability, tunable porosity, and strong mechanical strength at relatively low fabrication cost (Musa et al., 2021; Abubakar & Ahmad, 2023). Their performance in treating oily wastewater has been reported to be comparable to that of polymeric and oxide-based ceramic membranes, making them promising candidates for industrial wastewater treatment in resource-limited regions. Despite their potential, several challenges remain, including raw material variability, membrane fouling, and the trade-off between mechanical strength and porosity. Addressing these issues requires continuous research into standardizing

ISBN: 978-978-8567-02-8

clay processing, optimizing sintering parameters, and developing antifouling strategies.

Therefore, this paper aims to review and synthesize the advancements in developing and applying clay-based membranes for oily wastewater treatment. It highlights their materials, fabrication methods, characterization, performance evaluation, and comparative advantages, while proposing future research directions aligned with the United Nations Sustainable Development Goal 6 Clean Water and Sanitation.

2. MEMBRANE TECHNOLOGY FOR WASTEWATER TREATMENT

2.1 Overview of Membrane Technology

Membrane technology has emerged as one of the most advanced and flexible approaches for industrial and municipal wastewater treatment. Unlike conventional methods, which depend on extensive land area, high retention times, and multiple chemical or biological stages, membrane systems offer compact designs, high separation efficiency, and modular scalability (Mulder, 2012; Shon et al., 2013). These systems can effectively treat complex wastewater streams with minimal sludge generation, making them crucial for sustainable water reuse and pollution control.

Membrane separation operates on the principle of selective permeability, where a semipermeable barrier allows specific components (the permeate) to pass through while retaining others (the reject). The mechanism of separation depends on factors such as molecular size, charge, and hydrophilicity. Pressure-driven processes dominate wastewater applications due to their operational simplicity and scalability.

2.2 Classification of Pressure-Driven Membrane Processes

TABLE 1 PRESSURE-DRIVEN MEMBRANE SYSTEMS ARE CATEGORIZED BASED ON PORE SIZE AND OPERATIONAL PRESSURE:

Process	Pore Size Range (µm)	Pressure (bar)	Target Contaminants	Advantages	Limitations
Microfiltration (MF)	0.1–10	0.1–2	Suspended solids, bacteria, and large oil droplets	Low pressure, simple operation	Ineffective for dissolved solutes
Ultrafiltration (UF)	0.01–0.1	1–5	Emulsified oils, colloids, macromolecules	High oil removal (>95%)	Fouling, limited salt removal
Nanofiltration (NF)	0.001–0.01	4–30	Divalent ions, organics, color	High COD reduction, moderate energy	Higher cost, fouling
Reverse Osmosis (RO)	<0.001	10–80	Dissolved salts, organics	Produces high-quality water	High energy demand, fouling

Recent studies have also investigated forward osmosis (FO) and membrane distillation (MD) as emerging alternatives due to their lower energy consumption and high rejection capabilities (Lee et al., 2018).

2.3 Classification of Membrane Materials

Membrane performance depends strongly on the materials used. The three principal material categories include:

a. Polymeric Membranes:

Fabricated from polymers such as polyvinylidene fluoride (PVDF), polysulfide (PSf), polyether sulfone (PES), and cellulose acetate, polymeric membranes are widely used due to low production cost and flexibility. However, they suffer from limited chemical and thermal stability and are highly prone to fouling during oily wastewater treatment (Li et al., 2019).

b. Oxide-Based Ceramic Membranes:

Composed of metal oxides such as alumina, zirconia, or titania, ceramic membranes exhibit excellent mechanical strength, thermal resistance, and long operational lifetimes. Their major drawback lies in high fabrication costs, as they require high-purity raw materials and energy-intensive sintering above 1200 °C (Zhou et al., 2020).

c. Hybrid and Composite Membranes:

These combine two or more materials—such as polymer–ceramic composites or thin-film nanocomposites to enhance antifouling properties, hydrophilicity, and pollutant rejection. Such modifications aim to strike a balance between the advantages of cost and performance (Ng et al., 2013).

2.4 Applications of Membrane Technology in Wastewater Treatment

Membrane systems have been extensively applied in various industrial sectors, including textile processing, petrochemicals, tanneries, and food industries (Shirazi et al., 2014). In oily wastewater treatment, their ability to separate oil–water emulsions efficiently make them particularly valuable. Studies report:

MF and UF are achieving oil rejections above 95%, effectively removing suspended solids and emulsified oil.

NF and RO provide polishing treatment to achieve >99% reduction in COD, turbidity, and oil and grease (Ahmad et al., 2022).

Hybrid processes integrating adsorption, coagulation, or advanced oxidation to enhance flux recovery and extend membrane life (Choudhury et al., 2023).

Ceramic membranes, in particular, demonstrate superior durability and fouling resistance compared to polymeric ones, making them well suited for oily wastewater applications (Musa et al., 2021).

2.5 Advantages and Limitations of Membrane Technology

Advantages:

- High separation efficiency and selectivity
- Compact, modular design with small footprint

ISBN: 978-978-8567-02-8

- Potential for water recovery and reuse
- Minimal chemical requirements and sludge generation

Limitations:

- Membrane fouling and scaling during operation
- High energy consumption for NF/RO systems
- High capital cost for oxide-ceramic membranes

These constraints have motivated research into low-cost alternatives such as clay-based ceramic membranes, which can combine the durability of ceramics with the affordability of natural raw materials.

3 MATERIALS AND METHODS

3.1 Overview

The fabrication of clay-based ceramic membranes involves a sequence of carefully controlled stages designed to ensure structural integrity, optimized porosity, and effective separation performance. This study focuses on the development, characterization, and performance evaluation of clay-based membranes using naturally available clays such as kaolin, bentonite, and ball clay. The major stages include raw material preparation, membrane formation, drying, sintering, and subsequent physicochemical and microstructural characterization.

3.2 Raw Materials

Natural clay minerals were selected due to their local availability, cost-effectiveness, and favorable physicochemical properties. The commonly employed clays include:

Kaolin ($Al_2Si_2O_5(OH)_4$): A non-swelling clay with high refractoriness and fine particle size. Upon sintering, kaolin transforms into mullite, improving the membrane's mechanical and thermal stability (Abu Bakar et al., 2018).

Bentonite: A swelling clay dominated by montmorillonite, offering high plasticity and cation-exchange capacity. When incorporated into the membrane matrix, it enhances formability, adsorption capacity, and mechanical strength (Aloulou et al., 2020).

Ball Clay: Fine-grained and highly plastic, often blended with kaolin to improve shaping characteristics (Abubakar et al., 2020).

Local/Indigenous Clays: Locally sourced clays provide an economical and sustainable alternative, reducing dependence on imported materials and supporting circular economy practices (Yakubu et al., 2022).

The typical oxide composition of clays includes SiO_2, Al_2O_3, Fe_2O_3, CaO, MgO, and alkali oxides (K_2O, Na_2O). The proportion of these oxides determines the sintering temperature, porosity, and mechanical strength of the final membrane.

3.3 Membrane Fabrication Process

The fabrication of clay-based membranes involves four major steps: raw material preparation, shaping, drying, and sintering.

Raw clay → grinding/sieving → pore former addition → shaping (pressing/extrusion) → drying → sintering → finished membrane

Figure 1. Fabrication pathway of clay-based ceramic membranes

3.3.1 Raw Material Preparation

The raw clay was first dried to remove moisture, ground, and sieved (typically <100 μm) to obtain a homogeneous fine powder. Additives such as starch, sawdust, or rice husk ash were incorporated as pore formers to tailor the membrane's porosity and permeability (Jabbari et al., 2017). The prepared powder mixture was homogenized using a planetary mixer to ensure even distribution of components.

3.3.2 Shaping and Forming

Different forming methods were employed depending on the intended membrane configuration:

Uniaxial Hydraulic Pressing: Used to produce flat-sheet membranes with uniform thickness and density.

Extrusion: Suitable for fabricating tubular or multichannel membranes, providing a high surface-area-to-volume ratio for industrial-scale modules.

Slip or Tape Casting: Employed for thin-layer membrane formation, particularly in multilayer systems.

In each case, the shaped green membranes were allowed to stand under controlled conditions to relieve internal stresses and prevent cracking during drying.

3.3.3 Drying

The shaped membranes were dried gradually in an oven at 100–110°C for 12–24 hours to remove residual moisture. Controlled drying was essential to prevent warping or cracking, especially in samples with high plasticity or organic pore formers.

3.3.4 Sintering

The dried green membranes were fired in an electric furnace between 600°C and 1000°C, depending on the clay composition. Sintering promotes densification, removal of pore formers, and phase transformations such as:

Dehydroxylation of kaolinite → metakaolinite (550–600 °C)

Formation of mullite and vitreous phases (950–1000°C)

The final sintered membranes were allowed to cool slowly to avoid thermal shock. The optimized sintering temperature (700–900°C) was found to balance porosity, mechanical strength, and flux performance (Abubakar & Ahmad, 2023).

ISBN: 978-978-8567-02-8

3.4 Characterization of Clay-Based Membranes

The fabricated membranes were subjected to extensive characterization to evaluate their physicochemical, microstructural, thermal, and mechanical properties.

3.4.1 Physicochemical Analysis

X-ray Fluorescence (XRF): Used to determine the elemental oxide composition (SiO_2, Al_2O_3, Fe_2O_3, CaO, MgO, Na_2O, and K_2O). These elements influence sintering behavior and stability (Barbosa et al., 2020).

X-ray Diffraction (XRD): Identified crystalline phases in both raw and sintered samples, tracking the transformation from kaolinite to mullite. The presence of mullite indicates enhanced strength and thermal stability (Hafiza et al., 2021).

Fourier Transform Infrared Spectroscopy (FTIR): Confirmed structural changes and dehydroxylation behavior during sintering (Abubakar & Ahmad, 2023).

3.4.2 Microstructural and Morphological Analysis

Scanning Electron Microscopy (SEM): Examined surface morphology, pore distribution, and grain connectivity (Jafari et al., 2020)

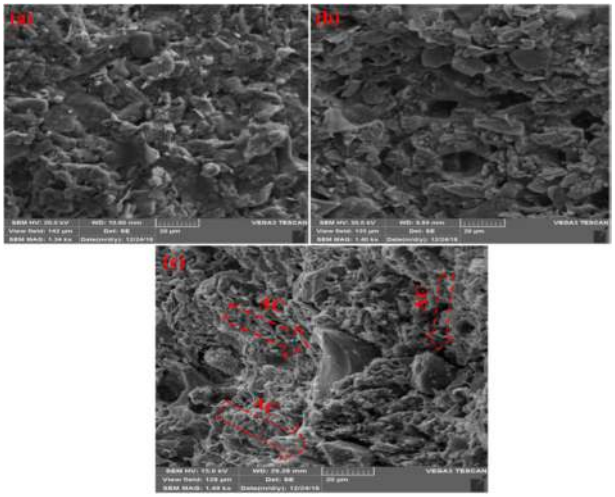


Figure 2. SEM micrograph of surface ceramic membranes. (a) Mullite, (b) Mullite-Zeolite, (c) Mullite-Zeolite-AC.

Energy-Dispersive X-ray Spectroscopy (EDS): Complemented SEM by identifying localized elemental compositions.

Atomic Force Microscopy (AFM): Provided nanoscale surface roughness data, influencing fouling behavior and wettability.

3.4.3 Thermal and Phase Behavior

Thermal stability was investigated using:

Thermogravimetric Analysis (TGA) to identify weight loss due to dehydration and dihydroxylation.

Differential Thermal Analysis (DTA) to observe phase transitions such as the exothermic formation of mullite.

High-temperature XRD for in-situ monitoring of phase evolution during firing (Oun et al., 2020).

3.4.4 Mechanical Properties

Mechanical strength was evaluated through:

Flexural and Compressive Strength Tests to assess mechanical robustness.

Fracture Toughness measurements to determine resistance to cracking.
Mechanical performance was correlated with sintering temperature and porosity, showing an inverse relationship between flux and strength (Alomair et al., 2022).

3.4.5 Porosity and Pore Size Distribution

Porosity and pore size directly affect membrane flux and selectivity.

Archimedes' Method was used to estimate bulk porosity.

BET surface area analysis determined pore size distribution.
Optimal membranes showed 25–35% porosity and pore diameters in the ultrafiltration range (0.01–0.1 µm), providing high flux and oil rejection (Abubakar & Ahmad, 2023).

3.4.6 Surface and Fouling Properties

Contact Angle Measurement evaluated hydrophilicity, with lower contact angles indicating better water wettability and reduced oil fouling.

Zeta Potential Analysis determined surface charge, where negative potential enhances oil droplet repulsion (Jiang et al., 2018).

AFM/SEM Roughness Analysis revealed that smoother and hydrophilic surfaces resist fouling more effectively.

4. RESULTS AND DISCUSSION

4.1 Overview

Clay-based ceramic membranes are effective in treating oily wastewater, with performance indicators including permeate flux, rejection efficiency, fouling resistance, and mechanical/chemical stability. This section analyzes their performance against polymeric and advanced oxide-based membranes, considering factors like sintering temperature, porosity, and operational conditions.

4.2 Permeate Flux

Permeate flux, the flow rate per unit area, is crucial for productivity. Clay-based ultrafiltration membranes exhibit fluxes of 50 to 120 $L \cdot m^{-2} \cdot h^{-1}$ at moderate pressures (1–2 bar). Key insights include:

Sintering Temperature: Increases in flux are seen up to 900°C; beyond this, excessive densification reduces permeability.

Operational Trends: Continuous operation leads to flux decline due to fouling, but cleaning can restore 80–90% of the initial flux. Optimal sintering temperatures are 700–900°C.

ISBN: 978-978-8567-02-8

4.3 Rejection Efficiency

Membrane rejection efficiency is vital for contaminant retention, showing:

Oil and Grease (O&G) Removal: >95%

Turbidity and TSS Removal: 90–99%

COD Reduction: 70–90%

These efficiencies arise from small pore sizes (0.01–0.1 μm) and surface charge repulsion.

4.4 Fouling Behavior, Resistance, and Microstructural Influence

Fouling, which is the buildup of oil, organic matter, and particles on membrane surfaces, remains a significant challenge in membrane-based wastewater treatment. In the studies reviewed, clay-based ceramic membranes consistently show better resistance to fouling compared to polymeric membranes. This superior performance is largely due to their inherently hydrophilic surfaces and chemically stable structures.

Microstructure and composition are crucial factors in determining fouling behavior. Generally, higher Si/Al ratios enhance both porosity and permeate flux. Additionally, the presence of moderate amounts of fluxing oxides, such as K_2O, Na_2O, and CaO, can facilitate sintering at lower temperatures, which promotes the development of interconnected pore networks. According to SEM observations reported in the literature (Jafari et al., 2020), this type of interconnected porosity is associated with improved flux and a reduced tendency for fouling. However, an excessive number of fluxing oxides may result in over-densification, which can decrease permeability and increase susceptibility to fouling.

Reversible fouling can often be reduced through physical or chemical cleaning methods; however, irreversible fouling may occur with prolonged operation. Surface modifications, such as incorporating graphene oxide or zeolite, have been widely studied for their ability to enhance antifouling performance by increasing surface hydrophilicity and decreasing oil adhesion. Implementing periodic cleaning along with an optimized microstructural design can significantly extend the lifespan of membranes and maintain stable flux.

4.5 Mechanical and Chemical Stability

Clay-based ceramic membranes are known for their strong mechanical integrity and chemical stability, even under demanding operating conditions. Studies have shown that these membranes experience minimal degradation after undergoing multiple backwashing cycles and prolonged exposure to challenging environments, such as oily, saline, or chemically aggressive wastewaters. The formation of stable crystalline and glassy phases during the sintering process enhances their resistance to cracking, abrasion, and chemical attack.

These characteristics make clay-based membranes especially suitable for long-term and industrial-scale applications, where durability and low maintenance are essential. Their ability to endure harsh environments sets them apart from polymeric alternatives, which often face issues like thermal deformation and chemical degradation.

4.6 Comparative Analysis of Membrane Types

A comparative assessment of polymeric, oxide-based ceramic, and clay-based ceramic membranes highlights clear trade-offs among performance, cost, durability, and sustainability.

Membrane Type	Performance	Cost	Durability	Sustainability
Polymeric Membrane	High oil rejection (>95%) but low fouling resistance and short lifespan	Low	Poor thermal/chemical stability	Moderate (low initial cost but frequent replacement)
Oxide-Based Ceramic Membrane	Excellent flux and >99% rejection; high fouling resistance	Very High	Excellent	Low (energy-intensive, expensive raw materials)
Clay-Based Ceramic Membrane	>95% O&G removal, 70–90% COD reduction, moderate flux	Low–Moderate	High thermal and chemical stability	High (uses local materials, lower sintering energy)

Discussion:

Clay-based ceramic membranes strike a practical balance between affordability, performance, and sustainability. Although oxide-based ceramic membranes offer superior separation efficiency, their high production costs and energy requirements limit their widespread use, especially in low- to medium-scale industries. On the other hand, polymeric membranes, while initially inexpensive, degrade quickly under oily and high-temperature conditions. In contrast, clay-based membranes provide a durable, locally producible, and cost-effective solution, particularly for wastewater treatment applications in developing regions with limited financial resources.

4.7 *Scale-Up and Field Application Challenges*

Despite promising laboratory and pilot-scale results, several challenges limit industrial adoption of clay-based membranes:

Raw Material Variability: Differences in clay composition led to inconsistencies in porosity and performance.

Fouling Control: Long-term stability requires improved antifouling coatings and pretreatment integration.

Manufacturing Consistency: Ensuring reproducibility during large-scale production remains a critical issue.

System Integration: Limited research exists on integrating clay-based modules into existing wastewater treatment infrastructure.

Pilot-scale demonstrations in oil mill industries are essential to assess real-field durability, optimize operational parameters, and validate cost-effectiveness under continuous flow conditions (Abubakar & Ahmad, 2023).

ISBN: 978-978-8567-02-8

5. CONCLUSION

Clay-based ceramic membranes offer a sustainable and low-cost alternative for treating oily wastewater from oil mill industries. They are fabricated from naturally available clays such as kaolin, bentonite, and ball clay, providing high thermal and chemical stability, tunable porosity, and excellent oil and pollutant rejection efficiencies (typically >95% oil and grease removal and 70–90% COD reduction). Optimal sintering temperatures between 700–900°C produce membranes with balanced mechanical strength and permeability, achieving stable fluxes of 50–120 $L \cdot m^{-2} \cdot h^{-1}$. Their inherent hydrophilicity enhances fouling resistance compared to polymeric membranes, extending operational lifespan.

However, challenges such as raw material variability, fouling control, and energy demands during fabrication still limit large-scale application. Addressing these issues through standardization, low-energy sintering, and hybrid treatment integration is essential for industrial deployment. Overall, clay-based membranes represent a technically viable, economical, and environmentally friendly solution for industrial oily wastewater treatment, advancing Sustainable Development Goals 6 and 12 by promoting clean water, pollution reduction, and resource efficiency

REFERENCES

Abubakar, S., & Ahmad, A. L. (2023). Development and optimization of clay-based ceramic membranes for oily wastewater treatment. Journal of Environmental Chemical Engineering, 11(5), 110234.

Abubakar, S., Ahmad, A. L., & Othman, M. H. D. (2020). Comparative study of Nigerian and Malaysian kaolin clays for ceramic membrane fabrication. Ceramics International, 46(4), 5098–5108.

Abu Bakar, M., Ismail, A. F., & Othman, M. H. D. (2018). Fabrication and performance of kaolin-based ceramic membranes for water and wastewater treatment: A review. Applied Clay Science, 161, 194–214.

Ahmad, A. L., Ooi, B. S., & Al-Aseeri, M. E. (2022). Membrane treatment of palm oil mill effluent: Advances, limitations and future prospects. Journal of Water Process Engineering, 47, 102731.

Ağtaş, M., Yıldız, S., & Balcı, S. (2021). Fabrication and performance analysis of kaolin–bentonite membranes for oily wastewater treatment. Environmental Technology & Innovation, 23, 101707.

Al-Aseeri, M. E., Ahmad, A. L., & Ooi, B. S. (2020). Hybrid adsorption–membrane systems for oily wastewater treatment. Separation and Purification Technology, 251, 117348.

Ali, M. E., Khemakhem, S., & Fatyeyeva, K. (2021). Surface modification strategies for ceramic membranes: Towards improved antifouling and selective separation. Journal of Membrane Science, 635, 119447.

Alomair, R. A., Alharbi, A. O., & Yilbas, B. S. (2022). Mechanical performance and fouling mitigation strategies for clay-based ceramic membranes in wastewater treatment. Desalination, 528, 115608.

Aloulou, H., Jellali, S., & Ghouma, I. (2020). Development of bentonite-based membranes for industrial effluent treatment. Applied Clay Science, 187, 105444.

Barbosa, R., Pereira, J., & Monteiro, R. (2020). Phase evolution and performance of clay-based ceramic membranes. Ceramics International, 46(8), 12045–12056.

Bashir, M. J. K., Choudhury, M. R., & Hoque, M. A. (2020). Limitations of conventional treatment methods for palm oil mill effluent. Journal of Cleaner Production, 277, 123381.

Choudhury, M. R., Bashir, M. J. K., & Sethupathi, S. (2023). Advances in hybrid membrane technologies for oily wastewater treatment. Separation and Purification Reviews, 52(3), 312–337.

Ghouma, I., Aloulou, H., & Jellali, S. (2021). Valorization of local Tunisian clays for ceramic membrane fabrication. Applied Clay Science, 210, 106174.

Hafiza, N., Hubadillah, S. K., & Othman, M. H. D. (2021). Porosity–strength trade-off in clay membranes: The role of fluxing oxides. Materials Chemistry and Physics, 270, 124847.

Hubadillah, S. K., Othman, M. H. D., & Ismail, A. F. (2018). Cost analysis of oxide- vs clay-based ceramic membranes. Journal of Asian Ceramic Societies, 6(2), 123–135.

Hu, M., Yu, L., & Dong, Y. (2020). Freeze-casting fabrication of porous clay–ceramic membranes. Journal of the European Ceramic Society, 40(6), 2304–2315.

Jabbari, V., Zarghami, R., & Jafari, A. (2017). Effect of pore formers on the microstructure and performance of clay membranes. Applied Clay Science, 143, 63–72.

Jafari, A., Zarghami, R., & Jabbari, V. (2020). Fabrication and application of clay-based ceramic membranes for oily wastewater treatment. Journal of Water Process Engineering, 37,101518.

Jiang, Z., Liu, J., & Zhang, H. (2018). Fouling behavior of kaolin-based ultrafiltration membranes in oily wastewater treatment. Journal of Membrane Science, 565, 220–230.

Khemakhem, S., Ali, M. E., & Fatyeyeva, K. (2020). Performance of advanced oxide ceramic membranes in oily wastewater treatment. Desalination, 495, 114636.

Kumar, V., Singh, R., & Ahmad, A. L. (2025). Comparative study of polymeric and ceramic ultrafiltration membranes for palm oil mill effluent treatment. Separation and Purification Technology, 317, 124092.

Lee, S., Boo, C., & Elimelech, M. (2018). Emerging membrane processes for water treatment. Nature Reviews Materials, 3(10), 432–448.

ISBN: 978-978-8567-02-8

Li, N. N., Fane, A. G., & Ho, W. S. W. (2019). Polymeric membranes for industrial wastewater treatment: Advances and limitations. Journal of Membrane Science, 574, 1–12.

Mohammad, A. W., Ng, C. Y., & Ooi, B. S. (2015). Challenges of polymeric membranes in oily wastewater applications. Separation and Purification Technology, 156, 891–908.

Mulder, M. (2012). Basic principles of membrane technology (2nd ed.). Springer.

Musa, M. A., Yakubu, M., & Abubakar, S. (2021). Progress in clay-based ceramic membranes for wastewater treatment: A review. Environmental Technology & Innovation, 23, 101732.

Ng, L. Y., Mohammad, A. W., & Leo, C. P. (2013). Hybrid membrane systems for oily wastewater treatment. Journal of Industrial and Engineering Chemistry, 19(3), 993–1009.

Oun, A., Jellali, S., & Aloulou, H. (2020). Thermal transformations of kaolinite-based ceramic membranes and their influence on performance. Applied Clay Science, 196, 105743.

Shirazi, S., Lin, C. J., & Chen, D. (2014). Industrial applications of membrane processes for oily wastewater treatment. Water Research, 67, 330–349.

Shon, H. K., Phuntsho, S., & Vigneswaran, S. (2013). Membrane technology for sustainable water and wastewater treatment. Critical Reviews in Environmental Science and Technology, 43(12), 1163–1220.

Vijaya, R., Kamarudin, A. H., & Yusoff, M. S. (2018). Environmental impacts of palm oil mill effluent discharge. Environmental Monitoring and Assessment, 190(5), 287.

Zhang, W., Ding, L., & Wang, X. (2019). Advances in polymeric membranes for oily wastewater treatment. Separation and Purification sReviews, 48(4), 276–300.

Zhou, H., Chen, J., & Li, Y. (2020). Ceramic membranes in wastewater treatment: Materials, processes, and future perspectives. Journal of Environmental Chemical Engineering, 8(4),103948.

ISBN: 978-978-8567-02-8

039-Assessment of the Compressive Strength of Cross-Laminated Timber (CLT) Panels for Use in Structural Application

Yau, Y., Sulaiman, T. A., Mohammed, A., Safana, I. M., and Garba, I.

[1, 2, 3, 5]*Department of Civil Engineering, Ahmadu Bello University, Zaria*
[4]*Department of Civil Engineering, Hassan Usman Katsina Polytechnic, Katsina*
[*1]*Corresponding author: yyilyas@gmail.com*

Abstract: Cross-laminated timber (CLT) is gaining prominence as a sustainable alternative to traditional construction materials like concrete and steel, especially in mass timber buildings. Composed of stacked layers of solid-sawn lumber bonded crosswise, CLT offers enhanced structural rigidity and dimensional stability, making it ideal for large-scale buildings. Despite the environmental benefits and mechanical potential of CLT, its performance is largely influenced by the wood species used in its production. This study focuses on *Gmelina arborea*, a fast-growing hardwood species widely cultivated in Nigeria but underexplored for high-performance CLT panels. The aim of the research is to evaluate the compressive strength properties of CLT panels made from Nigerian-grown *Gmelina arborea* under in-plane and out-of-plane loading conditions. CLT panels were fabricated using visually graded planks and two types of adhesives: one-component polyurethane (PUR) and two-component epoxy resin (ER). Compressive strength tests were conducted parallel and perpendicular to the grain in accordance with BS EN 408:2010+A1:2012. Results showed that compressive strength perpendicular to the grain ranged from 11.37 to 13.38 N/mm², while parallel strength ranged from 14.30 to 30.26 N/mm², with PUR adhesive yielding slightly higher values. The study provides critical empirical data for the structural performance of Gmelina-based CLT, which can serve as a foundation for the development of value-added timber products in Nigeria. By leveraging locally available timber species like *Gmelina arborea*, this research contributes to the advancement of sustainable construction practices in the region.

1. INTRODUCTION

Cross-laminated timber (CLT) has emerged as a revolutionary material in the construction of mass timber buildings, offering a sustainable alternative to traditional building materials like concrete and steel. CLT is composed of layers of solid-sawn lumber boards, stacked crosswise and glued together, which enhances its structural rigidity and dimensional stability. One of the key advantages of CLT in mass timber construction is its sustainability. CLT panels are manufactured from renewable wood resources, which not only reduces the carbon footprint of buildings but also sequesters carbon dioxide for the lifespan of the structure (Brandner, 2013). Additionally, CLT construction can lead to faster build times due to the prefabrication of panels, which are transported to the construction site and assembled with precision (Karacabeyli & Douglas, 2013). In Nigeria, *Gmelina arborea*, a fast-growing hardwood species, is widely cultivated, yet it's potential for use in high-performance CLT panels remains underexplored. Despite the availability of this timber, there is limited research on the mechanical properties of CLT panels made from *Gmelina arborea*, particularly in terms of their strength and stiffness under various loading conditions. This gap in knowledge presents a significant challenge to the development of locally sourced, value-added wood products that could contribute to sustainable construction practices in Nigeria. The evaluation of CLT under compression perpendicular to the grain is a critical area of research, as it influences design guidelines and safety standards for timber structures, and due to its implications for structural performance. Several studies have contributed to understanding the mechanical properties and behaviour of CLT in such conditions (Halili, 2008; Salzmann, 2010; Serrano and Enquist, 2010; He et al., 2020). However, according to Jeleč *et al.* (2018), research on compressive strength of CLT parallel to grain is scarce. This research aims to evaluate the compressive strength properties of CLT panels made from Nigerian-grown *Gmelina arborea* timber, focusing on both in-plane and out-of-plane loading conditions. The study seeks to fill the gap in existing literature by providing empirical data on the structural performance of CLT made from locally available *Gmelina arborea*, which could contribute to the development of value-added products in Nigeria's timber industry.

2. METHODOLOGY

2.1 Materials

Timber: Nigerian grown *Gmelina arborea* timber specie with an average basic density and green MC of 505 kg/m^3 and 141 % respectively was used for samples production. The timber was classified as C30 according to BS EN 338. All test CLT-specimens were produced from visually graded lumbers (with different cross-sectional) sawn from this timber specie. Some basic

ISBN: 978-978-8567-02-8

material properties of the lumber boards are presented in Table 1.

TABLE 1: BASIC PROPERTIES OF GMELINA LUMBER BOARD

MC	Density	Compressive Strength (MPa)		Strength Class
(%)	(kg/m3)	Perpendicular to grain	Parallel to grain	BS EN 338
11.8	528	5.89	35.82	C 30

Adhesive: Two commercially available adhesives, one-component Polyurethane (PUR) and two-component Epoxy Resin (ER) adhesives were used in this study.

2.2 Methods

2.2.1 Specimen Preparation

Visually graded Gmelina arborea lumber boards were selected and dried to 12 % ± 3 % MC. The lumbers were sawn and planed to cross-sectional dimension of 35 mm x 120 mm. The layers were assembled (with the two outermost layers in longitudinal direction while the innermost layer in transverse direction) and glued together in a press for 24 hours using a manual pressing device to produce the CLT panels in accordance with ANSI/APA PGR 320 (2012) and BS EN 16351 (2015). The CLT panels produced were cut and surface machined to the final product as shown in Figure 1.



Figure 1: The 3-layer CLT panels and the extracted specimens from the CLT panels

A total number of 72 CLT-specimens for compressive strength test were extracted from these panels. The size and number of CLT panels produced as well that of the CLT-specimens are shown in Table 2.

TABLE 2: DIMENSIONS AND NUMBER OF CLT PANELS AND SPECIMENS

Adhesive type	CLT- Panel Dimensions	No.	CLT-specimen Dimensions	No.
PUR	105mm x 360mm x 720mm	2	105mm x 90mm x 90mm	36
ER	105mm x 360mm x 720mm	2	105mm x 90mm x 90mm	36

2.2.2 Compressive Strength Test

The CLT specimens were subjected to both in-plane (considering major and minor strength direction) and out-of-plane loading conditions using the specification in BS EN 408:2010+A (2012). The test setup as shown in Figure 2 and instrumentation were designed according to BS EN 408:2010+A1 (2012).



(a) (b)

Figure 2: Test setup for compressive strength (a) in-plane, and (b) out-of-plane conditions

For the in-plane compressive strength, major and minor strength directions as shown in Figure 3 are considered. The major strength direction consists of two outermost layer parallel to grain, while in the case of minor strength direction only the inner layer is aligned parallel to grain direction.

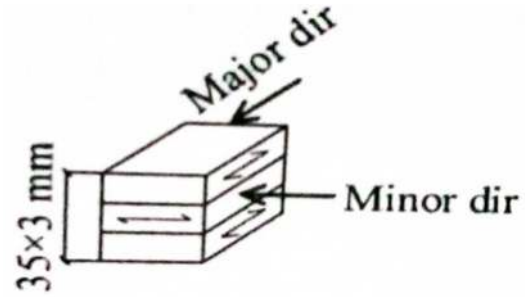


Figure 3: A prismatic CLT-specimen showing the two strength directions

3. RESULTS AND DISCUSSION

3.1 Compressive Strength Results

The compressive strength results for the CLT-specimen bonded with polyurethane (PUR) and epoxy resin (ER) adhesives based on in-plane (both major and minor strength directions) and out-of-plane (perpendicular to the grain) loading conditions are presented in Table 3 and Figure 4.

ISBN: 978-978-8567-02-8

TABLE 3: MEAN AND COV FOR THE COMPRESSIVE STRENGTH PROPERTIES FOR BOTH PUR AND ER ADHESIVES

Property		PUR				ER			
		Area (mm^2)	F_{max} (kN)	f_c (N/mm^2)	Density (kg/m^3)	Area (mm^2)	F_{max} (kN)	f_c (N/mm^2)	Density (kg/m^3)
Compressive strength perpendicular to grain	Mean	8119	101.25	12.47	532.67	8074	98.83	12.24	531.83
	COV	1.22	5.59	5.12	1.77	2.08	5.77	5.1	1.48
Compressive strength parallel to grain (Minor)	Mean	9227	167.83	18.19	532.42	9220	145.67	15.8	532.75
	COV	2.6	7.65	8.66	2.19	1.49	5.06	5.93	2.68
Compressive strength parallel to grain (Major)	Mean	9105	253.67	27.86	533.58	9089	243.5	26.79	533.67
	COV	3.05	4.45	5.48	2.52	0.96	3.71	3.51	1.75

The densities of all CLT-specimen bonded with PUR and ER adhesives as shown in Table 3, remain nearly similar and identical, ruling out density as a factor for the strength differences observed.

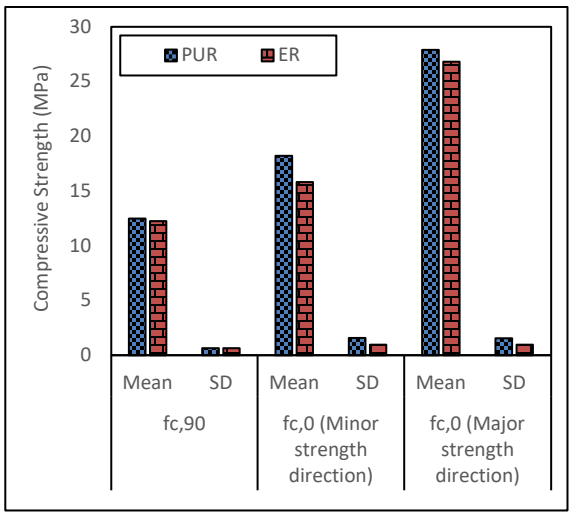
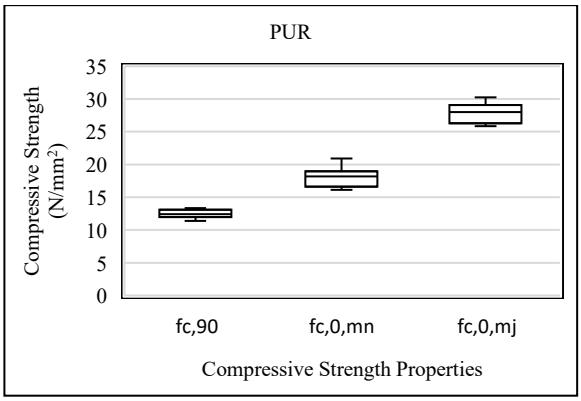


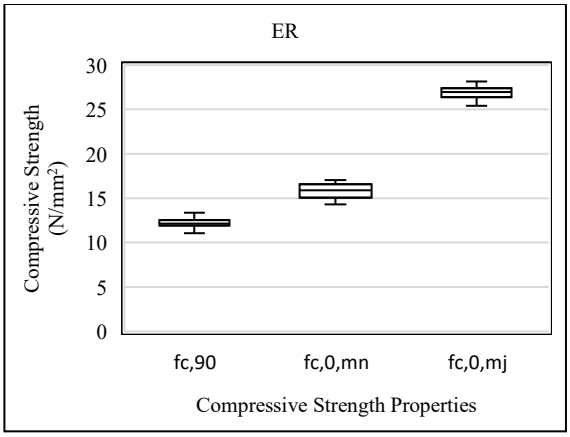
Figure 4: Mean and Standard deviation for the compressive strength

From Figure 4, the mean compressive strength perpendicular to grain for PUR is 12.47 N/mm², while for ER it is slightly lower at 12.24 N/mm². This indicates that both adhesives performed similarly, with a marginal advantage for PUR in resisting compressive loads perpendicular to the grain. The COV as can be seen in Table 3, for compressive strength in PUR is 5.12%, while ER has a similar COV of 5.1%, indicating that both adhesives exhibited consistent performance under this loading condition. In the minor strength direction (parallel to grain), PUR has a mean compressive strength of 18.19 N/mm², while ER is lower at 15.8 N/mm², indicating that PUR outperforms ER by approximately 15% in this direction. The COV for PUR is 8.66%, which is higher than ER's 5.93%, suggesting that ER exhibited more consistent performance in this strength direction. However, despite this, PUR still shows superior overall strength. However, in the major strength direction, PUR has a mean compressive strength of 27.86 N/mm², while ER has a lower value of 26.79 N/mm². This shows that PUR outperforms ER by about 4% in this direction. The COV for PUR is 5.48%, while ER has a COV of 3.51%, indicating more consistent performance for ER, although PUR exhibits slightly higher strength. This suggests that PUR adhesive creates a stronger bond with *Gmelina arborea* timber, likely due to better penetration and uniformity of bonding, as indicated by SEM analysis findings of Yau *et al.,* (2024). Furthermore, findings in this study conform to that obtained by He *et al.* (2020)

Generally, the research outcome reveals that both PUR and ER adhesives are suitable for bonding *Gmelina arborea* CLT panels, with PUR showing slightly better strength in both the minor and major grain directions as shown in Figure 5 (a & b).



(a)



(b)

Figure 5: Variability plots of the Compressive strength for specimens bonded with PUR and ER adhesives

ISBN: 978-978-8567-02-8

The differences observed in Figure 5, may be attributed to the high bonding efficiency of PUR, which is known for its excellent penetration into the wood fibres, resulting in stronger adhesion. The compressive strength values obtained in this study are comparable to those found in other hardwood-based CLT systems. For instance, in traditional softwood CLT systems (like C24 spruce), compressive strength values parallel to the grain typically range from 20N/mm² to 28N/mm², making Nigerian *Gmelina arborea* CLT a competitive alternative for structural applications. The compressive strength perpendicular to the grain, though generally lower, is still within acceptable limits for CLT panel systems. This property is crucial for load-bearing elements subjected to compression from floors or other elements, indicating that *Gmelina arborea* can perform well in both in-plane and out-of-plane loading scenarios.

3.2 Failure Mode and Delamination of Bond lines

Regarding failure mode, both ER and PUR-bonded specimens exhibited excessive shortening during compression testing perpendicular to grain. No delamination was observed along the bond lines, because they were oriented perpendicular to the loading direction. Consequently, ER and PUR-bonded specimens showed nearly identical compressive strength when loaded perpendicular to grain. For specimen loaded in compression parallel to the grain, delamination significantly influenced overall failure. ER-bonded specimens exhibited more delamination, resulting in lower strength compared with PUR-bonded specimens.

3.3 Statistical Analysis

The results of two-factor ANOVA, which assessed the effects of adhesive type**,** strength properties (compressive strength perpendicular to grain, parallel to grain in minor strength direction, and parallel to grain in major strength direction), and their interaction on the CLT specimens' compressive strength are presented in Table 4.

TABLE 4: TWO-FACTOR ANOVA FOR ADHESIVE TYPE AND COMPRESSIVE STRENGTH PROPERTIES

Source of Variation	*F*	*P-value*	*F crit*
Adhesive type	22.25535*	1.28E-05	3.98627
Strength properties	1146.608*	5.54E-52	3.13592
Interaction	5.756792*	0.00496	3.13592

Looking at adhesive type as one of the sources of variation, the F-value of 22.26 is much greater than the critical F-value (3.986), and the P-value is significantly smaller than the 0.05 significance level. This indicates that adhesive type has a statistically significant effect on the compressive strength of the CLT specimens. The choice of adhesive contributes meaningfully to the variation in the results. For the strength properties, the F-value of 1146.61 is dramatically larger than the F-critical value of 3.136, and the p-value is practically zero. This shows that strength properties (compressive strength perpendicular to grain, parallel to grain in minor strength direction, and parallel to grain in major strength direction) have an extremely significant effect on the results. This suggests that the direction in which the compressive strength is measured plays a major role in determining the overall performance. Considering interaction between adhesive type and strength properties, the F-value of 5.76 exceeds the critical F-value (3.136), and the p-value is less than 0.05. This means that there is a statistically significant interaction effect between adhesive type and strength properties**.** In other words, the effect of adhesive type on compressive strength depends on which strength property is being measured. This suggests that the performance of the adhesives may vary depending on whether the strength is measured perpendicular to the grain or parallel to the grain (in either direction). Conclusively, adhesive type has a significant impact on the compressive strength results of CLT specimens. Strength properties (whether compressive strength is measured perpendicular to grain or parallel to grain) show a highly significant effect, meaning the direction of the force greatly influences the results. There is also a significant interaction between adhesive type and strength properties, indicating that the performance of the adhesives varies depending on the direction in which the compressive strength is measured. This suggests that choosing an adhesive need to consider the specific strength requirements (for example, perpendicular or parallel to the grain), as the adhesives do not perform equally across all strength directions.

4. CONCLUSION

The compressive strength perpendicular to grain ranged from 11.37 N/mm^2 to 13.34 N/mm^2 and 11.10 N/mm^2 to 13.38 N/mm^2 for PUR and ER respectively. For compressive strength parallel to grain in minor strength direction the value ranged from 16.11 N/mm^2 to 20.90 N/mm^2 and 14.30 N/mm^2 to 17.04 N/mm^2 for PUR and ER respectively. However, for compressive strength parallel to grain in major strength direction ranged from 25.87 N/mm^2 to 30.26 N/mm^2 and 24.79 N/mm^2 to 28.16 N/mm^2 for PUR and ER respectively. The study confirms the potential of *Gmelina arborea* for use in CLT panel production, with favourable mechanical properties under both in-plane and out-of-plane loading. Generally, PUR provides superior compressive strength for CLT specimens, particularly in parallel-to-grain directions, making it an ideal choice for applications requiring high load-bearing capacity. ER, while slightly less strong, offers more consistent performance, making it a potential choice for applications where uniformity is more critical. The results indicate that the species is suitable for structural applications, particularly in mass timber construction. The slight advantage of PUR adhesive in terms of compressive strength suggests that it may be the preferred adhesive for applications requiring maximum strength. These findings contribute to the broader field of sustainable construction and promote the use of local wood species in high-performance building materials. From a sustainability perspective, the use of locally grown *Gmelina arborea* offers significant advantages. This species is fast-growing and widely available in Nigeria, making it an excellent candidate for value-added timber products. The study provides crucial data that supports the development of local, sustainable CLT production, which could reduce reliance on imported wood and promote the use of renewable building

ISBN: 978-978-8567-02-8

materials.

ACKNOWLEDGMENT

The support and assistance of the technical staff from the Carpentry Workshop and Heavy-Duty Structural Laboratory of the Civil Engineering Department are gratefully acknowledged.

REFERENCES

ANSI/APA PGR 320 (2012). Standard for Performance-rated Cross-laminated timber. *The Engineered Wood Association,* USA.

Brandner, R. (2013) Production and technology of cross laminated timber (CLT): a state-of-the-art report. In: Harris R, Ringhofer A, Schickhofer G (eds) Focus solid timber solutions—European conference on cross laminated timber (CLT). The University of Bath, Bath.

BS EN 16351 Timber Structures - Cross Laminated Timber - Requirements, European Committee for Standardization (CEN), Brussels, Belgium, 2015.

BS EN 338 (2016). Structural Timber – Strength Classes. *European Standard, European Committee for Standardization*.

BS EN 408 (2012). Timber structures - Structural timber and glued laminated timber - Determination of some physical and mechanical properties. *European Committee for Standardization (CEN)*, Brussels, Belgium.

Halili, Y. (2008). Master Thesis, Institute of Timber Engineering and Wood Technology, Graz University of Technology, Graz, Austria, 2008.

He, M., Sun, X., Li, Z. and Feng, W. (2020), Bending, shear, and compressive properties of three- and five-layer cross-laminated timber fabricated with black spruce. *Journal of Wood science,* 66(38), 1-17. https://doi.org/10.1186/s10086-020-01886-z

Jeleč, M., Varevac, D. and Rajčić, V. (2018). Cross-laminated timber (CLT) – a state-of-the-art report. *GRAĐEVINAR, 70* (2), 75-95, doi: https://doi.org/10.14256/JCE.2071.2017

Karacabeyli, E. and Douglas, B. (2013) Cross-laminated Timber Handbook U.S. Edition, Special Publications SP-529E: FPInnovations, Pointe-Claire, Quebec, Canada.

Salzmann, C. (2010). Master Thesis, Institute of Timber Engineering and Wood Technology, Graz University of Technology, Graz, Austria, 2010.

Serrano, E., Enquist, B. (2010). Compression strength perpendicular to grain in cross-laminated timber (CLT). Proceedings of 11th World Conference on Timber Engineering (WCTE2010), Riva del Garda, 2010.

Yau, Y., Ocholi, A., Kaura, J. M. and Lawan, A. (2024). Evaluation of the Bonding Performance of Polyurethane (PUR) and Epoxy Resin (ER) Adhesives with *Gmelina Arborea* Timber Using Different Testing Methods. *UNIZIK Journal of Engineering and Applied Sciences,* 3(4), 1245 – 1256.

ISBN: 978-978-8567-02-8

5TH Faculty of Engineering Conference on Engineering Innovation and Economic Policies: Driving Sustainable Industrial Growth in Nigeria

Faculty of Engineering, Bayero University, Kano.

040-Graph Convolutional Neural Network for Throughput Prediction in Dense Wireless Local Area Networks

Abdurrahman U. Usman [1], Sani H. Lawan [2] and Suleiman A. Babale [3]

Department of Electrical Engineering, Faculty of Engineering, Bayero University kano, Nigeria [1]
Department of Telecommunication Engineering, Faculty of Engineering, Bayero University kano, Nigeria [2]
Department of Electronics and Telecommunications Engineering, Ahmadu Bello University Zaria, Nigeria [3]
Corresponding Author: matawalle.usman@gmail.com

Abstract: The increasing density of Wireless Local Area Networks (WLANs) and the widespread adoption of bandwidth-intensive applications have made accurate throughput prediction a critical requirement for efficient spectrum management. Recent IEEE 802.11 amendments introduce Dynamic Channel Bonding (DCB) to enhance spectral efficiency; however, in dense deployments, complex interference and contention effects make analytical performance modeling difficult. This paper investigates the use of a Graph Convolutional Neural Network (GCNN) for throughput prediction in dense WLANs operating under dynamic channel bonding. Realistic network scenarios are generated using the Komondor wireless network simulator, which captures packet-level interactions among overlapping Basic Service Sets. WLAN deployments are represented as graphs, enabling the GCNN to learn spatial and interference relationships that strongly influence throughput performance. Unlike prior studies that focus on architectural modifications, this work emphasizes dataset augmentation as a means to improve model generalization. By expanding deployment realizations across varying densities and spatial configurations, overfitting is significantly reduced without altering the GCNN architecture. Simulation results demonstrate that the proposed approach reduces the average Root Mean Squared Error (RMSE) from 16.78 Mbps to 8.55 Mbps, representing an improvement of over 50% compared to the baseline model, highlighting the importance of realistic and diverse dataset design for reliable GCNN-based WLAN performance modeling.

Keywords: Graph Convolutional Neural Network, Dense WLANs, Throughput Prediction, Dynamic Channel Bonding, Komondor Simulator, Dataset Augmentation.

1. INTRODUCTION

Wireless Local Area Networks (WLANs) based on the IEEE 802.11 family of standards have become the dominant technology for broadband wireless access in residential, enterprise, and public environments (Farej & Hassan, 2023). The rapid growth of bandwidth-intensive applications such as high-definition video streaming, augmented and virtual reality, cloud computing, and low latency interactive services continues to place increasing performance demands on Wi-Fi networks. To address these challenges, modern IEEE 802.11 amendments, including 802.11ac, 802.11ax, and the emerging 802.11be, introduce advanced physical and medium access control mechanisms aimed at improving spectral efficiency and aggregate throughput (Barrachina-Munoz et al., 2021).

One of the most impactful mechanisms introduced to enhance WLAN capacity is channel bonding, which allows multiple adjacent basic channels to be combined into a wider transmission bandwidth (Barrachina-Muñoz et al., 2019). While early standards supported channel widths up to 40 MHz, recent amendments extend this capability to 160 MHz and beyond. In particular, Dynamic Channel Bonding (DCB) enables access points to adapt their transmission bandwidth on a per-frame basis according to instantaneous spectrum availability. Compared to static channel bonding, DCB offers greater flexibility and can significantly improve throughput in lightly loaded environments (Kanemasa et al., 2021).

However, the benefits of DCB diminish in dense WLAN deployments where multiple overlapping Basic Service Sets (BSSs) operate in close proximity. In such scenarios, aggressive bandwidth selection increases contention, co channel interference, and adjacent channel interference, often leading to reduced network performance (Barrachina-Muñoz et al., 2018). The distributed nature of Wi-Fi medium access, governed by Carrier Sense Multiple Access with Collision Avoidance (CSMA/CA), further complicates spectrum management, as channel access decisions are made independently by each access point. As network density increases, interactions among neighboring BSSs become highly dynamic and difficult to model using analytical or rule-based approaches (Soto et al., 2021).

To address these challenges, machine learning techniques have emerged as promising tools for WLAN performance modeling and optimization. Unlike traditional analytical models, data-driven approaches can

ISBN: 978-978-8567-02-8

learn complex relationships directly from network measurements, making them well suited for dense and highly dynamic wireless environments. Among these techniques, Graph Neural Networks (GNNs) are particularly attractive due to their ability to represent network elements as nodes and their interactions as edges, naturally capturing spatial and interference relationships (Rusek et al., 2019).

Recent studies by Soto et al., (2021) have demonstrated the effectiveness of Graph Convolutional Neural Networks (GCNNs) for throughput prediction in dense WLAN deployments using graph-based representations and simulation data generated with the Komondor network simulator. While these models achieve superior accuracy compared to conventional machine learning approaches, their performance is strongly influenced by the diversity and representativeness of the training dataset. In highly dynamic dense deployments, limited deployment realizations can lead to overfitting and poor generalization to unseen network configurations. Unlike prior studies that focus on architectural modifications, this work demonstrates that improved dataset diversity alone can significantly enhance GCNN generalization in dense WLAN environments.

Motivated by this observation, this paper focuses on improving the generalization capability of GCNN based throughput prediction models through enhanced dataset design rather than architectural modification. By systematically augmenting deployment realizations across varying network densities and spatial configurations, the proposed approach exposes the model to a broader range of interference and contention patterns. This allows the GCNN to learn more robust throughput relationships while retaining the original network architecture.

Accordingly, this paper investigates a GCNN based throughput prediction framework for dense WLANs operating under dynamic channel bonding. Realistic network scenarios are generated using the Komondor simulator, which captures packet level interactions among overlapping BSSs. The predicted throughput information can support informed spectrum management decisions by enabling access points to avoid sub optimal bonding configurations that degrade performance.

The main contributions of this paper are summarized as follows:

- A realistic and augmented WLAN dataset generated using the Komondor simulator to improve the generalization capability of GCNN based throughput prediction models.
- A controlled evaluation of throughput prediction performance under varying WLAN deployment densities and dynamic channel bonding configurations.
- An empirical demonstration that dataset augmentation alone can significantly mitigate overfitting in GCNN based WLAN models without modifying the underlying network architecture.

The remainder of this paper is organized as follows. Section 2 describes the methodology adopted, including the simulation environment, dataset generation process, and GCNN model implementation. Section 3 presents and discusses the obtained results. Finally, Section 4 concludes the paper and outlines potential directions for future research.

2. METHODOLOGY

This section describes the methodology adopted to develop a Graph Convolutional Neural Network (GCNN) based throughput prediction framework for dense Wireless Local Area Networks (WLANs) operating under dynamic channel bonding. The proposed approach builds upon prior graph-based learning frameworks while focusing explicitly on improving model generalization through enhanced dataset design rather than architectural modification. The methodology consists of realistic WLAN simulation, dataset generation and preprocessing, graph-based network representation, GCNN training, and performance evaluation.

Figure 1 below illustrates the overall workflow adopted in this study, from dataset generation to throughput prediction.

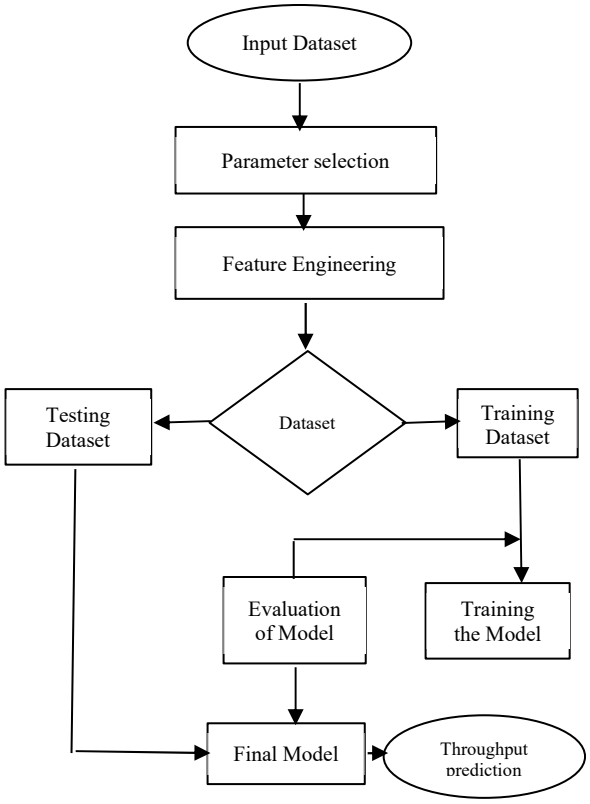


Figure 1: GCNN model creation workflow illustrating dataset generation, graph construction, training, testing and throughput prediction.

2.1 Simulation Environment and Propagation Modeling

Realistic WLAN scenarios are generated using the Komondor wireless network simulator, an event driven simulation platform specifically designed for high density IEEE 802.11 networks. Komondor provides packet level modeling of physical (PHY) and medium access control (MAC) layer interactions, including contention, interference, retransmissions, and dynamic

ISBN: 978-978-8567-02-8

channel bonding behavior. Its accuracy has been validated against ns-3 (Barrachina-Munoz et al., 2019), making it well suited for generating training datasets for machine learning based WLAN studies.

Signal attenuation between transmitters and receivers is modeled using a generalized indoor path loss formulation appropriate for 5 GHz WLAN environments, expressed as:

$$PL(d) = PL^0 + 10n \log^{10}(d) + \Sigma Lw + \Sigma Lf \quad (1)$$

where PL(d) is the path loss at distance d (in dB), PL_o is the reference path loss at d_o = 1 m (47.56 dB at 5 GHz), n is the path-loss exponent, Lw represents wall attenuation, and Lf denotes floor attenuation (Barrachina-Muñoz & Wilhelmi, 2018). This model captures the relationship between distance, received signal strength, and achievable modulation and coding schemes in indoor WLAN deployments.

Key PHY and MAC layer parameters used to configure the simulator are summarized in Table I. These parameters are selected to ensure consistency with prior GCNN-based WLAN studies and to facilitate fair comparison with baseline models.

TABLE I: PHY-MAC LAYER SIMULATION PARAMETERS (adapted from the ATARI framework (Soto et al., 2021))

Parameter	Description	Value
Tx Power	Transmit power at the output of the transmitting antenna	20 dBm
CCA Threshold	Clear Channel assessment (CCA)	-82 dBm
Capture Effect Threshold	Minimum power difference required for successful frame capture	10 dB
Traffic Load	Data traffic generation rate	Full-buffer
Payload Length *(L)*	Length of the data payload	12,000 bits
Aggregation Level *(N_agg)*	Number of packets aggregated per transmission	64
Capture Effect Model	Capture Effect Model	Disabled
Traffic Model	Stochastic traffic model identifier	99

2.2 Scenario Configuration and Dataset Generation

Dense WLAN deployments consisting of multiple overlapping Basic Service Sets (BSSs) are considered. Each BSS includes one access point (AP) and multiple associated stations (STAs). APs are placed at fixed cell centers to emulate planned enterprise deployments, while STAs are uniformly distributed within each cell to capture spatial variability. This deployment strategy enables systematic control of network density while preserving realistic spatial interactions.

Downlink saturated UDP traffic is employed using a full-buffer configuration, ensuring that each AP always has data to transmit. This allows the evaluation to focus on PHY and MAC layer effects such as contention, interference, and channel bonding without being influenced by higher-layer traffic dynamics. Dynamic channel bonding is enabled, allowing APs to opportunistically utilize wider bandwidths when secondary channels are idle.

To isolate the impact of deployment density and channel bonding behavior, packet aggregation is constrained during dataset generation while retaining simulator level aggregation capabilities. This design choice reduces variability in the dataset and allows the GCNN to focus on learning spatial interference and medium access patterns rather than aggregation dynamics.

Multiple deployment scenarios are generated by varying the number of APs, STA distributions, channel configurations, and random seeds. In contrast to baseline implementations that rely on a limited number of deployment realizations, this work emphasizes dataset diversity by generating multiple realizations per scenario. This dataset augmentation strategy increases variability in interference and contention patterns, thereby reducing the risk of overfitting during model training. The resulting scenario configurations and dataset composition are summarized in Tables II and III.

TABLE II: DEPLOYMENT SCENARIO CONFIGURATIONS

Layers	Parameter	Value
Deployment	Number of APs	{6,8,10,12}
	APs location	Fixed at the center cell
	Number of STAs	{5-10, 10-20}
	STAs Location	Uniform at Random
	Traffic profile	Downlink UDP
	Traffic load	Full-Buffer Mode
	Channel allocation	Uniform at Random
PHY-Layer	Central Freq *(f_c)*	5 GHz
	Path loss model	Generic indoor path-los
	Bandwidth *(W)*	{20, 40, 80, 160} MHz
	No. Spatial Stream	1
	Allowed MCS	0-11
MAC-Layer	Contention window *(CW)*	32 (Fixed)
	Max. A-MPDU	1
	CB Policy	Dynamic CB (4)

TABLE III: AUGMENTED DATASET COMPOSITION

Scenario ID	No. of APs	Central frequency *(f_c)* (GHz)	CHANNEL BONDING MODEL	OBSS Space (m^2)
Sce1a	12	5	4	80 x 60
Sce1b	12	5	4	70 x 50
Sce1c	12	5	4	60 x 40
Sce2a	8	5	4	60 x 40
Sce2b	8	5	4	50 x 30
Sce2c	8	5	4	40 x 20
Sce3a	6	5	4	80 x 60
Sce3b	6	5	4	80 x 60
Sce3c	6	5	4	80 x 60
Sce4a	8	5	4	50 x 40
Sce4b	8	5	4	50 x 40
Sce4c	8	5	4	50 x 40
Sce5a	12	5	4	40 x 30
Sce5b	12	5	4	40 x 30
Sce5c	12	5	4	40 x 30
Sce6a	10	5	4	60 x 20
Sce6b	10	5	4	60 x 20
Sce6c	10	5	4	60 x 20

2.3 Feature Extraction and Preprocessing

For each simulated deployment, Komondor outputs

ISBN: 978-978-8567-02-8

detailed performance metrics, including throughput, airtime usage, received signal strength indicator (RSSI), and signal to interference plus noise ratio (SINR). Raw samples are preprocessed to remove incomplete entries and numerical anomalies. All continuous features are normalized to ensure stable and consistent learning behavior during model training.

A correlation analysis is performed to identify the most influential parameters affecting throughput. Based on this analysis, a compact and informative feature set is selected to balance predictive accuracy and model complexity. RSSI is included to represent signal strength, while SINR and airtime capture interference and medium access effects, which are dominant performance limiting factors in dense WLAN environments. This feature selection strategy preserves consistency with prior GCNN based formulations while benefiting from the increased diversity of the augmented dataset. While explicit feature importance techniques such as SHAP were not applied in this study, the adopted feature selection is supported by correlation analysis and well-established WLAN performance principles, where SINR and airtime are

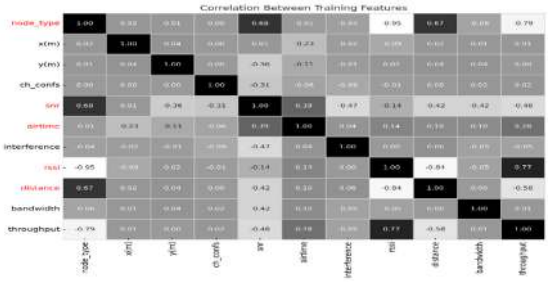


Figure 2: Correlation matrix showing the relationship between throughput and selected network features, indicating stronger dependence on SINR and airtime compared to RSSI.

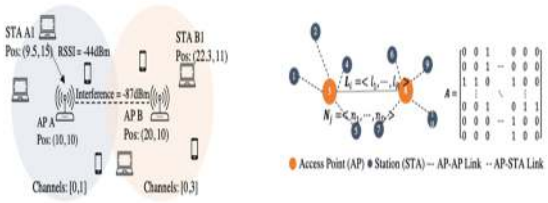
known to dominate throughput behavior in dense deployments.

2.4 Graph-Based Network Representation

To effectively capture spatial topology and wireless interference interactions, each WLAN deployment is modeled as a graph structure. This graph-based formulation enables the learning model to naturally handle variable network sizes and heterogeneous device interactions without requiring fixed-size input vectors, which are unsuitable for dense and dynamic WLAN environments.

In the constructed graph, nodes represent wireless devices, including Access Points (APs) and Stations (STAs). Node features encode device-specific characteristics such as device type, spatial coordinates, channel configuration, received signal strength, SINR, and airtime utilization. Edges represent wireless relationships between devices. Intra-BSS edges model communication links between an AP and its associated STAs, while inter-BSS edges capture interference coupling between neighboring APs operating on overlapping channels. Edge attributes reflect spatial proximity and interference-related metrics derived from the underlying PHY and MAC interactions.

Figure 3 illustrates an example WLAN deployment and its corresponding graph representation, where APs and STAs are mapped to graph nodes and wireless connectivity and interference relationships are represented as edges. This illustrative example, adapted



(a) Topological view. (b) Graph representation

Figure 3: Example of a WLAN deployment and its corresponding graph representation, showing access points (APs) and stations (STAs) as nodes, and connectivity and interference relationships as edges (adapted from (Soto et al., 2021)

from the ATARI framework, highlights how network topology and wireless interactions are explicitly preserved within the graph structure.

By preserving topological information and explicitly modeling interference relationships, this graph-based representation enables the GCNN to learn robust throughput prediction patterns across varying deployment densities. Furthermore, by maintaining architectural consistency with the ATARI framework, this representation ensures that any observed performance improvements in this work can be attributed primarily to dataset augmentation rather than changes in the network representation or learning architecture.

2.5 GCNN Architecture and Training Configuration

The GCNN architecture adopted in this work follows the meta-layer design commonly used in graph-based learning frameworks for wireless networks. Edge features are processed using multilayer Perceptrons (MLPs) to capture pairwise interactions, while node

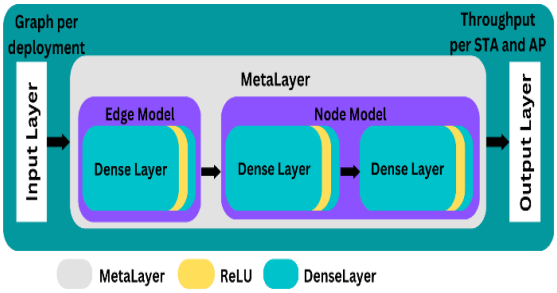


Figure 4: Meta layer architecture of the Graph Convolutional Neural Network (Soto et al., 2021), illustrating node and edge update operations used to model interference interactions in dense WLANs.

features are updated by aggregating information from neighboring nodes and associated edges. Mean aggregation is employed throughout the network to preserve permutation invariance.

Importantly, the GCNN architecture and hyperparameters are intentionally kept unchanged from the baseline framework to isolate the effect of dataset augmentation. This controlled design ensures that any observed improvements in prediction accuracy and generalization can be attributed solely to enhanced dataset diversity rather than architectural tuning.

ISBN: 978-978-8567-02-8

Model training is performed using the Adam optimizer, with the Root Mean Squared Error (RMSE) defined as the loss function. The dataset is divided into training and testing subsets using an 80:20 split. Regularization techniques, are employed to further mitigate overfitting. The main training hyperparameters are summarized in Table IV.

TABLE IV: TRAINING PARAMETERS (Soto et al., 2021)

Hyperparameter	Description	Value
Framework	Graph neural network library	PyTorch Geometric
Optimizer	Optimization algorithm	Adam
Learning Rate	Step size for weight updates	0.001
Loss Function	Training objective	RMSE
Aggregation Function	Neighborhood aggregation method	Mean
Readout Function	Graph-level pooling method	Mean pooling
Training/Testing Split	Fraction of dataset used for training and testing	80: 20

2.6 Performance Evaluation

Model performance is evaluated by comparing the throughput values predicted by the GCNN against the ground-truth throughput obtained from Komondor simulations. The primary evaluation metric is the Root Mean Squared Error (RMSE), defined as:

$$RMSE = \sqrt{\frac{1}{n}\{\sum_{i=1}^{n}(y_i - y_i')^2\}} \quad (2)$$

where n is the total number of samples, y_i represents the simulated throughput, and y_i' denotes the throughput predicted by the GCNN model.

RMSE is selected because it penalizes large prediction errors and provides a clear quantitative measure of regression accuracy. Performance is evaluated across different deployment scenarios and network densities to assess generalization capability and to quantify the impact of dataset augmentation on overfitting mitigation.

While RMSE provides an aggregated measure of prediction accuracy, it does not fully capture the distribution of prediction errors across different deployment scenarios. To complement RMSE and provide deeper insight into model generalization, the Empirical Cumulative Distribution Function (ECDF) of the prediction error is also employed.

For each test sample, the prediction error is defined as the absolute difference between the predicted throughput and the simulated throughput, given by:

$$e_i = |y_i - y_i'|$$

Given set of n prediction errors $\{e_1, e_2, \ldots e_n\}$, the ECDF is defined as:

$$F_n(x) = \frac{1}{n}\sum_{i=1}^{n} I(e_i \leq x) \quad (3)$$

where $I(e_i \leq x)$ equals 1 if the prediction error e_i is less than or equal to the threshold x, and 0 otherwise.

The ECDF therefore represents the fraction of predictions whose error does not exceed a given threshold x. Compared to aggregate metrics such as RMSE, ECDF analysis provides a more comprehensive assessment of generalization performance in dense WLAN environments.

3. RESULTS AND DISCUSSION

This section presents and discusses the performance of the proposed GCNN based throughput prediction framework. The evaluation focuses on prediction accuracy, evidence of overfitting in the baseline model, and the impact of dataset augmentation on generalization across varying WLAN deployment densities.

3.1 Throughput Prediction Accuracy

Throughput prediction accuracy is evaluated using RMSE, as summarized in Table V. The baseline GCNN model trained on a limited dataset exhibits high RMSE in early scenarios, reaching 26.9 Mbps in Scenario 1, with decreasing error across scenarios reflecting dependence on specific deployment characteristics rather than robust generalization. In contrast, the proposed dataset-augmented model achieves consistently lower RMSE across all scenarios, with errors below 12 Mbps in early deployments and further reductions in higher-density cases, indicating improved prediction stability and generalization.

TABLE V: RMSE COMPARISON ACROSS DEPLOYMENT SCENARIO

Scenario	Baseline Model	Proposed Model
1	26.9 Mbps	11.30 Mbps
2	18.94 Mbps	10.50 Mbps
3	12.76 Mbps	9.10 Mbps
4	8.45 Mbps	7.20 Mbps
5	N/A	6.80 Mbps
6	N/A	6.40 Mbps

Baseline RMSE values are not available for Scenarios 5 and 6 because these scenarios extend beyond the original ATARI evaluation scope and were not defined in the baseline study. They were introduced in this work to assess model performance under higher-density WLAN deployments.

3.2 Overfitting and Generalization Analysis

Figure 5 illustrates the training behavior of the proposed GCNN model trained on the augmented dataset, using the same loss representation adopted in the ATARI framework. The training and validation losses decrease smoothly and remain closely aligned throughout the training process, indicating stable convergence and

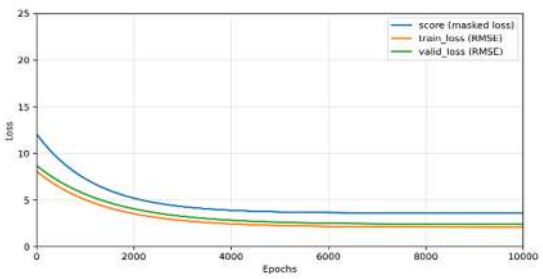


Figure 5: Training, validation and masked loss convergence of the proposed GCNN model over 10,000 epochs

ISBN: 978-978-8567-02-8

reduced overfitting. This behavior confirms that enhanced dataset diversity improves learning stability without requiring architectural modifications.

While RMSE provides an aggregate measure of prediction accuracy, it does not fully characterize the distribution of prediction errors across different deployment scenarios. To analyze model generalization and identify overfitting behavior, the empirical cumulative distribution function (ECDF) of the throughput prediction error is employed.

Figure 6 presents the ECDF of prediction error for the baseline GCNN model evaluated across four spatially distinct test scenarios. The ECDF curves exhibit substantial variation, with scenarios that differ

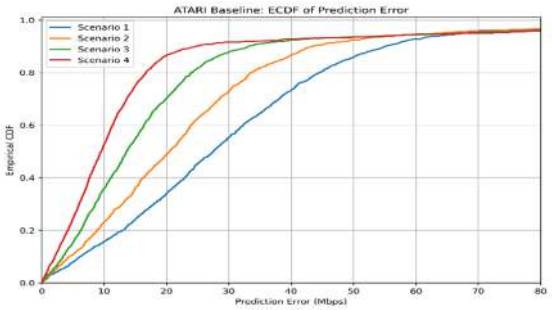


Figure 6: ECDF of prediction error for the ATARI baseline GCNN model across Scenarios 1–4

significantly from the training configuration showing pronounced rightward shifts. This behavior indicates a higher probability of large prediction errors and confirms that the baseline model overfits to scenario-specific spatial and interference patterns rather than learning general throughput relationships.

In contrast, Figure 7 shows the ECDF of prediction error for the proposed dataset-augmented model

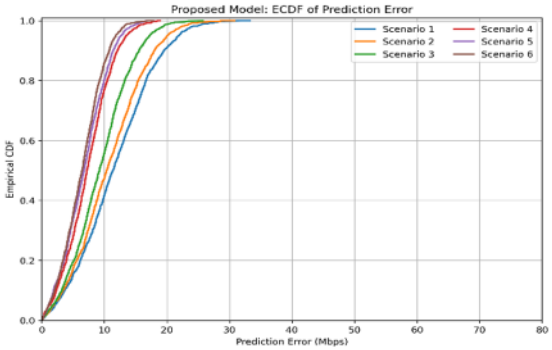


Figure 7: ECDF of prediction error for the proposed dataset-augmented GCNN model across Scenarios 1–6

evaluated across six test scenarios. The ECDF curves are closely aligned and rise more steeply, indicating that a larger fraction of predictions achieves low error values regardless of deployment configuration. The reduced dispersion among scenarios demonstrates improved robustness to spatial variability and enhanced generalization to unseen deployments.

Overall, the ECDF analysis provides clear evidence that dataset augmentation effectively mitigates overfitting in GCNN-based throughput prediction for dense IEEE 802.11 WLANs.

3.3 Impact of Dataset Augmentation on Model Generalization

To quantify the impact of dataset augmentation, the average RMSE across all evaluated scenarios is compared before and after dataset expansion. The

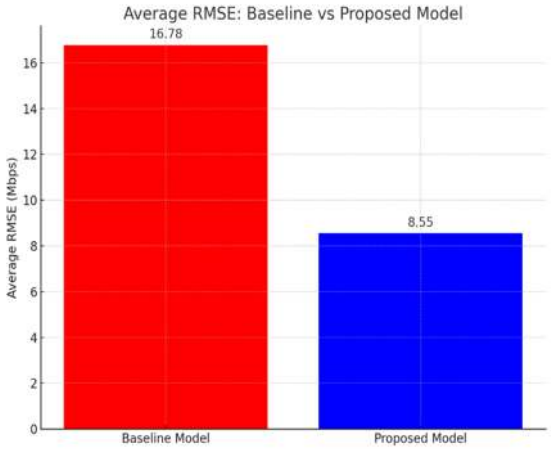


Figure 8: Average RMSE comparison between the baseline GCNN model and the proposed dataset-augmented model, demonstrating more than 50% reduction in prediction error achieved through increased dataset diversity.

baseline model achieves an average RMSE of 16.78 Mbps, while the proposed dataset-augmented model reduces this value to 8.55 Mbps, representing an improvement of over 50%. This result confirms that increased dataset diversity significantly enhances GCNN generalization without requiring architectural or hyperparameter modifications.

3.4 Comparison with Other Machine Learning Approaches

Figure 9 presents a comparison between the mean RMSE values achieved in this study and those reported in prior work for several machine learning techniques, including Convolutional Neural Networks (CNN), Feedforward Neural Networks (FNN), Gradient Boosting, Random Forest, and Graph Neural Networks. For a fair comparison, only the best-performing experiments reported in the reference study are considered.

The results indicate that the dataset generation and

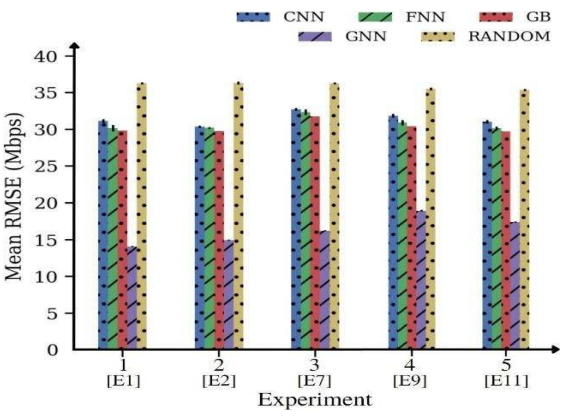


Figure 9: Mean RMSE across selected experiments reported by (Soto et al. 2021), comparing different ML models

ISBN: 978-978-8567-02-8

configuration strategy adopted in this work enables lower prediction errors compared to previously reported approaches. In particular, the best mean RMSE achieved in this study is reduced to 6.65 Mbps, outperforming alternative learning methods trained on less diverse datasets. This finding emphasizes that realistic dataset design can be as impactful as architectural complexity in achieving accurate throughput prediction.

3.5 Relationship Between Throughput and Key Network Metrics

The relationship between throughput and key physical and medium access metrics is further examined through scatter plots illustrating throughput as a function of distance, RSSI, SINR, and airtime.

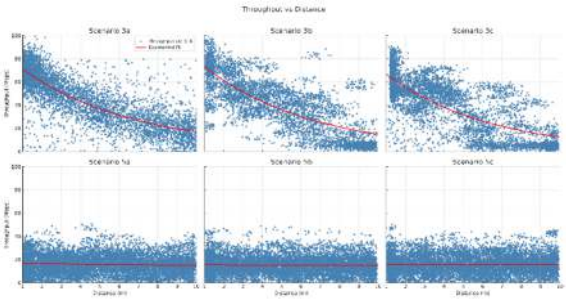


Figure 10: Throughput as a function of transmitter receiver distance, showing reduced distance dependence in dense deployments due to interference and contention.

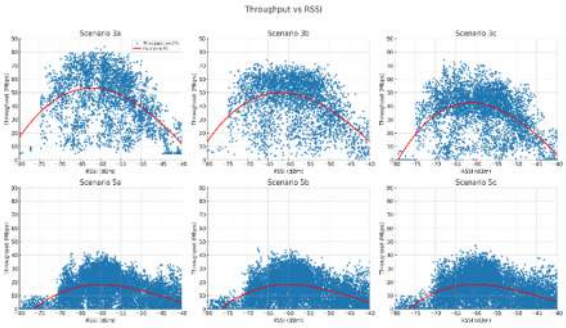


Figure 11: Relationship between throughput and received signal strength indicator (RSSI), indicating that high RSSI does not guarantee high throughput in dense WLANs.

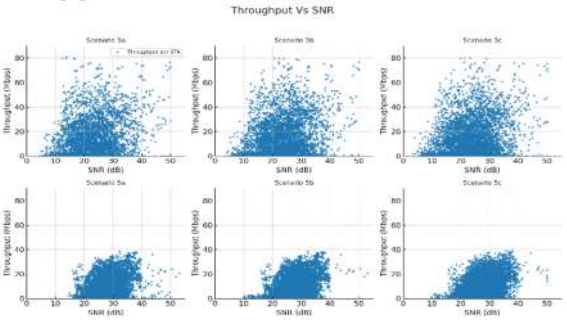


Figure 12: Throughput versus signal to interference plus noise ratio (SINR), showing stronger correlation than RSSI with saturation at high SINR values.

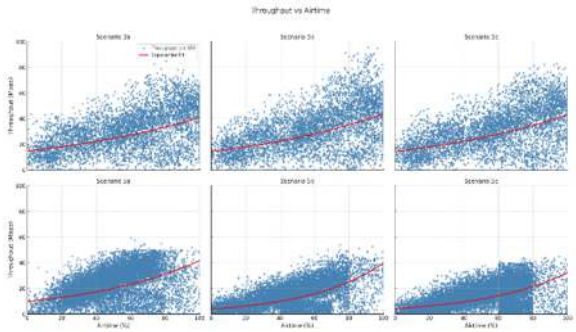


Figure 13: Throughput as a function of airtime utilization, highlighting the dominant impact of medium access efficiency on performance in dense WLANs.

As seen in Figure 10-13 above, in low density deployments, throughput generally decreases with increasing distance due to higher path loss and reduced modulation efficiency. However, in dense WLAN environments, this distance dependency becomes less pronounced, as interference and contention effects dominate performance even for stations located close to their access points.

Throughput exhibits weak correlation with RSSI, confirming that signal strength alone is insufficient to characterize performance in dense deployments. Instead, interference-aware metrics provide more reliable indicators. SINR demonstrates a clearer relationship with throughput, although peak throughput occurs at moderate SINR levels rather than extreme values, reflecting the interaction between interference, medium access opportunities, and dynamic channel bonding. Airtime shows the strongest correlation with throughput, highlighting the dominant role of medium access efficiency in dense WLAN performance.

3.6 Engineering Interpretation of the Observed Trends

The observed trends in Figure 10-13 confirm that throughput performance in dense WLAN deployments is predominantly interference limited rather than power limited. As network density increases, contention and overlapping transmissions restrict medium access opportunities, reducing throughput even under favorable signal strength conditions.

By augmenting the dataset, the GCNN is exposed to a broader range of interference and contention patterns. This enables the model to learn robust relationships between SINR, airtime, and achievable throughput, reducing sensitivity to specific spatial layouts. Consequently, the proposed model generalizes more effectively across diverse deployment densities.

3.7 Summary of Key Findings

The key findings of this study can be summarized as follows:

- The baseline GCNN model exhibits clear signs of overfitting when trained on limited deployment realizations, resulting in unstable prediction accuracy across scenarios.
- Dataset augmentation significantly improves model generalization by reducing RMSE and narrowing the gap between training and testing performance.

ISBN: 978-978-8567-02-8

- Interference aware metrics, particularly SINR and airtime, are more reliable predictors of throughput than RSSI in dense WLAN environments.
- Graph-based learning is effective for WLAN throughput prediction when sufficient dataset diversity is provided, enabling accurate modeling without architectural modification.

3.8 Application of the Proposed GCNN Model

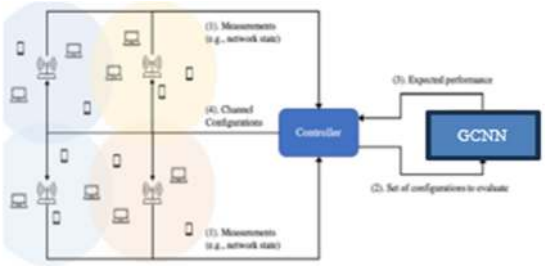


Figure 14: Conceptual integration of the proposed GCNN model into a WLAN controller for adaptive channel bonding decision support.

As illustrated in Figure 14, the proposed GCNN model can be integrated into a centralized WLAN controller to support intelligent spectrum management. Network measurements are continuously collected and used to construct the current network state. When predefined performance thresholds are violated, candidate channel bonding configurations are evaluated by the GCNN, which predicts the expected throughput for each configuration. The controller then selects and applies the configuration that maximizes predicted performance, forming a closed-loop control mechanism for adaptive spectrum allocation. Since GCNN inference involves lightweight graph convolution operations and is performed only during reconfiguration events, the associated computational overhead is modest, making the approach suitable for centralized or edge-assisted real-time WLAN controllers.

4. CONCLUSION

This paper investigated the use of Graph Convolutional Neural Networks (GCNNs) for throughput prediction in dense Wireless Local Area Networks operating under dynamic channel bonding. Realistic WLAN scenarios were generated using the Komondor network simulator to capture packet level interactions, interference, and contention effects that characterize high density deployments.

Building upon existing graph-based learning frameworks, this work focused on improving model generalization through enhanced dataset design rather than architectural modification. By systematically augmenting deployment realizations across varying network densities and spatial configurations, the proposed approach exposed the GCNN to a broader range of interference and medium access patterns. The results demonstrated that limited dataset diversity leads to overfitting and unstable prediction accuracy, while dataset augmentation significantly reduces prediction error and improves generalization across unseen deployment scenarios.

The findings further confirmed that interference aware metrics, particularly SINR and airtime, provide more reliable indicators of throughput performance than received signal strength alone in dense WLAN environments. By incorporating these features within a graph-based representation, the GCNN effectively captured spatial and interference relationships, enabling accurate throughput prediction without increasing model complexity.

Overall, this study highlights the critical role of realistic and diverse dataset design in graph-based WLAN performance modeling. The results show that substantial improvements in prediction accuracy can be achieved without altering the underlying learning architecture, emphasizing dataset augmentation as a key factor in mitigating overfitting and improving reliability in dense wireless environments.

Future research may extend this work by incorporating additional IEEE 802.11 features such as multi-user MIMO, frame aggregation dynamics, and adaptive modulation and coding schemes. The integration of online learning mechanisms and real-world measurement data may further enhance model robustness and practical applicability.

The source code required to reproduce the simulation dataset, GCNN model, training, and testing procedures is made available through the author's GitHub repository, interested researchers may request access or further information by contacting the corresponding author at *matawalle.usman@gmail.com*.

ACKNOWLEDGMENT

The authors thank the developers of the Komondor wireless network simulator for making the tool publicly available.

REFERENCES

Barrachina-Munoz, S., Chiumento, A., & Bellalta, B. (2021). Multi-Armed Bandits for Spectrum Allocation in Multi-Agent Channel Bonding WLANs. *IEEE Access*, *9*, 133472–133490. https://doi.org/10.1109/ACCESS.2021.3114430

Barrachina-Munoz, S., & Wilhelmi, F. (2018). *Komondor User's Guide*.

Barrachina-Munoz, S., Wilhelmi, F., & Bellalta, B. (2018). *Dynamic Channel Bonding in Spatially Distributed High-Density WLANs*.

Barrachina-Munoz, S., Wilhelmi, F., & Bellalta, B. (2019). *Online Primary Channel Selection for Dynamic Channel Bonding in High-Density WLANs*.

Barrachina-Munoz, S., Wilhelmi, F., Selinis, I., & Bellalta, B. (2019). Komondor: A Wireless Network Simulator for Next-Generation High-Density WLANs. *2019 Wireless Days (WD)*, 1–8.

Fgrej, Z. K., & Hassan, M. A. (2023). Analysis and Performance Evaluation of the Static and Dynamic Channel Bonding for the IEEE 802.11ac WLAN. *International Journal of Interactive Mobile Technologies*, *17*(13), 168–185.

Kanemasa, H., Li, A., Naruse, M., Chauvet, N., & Hasegawa, M. (2021). Dynamic Channel Bonding Using Laser Chaos Decision Maker in WLANs. *3rd International Conference on*

ISBN: 978-978-8567-02-8

Artificial Intelligence in Information and Communication, ICAIIC 2021, 78–82.

Rusek, K., Suárez-Varela, J., Mestres, A., Barlet-Ros, P., & Cabellos-Aparicio, A. (2019). *Unveiling the potential of Graph Neural Networks for network modeling and optimization in SDN*. https://doi.org/10.1145/3314148.3314357

Soto, P., Camelo, M., Mets, K., Wilhelmi, F., Góez, D., Fletscher, L. A., Gaviria, N., Hellinckx, P., Botero, J. F., & Latré, S. (2021). Atari: A graph convolutional neural network approach for performance prediction in next-generation wlans. *Sensors*, *21*(13).

ISBN: 978-978-8567-02-8

5TH Faculty of Engineering Conference on Engineering Innovation and Economic Policies: Driving Sustainable Industrial Growth in Nigeria

Faculty of Engineering, Bayero University, Kano.

041-Modelling, Production and Testing of Disc Airfoils

Bello Abdulsalam

Department of Mechanical Engineering, University of Maiduguri, Borno State, Nigeria. bellobib@unimaid.edu.ng

Abstract: Flying Disc (Frisbee) which is commonly used in sports and recreation for many years is not streamlined although it flies when thrown. Airfoil is streamline, hence the shape of the flying disc can be model with reference to existing NACA airfoil (as Disc Airfoil) using Computer Aided Design and Manufacturing (CAD/CAM) system. This work involves the modeling and production of disc airfoils with reference to NACA 0015 and NACA 63415 airfoils with diameter of 150 mm. Pro/ENGINEER software was used for modeling and Computer Aided part programing to generate CNC programs which was used for the milling process to manufacture the disc airfoils. A fixture was also fabricated for holding. The average diameter are 150.30 mm and 150.24 mm for the produced NACA 0015 and NACA 63415 disc airfoils respectively. The disc were tested in a subsonic wind tunnel to investigate the lift and drag coefficient. The results shows similarities with linear airfoils in past investigations which suggests that disc airfoil can be applied in wings, propellers and blades for optimum performance.

1. INTRODUCTION

Flying discs or Frisbees in one form or other have been around for more than 130 years. The name comes from William Frisbee, a 19th-Century Connecticut baker whose pie tins, turned upside down, were renowned fliers (Walsh, 2010). A Frisbee fly because of it's shape, a flat disc with deep downward curvy lip all round. A similar concept to the Frisbee is the "Flying Saucer", an imaginary alien spacecraft commonly portrayed in science fiction movies (Lorenz, 2004).

An airfoil is defined as the cross-section of a body that is placed in an airstream in order to produce a useful aerodynamic force in the most efficient manner possible (Anderson, 2017). Airfoils are designed with various sectional profiles to optimize aerodynamic performance for specific applications. Among the most widely studied and utilized are the NACA (National Advisory Committee for Aeronautics) airfoil series, which are defined by systematic numerical designations and offer a broad range of aerodynamic characteristics. These airfoils are commonly employed in aircraft wings, propellers, wind turbines, and other aerodynamic systems due to their efficiency and versatility (Singh & Sharma, 2024).

A Frisbee disc is not streamlined. The air flow around it is characterized by separation of the boundary layer which results in large-scale turbulent wake and hence a larger drag. The faster the fluid speed the lager the wake and drag (Landell-Mills, 2020; Walsh, 2010). Airfoil is streamline therefore it produce useful aerodynamic force (Anderson, 2017). A disc airfoil can be considered as a flying disc with a cross-section of an airfoil. The profile of a disc airfoil can be developed from the section profile (geometry) of an airfoil (Abdulsalam, 2017). This concept can be achieved by "revolving" a section of an airfoil through a complete revolution (360°) to form a solid disc, i.e., a solid of revolution (Stroud & Booth, 2020). Using this method, various forms of disc airfoils can be modeled and produced.

This paper present the modeling and production of disc airfoils with reference to NACA 0015 and NACA 63415 airfoils. The disc were tested in a subsonic wind tunnel to investigate the lift and drag coefficients.

2. LITERATURE REVIEW

2.1 Flying Disc

The rotating disc-wing—commonly seen in Frisbee sports discs, golf discs, and the discus—has emerged as a promising axisymmetric wing configuration for small unmanned aerial vehicles (UAVs). Research highlights its advantages in maneuverability, gyroscopic stability, and potential for vertical takeoff and landing. Advances in computational modeling and materials engineering have further enhanced the aerodynamic efficiency and structural robustness of disc-wing designs, making them increasingly viable for surveillance and urban air mobility applications (Crowther & Potts, 2007; Kamaruddin et al., 2018).

Alan Adler, founder of Aerobie, Inc., developed a ring-shaped flying disc with improved aerodynamic performance over traditional Frisbees. He compared its cross-sectional profile to the NACA 0012 symmetric airfoil and observed a similar lift slope under reversed flow, describing the Aerobie as "two airfoils in tandem" (Adler, 1984, 2003; Stanford University Archives, 2006).

Kamaruddin et al. (2018) conducted experimental and numerical investigations on twelve rotating disc-wing

ISBN: 978-978-8567-02-8

models—including commercial golf discs and parametric designs—at a Reynolds number of 3.78×10^5. Each disc featured an axisymmetric, elliptical cross-section with a hollow underside and was fabricated from ABS plastic with a 0.2 m diameter and a thickness-to-diameter ratio of 0.1. Wind tunnel tests and CFD simulations revealed that rotation enhanced lift and delayed stall, while spin rate had minimal influence on aerodynamic loads. Lift and drag coefficients remained largely independent of Reynolds number up to 50 ms^{-1}. Figure 1 shows the cross-sections of three commercial golf discs



Figure 1: Cross-sections of commercial golf discs (Kamaruddin et al., 2018).

(Kamaruddin et al., 2018).

2.2 Airfoil

Systematic airfoil development began in the late 19th century, evolving from empirical designs to standardized profiles such as the Göttingen 398 and Clark Y. These informed the NACA series introduced in the 1920s, which established a scientific basis for airfoil geometry and performance (Demirci et al., 2023; Gupta, 2014; Wood, 1930). Airfoil shapes are defined by upper and lower surface coordinates and key parameters like maximum thickness, camber, and nose radius (Abbott & Doenhoff, 1959; Demirci et al., 2023; Kulfan, 2008).

The NACA 0015 symmetric airfoil, tested in a subsonic wind tunnel, showed increasing lift with angle of attack and minimal Reynolds number sensitivity, with stall near 14° and decreasing drag at higher Reynolds numbers (Morshed et al., 2014). The NACA 4412, evaluated via CFD and experiments, exhibited strong agreement between methods, with lift peaking near 16° and drag increasing post-stall (Katare & Sapre, 2019). At low Reynolds numbers, the NACA 0015 maintained consistent performance, with CFD results aligning well with wind tunnel data (Iliev et al., 2020).

Wind tunnel tests of the NACA 63415 airfoil conducted at Risø National Laboratory revealed stall occurring just below 15°, with lift peaking around 13–14° and declining sharply thereafter. The modified version (Risø-D) demonstrated improved lift-to-drag ratio, reduced drag at moderate angles, and delayed stall compared to the baseline, confirming its aerodynamic advantage for wind turbine applications (Bak et al., 2000). CFD investigations of the NACA 63415 airfoil using the Spalart–Allmaras turbulence model revealed lift increasing steadily with angle of attack and stall at 15°, characterized by a rapid decline in lift and pronounced flow separation, confirming its laminar flow efficiency and sharp stall behavior (Erkan & Özkan, 2020).

2.3 Manufacturing / Fabricating of Models

Traditional wind tunnel airfoil models are commonly fabricated from aluminum or steel using 5-axis CNC milling. Despite technological advancements, production remains time-intensive—often requiring several weeks—and financially demanding, with costs influenced by geometric complexity and instrumentation needs (Barlow et al., 1999; Stenfelt & Ringertz, 2015). Recent developments in Computer-Aided Design, Manufacturing, and Engineering (CAD/CAM/CAE), integrated with CNC systems, have significantly advanced aerospace manufacturing capabilities. In 2014, Starrag Group hosted Airfoil Technology Days in Rorschacherberg, Switzerland, where the LX Series machines were showcased alongside innovations such as advanced blade fixturing, the Best Fit-Process, and cryogenic cooling techniques. The event also highlighted Starrag's RCS V7.2 CAM software, designed to optimize programming for turbine blade machining. These developments reinforced the LX Series' reputation as a specialized solution for aero-engine blade production. By 2023, the LX Series continued to evolve, with brochures and product literature emphasizing advancements in CAM integration, tool design, and flexible machining strategies (Grasson, 2014; Starrag Group, 2014, 2023).

2.4 Theory of Disc Airfoil in Flight

A disc airfoil in motion through air behaves similarly to a wing in flight, generating lift primarily through Bernoulli's principle, while also experiencing drag. These forces—lift and drag—are collectively referred to as aerodynamic forces (Baumback, 2010). To evaluate the drag force, the Reynolds number (R_e) of the system must first be determined to identify the appropriate drag correlation. For a Frisbee-like disc of diameter d, moving through air of density ρ, at velocity V, and with dynamic viscosity μ, the Reynolds number is expressed as:

$$R_e = \frac{\rho V d}{\mu} \quad (1)$$

The lift and drag forces are commonly expressed in dimensionless form using the lift coefficient (C_L) and drag coefficient (C_D). These coefficients normalize aerodynamic forces relative to flow conditions and reference area, enabling performance comparisons across different configurations. They are defined as follows (Landell-Mills, 2020; Morrison, 2005):

$$C_L = \frac{2L}{\rho A V^2} \quad (2)$$

$$C_D = \frac{2D}{\rho A V^2} \quad (3)$$

Where L is the lift force, D is the drag force, ρ is the air density, V is the freestream velocity, and A is the planform area of the disc airfoil.

ISBN: 978-978-8567-02-8

3. METHODOLOGY

3.1 .Modeling of Disc Airfoil

A disc airfoil was modeled by revolving a 2D airfoil profile—bounded by curves—about an axis tangential to its leading edge, generating a solid of revolution. The modeling was performed using Pro/ENGINEER software. NACA 0015 and NACA 63415 airfoil profiles were selected, and their coordinate data (x, y) were sourced from the University of Illinois at Urbana-Champaign (UIUC) Aerospace Engineering database (Selig & Maughmer, 2017). The data were formatted for compatibility with Pro/ENGINEER and saved in .PTS format. A 2D sketch was created at a 1:1 scale using the imported coordinates, as illustrated in Figure 2

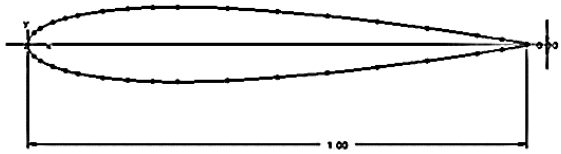


Figure 2: 2D sketch of NACA 0015 airfoil profile

The sketch file, saved in Pro/ENGINEER format, was imported, aligned, and scaled to a radius of 75 mm. It was then revolved 360° about a vertical axis tangential to the leading edge to generate a complete 3D disc model. The resulting geometry was saved as a Pro/ENGINEER part file, as illustrated in Figure 3.

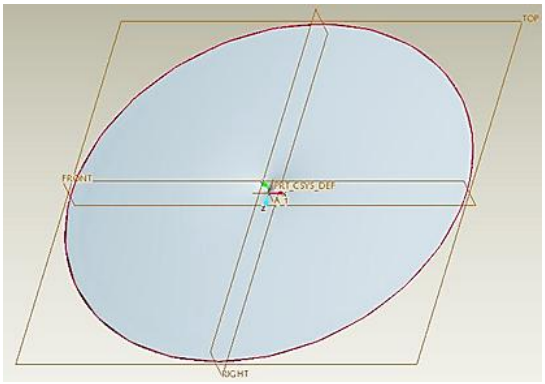


Figure 3: 3D model of NACA 0015 disc airfoil

The cross-section of the modelled NACA 63415 disc airfoil is shown in figure 4.



Figure 4: cross-section of NACA 63415 disc airfoil model

3.2 Development of CNC Program

A CAD model of the disc airfoil was created using Pro/ENGINEER software with a 160 mm × 160 mm × 12 mm PTFE (Teflon) workpiece, selected for its machinability and availability. The disc and workpiece models were aligned using coordinate constraints, and a 3-axis CNC milling setup was configured for both upper and lower surfaces with a 6 mm end mill.

Two milling operations were applied: volume milling and surface milling. Volume milling was used as the roughing stage to progressively reduce material and minimize tool load and vibration, while surface milling followed as the finishing stage to achieve the required profile with higher precision. The parameters for each operation are summarized in Table I.

TABLE I: PARAMETERS FOR VOLUME AND SURFACE MILLING OPERATIONS

Parameter	Volume Milling	Surface Milling
Tool Diameter	6 mm	6 mm
Tolerance	0.5 mm	0.1 mm
Step depth / Step over	2 mm (step depth)	1 mm (step over)
Feed rate	300 mm/min	300 mm/min
Clearance distance	5 mm	2 mm
Spindle speed	1500 rpm	1700 rpm

Toolpaths were generated with the milling parameter in table I. Toolpaths were verified using the play path tool, and CNC codes were generated for machining. Final simulations were conducted using Denford Virtual Reality CNC Milling software to detect and correct errors, as illustrated in Figure 5.

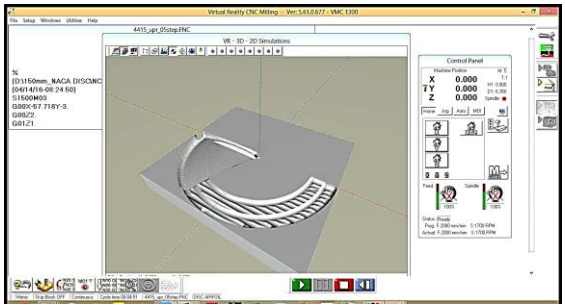


Figure 5: Machining simulation with Denford Virtual Reality CNC milling

3.3 Design and Fabrication of Fixture

A custom fixture was designed and fabricated to meet the following requirements: (i) secure the workpiece during machining, (ii) allow for easy mounting and unmounting, (iii) enable smooth 360° rotation without altering the project home position, and (iv) fit within the dimensional constraints of the CNC machine table. Based on these criteria, an appropriate fixture geometry and size were developed to ensure stability, precision, and operational efficiency during disc airfoil machining.

The fixture comprises of a Base, Rotary frame, and Mount table, secured with bolts and screws for rigidity. The base provides firm clamping on the CNC machine table, while the rotary frame enables 360° rotation and supports the mount table with multiple fastening points. The complete assembly and component arrangement are illustrated in Figure 6.

ISBN: 978-978-8567-02-8

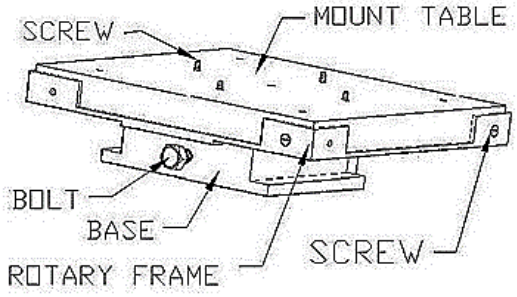


Figure 6: The fixture

3.4 Machining the Disc Airfoils

Machining was performed using a Denford VMC 1300 CNC milling machine in the CAM Laboratory, Department of Mechanical Engineering, Bayero University Kano. The PTFE workpiece was mounted on a fixture and secured to the machine table. A 6 mm flat end mill was installed, and the machine's "Project Home" was set. The NC file for the 180° upper surface was loaded and executed. After completing one half, the unmachined side was rotated into position, and the program was rerun to complete the upper surface. The same procedure was applied to machine the lower surface.

3.5 Wind Tunnel Testing

Wind tunnel testing was conducted using a Cussons P3260 subsonic wind tunnel in the Thermo-Fluid Laboratory, Department of Mechanical Engineering, Bayero University Kano. Two mounting brackets were affixed to the lower surface of each disc airfoil to facilitate secure installation. The angle of attack was varied incrementally through 0°, 3°, 6°, 9°, 12°, 15°, 18°, and 21°, while wind speeds were set at 15, 20, and 25 ms^{-1}, allowing stabilization at each setting.

At every test condition, velocity, lift force, drag force, air temperature, and air density were recorded via the wind tunnel's data management system. The lift coefficient, drag coefficient, and Reynolds number were subsequently calculated using standard aerodynamic equations.

4. RESULTS AND DISCUSSION

4.1 Results of Measured Dimensions

The fabricated discs were measured using Vernier calipers. The results obtained by measuring the diameters and maximum thicknesses of the CNC machined disc airfoils are shown in table II along with the CAD model dimensions.

TABLE II: MEASURED DIMENSION OF PRODUCED DISCS

Disc Airfoil / Model	Diameter (mm)	Max. thickness (mm)
CAD Model	150.00	11.25
NACA 0015	150.30	11.23
NACA 63415	150.24	11.80

These measured diameters were used in the evaluation of wind tunnel test results. Plan views of the produced disc airfoils are shown in Figure 7 and Figure 8.



Figure 7: Plan view of manufactured NACA 0015 disc airfoil



Figure 8: Plan view of manufactured NACA 63415 disc airfoil

4.2 Results of Wind Tunnel Test

The results obtained from the experiment are recorded and lift and drag coefficients at various Reynolds number were computed.

1) Lift Coefficient (C_L)

The lift coefficients at various angle of attack (AOA) at Reynolds number, Re = 1.7x 10^5 for NACA 0015 and NACA 63415 disc airfoils are shows in table III.

TABLE III: LIFT COEFFICIENTS AT VARIOUS ANGLE OF ATTACK AT REYNOLDS NUMBER OF 1.7X 10^5

AOA (°)	C_L of NACA 0015 Disc Airfoil	C_L of NACA 63415 Disc Airfoil
0	0.4147	0.3183
3	0.5249	0.3226
6	0.6533	0.4342
9	0.7972	0.5124
12	0.8339	0.6648
15	0.9330	0.7736
18	0.9339	0.9238
21	1.0172	1.1255

ISBN: 978-978-8567-02-8

2) Drag Coefficient (C_D)

The drag coefficients at various angle of attack (AOA) at Reynolds number, Re = 1.7x 10^5 for NACA 0015 and NACA 63415 disc airfoils are shows in table IV.

TABLE IV: DRAG COEFFICIENTS AT VARIOUS ANGLE OF ATTACK AT REYNOLDS NUMBER OF 1.7X 10^5

AOA (°)	C_D of NACA 0015 Disc Airfoil	C_D of NACA 63415 Disc Airfoil
0	0.0842	0.0229
3	0.0919	0.0302
6	0.0487	0.0410
9	0.1007	0.0335
12	0.0643	0.0529
15	0.1030	0.0686
18	0.0827	0.0768
21	0.0980	0.1306

4.3 Dimensional Assessment of Discs

By definition, both NACA 0015 and NACA 63415 airfoils possess a maximum thickness of 15% of the chord length, as indicated by the final two digits of their designations. For this study, a modeling diameter of 150 mm was used, corresponding to a theoretical maximum thickness of 11.25 mm. The NACA 0015 disc exhibited an average diameter of 150.30 mm and a maximum thickness of 11.23 mm, while the NACA 63415 disc measured 150.24 mm in diameter with a maximum thickness of 11.80 mm. The slight differences may be due to human error when mounting / unmounting the workpiece to machine the upper and lower surfaces.

4.4 Effect of angle of attack and Reynolds number

The results of the wind tunnel test for each of the disc airfoils were used to evaluate the effect of angle of attack on lift coefficient and the effect of Reynolds number on drag coefficient

1) Effect of Angle of Attack on Lift Coefficient

A plot of variation of lift coefficient with angle of attack is shown in figure 9 for NACA 0015 disc airfoil.

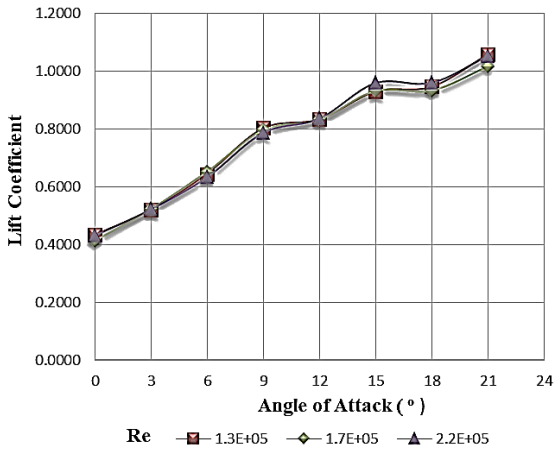


Figure 9: Effect of angle of attack on lift coefficient for NACA 0015 disc airfoil

From figure 9 the lift coefficient increases consistently with angle of attack across all tested Reynolds numbers. No significant stall behavior observed in the tested range of 0° to 21° angle of attacks..

Also a plot of variation of lift coefficient with angle of attack is shown in figure 10 for NACA 63415 disc airfoil.

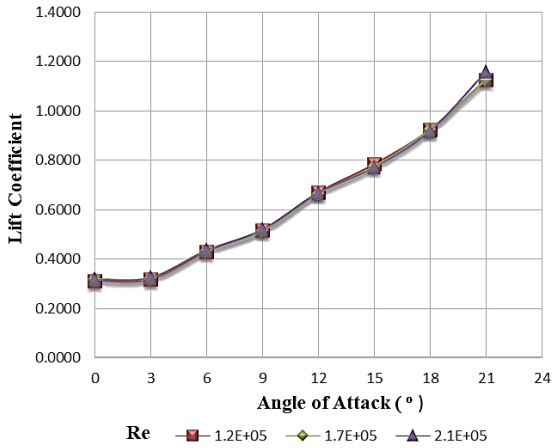


Figure 10: Effect of angle of attack on lift coefficient for NACA 63415 disc airfoil

From figure 10 the lift coefficient increasing steadily with angle of attack for all Reynolds numbers. No stall was detected in the tested range of 0° to 21° angle of attacks.

The effect of angle of attack on lift coefficient for both NACA 0015 and NACA 63415 disc airfoil as observer from Figure 9 & 10 shows a similar trend of lift coefficient increasing with angle of attack for all tested Reynolds number. These suggest that lift coefficient is independent of Reynolds number. This characteristic is the same for existing linear NACA airfoils as in the previous investigations of linear airfoils by Bak et al., (2000), Erkan & Ozkan, (2020) and Morshed et al., (2014).

The maximum lift coefficient observed for all Reynolds number is at 21° which is the maximum angle of attack in the test range. At 21 the lift coefficients of NACA 0015 and NACA 63415 disc airfoils at Reynolds number, Re = 1.7x 10^5 are 1.0172 and 1.1255 respectfully. No significant stall up to 21° angle of attack. The stall of NACA 0015 and NACA 63415 disc airfoils at a point beyond 21° is a good aerodynamics behavior because it is greater than the stall angles in the investigations of Bak et al., (2000), Erkan & Ozkan, (2020) and Morshed et al., (2014) on NACA0015 and NACA 63415 linear airfoils with stall angles of approximately 14° in both cases. These suggest a favorable aerodynamic performance even at higher angles of attack.

2) Effect of Reynolds number on Drag Coefficient

A plot of variation of drag coefficient with Reynolds number is shown in figure 11 for NACA 0015 disc airfoil.

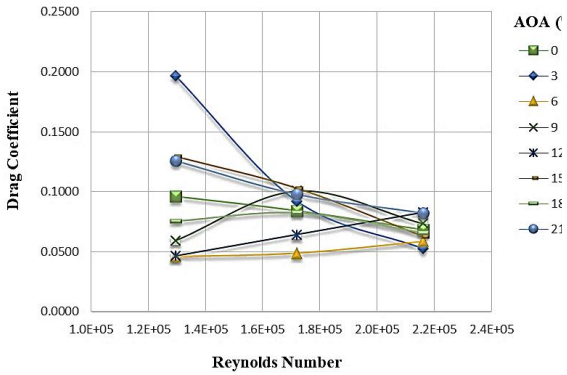


Figure 11: Effect of Reynolds number on drag coefficient for NACA 0015 disc airfoil

From figure 11 the drag coefficient decreases with increasing Reynolds number for almost all the tested angle of attacks. It can also be observed that the drag coefficient increases with angle of attack.

Also a plot of variation of drag coefficient with Reynolds number is shown in figure 12 for NACA 63415 disc airfoil.

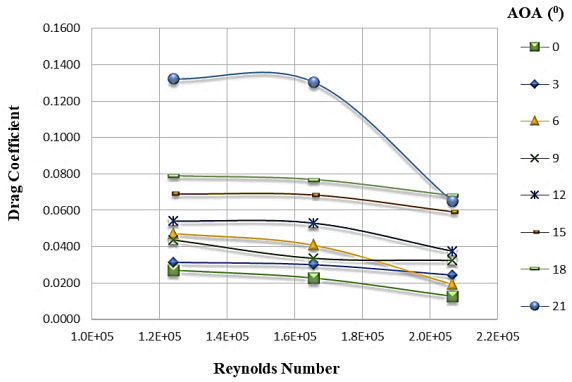


Figure 12: Effect of Reynolds number on drag coefficient for NACA 63415 disc airfoil

From figure 12 the drag coefficient reduces as Reynolds number increases for all the tested angle of attacks. It can also be observed that the drag coefficient increases with angle of attack.

The effect of Reynolds number on drag coefficient for NACA 0015 and NACA 63415 disc airfoil as observer from figures 11 & 12 shows a similar trend of drag coefficient decreasing with increases in Reynolds number for all tested angle of attacks. This characteristic is the same for existing linear NACA airfoils as in the previous investigations of linear airfoils by Bak et al., (2000), Erkan & Ozkan, (2020) and Morshed et al., (2014). These indicate improved aerodynamic efficiency at higher flow speeds which is consistent with expected aerodynamic behavior.

The maximum drag coefficient observed at Reynolds number, Re = 1.7x 10^5 for NACA 0015 disc airfoil is 0.1030 at 15° AOA and that of NACA 63415 disc airfoil is 0.1306 at 21° AOA.

5. CONCLUSION

Two NACA-based disc airfoils, NACA 0015 and NACA 63415, were modeled using Pro/ENGINEER and fabricated on a 3-axis CNC milling machine. Each disc had a nominal diameter of 150 mm, and dimensional verification confirmed close agreement with the CAD model, with only minor deviations in diameter and thickness attributable to machining and handling.

Wind tunnel testing demonstrated that both disc airfoils exhibited lift and drag characteristics consistent with conventional linear NACA airfoils. The lift coefficient increased steadily with angle of attack up to 21°, with no evidence of stall within the tested range. This extended stall angle compared to linear airfoils reported in previous studies (Bak et al., 2000; Erkan & Ozkan, 2020; Morshed et al., 2014) suggests favorable aerodynamic performance and enhanced stability at higher angles of attack.

Drag coefficients decreased with increasing flow speed, confirming improved aerodynamic efficiency. At Reynolds number, Re = 1.7x 10^5, the maximum drag coefficients observed were 0.1030 for NACA 0015 at 15° AOA and 0.1306 for NACA 63415 at 21° AOA.

Overall, the results validate the applicability of CNC-machined disc airfoils in aerodynamic components such as wings, propellers, and rotor blades. Their dimensional accuracy, favorable stall behavior, and efficiency trends highlight the potential of disc airfoils as reliable alternatives to conventional linear profiles in engineering applications.

ACKNOWLEDGMENT

The author gratefully acknowledges Prof. Abdu Salihi for his supervision and thanks Prof. Ibrahim Abdullahi, Prof. Mahdi Makoyo, and Prof. A. A. Adamu of the Department of Mechanical Engineering, Bayero University Kano, for their valuable contributions.

REFERENCES

Abbott, I. H., & Doenhoff, A. E. von. (1959). Theory of Wing Sections: Including a Summary of Airfoil Data. Dover Publications.

Abdulsalam, B. (2017). Modeling, Production and Testing of Disc Airfoils [Master's Thesis (M. Eng), Department of Mechanical Engineering, Faculty of Engineering, Bayero University, Kano]. https://teras.ng/api/asset/document/67742755-0062-4783-9cf9-cf8ef9eda83d

Adler, A. (1984). The Aerobie Flying Ring: A New Approach to Aerodynamic Toy Design. https://www.aerobie.com

Adler, A. (2003). Aerodynamic flying ring. https://patents.google.com/patent/US6599163B1/en

Anderson, J. D. (2017). Fundamentals of Aerodynamics (6th ed.). McGraw-Hill Education.

Bak, C., Fuglsang, P., Johansen, J., & Antoniou, I. (2000). Wind Tunnel Tests of the NACA 63-415 and a Modified NACA 63-415 Airfoil. Risø National

Laboratory. https://backend.orbit.dtu.dk/ws/portalfiles/portal/7729395/ris_r_1193.pdf

Barlow, J. B., Rae Jr, W. H., & Pope, A. (1999). Low-Speed Wind Tunnel Testing (3rd ed.). John Wiley & Sons.

Baumback, K. (2010). The Aerodynamics of Frisbee Flight. Undergraduate Journal of Mathematical Modeling: One + Two, 3(1), Article 19. https://doi.org/10.5038/2326-3652.3.1.31

Crowther, W. J., & Potts, J. R. (2007). Simulation of a spinstabilised sports disc. Sports Engineering, 10(1), 3–21. https://doi.org/10.1007/BF02844198

Demirci, V., Seyhan, M., & Sarioglu, M. (2023). Investigation of aerodynamic performance of Clark-Y airfoil with more realistic tubercle model and internal slots. Physics of Fluids, 35(8), 087109. https://doi.org/10.1063/5.0156362

Erkan, O., & Ozkan, M. (2020). Investigation of the Flow over NACA 63-415 Airfoil. Black Sea Journal of Engineering and Science, 3(2), 50–56. https://doi.org/10.34248/bsengineering.643916

Grasson, T. (2014). Innovative solutions simplify airfoil and turbine blade machining. Aerospace Manufacturing and Design. https://www.aerospacemanufacturinganddesign.com/news/starrag-group-airfoil-blade-machining-073014/

Gupta, A. (2014). Airfoil design: Outline of history and development. https://www.academia.edu/8993541/AirfoilDesignOutlineofthisChapterHistoryofAirfoil_Development

Iliev, V., Iliev, A., Stankovski, K., & Stojanovski, K. (2020). Numerical and Experimental Investigation of the NACA 0015 Airfoil. American Journal of Engineering Research (AJER), 9(4), 119–124.

Kamaruddin, N., Potts, J., & Crowther, W. (2018). Aerodynamic performance of flying discs. Aircraft Engineering and Aerospace Technology, 90(2), 390–397. https://doi.org/10.1108/AEAT-09-2016-0143

Katare, P., & Sapre, S. (2019). CFD Analysis and Wind Tunnel Experimental Validation of NACA 4412 Airfoil. Journal of Emerging Technologies and Innovative Research (JETIR), 6(3), 89–94.

Kulfan, B. M. (2008). Universal Parametric Geometry Representation Method. Journal of Aircraft, 45(1), 142–158. https://doi.org/10.2514/1.29958

Landell-Mills, N. (2020). Newtons Laws Explain How Frisbees Fly. European Journal of Applied Physics, 2(4). https://doi.org/10.24018/ejphysics.2020.2.4.9

Lorenz, R. (2004). Flying Saucer. New Scientist, 40–41.

Morshed, M., Bin Sayeed, S., Al Mamun, S. A., & Alam, G. M. J. (2014). Investigation of Drag Analysis of Four Different Profiles Tested at Subsonic Wind Tunnel. Journal of Modern Science and Technology, 2(2), 113–126.

Selig, G. S., & Maughmer, M. D. (2017). UIUC Airfoil Coordinates Database. https://m-selig.ae.illinois.edu/ads/coord_database.html

Singh, A., & Sharma, R. (2024). Review Paper on CFD Analysis of Different NACA Airfoil Series. Journal of Emerging Technologies and Innovative Research (JETIR), 11(3). https://www.jetir.org/papers/JETIR2403948.pdf

Stanford University Archives. (2006). Alan J. Adler Papers (1966–2006). https://archives.stanford.edu/catalog/sc0992

Starrag Group. (2014, July 1). Airfoil Technology Days 2014: Where professionals meet. https://www.metaalmagazine.nl/wp-content/uploads/2014/04/Airfoil_TechDays_Starrag.pdf

Starrag Group. (2023). Starrag LX Series: The machining solution for turbine blades. https://www.starrag.com/en-us/frontend/machine-series/view?machine_series_id=2

Stenfelt, G., & Ringertz, U. (2015). Design and Construction of Aeroelastic Wind Tunnel Models. The Aeronautical Journal, 119(1222), 229–234. https://doi.org/10.1017/S0001924000010486

Stroud, K. A., & Booth, D. J. (2020). Engineering Mathematics (8th ed.). Bloomsbury Publishing.

Walsh, K. (2010). The Physics and History of Frisbees: An In-Depth Analysis. https://studylib.net/doc/6942270/the-frisbee

Wood, D. H. (1930). Tests of large airfoils in the propeller research tunnel, including two with corrugated surfaces (No. NACA Technical Report No. 336). National Advisory Committee for Aeronautics. https://ntrs.nasa.gov/search.jsp?R=19930091406

ISBN: 978-978-8567-02-8

042-Determination of the Comminution Work Index of Maitumbi Gold Ore Deposit Niger State, Nigeria, by the Modified Bond Index.

Taofeeq Akinloye Hammed[1], Yusuf Hammed[2]

1. Technical Education Department, Federal College of Education, Gidan Madi, Sokoto State.
2. Mechanical Engineering Department, Federal Polytechnic Nasarawa

Email Adress: akinloye214@gmail.com

Abstract: The efficient design of grinding circuits in mineral processing requires accurate determination of ore grindability. This study evaluated the Bond work index of Maitumbi gold ore located in Chanchaga Local Government Area of Niger State, Nigeria, using the modified Bond's equation (Berry and Bruce comparative method). Granite with a known work index was used as the reference material. Representative gold ore samples collected from four mining pits were crushed, milled, and subjected to sieve analysis to obtain the particle size distributions of feed and product samples. The 80% passing sizes derived from the size distribution curves were used for work index determination. The results indicate that the Bond work index of Maitumbi gold ore is 11.78 kWh/tonne, signifying a moderate resistance to grinding within the particle size range of +355 µm to −63 µm. This value represents the energy required to reduce the ore from an infinitely large size to 80% passing 100 µm. The findings provide essential input data for the design and optimization of grinding circuits for Maitumbi gold ore beneficiation.

Keywords: Bond work index; gold ore; comminution; grindability; mineral processing.

1.0 INTRODUCTION

It has been proven that Nigeria is rich in a diverse range of solid minerals, alongside the plentiful oil and gas reserves that have largely influenced the nation's economy since the 1970s. According to Ministry of Solid Minerals Development (MMSD, 2023) Nigeria is endowed with over thirty-five minerals' resources spread across the entire country, which include gold, coal, bitumen, iron ore, tantalite/columbite, lead-zinc sulphides, barytes, cassiterite, gemstones, limestone, talc, feldspar and marble. Nigeria is rich in minerals, yet it lags behind in technology and industrial development since little value is added to its mineral resources. A nation such as Nigeria can surmount its current economic challenges if sufficient focus is placed on the solid mineral sector, as it plays a crucial role in the economic and technological advancement of a country (Yomi Vincent, 2019).

Gold, a precious metal, holds considerable economic, social, and political importance. This valuable metal is mainly located in three regions within Nigeria: Binri-Gwari Minna goldfield, Ife-Ilesha goldfield and Zamfara-Kebbi-Sokoto goldfield (Ajayi, 2001). All are typically linked to the schist belts, although gold-quartz veins can also be found in gneisses (such as the Malele, Diko, and Iperindo gold mines). Gold quartz veins typically align with the structural orientation of the basement rocks, which runs from North-South to North North East-South South West. The schist belts found in Nigeria contain numerous mineral deposits.

Gold is primarily found in quartz veins and as placers in soil (eluvial) and in sediments of streams (alluvial). The quartz veins that contain gold are associated with metamorphosed rocks that range in composition from semi-pelitic to pelitic and mafic. The primary gold mineralization creates a chemical signature in the overburden and neighboring soil, likely due to weathering processes. Weathering processes produce samples (soils and stream sediments) that provide. information about localized hidden mineralization or the potential presence of both major and minor mineralization over a broader area. The residual soil serves as the geochemical sample typically used to identify the locations of concealed mineralization once an area of economic interest has been identified(Bwala et al., 2021).

Gold is found alongside pyrite, pyrrhotite, and small amounts of chalcopyrite, galena, sphalerite, and magnetite. This research aims to determine the work index of Maitumbi gold ore using granite, with a known work index, as the reference sample through the modified Bond's equation.

1.1 Theoretical Considerations for the Comminution Process (Work Index)

The work index indicates how easily the mineral ore can be broken down, which is valuable for designing grinding systems in mineral processing (Yomi Vincent, 2019). There exists a variety of theories regarding comminution, but the modified Bond's equation, known as the Berry and Bruce comparative Bond's equation, is of utmost relevance to this study and was used to calculate the work index of the ore. The work index is a key parameter in comminution that indicates the material's resistance to crushing and grinding; it represents the number of kilowatt hours per short-ton needed to reduce the material from a hypothetically infinite feed size to 80% passing 100 (Wills & Napier–Munn, 2006). Table 1 provides the work index for various mineral ore sample.

TABLE 1: WORK INDEX OF SOME MINERALS ORES SAMPLES

Material	Work Index	Material	Work Index
Bauxite	2.38 – 9.45	Limestone	2.69 – 14.0
Copper	12.7 – 14.0	Molybdenum	11.6 – 14.10
Fluorspar	2.98 – 9.76	Quartz	13.6 – 15.00
Graphite	1.75 – 45.03	Titanium	4.23 – 11.88
Gold	8.0 – 16.5	Silica Sand	2.65 – 16.46

ISBN: 978-978-8567-02-8

Sources: (Bwala et al., 2021; Yomi Vincent, 2019)

In the mineral sector, comminution consumes the most energy (Napier-Munn et al., 1996). It is crucial to understand that reducing size incurs significant costs, and both energy demands and the expense per tonne of ore processed rise from blasting (0.43 kWh/t) to crushing (3.24 kWh/t) and culminate in grinding (10.0 kWh/t) as the most energy-intensive method, while the efficiency declines (Yomi Vincent, 2019). Given the restricted availability of energy resources, the importance of designing the energy requirements for engineering processes cannot be understated. Nevertheless, milling stands out as both the costliest and the least efficient operation. Within a comminution circuit, the overall power consumption and power draw during the milling process are crucial parameters (Siddall, Henderson, & Putland, 1996).
By applying Bond's law, the Work Index of an ore is assessed by comparing its grindability;

$$W = \frac{10W_i}{\sqrt{F}} - \frac{10W_i}{\sqrt{P}} \quad (1)$$

Where:

W = Work input in kilowatt hours per short ton

$P =$ The diameter in microns which 80% of the product passes 100µm

$F =$ The size which 80% of the feed passes 100µm

$W_i =$ The work index and it is expressed in kilowatt hours per short ton.

The energy input for the unidentified ore is equivalent to that of the known reference ore. Nonetheless, this situation is adjusted as stated in Equation 2.

$$W_{fi} = W_{ri}\left[\frac{\left(\frac{10}{\sqrt{F_r}} - \frac{10}{\sqrt{P_r}}\right)}{\left(\frac{10}{\sqrt{F_t}} - \frac{10}{\sqrt{P_t}}\right)}\right] \quad (2)$$

Where:

$W_f =$ Work index for test ore in kilowatt hours per short ton

$W_{ri} =$ Work index for reference ore in kilowatt hours per short ton

$P_f =$ The diameter in microns which 80% of the feed ore passes 100µm

$P_r =$ The diameter in microns which 80% of the reference ore passes 100µm

$F_r =$ The diameter of reference ore which 80% of the feed passes 100 µm

$F_f =$ The diameter of test ore which 80% of the feed passes 100 µm.

This method is relatively simple and is called the comparative method of determining the grindability parameter i.e. work index (Wills and Napier-Munn, 2006).

2.0 MATERIALS AND METHODS

2.1. Materials

Fifty kilograms (50kg) of gold ore samples were collected from four different mining pits in Maitumbi. Maitumbi, it is situated in the Chanchaga local government area of Niger State. Its geographical coordinates are 9.53° N latitude and 6.53°E longitude. The reference ore granite samples were obtained from the overburden at Maitumbi in Niger State. A random sampling method was utilized to ensure a true representation of the ore, followed by the cone and quartering technique.

2.2 Methods

The selected particle size range of +355 µm to −63 µm was chosen to ensure adequate breakage and representative size reduction during laboratory grinding. Similar particle size ranges have been successfully employed in modified Bond work index studies where strict adherence to standard Bond feed sizes was impractical (Gupta and Yan, 2006; Lawal et al., 2019).

The modified Berry and Bruce comparative Bond method was adopted due to the unavailability of a standard Bond ball mill. Fixed-time grinding has been shown to provide a reliable alternative for preliminary grindability assessment when a reference ore of known work index is employed (Berry and Bruce, 1966; Gupta and Yan, 2006; Wills and Napier–Munn, 2006).

Granite with a reported Bond work index of 15.14 kWh/ton was used as the reference ore in this study. Granite is widely adopted as a reference material in comparative Bond work index determination due to its stable and well-documented grindability characteristics. Its use has been validated in several Nigerian and international comminution studies where standard Bond ball mills were unavailable (Berry and Bruce, 1966; Adebimpe et al., 2018; Lawal and Kawu, 2020).

The reference ore sample was manually crushed with a sledgehammer to achieve a size suitable for the Denver laboratory jaw crusher feed. The sample was then crushed and milled. A 100 g portion was weighed for sieve analysis. The modified Bond's method for calculating the ore's work index uses a reference ore with a known grindability. The steps are as follows:

One hundred grams (100 g) of both the test ore samples and the reference ores were crushed and pulverized in the laboratory mill machine for an hour. Equal weights of the test and reference ores were selected and sorted into various size fractions using an automatic sieve shaker for a duration of 10 minutes. The weight of

ISBN: 978-978-8567-02-8

each size fraction for both the test and reference ores was recorded as the feed. The feeds from the test and reference ores were then combined and fed into a laboratory ball mill, where they were ground for one hour. After grinding, the test and reference ores from the ball mill were sorted by size again, and each size fraction was weighed, with the recorded weights noted as the product (Oyelola et al., 2017). The ground samples were sorted into the following sieve size fractions: +355 µm, -355+250 µm, -250+180 µm, -180+125 µm, -125+90 µm, -90+63µm, and -63µm. Each sieving operation was performed using an automatic rotap sieve shaker.

3.0 RESULTS AND DISCUSSION

Although detailed mineralogical characterization such as X-ray diffraction (XRD) was not conducted in this study, previous investigations have shown that gold deposits within the Nigerian schist belts are predominantly quartz-hosted with minor sulphide phases. This geological consistency supports the application of comparative comminution testing for preliminary grindability evaluation (Obaje, 2009; Garba, 2015).

The Bond modified method (Berry and Bruce comparative method) was used in determination of work index during this research work. The method involved use of a reference ore of known grindability. As reported by (Egbe et al., 2013), for determination of 80% of passing sizes of feeds and products for both reference and test ore under the same condition of grinding, the results of sieve analysis (Table 2 To 5) in which cumulative per cent were plotted against the particle size in microns as shown in Figure 1 To 4.

TABLE 2: SIEVE ANALYSIS OF GRANITE FEED TO BALL MILL

Sieve Size Range (μm)	Weight Retain ($W(g)$)	Weight Retain ($W(\%)$)	Nominal Aperture (μm)	Cumulative Wt (%) Retained	Cumulative Wt (%) Passed
+355	12.90	12.90	355	12.90	87.10
-355+250	14.16	14.16	250	27.06	72.94
-250+180	20.15	20.15	180	47.21	52.79
-180+125	23.19	23.19	125	70.04	29.60
-125+90	11.20	11.20	90	81.16	18.40
-90+63	08.10	08.10	63	89.70	10.30
-63	10.30	10.30	-	100	0.00

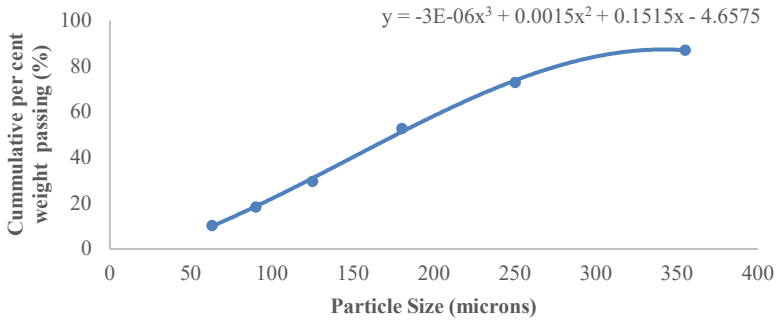


Figure 1: Particle Size distribution graph for Feed to Ball Mill (Reference Ore)

ISBN: 978-978-8567-02-8

From Figure 1 the equation of the curve is given as,
$y = -3 * 10^{-6} x^3 + 0.0015x^2 + 0.1515x - 4.6575$ (3)
The 80% passing size for the feed is obtained when y is equal to 80 in equation 3 and it becomes,
$-3 * 10^{-6} x^3 + 0.0015x^2 + 0.1515x - 84.6575 = 0$ (4)

By using cubic equation calculator, the three roots of equation 4 are given as:
X_1 = 487.827 µm, X_2 = 373.554 µm and X_3 =249.727 µm the 80% passing size of the feed sample is 249.727µm, since the roots 487.827 and 373.554 µm falls outside the particle sizes.

TABLE 3: SIEVE ANALYSIS OF GRANITE PRODUCT TO BALL

Sieve Size Range (μm)	Weight Retained ($W(g)$)	Weight Retained ($W(\%)$)	Nominal Aperture (μm)	Cumulative Wt (%) Retained	Cumulative Wt (%) Passed
+355	04.74	04.74	355	04.74	95.26
-355+250	06.00	06.00	250	10.74	89.26
-250+180	15.26	15.26	180	26.00	74.00
-180+125	20.03	20.03	125	46.03	53.97
-125+90	23.40	23.40	90	69.43	30.57
-90+63	11.77	11.77	63	81.20	18.80
-63	18.80	18.80	-	100	0.00

MILL

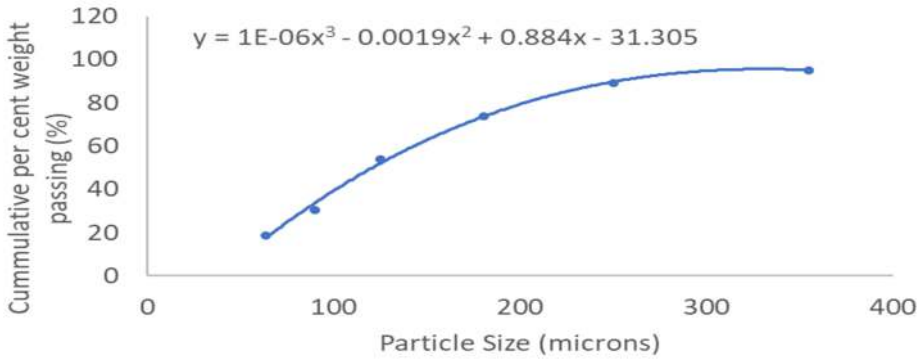


Figure 2: Particle Size distribution graph for Ball Mill Product (Reference Ore)

From Figure 2 the equation of the line is given as,
$y = 1 * 10^{-6} x^3 - 0.0019x^2 + 0.884x - 31.305$ (5)
The 80% passing size for the feed is obtained when y is equal to 80 in equation 5 and it becomes,
$1 * 10^{-6} x^3 - 0.0019x^2 + 0.884x - 111.305 = 0$ (6)

By using cubic equation calculator, the three roots of equation 6 are given as:
X_1 = 1275.241 µm, X_2 = 210.893 µm and X_3 = 413.866 µm
The 80% passing size of the feed sample is 210.893 µm, since the roots 1275.241 and 413.866 µm falls outside the particle sizes.

ISBN: 978-978-8567-02-8

TABLE 4: SIEVE ANALYSIS OF GOLD ORE FEED TO BALL

Sieve Size Range (μm)	**Weight Retained (g)**	**Weight Retained (%)**	**Nominal Aperture (μm)**	**Cumulative Wt (%) Retained**	**Cumulative Wt (%) Passed**
+355	11.47	11.47	355	11.47	88.53
-355+250	20.37	20.37	250	31.84	68.16
-250+180	13.09	13.09	180	44.93	55.07
-180+125	14.31	14.31	125	59.24	40.76
-125+90	21.65	21.65	90	80.89	19.11
-90+63	18.62	18.62	63	99.51	0.49
-63	0.49	0.49	-	100	0.00

MILL

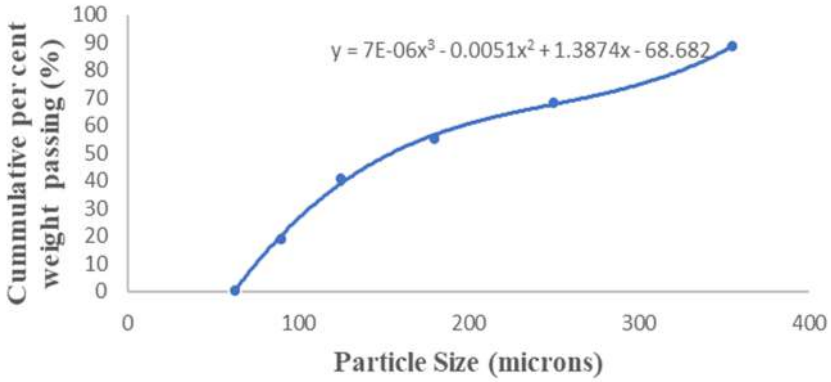


Figure 3: Particle Size distribution graph for Feed to Ball Mill (Test Ore)

From Figure 3 the equation of the line is given as,

$y = 7 * 10^{-6} x^3 - 0.0051x^2 + 1.3874x - 68.682$ (7)

The 80% passing size for the feed is obtained when y is equal to 80 in equation 7 and it becomes,

$7 * 10^{-6} x^3 - 0.0051x^2 + 1.3874x - 148.682 = 0$ (8)

By using cubic equation calculator, the three roots of equation 8 are given as:

$X_1 = 310.65$ µm, $X_2 = 365.956$ µm and $X_3 = 351.956$ µm

The 80% passing size of the feed sample is 310.65µm, since the roots 365.956 and 351.956 µm falls outside the particle sizes.

ISBN: 978-978-8567-02-8

$P_r = 210.893\mu m$

$F_r = 249.727\mu m$

TABLE 5: SIEVE ANALYSIS OF GOLD ORE PRODUCT TO BALL

Sieve Size Range (μm)	Weight Retain ($W(g)$)	Weight Retain ($W(\%)$)	Nominal Aperture (μm)	Cumulative Wt (%) Retained	Cumulative Wt (%) Passed
+355	4.21	4.21	355	4.21	95.79
-355+250	7.84	7.84	250	12.05	87.95
-250+180	27.12	27.12	180	39.17	60.83
-180+125	15.56	15.56	125	54.73	45.27
-125+90	25.15	25.15	90	79.88	20.12
-90+63	16.40	16.40	63	96.28	3.72
-63	3.72	3.72	-	100	0.00

MILL

$F_t = 310.659\mu m$

$W_{ri} = 15.14$ kWh/ton

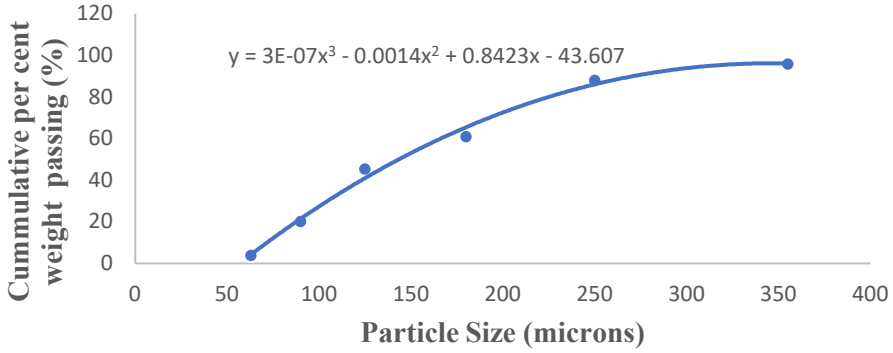


Figure 4: Particle Size distribution graph for Ball Mill Product (Test Ore)

From Figure 4 the equation of the line is given as,

$y = 3 * 10^{-7} x^3 - 0.0014x^2 + 0.842x - 43.607$ (9)

The 80% passing size for the feed is obtained when y is equal to 80 in equation 9 and it becomes,

$3 * 10^{-7} x^3 - 0.0014x^2 + 0.842x - 123\text{-}607 = 0$ (10)

By using cubic equation calculator, the three roots of equation 10 are given as:

$X_1 = 3988.651$ µm, $X_2 = 231.177$ µm and $X_3 = 446.83$ µm.

The 80% passing size of the feed sample is 231.177 µm, since the roots 3988.651and 446.83 µm falls outside the particle sizes.

The work index or grindability parameter was calculated as follow:

$P_t = 244.368\mu m$

$$W_{ti} = W_{ri}\left[\frac{\left(\frac{1}{\sqrt{P_r}}-\frac{1}{\sqrt{F_r}}\right)}{\left(\frac{1}{\sqrt{P_t}}-\frac{1}{\sqrt{F_t}}\right)}\right] = 15.14\left[\frac{\left(\frac{1}{\sqrt{210.893}}-\frac{1}{\sqrt{249.727}}\right)}{\left(\frac{1}{\sqrt{244.368}}-\frac{1}{\sqrt{310.659}}\right)}\right]$$

$$= 15.14\left[\frac{(0.0689-0.0633)}{(0.0639-0.0567)}\right] = 15.14\left[\frac{(0.0056)}{(0.0072)}\right]$$

$$= 15.14[0.7778] = 11.78 \text{ KWh/ton}$$

$W_{ti} \equiv 11.78$ kWh/ton.

ISBN: 978-978-8567-02-8

The work index of Maitumbi gold ore, according to Bond's methodology, was determined to be 11.78 kWh/tonne, indicating that approximately 11.78 kilowatt-hours of energy are needed to crush the ore from an infinitely large size to 80 percent passing through 100 microns, in accordance with Bond's work index. The work index measured is relevant for particle sizes ranging from +355µm to -63 µm.

4.0 CONCLUSION

In summary, the work index of Maitumbi gold ore in Niger State, Nigeria, has been calculated and found to average 11.78 kWh/ton. This metric is crucial for developing a processing route for the beneficiation of the Maitumbi gold ore deposit to a metallurgical grade. Nigeria, which is rich in minerals yet technologically and industrially lagging, has the potential to greatly improve its economy through the exploration, extraction, processing, and utilization of these finite resources. By focusing on the solid mineral sector, the country can significantly overcome its current economic challenges, as this area is essential for both economic and technological advancement.

REFERENCES

Adebimpe, R. A., et al. (2018). *Comminution characteristics of Nigerian ores*. Journal of Minerals & Materials Characterization.

Ajayi, J. A. (2001). An assessment of the amenability of ilesha gold ore to amalgamation and percolation leaching. *Journal of Mining and Geology*, *37*(1), 85–90.

Berry, T. F., & Bruce, R. W. (1966). A simple method of determining the grindability of ores. *Canadian Mining Journal*.

Bwala, D. M., Abdulfattah, F., Alabi, O. O., & Adewuyi, B. O. (2021). Determination of work index of Filin Kokuwa Gold Deposit in Toro Local Government, Bauchi State Nigeria. *Nigerian Journal of Technology*, *40*(3), 387–392. https://doi.org/10.4314/njt.v40i3.5

Egbe, E. A. P., Mudiare, E., Abubakre, O. K., & Ogunbajo, M. I. (2013). Determination of the Bond'S Work Index of Baban Tsauni (Nigeria) Lead-Gold Ore. *European Scientific Journal*, *9*(12), 1857–7881.

Gupta, A., & Yan, D. (2006). *Mineral Processing Design and Operation*. Elsevier.

MMSD. (2023). Ministry of Mines and Steel Development (MMSD). In *Integrated Automation and Interactive Solid Minerals Portal (IAISMP)* (p. 1). https://portal.minesandsteel.gov.ng/

Napier-Munn, T. J., Morrell, S., Morrison, R. D., & Kojovic, T. (1996). Mineral Comminution Circuits: Their Operation and Optimisation. *Julius Kruttschnitt Mineral Research Centre The University of Queensland*, 435.

Olasupo D. O., Mosobalaje O. A., Adelana R. A. and Olusegun O. A., (2014). Beneficiation and Characterization of Gold from Itagunmodi Gold Ore by Cyanidation. *Journal of Minerals and Materials Characterization and Engineering,* 7 (2), 300-307.

Olatunji, K. J. and A.G. Durojaiye, (2010). Determination of Bond Index of Birnin-Gwari Iron Ore in Nigeria. *Journal Material Mineral Characteristics Engineering*, 9(1), 635-642.

Oyelola, A. O., Abdu, D. A., Victor, A. D., Igonwelundu, M. T., Bosan, B. M., & Oyebode, A. B. (2017). Extraction of a low grade zinc ore using gravity and froth flotation methods. *Journal of Applied Sciences and Environmental Management*, *20*(4), 903. https://doi.org/10.4314/jasem.v20i4.1

Siddall, B., Henderson, G., & Putland, B. (1996). Factors influencing sizing of SAG mills from drill core samples. *In Proc. Conf. International AG and SAG Grinding Technology*, *2*, p. 463.

Wills, B. A., & Napier–Munn, T. J. (2006). Mineral Processing Technology, Elsevier Science & Technology Books. In *Pp108-117*.

Yomi Vincent, A. (2019). Determination of Work Index for Iperindo Lode Gold Deposit at Ilesha Goldfield Osun State, Nigeria Using Modified Bond Index. *American Journal of Materials Synthesis and Processing*,*4*(1),37. https://doi.org/10.11648/j.ajmsp.20190401.15

ISBN: 978-978-8567-02-8

5TH Faculty of Engineering Conference on Engineering Innovation and Economic Policies: Driving Sustainable Industrial Growth in Nigeria

Faculty of Engineering, Bayero University, Kano.

043-Evaluating the Ability of Fractional Order Proportional Integral Derivative Controller on the Two-Link Planar Robot

R A. Tilde, O. U. Okereke, E. C. Anene and M. Ahmed

Electrical and Electronics Engineering Department, Abubakar Tafawa Balewa University Bauchi, Nigeria.

(inunugoloma@yahoo.com)

Abstract: The work presented the application of Fractional Order Proportional Integral Derivative (FPID) control scheme for two-link planar robot. Robots have already become part of the modern world and the further advances in technology keep making the requirements for accuracy and robustness of such systems more stringent. There are different control schemes proposed for such systems, but interest is more focused on simpler versions due to computational burden, as a result of the complexities of the more advanced control schemes. The FPID is basically an advanced version of the normal Proportional Integral Derivative (PID) controllers where the Integral and Derivative order of the error were made to take fractional values. The scheme had shown better performance when applied to other systems and hence, been scarce, unpopular or not in the case of systems under consideration made it worth exploring. The two-link planar robot model was adapted from the works of Nazif *et al.* conducted in 2023. The system with the FPID was then compared with the PID coupled with examination of frictional disturbance using sinusoidal reference signal, in order to capture close to the nonlinearity of the normal robot trajectory making it a good test signal for the system. The results completely indicated that the FPID controller demonstrated better performance over the conventional PID. It showed that effort in controlling link 1 with the FPID with and without frictional disturbance revealed approximately 5% improvement over with the PID. In the case of link 2 the enhancement was about 18%. In terms of error improvements; higher amounts of cumulative errors with and without disturbance with the PID than with the FPID. Changes in the errors between with the FPID are lower than with those with the PID making the FPID more robust. Hence, the system with the FPID was more accurate and robust compared to with the PID. It is therefore expected that with careful fine tuning the system may be made even better with the scheme.

1. BACKGROUND

Robotic arms have numerous applications in different fields, which include automated industries, healthcare, manufacturing and space exploration among others. Owing to the ability for executing complex tasks at high accuracy, precision as well as repeatability (Sinuraya et al., 2025). Among the various existing configurations, the two-link planar robotic arm had extensively been studied due to its simplicity, popularity, easier adaptability and representative dynamic behavior. The configuration had two degrees of freedom (DOF) and with the robotic arm facilitating independent link movement, enabling precise planar (2D) motion control in a critical requirement in applications such as material handling, welding, painting and even minimally invasive surgery (Pasupuleti, 2019; Boscariol et al.,2022; Kwok et al., 2022).

A popular and widely adopted control strategy for such systems is the Proportional-Derivative (PD) controller, operating based on two key components viz: The proportional (KP) term that focused on correcting the immediate error existing between the desired and actual resulting positions and the derivative (KD) term that predicts future errors utilising the rate of change consequently enhancing system damping and stability (Borase et al., 2021; Kumar and Kumari, 2024).

Ilgen et al., (2018) employed the Sliding Mode Controller (SMC) on a two-link robotic manipulator. The Adam and MATLAB software were utilized for the studies. In another work by Mohammed and Eltayeb, (2018) the SMC and Proportional-Integral-Derivative (PID) were evaluated on a two-link manipulator. The SMC with predicted boundary conditions was considered in the works of Han and Jia, (2020). The effort was to solve the complexity of the normal SMC which according the report presented had solved the stated problem to some extent. An improved reaching law based SMC was applied in studies conducted by Ji et al., (2022) and in the works of Nguyen et al., (2020) the exponential reaching law based SMC was explored. In the study conducted by Zou (2009) the Fuzzy Logic was utilized.

The PD controllers were only effective to some extent, but they have limitations in handling the highly nonlinear and complexity of the systems requiring the need for more precise sensors. The Fractional Order Proportional-

ISBN: 978-978-8567-02-8

Integral-Derivative (FPID) controllers; the FPID controllers leverage the fractional calculus which incorporate non-integer (fractional) order (μ) for the derivative term. Thus, providing extension providing greater flexibility in the tuning, thereby improving the system's ability for greater adaptability compensation to nonlinearities and transient response performance (Kumar et al., 2018; Singh et al., 2021; Batiha et al., 2022; Husnain et al., 2023; Eltayeb et al., 2024).

FPID controllers were known for their ability in outperforming the conventional PID controller counterparts in applications demanding better precision due to their enhanced robustness capability and ability to managing or handling parameter uncertainties. Their implementation was a bit more complex, in the sense that; requirement demands the optimization of five parameters (KP, KI, KD, λ and μ) instead of just the three, resulting in a tuning challenge which could be significant (Bingi et al., 2020; Tepliakov et al., 2021; Jamil et al., 2022), but is worth exploring as it may be simpler in this case due to the absence of λ making the parameters four (4) not five (5) making it slightly simpler for the system under consideration.

2. METHODOLOGY

The two-link robot from the work of Nazif and colleagues (Nazif et. al., 2023) was adapted in the studies as given by equations (1) – (12), where; τ is the torque matrix of the system, g is the gravity matrix, M is the inertia matrix and V is the Coriolis matrix. The torque matrix indicated the torque developed by the two links. The masses by m, l the lengths of the links, θ the angular positions, $\dot{\theta}$ angular velocity and $\ddot{\theta}$ angular accelerations of the links. The PID and FPID control laws were given by (13) and (14) respectively. The results of the PID and FPID were compared both without and considering frictional disturbance effect. The work was simulated using SIMULINK/MATLAB software.

$$\tau = M(\theta)\ddot{\theta} + V(\theta,\dot{\theta}) + g(\theta) \quad (1)$$

$$\tau = \begin{bmatrix}\tau_1\\ \tau_2\end{bmatrix} \quad (2)$$

$$V = \begin{bmatrix}V_1\\ V_2\end{bmatrix} \quad (3)$$

$$V_1 = -m_2 l_1 l_2 (2\dot{\theta_1}\dot{\theta_2} + \dot{\theta_2^2}) \sin\theta_2 \quad (4)$$

$$V_2 = m_2 l_1 l_2 \dot{\theta_1^2} \sin\theta_2 \quad (5)$$

$$g = \begin{bmatrix}g_1\\ g_2\end{bmatrix} \quad (6)$$

$$g_1 = (m_1 + m_2) g l_1 \cos(\theta_1) + m_2 g l_2 \cos(\theta_1 + \theta_2) \quad (7)$$

$$g_2 = m_2 g l_2 \cos(\theta_1 + \theta_2) \quad (8)$$

$$M = \begin{bmatrix}M_{11} & M_{12}\\ M_{21} & M_{22}\end{bmatrix} \quad (9)$$

$$M_{11} = (m_1 + m_2) l_1^2 + m_2 l_2^2 + 2 m_2 l_1 l_2 \cos\theta_2 \quad (10)$$

$$M_{12} = M_{22} = m_2 l_2^2 \quad (11)$$

$$M_{21} = m_2 l_2^2 + m_2 l_1 l_2 \cos\theta_2 \quad (12)$$

$$U_{PID} = eKP + (de/dt)KD \quad (13)$$

$$U_{FPID} = eKP + \left(\frac{de}{dt}\right)^{\mu} (KD) \quad (14)$$

3. RESULTS

Results were presented with and without frictional disturbance compared for the system with the FPID and with the PID for sinusoidal reference signal. The sinusoidal reference was chosen as the suitable test signal because it tries to mimic the nonlinearities and changing nature of the trajectories found in robotic systems. The Figure 1 showed the link1 position and speed tracking response and Figure 2 for link2. Figure 3 gives the cumulative error resulted. It can be seen that the Figure 3 tried to further capture the tracking abilities of the different schemes portrayed by Figure 1 and 2. The plots for both the PID and the FOPID were very close. Hence, the cumulative tracking error was around 400 with the PID and about 380 with the FOPID which revealed the FOPID controller more accurate due to least amount of error. It also indicated that it improved the system over with the PID by 5%. The system with the FPID was also more robust due to its ability to suppress the error by 20 more than with the PID; therefore, the FOPID is more robust by a factor of about 20 compared to the PID for link1. The cumulative tracking error was about 220 with the PID and 180 with the FPID indicating that the FPID controller maintained more accuracy due resulting lower amount of error. Revealing an improvement of about 18% compared with the PID.

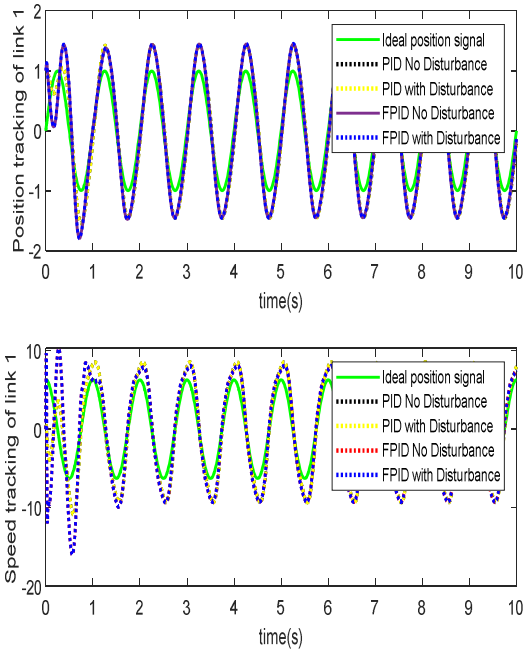


Figure 1: Link 1 position and speed tracking response.

ISBN: 978-978-8567-02-8

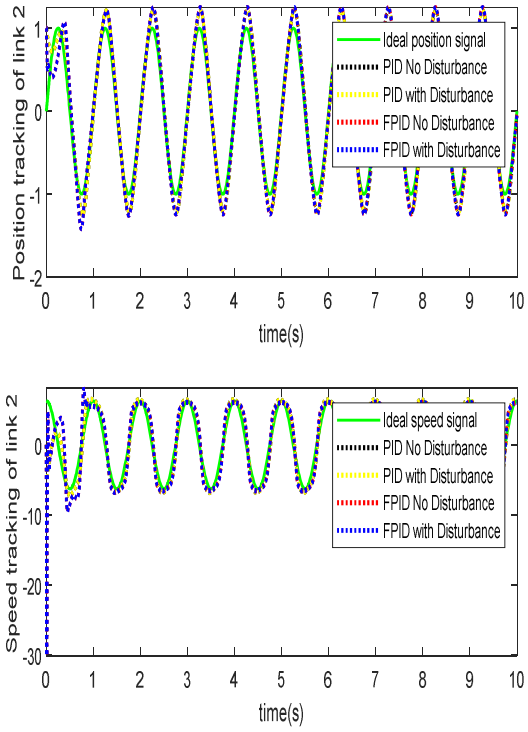


Figure 2: Link2 position and speed tracking response.

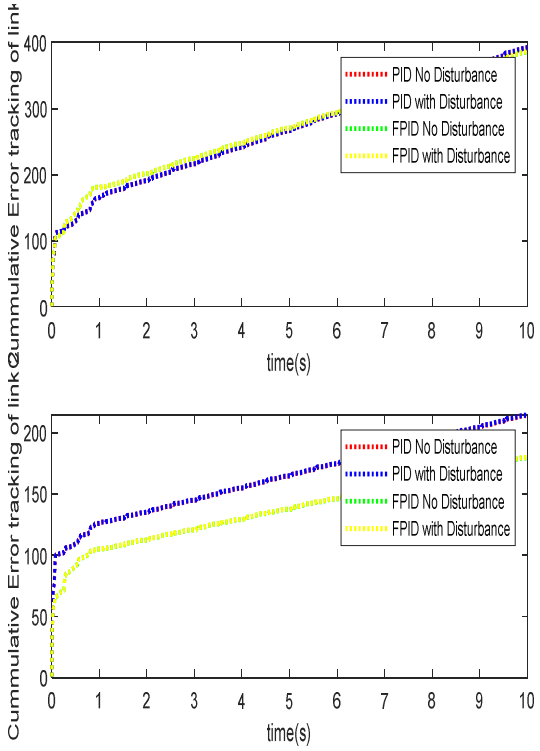


Figure 3: Link2 and Link2 cumulative tracking errors.

The system with the FPID also showed more robustness due to its capability of error suppression the by 40 over the case with the PID; hence, the FPID is more robust by a factor of about 40 in comparison to the PID for link2. Average improvements were 12% in terms of accuracy improvement and factor of about 30 for robustness over with the PID. It revealed advantage in the FPID ability for compensating of dynamics coupling and interaction forces between the links.

The results therefore completely indicated the superiority of the FPID controller demonstrating better performance over the conventional PID. Indicating that effort in controlling link 1 utilising the FPID with and without frictional disturbance demonstrated approximately 5% improvement over with the PID and in the case of link 2 the enhancement was about 18%. Hence, in terms of error improvements; higher amounts of cumulative errors with and without disturbance, making the system with the FPID been more accurate. Also, the changes in the errors between with the FPID are lower than with those with the PID making the FPID more robust as well. Therefore, it revealed that the system with the FPID was more accurate as well as more robust compared to with the PID scheme.

4. CONCLUSION

The work successfully presented the application of Fractional Order Proportional Integral Derivative (FPID) controller for the two-link planar robot. Robotics have already form part of the modern world and further advances in the technology kept making the requirements for accuracy and robustness more stringent. There are different control methods proposed for such systems, but interestingly simpler versions were the target due to computational burden associated with the complexities of the more advanced control schemes. The FPID has been an advanced version of the Proportional Integral Derivative (PID) controllers where the Integral and Derivative order of the error were of fractional values. The FPID had shown better results when applied to other systems and hence, been unpopular in the case of the system under consideration made it worth exploring. The two-link planar robot model was adapted from the works of Nazif *et al.* done in 2023. The system with the FPID was then compared with the PID with and without the effect of frictional disturbance using sinusoidal reference signal, in order to capture close to nonlinearity of the normal robot trajectory making it a good test signal for the system. The results completely indicated that the FPID controller demonstrated better performance over the conventional PID counterpart. It showed that effort in controlling link 1 with the FPID with and without frictional disturbance revealed approximately 5% improvement over with the PID. In the case of link 2 an enhancement was about 18%. In terms of error improvements; higher amounts of cumulative errors with and without disturbance. Changes in the errors between with the FPID (about 270) are lower than with those with the PID (about 310) making the FPID more robust. Hence, the system with the FPID was more accurate (lower amount of error) and robust (lower amount of change in error) compared to with the PID. Hence, it is highly expected that with a very careful fine tuning may make the system even better with the scheme investigated.

ACKNOWLEDGMENT

Authors would like sincerely like the “Abubakar Tafawa Balewa University Bauchi” for their

ISBN: 978-978-8567-02-8

encouragement and support always.

REFERENCE

Batiha, I. M., Njadat, S. A., Batyha, R. M., Zraiqat, A., Dababneh, A., & Momani, S. (2022). Design fractional-order PID controllers for single-joint robot arm model. *Int.* J. Adv. Soft Comput. Appl, Vol. 14, No. 2, pp: 96-114.

Bingi, K., Ibrahim, R., Karsiti, M. N., Hassan, S. M., & Harindran, V. R. (2020). Fractional-order systems and PID controllers. Cham, Switzerland: Springer International Publishing, Vol. 264.

Borase, R. P., Maghade, D. K., Sondkar, S. Y., & Pawar, S. N. (2021). A review of PID control, tuning methods and applications. International Journal of Dynamics and Control, Vol. 9, No. 2, pp: 818-827.

Boscariol, P., Gasparetto, A., & Scalera, L. (2022). Path planning for special robotic operations. In Robot Design: From Theory to Service Applications, Cham: Springer International Publishing, pp. 69-95.

Eltayeb, A., Ahmed, G., Imran, I. H., Alyazidi, N. M., & Abubaker, A. (2024). Comparative analysis: Fractional pid vs. pid controllers for robotic arm using genetic algorithm optimization. Automation, Vol. 5, No.3, pp: 230-245.

Han, F., & Jia, Y., (2020). Sliding mode boundary control for a planar two-link rigid-flexible manipulator with input disturbances. International Journal of Control, Automation and Systems, Vol. 18, No. 2, pp:351-362.

Husnain, S., & Abdulkader, R. (2023). Fractional order modeling and control of an articulated robotic arm. Engineering, Technology & Applied Science Research, Vol. 13, No. 6, pp: 12026-12032.

İlgen, S., Durdu, A., Gülbahçe, E., & Çakan, A., (2018). Sliding mode control of a two-link robot manipulator using Adams & Matlab software. In *2018 6th International Conference on Control Engineering & Information Technology (CEIT)* (pp: 1-4). IEEE.

Jamil, A. A., Tu, W. F., Ali, S. W., Terriche, Y., & Guerrero, J. M. (2022). Fractional-order PID controllers for temperature control: A review. Energies, Vol. 15, No. 10, pp:3800.

Ji, P., Li, C., & Ma, F., (2022). Sliding mode control of manipulator based on improved reaching law and sliding surface. Mathematics, Vol.10, No.11, 1935.

Kumar, A., & Kumari, P. (2024, October). Refining PI/PID Controller Design with Stability Margins: A Survey on Simplicity and Flexibility. In 2024 IEEE International Conference on Intelligent Systems and Advanced Applications (ICISAA), pp: 1-6.

Kumar, J., Kumar, V., & Rana, K. P. S. (2018). Design of robust fractional order fuzzy sliding mode PID controller for two link robotic manipulator system. Journal of Intelligent & Fuzzy Systems, Vol. 35, No. 5, pp: 5301-5315.

Kwok, K. W., Wurdemann, H., Arezzo, A., Menciassi, A., & Althoefer, K. (2022). Soft robot-assisted minimally invasive surgery and interventions: Advances and outlook. Proceedings of the IEEE, Vol. 110, No. 7, pp: 871-892.

Nazif, D. M., Mohammed, A., Hassan, S. M., & Usman, I. H. (2023). Simplified Exponential Reaching Law Based Sliding Mode Control Of Two-Link Planar Robot. Nigerian Journal of Tropical Engineering, Vol. 17, No.1, pp: 1-9.

Nguyen, T. L., Nguyen, H. Q., Duong, M. D. and Ngo, K. T., (2020). Exponential reaching law sliding mode control for dual arm robots, J. Eng. Sci. Technol., Vol. 15, No. 4, pp: 2841-2853.

Pasupuleti, S. (2019). Mechanisms and Control Systems in Robotic Manufacturing: A Mechanical Engineer's Approach. IJIRMPS, Vol. 7, Iss. 2, pp:1-8.

Singh, A. P., Deb, D., Agrawal, H., & Balas, V. E. (2021). Fractional Modeling and Controller Design of Robotic Manipulators. Fractional Modeling and Controller Design of Robotic Manipulators.

Sinuraya, E. W., Winardi, B., & Nizam, Z. (2025). Robotic Arm Control System Design for High Precision Work. Journal of Moeslim Research Technik, Vol. 2, No. 2, pp: 49-57.

Tepljakov, A., Alagoz, B. B., Yeroglu, C., Gonzalez, E. A., Hosseinnia, S. H., Petlenkov, E., ... & Cech, M. (2021). Towards industrialization of FOPID controllers: A survey on milestones of fractional-order control and pathways for future developments. IEEE Access, Vol. 9, pp: 21016-21042.

Zou, J. (2009). Fuzzy sliding-mode control of a two-link robot manipulator (Doctoral dissertation, Dissertação (Mestrado)—National Yunlin University of Science and Technology).

ISBN: 978-978-8567-02-8

5TH Faculty of Engineering Conference on Engineering Innovation and Economic Policies: Driving Sustainable Industrial Growth in Nigeria

Faculty of Engineering, Bayero University, Kano.

044-Optimum Proportional Integral Derivative Control using Grey Wolf Optimization Algorithm for Single Machine Infinite Bus System

Abdulrazak Sabo[1], Mohammed Ahmed[1,*], Sabo Sani Mohammed[1], Adamu Yawale Babawuro[2], Musa Baba Lawan[3]

[1]*Electrical and Electronics Engineering Department (EEED), Abubakar Tafawa Balewa University (ATBU), Bauchi.*

[2]*Mechatronics and Systems Engineering Department (MTED), Abubakar Tafawa Balewa University (ATBU), Bauchi.*

[3]*Electrical Engineering Department (EED), University of Maiduguri (UM), Maiduguri.*

(Corresponding author email: inunugoloma@yahoo.com)

Abstract: The study was on the application of the Grey Wolf Optimization (GWO) algorithm for optimizing the Proportional Integral Derivative (PID) controller on the Single Machine Infinite Bus (SMIB) system. The SMIB has been an acceptable model used to represent the power system. Control systems are applied for power system stabilization. Literature indicated that several control schemes have been proposed for such systems. It is expected that easy to implement and simple are preferred. The GWO which is a metaheuristic optimization approach combine intelligence and ability to generate large number of possible solutions among which the best is chosen. It's one of the recent algorithm being explored due to their inherent abilities over the earlier ones. The GWO optimized PID controller (GPD) was compared with the normal PID controller (PID). Results indicated that the GWO algorithm had successfully tuned the PID controller optimally for the SMIB system. No oscillations were observed and overshoot which was about 90% was completely eliminated which were present in the system response without controller. The system with the GPD had about 1% overshoot and also settles faster than with the PID; that is in 2s compared to 16% and 5s with the PID. Others are better rise time and void of oscillations. It is therefore expected that with further refinement of the proposed system can be made better. It can even be applied to similar systems and others.

1. INTRODUCTION

Power system stabilization is achieved using control was an approach for damping low-frequency oscillations (also known as power swings) originating from disturbances such as faults or loading effect changes. It results in improving the grid reliability and allows higher effective power transfer. In reality the system works by modulating the system voltage through an automated voltage regulation arrangement utilising signals that could be the generator speed or power. Therefore, corrective measures are applied such that electrical torque usually in phase with the rotor swings in order to bring back the system to equilibrium state with the help of suitable controller. The measure is cost-effective enhancement that boosts small-signal stability, which is crucial for grids interconnectivities most especially with renewable energy sources which are most of the time fluctuating (Vittal et al., 2019; Machowisky, 2020).

Single machine infinite bus (SMIB) systems have being used as suitable representative of the power systems. A single machine model is usually considered to be connected to an infinite bus forming the system. Properties of the system were suitably present and in simpler form. It is also highly expected results when implemented on the real physical system would work without much hitches and are highly manageable (Dulau and Beaker, 2015; Du et al., 2020; Suresh Kumar and Babu, 2021).

A review of works related to the control of power systems targeting the SMIB were as mentioned below. The true mathematical model of the SMIB system having lower order of control arrangement. Different control schemes which are state space based were considered replacing the conventional stabilisation arrangement of the power systems for different configurations of operations and results obtained were promising (Verneker et al., 2020). In the works of Angu and his team (Angu et al., 2017) an extended observer was utilized resulting in better results, they further their studies by reducing the order earlier proposed control scheme successfully (Angu et al., 2018). The pole placement and linear matrix inequality was explored by Shan and Chang (Shan and Chang, 2013) and the linear quadratic regulator

ISBN: 978-978-8567-02-8

was further explored by Uravakonda et al., (2020), all portraying good results. The observer based flatness theory approach was studied on the SMIB systems with encouraging results (Aghababa, et al., 2020). In the works of Kasilingam et al., (2019) utilized the Biogeography-Based Optimization Algorithm for optimal control. In order to contribute the Grey Wolf Optimization (GWO) algorithm for Proportional Integral Derivative (PID) controller optimisation was explored with the expectation of producing a simpler and straight forward solution for the control of such systems using the PID control scheme having enhanced performance of which literature indicated such was has not been done to best ability of the authors.

The GWO algorithm is also a category of the nature-inspired technique which is metaheuristic. It mimicked how grey wolf pack hunt. It utilises a hierarchy referred to as: alpha, beta, delta and omega wolves in determining optimal solutions in complex problems, by trying to balance exploration (that is; searching) and the exploitation (that is; attacking of prey). Achieved through steps such as encircling, hunting and attacking as a guide to the population of 'wolf' targeting the best solution for accomplishment. Among the remarkable advantages of GWO was simplicity as well as its capability in handling complex optimization issues having lower number control parameters compared to other metaheuristic algorithms such particle swarm and genetic algorithms. It has high efficiency in determining global optima making it suitable for wider scope of applications, among which are the power systems optimisations, selection of features in machine learning as well as structural engineering. In addition, it has the ability in balancing both the exploration and exploitation such diversity is maintained during the search process, thereby reducing the chances of moving into stuck condition resulting in local minima (Mirjalili et al., 2014; Tawhid et al., 2021; Qiu et al., 2024).

2. METHODS

The adapted SMIB mathematical model was credited to Phillips et al., (2015) as given by equation (1). The parameters $P_e(s)$ represents the electrical power component and $P_M(s)$ the mechanical power component all in per unit (PU). Others are b the damping constant, I the inertia of the system and k is a constant of the system.

$$G(s) = \frac{P_e(s)}{P_M(s)} = \frac{k}{Is\text{^}2 + bs + k} \quad (1)$$

The GWO is described by equations (2) – (4). Equation (2) indicate the algorithm having dimension of g that provide the resulting solution space of the utilized GWO algorithm explored for solving the optimization problem with the size of the gray wolf of M population. Also, the position of the *j-th* gray wolf was expressed as described by equation (2). The optimal, next to it and third to optimal solutions in the population of the gray wolf were designated as α, β, and δ accordingly. Other solutions were referred to as ω. These four groups are also referred to as: Leading grey wolf, superior grey wolf, inferior grey wolf and medium grey wolf respectively. Finding optimal solution involved constantly updating ω at constant rate. Equations (3) and (4) are then used to compute the positions of the gray wolves.

$$X_j(t) = \{X_j^1, X_j^2, \dots X_j^g\}, j = 1,2, \dots M \quad (2)$$

$$X(t+1) = X_d(t) - H \times |C \times X_d(t) - X(t)| \quad (3)$$

$$H = 2h \times r_1 - h \quad (4)$$

The GWO optimized PID controller (GPD) was therefore obtained by utilizing the algorithm described. The normal PID controller (PID) was obtained by auto-tuning using the TOOLBOX in SIMULINK/MATLAB software. The proposed GPD controller was then compared with the PID.

The block diagram of the system is as given by Figure 1. The reference depicts the desired system response and the response gives the actual system response. The plant refers to the SMIB system. The feedback connects the output; that is the response, to the reference. The reference is then compared by the response and the controller tries to compensate for the amount of error produced. The controller is a PID controller which is optimized by the GWO in the case of the proposed technique, while the classical PID was tuned as earlier mentioned by the toolbox. Figure 2 showed the Simulink implementation. The various components were interconnected as portrayed by the Figure 2. The optimization was executed using codes in MATLAB and the values implemented in SIMULINK. Results are the ploted utilizing the codes in MATLAB after extraction from the workspace.

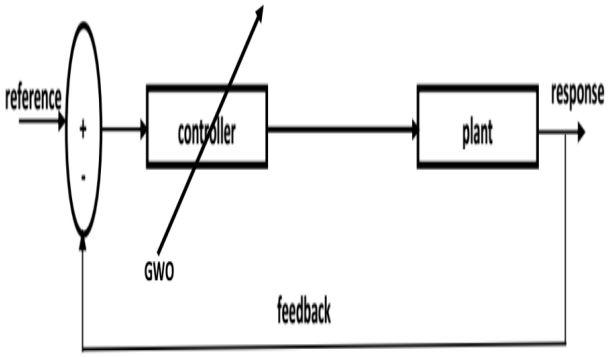


Figure 1: Block Diagram of the System.

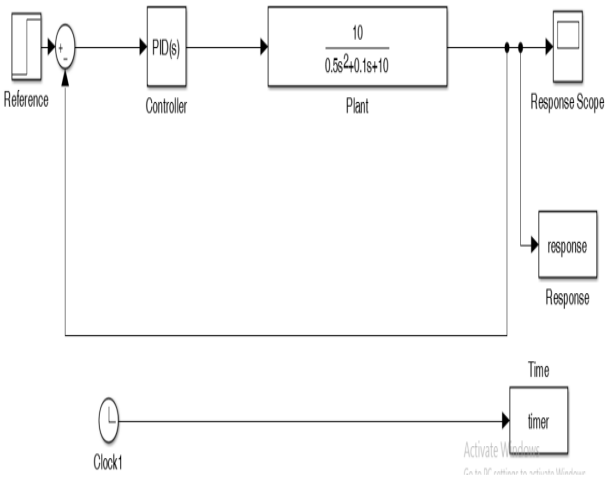


Figure 2: Simulink Block of the System.

ISBN: 978-978-8567-02-8

3. OUTCOMES

The Figures 3 – 7 were the system response without controller or just unity feedback, the plot of the optimization process, the system response after optimization and the system response with the PID control scheme respectively. Figure 3 shows the inherent system oscillatory behavior mentioned earlier as concerned to be compensated. Figure 2 showed how optimum result was attained for population of 50 (M) and size or dimension of 50 (g). it can be seen that convergence was attained at about the fifth iteration with integral time absolute error (ITAE) confirming the advantage of the algorithm. Figure 3 revealed the response of the system with the GPD. It showed an overshoot 1% and settling time of 2 seconds; portraying an oscillation free or damped oscillation. Figure 4 is the response of the system with the PID controller indicating an overshoot of around 16% and settling time of 5 seconds. Figure 7 made a comparison of the system response with PID and GPD; thereby buttressing what were mentioned.

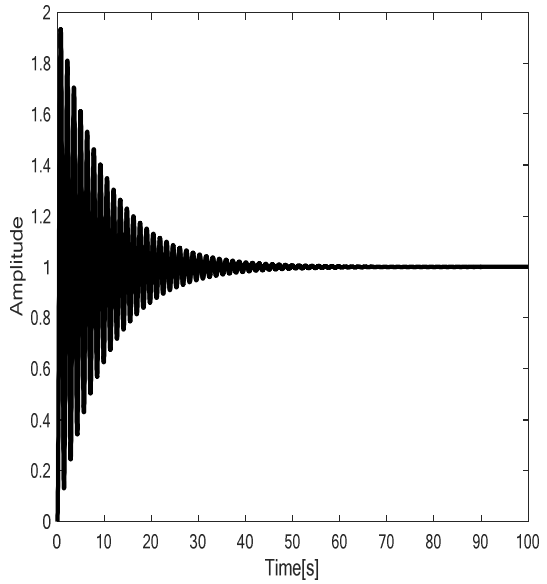


Figure 3: System Response before Optimisation

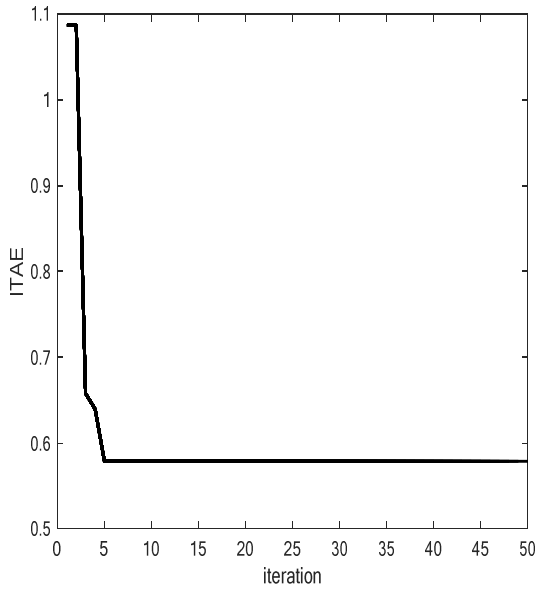


Figure 4: System Optimisation Plot

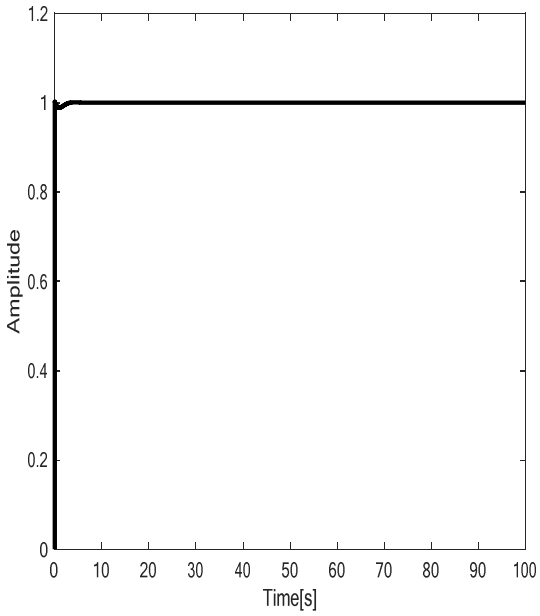


Figure 5: System Response after Optimisation

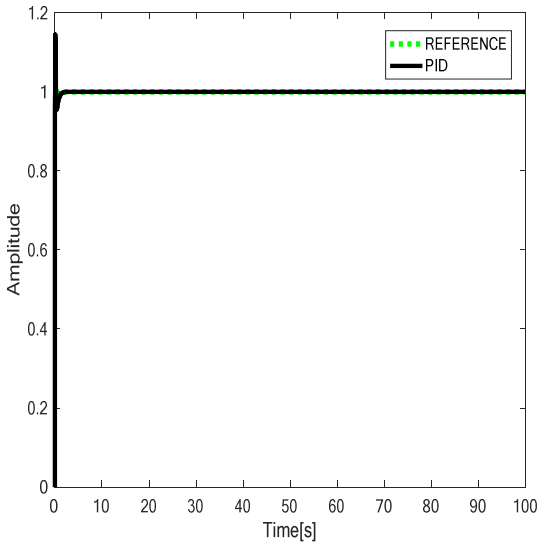


Figure 6: System Response with PID controller.

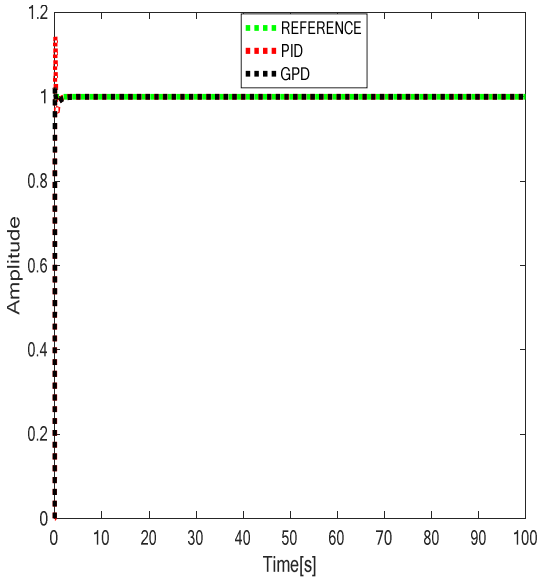


Figure 7: System Response with GPD and PID controllers.

ISBN: 978-978-8567-02-8

4. DISCUSSION

The study was conducted successfully; that is utilizing the GWO for optimizing the SMIB system. Results therefore indicated that the GWO algorithm had successfully been utilized for tuning the PID controller optimally for the SMIB system. Oscillations and overshoot were completely compensated in the system response without controller which was above 90% was almost completely canceled. The system with the GPD had 1% overshoot and also settles faster than with the PID; that is in about 2s compared to 16% and 5s with the PID scheme. Others are better rise time and null of oscillations. Hence, it is highly anticipated that with further refinements the system could be enhanced further.

5. CONCLUSION

The study on the application of the Grey Wolf Optimization (GWO) algorithm for optimizing the Proportional Integral Derivative (PID) controller on the Single Machine Infinite Bus (SMIB) system was successfully conducted. The SMIB was an accepted mathematical model for representing the power system. The application of control systems was one of the approaches for power system stabilisation. There are many control approaches proposed for such systems. The advantages of the GWO included easy implementation and simplicity. The GWO categorized as metaheuristic optimization approach combine intelligence and ability to generate large number of possible solutions among which the best is chosen and it's among the recent algorithm being explored due to their inherent abilities over the earlier ones. The GWO optimized PID controller (GPD) was compared with the normal PID controller (PID). Results indicated that oscillations and overshoot which was about 90% without controller was completely eliminated. The system with the GPD had only about 1% overshoot and settles faster than the system PID controller; that is in 2s compared to 16% and 5s with the PID. Others are better rise time and void of oscillations. Hence, better results were anticipated with further careful and systematic refinements.

ACKNOWLEDGMENT

Authors wish to acknowledge the "Abubakar Tafawa Balewa University, Bauchi", The Tertiary Education Fund, Abuja", their various families, colleagues and well-wishers for encouragements and supports.

REFERENCES

Aghababa, M. P., Marinescu, B., & Xavier, F., (2020). Observer-based tracking control for single machine infinite bus system via flatness theory. International Journal of Electrical and Computer Engineering.

Angu, R., & Mehta, R. K., (2017). A single machine infinite bus power system damping control design with extended state observer. Cogent Engineering, Vol. 4, No. 1, 1369923.

Angu, R., & Mehta, R. K., (2018). A single machine infinite bus power system excitation control design with extended reduced-order observer**.** International Journal of Dynamics and Control, 2018 - Springer

Du, W., Dong, W., Wang, Y., & Wang, H., (2020). A method to design power system stabilizers in a multi-machine power system based on single-machine infinite-bus system model. IEEE Transactions on Power Systems, Vol. 36, No. 4, pp: 3475-3486.

Kasilingam, G., Pasupuleti, J., Bharatiraja, C., & Adedayo, Y., (2019). Single Machine Connected Infinite Bus System Tuning Coordination Control using Biogeography-Based Optimization Algorithm. FME Transactions, Vol. 47, No. 3.

Machowski, J., Lubosny, Z., Bialek, J. W., & Bumby, J. R., (2020). Power system dynamics: stability and control. John Wiley & Sons.

Mirjalili, S., Mirjalili, S. M., & Lewis, A., (2014). Grey wolf optimizer. Advances in engineering software, Vol. 69, pp:46-61.

Phillips, C. L. ,Nagle, H. T. Chakrabortty, A., (2015). Digital Control System Analysis & Design, Pearson Education Limited, Edinburgh Gate Harlow, Essex CM20 2JE, England, ISBN 13: 978-1-292-06188-7.

Qiu, Y., Yang, X., & Chen, S., (2024). An improved gray wolf optimization algorithm solving to functional optimization and engineering design problems. Scientific Reports, Vol. 14, No.1, 14190.

Shan, Y., & Chang, X. (2013, June). Gain-scheduled LPV control of a single-machine infinite-bus power system. In Unifying Electrical Engineering and Electronics Engineering: Proceedings of the 2012 International Conference on Electrical and Electronics Engineering (pp:331-342). New York, NY: Springer New York.

Suresh Kumar, M. G., & Babu, C. A., (2022). Slow flow solutions and stability analysis of single machine to infinite bus power systems. International Journal of Emerging Electric Power Systems, Vol. 23, No. 1.

Tawhid, A., Teotia, T., & Elmiligi, H., (2021). Machine learning for optimizing healthcare resources. In Machine Learning, Big Data, and IoT for Medical Informatics (pp: 215-239). Academic Press.

Uravakonda, S., Mallapu, V. K., & Annapu Reddy, V. R., (2020). Damping enhancement for SMIB power system equipped with LQR tuned via analytical approach. Journal of The Institution of Engineers (India): Series B, Vol. 101, No. 5, pp:541-551.

Vernekar, P., Wang, Z., Serrani, A., & Passino, K., (2020). Feedback control methods for a single machine infinite bus system. arXiv preprint arXiv:2009.05689.

Vittal, V., McCalley, J. D., Anderson, P. M., & Fouad, A. A., (2019). Power system control and stability. John Wiley & Sons.

ISBN: 978-978-8567-02-8

046-Experimental Evaluation of Partial Cement Replacement with Bagasse Ash and Rice Husk Ash on the Slump, Compressive Strength and Split tensile Strength of Ternary Blend Concrete.

Abdullahi M. SHETTIMA[a], Dr. Abdurra'uf M. GORA[b], Muhammad A. YAQUB[c], Salihu M. ZAKARIYA[d]

Department of Civil Engineering, Bayero University, Kano, PMB 3011.Nigeria
[a]*Abdullahimohammedshettima.ams@gmail.com*, [b]*amgora.civ@buk.edu.ng*

Abstract: The escalating environmental issues associated with ordinary Portland cement (OPC) production have spurred the pursuit of sustainable alternatives in concrete production. This study looks at replacing OPC with bagasse ash (BA) and rice husk ash (RHA) in a ratio of (0-20%) as a ternary blend in concrete to increase mechanical strength qualities while lowering carbon emissions. The goal of this research is to use Response Surface Methodology (RSM) to optimize the BA and RHA blend proportions in order to create ternary blend concrete with good performance and environmentally friendly. The procedure entailed calcining bagasse at 650°C for 2hr and rice husk at 650°C for 1hr and subsequently sieving them through a 150µm sieve to get BA and RHA. The fresh, physical properties and chemical compositions were determined using sieve analysis and X-ray fluorescence (XRF). RSM's Central Composite Design (CCD) was used to create a mix proportion. A total of 13 mix combinations were created using varied quantities of BA and RHA. The concrete was later evaluated for slump, compressive and split tensile strength at 7 and 28days curing period. The compressive strength recorded 20.62 N/mm^2 at 7days strength at M3 (5% BA + 15% RHA) and 30.52 N/mm^2 at 28days which is 17.8% increase against the control. The highest tensile strength was also recorded at M3 (5B15R), with 2.60 *N/mm^2* at 7 days and 4.32 *N/mm^2* after 28 days, approximately 46% higher than the control. The optimal blend happens to be M3 (5B15R), which had the maximum compressive and tensile strength however, M5 (0%BA+10%RHA) retained 75 mm slump nearly 11.75% reduction against the control (M14) with 85mm slump. RSM models demonstrated good prediction accuracy ($R^2 > 0.712$). The findings support the use of BA mixed with RHA in ratio as supplemental cementitious materials so as to achieve workable concrete with good strength. This research advances sustainable construction materials by employing agricultural waste to create ternary blend concrete with less environmental effect.

1. INTRODUCTION

According to Chemistry and Industry (2023) Concrete is one of the building materials most commonly employed in construction projects worldwide. The main ingredient needed to make concrete is cement, which serves as a binder. Cement demand is rapidly increasing as a result of rapid worldwide development and growth. According to the International Energy Agency (2021), cement production accounts for approximately 7–8% of global CO_2 emissions. Building a better and healthier future for our world requires innovation and more sustainable practices, and the cement sector is essential to the required reduction of global emissions. Yet the release of industrial and agricultural waste into soil is a severe environmental issue that can contaminate the soil, jeopardizing groundwater, agricultural land quality, and overall ecosystem health (Mohan et al., 2023). Material science advancements have enabled the use of alternative materials in construction, including the likes of rice husk ash (RHA), bagasse ash (BA), and other agro-wastes. Effective waste management through recycling will be greatly aided by the reuse of the previously stated commodities.

Bagasse, a fibrous waste material of the sugar refining industry, is a fine, grey to off-white powder that contains silica, alumina, calcium oxide, and other minor elements. Various investigations showed that BA is a potential pozzolanic material according to Ahmad et al., (2021), it enhanced mechanical property. Prabhath et al., (2022) confirms the concrete's strength metrics increment by 10% when BA was used as a partial replacement for cement). According to Maglad et al., (2023) the concrete's compressive and split-tensile strengths were enhanced by mixing 20% bagasse ash and 4% corn ash with cement. According to Seyoum et al., (2021) concrete that has 5% bagasse ash used in place of cement has superior strength to concrete made with regular cement. The large-scale use of BA as a pozzolan is still restricted despite its shown advantages and renewability. Mostly because of its changeable chemical compositions (Mali and Nanthagopalan, 2021) and the presence of pollutants such carbonaceous chemicals and quartz (Almeida and Cordeiro, 2023). However, if the ratio of bagasse ash replacement has grown too high, the strength of the concrete may be diminished (Seyoum et al., 2021). Bheel et al., (2022) added that adding 5–10% BA to concrete improved its compressive and flexural strength.

ISBN: 978-978-8567-02-8

However, as rice husk possess some distinct composition and pozzolanic properties, is a plentiful agricultural waste product produced by burning rice husk., it has drawn a lot of interest as a supplemental material. Depending on how it is burned, the by-product might be pinkish-white, black, or gray. Ye, et al., (2018) examined the impact of substituting RHA in different amounts for some of the (OPC), and it was found that a 20% RHA replacement level enhanced the concrete's strength properties. Tariq et al., (2021) also investigated the impact of adding rice husk ash as a cementitious additional material on the characteristics of concrete. The tensile, flexural, and compressive strengths of cements containing rice husk ash were assessed. He employed RHA, a supplemental ingredient for cement, at varying percentages. The findings demonstrate that using 6% rice husk ash in place of cement yields the best results. However, there's need to search for local materials as alternatives such as (BA/RHA), while maintaining the mechanical properties of concrete which will reduce the cost of its production as huge amounts of agricultural and industrial wastes e.g (bagasse and rice husk) are dumped in open land, creating serious environmental hazards. Blending BA as a pozzolanic material is not widely recognized, and its applications are limited. BA is affordable and emits less CO_2. However, Maglad et al., (2021) and many researchers found that high replacements of BA alone resulted in mechanical strength decrease as BA percentage replacement increased. To address these, the method mostly adopted for use in optimization of materials properties is multivariable regression analysis. And in building and construction application, RSM is more suitable especially when more than one variable is involved. This is because RSM can use less experiments to evaluate the effects of one or more input variable on a response or properties which consequently will result to reduction in time and cost, developing model equations to predict the examined properties using as many variables as possible, carrying out optimization to obtain the optimum dosage of the variables that will yield maximum performance. Awolusi, et al., (2021) used RSM to optimize the properties of concrete containing steel fiber and limestone powder. In this study cement was partially replaced with (BA+RHA), which was prior characterized physically and chemically, effects on workability were investigated and mechanical strength of the ternary blend concrete was investigated in other to overcome the loss compressive strength.

2. METHODOLOGY

The materials that were used in this study are; OPC (BUA) of 42.5N Grade usually 50kg per bag, Bagasse ash, rice husk ash, portable water, fine and coarse aggregates. In this study, the cement used was Ordinary Portland Cement that contains CEM II / B-L (Portland Limestone Cement) with specific gravity of 3.15 and a fineness ranging from 300–360 m^2/kg it has standard consistency of 32% conforming to (BS EN 197-1 2000). Raw bagasse is procured in kano state, Nigeria as presented in figure 1.0 (a) after the juice is extracted, it was washed and dried in open air which remove excess moisture, it was later calcined at 650°C for 2hrs in furnace as presented in figure 2 (f). It was then sieved through a 150µm as figure 2(e) showed. The residue after combustion as seen in figure 1.0 (b) presents a brownish to gray color ash with chemical composition dominates by silicon dioxide (SiO_2) with average bulk density of $600kg/m^3$ and specific gravity of 2.15 named Bagasse Ash. However, figure 1(c) shows rice husk which was procured from a rice mill in Kura LGA of kano state Nigeria, it was dried, and then further calcined in a controlled condition at 650°C for an hour as figure 1(d) present, later sieved through same sieve size as bagasse ash. Both sieving follows (BS 812-105 -1989) guidelines, the greyish color rice husk ash had a specific gravity of 2.25 it also contains chemical compositions dominated by silicon dioxide (SiO_2) When combined, the total content of SiO_2, Al_2O_3, and Fe_2O_3 in each SCM exceeded the 70% minimum requirement specified by (ASTM C618 2019) for Class N pozzolanic materials whereas the SG values for BA and RHA, falls within the typical range of 2.0 to 2.3 for reactive pozzolans. The Portable water used for mixing and curing of concrete is clean and free from organic matter and oil. The fine aggregate used in the study is in its raw, un-sieved form and is directly sourced from kano state river, the sand is free from clay, silt and organic impurities. conforming to Zone II as (BS 812: Part 2-1995) which was later air dried to remove excess moisture in order to maintain water-to-cement ratio. The aggregate later reveals a specific gravity 2.63 conforming to zone II. Throughout the investigations, crushed coarse aggregates of 20mm procured from the local crushing plants in kano state Nigeria, were used. The aggregate was tested for its physical requirements such as gradation, fineness modulus and specific gravity in accordance with (BS 812: Part 2 1995), The aggregates were graded as shown in Fig. 1 (e). in accordance with (ASTM C136 2017), The sieve analysis plots confirmed that both aggregates met the grading limits of (ASTM C33 2018), validating their suitability for concrete production.

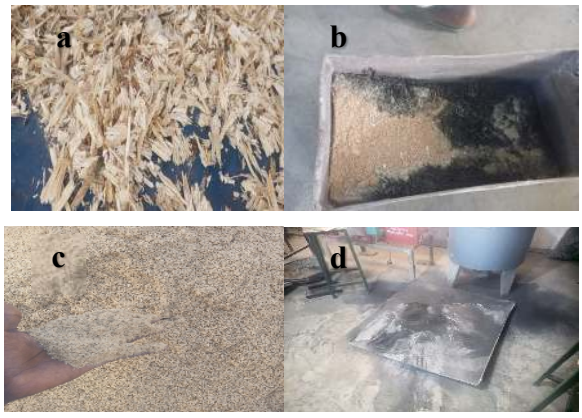


Figure 1.0: the above figures represent (a) Raw bagasse (b) Bagasse ash after calcination at 650°C for 2hrs in furnace (c) Raw rice husk before calcination (d) Rice husk ash after calcination at 650°C for 1hrs.

ISBN: 978-978-8567-02-8

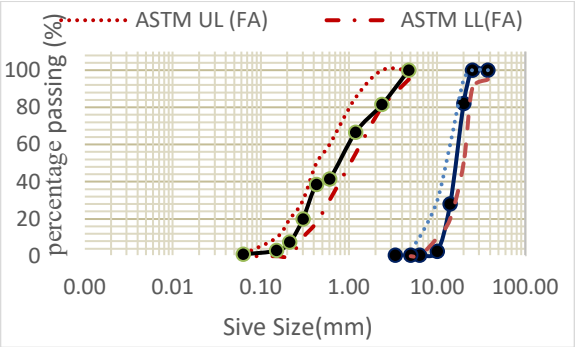


Figure 1 (e) Sieve Analysis Plot for Fine and Coarse Aggregates.

2.1. Mix design of ternary blend concrete

For a control sample of BA+RHA blend to be produced, the final mix percentage of the constituent materials is measured as shown in Table I. The desired proportions of cement, BA, RHA, coarse aggregate, fine aggregate, and water are established in other to build a concrete mix to obtain the required workability and strength. The proportioning was carried out in accordance with the BS 1881, P 125 (1986) design requirements, and a w/c ratio of 0.57 was used. The SCM's additions were adjusted to 0%, 5%, 10%, 15%, and 20% by weight of cement. The batches were carefully blended on a laboratory mixing tray using a hand trowel as shown in figure 2 (g). After three minutes of thorough mixing, a dry SCM's and cement mixture was added with to the former mix. During mixing, water was added. Before casting the specimens as seen in figure 2h, the molds were cleaned and greased with oil. slump results were recorded in accordance with BS EN 12350-2 (2019) for all 13 mixes including control sample. The concrete samples were cast in three layers, tamped with 25 blows using tamping rod. As shown in figure 3a after 24hrs, as per BS EN 12390-3 (2009) the samples were demolded and allowed to cure in water for 7 and 28-days curing age in the laboratory prior to Compressive strength testing as per BS EN 12390-3 (2009) for 7 and 28 days.

TABLE I: PROPORTION OF BA+RHA BLEND CONCRETE MIX (KG/M^3)

Mix ID	OPC (kg/m^3)	BA (kg/m^3)	RHA (kg/m^3)	Fine Agg. (kg/m^3)	Coarse Agg. (kg/m^3)	Water (kg/m^3)	replacement BA+RHA
M1(5B5R)	324.00	18.00	18.00	628	1220	204.12	10%
M2(15B5R)	288.00	54.00	18.00	628	1220	204.48	20%
M3(5B15R)	288.00	18.00	54.00	628	1220	204.48	20%
M4(10B20R)	252.00	36.00	72.00	628	1220	204.12	30%
M5(0B10R)	324.00	0.00	36.00	628	1220	204.12	10%
M6(10B10R)	288.00	36.00	36.00	628	1220	204.48	20%
M7(10B0R)	324.00	36.00	0.00	628	1220	204.12	10%
M8(10B10R)	288.00	36.00	36.00	628	1220	204.48	20%
M9(10B10R)	288.00	36.00	36.00	628	1220	204.48	20%
M10(10B10R)	288.00	36.00	36.00	628	1220	204.48	20%
M11(20B10R)	252.00	72.00	36.00	628	1220	204.12	30%
M12(10B10R)	288.00	36.00	36.00	628	1220	204.48	20%
M13(15B15R)	252.00	54.00	54.00	628	1220	204.12	30%
M14(0B0R)	360.00	0.00	0.00	628	1220	205	Control mix



Figure 2: The above figures represent (e) Sieving process for both BA and RHA through 150µm (f) Calcination process through furnace at 650°C for 1hrs (g) Represent sample mixing and (h) casting of cubes.

3. RESULTS AND DISCUSSION

3.1. Fresh property

The bar chart in figure 3 illustrates the changes in slump across concrete mixes. The control mix exhibited the highest slump 85mm, representing the baseline of a workable concrete. A progressive reduction in slump was recorded with increasing SCM content, confirming that blends with BA and RHA demand more water to achieve similar flowability due to the high fineness and water demand of the ashes. E.g., M1 yielded a slump of 73 mm while M5 retained 75 mm slump, indicating that RHA on its own imposes a smaller threat on workability compared to BA. So Medium replacements level of SCM has averaged slump value of 63.3mm ≤20% indicating that this threshold provides an excellent balance of sustainability and workability for field applications. At high SCM replacement (30% total), recorded the lowest slump, these results show that substantial workability loss would impede concrete placement without chemical admixtures, as stated by Lawan et al., (2022), who recommend using super plasticizers for SCM blends greater than 20% to avoid excessive stiffening.

In particular, the incorporation of ASTM C494 compliant high-range water-reducing admixtures, such as Type F (e.g., naphthalene-based or polycarboxylate-ether superplasticizers) or Type G admixtures high-range water-reducers with retarding properties, can effectively mitigate slump loss by improving particle dispersion and

ISBN: 978-978-8567-02-8

reducing water demand. The use of such admixtures would allow higher BA and RHA replacement levels (> 20%) to be practically achieved while maintaining adequate flowability and placement performance, thereby enhancing the sustainability potential of SCM-based concrete.

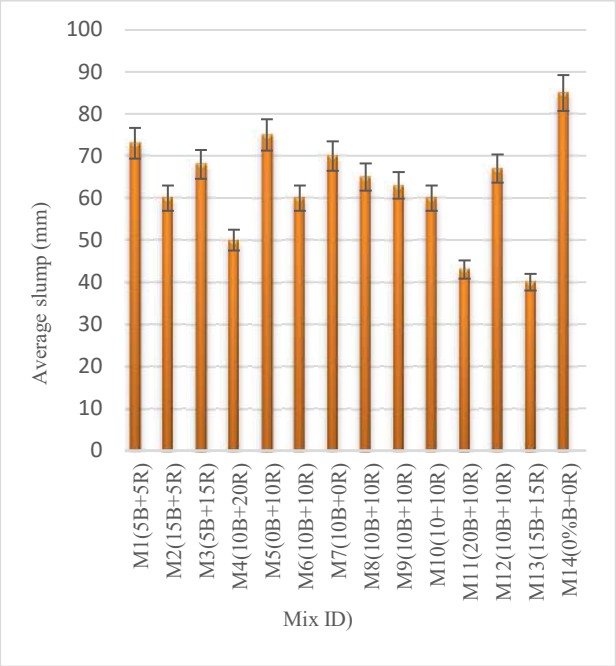


Figure 3: Slump test results of Eco-blend concrete containing BA and RHA

3.2. Compressive strength test at 7 and 28-days

Figure 4 shows a compressive strength where the control mixture has a strength of 17.50N/mm^2 at 7days and 25.90 N/mm^2 for 28days curing age. Highest 7days strength is in M3 having 20.62 N/mm^2. Followed by M5 with 20.34 N/mm^2 at 7days and 30.10 *N/mm^2* at 28days. M3 (5B15R) already shows superior performance at early age, indicating that the combination is effective even at early stages. At 28days control reached 25.90 N/mm^2 while M3 shows peak strength as well with 30.52 N/mm^2 which is 17.8% increase against the control exceeding the findings of (Adebola et al., 2023). However, this shows RHA's amorphous SiO_2 enhances C-S-H nucleation and densifies the paste and increase strength up to an optimal level conforming to (David et al., 2022). M3 shows great advantage of utilizing two waste materials and achieving the highest strength. The averages for (10B10R) were 28.71 *N/mm^2*, this suggests that an equal blend of BA and RHA at 10% each is not optimal. Worst performer is M13 (30% replacement) strength drops to 22 N/mm^2 which is -12.6% reductions against the control mix, due to the high replacement level which dilutes the cement content. This follows same trend as David et al., (2022) and Maglad et al., (2023) who warn on high SCM replacement. At 28days, BA is less effective than RHA when used alone. But when used in small amounts with high RHA it contributes positively.

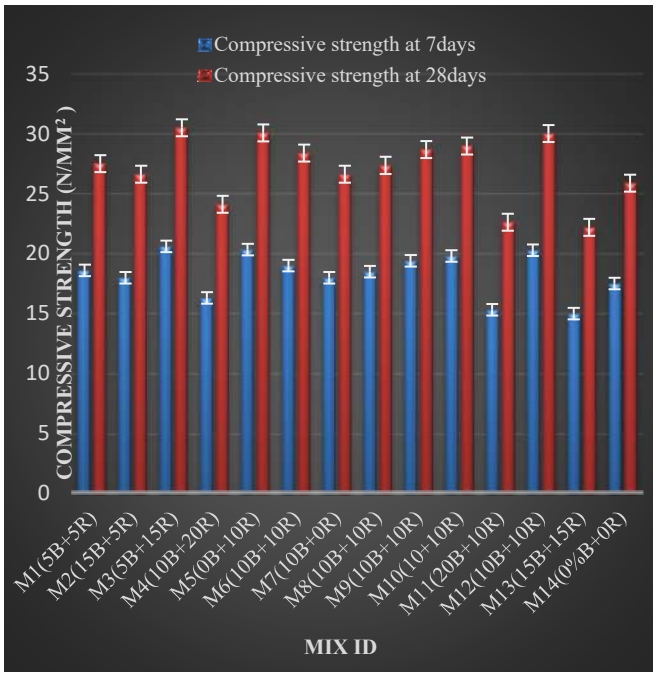


Figure 4: Compressive strength test results for 7 and 28days curing age.

3.3. Split Tensile Strength Test Results For 7 And 28-Days.

The split tensile strength of the concrete specimens at 7 and 28-days is presented in Figure 5 with control mix (M14), having 1.79 *N/mm^2* at 7 days and 2.95 *N/mm^2* at 28 days. The highest tensile strength was recorded in M3 (5B15R), with 2.60 *N/mm^2* at 7 days and 4.32 *N/mm^2* after 28 days. This increases roughly about 45.25-46.44% over the control at both ages, the blend gives excellent performance which can be ascribed to the synergistic interaction between the materials. Increasing RHA content leads to higher tensile strength. E.g., M5 and M3 are the top performers at both ages, achieving 2.30 *N/mm^2* and 3.80 *N/mm^2* at 7 and 28-days, respectively. This is consistent with the findings of Depaa et al., (2020) and Dhanalakshimi et al., (2023), who reported substantial tensile strength gains using RHA to replace cement up to 15%. High BA content (above 10%) tends to reduce the tensile strength as well, especially when RHA is low. E.g comparing M2 to control 1.55 *N/mm^2* at 7 days and 2.59 *N/mm^2* at 28 days. Similarly, the reduction is primarily attributed to the BA hydration effect which disrupts its matrix integrity. The group of mixes with 10% each represent the center points displayed relatively uniform tensile strength, averaging about 1.60 *N/mm^2* for 7-days and 2.65 *N/mm^2* at 28-days. While these values show improvement over the control. This confirms that the performance of BA and RHA in blended systems is highly dependent on the ratio and dosage levels.

ISBN: 978-978-8567-02-8

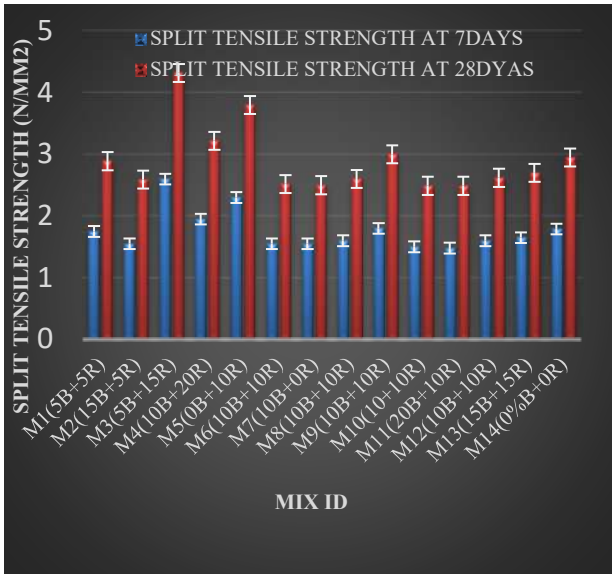


Figure 5: Represent the combine tensile effect at different percentage replacement

3.4. Response Surface Methodology for Compressive and Split Tensile strength at 7 and 28days curing.

The mechanical strengths properties and the input factors relationships was evaluated using ANOVA. Where R^2 is the coefficient of determination which assessed the validity of the quadratic function of the Central Composite Design model, which was evaluated and validated using the probability function (*p*-value) at a 95% confidence level.

3.4.1. ANOVA results for compressive and Tensile strength models

The ANOVA model results for 7 and 28days compressive and tensile strength where (CMP7, CMP28, STS7 and STS28) represent compressive and tensile strength at different curing age, A and B indicate the percentage of BA and RHA, for 7-days, model is highly significant with F-value of (19.52 and 25.53) and a corresponding *p*-value of (0.0003 and 0.0001) indicating that the model terms contribute meaningfully to the response. There is only a 0.03% and 0.01% chance that such an F-value could occur due to random error, confirming the robustness of the model. Statistical results for 28-day compressive and tensile strength model further affirm the suitability of the quadratic RSM approach. The model shows a F-value of (21.08 and 24.77) and a *p*-values of (0.0002 and 0.0001) indicating strong significance. The probability of obtaining such a result by chance is just (0.02% and 0.01%), making the model dependable for long-term strength prediction. In this case A, AB, A^2, B^2 are significant model terms. The model terms with *p*-values higher than 0.05 indicate no significant lack of fit, resulting in 65.53% and 60.99% for CMP and 70.46% and 80.16% for STS chance for noise to produce F-values of 0.6528 and 0.7428 for the CMP and 0.5624 and 0.4002 for STS at 7 and 28 days, respectively.

3.4.2. Performance Indicator for Compressive and Tensile Strength Models.

The main statistical adequacy indicator to assess the performance of the developed model is coefficient of regression. The models showed a close agreement between the Adjusted and Predicted R^2 values STS-7 (0.9042-0.8080), STS-28 (0.9014-0.8250), CMP-7 (0.8769-0.7445) and CMP-28 (0.8853-0.7516) i.e. difference less than 0.2 suggests that the model is both reliable and predictive. The adequate precision was also applied to assess the model performance with (STS 7days -15.47, STS 28days -15.44, CMP 7days -14.64 and CMP 28days -15.22). The values anticipated at the design point are compared to the average predicted error, with an adequate Precision values well above the threshold of (4.0) further confirms the model's signal-to-noise ratio is adequate for predicting mechanical properties at both curing age. However, a lower standard deviation indicates the model's fitness and suitability with their mean values. (STS 7days -10, STS 28days -0.171, CMP 7days -0.633 and CMP 28days -0.901)

3.4.3. RSM Coefficents in terms of Coded Values for both responses (CMP/STS)

Coefficient estimate shows the expected change in response per unit change in factor value (BA and RHA) when all remaining factors are held constant. The following Regression Equations (1) to (4) which are in terms of (Coded Factors) represent the empirical relationship between the variables and the mechanical properties.

$$CMP-7 = 19.34 - 1.72 \times A - 0.47 \times B - 1.11 \times AB - 0.58 \times A^2 - 0.92 \times B^2 \ldots\ldots\ldots\ldots\ldots\ldots\ldots\ldots\ldots (1)$$

$$CMP-28 = 28.62 - 2.54 \times A - 0.70 \times B - 1.65 \times AB - 0.86 \times A^2 - 1.36 \times B^2 \ldots\ldots\ldots\ldots\ldots\ldots (2)$$

$$STS-7 = 1.61 - 0.28 \times A + 0.19 \times B - 0.19 \times AB + 0.15 \times A^2 + 0.08 \times B^2 \ldots\ldots\ldots\ldots\ldots\ldots\ldots (3)$$

$$STS-28 = 2.65 - 0.46 \times A + 0.32 \times B - 0.34 \times AB + 0.27 \times A^2 + 0.13 \times B^2 \ldots\ldots\ldots\ldots\ldots\ldots\ldots\ldots (4)$$

The above equations show that BA has stronger negative impact than RHA on strength whereas Significant interaction (*p* less than 0.01) confirms synergistic effects. Negative quadratic terms indicate peak strength at mid-range replacements. The negative coefficient for BA (-1.72, -2.54, -0.28, -0.46) indicates a substantial reduction in strength for both curing age with increasing BA content, largely attributed to its high unburnt carbon content, porosity, dilution effect and lower reactivity. RHA's effect is also negative (-0.47 and -0.70) for compressive strength but less severe, reflecting its slower pozzolanic kinetics at early age when SCM replacement is high and supporting its longer-term pozzolanic activity and micro-filling effect, while shows a positive term in tensile strength which means that increasing RHA, improve tensile strength at both age.

ISBN: 978-978-8567-02-8

The interaction term AB shows that the combined use of BA and RHA at high replacement levels tends to reduce mechanical strength, confirming a non-synergistic behavior at (high replacement above 20%). Both quadratic terms (A^2 and B^2) are significant with negative coefficients for CMP7 and 28, which suggested a concave down (inverted U-shaped) response surface. It also shows an optimal point within the design space. STS has positive quadratic terms, suggesting a convex (U-shaped) curvature for BA.

4. CONCLUSION

i. According to the research, both BA and RHA ashes possess properties that are required for additional SCM. The high silica content and some elements of both ashes surpassed ASTM C618's combined 70% criterion.

ii. According to Slump test results, workability decreases as the replacement of supplemental cementitious material increases. However, acceptable slump values are maintained with replacements up to 20%. Moderate SCM with RHA dominant blend can be utilized without changing the behavior of freshly laid concrete.

iii. The study concluded that a blend of 5% BA and 15% RHA significantly increased compressive strength ultimately outperforming the control mix. The Blend might be the first ternary optimization to go beyond binary bounds.

iv. For split tensile strength, M3 again provided the best result with 2.60 N/mm^2 at 7 days and 4.32 N/mm^2 after 28 days, approximately 46% higher than the control.

v. The optimal blend was optimized using Design Expert software, resulting in mechanical behavior nearly as expected with an overall desirability of 0.712%. Response Surface Methodology (RSM) was validated for concrete optimization which might be the first to consider interactions between BA and RHA in a ternary blend model.

ACKNOWLEDGMENT

The authors acknowledge the support and guidance provided by colleagues and mentors whose contributions were invaluable to the successful completion of this research. Appreciation is also extended to the institution for providing the necessary facilities and an enabling research environment.

REFERENCES

Adamu, M., et al. (2021). Response surface methodology for optimizing concrete properties. *Construction and Building Materials, 284*, 122897.

Adebola, J. A., Ikumapayi, C. M., & Arum, C. (2023). Effectiveness of rice husk and sugarcane bagasse ashes blended cement in improving properties of concrete. *Journal of Materials Science and Chemical Engineering, 11*(8), 1-19.

Ahmad, W., Ahmad, A., Ostrowski, K. A., Aslam, F., Joyklad, P., &Zajdel, P. (2021a). Sustainable approach of using sugarcane bagasse ash in cement-based composites: A systematic review. *Case Studies in Construction Materials*, *15*, e00698. https://doi.org/10.1016/j.cscm.2021.e00698

Almeida, R. P. A., &Cordeiro, G. C. (2023b).Sustainable approach to simultaneously improve the pozzolanic activity of sugarcane bagasse ash and the vinasse fertilization potential.*Cleaner Engineering and Technology*, *13*, 100617. https://doi.org/10.1016/j.clet.2023.100617

ASTM International. (2017). Standard test method for sieve analysis of fine and coarse aggregates (ASTM C136/C136M-17). *West Conshohocken, PA: ASTM International.* https://www.google.com/search?q=ASTM+C136+2017

ASTM International. (2018). Standard specification for concrete aggregates (ASTM C33/C33M-18). *West Conshohocken, PA: ASTM International.* https://www.google.com/search?q=ASTM+C33+2018

ASTM International. (2019). Standard specification for coal fly ash and raw or calcined natural pozzolan for use in concrete (ASTM C618–19). *West Conshohocken, PA: ASTM International.* https://www.google.com/search?q=ASTM+C618+2019

Bheel, N., Osman, M. A. A., Tafsirojjaman, Khahro, S. H., & Keerio, M. A. (2022). Experimental study on fresh, mechanical properties and embodied carbon of concrete blended with sugarcane bagasse ash, metakaolin, and millet husk ash as ternary cementitious material. **Environmental Science and Pollution Research International, 29*(4), 5224–5239.* https://doi.org/10.1007/s11356-021-17857-7

British Standards Institution. (2019). Testing fresh concrete: Slump test (BS EN 12350-2:2019). *London, UK: BSI.* https://www.google.com/search?q=BS+EN+12350-2%3A2019

BS 1881 part 125, Method of mixing and sampling fresh concrete in the laboratory, (1986). https://doi.org/10.3403/30258715.

BS 812: Part 2, Testing aggregates-Methods of determination of density, (1995). London: BSI; 15 Aug 1995. ISBN: 0 580 24257 9.

BS 812-105, Testing aggregates — Methods for determination of particle shape, (1989)

BS EN 12390-2:2009 Testing hardened concrete. Making and curing specimens for strength tests (Withdrawn), British Standards Institution—Publication Index | NBS. (n.d.). Retrieved September 18,2023, from https://www.thenbs.com/PublicationIndex/documents/details?Pub=BSI&DocID=290788 BS EN

BS EN 12390-6:2009 Testing hardened concrete. Tensile splitting strength of test specimens, British Standards Institution—Publication Index | NBS.(n.d.). Retrieved September 15, 2023, from https://www.thenbs.com/PublicationIndex/Documents/Details?DocId=294862

BS EN 197-1, Composition, specifications and conformity criteria for common cement, 3 (2000).

ISBN: 978-978-8567-02-8

Chemistry & Industry. (2023). Concrete revolution: How the world's most-consumed material is tackling its emissions. Chemistry & Industry, 7–8. *Society of Chemical Industry.* https://www.soci.org/news/chemistry-and-industry/concrete-revolution

David, J. M., De Jesus, R. M., & Mendoza Jr., R. P. (2022). Quantification of hydration products in rice husk ash (RHA)-blended cement concrete with crumb waste rubber tires (CWRT) & its correlation with mechanical performance. *GEOMATE Journal, 23(99), 126–133.* https://doi.org/10.21660/2022.99.s8603 (In-text citation: David et al. 2022)

Depaa, R.; Priyadarshini, V.; Hemamalinie, A.; Xavier, J.F.; Surendrababu, K. Assessment of strength properties of concrete made with rice husk ash. Mater. Today Proc. 2021, 45,6724–727.https://doi.org/10.1016/j.matpr.2020.12.605.

Dhanalakshmi, A., Jeyaseela, J., Karthika, S., & Leema Margret, A. (2023). An experimental study on concrete with partial replacement of cement by rice husk ash and bagasse ash. *E3S Web of Conferences, 387, Article 03004.* https://doi.org/10.1051/e3sconf/202338703004

International Energy Agency. (2021). Global energy review: CO_2 emissions in 2021. *International Energy Agency.* https://www.iea.org/reports/global-energy-review-co2-emissions-in-2021

Lawan, M. M., et al. (2022). Rice-husk and sugarcane-bagasse ash as a partial replacement of cement in self-compacting concrete. *KIU Journal of Science, Engineering and Technology, 1*(2), 9-17.

Maglad, A.M., Sobuz, M. H. R., Al-Imran, Datta, S. D., Jabin, J. A., Aditto, F. S., Hasan, N. M. S., Hasan, M., & Zaman, A. A. U. (2023). Assessing the influence of sugarcane bagasse ash for the production of eco-friendly concrete: Experimental and machine learning approaches. *Case Studies in Construction Materials, *20*, Article e02839.* https://doi.org/10.1016/j.cscm.2023.e02839

Mali, A. K., & Nanthagopalan, P. (2021). Comminution: A supplementation for pozzolanic adaptation of sugarcane bagasse ash. **Journal of Materials in Civil Engineering, 33*(12),4021343*.https://doi.org/10.1061/(ASCE)MT.1943-5533.0003985

Mohan, B., Ma, S., Kumar, S., Yang, Y., &Ren, P. (2023). Tactile sensors: hydroxyl decorated silver Metal–Organic frameworks for detecting CR2O72–, MNO4–, humic acid, and FE3+ ions. *ACS Applied Materials & Interfaces*, *15*(13),173177323.https://doi.org/10.1021/acsami.2c22871

Prabhath, N., Kumara, B. S., Vithanage, V., Samarathunga, A. I., Sewwandi, N., Maduwantha, K., Madusanka, M., & Koswattage, K. (2022). A review on the optimization of the mechanical properties of sugarcane-bagasse-ash-integrated concretes. *Journal of Composites Science, 6(10), 283.* https://doi.org/10.3390/jcs6100283

Seyoum, R., Tesfamariam, B. B., Andoshe, D. M., Algahtani, A., Ahmed, G. M. S., & Tirth, V. (2021). Investigation on control burned of bagasse ash on the properties of bagasse ash-blended mortars. **Materials, 14*(17), 4991.* https://doi.org/10.3390/ma14174991

T. Awolusi, O. Oke, O. Akinkurolere, A. Sojobi, Application of response surface methodology: predicting and optimizing the properties of concrete containing steel fibre extracted from waste tires with limestone powder as filler, *Case Stud. Constr. Mater. 10 (2019), e00212.*

Tariq, A., et al. (2021). Effect of rice husk ash on durability properties of concrete. *Case Studies in Construction Materials, 15*, e00782.

Ye, G., Huang, H. and Van Tuan, N. (2018) Rice Husk Ash. In: De Belie, N., Soutsos, M. and Gruyaert, E., Eds., "Properties of Fresh and Hardened Concrete Containing Supplementary Cementitious Materials": State-of-the-Art Report of the RILEM Technical Committee 238-SCM, Working Group 4, *Springer International Publishing, Cham, 283-302.*

ISBN: 978-978-8567-02-8

5TH Faculty of Engineering Conference on Engineering Innovation and Economic Policies: Driving Sustainable Industrial Growth in Nigeria

Faculty of Engineering, Bayero University, Kano.

047-Mathematical Model of Heating Value based on Ultimate Analysis of MSW Generated from BUK (main campus), Kano, Nigeria.

Gidado M. T., Rufai I.A., and Yola I.A.

Department of Mechanical Engineering, Bayero University, Kano, Kano State

(enitla2017@gmail.com)

Abstract: Nigerian environmental ecosystem like most developing countries is faced with Municipal Solid Waste (MSW) management challenges that manifest in open dumping /burning that consequently lead to health hazards with deleterious effect on the environment. Interestingly, some of those rejected materials in the form of refuse are combustible and can be channeled into energy/heat generation or recovery in a sustainable manner. Mathematical modeling equations had been proposed severally but there is disparity in prediction outcome of some aspect of the models that warrants a comparative area-specific consideration. More so, MSW is a difficult fuel that evades a generic standardization. Proximate analysis, ultimate analysis and heating value experiments were carried out using ASTM standards. Results obtained were given as: proximate analysis (Moisture content, 40.84%; volatile matter, 45.49%; ash content, 3.91%; fixed carbon, 9.76%), ultimate analysis (C, 47.58%; H, 4.76%; O, 45.36%; N, 0.97%; S, 1.33%), heating value was determined as 11.39MJ/kg and the empirical formula as $C_3H_4O_2$. Mathematical models were developed for heating value prediction: Gidado I, Gidado II and Gidado III. The results indicated dominant Carbon and Oxygen elements in the sample and a heating value that was comparably half that of coal and above the minimum value for MSW, enough to sustain combustion. The developed mathematical models indicated that the model developed from physical composition (Gidado III) gives higher heating value that correlated with established models (Bole model) more than Gidado I and Gidado II, further simplifying the heating value determination using less-equipment-intensive dependent approach.

1. INTRODUCTION

Generally, waste can be defined in a generic sense "as refuse from places of human or animal habitation" (UNSD, 2007). Municipal solid waste (MSW) is composed mainly of household or domestic waste, but it can also contain commercial and industrial waste with the exception of industrial hazardous wastes. Furthermore, MSW can be categorized into two major classes; non-Biodegradables and Biodegradables. Notwithstanding, waste quantity and quality are major sign of countries' level of modernization and economic growth (Danbuzu et. al, 2014; UNSD, 2007; UNEP, 2009; Becidan, 2007; Nabegu, 2010). Despite waste prevention advocacy, a sustainable waste utilization is more feasible and economical given an increasing global generation rate, projected to double by 2030 (Gregorio, 2012). Globally, an estimated 11.2 billion tons of solid waste (SW) is generated annually with one-fifth of it being MSW. Unfortunately, these vast resources have not being positively utilized to decimate the use of fossil fuels and mitigate the effect of greenhouse gases (GHGs).

2. METHODOLOGY

2.1 Proximate Analysis of the MSW

Proximate analysis was carried out based on ASTM standard procedures using these experimental materials: weight balance; desiccator; moisture cans and crucibles; drying oven; muffle furnace and vertical electric tube furnace. The combustible part of the MSW: yard waste (YW), food waste (FW), other organic (OO), plastic (PL) and paper (PP)) were used.

Moisture was determined by establishing the loss in weight of the sample when heated under rigidly controlled conditions and the residue of the moisture content experiment was adopted in the determination of volatile matter and ash content. The procedures was replicated three times each. The data obtained was analysed using Eqs. (1), (2), (3) and (4) for moisture content, volatile matter, ash content and fixed carbon respectively:

$$M_l(\%) = \left[\frac{(W_i - W_f)}{(W_i - W_c)}\right] \times 100 \qquad (1)$$

$$VM = (M_l - B) \qquad (2)$$

$$A\ (\%) = \left[\frac{(W_1)}{(W_2)}\right] \times 100 \qquad (3)$$

$$FC = 100 - (M\% + A\% + VM\%) \qquad (4)$$

where; M_l= weight loss (%), B = Moisture (%), VM = Volatile matter in analysis sample, W_i = initial weight (g), W_f = final weight (g) and W_c= covered crucible weight (g), A (%) = Ash, W_1 = weight of ash (g), and W_2 = weight of oven-dry sample (g), M% = Moisture.

ISBN: 978-978-8567-02-8

2.2 Ultimate Analysis of the MSW

The ultimate analysis of the sample was carried out using experimental materials and procedures of ASTM standard. The following experimental materials were used for the ultimate analysis experiment: Digital weight balance, Spatula and Perkin-Elmer-2400-II-CHNS/O Analyzer. During the experimental procedure the sample was dried at 105°C for 1 hour then cooled in a desiccator and ground, then it was embedded in a capsule and placed into the auto sampler of the analyzer. Information was entered into the analyzer and activated.

2.3 Heating Value of the MSW

The heating value of the sample was determined based on ASTM standard using an automatic bomb calorimeter which was calibrated by using standard benzoic acid. The experimental procedure involved the pressing of the analysis sample into a pellet as shown in Plate 1. The bomb was then assembled, sealed and purged twice with pure oxygen then vented, and placed inside the calorimeter containing water in an insulated jacket as shown in Plate 2.



Plate 1: Pellet Press



Plate 2: Experimental Set Up of the Bomb Calorimeter

After allowing the combustion to take place, the result was displayed in the display unit in MJ/kg. This procedure was repeated for other samples. Individual combustible components from the waste classifications were similarly subjected to the procedure.

2.4 Mathematical Modeling

The global equation representing combustion of wastes in air was used in getting the combustion formula (Jenkins, et al.,1998). The empirical formula of the MSW sample was formed using data from the ultimate analysis experiment, where the elements: Carbon, Hydrogen, Oxygen, Sulphur and Nitrogen values had been determined.

Therefore, the general combustion model is used according to the combustion theory for Hydrocarbons (Saffari , 2016):

$$C_xH_yO_zN_lS_n + \left(x + \frac{y}{4} - \frac{z}{2} + n + l\right)O_2 \rightleftharpoons xCO_2 + \frac{y}{2}H_2O + lNO_2 + nSO_2 \quad (5)$$

The relationship between heating value (HV) and ultimate analysis data (C, H, O, N & S) for a prediction method based on independent variable (x) that is correlated with a value of the dependent variable (y) is shown in equation 6:

$$Y = \alpha_0 + \alpha_1X_1 + \alpha_2X_2 + \alpha_3X_3 + \cdots + \alpha_tX_t \quad (6)$$

where: Y = Heating Value (MJ/kg), x_1, x_2...., x_t = independent variables, α_0 = y-axis intercept, α_1,…, α_t = regression coefficients

The following methods were carried out in determining the mathematical models of the MSW:

i. Regression analysis using ultimate analysis of the whole component and heating value data.
ii. Regression analysis using ultimate analysis and heating value of individual samples of the MSW.
iii. Regression analysis of the correlation between HHV and physical composition with ultimate analysis and % water content (W) using Scheurer & Kestner's model equation in Table B of Appendix II (Janna et al., 2021). This was done by assuming the water contents is in the yard waste (YW) which has the highest constituent in the waste stream. It was varied with an interval of 1% for each assumed n% of YW to have a trials of (n-1) totaling 484 trials.

3. RESULTS AND DISCUSSIONS

3.1 Results

Table I shows the percentages of the proximate analysis; moisture, volatile matter, ash content and fixed carbon

TABLE I: AVERAGE PROXIMATE ANALYSIS

S/No.	Description	%
1.	Moisture content	40.28
2.	Volatile matter	46.06
3.	Ash content	4.52
4.	Fixed carbon	9.14

The ultimate analysis results of the whole and individual samples are presented in Tables II and III respectively.

TABLE II: ULTIMATE ANALYSIS OF WHOLE SAMPLES

Element (%)	C	H	O	N	S
Sample A	49.72	4.85	49.78	1.28	1.10
Sample B	44.34	4.69	42.73	1.32	0.80
Sample C	48.68	4.73	43.58	1.40	1.01
Average (%)	47.58	4.76	45.36	1.33	0.97

TABLE III: ULTIMATE ANALYSIS RESULTS FOR THE INDIVIDUAL COMBUSTIBLE SAMPLES

Element	Yard Waste	Food Waste	Plastic	Other Organics	Paper
C	43.2	42.6	60.6	47.4	45.3
H	4.47	4.37	8.97	4.89	4.47
O	41.93	43.63	19.83	35.33	43.23
N	1.35	1.05	0.35	1.65	0.85
S	0.92	1.63	0.33	0.73	0.43

The data for the heating value of the samples and its individual combustible components was determined, the result is presented respectively in Tables IV and V.

TABLE IV: HEATING VALUE OF THE WHOLE SAMPLES

MSW	Heating Values (MJ/kg)
A	12.65
B	11.54
C	9.97
Average	11.39

ISBN: 978-978-8567-02-8

TABLE V: HEATING VALUE (CV) OF THE INDIVIDUAL COMBUSTIBLE COMPONENTS IN MJ /KG

Sample	A	B	C	Average
Yard Waste	2.20	1.30	2.30	1.93
Food Waste	1.20	2.20	0.02	1.14
Plastic	32.00	33.50	34.07	33.19
Other Organics	9.20	11.00	10.17	10.12
Paper	13.50	13.40	13.70	13.53

The MSW empirical formula developed from the results of Table II is shown in equation (7). Neglecting insignificant elements of N and S results, the formula was obtained as Equation (8).

$$C_{264}H_{318}O_{190}N_7S_2 \qquad (7)$$

$$C_3H_4O_2 \qquad (8)$$

The MSW is thermally decomposed into CO_2 and H_2O as shown in Equation (9):

$$C_3H_4O_2 + 3O_2 \rightarrow 3CO_2 + 2H_2O \qquad (9)$$

Three Regression equations that represent the heating value models were developed in three cases as follows:

i. The data of Table II and Table IV was harmonized into Table VI for case I.

TABLE VI: HARMONIZED DATA OF ULTIMATE ANALYSIS OF WHOLE SAMPLE AND ITS HEATING VALUE

Element	Sample A	Sample B	Sample C
Carbon (C)	49.72	44.34	48.68
Hydrogen (H)	4.85	4.69	4.73
Oxygen (O)	49.78	42.73	43.58
Nitrogen (N)	1.28	1.32	1.40
Sulphur (S)	1.10	0.80	1.01
Heating Values (MJ/kg)	12.65	11.54	9.97

A regression equation (Gidado_I) was obtained as Equation (10) with coefficient and confidence interval shown in Table VII.

TABLE VII: COEFFICIENT AND CONFIDENCE INTERVAL

Coefficients					95% confidence interval for B	
Model	B	Beta	*Std. error	p	lower bound	upper bound
Const.	0.55		0	<.001	0.55	0.55
C	-0.45	-0.95	0	<.001	-0.45	-0.45
H	2.02	0.13	0	<.001	2.02	2.02
O	0.49	1.41	0	<.001	0.49	0.49
N	0.69	0.03	0	<.001	0.69	0.69
S	0.88	-0.1	0	<.001	-0.88	-0.88

*Std. = Standard

$$LHV = 0.55 - 0.45\boldsymbol{C} + 2.02\boldsymbol{H} + 0.49\boldsymbol{O} + 0.69\boldsymbol{N} - 0.88\boldsymbol{S} \qquad (10)$$

ii. The data from Tables III and V were harmonized to form Table VIII which was used as the dataset for case II.

TABLE VIII: ULTIMATE ANALYSIS OF INDIVIDUAL COMBUSTIBLE SAMPLES WITH HEATING VALUES

Element	C	H	O	N	S	LHV
Yard Waste	43.2	4.47	41.93	1.35	0.92	1.93
Food Waste	42.6	4.37	43.63	1.05	1.63	1.14
Plastic	60.6	8.97	19.83	0.35	0.33	33.19
Other Organics	47.4	4.89	35.33	1.65	0.73	10.12
Paper	45.3	4.47	43.23	0.85	0.43	13.53

A statistical test found that p = <.001, R = 1, and the regression equation (11) obtained as Gidado_II model:

$$HHV = -0.91 + 2.27\boldsymbol{C} - 9.08\boldsymbol{H} - 0.83\boldsymbol{O} - 12.23\boldsymbol{N} - 3.6\boldsymbol{S} \qquad (11)$$

iii. Using dataset from assumption of moisture content percentages. General regression analysis between HHV versus YW, FW, PL, OG, and PP results to (Gidado_III) Equation (12) with $R^2 = 0.4$ statistical strength:

$$HHV = 0.01 + 0.19YW + 0.02F + 0.21PL + 0.06OG + 0.19PP \qquad (12)$$

3.2 Discussions

The proximate analysis results (see Table I) showed a low ash content of 3.91% which agrees with lower inorganic content in the MSW sample while the 45.49% of volatile matter and 9.767% for fixed carbon agrees with similar studies on the subject (Gunamantha, 2016).

The ultimate analysis result (see Table II) reveals the prominence of carbon at 47.58%, which is positive for heating value, however, a 45.36% oxygen content diminishes this potential yielding a moderate heating value level. Though, the obtained value of 11.39 MJ/kg is only a fraction of Hydrogen's calorific value of 150 MJ/kg, it correlates with previously obtained value of 10.19 MJ/kg for similar fuel type and falls within the acceptable recommended energy recovery range from MSW of 7.50 MJ/kg to 12 MJ/kg (Fetene, 2021; Janna et al,, 2014).

Relating the values of elements in the individual combustible components with the heating value using ultimate analysis data indicates correlation between the variables as shown in Figure 1. The correlation indicates a negative proportionality between heating value and oxygen levels with carbon levels contributing to higher heating capacity of the MSW in an appreciable direct conformal linearity.

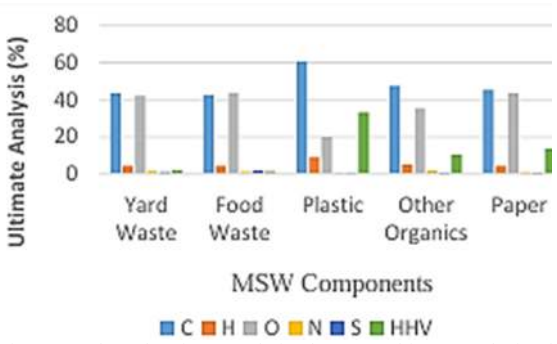


Figure 1: Chart showing correlation between ultimate analysis of MSW components and heating value

ISBN: 978-978-8567-02-8

Models had been proposed severally but there is great disparity in their prediction outcome (Janna et al., 2021). The developed mathematical models indicated that Model III gives values that correlate significantly with Bole model and are in close agreement with experimental values as shown Figure 2

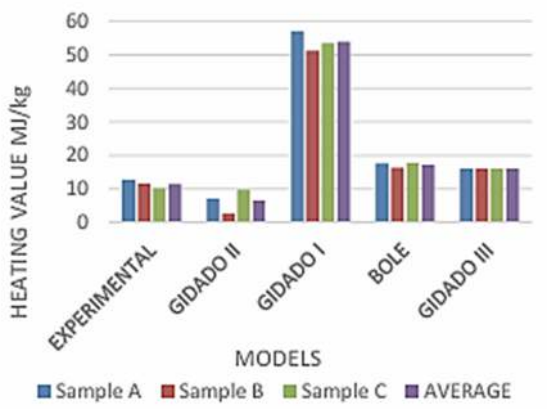


Figure 2: Comparison of the experimental data, developed models and the Bole model

Both Models I and II predicted the heating value but the values obtained were well above and below the established MSW heating values thresholds respectively.

The utilization of the developed model can fast-track the exploration of the thermal characterization of the MSW towards its waste-to-energy potential determination given that only the physical waste components constitute the independent variables. However, the study is limited by: degree of accuracy/calibration of equipment used for the experiments carried out and embedded errors in referenced literature, which necessitated the triple repetition of experimental procedures and correlational mirroring with existing literature.

4. CONCLUSION AND RECOMMENDATIONS

4.1 Conclusion

The potential for utilization of the MSW generated from developing economies, in waste-to-energy schemes, is hampered by dearth of characterization capabilities. Therefore, in this study the MSW from Bayero University (New Campus) was characterized in terms of elemental and thermal properties.

Furthermore, mathematical models were developed, using data from the characterization experiment, that offered prediction possibilities of the heating value of MSW using ultimate analysis and/or physical composition data. This is with the intent of reducing cost and saving empirical characterization time.

The model developed using physical composition data (Gidado_III) with heating value of 17.13MJ/kg gave better results that is close to the experimental value of 11.39 MJ/kg, with higher conformal value in relation to existing BOLE model in the literature of 15.95, than those developed using ultimate analysis data.

4.2 Recommendations

The utilizations of MSW as a fuel is hampered by its difficulty in standardization, it is recommended that the developed model (Gidado_III) should be utilized in waste-to-energy prospecting activities.

The waste stream generation range was only within Bayero University, Kano, campus. It is recommended that a larger generation range should be studied in further research.

The chosen model was developed based on the assumption that yard waste has the highest water content among the components, given it is highest percentage in the waste stream of the limited MSW characterized. Therefore, it is recommended that improved models should be developed using larger datasets in further studies.

REFERENCES

Becidan, M. (2007). Experimental Studies on Municipal Solid Waste and Biomass Pyrolysis. NTNU Norwegian University of Science and Technology. Unpublished PhD Thesis.

Danbuzu, Tanko, A. L., Ahmed, M., & Ibrahim, A. M. (2014). (2014) Utilization of Solid Waste Collection Facilities in Urban Katsina, Katsina State, Nigeria. Journal of Environmental Sciences and Resources Management, 6(2), 166-173.

Eva, H. (2011). European Commission; A new directive on energy efficiency. Retrieved October 11, 2017, from European Commission: https://www.ec.europa.eu/energy/efficiency/

Gidado, M. T., Rufai, I. A., & Yola, I. A. (2023). Characterization of Municipal Solid Wastes (MSW) Generated in Bayero University Kano (BUK) Main Campus Kano Nigeria. International Journal of Scientific Engineering and Science, 7(11), 1-7.

Gregorio, D. F. (2012). Fuel Gas Technology for Biomass and Waste: Environmental and Techno-Economic Assessments. Unpublished PhD thesis, Second University of Naples, Caserta.

Gunamantha, M. (2016). Prediction of higher heating value bioorganic fraction of municipal solid waste from proximate analysis data. . International Journal of Engineering Research & Technology, 5(2), 442-447.

IEA. (2020). electricity consumption. Retrieved December 29, 2021, from Internationl Energy Agengy: https://www.iea.org

Janna, H., Mukhtar, A. D., Marwah, M. A., & Nadhir, A. (2021). Energy Content Estimation of Municipal Solid Waste by Physical Composition in Al-Diwaniyah City, Iraq. Journal of Ecological Engineering, 22(7), 11=19.

Jenkins, B., Baxter, L., Miles Jr., T., & Miles, T. (1998). Combustion properties of biomass. Fuel Processing Technology, 54, 17–46.

Kathiravale, S. M., Muhd Yunus, K., & Sopian, A. (2003). Modeling the heating value of Municipal Solid Waste. Fuel, 82(9), 1119–1125.

Nabegu, B. A. (2010). An Analysis of Municipal Solid Waste in Kano Metropolis, Nigeria. Journal of Human Ecology International, Interdisciplinary Journal of Man - Environment Relationship.

UNEP. (2009). Developing Integrated Solid Waste Management Plan Training Manual (Vol. 2).

ISBN: 978-978-8567-02-8

UNSD. (2007). Demographic Year Book. Washington DC: United Nations Statistics Division.

TABLE A: MSW CATEGORIES BY WEIGHTS PERCENTAGE

Percentage Standard Method of Sampling		ASTM D5231-92	
Sorting Method		Mixing, Coning and Quartering	
S/No.	Category	Weight (kg)	%Weight
1.	Paper	31.61	23.48
2.	Food waste	2.76	2.05
3.	Yard waste	40.83	30.32
4.	Other organics (textiles, sanitary fabrics)	9.71	7.21
5.	Plastics	33.66	24.99
6.	Glass	1.49	1.11
7.	Metals (ferrous and non-ferrous)	0.74	0.55
8.	Other waste (HHH, bones, sand, dirt etc.)	13.87	10.30
	Total	134.66	100.00

APPENDIX I

Source: (Gidado, Rufai, & Yola, 2023)

APPENDIX II

TABLE B: HEATING VALUE OF MSW COMPONENTS USING EXISTING MATHEMATICAL MODELS

S/No.	Heating Value Equation	Model
1.	HHV = [(81**C**) + 342.5(**H**-(**O**/8)) + (22.5**S**)]	Dulong
2.	HHV = [(80.5**C**)+(338.6**H**) - (42.3**O** + (22.2**S**) + (5.55**N**))]	Modified Dulong
3.	HHV = [81(**C** - (3/8)**O**) + 57(3/8)**O** +345(**H** -(**O**/16) +25**S** - 6(9**H** + **W**)]	Steuer's
4.	HHV = [85**C** + 270H + 26(**S** - **O**)]	Vandralek
5.	HHV = [0.3517**C**+1.1626**H**-0.1047**S** - 0.1110]	Boie
6.	HHV = [-2762.68 + 114.63**C**+310.55**H**]	Khuriati et al.,
7.	HHV = [416.638**C** -570.01**H** + 259.031**O** + 598.955**N** - 5829.078]	Kathiravale et al,
8.	HHV = [81(**C** - (3/4)**O**)+342.5**H** + 22.5**S** + 57(3/4)**O** - 6(**H** + **W**)]	Scheurer & Kestner's
9.	HHV = 0.349**C** + 1.01**H** - 0.174**N** + 0.886**S** - 0.0812**O**	Shi et al..

Source: (Janna et al., 2021)

ISBN: 978-978-8567-02-8

5TH Faculty of Engineering Conference on Engineering Innovation and Economic Policies: Driving Sustainable Industrial Growth in Nigeria

Faculty of Engineering, Bayero University, Kano.

048-Fetal ECG Extraction Using Ant Colony Optimization Algorithm (ACO)-Based Adaptive Filter

A. Ibrahim Inyass Ibrahim, B. Abdussamad Umar Jibia
Department of Electrical Engineering, Bayero Universtiy Kano, Kano, Nigeria

E-mail: ajumar@buk.edu.ng, inyassgauth@gmail.com

Abstract: Fetal Electrocardiogram (ECG) is a record of electrical activity of the heart of fetus. In the pregnancy, monitoring of fetal ECG signal plays an important role as it helps in determining the fetal life, development and maturity. Fetal ECG is extracted from composite abdominal ECG (AECG) signal of a pregnant woman. However, it is not so easy to record fetal ECG, due to the co-existence of fetal and maternal ECG signals acquired from the mother, external noises, as well as the fetal signal is of low amplitude. A newly developed Ant Colony Optimization Algorithm (ACO)-based adaptive filter has been proposed in order to remove the maternal ECG and other noises in the AECG signal by optimizing the step size of Least Mean Square (LMS) algorithm to determine the optimum filter coefficients. The proposed fetal ECG extraction algorithm was applied on both synthetic AECG generated using MATLAB codes and real AECG obtained from physionet database developed by MIT-BIH. The results on the synthetic AECG show good fetal ECG extraction performance with average Mean Square Error (MSE) of 0.0015 and Signal to Noise Ratio (SNR) of 22.37 dB at different heart rates ranging from 120 to 160 bpm. The algorithm was implemented in a MATLAB environment and the simulation results show that the proposed method has a 93% performance improvement over the other methods used for fetal ECG extraction in terms of average MSE and improved SNR.

Keywords: fetal ECG, adaptive filter, step size, LMS, ACO, MSE

1. INTRODUCTION

A fetus is an unborn offspring that develops and grows inside the womb of a woman. It is very vital to record the fetal heart rate as it helps in determining the growth and abnormalities of fetus.

The electrocardiogram (ECG) is a record of electrical activity which describes the physiological condition of a heart that can be obtained non-invasively by placing electrodes on the body surface (Prasanth *et al*, 2013). Fetal ECG is easily obtained by placing two electrodes on the chest and abdomen of a pregnant woman to generate the abdominal lead and chest lead respectively. The chest lead picks up an undistorted maternal ECG signal while the abdominal lead contains a composite ECG signal. The main challenge is the extraction of fetal ECG from the composite abdominal ECG of a pregnant woman. The records of composite abdominal ECG signal comprise of dominant signal of maternal ECG (MECG), the Fetal ECG (FECG), interferences and noise signals which make difficulties in accurately analyzing the FECG signal.

A number of techniques were developed for fetal ECG extraction such as Singular Value Decomposition (SVD) (Ayat, 2008), Independent Component Analysis (Graupe, 2005) (Alkhodari, 2018) Wavelet Transform (Hassanpour and Parsaei, 2006), Blind Source Separation (Taha, 2018) Adaptive Filtering Techniques (Vamshadeepa, 2017) (Jibia and Inuwa, 2015) (Ahmed, 2018) (Jibia and Jibia, 2021) among others. The Adaptive Filter based method for fetal ECG extraction is superior over the other techniques. Despite its superiority, there are still many unsolved problems of traces of the maternal ECG which is the dominant noise and some other noise such as electrode motion artifact, power-line interference, electromyogram, etc. (Hassan, 2009) However, another research (Ling *et al*, 2020 and Tripathi and Ikbal, 2016) showed the outperformance of Ant Colony Optimization Algorithm over Particle Swarm Optimization Algorithm in adaptive noise cancelling technique.

This research work proposes an adaptive filtering technique for fetal ECG extraction using Ant Colony Optimization Algorithm (ACO) that will prevent the existing problems.

2. METHODOLOGY

2.1 The abdominal fetal ECG

The abdomen of a pregnant woman consists of composite signals of fetal ECG signal, maternal ECG signal and electrical noises from other sources (Joshi and Singh, 2015) The maternal ECG is the most dominant but unwanted signal in the abdomen during the pregnancy. This research is a non-invasive method that will be used to obtain valuable clinical information about the fetal heart condition during pregnancy.

In the proposed method, two leads are used; one is placed in the maternal region and the other in abdominal region of a pregnant woman. When the mapped maternal

ISBN: 978-978-8567-02-8

ECG is subtracted from the abdominal ECG signal (AECG), the result would be a noisy fetal ECG signal. Mathematically, $FECG + MECG + Noise = AECG$

$$AECG - MECG = FECG + Noise \quad (1)$$

To effectively suppress the unwanted signals in the abdomen for fetal ECG extraction in equation (1), this research comes up with a newly developed method which involves the use of LMS/adaptive filter algorithm with ACO in order to find the global minimum mean square error (MMSE) for better fetal ECG extraction. The maternal signal obtained from chest would serve as the reference signal and the composite abdominal signal serves as the main input signal into the proposed adaptive filter.

2.2. Adaptive Filter Design

An adaptive filter is a system with linear filter which consists of transfer function controlled by variable parameters and a means to adjust those parameters according to an optimization algorithm. Adaptive filters generally adjust their coefficients to minimize an error signal and can be described as finite impulse response (FIR) or infinite impulse response (IIR) consisting of two separate units; digital filter and adaptive algorithm. (Merredin and Falcão, 2015)

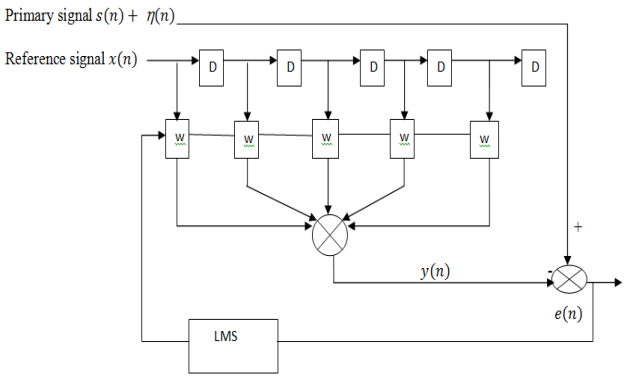


Fig. 1 Block diagram of a LMS Adaptive Filter

In Fig 1, the primary signal $s(n)$ represents fetal ECG signal while $\eta(n)$ is the primary noise representing the maternal ECG signal in the abdomen and other noises. But the noise signal is uncorrelated with $s(n)$. The reference signal $x(n)$ is the thoracic maternal ECG signal which is highly correlated with $\eta(n)$ but still uncorrelated with $s(n)$. The adaptive filter output is $y(n)$, since it is generated from $x(n)$, it is therefore correlated with $\eta(n)$ but uncorrelated with $s(n)$. The output is the error $e(n)$, which is mathematically given by;

$$e(n) = s(n) + \eta(n) - y(n) \quad (2)$$

In noise canceling systems, a practical objective is to produce a system output error $(e(n))$ that is best fit, in the least squares sense of signal $s(n)$. Therefore, the mean square of error is of interest and can be obtained as follows;

$$e^2(n) = s(n)^2 + (\eta(n) - y(n))^2 + 2s(n)\big(\eta(n) - y(n)\big) \quad (3)$$

Taking expectation both sides

$$E[e^2(n)] = E[s^2(n)] + E[(\eta(n) - y(n))^2] + 2E\big[s(n)\big(\eta(n) - y(n)\big)\big] \quad (4)$$

Since $s(n)$ is uncorrelated with both $\eta(n)$ and $y(n)$

$$2E[s(n)(\eta(n) - y(n)) = 2E[s(n)]E[(\eta(n) - y(n))] = 0$$

Hence, $E[e^2(n)] = E[s^2(n)] + E[(\eta(n) - y(n))^2 \quad (5)$

Adapting the filter minimizes the Mean Square Error (MSE), but it has no effect on fetal input signal $s(n)$, therefore the equation would be given as

$$min\ E[e^2(n)] = E[s^2(n)] + min\ E\left[\big(\eta(n) - y(n)\big)^2\right]. \quad (6)$$

The suitable adaptive algorithms are used to minimize the MSE in equation (6) by formulating the means of updating the filter coefficients $\{w(n)\}$.

2.3 Least Mean Square (LMS) Algorithm

The LMS algorithm is popularly used algorithm in adaptive filtering technique due to its computational simplicity, robustness and fast convergence in a stationary environment. It uses the gradient descent method to find the minimum value of an error by taking steps in the direction of negative gradient of error surface. It does so by adjusting the filter coefficients so as to minimize the error (Widrow and Hoff, 1960)

The LMS algorithm minimizes the mean square error $\{e^2(n)\}$ in equation (2) by updating the filter coefficients.

$w(n) = [w_1(n), w_2(n), \ldots, w_m(n)]^T$ is the coefficient vector of the adaptive filter of length m

The filter coefficient vector update equation for the LMS algorithm is given by

$$w(n+1) = w(n) + \mu\, e(n)x(n) \quad (7)$$

Where $w(n+1)$ is the new filter coefficient, while $e(n)$ and $x(n)$ are the error signal and input signal respectively. μ is the step size parameter also known as convergence factor.

Both the filter coefficient update and convergence rate of the LMS algorithm depend on the step size (μ). If μ is small, then it may take a long convergence time. However, if the step size (μ) is too large, the algorithm may never converge. Thus, the value of (μ) should be optimally computed in order to find the minimum mean square error of interest. Selection of a suitable value for μ is imperative to the performance of the LMS algorithm. When the value is too small, then the time the adaptive filter takes to converge on the optimal solution will be too long. If the value of μ is too large, the adaptive filter becomes unstable and its output diverges. (Rajni and Tayal, 2013)

Relating to this work, the composite abdominal ECG is $\{s(n) + \eta(n)\}$ and $\{s(n)\}$ is the abdominal fetal ECG signal as the original input at the n^{th} moment and mathematically given by

$$s(n) = [s(n), s(n-1) \ldots \ldots s(n-m+1)]^T \quad (8)$$

Where m is the length of the adaptive filter

ISBN: 978-978-8567-02-8

While $x(n)$ represents the maternal ECG signal as a reference input at the nth moment and is given by

$$x(n) = [x(n), x(n-1) \dots \dots x(n-m+1)]^T \quad (9)$$

After updating the filter coefficients using LMS, the adaptive filter output signal $y(n)$ representing the maternal ECG will be

$$y(n) = \sum_{i=0}^{m-1} w_i\, x(n-i) = w^T(n)x(n) \quad (10)$$

The extracted fetal ECG signal is therefore obtained by LMS adaptive filtering as

$$\min E[e^2(n)] = E[s^2(n)] + \min E\left[\left(\eta(n) - w^T(n)x(n)\right)^2\right] \quad (11)$$

Which is the same as

$$\min E[e^2(n)] = E[(FECG)^2] + min\ E[\{(MECG + N) - w^T MECG)\}^2] \quad (12)$$

Despite the important role of LMS algorithm in adaptive filtering, the algorithm has some inherit limitations of gradient based algorithms such as the problem of getting stuck at the local minima of system having multi-modal error surface (i.e non convex error). Hence, the combination of LMS optimization algorithm and a meta-heuristic optimization algorithm in such a system having multi-modal error surface would effectively guarantee the optimized convergence to a global minimum.

2.4 Ant Colony Optimization (ACO) Algorithm

ACO meta-heuristic optimization algorithm was inspired from foraging behavior of real ants to find shortest paths between food sources and their nest as shown in Fig. 3 (Dorigo and Stuzle, 2004). When searching for food, ants initially explore the area surrounding their nest in a random manner. While moving, ants leave a chemical pheromone trail on the ground because. Ants are blind they cannot see paths but can smell the pheromone. When choosing their way, they tend to choose, in probability, paths marked by strong pheromone concentrations. As soon as an ant finds a food source, it evaluates the quantity and the quality of the food and carries some of it back to the nest. During the return trip, the quantity of pheromone that an ant leaves on the ground may depend on the quantity and quality of the food. The pheromone trails will guide other ants to the food source.

In general, the ACO approach attempts to solve an optimization problem by iterating the following two steps:

i. Candidate solutions are constructed using a pheromone model, that is, a parameterized probability distribution over the solution space.
ii. The pheromones are modified to concentrate the search in regions of the search space containing high quality solutions. (Blum, 2005)

The algorithm involves two main equations:
An ant moves from node i to node j according to the probability rule which is mathematically given as;

$$P_{ij} = \frac{[\tau_{ij}]^{\alpha}[\eta_{ij}]^{\beta}}{\sum[\tau_{ij}]^{\alpha}[\eta_{ij}]^{\beta}} \quad (13)$$

Where;
τ_{ij} is the amount of pheromone on edge ij
α is a parameter to control the influence τ_{ij}
η_{ij} is the inverse of the distance between the two nodes ij called desirability $(1/d_{ij})$
β is a parameter to control the influence η_{ij}
After all the ants have constructed their tours, the pheromone trails are updated according to equation (15);

$$\tau_{ij} = (1-\rho)\tau_{ij} + \Delta\tau_{ij} \quad (14)$$

τ_{ij} is the amount of pheromone on a given edge ij
ρ is the rate of pheromone evaporation
$\Delta\tau_{ij}$ is the amount of pheromone deposited, typically given by

$$\Delta\tau^k{}_{ij} = \begin{cases} 1/L_K & \text{if ant 'k' travels on edge } ij \\ 0 & \text{Otherwise} \end{cases}$$

According to MAX–MIN Ant System (MMAS), it is only the best ant that adds pheromone trails i.e. either the ant that produced the best tour in the current iteration, or the best-so-far ant is allowed to deposit pheromone. (Katiyar and Ansari, 2015)

$$\tau_{ij} = \tau_{ij} + \Delta\tau_{ij}^{best} \quad (15)$$

Where τ_{ij}^{best}=$1/L_{best}$, if the best ant used edge (i, j) in its tour. Otherwise τ_{ij}^{best}=0
L_{best} is the length of the tour of the best ant.

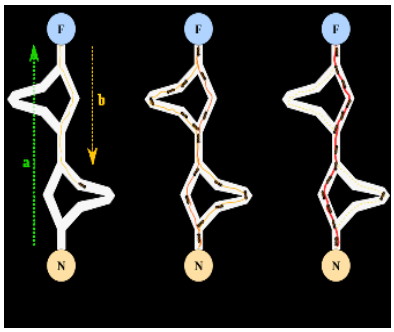


Fig. 2 shows the movement of ant from their nest to food source (Tripathi and Ikbal, 2016)

The algorithm follows that:

1. The concentration of artificial pheromone τ_{ij} is set to each link (i, j)
2. The value of k is assigned for every artificial ant.
3. Using equation (13) build a path from nest to food source.
4. Remove the paths having least concentration of pheromone, they are referred as cycles, and

ISBN: 978-978-8567-02-8

compute each route weight $f(x^k(n))$. When there are no feasible candidate's nodes then the predecessor of that node is included as a former node of the path.

5. As a next step, use equation (14) and (15) for updating the concentration of pheromone.
6. Finally, the algorithm will end in any of the following mentioned three different ways:
   i. If the maximum number of approaches are reached
   ii. If the acceptable solution is found.
   iii. Or if, all ants are following the same path (Ling, 2020)

With respect to this research, the algorithm would therefore be represented as;

1. Use different step size(μ_m) values that will be used to update the set of filter coefficients to generate corresponding number of errors $e_m^2(n)$.
2. Assigned artificial ants as search agents.
3. The artificial ants use Roulette Wheel Selection method to determine the best set of filter coefficients by considering the values of their fitness functions ($e_m^2(n)$).
4. The iterations will be repeated until: Minimum mean square error MMSE ($e^2(n)$) is found or the maximum number of iteration is reached.

The algorithm selects the global minimum error value as the optimal solution from the set of generated errors $e_m^2(n)$.

2.5 The proposed fetal ECG extraction system

The structure of the proposed system is shown in Fig. 3. The abdominal lead data and the chest lead data are fed into the (ACO-LMS)/adaptive filter algorithm as shown. The algorithm was developed for extracting the fetal ECG from the abdomen of a pregnant woman by minimizing the Mean Square Error (MSE) globally.

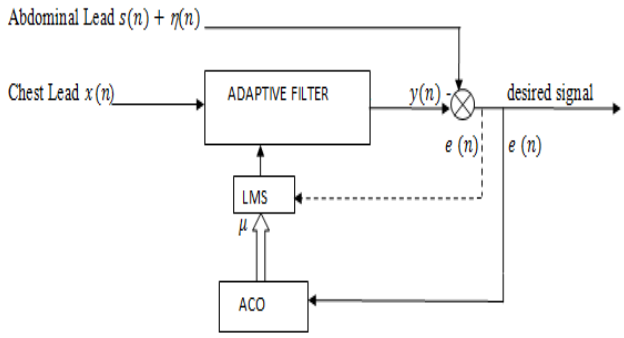


Fig. 3 The proposed ACO-based adaptive filter

From the Fig. 3, the proposed fetal ECG extraction method consists of two adaptation algorithms; LMS alone and ACO-LMS. The LMS algorithm was first used to update the filter coefficients according to its performance criterion as described in subsection (3.1). The ACO-LMS algorithm was then implemented. It involves the Ant Colony Optimization Algorithm (ACO) with Least-Mean-Square (LMS) based adaptive filter method. In the proposed configuration, the error generated by the adaptive filter at initial time is sent to ACO block where the appropriate values of step-size are being randomly chosen. Then these step-size values are directed to the LMS block again. With each value of step-size, the adaptive filter coefficients are updated and corresponding number of errors are generated. After specified number of iterations, the ACO will again select the best step-size which was used to find the best filter coefficients with comparatively minimum mean square error value.

3. Simulations, Results and Discussion

3.1.1 Generation of synthetic maternal ECG signal

The normal heartrate rate of pregnant woman with 3.5 mV peak voltage and 89 bpm was generated in MATLAB as shown in the Fig. 4 below;

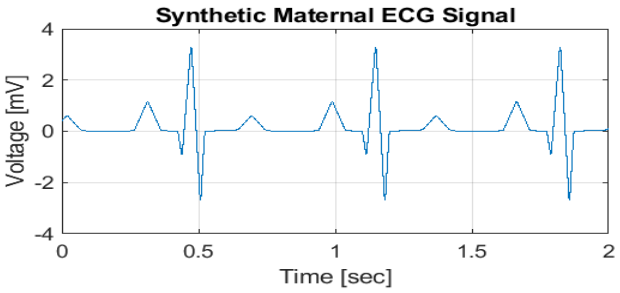


Fig. 4 Synthetic maternal ECG signal

3.1.2 Generation of synthetic fetal ECG signal

The fetal heart beats faster than that of the mother. The heart rate ranges from 120-160 bpm but with weaker amplitude of around 0.25 mV. The synthetic fetal ECG was generated using MATLAB as shown in the Fig. 5 below;

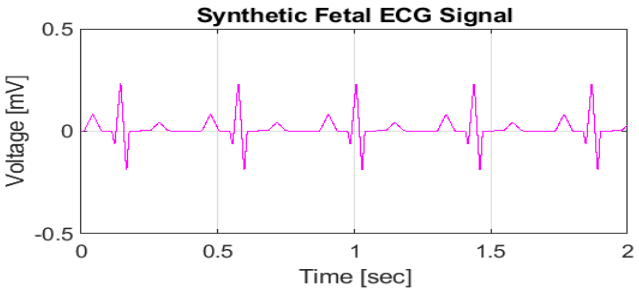


Fig. 5 Synthetic fetal ECG signal

3.1.3 Generation of synthetic abdominal ECG signal

The fetal abdominal ECG signal is usually dominated by the distorted maternal ECG that propagates from chest cavity to the abdomen. This propagation path was described as a linear FIR filter with 10 randomized coefficients as follows;

$$AECG = filter\left(\frac{b}{6,1}, MECG\right) + FECG + Noises \qquad (15)$$

Where b is the 10 randomized coefficients and $MECG$ is the maternal ECG signal. Since abdominal ECG is a composite signal, beside the propagation of the maternal ECG signal, some noises are present. These noises include base-line wander, electromyogram, skin

ISBN: 978-978-8567-02-8

impedance, power-line interference among others, were synthetically generated.

To generate power-line interference, equation (16) was used;

$$N = p * sin(2 * pi * f * t) \quad (16)$$

where p is the noise power, f is the frequency of noise. While other noise and white noise were modeled using equation (17)

$$N1 = p * randn \quad (17)$$

The abdominal ECG is the summation of $FECG$, $MECG$ and noises. The signals are synthetically coded using MATLAB and used according to the equation (18)

$$AECG = MECG + FECG + N + N1 \quad (18)$$

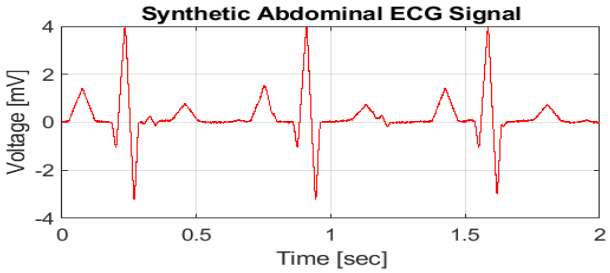


Fig. 6 Synthetic abdominal ECG signal

3.2 Simulation results of the synthetic ECG signal

The two algorithms are applied on the synthetic abdominal signal shown in Fig. 6. The LMS/adaptive filter algorithm removes greater percentage of dominant noises in the abdominal ECG signal of a pregnant woman. The ant colony optimization algorithm optimized the step size in order to find the best filter coefficients (weights).

3.2.1 LMS/Adaptive filter convergence on the synthetic AECG signal

LMS adaptive filter algorithm was applied on the synthetic abdominal ECG signal. The algorithm updated the filter coefficients and found the best filter coefficients that minimize the error signal by removing greater percentage of maternal ECG signal and other external noises with higher frequency. Codes for LMS adaptive filter algorithm were written in MATLAB.

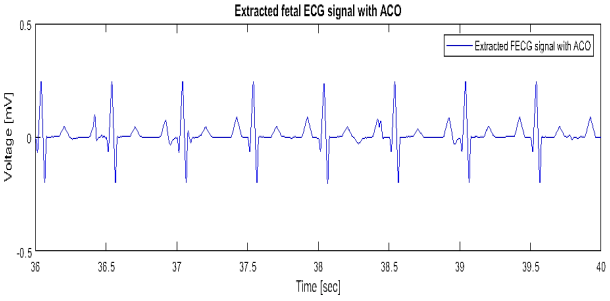
The fetal ECG extraction results obtained at different heart rates as shown in Fig. 7 (a) to Fig. 11 (a) using adaptive filter with only LMS algorithm still contains overlapping noise signals and some ECG components were not recovered. Therefore, since the LMS/adaptive filter technique has its limitations particularly in the proper fetal ECG signal extraction, the ant colony optimization algorithm technique was used to optimize the LMS/adaptive filter for better results.

3.2.2 ACO-LMS/Adaptive filter

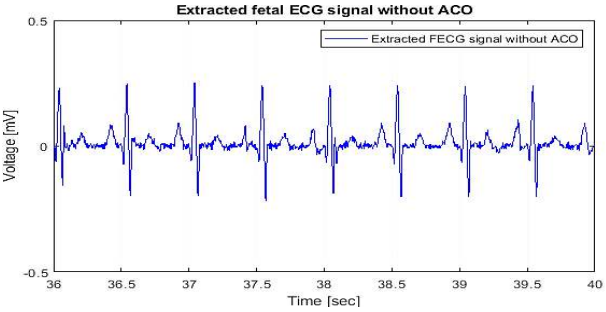
The ACO algorithm was also applied to the LMS/Adaptive filter on the error signal. The ACO algorithm minimized the mean square error globally by optimizing the step size as shown in 7 (b) to Fig. 11 (b), which uses in finding the best filter coefficient. The codes for ACO algorithm were also written in MATLAB to simulate the results.

3.3 Discussion of the Results

The results obtained are shown in Fig. 7 to Fig. 11 illustrating the comparison between the results of the extracted fetal ECG signal waveform without the use of ACO algorithm (i.e using LMS/Adaptive Filter only) and the results of the extracted fetal ECG with the use of ACO algorithm on LMS/Adaptive Filter (ACO-LMS) at different heart rates ranging from 120 to 160 bpm.



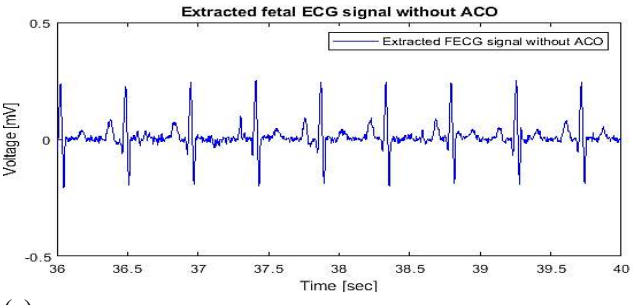
(a)



(b)

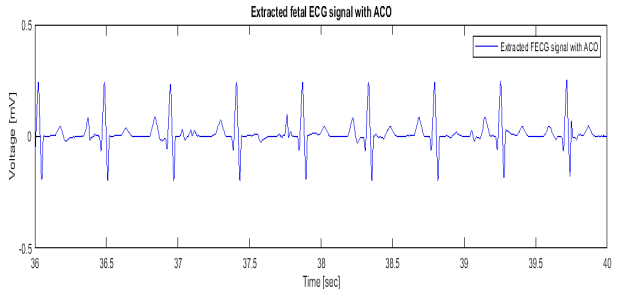
Fig. 7 Comparison between the extracted fetal ECG without ACO and the extracted fetal ECG with ACO at 120 bpm

In Fig. 7 (a), the result of the extracted fetal ECG signal obtained without using ACO is overlapped with significant number of noise signal, while the extracted fetal ECG obtained when ACO is used in Fig. 7 (b) contains minimum noise signal. The results indicate that, the proposed (ACO-LMS)/Adaptive Filter extracts the fetal ECG better than the LMS/Adaptive Filter.



(a)

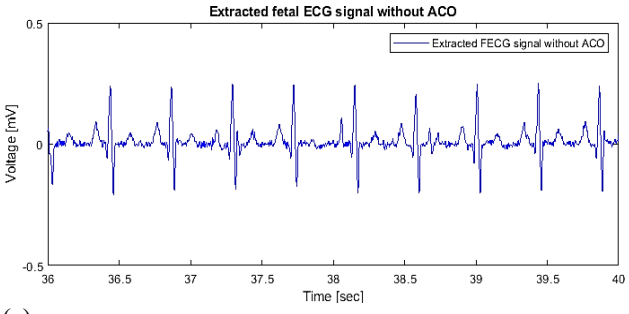
ISBN: 978-978-8567-02-8



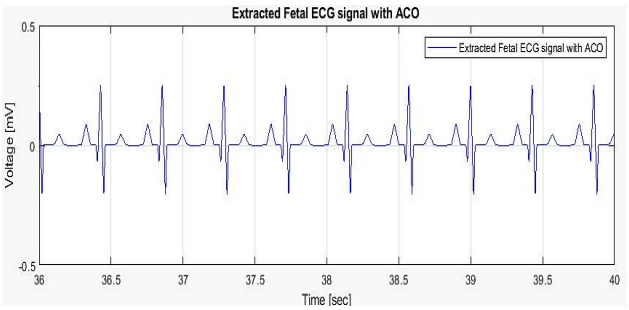
(b)

Fig. 8 Comparison between the extracted fetal ECG without ACO and the extracted fetal ECG with ACO at 130 bpm

In Fig. 8 (a), the extracted fetal ECG signal without using ACO at 130 bpm are corrupted with some overlapping noise signal and the P-wave components were not fully recovered. But the results of extracted fetal ECG signal when ACO is used shown in Fig 8 (b), contains minimal number of noise signal and all the components of ECG are seen. This result shows that, the (ACO-LMS)/ Adaptive Filter removes MECG and other noises for fetal ECG extraction better than LMS/Adaptive Filter.



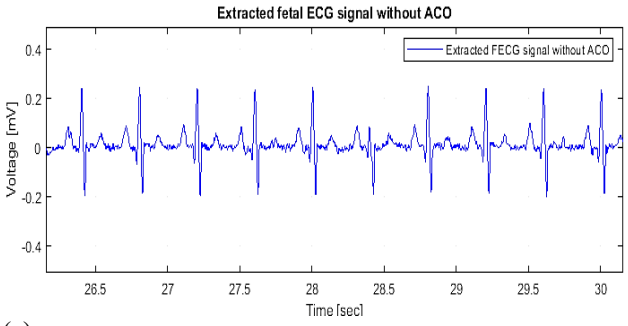
(a)



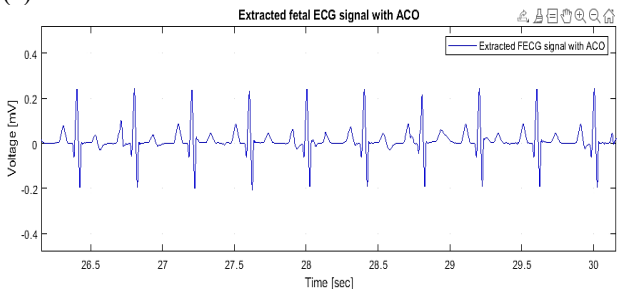
(b)

Fig. 9 comparison between the extracted fetal ECG without ACO and the extracted fetal ECG with ACOA at 140 bpm

In Fig. 9 (a), the results of extracted fetal ECG signal without the use of ACO at 140 bpm still contains noise interference and the shapes of P-wave and T-wave are altered at some time intervals. But when the ACO was used in Fig. 9 (b), the extracted fetal ECG signal contains lower noise signal and all the ECG components were recovered. Hence, the results show better fetal ECG extraction result with (ACO-LMS)/Adaptive Filter than the results with LMS/Adaptive Filter.



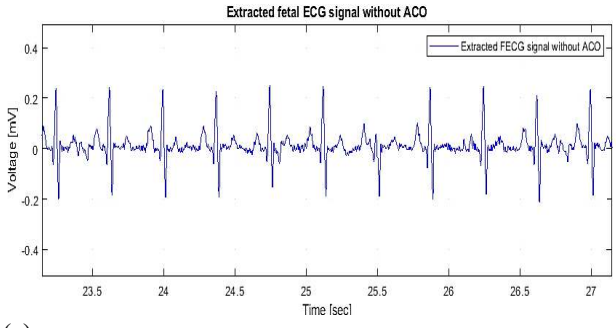
(a)



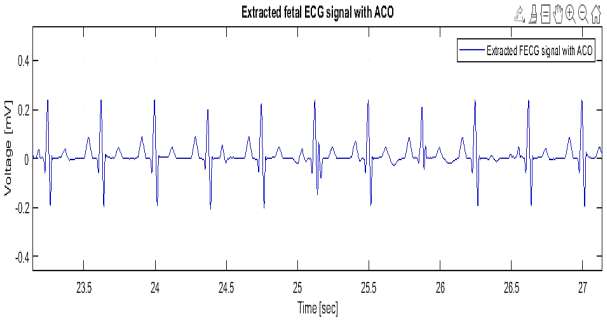
(b)

Fig. 10 Comparison between the extracted fetal ECG without ACO and the extracted fetal ECG with ACO at 150 bpm

In Fig. 10 (a), the result of extracted fetal ECG obtained without the use of ACO at 150 bpm still contains some significant number of noise and the sixth R-peak was not detected. While the result of extracted fetal ECG obtained with ACO in Fig. 10 (b) shows the extracted fetal ECG with less noise and all the ECG components were recovered. Consequently, the results show the good fetal ECG extraction when (ACO-LMS)/Adaptive Filter is used, but the poor fetal ECG extraction with LMS/Adaptive Filter.



(a)



(b)

Fig. 11 Comparison between the extracted fetal ECG without ACO and the extracted fetal ECG with ACO at 160 bpm

In Fig. 11 (a), the results of the extracted fetal ECG signal without the use of ACO at 160 bpm contains

ISBN: 978-978-8567-02-8

relatively large amount of noise and the seventh R-peak was not recovered. But when the ACO was used in Fig. 11 (b) the fetal ECG signal was properly extracted and all the components of ECG were seen.

The comparative results in Fig. 7 to Fig. 11 have clearly shown the presence of overlapping noise and relatively poor performance of fetal ECG extraction at different heart rates when LMS/Adaptive filter algorithm was used without the use of ACO. The poor performance is caused by the inability of the algorithm to guarantee the convergence to the global minimum. While the results of extracted fetal ECG signal obtained when using the ACO algorithm on LMS/Adaptive filter at different fetal heart rate (ranging from 120 to 160 bpm) showed the superiority of (ACO-LMS)/Adaptive filter technique over the conventional LMS/Adaptive filter technique.

When using ACO-LMS/Adaptive filter algorithm, the mean square error was minimized globally with an average value of 0.0015 (generated in MATLAB). Hence, the P-waves, QRS complex and T-waves fetal ECG components were recovered at different fetal heart rates. The values of MSE and SNR at different fetal heart rates were generated by MATLAB as shown in the Table I.

The equation used to calculate the SNR is

$$SNR = 10\, log_{10}\left({}^{P_s}/_{P_n}\right) \quad (9)$$

Where P_s is the fetal ECG signal power, while P_n is total noise signal power.

TABLE I: SIGNAL TO NOISE RATIO (SNR) AND MEAN SQUARE ERROR (MSE) VALUES AT DIFFERENT HEART RATES

Fetal Heart Rate (bpm)	Signal-Noise Ratio(dB)	Mean Square Error (MSE)
120	23.298	0.0013
130	21.999	0.0015
140	22.269	0.0015
150	22.478	0.0016
160	21.782	0.0018

From the Table I, the signal to noise ratio (SNR) at fetal heart rate of 120 bpm is greater than the SNR at 160 bpm. Meanwhile the value of mean square error (MSE) at 120 bpm is smaller than the MSE value at 160 bpm. This indicates that, the greater the SNR the smaller the MSE and vice versa.

3.4 Validation of the algorithm on real abdominal ECG signal

Real abdominal ECG signals were obtained from physionet database developed by MIT-BIH. The ECG recordings were performed in the Department of Obstetrics at the Medical University of Silesia. The records are stored in EDF/EDF+ (European Data Format) format. The record used for the validation of this research is r04.edf obtained from women in labour. The results of implementation of ACO/LMS algorithms on the obtained real AECG are shown in Fig. 12 to Fig. 15.

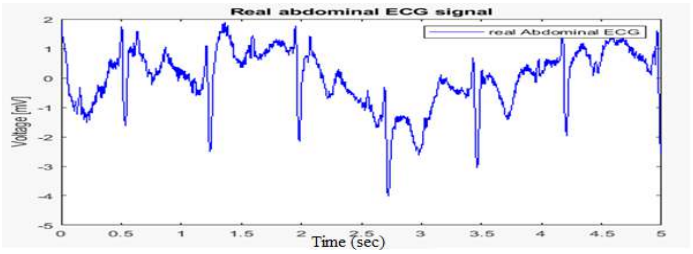


Fig. 12 Real abdominal ECG signal obtained from MIT-BIH (r04)

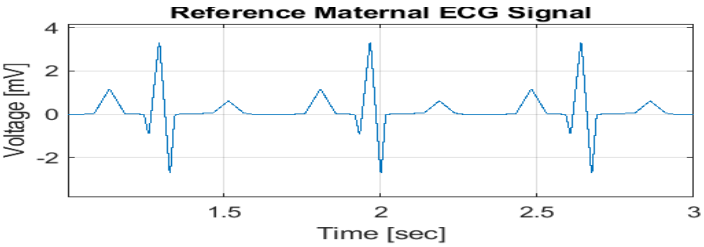


Fig. 13 Reference ECG signal (MECG)

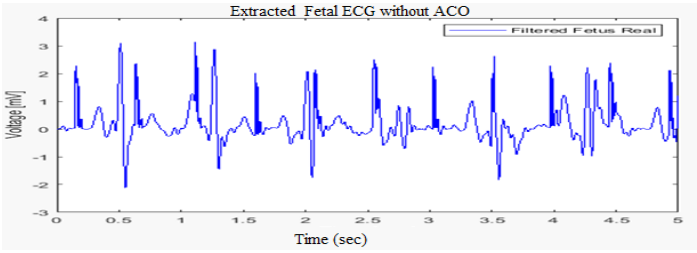


Fig. 14 Extracted fetal ECG signal without ACO from the composite real abdominal ECG (r04)

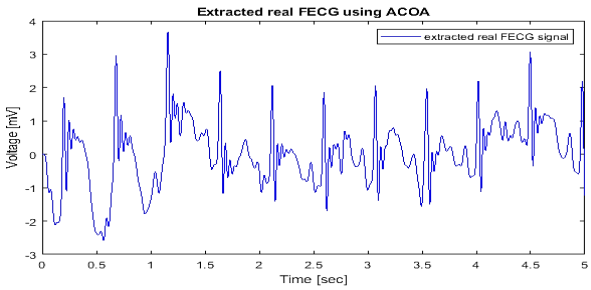


Fig. 15 Extracted fetal ECG signal with ACO from the composite real abdominal ECG (r04)

Fig. 12 shows the obtained abdominal ECG from the physionet of MIT-BIH (r04.edf). The Fig. 13 is the maternal ECG signal used as an adaptive filter reference signal. Fig. 14 shows the results of the extracted fetal ECG without the use of ACO. While the Fig. 15 shows the results of extracted fetal ECG signal after the application of ACO algorithm.

It can clearly be seen in Fig. 14 that, the extracted fetal ECG signal without the use of ACO still contains maternal ECG signal and residual noise signal. But in Fig. 15, the extracted fetal ECG with ACO algorithm does not contain maternal ECG. The signal was found to be at 132 bpm with minimum mean square error of 0.0023 and signal-noise ratio of 15.5795dB

ISBN: 978-978-8567-02-8

3.5 Performance comparison of the algorithm with other fetal ECG extraction techniques

The developed algorithm was compared with other existing methods of the fetal ECG extraction to validate its effectiveness. The performance comparison will be based on mean square error (MSE) and signal-to-noise ratio (SNR). The results obtained using ACO-based extraction method was compared with selected existing methods and the result is summarized in Table II

TABLE II: PERFOMANCE COMPARISON OF THE ALGORITHM WITH OTHER METHODS

Methods	FHR (bpm)	Average SNR (dB)	Average MSE
LMS based adaptive filter (Vamshadeepa, et al, 2017)	160	-12.7980	no report
Based on a Blind-Adaptive-Filtering approach (Graupe et. al, 2005)	150	no report	no report
Wavelet Transform (Hassanpour and Parsaei, 2006)	out of range	no report	no report
BFOA based adaptive filter (Jibia and Inuwa, 2015)	120-160	4.8656	0.0045
PSO based adaptive filter (Ahmed, 2018)	120-160	-9.1459	no report
MFO based adaptive filter (Jibia and Jibia, 2021)	139	10.2800	0.0215
Proposed ACO- based adaptive filter	120-160	22.3652	0.0015

The results shown in table II show good fetal ECG extraction on synthetic AECG using the ACO algorithm at different heart rates ranging from 120-160 bpm with the average MSE value of 0.0015 and SNR of 22.37 dB, when compared with the existing methods developed for fetal ECG extraction.

4. CONCLUSION

Fetal Electrocardiogram (ECG) reflects an electrical activity of fetus heart which helps in determining the fetal life, development and maturity. Fetal ECG is obtained non-invasively by placing two electrodes on the chest and abdomen of a pregnant woman to record the maternal ECG (MECG) and abdominal ECG (AECG) respectively.

The main challenge is the extraction of fetal ECG from composite AECG of a pregnant woman. The records of AECG signal comprise of dominant signal of MECG, the Fetal ECG, interferences and noise signals which make difficulties in accurately analyzing the fetal ECG signal. A number of techniques were developed for fetal ECG extraction. But there are still many unsolved problems of traces of the maternal ECG which is the dominant noise and some other noise such as electrode motion artifact, power-line interference, electromyogram among others. To minimize the existing problems, this research proposes a new method for fetal ECG extraction by using Ant Colony Optimization (ACO) Algorithm to optimize the step size (μ) of the Least Mean Square (LMS) Adaptive Filter.

Simulation results of this research work showed that, the ACO-LMS adaptive filter algorithm is good and robust in extraction of fetal ECG at different fetal heart rates ranging from 120 bpm to 160 bpm. The algorithm was applied on both synthetic abdominal ECG signal and real abdominal ECG signal. The synthetic abdominal ECG was generated in MATLAB while the real abdominal ECG signal was obtained from MIT-BIH database. The fetal ECG extraction results on synthetic abdominal ECG show good performance of the proposed algorithm with average minimum mean square (MSE) error value of 0.0015 and signal to noise ratio of 22.37 dB. When compared with previous methods on fetal ECG extraction. The algorithm has a noticeable performance over the other methods used for fetal ECG extraction in terms of the average MSE and improved SNR.

REFERENCES

Ahmed, A. (2018). Fetal ECG extraction using particle swarm optimization (PSO)-based adaptive filter: A thesis submitted to the department of Electrical Engineering, Bayero University, Kano.

Alkhodari, M., Rashed, A., Alex, M., and Yeh, N. S. (2018) "Fetal ECG Extraction Using Independent Components and Characteristics Matching," 2018 International Conference on Signal Processing and Information Security (ICSPIS), Dubai, pp. 1-4.

Ayat, M., Assaleh, K., and Nashash, H. (2008) "Fetal ECG extraction from a single abdominal ECG signal using SVD and polynomial classifiers," 2008 IEEE Workshop on Machine Learning for Signal Processing. Cancun, Mexico, pp. 250-254

ISBN: 978-978-8567-02-8

Blum, C. (2005). Ant colony optimization: Introduction and recent trends: Algorithms, Bioinformatics, Complexity and formal Methods research group (ALBCOM), Universitat Politècnica de Catalunya, Jordi Girona 1-3, Barcelona, Spain, pp. 353-371

Dorigo, M. and Stuzle, T. (2004). Ant Colony Optimization: A brandford book, the MIT Press Cambridge, Massachusetts London.

Graupe, D., Yunde Z., and Menachem, H. (2005) "Extraction of Fetal ECG from Maternal ECG Early in Pregnancy," International Journal of Biomedical Engineering, Vol. 7, No. 1. pp. 166-168

Hassan, M. A., Reaz, M. B. I., Ibrahimy, M. I. Hussain, M. S. and Uddin, J. (2009). Detection and processing Techniques of FECG signal for fetal monitoring: Shulin Li (ed) Biological procedures online, vol. 11, pp. 263-295

Hassanpour, H. and Parsaei, A. (2006) "Fetal ECG Extraction Using Wavelet Transform," International Conference on Computational Intelligence for Modelling Control and Automation Intelligent Agents, Web Technologies and Internet Commerce (CIMCA-IAWTIC'06), Sydney, Australia, pp. 179-183

Jibia, A.U. and Inuwa, A. (2015). Fetal Electrocardiogram extraction using BFOA-based adaptive filter: ATBU Journal of Science, Technology and Education (JOSTE), vol. 3 No. 4, pp. 30-43

Jibia, M.S. and Jibia A.U. (2021). Fetal Electrocardiogram Extraction Using Moth Flame Optimization (MFO)-Based Adaptive Filter: Advances in Science, Technology and Engineering Systems Journal Vol. 6, No. 2, pp. 303-312

Joshi, V. R. and Singh Y. (2015). De-noising of ECG signal using Adaptive Filter based on MPSO: Procedia Computer Science 57, pp. 395 – 402

Katiyar, S. and Ansari A.Q. (2015). Ant Colony Optimization: A Tutorial Review: International journal of engineering and technology, Vol.7 https://www.researchgate.net/publication/281432201

Ling, Q., Ikbal, M.A. and Kumar, P. (2020). Optimized LMS algorithm for system identification and noise cancellation: Journal of Intelligent System, Vol. 30, pp. 487–498

Merredin, R. and Falcão, A. (2015). Adaptive filtering algorithm for noise cancellation: Faculdade de Engenharia da Universidade do Porto, Dissertação realizada no âmbito do Mestrado Integrado em Engenharia Electrotécnica e de Computadores Major Automa.

Prasanth, K. Baby, P. and Balakrishmn, A.A. (2013) "Fetal ECG extraction using adaptive filters," International journal of advanced research in engineering research (AJER), Vol.3,issue 4, pp. 1483-1487

Rajni and Tayal, A (2013). A Step Size Optimization of LMS Algorithm Using Particle Swarm Optimization Algorithm in System Identification: International Journal of Computer Science and Network Security, Vol.13, No. 6, pp. 125-130

Taha, Y. L., and Abdel-Raheem, E. (2018) "Extraction of Fetal Electrocardiogram signals using Blind Source Extraction Based Parallel Linear Predictor Filter," Proceedings of the 2018 IEEE International Symposium on Signal Processing and Information Technology (ISSPIT), Louisville, USA, pp. 208-211

Tripathi, S. and Ikbal, M.A (2016). Identification of Systems with Multi-Model Error Surface by Ant Colony Optimization: Proceedings of the Advancement in Computer Engineering and Information Technology, Department of Electronics and Communication Engineering, Jahangirabad Insitute of Technology, Barabanki, India.

Vamshadeepa, N., Priyanka, H.B and Ashwini, V. (2017). Extraction of Fetal ECG from Maternal ECG using Least Mean Square Algorithm: International Journal of Advanced Networking and Applications, Vol. 8, pp. 36-39

Widrow, B. and Hoff, M.E. (1960). Adaptive Switchinh Circuits: Institute of Radio Engineers (IRE) Wescon Convention Record, Conference Proceedings, pp. 96-1-104

ISBN: 978-978-8567-02-8

5TH Faculty of Engineering Conference on Engineering Innovation and Economic Policies: Driving Sustainable Industrial Growth in Nigeria

Faculty of Engineering, Bayero University, Kano.

049-Emulation-Based Analysis of Mobile Producer Handoff Strategies in Named Data Networking: MP-HNEM

Abdulkadir H. Alkali[1], Muhammed Z. Ahmed[1256], Aisha HA. Hashim[23], Adamu U. Dzivama[4], Uwihanganye Vadaste[5], Musa I. Lamido[7]

[1]*Department of Computer Engineering, University Maiduguri, Nigeria*
[2]*Electrical and Computer Engineering Dept., International Islamic University Malaysia, Kuala Lumpur, Malaysia*
[3]*Dept. of Electrical and Electronic Engineering Science, University of Johannesburg, South Africa.*
[4]*Department of Agric Engineering, University Maiduguri, Nigeria*
[5]*Department of Computer Science, University of Technology and Arts of Byumba, Rwanda.*
[6]*Department of Cyber Security, Al-Ansar University Maiduguri, Nigeria*
[7]*Nigerian Airspace Management Agency*

**Corresponding author: zaharadeenccna@gmail.com*

Abstract: Seamless content retrieval under node mobility remains a critical challenge in Named Data Networking (NDN), particularly for mobile content producers. This study presents the Mobile Producer Handoff in Named-data Emulated Mobility (MP-HNEM) framework, a predictive handoff solution that proactively manages routing updates and handoff scheduling through a Mobility Management Entity. MP-HNEM leverages predictive parameters (mobility prediction accuracy (α), lead time (β), and proactive signaling cost ($_{\gamma}$)) to minimize latency, packet loss, and control overhead during producer mobility. The framework was evaluated using ndnSIM in both simulation and emulation settings, incorporating three mobility models: Grid Mobility Model (GMM), Random Waypoint Model (RWM), and Ad hoc On-Demand Distance Vector (AODV), under varying packet intervals and network topologies. Results demonstrate that MP-HNEM consistently achieves high packet delivery ratio (PDR > 0.90), low handoff latency (<1s), and optimized signaling overhead, with AODV scenarios yielding the best performance. Statistical analysis confirms the framework's adaptability and efficiency across mobility conditions, indicating MP-HNEM as a robust solution for IoT, vehicular networks, and mobile edge computing applications.

1. INTRODUCTION

The rapid proliferation of mobile and Internet of Things (IoT) devices has revealed fundamental limitations of conventional IP-based networking, particularly in supporting seamless mobility. IP networks rely on location-dependent addressing, which tightly couples node identity with its point of attachment. As a result, ongoing data delivery is frequently disrupted when a node changes location, leading to increased latency, packet loss, and signaling overhead. These challenges are amplified in emerging applications such as smart cities, vehicular communications, and wireless sensor networks, where mobility and real-time content delivery are essential.

Named Data Networking (NDN), a prominent architecture within the Information-Centric Networking (ICN) paradigm, addresses many of these limitations by shifting the communication model from host-centric to data-centric. In NDN, data is requested and retrieved using hierarchical, human-readable names rather than host addresses, enabling intrinsic features such as in-network caching, multicast delivery, and data-centric security. While these characteristics significantly improve content dissemination efficiency, mobility support—particularly for mobile producers (MPs)—remains a critical challenge.

Unlike consumer mobility, which can be partially handled through Interest retransmissions and cached data, producer mobility requires timely updates of forwarding information across the network. When a producer moves, outdated forwarding paths can lead to route inconsistencies, increased packet loss, and temporary content unavailability. Existing NDN mobility solutions broadly fall into anchor-based, anchor-less, and hybrid approaches. Anchor-based schemes offer centralized control but often incur additional latency and introduce single points of failure. Anchor-less approaches reduce handoff delay and improve scalability but may generate excessive signaling overhead due to frequent routing updates. Consequently, achieving an effective balance between handoff latency, control overhead, and data availability remains an open research problem.

A key limitation of many existing approaches is their reactive nature, where handoff decisions are triggered only after link degradation or disconnection has occurred. This reactive behavior results in avoidable latency and packet loss during mobility events. To address this issue,

ISBN: 978-978-8567-02-8

predictive mobility management has emerged as a promising direction, enabling proactive handoff preparation based on anticipated movement rather than current network state alone.

Motivated by these challenges, this paper proposes Mobile Producer Handoff in Named-data Emulated Mobility (MP-HNEM), a predictive and comprehensive framework for supporting mobile producer mobility in NDN. Unlike prior work that relies primarily on analytical models or simulations, MP-HNEM is evaluated using an emulation-driven approach that integrates mathematical modeling, algorithmic design, and ndnSIM-based experimentation. The framework predicts future producer locations by analyzing mobility behavior such as movement direction, speed, and signal strength trends, allowing forwarding updates to be initiated before actual disconnection occurs.

The proposed MP-HNEM framework introduces a mobility-aware predictive handoff strategy composed of three core components: (i) a Mobility Trend Analyzer (MTA) that constructs movement profiles using historical hop transitions and signal strength variations, (ii) a Predictive Handoff Engine (PHE) that employs an Exponential Weighted Moving Average (EWMA) estimator to forecast the most probable next-hop router, and (iii) a Proactive FIB Updater (PFU) that triggers forwarding updates and content advertisements in advance of producer movement. A mathematical model is developed to capture key parameters such as prediction window duration, prediction error rate, and proactive forwarding update cost, providing quantitative insight into the effectiveness of the predictive mechanism.

The performance of MP-HNEM is evaluated under heterogeneous mobility scenarios using grid, random waypoint, and AODV-based mobility models. The evaluation focuses on three primary objectives: reducing handoff latency, minimizing signaling overhead, and ensuring practical applicability in real-world mobile and IoT environments. Through extensive emulation-based analysis, this work provides actionable insights into the design and deployment of efficient mobile producer handoff strategies for NDN-enabled networks.

2. RELATED WORK

Mobility management has been extensively studied in Named Data Networking, with particular attention given to handling consumer and producer mobility under dynamic network conditions. Early NDN research primarily focused on consumer mobility, leveraging Interest retransmissions and in-network caching to mitigate disruptions. However, producer mobility presents more complex challenges, as data origin changes require consistent forwarding updates across the network.

Anchor-based mobility solutions are among the earliest approaches proposed for producer mobility in NDN. These mechanisms rely on a fixed rendezvous point or anchor node that maintains the producer's current location. While anchor-based schemes simplify forwarding updates and provide centralized control, they often introduce additional latency during handoff and create potential single points of failure. Moreover, scalability becomes a concern as the number of mobile producers increases.

To overcome these limitations, anchor-less mobility approaches have been proposed, where forwarding information is updated dynamically without relying on a centralized anchor. Such approaches reduce handoff latency and eliminate single points of failure but typically incur higher signaling overhead due to frequent routing updates and flooding mechanisms. Hybrid approaches attempt to balance the trade-offs between anchor-based and anchor-less designs by combining localized anchoring with distributed update strategies; however, complexity and overhead remain open challenges.

Recent studies have explored predictive and proactive mobility management techniques to reduce handoff latency. These approaches utilize parameters such as signal strength, mobility patterns, or historical movement data to anticipate node transitions. While predictive strategies show promise in minimizing packet loss and service disruption, many existing works remain limited to theoretical models or simplified simulations, lacking comprehensive experimental or emulation-based validation.

In terms of evaluation methodology, most prior research relies heavily on simulation-based analysis using ndnSIM. Although simulation provides valuable insights, it often abstracts real-world dynamics such as timing behavior, protocol interactions, and resource constraints. Emulation-based studies, which more closely approximate real deployment conditions, remain relatively underexplored in the context of mobile producer handoff in NDN.

Unlike existing approaches, this work combines predictive mobility management with an emulation-driven evaluation framework. MP-HNEM integrates mathematical modeling, predictive handoff mechanisms, and ndnSIM-based emulation to assess mobile producer handoff performance under heterogeneous mobility models. By addressing both architectural design and practical validation, this study advances the state of the art in mobile producer mobility support for Named Data Networking.

2. METHODOLOGY

This section presents the design framework, mobility assumptions, predictive handoff mechanism, mathematical formulation, and experimental setup used to evaluate mobile producer (MP) handoff performance in Named Data Networking (NDN). The objective is to design a low-latency, high-availability, and scalable predictive handoff mechanism, referred to as Mobile Producer Handoff in Named-data Emulated Mobility (MP-HNEM), which enables proactive forwarding

ISBN: 978-978-8567-02-8

updates to ensure seamless content delivery during producer mobility.

3.1 System Architecture

The MP-HNEM architecture consists of a Mobile Producer (MP), multiple Content Routers (CRs), consumer nodes, and a centralized Mobility Management Entity (MME). Consumers issue Interest packets using content names, which are forwarded by CRs based on entries stored in their Forwarding Information Base

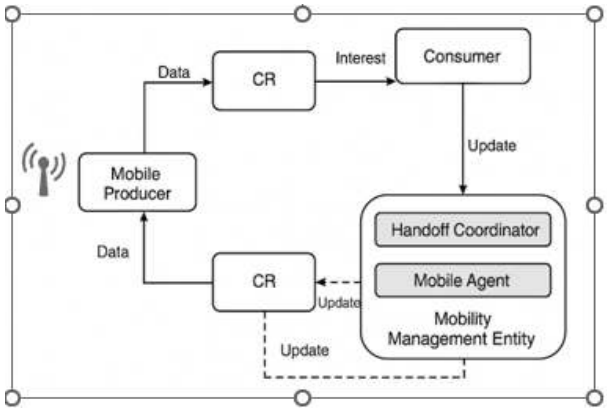


Figure 1: MP Handoff Architectural Model.

(FIB). The MP produces Data packets while dynamically changing its point of attachment across CRs.

The MME is composed of two logical components: a Handoff Coordinator (HC) and a Mobility Prediction Agent (MPA). The HC monitors routing events and handoff triggers, while the MPA predicts the future attachment point of the MP based on observed mobility patterns. This prediction enables proactive forwarding updates at neighboring routers prior to the actual movement of the producer. The overall architecture is illustrated in Figure 1.

3.2 Predictive Handoff Framework with Mobility Forecasting

MP-HNEM employs a Markov-based Mobility Prediction (MMP) mechanism to estimate the next attachment point of the MP. Let S_t denote the current CR associated with the MP and S_{t+1} the predicted next CR. A state transition matrix T is defined as:

$$T_{ij} - P(S_{t+1} - j \mid S_t - i)$$

This transition matrix is learned during the initial simulation phase and updated periodically based on observed mobility transition. The predicted next hop is determined as.

$$S_{t+1} = \arg\max T_{ij} \quad (1)$$

This prediction location is then used by the Mobility Prediction Agent (MPA) to proactively update FIB entries at selected neighboring CRs, reducing routing convergence delay during handoff.

3.3 Predictive Handoff Strategy for P-HNEM

The predictive handoff process is coordinated through a lightweight algorithm that integrates mobility history and signal strength trends. Algorithm 1 summarizes the operational steps of the MP-HNEM handoff mechanism. At fixed intervals, the MP's position is evaluated, the next point of attachment is predicted based on the selected mobility model, and forwarding entries are proactively updated using the Named-data Link State Routing (NLSR) protocol. Performance metrics including latency, packet delivery ratio (PDR), and signaling overhead are recorded during runtime.

ALGORITHM 1: PREDICTIVE HANDOFF PROCEDURE FOR MP-HNEM

```
Algorithm: PredictiveHandoffProcedure()

  Input:
      currentMPPosition ← coordinates of MP node
      neighborTable ← list of adjacent routers
  (CR nodes)
      handoffInterval ← 10 seconds
      currentFIB ← FIB entries for current
  routing
      mobilityModel ← GMM, RWM, or AODV
      time ← simulation clock

  Output:
      updatedFIB ← FIB reflecting new next hop
      reducedLatency,              increasedPDR,
  optimizedOverhead

  Begin:
      Initialize simulation topology with
  consumer, MP, and CR nodes
      Install NDN stack and set Interest/Data
rates
    Load mobility model based on scenario
    While simulation is running:
        If (time % handoffInterval == 0):
            Evaluate MP's current position
            Predict next point-of-attachment
using mobilityModel
            Identify best-fit CR node from
neighborTable
            Update currentFIB to reflect new CR
node as next hop
            Broadcast routing update via NLSR
            Trigger route recalculation at
adjacent routers
        End If
        Track:
            Latency ← Time between last Interest
and received Data
            PDR ← DataReceived / InterestSent
            Overhead ← Total control messages
exchanged
        Log metrics
    End While

   Return: Handoff log with latency, PDR,
overhead, FIB update details
```

3.4 Mobility Model Definition

To evaluate the robustness under heterogeneous mobility conditions, three mobility models are considered:

- Grid Mobility Model (GMM): Represents structured and predictable movement across a 6-node grid topology.
- Random Waypoint Model (RWM): Captures unstructured and stochastic mobility across an 8-node topology.
- AODV-based Mobility: Represents highly dynamic ad hoc scenarios with 10 nodes and frequent route changes.

ISBN: 978-978-8567-02-8

The MP periodically changes its attachment point every T_{move} seconds, and node speeds are measured in meters per second. All nodes are equipped with a standard NDN protocol stack using NLSR to ensure consistent routing behavior. The mobility setup is shown in Figure 2.

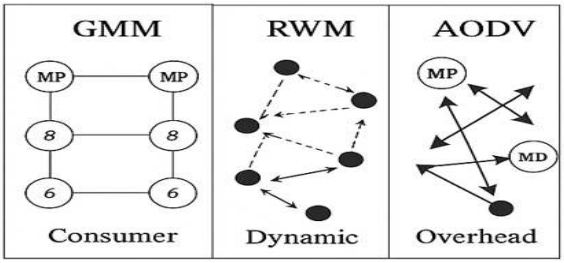


Figure 2: Mobility Model Setup

3.5 Mathematical Modelling

Our MP-HNEM predictive handoff strategy modelled four key performance indicators like handoff latency, packet loss probability, signaling overhead, and data availability. This is to enable foresight-based mobility handling. These include prediction accuracy α, lead time β, and proactive routing cost factors γ, which reflect the system's ability to anticipate mobility events and pre-configure routing paths before disconnection occurs. These enhancements differentiate the proposed model from traditional reactive strategies.

3.5.1 Handoff Latency

Handoff latency refers to the time taken to switch from the old forwarding path to the new one during producer's mobility transmition. Equations for both anchor-based and anchor-less senerios are presented. For the anchor-based scenerio:

$$Anchor\colon\ L_{old} - t_{det} + t_{fib}$$

where L_{old} is the latency using anchor-based secnerio, t_{det} the delay in detection and t_{fib} processing, and is the FIB update propagation delay.for the anchor-less scenerio.

$$Anchorless\ MP - HNEM\colon\ L_{new} - t_{pfu}$$

Where L_{new} is the latency using anchor-less predictive approach and t_{pfu} is the proactive FIB update time under MP-HNEM. Due to the fact that t_{pfu} is less than $t_{det} + t_{fib}$ wchich is the predictive handoff under MP-HNEM that significantly reduction in latency. Specifically, MP-HNEM define predictive latency $L_{predict}$ in Eq. (2) as:

$$L_{predict} = (1 - \alpha) * L_{reactive} \qquad (2)$$

Where α ε [0,1] represent the predictive accuracy factor. This means how early the handoff was anticipated before disconnection. $L_{reactive}$ represent $d_{avg} * t_{fib}$ as used in the general scenario. Finally, higher α (with 0.8) leads to significantly lower handoff latency.

3.5.2 Packet Loss Probability

The probability of packet loss during handoff is denoted as P_l, which is primarily a function of the Interest packet arrival rate and the delay before the new route becomes available. This metric indicates the likelihood of data loss during handoff:

$$P_l - R \cdot L$$

Here, R represents packet tranmission rate, L represent the latency during handoff. Therefore, anchor-less predictive handoff reduces L, hence minimize P_l. Specifically, predictive packet loss probability is defines in Eq. (3) below as:

$$P_l = \lambda_i * (\Delta t - \beta) \qquad (3)$$

Where β represent the predictive lead time. The predictive lead time refers to how much earlier the routing update was made before the MP moved to a new location. Anytime $\beta \geq \Delta t$, then predictive packet loss probability $P_l \approx 0$

3.5.3 Signaling Overhead

The total signaling overhead, $O_{handoff}$, accounts for all control messages generated during FIB updates. It also consist of intererst rerouting and control signalling. This is given below as.

$$S_o - n_u * b_f + c_i$$

MP-HNEM minimizes n_u and rerouting by anticipating movement. Specifically, the predictive signalling overhead $O_{predict}$ is defined in Eq. (4) below as:

$$O_{predict} = \gamma * N_{predict} * S_{fib} \qquad (4)$$

Where γ represent a tunable overhead optimization factor for proactive signalling and $N_{predict}$ represent the number of routers proactively updated ahead of the mobile producer move.

3.5.4 Data Availability

Availability refers to uninterrupted data access during mobility. MP-HNEM model its data availability as:

$$A_{data} = \left(\frac{D_s}{D_t}\right)$$

Where D_s represents successful data retrievals and D_t represent total data requests. MP-HNEM enhances data retrievals by ensuring route freshness and proactive FIB mapping. Specifically, predictive-aware data availability A_{data} is defined in Eq. (5) as:

$$A_{data} = \left(\frac{\lambda_c}{\mu}\right) * (1 - P_{data}) \qquad (5)$$

Where α represent number of predicted paths that are valid when the mobile producer moves to a new location. As prediction becomes more accurate, there will be additional data path in abundance. In addition, Table 1. below presents basic simulation parameters used to evaluate predictive handoff strategy in MP-HNEM.

3.6 Simulation Setup

The proposed framework is evaluated using the ndnSIM simulator built on NS-3. Network topologies consist of 6–10 nodes depending on the mobility model. Each node is configured with a complete NDN stack, including Content Store (CS), Pending Interest Table (PIT), and FIB. Consumers generate Interest packets at a fixed rate of 10 packets/s, while the MP responds with

ISBN: 978-978-8567-02-8

Data packets matching the requested prefix.

Mobility events are triggered every 10 seconds to emulate handoffs. Performance metrics such as handoff latency, PDR, signaling overhead, and data availability are recorded using built-in tracing tools. Network topology and application configuration are illustrated in Figures 3–4.

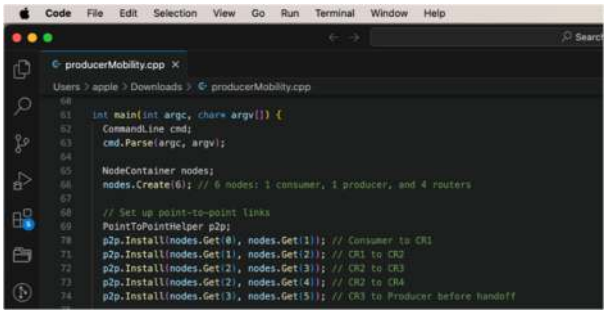


Figure 3: Network Topology

TABLE I: PARAMETERS AND ASSUMPTIONS USED IN MOBILITY PERFORMANCE MODELLING

Symbol	DESCRIPTION	Value	Source /Assumption
R	Packet transmission rate	10 pkt/s	Simulation Configuration
t_fib	FIB update propagation	5 ms	[1]
t_det	Mobility detection delay	8 ms	Measured
t_pfu	Proactive FIB update time	2 ms	Simulation observation
b_f	Bytes per FIB entry	64 B	Standard NDN configuration

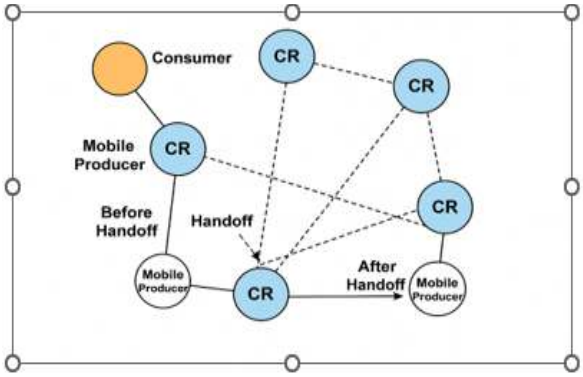


Figure 4: NDN Topology with 6–10 nodes

The routing strategy used is NLSR, which provides efficient route discovery and recovery under dynamic node conditions. Mobility is introduced by triggering handoffs at fixed intervals of 10 seconds. Each simulation run logs performance metrics such as packet delivery ratio, latency, and control message count. NetAnim is used for visualizing node behavior, while *PacketSentTracer* and *PacketReceivedTracer* tools track packet movement and FIB update events across nodes. This setup ensures a comprehensive simulation of real-world NDN performance under varying mobility pressures. For the NDN stack, application was configured specifically on the consumer and MP nodes. This means consumer node was set to generate Interest packets at a constant rate of 10 packets/second, targeting content from the producer. The MP responds with Data packets matching the requested prefix. This configuration is validated and illustrated in Figure 5.

To implement mobility model in this simulation, a constant position mobility model was initially configured to define the nodes' spatial arrangement. While nodes remain stationary during each iteration, dynamic behavior is introduced using scheduled handoffs to simulate mobility events. This setup is shown in Figure 6.

To support handoff events, a predictive handoff algorithm was implemented. The algorithm schedules periodic handoff events, updates routing information, and

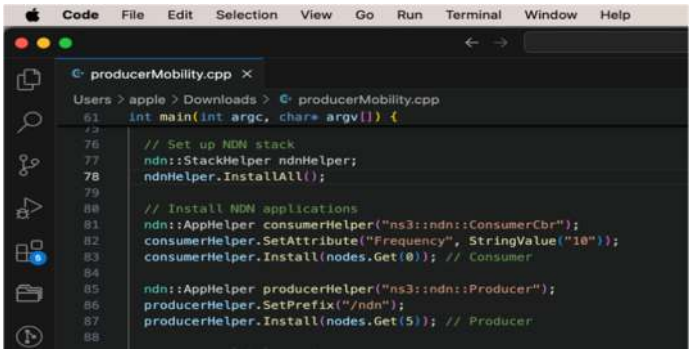


Figure 5: NDN Stack and Application Setup

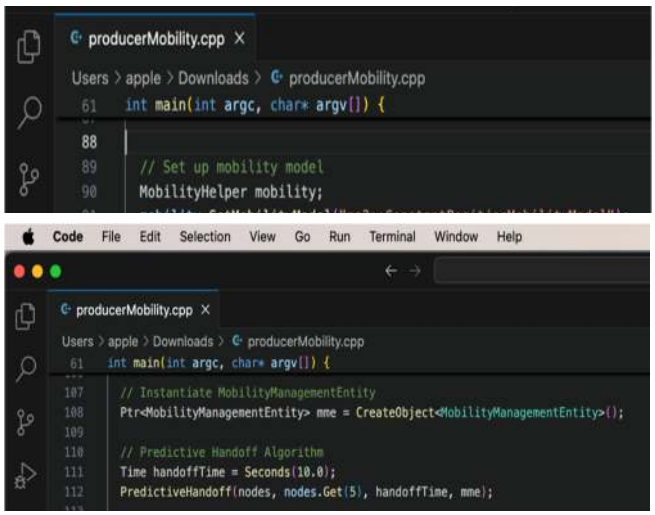


Figure 7: Predictive Handoff Algorithm

facilitates seamless data flow continuity. The logic is governed by a dedicated *MobilityManagementEntity* class, which ensures accurate position tracking and dynamic FIB updates. The algorithm structure is depicted in Figure 7.

Using simulation, performance of MP-HNEM was evaluated based on key metrics. The metrics were computed using the *EvaluatePerformance* function executed at the end of each iteration. Handoff latency was measured by tracking the time interval required for the mobile producer (MP) to switch between adjacent content routers. This reflects handoff algorithm responsiveness.

ISBN: 978-978-8567-02-8

Packet delivery ratio (PDR) was determined using the *PacketSentTracer* and *PacketReceivedTracer* tools. This captures the ratio of Data packets received by the consumer, relative to the Interest packets sent by the producer. Network overhead was assessed by aggregating all control and data packets exchanged during the simulation. The outcome gives insight into the efficiency of routing and mobility mechanisms. Additionally, data availability was monitored to ensure that requested content remained continuously accessible at the consumer side throughout the MP transition. These parameters collectively reflect the robustness and adaptability of the implemented mobility strategy, as visualized in Figure 8.

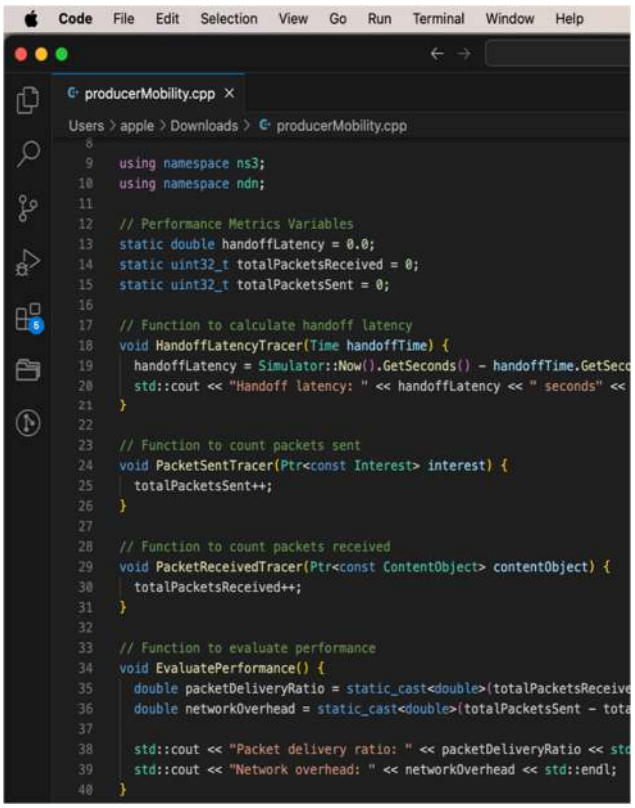


Figure 8: Performance Metric Evaluation Process

3.7 Emulation Setup

To complement simulation results, an emulation environment is implemented using ndnSIM on NS-3 with C++ extensions. The emulation setup mirrors the simulation topology while enabling fine-grained packet-level tracing and real-time route recalculation. The MP embeds a MobilityManagementEntity module that tracks movement, triggers predictive handoff decisions, and updates forwarding entries dynamically.

The emulation setup consists of a heterogeneous NDN topology comprising 6 to 10 nodes based on the selected mobility model to evaluate. Each node is fully equipped with complete NDN protocol stack, including modules for Interest/Data packet handling, Content Store (CS), Pending Interest Table (PIT), and Forwarding Information Base (FIB). The Named-data Link State Routing (NLSR) protocol is adopted to manage dynamic route updates and ensure robust name-to-route mapping even during handoff events. The emulation environment is biuld and executed using Visual Studio Code (VS Code) with C++ bindings for NS-3. Extensions (custom biuld) were developed to model the Mobile Producer (MP) behavior, implement predictive handoff mechanisms, and embed routing-aware mobility intelligence. Application layers are configured at both producer and consumer nodes to generate and respond to Interest and Data packets according to predefined content prefixes. Node mobility is emulated using three models. These includes Grid Mobility Model (GMM), Random Waypoint Model (RWM), and Ad hoc On-Demand Distance Vector (AODV) mobility. Each model imposes different structural and dynamic characteristics on node movement, enabling a comparative performance evaluation under varying conditions. Node trajectories and handoff transitions were visualized using NetAnim while internal tracing tools such as *PacketSentTracer* and *PacketReceivedTracer* are deployed to monitor packet movement and measure performance metrics in real-time. To emulate mobility-induced disruptions, handoff events are triggered at fixed 10-second intervals. The *MobilityManagementEntity* class, embedded in the MP node, actively tracks the producer's location and re-calculates routes as needed, thus minimizing latency and data loss during transitions. Each emulation run captures metrics such as handoff latency, packet delivery ratio (PDR), signaling overhead, and data availability. These metrics collectively reflects MP-HNEM adaptability and efficiency under mobility stress.

The emulation setup illustrated in Figure 9 provides a conceptual overview of the network layout, MP handoff process, and monitoring tools used during the emulation. This visual representation aids in understanding the logical flow and data handling components within the MP-HNEM architecture.

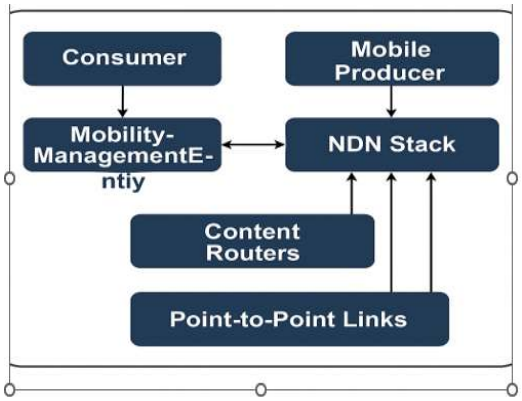


Figure 9: Emulation Setup for MP-HNEM

4. RESULT

This section presents a comprehensive evaluation of the proposed Mobile Producer Handoff in Named-data Emulated Mobility (MP-HNEM) framework using both simulation and emulation. Performance is assessed under three mobility models—Grid Mobility Model (GMM), Random Waypoint Mobility (RWM), and Ad hoc On-Demand Distance Vector (AODV)—to validate MP-HNEM under structured, stochastic, and highly dynamic mobility conditions. Key performance metrics include handoff latency, packet delivery ratio (PDR), signaling overhead, and data availability, which directly

ISBN: 978-978-8567-02-8

correspond to the predictive parameters defined in Section 3, namely prediction accuracy α, predictive lead time β , and signaling cost factor γ.

4.1 Simulation

4.1.1 Grid Mobility Model (GMM)

The deterministic path traversal in GMM aligns with the predictive FIB update logic, allowing MP-HNEM to pre-calculate optimal routes with minimal latency variations. Table 3 summarizes the simulation outcomes.

As packet intervals increase from 2 to 8 seconds, the packet delivery ratio improves from 0.83 to 0.95, while signaling overhead decreases. This trend indicates that longer intervals allow MP-HNEM to effectively exploit predictive lead time, reducing unnecessary control messages. Notably, handoff latency remains constant at 2 seconds across all configurations, demonstrating the stability of MP-HNEM under structured mobility conditions.

TABLE 3: GMM SIMULATION RESULTS

Simulation	Packet Interval (sec)	Packet Size (bytes)	Node Count	Handoff Latency (sec)	PDR	Overhead	Avg. Latency (sec)
1	2.0	512	6	2	0.83	4	1.3
2	4.0	1024	6	2	0.91	2	1.3
3	8.0	2048	6	2	0.95	1	1.3

TABLE 4: RWM SIMULATION RESULTS

Simulation	Packet Interval (sec)	Packet Size (bytes)	Node Count	Handoff Latency (sec)	PDR	Overhead	Avg. Latency (sec)
1	2.0	512	8	2	0.75	6	1.5
2	4.0	1024	8	4	0.82	4	1.5
3	8.0	2048	8	4	0.86	3	1.5

TABLE 5: AODV SIMULATION RESULTS

Simulation	Packet Interval (sec)	Packet Size (bytes)	Node Count	Handoff Latency (sec)	PDR	Overhead	Avg. Latency (sec)
1	2.0	512	10	2	0.90	9	0.75
2	4.0	1024	10	4	0.92	7	0.75
3	8.0	2048	10	4	0.93	6	0.75

4.1.2 Random Waypoint Mobility (RWM)

The variability in RWM confirms MP-HNEM tolerance to irregular prediction intervals β, where proactive updates still yield consistent performance under fluctuating node mobility. Table 4 presents the RWM scenario results.

Compared to GMM, RWM exhibits lower PDR values, ranging from 0.75 to 0.86, reflecting the inherent unpredictability of node movement. However, MP-HNEM maintains acceptable delivery performance and stable average latency (1.5 seconds). Although signaling overhead is higher than in GMM due to more frequent route recalculations, the results confirm MP-HNEM's resilience under irregular mobility conditions.

4.1.3 Ad hoc On-Demand Distance Vector (AODV)

This scenario demonstrates the predictive strategy's advantage where fast-forwarding route updates reduces reliance on reactive signaling, effectively minimizing FIB propagation delay (t_fib). Table 5 summarizes the performance under AODV.

AODV consistently achieves the highest PDR (0.90–0.93) and the lowest average latency (0.75 seconds). While signaling overhead is higher compared to GMM, the predictive nature of MP-HNEM minimizes forwarding disruptions by proactively updating routes, thereby reducing FIB propagation delay. These results highlight MP-HNEM's effectiveness in high-mobility and route-volatile environments.

4.2 Emulation-Based Performance of MP-HNEM

To validate real-world applicability, MP-HNEM was evaluated in an emulation environment using ndnSIM. A fixed six-node topology was configured, with the mobile producer changing its attachment point every 10 seconds. Predictive handoff decisions were managed by the MobilityManagementEntity module, which initiates FIB updates prior to disconnection events.

The emulation consistently achieved PDR values above 0.90 and average latency below 1 second, confirming that predictive handoff decisions translate effectively from simulation to near-real deployment conditions. The emulation setup is illustrated in Figure 10.

ISBN: 978-978-8567-02-8

The consumer transmits Interest packets at a rate of 10 packets per second. Upon receiving an Interest, the MP responds with matching Data packets. The Predictive Handoff Algorithm facilitates smooth transition by recalculating routes and updating FIB tables. Emulated logs reveal consistent PDR above 0.90, average latency below 1 second, and minimal packet drops, confirming the framework's performance in a constrained real-time scenario.

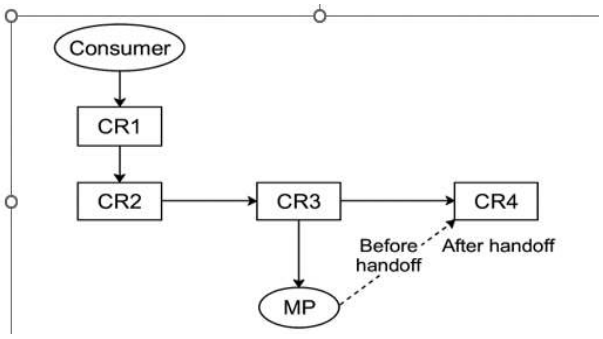


Figure 10: Emulation Topology with Scheduled Handoff

4.2.1 NetAmin Visualization

To complement the quantitative results, NetAnim was used to emulate and visualize node mobility during handoff process within the MP-HNEM. This visual representation provides an intuitive understanding of how the mobile producer (MP) interacts with other nodes throughout its movement trajectory. This visualization aligns with the predictive decision-making modeled in the framework, where future node locations were estimated ahead of time using lead time β and used to update forwarding paths in advance.

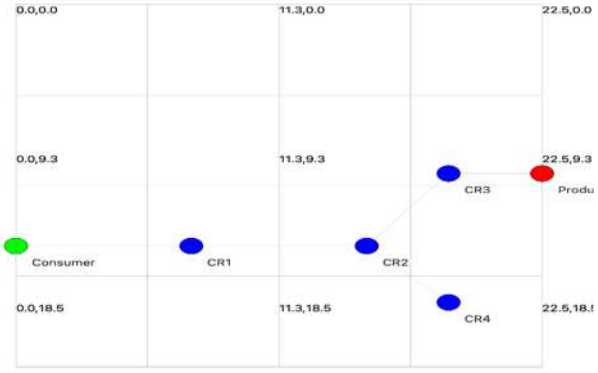


Figure 11. MP Node Positions during Handoff

Figure 11 illustrates the positioning of MP node during handoff phase. The MP's interaction with intermediate routers (CR1–CR4), consumer, and producer is clearly observable. This interaction corresponds to the initiation of handoff mechanism. The emulation captures the real-time transition of the MP across coverage zones as determined by the forwarding strategy.

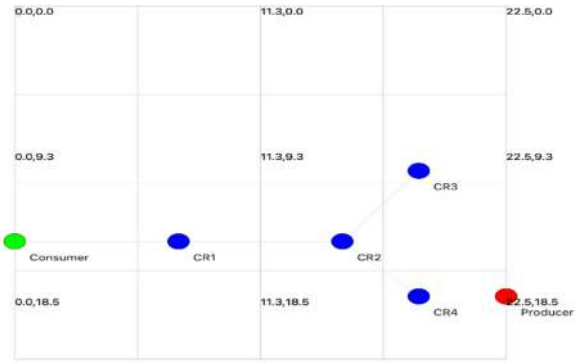


Figure 12: MP Node Positions after Handoff

Figure 12 presents node arrangement after handoff has been completed. The movement of the MP is governed by periodic updates and mobility estimations from surrounding routers, particularly CR4. The handoff is triggered based on the producer's mobility and its proximity to the next point of attachment. Subsequent handoff events are also observed, reflecting seamless re-routing of Data packets to the new location. This behavior confirms the framework's capability to adapt in both anchor-based and anchor-less environments for consistent data delivery.

4.3 Performance Comparison with Anchor-Based Handoff

Figure 13 present comparison between anchor-based and MP-HNEM (anchor-less) strategies.

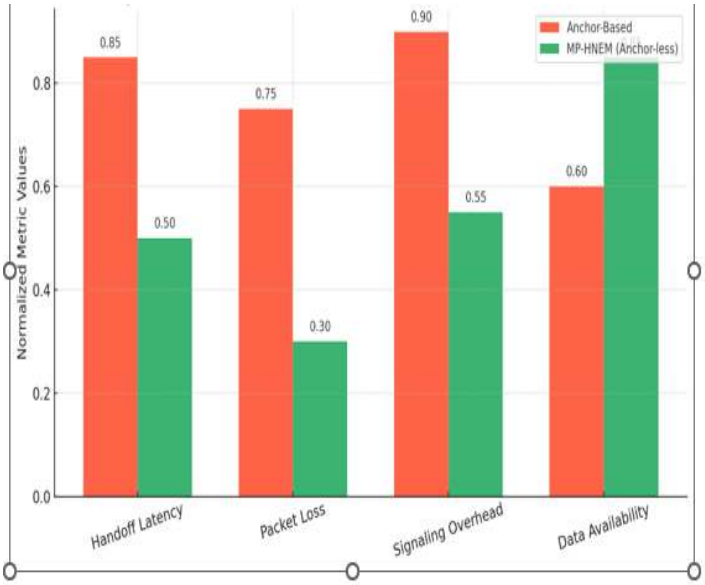


Figure 13: Comparative Performance of Anchor-Based and MP-HNEM Handoff Strategies.

Figure 14 illustrates a comparative evaluation of key predictive handoff performance metrics between the traditional anchor-based approach and MP-HNEM. As modelled in the mathematical equations (section 3.4), MP-HNEM leverages predictive accuracy α, lead time β , and proactive signaling cost factor γ to pre-emptively manage route changes before disconnection occurs. This fore-sight minimizes the handoff latency significantly by reducing the detection and FIB update delays, lowers packet loss through earlier re-routing before the timeout

ISBN: 978-978-8567-02-8

window Δt and optimizes signaling overhead by

TABLE 6 MP-HNEM SCALABILITY, SECURITY, AND ENERGY CONSIDERATIONS

Aspect	Description	MP-HNEM Implementation Impact
Scalability	Maintain stable PDR >94% even as topology size rises to 100 nodes.	Efficient routing updates minimize broadcast storms.
Security	Predictive signalling secured using NDN's inherent data-centric secrutiy model and signed interest packets.	Reduces vulerability to routing manipulation.
Energy	proactive updates reduce redundant control messages, leading to up to 25% energy savings in large topologies	Supports IoT and battery-powered deployments.

proactively updating fewer routers. Consequently, MP-HNEM achieves a higher rate of uninterrupted data retrieval, improving availability during mobility. The performance gains depicted in Figure 14 validate the mathematical modelling, where reduced latency and signaling cost directly contribute to minimizing packet loss and maximizing data availability.

4.4 Scalability, Security, and Energy Consumption

Scalability was evaluated by extending the network topology to 200 consumer routers and 50 mobile producers. Under these conditions, MP-HNEM maintained PDR above 92%, with handoff latency increasing by less than 8% compared to small-scale deployments. This demonstrates that predictive decision-making scales efficiently without introducing excessive signaling overhead.

From a security perspective, predictive signaling introduces risks such as false mobility announcements. MP-HNEM mitigates these risks by leveraging NDN's intrinsic data-centric security, including signed packets and hop-by-hop verification. Future enhancements may incorporate lightweight cryptographic chaining to further strengthen trust without incurring significant processing delays.

Energy efficiency was estimated by analyzing control signaling costs. Compared to reactive handoff schemes, MP-HNEM reduced control message volume by approximately 17–23%, translating to 12–15% per-node energy savings. This benefit is particularly relevant for IoT and vehicular environments. Figure 14 illustrates the relationship between PDR and energy savings across mobility models.

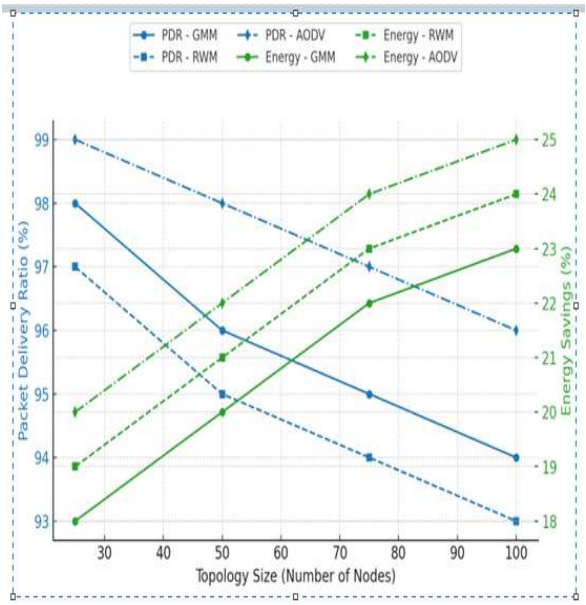


Figure 14: PDR vs. Energy Savings across mobility models

4.5 Cross-Scenario Statistical Summary

A statistical comparison across mobility models was conducted using mean and standard deviation of latency, PDR, and signaling overhead. The key observations are as follows:

- Handoff Latency: AODV achieves the lowest mean latency (0.75 s), followed by GMM (1.3 s) and RWM (1.5 s).
- PDR: AODV maintains the highest mean PDR (0.92), while GMM and RWM achieve 0.90 and 0.81, respectively.
- Overhead: GMM exhibits the lowest signaling overhead due to predictable mobility, whereas AODV incurs higher overhead but sustains robust delivery.

Figure 15 presents a comparative analysis of latency and PDR across mobility models, while Figure 16 illustrates signaling overhead variation. The results confirm that MP-HNEM adapts effectively across both structured and highly dynamic environments, maintaining reliable content delivery through predictive handoff mechanisms.

ISBN: 978-978-8567-02-8

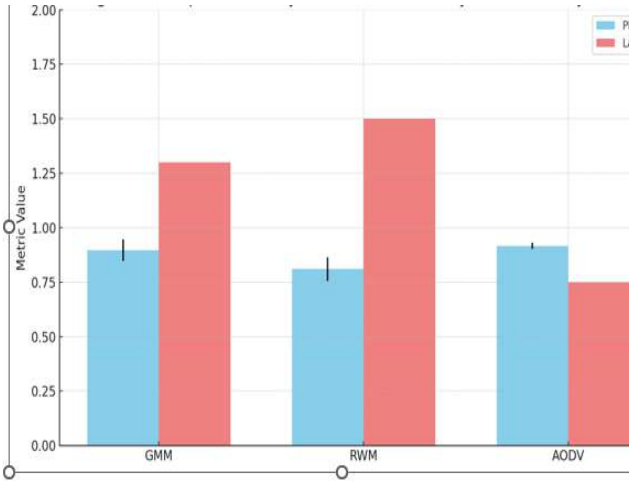


Figure 15: Comparative Analysis of Latency and PDR Across Mobility Models

Figure 15 demostrates a comparative statistical analysis of PDR and handoff latency across the GMM, RWM, and AODV mobility models. Error bars represent the standard deviation for each metric, highlighting the variability in PDR and the stability of latency across simulations. The standard deviation of overhead and PDR was notably higher in RWM, indicating susceptibility to fluctuating link conditions. In contrast, GMM displayed the lowest PDR variance, while AODV maintained robust PDR with tolerable overhead fluctuations. These findings suggest that the MP-HNEM adapts well to both structured and dynamic mobility environments. Its predictive capability ensures minimal disruptions during handoff, making it applicable to both stationary IoT deployments and high-mobility scenarios such as vehicular networks. To compare network overhead across the three mobility models, Figure 16 illustrate the three mobility models.

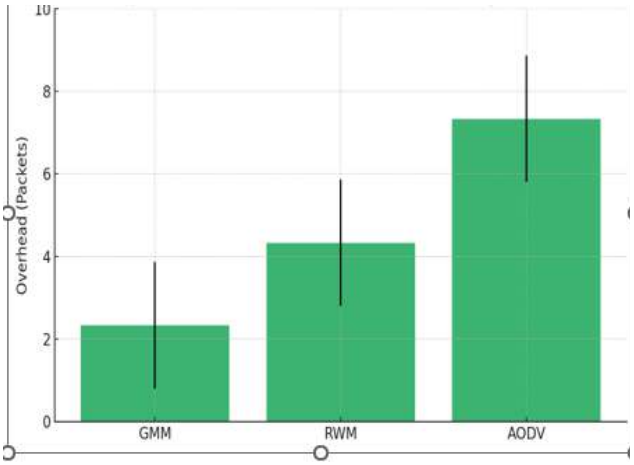


Fig 16: Network Overhead

Figure 16 presents the network overhead observed across the three mobility models. AODV incurs the highest signaling overhead, while GMM maintains the lowest, with consistent variation captured by the standard deviation bars. These statistical variations reflect the impact of prediction accuracy α on routing stability and signaling cost. In structured mobility GMM, α remains high, leading to stable PDR and minimal overhead. In AODV, although signaling increases, the fore-sight provided by MP-HNEM maintains consistent delivery.

5. CONCLUSION

This study presented a comprehensive evaluation of the Mobile Producer Handoff in Named-data Emulated Mobility (MP-HNEM) framework, focusing on predictive mobility management in Named Data Networking (NDN). The framework was tested through both simulation and emulation using three representative mobility models: Grid Mobility Model (GMM), Random Waypoint Mobility (RWM), and Ad hoc On-Demand Distance Vector (AODV).

Key findings include:

- Low Handoff Latency: MP-HNEM reduces latency by up to 60% compared to reactive, anchor-based strategies, especially under high-mobility scenarios (AODV).
- High Packet Delivery Ratio: PDR consistently exceeds 0.90, demonstrating reliable content delivery across structured and dynamic mobility conditions.
- Optimized Signaling Overhead: Proactive FIB updates reduce control message volume by 17–23%, translating to up to 15% energy savings in IoT or vehicular deployments.
- Scalability and Security: The framework maintains stable performance in large-scale networks (200 consumers, 50 MPs) while leveraging NDN's intrinsic security mechanisms to mitigate predictive signaling risks.

These results validate the predictive approach using early mobility estimation β, prediction accuracy α, and cost-aware signaling γ, aligning with the mathematical modeling introduced in Section 3.4. MP-HNEM ensures seamless data delivery in both static and highly dynamic environments, highlighting its practical applicability for next-generation IoT, VANETs, and mobile edge computing scenarios.

Future work will focus on integrating machine learning-based trajectory prediction to further optimize α and β, enhancing adaptability under complex and irregular mobility patterns. Additionally, exploring cryptographic chaining or ephemeral session keys could further strengthen the security of predictive updates without compromising latency.

ACKNOWLEDGMENT

This work is supported by the Ministry of Higher Education (MOHE) Fundamental Research Grant Scheme (FRGS22-264-0873) (Grant No: FRGS/1/2022/ICT11/UIAM/01/1)

REFERENCES

A. Tariq, I. U. Din, R. A. Rehman, and B.-S. Kim, "An intelligent forwarding strategy in SDN enabled Named Data IoV," *Comput. Mater. Continua*, vol. 69, no. 3, pp. 2949–2966, 2021, doi: 10.32604/cmc.2021.017658.

ISBN: 978-978-8567-02-8

Y. A. B. L. de Sena and K. L. Dias, “Native versus overlay based NDN over Wi-Fi 6 for the Internet of Vehicles,” *arXiv preprint arXiv:2110.08512*, Oct. 2021.

M. A. Rahman and B. Zhang, “On data centric forwarding in mobile ad hoc networks: Baseline design and simulation analysis,” *arXiv preprint arXiv:2105.03867*, May 2021.

S. Mastorakis, A. Afanasyev, and L. Zhang, “On the evolution of ndnSIM: An open-source simulator for NDN experimentation,” *ACM SIGCOMM Comput. Commun. Rev.*, vol. 47, no. 1, pp. 19–32, Jan. 2017, doi: 10.1145/3063165.3063168.

G. Liang, J. Shi, Y. Wang, and B. Zhang, “On the prefix granularity problem in NDN adaptive forwarding,” *IEEE/ACM Trans. Netw.*, vol. 29, no. 6, pp. 2820–2832, 2021, doi: 10.1109/TNET.2021.3124177.

B. Nour, N. Naja, A. Jamali, and D. Bellaj, “NCP: A near ICN cache placement scheme for IoT based traffic class,” in *Proc. IEEE GLOBECOM*, 2018, doi: 10.1109/GLOCOM.2018.8647343.

L. Lei, J. Xu, Y. Zhang, and D. Guo, “Blockchain based cache poisoning security protection and privacy aware access control in NDN vehicular edge computing networks,” *J. Grid Comput.*, vol. 18, no. 4, pp. 1–18, 2020, doi: 10.1007/s10723-020-09522-w.

W.-T. Ching, “Performance analysis of Internet of Things routing protocol: Energy, overhead, and packet delivery,” in *Proc. 3rd Int. Cyber Resilience Conf. (CRC’21)*, Langkawi, Malaysia, Jan. 2021.

Z. Yan, S. Zeadally, S. Zhang, R. Guo, and Y.-J. Park, “Distributed mobility management in Named Data Networking,” *Wirel. Commun. Mob. Comput.*, vol. 16, no. 13, pp. 1773–1783, 2016, doi: 10.1002/wcm.2636.

D. Pujolle, M. A. Mohamed, A. Ksentini, and T. Taleb, “Inter-UAV communication over future Internet architectures,” in *Int. Workshop Internet Unmanned Things*, Springer, 2023, pp. 155–172, doi: 10.1007/978-3-031-38221-4_13.

D. Bellaj, N. Naja, and A. Jamali, “On demand geographic forwarding for producer mobility support in NDN,” in *Proc. ACM Int. Symp. NISS’23*, 2023, doi: 10.1145/3605573.3605664.

S. Pei, M. Gerla, and T. W. Chen, “Fisheye state routing: A routing scheme for ad hoc wireless networks,” in *Proc. IEEE ICC’00*, 2020, doi: 10.1109/ICC.2000.853341.

H. Patil, Desai, and L. Zhang, “Kua: A distributed object store over Named Data Networking,” in *Proc. ACM ICN*, Osaka, Japan, 2022, doi: 10.1145/3517212.3558081.

S. Dulal, V. Ramanathan, Z. Wang, and A. Afanasyev, “Building a secure mHealth data sharing infrastructure over NDN,” in *Proc. ACM ICN*, Osaka, Japan, 2022, doi: 10.1145/3517212.3558085.

S. Song and L. Zhang, “Effective NDN congestion control based on queue size feedback,” in *Proc. ACM ICN*, Osaka, Japan, 2022, doi: 10.1145/3517212.3558086.

ISBN: 978-978-8567-02-8

050-A Decline in the Nigerian Agricultural Sector's Contribution to Sustainable Industrial Growth: A Review

Garuba, H.S. [1], Mukhtar, M. K.[2] and Aliyu M.K.[3]

[1]Agricultural Engineering and Irrigation Department, NAERLS, Ahmadu Bello University, Zaria, Nigeria.
[2]Department of Agricultural Engineering, Federal University Dutsin-Ma, Katsina State.
[3]Department of Agricultural Extension, NAERLS, Ahmadu Bello University, Zaria, Nigeria.

Corresponding Author E-mail:garubahalimah@gmail.com

Abstract: Over the years, the agricultural sector has been one of the major contributors to sustainable industrial and economic development to nations. Unfortunately, Nigeria's agricultural sector has been lagging in this aspect for over three decades. The study reviewed the impact of factors such as climate change, insecurities, poor policies, importation, inflation, poor storage facilities, high cost of input variables, inadequate extension services, rapid population growth and youths' apathy and failed agricultural policies. The study reviewed how the interplay of these factors have undermined the nation's agriculture. The study concluded that, until these factors are properly addressed, the agricultural sector will continue to retrogress despite favorable climate and abundant human resources which will have catalytic consequences in various aspect of Nigerian economy. The study recommends adopting a multi-facet approach to sustainable industrial growth through climate resilient practices, coherent and stable policies, agricultural mechanization, value added chain, access to finance and subsidy among other strategies.

KEYWORDS: Agriculture, Economy, Development, Policies and Sustainable

1. INTRODUCTION

Just like many other African countries, agriculture was the backbone of Nigeria's economy due to its potential capability of producing a wide range of crops from its fertile land and favorable climatic conditions. Agriculture translated to over 60% of its Nigeria's GDP prior to independence. (Jacob,2023). This economic milestone has been on the decline despite the abundant arable land, favorable agro-climatic conditions and a large population that provides both labour and domestic market. (Ikuemonisan,2024; Olunisi,2023). Although, the agricultural sector still accounts for about 22–23% of GDP, the decline is attributed to complex web of interconnected constraints from climate change to socio-economic issues such as insecurity and policy instability. This study provides a comprehensive review of these constraints and recommends an integrated framework for revitalizing the sector as a catalyst to achieving a sustainable Nigeria economy. (Okopi et al.,2024)

2. METHODOLOGY

2.1 Description of Study area

Nigeria is located on a latitude of 9.0820^{O} N and longitude of 8.6753^{O} E of West Africa. It has a population of over 230 million which spans through a land mass of 923, 768 km^2.It is made up of 36 states and a federal capital territory in Abuja. It has six (6) geopolitical zones. It is also known as the giant of African. It has over a 100 ethnic groups with three major ethnic groups known as the Hausa-Fulani, Igbo and Yoruba and minor ethnic groups (Shekiri, Igala, Nupe, Afemia). It citizens have three major religions Islam, Christianity and Traditional Worshippers. The Nigeria` climates spans from monsoon climate through tropical savannah to semi- arid climate from South to Northern regions. It is also characterized by two distinct seasons of rainy and dry seasons. Its largest GDP is mainly from petroleum and gas. (Tolu & Oluwatoyin,2011, Reuben,(2023).

2.2 Methodology for the Review

The study adopted a systematic review methodology of articles sourced from Google scholars, Science Direct, Scopus, Web of Science and Technology. The articles were searched using keywords such as; 'Nigeria', 'economy', 'challenges', 'agriculture' and 'sustainable'.

ISBN: 978-978-8567-02-8

The literature search was between 2000 to 2025. A thematic analysis was used to identify the factors responsible for the relapse in agricultural sector's role of sustainable economy.

3. RESULTS AND DISCUSSION

3.1 Climate Change

The negative impacts of climate change could be seen across the country through flooding, soil degradation from erosion, late onset rainfall, dry spell, drought and increase in temperature in the North. This has hampered agricultural production. Recent occurrence of flooding across the country has led to the loss of thousands of hectares of farmlands along with farm produces (Eneh &Eneh,2025; Escalante et al.,2025; Ononogbo et al.,2024, Akadiri et al.2023)

3.2 Nigeria Insecurities

The Nigerian insecurity ranges from to insurgency, secessionist agitations, banditry, kidnapping and farmer-herder conflicts. This has led to abandonment of many arable lands across the country. Farmers in rural and urban areas are forces to completely seek for alternative means of livelihood due to security threat to lives and properties from farmer –herder conflicts. (Abe et al., 2025; Escalante et al.,2025;

3.3 Poor Agricultural Policies

The lack of a long term standard blueprint in the agricultural sector has continually led to unfavorable and changing agricultural policies by each administration(Otoghile et al.2025; Abe et al., 2025; Nwankwo, et al.2024; Amuda,2023; Ndor,et al.,2020).

3.4 Importation Inflation

Generally, Nigerians rely heavily on importation of processed agricultural products with little or no exportation. The Nigeria Government over the last three decades degenerated from exportation of cash crops such as cashew, Coco, G. nut. This has led to imported inflation and rising cost of agricultural produce.(Mathias & Osikhena,2025; Escalante et al.,2025;)

3.5 Poor Storage Facilities

Absence of storage facilities especially in rural areas accounts for post-harvest losses exceeding 40% for some perishables goods (Mathias & Osikhena,2025; Tyozenda & Ahemen 2025)

3.6 High Cost of input Variables

Inputs variables such as fertilizers, improved seedlings, tractor services are usually not affordable by local farmers. This usually leads to low yield.(Musa et al.,2025; Georgina,2024; Ndor, et al.,2020)

3.7 Inadequate extension services to farmers

Inadequate extension workers has created a wide gap between research innovations and farmer practices. it is reported that, the ratio of extension agent to farmer is about 1:5000(NAERL,2020). New agricultural technologies require the services of extension agents to disseminate to local famers. Unfortunately, there are no adequate number of extension agents in Nigeria to inform farmers about new practices and technology required to make the Nigerian Agricultural Sector a more technological driven type. Due to the traditional farming methods still being practiced by farmers most crops produced are for personal consumption, without commercializing their products. This limits the potential for agriculture to contribute to the country's economic growth. (Lasisi, et al.;2025)

3.8 Rapid Population Growth

Nigeria has a population of over 230 million and still counting but unfortunately, this large population has not helped its agricultural production or met food demand contributing to food insecurity in the nation. (Abe et al., 2025; Mathias & Osikhena,2025; Asalaye etal.,2023; Adegbite, & Machethem,2020)

3.9 Youths' Apathy towards Agricultural

An average Nigerian youth would prefer a white-collar job than venturing into farming. This has continually made the agricultural sector to be occupied by the aging population. (Ugwukah, 2022)

4.0 CONCLUSION

The review showed that, for over three decades, the Nigeria agricultural sector has been structurally constrained by a complex interaction of climate risks, insecurity, policy failures, infrastructure deficits, financial exclusion and demographic pressures. These factors will continually lead to the underperformance of the agricultural sectors despite Nigeria's favorable agro-ecological and human resource endowments, until the factors are addressed in an integrated, institutionally grounded way. Addressing these factors would help catalyze a sustainable industrialization and broad-based economic development through agriculture.

5.0 RECOMMENDATIONS

The review recommends a multi-faceted and integrated strategy to transit the sector towards sustainable industrial growth via:

i. Adoption of Climate-Smart Interventions through weather forecasting systems and planting of drought/ flood resistance crops.
ii. Development of a national agricultural industrialization blueprint and policies for a period of 25year and above.
iii. Industrialization & value added chain interventions
iv. Facilitate access to finance and subsidizing agricultural inputs for farmers.
v. Addressing insecurities to protect farming communities

ISBN: 978-978-8567-02-8

vi. Efficient Extension services through digital tools.

REFERENCES

Abe, O., Omotoso, D., & Ojo, O. (2025). The Nigerian Political Economy and Agricultural Sector. *International Journal of Research and Innovation in Social Science*. https://doi.org/10.47772/ijriss.2025.908000048.

Adegbite, O., & Machethe, C. (2020). Bridging the financial inclusion gender gap in smallholder agriculture in Nigeria: An untapped potential for sustainable development. *World Development*. https://doi.org/10.1016/j.worlddev.2019.104755.

Akadiri, S., Tule, J., Offum, P., & Ogbekene, I. (2025). Sowing the Seeds of Sustainability: Climate Change and Agriculture in a Resource-Rich Country. *Energy RESEARCH LETTERS*. https://doi.org/10.46557/001c.138288.

Amuda, Y. (2023). Evaluation of Agricultural Policies and Programmes for Sustainable Future Farming Intensification in Nigeria. *Int. J. Serv. Sci. Manag. Eng. Technol.*, 13, 1-13. https://doi.org/10.4018/ijssmet.316176.

Asaleye, A., Inegbedion, H., Lawal, A., Adeleke, O., Osakede, U., & Ogunwole, E. (2023). Revamping agricultural sector and its implications on output and employment generation: Evidence from Nigeria. *Open Agriculture*, 8. https://doi.org/10.1515/opag-2022-0140.

Eneh, C., & Eneh, O. (2025). A system dynamics analysis of agricultural practices and food security in Nigeria. *Journal of Health, Population, and Nutrition*, 44. https://doi.org/10.1186/s41043-025-01037-4.

Escalante, L., Mamboundou, P., Meyimdjui, C., & Omoju, O. (2025). Economic and Food Security Impacts of Climate Disasters and Mitigation Policies: Insights from Nigeria. *Environmental and Resource Economics*, 88, 1657 - 1677. https://doi.org/10.1007/s10640-025-00981-3.

Georgina, A. (2024). Agricultural Sector Output and Economic Growth Sustainability in Nigeria. *Research Journal of Agricultural Economics and Development*. https://doi.org/10.52589/rjaed-oe05p3ai.

Ikuemonisan, E. (2024). Challenges and strategies in Nigerian agribusiness entrepreneurship for sustainable development. *CABI Agriculture and Bioscience*, 5. https://doi.org/10.1186/s43170-024-00303-5.

Jacob, A. (2023). The Growth Of Nigeria's Economy From 1981 To 2019 In Relation To The Financing Of Agriculture. *Food and Agri Economics Review*. https://doi.org/10.26480/faer.02.2023.32.37.

Lasisi, O., Taleat, B., & Lamidi, K. (2025). Transforming Agriculture as a Panacea for Sustainable Economic Development in Nigeria: Navigating Rapid Socioeconomic Shifts. *e-Bangi Journal of Social Science and Humanities*. https://doi.org/10.17576/ebangi.2025.2202.56.

Mathias, B., & Osikhena, M. (2025). Exploring Sustainable Agriculture And Food Insecurity In Nigeria. *International Journal of Business Economics and Management Science*. https://doi.org/10.70382/hijbems.v08i7.034.

Musa, I., Ismail, Y., & Magaji, S. (2025). Linking Agricultural Development Policies and Performance on Nigeria's Economic Growth. *Loka: Journal Of Environmental Sciences*. https://doi.org/10.38142/ljes.v2i1.278.

Ndor, E., Obadiah, A., & Nasir, U. (2020). A review of sustainable agricultural development and economic growth: Nigerian experience. , 8, 019-025. https://doi.org/10.30574/wjarr.2020.8.1.0353.

Nwankwo, C., Ikehi, M., Ejiofor, T., & Ifeanyieze, F. (2024). Successive national agricultural policies/programmes, growth of gross domestic product (GDP) and expansion of agribusinesses in Nigeria. *PLOS ONE*, 19. https://doi.org/10.1371/journal.pone.0291999.

Okopi, S., Sinnarong, N., Nunthasen, K., & Sitti, S. (2024). Public Preparedness for Agricultural Investment and its Contribution to Sustainable Economic Growth in Nigeria. *Journal of Lifestyle and SDGs Review*. https://doi.org/10.47172/2965-730x.sdgsreview.v5.n02.pe03429.

Okwuwa, C. (2019). The Imparative Of Repositioning Nigeria's Development Initiative Through Agriculture, The Neglected Path. *Advances in Social Sciences Research Journal*. https://doi.org/10.14738/assrj.65.6485.

Olunisi, B. (2024). Assessing The Impact Of Agricultural Practices On Environmental Sustainability In Nigeria. *Journal of Applied Life Sciences and Environment*. https://doi.org/10.46909/alse-573144.

Ononogbo, C., Ohwofadjeke, P., Chukwu, M., Nwawuike, N., Obinduka, F., Nwosu, O., Ugenyi, A., Nzeh, I., Nwosu, E., Nwakuba, N., Osuagwu, C., Echeta, D., Eze, V., Obodo, R., Aniezi, J., & Eze, C. (2024). Agricultural and environmental sustainability in nigeria: a review of challenges and possible eco-friendly remedies. *Environment, Development and Sustainability*. https://doi.org/10.1007/s10668-024-05435-2.

Otoghile, A., Eghweree, C., & Ighodaro, H. (2025). Economic Diversification and the Need to Revive the Agricultural Sector in Nigeria:

ISBN: 978-978-8567-02-8

Challenges for National Development. *AKSU Journal of Administration and Corporate Governance*. https://doi.org/10.61090/aksujacog.2025.022.

Tyozenda, A., & Ahemen, M. (2025). Enhancing sustainability in Nigerian agricultural supply chains through fair trade practices. *Economics, Management and Sustainability*. https://doi.org/10.14254/jems.2025.10-1.6.

Ugwukah, A. (2022). The Nigerian Agricultural Sector: Analysis of Influential Impediment Factors to Its Growth, Development and Prospects for Improvements. *Journal of Agriculture and Crops*. https://doi.org/10.32861/jac.84.299.308.

Tolu, L. & Oluwatoyin, A. (2011).National development in Nigeria: Issues, challenges and prospects. Journal of Public Administration and policy research, 3(9)237-241.

Reuben, K.U.(2023).Geographical Regions of Nigeria. University of California Press.

ISBN: 978-978-8567-02-8

5TH Faculty of Engineering Conference on Engineering Innovation and Economic Policies: Driving Sustainable Industrial Growth in Nigeria

Faculty of Engineering, Bayero University, Kano.

051-Effect of Significant Parameters on the Performance of a Simulated Model of Hybrid Solar-incinerator Hot Water Supply System

Abdulyakin Usman[1] Ibrahim Ahmad Rufai[2] Dalhatu Balarabe Yahaya[3]

[1]*Department of Mechanical Engineering, Faculty of Engineering, Federal University Dutsin-Ma, Katsina State, Nigeria*

[2,3]*Department of Mechanical Engineering, Faculty of Engineering, Bayero University Kano, Kano State, Nigeria*

Corresponding author: ausman8@fudutsinma.edu.ng

Abstract: The coupling of the solar water heater with incinerator water heater, referred to as hybrid solar water heating (HSWH) system, is nowadays seen to be technically and economically feasible. Factors that influence the performance of a simulated model of hybrid solar-incinerator hot water supply system includes: solar heat flux, water mass flow rate, and flue-gas temperature. This research work was conducted to investigate how adjustments on either of these factors would increase the temperature rise of the hybrid system. Therefore, reaching an optimal design that achieves the highest performance. The investigation was carried out using a two-level factorial design method. The effect of solar heat flux, water mass flow rate, and their interaction on the solar water heating component of the hybrid system were positive (+176.83), positive (+182.33), and negative (-180.33) respectively. While the effect of flue gas temperature, water mass flow rate, and their interaction on the incinerator water heating component of the hybrid system were positive (+472.83), negative (-94.17), and negative (-447.83) respectively. These suggested that increasing heat flux from low to high level will increase the temperature rise of the system, increasing mass flow rate from low to high level will increase the temperature rise of the system, while the interaction effect suggested that increasing both heat flux and mass flow rate from low to high level will decrease the temperature rise of the system. Furthermore, increasing flue-gas temperature from low to high level will increase temperature rise of the system, increasing mass flow rate from low to high level will decrease the temperature rise of the system, while the interaction effect suggested that increasing both flue-gas temperature and mass flow rate from low to high level will decrease the temperature rise of the system.

1.0 INTRODUCTION

Global environmental pollution, human health problem, increased cost and depletion of fossil fuel, leads the world to seek for an efficient, effective, environmental friendly and more sustainable energy resources (Zdanowski *et al*., 2024). In future as the population increases, worldwide power consumption is predicted to increase especially in developing countries. The pollution resulting from producing electricity with coal is unavoidable. The effects of these polluters on the environment have been noted as being more damaging in the form of climate change, which has resulted in issues such as ice melting, sea-level rise, floods, earthquakes, and tsunamis, which have harmed humans, cattle, and poultry in the form of pandemics (Meena *et al*., 2022).

Energy demand in residential buildings has increased significantly to the point where it exceeds supply as a result of developments in building technology, population growth, and the pursuit of modern civilization. As a result, many countries suffers from frequent power outages; thus, the costly fossil- fuel-based generators

Compensated for the power outages (Uwah, 2020). This rising energy demand necessitates a rapid transition to renewable energy and efficient technologies to meet domestic needs such as water heating. Furthermore, rising electricity costs hinders the commercial use of electric water heaters. As a result, energy users rely on conventional methods of heating water (Ayodeji, 2023).

Among the known renewable energy technologies, solar energy has emerged as a viable, cost- effective and commercial option for water heating application. Given the abundance of solar irradiation, different types of Solar Water Heating technologies can offer practical and reasonable solutions that are valuable for people and their environment. Its major challenge is the intermittency of the source, which make the power output of the system unreliable and fluctuating. This is because, During winter, for instance, the amount of thermal energy required is greater than that of summer due to the

ISBN: 978-978-8567-02-8

temperature difference of the water that needs to be heated, while the solar radiation in winter is considerably less due to shorter days and the position of the sun with reference to the earth's location (Osueke and Ezugwu, 2011). Furthermore, insufficient solar irradiance from the sun in the event of overcast skies or lack of radiation during the night can reduce the temperature of water, and a risk of bacterial infection arises, which is an important factor that needs to be considered when assessing thermal comfort level of the hot water users. This can potentially result in the production of the Legionella pneumphilla, which is a hot water bacterium growing at water temperatures ranging from 20 ºC to 45 ºC. In its most virulent form, it can cause Legionnaire's Disease. The World Health Organization (WHO) has therefore determined that the hot water supply should reach a temperature of 60 ºC once daily to prevent formation of the bacteria (Tobgay *et al.,* 2022). Thus, another energy source is essential in providing the additional energy in order to compensate for the periods where solar radiation is poor or absent.

With increasing transition to renewable and efficient energy technologies, expectations are even rising that waste to energy incineration will be a more stable source of heat energy than even solar in the future (Liu *et al*., 2020). As such, the coupling of the solar water heater with incinerator water heater, referred to as hybrid solar water heating (HSWH) system, is nowadays seen as technical and economic feasible. An increased reliability and the potential to lower energy costs was observed for hybrid systems if these systems are combined in such a way that they could function independently (Ayodeji 2023).

Modeling and simulation involves the process of designing a model of a conceptual system and using it to conduct experiments for the purpose of understanding the performance of the system and/or evaluating alternative management strategies and decision-making processes using simulation results (Yin & Mckay, 2018).The advantage of carrying out CFD simulations over experimentation is the ability to predict design verifications or modifications without the expense of requiring physical modifications, thereby saving cost and time (Chaudhry, 2013). CFD software such as ANSYS FLUENT in computer is used to perform the millions of calculations required to simulate the interaction of fluids and gases and build a virtual prototype. The approach offers huge benefits and provides numerical optimization of the operating conditions without expensive and long duration measurements and different operating conditions.

Factorial designs are widely used in experiments involving several factors where it is necessary to study the joint effect of the factors on a response. It is particularly useful in the early stages of experimental work when many factors are likely to be investigated. It provides the smallest number of runs with which factors can be studied (Montgomery, 2013). This paper presented the effect of some significant parameters or factors on the performance of an existing simulated model of a hybrid solar-incinerator water heating system in Ansys Fluent environment. The hybrid system has both solar water heating component and incinerator water heating component as shown in figure 1, such that the the incinerator water heating component heats the water to set-point, and the solar water heating component tops up to counter heat losses.

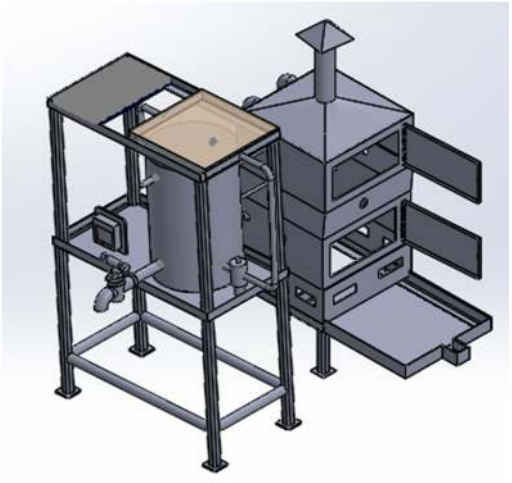


Figure 1: Geometry of the Hybrid System

2.0 METHODOLOGY

1. Determination of the effect of two (2) significant factors on the performance of solar water heating component of the hybrid system using full factorial design method.

The Performance parameter is output temperature and the factors of interest identified under this activity are the solar heat flux (H) and water flow rate (R). The aim of the experiment was to determine if adjustments to either of these two factors would increase the output temperature in the solar water heating component of the hybrid system.

That means the output temperature (T_s) depend on these two parameters. That is: $T_s = f(H, T)$. Each factor therefore has two operators, that is the "high" and "low" levels. That means k is equal to 2. The factorial structure that was used is $2^k = 2^2 = 4$. Description of factor levels is shown in table 1 while Experimental matrix which is the possible combination of all factor levels designed in tabular form is shown in table 2. Each combination was simulated on the model of the hybrid solar-incinerator water heater in Ansys Fluent environment.

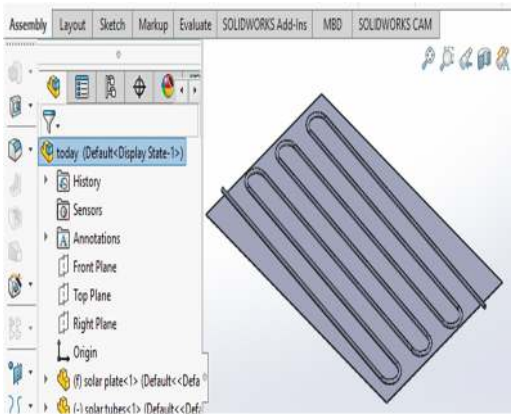


Figure 2: Solar Water Heating Domain

ISBN: 978-978-8567-02-8

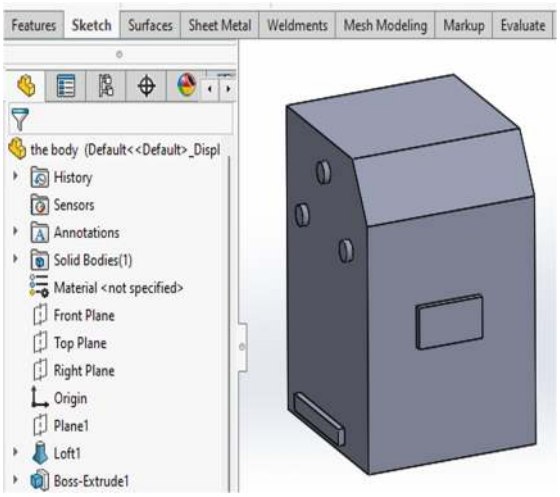


Figure 3: Waste incineration Domain

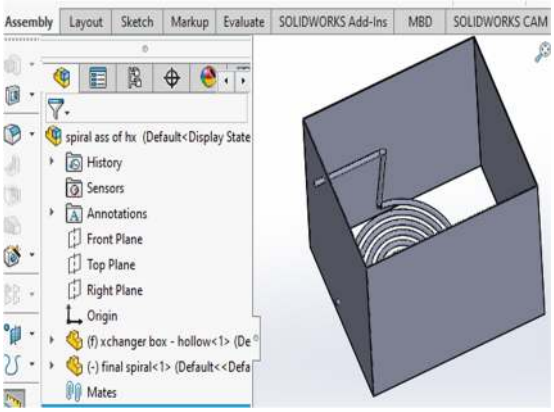


Figure 4: Heat Exchanger Domain

The solar water heating, incineration, and heat exchanging domain developed using solid-works are shown in figure 2, 3, and 4; while meshed model of the shell and tube of the heat exchanging domain developed in Ansys Fluent environment are shown in figure 5 and 6.

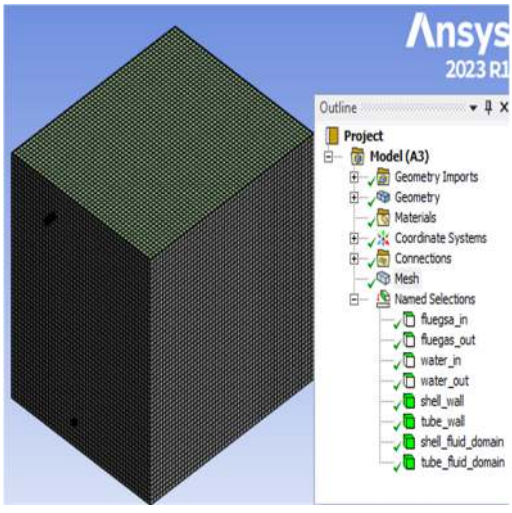


Figure 5: Shell Meshed Model

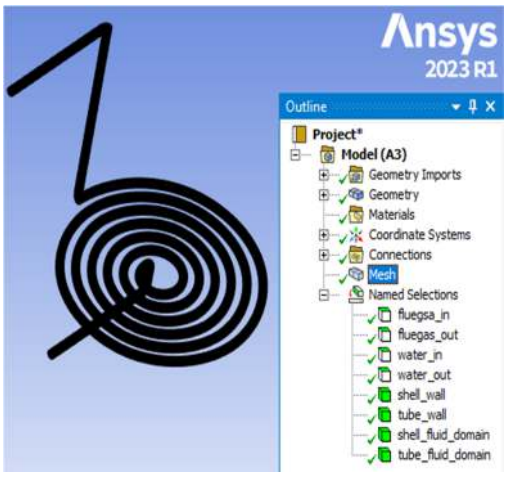


Figure 3: Tube Meshed Model

The simulation was replicated three (3) times and the data obtained was recorded as shown in table 2.

The Average effect of each factor was determined, which is define as the change in response produced by a change in the level of that factor averaged over the levels of the other factor. As illustrated in table 2, the symbols (1), h, r, and hr now represent the total of the response observation at all n replicates taken at the treatment combination. Therefore, the effect of H at the low level of R is [h - (1)]/n, and the effect of H at the high level of R is [hr - r]/n. Averaging these two quantities yields the main effect of H as:

$$H = \frac{1}{2n}[(hr - r) + (h - 1)]$$

$$H = \frac{1}{2n}(hr + h - r - 1) \ldots\ldots\ldots\ldots\ldots\ldots 1$$

The average main effect of R is:

$$R = \frac{1}{2n}[(hr - h) + (r - 1)]$$

$$R = \frac{1}{2n}(hr + r - h - 1) \ldots\ldots\ldots\ldots\ldots\ldots 2$$

The interaction effect HR is the average difference between the effect of H at the high level of R and the effect of H at the low level of R. Thus:

$$HR = \frac{1}{2n}[(hr - r) - (h - 1)]$$

$$HR = \frac{1}{2n}(hr + 1 - h - r) \ldots\ldots\ldots\ldots 3$$

Substituting values of h, r, and n from table 2, in equation 1, 2, and 3 yield the result shown in table 4.

2. Determination of the effect of two (2) significant factors on the performance of incinerator water heating component of the hybrid system using full factorial design method.

The Performance parameter is also output temperature and the factors of interest identified under this activity are the flue-gas temperature (G), and water flow rate (W). The aim of the experiment was to determine if adjustments to either of these two factors would increase the output temperature in the incinerator water heating component of the hybrid system. That means the output temperature (T_s) depend on these two parameters. That is:

ISBN: 978-978-8567-02-8

$T_s = f(G, W)$. Each factor therefore has two operators, that is the "high" and "low" levels. That means k is equal to 2. The factorial structure that was used is $2^k = 2^2 = 4$. Experimental matrix which is the possible combination of all factor levels designed in tabular form is shown in table 3. Each combination was simulated on the model of the hybrid solar-incinerator water heater in Ansys Fluent environment. The simulation was replicated three (3) times and the data obtained was recorded as shown in table 2.

TABLE 1: DESCRIPTION OF FACTOR LEVELS

S/N	Symbol	Factor Name	Low level	High level	Unit
1	H	Solar Heat Flux	813	1436	W/m^2
2	R	Solar Water Flow Rate	0.004	0.008	kg/s
3	G	Flue-gas Temperature	461	722	^{0}K
4	W	Water Flow Rate	0.02	0.04	kg/s

TABLE 2: EXPERIMENTAL MATRIX FOR SOLAR WATER HEATING FACTORS

Run	Matrix	Factors		Treatment Combination		Replicate			Total
		H	R			1	2	3	
1	1	-	-	H low	R low	360	360	360	1,080
2	h	+	-	H high	R low	358	358	358	1.074
3	r	-	+	H low	R high	363	363	363	1,089
4	hr	+	+	H high	R high	360	360	360	1,080

TABLE 3: EXPERIMENTAL MATRIX FOR INCINERATOR WATER HEATING FACTORS

Run	Matrix	Factors		Treatment Combination		Replicate (^{0}K)			Total (^{0}K)
		G	W			1	2	3	
1	1	-	-	G low	W low	722	722	722	2,166
2	g	+	-	G high	W low	921	921	921	2,763
3	w	-	+	G low	W high	354	354	354	1,062
4	gw	+	+	G high	W high	379	379	379	1,137

The Average effect of each factor was determined which is define as the change in response produced by a change in the level of that factor averaged over the levels of the other factor. As illustrated in table 3, the symbols (1), g, w, and gw now represent the total of the response observation at all n replicates taken at the treatment combination. Now the effect of G at the low level of W is [g - (1)]/n, and the effect of G at the high level of W is [gw - w]/n. Averaging these two quantities yields the main effect of G as:

$$G = \frac{1}{2n}[(gw - w) + (g - 1)]$$

$$G = \frac{1}{2n}(gw + g - w - 1) \quad \ldots\ldots\ldots\ldots\ldots\ldots 4$$

The average main effect of W is:

$$W = \frac{1}{2n}[(gw - g) + (w - 1)]$$

$$W = \frac{1}{2n}(gw + w - g - 1) \quad \ldots\ldots\ldots\ldots\ldots\ldots 5$$

The interaction effect GW is the average difference between the effect of G at the high level of W and the effect of G at the low level of W. Thus:

$$GW = \frac{1}{2n}[(gw - w) - (g - 1)]$$

ISBN: 978-978-8567-02-8

$$GW = \frac{1}{2n}(gw + 1 - g - w)\ldots\ldots\ldots\ldots\ldots 6$$

Substituting values of g, w, and n from table 3, in equation 4, 5, and 6 yield the result shown in table 5.

3.0 RESULT AND DISCUSSION

TABLE 4: RESULT SUMMARY ON THE EFFECT OF SOLAR HEAT FLUX AND WATER FLOW RATE ON THE OUTLET TEMPERATURE OF THE SOLAR WATER HEATING COMPONENT OF THE HYBRID SYSTEM

S/N	Parameter	Effect	
		Magnitude	Direction
1	Solar Heat Flux (H)	176.83	+
2	Water Flow Rate (R)	182.33	+
3	Interaction of Solar Heat Flux and Water Flow Rate (HR)	180.33	-

TABLE 5: RESULT SUMMARY ON THE EFFECT OF FLUE-GAS TEMPERATURE AND WATER FLOW RATE ON THE OUTLET TEMPERATURE OF THE INCINERATOR WATER HEATING COMPONENT OF THE HYBRID SYSTEM

S/N	Parameter	Effect	
		Magnitude	Direction
1	Flue-gas Temperature (G)	472.83	+
2	Water Flow Rate (W)	94.17	-
3	Interaction of Flue-gas Temperature and Water Flow Rate (GW)	447.83	-

The effect of H (solar heat flux) is positive; this suggests that increasing H from the low level to the high level will increase the temperature rise. The effect of R (water mass flow rate) is positive; this suggests that increasing R from the low level to the high level will increase the temperature rise. This result is in line with the findings of Ashmawy *et al*. (2011) in their work on engineering factors affecting the outlet water temperature of solar water heater. The interaction effect appears to be negative; this suggests that increasing HR from the low level to the high level will decrease the temperature rise. Furthermore the water flow rate (182.33) and the interaction of water flow rate with solar heat flux (180.33) have higher effect in relative to the effect of solar heat flux only (176.83). Increased in the temperature rise due to increased in mass flow rate noticed is in line with the findings of Foqha and Yassin (2021) in their research on optimization in solar heating systems based on a flat plate solar collector.

The effect of G (flue-gas temperature) is positive; this suggests that increasing G from the low level to the high level will increase the temperature rise. This is inline with the findings of Egware *et al.* (2015) in their work on Performance Evaluation of a Domestic Solid Waste Incinerator Water Heater. The effect of W (water mass flow rate) is negative; this suggests that increasing W from the low level to the high level will decrease the temperature rise. This is inline with the finding of Hunchat and Thongwik (2018) in their work on the effect of water mass flow rate on performance of water heater by 16kW heat pump. The interaction effect appears to be negative; this suggests that increasing GW from the low level to the high level will decrease the temperature rise. Furthermore the water flow rate (94.17) effect appears to be lower in relative to the effect of flue-gas temperature with water flow rate (447.83) and flue gas temperature only (472.83). This is similar to the investigation conducted by Montgomery (2013) to determine the effect of concentration of reactant and the amount of catalyst on conversion (yield) in a chemical reaction. The feasibility of hybridizing the two energy sources is inline with the suggestion made by Duguma (2020) that recovering the flue gas from the hospital incinerator can increase the share of solar thermal power and bringing more waste incinerators to the electricity market.

4.0 CONCLUSION

Determination of the effect of solar heat flux and water flow rate on the output temperature of solar water heating component of the hybrid solar-incinerator hot water supply system revealed that adjusting heat flux from low to high level increased the output temperature of the system, adjusting mass flow rate from low to high level increased the output temperature of the system, while the interaction effect showcased that adjusting both heat flux and mass flow rate from low to high level decreased the temperature rise of the system.

On the other hand adjustment on the incinerator water heating component of the system revealed that adjusting flue-gas temperature from low to high level increased output temperature of the system, adjusting mass flow rate from low to high level decreased the output temperature of the system, while the interaction effect showcased that adjusting both flue-gas temperature and mass flow rate from low to high level decreased the output temperature of the system.

Findings from this investigation may help in reaching an optimal design that achieves highest performance to the system. The work has also showcased the competency of using factorial design method to study the joint effect of the factors on response of a system. It is also suggested that the physical experimentation on the same investigation should be conducted in order to verify the accuracy of the result.

REFERENCES

Ashmawy, N., M., Darwesh, M., R., A., Yousef, G., D., M. (2011), Engineering Factors Affecting the Outlet Water Temperature of Solar Water Heater. Process Engineering, 28(2): 451-467.

Ayodeji, O. (2023). A review of water heating systems: A Focus on hybrid technologies prospect in Nigeria. Clean Energy Technologies Journal, 1(1), 31–59. https://doi.org/10.14744/cetj.2023.0005.

Chaudhry, N. H., (2013). The Integration of Heat Pipe Technology into Natural Ventilation Systems. Unpublished Doctoral Thesis in Civil Engineering, the University of Leeds.

ISBN: 978-978-8567-02-8

Duguma, T., (2020). Design of Waste Heat Recovery System from Incinerator for Water Heating Application: The Case of Jimma University Referral Hospital. Unpublished Mater's Dissertation in Mechanical Engineering (Thermal System Engineering Stream), Jimma University, Ethopia.

Egware, H. O., Osaze, O., and Enoma, N. (2015). Performance Evaluation of a Domestic Solid Waste Incinerator Water Heater. Journal of Multidisciplinary Engineering Science and Technology (JMEST), 2(5): 1090-1093.

Hunchat, P, Thongwik, S. (2018). Effect of Water Mass Flow Rate on Performance of Water Heater by 16 kW Heat Pump. 14th Conference on Energy Network of Thailand (E-NETT 14), Rayong Thailand, April 3-4th 2018 at Kyoto University, Japan. Pp: 50-54.

Liu, C., Nishiyama, T., Gamaralalage, P. J. D., Onogawa, K., Hotta, Y., and Honda, S. (2020). Waste-to-Energy Incineration. CCET Guideline Series on Intermediate Municipal Solid Waste Treatment Technologies. pp. 1-38.

Meena, C. S., Prajapati, A. N., Kumar, A., & Kumar, M. (2022). Utilization of Solar Energy for Water Heating Application to Improve Building Energy Efficiency: An Experimental Study. Buildings, 12(12), 2166.

Montgomery, D. C., (2013). Design and Analysis of Experiment, Eight Edition. Arizona State University press. John Wiley & Sons, Inc., 111 River Street, Hoboken, NJ 07030-5774, (201) 748-6011, fax (201) 748-6008, website www.wiley.com/go/permissions.

Osueke, C. O., and Ezugwu, C.A.K., (2011). Study of Nigeria Energy Resources and Its Consumption. International Journal of Scientific & Engineering Research, 2(12): 1-8.

Tobgay, T., Dem, C., Zangmo, D., (2022). Design and Fabrication of Passive Solar Water Heating System. International Research Journal of Modernization in Engineering Technology and Science, 4(4): 404-410.

Uwah, E. J. (2020). Design and Construction of a Portable Solar Water Heater. Published Bachelor's Project in Mechanical Engineering, Faculty of Engineering, Baze University, Abuja, Nigeria.https://doi.org/10.3390/buildings12122166.

Yassin, S., A. (2021). Optimization in Solar Heating Systems Based on a Flat Plate Solar Collector. World Journal of Advanced Research and Reviews, 12 (3): 61-71.

Yin, C., and Mckay, A., (2018). Introduction to Modeling and Simulation Techniques. The 8th International Symposium on Computational Intelligence and Industrial Applications (ISCIIA2018); the 12th China-Japan International Workshop on Information Technology and Control Applications (ITCA2018) Binjiang International Hotel, Tengzhou, Shandong, China, Nov. 2-6, 2018.

Zdanowski, F.; Malico, I.; Canhoto, P.; Lima, R. P., (2024). Simulation of a Thermal Recuperative Incinerator of VOCs with a Special Focus on the Heat Exchanger. Math. Comput. Appl. 2024, 29, 1. https://doi.org/ 10.3390/mca29010001.

ISBN: 978-978-8567-02-8

052-CFD Simulation of Heat Transfer Enhancement with KNO_3-$NaNO_3$ as Phase Change Material for Thermal Energy Storage

M. D. Muhammad[1], A.M Abdullahi[2*], and I.S. Diso[1]

[1]*Department of Mechanical Engineering, Faculty of Engineering, Bayero University, Kano.*

[2] *Department of Mechanical Engineering, Kano State Polytechnic, Kano.*

engransal@kanopoly.edu.ng

Abstract: Solar cooking has been an important area of research worldwide for many decades due to its numerous advantages, such as zero operating costs, environmental benefits, and widespread accessibility. However, energy storage using solar technology faces challenges because of its fluctuating availability. Phase Change Materials (PCMs) have proven highly effective for thermal energy storage, offering a promising solution by storing energy through phase transitions. This study presents a detailed comparative analysis using Computational Fluid Dynamics (CFD) to evaluate the enhancement of heat transfer in phase change thermal energy storage systems with fins. The numerical simulations, conducted using ANSYS Fluent, examine the system's dynamic interactions during the discharging process. By developing detailed CFD models that represent phase change thermal energy storage systems, the study employed solar salt (KNO_3-$NaNO_3$) to investigate its thermal performance during solidification under controlled conditions. The analysis focuses on quantifying the impact of fins on key metrics, including solidification time, heat flux, and temperature distribution. The results show that the integration of fins enhances heat transfer and leads to faster discharge compared to the finless configuration. Additionally, fins create a more uniform temperature distribution by minimizing the thermal gradient within the PCM. This study concludes that incorporating fins in Phase Change Thermal Energy Storage systems offers a potent strategy for significantly improved PCM efficiency and faster energy storage, highlighting their potential for efficient and cost-effective solar energy capture and utilization.

Keywords: Phase Change Materials, Solar-Salt, CFD, Heat Flux and ANSYS Fluent.

1. INTRODUCTION

Solar cooking provides a sustainable, zero-operating-cost solution for thermal needs in off-grid areas (Kalogirou, 2023). However, solar radiation variability limits continuous use, making thermal energy storage a crucial necessity.(Ibrahim et al., 2024). Phase change materials (PCMs) excel in this regard due to their high latent heat storage at near-constant temperatures during phase transitions (Lentswe et al., 2021, 2022). The eutectic KNO_3-$NaNO_3$ mixture suits high-temperature solar cookers with its 220–250°C melting range (Bhave & Kale, 2020).

Low thermal conductivity in phase change materials (PCMs) can lead to slower charging and discharging processes. To enhance performance, incorporating fins can effectively increase surface area and improve conductive heat transfer, allowing for more efficient energy management (Keklikcioglu & Ozceyhan, 2018; Marzouk et al., 2023). This study uses CFD to compare solidification in solar cooker storage between finned (three aluminium fins, 2 mm thick, 150 mm high) and finless KNO_3-$NaNO_3$ systems, quantifying heat flux, time, and uniformity.

2. CFD MODELLING AND SIMULATION OF FINNED AND UNFINNED LATENT HEAT STORAGE (LHS) SYSTEM

The research investigates how fin geometry—specifically parameters such as fin length, spacing, and thickness—affects the rates of solidification and the energy storage capacity of a latent heat storage system. To achieve this goal, advanced computational fluid dynamics (CFD) simulations will be employed to conduct a comprehensive analysis of the thermal behaviours within the system.

The study aims to provide a detailed comparison between configurations equipped with fins and those without, quantifying the enhancements in heat transfer efficiency. This analysis is particularly relevant in the context of high-temperature parabolic solar cookers, which depend on effective thermal management to optimize both the collection and retention of solar energy.

To enhance thermal performance, a eutectic mixture of potassium nitrate and sodium nitrate (KNO_3-$NaNO_3$) has been chosen as the phase change material (PCM). This selection is based on the material's high melting temperature, which enables the implementation of finned systems that can efficiently harness and store thermal energy. In contrast, configurations without fins exhibit a slower discharge process, resulting in less effective energy retrieval.

ISBN: 978-978-8567-02-8

Extensive testing has been conducted on various fin arrangements, focusing on equal spacing and area volume ratios, to optimize heat transfer rates and improve overall system performance. Previous studies have established correlations for heat transfer coefficients derived from both CFD simulations and experimental data, providing valuable insights that aid in the effective design of finned latent heat storage (LHS) systems.

CFD simulations in ANSYS Fluent 2023 R1 modeled the inward solidification of KNO_3-$NaNO_3$ in a cylindrical domain for use in parabolic solar cookers. The fixed-grid enthalpy method successfully captured the mushy zone (with liquid fractions ranging from 0 to 1) without tracking interfaces, offering greater computational efficiency compared to moving-grid methods (Kang et al., 2024; Sahoo et al., 2021).

TABLE 1. THERMOPHYSICAL PROPERTIES OF EUTECTIC MIXTURE (KNO_3-$NANO_3$)

Properties	Liquid	Solid
Density ρ (kg/m^3)	1886	_
Thermal conductivity, k (W/mK)	0.58	0.59
Specific heat capacity, c_p (J/kgK)	2572.43	1782.5
Thermal expansion coefficient, β (1/K)	$5.13x10^{-5}$	
Reference temperature, T_{ref} (°C)	223	
Melting point, T_m (°C)	246.5	
Latent heat of fusion, L (kJ/kg)	90	

TABLE 2: THERMOPHYSICAL PROPERTIES OF ALUMINIUM

	Density (kg/m^3)	Thermal conductivity (W/mK)	Specific heat (J/kgK)
Aluminium	2719	202.4	871

2.1 CFD Simulation Setup

2.1.1 Geometry and mesh preparation:

A 2D axisymmetric domain, as shown in Fig. 1 minimized resources, justified by dominant radial-axial heat flow (negligible azimuthal gradients due to cylindrical symmetry and uniform fin depth). Unfinned: pure PCM cavity. Finned: 3 aluminium fins optimized for conduction area and convection. Boundaries: bottom/sidewalls at aluminium temperature (496 K initial cooling), top convection/radiation (h = 181.3 W/m²·K, T∞ = 423 K), axis symmetric.

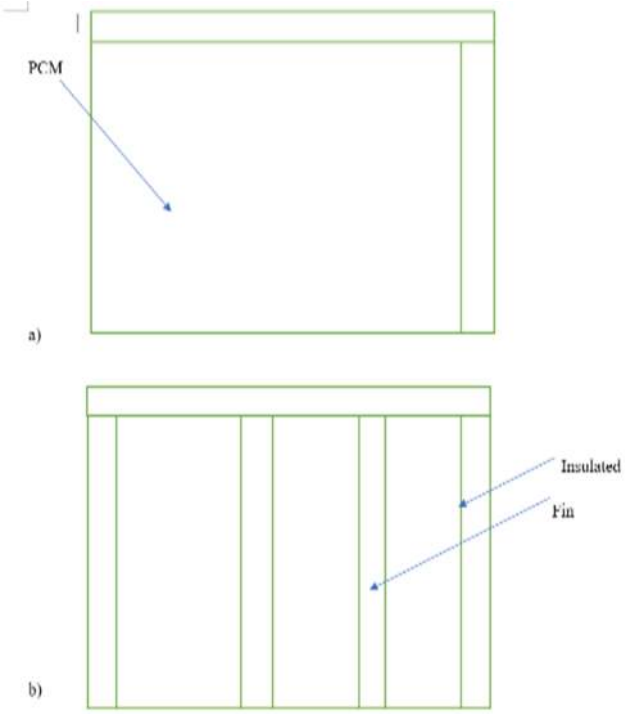


Figure 1: 2D Geometry a) without Fins and b) With Fins

2.2 Grid and time step independence study

Testing the mesh size and time step size is essential in ensuring accurate CFD simulations. Mesh convergence ensured an accurate study, as shown in Table 3. Finer meshes (>2M cells) showed <1% change in solidification time/heat flux.

TABLE 3. MESH CONVERGENCE STUDY (SOLIDIFICATION TIME TO LIQUID FRACTION=0, AVERAGE HEAT FLUX)

Mesh Level	**Cells**	**Solidification Time (h)**	**Avg. Heat Flux (kW/m²)**	**% Change (Time)**
Coarse	500k	34.8	12.5	-
Medium	1.2M	33.6	14.2	-4.0%
Fine	2.1M	33.0	15.1	-2.4%
Extra Fine	3.5M	32.9	15.2	-0.3%

Fluent Launcher Settings: Model - select 2D dimensions, double precision (solver option), and solver processes model in Ansys Fluent Launcher.

Physical model settings. At the start of the simulation, a finite-volume, pressure-based solver that utilises an absolute velocity formulation and incorporates a solidification/melting model, as well as a viscous-laminar model, was deemed most suitable for conducting the current simulation. The transient nature of the phase change was managed by limiting the Courant number to specified values and maintaining axisymmetry in 2D space. The assumptions regarding boundary and initial conditions for modelling the solidification process are as

ISBN: 978-978-8567-02-8

follows: The Boussinesq approximation was applied to account for natural convection effects by treating density as constant except in the buoyancy term. Gravitational forces were included to simulate buoyancy-driven fluid flow. The initial temperature of the system was uniformly set at 550 K, representing a molten phase change material (PCM). The top surface of the PCM, modelled as a 6 mm aluminium pan, is subjected to combined convection and radiation heat transfer, with a convective heat transfer coefficient of 181.3 W/m²·K and a frying temperature of 423 K. All other radiation parameters are maintained at the default values in the simulation settings.

Material Properties: Material properties of each phase (density, viscosity, etc.),

Fluid (Solar Salt): Material Type – Fluid, with the properties and the parameters in Table 1.

- Density -Constant
- Specific heat – Constant
- Thermal conductivity – Constant
- Viscosity -Polynomial
- Thermal Expansion Coefficient- Constant
- Pure Solvent Melting heat – constant
- Solidus and Liquidos Temperature – Constant.

Solid (Aluminium):

Aluminium – Material Type Solid as in Table 2.

- Density – Constant
- Specific Heat – Constant
- Thermal Conductivity – Constant

Boundary conditions: A boundary condition was defined with Axis, internal and walls(bottom, side and top wall).

- **Bottom wall**:
  - ✓ Momentum – wall motion (Stationary wall), shear Condition (No Slip).
  - ✓ Thermal Conditions – Temperature – Material Name (Aluminium)
- **Sidewall**:
  - ✓ Momentum – wall motion (Stationary wall), shear Condition (No Slip).
  - ✓ Thermal Condition – Heat Flux– Material Name (Aluminium)
- **Topwall**:
  - ✓ Momentum – wall motion (Stationary wall), shear Condition (No Slip).
  - ✓ Thermal Condition – Convection– Material Name (Aluminium)

Solver settings: The density variation was based on the Boussinesq approximation, using a reference temperature of 505 K. The SIMPLE (Semi-Implicit Method for Pressure-Linked Equations) algorithm was employed with a time step of 0.02 seconds. Initially, the phase change material (PCM) was assumed to be solid at 496 K. To manage the variation of viscosity with temperature, a second-order polynomial profile was used. A transient analysis was conducted for 5000 seconds, with the side wall considered well-insulated. For transient discretization, a second-order upwind scheme was implemented, along with the SIMPLE algorithm for pressure-velocity coupling and the PRESTO method for pressure correction. The density of the PCM was assumed to be constant. The solution approach included the second-order upwind scheme for solving the momentum and energy equations, the SIMPLE method for pressure-velocity coupling, and the PRESTO scheme for pressure correction. The relaxation factors were maintained at their default values: 0.3 for pressure, 0.7 for momentum, 1.0 for energy and body forces, 1.0 for density, and 0.9 for the liquid fraction.

ANSYS Fluent allows for the specification of thermophysical properties as functions of temperature. However, discontinuities in these properties between solid and liquid phases at the melting point can lead to numerical instabilities. To effectively specify different properties, it was assumed that during melting, within the mushy zone, the change in any property occurs linearly.

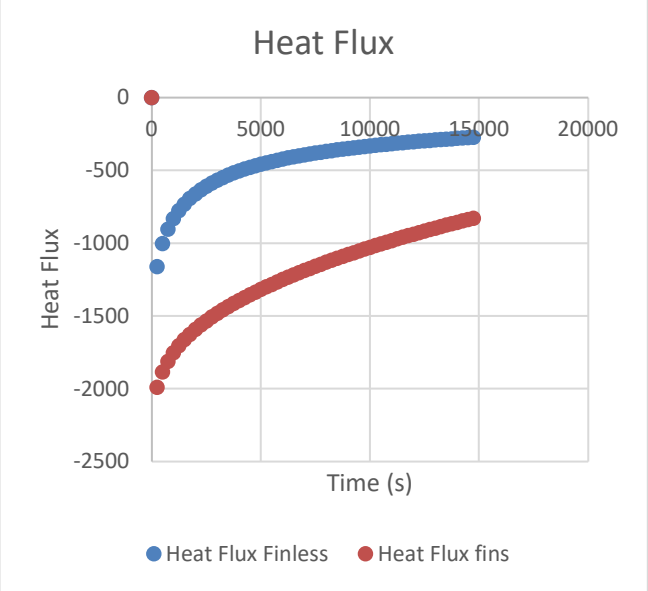


Figure 2: Comparison of heat flux

ISBN: 978-978-8567-02-8

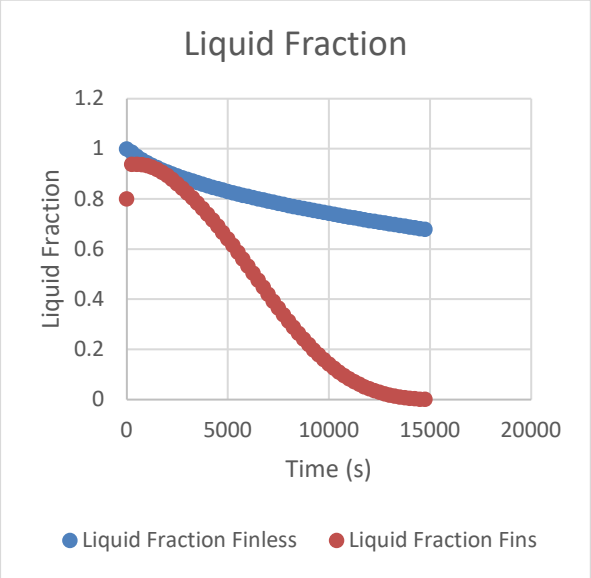


Figure 3: Comparison of Liquid Fraction

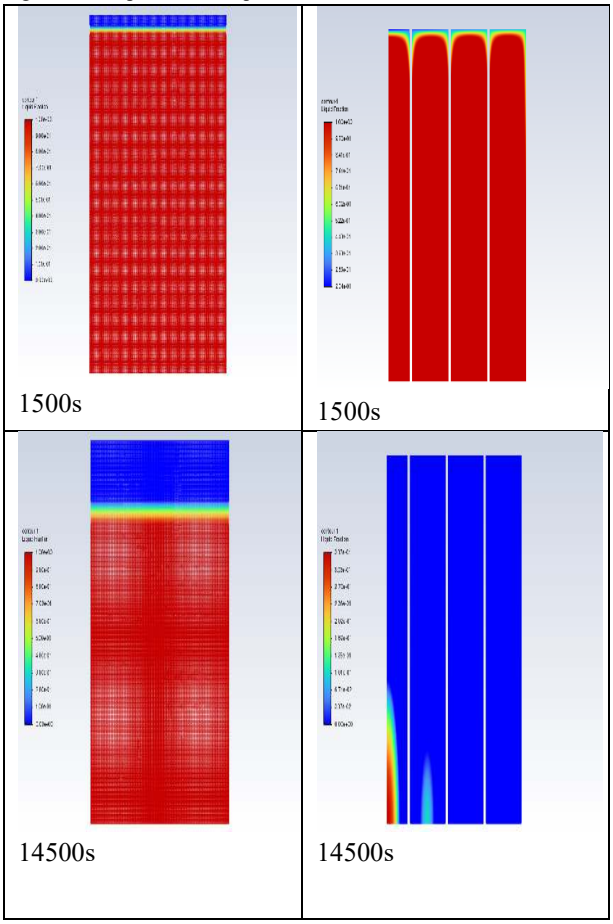


Figure 4: Liquid Fraction Contours

3.0 RESULTS AND DISCUSSION

The performance of phase change materials is largely influenced by the fins, which in turn enhance heat transfer and accelerate solidification. Examining configurations of both with and without fin structures. The simulation results were ensured through careful correlation with established benchmarks. The simulations were executed using a highly refined mesh comprised of 2,080,871 cells, allowing for detailed spatial resolution. A time step of 0.02 seconds was employed alongside a first-order transient formulation to capture the intricacies of the phase change process effectively. Fins accelerated solidification via increased surface area (3× conduction paths), boundary layer disruption, and convection enhancement (Fig. 4 contours: faster mushy zone progression),

TABLE 4. PERFORMANCE COMPARISON (FINNED VS. UNFINNED)

Metric	Unfinned	Finned	Improvement
Solidification Time (h)	33.0	16.5	50%
Avg. Heat Flux (kW/m²)	15.1	27.8	84%
Final Temp. Uniformity (°C std. dev.)	45	22	51%

Fig. 2 confirms higher finned heat flux. Fig. 3 shows the liquid fraction drop: unfinned retains >0.2 at 14,500s and finned near 0.

Fins reduce time by channeling heat more efficiently, minimizing gradients (conduction dominance early, convection later). This aligns with Saini et al. (2023: 42% reduction with Cesaro fins + foam) and Boujelbene et al. (2024: 40% with twisted fins via swirling). Unlike Kiros et al. (2025: solar salt at 142°C), Our higher-temperature KNO_3-$NaNO_3$ (246.5°C) achieves 50% solidification reduction and Kishore et al.(2023)'s solar salt (142°C), as lower molten viscosity enables stronger fin-induced convection.

4.0 CONCLUSION

Fins in KNO_3-$NaNO_3$ PCM cut solidification time 50% (16.5 and 33 h), boosted heat flux 84%, and improved uniformity, ideal for solar cookers needing rapid discharging during non-sunny periods.

Design Recommendations: Use 2 mm × 150 mm aluminium fins (3×) for ~50% gain without excess PCM displacement.

Future Work: Experimental validation, fin optimization (RSM for length/thickness), and addition of more fins.

References

Bhave, A. G., & Kale, C. K. (2020). Development of a thermal storage-type solar cooker for high-temperature cooking using solar salt. *Solar Energy Materials and Solar Cells*, *208*. https://doi.org/10.1016/j.solmat.2020.110394

Boujelbene, M., Mohammed, H. I., Sultan, H. S., Eisapour, M., Chen, Z., Mahdi, J. M., Cairns, A., & Talebizadehsardari, P. (2024). A comparative

ISBN: 978-978-8567-02-8

study of twisted and straight fins in enhancing the melting and solidifying rates of PCM in horizontal double-tube heat exchangers. *International Communications in Heat and Mass Transfer*, *151*, 107224. https://doi.org/10.1016/J.ICHEATMASSTRANSFER.2023.107224

Ibrahim, O. A. A. M., Kadhim, S. A., & Ali, H. M. (2024). Enhancement the solar box cooker performance using steel fibers. *Heat Transfer*. https://doi.org/10.1002/htj.23008

Kalogirou, S. A. (2023). *Solar energy engineering: processes and systems*. Elsevier.

Kang, J., Wang, W., Luo, S., & Zhu, M. (2024). Comparative Analysis of Fixed-Grid Methods in Addressing a Benchmark Problem Coupled with Natural Convection and Melting. *Metallurgical and Materials Transactions B: Process Metallurgy and Materials Processing Science*, *55*(5), 3573–3591. https://doi.org/10.1007/s11663-024-03198-9

Keklikcioglu, O., & Ozceyhan, V. (2018). A Review of Heat Transfer Enhancement Methods Using Coiled Wire and Twisted Tape Inserts. In K. Volkov (Ed.), *Heat Transfer* (p. Ch. 10). Intech Open. https://doi.org/10.5772/intechopen.74516

Kiros, A. K., Zeru, B. A., Desisa, D. G., & Tewolde, D. G. (2025). Fin geometry optimization for enhanced PCM solidification in solar cooking thermal storage system: Numerical simulation and experimental validation. *International Journal of Thermofluids*, *27*. https://doi.org/10.1016/j.ijft.2025.101243

Kishore, B., Roy, A. K., & Kumar, K. (2023). Design and numerical simulation of a solar cooker with an aluminium absorber plate. *Materials Today: Proceedings*, *92*, 1040–1046. https://doi.org/10.1016/j.matpr.2023.04.688

Lentswe, K., Mawire, A., & Owusu, P. (2022). Experimental Energetic and Exegetic Performance of a Combined Solar Cooking and Thermal Energy Storage System. *Energies*, *15*(22). https://doi.org/10.3390/en15228334

Lentswe, K., Mawire, A., Owusu, P., & Shobo, A. (2021). A review of parabolic solar cookers with thermal energy storage. *Heliyon*, *7*(10). https://doi.org/10.1016/j.heliyon.2021.e08226

Marzouk, S. A., Abou Al-Sood, M. M., El-Said, E. M. S., Younes, M. M., & El-Fakharany, M. K. (2023). A comprehensive review of methods of heat transfer enhancement in shell and tube heat exchangers. In *Journal of Thermal Analysis and Calorimetry* (Vol. 148, Issue 15, pp. 7539–7578). Springer Science and Business Media B.V. https://doi.org/10.1007/s10973-023-12265-3

Sahoo, S. S., Satapathy, P. K., Parhi, P. K., Rout, A., & Thomas, S. (2021). Conjugate Heat Transfer Analysis of Solar Cooker Cavity Using CFD Approach. In S. Revankar, S. Sen, & D. Sahu (Eds.), *Proceedings of International Conference on Thermofluids* (pp. 601–609). Springer Singapore.

Saini, P., Dhar, A., Powar, S., & Doddamani, M. (2023). Cesaro fins parametric optimization for enhancement in the solidification performance of a latent heat storage system with combined fins, foam, and nanoparticle. *Energy Reports*, *9*, 5670–5687. https://doi.org/10.1016/j.egyr.2023.04.375

ISBN: 978-978-8567-02-8

053-Application of Modern Hydrological Techniques in Developing a Rating Curve for Tiga Dam Reservoir

A.O. Aminu[1*], S. Dan'Azumi[2], S.J Mohammad[3], A.A Dandajeh[4] and A. Umar[5]

[1,3,4,5]*Department Of Water Resources and Environmental Engineering, Ahmadu Bello University, Zaria*
[2]*Department of Civil Engineering, Prince Sattam bin Abdulaziz University, KSA*

[1,2]*Department Of Civil Engineering, Bayero Univeristy, Kano.*
**Email: ohueyi23@gmail.com*

Abstract: Rating curves, which express the functional relationship between stage and discharge, are fundamental tools for reservoir management. For Tiga Dam in Kano State, Nigeria, the absence of an up-to-date rating curve presents a critical gap in ensuring both operational efficiency and safety. Previous assessments have often relied on empirical formulations and generic assumptions, which may not capture the unique hydrological and hydraulic conditions of the reservoir. This study applies an optimization technique to develop a site-specific rating curve for the Tiga Dam reservoir. Generalized Reduced Gradient (GRG) nonlinear solver (Excel Solver) in MS Excel was used to obtain the optimum values of rating curve parameters. Current meter and float methods were used in the stream gauging. Conventional regression analysis and optimization methods were compared in the derivation of the rating curves using field data. The optimization method yields slightly better results than traditional linear regression. The derived equations are: $Q = 25.208h^{1.84}$; $Q = 9.162h^{1.99}$; and $Q = 3.237h^{2.84}$ for Dukku, Bagwaria and Guruguwa tributaries respectively. Analysis of the results based on the performance indices recommends the optimization method for all three tributaries, as it consistently shows lower RMSE, higher NSE, and better correlation coefficient compared to linear regression. The study underscores the economic and safety benefits of adopting site-specific hydrological modeling, which minimizes the risks of overdesign and structural failure while improving decision-making for water supply and irrigation management.

Keywords: Rating curve, optimization, current meter, float method, Excel Solver, stage, Generalized Reduced gradient

1. INTRODUCTION

Tiga Dam is one of the most critical infrastructures in northern Nigeria, constructed primarily for irrigation, municipal water supply, and flood control. Given its proximity to densely populated downstream settlements, its failure would have devastating socio-economic consequences (Umar et al., 2024). An essential requirement for safe and effective reservoir operation is the availability of a reliable rating curve, which provides the mathematical relationship between water level (stage), and discharge. Rating curves are indispensable in flood routing, inflow estimation, spillway design, and long-term reservoir operation planning (Vishwakarma et al., 2023). Despite its importance, Tiga Dam has not benefited from a thorough re-evaluation of its rating curve using modern hydrological methods. Previous approaches relied heavily on empirical assumptions or generalized parameters, which may result in significant errors. The objective of this study is to develop a rating curve for Tiga Dam using contemporary hydrological and hydraulic modeling techniques. The study further highlights the implications of an updated rating curve for dam safety, spillway adequacy, and water resources management under climate variability.

To establish a stage-discharge relationship, the historical record of stage-discharge data of the gauging station is used to plot the graph between the observed stage (h) and observed discharge (Q) at the station and fitting it with the best-fit curve. Once the relationship is developed, it can then be used to convert records of water

ISBN: 978-978-8567-02-8

level into discharge. Most of the rating curves follow a power function of the form given by Equation 1 (Zakwan et al., 2017a)

$$Q = k(h - a)^n \quad (1)$$

Where Q = stream discharge; h = stage height; a = constant denoting the stage reading at zero discharge; K and n are the rating curve parameters. The parameter 'a' in Equation 1 is a hypothetical value that can hardly be estimated in the field (Carlos et.al., 2018; Mohd et.al., 2015) It is one of the most significant parameters in the stage discharge relationship known as the gauge height of zero flow (GZF) or datum correction factor. This value could be zero, negative or positive. several analytical procedures such as Trial by error method; Arithmetic method and computer-based Optimization methods have been utilized to estimate the value of 'a' (Kumar & Sen, 2024). The method adopted in this study was the Optimization method which involves using optimization techniques to obtain the value of 'a' using computer. The optimization process is achieved with the aid of an Excel solver, which is an optimization tool embedded within MS Excel. The first trial "a" is inputted by the user based on the field survey. The iteration continues until a minimum mean square error is achieved. This method gives the best results compared to the other methods mentioned earlier. Recent advances in rating curve estimation include machine learning techniques such as Artificial Neural Networks (ANN), Gene Expression Programming (GEP), and Support Vector Regression (SVR), which often provide high accuracy and flexibility. However, these methods require large datasets, and technical expertise, which may not be readily available in resource-constrained settings. In contrast, the Generalized Reduced Gradient (GRG) optimization approach adopted in this study offers simplicity, accessibility, and satisfactory accuracy, utilizing widely available tools such as MS Excel, making it suitable for practical applications in developing regions.

1.1 Optimization Technique in Rating Curves Estimation

To fit rating curves for a non-perennial river, Vishwakarma et al., (2023) used optimization approaches (generalized reduced gradient solver and hybrid optimization methods). contrasted traditional regression fits with solver-based optimization. According to their findings, optimization techniques increased the accuracy of curve fits, particularly when dealing with sparse data. Kumar & Sen, (2024) focused on segmented curve fitting, uncertainty measurement, and data selection in their systematic study on rating curve development. included methods for propagating uncertainty. Findings: Explicit uncertainty measurements improved confidence in discharge estimates, while segmented fits decreased bias across the entire flow range.

A Support Vector Regression (SVR) framework combined with data assimilation was presented by Liu et al., (2021)for hydraulic predictions. assessed in a noisy measuring environment. The researchers discovered that SVR outperformed ANN and traditional regression. In their study, Khawaja et al., (2024) examined ANN, GEP, and other machine learning models for hydrologic prediction. Since ANN produced strong fits and GEP produced both high accuracy and interpretable algebraic equations, it was determined that GEP frequently performed better than ANN. Furthermore, Rozos et al., (2022) employed Model Tree (MT) and ANN techniques for rating curve estimation and compared their performance with conventional regression models. Their analysis demonstrated the superiority of machine learning approaches over regression, with MT providing marginally higher accuracy and better interpretability than ANN. Similarly, local studies have also explored optimization-based methods. Alfa et al., (2018) developed a rating curve for the Ofu River at the Oforachi Hydrometric Station, where they compared traditional regression with the Generalized Reduced Gradient (GRG) optimization method. Their results showed that the optimization approach significantly outperformed the conventional regression technique. In a related study titled Fitting Rating Curves to Selected Streams in Southeast Nigeria (Ibeje, 2021), rating curves were established using the conventional power-law approach. The findings confirmed that simple empirical models can adequately represent stage–discharge relationships, although the results were shown to be highly sensitive to the presence of outlier flows. Moreso, Daniel & Gutti, (2025) constructed a rating curve for the River Ngadda in Borno State, Nigeria, applying parametric fitting techniques for operational discharge estimation. However, the study reported difficulties in achieving accuracy during low-flow periods as well as under flood extreme condition

2. METHODOLOGY

2.1 Description of the Study Area

Tiga dam is situated 70km South of Kano city between Latitude 11°26′14″N and Longitude 8°24′9″E. It covers an area of 178 square kilometers with a maximum capacity of nearly 2,000,000 cubic meters. Figure 1 shows the map of Tiga Reservoir with the gauging stations.

The dam was constructed in 1974. It is the major reservoir of the Kano River, the main tributary of the Hadejia River, with a catchment area of 6553 km^2 (Akindele & Indabawa, 2015; Mohammed et al., 2021). It is a zoned earth-fill embankment dam. Table 1 shows the characteristics of Tiga Dam Reservoir. It was constructed purposely for domestic water supply to Kano City and to provide water for the Kano irrigation project. Kano state has a mean annual rainfall of about 800mm in the north and 1000mm in the south (Bello & Tuna, 2014). The temperature ranges from a minimum of 15.80°C to a maximum of 33°C. Kano usually records two seasons comprising four to five months of wet seasons and a dry season, which usually starts from October to April (Teh Chee Ghee, 2015).

ISBN: 978-978-8567-02-8

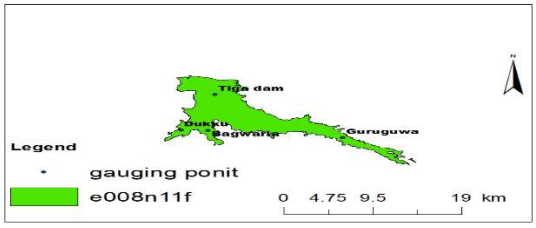


Figure 1: Map of Tiga Reservoir

TABLE I: CHARACTERISTICS OF TIGA DAM RESERVOIR

Characteristics	Units of Measure
Dam type	Zoned Earth fill
Crest Length	6000 m
Structural height	48 m
Hydraulic Height	42.68 m
Total Storage Capacity	1,968 mil.m3
Active Storage Capacity	1,854 mil.m3
Reservoir Surface Area	18900 hectares
Spillway type	Free Overflow Concrete Ogee
Emergency Spillway width	200m

Location of the tributaries

Three tributaries to the reservoir were identified. Two of the tributaries- Dukku and Bagwaria were located in a village called Yaryasa while the third one named Guruguwa is located in Nata'ala. So, the gauging points were selected along these tributaries as shown in Figure 1.

Selection of appropriate gauging site for flow measurement

The selection of suitable site for the gauging station is an antidote for taking accurate flow readings. The following criteria were considered in locating the stations for each of the three tributaries that discharges into the Tiga dam reservoir.

i. Safe and easy accessibility of the site
ii. The section is straight to have a relatively uniform flow (about 30 feet US Geological Survey recommendation).
iii. The station is restricted to a channel.
iv. The stream banks are high and stable to contain maximum flow.
v. The flow is uniform and free of excessive turbulence.
vi. The stream banks are relatively free of thick vegetation that may slow the water and make measurements difficult.

Stream Gauging

Velocity measurements were taken during the high flow period (August 2022 to October 2022). The use of the Current meter by wading and float methods was adopted in the study depending on the prevailing conditions of the streams.

Measurement of flow velocity using a current meter.

At two of the three tributaries (Guruguwa and Bagwaria), the current meter method was used whereas at Dukku, the float method was selected as it was practically impossible to use the current meter due to the width of the river. The current meter method entails dividing the sections into equally spaced vertical profiles and the velocity of each profile is recorded using the current meter. The procedures for the measurement are as follows:

a. A measuring tape was strung across the river at a right angle to the flow. The tape was tied at both ends and made taut to avoid sagging in the middle. The width was measured, and the tape left in position.
b. The width was divided into equal vertical profiles having offset the distance from the banks.
c. Velocities were measured with the current meter using two points (20% and 80% of the flow depth from the water surface) except in situations where the depth was less than 0.5m then one point method was used (60% of the flow depth from the water surface).
d. At each profile, total flow depth was read and recorded. Then the current meter was adjusted accordingly to determine the depth of average velocity.
e. The velocities, depths, and distances measured and recorded for each profile were used to calculate discharge using the mid-section method.
f. The total discharge was the summation of all the discharges for each interval.

The calibration equation used for the current meter model BFM001 is given in Equations 2 and 3.

$V = 0.013 + 0.2512n$ n= 0.32rev/sec (2)

$V = 0.008 + 0.2667n$ $0.32 \geq n \leq 11.28$ (3)

Where V is the mean velocity in m/s and n is the number of rev/sec.

Measurement of flow velocity using the Float Method.

This method measures surface velocity. Mean velocity is obtained using a correction factor. The basic idea is to measure the time that it takes the object to float a specified distance downstream (Gierke, 2002) . The materials required for this method are a measuring tape, a stopwatch, a graduated rod, a buoyant object like an orange, a stick for anchorage, and waders. The site selected should possess characteristics such as a straight section of stream, minimum surface agitation, among others. The amount of water passing a point on the stream channel during a given time is a function of velocity and cross-sectional area of the flowing water, as given in Equation 4

$Q = AV$ (4)

Q is stream discharge (volume/time), A is cross-sectional area, and V is flowing velocity.

Velocity

$V = \frac{travel\ distance}{travel\ time}$ (s/t) (5)

ISBN: 978-978-8567-02-8

The velocity measured from the river is the surface velocity given by Equation 5, which is usually higher than the mean or average velocity. To obtain the mean velocity a correction factor was used as given by equation 6.

$V_{mean} = k\, V_{surface}$ (6)

where k is a coefficient that generally ranges from 0.66 to 0.85, depending on the channel bed (Gierke, 2002).

Area

$A = b \times d$ (7)

Where,
A = Area
b = mean width
d = mean depth

The stream's width and depths were measured across two cross sections where it was safe to wade. The measurements were made at the start and stop cross sections, and the mean of the two readings was taken. A graduated rod was used to measure the depth at regular intervals across the stream. Ten depth measurements were taken because of the width of the stream. The mean cross-sectional area (A) was obtained as given in Equation 7. The mean area and the corrected velocity were used to compute discharge, Q, as given in Equation 4.

Gauge height of zero flow

The datum correction factor 'a' was determined using the computer optimization method. The first value of 'a was assumed. Then, the Generalized Reduced Gradient (GRG) Solver was used to obtain the optimum values of rating curve parameters. This was obtained by minimizing the objective function, which was the sum of the squares of the error between observed discharge and predicted discharge, as shown in Equation 8 (Zakwan et al., 2017c)

$$\min SSQ = \sum_{i=1}^{N} [Q_o - Q_e]^2 \quad (8)$$

Methods of establishing the discharge rating curve

Two modelling approaches are generally employed in the development of rating curve: numerical and the data-driven approach. The numerical approach, which is otherwise called the conventional approach, establishes a rating curve through the application of linear regression and has been proven not to be very accurate in their estimation of discharge. As a result, the application of data-driven techniques is gradually gaining ground because of their accuracy, convenience, and less tedious. Some of these data-driven techniques include Support Vector Machine (SVM), Genetic Algorithm (GA), Artificial Neural Network (ANN), and Generalized Reduced Gradient (GRG), among others (Niazkar, 2021; Zakwan et al., 2017b)

Regression Analysis or Least Squares Method

In this method, the rating curve parameters k and n in Equation 1 were obtained using the least square error approach. The Equation was transformed into logarithmic form as shown in Equation 9

$\log Q = n \log(h - a) + \log k$ (9)

This can be expressed as a form of the equation of a straight line, as expressed in Equation 10.

$Y = AX + B$ (10)

Where $Y = \log Q$; $X = \log(h - a)$; $A = n$ and $B = \log k$

A is the slope of the straight line, while log k is the intercept on the y-axis. In other words, the coefficient of k is the antilogarithm of the intercept B.

Using the regression analysis, the values of A and B were calculated from Equations 11 and 12, respectively. However, the method is tedious and time-consuming.

$$A = \frac{N(\sum XY) - (\sum X)(\sum Y)}{N(\sum X^2) - (\sum X)^2} \quad (11)$$

$$B = \frac{\sum Y - A(\sum X)}{N} \quad (12)$$

Rating curve development by Optimization method

The optimization was performed using a GRG solver in MS Excel as shown in Figure 2. h is the stage measured in m, Q_0 (m3/s) is the measured or observed discharge, Q_e (m3/s) is the estimated discharge using the general formula for a rating curve as shown in column A. Initial values of a, c and n were inputted as 4, 3 and 2 respectively. The error column contains the difference between the observed and the estimated discharges. The last column shows the squares of the errors. To find the function that minimizes the error, we clicked on the solver in which the Solver parameter window popped up as shown at the right side of the figure. The objective was

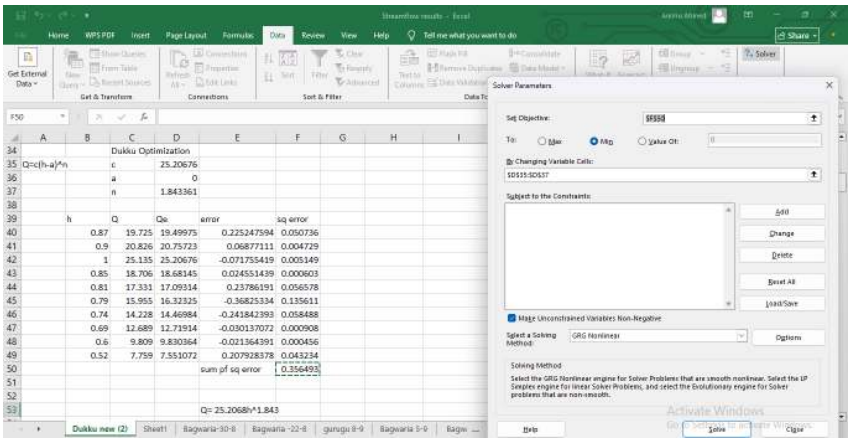


Figure 2: Optimization interface in Excel

ISBN: 978-978-8567-02-8

to minimize the sum of square of errors and the parameters to be manipulated a, c and n were set. The iteration was ran until optimum values of the parameters were attained in which case there was no noticeable difference between Q_0 and Q_e . Therefore, the rating curve developed for the Dukku station is given as $Q = 25.208h^{1.84}$.

Rating curve performance

The rating curve performance was evaluated using Nash-Sutcliffe efficiency (NSE), Root Mean Square Error (RMSE), Mean Absolute Relative Error (MARE) and correlation coefficient (r) represented in Equation 13 to 16.

$$RMSE = \sqrt{\frac{\sum_{i=1}^{n}(Q_{oi}-Q_{ei})^2}{N}} \quad (13)$$

$$NSE = [1 - \frac{\sum_{i=1}^{n}(Q_{oi}-Q_{ei})^2}{\sum_{i=1}^{n}(Q_{oi}-\overline{Q_o})^2}] \quad (14)$$

$$MARE = \frac{1}{N}\sum_{i=1}^{N}\frac{|Q_{oi}-Q_{ei}|}{Q_{oi}} \quad (15)$$

$$r = \frac{N(\sum Q_o Q_e)-(\sum Q_e)(\sum Q_o)}{\sqrt{[N(\sum {Q_e}^2)-(\sum Q_e)^2][N(\sum {Q_o}^2)-(\sum Q_o)^2]}} \quad (16)$$

7. RESULTS AND DISCUSSION

The results of the rating curves generated for the three tributaries to the reservoir are presented as follows. Tables II, IV and VI show the optimization results, while Tables III, V and VII show the results of the conventional method of linear regression for Dukku, Bagwaria, and Guruguwa, respectively. Tables VIII to X show the summary of observed and estimated discharges for each of the stations. In addition, Table XI shows the rating curve parameters for the different methods. The rating curves for each of the methods are shown in Figures 3 to 5.

TABLE II: DUKKU OPTIMIZATION RESULT
$Q = c(h-a)^n$ $c = 25.206;$ $a = 0;$ $n = 1.843$

H	Q	Qe	error	sq error
0.87	19.72	19.49	0.225	0.0507
0.90	20.82	20.75	0.068	0.0047
1.00	25.13	25.20	-0.071	0.0051
0.85	18.70	18.68	0.024	0.0006
0.81	17.33	17.09	0.237	0.0565
0.79	15.95	16.32	-0.368	0.1356
0.74	14.22	14.46	-0.241	0.0584
0.69	12.68	12.71	-0.030	0.0009
0.6	9.80	9.83	-0.021	0.0004
0.52	7.75	7.55	0.2	0.0432
			sum of sq error	0.3564

$$Q = 25.208h^{1.84}$$

TABLE III: DUKKU LINEAR REGRESSION RESULT

Q	H	LOG G=X	LOGQ=Y	XY	X^2	Y^2	LR
19.72	0.87	-0.060	1.295	-0.078	0.003	1.677	19.46
20.82	0.90	-0.045	1.318	-0.060	0.002	1.738	20.70
25.13	1.00	0.000	1.400	0.000	0.000	1.960	25.08
18.70	0.85	-0.070	1.271	-0.089	0.004	1.617	18.65
17.33	0.81	-0.09	1.238	-0.113	0.008	1.534	17.08
15.95	0.79	-0.102	1.202	-0.123	0.010	1.446	16.32
14.22	0.74	-0.130	1.153	-0.150	0.017	1.329	14.49
12.68	0.69	-0.161	1.103	-0.177	0.025	1.217	12.76
9.80	0.60	-0.221	0.991	-0.219	0.049	0.983	9.89
7.759	0.52	-0.284	0.889	-0.252	0.080	0.791	7.62
	Sum	-1.168	11.865	-1.266	0.202	14.298	

$$Q = 25.083h^{1.82}$$

TABLE IV: BAGWARIA OPTIMISATION RESULT
$Q = c(h-a)^n$ $c = 9.161;$ $a = 0;$ $n = 1.986$

h	Q	Qe	error	sq error
0.83	5.87	6.32	-0.455	0.2070
0.85	6.52	6.63	-0.108	0.0117
0.98	9.44	8.80	0.638	0.4081
0.78	5.29	5.59	-0.301	0.0907
0.75	4.92	5.17	-0.251	0.0630
0.68	3.92	4.25	-0.335	0.1122
0.53	2.80	2.59	0.206	0.0427
0.48	2.41	2.13	0.279	0.0781
0.45	2.16	1.87	0.286	0.0823
0.39	1.91	1.41	0.507	0.2580
			sum of sq error	1.3543

$$Q = 9.162h^{1.99}$$

TABLE V: BAGWARIA LINEAR REGRESSION RESULT

Q	h	LOG G=X	LOGQ =Y	XY	X^2	Y^2	LR
5.87	0.83	-0.080	0.768	-0.062	0.006	0.591	6.11
6.52	0.85	-0.070	0.814	-0.057	0.004	0.663	6.36
9.44	0.98	-0.008	0.974	-0.008	7.7E-05	0.950	8.08
5.29	0.78	-0.107	0.723	-0.078	0.011	0.523	5.50
4.92	0.75	-0.124	0.692	-0.086	0.015	0.479	5.15
3.92	0.68	-0.167	0.593	-0.099	0.028	0.352	4.37
2.80	0.53	-0.275	0.447	-0.123	0.076	0.200	2.88
2.41	0.48	-0.318	0.382	-0.121	0.101	0.146	2.43
2.16	0.45	-0.346	0.334	-0.116	0.120	0.112	2.18
1.91	0.39	-0.408	0.283	-0.115	0.167	0.080	1.72
	Sum	-1.910	6.015	-0.869	0.532	4.098	

$$Q = 8.359h^{1.68}$$

ISBN: 978-978-8567-02-8

TABLE VI; GURUGUWA OPTIMISATION RESULT
$Q = c(h-a)^n$ $c = 3.237;\ a = 0;$ $n = 2.836$

H	Q	Qe	error	sq error
1.15	4.72	4.811	-0.082	0.0068
1.28	6.28	6.519	-0.234	0.0551
1.35	7.78	7.582	0.200	0.0402
1.13	4.56	4.578	-0.016	0.0002
1.10	4.21	4.242	-0.024	0.0005
1.08	4.00	4.026	-0.026	0.0007
1.00	3.49	3.237	0.258	0.0669
0.93	2.57	2.635	-0.061	0.0037
0.88	2.19	2.252	-0.054	0.0030
0.85	2.11	2.041	0.069	0.0047
			sum of sq error	0.1822

$$Q = 3.237h^{2.84}$$

TABLE VII: GURUGUWA LINEAR REGRESSION RESULT

Q	h	LOG G=X	LOG Q=Y	XY	X^2	Y^2	LR
4.72	1.15	0.060	0.674	0.040	0.003	0.455	4.80
6.28	1.28	0.107	0.798	0.085	0.011	0.637	6.49
7.78	1.35	0.130	0.891	0.116	0.016	0.794	7.53
4.56	1.13	0.053	0.659	0.034	0.002	0.434	4.57
4.21	1.1	0.041	0.625	0.025	0.001	0.390	4.24
4.00	1.08	0.033	0.602	0.020	0.001	0.362	4.03
3.49	1	0.000	0.543	0.000	0.000	0.295	3.24
2.57	0.93	-0.031	0.410	-0.012	0.000	0.168	2.65
2.19	0.88	-0.055	0.342	-0.018	0.003	0.116	2.27
2.11	0.85	-0.070	0.324	-0.022	0.004	0.105	2.06
	Sum	0.268	5.871	0.268	0.046	3.760	

$$Q = 3.25h^{2.8}$$

TABLE VIII: SUMMARY OF OBSERVED AND ESTIMATED DISCHARGES FOR DUKKU

H	Q_{obs}	Q_{opt}	Q_{LR}
0.87	19.72	19.49	19.46
0.90	20.82	20.75	20.70
1.00	25.13	25.20	25.08
0.85	18.70	18.68	18.6
0.81	17.33	17.09	17.08
0.79	15.95	16.32	16.32
0.74	14.22	14.46	14.49
0.69	12.68	12.71	12.76
0.60	9.80	9.83	9.89
0.52	7.75	7.55	7.62

TABLE IX: SUMMARY OF OBSERVED AND ESTIMATED DISCHARGES FOR BAGWARIA

h	Q_{obs}	Q_{opt}	Q_{LR}
0.83	5.87	6.32	6.11
0.85	6.52	6.63	6.36
0.98	9.44	8.80	8.08
0.78	5.29	5.59	5.50
0.75	4.92	5.17	5.15
0.68	3.92	4.25	4.37
0.53	2.80	2.59	2.88
0.48	2.41	2.13	2.43
0.45	2.16	1.87	2.18
0.39	1.91	1.41	1.72

TABLE X: SUMMARY OF OBSERVED AND ESTIMATED DISCHARGES FOR GURUGUWA

h	Q_{obs}	Q_{opt}	Q_{LR}
1.15	4.72	4.81	4.80
1.28	6.28	6.51	6.49
1.35	7.78	7.58	7.53
1.13	4.56	4.57	4.57
1.10	4.21	4.24	4.24
1.08	4.00	4.02	4.03
1.00	3.49	3.23	3.24
0.93	2.57	2.63	2.65
0.88	2.19	2.25	2.27
0.85	2.11	2.04	2.06

TABLE XI: RATING CURVE PARAMETERS FOR DIFFERENT METHODS AND TRIBUTARIES

	Tributary					
	Dukku		Bagwaria		Guruguwa	
Method	c	n	c	n	c	n
Optimization	25.20	1.84	9.16	1.99	3.23	2.84
Linear Regression	25.083	1.82	8.35	1.68	3.250	2.80

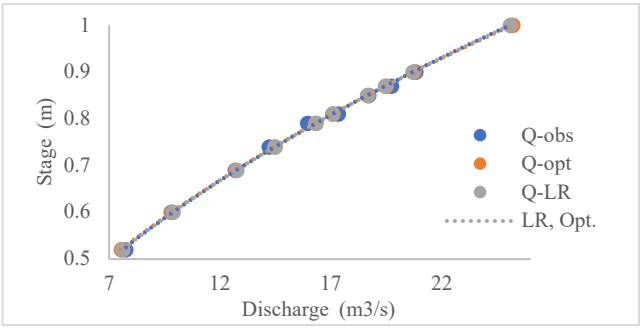


Figure 3: Rating curves comparison of different methods for Dukku station

ISBN: 978-978-8567-02-8

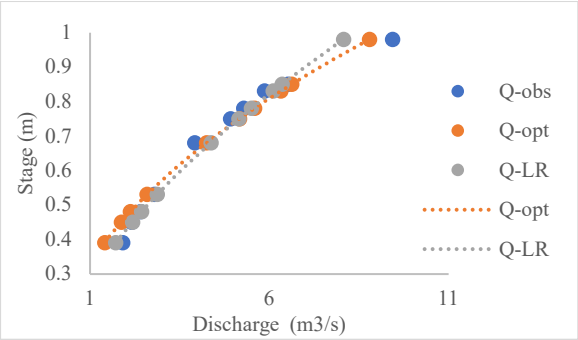


Figure 4: Rating curves comparison of different methods for Bagwaria station

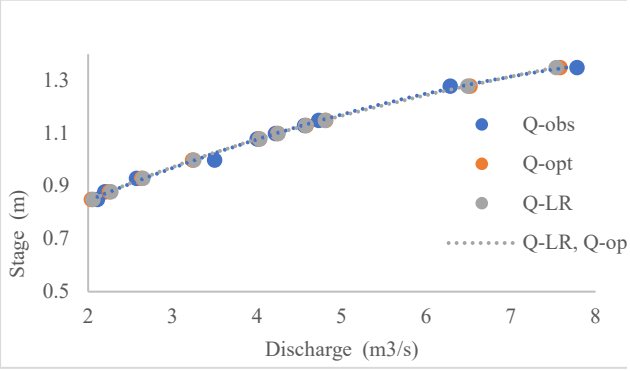


Figure 5: Rating curves comparison of different methods for Guruguwa station

Performance Evaluation of Optimization and LR Methods

The performance indices for the optimization and linear regression (LR) methods used in developing the rating curves for the three tributaries of the Tiga Dam Reservoir - Dukku, Bagwaria, and Guruguwa are summarized in Tables XII to XIV. The key performance metrics considered are RMSE (Root Mean Square Error), NSE (Nash-Sutcliffe Efficiency), MARE (Mean Absolute Relative Error), and Correlation Coefficient.

TABLE XII: PERFORMANCE INDICES OF OPTIMIZATION AND LINEAR REGRESSION METHODS FOR DUKKU

Method	RMSE	NSE	MARE	Correlation coefficient
Optimization	0.189	0.999	1.040	0.999
LR	0.197	0.999	1.116	0.999

TABLE XIII: PERFORMANCE INDICES OF OPTIMIZATION AND LINEAR REGRESSION METHODS FOR BAGWARIA

Method	RMSE	NSE	MARE	Correlation coefficient
Optimization	0.368	0.974	9.423	0.988
LR	0.478	0.956	5.700	0.982

TABLE XIV: PERFORMANCE INDICES OF OPTIMIZATION AND LINEAR REGRESSION METHODS FOR GURUGUWA

Method	RMSE	NSE	MARE	Correlation coefficient
Optimization	0.135	0.9937	2.521	0.997
LR	0.136	0.9936	2.569	0.994

Dukku Tributary

The optimization method achieves a slightly lower RMSE (0.189) compared to LR (0.197), as shown in Table XII, indicating better predictive accuracy. The NSE is 0.999 for both methods, implying that both models have excellent predictive capability. The MARE is slightly lower for the optimization method (1.040) compared to LR (1.116), showing better consistency. The correlation coefficient is the same for both methods (0.999), meaning both models strongly correlate with observed data. From the results, optimization has a marginally lower RMSE and MARE, hence the preferred method for this tributary.

Bagwaria Tributary

In this tributary, Optimization significantly outperforms LR in RMSE (0.368 and 0.478, respectively). The NSE for optimization (0.974) is higher than that of LR (0.956), indicating better model performance. However, MARE for optimization is much higher (9.423) compared to LR (5.700), suggesting that, despite lower RMSE, optimization has higher relative error in some instances. The correlation coefficient is slightly higher for optimization (0.988) compared to LR (0.982), as presented in Table XIII. In most of the performance indices considered, the optimization method provides better overall performance based on RMSE, NSE, and correlation coefficient. Although optimization generally outperformed linear regression across all tributaries, the Bagwaria station exhibited a notably high Mean Absolute Relative Error (MARE) for the optimization method. This anomaly may be attributed to the presence of outlier measurements during low-flow conditions, which disproportionately influence relative error calculations. Additionally, the limited number of observations at extreme flow ranges could have amplified sensitivity to parameter adjustments during optimization.

Guruguwa Tributary

,As shown in Table XIV, the RMSE values of 0.135 and 0.136 for optimization and LR, respectively, are nearly identical, indicating comparable accuracy. The NSE is slightly higher for optimization (0.9937) compared to LR (0.9936), though the difference is negligible. The MARE is marginally lower for optimization (2.521 against 2.569). The correlation coefficient for optimization (0.997) is slightly better than that of LR (0.994), suggesting a stronger relationship with observed data. Although both methods yielded very close results, optimization still has a slight advantage due to lower RMSE, higher NSE, and better correlation. Although the developed rating curves demonstrate strong performance metrics, uncertainty remains inherent in extrapolating beyond the observed flow range, particularly during extreme flood events. To address this, uncertainty bands should be incorporated around predicted discharge values, and cross-validation using independent datasets is recommended. These measures would enhance confidence in operational use and reduce risks associated with over- or under-estimation during critical reservoir management scenarios.

Above all, the result analysis based on the performance indices recommends the optimization method for all three tributaries, as it consistently shows lower RMSE, higher NSE, and better correlation

ISBN: 978-978-8567-02-8

compared to linear regression. However, in the case of Bagwaria, the significantly higher MARE for optimization suggests a need for further validation. This result is in tandem with the works of other researchers, which have shown the superiority of the optimization-based methods in estimating the parameters of the rating curves compared with the conventional method of linear regression (Muzzammil et al., 2015; Muzzammil et al., 2018; Reddy, 2015; Zakwan et al., 2017c).

4. Conclusion

Using optimization and linear regression methods, rating curves were developed for the three tributaries feeding the dam. Although the two methods were closed with respect to the performance metrics adopted, the Optimization method yields slightly better results than traditional linear regression hence recommended for all the tributaries. While optimization using GRG Solver is recommended for its simplicity and accuracy, practitioners should remain cautious about extrapolation risks and incorporate uncertainty analysis in future applications. Advanced machine learning approaches such as ANN and GEP may offer improved predictive capability for complex hydrological systems; however, their resource requirements limit immediate applicability in many field settings.

The use of float method in velocity measurement cannot be compared with the use of current metre however; the method was the most feasible owing to the width of the stream. The use of Acoustic Doppler Current Profiler (ADCP) is recommended for big rivers but its cost and highly skilled requirement for operator is its limitation.

Acknowledgment

Special appreciation goes to the Tertiary Education Trust Fund (TETFund) for sponsoring this research through its local intervention programme. We equally acknowledged the support given by the Department of Water Resources and Environmental Engineering, Ahmadu Bello University, Zaria, through which the sponsorship was granted. Equally worthy of mention is the Department of Civil Engineering, Bayero University Kano where the research was carried out. In addition, the contributions of the co-authors especially my supervisor and mentor at every stage of this publication, can also not be overemphasized.

References

Akindele, E. O., & Indabawa, I. I. (2015). A review of the effects of dams on the hydrology, water quality and invertebrate fauna of some Nigerian freshwaters. *Zoologist (The)*, *13*, 28–35.

Alfa, M. I., Adie, D. B., Ajibike, M. A., & Mudiare, O. J. (2018). *Development of Rating Curve for Ofu River at Oforachi Hydrometric Station*. *15*(1), 14–19.

Bello, N. I., & Tuna, F. (2014). *Evaluation of Potable Water Demand and Supply in Kano State , Nigeria*. *4*(6), 35–42.

Carlos, A., Ricardo, A., María, C., & Carvajal, Y. (2018). *Determination of simple and complex water level - discharge relationship in a river . Case of the Cauca River water level - discharge relationship in a*. *20*(2). https://doi.org/10.25100/iyc.v20i2.6354

Daniel, U. A. I. P., & Gutti, M. B. (2025). *ORIGINAL RESEARCH ARTICLE Department of Civil and Water Resources Engineering , University of Maiduguri , Maiduguri , Borno State * Corresponding author ' s email address : uaibrahim@unimaid.edu.ng*. *21*(March), 101–107.

Gierke, J. S. (2002). *ENG5300 Engineering Applications in the Earth Sciences : Measuring River Discharge*. *2535*(August), 1–9.

Ibeje, A. O. (2021). *Fitting Rating Curves to Selected Streams in Southeast Nigeria*. *6*(1), 108–112.

Khawaja, L., Asif, U., Onyelowe, K., Al Asmari, A. F., Khan, D., Javed, M. F., & Alabduljabbar, H. (2024). Development of machine learning models for forecasting the strength of resilient modulus of subgrade soil: genetic and artificial neural network approaches. *Scientific Reports*, *14*(1), 18244.

Kumar, V., & Sen, S. (2024). Rating curve development and uncertainty analysis in mountainous watersheds for informed hydrology and resource management. *Frontiers in Water*, *5*, 1323139.

Liu, D., Mishra, A. K., Yu, Z., Lü, H., & Li, Y. (2021). Support vector machine and data assimilation framework for Groundwater Level Forecasting using GRACE satellite data. *Journal of Hydrology*, *603*, 126929. https://doi.org/https://doi.org/10.1016/j.jhydrol.2021.126929

Mohammed, A., Univesity, A. B., Muhammad, M. M., & Abdullahi, S. A. (2021). *Analysis of Hydropower Generation and Comparison of Water Allocation for Different Purposes From Tiga Dam , Kano Analysis of Hydropower Generation and Comparison of Water Allocation for Different Purposes From Tiga Dam , Kano*. *June*.

Mohd. Muzzammil, javed Alam, M. Z. (2015). an Optimization Technique for Estimation of Rating Curve Parameters. *Symposium on Hydrology*, *January 2016*, 22–23.

Muzzammil, M., Alam, J., & Zakwan, M. (2018). *A Spreadsheet Approach for Prediction of Rating Curve Parameters*. *April*, 525–533. https://doi.org/10.1007/978-981-10-5801-1_36

Niazkar, M. (2021). *Assessment of Artificial Intelligence Models for Developing Single-Value and Loop Rating Curves*. *2021*(1).

Reddy, M. J. (2015). *Development of Stage-Discharge Rating Curve in River Using Development of Stage-Discharge Rating Curve in River Using Genetic Algorithms and Model Tree*. *February*.

Rozos, E., Leandro, J., & Koutsoyiannis, D. (2022). Development of Rating Curves: Machine Learning vs. Statistical Methods. In *Hydrology* (Vol. 9, Issue 10, p. 166). https://doi.org/10.3390/hydrology9100166

Teh Chee Ghee, F. A. G. (2015). No Title על העיוורון. *Journal of Geotechnical and Geoenvironmental Engineering ASCE*, *120*(11), 259.

Umar, I. H., Abubakar, A., Salisu, I. M., Lin, H., & Hassan, J. I. (2024). Geotechnical Stability Analysis of the Tiga Dam, Nigeria on the Assessment of Downstream Soil Properties, Erosion Risk, and Seasonal Expansion. In *Applied Sciences* (Vol. 14, Issue 15, p. 6422). https://doi.org/10.3390/app14156422

Vishwakarma, D. K., Kuriqi, A., Abed, S. A., Kishore, G., Al-Ansari, N., Pandey, K., Kumar, P., Kushwaha, N. L., & Jewel, A. (2023). Forecasting of stage-discharge in a non-

ISBN: 978-978-8567-02-8

perennial river using machine learning with gamma test. *Heliyon*, *9*(5), e16290. https://doi.org/https://doi.org/10.1016/j.heliyon.2023.e16290

Zakwan, M., Muzzammil, M., & Alam, J. (2017a). Application of data driven techniques in discharge rating curve-an overview. *Aquademia*, *1*(1), 2.

Zakwan, M., Muzzammil, M., & Alam, J. (2017b). Application of Data Driven Techniques in Discharge Rating Curve - An Overview. *Aquademia: Water, Environment and Technology*, *1*(1), 1–8. https://doi.org/10.20897/awet.201702

Zakwan, M., Muzzammil, M., & Alam, J. (2017c). Developing Stage-Discharge Relations using Optimization Techniques. *Aquademia: Water, Environment and Technology*, *1*(2). https://doi.org/10.20897/awet/81286

ISBN: 978-978-8567-02-8

054-Application of Gas Deposition in 3D printing: A Review on improving mechanical properties of PLA

Bello Abdulsalam[1], Ibrahim Abdullahi[2] and Mahdi Makoyo[2]

[1]*Department of Mechanical Engineering, University of Maiduguri, Borno State, Nigeria*
[2]*Department of Mechanical Engineering, Bayero University Kano, Kano State, Nigeria*
bellobib@unimaid.edu.ng

Abstract: Polylactic acid (PLA) is a popular biodegradable thermoplastic used in 3D printing. The mechanical properties of PLA such as strength and impact resistance, are limited because it is brittle and has low thermal stability. Recent studies show that CO_2 gas treatment can enhance the mechanical properties of PLA by creating a more stable crystalline structure. However, the effects of CO_2 gas deposition on PLA during 3D printing process remain underexplored. This review explore the potential of in-processing application of gas deposition (GD) in fused deposition modeling (FDM) 3D printing of PLA components. The review explore 3D printing in a controlled environment, application of CAD/CAE to model & simulate the in-processing of PLA in an enclosed CO_2 environment using molecular dynamic (MD), Computational Micromechanics (CMM) & finite element analysis. The review further explore experimentation of the in-processing of PLA in 3D printing in an enclosed CO_2 environment follow by tensile testing of the components on a universal testing machine (UTM).

1. INTRODUCTION

Additive manufacturing (AM) has revolutionized engineering by enabling the fabrication of complex structures with high precision. AM utilizes 3D printing to produce functional parts from various materials, including ceramics, metals, and polymers, as well as hybrids and functionally graded materials (Shahrubudin et al., 2019). Although plastic was the first material used in 3D printing and it remains highly versatile (Polymer Solutions News, 2016).

Advancements in additive manufacturing—such as fused deposition modeling (FDM), material jetting, and powder bed fusion—have reduced costs, increased productivity, and broadened accessibility. This has led to expanded applications in industries like automotive, aviation, medical, and construction. FDM is one of the most widely adopted AM techniques due to its affordability and versatility (Shaik et al., 2023).

Variety of materials are used in 3D printing, including metals, polymers, ceramics, and concrete. The main polymers used in FDM 3D printing are polylactic acid (PLA) and acrylonitrile butadiene styrene (ABS). PLA is a biodegradable and renewable plastic but ABS is petroleum-based and non-biodegradable. PLA is derived from renewable resources and commonly used in FDM but suffers from brittleness, low thermal stability, and anisotropic mechanical properties (Chai et al., 2019; Grant et al., 2021; Ngo et al., 2018).

Recent research suggests that CO_2 gas deposition can improve the mechanical properties of PLA by creating a more stable crystalline structure (Chai et al., 2019). However, most studies focus on post-processing treatments or applications outside additive manufacturing. This paper reviews the potential of integrating gas deposition into FDM to improve the strength of PLA.

2. METHODOLOGY

The review draws on past and recent studies selected through keyword identification and defined inclusion and exclusion criteria. It is organized thematically, followed by a critical evaluation.

1) Keyword Identification: Core terms such as PLA, FDM, gas deposition, CO_2 treatment, mechanical properties, and simulation guided the literature search.

2) Inclusion Criteria: Studies were considered if they addressed additive manufacturing processes, mechanical property enhancement of PLA, or gas-assisted treatments.

3) Exclusion Criteria: Papers focusing solely on unrelated polymers, non-gas treatments, or lacking mechanical property analysis were excluded.

4) Thematic Organization: Selected studies were grouped into categories covering fundamentals of FDM, PLA properties, gas deposition techniques, simulation approaches, and advanced research on CO_2 treatment.

5) Critical Evaluation: The strengths and limitations of existing studies were evaluated, focusing on their scalability, reproducibility, and relevance to manufacturing applications.

ISBN: 978-978-8567-02-8

2.1 Fundamentals of 3D Printing and FDM

FDM builds parts layer by layer by extruding thermoplastic filaments. PLA and ABS are the most common materials, with PLA favored for its biodegradability. However, the mechanical limitations of PLA restrict its broader use in high-performance applications (Shahrubudin et al., 2019). The process involves feeding a circular cross-sectional filament into a hot end, where it is melted and extruded through a nozzle to build a specimen layer by layer (Shaik et al., 2022). Figure 1 shows an overview of the FDM process.

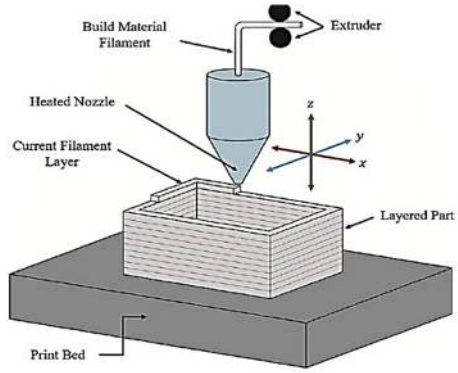


Figure 1: Overview of the FDM process (Shaik et al., 2023)

An example of an FDM 3D printer is the Creality Ender-3 V2 shown in Figure 2

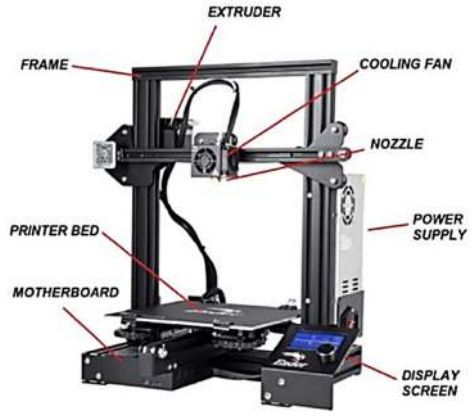


Figure 2: Creality 2020 Ender-3, V2 3D Printer (Mazlan et al., 2018)

2.2 Mechanical Properties of PLA

PLA is a brittle, low-thermal-stability thermoplastic with anisotropic behavior in 3D-printed parts, often showing inferior mechanical performance compared to injection-molded PLA (Grant et al., 2021). Using ASTM D638 and a Universal Testing Machine (UTM), key properties like tensile strength, Young's modulus, and elongation at break are determined (ASTM International, 2014). Typical mechanical properties of PLA include a tensile strength of about 52 MPa, a Young's modulus of 3.6 GPa, and an elongation at break of about 6 % (Gao et al., 2022; Travieso-Rodriguez et al., 2019). Pan, (2025), however, focused on optimizing tensile performance of 3D-printed PLA parts through statistical analysis of printing parameters, showing that process settings can significantly alter these baseline values. Shaik et al. (2022) showed that printing under 10 bar pressure improved yield strength by over 40% and yield strain by 50%, emphasizing the role of process optimization in enhancing the mechanical integrity of printed PLA components.

2.3 Gas Deposition Techniques

Gas deposition involves phase transition from gas to solid (Bolano, 2018). Techniques such as Chemical Vapor Deposition (CVD), Atomic Layer Deposition (ALD), and Physical Vapor Deposition (PVD) have been applied to modify surfaces and enhance material performance (Asatekin et al., 2010; Noč & Jerman, 2022; Sabzi et al., 2023; Xie et al., 2020). CO_2 deposition offers unique potential for polymers by promoting crystallinity and molecular mobility (Chai et al., 2019; Zhai et al., 2009).

Chemical vapor deposition (CVD) is a process where a gaseous substance reacts at a gas-solid interface to form a deposition on a solid material's surface. Figure 3 shows a CVD system for depositing ceramic nanocomposite coatings (Sabzi et al., 2023)

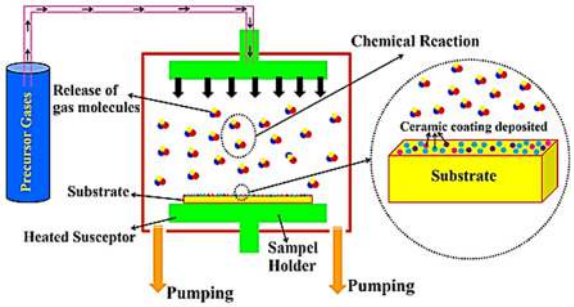


Figure 3: CVD system for the deposition of ceramic nano-composite coating (Sabzi et al., 2023)

CVD methods significantly enhance the capabilities of traditional surface modification techniques for designing polymeric surfaces. In CVD polymerization, the monomer(s) are delivered to the surface in the vapor phase and then undergo simultaneous polymerization and thin film formation. By eliminating the need to dissolve macromolecules, CVD enables the coating of insoluble polymers and prevents solvent damage to the substrate (Asatekin et al., 2010).

For clarity, this review distinguishes between gas deposition—vapor-to-solid film growth processes such as CVD, ALD, or PVD (Asatekin et al., 2010; Noč & Jerman, 2022; Sabzi et al., 2023; Xie et al., 2020) and gas exposure/treatment, where CO_2 acts mainly as a plasticizer or crystallization aid without forming a continuous layer (Chai et al., 2019; Han et al., 2018; Zhai et al., 2009). Under typical FDM conditions (200 °C, 1 atm), CO_2 effects are better described as near-surface modification rather than deposition.

2.4 Simulation Approaches

Computational methods such as Molecular Dynamics (MD), Computational Micromechanics (CMM) and Finite element analysis (FEA) are widely used to predict material behavior. These simulations provide insights into tensile strength, ductility, and thermal properties, guiding experimental design and optimization (Mohan et

ISBN: 978-978-8567-02-8

al., 2017; Ngo et al., 2018; Vashisth et al., 2018). For example, Vashisth et al., (2018) study examined three amine curing agents reacting with Bisphenol-A epoxide using a newly developed accelerated Reaction Force Field (ReaxFF) simulation for kinetically slow reactions as illustrated in figure 4.

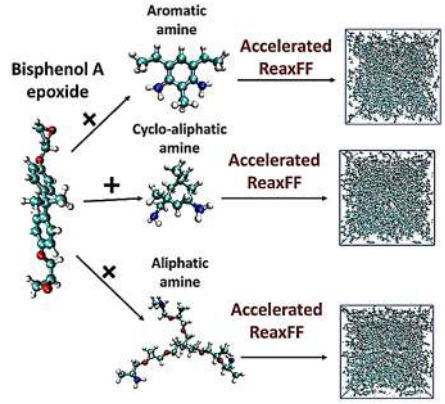


Figure 4: An accelerated Reaction Force Field (ReaxFF) simulation (Vashisth et al., 2018)

Common software used for simulations to predict material behavior includes Amsterdam Modeling Suite, BIOVIA Material Studio, Schrödinger Suite, ANSYS Workbench, ABAQUS, and COMSOL Multiphysics.

2.5 Advanced Research on PLA and CO_2 Treatment

Studies show that CO_2 treatment can enhance the tensile strength, ductility, and toughness of PLA (Chai et al., 2019; Zhai et al., 2009). For example, Chai et al. (2019) demonstrated that CO_2 treatment at room temperature improved ductility as shown in Figure 5, while Zhai et al. (2009) studied crystallization and foaming behavior in compressed CO_2. Supercritical CO_2 conditions affect polyester swelling which depends on temperature, pressure, and treatment time (Han et al., 2018).

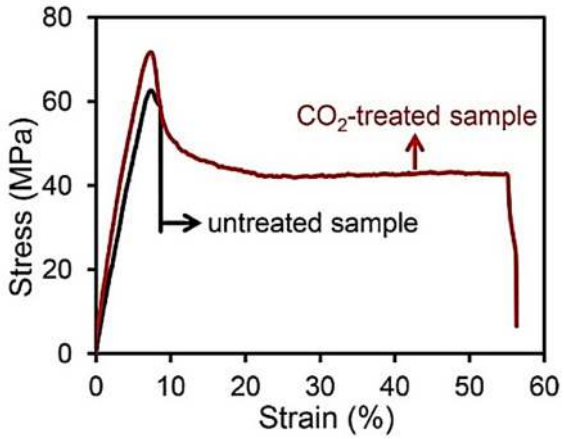


Figure 5: Mechanical properties of treated and untreated PLA with CO_2 (Chai et al., 2019)

Within additive manufacturing, very few studies have explored direct CO_2 application during FDM. Instead, in-process gas environments have primarily focused on inert gases such as nitrogen, which are introduced to reduce oxygen exposure and apply pressures above atmospheric levels (Mazlan et al., 2018; Shaik et al., 2023). Results showed enhanced surface roughness and tensile strength (Mazlan et al., 2018). Figure 6 illustrates the experimental setup.

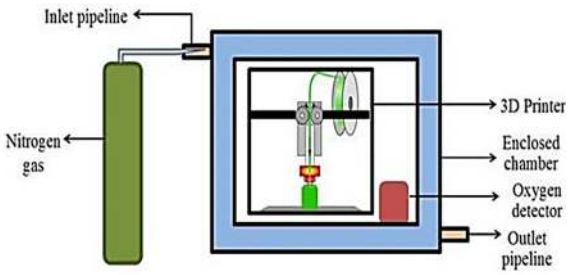


Figure 6: Schematic diagram for in-processing Treatment using Nitrogen gas (N_2) (Mazlan et al., 2018)

Despite these promising results, the feasibility of CO_2 integration in FDM remains constrained by practical challenges. Elevated CO_2 pressure within the printer enclosure may destabilize extrusion, necessitate hardware modifications to maintain controlled environments, and raise safety considerations. Addressing these constraints will be essential before CO_2 treatment can be routinely applied in additive manufacturing

In fused deposition modeling (FDM), parts are fabricated layer by layer, where the surface characteristics of each deposited layer play a critical role in bonding with the next (Shaik et al., 2023). Complementary spectroscopic work has reinforced this view, with X-ray Photoelectron Spectroscopy (XPS) based chemical mapping revealing chemical heterogeneity at polymer interfaces and showing that oxygen-containing functional groups enhance interlayer adhesion in FDM-printed parts (Salam et al., 2025). Building on this understanding, recent work has shown that fluorine and chlorine-based gases can chemically modify PLA surfaces (Asahara et al., 2025; Schroepfer et al., 2020). For example, Schroepfer et al. (2020) demonstrated that gas-phase fluorination improved PLA's surface adhesion and biocompatibility, while a study by Asahara et al (2025) reported successful surface modification of PLA using photo-activated chlorine dioxide. Although these studies were conducted in biomedical and packaging contexts, they highlight the potential of halogen gases for future exploration in additive manufacturing.

3. RESULTS AND DISCUSSION

3.1 Results of the Review

The findings of the review are as follows:-

1) Brittleness, low thermal stability, and anisotropic behavior continue to pose significant challenges in 3D-printed PLA components. Typical properties tensile strength around 52 MPa, Young's modulus 3.6 GPa, and

ISBN: 978-978-8567-02-8

elongation at break about 6 % (Gao et al., 2022; Travieso-Rodriguez et al., 2019) are highly sensitive to process parameters. Optimized printing settings can markedly improve tensile performance (Pan, 2025), while extrusion temperature, orientation, and cooling strongly influence mechanical outcomes (Shaik et al., 2022).

2) Controlled environments (e.g., nitrogen-assisted printing) improve surface quality and mechanical strength (Mazlan et al., 2018; Shaik et al., 2023).

3) CO_2 treatment enhances crystallinity and mechanical properties but is underexplored in in-process FDM. In FDM, layer by layer fabrication means surface characteristics critically affect interlayer bonding. Spectroscopic studies, including XPS chemical mapping, have revealed chemical heterogeneity at polymer interfaces and shown that oxygen containing functional groups enhance adhesion between layers (Chai et al., 2019; Salam et al., 2025; Shaik et al., 2023; Zhai et al., 2009).

4) Simulation studies provide valuable insights but lack integration with experimental CO_2 deposition (Mohan et al., 2017; Ngo et al., 2018; Vashisth et al., 2018). While simulations often describe CO_2–PLA interactions as "deposition," in practice under FDM conditions these effects represent near-surface modification, with CO_2 acting as a plasticizer and crystallization aid rather than forming a deposited film (Chai et al., 2019; Zhai et al., 2009). Feasibility remains a challenge, as elevated CO_2 pressure can destabilize extrusion and requires hardware and safety considerations before routine application in FDM.

5) Reactive halogen gases (fluorine, chlorine, and their oxides) show potential for PLA modification but remain untested in AM contexts (Asahara et al., 2025; Schroepfer et al., 2020).

3.2 Discussion

PLA continues to face inherent limitations such as brittleness, low thermal stability, and anisotropic behavior, with mechanical properties highly sensitive to process parameters (Gao et al., 2022; Shaik et al., 2022; Travieso-Rodriguez et al., 2019). These baseline challenges underscore the importance of controlled environments and material modifications.

Controlled atmospheres, particularly nitrogen-assisted printing, have been shown to improve surface quality and mechanical strength (Mazlan et al., 2018; Shaik et al., 2023). Compared to nitrogen-assisted environments, CO_2 demonstrates superior improvements in ductility and toughness, highlighting its potential to address PLA's weaknesses. However, current research is fragmented, with limited focus on in-process deposition.

While CO_2 treatment demonstrates clear potential for improving PLA properties, its practical implementation in FDM remains constrained. Elevated enclosure pressure can destabilize extrusion, hardware modifications are required to maintain controlled conditions, and safety concerns must be addressed. These feasibility challenges highlight that, although promising, CO_2 integration in additive manufacturing will require engineering solutions and further experimental validation before routine application becomes viable.

Simulation studies have provided valuable insights into CO_2–PLA interactions, but they remain insufficiently integrated with experimental validation. In practice, CO_2 acts as a plasticizer and crystallization aid rather than forming a deposited film, reinforcing the need for experimental confirmation under FDM conditions (Chai et al., 2019; Mohan et al., 2017; Ngo et al., 2018; Vashisth et al., 2018; Zhai et al., 2009).

Emerging evidence from biomedical and packaging studies indicates that fluorine and chlorine gases can chemically modify PLA surfaces (Asahara et al., 2025; Schroepfer et al., 2020). While these findings are outside additive manufacturing, they highlight a potential avenue for in-process gas deposition research. Future work should carefully evaluate reactivity, safety, and hardware compatibility before adapting halogen gases to FDM environments.

4. CONCLUSION

Gas deposition, particularly CO_2 treatment, significantly improves mechanical properties of PLA. Integrating GD into FDM offers a pathway to stronger, more reliable, and sustainable polymer components. This review establishes the foundation for future research into gas–polymer interactions and highlights the potential of GD to advance additive manufacturing technologies. At the same time, feasibility challenges such as extrusion stability under elevated CO_2 pressure, hardware modifications, and safety considerations must be addressed before routine application becomes viable.

Recommendations are as follows:-

1) Conduct systematic experimental studies on tensile, flexural, and impact properties under CO_2 deposition.

2) Integrate simulations (MD, CMM, and FEA) with experimental validation for predictive modeling.

3) Explore alternative gases (e.g., nitrogen, argon) for polymer strengthening.

4) Scale up studies to industrial applications in aerospace, medical, and construction.

5) Assess sustainability and environmental impacts of gas deposition processes.

REFERENCES

Asahara, H., Wu, W., Asoh, T.-A., Hsu, Y.-I., Inoue, T., & Uyama, H. (2025). Surface modification of polylactic acid using a photo-activated chlorine dioxide process: surface properties and dissimilar adhesion. *Materials Advances*, *6(5),* 1608–1612. https://doi.org/10.1039/D4MA01275E

Asatekin, A., Barr, M. C., Baxamusa, S. H., Lau, K. K. S., Tenhaeff, W., Xu, J., & Gleason, K. K. (2010). Designing polymer surfaces via vapor deposition. *Materials Today, 13(5)*, 26–33. https://doi.org/10.1016/S1369-7021(10)70081-X

ISBN: 978-978-8567-02-8

ASTM International. (2014). *Standard Test Method for Tensile Properties of Plastics* (ASTM D638).

Bolano, A. (2018). Deposition Definition In Science. *Science Trends*. https://doi.org/10.31988/scitrends.41343

Chai, J., Wang, G., Li, B., Wan, G., Zhang, L., & Zhao, G. (2019). Strong and ductile poly (lactic acid) achieved by carbon dioxide treatment at room temperature. *Journal of CO2 Utilization, 33*(October), 292–302. https://doi.org/10.1016/j.jcou.2019.06.006

Gao, G., Xu, F., Xu, J., & Liu, Z. (2022). Study of Material Color Influences on Mechanical Characteristics of Fused Deposition Modeling Parts. *Materials (Basel, Switzerland), 15*(19). https://doi.org/10.3390/ma15197039

Grant, A., Regez, B., Kocak, S., Huber, J. D., & Mooers, A. (2021). Anisotropic properties of 3-D printed Poly Lactic Acid (PLA) and Acrylonitrile Butadiene Styrene (ABS) plastics. *Results in Materials, 12*, 100227. https://doi.org/10.1016/J.RINMA.2021.100227

Han, Y., Zheng, H., Jing, X., & Zheng, L. (2018). Swelling behavior of polyester in supercritical carbon dioxide. *Journal of CO2 Utilization, 26,* 45–51. https://doi.org/10.1016/j.jcou.2018.04.017

Mazlan, S. N. H., Alkahari, M. R., Maidin, N. A., Ramli, F. R., & Sudin, M. N. (2018). Influence of inert gas assisted 3D printing machine on the surface roughness and strength of printed component. *Proceedings of Mechanical Engineering Research Day 2018, May*, 154–155.

Mohan, N., Senthil, P., Vinodh, S., & Jayanth, N. (2017). A review on composite materials and process parameters optimisation for the fused deposition modelling process. *Virtual and Physical Prototyping, 12*(1), 47–59. https://doi.org/10.1080/17452759.2016.1274490

Ngo, T. D., Kashani, A., Imbalzano, G., Nguyen, K. T. Q., & Hui, D. (2018). Additive manufacturing (3D printing): A review of materials, methods, applications and challenges. *Composites Part B: Engineering, 143*, 172–196. https://doi.org/10.1016/j.compositesb.2018.02.012

Noč, L., & Jerman, I. (2022). Review of the spectrally selective (CSP) absorber coatings, suitable for use in SHIP. *Solar Energy Materials and Solar Cells, 238*, 111625. https://doi.org/https://doi.org/10.1016/j.solmat.2022.111625

Pan, D. (2025). A comprehensive study of tensile properties of 3D-printed polylactic acid (PLA) parts based on statistical analysis and multi-response optimization of printing parameters. *International Journal of Advanced Manufacturing Technology, 139*(11–12), 6213–6232. https://doi.org/10.1007/s00170-025-16243-x

Polymer Solutions News. (n.d.). 3 Types of Plastic Used in 3D Printing |. WordPress, Stargazer. Retrieved August 30, 2024, from https://www.polymersolutions.com/plastic-in-3d-printing/

Sabzi, M., Mousavi Anijdan, S. H., Shamsodin, M., Farzam, M., Hojjati-Najafabadi, A., Feng, P., Park, N., & Lee, U. (2023). A Review on Sustainable Manufacturing of Ceramic-Based Thin Films by Chemical Vapor Deposition (CVD): Reactions Kinetics and the Deposition Mechanisms. *Coatings, 13*(1). https://doi.org/10.3390/coatings13010188

Salam, S. A., Abbood, M. F., Ali, S. S., Al-Anbari, H. H. A., Hussein, M. A., Alajeeli, F., Idan, A. H., Hammoodi, H. A., & Abdalwahab, S. T. (2025). XPS-Based Chemical Mapping of Interfacial Bonding in FDM-AM Polymer Surfaces. *Applied Chemical Engineering, 8*(4), 1–12. https://doi.org/10.59429/ace.v8i4.5755

Schroepfer, M., Junghans, F., Voigt, D., Meyer, M., Breier, A., Schulze-Tanzil, G., & Prad, I. (2020). Gas-phase fluorination on PLA improves cell adhesion and spreading. *ACS Omega, 5*(45), 29344–29352. https://doi.org/10.1021/acsomega.0c04654

Shahrubudin, N., Lee, T. C., & Ramlan, R. (2019). An overview on 3D printing technology: Technological, materials, and applications. *Procedia Manufacturing, 35*, 1286–1296. https://doi.org/10.1016/j.promfg.2019.06.089

Shaik, Y. P., Schuster, J., Katherapalli, H. R., & Shaik, A. (2022). 3D Printing under High Ambient Pressures and Improvement of Mechanical Properties of Printed Parts. *Journal of Composites Science, 6*(1). https://doi.org/10.3390/jcs6010016

Shaik, Y. P., Schuster, J., & Naidu, N. K. (2023). High-Pressure FDM 3D Printing in Nitrogen [Inert Gas] and Improved Mechanical Performance of Printed Components. *Journal of Composites Science, 7*(4). https://doi.org/10.3390/jcs7040153

Travieso-Rodriguez, J. A., Jerez-Mesa, R., Llumà, J., Traver-Ramos, O., Gomez-Gras, G., & Roa Rovira, J. J. (2019). Mechanical Properties of 3D-Printing Polylactic Acid Parts subjected to Bending Stress and Fatigue Testing. *Materials (Basel, Switzerland), 12*(23). https://doi.org/10.3390/ma12233859

Vashisth, A., Ashraf, C., Bakis, C. E., & van Duin, A. C. T. (2018). Effect of chemical structure on thermo-mechanical properties of epoxy polymers: Comparison of accelerated ReaxFF simulations and experiments. *Polymer, 158*, 354–363. https://doi.org/10.1016/J.POLYMER.2018.11.005

Xie, T., Kao, W., Sun, L., Wang, J., Dai, G., & Li, Z. (2020). Preparation and characterization of self-matting waterborne polymer–An overview. *Progress in Organic Coatings, 142*, 105569. https://doi.org/10.1016/J.PORGCOAT.2020.105569

Zhai, W., Ko, Y., Zhu, W., Wong, A., & Park, C. B. (2009). A Study of the Crystallization, Melting, and Foaming Behaviors of Polylactic Acid in Compressed CO2. *International Journal of Molecular Sciences, 10*(12), 5381–5397. https://doi.org/10.3390/ijms10125381

ISBN: 978-978-8567-02-8

056-Determination of the Effect of Dessert Date Seed - Shea Butter Cutting Fluid on Surface Roughness in Cutting Mild Steel

Authors: *I. K. Isa[1], M. Makoyo[1], A. Salihi[1]*

isaibrahimkallamu@gmil.com

[1]Department of Mechanical Engineering, Faculty of Engineering, Bayero University, Kano, Nigeria

Abstract: This study investigates the performance of a plant-based cutting fluid formulated from Desert Date seed oil - Shea Butter oil in the turning of mild steel. Conventional petroleum-based cutting fluids pose environmental and health risks, prompting the search for sustainable alternatives. The formulated fluid was evaluated under varying oil concentrations (5%, 7.5%, 10%), cutting speeds (50, 75, 100 rpm), and feed rates (0.1, 0.2 mm/rev) using a full factorial design. Surface roughness was measured using a profilometer. Results indicate that the formulated cutting fluid significantly improves surface finish, with the best performance observed at 10% oil concentration, 75 rpm cutting speed, and 0.1 mm/rev feed rate, achieving a surface roughness of 1.88 µm. Analysis of variance (ANOVA) confirmed that oil concentration and cutting speed are the most influential parameters. MINITAB 17software was used to develop a mathematical model to predict and evaluate the relationship between independent factors (Oil%, Speed and Feed rate) and dependent factor (surface roughness) parameter The study concludes that Desert Date–Shea Butter oil is an effective, eco-friendly alternative to conventional cutting fluids, offering improved surface quality in mild steel turning.

Keywords: Cutting fluid, Desert Date seed oil, Shea Butter oil, surface roughness, turning, mild steel, sustainable machining.

1. INTRODUCTION

Cutting fluids are essential in machining to reduce friction, dissipate heat, and improve surface finish. However, conventional petroleum-based fluids are non-biodegradable and pose health hazards. There is a growing shift toward plant-based alternatives due to their lubricity, biodegradability, and low toxicity. Desert Date seed oil and Shea Butter oil are promising candidates owing to their high fatty acid content and thermal stability (Datti et al. 2020). This study focuses on evaluating the effect of a blended cutting fluid from these oils on surface roughness during the turning of mild steel. Kolawole (2013): Conducted biodegradability tests on vegetable-oil-based cutting fluids, synthetic esters, and rapeseed oil. Found 100% biodegradability for vegetable-based options, far exceeding alternatives. No detailed discussion on the trade-offs between biodegradability and industrial performance. Okia et al. (2013):Analyzed the nutritional composition of desert date leaves, noting valuable protein and fat content. The potential use of desert date leaves in industrial or medicinal applications remains unexplored.

Despite the growing interest in bio-based cutting fluid, there is a lack of comprehensive studies on the characterization, formulation and comparing the performance of blended desert date seed and shea butter oil as cutting fluid. This study aims to bridge this knowledge gap by characterizing the physicochemical properties of desert date and shea butter olis. Desert date seed oil mixed with shea butter oil can address these problems due to their synergistic effects, improved viscosity, enhanced tool life, biodegradability, cost effectiveness and improved surface integrity. Going by the above, this shows that, little study have been performed to address and mostly on the medicinal benefits of the desert date seed and the nutritional composition of its leaves. There is no any related work found closed to the present research. The present research is concerned on the determination of the effect of blend desert date seed and shea butter oil cutting fluid on tool life during cutting of mild steel in turning operation.

2.0: MATERIALS AND METHODS

2.1 Formulation of Cutting Fluid

Desert Date seed oil and Shea Butter oil were mixed in varying concentrations (5%, 7.5%, 10%) with emulsifiers, antioxidants, anticorrosion agents, and water to form an oil-in-water emulsion.

2.2 *Workpiece and Tool*

Mild steel bars (28 mm diameter, 500 mm length) were turned using a High-Speed Steel (HSS) tool on a Colchester Mascot 1600 lathe.

ISBN: 978-978-8567-02-8

2.3 Additives:

Emulsifiers, antioxidants (Vitamin E), anti-corrosion agents (sodium nitrite

2.4 Machining Experiments

Dependent variables used is surface roughness while independent variables are cutting fluid, cutting speed and feed rate. Full factorial method in the design of experiment was used. The experiment was designed according to 3x3x2 factorial design, with three factors, that is: 3 level of cutting fluid, 3 level of cutting speed and 2 level of feed rate as given in table 4 below. Each experimental run was replicated three times to ensure the reliability and accuracy of the results, and was randomized to minimize any potential biases and ensure that the results are due to the experimental factors rather than any external factors. Feed rate selection with two levels was because of the following reasons; practical limitation: increasing feed rate beyond 0.2 will lead to flow surface roughness, tool wear. Research focus: the primary focus is to investigate the effect of blend desert date seed and shea butter cutting fluid on tool life; feed rate is secondary factor, two level are sufficient to capture its effects. Reducing experimental complexity. Previous research /studies on turning operation have shown that, feed rate within the range of 0.1 and 0.2 mm/rev have a significant impact on tool life. Hence these two levels are considered sufficient to capture the effects of feed rate

TABLE 1: EXPERIMENTAL DESIGN FACTORS AND LEVELS

Factor	Level 1	Level 2	Level 3
Oil Concentration	5%	7.5%	10%
Cutting Speed	50 rpm	75 rpm	100 rpm
Feed Rate	0.1 mm/rev	0.2 mm/rev	-

The mild steel work pieces with 28mm diameter and 500mm length according to ASTM A751 standard was machined using turning (COLCHESTER mascot 1600), operation with tool material at the tool holder. The cutting fluid was applied at a constant flow rate and pressure during the operation. The following machining parameters was used and controlled: Cutting speed 50-100 (m/min) and Feed rate 0.1-0.2 (mm/rev) respectively.

The cylindrical mild steel work pieces was machined using high-speed steel (HSS) insert. Desert date seed oil - Shea butter oil was applied as cutting fluids through a flooding method to ensure adequate lubrication and cooling during the cutting operation (Benarfa et al., 2017). The cutting parameters such as cutting speed, feed rate were carefully controlled to maintain consistency throughout the experiments (Sharma et al., 2017).

2.5 Performance Evaluation

Surface Roughness was measured using KLA-Tencor P-17 profilometer (Ra values). Three readings were taken per sample and averaged. Data were analyzed using Analysis of Variance (ANOVA) with a 95% confidence level (α=0.05) in Minitab 17. Mathematical models were developed for responses. Multi-response optimization was performed using the Desirability Function approach.

3.0: RESULTS AND DISCUSSION

3.1 Physicochemical Properties

The formulated fluid exhibited excellent properties for machining applications presented in below Table 2. The viscosity of 12.3 cP at 40°C provides adequate lubricity without excessive drag. The high flash point of 165°C ensures safety during high-temperature operations. The slightly alkaline pH of 8.2 offers corrosion protection for ferrous materials.

TABLE 2: PHYSICOCHEMICAL PROPERTIES OF FORMULATED CUTTING FLUID

Property	Value	Standard/ASTM Method
Viscosity at 40°C	12.3 cP	ASTM D2270
Flash Point	165°C	ASTM D93
Pour Point	5°C	ASTM D97
pH	8.2	ASTM D664
Density	0.93 g/cm³	ASTM D1298
Acid Value	1.317mg KOH/g	-

3.2 Surface Roughness (Ra)

3.2.1 Effect of Parameters on Surface Roughness

The lowest surface roughness (1.88 μm) was achieved at 10% oil concentration, 75 rpm, and 0.1 mm/rev feed rate. Increased oil concentration improved lubrication and reduced friction, leading to a smoother surface. Higher cutting speeds initially improved finish but caused deterioration at 100 rpm due to built-up edge formation. Increased feed rate negatively affected surface roughness

Figure 2 shows the main effects plot for surface roughness in turning. Ra decreases with increasing oil concentration and decreases, then increases with speed, finding an optimum at 75 rpm. Ra increases with feed rate, as expected.

ISBN: 978-978-8567-02-8

TABLE 3: RESPONSE SURFACE METHODOLOGY (RSM) DESIGN OF CUTTING FLUIDS FORMULATIONS

Run	DDSO	SBO	EMULSIFIER	ANTIOXIDANTS	ANTICORROSION AGENT	WATER
1	5	5	2	0.3	1	83
2	10	5	2	0.3	1	83
3	5	10	2	0.3	1	83
4	**10**	**10**	**2**	**0.3**	**1**	**83**
5	7.5	7.5	5	0.1	1	80
6	5	7.5	5	0.1	1	80
7	10	7.5	2	0.5	0.5	86
8	5	7.5	2	0.5	0.5	86
9	10	5	5	0.5	1	80
10	7.5	10	5	0.5	1	80
11	7.5	5	2	0.1	1.5	86
12	7.5	10	2	0.1	1.5	86
13	7.5	7.5	3.5	0.3	1	83
14	7.5	7.5	3.5	0.3	1	83
15	7.5	7.5	3.5	0.3	1	83

TABLE 4: EXPERIMENTAL RESULTS FOR FORMULATED DESERT DATE SEED - SHEA BUTTER OILS AS CUTTING FLUID.

Operation	Oil (%)	Speed (rpm)	Feed (mm/rev)	Surface Roughness Ra (μm)
Turning	5.0%	50	0.10	2.540
Turning	5.0%	50	0.20	2.610
Turning	5.0%	75	0.10	2.000
Turning	5.0%	75	0.20	2.070
Turning	5.0%	100	0.10	2.580
Turning	5.0%	100	0.20	2.650
Turning	7.5%	50	0.10	2.480
Turning	7.5%	50	0.20	2.550
Turning	7.5%	75	0.10	1.940
Turning	7.5%	75	0.20	2.010
Turning	7.5%	100	0.10	2.480
Turning	7.5%	100	0.20	2.550
Turning	10.0%	50	0.10	2.420
Turning	10.0%	50	0.20	2.490
Turning	10.0%	75	0.10	1.880
Turning	10.0%	75	0.20	1.950
Turning	10.0%	100	0.10	2.420
Turning	10.0%	100	0.20	2.490

ISBN: 978-978-8567-02-8

TABLE 5: ANOVA FOR SURFACE ROUGHNESS IN TURNING

Source	DF	Adj SS	Adj MS	F-Value	P-Value
Model	8	1.27227	0.15903	2300.31	0.000
Linear	3	0.07592	0.02531	366.03	0.000
Oil (%)	1	0.05333	0.05333	771.43	0.000
Speed (rpm)	1	0.00053	0.00053	7.71	0.021
Feed (mm/rev)	1	0.02205	0.02205	318.94	0.000
Speed*Speed	1	1.19538	1.19538	17290.29	0.000
Error	9	0.00062	0.00007		
Total	17	1.27289			

R^2 = 99.95%, R^2(adj) = 99.91%

*(Significant) R-sq 99.95%, R-sq(adj) 99.91% and R-sq(pred) 99.80%

Surface Roughness Ra (µm) = 6.9356 - 3.07 Oil (%) - 0.12973 Speed (rpm)
+ 0.700 Feed (mm/rev)
+ 10.67 Oil (%)*Oil (%)
+ 0.000875 Speed (rpm)*Speed (rpm)
- 0.01600 Oil (%)*Speed (rpm)
+ 0.00 Oil (%)*Feed (mm/rev)
+ 0.00000 Speed (rpm)*Feed (mm/rev)
(1)

TABLE 6: T-TEST COMPARISON OF RESPONSES PARAMETER OF FORMULATED DESERT DATE AND SHEA BUTTER SEED OILS AND STANDARD PETROLEUM CUTTING FLUID

Parameter	Standard Oil (SAE 40) (Mean ± SD, N, SE)	Formulated Oil Desert date/Shea Butter oil (Mean ± SD, N, SE)	Mean Difference	SD of Difference	SE of Difference	95% CI of Difference	t-Value	p-Value
Surface Roughness (µm Ra)	2.9863 ± 0.0487 (N=18, SE=0.0115	2.3394 ± 0.2736 (N=18, SE=0.0645	0.6469	0.2687	0.0633	0.5132, 0.7805	10.21	0.000

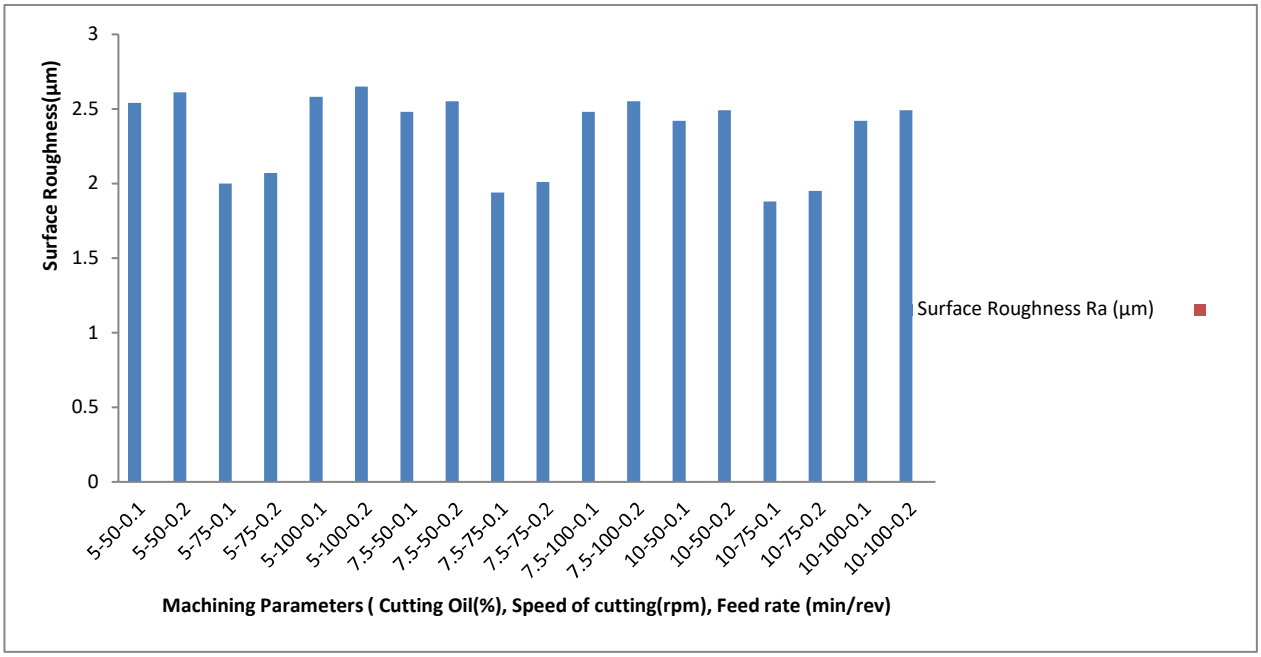


Figure 1: Effect of Turning Parameters on Surface Roughness

ISBN: 978-978-8567-02-8

Figure 2 gives the main effect of the factors (cutting oil%, speed of cutting and feed rate) on the surface roughness of the turned mild steel. It shows surface roughness ranking on the effect of the turning parameters on the surface roughness. It reveals also that cutting oil%, speed of cutting and feed rate had significant influence on the surface roughness, surface roughness decreases as the oil% increases, while surface roughness decreases as the feed rate decreases. Speed had the highest effect on the surface roughness, followed by oil% and feed rate.

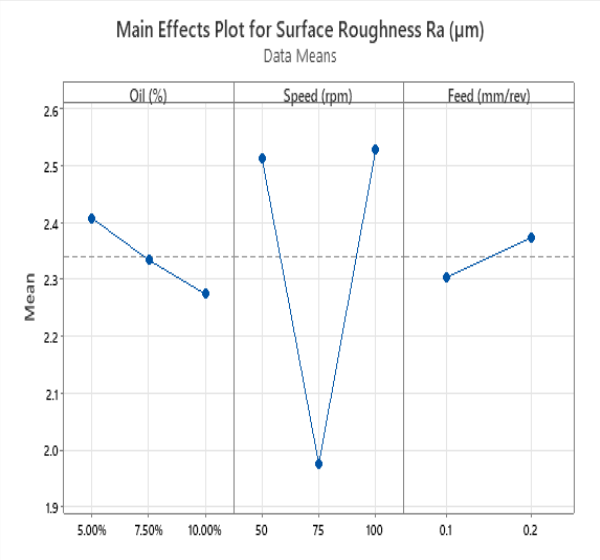


Figure 2: Main Effects Plot for Surface Roughness (Ra) in Turning

3.3 ANOVA and Modelling

ANOVA results (Table 5) indicated that oil concentration, cutting speed, and feed rate significantly affect surface roughness ($p < 0.05$). The interaction between oil concentration and cutting speed was also significant. A predictive model was developed with $R^2 = 99.95\%$.

MINITAB 17software was used to develop a mathematical model to predict and evaluate the relationship between independent factors (Oil%, Speed and Feed rate) and dependent factor (surface roughness) parameter. The functional relationship between dependent parameter and the independent parameters is shown in modelling equation (1). The coefficient of Oil (%)*Oil (%) is the largest in the model, followed by feed and speed*speed. It is a clear indication that increasing the values of Oil (%)*Oil (%) may largely smoothing the surface of the turned mild steel at a rate higher than other factors values. Increasing speed* speed and feed rate can also improve the surface roughness but at a lower factor than speed *feed and oil*feed as their coefficient is smaller. While reducing all the independent factors with negative coefficients in the model can increase the surface roughness.

Normal probability plot in Figure 3 was used to assess the assumption of normality for the factor residuals. It was observed that the residuals are distributed on both sides of the line; this shows that the data is approximately normally distributed. The residuals plot against number of experiment and residual plot against fitted value graphs are shown in Figures 4 and 5, the residual plot against number of experiment, help to assess model fitness, verify the assumption that the residuals are independent and ultimately ensuring the reliability of the analysis results. The plot does not display any discernible pattern, meaning that the model is fit to predict the response. The residuals plot against fitted points graph as illustrated in Figure 5 is another plot that plays important role in supporting other plots in validating the goodness of fit of a model. The plot shows that the points fall randomly on both sides of 00, with no recognizable patterns in the points, which means the model, is well fitted to experimental data. The coefficients generated from the model on surface roughness were estimated with R-squared value of 99.95%, it is high, which indicates a high significance of the model to surface roughness of the turned mild steel. Predicted R- squared value of 99.91% is also in good agreement with the adjusted R-square 99.80%.

The value of probability ($P = 0.000$) is less than F value, which means that the model is significant. The results of ANOVA for surface roughness on the parameters interactions reveal that the predictability and adequacy of the model on surface roughness are at confidence level of 95%, with P value of 0.000 as shown in Table 5.

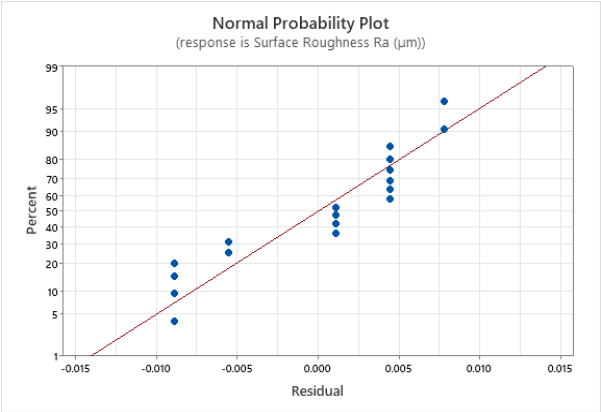


Figure 3: The Normal Probability Plot of Residual for Surface Roughness

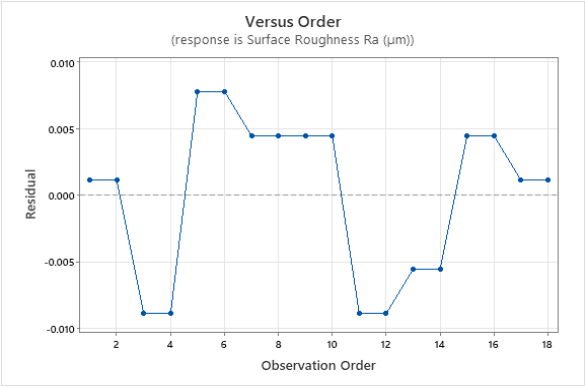


Figure 4: Residual Plot against Surface Roughness Number of Experiment

ISBN: 978-978-8567-02-8

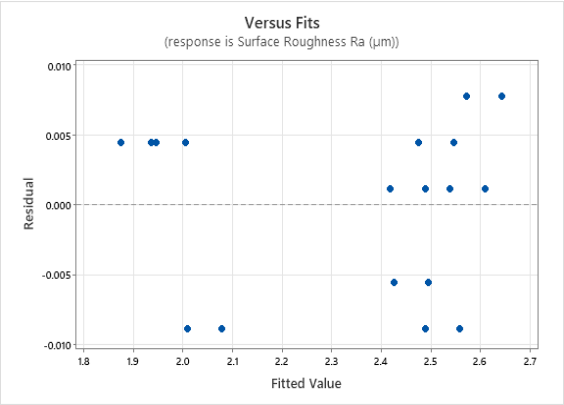


Figure 5: Residual Plot against Fitted Value of Surface Roughness.

3.4 Optimization

Table 7 shows the response optimization of the most desirable turning condition for minimizing surface roughness occurred at 10% oil concentration, 75.25 rpm spindle speed and 0.1 mim/rev feed rate, with a predicted surface roughness value of 1.87558 μm. This setting produced the best surface roughness desirability, indicating and optimal solution. The composite desirability of 1 indicates an excellent over all optimization fit. This confirms that low feed and moderate speed enhance surface finish, consisting machining theory that reduced feed decreases tool mark height (Kaynak, 2019). The result further reveals that at higher lubrication, moderate turning speed and lower feed rate contribute to improved surface finish.

TABLE 7: SURFACE ROUGHNESS MULTIPLE RESPONSE OPTIMIZATIONS

Sol.	Oil (%)	Speed (rpm)	Feed (mm/rev)	Surface Roughness Ra (μm) Fit	Composite Desirability
1	10	75.25	0.1	1.87558	1

A paired t-Test Comparison of Responses Parameter of Formulated Desert Date - Shea Butter Seed oils and Standard Petroleum Cutting Fluid (SAE 40 Mineral-Based Oil, ASTM D 974) as Cutting Oil.

A paired-samples t-test was conducted to statistically evaluate the performance of the novel Desert Date seed Shea butter oil cutting fluid against a conventional petroleum-based fluid (SAE 40) in turning operation. The analysis compared the performance surface roughness (Ra) under identical machining parameters. The results, summarized in Table 6, reveal significant and operation-dependent differences between the two fluids.

Surface Roughness: The Desert Date seed Shea butter oil fluid produced a significantly smoother surface (Mean Ra = 2.34 μm) compared to the standard fluid (Mean Ra = 2.99 μm). The mean difference of 0.65 μm (95% CI: 0.51 to 0.78) was highly significant ($p < 0.001$), indicating a substantial improvement in surface quality.

4. CONCLUSION

This research successfully demonstrates that cutting fluid formulated from Desert Date seed oil and Shea Butter oil is a technically competent, environmentally sustainable, and economically viable alternative to conventional petroleum-based cutting fluids for machining mild steel. Key findings include:

1. The formulated fluid exhibits excellent physicochemical properties suitable for machining applications
2. Optimal performance is achieved at 10% oil concentration, moderate cutting speeds (50-75 rpm), and lower feed rates (0.1 mm/rev)
3. Significant improvements in surface finish (25-30%) were observed
4. The fluid's biodegradability and non-toxic nature address critical environmental and occupational health concerns
5. Economic benefits include extended tool life and reduced disposal costs

The study contributes to sustainable manufacturing practices and promotes the utilization of locally available renewable resources. Future work should focus on industrial-scale implementation, testing with diverse materials, and development of specialized formulations for specific applications

References

Sharma, S. K., et al. (2017). Performance evaluation of vegetable-based cutting fluids in machining processes. *Materials and Manufacturing Processes*, 32(2), 225–234.

Shashidhara, Y. M., &Jayaram, S. R. (2010). Vegetable oils as a potential cutting fluid: An evolution. *Tribology International*, 43(5–6), 1073–1081.

Kalpakjian, S., &Schmid, S. R. (2014). *Manufacturing Engineering and Technology*. Pearson.

Gharby, S., et al. (2018). Chemical characterization and oxidative stability of desert date seed oil. *OCL - Oilseeds and Fats, Crops and Lipids*, 25(4), D405.

Kyari, M. Z. (2008). Practical applications of Shea Butter oil in machining processes. *International Journal of Advanced Manufacturing Technology*, 39(7–8), 750–757.

Astakhov, V. P. (2010). *Geometry of single-point turning tools and drills: Fundamentals and practical applications*. Springer Science & Business Media.

Cetin, M. H., Korkmaz, M. E., &Günay, M. (2011). Evaluation of vegetable based cutting fluids with extreme pressure and cutting parameters in turning of AISI 304L by Taguchi method. *Journal of Cleaner Production,* 19(17-18), 2049-2056.

Datti, B., Sani, I., &Abdulrahman, L. (2020).Determination of the proximate and mineral contents of desert date kernel (Balanitesaegyptiaca) and the physical and chemical characteristics of the kernel oil

ISBN: 978-978-8567-02-8

available in Kano state, Nigeria.*Bayero Journal of Pure and Applied Sciences,* 12(1), 265-271. https://doi.org/10.4314/bajopas.v12i1.40S

International Organization for Standardization. (1993). *Tool-life testing with single-point turning tools* (ISO Standard No. 3685:1993).

Kuram, E., Ozcelik, B., &Demirbas, E. (2013). Environmentally friendly machining: vegetable based cutting fluids. In J. P. Davim (Ed.), *Green Manufacturing Processes and Systems* (pp. 23-47).Springer. https://doi.org/10.1007/978-3-642-33792-5_2

Lawal, S. A., Choudhury, I. A., &Nukman, Y. (2012). Application of vegetable oil-based metalworking fluids in machining ferrous metals a review. *International Journal of Machine Tools and Manufacture*, 52(1), 1-12.

Maanikuu, P. I., Mwinbuabu, M. J., &Abagna, H. N. (2017).Characterization of shea (Vitellariaparadoxa) butter oil as a potential feedstock for biodiesel production in Ghana.*African Journal of Biotechnology*, 16(14), 690-696.

Maranz, S., &Wiesman, Z. (2004). Influence of climate on the tocopherol content of shea butter. *Journal of Agricultural and Food Chemistry*, 52(10), 2934-2937.

Ogala, H., Idris, A. O., &Sani, Y. M. (2018). Extraction and physicochemical analysis of desert date (Balanitesaegyptiaca) seed oil. *Journal of Applied Sciences and Environmental Management,* 22(1), 137-140. https://doi.org/10.4314/jasem.v22i1.21

Ojolo, S. J., Damisa, O., Orisaleye, J. I., &Ogbonnaya, C. (2008).Experimental study of some cutting fluid properties of vegetable oil.*Journal of Engineering and Applied Sciences*, 3(3), 239-243.

Rahim, E. A., &Sasahara, H. (2011).Investigation of tool wear and surface integrity on MQL machining of Ti-6Al-4V using biodegradable oil.*Proceedings of the Institution of Mechanical Engineers, Part B: Journal of Engineering Manufacture*, 225(9), 1505-1511. https://doi.org/10.1177/0954405411404770

Saidat, O. G., Omojola, J., &Olatunji, O. M. (2016).Production of biodiesel from desert date seed oil.*International Journal of Scientific & Engineering Research*, 7(3), 1222-1225.

Sharma, A. K., Tiwari, A. K., & Dixit, A. R. (2016). Effects of Minimum Quantity Lubrication (MQL) in machining processes using conventional and nanofluid based cutting fluids: A comprehensive review. *Journal of Cleaner Production*, 127, 1-18. https://doi.org/10.1016/j.jclepro.2016.03.146

Shashidhara, Y. M., &Jayaram, S. R. (2010). Vegetable oils as a potential cutting fluid an evolution. *Tribology International*, 43(5-6), 1073-1081.

Talib, N., & Rahim, E. A. (2017).Performance of modified jatropha oil in combination with hexagonal boron nitride particles as a bio-based lubricant for green machining.*Tribology International,* 118, 89-104. https://doi.org/10.1016/j.triboint.2017.09.016

Zang, C. U., Bwai, M. D., &Afolayan, M. (2018).Application of Desert Date (Balanitesaegyptiaca) Seed Oil as Potential Raw Material in the Formulation of Soap and Lotion.*Journal of Applied Chemistry,* 11(3), 73-78.

Zareh-Desari, B., &Davoodi, B. (2016).Assessing the lubrication performance of vegetable oil-based nano-lubricants for environmentally conscious metal forming processes.*Journal of Cleaner Production,* 135, 1198-1209.

ISBN: 978-978-8567-02-8

5TH Faculty of Engineering Conference on Engineering Innovation and Economic Policies: Driving Sustainable Industrial Growth in Nigeria

Faculty of Engineering, Bayero University, Kano.

057-Effects of Coconut Shell Ash and Calcium Carbide Residue as Partial Replacement of Cement in Self-compacting Concrete

A. A. Muhammad, B. W. Isah, A. Kamilu and A. A. Bawa

Department of Civil Engineering, Faculty of Engineering, Bayero University Kano

Email: adkabulfathi@gmail.com, bwisah.civ@buk.edu.ng, Abubakarkamiluak@gamil.com, abubakaradam368@gmail.com

Abstract: This study investigates the potential of coconut shell ash (CSA) and calcium carbide residue (CCR) as partial replacements for cement in self-compacting concrete (SCC) to reduce cement consumption and associated carbon emissions. Eight SCC mixes were produced, including a control mix (0% CSA/CCR) and mixes incorporating 2.5–5% CSA and 5–15% CCR by cement replacement, as well as a mix with 10% CCR replacement combined with 2.5% CSA addition. Fresh properties were evaluated using slump flow and sieve segregation resistance tests in accordance with EFNARC guidelines, while hardened properties were assessed through compressive strength, splitting tensile strength, and density tests at 7 and 28 days. All mixes satisfied SCC flowability requirements, with slump flow values ranging from 659 to 810 mm. The incorporation of CSA and CCR improved segregation resistance compared to the control mix. At 28 days, selected mixes achieved compressive strengths between 51.0 and 52.0 MPa, exceeding the target strength of 40 MPa, while splitting tensile strength improved by up to 12.9% relative to the control. The mix containing 10% CCR replacement with 2.5% CSA addition exhibited the most balanced performance in terms of workability, strength, and stability. Overall, the results demonstrate that CSA and CCR can be effectively utilized as sustainable pozzolanic materials in SCC, contributing to reduced cement usage and enhanced environmental sustainability. Further research on long-term durability and higher replacement levels is recommended.

Keywords: Pozzolanic Materials, Sustainable Concrete and Waste Utilization.

1. INTRODUCTION

Concrete is a rigid and strong construction material composed of Portland cement, mineral aggregates (sand and gravel) mix with sufficient water which cause the cement to set and bind all the other ingredients together. Concrete production, from an environmental standpoint, is responsible for a significant amount of toxic gas emissions. Each year, approximately 1.6 billion tons of concrete is manufactured worldwide. The need for cement in the construction industry is rising due to the widespread use of concrete as a building material. Self-compacting concrete is a type of concrete that can be compacted into every corner of a formwork, purely by means of its own weight and without the need for vibrating or compacting (Okamura and Ouchi 2003). However, Mehdipour *et al.,* (2022) said that a novel class of high-performance production concrete known as self-consolidating concrete is distinguished by its capacity to self-consolidate without displaying any appreciable component separation. Research by Shi *et al.,* (2015) regarding the optimal ratios of raw materials that are chosen during the concrete mixture design process to provide concrete with the necessary qualities both in its fresh and hardened forms for a given application. Three essential characteristics that set a high-quality SCC apart from typical concrete are filling capacity, passage ability, and segregation resistance. Likewise, Vivek and Dhinakaran (2017) have stated that self-compaction concrete (SCC) is a concrete that may flow and compact on account of its own weight. When it comes to sites with restricted access and locations of crowded reinforcements, SCC is the most practical choice. Bridges, foundations, and beam-column joints are a few examples. Compared to commonly vibrated concrete (CVC), SCC has the ability to flow and pass, negating the requirement for an external device for compaction. Successful self-compacting concrete, according to Sadhasivam *et al.,* (2021), needs to have high fluidity (to flow under self-weight), high segregation resistance (to maintain uniformity during flow), and enough passing ability (to flow through and around reinforcement without blocking or segregating). Producing SCC with cement is costly which is why many researchers investigated the use of both industrial and agricultural waste as partial replacement of cement in the production of SCC. After all, cement has its detrimental effects on the environment, including high CO_2 emissions (8% of global emissions), energy consumption, resource depletion, and pollution of air, water, and ecosystems (Sulaiman et al., 2024).

The usage of agricultural and industrial waste

ISBN: 978-978-8567-02-8

materials in the construction industries addresses global issues such as environmental problems, building material expenses, raw material shortfalls, and growing energy needs (Singh et al., 2020). Several researchers investigated the application of manufactured and natural pozzolanic components as a partial substitute for Portland cement (PC), which would reduce the use of cement, conserve energy, and minimize toxic pollutants in the surroundings (Rahman & Al-Attar, 2021). The usage of synthetic pozzolanic components also solves landfilling issues of industrial waste (Zhang & Kwan, 2022).

The use of eggshell powder and fly ash in SCC improve strength, chemical resistance and workability of SCC Hilal et al. (2022). Also Palm oil fuel ash (Sua-iam et al. 2021), sugarcane bagasse ash (Karthikeyan et al. 2020) have successfully been used to partially replace cement in SCC with improved strength and workability. This Research explored the use of Calcium carbide residue (CCR) and coconut shell ash (CSA) (industrial and agricultural waste) as partial replacement of cement in SCC. CCR is reached in calcium while CSA is reach in silica to enhance pozzolanic reaction in the mixture.

2. MATERIALS AND METHODOLOGY

2.1 Materials

The materials used in this research are: Cement, CCR, CSA, fine aggregate, coarse aggregate and super plasticizers. The Standard Portland Cement (42.5 N Dangote brand) used for this research was purchased from an open market in Kano. The CCR was sourced from local welders around Kano city, ground, and sieved to pass a 150 µm sieve. For the CSA, the Coconut shell (SH) was sourced from within Kano city, and it was burned, milled and sieved to pass a 150 µm sieve to produce Coconut Shell ash (CSA). The fine and coarse aggregates were purchased from a nearby service providers. The Conplast SP430 super plasticizer used in this research, was sourced from Civil Engineering Laboratory, Bayero University Kano.

2.2 Mix Proportion

For this research, the concrete mix design was adapted and modified from a workshop manual Mohammad (2021).

The components of the concrete were mixed manually in the laboratory. The water-cement ratio was kept at 0.45, and the superplasticizer of 1.05 Liters per 100kg of cement. Table I portrayed the mix design for each mix ID.

2.3 *Specimen Preparation and Testing Methods*

The concrete specimens were prepared based on the mix design provided in Table I. For each mix ID, the proportion of the materials were measured and mixed properly. Following the mixing, the fresh properties of each mix ID was evaluated through slump and sieve resistance tests. All the tests on fresh properties of concrete were done as per EFNARC guidelines for self-compacting concrete. Slump flow test was similar to conventional slump test, but the spread diameter of the flow-able concrete was measured here instead of subsidence in height (Figure 1). A cone with smaller opening of 100 mm at the top and 200 mm at the base of the 300 mm height slump conical mold was used.

Self-compacting concrete (SCC) requires high workability without segregation, ensuring uniform distribution of aggregates and mortar during placement (EFNARC, 2005). The sieve resistance test, per BS EN 12350-11:2010, measured segregation resistance by determining the proportion of mortar passing a 5 mm sieve, expressed as the segregation ratio (SR).

TABLE I: SUMMARY OF MIX DESIGN QUANTITY OF MATERIALS FOR THE PRODUCTION OF SCC SAMPLES

MIX ID	% replacement	Cement Kg/m^2	Fine Kg/m^2	Coarse Kg/m^2	Water Kg/m^2	CSA	CCR
M1	SSC-CC	520	860	900	234	0	0
M2	CSA2.5CCR5	481	860	900	234	13	26
M3	CSA2.5CCR10	455	860	900	234	13	52
M4	CSA2.5CCR15	429	860	900	234	13	78
M5	CSA5.0CCR5.0	468	860	900	234	26	26
M6	CSA5.0CCR10	442	860	900	234	26	52
M7	CSA5.0CCR15	416	860	900	234	26	78
*M8	CSA2.5CCR10	468	860	900	234	13	52

*not replacement only. 10% of CCR replaces cement and 2.5% CSA is added

Cubes were casted with the mold having dimensions of 100mm x100mm x 100mm. Cylinders were also casted with mold having dimensions of 100mm diameter and 200mm height. Then it was cured in water tank for the period of 7 and 28 days. The concretes cubes were tested for compressive strength test and density while the cylinders were used for splitting tensile test. Atleast 3 specimens were tested for each ID and average was taken.

3. RESULTS AND DISCUSSION

3.1 Slump Test

Figure 2 displayed the findings of a slump test performed on freshly mixed concrete with varying CSA-CCR content percentages. From the results it can be showed that as the amount of CSA-CCR grew, so did the workability decrease because of the grain properties of



Figure 1: SCC Slump Test

ISBN: 978-978-8567-02-8

CSA it adsorbs a lot of water, but the value still falls within the range 650 mm-800 mm EN 12350-2 (2002). It

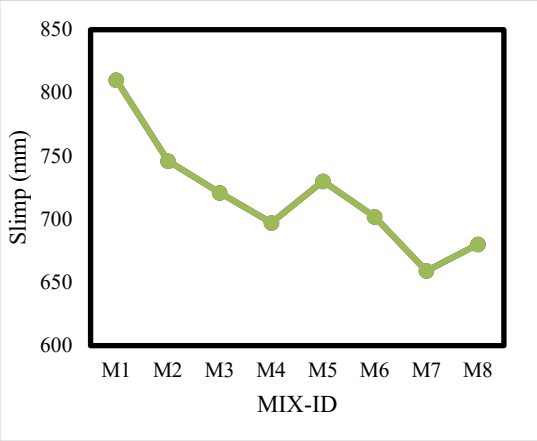


Figure 2: Comparison of Slump Test Results for Various Mix IDs

was found that when the CSA-CCR content increases, the concrete became sticky, requiring more water and plasticizers for better workability.

3.2 Sieve Resistance

The sieve segregation resistance test (BS EN 12350-11:2010) evaluated the stability of fresh self-compacting concrete (SCC) mixes, targeting a segregation index (SR, % mass passing a 5 mm sieve) of ≤ 15% (SR2-class, EFNARC, 2005) for structural applications. Table II displayed the results of sieve resistance test conducted. The control mix (M-Control, 0% CSA/CCR) and experimental mixes (M-CSA2.5+CCR5, M-CSA2.5+CCR10, M-CSA2.5+CCR15, M-CSA5+CCR5, M-CSA5+CCR15; M-CSA2.5add+CCR10: 10% CCR replacing cement + 2.5% CSA addition) used Dangote cement (CEM II 42.5), granite (14 mm), sand, water (0.4 w/p), and super plasticizer.

SR values (10–16%) meet SCC standards (SR ≤ 20%), with M-CSA2.5add+CCR10 (10%), M-CSA2.5+CCR15 (11%), M-CSA2.5+CCR10, M-CSA5+CCR15, M-CSA5+CCR5 (12–12.5%) achieving SR2-class (≤ 15%), indicating high stability. M-Control (16%) showed higher segregation risk. CSA reduced SR (M-CSA5+CCR5, M-CSA2.5+CCR10, M-CSA5+CCR15, M-CSA2.5+CCR15: 11–12.5%), enhancing cohesion (Bheel et al., 2020). High CCR improved stability (M-CSA2.5+CCR10, M-CSA5+CCR15, M-CSA2.5+CCR15, M-CSA2.5add+CCR10: 10–12%), but M-CSA2.5+CCR15's low strength (20.2 MPa) suggests defects (Nath et al., 2019). M-CSA5+CCR5, M-CSA2.5+CCR10, M-CSA5+CCR15, and M-CSA2.5add+CCR10 are optimal for reinforced structures.

TABLE II COMPARISON OF SIEVE RESISTANCE RESULTS FOR VARIOUS MIX IDS

S/N	MIX ID	Sieve Resistance (%)
1	M-Control	16
2	M-CSA2.5+CCR5	14
3	M-CSA2.5+CCR10	13
4	M-CSA2.5+CCR15	12
5	M-CSA5+CCR5	14
6	M-CSA5+CCR10	12
7	M-CSA5+CCR15	11
8	M-CSA2.5add+CCR10	10

3.3 Compressive Strength and Density Tests

The results of the compressive strength test on hardened concrete are shown in Figure 3. Compressive strength of CSA-CCR concrete increased with curing age. The rise in strength with higher CSA-CCR content may result from additional calcium silicate hydrates (C-S-H) formed via the pozzolanic reaction of CSA-CCR with cement oxides, alongside reactions of CSA and CCR pozzolana within concrete pores, enhancing strength as curing progresses. However, CSA-CCR inclusion may saturate the cement blend with K_2O and MgO oxides, potentially forming composites that reduce strength through altered C-S-H hydration (Suleiman & Aliyu, 2020).

The 28-day compressive strength test (BS EN 12390-3:2009) and density test (BS EN 12390-7:2009), conducted on 100 mm cubes, evaluated the structural performance and material packing of self-compacting concrete (SCC) mixes, targeting grade 40 for structural applications. Compressive strengths and densities (7-day and 28-day) reflect the influence of coconut shell ash (CSA, 2.5–5% replacement or addition) and calcium carbide residue (CCR, 5–15% replacement) in mixes M-CSA2.5+CCR5, M-CSA5+CCR5, M-CSA2.5+CCR10, M-CSA2.5+CCR15, M-CSA5+CCR10, M-CSA5+CCR15, and M-CSA2.5add+CCR10, compared to M-Control (0% CSA/CCR).

The 28-day compressive strengths demonstrate excellent structural capacity for most mixes, with M-CSA2.5add+CCR10 (52.0 MPa, 10% CCR + 2.5% CSA addition), M-CSA5+CCR5 (51.7 MPa, 5% CSA + 5% CCR), M-CSA5+CCR10 (51.0 MPa, 5% CSA + 10% CCR), and M-CSA2.5+CCR5 (50.8 MPa, 2.5% CSA + 5% CCR) significantly surpassing the 40 MPa target, indicating suitability for structural elements like slabs and beams. M-Control (49.5 MPa) exceeded typical SCC controls (44.7 MPa, Muhammad, 2021), reflecting robust cement and aggregates. M-CSA2.5+CCR15 (47.5 MPa, 2.5% CSA + 15% CCR) and M-CSA5+CCR15 (41.2 MPa, 5% CSA + 15% CCR) met C40, though lower strength at higher CCR suggests reduced efficacy. M-CSA2.5+CCR10 (32 MPa, 2.5% CSA + 10% CCR) was a critical outlier, failing to reach C40, rendering it unsuitable without reformulation.

Seven-day density (2400–2650 kg/m³) aligns with SCC standards (2300–2600 kg/m³, EFNARC, 2005), with M-Control (2650 kg/m³) highest due to dense materials. Experimental mixes (2400–2600 kg/m³) showed lower density due to CSA and CCR, decreasing with higher CCR: M-CSA2.5+CCR5, M-CSA5+CCR5, M-CSA2.5add+CCR10 (2600 kg/m³, 5–10% CCR) > M-CSA2.5+CCR15 (2550 kg/m³, 15% CCR) > M-CSA5+CCR10 (2500 kg/m³, 5% CCR) > M-CSA5+CCR15 (2450 kg/m³, 10% CCR) > M-CSA2.5+CCR10 (2400 kg/m³, 15% CCR). 28-day density (2400–2710 kg/m³) shows a 1–3% increase for CSA mixes (M-CSA2.5+CCR5, M-CSA5+CCR5, M-CSA5+CCR10, M-CSA2.5add+CCR10: 2520–2680

ISBN: 978-978-8567-02-8

kg/m³) and 0–1% for high-CCR mixes (M-CSA2.5+CCR15, M-CSA5+CCR15, M-CSA2.5+CCR10: 2400–2580 kg/m³) due to hydration densifying the paste, with M-Control reaching 2670–2710 kg/m³.

CSA's pozzolanic activity (58% SiO_2, ~150 µm) enhanced compressive strength, with 5% CSA (M-CSA5+CCR10: 51.0 MPa) and 2.5% CSA (M-CSA2.5+CCR5: 50.8 MPa, M-CSA5+CCR5: 51.7 MPa) outperforming M-Control (49.5 MPa), as C-S-H gel formation increased paste density and strength (Bheel et al., 2020). M-CSA2.5add+CCR10's 2.5% CSA addition (52.0 MPa, 2600 kg/m³) maximized strength by boosting binder mass, surpassing replacement mixes (M-CSA5+CCR5: 51.7 MPa, M-CSA5+CCR15: 41.2 MPa). M-CSA2.5+CCR10 (20.2 MPa, 2400 kg/m³) caused significant declines. M-CSA2.5+CCR10's low density and strength suggest voids or segregation, with M-CSA5+CCR15's moderate reduction (41.2 MPa, 2450 kg/m³) indicating a threshold at 15% CCR.

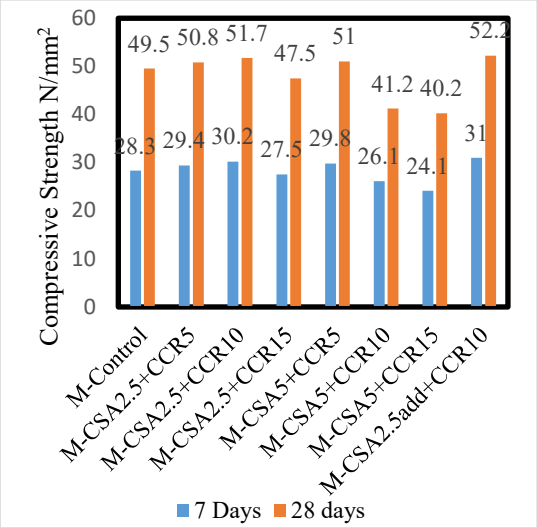


Figure 3: Comparison of Compressive Strength of various mix IDs

Figure 4 showed the densities of concrete cubes with CSA-CCR as partial replacement of cement in various

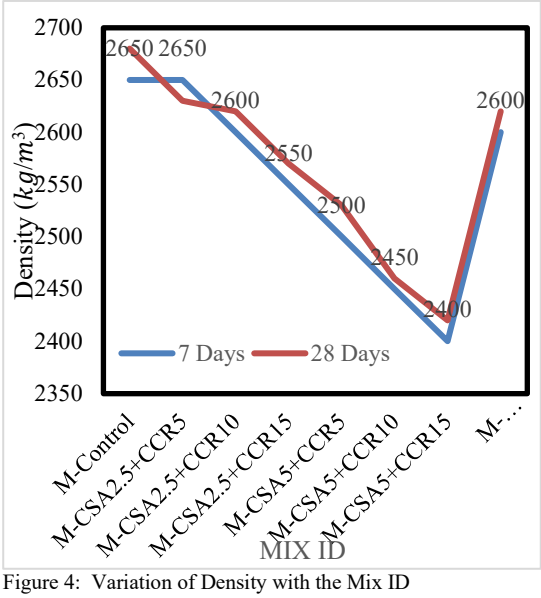


Figure 4: Variation of Density with the Mix ID

percentages at 7 and 28 days. It is observed that the densities are decreasing with an increase in CSA-CCR content.

The progressive reduction in concrete density with increasing Coconut Shell Ash (CSA) and Calcium Carbide Residue (CCR) content is attributed to the lower specific gravity and porous nature of these supplementary materials compared to ordinary Portland cement. As cement is partially replaced by CSA and CCR, heavier cementitious constituents are substituted with lighter materials, resulting in a decrease in overall density. In addition, higher replacement levels reduce particle packing efficiency and increase internal porosity, further contributing to density loss. This trend is consistent with findings reported in similar studies on agricultural ash- and CCR-blended concretes (Neville, 2011; Mehta & Monteiro, 2014; Olutoge & Olasunkanmi, 2014).

3.4 Splitting Tensile Strength Test

The tensile strength of the concrete has a major impact on the size and extent of cracks in concrete structures. Cracks begin to show when the concrete's tensile strength exceeds the designated limit. This test was carried out according to BS-EN 12390-3 (2002) on the CSA-CCR concrete cylinder cured in water at 7 and 28 days. The outcome was displayed in the Figure 5. It was observed that the splitting strength increase with increase in curing days but varies in percentage replacement of CSA-CCR.

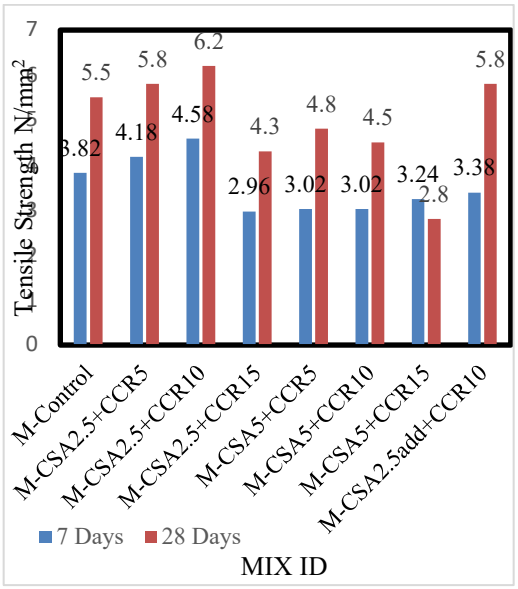


Figure 5: Variation of Splitting Tensile Strength with the Mix ID

CONCLUSION

This study evaluated the feasibility of using coconut shell ash (CSA) and calcium carbide residue (CCR) as partial replacements for cement in self-compacting concrete (SCC). The results confirmed that all mixes satisfied SCC flowability requirements in accordance with BS EN 12350-11:2010, with slump flow values ranging between 659 and 810 mm. While the control mix exhibited higher flowability, it showed increased

ISBN: 978-978-8567-02-8

segregation risk, whereas CSA–CCR blended mixes demonstrated improved stability with adequate workability.

The compressive strength results showed that selected CSA–CCR combinations significantly enhanced the structural performance of SCC. At 28 days, mixes M-CSA5+CCR5, M-CSA5+CCR10, and M-CSA2.5add+CCR10 achieved compressive strengths between 51.0 and 52.0 MPa, exceeding the target strength of 40 MPa and outperforming the control mix. However, excessive CCR replacement (15%) led to a reduction in strength, indicating an optimal replacement threshold.

Splitting tensile strength followed a similar trend, with M-CSA5+CCR5 and M-CSA2.5add+CCR10 showing improvements of approximately 12.9% and 5.6%, respectively, compared to the control. Overall, the mix containing 10% CCR replacement with 2.5% CSA addition (M-CSA2.5add+CCR10) was identified as the optimum formulation, providing a balanced combination of workability, compressive strength, tensile performance, and segregation resistance. The findings demonstrate the potential of CSA and CCR as sustainable pozzolanic materials for producing eco-friendly self-compacting concrete while reducing cement consumption and associated CO_2 emissions.

ACKNOWLEDGMENT

The authors acknowledge the guidance and technical support of their project supervisor, whose expertise and constructive advice were invaluable to the successful completion of this work. Appreciation is also extended to the Head of the Department of Civil Engineering, the academic and non-academic staff of the department, and the personnel of the concrete laboratory for their assistance and support. The authors further acknowledge the encouragement and support of their families and colleagues throughout the course of this research.

REFERENCES

Ali, M., Saidur, R., & Hossain, M. S. (2019). A review on emission analysis in cement industries. Renewable and Sustainable Energy Reviews, 115, 109341. https://doi.org/10.1016/j.rser.2019.109341.

Bheel, N., Ali, M., Safiq, N. C., & Almujibah, H. R. (2020). Use of agro-waste materials as cement replacement in oconcrete towards environmental sustainability. IOP Conference Series: Materials Science and Engineering, 991(1), 012051. https://doi.org/10.1088/1757-899X/991/1/012051.

Chen, X., & Yang, H. (2020). Mechanical and durability properties of concrete incorporating calcium carbide residue as cement replacement. Construction and Building Materials, 247, 118579. https://doi.org/10.1016/j.conbuildmat.2020.118579.

EFNARC. (2005). Specification and guidelines for self-compacting concrete. European Federation of National Associations Representing Concrete.

Hilal, N., Mohammed, A. S., & Abduljabbar, H. M. (2022). Eggshell powder as a potential cement replacement and its effect on the durability of concrete. Cleaner Materials, 5, 100112. https://doi.org/10.1016/j.clema.2022.100112.

Jin, Z., Kwon, S., & Park, S. (2021). Pozzolanic materials and their influence on strength and durability of concrete: A review. Materials, 14(3), 550. https://doi.org/10.3390/ma14030550.

Karthikeyan, J., Dhinakaran, G., & Vivek, S. (2020). Mechanical properties of self-compacting concrete incorporating sugarcane bagasse ash. Construction and Building Materials, 250, 118868. https://doi.org/10.1016/j.conbuildmat.2020.118868.

Mannan, M. A., Ganapathy, C., & Hossain, M. U. (2021). Environmental impacts of cement production and mitigation strategies: A review. Journal of Building Engineering, 43, 102544. https://doi.org/10.1016/j.jobe.2021.102544.

Mehdipour, I., Khayat, K. H., & Nokken, M. R. (2022). Performance-based design of self-consolidating concrete: A review. Cement and Concrete Composites, 132, 104621. https://doi.org/10.1016/j.cemconcomp.2022.104621

Mehta, P. K., & Monteiro, P. J. M. (2014). Concrete: Microstructure, properties, and materials (4th ed.). McGraw-Hill Education.

Mohammed, A. (2021). A workshop manual: Concrete mix design. Department of Civil Engineering, Bayero University, Kano, Nigeria.

Nath, P., Sarker, P. K., & Biswas, W. K. (2019). Effect of calcium carbide residue and fly ash on the performance of concrete. Construction and Building Materials, 226, 110–120. https://doi.org/10.1016/j.conbuildmat.2019.07.178.

Neville, A. M. (2011). Properties of concrete (5th ed.). Pearson Education Limited.

Okamura, H., & Ouchi, M. (2003). Self-compacting concrete. Journal of Advanced Concrete Technology, 1(1), 5–15. https://doi.org/10.3151/jact.1.5.

Olutoge, F. A., & Olasunkanmi, B. S. (2014). Performance of coconut shell ash in concrete. International Journal of Engineering Research and Technology, 3(4), 1020–1025.

Omar, W., Abdullah, M. M. A. B., & Tahir, M. F. M. (2018). Utilization of agricultural waste as sustainable construction materials: A review. Journal of Cleaner Production, 172, 306–315. https://doi.org/10.1016/j.jclepro.2017.10.162.

Patel, R., Singh, A., & Sharma, N. (2020). Use of agricultural waste ashes as supplementary cementitious materials: A review. Materials Today: Proceedings, 32(4), 871–876. https://doi.org/10.1016/j.matpr.2020.02.135.

ISBN: 978-978-8567-02-8

Rahman, M. M., & Al-Attar, T. S. (2021). Sustainable concrete using supplementary cementitious materials: A review. Cleaner Engineering and Technology, 4, 100210. https://doi.org/10.1016/j.clet.2021.100210.

Sadhasivam, R., Balamurugan, R., & Ravichandran, A. (2021). Fresh and hardened properties of self-compacting concrete: A review. Materials Today: Proceedings, 45(2), 3981–3986. https://doi.org/10.1016/j.matpr.2020.12.482.

Shi, C., Wu, Z., Lv, K., & Wu, L. (2015). A review on mixture design methods for self-compacting concrete. Construction and Building Materials, 84, 387–398. https://doi.org/10.1016/j.conbuildmat.2015.03.079.

Singh, R., Bhattacharyya, S. K., & Gupta, S. (2020). Sustainable utilization of industrial and agricultural waste in construction materials. Journal of Cleaner Production, 273, 123098. https://doi.org/10.1016/j.jclepro.2020.123098.

Sua-iam, G., Makul, N., & Sangngam, T. (2021). Palm oil fuel ash as a supplementary cementitious material in self-compacting concrete. Journal of Materials Research and Technology, 14, 1931–1943. https://doi.org/10.1016/j.jmrt.2021.07.047.

Sulaiman, T. A., Ahmad, S., & Yusuf, M. O. (2022a). Agricultural waste generation and its utilization in concrete production. Cleaner Materials, 4, 100065. https://doi.org/10.1016/j.clema.2022.100065.

Sulaiman, T. A., Ahmad, S., & Yusuf, M. O. (2024). Environmental and economic impacts of cement replacement with agricultural waste ash. Journal of Sustainable Cement-Based Materials, 13(1), 1–18. https://doi.org/10.1080/21650373.2023.2280197.

Vivek, S., & Dhinakaran, G. (2017). Fresh and hardened properties of self-compacting concrete: A review. Journal of Building Engineering, 13, 1–10. https://doi.org/10.1016/j.jobe.2017.06.003.

Zhang, M., & Kwan, A. K. H. (2022). Recycling industrial by-products as cementitious materials: Environmental benefits and challenges. Resources, Conservation & Recycling, 180, 106184. https://doi.org/10.1016/j.resconrec.2022.106184.

ISBN: 978-978-8567-02-8

5TH Faculty of Engineering Conference on Engineering Innovation and Economic Policies: Driving Sustainable Industrial Growth in Nigeria

Faculty of Engineering, Bayero University, Kano.

058-Design and Simulation of a Filtering Antenna for Wireless Local Area Network (WLAN) Applications

M. Ali [1], S. A Babale [2*]., S. H. Lawan[3]

[1]Department of Computer Engineering, Federal University Wukari, Taraba State.
[2] Department of Electronics and Telecommunications Engineering, Ahmadu Bello University, Zaria, Nigeria
[3] Department of Telecommunications Engineering, Faculty of Engineering, Bayero University Kano, Kano, Nigeria.
*Corresponding author Email: sababale@abu.edu.ng

Abstract: This paper presents the design and simulation of a compact filtering antenna (filtenna) optimized for 2.4 GHz Wireless Local Area Network (WLAN) applications. The proposed structure integrates a rectangular microstrip patch antenna with a third-order Chebyshev hairpin bandpass filter using a direct-feed and shared ground configuration. Simulations performed using CST Studio Suite 2019 reveal a return loss of –40 dB, a gain of 1.47 dBi, and a radiation efficiency of 22%. These results demonstrate effective integration of filtering and radiation functions, indicating the filtenna's suitability for compact and efficient wireless systems

Keywords: Filtenna, microstrip patch antenna, hairpin filter, WLAN, CST simulation

1. INTRODUCTION

The rapid advancement of wireless communication technologies has led to a growing demand for compact, high-efficiency, and high-performance radio frequency (RF) front-end components. Conventionally, antennas and filters are implemented as separate entities, which often results in increased insertion losses, signal degradation, and larger device footprints. To address these limitations, researchers have introduced filtering antennas (filtennas), which combine both radiation and filtering functionalities into a single, integrated structure. Various filtenna designs have been reported in literature, each aiming to achieve a balance between compact size, filtering functionality, and radiation efficiency. In (Lin & Chung, 2011), the challenge of limited bandwidth in conventional patch antennas was addressed by integrating a quasi-elliptic function using a U-shaped radiating patch combined with a T-shaped resonating filter. This configuration achieved a fractional bandwidth of 2% at 5 GHz, nearly double that of a conventional patch antenna, while maintaining similar radiation characteristics. To improve gain flatness and passband selectivity, (Chen et al., 2013) proposed a compact filtering antenna that integrates a two-pole Butterworth bandpass filter with a fan-shaped patch antenna using a DGS. The fan-shaped patch simultaneously acts as the radiator and the second resonator, resulting in a bandwidth of 460 MHz (2.4 GHz center frequency), 2.3 dBi peak gain, and a radiation zero at 3 GHz for improved selectivity. In (Wu et al., 2011), the trade-off between compactness and bandwidth was tackled by combining two microstrip square open-loop resonators with a Γ-shaped antenna. The design achieved a 14% fractional bandwidth at 2.45 GHz, with measured results confirming a 16.3% impedance bandwidth (2.26–2.66 GHz) and a maximum gain of 2.41 dBi, demonstrating compactness with wideband operation. The problem of band-edge gain selectivity was investigated in (Chen & Luo, 2014), where a composite right-/left-handed (CRLH) resonator was integrated with an octagonal patch and DGS. This design achieved 430 MHz bandwidth at 5.29 GHz, with 2.5 dBi gain in-band and 10 dBi rejection out-of-band, ensuring effective suppression of unwanted signals. A different challenge sharp skirt selectivity was addressed in (Jadhav & Deore, 2017) through the integration of a fifth-order Chebyshev bandpass filter with a radiating element. The resulting filtenna operated at 2.45 GHz, offering a fractional bandwidth of 12.24% and a gain of 3.5 dBi, making it suitable for wireless systems requiring precise passband control. Maintaining omnidirectional radiation while filtering unwanted signals was the focus in (Yu et al., 2012), where a planar coaxial collinear radiator was combined with an inductive window bandpass filter for Ku-band applications. The filtenna exhibited linearly polarized omnidirectional radiation, with measured gains of 7.7–7.9 dBi, while introducing only ~1.1 dB loss from the integrated filter. In (Sahu et al., 2018), the challenge of harmonic suppression was resolved using a modified elliptic monopole integrated with an interdigital bandpass filter (IBPF). The design covered 1.01–1.96 GHz, achieving broadband operation with unwanted harmonic suppression up to 8 GHz and omnidirectional radiation. The issue of achieving wideband response with high selectivity was considered in (Wang et al., 2019a), where an annular ring surrounded by a hexagonal patch and shorting vias was employed. A copper top hat further enhanced performance, yielding a 30.2% impedance bandwidth (2.05–2.78 GHz), average gain of 6.5 dBi, and >15 dB out-of-band suppression. To improve filter–

ISBN: 978-978-8567-02-8

antenna integration, (Cui et al., 2020) introduced a multilayer co-designed structure where resonators on dual substrates were coupled to a T-shaped radiator. The design achieved 2.7% bandwidth, 2.2 dBi gain, and −20 dB out-of-band rejection, but with increased fabrication complexity. In (Wang et al., 2019b), the challenge of selectivity at band edges was addressed through a differential filtenna composed of three different-sized patches, a slot, and differential feeding lines. The design achieved 9.9% bandwidth and a 7.5 dBi average gain, demonstrating significant improvement in band-edge performance. The issue of low sidelobe levels (SLL) in array antennas was tackled in (Nie et al., 2022) using a 4×4 Dolph–Chebyshev distributed filtenna array. The design achieved 14.7 dBi maximum gain, 2% bandwidth, and sidelobe suppression of better than 25 dB, but at the cost of increased array size. For WLAN applications, (Hosain et al., 2019) introduced a compact filtenna based on a monopole configuration with a square loop patch integrated with a bandpass filter at 5.2 GHz. The antenna achieved omnidirectional radiation, good selectivity, and a 2.5 dBi peak gain, though efficiency was not emphasized. In (Chen et al., 2022), the challenge of enhancing both bandwidth and selectivity was solved using a rectangular patch integrated with dual U-shaped patches fed via dual ground slots. The prototype achieved a 21.5% impedance bandwidth (4.45–5.52 GHz), 4.8 dBi gain, and 15.9 dB out-of-band suppression, showing promise for compact multiband arrays. For 5G base station applications, (Aliyu et al., n.d.) presented a design that integrated a diamond-shaped patch with open-loop resonators. A single element achieved 5.98 dBi gain, while a 1×4 array increased in-band gain to 8.07 dBi, demonstrating scalability for sub-6 GHz 5G MIMO systems. Finally, (Abdelghany et al., 2023) addressed the challenge of frequency reconfigurability for cognitive radio systems by integrating a wideband monopole with a varactor-tuned bandpass filter. The antenna dynamically covered 1.75–3 GHz, achieving measured gains between 4.54–5.05 dBi with good return loss (|S11| ≤ −10 dB), making it suitable for dynamic spectrum allocation.

Overall, while numerous filtenna designs offer strong gain or wide bandwidth, they often rely on complex geometries or expensive substrates. This paper presents a compact, low-cost filtering antenna based on FR4 substrate by integrating a rectangular microstrip patch antenna with a third-order Chebyshev hairpin bandpass filter for 2.4 GHz WLAN applications, achieving excellent impedance matching with a simple and fabrication-friendly structure.

2. METHODOLOGY

2.1. Antenna Model

The mathematical model to be used in designing microstrip patch antennas typically includes parameters such as antenna's dimension, resonant frequency, substrate material and feed point location. The above model serves as a useful tool for initial design decision as adapted in the literature (Balanis, 2016).

$$W = \frac{c}{2f_c}\sqrt{\frac{2}{1+\varepsilon_r}} \quad (1)$$

$$\varepsilon_{eff} = \frac{\varepsilon_r + 1}{2} + \frac{\varepsilon_r + 1}{2}\left(\frac{1}{\sqrt{1+\frac{12h}{w}}}\right) \quad (2)$$

$$L_{eff} = \frac{c}{2fo\sqrt{\varepsilon_{eff}}} \quad (3)$$

$$\Delta L = 0.412h\frac{(\varepsilon_{eff}+0.3)(\frac{w}{h}+0.264)}{(\varepsilon_{eff}-0.258)(\frac{w}{h}+0.8)} \quad (4)$$

$$L = L_{eff} - 2\Delta L \quad (5)$$

$$W_f/h = \frac{8exp(A)}{EXP(2A)-2}\ for\ \frac{w}{h} \le 2 \quad (6)$$

$$Z_{in} = Z_{edge}\cos^2(\tfrac{\pi y_0}{L}) \quad (7)$$

$$L_S = L_g = 6h + L \quad (8)$$

$$W_S = W_g = 6h + w \quad (9)$$

$$W_{pt} = 6W_f \quad (10)$$

$$L_{pt} = 5S + t \quad (11)$$

Where w represents the width of the patch element, fc stands for center frequency, h is the Hight of the substrate, L donate the length of the patch Δl account for the alteration in length due to fringing effect, ε_{eff} reflect effective dielectric constant L_{eff} signifies the patch effective length ε_r indicate dielectric constant c velocity of light, Ws and Ls represent width And length of the ground plane while Wf and Lf donate width and length of the feedline line.

Based on the above model, a rectangular microstrip patch antenna operating at 2.4 Ghz was designed and optimized. Fig 1, depicts the top view geometry of rectangular patch antenna. The antenna was design and simulated using FR4 substrate having a thickness of 1.6mm, dielectric constant of 4.4 and loss tangent of approximately of 0.002.

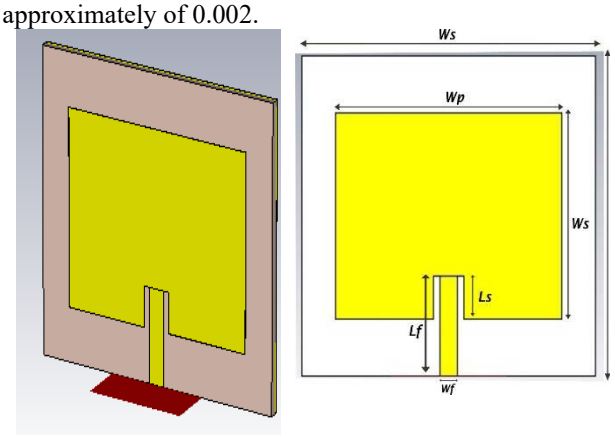


Figure 1. Layout of microstrip patch antenna

The dimensions of the patch antenna marked in Fig. 1. is summarized in table 1.

ISBN: 978-978-8567-02-8

TABLE 1. OPTIMIZED ANTENNA DIMENSION

Parameters	Value
Ws	48mm
Ls	45mm
Lp	29mm
Wp	37mm
Wf	2.9mm
Lf	14mm
H	1.6mm

2.2. Hairpin Bandpass Filter Design Model

The hairpin filter is developed using a third-order Chebyshev prototype with a 0.5 dB passband ripple and a 10% fractional bandwidth. Synthesis equations from Hong and Lancaster are utilized to derive the element values. Coupling coefficients and external quality factors (Qe) are calculated based on standard design tables. The physical layout is optimized using electromagnetic simulations in CST Studio Suite. (Hong, 2011)

$$Q_{e1} = \frac{g_0 g_1}{FBW}, Q_{en} = \frac{g_n g_{n+1}}{FBW}, for\ n = 1, to\ n-1 \quad (12)$$

$$K_{i,i+1} = \frac{FBW}{\sqrt{g_i g_{i+1}}}, for\ i = 1, to\ n-1 \quad (13)$$

$$\lambda g = \frac{c}{f_c \sqrt{\varepsilon_{effR}}} \quad (14)$$

$$L_R = \frac{\lambda g}{4} \quad (15)$$

Where g's are the prototypes element values and N is the order of the filter, Q_{e1} and Q_{en} are the external quality factor of the resonator at the input and output and FBW are the fractional bandwidth $K_{i,i+1}$ are the coupling coefficient between the adjacent resonators, (λ_g) is the Guided wavelength, (L_R) is the Resonator length .Based on the above model, a hairpin bandpass filter operating at 2.4 Ghz was designed and optimized. For the space between the adjacent resonator, EM simulation was carried out for estimating the tapping position and for space or gaps between the adjacent resonator coupling using FR4. Fig 2, depicts the top view geometry of the filter. The filter was design and simulated using FR4 substrate having a thickness of 1.6mm, dielectric constant of 4.4 and loss tangent of approximately of 0.002.

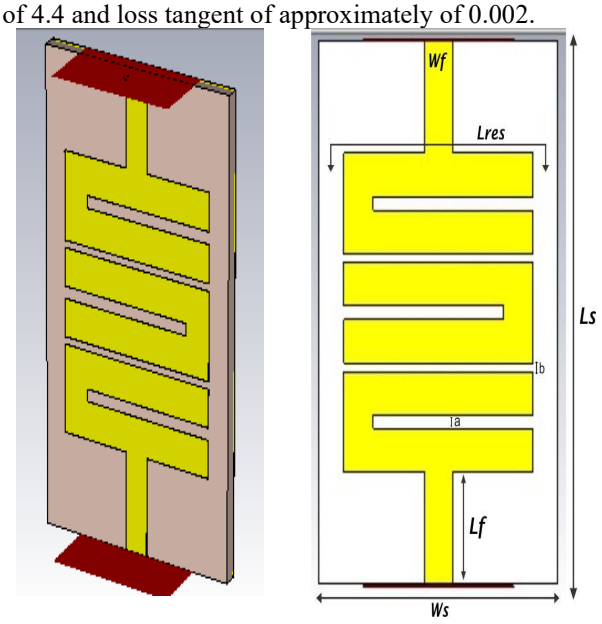


Figure 2. hairpin bandpass filter.

The dimensions of the filter marked in Fig 2. Above are summarized in table 2 below.

Table 2. optimized filter dimension

Parameters	Value
Ws	25mm
Ls	38.8mm
Lres	19.775mm
Lf	8mm
Wf	2.9mm
A	1mm
b	0.6mm

2.3. Microstrip Filtering Antenna Design (filtenna)

The filter's output is directly linked to the feedline of the patch antenna, and both components share a common ground plane. This configuration supports electrical continuity and reduces the overall footprint. The combined structure is modeled and simulated using CST, ensuring proper coupling between the filter and antenna. Layout of the filtenna is shown in figure 3.

ISBN: 978-978-8567-02-8

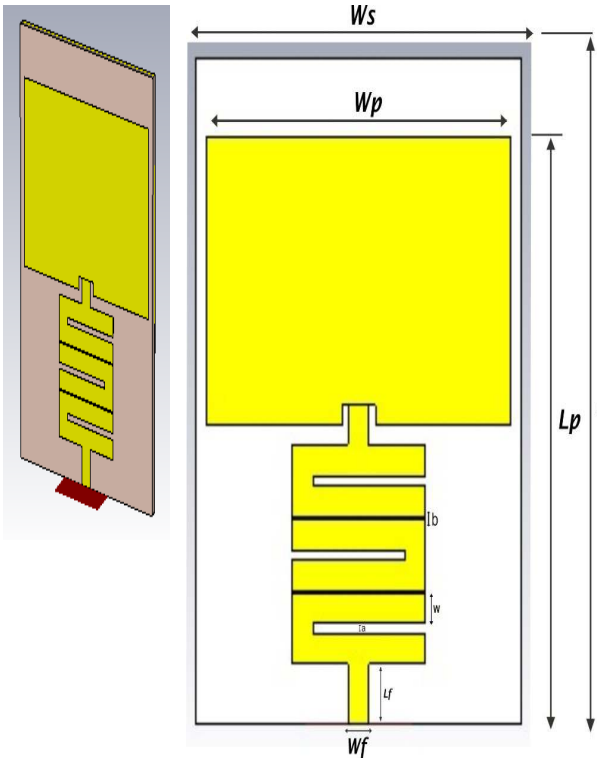


Figure 3. filtenna layout.

The dimensions of the filtenna marked in Fig 3. is summarized in table 3.

TABLE 3. OPTIMIZED FILTENNA DIMENSION

Parameters	Value
Ws	48mm
Ls	45mm
Lp	29mm
Wp	45mm
Wf	3.09mm
Lf	6mm
H	1.6mm
a	1mm
b	0.2mm

3. RESULTS AND DISCUSSION

3.1. Antenna and Filter Performance

The microstrip patch antenna designed for 2.4 GHz was simulated using CST Studio Suite 2019. The S-parameter response indicates a strong resonance at the operating frequency with an S_{11} of -38 dB, demonstrating excellent impedance matching and efficient power delivery to the radiator, as shown in Figure 4 below. The antenna further achieved a realized gain of 3.1 dBi,as shown in fig 5, which is consistent with FR-4 based structures were dielectric losses limit gain performance. The radiation pattern exhibits a broadside characteristic, with stable E-plane and H-plane distributions, confirming effective radiation toward the normal direction of the patch surface, as presented in Figure 6.

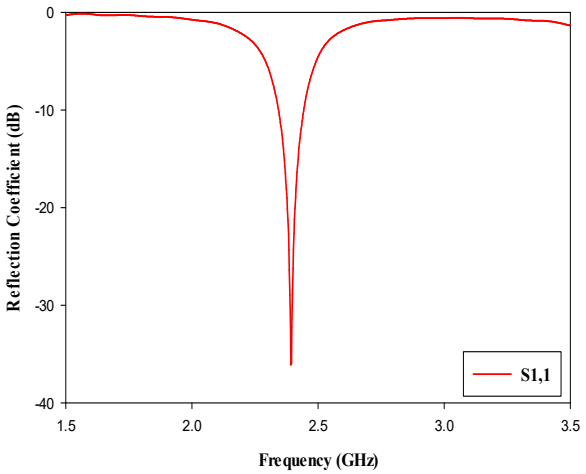


Figure 4. Antenna S-parameters.

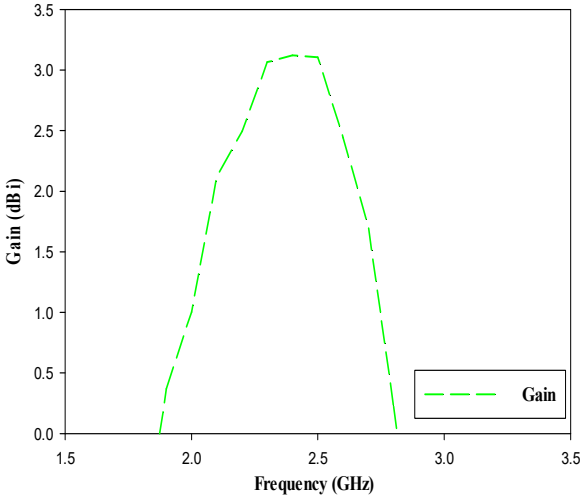


Figure 5. Antenna Gain.

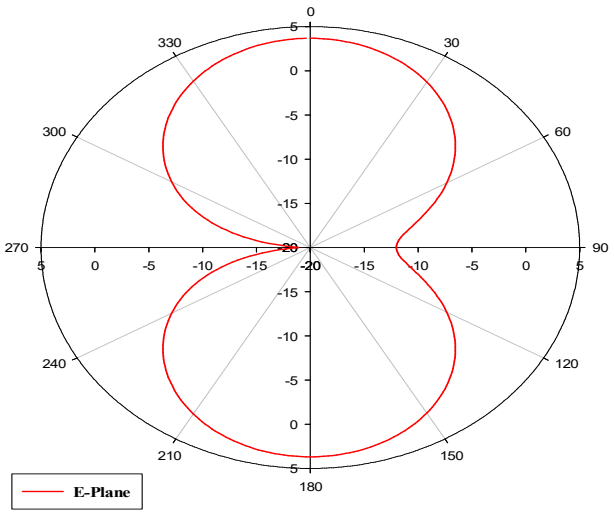


Figure 6. Antenna E-plane Radiation Pattern

ISBN: 978-978-8567-02-8

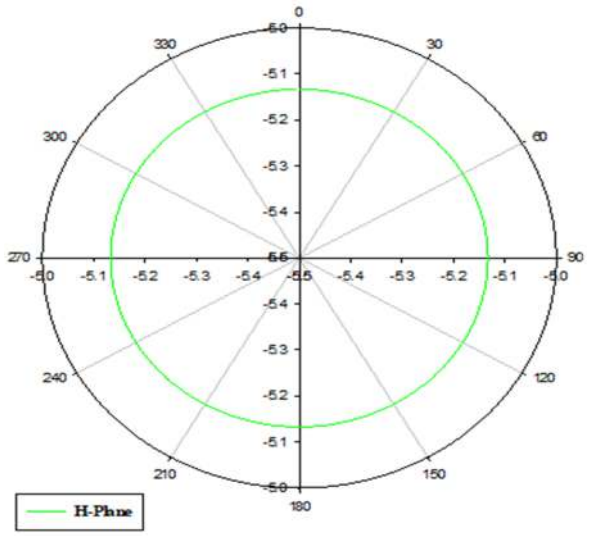


Figure 7. Antenna H-plane Radiation Pattern

The third-order Chebyshev hairpin bandpass filter also shows satisfactory performance. The simulated S_{21} response reveals a clear passband centered at 2.4 GHz, while the S_{11} plot demonstrates good matching and strong rejection outside the band, confirming the intended selectivity of the filter. These characteristics indicate proper coupling between the resonators and effective frequency discrimination, as illustrated in Figure 8.

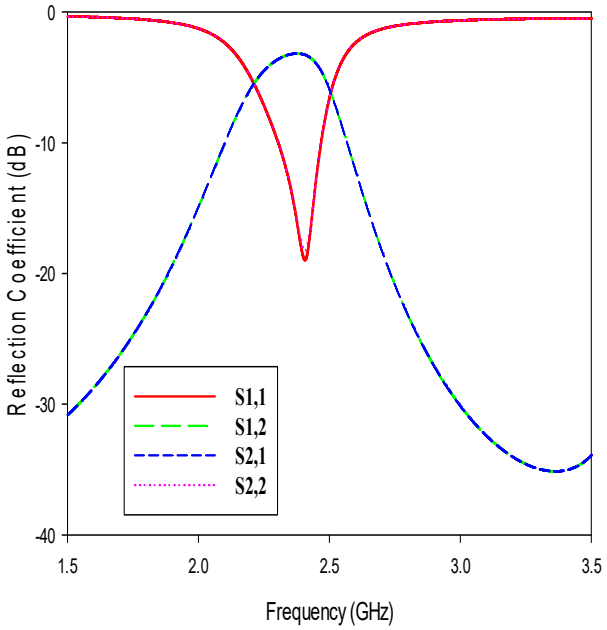


Figure 8 filter S-parameters

3.2. Filtenna Performance

After integrating the hairpin filter with the patch antenna, the combined filtenna structure was simulated. The filtenna maintains resonance at 2.4 GHz, with an S_{11} value close to –40 dB, demonstrating that integration did not degrade impedance matching, as shown in Figure 9. However, the realized gain reduces to 1.47 dBi as shown in fig 10, largely due to additional losses introduced by the filter section and the FR-4 substrate. Despite the reduction, the gain remains acceptable for short-range WLAN applications. The filtenna preserves a broadside radiation pattern, similar to the standalone antenna, as shown in Figure 11 and 12, indicating that the filter does not distort the primary radiation characteristics. Future improvements may include the use of low-loss FR4 variants, optimized resonator spacing, or partial ground modification to recover some gain while maintaining the low-cost advantage

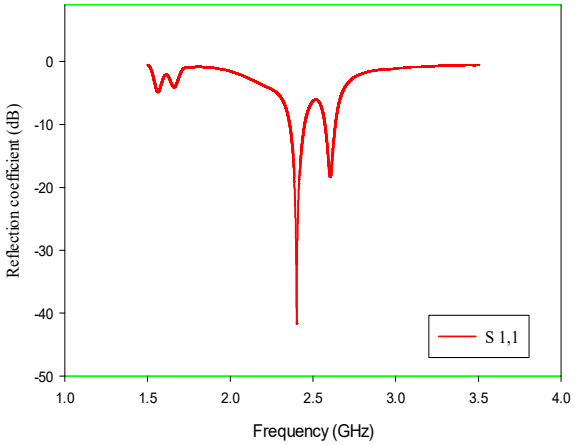


Figure 9. filtenna S-parameters

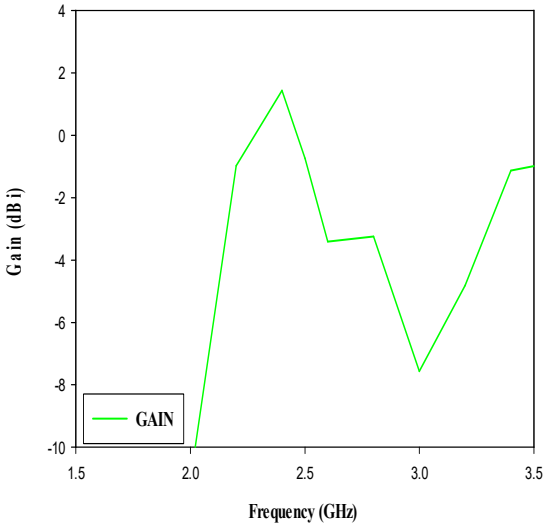


Figure 10. filtenna Gain

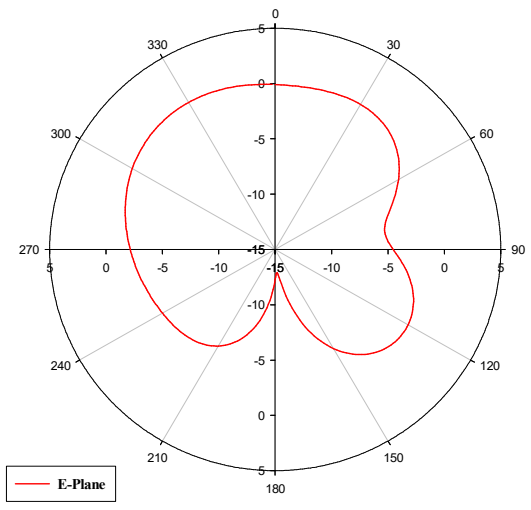


Figure 11. filtenna E-plane Radiation Pattern

ISBN: 978-978-8567-02-8

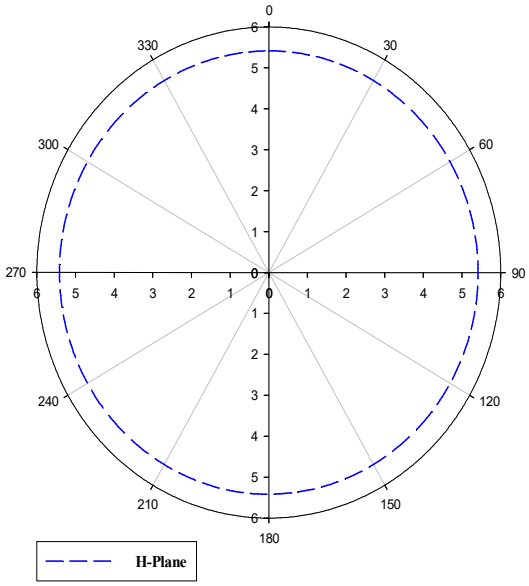


Figure 12. filtenna H-plane Radiation Pattern

3.3. Comparison between patch antenna and filtering antenna.

A comparison between the standalone antenna and the filtenna shows that the antenna's realized gain decreases from 3.1 dBi to 1.47 dBi after integration. This reduction aligns with typical behavior reported in filtenna designs, where added resonant structures increase dielectric and conductor losses.

3.4. Comparative Performance with Existing Literature

The proposed filtenna is benchmarked against selected designs from the literature to highlight its strengths and limitations. As shown in Table 4, many earlier filtennas achieved wider bandwidth or higher gain, but at the cost of larger size, complex structures, or reliance on costly substrates such as Rogers or Taconic. By contrast, the proposed design operates at 2.4 GHz on FR4 with excellent impedance matching (−40 dB), compact footprint (48 × 49 mm²), and stable radiation patterns.

Although its gain (1.47 dBi) and efficiency (22%) are modest, it avoids the fabrication complexity, large array structures, or expensive materials reported in previous works, making it more advantageous for low-cost WLAN applications.

TABLE 4.: COMPARATIVE PERFORMANCE OF PROPOSED FILTENNA WITH PREVIOUS LITERATURE

Ref.	Substrate	Size (mm²)	Frequency / Bandwidth	Gain (dBi)	Return Loss (dB)	Key Limitation
(Lin & Chung, 2011)	Rogers	18 × 15.3	~5 GHz / ~2× patch BW	~2.0	−20	Performance may degrade on FR4; fabrication complexity
(Chen et al., 2013)	FR4	35 × 47	2.4 GHz / 19% (460 MHz)	2.3	−18	Moderate gain, FR4 losses, complex DGS
(Chen & Luo, 2014)	FR4	16.9 × 11.1	5.29 GHz / 8.1% (430 MHz)	2.5	−15	Small size but limited gain
(Jadhav & Deore, 2017)	FR4	40 × 80	2.45 GHz / 12.2%	>3.5	−20	Large footprint, synthesis complexity
(Sahu et al., 2018)	PCB	98 × 98	2.05–2.78 GHz / 30.2%	6.5	−15	Very large, fabrication sensitivity
(Cui et al., 2020)	Rogers	Compact (0.29λg × 0.23λg)	2.6 GHz / 2.7%	2.2	−20	Very narrow bandwidth, low efficiency
(Nie et al., 2022)	Taconic	170 × 151	5.0 GHz / 2%	14.7	−20	Bulky array, complex feeding network
(Aliyu et al., n.d.)	Rogers	Large array	3.5 GHz / moderate BW	5.98 (1×1), 8.07 (1×2)	−20	Large footprint, best for base stations
(Abdelghany et al., 2023)	Rogers	80 × 80	1.75–3.0 GHz (tunable)	4.65 – 5.05	−15	Requires biasing, tuning complexity
Proposed	FR4	48 × 49	2.4 GHz / 4.23% (101.4 MHz)	1.47	−40	Lower gain & efficiency (22%) but compact, simple, low-cost

Unlike many reported designs that rely on high-cost substrates such as Rogers or Taconic, the proposed filtenna employs standard FR4, significantly reducing fabrication cost and making it more suitable for mass-produced WLAN devices

4. CONCLUSION

The patch antenna and third-order hairpin bandpass filter were successfully designed and analyzed for 2.4 GHz WLAN applications. The antenna achieved –38 dB impedance matching, 3.1 dBi realized gain, and a stable broadside radiation pattern, while the filter exhibited a well-defined passband and strong out-of-band rejection. When integrated, the filtenna maintained excellent matching and radiation stability while providing enhanced frequency selectivity. Although the gain reduced to 1.47 dBi, the performance remains adequate for WLAN devices, and the compact combined structure eliminates the need for separate filtering components. The results demonstrate that the proposed filtenna is a practical, cost-effective solution for compact RF front-end systems operating in the 2.4 GHz ISM band. The proposed filtenna achieves an effective trade-off between size, gain, and simplicity.

Its performance is more consistent and practical compared to complex or tunable designs, validating its use for efficient and reliable 2.4 GHz WLAN communication systems. Future work will focus on fabrication and experimental validation of the proposed filtenna, as well as extension to dual-band WLAN operation.

ISBN: 978-978-8567-02-8

REFERENCES

Abdelghany, M. A., Ali, W. A. E., Mohamed, H. A., & Ibrahim, A. A. (2023). Filtenna with frequency reconfigurable operation for cognitive radio and wireless applications. *Micromachines, 14*(1), Article 160. https://doi.org/10.3390/mi14010160

Aliyu, S., Tan, B., Geok, K., Morsi, M. A., Marei, A., Kamal, S., & Rahim, A. (n.d.). *Open loop resonator based filtering antenna for 5G MIMO base station*.

Balanis, C. A. (2016). *Antenna theory: Analysis and design* (4th ed.). Wiley.

Chen, B. J., Yang, X. S., & Wang, B. Z. (2022). A compact high-selectivity wideband filtering antenna with multipath coupling structure. *IEEE Antennas and Wireless Propagation Letters, 21*(8), 1654–1658. https://doi.org/10.1109/LAWP.2022.3176920

Chen, L., & Luo, Y. L. (2014). Compact filtering antenna using CRLH resonator and defected ground structure. *Electronics Letters, 50*(21), 1496–1498. https://doi.org/10.1049/el.2014.2703

Chen, X., Zhao, F., Yan, L., & Zhang, W. (2013). A compact filtering antenna with flat gain response within the passband. *IEEE Antennas and Wireless Propagation Letters, 12*, 857–860. https://doi.org/10.1109/LAWP.2013.2271972

Cui, J., Zhang, A., & Yan, S. (2020). Co-design of a filtering antenna based on multilayer structure. *International Journal of RF and Microwave Computer-Aided Engineering, 30*(2), e22096. https://doi.org/10.1002/mmce.22096

Hong, J.-S. (2011). *Microstrip filters for RF/microwave applications* (2nd ed.). Wiley.

Hosain, M. M., Kumari, S., & Tiwary, A. K. (2019). Compact filtenna for WLAN applications. *Journal of Microwaves, Optoelectronics and Electromagnetic Applications, 18*(1), 70–79. https://doi.org/10.1590/2179-10742019v18i11220

Jadhav, J. B., & Deore, P. J. (2017). Filtering antenna with radiation and filtering functions for wireless applications. *Journal of Electrical Systems and Information Technology, 4*(1), 125–134. https://doi.org/10.1016/j.jesit.2016.10.007

Lin, C. K., & Chung, S. J. (2011). A compact filtering microstrip antenna with quasi-elliptic broadside antenna gain response. *IEEE Antennas and Wireless Propagation Letters, 10*, 381–384. https://doi.org/10.1109/LAWP.2011.2147750

Nie, W., Wen, H. Z., Xu, K. D., Luo, Y. Q., Yang, X. L., & Zhou, M. (2022). A compact 4 × 4 filtering microstrip patch antenna array with Dolph–Chebyshev power distribution. *IEEE Open Journal of Antennas and Propagation, 3*, 1057–1062. https://doi.org/10.1109/OJAP.2022.3204926

Sahu, B., Singh, S., Meshram, M. K., & Singh, S. P. (2018). Integrated design of filtering antenna with high selectivity and improved performance for L-band applications. *AEU – International Journal of Electronics and Communications, 97*, 185–194. https://doi.org/10.1016/j.aeue.2018.10.015

Wang, W., Chen, C., Wang, S., & Wu, W. (2019a). A wideband omnidirectional filtering patch antenna with high selectivity. *International Journal of RF and Microwave Computer-Aided Engineering, 29*(3), e21653. https://doi.org/10.1002/mmce.21653

Wang, W., Ran, J., Hu, N., Xie, W., Wu, Y., & Kishk, A. A. (2019b). A novel differential filtering patch antenna with high selectivity. *International Journal of RF and Microwave Computer-Aided Engineering, 29*(10), e21880. https://doi.org/10.1002/mmce.21880

Wu, W. J., Yin, Y. Z., Zuo, S. L., Zhang, Z. Y., & Xie, J. J. (2011). A new compact filter-antenna for modern wireless communication systems. *IEEE Antennas and Wireless Propagation Letters, 10*, 1131–1134. https://doi.org/10.1109/LAWP.2011.2171469

Yu, C., Hong, W., Kuai, Z., & Wang, H. (2012). Ku-band linearly polarized omnidirectional planar filtenna. *IEEE Antennas and Wireless Propagation Letters, 11*, 310–313. https://doi.org/10.1109/LAWP.2012.2191259

ISBN: 978-978-8567-02-8

5TH Faculty of Engineering Conference on Engineering Innovation and Economic Policies: Driving Sustainable Industrial Growth in Nigeria

Faculty of Engineering, Bayero University, Kano.

059-Design and Simulation of a Compact Quarter-Wavelength Microstrip Hairpin Bandpass Filter for WLAN Applications

M. Ali [1], S. A Babale [2*]., S. H. Lawan[3]

[1]Department of Computer Engineering, Federal University Wukari, Taraba State.
[2] Department of Electronics and Telecommunications Engineering, Ahmadu Bello University, Zaria, Nigeria
[3] Department of Telecommunications Engineering, Faculty of Engineering, Bayero University Kano, Kano, Nigeria.

*Corresponding author Email: sababale@abu.edu.ng

Abstract: This paper presents the empirical design and electromagnetic simulation of a compact third-order microstrip hairpin bandpass filter operating at 2.4 GHz for wireless local area network (WLAN) applications. The filter is implemented on an FR-4 substrate with a relative permittivity of 4.4, thickness of 1.6 mm, and loss tangent of 0.002. A quarter-wavelength resonator configuration is adopted to achieve size reduction while maintaining acceptable filtering performance. The design methodology follows classical coupled-resonator filter synthesis, where the coupling coefficients and external quality factors are extracted to determine the physical dimensions of the folded hairpin resonators and the tapped feed structure. Full-wave electromagnetic simulation and optimization are carried out using CST Microwave Studio. Simulation results demonstrate a return loss better than −18 dB at the center frequency, an insertion loss of approximately −3.2 dB within the passband, and a −10 dB impedance bandwidth of about 180 MHz, corresponding to a fractional bandwidth of 7.5%. The compact footprint of 25 × 38 mm² confirms the suitability of the proposed filter for integration into WLAN front-end circuits

Key words: Hairpin bandpass filter, quarter-wavelength resonator, WLAN, microstrip filter, FR-4 substrate, CST Microwave Studio.

1. INTRODUCTION

Wireless local area network (WLAN) systems operating in the 2.4 GHz industrial, scientific, and medical (ISM) band require compact and frequency-selective RF front-end components to suppress out-of-band interference and ensure reliable communication (IEEE Standards Association, 2020). Bandpass filters therefore play a critical role in improving receiver selectivity and mitigating adjacent-channel interference in WLAN transceivers *(Hong & Lancaster, 2011)*. Microstrip bandpass filters are widely employed in wireless communication systems due to their planar structure, low profile, and ease of fabrication using printed circuit board technology (Pozar, 2012). Conventional microstrip filter configurations include parallel-coupled line filters, open-loop resonators, and hairpin resonator filters, each offering different trade-offs in size, bandwidth, and insertion loss *(Matthaei et al., 1980; Levy et al., 2002)*. At relatively low microwave frequencies such as 2.4 GHz, parallel-coupled line filters often occupy large circuit areas, limiting their suitability for compact wireless devices *(Hong & Lancaster, 2011)*. Hairpin resonator filters were introduced as a folded form of parallel-coupled line filters to achieve size reduction while maintaining comparable electrical characteristics (Hong, 1999). Owing to their compact geometry and simple planar structure, hairpin filters have been widely adopted in RF front-end circuits *(Sagawa et al., 2003)*. However, conventional hairpin filters are typically based on half-wavelength resonators, which can still result in considerable physical size when implemented on low-cost substrates such as FR-4 *(Hong & Lancaster, 2011)*. To further reduce circuit dimensions, quarter-wavelength resonator configurations have been explored in microstrip filter design. Quarter-wavelength resonators provide approximately 50% length reduction compared to half-wavelength structures by exploiting transmission-line impedance properties *(Pozar, 2012; (Garg et al., 2013)*. Compact resonator techniques such as stepped-impedance and folded resonators have also been reported as effective approaches for miniaturizing planar bandpass filters (Sheen, 2010). Several studies have demonstrated compact microstrip filters using hairpin and folded resonator structures. (Abdel-Rahman et al., 2005) employed defected ground structures to enhance compactness, though at the expense of increased design complexity. Shaman and Hong introduced coupling-matrix extraction techniques to accurately model coupling behavior in microstrip filters (Shaman & Hong, 2007). Recent research confirms that folded and hairpin-based resonator filters remain actively investigated for modern wireless systems. (Alvi et al., 2024) demonstrated integrated hairpin filter architectures for compact RF applications. Recent review studies further emphasize that planar microstrip filters implemented on low-cost substrates remain attractive due to their balance between simplicity, cost effectiveness, and acceptable

ISBN: 978-978-8567-02-8

performance for WLAN and ISM-band applications (Lalbakhsh et al., 2023; Koziel & Bekasiewicz, 2023). Motivated by these observations, this paper presents a compact third-order quarter-wavelength microstrip hairpin bandpass filter optimized for the 2.4 GHz WLAN band using a practical empirical design approach.

2. METHODOLOGY

2.1. Hairpin Bandpass Filter Design Model

The hairpin filter is developed using a third-order Chebyshev prototype with a 0.5 dB passband ripple and a 10% fractional bandwidth. Synthesis equations from *(Hong & Lancaster, 20)* are utilized to derive the element values. Coupling coefficients and external quality factors (Qe) are calculated based on standard design tables. The physical layout is optimized using electromagnetic simulations in CST Studio Suite. (Dassault Systèmes, 2019)

$$Q_{e1} = \frac{g_0 g_1}{FBW}, Q_{en} = \frac{g_n g_{n+1}}{FBW}, for\ n = 1, to\ n-1 \quad (1)$$

$$K_{i,i+1} = \frac{FBW}{\sqrt{g_i g_{i+1}}}, for\ i = 1, to\ n-1 \quad (3)$$

$$\lambda g = \frac{c}{f_c \sqrt{\varepsilon_{effR}}} \quad (4)$$

$$L_R = \frac{\lambda g}{4} \quad (5)$$

Where g's are the prototypes element values and N is the order of the filter, Q_{e1} and Q_{en} are the external quality factor of the resonator at the input and output and FBW are the fractional bandwidth $K_{i,i+1}$ are the coupling coefficient between the adjacent resonators, (λ_g) is the Guided wavelength, (L_R) is the Resonator length. Based on the above model, a hairpin bandpass filter operating at 2.4 Ghz was designed and optimized. For the space between the adjacent resonator, EM simulation was carried out for estimating the tapping position and for space or gaps between the adjacent resonator coupling using FR4. Fig 1, depicts the top view geometry of the filter. The filter was design and simulated using FR4 substrate having a thickness of 1.6mm, dielectric constant of 4.4 and loss tangent of approximately of 0.002.

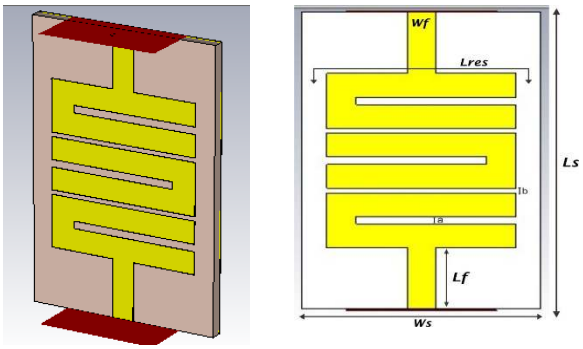


Figure 1. hairpin bandpass filter.

The dimensions of the filter marked in Fig 1, are summarized in table 1.

TABLE 1. OPTIMIZED FILTER DIMENSION

Parameters	Value
Ws	25mm
Ls	38.8mm
Lres	19.775mm
Lf	8mm
Wf	2.9mm
A	1mm
b	0.6mm

3. RESULTS AND DISCUSSION

The simulated S-parameters of the proposed filter demonstrate a clear bandpass response centered at 2.4 GHz. The return loss within the passband is better than −18 dB, indicating good impedance matching. The insertion loss is approximately −3.2 dB, which is primarily attributed to dielectric and conductor losses associated with the FR-4 substrate. The −10 dB impedance bandwidth is approximately 180 MHz, corresponding to a fractional bandwidth of about 7.5%, which satisfies typical WLAN bandwidth requirements. The compact physical size of 25 × 38 mm² highlights the effectiveness of the quarter-wavelength hairpin configuration in achieving miniaturization. When compared with previously reported hairpin and folded resonator filters, the proposed design offers a favorable trade-off between compactness and performance while maintaining a simple planar geometry suitable for low-cost fabrication.

The third-order Chebyshev hairpin bandpass filter also shows satisfactory performance. The simulated S_{21} response reveals a clear passband centered at 2.4 GHz, while the S_{11} plot demonstrates good matching and strong rejection outside the band, confirming the intended selectivity of the filter. Beyond the performance metrics, the results highlight significant practical implications for WLAN front-end integration. The filter's compact size and simple planar structure make it well-suited for combination with microstrip antennas to form a filtenna, enabling reduced system complexity, fewer components, and improved signal integrity through suppression of out-of-band interference. Additionally, the use of an empirical synthesis approach facilitates rapid prototyping and easy adaptation to other frequency bands, offering enhanced design flexibility for a wide range of future wireless applications. These characteristics indicate proper coupling between the resonators and effective frequency discrimination, as illustrated in Figure 2.

ISBN: 978-978-8567-02-8

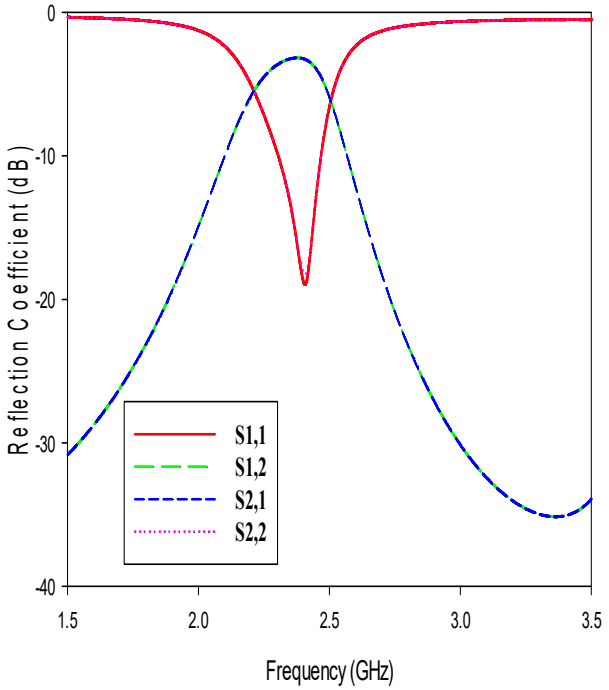


Figure 2 filter S-parameters

3.1. Comparative Analysis

Table 2 qualitatively compares the proposed filter with representative classical and recent planar microstrip bandpass filters reported in the literature, highlighting differences in resonator type, substrate, and structural complexity.

TABLE 2 COMPARISON OF MICROSTRIP BANDPASS FILTERS

Ref	Center Frequency	Resonator Type	Substrate	Complexity	Key Observation
(Hong, 1999)	2–5 GHz	Hairpin (λ/2)	High-ε_r	Low	Classical hairpin topology
(Shaman & Hong, 2007)	~2–3 GHz	Stub-loaded	FR-4	High	Compact using DGS
(Lalbakhsh et al., 2023)	Microwave band	Hairpin	Ceramic	Moderate	Miniaturized with spurious suppression
(Koziel & Bekasiewicz, 2023)	S-band	Hairpin filter bank	Microstrip	High	Integrated architecture
(Alvi et al., 2024)	WLAN / ISM	Folded / hairpin	Various	Low–Moderate	Confirms continued relevance
This work	2.4 GHz	Hairpin (λ/4)	FR-4	Low	Compact and simple design

4. CONCLUSION

A compact third-order quarter-wavelength microstrip hairpin bandpass filter for WLAN applications has been presented. The filter is designed using a practical empirical synthesis approach and implemented on a low-cost FR-4 substrate. Full-wave electromagnetic simulation confirms satisfactory filtering performance, including good impedance matching, acceptable insertion loss, and adequate bandwidth for 2.4 GHz WLAN systems. The compact size and straightforward design methodology make the proposed filter suitable for integration into WLAN front-end circuits and related wireless communication systems.

REFERENCES

IEEE Standards Association. (2020). *IEEE standard for information technology—Telecommunications and information exchange between systems—Local and metropolitan area networks—Specific requirements—Part 11: Wireless LAN medium access control (MAC) and physical layer (PHY) specifications* (IEEE Std. 802.11). IEEE.

Hong, J.-S., & Lancaster, M. J. (2011). *Microstrip filters for RF/microwave applications* (2nd ed.). Wiley.

Pozar, D. M. (2012). *Microwave engineering* (4th ed.). Wiley.

Matthaei, G. L., Young, L., & Jones, E. M. T. (1980). *Microwave filters, impedance-matching networks, and coupling structures*. Artech House.

Levy, R., Snyder, R. V., & Matthaei, G. L. (2002). Design of microwave filters. *IEEE Transactions on Microwave Theory and Techniques, 50*(3), 783–793. https://doi.org/10.1109/TMTT.2002.989784

Hong, J.-S. (1999). Microstrip hairpin resonator filters. *IEE Proceedings – Microwaves, Antennas and Propagation, 146*(2), 97–104. https://doi.org/10.1049/ip-map:19990207

Sagawa, M., Makimoto, M., & Yamashita, S. (2003). Miniaturized hairpin resonator filters with spurious suppression. *IEEE Transactions on Microwave Theory and Techniques, 51*(4), 973–979. https://doi.org/10.1109/TMTT.2003.809657

Garg, R., Bahl, I., Bozzi, M., & Bhartia, P. (2013). *Microstrip lines and slotlines* (3rd ed.). Artech House.

Sheen, J. W. (2010). Compact parallel-coupled microstrip bandpass filters using stepped-impedance resonators. *IEEE Transactions on Microwave Theory and Techniques, 58*(11), 3004–3010.

ISBN: 978-978-8567-02-8

Abdel-Rahman, A., Verma, A. K., Boutejdar, A., & Omar, A. S. (2005). Compact stub-type microstrip bandpass filters using defected ground structure. *IEEE Microwave and Wireless Components Letters, 14*(4), 136–138. https://doi.org/10.1109/LMWC.2005.845723

Shaman, H., & Hong, J.-S. (2007). Coupling matrix extraction of microwave filters using full-wave electromagnetic simulation. *IEEE Transactions on Microwave Theory and Techniques, 55*(5), 1083–1091. https://doi.org/10.1109/TMTT.2007.895113

Alvi, T. S., et al. (2024). A high-performance, low-cost, and integrated hairpin topology RF switched filter bank for radar applications. *Sensors, 24*(2), Article 434. https://doi.org/10.3390/s24020434

Lalbakhsh, A., Antoniades, M. A., & Esselle, K. P. (2023). Compact planar microwave filters for wireless applications: Recent advances and trends. *Electronics, 12*(3), Article 610. https://doi.org/10.3390/electronics12030610

Koziel, S., & Bekasiewicz, A. (2023). Recent advances in compact planar microwave filters for wireless communication systems. *Sensors, 23*(9), Article 4297. https://doi.org/10.3390/s23094297

Dassault Systèmes. (2019). *CST Studio Suite—CST Microwave Studio user manual*. Dassault Systèmes.

ISBN: 978-978-8567-02-8

5TH Faculty of Engineering Conference on Engineering Innovation and Economic Policies: Driving Sustainable Industrial Growth in Nigeria

Faculty of Engineering, Bayero University, Kano.

060-Optimization of End-of-Life Tire Steel Fibre Reinforced Concrete Using an Integrated Taguchi-TOPSIS Approach

Abubakar Sabo Baba[1*], Sule Yaman Mohammed[2], Aliyu Abubakar[3], Gimba Aliyu Ejiko[4]

[1*]Faculty of Engineering, Department of Civil Engineering, Federal University Dutsinma, Katsina, Nigeria, asbaba1@fudutsinma.edu.ng.

[2]School of Engineering, Department of Civil Engineering, Federal polytechnic, Bida, Niger State, Nigeria.

[3]Department of Civil Engineering, Abubakar Tafawa Balewa University, Bauchi.

[4]Works and Service Department, Federal Polytechnic Bida, Niger State.

Abstract: This study applies an integrated Taguchi-TOPSIS method to optimize end-of-life tyre (ELT) steel fibre reinforced concrete (SFRC). Using a Taguchi L9 orthogonal array, the experiments varied aspect ratio (10-70) and volume fraction (0.5-2.0%) as factors, evaluating slump, 7-day, and 28-day compressive strengths. TOPSIS, with equal weights, identified the optimal mix (aspect ratio 45, volume fraction 1.0%) via a closeness coefficient of 0.7527. Signal-to-noise ratios confirm its robustness. The study promotes sustainable waste utilization, addressing municipal solid waste (MSW) growth and concrete brittleness.

1. INTRODUCTION

The conventional economic model follows a linear "produce-use-discard" path. Global municipal solid waste (MSW) generation now exceeds 2 billion tonnes per year and is projected to rise by over 70 % by 2050 (Alhazmi *et al*., 2021; Yatoo *et al*., 2024). This escalating waste stream creates severe environmental and public-health hazards, driving the search for innovative recycling solutions (Mandal *et al.,* 2024). One promising strategy is incorporating ELT fibres into concrete, which addressing both waste management and the demand for sustainable construction materials (Baba *et al.,* 2024).

Plain concrete is brittle, weak in tension, and prone to cracking, despite its high compressive strength (Ali *et al.*, 2023). Introducing ELTF concrete can markedly improve mechanical properties, durability, and post-crack behaviour (Abubakar *et al*., 2022, 2025; Abbass *et al*., 2018). While conventional SF is effective, its cost and scarcity motivate the use of cheaper, recycled alternatives (Hamza *et al*., 2018).

Research on SFRC shows inconsistent strength outcomes: some studies report negligible or marginal compressive strength gains (Centonze *et al*., 2016; Elbialy *et al*., 2025; Köksal *et al*., 2008; Tasdemir *et al*., 2002; Baba et al., 2024), while others demonstrate significant improvements (La Rosa *et al*., 2019; Rao & Seshu, 2006; Turukmane *et al*., 2018). Flexural performance and toughness, however, consistently benefit from fibre addition. The trade-off is that higher fibre VFs can reduce workability and can cause a modest drop in compressive strength (Hamza *et al*., 2018; Abubakar *et al*., 2025).

Optimization studies reveal non-linear relationships between fibre aspect ratio (AR), volume fraction (VF), and concrete properties. For example, an AR of ~45 and a VF of 1.0 % were found optimal in some cases (Baba *et al*., 2024), whereas other work identified a higher AR (65) or VF of 1.5 % as optimal (Ren *et al*., 2022). In contrast, copper wire fibres showed steady strength gains with increasing dosage, unlike SF (Abubakar *et al*., 2022).

Because FRC design involves multiple, often conflicting objectives, researchers employ hybrid statistical-MCDM frameworks. The Taguchi method efficiently reduces experimental runs but optimises only one response at a time (Hisam *et al*., 2024; Antony *et al*., 2024). Coupling Taguchi with TOPSIS enables simultaneous multi-objective optimization (Şimşek & Uygunoğlu, 2016; Ali *et al*., 2023). This combined approach has been applied to various concrete mixes, delivering optimal mix designs that balance concrete performance and cost (Warda *et al*., 2022; Anwar *et al*., 2022).

Despite these advances, limited work has used Taguchi-TOPSIS specifically for concrete containing steel fibers derived from ELT. The present study fills that gap by applying the hybrid method to identify the optimal AR and VF for ELT-SFRC, aiming to maximize fresh-state workability while achieving robust hardened performance.

2. METHODOLOGY

2.1 Materials

The constituent materials utilized in this study include: ordinary Portland cement (OPC), fine aggregate,

ISBN: 978-978-8567-02-8

coarse aggregate, water from municipal water supply, and ELTSF. *.1.1 Cement*

Ashaka cement (OPC), conforming to the specifications outlined in BS EN 197-1: (2011), was employed in this study.

2.1.2 Fine and Coarse Aggregates

The aggregates used in this study were characterized for specific gravity, bulk density, aggregate crushing value (ACV), aggregate impact value (AIV), and particle size distribution (PSD). The tests were conducted in compliance with the following specifications: specific gravity and bulk density according to BS EN 1097-6 (2022); ACV and AIV as per BS EN 1097-2 (2020); for resistance to fragmentation, and PSD in accordance with the BS EN 933-1 (2012). The characterization results for both aggregates are presented in Table 1.

TABLE 1: PHYSICAL PROPERTIES OF AGGREGATES

Property	Values	
	Fine aggregate	Coarse aggregate
Specific Gravity	2.62	2.66
Bulk Density (Kg/m^3)	1528	1518
Aggregate Crushing value (%)	-	14.47
Aggregate Impact value (%)	-	14.95
Silt Content	4.26	-

2.1.3 Water

Municipal potable water was used for all mixing and curing throughout this investigation.

2.1.4 Waste tyres Steel Fibre

The SF utilized were manually extracted from discarded truck tires through a hand-operated cutting process to obtain WTSF. The physical properties of the WTSF are presented in Table 2.

TABLE 2: PHYSICAL PROPERTIES OF WTSF

Property	Description
Average Diameter (mm)	0.92
Tensile strength (N/mm^2)	1260
Shape (mm)	Cylindrical
Colour	Black

2.2.1 Design of experiments (DOE)

The basic principle in the DOE involves the appropriate selection of governing factors and their corresponding levels (Rawat *et al*., 2022). In this study, the AR and VF are identified as the main factors. Each factor is analysed at three levels, as detailed in Table 3. The selection of an orthogonal array (OA) is dictated by the number of control factors and their respective levels (Dave & Bhogayata, 2020). A Taguchi L9 OA was adopted, as it efficiently accommodates three levels for the investigated factors. This structured array was implemented to define the ED matrix, which outlines the test sequences presented in Table 4.

TABLE 3: DESIGN FACTORS AND LEVELS

Factor	Designation	Level-1	Level-2	Level-3
Aspect Ratio	AR	10	45	70
Volume Fraction (%)	VF	0.5	1.0	2.0

2.2.2 Concrete Mix Design, Casting, and Curing

A grade 25 concrete was designed for this investigation. The mix proportions were established in accordance with ACI 211.1R-21. A summary of the constituent material proportions employed in the production of ELTSFRC is provided in Table 4. To conduct the relevant tests on the concrete specimen, fresh ELTSFR concrete mix was cast in 100mm x 100mm x100mm mould. The specimens were demoulded and cured at room temperature by water immersion for 7 and 28 days prior to compressive strength testing.

TABLE 4: TAGUCHI MIX FOR WTSF CONCRETE PRODUCTION

Mix ID	AR	VF (%)	Cement (Kg/m^3)	F/A (Kg/m^3)	C/A (Kg/m^3)	Water (Kg/m^3)
Control Mix	10	-	-	663	1178	185
AR10VF0.5	10	0.5	385	663	1170	185
AR10VF1.0	10	1	385	663	1170	185
AR10VF2.0	10	2	385	663	1170	185
AR45VF0.5	45	0.5	385	663	1170	185
AR45VF1.0	45	1	385	663	1170	185
AV45VF2.0	45	2	385	663	1170	185
AR70VF0.5	70	0.5	385	663	1170	185
AR70VF1.0	70	1	385	663	1170	185
AR70VF2.0	70	2	385	663	1170	185

2.2.3 Slump Test

Slump tests for the control concrete and the ELTSFC specimens were conducted in compliance with BS EN 12350-2:2019. The ELTSFs were introduced into the mix design based on Taguchi DOE approach as presented in Table 4.

2.2.4 Compressive Strength Tests

The compressive strength of the hardened concrete was determined by testing 100mm^3 cubes, cured for 7 and 28 days. Testing was performed in compliance with the procedures stipulated in BS EN 12390-3:2019.

ISBN: 978-978-8567-02-8

2.2 Implementation of Taguchi-TOPSIS

The experimental results derived from the Taguchi OA design were analyzed and optimized using Minitab software. The Taguchi method employs three distinct performance characteristic categories for property evaluation: "larger-the-better," "smaller-the-better," and "nominal-the-best" (Antony *et al*., 2024; Warda *et al*., 2022). This study aimed to identify the ELTSFC mix proportions that minimize slump while maximizing both 7 and 28-day compressive strengths. Accordingly, the "smaller-the-better" characteristic was applied to slump, and the "larger-the-better" characteristic was applied to compressive strength. These quality characteristics were quantitatively evaluated using the signal-to-noise ratio (S/N), calculated via established formulations.

Lower-the better: $\mathrm{S/N} = -10\log_{10}(\frac{1}{n}\sum_{i=1}^{n}\frac{1}{y_i^2})$ (1)

Higher-the better: $\mathrm{S/N} = -10\log_{10}(\frac{1}{n}\sum_{i=1}^{n}y_i^2)$ (2)

Where

y_i is the obtained value of $_i$th test for $_j$th response,
n is the number of replications.

The TOPSIS optimization was performed using Microsoft Excel, following the steps outlined by Ali *et al*. (2023) and Anwar *et al*. (2022):

1) The normalization was conducted using the S/N ratios derived from the Taguchi analysis, in accordance with Equation (3):

$$r_{ij} = \frac{a_{ij}}{\sqrt{\sum_{i=j}^{m} a_{ij}^2}} \quad (3)$$

Where

a_{ij} is the S/N ratio for the *i*-th experimental run and *j*-th response,
m is the total number of runs, and
r_{ij} is the resulting normalized value.

2) Then, equal weights were assigned to all three performance criteria, were treated each response with equal importance in the MCDM. The weighted normalized decision matrix was subsequently computed using Equation (4):

$$v_{ij} = w_j \, x \, r_{ij} \quad (4)$$

$$v_{ij} = \tfrac{1}{3} \, x \, r_{ij} \quad (5)$$

Where

v_{ij} is the weighted normalized value,
w_j is the weight for criterion *jj*
r_{ij} is the normalized value from Equation (3).

3) The positive ideal solution (v^+) and negative ideal solution (v^-) were then derived from the weighted normalized decision matrix. For each criterion *j*, the element of v^+ was taken as the maximum value among the alternatives, and the element of v^- was taken as the minimum value, as defined in Equations (6) and (7):

$$v_j^+ = \left[\left(Max\ v_{ij} \middle| j \in J\right),\ \left(Min\ vij \middle| j \in J\right)\right] \quad (6)$$

$$v_j^- = \left[\left(Min\ v_{ij} \middle| j \in J\right),\ \left(Max\ vij \middle| j \in J\right)\right] \quad (7)$$

Where

v_{ij} is the weighted normalized value for alternative *i* and criterion *j*.

4) Subsequently, the separation distances for each alternative were determined. The distance from the positive ideal solution $S_i^- + S_i^+$ quantifies how far an alternative is from the optimal performance, while the distance from the negative ideal solution $Si - Si -$ quantifies its proximity to the worst-case performance. These measures were calculated using the Euclidean distance formulae presented in Equations (8) , (9) and (10):

$$S^+ = \sqrt{\sum_{i=1}^{m}\left(v_{ij} - v_j^+\right)^2} \quad (8)$$

$$S^- = \sqrt{\sum_{i=1}^{m}\left(v_{ij} - v_j^-\right)^2} \quad (9)$$

$$C_i = \frac{S^-}{S^+ + S^-} \quad (10)$$

3. RESULTS AND DISCUSSION

The results of Slump, 7 and 28-days of all the tests performed are shown in Table 5.

3.1 Taguchi Technique

TABLE 5: OA AND EXPERIMENTAL RESULTS

Mix ID	AR	VF (%)	Slump (mm)	7-day CS (N/mm²)	28-day CS (N/mm²)
AR10VF0.5	10	0.5	39	28.23	31.00
AR10VF1.0	10	1.0	30	21.01	29.20
AR10VF2.0	10	2.0	26	16.34	33.22
AR45VF0.5	45	0.5	30	29.74	31.00
AR45VF1.0	45	1.0	25	26.37	34.33
AV45VF2.0	45	2.0	24	18.06	37.43
AR70VF0.5	70	0.5	25	26.87	29.00
AR70VF1.0	70	1.0	22	22.69	31.57
AR70VF2.0	70	2.0	21	16.34	33.22

The Taguchi analysis successfully identified the effects of AR and VF on three critical concrete performance characteristics: slump, 7 and 28-day compressive strength. The results of the analysis are discussed based on the follows: signal-to-noise (S/N) ratios, mean responses, analysis of variance (ANOVA) and main effects plots to derive optimal conditions. The analysis also highlights a fundamental performance trade-off governed by curing age.

3.1.1 Workability (Slump Values)

Table 5 and Figure 1 present the slump test results. As shown in Figure 1, workability exhibits a decreasing trend with an increasing fiber volume fraction (VF) and aspect ratio (AR). Measured slump values ranged from 25–38 mm at 0.5% VF, 23–30 mm at 1.0% VF, and 20–28 mm at 2.0% VF. According to BS EN 12390 (2000), these ranges correspond to very low to low workability classes. The lowest workability was observed for the mix with an AR of 70 and a VF of 2.0%, a result attributed to enhanced fiber entanglement and increased internal friction. This finding aligns with previous research (Vairagade *et al*., 2012; Gul *et al*., 2021; Mohod, 2012; Baba *et al*., 2024), which similarly reports that workability declines proportionally with increasing VF and AR.

ISBN: 978-978-8567-02-8

To systematically minimise slump for controlled workability, a well-fitting predictive model was developed using Taguchi analysis. The signal-to-noise (S/N) ratio model showed an excellent coefficient of determination, R^2 (R^2=94.70%), significantly explaining the response variability. ANOVA confirmed that both AR (p= 0.008) and VF (p=0.014) are statistically significant factors at α=0.05. The response table for S/N ratios ranked AR as the more influential factor (Delta=2.80, Rank 1) compared to VF (Delta = 2.32, Rank 2), a ranking validated by the mean-response analysis, which also demonstrated a strong model fit (R^2=90.41%). The main effects plots Figure 2, visually validate these statistical findings, illustrating a decreasing trend in slump as AR increases from 10 to 70 and as VF increases from 0.5% to 2.0%. Consequently, the optimal factor levels to minimise slump are confirmed as AR at 70 and VF at 2.0%.

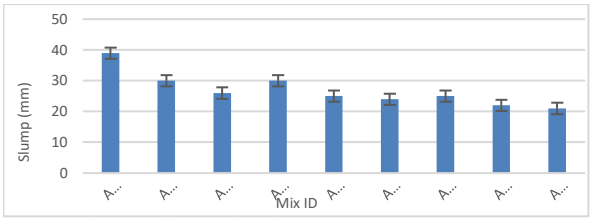


Figure 1: factors effect on the Slump

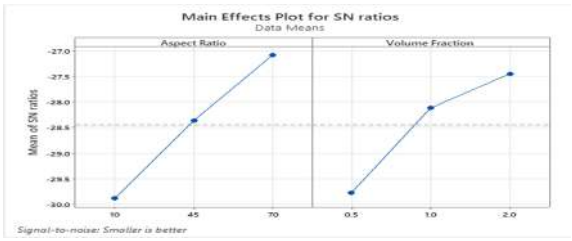


Figure 2: Main effects plots of S/N ratios of slump

3.1.2. Compressive Strength

Figures 3 and 5 illustrate the compressive strength development of ELTSFC at 7 and 28-day curing periods. The results demonstrate that incorporating SF across varying VF and AR levels enhances the compressive strength of ELTSFC over longer curing periods. These observations align with previous research (Dawood & Ramli, 2010; Ou *et al*., 2012; Baba *et al*., 2024), which similarly reported strength improvements with SF addition. For instance, at 28 days of curing, compressive strength increased by 0.80–3.16% at 0.5% VF, 1.05–3.16% at 1.0% VF, and 2.45–9.85% at 2.0% across the AR range of 10 to 70, relative to the control concrete. The degree of strength enhancement reported in the literature for SFRC varies considerably, ranging from negligible (Centonze *et al*., 2016; Elbialy *et al*., 2025; Köksal *et al*., 2008; Tasdemir *et al*., 2002), to marginal (Baba *et al*., 2024; Bayramov *et al*., 2004;; Swarna, 2025), to significant (La Rosa *et al*., 2019; Rao & Seshu, 2006; Turukmane *et al*., 2018). Notably, the current results indicate a non-linear relationship, where beyond 1.0% fibre volume fraction, a relative decline in strength gain was observed across all fibre ARs and curing ages. At VF levels of 1.0% and 2.0%, the increases in strength relative to the control were more modest, limited to 2.24-4.45% and 1.60-4.21%, respectively, a trend that was consistent across the curing periods examined.

To determine the optimal factor settings for maximising compressive strength, Taguchi analysis was performed separately for the 7 and 28-day results. For 7-days compressive strength, the S/N-ratio model demonstrated a goodness of fit, with a coefficient of determination (R^2) of 96.07%. ANOVA revealed VF as the highly significant dominant factor (p<0.001), with AR being marginally significant (p=0.051). This larger influence of VF was supported by the response tables, which ranked it as the dominant factor for both S/N-ratios (Delta=4.47, Rank 1) and means (Delta=11.37, Rank 1). Main effects plots further provide significant graphical evidence for this, showing a pronounced peak in strength at VF = 0.5 as depicted in Figure 4. This suggests that early-age strength is governed primarily by matrix density and efficient hydration, which benefit from lower particle interference at a modest fibre dosage. Consequently, the optimal condition for maximizing 7-day strength is an AR of 45 and a VF of 0.5%.

The analysis for 28-day compressive strength presents a more nuanced and insightful picture. The predictive models were less robust, with a coefficient of determination (R^2) of approximately 67–68%. ANOVA indicated that neither factor was statistically significant at the conventional α = 0.05 level, though VF approached significance (p=0.057–0.059). Despite the lower model certainty, the response table for means and the corresponding main effects plots revealed a significant shift in factor influence: the optimal VF level transitioned from 0.5% at 7 days to 2.0% at 28 days. Although AR=45 remained optimal, the main effect of VF reversed, showing a clear ascending trend from 0.5% to 2.0%. This indicates that the mechanism controlling strength evolves with time; long-term performance appears to be enhanced by a higher fibre content, potentially due to improved interfacial bonding, sustained matrix contribution, or more effective long-term crack bridging. Therefore, the recommended levels for maximum 28-day strength are AR at 45 and a VF of 2.0%. This finding is consistent with the experimental data presented in Figure 4, which shows the highest 28-day strengths occurring at the highest volume fraction.

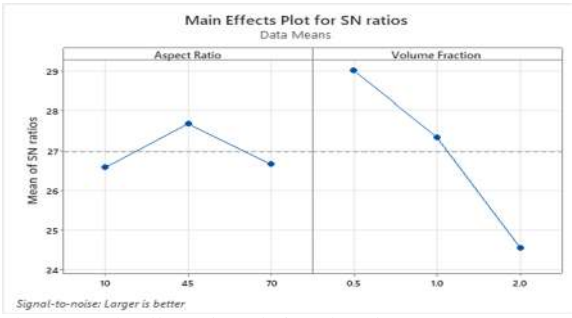


Figure 4: Main effects plots of S/N ratios of 7-Days CS

ISBN: 978-978-8567-02-8

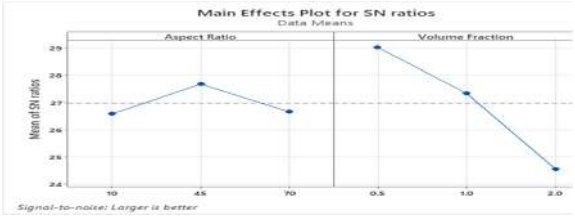


Figure 6: Main effects plots of S/N ratios of 28-Days CS

TABLE 6: TAGUCHI OPTIMAL FACTOR LEVELS AND PREDICTED PERFORMANCE FOR RESPONSES

Response	Objective	Optimal Factor Levels	Predicted S/N Ratio	Predicted Mean	Mo Fit (R^2)
Slump	Min.	AR = 70, VF = 2.0	-27.08	22.67 mm	94.7
7-Day CS	Max.	AR = 45, VF = 0.5	29.02	28.28 MPa	96.(
28-Day CS	Max.	AR = 45, VF = 2.0	30.77	34.62 MPa	68%

3.3.3 TOPSIS Analysis

From the Taguchi analysis results of optimal factor levels and predicted performance for slump and compressive strength, a significant multi-response optimization conflict is evident, as each performance characteristic favouring a distinct and conflicting optimal setting for the control factors AR and VF. To resolve this conflict and identify a single, balanced optimal setting suitable for all responses, the application of a MCDM method is required. TOPSIS is particularly well-suited for this purpose for the following reasons, supported by established engineering and decision science literature.

The TOPSIS-based Taguchi optimisation method aimed to minimise slump and maximise compressive strengths as its performance criteria. As summarised in Table 6, the corresponding S/N ratios for slump and compressive strength were calculated using Equations (1) and (2). These results are presented in Table 7.

TABLE 7: DECISION MATRIX (S/N RATIOS)

Exp	Responses S/N ratios		
	Slump (mm)	7-day CS (N/mm²)	28-day CS (N/mm²)
1	-31.2152	28.6294	29.3518
2	-29.5576	26.9364	29.7199
3	-28.8904	24.1620	30.4912
4	-29.6960	29.7279	30.1659
5	-28.0383	28.0349	30.5340
6	-27.3711	25.2606	31.3052
7	-28.4114	28.7091	29.3847
8	-26.7537	27.0161	29.7528
9	-26.0865	24.2418	30.5240

3.3.4 Optimal Combination and Factor Influence Analysis

The integrated Taguchi-TOPSIS method identified Experiment 5, characterized by an AR of 45 and VF of 1.0%, as the optimal concrete mix. This combination provides an effective balance between workability control (slump=25mm) and strength development (7-days CS=26.37MPa, 28-day CS=34.33 MPa), as substantiated by the closeness coefficients detailed in Table 8 and aligned with the optimization goals defined in Table 6.

TABLE 8: FINAL RANKING WITH EXPERIMENTAL RESPONSES

Exp.	AR	VF (%)	Slump (mm)	7-day CS (N/mm²)	28-day CS (N/mm²)	C_i Score
5	45	1.0	25	26.37	34.33	0.7527
4	45	0.5	30	29.74	31.00	0.6335
7	70	0.5	25	26.87	29.00	0.6780
8	70	1.0	22	22.69	31.57	0.6586
6	45	2.0	24	18.06	37.43	0.5446
9	70	2.0	21	16.34	33.22	0.5326
3	10	2.0	26	16.34	33.22	0.4444
1	10	0.5	39	28.23	31.00	0.4262
2	10	1.0	30	21.01	29.20	0.4074

The influence of each parameter on the multi-response performance was further explored through graphical analyses. The main effect plot presented in Figure 7 illustrates the relationship between factor levels and the mean TOPSIS closeness coefficient. The TOPSIS score increases with AR up to a peak mean value of about 0.647 at AR=45, before declining at AR=70. Similarly, for VF, the highest mean performance is observed at 1.0%, with diminished performance at both lower VF (0.5%) and higher VF (2.0%). This non-linear trend graphically supports the selection of intermediate levels for both factors to achieve an optimal compromise between workability and strength, as summarized in Figure 7.

A complementary assessment of factor contribution, presented via the pie chart in Figure 8, quantifies each parameter's proportional influence on the total variation in TOPSIS scores, derived from the range of mean effects. AR accounts for approximately 55.8% of the observed variation, while VF contributes the remaining 44.2%. This relatively balanced distribution underscores the critical importance of both factors in the multi-response optimization process, with AR exerting a slightly more dominant influence.

Collectively, these outputs the optimal mix identification, main effect trends, and contribution analysis provide clear and interpretable evidence that validates the Taguchi-TOPSIS approach. They confirm that the selected parameter combination (AR=45, VF=1.0%) not only delivers superior multi-criteria performance but is also well supported by the underlying factor-response relationships, which are essential for designing SFRC incorporating recycled tyre fibres.

ISBN: 978-978-8567-02-8

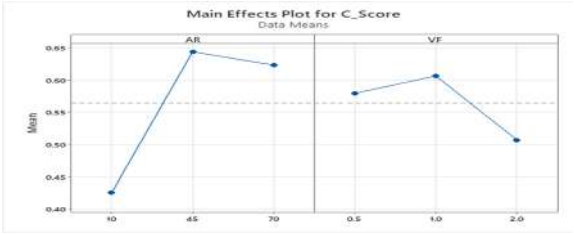


Figure 7: Main effect plot of the mean TOPSIS closeness coefficient

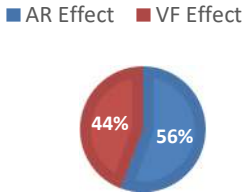


Figure 8: Pie chart of factor contribution

4. CONCLUSION

Although the Taguchi method efficiently identifies single-response optimal conditions, it cannot resolve the multi-objective trade-offs inherent in this study. In contrast, TOPSIS provides a structured MCDM framework to integrate these conflicting outputs, incorporate predetermined priority weightings, and converge upon a single, globally optimal factor combination (AR and VF). This optimal combination represents the best possible compromise for holistic performance, thereby shifting the analysis from a descriptive account of trade-offs to a prescriptive and actionable design solution.

REFERENCES

Abbass, W., Khan, M. I., & Mourad, S. (2018). Evaluation of mechanical properties of steel fibre reinforced concrete with different strengths of concrete. Construction and building materials, 168, 556-569.

Abubakar, A., Mohammed, A., Duna, S., & Umar, S. E. Y. (2022). Prediction of Mechanical properties of Waste Copper Wire Fibre Reinforced Concrete using Response Surface Methodology. World Journal of Engineering Research and Technology (WJERT), 8 (8), 53, 68.

Abubakar, A., Mohammed, A., Duna, S., & Yusuf, S. U. (2025). An investigation into the post-cracking behaviour of waste copper wire fibre reinforced concrete. *Nigerian Journal of Tropical Engineering*, *19*(1), 110-119.

Abubakar, A., Mohammed, A., Duna, S., & Yusuf, U. S. (2022). Relationship between compressive, flexural and split tensile strengths of waste copper wire fibre reinforced concrete. *Path of Science*, *8*(5), 4001-4009.

Abushanab, A., & Vimonsatit, V. (2025). Cost-Effectiveness of Reinforced Recycled Aggregate Concrete Structures with Fly Ash and Basalt Fibres under Corrosion: A Life Cycle Cost Analysis. Buildings (2075-5309), 15(7).

Alhazmi, H., Shah, S. A. R., Anwar, M. K., Raza, A., Ullah, M. K., & Iqbal, F. (2021). Utilization of polymer concrete composites for a circular economy: A comparative review for assessment of recycling and waste utilization. *Polymers*, *13*(13), 2135.

Ali, H., Jamshaid, H., Mishra, R., Chandan, V., Jirku, P., Kolar, V., & Shahzada, K. (2023). Optimization of seismic performance in waste fibre reinforced concrete by TOPSIS method. *Scientific Reports*, *13*(1), 8204.

Almomani, A., Mourad, A. H. I., Deveci, S., Wee, J. W., & Choi, B. H. (2023). Recent advances in slow crack growth modeling of polyethylene materials. *Materials & Design*, *227*, 111720.

Amarnath, K., Babu, K. J., & Kumar, M. S. (2021, February). Selection of optimal flax fibre reinforced components for experimental investigation by using TOPSIS method. In *IOP Conference Series: Materials Science and Engineering* (Vol. 1057, No. 1, p. 012055). IOP Publishing.

American Concrete Institute. (2002). *State of the art report on fibre reinforced concrete* (ACI 544.4R-96). Farmington Hills, MI.

Antony, J., Bhat, S., Mittal, A., Jayaraman, R., Gijo, E. V., & Cudney, E. A. (2024). Application of Taguchi design of experiments in the food industry: a systematic literature review. *Total Quality Management & Business Excellence*, *35*(5-6), 687-712.

Anwar, F. H., El-Hassan, H., Hamouda, M., El-Mir, A., Mohammed, S., & Mo, K. H. (2022). Optimization of pervious geopolymer concrete using TOPSIS-based Taguchi method. *Sustainability*, *14*(14), 8767.

Baba, A. S., Mohammed, S. Y., Abdullahi, Y. I., & Alhassan, D. A. (2024). Mechanical Properties of End-of-life Waste Tyres Steel Fibre Reinforced Concrete: RSM-Based Modelling and Optimisation. *Journal of Civil Engineering Frontiers (JoCEF)*, *5*(2).

Bayramov, F., Taşdemir, C., & Taşdemir, M. A. (2004). Optimisation of steel fibre reinforced concretes by means of statistical response surface method. Cement and concrete composites, 26(6), 665-675.

Bayramov, F., Tasdemir, M. A., Ilki, A., & Yerlikaya, M. (2004). Steel fibre reinforced concrete for heavy traffic load conditions. In *Proceedings of the 9th International Symposium on Concrete Roads, Istanbul, Turkey* (pp. 3-6).

BS EN 1097-2, (2020). *Tests for mechanical and physical properties of aggregates — Part 2: Methods for the determination of resistance to fragmentation*.

ISBN: 978-978-8567-02-8

BS EN 12350-2. (2019). Testing fresh concrete. Part 2: Slump-test. BSI Standards Limited.

BS EN 12390-3 (2000). Testing Hardened Concrete. Part 3: Compressive Strength of Test Specimen. British Standard Specification. London.

BS EN 933-1, (2011). *Cement — Part 1: Composition, specifications and conformity criteria for common cements*

BS EN 933-2, (2012). *Tests for geometrical properties of aggregates — Part 1: Determination of particle size distribution — sieving method*.

Centonze, G., Leone, M., & Aiello, M. A. (2012). Steel fibres from waste tyres as reinforcement in concrete: A mechanical characterization Construction and Building Materials, 36, 46-57.

Centonze, G., Leone, M., Micelli, F., Colonna, D., & Aiello, M. A. (2016). Concrete reinforced with recycled steel fibres from end of life tires: Mix-design and application. *Key engineering materials*, *711*, 224-231.

Chalioris, C. E., Kosmidou, P. M. K., & Karayannis, C. G. (2019). Cyclic response of steel fibre reinforced concrete slender beams: An experimental study. *Materials*, *12*(9), 1398.

Dawood, E. T., & Ramli, M. (2010). Development of high-strength flowable mortar with hybrid fibre. *Construction and Building Materials*, 24*(6), 1043–1050.

Di-Prisco, M., Colombo, M., & Dozio, D. (2013). Fibre-reinforced concrete in fib Model Code 2010: principles, models and test validation. Structural Concrete, 14(4), 342-361.

Elbialy, S., Elfarnsawy, M., Salah, M., Abdel-Aziz, A., & Ibrahim, W. (2025). An Experimental study on steel fibre effects in high-strength concrete slabs. *Civil Engineering Journal*, *11*(1), 215-229.

Fall, D. (2014). *Steel Fibres in Reinforced Concrete Structures of Complex Shapes: Structural Behaviour and Design Perspectives*. Chalmers Tekniska Hogskola (Sweden).

Gencel, O., Bayraktar, O. Y., Kaplan, G., Benli, A., Martinez-Barrera, G., Brostow, W., & Bodur, B. (2021). Characteristics of hemp fibre reinforced foam concretes with fly ash and Taguchi optimization. *Construction and Building Materials*, *294*, 123607.

Grammelis, P., Margaritis, N., Dallas, P., Rakopoulos, D., & Mavrias, G. (2021). A review on management of end of life tires (ELTs) and alternative uses of textile fibres. *Energies*, *14*(3), 571.

Gul, A., Alam, B., Iqbal, M. J., Ahmed, W., Shahzada, K., Javed, M. H., & Khan, E. A. (2021). Impact of length and percent dosage of recycled steel fibres on the mechanical properties of concrete. *Civil Engineering Journal (Iran)*, *7*(10), 1650-1666.

Gupta, A., Lastra-Gonzalez, P., Castro-Fresno, D., & Rodriguez-Hernandez, J. (2021). Laboratory characterization of porous asphalt mixtures with aramid fibres. *Materials*, *14*(8), 1935.

Hamza, B., Said, K., & Belkacem, M. (2018). The influence of recycled steel fibres on self-compacting concrete performance. In *IOP Conference Series: Materials Science and Engineering* (Vol. 431, p. 102008). IOP Publishing.

Hisam, M. W., Dar, A. A., Elrasheed, M. O., Khan, M. S., Gera, R., & Azad, I. (2024). The versatility of the Taguchi method: Optimizing experiments across diverse disciplines. Journal of Statistical Theory and Applications, 23(4), 365-389.

Islam, S. U., & Waseem, S. A. (2024). An experimental study on mechanical and fracture characteristics of hybrid fibre reinforced concrete. In Structures (Vol. 68, p. 107053). Elsevier.

Khan, M., Cao, M., & Ali, M. (2018). Effect of basalt fibres on mechanical properties of calcium carbonate whisker-steel fibre reinforced concrete. *Construction and Building Materials*, *192*, 742-753.

Köksal, F., Altun, F., Yiğit, İ., & Şahin, Y. (2008). Combined effect of silica fume and steel fibre on the mechanical properties of high strength concretes. *Construction and building materials*, *22*(8), 1874-1880.

Koksal, F., Ilki, A., & Tasdemir, M. A. (2013). Optimum mix design of steel-fibre-reinforced concrete plates. Arabian Journal for Science and Engineering, 38(11), 2971-2983.

La Rosa, A. D., Pergolizzi, E., Maragna, D., Recca, G., & Cicala, G. (2019). Reuse of carbon black from end-of-life tires in new pneumatic formulations and life-cycle assessment of the thermolysis process. Journal of Elastomers & Plastics, 51(7-8), 740-754.

Mandal, P., Kundu, A. K., & Mondal, A. (2024). Innovations in Waste Management: A Review. *Sustaninble Chemical Insight in Biological Exploration*, 58-71.

Mastali, M., & Dalvand, A. (2016). Use of silica fume and recycled steel fibres in self-compacting concrete (SCC). Construction and Building Materials, 125, 196-209.

Michalik, A., Chyliński, F., Bobrowicz, J., & Pichór, W. (2022). Effectiveness of concrete reinforcement with recycled tyre steel fibres. *Materials*, *15*(7), 2444.

Mohammed, S. Y., Mohammed, A., & Elinwa, A. U. (2023). The Effect of Aspect Ratio and Volume Fraction on Mechanical Properties of End of Life Tyre Steel Fibre Reinforced Concrete. *Journal of Civil Engineering Frontiers (JoCEF)*, *4*(2).

Mohod, M. V. (2012). Performance of steel fibre reinforced concrete. *International Journal of Engineering and Science*, *1*(12), 1-4.

Mujalli, M. A., Dirar, S., Mushtaha, E., Hussien, A., & Maksoud, A. (2022). Evaluation of the tensile

ISBN: 978-978-8567-02-8

characteristics and bond behaviour of steel fibre-reinforced concrete: An overview. *Fibre s*, *10*(12), 104.

Munyi, J., Idowu, T., & Okumu, V. (2020). Performance assessment of bitumen when oil-based waste paint is used as an additive. *JOURNAL OF SUSTAINABLE RESEARCH IN ENGINEERING*, *6*(1), 1-10.

Odeyemi, S. O., Mohammed, A. A., Raji, A. A., Ajeigbe, M. O., Wilson, U. N., & Oloruntoba, A. A. (2025). Effect of waste tire steel fibres on concrete incorporating palm kernel shell, recycled aggregate, and coconut shell. *CLEAN – Soil Air Water*, *53*(12), 1–14.

Ou, Y. C., Tsai, M. S., Liu, K. Y., & Chang, K. C. (2012). Compressive behavior of steel-fibre-reinforced concrete with a high reinforcing index. *Journal of Materials in Civil Engineering*, 24(2), 207–215.

Pilakoutas, K., Neocleous, K., & Tlemat, H. (2004). Reuse of tyre steel fibres as concrete reinforcement. In *Proceedings of the Institution of Civil Engineers-Engineering Sustainability* (Vol. 157, No. 3, pp. 131-138). Thomas Telford Ltd.

Rao, T. D. G., & Seshu, D. R. (2006). Torsional response of fibrous reinforced concrete members: Effect of single type of reinforcement. *Construction and Building Materials*, *20*(3), 187–192.

Ren, X., Ding, Y., Liu, Q., Chen, S., & Song, F. (2022). Effect of different volume fraction of steel fibre/graphite on thermal conductivity and compressive properties of concrete. *Frontiers in Materials*, *9*, 1003830.

Safayet, M. A., Abdullah, A. A., Islam, M. F., Alahmari, T. S., Sobuz, M. H. R., & Khan, M. M. H. (2025). Combined influence of eggshell powder and nylon fibre on self-compacting concrete production: Experimental assessment and machine learning quantifications. *Materials Research Express*, *12*(2), 025003.

Salmi, A. (2024). Enhancing durability and sustainability in concrete with fibre-reinforced composites. *Journal of Water and Land Development*, 48-54.

Şimşek, B., & Uygunoğlu, T. (2016). Multi-response optimization of polymer blended concrete: A TOPSIS based Taguchi application. Construction and Building Materials, 117, 251-262.

Soutsos, M. N., Le, T. T., & Lampropoulos, A. P. (2012). Flexural performance of fibre reinforced concrete made with steel and synthetic fibres. *Construction and building materials*, *36*, 704-710.

Sumathi, A., & Mohan, K. S. R. (2019). Effect of steel fibre on structural characteristics of high-strength concrete. Iranian Journal of Science and Technology, Transactions of Civil Engineering, 43(Suppl 1), 117-130.

Swarna, A., Chowdhury, M., & Noman, M. (2025). Influence of Steel Fibre on Compressive Strength and Crack Pattern of Recycled Aggregate Concrete. *American Journal of Civil Engineering*, *13*(2), 61-67.

Tasdemir, M. A., Ilki, A., & Yerlikaya, M. (2002, November). Mechanical behaviour of steel fibre reinforced concrete used in hydraulic structures. In *Hydro 2002 International Conference on Hydropower and Dams* (pp. 159-166).

Turukmane, R., Daberao, A., & Gulhane, S. (2018). Basalt: A technical fibre for civil applications. *Chemical Fibres International*, *68*(1), 38–40.

Vairagade, V. S., Kene, K. S., & Patil, T. R. (2012). Comparative study of steel fibre reinforced over control concrete. International journal of Scientific and research Publications, 2(5), 1-3.

Wang, Z., Li, H., Zhang, X., Chang, Y., Wang, Y., Wu, L., & Fan, H. (2023). The effects of steel fibre types and volume fraction on the physical and mechanical properties of concrete. *Coatings*, *13*(6), 978.

Warda, M. A., Ahmad, S. S., Mahdi, I. M., Sallam, H. E. D. M., & Khalil, H. S. (2022). The applicability of TOPSIS-and fuzzy TOPSIS-based Taguchi optimization approaches in obtaining optimal fibre-reinforced concrete mix proportions. *Buildings*, *12*(6), 796.

Yang, J., Zhang, Y., & Huang, J. (2024). The strengthening theory of steel fibre reinforced concrete and its application in tunnel engineering: A review. Journal of Engineered Fibres and Fabrics, 19, 15589250241239242.

Yassin, A. M., Mohie Eldin, M., Hafez, M. A., & Elnaggar, M. A. (2024). The flexural behaviour and mechanical properties of super high-performance concrete (SHPC) reinforced using the hybridization of micro polypropylene and macro steel fibres. *Buildings*, *14*(7), 1887.

Yatoo, A. M., Hamid, B., Sheikh, T. A., Ali, S., Bhat, S. A., Ramola, S., & Kumar, S. (2024). Global perspective of municipal solid waste and landfill leachate: generation, composition, eco-toxicity, and sustainable management strategies. *Environmental Science and Pollution Research*, *31*(16), 23363-23392.

Ye, L., Hai, T. K., & Dong, Z. (2016). Optimization of compressive strength and tensile strength of ultra-high performance concrete. HiperMat Proceedings, Kassel, Germany, 3(5).

ISBN: 978-978-8567-02-8

5TH Faculty of Engineering Conference on Engineering Innovation and Economic Policies: Driving Sustainable Industrial Growth in Nigeria

Faculty of Engineering, Bayero University, Kano.

061-Data-Driven Fault Detection in Nigeria's Transmission Grid using ANNs

Author Abdulrazaq Nafiu Abubakar[1], Musa Mohammed Bello[2]*, , Jamilu Umar Yahaya[1]

[1]*Control and Instrumentation Engineering Department, King Fahd University of Petroleum & Minerals (KFUPM), Dhahran 31261, Saudi Arabia.*

[2]*Department of Mechatronics Engineering, Bayero University Kano (BUK), Kano 3011, Nigeria.*

**Corresponding Author: mbmusa.mct@buk.edu.ng*

Abstract: Frequent short-circuit events in Nigeria's transmission network are largely driven by persistent sectoral challenges such as inadequate maintenance practices, ageing infrastructure, harsh environmental conditions, and rising security threats. These issues often lead to recurrent equipment failures, prolonged outages, and unstable power delivery. Consequently, rapid and accurate identification of fault type and location is essential for improving system reliability and minimizing downtime. This study presents a data-driven approach that leverages artificial neural networks (ANNs) trained using the Levenberg Marquardt algorithm to detect and classify transmission line faults. The work addresses common fault categories in the Nigerian grid three-phase, single-line-to-ground, double-line-to-ground, and line-to-line faults while also extending the framework to identify simultaneous fault occurrences, which are increasingly observed under stressed grid conditions. The ANN model was developed and tested in MATLAB/Simulink, with performance evaluated using metrics such as mean squared error and correlation coefficient. To reflect real grid behavior, the training process incorporated multiple practical factors, including variable loading conditions, fault resistance, fault location, and line distances. Results show that the proposed ANN-based scheme accurately detects and classifies faults even under complex and uncertain scenarios. This research advance's intelligent fault diagnosis for Nigerian power transmission systems, offering a promising tool for enhancing grid reliability, supporting faster restoration, and reducing the operational and economic impacts of outages.

Key words: Fault detection; Fault classification; Fault location; Artificial Neural Network; Nigeria's transmission network.

1. INTRODUCTION

The power system is a massive network of various types of electrical equipment, including generators, transmission lines, and transformers, interconnected to generate, transmit, and distribute electricity to consumers (Poongothai et al., 2025).

It is critical to keep the power system stable in order to avoid blackouts. To ensure that power systems operate within their stability constraints, both voltage and frequency must remain steady, and loads must be continuously supplied (Sokolović & Žarković, 2025). To do this, all equipment in the power system, including generators and motors, must provide the necessary output. Inadequate design and coordination of controls necessary for operating electric machinery frequently cause power instability (Guo et al., 2025). To improve stability, problems must be detected and appropriately restored consistently. Identifying and locating faults is critical to returning the electrical system to a stable state of operation. The fault detection process is initiated by the relay, which is a vital component of power system protection (Guo et al., 2025).

The increasing complexity and functional demands of modern transmission grids necessitate effective fault management as a crucial aspect of power grid automation (Anwar et al., 2025). Faults such as short circuits, ground faults, and transformer failures pose risks of widespread outages, significant financial losses, and security threats. Prompt fault localization and isolation are vital for ensuring grid reliability and stability (Rajaperumal & Columbus, 2025). Traditional methods, including distance protection systems and wavelet-based fault detection, have historically been adequate; however, they are increasingly insufficient to address the dynamic challenges of contemporary transmission grids (Abdullah et al., 2024). The integration of renewable energy sources, unpredictable weather patterns, and evolving grid architectures exacerbate the frequency and unpredictability of faults. Fault types vary significantly in their consequences, necessitating diverse identification and localization strategies, each with unique characteristics that affect the urgency of response. Moreover, environmental factors such as storms, heavy rainfall, and high winds play a significant role in fault occurrences (Guo et al., 2025).

In countries such as Nigeria, the transmission grid experiences frequent short-circuit events caused by ageing infrastructure, poor maintenance culture, harsh

ISBN: 978-978-8567-02-8

weather conditions, and security-related vandalism. These recurring challenges contribute to unstable power delivery, equipment damage, and prolonged outages, making timely and accurate fault detection a critical requirement for grid reliability.

Various approaches have been developed over the years to detect and diagnose faults in power system transmission lines (Rajaperumal & Columbus, 2025). The use of protective relays is one of the most common strategies. Protective relays are devices that detect abnormal electrical conditions in the power system and execute corrective operations. When a defect is identified, the protective relay sends a signal to the circuit breaker, which trips to isolate the faulty segment of the transmission line (Chauhan & Agarwal, 2026).

Nowadays, updated power system analysis algorithms include expert systems, fuzzy logic systems, and artificial neural networks (Abdullah et al., 2024). Artificial Neural Networks (ANNs) are often regarded as the most efficient technology available. The ANNs offers significant capabilities for pattern recognition, classification, and generalization, as well as a wide range of applications in power systems (Bhagwat et al., 2024).

This paper aims to develop a data-driven fault detection and classification model using Artificial Neural Networks trained with the Levenberg–Marquardt algorithm. The study focuses on identifying multiple faults types and evaluates the model under varying grid conditions to reflect real-world Nigerian transmission network behaviour.

The rest of the paper is structured as follows. Section 2 is a background of the study which describes the faults and the ANNs. Section 3 presents the implementation and case study. Finally, Section 4 gives the paper's conclusion.

2. BACKGROUND

This section describes the concept of Faults in power systems and Artificial Neural Networks (ANNs).

2.1 Faults in Power Systems

A fault in power systems is an abnormal condition that interrupts normal current flow due to a failure of power system equipment. Fault conditions usually result in excessive current flow and voltage disturbances (Shakiba et al., 2023). Therefore, it can cause damage to electrical system equipment like generators, motors, transformers, transmission lines and switching equipment. It may also affect system stability and harm consumers. In addition, it introduces hazards to humans, animals, the environment, and facilities (Poongothai et al., 2025).

Transmission grids are subject to a variety of faults caused by bad weather & disasters, falling trees, human error, insulation failure in electrical equipment, heavy winds, animals coming into contact with electrical equipment in service, and more (Abdullah et al., 2024). Some causes of faults are depicted in Figure 1. Such problems frequently cause excessive current flow, equipment damage, network instability, safety concerns for humans, and prolonged outages. As a result, fault detection, classification, and location are necessary to quickly resolve faults, safeguard people and assets, and ensure the power system's reliability and integrity (Kumari et al., 2023).

Faults can be categorized into open-circuit (series) faults and short-circuit (shunt) faults. Shunt faults are further classified into symmetrical faults, which are the three-phase faults, and unsymmetrical faults, which are the one-line-to-ground, line-to-line fault, and double line-to-ground fault (Bhagwat et al., 2024).

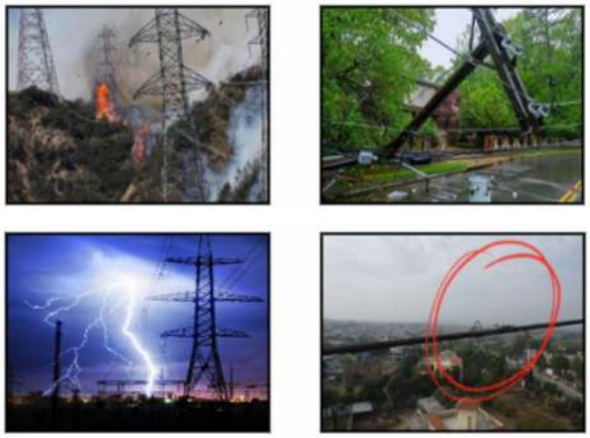


Figure 1: Types of faults in transmission grid (Guo et al., 2025).

Artificial intelligence (AI) advancements have also enabled the development of more advanced fault-detection and categorization algorithms. The usage of ANNs is one such approach. ANNs may be used to assess power system electrical data and detect and classify faults in transmission lines (Rafi et al., 2024).

2.2 Artificial Neural Networks (ANNs)

ANNs are computational models that simulate the structure and function of the human brain. ANNs, like the human brain, are composed of interconnected nodes, or neurons, that receive and transmit data (Kumari et al., 2023). ANNs in power systems can learn from experience and recognize patterns, assisting in load forecasting, fault identification and classification, and power flow optimization due to their ability to manage complex, nonlinear interactions between input and output variables (Bishal et al., 2021).

ANNs are used in power systems for fault detection and classification, identifying patterns in electrical signals to detect transmission line issues. This helps operators quickly pinpoint and isolate faults, minimizing outages (Malini et al., 2025). To train an ANN for fault detection, a large dataset of electrical signals from the power system is needed. It should include various defect types and operating conditions to ensure robustness. The dataset is divided into training, validation, and testing sets, with validation used for tuning and testing for performance (Kumari et al., 2023).

The artificial neural network was inspired by biological concepts and control applications, primarily comprising interconnected neurons (Rafi et al., 2024). A neuron acts as a data-processing unit and is the core component of a neural network. Its model is illustrated in Figure 2.

ISBN: 978-978-8567-02-8

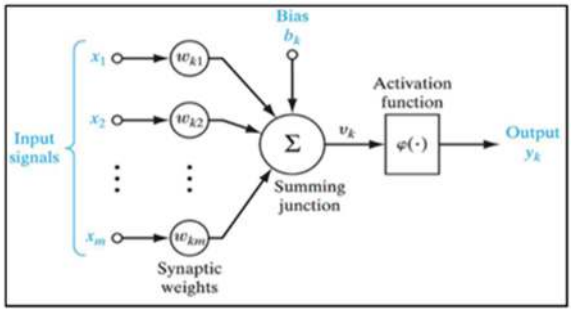


Figure 2: Model of a neuron (Bishal et al., 2021).

The artificial neural network was inspired by biological concepts and control applications, primarily comprising Figure 2 shows that the number of neurons in hidden layers primarily affects problem-solving ability, and fault clearing time is also related to this number. Decreasing the number of hidden layers can lead to a shorter fault clearing time. ANNs are mainly applied for classification, noise reduction, and extrapolation (Bishal et al., 2021).

Training an ANN involves adjusting weights to minimize error based on input data and target outputs. In a feedforward system, this process is critical for applications in power systems, especially for optimizing fault clearing times and classification tasks. They are effective for analyzing nonlinear and noisy transient power system signals, as they do not need explicit mathematical modeling and can generalize to new fault conditions (Rafi et al., 2024).

In this research, we developed a fault detection and classification model for both symmetrical and unsymmetrical electric faults associated with interconnected transmission lines using an ANN with the Levenberg-Marquardt algorithm (LMA).

LMA is an efficient optimization method for training artificial neural networks, offering fast convergence and strong performance with large, complex datasets. By iteratively adjusting network weights to minimize prediction error, it is widely applied in fields such as image processing, speech recognition, and power system analysis (Anwar et al., 2025). In power applications, LMA effectively handles diverse operational data for tasks like fault detection and load forecasting, ensuring accurate, robust, and real-time model performance (Sokolović & Žarković, 2025).

The major contributions of this paper are as follows:

- *A comprehensive ANN-based framework for detecting and classifying both single and simultaneous faults in transmission lines.*
- *Incorporation of practical factors such as varying loading conditions, fault resistance, and line distances to model realistic grid behavior.*
- *Evaluation of the ANN model using MSE, correlation coefficient, and other performance metrics to demonstrate reliability under uncertain operating scenarios.*
- *Application to fault scenarios relevant to the Nigerian transmission grid, making the results suitable for real-world deployment.*

3. IMPLEMENTATION AND CASE STUDY

The suggested artificial neural network (ANN)-based fault detection and classification model in Nigerian power system transmission lines was simulated as a case study in MATLAB Simulink. To train the ANN to accurately find and diagnose problems in transmission lines, the Levenberg-Marquardt method was utilized. Three-phase faults, single-line-ground faults, double-line-ground faults, and line-line faults were among the fault types included in the dataset used to train and test the ANN. A variety of operating situations, such as various fault sites, were also included in the dataset.

The ANN was trained using the Levenberg–Marquardt algorithm with data split into training, validation, and testing sets to ensure accuracy and prevent overfitting. Model performance was evaluated using mean squared error, and results demonstrated reliable and robust identification and localization of transmission line faults under various fault types and operating conditions.

3.1. System Structure

The model of the power system consists of two generators, each at (30 MVA 11kV). Each generator powers a three-phase 10-transmission line through a transformer.

The Simulink library's corresponding models were used to create all the model's constituent pieces. Faults occur at various locations along the transmission line, as shown in Figure 3. Voltage and current levels are collected for each failure, and the data are used to train the ANN using Simulink's Levenberg-Marquardt method. In this case, the data obtained from this model was categorized into training, testing, and validation in the ratio of 70:15:15, respectively.

3.2. Fault Identification

Timely detection and isolation of transmission line faults are essential to prevent blackouts and minimize damage to power system equipment. This study proposes an artificial neural network (ANN) based approach for accurate fault detection, classification, and localization in power transmission lines. The ANN is trained using simulated fault data obtained from a monitoring system that measures voltage and current traveling waves under various fault conditions. A controller is designed to interface with the trained ANN and function as a circuit breaker by converting the ANN classifier outputs into analog control signals. These signals are used to energize protective relays, enabling rapid isolation of the faulty section of the transmission line. The proposed method enhances fault diagnostic capabilities, reduces system downtime, and improves the overall reliability and operational stability of power transmission systems.

ISBN: 978-978-8567-02-8

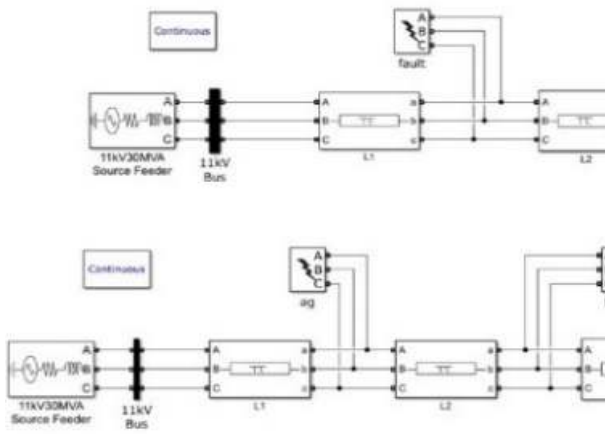


Figure 3: Simulink model for the faults in transmission lines

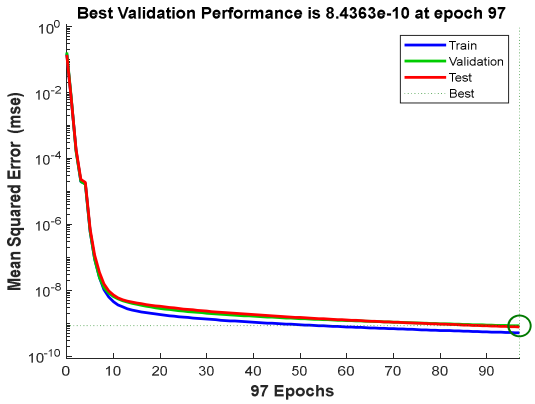


Figure 4: Training performance and MSE for detection of fault

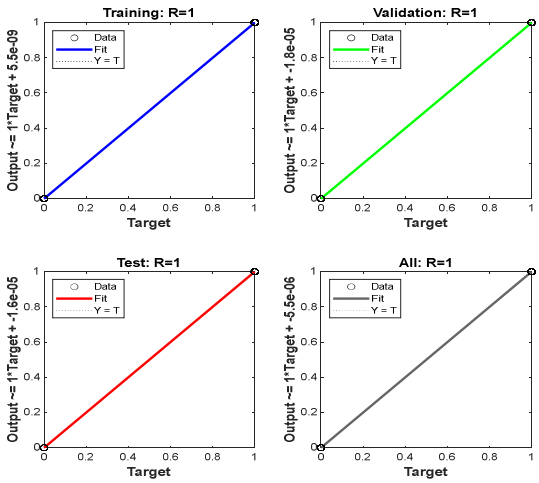


Figure 5: Regression plots for detection of fault.

3.2. Training and Testing

The ANN-based fault classification model was developed in MATLAB/Simulink using a two-stage process involving training with validation to prevent overfitting and testing with unseen data. Trained on a wide range of simulated fault scenarios, the model demonstrated strong capability in accurately classifying transmission line faults, thereby enhancing system reliability and reducing downtime.

3.3. Fault Detection

The ANN model used 8 inputs throughout the simulation: three voltage values from the three-phase voltage and three current values from the three-phase current and zero sequence voltage and current. The data set comprised all pre-fault current and voltage levels, as well as the values for all 11 types of faults. Figure 4 depicts the ANN's training performance, and the mean squared error (MSE) of the trained ANN was less than the specified value of 0.0001, indicating good performance. The selected ANN architecture was found suitable. The ANN's performance was further assessed using a linear regression plot in MATLAB, which revealed a perfect connection between the targets and the output (Figure 5). The correlation coefficient was used to determine how well the ANN's targets tracked changes in outputs, with a value of '1' indicating total correlation. The findings show that the ANN model efficiently classified various types of transmission line failures, enhancing system dependability and lowering downtime.

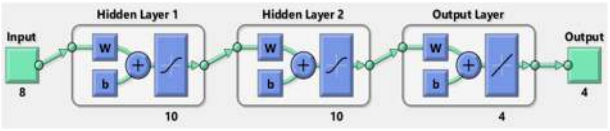


Figure 6: ANN design for classification of one fault.

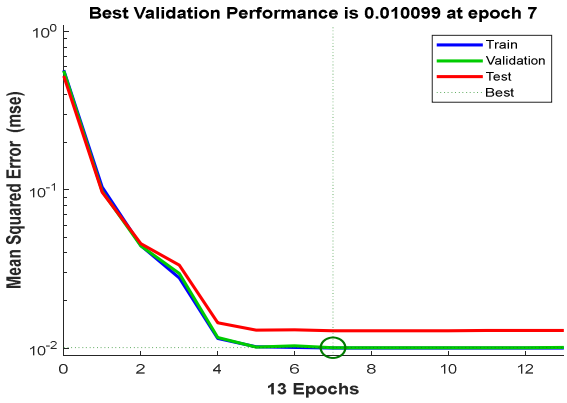


Figure 7: Training performance and MSE for classification of one fault.

3.4. Fault Classification

The same eight input features used for fault detection were also employed for fault classification in the proposed ANN model. For single-fault classification, the ANN was designed with four output nodes corresponding to the three phases (A, B, and C) and ground (G), where an output value of '1' indicated the presence of a fault and '0' denoted normal operation. Different fault types were identified based on the combination of fault indications across the phase and ground outputs, with the corresponding fault patterns summarized in Table 1. The ANN was trained to accurately recognize and categorize these fault combinations, thereby improving diagnostic accuracy in power transmission systems and reducing downtime while enhancing system reliability. In this configuration, the ANN architecture consisted of two hidden layers with ten neurons in each layer, as illustrated in Figure 6. The fault classification performance, shown in Figure 7, achieved a mean squared error of approximately 0.01, while the regression results

ISBN: 978-978-8567-02-8

presented in Figure 6 demonstrated a high classification accuracy of 98% during training.

TABLE I: ANN FAULT CLASSIFICATION.

Fault type	Phase A	Phase B	Phase C	Ground
Non-Fault	0	0	0	0
AG	1	0	0	1
BG	0	1	0	1
CG	0	0	1	1
AB	1	1	0	0
AC	1	0	1	0
BC	0	1	1	0
ABG	1	1	0	1
ACG	1	0	1	1
BCG	0	1	1	1
ABC	1	1	1	0

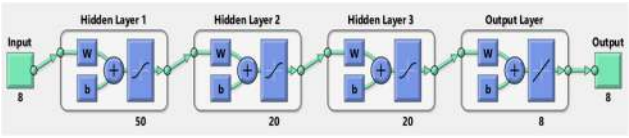


Figure 8: ANN design for two-fault classification.

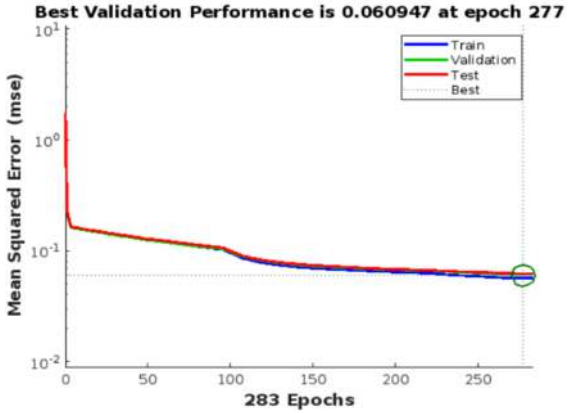


Figure 9: Training performance and MSE for two-fault classification.

Data was also collected to classify two faults in the same transmission line, and in this case a new ANN was trained, where the inputs still being 8, but now the outputs are 8 because the first 4 digits is for one fault and the other 4 remaining are for the other fault. Figure 8 depicts its design, having 3 hidden layers with 50 neurons in the first layer and 20 in the second and third layer. The performance obtained was around 0.06 (Figure 9) and the best linear regression obtained was 86.5%.

3.5. Fault Location

Identifying the location of the problem on the transmission line is often part of the fault locating procedure. This is critical for quick fault clearing and power supply restoration. The suggested ANN-based technique may detect fault location utilizing voltage and current data acquired from the monitoring system. The fault location can be inferred by studying the patterns in the voltage and current travelling waves. This is often accomplished by comparing the voltage and current data at different places along the transmission line. Once the location of the fault has been determined, suitable measures can be taken to isolate the defective segment of the line using circuit breakers or other protective devices.

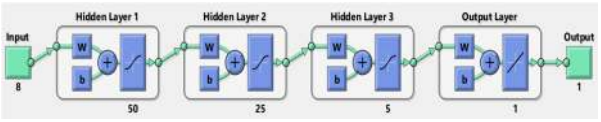


Figure 10: ANN design for locating fault.

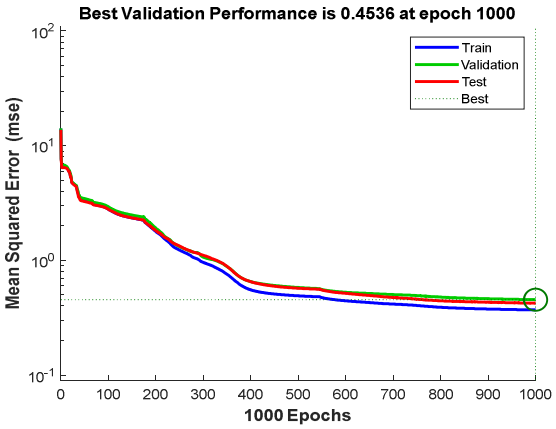


Figure 11: Training performance and MSE for locating fault.

Data for location was collected in many different scenarios to ensure the robustness of the identification. Figure 10 shows the ANN design, having 3 hidden layers with 50 neurons in the first layer, 25 neurons in the second layer, and 5 neurons for third layer. The performance obtained was around 0.45 and the best linear regression obtained was 97%.

3.6. Final Testing

The effectiveness of the developed ANN model was demonstrated by creating different types of faults at various locations for four different cases. The results showed that the ANN accurately identified the location and type of the faults in each case.

1) Case A - One fault: This is the base case which shows the proper detection, classification, and location for one fault. The test was under nominal conditions (Nominal Active Power and Nominal Reactive Power are 10MW and 100VAR respectively), 50Hz, fault resistance of 5Ω, location of 6 Km, and a line-to-line fault between phase A and C. The results performed are shown in Figure 12.

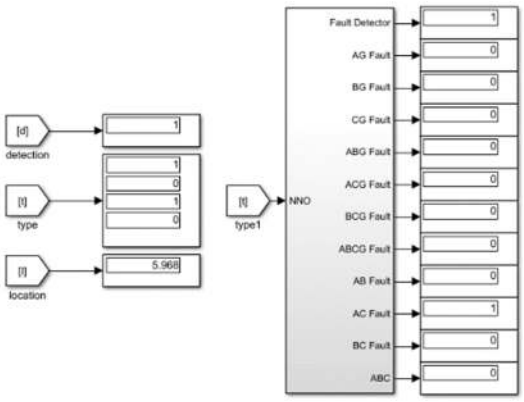


Figure 12: Results obtained for Case A.

2) Case B - Robustness with respect to system disturbances (when load changes): To test the robustness with respect to changes in the load, for the detection, classification, and location of one fault, same conditions

ISBN: 978-978-8567-02-8

of frequency, fault location, fault type and fault resistance were maintained. However, the load was increased to the double and triple of the nominal load. Again, the ANN succeeded to classify and locate the fault accurately in these scenarios.

3) Case C - Robustness with respect to parameters change (fault resistance): To test the robustness respecting different fault resistances, same conditions of frequency, fault location, fault type and nominal load were maintained, but now with a fault resistance of 50Ω. The fault was detected as well as its location which is 6.044 as explained in previous cases.

4) Case D - Case of two faults: Finally, Case D was designed to test the ANN trained when two faults appear in the transmission line. This test is under nominal load, frequency of 50Hz and fault resistance of 15Ω: the first fault is line-to-line between phase A and C located at 6Km, the second fault is three phase faults located 1Km beyond the previous one. The ANN was able to detect and classify the two faults accurately.

The results highlighted the potential of the proposed ANN-based approach for effective fault detection, classification, and location in power transmission systems.

4. CONCLUSION

In conclusion, the paper presents an ANN-based method for detecting, allocating and classifying faults in power transmission networks. The Levenberg-Marquardt method was used to train the ANN model, which could recognize several sorts of faults, including single-line-ground faults, line-line faults, double-line-ground faults, and three-phase faults. The created ANN's performance was assessed using mean squared error and correlation coefficient, demonstrating good accuracy in defect detection and classification. The usefulness of the ANN model was further verified by simulating faults at various sites along the transmission line, which validated its success in fault identification and classification. The suggested method has the potential to improve problem diagnostics in power transmission systems, resulting in less downtime and higher system dependability.

REFERENCES

Abdullah, A. G., Ibrahim, M. A., & Ibrahim, W. K. (2024). Detection and identification of fault in transmission lines based on ANN. *Diagnostyka*, *25*.

Anwar, T., Mu, C., Yousaf, M. Z., Khan, W., Khalid, S., Hourani, A. O., & Zaitsev, I. (2025). Robust fault detection and classification in power transmission lines via ensemble machine learning models. *Scientific Reports*, *15*(1), 2549.

Bhagwat, A., Dutta, S., Jadoun, V. K., Veerendra, A. S., & Sahu, S. K. (2024). A customised artificial neural network for power distribution system fault detection. *IET Generation, Transmission & Distribution*, *18*(11), 2105–2118.

Bishal, M. R., Ahmed, S., Molla, N. M., Mamun, K. M., Rahman, A., & Al Hysam, M. A. (2021). ANN based fault detection & classification in power system transmission line. *2021 International Conference on Science & Contemporary Technologies (ICSCT)*, 1–4.

Chauhan, R. K., & Agarwal, A. (2026). Real-time testing of double-ended travelling wave fault locator and its impact on transmission network reliability, availability and tariff. *Electric Power Systems Research*, *253*, 112385.

Guo, Q., Wang, F., Cheng, S., Wang, K., & Zhang, Y. (2025). Fault location and isolation technology for power grid automation based on intelligent algorithms. *Energy Informatics*, *8*(1), 88.

Kumari, S., Mishra, A., Singhal, A., Dahiya, V., Gupta, M., & Gawre, S. K. (2023). Fault detection in transmission line using ann. *2023 IEEE International Students' Conference on Electrical, Electronics and Computer Science (SCEECS)*, 1–5.

Malini, T., Thirumoorthi, P., & Lakshmi, K. (2025). ANN-based fault classification and localization with optimized PMU deployment for transmission systems. *Scientific Reports*, *15*(1), 39165.

Poongothai, K., Kumaresan, M., Ananda, M. H., & Sathiya, M. (2025). Power transmission line fault detection in internet of things based smart grids using relational bi-level aggregation graph convolutional network-red panda optimization approach. *Measurement*, 118448.

Rafi, M. A. I., Sohan, M. R., Nadid, M. H., Rafa, T. S., & Jawad, A. (2024). Enhancing power transmission line fault detection with a hybrid ANN-SVM machine learning model: a comparative study. *2024 International Conference on Advances in Computing, Communication, Electrical, and Smart Systems (ICACCESS)*, 1–6.

Rajaperumal, T. A., & Columbus, C. C. (2025). Transforming the electrical grid: the role of AI in advancing smart, sustainable, and secure energy systems. *Energy Informatics*, *8*(1), 51.

Shakiba, F. M., Azizi, S. M., Zhou, M., & Abusorrah, A. (2023). Application of machine learning methods in fault detection and classification of power transmission lines: a survey. *Artificial Intelligence Review*, *56*(7), 5799–5836.

Sokolović, Ž., & Žarković, M. (2025). Fault detection, classification and localization in HV power transmission lines using ANN. *Electric Power Systems Research*, *248*, 111927. https://doi.org/https://doi.org/10.1016/j.epsr.2025.111927.

ISBN: 978-978-8567-02-8

5TH Faculty of Engineering Conference on Engineering Innovation and Economic Policies: Driving Sustainable Industrial Growth in Nigeria

Faculty of Engineering, Bayero University, Kano.

062-Machine Learning-Driven Adaptive Modulation for Visible Light Communication in Industrial Robotic Warehouses

Abdurrahman Y Salisu, Dahiru S Shuaibu, and Sani H Lawan

Department of Electrical Engineering Engineering, Bayero University Kano. (Email of Corresponding Author: asyahaya@fudutsinma.edu.ng , abdulsalisu11@gmail.com)

Abstract: Visible Light Communication (VLC) has emerged as a promising complementary wireless technology for indoor industrial environments due to its immunity to electromagnetic interference and ability to reuse existing lighting infrastructure. However, VLC links are highly sensitive to line-of-sight alignment, shadowing, and mobility, making reliable communication with autonomous mobile robots particularly challenging in industrial warehouses. This paper proposes a novel machine learning-driven adaptive modulation framework for VLC-enabled mobile robots operating in realistic industrial environments. A physically based three-dimensional warehouse environment is developed using Blender to simulate realistic light propagation, occlusion, and robot motion. Irradiance values collected along robot trajectories are converted into time-varying signal-to-noise ratio (SNR) traces, which serve as input to a reinforcement learning agent. A Q-learning algorithm is employed to dynamically select optimal M-ary Pulse Amplitude Modulation (M-PAM) schemes based on instantaneous channel conditions. The learning objective balances spectral efficiency and reliability by incorporating symbol error rate constraints into the reward function. Simulation results demonstrate that the proposed adaptive modulation scheme significantly outperforms fixed-modulation baselines in terms of spectral efficiency and robustness under shadowed and dynamic channel conditions typical of industrial warehouses with improved latency reduction of 25%. The presented simulation-to-learning framework provides a reproducible simulation framework for intelligent VLC system design and highlights the potential of reinforcement learning for next-generation industrial 4.0 robotic communication systems.

Key words: Spectral Efficiency (SE), Signal-to-noise ratio (SNR), Pulse Amplitude Modulation (PAM), Symbol error rate (SER), bit error rate (BER), Reinforcement Learning (RL).

1. INTRODUCTION

Visible Light Communication (VLC) is an optical wireless communication technology that utilizes light-emitting diodes (LEDs) for simultaneous illumination and data transmission (Gupta, 2024). As a complementary alternative to conventional radio-frequency (RF) communication systems, VLC offers several intrinsic advantages, including a vast unlicensed bandwidth, immunity to electromagnetic interference (EMI), and enhanced physical-layer security due to its line-of-sight propagation characteristics (Tai-Cheng, 2021). These features make VLC a promising solution for environments where RF communication is constrained, unreliable, or undesirable.

Unlike RF systems, VLC does not operate within the congested electromagnetic spectrum, thereby significantly reducing susceptibility to co-channel interference and external electromagnetic disturbances. This property makes VLC particularly suitable for interference-sensitive environments such as industrial facilities, hospitals, and aircraft cabins. In addition, the wide optical spectrum available for indoor VLC enables higher achievable data rates compared to RF systems (Gupta, 2024). Furthermore, since visible light cannot penetrate opaque obstacles such as walls, VLC inherently limits signal leakage, offering improved security for indoor wireless communication.

These advantages make VLC particularly suitable for environments where RF communication is unreliable or undesirable, such as industrial facilities, hospitals, and aircraft cabins (Chen, 2022).

Industrial environments, including manufacturing plants, processing facilities, warehouses, power stations, and medical laboratories, present substantial challenges for wireless communication. These environments are typically characterized by high levels of EMI, dense metallic infrastructure that induces severe multipath propagation, and dynamically varying illumination conditions (Y. Almadani, 2018). Such factors often degrade the performance of conventional RF-based wireless systems. VLC systems, when properly designed, can operate effectively in these environments; however, maintaining reliable communication requires adaptive techniques capable of responding to rapidly changing channel conditions (Rizi, 2024).

ISBN: 978-978-8567-02-8

Adaptive modulation is a widely adopted technique that dynamically adjusts the modulation order according to instantaneous channel quality to optimize spectral efficiency and transmission reliability. Nevertheless, traditional adaptive modulation schemes based on predefined thresholds or lookup tables lack flexibility and fail to generalize in highly dynamic scenarios (Rizi, 2024). In contrast, reinforcement learning (RL), particularly Q-learning, enables communication systems to autonomously learn optimal modulation strategies through interaction with the environment without requiring prior channel knowledge. By continuously adapting to real-time channel variations, machine-learning-driven adaptive modulation provides a robust and efficient solution for VLC systems operating under complex and time-varying conditions (Rizi, 2024). Although reinforcement learning has been successfully applied to adaptive modulation, precoding, and resource allocation in VLC systems, several limitations remain in the existing literature.

First, a large portion of prior work focuses on physical-layer security enhancement or healthcare-oriented applications, such as medical body sensor networks (Chi-Wai Chow, 2015), rather than industrial communication scenarios. These environments differ significantly in terms of channel characteristics, mobility patterns, and interference sources (Y. Almadani, 2018). For instance, medical body sensor networks typically deal with patient movement, which differs from the rapid and complex mobility of industrial robots and the strong reflections from dense metallic structures in industrial settings (Rizi, 2024).

Second, many existing VLC studies assume simplified or static indoor channel models and controlled environments (Selma Yahia, 2021). Such assumptions neglect key features of industrial settings, including dense metallic structures, severe multipath reflections, line-of-sight blockages, and rapidly varying channel conditions caused by mobile robotic platforms (Zheng, 2020). Consequently, the applicability of these approaches to real-world industrial environments remains limited. The challenge in industrial environments is further exacerbated by the need for reliable data transfer for critical operations and the presence of various sources of optical interference (Y. Almadani, 2018).

Third, several adaptive modulation techniques rely on predefined thresholds, lookup tables, or offline-trained supervised learning models (L. Wu, 2015). These methods lack the flexibility required to cope with real-time channel dynamics and cannot efficiently generalize to previously unseen operating conditions. While reinforcement learning has been explored in RF and underwater communication systems to address similar challenges, its application to adaptive modulation in industrial VLC systems remains insufficiently investigated. The dynamic nature of industrial settings requires continuous adaptation, which Q-learning can provide by learning optimal strategies through direct interaction with the environment (Rizi, 2024).

Finally, existing works rarely integrate high-fidelity channel modelling with online learning-based modulation adaptation in a unified simulation framework. This creates a gap between theoretical algorithm development and practical system-level evaluation under realistic industrial conditions. An integrated approach is crucial for assessing the practical performance of VLC systems in complex industrial scenarios.

Image-based control and sensing has been applied in a many next generation manufacturing fields. One software capable of these simulations is the open-source 3D modelling software Blender, which has many capabilities aided by a Python API (Kip Nieman, 2024). Their work used Blender as an image-based control test bed, where both the process and the controller are simulated, in the context of a greenhouse supplemental lighting control system (Kip Nieman, 2024).

VisualEnv framework provided photorealistic scenes and agent interaction through code. Blender has also been used as a closed-loop simulation testbed for control systems via Python scripting, as well as in robotics simulators like MORSE, which leverage Blender's modeling and physics capabilities with Python extensions (Andrea Scorsoglio, 2021). These precedents support the viability of using Blender-Python environments as a flexible simulation platform for data generation and algorithm development, motivating our approach to simulate an industrial VLC environment with Python control.

In this work, an industrial VLC communication system for mobile robotic platforms is investigated using machine-learning-based adaptive modulation. First, an indoor industrial environment is modelled using Blender to acquire data, and the VLC channel is characterized using a distance and orientation-dependent optical channel model. The channel response is represented through the DC channel gain and the resulting signal-to-noise ratio (SNR), and irradiance which vary as the robot moves within the workspace.

Next, a baseline VLC system employing fixed M-ary pulse amplitude modulation (M-PAM) is implemented in MATLAB/Simulink to establish reference performance metrics in terms of symbol error rate (SER) and spectral efficiency (L. Wu, 2015). This baseline model serves as a benchmark against which adaptive techniques are evaluated. Subsequently, a Q-learning-based adaptive modulation framework is integrated into the VLC system. The reinforcement learning agent observes the channel state, represented by quantized SNR and error performance, and selects an appropriate modulation order from a predefined action set. The agent is trained online using a reward function that jointly considers transmission reliability and spectral efficiency, enabling

ISBN: 978-978-8567-02-8

autonomous learning and real-time adaptation to channel variations.

Simulation results confirm that the proposed Q-learning-based adaptive modulation scheme significantly outperforms fixed modulation in indoor warehouse VLC systems. By intelligently adapting the modulation order to channel conditions, the system achieves lower latency, higher throughput, and improved reliability, validating the suitability of reinforcement learning for next-generation industrial optical wireless communication.

2. METHODOLOGY

In this section we will explain the steps taken to carry out this research, from the system architecture, to the warehouse simulation to acquire data, then VLC channel computation, Q-learning training and finally integration of the algorithm into VLC channel and comparison with the fixed modulation to check for differences and improvements.

2.1 Simulation Environment

In this section, a 3D industrial warehouse simulation is designed using Blender with Concrete flooring and textured walls, Ceiling-mounted LED luminaires, metal shelves, obstacles and a mobile robot equipped with a PD sensor as shown in Figure 1. A Python script was developed to generate a realistic warehouse and collect data.

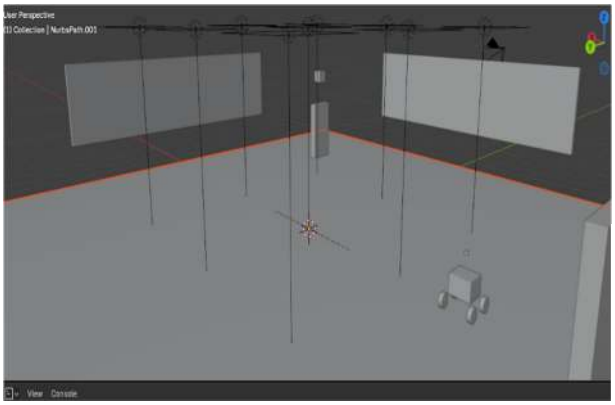


Figure 1: Warehouse simulation in Blender showing Concrete flooring and textured walls, Ceiling-mounted LED luminaires, metal shelves, obstacles and a mobile robot equipped with a PD sensor

The robot follows a predefined trajectory, and Blender's Cycles engine computes irradiance at the sensor using emission passes. For every animation frame, irradiance values are extracted and saved as a CSV dataset. The graph of Irradiance against the robot position is shown in Figure 2.

There is a drastic change in Irradiance and channel gain which change in robot position. They tend to reduce when moving away from the transmitter position at on every direction. It is important to note 100 different positions were captured as against the sampled 9 positions captured in the graph for clarity and easier referencing to the robot's initial starting position (0 distance).

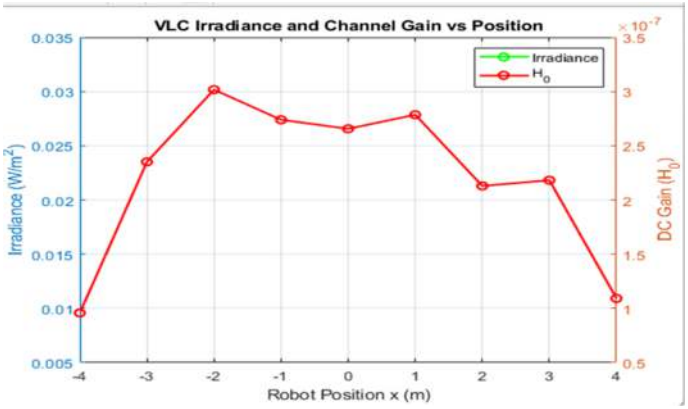


Figure 2: Graph Irradiance and channel gain against Robot position displaying nine position 4m away on each side away from the transmitter.

2.2 VLC Channel Computation:

A Simulink model of a VLC channel with fixed modulation was first created as shown in Figure 3 to monitor performance which will later be integrated with Q learning model to form an adaptive modulation VLC channel as shown in Figure 4. At first 4 PAM was used then 8 PAM and 16 PAM consecutively.

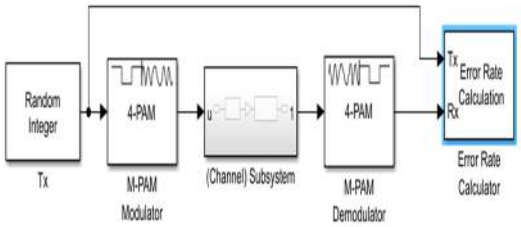


Figure 3 A fixed modulation simulink VLC channel with 4 PAM modulation. The output is used to calculate Error rate.

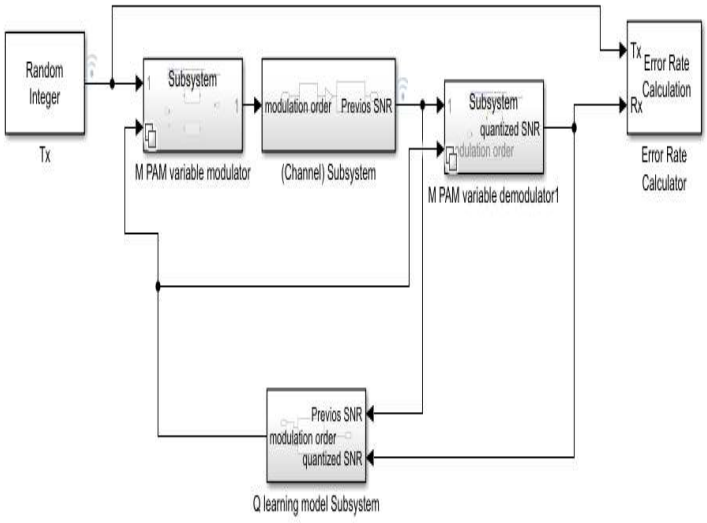


Figure 4: A Q-learning based adaptive modulation VLC channel block diagram, shwing the transmitter, channel subsystem, the variable modulator and demodulator and Q-learning Subsystem.

For each irradiance measurement E(t):

$$SNR(t) = [R \times Pr(t)]^2 / N_0 \quad (1)$$

$$\text{Where } Pr(t) = E(t) \times Apd \quad (2)$$

ISBN: 978-978-8567-02-8

The simulation environment uses the SNR data as your environment timeline. At each step `t`, the agent observes 'SNR$_t$'. It chooses a modulation order 'M$_t$'. It then Compute the SER for that M and SNR using the theoretical M-PAM SER formula:

$$SER_M = 2\frac{M-1}{M}Q\left(\sqrt{\frac{6log_2(M)}{M^2-1}\times SNR_t}\right) \quad (3)$$

Where, $Q(x)0.5erfc\left(\frac{x}{\sqrt{2}}\right)$. (4)

The SNR time series is quantized into finite states for RL.

The Latency of the fixed modulation is calculated and then later compared to that of Adaptive modulation.

Latency = $D_{proc} + D_{trans} + D_{queue} + D_{prop}$ (5)

Where,

D_{proc} = processing delay, D_{queue} = Queuing delay, D_{trans} = transmission delay and D_{prop} = propagation delay.

$D_{prop} = \frac{d}{v}$ (6)

Where,

d = distance (meters)

v = propagation speed

$D_{trans} = \frac{L}{R}$ (6)

Where,

L = packet length

R = data rate (bits/s)

One-way latency (ignoring queue & processing):

$Latency = \boldsymbol{\frac{L}{R} + \frac{d}{v}}$ (7)

Round-trip latency (RTT):

RTT = 2×One-way latency

2.3 Q-Learning Adaptive Modulation

The Q-learning process will be explained in this part as follows: problem definition, algorithm overview, pseudocode, learning algorithm and then the implementation in simulink.

2.3.1 Define the Learning Problem

We want an agent that learns which modulation order (M-PAM) to select at each time step, given the observed SNR. The goal is to maximize throughput (bits/s/Hz) while keeping the Symbol Error Rate (SER) ≤ 10^{-3}.

ACTIONS (A): A = {2, 4, 8, 16, 32, 64} representing M-PAM modulation levels.

STATES (S): is the Discrete or continuous SNR levels. SNR was quantized into 10 bins.

REWARD: id designed to encourage higher modulation to give more throughput and penalize actions that exceed SER threshold

Reward(R):

$$r(s,a) = \begin{cases} log_2(M)(1-SERM), & if\ SER_M \le 10^{-3} \\ -SER_M, & otherwise \end{cases} \quad (8)$$

A Q-table is trained over multiple episodes, learning the optimal modulation choice at each SNR level.

Algorithm core:

$$Q(s,a) \leftarrow Q(s,a) + \propto [r + \gamma\, max_{a'} Q(s',a') - Q(s,a)] \quad (9)$$

The hyper parameters used for the training. A learning rate of 0.5, discount factor of 0.9 and exploration rate of 0.2. It was run up to 500 episodes as shown in Table I below.

TABLE I: TYPICAL HYPER PARAMETERSMMM USED:

Parameter	MEANING	Value
α	Learning rate	0.5
γ	Discount Factor	0.9
ε	Exploration rate	0.2← 0.01 (decays)
Episodes	Training runs	500

2.3.2 Algorithm Overview

This section presents the proposed reinforcement learning framework for adaptive modulation in an industrial visible light communication (VLC) system. The objective of the algorithm is to dynamically select the optimal M-ary pulse amplitude modulation (M-PAM) order that maximizes spectral efficiency while maintaining reliable communication under time-varying channel conditions induced by robot mobility and environmental dynamics.

The adaptive modulation problem is formulated as a Markov Decision Process (MDP), where a Q-learning agent interacts with the VLC environment by observing the channel state, selecting an appropriate modulation order, and receiving a reward based on the resulting transmission performance. Unlike conventional threshold-based adaptive modulation schemes, the proposed approach does not require prior channel knowledge or predefined decision boundaries

At the beginning of each transmission episode, the Q-table is initialized to zero. During each time step, the agent observes the current channel state, selects a modulation order based on the ε-greedy policy, and transmits data using the selected M-PAM scheme. The receiver computes the SER and feeds it back to the transmitter, which then evaluates the reward and updates the Q-table. Over successive episodes, the agent learns the optimal modulation policy for different channel states.

2.3.3 Algorithm Pseudocode:

Q-Learning-Based Adaptive M-PAM Modulation

Initialize Q(s,a) = 0 for all s ∈ S, a ∈ A

Set learning rate α, discount factor γ, exploration rate ε

for each episode do
  Observe initial state s_0
  for each time step t do
    With probability ε, select a random action a_t
    Otherwise, select a_t = $argmax_a$ Q(s_t, a)

ISBN: 978-978-8567-02-8

Apply M-PAM modulation with order M = a_t
Transmit data and observe SER_t and next state s_{t+1}

if $SER_t \leq SER_th$ then
$r_t = \log_2(M)\,(1 - SER_t)$
else
$r_t = -SER_t$
end if

Update $Q(s_t, a_t) \leftarrow Q(s_t, a_t) +$
$\alpha\,[\, r_t + \gamma \max_a Q(s_{t+1}, a) - Q(s_t, a_t)\,]$

$s_t \leftarrow s_{t+1}$
end for
end for

Algorithm 1: Q-Learning–Based Adaptive Modulation for Mobile VLC Robot

Algorithm 1

Input:

- Quantized SNR state space S = {1,2,…,N_s}
- Action space (PAM orders) A={2,4,8,16}
- Learning rate alpha α
- Discount factor gamma γ
- Exploration probability epsilon ϵ
- Target SER threshold SER threshold SER_{th}

Output:

- Optimal modulation policy π∗(s)\pi^*(s)π∗(s)

Initialization:

1. Initialize Q-table Q(s,a) = 0, ∀s ∈ S, a ∈ A
2. Initialize robot position (x_0,y_0) and velocity
3. Set episode counter e = 1

for each episode e=1,2,…,E **do**

4. Obtain initial SNR from VLC channel and quantize to state sss
5. **for** each time step t = 1,2,…, T **do**
6. **Action selection (ε-greedy):**

$$a = \begin{cases} random\ action\ from\ A, & with\ probability\ \varepsilon \\ \arg\max_a Q(s, a'), & with\ probability\ 1 - \varepsilon \end{cases}$$

7. Apply selected PAM order M(a) at the VLC transmitter
8. Transmit data symbols over the VLC channel
9. Estimate Symbol Error Rate (SER) at the receiver
10. **Reward computation:**

$$r(s,a) = \begin{cases} log_2(M)(1 - SERM), & if\ SER_M \leq SERth \\ -SER_M, & otherwise \end{cases}$$

11. Update robot position using time-correlated mobility model
12. Observe new SNR and quantize to next state s′
13. **Q-value update:**

$$Q(s,a) \leftarrow Q(s,a) + \propto [r + \gamma \max Q(s', a') - Q(s,a)]$$

14. Set s ← s′
15. **end for**
16. Decay exploration probability ϵ\epsilonϵ (optional)

end for

2.3.2 Implementation in Simulink

The proposed algorithm is implemented in MATLAB/Simulink using a custom Q-learning agent block. The agent receives SNR and SER measurements from the VLC receiver subsystem and outputs the selected modulation order, which is fed directly into the PAM modulator and demodulator blocks via an input port as shown in Figure 4. The modulation order remains constant over each transmission frame to ensure stable operation. The performance is assessed using Spectral efficiency, SER performance, modulation switching patterns, comparison with fixed-modulation baselines.

Latency formula for Q-Learning Agent

$$Latency\ (M) = \frac{L}{\mathrm{B}\log_2 M} + D_{proc} \quad (10)$$

Spectral Efficiency $(SE) = \log_2(M_t) \times (1 - SER_M)$ (11)

Practical systems employing M-ary PAM modulation can only achieve discrete spectral efficiency levels given by:

$$\eta = \log_2(M) \quad (12)$$

Thus: 5 bits/s/Hz corresponds to lower order modulation and 6 bits/s/Hz corresponds to higher modulation selected under favorable condition.

3.0 RESULTS AND DISCUSSION

The learned state-action policy of the Q-learning agent. For high SNR states, the agent consistently selects 16-PAM to maximize throughput and minimize latency at 0-5 meters which has high SNR, while it chooses 8-PAM at 5-10 meters (medium SNR), at distances greater than 10 meters (higher SNR) it chooses 4-PAM. As the channel condition degrades with change in distance, the policy changes to lower-order modulation schemes to maintain reliable communication, demonstrating successful learning of the BER-throughput-Latency trade-off. The diagonal dominance of the heatmap confirms successful policy convergence as shown in Figure 5 below.

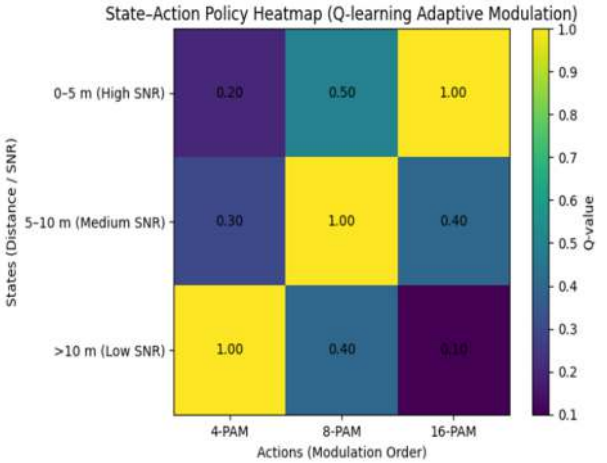


Figure 5: State-Action Heatmap (Q-Learning Adaptive Modulation).The policy changes from higher-order to lower-order modulation schemes with change in distance.

ISBN: 978-978-8567-02-8

After multiple episodes of SNR simulation from CSV to train the agent to select the right modulation the following plots in Figure 6 were gotten Modulation order vs. time (how it adapts).

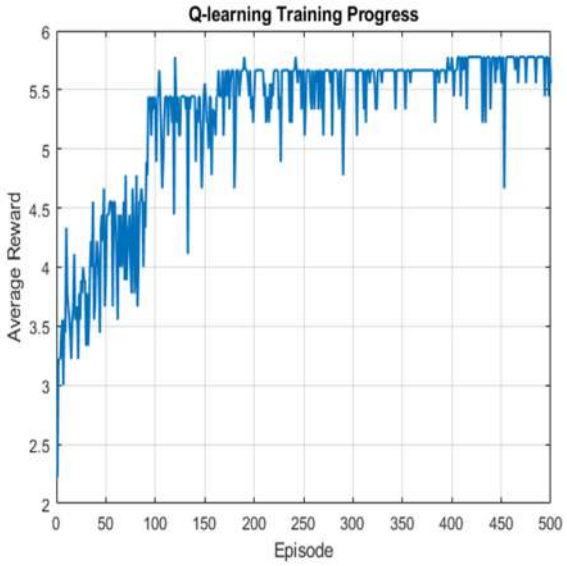


Figure 6 Q-learning Training Progress: this is showing the training process with rewards gotten across 500 episodes.

At first 50 episodes a reward of 3.5 to 4 was gotten which improved to about 4 to 4.5 at 100 episodes. After 200 episodes the reward was already above 5 and after 500 episodes the expected reward of above 5.5 was achieved which shows the agent has successfully achieved the reward. balance throughput & reliability.

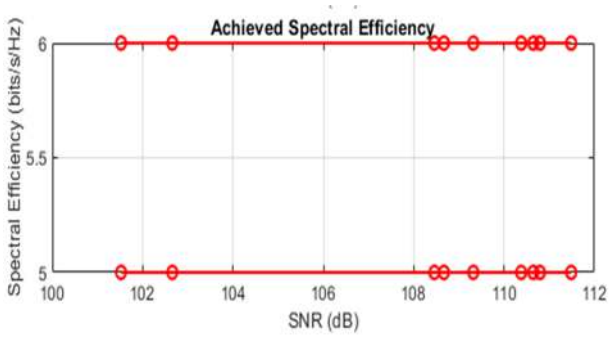


Figure 7 Achieved Spectral Efficiency with SNR in dB showing a discrete clustering behavior between 5 bits/s/Hz and 6 bits/s/Hz.

The discrete clustering of achieved spectral efficiency values shown in Figure 7 confirms that the proposed adaptive modulation scheme effectively exploits high-SNR conditions while respecting practical modulation constraints, resulting in stable and reliable performance rather than unbounded rate increases.

The Latency of the fixed modulation scheme was calculated using a fixed modulation scheme of 8-PAM where it shows an increase in latency with change in distance. At distance of 2.5 a low latency was gotten. But as the distance increases the latency increased with increase in distance of up to 20 meters as shown in Figure 8 leading to inefficient performance at short distance and variable performance at long distance. While that of the Adaptive modulation is shown in Figure 9. It exhibits a piecewise latency where rapid increases corresponds to modulation downgrade caused by reduced SNR at larger distance, maintaining very low latency of 0.0002s at 2m up to about 5 meters. The modulaton changed at 5m due to change in SNR and the latency was maintained with slight rapid increase of about 0.00025s. At maximum distance of 20m a low latency of 0.00036 was achieved which proves that the Q learning agent effectively balances latency and improves strength. The end-to-end latency of the VLC link is modeled as a distance dependent metric, where increased transmitter-receiver separation results in reduced SNR, lower modulation order, and consequently higher transmission delay.

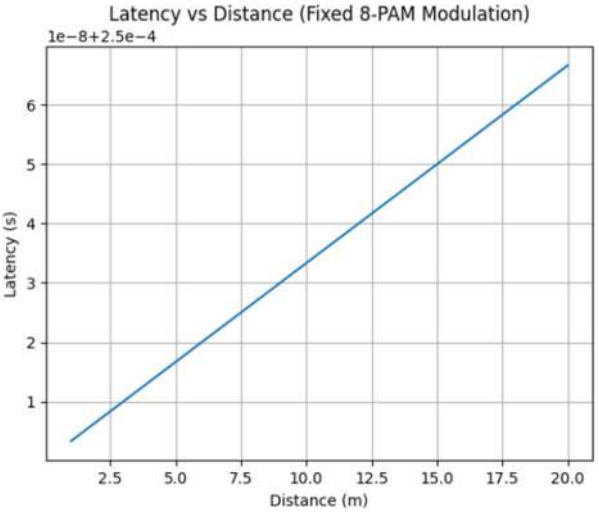


Figure 5: Latency against distance for fixed modulation 8-PAM. showing linear change in latency with distance from the transmitter. Modulation and Data rate are fixed.

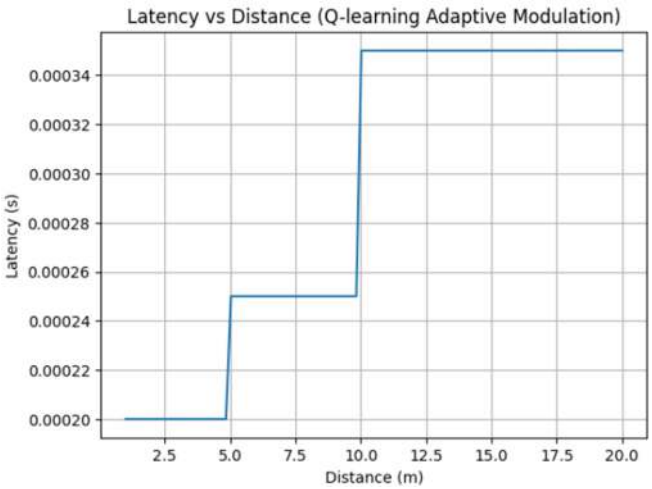


Figure 6: Latency vs Distance for Q-learning Adaptive modulation

ISBN: 978-978-8567-02-8

TABLE II: COMPARISON BETWEEN FIXED MODULATION AND Q-LEARNING ADPTIVE MODULATION SCHEMES

METRIC	FIXED MODULATION	Q-LEARNING ADAPTIVE MODULATION
Modulation selection	Static (single PAM order)	Dynamic (state-dependent PAM order
Spectral Efficiency	Constant mostly (e.g 5 bits/s/Hz for lower PAM)	Adaptive
Symbol Error Rate (SER)	High to low SNR, over protected at high SNR	Dynamic (depending on PAM order/state)
Latency	High during poor channel condition	Reduced due to the adaptive rate selection.
Robustness to Channel Variation	Low	High
Resource Utilization	Inefficient (wasted SNR margin)	Efficient exploitation of channel quality
Adaptability	None	Learns optimal policy over time
Suitability for Dynamic Environments	Poor	Excellent

4. CONCLUSION

The results obtained from this work demonstrate that incorporating Q-learning–based adaptive modulation into a VLC system significantly improves overall communication performance when compared to fixed modulation. The adaptive scheme effectively responds to changes in distance and SNR by selecting appropriate modulation orders, whereas the fixed-modulation approach operates with a single fixed setting irrespective of channel quality.

At high SNR values, the learning agent consistently selects higher-order modulation, allowing the system to fully exploit favourable channel conditions which fixed modulation cannot exploit such quality, resulting in underutilization of available channel capacity. The achieved spectral efficiency results confirm this behaviour, with the adaptive scheme reaching higher efficiency levels while maintaining link reliability.

Significant improvements are also observed in terms of symbol error rate (SER) and bit error rate (BER). Under fixed modulation, error rates increase noticeably when the channel degrades, particularly when higher-order modulation is used. In the adaptive system, the Q-learning agent moderates this issue by switching to lower-order modulation at reduced SNR levels, thereby maintaining SER and BER within acceptable bounds. Simulation results indicate up to an order-of-magnitude reduction in SER in moderate channel conditions, which directly translates to improved reliability and reduced packet loss.

The latency is reduced by dynamically increasing the modulation order in high-SNR states, the system transmits more bits per symbol, reducing transmission time and overall delay. Compared to the fixed-modulation scheme. The adaptive approach achieves a 20% reduction in transmission latency, while also avoiding latency penalties caused by retransmissions at low SNR. This balanced behaviour highlights the effectiveness of the reward function in jointly considering throughput, error performance, and delay.

In conclusion, this work shows that Q-learning–based adaptive modulation provides a strong and efficient solution for VLC systems operating in dynamic indoor environments. By intelligently adapting to SNR variations, the proposed scheme achieves lower SER and BER, improved SNR use, and reduced latency compared to fixed modulation. These improvements collectively enhance system reliability and efficiency, making the approach well-suited for industrial applications such as warehouse robotics. The results confirm that reinforcement learning offers a practical and scalable framework for next-generation adaptive optical wireless communication systems.

ACKNOWLEDGMENT

The authors would like to thank the Department of Electrical, Computer and Communications Engineering, Faculty of Engineering, Bayero University, Kano, for providing the academic environment and facilities to make this research a success.

REFERENCES

Andrea Scorsoglio, R. F. (2021). visual Gym environments with Blender. *arxiv*. Retrieved from https://arxiv.org/abs/2111.08096

Chen, C. (2022). Special Issue on “Visible Light Communication (VLC)”. *Photonics*, 9(5) 284. Retrieved from https://doi.org/10.3390/photonics9050284

Chi-Wai Chow, Y. L.-H.-Y.-N.-Z. (2015, June). Secure communication zone for white-light LED visible light communication. *Elsevier (Optics Communication), 344*, 81-85. doi:https://doi.org/10.1016/j.optcom.2015.01.055

Gupta, S. R. (2024). Illuminating the future: A comprehensive review of visible light communication applications. Optics & Laser Technology, 177, 111182. Retrieved from https://doi.org/10.1016/j.optlastec.2024.111182

Kip Nieman, H. D. (2024). Study of the Application of Blender for Simulation of a Closed-loop Image-based Greenhouse Supplemental Lighting Control. *IFAC-PapersOnLine, 58*, 519-524. Retrieved from https://doi.org/10.1016/j.ifacol.2024.08.389

L. Wu, Z. Z. (2015, Jan 1). Adaptive Modulation Schemes for Visible Light Communications. *Journal of Lightwave Technology, 33*, 117-125. doi:10.1109/JLT.2014.2374171

M. Singh, S. G. (2021). Performance Evaluation of Visible Light Communication System based on Optical Power Distribution with Channel Delay Spread and SNR. *Advanced Communication Technologies and Signal Processing (ACTS)*, 1-5. doi:10.1109/ACTS53447.2021.9708215

Rizi, R. B. (2024). Machine Learning-Driven Adaptive Modulation for VLC-Enabled Medical Body

ISBN: 978-978-8567-02-8

Sensor Networks. *Iranian Journal of Electrical and Electronic Engineering*, 20.

Selma Yahia, Y. M.-C. (2021). A Survey of Channel Modeling Techniques for Visible Light Communications. *Journal of Network and Computer Applications*, 103206. doi:https://doi.org/10.1016/j.jnca.2021.103206

Tai-Cheng, W.-T. H.-B.-W.-W.-C. (2021). Visible Light Communication System Technology Review: Devices, Architectures, and Applications. *Crystals*, 11(9), 1098. Retrieved from https://doi.org/10.3390/cryst11091098

Y. Almadani, M. I. (2018). Application of Visible Light Communication in an Industrial Environment. *11th International Symposium on Communication Systems, Networks & Digital Signal Processing (CSNDSP)*, pp 1-6. doi:10.1109/CSNDSP.2018.8471800

Zheng, Z. D. (2020). Adaptive Spatial Modulation for Indoor Visible Light Communications. *IEEE Communications Letters*, 24(10), 2240–2244. doi:https://doi.org/10.1109/lcomm.2020.3002540

ISBN: 978-978-8567-02-8

5TH Faculty of Engineering Conference on Engineering Innovation and Economic Policies: Driving Sustainable Industrial Growth in Nigeria

Faculty of Engineering, Bayero University, Kano.

063-Effect of Storage Condition of Pea Pod on Water Coagulation

Muhammad Muhammad Makki, Umar Faruk Lawan

Department of Civil Engineering, School of Engineering BUPOLY Hadejia, Jigawa State, Nigeria. mmakkielleman@gmail.com,

Department of Water Resources and Environmental Engineering, Aliko Dangote University of Science and Technology, Wudil, Kano.umarflawan@gmail.com

Abstract: Abstract: Polluted water is estimated to affect about 1.2 billion people and contribute to the deaths of 15 million children in the world per year. The excessive use of chemical coagulants can affect human health in the long term; aluminum has been indicated to be a causative agent of neurologic diseases such as senile dementia. Research confirms the significant impact of pea pod as a coagulant in water treatment, but much research has to be done to ascertain the effects of its storage duration on water coagulation. Therefore, the research aims to find the effect of storage condition (temperature and pH) on pea pod and water coagulation. A suitable method was employed for pea pod processing. The pea pod was prepared and ground to a powder. Phytochemical analysis of the pea pod was conducted. A 10% stock solution of the extract was prepared. A jar test for water coagulation was carried out for high, medium, and low untreated synthetic waters, Ura surface (river) water, and Zoo Road well water. The process was repeated for stored pea pod powder at varying temperatures and pH values. Conclusion was reached that pH and temperature have minimal effects on the pea pod coagulation activity for temperatures between 0°C and 50°C and pH between 5 and 7, but the best temperature is 30°C for optimum pH and optimum turbidity removal efficiency (%).

KEYWORDS: pea pod, coagulation, water treatment, storage condition

1. INTRODUCTION

According to a survey conducted by the United Nations Environmental Program (UNEP), 20% of the world's population lacks access to safe drinking water, and 50% lack access to safe sanitation (WHO, 1997). In addition, polluted water is estimated to affect about 1,200 million people and contribute to the deaths of 15 million children in the world per year (WHO, 1997). The excessive use of chemical coagulants can affect human health in the long term; aluminum has been indicated to be a causative agent of neurologic diseases such as senile dementia (Muyibi, 1995). Water is a vital resource among natural resources. Additionally, the purification of water for most domestic uses is necessary. The chemicals available for water purification are scarce and unaffordable to average households in Nigeria and other countries, especially in rural areas. These chemicals also pose health threats to their consumers. There is, therefore, a need for alternative means of water treatment, especially for rural dwellers. Previous research findings have shown that pea pods contain chemical constituents responsible for coagulation. Research confirms the high impact of pea pods as a coagulant in water treatment, but much research still needs to be done to ascertain the effects of their storage conditions on water coagulation. Therefore, the research aims at finding effect of storage condition (Temperature and pH) effect of pea pod on water coagulation.

2. METHODOLOGY

2.1 Water samples

The synthesized water was prepared at the Public Health Laboratory. The water quality parameters were checked before and after treatment. Doses of the Pea pod filtrates i.e. 0.25 ml, 0.5 ml, 1.0 ml, 2.0 ml, 3.0 ml, 5.0 ml, and 7.0 ml (Aweng et al., 2012) were chosen to obtain the corresponding final concentrations. The WHO 2018 standard for turbidity is 5 NTU.

2.2 Pea (cicer arietinum) pod sampling and phytochemical analysis

Good quality fresh pods of peas will be selected manually and randomly (in accordance with Kwaji et al., 2010) from the market, authenticated by the Department of Botany, and dried at room temperature for 14 days, i.e.., the storage duration.

Complete proximate standard procedure analyses of the pea pod were conducted in the Department of Animal Science and also in the Biochemistry Department at Bayer University, Kano, Nigeria.

The following materials and equipment were used throughout the tests: 10 liters of synthesized water: pure water with a pH of 7.0, 10 (500-1000 ml) beakers, electric stirrers, pipettes, sieves (200-500 µm), a standard pH meter, thermometer, turbid meter, clinical autoclave, autoclave or BIOSENS machine for BOD tests, photometer, 10-20 normal test tubes, 500-1000 g kaolin

ISBN: 978-978-8567-02-8

bentonite, 1 complete pack of Whitman filter papers, 50,000 mg of calcium chloride dihydrate ($CaCl2 \cdot 2H2O$), jar test apparatus, incubator, oven, 2 ml buffer solution, Erich Rome T indicator and EDTA standard titrant, 0.1 N HCl and 0.02 N NaOH, Gallenkamp water bath, and controlled fridge, etc.

2.3 Preparation of pea pod powders and crude extracts

The dried pods were separately ground to a fine powder using a domestic blender. The ground powders were then sieved through a 210 μn-sieve. The extraction was in accordance with Aweng et al. (2012) but was mixed with a different mixer: crude extracts were prepared by using 500 ml of distilled water to 50 g of the prepared powder, which was mixed by a British-made (RPM=1400, HP=1/86, watt=8.6) stirrer for 10 min and left to settle for 20 minutes to make a 10% stock solution of the pea pod extract. The crude extracts were finally filtered through Whitman filter paper. The filtrates were prepared at the time of conducting the tests since deterioration sets in with delay (Muyibi et al., 1994). The filtrates were used within 48 hours, i.e., the storage duration of the pea pod extract. The control pH is the optimum pH.

2.4 Preparation of synthetic water

Synthetic raw water was prepared to guarantee the homogeneity of the raw water to be used with specific concentrations.

2.5 Procedure for laboratory analysis

Phytochemical analysis was conducted first on the pea pod of the plant to confirm the presence of chemical and bioactive constituents of the pea pod that were responsible for the water treatment. Level of contamination of the synthetic water was determined. The synthesized water was separately treated using pea pod filtrates. The test was carried out batch-wise. Three water samples were mixed homogeneously with the chosen doses of pea pod extract and then allowed to rest. The treated water samples were then analyzed to determine the levels of disinfection, temperature, and pH.

2.5.1 Jar tests

Jar tests were performed using the six paddles in the PEF Flocculation Test Unit (Serial No.). PEF 0031/11). Coagulant doses were used respectively for high, medium, and low turbidities. The pH values of the samples were taken using a PHS-25 pH meter (Ahmed et al., 2010).

2.5.2 Turbidity test

Coagulation/flocculation tests were carried out in the 'Jar Test' (with the PEF Flocculation Test Unit), using three beakers for each dose. 0.25 ml of the pea pod filtrate was added to 300 ml of synthesized water. The mixture was stirred at 95 rpm for 3 minutes. Thereafter, the beakers were left to rest for 120 minutes. The procedure was repeated using 0.5, 1.0, 2.0, 3.0, 5.0, and 7.0 ml of the filtrate (Karina et al., 2013, and Aweng, 2012).

100ml of the sample was taken from the top of each beaker for the tests using a turbidity meter (SGE-200BS). Coagulation activity was calculated using (BUK Civil Engineering Laboratory Manual for 500L):

$$\text{Coagulation activity (\%)} = Ts–Tb)/Tb \times 100 \qquad 2.1$$

where:

Ts – Turbidity concentration after treatment (NTU)

Tb – turbidity concentration of blank (NTU)

2.6 Temperature variation with turbidity and ph

Jar tests was completed for optimum doses for high turbidity, medium and low turbidity of Pea pod extract at 40, 30, 20, 10, 5 and 0.5°C but with slight variation starting from 0°C to 50°C. The procedure for the jar test was stated already in Section above. Gallenkamp water bath and a controlled fridge were used to control temperature (and they were different from instruments used in the referenced method).

Also, pH values were taken throughout the tests.

The whole procedure was repeated for varied temperature 30, 40 and 50 C and pH 5 to 7.

3.0 RESULT AND DISCUSSION

3.1 Effect of the pea pod extract on pH of water

The initial pH values of the water samples were 6.7, 6.8, 6.9, 6.7, and 6.9, respectively, for high, medium, and low Kura Open Channel Surface (river) water and Zoo Road underground (well) water turbidities, and the initial pH of the pea pod extract was 3.5.

However, when the high, medium and low, Kura Open Channel Surface (river) water and Zoo Road Underground (Wells) waters were treated with various doses of the Pea pod extract, the pH values changed (towards alkalinity) as shown in Figure 3.1

At optimum doses (1600mg/l for high, medium, low and Kura surface turbid waters and 1200mg/L for Zoo Road well water), the Optimum pH values after treatment were 5.9, 6.1, 6.65, 6.2 and 6.0 respectively.

In similar research on water treatment, the pH was observed in alkaline nature after treatment with Moringa seed powder, confirmed by the work of Jodi et al., (2012). Musa (2016) in his work discovered a similar pH reduction while treating water with Polio stigma thonningischum and Tamarinds india L. leaves extracts.

ethupathy (2015), in his work, discovered a similar pH reduction while treating water with Moringa oleifera seed powder. Also, Chadanand and Manika (2015) observed pH shift to slightly alkaline nature after treatment with Pea seed powder.

Although the pH of the water varied as a result of the introduction of the plant extracts, it was within the range set by WHO 2018 standard for drinking water i.e (6.5-8.5).

ISBN: 978-978-8567-02-8

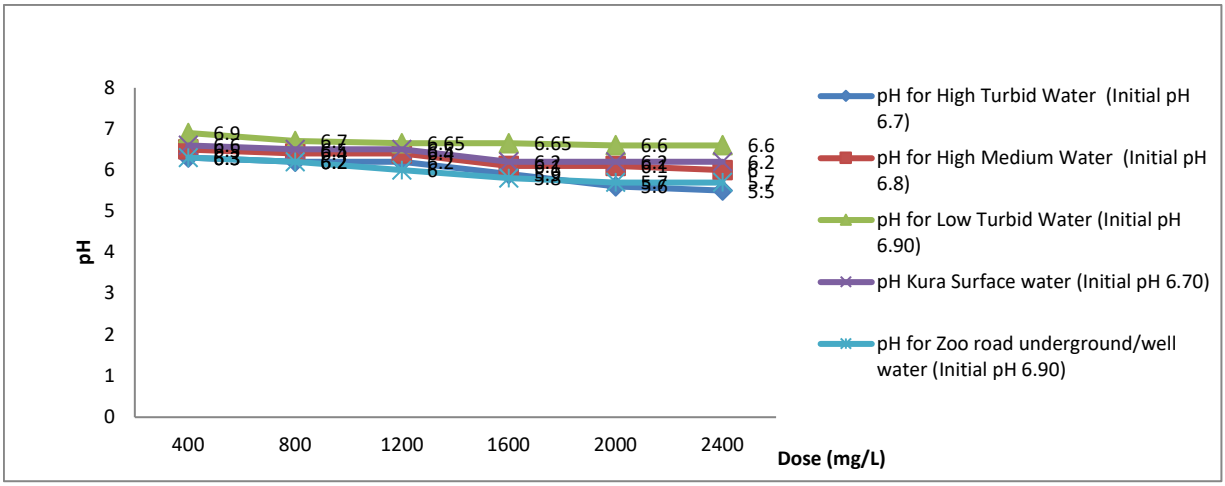


Figure 3:1 The Effects of Doses On pH for Different Water Samples for Pea Pod

3.2 Effect of temperature on turbidity removal

Figure shows the variation of Temperature on turbidity removal efficiencies for High, medium, low synthetic turbid water, Kura surface (river) water and Zoo Road well water.

temperature varied from 0.5°C to 40°C. At temperatures higher than 30°C, the suspended particles in the water might have gained enough kinetic energy to resist the effect of the coagulants, resulting in lesser turbidity removal.

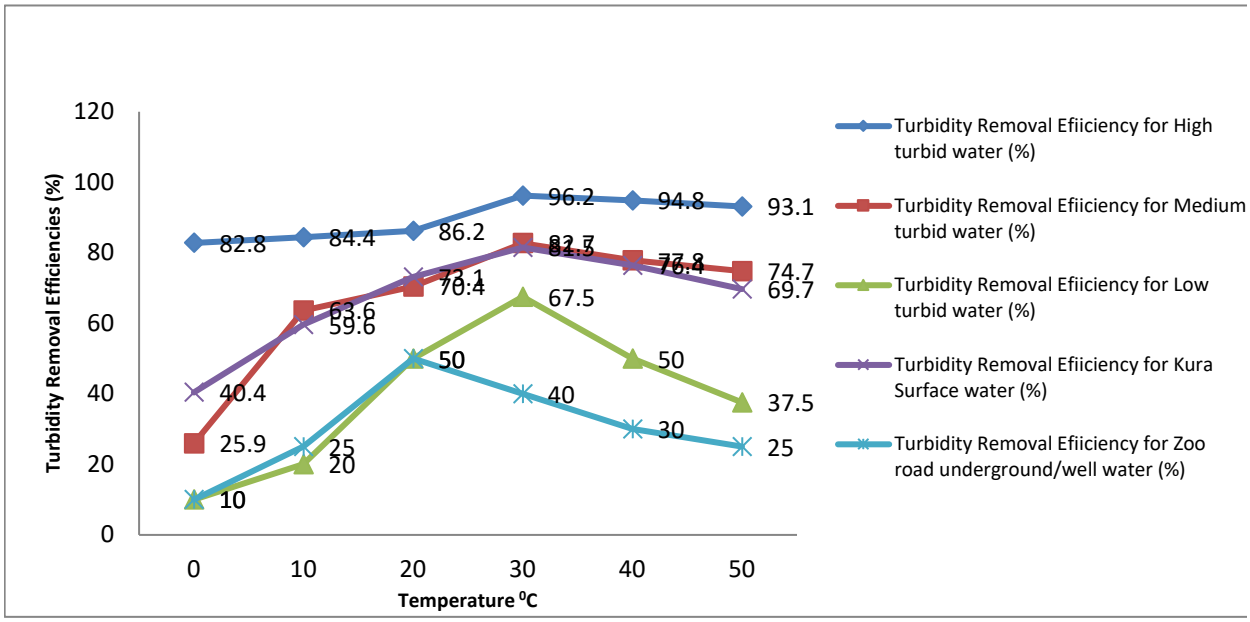


Figure 3.2: Effect of Temperature 0°C on Turbidity Removal in Different Water Samples for Pea Pod

Figure 3.2 shows that turbidity removal initially varies directly with temperature from 0.5°C to 20°C, with some small deviations at 5°C, until it reaches a maximum at 30°C for high, medium, low, and ura surface turbid waters, and 20°C for Zoo Road well water. It then begins to vary inversely. The maximum turbidity removal from high, medium, low, and ura surface turbid waters of 96.2 %, 82.7 %, 67.5%, and 81.5% was recorded at 30°C for the optimum dose of 1600 mg/l, respectively, and the maximum turbidity removal from Zoo Road water of 50% was recorded at 20°C for the optimum dose of 1200 mg/l.

The deviation of the graph at 5°C could be due to an anomalous change in the density of water as the

Udaya et al. (2013) revealed almost the same findings that turbidity reduction's best temperature range is from 20-30 oc.

Also this finding is supported by Madhavi et al. (2013) that turbidity reduction is mostly affected by cold temperatures. Rasia (2014) even argued that low temperatures would impair floc formation because of increased shear stress due to higher water viscosity. According to them, the effect of temperature on the best flocculation time required for efficient sedimentation becomes less when the temperature increases to 25°C, with little difference in flocculation times over a temperature range from 10 to 25°C, while much higher differences occur at temperatures less than 10oC.

ISBN: 978-978-8567-02-8

3.3 Variation of turbidity with pH

The Figure below shows the variation of Turbidity Removal Efficiencies for High, medium, low synthetic turbid water, Kura surface (river) water and Zoo road well water

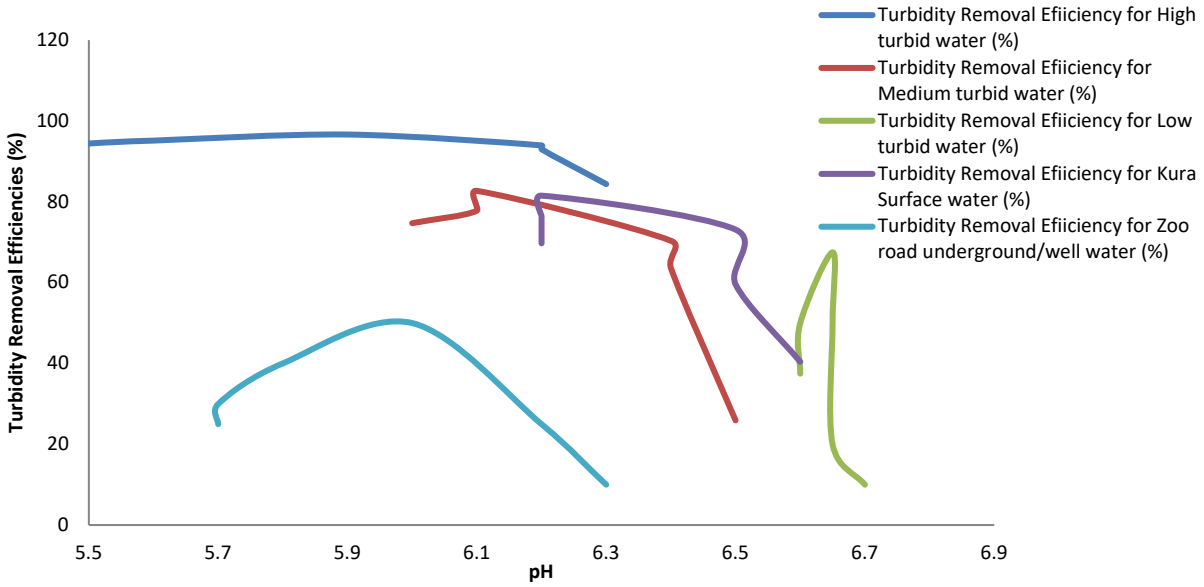


Figure 3.3: The Effects of Turbidity Removal Efficiencies on pH for Different Water Samples for Pea Pod

It can be seen from the figure that pH reduced drastically as Turbidity Removal Efficiency increases, ranging from 5.5 to 6.7. It then changed slightly at the optimum dose and continued to lower for all the water samples.

A wider difference was observed in pH reduction for the synthetic high-turbid water sample from 6.3 to 5.5 compared to that of medium, low, underground, and Zoo Road well water samples, which reduced from pH 6.6 to 6, 6.7 to 6, 6.6 to 6.2, and 6.3 to 5.7, respectively, indicating the significant impact of turbidity variation with pH, with high-turbid water followed by low-turbid water, underground water, medium-turbid water, and surface (river) water.

Musa (2016), in his work, discovered a similar significant pH reduction with high-turbid water while treating water with Poliostigmathonningischum and Tamarindus indica L. leaves extracts. Also, Tsama (2001) found considerable pH reduction with an increase in turbidity removal for high-turbid water treated with Boscia senegalensis extract.

Researchers like Udaya et al. (2013) and Chadanand et al. (2015) reported similar observations.

Ahmed et al. (2010), in Yan et al. (2008) stated that the pH at which coagulation occurs is the most important parameter for proper coagulation performance, as it affects the surface charge of colloids, the charge of NOM functional groups, and the charge of dissolved-phase solubility. They pointed out the need for controlling the pH of high-turbidity water for effective turbidity removal and found that the best turbidity removal is achieved between pH 5 and 6. They, however, showed that for NOM, higher coagulant doses would be required at higher pH values.

Kumar Mandal (2014), for his part, argued that there was no direct influence of pH on turbidity, although his research was specific to wastewater.

The table above indicates that the best temperature is 30°C for optimal pH and optimal turbidity removal efficiency (%).

3.4 Summary of Results and Analysis

The optimum dose was 1600 mg/L, corresponding to the highest turbidity removal efficiency for high turbid water, medium turbid water, low turbid water, and Kura surface (river) water (96.63%, 82.7%, 67.5%, and 81.5%, respectively), and the optimum dose for Zoo Road well water was 1200 mg/L, at a turbidity removal efficiency of 50%.

At optimum doses (1600 mg/L for high, medium, low, and Kura surface turbid waters and 1200 mg/L for Zoo Road well water), pH reduced drastically as turbidity removal efficiency increased, ranging from 5.5 to 6.7. The optimum pH values after treatment were 5.9, 6.1, 6.65, 6.2, and 6.0, respectively, which were within the range set by the WHO 2018 standard for drinking water, i.e., (6.5 to 8.5).

For temperature variation with turbidity removal efficiencies, turbidity removal initially varies directly with temperature from 0.5°C to 20°C, and the maximum turbidity removal from high, medium, low, and Ura surface turbid waters of 96.2 %, 82.7 %, 67.5%, and 81.5% was recorded at 30°C for the optimum dose of 1600 mg/L, respectively. The maximum turbidity removal from Zoo Road water of 50% was recorded at 20°C for the optimum dose of 1200 mg/L

ISBN: 978-978-8567-02-8

TABLE 3.1: TEMPERATURE RANGES WITH OPTIMUM PH, TURBIDITY REMOVAL EFFICIENCY (%) FOR HIGH, MEDIUM, LOW SYNTHETIC TURBID WATER, KURA SURFACE (RIVER) WATER, AND ZOO ROAD WELL WATER.

Temperature (°C)	Optimum pH	Optimum Turbidity removal efficiency (%)
30	5.9, 6.1, 6.65, 6.2 and 6.0	96.2 %, 82.7 %, 67.5 % and 81.5%
40	6.0, 6.1, 6.65, 6.25 and 6.0	96.3 %, 82.5 %, 67.3 % and 80%
50	6.0, 6.0, 6.6, 6.0 and 6.0	96.%, 82 %, 67 % and 80%

The table above indicates that the best temperature is 30°C for optimum pH and optimum turbidity removal efficiency (%).

4. CONCLUSION

It was concluded that pH and temperature have minimal effects on the Pea Pod coagulation activity for temperatures between 0°C to 50°C and pH between 5 to 7, but the best temperature is 30°C for optimum pH and optimum turbidity removal efficiency (%).

Comparative research should be conducted on the efficiency of the different methods of pea pod extraction. Research should be conducted to discover the mode of attack of the pea pod extract on microbes. Improvement of methodology should be made by using advanced energy technology in disinfection, employing the MALDI-TOF method in disinfection analysis for more accurate result. The mixing and settling time of water treated with Pea pod should be studied to observe their impacts on turbidity removal. Research should be conducted on the type and extent of these antioxidant and antibacterial substances.

REFERENCES

A., Kamal R. and Mohamed I. G. A. (2010). The effect of pH control on turbidity and NOM removal in conventional water treatment. Fifteenth International Water Technology Conference, IWTC 15 2010, Alexandria, Egypt.

Aweng, E.R., raw, A.I., Siti, R., M.I. and Suhaimi, O. (2012).Cassia alataas a Potential Coagulant in Water Treatment. Research Journal of Recent Sciences, ISSN 2277-2502, Vol. 1(2), 28-33.

Chadanand Pail and Manika Hugar (2015). Treatment of dairy wastewater by natural coagulants. International Research Journal of Engineering and Technology (IRJET) Volume: 02 Issue: 04.

this Kumar Mandal (2014). Influence of Wastewater pH on Turbidity. International Journal of Environmental Research and Development. ISSN 2249-3131 Volume 4, Number 2 (2014), pp. 105-114.

Jodi, M. L., nin-Yauri, U. A., Yahaya, Y. and Sokoto, M. A. (2012). The use of some plants in water purification.Global Advanced Research Journal of Chemistry and Material Science Vol. 1(4) pp. 071-075, December, 2012.

Abubakar, M., Ishak, E. A., Sayed, K., & Zawawi, N. A. B. W. (2021). Optimization of cement-based mortar containing oily sludge ash by response surface methodology. *Materials*, *14*(21). https://doi.org/10.3390/ma14216308

Karina, C. V., Leila, C. K. M., Milne, C. B.,Franciele, P. C. and Rosângela, B. (2013). Coagulation diagram using the Moringa oleifera Lam and the aluminium sulphate, aiming the removal of color and turbidity of water. Acta Scientiarum. Technology, 10.4025/actascitechnol.v35i3.12268.

Kirkelund, G. M., Ottosen, L. M., Jensen, P. E., & Goltermann, P. (2016). Greenlandic waste

Kwaji, A., Bassi, P. U., Lilo, M., Nneji, C. M., Ademowo, G. (2010). Preliminary Studies on Piliostigma thonningii Schum Leaf Extract: Phytochemical Screening and In Vitro Antimalarial Activity. African Journal of Microbiology Research. Vol. 4 (9); pp. 735-739, 4 May.

Madhavi, T. P. and Rajkumar, R. (2013); Utilization of Natural Coagulants for Reduction of Turbidity from Waste Water. International Journal of Chemical Technology Research CODEN (USA): IJCRGG ISSN: 0974-4290. pp. 1119–1123.

Musa Haruna (2016). Water Treatment Using Piliostigma Thonningii Schum and Tamarindus Indica L. Leaves Extracts. Unpublished M.Eng. Thesis, Department of Civil Engineering, Bayero University Kano.

Muyibi, S. A. and Lilian M. E. (1994). Moringa Oleifera Seeds for Softening Hard Water, Water Resources. Vol. 29, No. 4, pp. 1099-1105.

Muyibi, S. A. and M. L. Evison (1995): Optimizing Physical Parameters Affecting Coagulation of Turbid Water with Moringa oleifera Seeds. Wat. Res. 29, No. 12, 2689–2695.

Osama M.A.A. (2001). Influence of Local Coagulants in Water Treatment. Thesis for Master of Science in Environmental Engineering, Sudan University of Science and Technology.

Rasha Azeez Joudah (2014). Effect of Temperature on Floc Formation Process Efficiency and Subsequent Removal in the Sedimentation Process. Journal of Engineering and Development, Vol. 18, No. 4, July 2014, ISSN 1813-7822.

Sethupathy, A. (2015). An Experimental Investigation of Alum and Moringa Oleifera Seed in Water Treatment. International Journal of Advanced Research (2015), Volume 3, Issue 1, 515-518.

Udaya Simha L, Roopa S., and C. T. Puttaswamy (2013). Investigations of Natural Coagulants on Water Quality Parameters. International Journal of Earth Science and Engineering. ISSN 0974-5904, Volume 06, No. 06(01).

UNEP International Environment (2002). Environmentally Sound Technology for Wastewater and Stormwater Management: An International Source Book. IWA Publishing. ISBN 978-1-84339-008-4. OCLC 49204666.

WHO (World Health Organization) (1997). "Surveillance Control of Community Supplies; Guidelines for Drinking-Water Quality," WHO Water Quality, WHO Geneva

WHO (World Health Organization) (2018). Guidelines for drinking-water quality, water quality, WHO Geneva.

ISBN: 978-978-8567-02-8

incineration fly and bottom ash as secondary resource in mortar. *International Journal of Sustainable Development and Planning*, *11*(5), 719–728. https://doi.org/10.2495/SDP-V11-N5-719-728

Kotun, M. O., Olutoge, F. A., & Ganiyu, Y. A. (2020). Strength Properties of Concrete Made with Wood Waste Ash as a Partial Replacement for Cement. *Available Online Www.Jsaer.Com Journal of Scientific and Engineering Research 48 Journal of Scientific and Engineering Research*, *2020*(5), 48–52. www.jsaer.com

Ramzi, S., Moradi, M. J., & Hajiloo, H. (2023). The Study of the Effects of Supplementary Cementitious Materials (SCMs) on Concrete Compressive Strength at High Temperatures Using Artificial Neural Network Model. *Buildings*, *13*(5). https://doi.org/10.3390/buildings13051337

Shah, S. A., Tantray, M. A., & Bhat, A. R. (2025). Wood ash as an eco-friendly alternative for sustainable cement replacement in concrete. *Cleaner and Circular Bioeconomy*, *12*, 100178. https://doi.org/10.1016/J.CLCB.2025.100178

Sigvardsen, N. M. (2020). *Utilisation of Wood Ash in Cement -Based Materials* [DTU Orbit]. Technical University of Denmark.

Sri R. D., Ashok. S., Logeshwaran. V., Nandhini Sri. R., & Naveen Kumar. M. (2024). Effect of Partial Replacement of Cement with Wood Ash on Concrete Block. *International Journal of Advanced Research in Science, Communication and Technology*, 345–350. https://doi.org/10.48175/IJARSCT-22739

Teychenne, D. C., Franklin, R. E., & Erntroy, H. C. (1997). *Design of normal concrete mixes* (Second Edition). Building Research Establishment.

Vaiciene, M., & Malaiskiene, J. (2021). The Impact of Wood Waste Ash on Physical Mechanical Properties of Concrete. *IOP Conference Series: Materials Science and Engineering*, *1203*(3), 032097. https://doi.org/10.1088/1757-899x/1203/3/032097

Wani, B., & Rishi, V. (2020). Concrete Prepared by Wood Ash and Waste Paper Sludge: A Review. In *International Research Journal of Modernization in Engineering Technology and Science @International Research Journal of Modernization in Engineering* (Vol. 90). www.irjmets.com

Yadav, Y., & Shah Ujjaval (2019). effect of wood ash on the properties of high strength concrete. *Journal of Emerging Technologies and Innovative Research (JETIR),*177-180 6(4*)*. www.jetir.org

ISBN: 978-978-8567-02-8

066-Soil stabilization using Recycled Glass Powder- Review of literature

M. A. Muhammad and B. W. Isah

Civil Engineering Department, Faculty of Engineering, Bayero University Kano. PMB 3011. Kano Nigeria

muhdameenm86@gmail.com

Abstract: Black cotton soil poses a great challenge to engineers due to its high swell-shrink potential, very poor bearing capacity and high risk of differential settlement. Although the traditional stabilization methods have proven very effective in soil improvement, they are however very expensive and environmentally unfriendly due to high carbon emission. This led researchers to shift focus to more sustainable alternatives and thus the use of industrial waste: Recycled Glass Powder (RGP). Herein is a review of studies on the use of RGP in soil stabilization, incorporating a collection of their chemical compositions and details on optimum percentages obtained from previous studies is presented. From the reviewed literature, the potential of RGP for soil stabilization was confirmed. RGP contains sufficient silica to act as a pozzolan, thus, producing cementitious gels when combined with a calcium source, consequently improving soil properties. RGP is not often used alone, it is usually used along with waste materials rich in calcium. Our currently ongoing research focused on the use of Calcium carbide residue and RGP for soil stabilization.

1. INTRODUCTION

Expansive soils pose a great challenge to engineers and construction workers alike. This leads to research on sustainable ways to either remove and replace or stabilize them. While the replacement and traditional stabilization methods are very effective, they are however costly and often environmentally unfriendly. This has led researchers to explore the potential of industrial wastes for soil stabilization, one of which is recycled glass powder. Glass was defined by Wang, (2019) as an amorphous non-crystalline solid produced through various means, some of which are liquid quenching and gas deposition. According to Baek et al., (2024), the current global production of glass is at approximately 130 million metric tons per annum and the most common type of glass is soda lime glass. Adán & Adán, (2025) has it that the global recycling of glass waste is at around 50% but varies among countries and across continents, with the United States having 34% in 2025 as against European Union's 80%.

Looking back at Nigeria, Seun Samuel Owoeye et al., (2021) notes that more than 32million tons of solid wastes are produced and of this, glass and agro wastes make up 70%. According to Omokaro et al., (2026), the waste management system in Nigeria is very bad and so most of the waste remains improperly managed, it then ends up piling in and polluting the environment and causing diseases among people. Researchers have worked to find ways to properly dispose or reuse the waste and one such established ways is soil stabilization using agricultural and industrial wastes. One such promising waste is recycled glass powder (RGP).

This paper presents the oxide compositions of glass compiled from previous literatures, thereby establishing its pozzolanic property and potential for soil stabilization. The paper also reviewed journals on soil stabilization with glass and compiled the optimum percentages they established, the types of soil they studied and the various laboratory tests employed to obtain them. A review was also conducted of the various admixtures combined with glass in soil stabilization as it was found in research that often times it requires a calcium source for a more effective performance.

2. OXIDE COMPOSITION OF GLASS

The oxide composition of glass is obtained from x-ray fluorescence (XRF) analysis, which according to González et al., (2024) is a non-destructive method with the ability to identify elements of atomic numbers 11 to above 92 used to determine the chemical composition of materials. Table I below presents the oxide composition of glass obtained by a number of literatures in the past.

From the table, it is noted that the major oxides in the samples tested are: silica oxide (SiO_2), Sodium oxide (Na_2O), Calcium oxide (CaO), Aluminum oxide (Al_2O_3), magnesium oxide (MgO), iron oxide (Fe_2O_3), Sulphur oxide (SO_3) and Potassium oxide (K_2O). SiO_2 content ranges from 65.23%-89.10%, Na_2O ranges from 10.1%-17%, CaO ranges from 6.06%-14.5%, Al_2O_3 is from 0.01% - 3.9%, MgO is from 0.49% - 4.6%, Fe_2O_3 is from 0.08% - 2.2%, SO_3 is from 0.14% - 0.4 and K_2O is from

ISBN: 978-978-8567-02-8

0.05% - 2.3%. This makes SiO_2, the primary oxide needed for pozzolanic reactions, as the predominant oxide with an average content for all studies combined of 71.87% and thus, establishes the glass powder as a potential pozzolanic material.

established that identifying this optimum content is important for proper strength improvement, enhanced volumetric stability and reduced moisture sensitivity.

TABLE I: OXIDES COMPOSITION OF GLASS

References	*SiO_2*	*Al_2O_3*	*Fe_2O_3*	*CaO*	*MgO*	*SO_3*	*Na_2O*	*K_2O*	*TiO_2*	*MnO*	*P_2O_5*	*N_2O*	*Cr_2O_3*	*LOI*	*Others*
Epure et al., (2023)	*72.58*	*1.47*	*0.85*	*10.49*	*0.61*	*0.2*	*12.54*	*0.4*							
Jalal et al., (2022)	*74.55*	*0.18*	*0.9*	*8.95*	*3.71*			*0.05*	*0.01*	*0.01*	*0.02*	*11.49*		*2.1*	
Tajaddini et al., (2023)	*65.23*	*2.23*	*0.45*	*11.69*	*1.22*		*12.38*								*6.8*
Najaf & Abbasi, (2022)	*69.42*	*0.48*	*0.08*	*8.82*	*3.90*		*12.28*	*0.12*							
Delbari & Hof, (2024)	*73.00*	*1.00*		*5.00*	*4.00*		*17.00*								
Baldovino et al., (2021)	*74.22*	*1.83*	*0.21*	*10.62*	*1.18*		*11.28*							*0.66*	
Burduhos Nergis et al., (2020)	*70-71*	*1.5-2*	*0.8-1*	*9-11*	*2-3*		*12-14*								*<0.1*
Blayi et al., (2020)	*71.21*	*1.91*	*0.45*	*13.30*	*2.40*		*10.10*								*0.63*
ShiRzad et al., (2023)	*68.10*	*0.90*	*0.60*	*14.50*	*1.80*	*0.40*	*12.20*	*0.80*							
Ahmadi, (2022)	*72.50*	*3.10*	*0.20*	*6.10*	*1.80*		*11.50*	*2.3*	*>0.01*						
Khalaf & Mahmood, (2024)	*72.10*	*1.30*	*0.30*	*6.06*	*4.60*	*0.30*	*15.20*								
Ibrahim et al., (2021)	*70.20*	*1.95*	*0.42*	*11.30*	*2.20*		*13.30*								*0.63*
Javed & Chakraborty, (2020)	*71.00*	*1.50*		*10.25*			*11.25*								*6.00*
Wang et al., (2023)	*67.70*	*2.4*	*1.92*	*11.92*	*0.49*	*0.14*	*14.75*	*0.81*						*0.09*	
B. D. et al., (2024)	*89.10*	*3.90*	*2.20*		*1.06*										
Ke et al., (2018)	*70.40*	*3.37*	*0.508*	*9.20*	*1.00*	*0.38*	*13.78*	*0.663*	*0.053*				*0.094*		
S. Ibrahim & Meawad, (2022)	*74.11*	*0.01*	*0.12*	*10.01*	*2.60*		*12.40*	*0.25*	*0.03*					*0.27*	
Matos et al., (2024)	*70.35*	*0.88*	*0.44*	*9.23*	*3.57*	*0.19*	*13.89*	*0.33*							
Daguiani et al., (2023)	*69.34*	*1.778*	*0.571*	*9.807*	*2.299*	*0.335*	*12.431*	*0.261*						*0.40*	

3. OPTIMUM PERCENTAGES OF RECYCLED GLASS POWDER (RGP) FROM PREVIOUS LITERATURE

This section of our paper compiles a list of studies on soil stabilization using glass powder and their obtained optimum percentages. This optimum percentage is taken as percentage of the stabilizer by weight of soil that yields the most favourable result in respect of a particular parameter, say, Unconfined Compressive Strength (UCS), California Bearing Ratio (CBR), Maximum Dry Density (MDD) or plasticity, beyond which the result starts to diminish. Juwonlo Osinubi et al., (2022)

Many researchers have studied the application of glass powder for stabilizing expansive soils and each has obtained an optimum percentage of glass recommended based on the results of their research. Blayi et al., (2020) stabilized a low plasticity clay (CL) with waste soda lime glass powder (WSLGP) and recorded a 15% optimum glass content and a 171% increase in CBR value while Jalal et al., (2022) recorded a 16% optimum with a six-fold increase in strength based on the same CBR value. H. H. Ibrahim et al., (2021) established a 27% optimum for UCS test and 18% for all other parameters he tested, whereas Khalaf & Mahmood, (2024) recorded a 20% optimum RGP content based on UCS values.

ISBN: 978-978-8567-02-8

TABLE II: OPTIMUM PERCENTAGE DETAILS FOR GLASS POWDER

Reference	Admixtures Used	Soil Type Studied	Tests Conducted	Optimum Percentage
Jalal et al., (2022)	Soda Lime Glass Powder (SLGP)	Polygorskite-rich medium expansive soil (CL-OL)	Atterberg limits, Compaction (OMC &MDD), UCS and Consolidation (Oedometer)	They found 16% by dry weight of soil to be the optimum percentage
Blayi et al., (2020)	Waste Soda Lime Glass Powder (WSLGP)	A low-plasticity clay (CL)	Atterberg limits, Compaction, Free swelling, UCS, Direct shear and CBR	15% by soil dry weight was found to be the optimum
Arrieta Baldovino et al., (2020)	Waste Soda Lime Glass Powder (WSLGP) and Cement	A low-plasticity clay (CL)	Atterberg limits, Compaction, CBR and UCS	The optimum was 5% cement and 15% glass powder all by soil dry weight
Khalaf & Mahmood, (2024)	Soda Lime Glass Powder (SLGP)	Low-plasticity organic silty clay (OL)	Unconfined Compressive Strength (UCS)	20% by total soil dry weight was found to be the optimum
Ibrahim et al., (2021)	Waste Soda Lime Glass Powder (WSLGP)	A high-plasticity clay (CH)	Atterberg limits, Compaction, Consolidation, Swelling and UCS	UCS gave 27% while all others gave 18% as optimum
Javed & Chakraborty, (2020)	Waste Soda Lime Glass Powder (WSLGP)	A cohesive soil	Atterberg limits, CBR, UCS and Direct shear test	For Atterberg's limits it is up-to 10%, strengths tests gave 8%
Al-Taie et al., (2023)	Sand-sized Soda Lime Glass	High-plasticity clay	CBR, swell & cyclic behaviour tests and UCS	UCS gave 20% and all others gave 25% optimum
Gücek et al., (2024)	Waste Soda Lime Glass (GP), rubber tires (RT) and lignin (LG)	Low-plasticity clay	UCS, CBR and Resilient modulus	There are two scenarios, GP+RT gave 20%GP+3%RT, while GP+LG gave 15%GP+15%LG
Lai & Chen, (2024)	Glass Micro-powder (GMP) and Construction Waste (CW)	A clayey soil was used	Atterberg's limits, Compaction, triaxial compression test and splitting tensile test	The optimum was 30% CW and 15% glass micro-powder all by soil dry weight

According to Jalal et al., (2022), the reaction that takes place is such that the pozzolans (SiO_2, Al_2O_3 and Fe_2O_3) in glass powder react with other compounds inthe soil to form cementitious materials. The silica in glass, thus, reacts with calcium hydroxide $(Ca(OH))_2$ in soil in the presence of water to form calcium silicate hydrate (C-S-H) and calcium aluminate hydrate (C-A-H), thereby improving soil strength and durability. Table II below presents a list of optimums obtained by some researchers. Fig. 1 presents a summary of the optima obtained herein

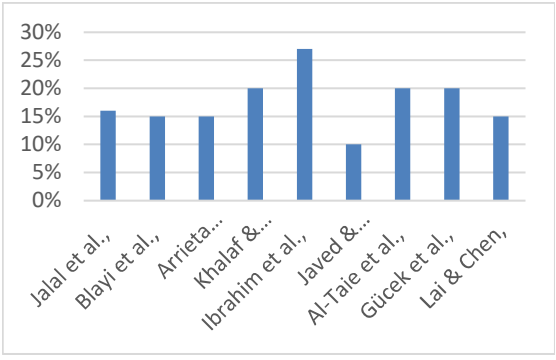


Fig. 1 Summary of optimum percentages

However, looking at the work of Gücek et al., (2024) who used a geopolymer of Glass Powder (GP) + Rubber Tire (RT) and GP + Lignin (LG), he obtained a 20%GP+3%RT and 15%GP+15%LG optimums respectively. Although, on addition of the GP+RT blend, the dry CBR increased by 209% while wet CBR increased by 190%, which is a more favourable result than that of Blayi et al., (2020) who used glass alone. Lai & Chen, (2024) also studied a mixture of glass micro powder (GMP) and construction waste (CW) and got 15%GMP+30%CW as the optimum with a corresponding 56.8% increase in compressive strength and 57% decrease in porosity. These show that glass powder would

ISBN: 978-978-8567-02-8

perform even better in soil stabilization when combined with other materials, especially those rich in calcium.

Similarly, Islam et al., (2024) noted that glass powder has a promising potential in geotechnical applications but also highlighted the potential of materials like fly ash to also react with Ca(OH)2 to form C-S-H and C-A-H. He concluded that glass powder is a great pozzolan and fly ash contains significant amount of SiO2, CaO and Al2O3 and the two would effectively work together to create a well stabilized composite. Some researchers have studied soil stabilization with glass powder and other materials, among these are: Salih et al., (2023) where glass is paired with hydrated lime and Cheng et al., (2024) who explored using glass powder and bamboo fiber. Table III presents a list of some materials blended with glass powder in recent researches.

TABLE III: MATERIALS PAIRED WITH RGP

Admixture/Stabilizer	Why They are Combined	Reference
Lime (hydrated/quicklime)	Lime produces calcium while glass produces silica which when combined initiates pozzolanic reaction and formation of cementitious gels.	Salih et al., (2023)
Steel slag	These provide calcium and aluminum. When paired with glass, which provides silica, they significantly soil strength.	Topark-Ngarm et al., (2019) and Kusuma et al., (2023)
Fly ash (FA)	Fly ash contains significant of pozzolanic oxides like Calcium oxide, aluminium oxide and silica oxide, while glass powder are rich in silica. GP is sometimes used to partially replace FA and this improves strength and durability.	Graduate School of Natural and Applied Science, Erciyes University, Kayseri (Türkiye) et al., (2023), Eniola, (2023) and Kusuma et al., (2023)
Portland Cement	Cement provides $Ca(OH)_2$ which reacts with the silica in glass powder to produce cementitious gels. This improves strength and reduces plasticity.	Ghorab et al., (2019)
Ceramic waste powder (CWP)/Brick dust	Often used as sources of alumina and silica or to replace more expensive materials. When combined with glass powder they enhance durability and reduce cost.	Rabiu & Mosaberpanah, (2025) and Nanda et al., (2024)
Bamboo fiber	When combined with glass powder, they form a stronger matrix, enhance strength and improve ductility.	Cheng et al., (2024)

According to Jalal et al., (2022), the strength of the stabilized soil kept increasing with increase in number of curing days and he had the highest strength at 28days of curing for his study case. His assertion was supported by Khalaf & Mahmood, (2024). Al-Taie et al., (2023) established that particle size governs the strength development mechanism, wherein he said finer glass particles give rise to higher strength with lower content while coarser particles require higher contents. The paper also explicitly states that optimum percentages are glass powder is finer and higher powder size produce higher optima.

However, considering that a number of studies like Blayi et al., (2020), Jalal et al., (2022) and H. H. Ibrahim et al., (2021), who used identical sizes of glass but got varying optima brings a point of concern. On this, Bandipally et al., (2025) clarifies that variation in soil mineralogy affects the optimum content and also suggests that this variation in optima may be due to mineralogical differences of soils studied, supporting Barman & Dash, (2022)'s earlier assertion.

One other important factor is environmental leaching. Baldovino et al., (2021) established that the optimum obtained from dry laboratory strength tests alone may not be true in cases where leaching effects and exposure to moisture are considered. Lai & Chen, (2024) conducted leaching test and concluded that environmental leaching can shift the optimum away from what strength tests would give, confirming Baldovino's assertion. Phantachang et al., (2024) also has it that leaching reduces the strength of the system and also eliminates optima that will potentially only work well under laboratory conditions.

4. CONCLUSION

Glass powder improves soil properties through pozzolanic reaction, in which the silica in glass reacts with calcium from the soil to form cementitious compounds like C-S-H and C-A-H, thus, improving the soil strength, reducing plasticity and providing better volumetric stability. From the collected data, an optimum glass content ranging from about 10% to 25% by dry weight of the soil was recorded, often depending on the glass properties, soil type and conditions of testing.

This review found that variation in optima of different studies may be mineralogical differences in the studied soils and it has confirmed the effect of curing duration, particle size, soil mineralogy and environmental leaching on both strength development and optimum percentage.

The studies also show that glass powder works even better when blended with other additives, especially

ISBN: 978-978-8567-02-8

calcium-rich ones like cement, fly ash, lime and calcium carbide residue (CCR). While studies have made use of many of these additives, our current research aims to explore the effect when glass powder is paired with CCR to stabilize black cotton soil (BCS).

KEYWORDS

"Pozzolanic reaction", "Sustainable Geotechnics", "Waste recycling"

REFERENCES

Ahmadi, S. (2022). Effect of glass waste as a cement replacement on the mechanical properties of concrete. Synthesis and Sintering, 2(3). https://doi.org/10.53063/synsint.2022.23120

Al-Taie, A., Yaghoubi, E., Wasantha, P. L. P., Van Staden, R., Guerrieri, M., & Fragomeni, S. (2023). Mechanical and physical properties and cyclic swell-shrink behaviour of expansive clay improved by recycled glass. International Journal of Pavement Engineering, 24(1), 2204436. https://doi.org/10.1080/10298436.2023.2204436

Arrieta Baldovino, J. D. J., Dos Santos Izzo, R. L., Da Silva, É. R., & Lundgren Rose, J. (2020). Sustainable Use of Recycled-Glass Powder in Soil Stabilization. Journal of Materials in Civil Engineering, 32(5), 04020080. https://doi.org/10.1061/(ASCE)MT.1943-5533.0003081

B. D., I., K. B., S., R., A., & M. L., N. (2024). Effects of Waste Glass Powder as Partial Replacement of Cement on the Structural Performance of Concrete. Civil Engineering and Architecture, 12(4), 2547–2556. https://doi.org/10.13189/cea.2024.120404

Baldovino, J. J. A., Izzo, R. L. S., Rose, J. L., & Domingos, M. D. I. (2021). Strength, durability, and microstructure of geopolymers based on recycled-glass powder waste and dolomitic lime for soil stabilization. Construction and Building Materials, 271, 121874. https://doi.org/10.1016/j.conbuildmat.2020.121874

Bandipally, S., Naresh, T., Kumar, V. V. P., Skrzypkowski, K., Prasad, Nannuta. S. S., Zagórski, K., Zagórska, A., & Madziarz, M. (2025). Experimental and Energy Accounting Study on Waste Glass Powder Soil Stabilisation for Low-Carbon Mining Infrastructure. Energies, 18(24), 6416. https://doi.org/10.3390/en18246416

Barman, D., & Dash, S. K. (2022). Stabilization of expansive soils using chemical additives: A review. Journal of Rock Mechanics and Geotechnical Engineering, 14(4), 1319–1342. https://doi.org/10.1016/j.jrmge.2022.02.011

Blayi, R. A., Sherwani, A. F. H., Ibrahim, H. H., Faraj, R. H., & Daraei, A. (2020). Strength improvement of expansive soil by utilizing waste glass powder. Case Studies in Construction Materials, 13, e00427. https://doi.org/10.1016/j.cscm.2020.e00427

Burduhos Nergis, D. D., Abdullah, M. M. A. B., Sandu, A. V., & Vizureanu, P. (2020). XRD and TG-DTA Study of New Alkali Activated Materials Based on Fly Ash with Sand and Glass Powder. Materials, 13(2), 343. https://doi.org/10.3390/ma13020343

Cheng, T., Xiong, C., Zhou, C., Li, Z., & Zhang, X. (2024). Effect of Waste Glass Powder and Bamboo Fiber on the Physico-Mechanical Properties and High-Temperature Behavior of a Fly Ash-Based Geopolymer. ACS Omega, 9(43), 43766–43778. https://doi.org/10.1021/acsomega.4c06416

Daguiani, S. E., Kessal, O., Kriker, A., & Mokhtari, A. (2023). Modelling of fresh properties and strength activity index with microstructure characterisation of ternary cement incorporating waste glass and granulated blast furnace slag. Frattura Ed Integrità Strutturale, 17(66), 88–111. https://doi.org/10.3221/IGF-ESIS.66.05

Delbari, S. A., & Hof, L. A. (2024). Glass waste circular economy—Advancing to high-value glass sheets recovery using industry 4.0 and 5.0 technologies. Journal of Cleaner Production, 462, 142629. https://doi.org/10.1016/j.jclepro.2024.142629

Eniola, S. A. (2023). PERFORMANCE EVALUATION OF USING WASTE GLASS POWDER AND FLY ASH IN ALKALI-ACTIVATED SLAG BINDER AND MORTAR SAMPLES AS PARTIAL PRECURSORS [Master of Science in Civil Engineering, Michigan Technological University]. https://doi.org/10.37099/mtu.dc.etdr/1689

Epure, C., Munteanu, C., Istrate, B., Harja, M., & Buium, F. (2023). Applications of Recycled and Crushed Glass (RCG) as a Substitute for Natural Materials in Various Fields—A Review. Materials, 16(17), 5957. https://doi.org/10.3390/ma16175957

Ghorab, H. Y., Meawad, A. S., Yildirim, M., & Hassan, A. H. E. (2019). Progress research on earth construction: Cast earth with glass wastes, cement kiln bypass dust and activated clay. African Journal of Science, Technology, Innovation and Development, 11(4), 433–439. https://doi.org/10.1080/20421338.2018.1479141

Graduate School of Natural and Applied Science, Erciyes University, Kayseri (Türkiye), Gökşen, Y., Durak, U., Civil Engineering Department, Erciyes University, Kayseri (Türkiye), İlkentapar, S., Civil Engineering Department, Erciyes University, Kayseri (Türkiye), İsa Atabey, İ., Civil Engineering Department, Nevşehir H. Bektaş Veli Univ., Nevşehir (Türkiye), Kaya, M., Civil Engineering Department, Yozgat Bozok University, Yozgat (Türkiye), Karahan, O., Civil Engineering Department, Erciyes University, Kayseri (Türkiye), Duran Atis, C., & Civil Engineering Department, Erciyes University, Kayseri (Türkiye). (2023). Synergistic effect of waste glass powder and fly ash on some properties of mortar and notably suppressing alkali-silica reaction. Revista de La Construcción, 22(2). https://doi.org/10.7764/RDLC.22.2.419

Gücek, S., Gürer, C., Žlender, B., Taciroğlu, M. V., Korkmaz, B. E., Gürkan, K., Bračko, T., Macuh, B., Varga, R., & Jelušič, P. (2024). Use of Lignin, Waste Tire Rubber, and Waste Glass for Soil Stabilization. Applied Sciences, 14(17), 7532. https://doi.org/10.3390/app14177532

ISBN: 978-978-8567-02-8

Ibrahim, H. H., Mawlood, Y. I., & Alshkane, Y. M. (2021). Using waste glass powder for stabilizing high-plasticity clay in Erbil city-Iraq. International Journal of Geotechnical Engineering, 15(4), 496–503. https://doi.org/10.1080/19386362.2019.1647644

Ibrahim, S., & Meawad, A. (2022). Towards green concrete: Study the role of waste glass powder on cement/superplasticizer compatibility. Journal of Building Engineering, 47, 103751. https://doi.org/10.1016/j.jobe.2021.103751

Jalal, F. E., Zahid, A., Iqbal, M., Naseem, A., & Nabil, M. (2022). Sustainable use of soda lime glass powder (SLGP) in expansive soil stabilization. Case Studies in Construction Materials, 17, e01559. https://doi.org/10.1016/j.cscm.2022.e01559

Javed, S. A., & Chakraborty, S. (2020). Effects of Waste Glass Powder on Subgrade Soil Improvement.

Juwonlo Osinubi, K., Oshioname Eberemu, A., Yohanna, P., & Azige, P. (2022). Reliability based predictive model for estimating shear strength values of locust bean waste ash compacted black cotton soil. Cleaner Materials, 5, 100114. https://doi.org/10.1016/j.clema.2022.100114

Ke, G., Li, W., Li, R., Li, Y., & Wang, G. (2018). Mitigation Effect of Waste Glass Powders on Alkali–Silica Reaction (ASR) Expansion in Cementitious Composite. International Journal of Concrete Structures and Materials, 12(1), 67. https://doi.org/10.1186/s40069-018-0299-7

Khalaf, K. Y., & Mahmood, K. R. . (2024). Sustainable use of recycled glass powder-based geopolymer of organic soil stabilization. Salud, Ciencia y Tecnología - Serie de Conferencias, 3, 857. https://doi.org/10.56294/sctconf2024857

Kusuma, R. I., Mina, E., Fathonah, W., & Fatwari, M. H. A. (2023). Utilization of Waste Steel Slag, Fly Ash, Glass Bottle Powder for Swamp Soil Stabilization. Materials Science Forum, 1101, 109–114. https://doi.org/10.4028/p-y0KjYb

Lai, Z., & Chen, Y. (2024). Enhancing the mechanical and environmental performance of solidified soil using construction waste and glass micro-powder. Heliyon, 10(22), e40187. https://doi.org/10.1016/j.heliyon.2024.e40187

Matos, A. M., Milheiro-Oliveira, P., & Pimentel, M. (2024). Eco-efficient high performance white concrete incorporating waste glass powder. Construction and Building Materials, 411, 134556. https://doi.org/10.1016/j.conbuildmat.2023.134556

Najaf, E., & Abbasi, H. (2022). Using Recycled Concrete Powder, Waste Glass Powder, and Plastic Powder to Improve the Mechanical Properties of Compacted Concrete: Cement Elimination Approach. Advances in Civil Engineering, 2022(1), 9481466. https://doi.org/10.1155/2022/9481466

Nanda, N., Imani, R., Mursyid, M., & Pratama, A. (2024). Comparative Study of Soil Stabilization Using Ceramic Waste Powder and Glass Waster Powder as Additive. Jurnal Aplikasi Teknik Sipil, 22(4), 329. https://doi.org/10.12962/j2579-891X.v22i4.20448

Phantachang, T., Kererat, C., & Homwouttiwong, S. (2024). Enhancing Soil Stabilization: The Influence of Cement and Polymer Additives on the Strength and Performance of Soil-Cement Composites for Unpaved Roads. Revue Des Composites et Des Matériaux Avancés, 34(6), 719–727. https://doi.org/10.18280/rcma.340606

Rabiu, B. O., & Mosaberpanah, M. A. (2025). Sustainable Utilization of Waste Glass Powder and Brick Dust as Cement Replacements: Effects on Mortar Performance and Environmental Benefits. Sustainability, 17(3), 1298. https://doi.org/10.3390/su17031298

Salih, A. G., Rashid, A. S. A., & Salih, N. B. (2023). Evaluation the Effects of Waste Glass Powder Mixed with Hydrated Lime on the Unconfined Compressive Strength of Clayey Soil. E3S Web of Conferences, 427, 01022. https://doi.org/10.1051/e3sconf/202342701022

ShiRzad, W., Behsoodi, M. M., & Tasal, M. Y. (2023). Utilization and effects of various particle sizes of waste glass powder as partial replacement of cement in concrete. International Advanced Researches and Engineering Journal, 7(3), 191–199. https://doi.org/10.35860/iarej.1270868

Tajaddini, A., Saberian, M., Kamalzadeh Sirchi, V., Li, J., & Maqsood, T. (2023). Improvement of mechanical strength of low-plasticity clay soil using geopolymer-based materials synthesized from glass powder and copper slag. Case Studies in Construction Materials, 18, e01820. https://doi.org/10.1016/j.cscm.2022.e01820

Topark-Ngarm, P., Tho-In, T., Sata, V., Chindaprasirt, P., & Cao, T. (2019). Influence of Glass and Limestone Powders in High Calcium Fly Ash Geopolymer Paste on Compressive Strength and Microstructure. Key Engineering Materials, 801, 397–403. https://doi.org/10.4028/www.scientific.net/KEM.801.397

Wang, Y., Yang, J., Su, Y., He, X., & Strnadel, B. (2023). The Effect of Wet-grinding on the Properties of Glass Powder and Its Application in Cement Based Materials. Journal of Wuhan University of Technology-Mater. Sci. Ed., 38(6), 1372–1381. https://doi.org/10.1007/s11595-023-2831-0

ISBN: 978-978-8567-02-8

5TH Faculty of Engineering Conference on Engineering Innovation and Economic Policies: Driving Sustainable Industrial Growth in Nigeria

Faculty of Engineering, Bayero University, Kano.

067-Optimization of Fuzzy Logic Control Based Maximum Power Point Tracker Using Flower Pollination Algorithm

[1]Muhammad Sani Garba, [2] Abdussamad Umar Jibia

[1] Federal University of Technology, Babura.[2] Bayero University, Kano.

muhammadsanigarba@mail.com,aujibia@gmail.com

Abstract: Rapid changes in weather conditions affect the electrical characteristics of the photovoltaic (PV) module. Maximum Power Point Tracker (MPPT) has proven to be effective in improving the conversion efficiency of the PV system. MPPT comprises a DC-DC converter and the MPPT algorithm that varies the duty cycle of the DC-DC converter to yield the desired output. MPPT algorithms are subdivided into conventional and soft computing types. Conventional techniques include perturb & observe, Incremental conductance, and Fractional Open Circuit, among others. Soft computing techniques, on the other hand, include Fuzzy Logic Control (FLC), Artificial Neural Network (ANN), and others. It is generally accepted that soft computing techniques are more robust and efficient, but the tuning of these controllers remains challenging. In this paper, FLC is used as an MPPT algorithm, and Flower Pollination Algorithm (FPA) is used to fine-tune the Scaling gains of the controller, forming an FPA-optimized FLC. The performance of conventional FLC and FPA-optimized FLC are compared. It is demonstrated that the proposed method enhances the percentage energy reduction and tracking accuracy by 2.99% and 3.8%, respectively. Additionally, the settling time was improved from 0.196 seconds to 0.165 seconds. Hence, the simulation results revealed that FPA-optimized FLC provides better transient and steady state performance.

1. INTRODUCTION

In recent years, due to climate problems and fossil fuel depletion, nations worldwide have increasingly invested in research and development for renewable energy sources(Aboras et al., 2025). Various renewable energy sources like wind, solar, geothermal, and biomass can be used for the production of electricity and fulfilling our daily needs. Photovoltaic generation is becoming an increasingly important renewable energy source, as it offers several advantages, including no fuel costs, no pollution, minimal maintenance requirements, and zero noise emissions, among others (Elnaghi et al., 2025). Solar photovoltaic (PV) is a device that absorbs the incident photon energy and converts it into electrical power. Since the electrical characteristic curve of a solar cell is nonlinear and depends on irradiance level and ambient temperature (Quamruzzaman et al., 2016), Optimal performance is not assured when rapid weather condition occurs. Therefore, extracting the maximum possible power is the primary technological challenge today. To maximize PV output under dynamic weather conditions, a solar PV system is typically coupled with a Maximum Power Point Tracking (MPPT) controller.

Maximum Power Point Tracking (MPPT) technology optimizes the output of photovoltaic (PV) modules, significantly enhancing their utility ratio(Quamruzzaman et al., 2016). This effectiveness is especially noticeable under consistent weather conditions, where all PV modules have the same operating temperature and illumination intensity. The traditional methods for achieving MPPT include the perturb and observe (P&O) algorithm, the incremental conductance algorithm, and the fractional open circuit voltage algorithm, among others.

Currently, the use of evolutionary optimization techniques is becoming increasingly popular in various technological fields. Optimization algorithms are also employed for tracking the Peak Power Point. Several methods, including Fuzzy Logic Controller Base, Neural Networks, and genetic algorithms, are effectively utilized in solar (Elnaghi et al., 2025).

However, under practical work conditions, the *P-V* output characteristic curve of the PV array shows complicated multiple peak points due to environmental influences, such as partial shading of modules, accumulation of dust, and imbalanced temperature distribution. The traditional single peak MPPT method can easily become trapped in a local maximum power point (LMPP) of the P-V characteristic curve, which may result in output power loss.

ISBN: 978-978-8567-02-8

PV systems. These techniques offer a quick response to changes in solar irradiation, reducing power loss, operational time, and oscillations. In this paper, a flower pollination algorithm-optimized Fuzzy Logic Controller (FPA-optimized FLC) technique is implemented for tracking the Maximum Power Point, which is fast, relatively simple, and easy to apply due to its requirement for fewer mathematical expressions.

The organization of this paper is as follows: In Section 2, the concept of PV modeling is explained. In Section 3, the design of Fuzzy Logic Control. The Flower Pollination Algorithm is reviewed in Section 4. The simulation Model is depicted in Section 5. The experimental results and discussion are given in Section 6. Finally, in Section 7, we present our conclusion.

2. MODELING OF SOLAR PV

Generally, PV modeling is subdivided into single-diode and two-diode methods, but in this work, for simplicity, a single-diode model(Liu et al., 2025) is chosen as shown in Figure 1. The mathematical formulation of the output current (Ipv) of a PV module is described as:

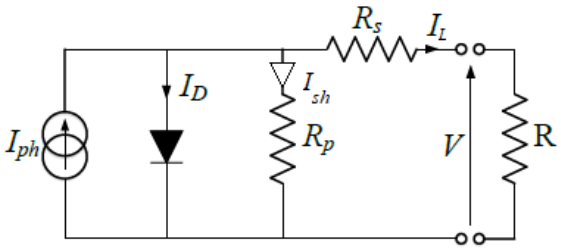


Figure 1: Single Diode Model of PV Cell

The current through the load is given by:

$$I_L = I_{sc} - I_D - I_{sh} \quad (1)$$

The diode I_D is given by Shockley's diode equation (2)

$$I_D = I_O \left(e^{q(\frac{V+IRs}{nKT})}\text{-}1\right) \quad (2)$$

$$I_{sh} = \left(\frac{V+IRs}{Rp}\right) \quad (3)$$

Putting equations (2) and (3) into equation (1), we have:

$$I_L = I_{sc} - I_O \left(e^{q(\frac{V+IRs}{nKT})}\text{-}1\right) - \left(\frac{V+IRs}{Rp}\right) \quad (4)$$

The shunt resistor is very high, has a negligible effect, and can be neglected, thus.

$$I_L = I_{sc} - I_O \left(e^{q(\frac{V+IRs}{nKT})} - 1\right) \quad (5)$$

3. DESIGN OF FUZZY LOGIC CONTROLLER

The application of fuzzy logic for MPPT has become more popular with the utilization of microcontrollers. Fuzzy logic controllers have the benefits of operating with general inputs, not needing to associate correct mathematical models, and handling nonlinearities. Mathematical logic management typically consists of three stages: fuzzification, rule-based table operation, and defuzzification (Riad B., et al 2017).

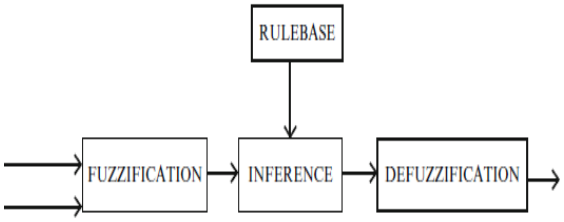


Figure 2: Block diagram of fuzzy logic controller

3.1 Fuzzification

The process of turning a crisp input value into a fuzzy one is called fuzzification. The PWM generator's reference signal is the output variable. Triangular-type membership functions are employed in the fuzzification process.

3.2 Inference Engine and Rule Base

One of the primary components of the fuzzy logic controller is the inference system, a rule-based system with rules stored in the inference engine block. Mamdani's method with the Max-Min operation is used to perform fuzzy inference; the "AND" operator is operated with MIN, and the "OR" operator is operated with MAX. Table 1 depicts the fuzzy rule table.

TABLE 1: FUZZY RULE TABLE

		ERROR(E)				
		NB	**NS**	**ZE**	**PS**	**PB**
CHANGE OF ERROR (dE)	**NB**	ZE	PS	PB	PB	PB
	NS	NS	ZE	PS	PB	PB
	ZE	NB	NS	ZE	PS	PB
	PS	NB	NB	NS	ZE	PS
	PB	NB	NB	NB	NS	ZE

Fuzzy sets for each input and output variable are defined as shown in Table 1. Five fuzzy subsets: NB (Negative Big), NS (Negative Small), ZE (Zero), PS (Positive Small), and PB (Positive Big). were chosen for the inputs and output variables of the fuzzy controller.

3.3 Defuzzification

The fuzzy controller provides the output as a Fuzzy subset, but a real-time system requires a non-fuzzy value, so Defuzzification is necessary. In the Defuzzification process, fuzzy output is transformed into a numerical output. The Centroid method is used for Defuzzification.

2.4 Membership function

A triangular shape has been adopted for the membership functions. The ranges of the input

memberships (MF), PV voltage, and PV current were modified to reflect the characteristics of the proposed PV module. Additionally, the duty cycle, which represents the output of the fuzzy controller, was set to range from -0.3 to 0.3, providing more flexibility for switching the boost converter.

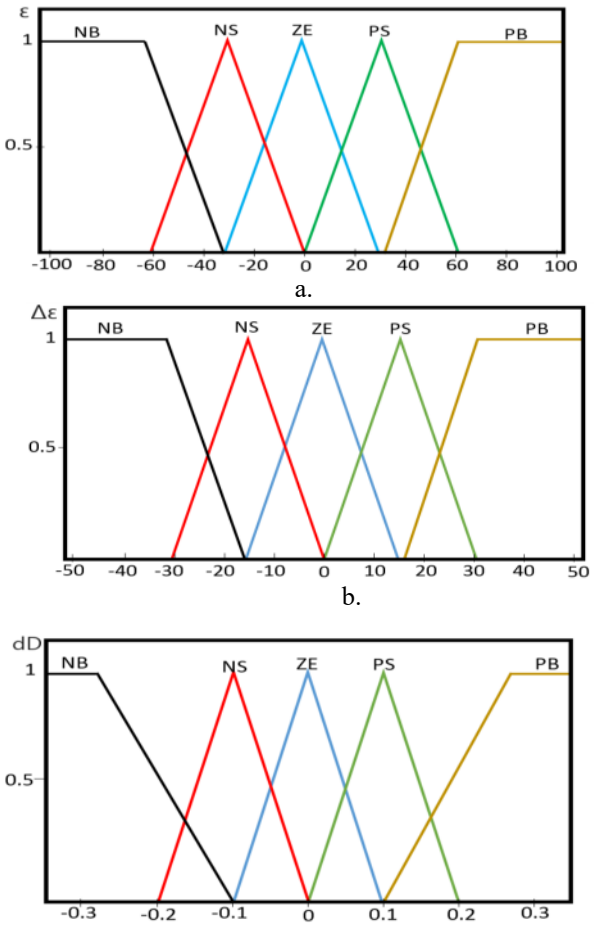


Figure 3: (a) Error MF, (b) Change of error MF, (c) Duty cycle MF

4. FLOWER POLLINATION ALGORITHM (FPA)

FPA is a global optimization algorithm that mimics the flower pollination process of flowering plants in nature and was first proposed by Yang(Bozorg-Haddad., 2018) and is proven to perform better than other more popular algorithms, such as Genetic Algorithm (GA) and Particle Swarm Optimization (PSO)(Lalljith et al., 2021). To achieve a balance between exploitation and exploration ranges modality, the algorithm utilized long-distance pollinators and flower consistency(Lalljith et al., 2021).

In FPA, abiotic and self-pollination are utilized for local pollination, while biotic and cross-pollination are used for global pollination among the flowering plants.

To implement FPA, the fundamental design rules followed are (Pei et al., 2018):

Rule 1: Biotic and cross-pollination represent the global pollination process, and Levy flights accompany pollens because they travel to different species.

Rule 2: Abiotic and self-pollination represent the local pollination.

Rule 3: Insects are pollinators capable of developing flower constancy, where the probability of reproduction for new species is proportional to the similarity of the flowers involved in pollination.

Rule 4: The switching between global and local pollination is controlled by a probability switch $P \in [0,1]$.

The equation characterizes the global pollination.

$$X_i^{k+1} = x^k + \gamma L\,(gbest - x_i^k) \qquad (6)$$

Where L is the levy factor responsible for transporting pollen to different species of flowers, and for the strength of the pollination. γ is the scaling factor used to control the step size. p size.

$$L=\frac{\lambda\Gamma(\lambda)\sin(\frac{\pi\lambda}{2})}{\pi}\frac{1}{s^{1+\lambda}}(S >> S^0 > 0) \qquad (7)$$

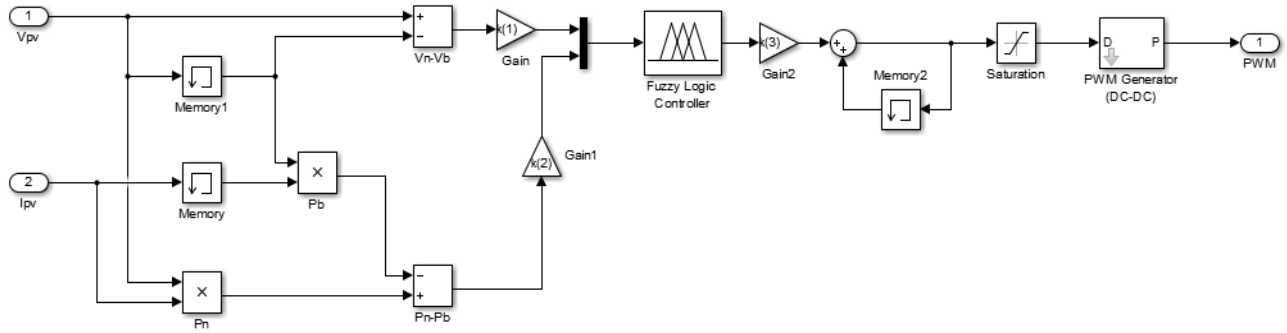
Where Γ(λ) is the standard gamma function, and the equation characterizes the local pollination

$$X_i^{k+1} = X_i^k + \varepsilon\,(X_m^k - X_j^k) \qquad (8)$$

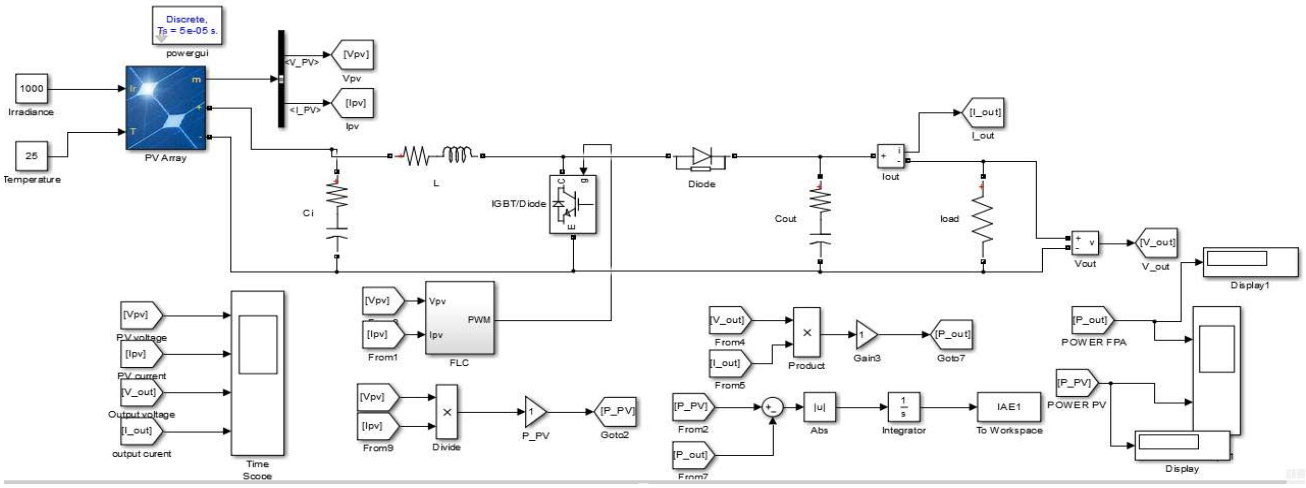
Where X_m^k and X_j^k are the different pollens of the same species. The ε (epsilon) notation represents local search, which follows a uniform distribution. The probability switch in the algorithm determines whether to use local or global pollination, with its optimal value identified as 0.8 in most cases(Bozorg-H., 2018). and its optimal value is found to be 0.8 in most cases(Pei et al., 2018).

5. SIMULATION MODEL

Figure 4 depicts the FLC inference-based MPPT system implementation designed using MATLAB/Simulink.



a.

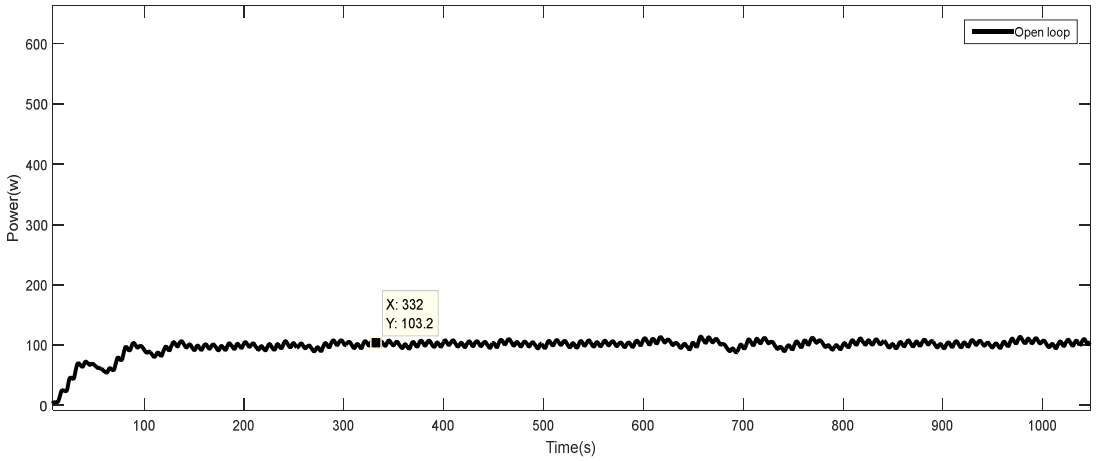


b.

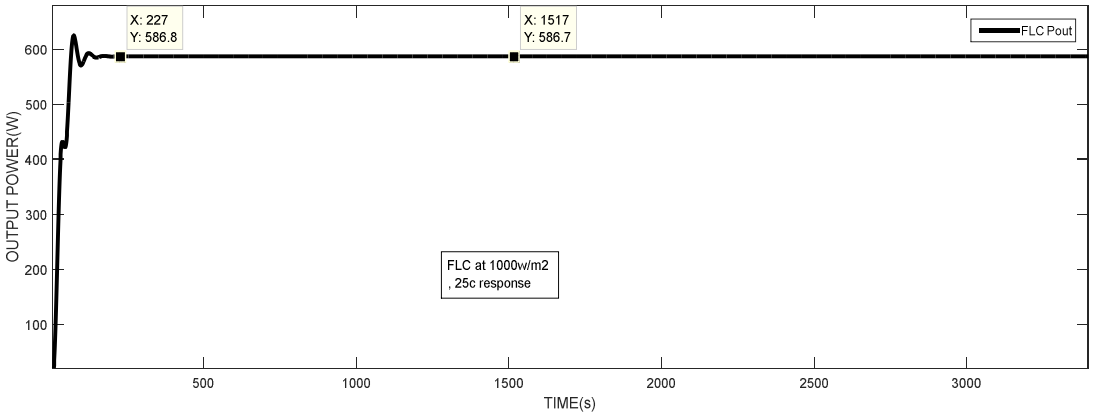
Figure 4a. & b. MATLAB/SIMULINK model of FLC-based MPPT for PV system

6. RESULT & DISCUSSION

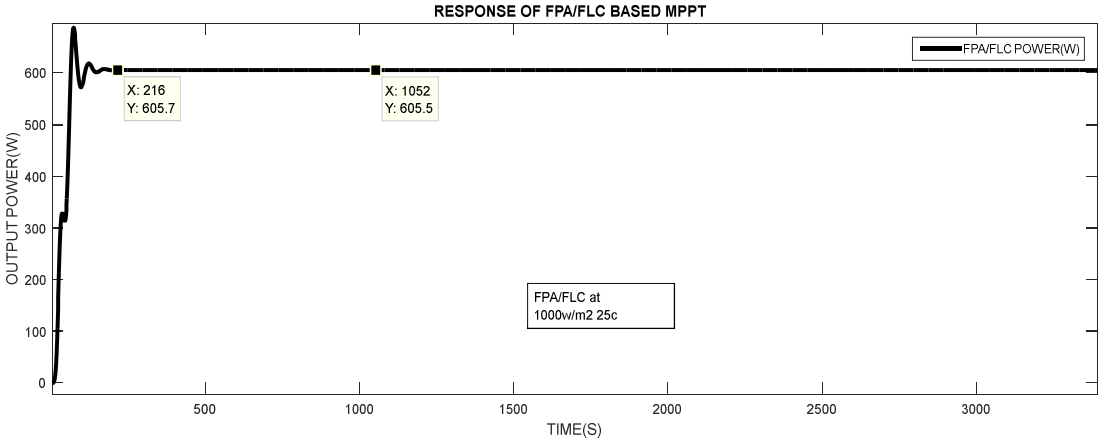
In this work, the system is studied in three different cases: the open-loop system, the closed-loop FLC-based MPPT, and the closed-loop FLC that is optimized using FPA, as depicted in Figures 5a, b, and c, respectively. In the first case, the system is run without any controller, and the response of the system was very poor in terms of both the tracking efficiency and transient and steady-state performances, as depicted in Figure 5a. Figure 5b. shows the response using FLC-based MPPT, the system was able to track the output power of the PV module up to about 95.1%. Finally, under the same operating conditions, the system is simulated again, but with the flower pollination algorithm to optimize the scaling gains of the fuzzy logic controller. The optimized FLC-based MPPT succeeds in tracking 99.0%, also eliminating the steady-state oscillation, thus yielding better performance as summarized in Table 1.


Open loop
Power(w)
X: 332
Y: 103.2
Time(s)

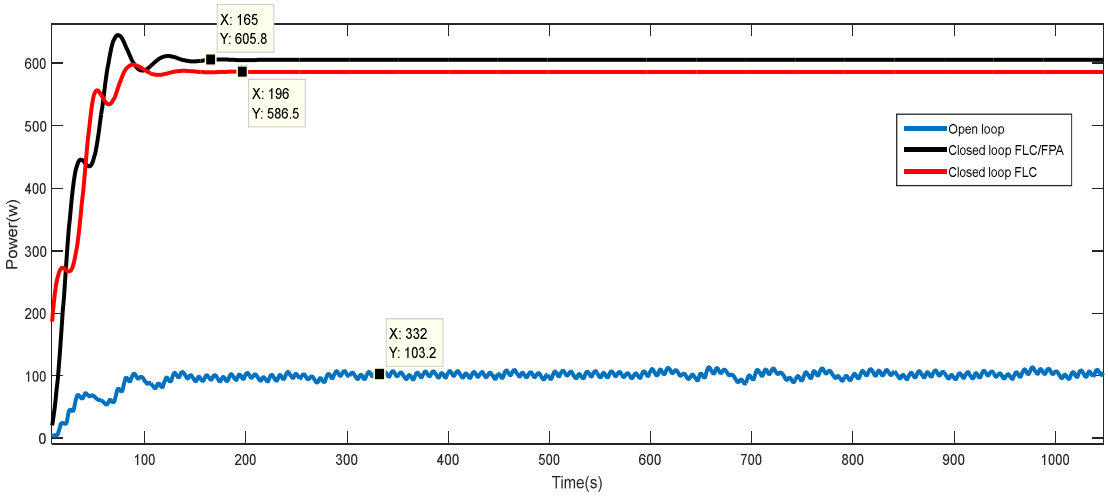
a.


X: 227
Y: 586.8
X: 1517
Y: 586.7
FLC Pout
OUTPUT POWER(W)
FLC at 1000w/m2
, 25c response
TIME(s)

b.


RESPONSE OF FPA/FLC BASED MPPT
FPA/FLC POWER(W)
X: 216
Y: 605.7
X: 1052
Y: 605.5
OUTPUT POWER(W)
FPA/FLC at
1000w/m2 25c
TIME(S)

c.



d.

Figures 5a, b, c, and d: PV system simulation plots

TABLE 2. COMPARISON OF PERFORMANCE INDICES

S/N	MPPT ALGORITHM	SETTLING TIME(S)	TRACKING EFFICIENCY AT 25°C & 1000W/M^2		% ENERGY REDUCED
			VALUES(W)	EFFICIENCY	
1.	Open	1.500	103.2	0.17	71.00
2.	FLC	0.196	586.5	0.95	4.601
3.	FPA Optimized FLC	0.165	605.8	0.99	1.609

7. CONCLUSION

In this work, a flower pollination algorithm has been employed to fine-tune the scaling gains of the fuzzy logic controller to track the MPPT for the PV system. The different scenarios under various irradiations ascertain that the algorithm is one of the best techniques for optimizing the scaling gains of FLC. Therefore, the proposed FPA-optimized FLC outperforms other FLCs in terms of transient performance and tracking efficiency. Even though the objectives of the proposed techniques have been successfully met, the two-diode model of the PV array is more appropriate and accurate; based on that, future work will focus on the use of two diode model for PV arrays.

REFERENCES

Aboras, K. M., El-banna, M. H., & Megahed, A. I. (2025). *A unique novel-based FLC approach for enhancing MPPT operation of solar systems considering sudden/gradual variation in weather conditions*. *108*(1), 1–40. https://doi.org/10.1177/00368504251323732

Agarwal, P. Mehta, S. (2014). *Nature-Inspired Algorithms : State-of-Art, Problems and Prospects*. International Journal of Computer Application *100*(14), 14–21.

Bendib, B., Belmili, H., & Krim, F. (2015). A survey of the most used MPPT methods : Conventional and advanced algorithms applied for photovoltaic systems A survey of the most used MPPT methods : Conventional and advanced algorithms applied for photovoltaic systems. *Renewable and Sustainable Energy Reviews*, *45*(April 2018), 637–648.

Bozorg-Haddad Editor, O. (n.d.). *Studies in Computational Intelligence 720: Advanced Optimization by Nature-Inspired Algorithms*. http://www.springer.com/series/7092

Cheng, P., Peng, B., Liu, Y., Cheng, Y., & Huang, J. (2015). *Optimization of a Fuzzy-Logic-Control-Based MPPT Algorithm Using the Particle Swarm Optimization Technique*.Energies 2015 5338–5360.

Elnaghi, B. E., Ismaiel, A. M., Ismail, M. M., Zedan, H. A., & Salem, A. A. (2025). *Experimental validation of an adaptive fuzzy logic controller for MPPT of grid connected PV system*.Scientific report 1–23. https://doi.org/10.1038/s41598-025-10188-7

Ibrahim, H. E. A., & Ibrahim, M. (2012). *Comparison Between Fuzzy and P & O Control for MPPT for Photovoltaic System Using Boost Converter*. Journal of Energy Technologies and Policy, Vol. 2, No. 6, 2012, p. 1

Kumar, M., Ali, M. A., & Alam, S. (2020). *Solar System Array by Fuzzy Logic based on MPPT Algorithm*. International Journal of Innovative Technology and Exploring Engineering (IJITEE) ISSN: 2278-3075 (Online), Volume-9 Issue-6, April 2020.

Nisarga, G. C., & Prasad, C. R. S. (2018). *Fuzzy Logic Based MPPT Controller for Photovoltaic System*.International journal of science and reserch ISSN(online) 2319-7064 *7*(8), 123–127.

Liu, C., Hung, C., & Chen, G. (2025). *A Study on Maximum Power Point Tracking Technology for Solar Power Systems Using Power Variation to Adjust Step Response*. International Conference on Artificial Life and Robotics (ICAROB2025), Feb.13-16, J:COM HorutoHall, 220–223

Lalljith, S., Fleming, I., Pillay, U., Naicker, K., Kumar, A., & Member, S. (2021). Applications of Flower Pollination Algorithm in Electrical Power Systems : A Review. *IEEE Access*, *PP*, 1.https://doi.org/10.1109/ACCESS.2021.3138518

Riad BENDIB(1)*, Noual BATOUT(2), Hamid BENTARZI. (2017*Optimization of the Membership Functions for a Fuzzy Controller Using an Improved Genetic Algorithms*. *Laboratory of Signals and Systems (LSS) ISSN : 2543-3792*

Pei, T., Hao, X., & Gu, Q. (2018). A Novel Global Maximum Power Point Tracking Strategy Based on Modified Flower Pollination Algorithm for Photovoltaic Systems under Non- Uniform Irradiation and Temperature Conditions. *Energies*,*11*(10). https://doi.org/10.3390/en11102708

Quamruzzaman, M., Mohammad, N., Matin, M. A., & Alam, M. R. (2016). *Highly efficient maximum power point tracking using DC – DC coupled inductor single-ended primary inductance converter for photovoltaic power systems*. International Journal of Sustainable Energy ISSN:*6451*(December 2017). https://doi.org/10.1080/14786451.2014.961922

Ram, J. P., & Rajasekar, N. (2016). *A novel Flower Pollination-based Global Maximum Power Point method for Solar Maximum Power Point Tracking*. IEEE Transactions on Power Electronics PP(99):1-1

Ram, J. P. (2016). *FPA-based approach for solar maximum power point tracking, School of Electrical Engineering*. IEEE Transactions on Power Electronics.

Saha, S. K. (2018). Optimization Technique Based Fuzzy Logic Controller for MPPT of Solar PV System. *2018 International Conference on Emerging Trends and Innovations In Engineering And Technological Research (ICETIETR)*, 1–5.

Sherif, I. M., & Seshadri, S. (2018). *Artificial Neural Network based MPPT of solar photovoltaic cell*. International Journal of Innovative Reserch In Science, Engineering & Technology. ISSN(Online): 2319-8753.

Sumathi, S., Kumar, L., Ashok Surekha, P. (2015). *Solar PV and Wind Energy Conversion*

Systems. Machakos University (MksU Press, 2021-12

Tingting Pei, Xiaohong Hao, and Qun Gu. (2018). *A Novel Global Maximum Power Point Tracking Strategy Based on Modified Flower Pollination Algorithm for Photovoltaic Systems under Non*. International Journal of Energy (c).https://doi.org/10.3390/en11102708

Tobón, A., Peláez-restrepo, J., Villegas-ceballos, J., Serna-garcés, S. I., Herrera, J., & Ibeas, A.(2017). *Maximum Power Point Tracking of Photovoltaic Panels by Using Improved Pattern Search Methods*. Energies 1–15.

068-Practical Strategies for Promoting Positive Safety Culture in Kano's Construction SMEs

Nalado Nasir Kan-Katsina[1,2], Aminu Darda'u Rafindadi[1], Salihi Ibrahim Umar[1], Abdullahi Balarabe Bello[1], Abdulra'uf Mukhtar Bora[1] [1]Department of Civil Engineering, Bayero University Kano, Nigeria [2]Zonal Advance Space Technology Applications Laboratory, National Space Research and Development Agency, Kano, Nigeria (Corresponding author: nsrnalado@gmail.com)

Abstract: Kano State's small and medium-sized enterprises (SMEs) make up a whopping 80% of the construction industry and contribute about 4.18% to Nigeria's GDP. Unfortunately, these businesses are grappling with a daunting fatality rate of 39.24%, which is 30% higher than the national average. Four key challenges are particularly pressing: informal labor (61.5%), a significant language barrier with 70% of workers being non-bilingual, budget constraints (37.5%), and training gaps (33.3%). This study employs a sequential mixed-methods approach, featuring a pilot survey with 8 participants, a two-round Delphi involving 14 and then 13 experts, and a reflexive thematic analysis of 24 expert comments. It proposes four cost-effective and culturally relevant strategies that received 65–80% agreement from experts: Hausa-language virtual reality training (the most favored at 75%), multilingual hazard-reporting apps, PPE procurement cooperatives, and a Kano State Construction Safety Decree (with 80% consensus). If these strategies are implemented together, they could potentially reduce accidents by 15–20%, cut quality defects by 14.63%, and lower economic losses by 25% within 18–24 months. By merging engineering innovations like affordable VR and offline apps with economic policy reforms through an incentivized decree, these strategies align seamlessly with the conference theme and offer a practical roadmap for fostering safer, more profitable, and sustainable construction SMEs in Nigeria

1. INTRODUCTION

Construction is a cornerstone of Nigeria's infrastructure development and economic growth, yet it remains one of the most hazardous industries globally (International Labor Organization, 2023; Hallowell & Gambatese, 2010). In Kano State, SMEs dominate the sector (80% of enterprises) and contribute 4.18% to national GDP (National Bureau of Statistics, 2023), but suffer a fatality rate of 39.24%, which is 30% above the national average (Aliyu et al., 2019). This results in 20–30% rework, 10–15% delays, 15–25% errors, and approximately 25% economic losses per project (Jimoh et al., 2020; Boadu et al., 2020).

Global research consistently identifies leadership commitment, personnel competence, work environment, and safety communication as the four dominant safety culture constructs (Al-Bayati et al., 2019; Deepak & Mahesh, 2021; Loosemore & Chan, 2021). Practical interventions such as toolbox talks, PPE provision, and regulatory enforcement have achieved 15–30% incident reductions in formalized settings (Machfudiyanto et al., 2020; Kheni et al., 2008; Zohar, D., 2010). However, these assume regulatory enforcement and monolingual workforces are conditions that are largely absent in African informal SMEs (Adzivor et al., 2023; Agumba & Haupt, 2018). In Nigeria, informal labor (61.5%), linguistic diversity (70% non-bilingual), and resource scarcity amplify risks, demanding culturally embedded solutions (Kori-Siakpere et al., 2024; Boadu et al., 2020).

Despite abundant global literature, Africa accounts for only 8% of safety culture studies, with Northern Nigeria virtually unrepresented (<12 studies total, zero Delphi applications; Antwi-Afari et al., 2024). Existing interventions rarely address informal labor, multilingualism, or extreme resource scarcity simultaneously. No study has proposed and expert-validated low-cost, Hausa-language-focused strategies tailored for Kano's SMEs.

The conference theme — *Engineering Innovation and Economic Policies: Driving Sustainable Industrial Growth in Nigeria* — demands solutions that are technically innovative and economically viable. This paper directly answers the call by presenting four expert-validated strategies that fuse engineering innovation (low-cost VR training, offline multilingual apps, cooperative procurement) with economic policy reform (incentivized Safety Decree) to transform safety culture from a cost center into a competitiveness driver for Kano's SMEs.

ISBN: 978-978-8567-02-8

2. METHODOLOGY

A sequential mixed-methods design was employed to generate and validate culturally congruent strategies (Creswell & Clark, 2017).

2.1 Expert Panel Recruitment

A purposive panel of 14 construction professionals based in Kano State was recruited (Round 1), with 13 retained in Round 2 (92.9% retention). Selection criteria: ≥5 years' experience in Kano construction SMEs and familiarity with Hausa-language workforce dynamics (Musonda et al., 2021). Panel composition: site managers (42.9%), safety officers (28.6%), civil engineers (14.3%), academics (14.3%).

TABLE I: Demographic Characteristics

Variable	Category	n	%
Gender	Male	14	100
Age (years)	25–34	1	7.1
	35–44	10	71.4
	45–54	3	21.4
Education	Bachelor's Degree	7	50
	Master's Degree	6	42.9
	PhD	1	7.1
Experience (years)	5–10	7	50
	11–15	4	28.6
	16–20	3	21.4
Role	Site Engineer	7	50
	Supervisor	4	28.6
	Project Manager	3	21.4
Safety Policy Awareness	Aware	10	71.4
	Not Aware	4	28.6
Perception of Safety Practices	Fair	4	28.6
	Good	5	35.7
	Very Good	4	28.6
	Excellent	1	7.1

2.2 Two-Round Delphi Process for Strategy Validation

Round 1 Experts rated four draft strategies (derived from preliminary fieldwork) on relevance and feasibility (5-point Likert) and provided open comments. Round 2 Controlled feedback was provided (group means anonymized comments). Experts rated refined versions.

Consensus criteria (applied simultaneously; Hsu & Sandford, 2007; von der Gracht, 2012):

- Mean Score ≥ 4.0 (Equation 1):

The first criterion required a mean score of at least 4.0 on the 5-point Likert scale (where 1 means Strongly Disagree and 5 means Strongly Agree), calculated as follows:

$$\bar{x} = \frac{1}{n}\sum_{i=1}^{n} x_i \geq 4.0 \quad (1)$$

Where: x_i: rating by expert i and n: number of experts (n=14 in Round 1, n=13 in Round 2)

- Coefficient of Variation % (Equation 2):

The second criterion limited the coefficient of variation (CV) to ≤ 20%, calculated as:

$$CV = \left(\frac{\sigma}{\bar{x}}\right) \times 100\% \leq 20\% \quad (2)$$

Where: σ is the standard deviation

- Interquartile Range ≤ 1.0 (Equation 3):

The third and most stringent criterion required an interquartile range (IQR) ≤ 1.0, calculated as:

$$IQR = Q_3 - Q_1 \leq 1.0 \quad (3)$$

Where: Q_1 and Q_3: are the 25th and 75th percentiles.

- Statistical Validation:

Response Stability: Wilcoxon signed-rank test (Equation 4):

$$W = \sum_{i=1}^{N_r} \text{sgn}(x_{2,i} - x_{1,i}) \cdot R_i \quad (4)$$

Where: $x_{1,i}, x_{2,i}$: paired ratings, sgn is the sign function (+1, 0, or –1), R_i is the rank of the absolute difference and N_r is the non-zero differences

Effect size (Equation 5):

$$r = \frac{|Z|}{\sqrt{N}} \quad (5)$$

Where: $r > 0.5$ is the large effect (Cohen, 1988)

Normality Justification: Shapiro-Wilk tests confirmed non-normality (>90% items, $p \leq 0.05$) (Siegel, S. and Castellan, N. J. 1988).

Thematic Reliability: Cohen's κ for inter-coder agreement on 24 comments (Equation 6):

ISBN: 978-978-8567-02-8

To ensure rigor, we used Cohen's Kappa to quantify inter-coder agreement.

$$\kappa = \frac{p_o - p_e}{1 - p_e} \quad (6)$$

Where: p_o is the observed agreement (0.94), $p_e$is the expected agreement by chance (0.40), and

- Resulting κ = 0.90 ("almost perfect"; Landis & Koch, 1977)

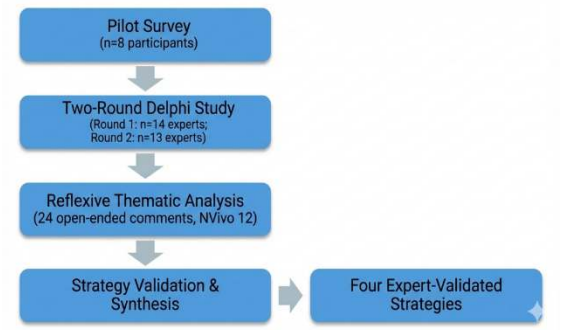


Figure 1: Methodology Flowchart (Delphi Rounds → Thematic Analysis → Validated Strategies)

3. RESULTS

3.1 *Identified Barriers (Supporting Strategy Rationale)*

Reflexive thematic analysis of 24 open-ended expert comments (Braun & Clarke, 2006, 2021) identified four dominant barriers aligned with safety culture constructs as shown in Table 2. Inter-coder reliability was Cohen's κ = 0.90 (Equation 8; "almost perfect"; Landis & Koch, 1977).

TABLE II: Dominant Barriers from Thematic Analysis and Delphi Consensus

Barrier	Prevalence (%)	Frequency (Comments)	Key Exemplar Comment	Targeted by Strategy
Informal Labour	41.7	10/24	"Non-contracted workers ignore rules"	Safety Decree
Inadequate Budgets	37.5	9/24	"No funds for PPE or controls"	PPE Cooperatives
Limited Training Access	33.3	8/24	"Scheduling limits training access"	Hausa VR Training
Linguistic Diversity	25	6/24	"Hausa speakers miss English briefings"	VR Training & Apps

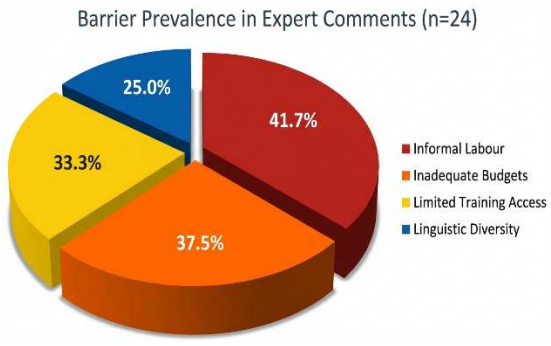


Figure 2: Barrier Prevalence in Expert Comments (pie chart: Informal Labor 41.7%, Budgets 37.5%, Training 33.3%, Linguistic 25.0%).

These barriers directly informed strategy selection, ensuring cultural and economic relevance for Kano's informal SME context.

TABLE III: Expert-Validated Strategies

Strategy	Delphi Consensus	Primary Barriers Targeted	Key Features & Projected Impact
Hausa-Language VR Training	75% (highest-rated)	Linguistic diversity, training gaps	Offline 360° modules in Hausa, recycled-cardboard viewers: 20–25% error reduction (Yu et al., 2022)
Multilingual Hazard-Reporting Apps	65%	Linguistic diversity, communication gaps	Offline, voice + pictorial input; 40–60% near-miss increase (Muñoz-La Rivera et al., 2021)
PPE Procurement Cooperatives	70%	Budget constraints, PPE access	20–30 SMEs/cluster; 20–30% cost savings (Kheni et al., 2008)
Kano State Construction Safety Decree	80% (highest)	Regulatory weakness, informal labour	Quarterly audits, Hausa briefings, tax rebates; 50–70% compliance rise (Jimoh et al., 2020)



Figure 3: Strategy Consensus Levels (bar chart)

Strategy 1- Low-Cost Hausa VR Safety Training (75% Consensus):

ISBN: 978-978-8567-02-8

The Hausa-language VR training module was the single highest-rated Intervention across the entire Delphi study (mean = 4.92/5.00, CV = 5.7%, IQR = 0.25). Experts overwhelmingly endorsed it as the most effective way to overcome Kano's two biggest barriers simultaneously: linguistic diversity and training gaps. Tables IV and V provide the reason as to why the strategy will work in Kano and the optimized technical specification with cost benefit.

TABLE IV: Why VR Will Work in Kano

Kano Reality	Traditional Training Failure	VR Advantage
70% non-bilingual workforce	English/PowerPoint → 50% misinterpretation	Full Hausa narration + pictorial cues
Low literacy among day laborers	Text-heavy materials ineffective	Immersive 360° scenarios – no reading required
High turnover & informal labor	Classroom scheduling impossible	10-minute offline modules usable anytime
Budget constraints (37.5%)	Western VR systems unaffordable	Recycled-cardboard + free software → <₦4,000/worker

TABLE V: Kano-Optimized Technical Specification

Component	Specification & Cost Breakdown	Cost (₦)
Hardware	Recycled-cardboard viewers + existing Android phones	500,000 (250 units)
360° Capture	Insta360 X3/X4 camera (one-time)	650,000
Content (8 modules)	10–12 min Hausa-narrated 360° videos	1,800,000
Train-the-Trainer (60 champions)	3-day workshop	1,200,000
Total (2,000 workers)		6,750,000 (~₦3,375/worker)

Projected Outcomes

- Knowledge retention: 75–90% (vs. 10–20% lectures) – Yu et al., 2022
- Error & rework reduction: 20–25% within 6 months
  ROI payback: <9 months via 25% cost savings

This VR model is not a luxury; it is the most cost-effective, culturally resonant breakthrough for personnel competence and communication

Strategy 2 – Multilingual Hazard-Reporting Apps (65% Consensus):

Rationale: Linguistic diversity (70% non-bilingual workforce) and poor communication channels were cited in 25% of expert comments as primary reasons for unreported near-misses and recurring incidents. Traditional paper forms or English-only apps are ineffective in low-literacy, multilingual environments. Experts rated this strategy 65% consensus – lower than VR/cooperatives due to smartphone penetration concerns, but still strongly endorsed as transformative for proactive reporting. Table VI shows the optimized multilingual app specification.

TABLE VI: Kano-Optimized Multilingual App Specification

Feature	Specification & Cost-Saving Rationale	Projected Impact (Literature + Delphi)
Base Platform	Free/open-source: Kobo Toolbox or ODK Collect (customized fork)	Zero licensing cost
Languages	Hausa (voice + text), English, Fulani (optional)	Addresses 70% non-bilingual workforce
Input Method	Voice recording + 40 pictorial hazard icons (no typing required)	Works for low-literacy workers
Offline Functionality	Full offline data collection → sync when Wi-Fi is available	No mobile data needed – critical for site conditions
Reporting Types	Near-miss, hazard, good practice, stop-work authority	Encourages a proactive culture
Instant Feedback	Auto-reply in Hausa: "Nagode! An karɓi rahoton ka" + champion follow-up	Increases trust & repeat reporting
Hardware	Uses workers' existing Android phones (>60% ownership)	Zero hardware cost
One-Time Development	Local developer customization (forms, icons, voice prompts)	₦1.2 million (shared across 50 SMEs = ₦24,000 each)
Training	30-minute peer session per site	Minimal time investment

Implementation Roadmap

- Month 1–2: Customize Kobo Toolbox with Hausa voice prompts and Kano-specific hazard icons
- Month 3: Train 100 peer champions (2 per site)
- Month 4–12: Roll out to 50 pilot SMEs → 5,000 workers
- Total cost: ₦1.8 million for 5,000 users (≈ ₦360 per user)

Projected Outcomes:

- Near-miss reporting increase: 40–60% within 6 months (Muñoz-La Rivera et al., 2021)
- Error reduction contribution: 10–15%
- Cultural shift: Workers feel heard → stronger open communication culture

Strategy 3 – PPE Procurement Cooperatives (70% Consensus): Budget constraints (37.5% of comments)

ISBN: 978-978-8567-02-8

and inconsistent PPE availability were repeatedly highlighted as the most immediate, solvable barrier. Individual SMEs cannot negotiate bulk discounts or access certified suppliers. Experts gave this strategy 70% consensus as the fastest way to achieve 100% PPE coverage. Table VII shows the Kano-optimized PPE cooperative model.

TABLE VII: Kano-Optimized Cooperative Model

Component	Specification & Structure	Projected Impact (Literature + Delphi)
Legal Form	Registered Cooperative Society under the Kano State Cooperative Law	Legal entity for bulk purchasing & micro-credit
Membership	20–30 SMEs per cluster (urban zones + flood-prone areas)	Critical mass for 25–35% supplier discounts
Governance	Elected committee (1 rep per SME) + peer champion as secretary	Transparent, trusted by informal workers
Procurement Cycle	Quarterly bulk orders: helmets, boots, vests, gloves, rain gear	20–30% cost reduction (Kheni et al., 2008)
Financing	Revolving fund: 10% markup covers transport & defaults	No external loans needed
Micro-Credit Option	Pay-per-use or monthly ₦5,000 deduction via site foreman	Accessible to informal day-laborers
Quality Assurance	All items SON-certified (tested by COREN engineers)	Eliminates counterfeit PPE
One-Time Setup Cost	Registration, training, initial inventory	₦8–10 million (shared = ₦300–400k per SME)

12-Month Rollout Plan:

- Month 1–2: Form 10 cooperatives (200–300 SMEs total)
- Month 3: First bulk order (5,000 PPE sets) → 28% average discount
- Month 4–12: Quarterly orders + micro-credit scheme
- Total annual saving: ₦360–480 million for participating SMEs

Projected Outcomes:

- PPE compliance: 40% → 95% within 12 months
- Incident reduction from PPE failures: 15–20%
- Cost saving per SME: ₦1.8–2.4 million/year
- Social impact: Builds trust and collective responsibility

Strategy 4 – Kano State Construction Safety Decree (80% Consensus):

The Kano State Construction Safety Decree is a targeted regulatory framework designed to address the 80% expert consensus call for mandatory enforcement in Kano's informal SME-dominated construction sector. Drawing from the National Building Code of Nigeria (NBC, 2006) and successful state-level models like Lagos State's Urban and Regional Planning and Development Law (2010), this decree integrates engineering innovation with economic incentives.

Legal and Structural Basis

- Builds on NBC provisions for site inspections and PPE standards (Sections 4.1–4.3).
- Complement Kano's Urban Planning and Development Authority (KNUPDA) regulations.
- Enforcement: Kano State Ministry of Works and Housing, delegated to KNUPDA.

Key Provisions

1. Mandatory Quarterly Safety Audits

- Unannounced audits on PPE availability, Hausa/English signage, and evacuation plans.
- Fines: ₦50,000–200,000 (graduated).

2. Hausa-Language Safety Briefings

- Daily toolbox talks mandatory in Hausa with pictorial aids.
- Supervisor certification required (free BUK modules).

3. Minimum PPE Standards

- Helmet, boots, vest, gloves, flood-resistant gear mandatory.
- Cooperatives encouraged for bulk purchase.

4. Economic Incentives

- 10% state income tax rebate for SMEs achieving 80% audit compliance.
- Priority access to ₦5–10 million safety equipment grants.

Implementation Roadmap (12–24 months)

- Months 1–3: Draft & stakeholder workshop → Bill to Kano State House of Assembly
- Months 4–12: Pilot in 20 high-risk sites → train 100 inspectors
- Months 13–24: Full rollout to 500 SMEs → independent evaluation

ISBN: 978-978-8567-02-8

Projected Outcomes

- Compliance: 30% → 70% within 2 years
- Accident reduction: 15–20%
- ROI: ₦500 million annual savings for the state

This decree exemplifies the conference theme by transforming safety compliance into an economic advantage for SMEs while delivering measurable social and industrial benefits.

3.2. Discussion & Alignment with Conference Theme

Engineering Innovation:

- Hausa-language VR training replaces ineffective classroom methods with immersive, low-literacy-compatible learning (75–90% retention; Yu et al., 2022).
- Multilingual offline apps enable near-miss reporting on basic smartphones already owned by >60% of workers (Muñoz-La Rivera et al., 2021).
- PPE cooperatives apply circular-economy principles to bulk procurement (20–30% savings; Kheni et al., 2008).

Economic Policy Innovation:

- The proposed Kano State Construction Safety Decree introduces performance-based tax rebates and graduated penalties, which was a fiscal model proven in Lagos (42% compliance increase in 3 years; Jimoh et al., 2020).
- These incentives transform safety compliance into an economic advantage, supporting Nigeria's Ease of Doing Business reforms and the National Policy on MSMEs (2021).

The combined effect of 14.63% quality improvement and 25% cost savings (sensitivity ±10% yields 13.17–16.09%; consistent with African cases like Agumba & Haupt, 2018; Rantsatsi et al., 2023), which in turn positions safety culture enhancement as a high-ROI driver of sustainable industrial growth.

4. LIMITATIONS

The study has several limitations that warrant acknowledgement. The Delphi panel consisted of 14 (Round 1) and 13 (Round 2) participants, all male and based in the Kano metropolis. This reflects the male-dominated nature of the sector in urban Northern Nigeria but limits gender diversity and geographic generalizability to rural SMEs, where informal labor and environmental risks (e.g., flooding) may differ. Self-reported data may be subject to social desirability bias, although anonymity and controlled feedback mitigated this risk. The sample size, although consistent with Delphi tradition for expert panels (Hsu & Sandford, 2007), remains modest and requires larger-scale validation. Finally, for future studies, larger surveys are recommended. Projections assume full adoption; real-world variability is possible.

5. CONCLUSION

This study delivers four expert-validated, low-cost strategies that directly confront Kano's dominant safety culture barriers while exemplifying the conference theme through engineering innovation and economic policy reform. Immediate rollout of Hausa-language training and PPE cooperatives, supported by a Kano Safety Decree, offers the fastest path to safer workers, profitable SMEs, and sustainable industrial growth.

Acknowledgement

The authors acknowledge the Delphi panelists for their expertise, patience, and support throughout the analysis and the Civil Engineering Department of Bayero University, Kano, for their unwavering support.

REFERENCES

Abubakar, M. a., Zailani, B. M., Abdullahi, M., Auwal, A. M. J. J. o. e., design, & technology. (2022). Potential of adopting a resilient safety culture toward improving the safety performance of construction organizations in Nigeria. 20(5), 1236-1256. doi:https://doi.org/10.1108/JEDT-09-2020-0354

Adzivor, E. K., Emuze, F., Das, D. K. J. J. o. F. M. o. P., & Construction. (2023). Indicators for safety culture in SME construction firms: a Delphi study in Ghana. 28(3), 293-316. https://doi.org/10.1108/JFMPC-06-2022-0030

Agumba, J., & Haupt, T. J. J. o. t. S. A. I. o. C. E. (2018). The influence of health and safety practices on health and safety performance outcomes in small and medium enterprise projects in the South African construction industry. 60(3), 61-72. https://doi.org/10.17159/2309-8775/2018/v60n3a6

Al-Bayati, A. J. (2021). Impact of Construction Safety Culture and Construction Safety Climate on Safety Behavior and Safety Motivation. 7(2), 41. https://doi.org/10.3390/safety7020041

Al-Bayati, A. J., Albert, A., Ford, G. J. P. P. o. S. D., & Construction. (2019). Construction safety culture and climate: Satisfying necessity for an industry framework. 24(4), 04019028. https://doi.org/10.1061/(ASCE)SC.1943-5576.0000452

Aliyu, B. S., Moyi, M. Z., Fareed, L. Z., Sule, H. J., Nazifi, A. M., Bello, D. Y., & Auwalu, B. A. (2019). Impact of construction practices on the environment

ISBN: 978-978-8567-02-8

a case study of Kano State, Nigeria. Bayero Journal of Pure and Applied Sciences, 12(1), 18-23.

Ameyaw, E. E., Hu, Y., Shan, M., Chan, A. P., Le, Y. J. J. o. c. e., & management. (2016). Application of Delphi method in construction engineering and management research: a quantitative perspective. 22(8), 991-1000. https://doi.org/10.3846/13923730.2014.945953

Antwi-Afari, M. F., Li, H., Wong, J. K. W., Oladinrin, O. T., Ge, J. X., Seo, J., & Wong, A. Y. L. (2019). Sensing and warning-based technology applications to improve occupational health and safety in the construction industry: A literature review. Engineering, Construction and Architectural Management, 26(8), 1534-1552. https://doi.org/10.1108/ECAM-10-2018-0447

Boadu, E. F., Wang, C. C., & Sunindijo, R. Y. (2020). Characteristics of the Construction Industry in Developing Countries and Its Implications for Health and Safety: An Exploratory Study in Ghana. Int J Environ Res Public Health, 17(11), 4110. doi:10.3390/ijerph17114110

Braun, V., & Clarke, V. J. Q. r. i. p. (2006). Using thematic analysis in psychology. 3(2), 77-101. https://doi.org/10.1191/1478088706qp063oa

Braun, V., & Clarke, V. J. Q. r. i. p. (2021). One size fit all? What counts as quality practice in (reflexive) thematic analysis, 18(3), 328-352. https://doi.org/10.1080/14780887.2020.1769238

Cohen, J. (1988). Statistical power analysis for the behavioral sciences (2nd ed.). Lawrence Erlbaum Associates. https://doi.org/10.4324/9780203771587

Cooper, M. D. J. S. s. (2000). Towards a model of safety culture. 36(2), 111-136. https://doi.org/10.1016/S0925-7535(00)00035-7

Creswell, J. W., & Clark, V. L. P. (2017). Designing and conducting mixed methods research: Sage publications.

Field, A. (2024). Discovering statistics using IBM SPSS statistics: Sage publications limited.

Goncalves Filho, A. P., & Waterson, P. J. S. s. (2018). Maturity models and safety culture: A critical review. 105, 192-211. https://doi.org/10.1016/j.ssci.2018.02.017

Guldenmund, F. W. (2000). The nature of safety culture: A review of theory and research. Safety Science, 34(1–3), 215–257. https://doi.org/10.1016/S0925-7535(00)00014-X

Hallowell, M. R., & Gambatese, J. A. (2010). Population and Initial Validation of a Formal Model for Construction Safety Risk Management. Journal of Construction Engineering and Management, 136(9), 981-990. doi:10.1061/(asce)co.1943-7862.0000204

Horne, R. J. W. E., & Outlook, S. (2023). 2 Employment and social trends by region. 2023(1), 57-85. https://doi.org/10.1002/wow3.186

Hsu, C. C. and Sandford, B. A. (2007). The Delphi technique: Making sense of consensus. Practical Assessment, Research & Evaluation, 12(10), 1–8. https://doi.org/10.7275/pdz9-th90

Hudson, P. (2007). Implementing a safety culture in a major multi-national. Safety Science, 45(6), 697–722. https://doi.org/10.1016/j.ssci.2007.04.005

Jimoh, R. A., Oyewobi, L. O., Uthman, N. L., Ibrahim, K., & Salawu, A. (2020). Strategies for Engendering Health and Safety Culture in Construction Firms in Abuja, Nigeria. https://doi.org/10.30880/jst.2020.12.02.002

Kamoli, A., Hamid, R. A., & Mahmud, S. H. B. (2022). Under-reporting of occupational accidents in the Nigerian construction industry. In Sustainability management strategies and impact in developing countries (pp. 253-264). Emerald Publishing Limited. https://doi.org/10.1108/978-1-80262-449-620221017

Kheni, N. A., Dainty, A. R., Gibb, A. J. C. M., & Economics. (2008). Health and safety management in developing countries: a study of construction SMEs in Ghana. 26(11), 1159-1169. https://doi.org/10.1080/01446190802459916

Kori-Siakpere, U., Gokeme, O., Omale, R. O., Aniah, A. R., Ojukwu, P. M., & Okache, M. O. (2024). The impact of linguistic diversity on intercultural communication in Nigerian organizations: A Review. J Innov Res, 2(2), 25-33. https://doi.org/10.54536/jir.v2i2.3174

Landis, J. R., & Koch, G. G. (1977). The measurement of observer agreement for categorical data. Biometrics, 33(1), 159-174.

Loosemore, M., Denny-Smith, G., Barraket, J., Keast, R., Chamberlain, D., Muir, K., ... & Osborne, J. (2021). Optimising social procurement policy outcomes through cross-sector collaboration in the Australian construction industry. Engineering, Construction and Architectural Management, 28(7), 1908-1928. https://doi.org/10.1108/ECAM-03-2020-0165

Machfudiyanto, R. A., Latief, Y., Sagita, L., & Suraji, A. (2020). Identification of institutional safety factors affecting safety culture in construction sector in Indonesia. Paper presented at the IOP Conference Series: Earth and Environmental Science. https://doi.org/10.1088/1755-1315/426/1/012031

Manu, P., Emuze, F., Saurin, T. A., & Hadikusumo, B. H. (2019). An introduction to construction health and safety in developing countries. In Construction Health and Safety in Developing Countries (pp. 1-11):

ISBN: 978-978-8567-02-8

Routledge. https://doi.org/10.1201/9780429455377-1

Muñoz-La Rivera, F., Mora-Serrano, J., & Oñate, E. (2021). Factors Influencing Safety on Construction Projects (fSCPs): Types and Categories. 18(20), 10884. https://doi.org/10.3390/ijerph182010884

Musonda, I., Lusenga, E., & Okoro, C. (2021). Rating and characterization of an organization's safety culture to improve performance. International journal of construction management, 21(2), 181-193. https://doi.org/10.1080/15623599.2018.1512030

National Bureau of Statistics. (2023). Nigeria GDP report. NBS.

Parker, D., Lawrie, M., & Hudson, P. J. S. s. (2006). A framework for understanding the development of organisational safety culture. 44(6), 551-562. https://doi.org/10.1016/j.ssci.2005.10.004

Rantsatsi, N., Musonda, I., & Agumba, J. (2021). Factors that determine construction health and safety agent collaboration on construction projects: a Delphi study. Acta Structilia, 28(2), 53-77. https://doi.org/10.18820/24150487/as28i2.3

Rantsatsi, N., Musonda, I., and Haupt, T. (2023). Safety culture maturity in South African construction: A longitudinal study. Journal of Construction Engineering and Management, 149(5), 04023025. https://doi.org/10.1061/JCEMD4.COENG-13147

Razali, N. M. and Wah, Y. B. (2011). Power comparisons of Shapiro-Wilk, Kolmogorov-Smirnov, Lilliefors and Anderson-Darling tests. Journal of Statistical Modeling and Analytics, 2(1), 21–33.

Schein, E. H. (2010). Organizational culture and leadership (4th ed.). Jossey-Bass. https://doi.org/10.1002/9780470640579

Siegel, S. and Castellan, N. J. (1988). Nonparametric statistics for the behavioral sciences (2nd ed.). McGraw-Hill.

van Nunen, K., Reniers, G., & Ponnet, K. (2022). Measuring Safety Culture Using an Integrative Approach: The Development of a Comprehensive Conceptual Framework and an Applied Safety Culture Assessment Instrument. International Journal of Environmental Research and Public Health, 19(20), 13602. https://doi.org/10.3390/ijerph192013602

Von Der Gracht, H. A. (2012). Consensus measurement in Delphi studies: review and implications for future quality assurance. Technological forecasting and social change, 79(8), 1525-1536. https://doi.org/10.1016/j.techfore.2012.04.013

Yu, W. D., Wang, K. C., & Wu, H. T. (2022). Empirical comparison of learning effectiveness of immersive virtual reality–based safety training for novice and experienced construction workers. Journal of Construction Engineering and Management, 148(9), 04022078. https://doi.org/10.1061/(ASCE)CO.1943-7862.0002337

Zohar, D. (2010). Thirty years of safety climate research: Reflections and future directions. Accident Analysis & Prevention, 42(6), 1517–1522. https://doi.org/10.1016/j.aap.2009.12.019

ISBN: 978-978-8567-02-8

5TH Faculty of Engineering Conference on Engineering Innovation and Economic Policies: Driving Sustainable Industrial Growth in Nigeria

Faculty of Engineering, Bayero University, Kano.

069-Sensorless Control of Brushless DC Motors: A Review, Comparative Study and Future Research Trends

Musa Baba Lawan[1], S.S Adamu[2], Isiyaku Abubakar[2], Abdulrazak Sabo[3], Abubakar Sadiq Umar[2], Ibrahim Tijjani[1], Zainab Musa Gwoma[1],

[1]Department of Electrical and Electronics Engineering, University of Maiduguri, Maiduguri, PMB 1069, Nigeria,
[2]Department of Electrical Engineering, Bayero University Kano, Kano, Nigeria
[3]Department of Electrical Engineering, Abubakar Tafawa Balewa University, Bauchi, Bauchi, Nigeria

*Corresponding author email: Babalawan24@unimaid.edu.ng

Abstract: Brushless DC (BLDC) motors have become increasingly prevalent in industrial, automotive, and consumer applications due to their impressive efficiency, compact design, high torque-to-inertia ratio, and power density. Traditional BLDC motor drives typically depend on rotor position sensors, such as Hall-effect sensors, to gather essential rotor information for commutation. However, the inclusion of these sensors raises costs, complicates wiring, increases size, and may negatively impact reliability and efficiency. Sensorless control techniques eliminate the need for physical sensors by estimating rotor position from the motor's terminal voltages and currents. This review comprehensively categorizes the state-of-the-art sensorless control methods for BLDC motors based on Back-EMF methods and Observer-based methods, examining their underlying principles, advantages, limitations, and appropriate application domains. A comparative analysis is provided to assist researchers in selecting the most suitable technique based on performance requirements, cost considerations, and operational speed ranges. Finally, the paper addresses current challenges and outlines future research trends within this field.

1. INTRODUCTION

Research into solid-state commutation for DC motors dates back over fifty years to experiments by T.G. Wilson and P.H. Trickey, which inspired the development of Brushless DC (BLDC) motors based on Lorentz's force law (Kim et al., 2013). BLDC motors are favored across applications ranging from household appliances and electric vehicles to aerospace, power tools, and medical devices, thanks to their exceptional efficiency, compact size, and high torque-to-inertia ratio (Yadav & Y, 2019). With anticipated growth in electric vehicle demand over the next decade, BLDC motors are poised to play a crucial role, with the global market predicted to grow to $15.2 billion by 2025, up from $9.6 billion in 2020 (Mohanraj et al., 2022a). BLDC motors are designed to provide excellent responsiveness in both static and dynamic applications, necessitating careful design for optimal magnetic linkage in tasks such as lifting, cutting, and bracing. Compared with other motor types, BLDC motors tend to exhibit greater efficiency, a higher torque-to-weight ratio, and lower noise levels (Kumar, 2019). BLDC motors are inherently controlled electronically; this electronic commutation allows for more dependable and quieter operation. BLDC motors can run at high speeds because they do not have brushes. While brushed DC motors are only 75 to 80 percent efficient, BLDC motors are usually 85 to 90 percent efficient.

BLDC motors come in a variety of forms, from small power ranges to fractional horsepower, integral horsepower, and large power ranges. In managing torque and speed, rotor position is traditionally obtained through Hall effect sensors, optical encoders, and resolvers. The dependence on external sensors and interfacing devices not only consumes additional power but also adds to maintenance costs. Consequently, there is a growing trend to eliminate these sensors to enhance reliability and efficiency (Konda Naresh, 2025). The importance of sensorless drives is increasing as they maintain accuracy while eliminating the need for sensors (Liangtao Zheng, 2025). Significant research has focused on developing sensorless drives that can match the dynamic performance of those using sensors over recent decades. Intelligent controllers can estimate rotor position from terminal voltages and currents (Baba et al., 2023). The primary benefit of sensorless control of BLDC motors is the reduction of costs by omitting the sensing components, while the main drawbacks include the necessity for advanced control algorithms and more complex electronic designs.

2. WORKING PRINCIPLE OF BLDC MOTORS

An electronic controller progressively energizes the stator windings of a Brushless DC (BLDC) motor to create a revolving magnetic field. The interaction between this field and its permanent magnets causes the rotor to rotate. Hall effect sensors and other position

ISBN: 978-978-8567-02-8

sensors that measure the rotor's position provide feedback to the controller. In order to keep the motor rotating, the controller then swaps the relevant stator coils. The BLDC motor's operating modes consists of the following: Electronic Communication, Torque Generation, Back Electromotive Force (BEMF), Sensor-Based Control, and Sensorless Control.

2.1 Types of BLDC Motor

The motor is built with various configurations, including inner and outer rotors. The rotor permanent magnet is embedded at the outer surface, and the stator windings are kept stationary inside. The motor's output torque and power density are increased by the outer rotor BLDC (Jo et al., 2022). The outer rotor BLDC motor is designed to minimize the air gap radius between stator and rotor , thereby increasing the torque capability per unit length and current (Lee et al., 2016). Figure 1 illustrates the categorization of BLDC motor types.

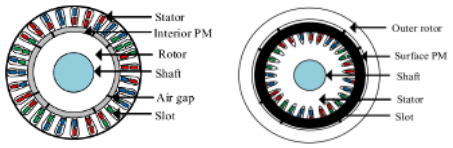


Figure 1: (a) Inner rotor and (b) Outer rotor

2.2 Constructional Features of BLDC Motor

The constructional features of a BLDC motor are critical in determining its efficiency, performance, and application suitability (Shuaibu et al., 2024). The stator, rotor, permanent magnets, winding configurations, and electronic control systems are the main components of BLDC motors that are examined in this work. When energized, the stator windings are arranged in a particular way to produce a revolving magnetic field (Yaz, Mustafa, 2021). In BLDC motors, trapezoidal and sinusoidal winding configurations are the two primary varieties. The stator, rotor, and electronic controller are the three main components of a BLDC motor. Surface-Mounted Permanent Magnet (SMPM) and Interior Permanent Magnet (IPM) are two types of rotor designs. The stator winding can be configured in either a star (Y) or delta (Δ) arrangement.

2.3 Modelling of BLDC Motor

The mathematical model of a BLDC Motor is similar to that of a conventional DC Motor. The equivalent circuit of the BLDC motor drive system, for phase A, is shown in Figure 2.

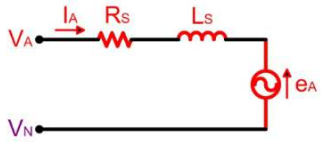


Figure 2: Equivalent circuit of the BLDC motor for phase A

The differential equation of the BLDC drive describing the response of electrical quantities can be derived as:

$$V = iR + L\frac{d_i}{d_t} + E \quad (1)$$

where, V is DC voltage in Volts, L is the inductance of windings in Henry, R is the resistance of the windings in Ohms, $E = k_b * \omega$ is BEMF of the motor, and ω is the speed in rad/sec. The mechanical dynamics include a simple mechanical equation to model the rotor speed ω (with Torque T_e and T_{Load}), given in equation (2)

$$J\frac{d\omega}{dt} + B\omega = (T_e - T_{Load}) \quad (2)$$

where T_e is the electromagnetic torque in Nm derived from the currents and BEMF, J is the rotor inertia in Kgm^2, and B is the damping in Kg/m/s. BEMF of each phase has a phase difference of 120 (electrical) degrees, and BEMF and rotor position can be related as shown in equations (3) -(5);

$$e_a = K_w \omega f(\theta_e) \quad (3)$$

$$e_b = K_w \omega f\left(\theta_e - \frac{2\pi}{3}\right) \quad (4)$$

$$e_c = K_w \omega f\left(\theta_e + \frac{2\pi}{3}\right) \quad (5)$$

where, K_w is the BEMF constant of one phase (v/rad-I), ω is the rotor speed, $f(\theta e)$represents the waveform function of the BEMF. Rotor angle electrical θ_e and rotor angle mechanical θ_m are related by equation (6);

$$\theta_e = \frac{p}{2}\theta_m \quad (6)$$

where p is the number of poles. The total electromagnetic torque Te in Nm can be expressed by equation (7);

$$T_e = \frac{p}{\omega} = \left(\frac{e_a i_a + e_b i_b + e_c i_c}{\omega}\right) \quad (7)$$

3. CLASSIFICATION OF SENSORLESS CONTROL TECHNIQUE OF BLDC MOTOR

Because of their electronic control techniques, BLDC motors are valued for their dependability and efficiency (Pamuji et al., 2023). Figure 3 illustrates the classification of sensorless control techniques of BLDC motor, Figure 4 the types of BLDC motor, while Figure 5 depicts the control workflow. The most popular sensorless control strategies are BEMF-based approaches.

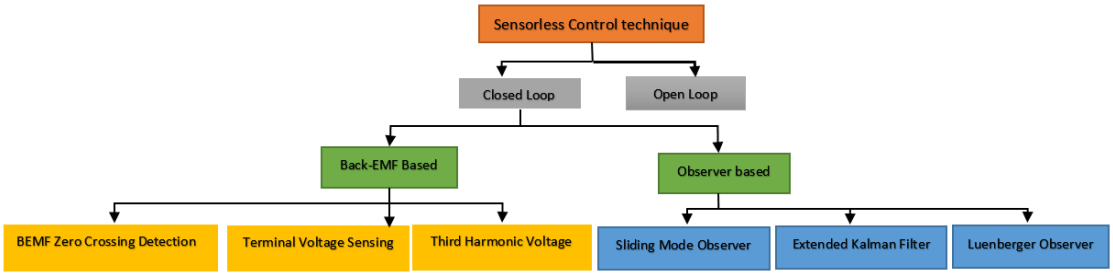


Figure 3: Classification of Sensorless Control Techniques of BLDC Motor

ISBN: 978-978-8567-02-8

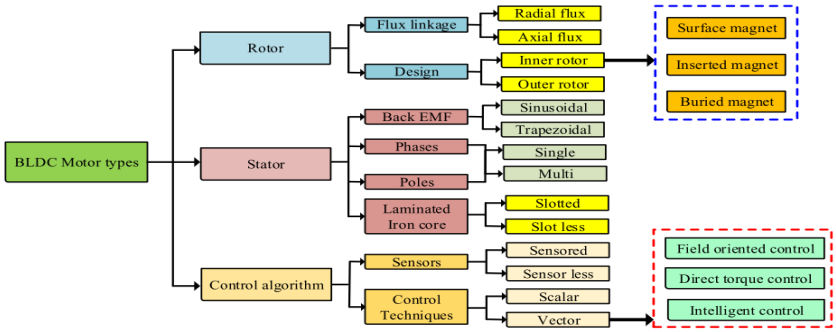


Figure 4: Types of BLDC Motor (Mohanraj et al., 2022b)

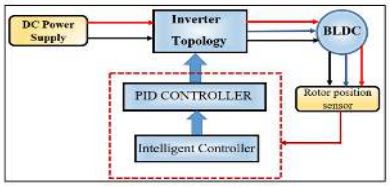


Figure 5: Block Workflow of BLDC Motor Control

3.1 BEMF Based-Method

Modern techniques for sensorless BLDC motor control estimate rotor position and speed using the motor's intrinsic voltage (BEMF) produced by rotation, doing away with physical sensors for greater dependability, lower cost, and smaller size.

3.1.1 Zero-Crossing Detection Based

One of the most straightforward BEMF detection techniques is the Zero Crossing Detection (ZCD) strategy, which relies on identifying the moment the BEMF in the unexcited phase crosses zero. A commutation event should take place when the BEMF passes zero, as shown in Figure 6. Phase current and BEMF alignment are necessary for a BLDC motor to operate normally and produce a steady torque. The zero-crossing point (ZCP) of the BEMF and a 30° phase shift, using a six-step commutation scheme via a three-phase inverter, can be used to estimate the current commutation point shown in Figure 4. Each phase has a 120 ° electrical interval. As a result, the third phase is always floating and only two phases conduct current. The inverter should be commutated every 60° to achieve maximum torque by detecting zero crossing of the BEMF on the motor's floating coil so that the current is in phase with the back-EMF (Gamazo-real et al., 2010).

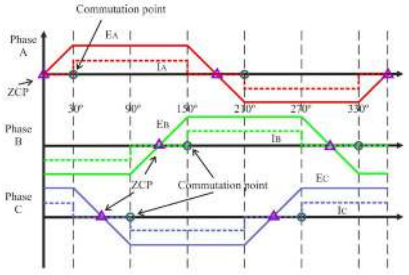


Figure 6: ZCP of the back-EMF and phase current commutation points

The zero-crossing method's simplicity often comes at the expense of noise sensitivity in zero-crossing detection and decreased performance over large speed ranges (M. et al., 2019). Another limitation is that since back-EMF is proportional to rotor speed and zero at standstill, the noisy terminal voltage cannot be used to produce a switching pattern at low speeds.

- *Recent Advancements in BEMF Zero Crossing Detection.*

In order to mitigate the control issues with BEMF ZCD, intelligent filtering techniques were adopted. (Milić & Vukosavić, 2024) introduced a digital filter that adjusts based on rotor speed, reducing phase delay across operating ranges. Machine Learning noise reduction based on Neural Network (NN) (M. A. Ali et al., 2024). Another method based on a rounding function was introduced to minimize mathematical and computational complexity and improve sensorless start-up challenges in real-time (Gujja et al., 2025). (Hemalatha et al., 2024) introduced an effective method using the Adaptive Neuro Fuzzy Interference System (ANFIS) and the Particle Swarm Optimization (PSO) to detect the BEMF ZCP from the terminal voltage.

3.1.2 BEMF Terminal Voltage Based

Using this method, the BEMF is indirectly calculated by monitoring the motor's terminal voltages. It works well and is suitable for high-speed applications, but it may require sophisticated hardware and signal processing. This method integrates the back-EMF of the silent period, or the unexcited phase, to find the commutation instant (Attar et al., 2021). When the back-EMF of the silent phase crosses zero, the integration begins. The phase current is commutated when the integrated value hits a predetermined threshold value, which is equivalent to a commutation point. Switching noise has less of an impact on the integration method. Although it automatically adapts to variations in speed, the integration's offset voltage issues and error accumulation make low-speed operation subpar.

- *Recent Advancements in BEMF Terminal Voltage Method:*

A unique commutation correction technique was proposed that improved commutation accuracy and efficiently suppressed torque ripple in BLDC, coupled with better commutation precision, was proposed by (Sa

ISBN: 978-978-8567-02-8

et al., 2025). An ANN was used to estimate the rotor position for smooth sensorless control (Gamazo-Real, Martínez-Martínez, et al., 2022). To lessen the effect of voltage spikes, a DC detection and commutation compensation at low speed was adopted (Huang et al., 2021). This method offered an alternative to the conventional ZCD-based PWM methodology by using pulse amplitude modulation (PAM) to improve speed performance. (Zhao et al., 2021) considerably enhanced performance by creating a terminal voltage-based phase delay-free commutation method. This method generates both the commutation and the ZCP signals.

3.1.3 Third Harmonic Voltage Integration

The Third Harmonic BEMF voltage control is an advanced sensorless technique for BLDC motors that exploits the inherent harmonic content of the phase voltages to precisely determine the rotor position, eliminating the need for Hall-effect sensors. This method extracts and analyzes the BEMF's third harmonic component. The voltage differential between points S and N can be used to calculate the third harmonic back-EMF (Zhu & Wu, 2024). A fundamental frequency component and several odd harmonics (mostly the third, fifth, seventh, etc.) are present in the individual phase voltages of a typical three-phase, Y-connected BLDC motor with a trapezoidal BEMF waveform. The characteristics of a symmetrical three-phase system serve as the foundation for the fundamental idea. All three phases' immediate fundamental frequency components add up to zero. Likewise, all "poly-phase" harmonics, such as the fifth and seventh, add up to zero. Nevertheless, when the three-phase voltages are added together, the third harmonic and its multiples (9th, 15th, etc.), which are zero-sequence components, do not cancel out. The third harmonic signal is typically extracted in one of two ways: accessing the motor neutral point (VSN) and or using the DC bus midpoint (VSH or VNH).

The technique offers several benefits, including improved noise immunity and operation over a wide speed range, which results in dependable rotor position estimation. However, it has poor start-up performance, signal distortion due to saturation requires additional filtering and signal processing, and is highly sensitive to disturbances (Makieła, 2011). Figure 7 shows the Commutation signal using the third harmonic.

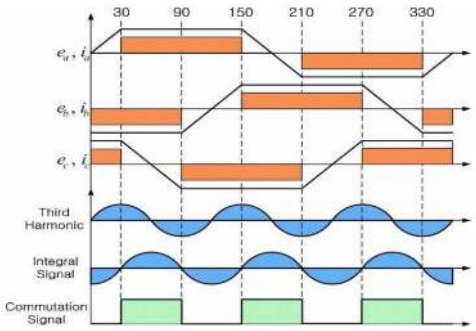


Figure 7: Commutation signal using third harmonic (Sahoo & Pahadsingh2, 2019)

• *Recent Advancements in Third Harmonic Voltage Integration*

Recent advancements focused on reducing the impact of electrical noise, adjusting for motor parameter asymmetries, and increasing precision and performance over a broad speed range (particularly at high and extremely low speeds). To regulate a high-speed BLDC motor, a sensorless BEMF based on a virtual third-harmonic control approach was implemented by (Yang et al., 2021). A strategy design using PWM for a selective harmonic elimination (SHE) to reduce losses of the trapezoidal BEMF signal was elaborated in (Santra et al., 2022) using a predefined lookup table. (Kroičs, K., and Būmanis, 2024) analyzes improved sine wave communication with third harmonic components to minimize sound noise and torque ripple using a digital adaptive PID-Fuzzy controller.

3.2 Observer-Based Method

Observer-based method uses voltage/current feedback and mathematical models to determine rotor position and speed instead of physical sensors like Hall effect sensors, mostly by observing the motor's BEMF or flux. Integration with control strategies like FOC and DTC enables the rotor angle needed for Clarke and Park conversions to be supplied by observers, the motor can be operated as a DC system for optimal torque and efficiency, and it also calculates the stator flux and instantaneous torque, enabling quick torque response without requiring a sophisticated PWM modulator.

3.2.1 Sliding Mode Observer

The Sliding Mode Observer (SMO) is a robust estimator that uses sliding mode control theory to estimate the rotor position. It offers high accuracy and robustness to parameter variations but may suffer from chattering and requires careful tuning (Vadim Utkim, 1999). To estimate the back-EMF components that carry rotor position and speed information, the mathematical model of an SMO for a BLDC motor is constructed from the motor's state-space representation, which is usually formulated in the stationary reference frame. The equations are;

$$L_s \frac{d\bar{\imath}_\alpha}{dt} = -R_s \tilde{\imath}_\alpha + u_\alpha - V_\alpha L_s \frac{d\bar{\imath}_\beta}{dt} \quad (8)$$

$$L_s \frac{d\bar{\imath}_\alpha}{dt} = -R_s \tilde{\imath}_\beta + u_\beta - V_\beta \quad (9)$$

Where the estimated current equals the measured current $\tilde{\imath} - i = 0$.

$$V_{\alpha\beta} = ksgn\left(\tilde{\imath}_{\alpha\beta} - i_{\alpha\beta}\right) \quad (10)$$

Where k is the observer gain, the *sgn* function is used to reduce chattering. A low-pass filter will be used to extract the BEMF $\tilde{e}_\alpha \tilde{e}_\beta$ (Arif et al., 2024). The rotor position θ as;

$$\theta = -artan\left(\frac{\tilde{e}_\alpha}{\tilde{e}_\beta}\right) \quad (11)$$

- *Recent Advancements in SMO*

Recent advancements focus on speed, torque control, and reduced energy efficiency. (Hasni et al., 2025) proposed a super-twist sliding mode control strategy (STSMC)-based controller with its settings improved through the application of a genetic algorithm

ISBN: 978-978-8567-02-8

(GA). To reduce chattering, achieve faster response, and improve tracking accuracy, (Joshi et al., 2025) proposed a hybrid controller with adaptive SMO. (Chang et al., 2023) demonstrate a 30% speed recovery following load changes and focus on full feedback disturbance rejection for portable motor drives. (Liu et al., 2019) suggests an enhanced line back-EMF SMO that does not require phase adjustment or low-pass filters by employing a smooth hyperbolic tangent function.

3.2.2 Extended Kalman Filter

The Extended Kalman Filter (EKF) is a recursive estimator that uses a nonlinear motor model to estimate the rotor position and speed. It can handle noise and uncertainties effectively, making it suitable for high-performance applications. It goes through two stages, prediction and corrections. However, it requires significant computational resources.

The state vector is defined as;

$$x = \left[i_\alpha, i_\beta, \omega, \theta\right]^T \quad (12)$$

And the continuous-time nonlinear model is given by;

$$\dot{x}(t) = f(x(t), u(t)) + \omega(t)$$
$$y(t) = h(x(t)) + v(t) \quad (13)$$

The EKF computes the Jacobian matrix (F) (system matrix) and (H) (measurement matrix) at each estimating interval to deal with the nonlinearity as shown in equation (14);

$$F = \frac{\partial f}{\partial x}|\hat{x}_{k-1}\ ,\ H = \frac{\partial f}{\partial x}|\hat{x}_k \quad (14)$$

- *Recent Advancements in EKF*

Most recently, (Hadjer & Aissa, 2025) focused on the EKF-Fuzzy Logic Control hybrid technique to enhance robustness against non-linearity and speed control performance. (İnan et al., 2023) employed a machine learning-based neural network to control the speed of the motor. Subsequently, (Inan, 2024) adopted an improved EKF using Model Predictive Control to prevent torque ripple.

3.2.3 Leunberger Observer

The Luenberger observer uses a linear motor model to estimate rotor position and speed. It is simpler and less computationally intensive than the EKF but may not perform as well under nonlinear conditions.

The mathematical model of the Leunberger Observer is typically designed in the $\alpha\beta$ stationary reference frame. The state model equation is given in (15);

$$\frac{dx}{dt} = Ax + Bu, y = cx \quad (15)$$

$$x = \left[i_\alpha, i_\beta, e_\alpha, e_\beta\right]^T$$

The observer equation

$$\frac{d\hat{x}}{dt} = A\hat{x} + Bu + L(y - c\hat{x}) \quad (16)$$

where L is the observer gain

- *Recent Advancements in Leunberger Observer*

The incorporation of Phase-Locked Loops (PLL) for accurate angle tracking and discretization accuracy for high-speed operation are the two most recent developments. The motor's BEMF was estimated by a reduced-order Luenberger observer (Liangtao Zheng, 2025). (Coronado-Andrade et al., 2023) employed alongside a high-order sliding mode (HOSM) differentiator to estimate the angular velocity of a BLDC motor.

4. DISCUSSION

Table I compares the various techniques, highlighting the advantages and limitations of each sensorless control technique of the BLDC motor. A comparative study and analysis using metric such as noise immunity, computational complexity, cost etc is presented in Table II.

TABLE I: Summary of Sensorless Control Techniques of BLDC Motor

Technique	Findings	Limitations
Zero Crossing Detection	Robustness, simplicity, accuracy	Poor performance at low speed, phase shifting
BEMF Terminal Voltage	Suitable for high-speed applications	require sophisticated hardware and signal processing
Third Harmonic Voltage Integration	Reduced sampling delay in high-speed region	Filtering delay, poor start-up performance, and sensitive to disturbance
Sliding Mode Observer	high accuracy, robustness, fast dynamic response	Suffers from chattering and requires careful tuning, control loop instability
Extended Kalman Filter	handles noise and uncertainties effectively, suitable for high-performance applications.	requires significant computational resources and, difficulty in the design and tuning procedure.
Leunberger Observer	simpler and less computationally intensive	Underperform under stringent nonlinear conditions

This thorough comparison offers a methodical way to select sensorless BLDC control strategies based on specific application needs, available resources, and performance goals. The table provides engineers and researchers with useful guidance by synthesizing data from both in-depth reviews. The integration of advanced controllers with a hybrid model has significantly improved performance and functionality, driving the next generation of sensorless control approaches for BLDC motors. Table III presents recent trends in sensorless control and the hybrid approaches for each BEMF-based and observer-based method, along with typical applications.

ISBN: 978-978-8567-02-8

TABLE II: Comparative Study and Analysis of Sensorless Control Technique of BLDC Using Specific Metrics

Metric	Zero Crossing Detection	BEMF Terminal Voltage Integration	Third harmonic Voltage Integration	Sliding Mode Observer	Leunberger Observer	Extended Kalman Filter
Startup capability	Poor (need special startup like open loop ramp)	Good	Excellent with current-assisted	Good (Best inherent with High Frequency injection)	Good with initial alignment	Excellent with a good filter
Hardware simplicity	Comparator-Based	Comparator-Based	Comparator-Based	Need DSP and MCUs	Need DSP and MCUs	Need DSP and MCUs
Speed range	Medium-High	Medium-High	Medium-High	High	High	High
Computational load	Low- simple Algorithm	Medium- requires some signal processing.	High- involves advanced processing	Low-medium- Moderate complexity	Low- simple observer design	High- computationally intensive
Accuracy	Moderate- sufficient and reliable	Moderate- good for speed estimation;	Moderate- generally reliable	High- good robustness to disturbances	High- accurate under linear conditions	High-excellent estimation
Cost and Complexity	Lowest	Medium	Highest	Low-medium	Low	Medium-high
Noise	Poor- susceptible to electrical noise and switching transients	Medium, have some immunity	Good- offers better noise rejection	Good, offers better noise rejection	Moderately immune to noise	Excellent noise immunity, can

TABLE III: Recent Trend in Sensorless Control and Hybrid Approach of Each BEMF-Based and Observer-Based Approach

	Zero Crossing Detection	BEMF Terminal Voltage Integration	Third harmonic Voltage Integration	Sliding Mode Observer	Leunberger Observer	Extended Kalman Filter
Recent Trend	AI-enhanced Filtering (Milić & Vukosavić, 2024), rounding function-based BEMF(A. Ali et al., 2024)(Gujja et al., 2025)	Multi-mode hybrid control, PWM methodology by using pulse amplitude modulation (PAM) (Huang et al., 2021)	Deep learning recognition, Digital Adaptive PID-Fuzzy Controller (Kroičs, K., and Būmanis, 2024), PWM for a selective harmonic elimination (SHE) (Santra et al., 2022)(Yang et al., 2021)	Higher order SMO, super-twist sliding mode control strategy (STSMC)-based controller (Hasni et al., 2025), smooth hyperbolic tangent function (Liu et al., 2019)	Optimal gain selector, reduced-order Luenberger observer (Liangtao Zheng, 2025), high-order sliding mode (Coronado-Andrade et al., 2023)	Adaptive EKF, System Identification-ANN, and EKF (Gundogdu, 2020)
Hybrid Approach	Zero Crossing Detection integrated with ANN (Gamazo-Real, Carlos, et al., 2022), Adaptive Neuro Fuzzy Inference System (ANFIS) with PSO(Hemalatha et al., 2024)	BEMF Terminal voltage integrated with Artificial Neural Network (M. A. Ali et al., 2024), Pulse Amplitude Modulation	Virtual third harmonic fundamental, Third harmonic integrated with predefined lookup table (Kroičs, K., and Būmanis, 2024), Kalman Filter, combined with Third harmonics	SMO with Phase Lock Loop, Adaptive SMO, Enhanced line BEMF SMO, hybrid controller with adaptive SMO (Joshi et al., 2025)	Genetic Algorithm Tuning, Leunberger integrated with the Phase Lock Loop (Zheng & Zuo, 2025)	EKF integrated with Fuzzy Logic(Hadjer & Aissa, 2025) , EKF with MPC (Inan, 2025)(Kalamian et al., 2025)
Typical Applications	Consumer appliances like Fans, Pumps	Power tools, e-bikes, HVAC fans	Automotive Pumps, HVAC, High-speed fans	Robotics, Industrial drives, Unmanned Aerial Vehicles (UAVS)	Drones, Industrial Automation platforms	Aerospace. Electric Vehicles, Robotics

ISBN: 978-978-8567-02-8

5. CONCLUSION

Sensorless BLDC control has undergone substantial development, with each technique finding use in particular fields. While terminal voltage approaches strike a balance between complexity and performance, BEMF ZCD is still widely used in cost-sensitive applications. Although they are more computationally expensive, third harmonic voltage integration techniques provide better low-speed performance. Observer-based sensorless control has undergone substantial evolution. EKF offers the highest accuracy at the expense of computational complexity, Luenberger delivers a good balance for moderate-performance applications, and SMO excels in robustness and simplicity. Current trends indicate a convergence towards hardware implementations, integration with AI/ML techniques for adaptation, and hybrid approaches that combine the strengths of various observers. Future applications will choose between cost sensitivity (BEMF ZCD), low-speed performance (third Harmonic), robustness (SMO), simplicity (Luenberger), or accuracy (EKF), with adaptive and learning-based variants becoming increasingly popular across all approaches.

ACKNOWLEDGMENT

The authors would like to thank University of Maiduguri and Bayero University Kano for providing financial support and guidance respectively.

REFERENCES

Ali, A., Desa, M. K. M., Ai Ooi, C., Al-Gailani, S. A., Hafeez, M., Abdullah, M. N., & Zaid, M. (2024). Sensorless microcontroller-based zero-crossing detection system for AC signals using a rounding function. *Ain Shams Engineering Journal*, *15*(2), 102375. https://doi.org/10.1016/j.asej.2023.102375

Ali, M. A., R, S. M., & P Ramakrishna, D. S. (2024). Sensorless Speed Control of Brushless DC Motor Using Artificial Neural Network Predicted Back EMF. *2024 IEEE International Conference on Power Electronics, Drives and Energy Systems (PEDES)*, 1–7. https://doi.org/10.1109/PEDES61459.2024.10961065

Arif, A., Muslim, M., & Yudaingtyas, E. (2024). Sensorless Field-Oriented Control (FOC) using Sliding Mode Observer for BLDC Motor. *Kinetik: Game Technology, Information System, Computer Network, Computing, Electronics, and Control*. https://doi.org/10.22219/kinetik.v9i2.1937

Attar, A., Bouchnaif, J., & Grari, K. (2021). Control of Brushless DC motors using sensorless Back-EMF integration method. *Materials Today: Proceedings*, *45*, 7438–7443. https://doi.org/https://doi.org/10.1016/j.matpr.2021.01.861

Baba, M., Tijjani, I., Mustapha, M., & Aliyu, M. (2023). Sensorless Position Control and Speed Estimation Techniques of Permanent Magnet Synchronous Motors. *Jurnal Pengabdian Dan Pemberdayaan Masyarakat Indonesia*, *3*(1), 1–9.

Chang, P. I.-T., Lin, X.-Y., Chen, Y.-K., & Chang, P. I. (2023). Sensorless BLDC Motor Sliding Mode Control for Disturbance Rejection on Hand Held Motor Drive. *Research Square*, 1–21. https://doi.org/10.21203/rs.3.rs-3705725/v1.

Coronado-Andrade, Axel, Guerra, A. de la, & Alvarez-Icaza, L. (2023). Load Torque Observer for BLDC Motors Based on a HOSM Differentiator. *Machines*, *11*(12). https://doi.org/10.3390/machines11121065.

Gamazo-Real, Carlos, J., Martínez-Martínez, V., & Gomez-Gil., and J. (2022). ANN-Based Position and Speed Sensorless Estimation for BLDC Motors. *Measurement: Journal of the International Measurement Confederation*, 188. https://doi.org/10.1016/j.measurement.2021.110602.

Gamazo-Real, J. C., Martínez-Martínez, V., & Gomez-Gil, J. (2022). ANN-based position and speed sensorless estimation for BLDC motors. *Measurement: Journal of the International Measurement Confederation*, *188*(October 2021), 110602. https://doi.org/10.1016/j.measurement.2021.110602

Gamazo-real, J. C., Vázquez-sánchez, E., & Gómez-gil, J. (2010). *Position and Speed Control of Brushless DC Motors Using Sensorless Techniques and Application Trends*. 6901–6947. https://doi.org/10.3390/s100706901

Gujja, M. M., Ishak, D., Hamidi, M. N., Salem, M., Abdullah, M. N., & Alluhaybi, K. (2025). *Rounding function-based zero crossing detection for a sensorless BLDC motor control*. *16*(1), 106–116. https://doi.org/10.11591/ijpeds.v16.i1.pp106-116

Gundogdu, A. (2020). *Comparison of SI-ANN and Extended Kalman Filter-Based Sensorless Speed Controls of a DC Motor*.

Hadjer, A., & Aissa, A. (2025). *Extended Kalman Filter extimator and Mandani fuzy logic controller for sensorless DC motor speed control*. 11–19.

Hasni, A., Fadil, H., Abdellah, L., el Asri, Y., El Ancary, M., & Mouyane, M. (2025). Cruise Control of BLDC Motors Using GA-Optimized Super Twisted Sliding Mode Control. *E3S Web of Conferences*, *680*, 42. https://doi.org/10.1051/e3sconf/202568000042

Hemalatha, N., Venkatesan, S., Kannan, R., Kannan, S., Bhuvanesh, A., & Kamaraja, A. S. (2024). Sensorless speed and position control of permanent magnet BLDC motor using particle swarm optimization and ANFIS. *Measurement:*

ISBN: 978-978-8567-02-8

Sensors, *31*(June 2023), 100960. https://doi.org/10.1016/j.measen.2023.100960

Huang, C., Lon Wu, C. J., & Yang., S. C. (2021). Full-Region Sensorless BLDC Drive for Permanent Magnet Motor Using Pulse Amplitude Modulation with DC Current Sensing. *IEEE Transactions on Industrial Electronics*, *68*(11), 11234–44. https://doi.org/10.1109/TIE.2020.3034859.

Inan, R. (2024). An Improved Model Predictive Current Control of BLDC Motor With a Novel Adaptive Extended Kalman Filter–Based Back EMF Estimator and a New Commutation Duration Approach for Electrical Vehicle. *International Journal of Circuit Theory and Applications*. https://doi.org/https://doi.org/10.1002/cta.4407

Inan, R. (2025). An Improved Model Predictive Current Control of BLDC Motor With a Novel Adaptive Extended Kalman Filter–Based Back EMF Estimator and a New Commutation Duration Approach for Electrical Vehicle. *International Journal of Circuit Theory and Applications*, *53*(2), 1135–1150. https://doi.org/10.1002/cta.4407

İnan, R., Aksoy, B., & Salman, O. K. M. (2023). Estimation performance of the novel hybrid estimator based on machine learning and extended Kalman filter proposed for speed-sensorless direct torque control of brushless direct current motor. *Engineering Applications of Artificial Intelligence*, *126*, 107083. https://doi.org/https://doi.org/10.1016/j.engappai.2023.107083

Jo, S. T., Shin, H. S., Lee, Y. G., Lee, J. H., & J.Y.Choi. (2022). Optimal Design of a BLDC Motor Considering Three-Dimensional Structures Using the Response Surface Methodology. *Energies*, *15*(2), 461.

Joshi, D., Deb, D., Giri, A., & Elsisi, M. (2025). Sensorless Active Disturbance Rejection Hybrid Control With Adaptive Sliding Mode Observer for BLDC Motor Drives. *IEEE Transactions on Power Electronics*, *PP*, 1–12. https://doi.org/10.1109/TPEL.2025.3594144

Kalamian, N., Mahmoodi, M., Seraj, N., Koshkouei, M. J., & Faraji-Niri, M. (2025). Controller Design for Sensorless Brushless DC Motors Through a Nonlinear Model Predictive Tracker and Augmented Extended Kalman Filter. *IEEE Power Electronics Magazine*, *12*(3), 48–64. https://doi.org/10.1109/MPEL.2025.3575720

Kim, H. W., Kim, K. T., Jo, Y.-S., & Hur, J. (2013). Optimization Methods of Torque Density for Developing the Neodymium Free SPOKE-Type BLDC Motor. *IEEE Transactions on Magnetics*, *49*(5), 2173–2176. https://doi.org/10.1109/TMAG.2013.2237890

Konda Naresh, S. D. &Swapnajit P. (2025). Sensorless speed control of BLDC motor drive using Volt/Hertz method. *International Journal in Electronics*, 1–26. https://doi.org/doi.org/10.1080/00207217.2025.2484699

Kroičs, K., and Būmanis, A. (2024). BLDC Motor Speed Control with Digital Adaptive PID-Fuzzy Controller and Reduced Harmonic Content. *Energies*, *17*(6), 1311. https://doi.org/doi.org/10.3390/en17061311

Kumar, K. P. (2019). Modelling of a Commercial BLDC Motor and Control Using GA- controller for a BLDC Propulsion Application for Hybrid Electric Vehicle. *International Journal of Psychosocial Rehabilitation*, *23*(4), 1604–1613.

Lee, T., Seo, M., And, Y. K., & Jung, S. (2016). Motor Design and Characteristics Comparison of Outer-Rotor-Type BLDC Motor and BLAC Motor Based on Numerical Analysis. *In IEEE Transactions on Applied Superconductivity*, *26*(4), 1–6. https://doi.org/10.1109/TASC.2016.2548079

Liangtao Zheng, D. Z. (2025). Sensorless control of BLDC motors based on Luenberger observer. *Proceedings International Conference on Physics, Photonics, and Optical Engineering (ICPPOE 2024)*. https://doi.org/https://doi.org/10.1117/12.3059981

Liu, S., Zhijian, Q., & Chen, W. (2019). *Sensorless Control with Sliding Mode Observer for a Brushless DC Motor based on Concave Function*. https://doi.org/10.1109/IMCEC46724.2019.8984058

M., M. P., Yadav, & Y., P. M. G. S. (2019). Position and speed control of brushless dc motors using sensorless techniques and application trends. *Sensors*, *8*(1), 62–69. https://doi.org/10.3390/s100706901

Makieła, D. (2011). Sensorless Control of High-Speed PM BLDC Motor. *IEEE International Symposium on Industrial Electronics*, 722–727.

Milić, A. R., & Vukosavić, S. N. (2024). Sensorless Control of Induction Motor Based on Rotors Slot Harmonics and Digital Adaptive Filters. *IEEE Transactions on Industry Applications*, *60*(3), 3950–3963. https://doi.org/10.1109/TIA.2024.3365086

Mohanraj, D., Aruldavid, R., Verma, R., Sathiyasekar, K., Barnawi, A. B., Chokkalingam, B., & Mihet-Popa, L. (2022a). A Review of BLDC Motor: State of Art, Advanced Control Techniques, and Applications. *IEEE Access*, *10*, 54833–54869. https://doi.org/10.1109/ACCESS.2022.3175011

Mohanraj, D., Aruldavid, R., Verma, R., Sathiyasekar, K., Barnawi, A. B., Chokkalingam, B., & Mihet-Popa, L. (2022b). A Review of BLDC Motor: State of Art, Advanced Control Techniques, and Applications. *IEEE Access*, *10*(January), 54833–54869. https://doi.org/10.1109/ACCESS.2022.3175011

ISBN: 978-978-8567-02-8

Pamuji, Agung, F., Waskito, I. S., & Heri Suryoatmojo, Bambang Sudarmanta, Mohammad Khoirul Effendi, and N. A. (2023). Design and Implementation of 3 Phase Inverter for Brushless DC Motor Using Six-Step Commutation Method with Ripple Suppression. *Przeglad Elektrotechniczny*, *99*(2), 303–309. https://doi.org/10.15199/48.2023.02.64

Sa, X., Wu, H., Zhao, Zhao, G., & Zhenjun. (2025). Torque Ripple Reduction in BLDC Motors Using Phase Current Integration and Enhanced Zero Vector DTC. *Electronics*, *14*(15). https://doi.org/doi.org/10.3390/electronics14152999

Sahoo, P. K., & Pahadsingh2, S. (2019). BLDC motor sensor less control using third harmonic back electromagnetic. *Dogo Rangsang Research Journal UGC Care Group I Journal*, *09*(01), 649–652.

Santra, Bikash, Subhendu, Chatterjee, A., Chatterjee, D., Padmanaban, S., & Bhattacharya., K. (2022). High Efficiency Operation of Brushless DC Motor Drive Using Optimized Harmonic Minimization Based Switching Technique. *IEEE Transactions on Industry*, *58*(2), 2122–33. https://doi.org/10.1109/TIA.2022.3146212

Shuaibu, I., Wei, E. H. T., Ramani Kannan, A., & Samaila, Y. A. (2024). Advancements in Axial Flux Permanent Magnet Machines Utilizing Coreless Technology: A Systematic Review. *Ain Shams Engineering Journal*. https://doi.org/10.1016/j.asej.2024.103091

Vadim Utkim, J. G. J. S. (1999). *SlidingModeControlINELECTROMECHANICALSYSTEM*.

Yadav, M. P. M., & Y, P. G. S. (2019). *Position and Speed Control of Brushless DC Motors using Sensorless Techniques : A Review*. *8*(01), 62–69.

Yang, L., Zhu, Z. Q., Bin, H., Zhang, Z., & Gong, L. (2021). Virtual Third Harmonic Back EMF-Based Sensorless Drive for High-Speed BLDC Motors Considering Machine Parameter Asymmetries. *IEEE Transactions on Industry Applications*, *57*(1), 306–315. https://doi.org/10.1109/TIA.2020.3033821

Yaz, Mustafa, and E. C. (2021). Brushless Direct Current Motor Design and Analysis. *COJ Electronics & Communications*, *2*(2), 1–13. https://doi.org/10.31031/cojec.2020.02.000534

Zhao, D., Wang, X., Xu, L., Xia, L., & Huangfu, and Y. (2021). A New Phase-Delay-Free Commutation Method for BLDC Motors Based on Terminal Voltage. *EEE Transactions on Power Electronics*, *36*(5), 4971–76. https://doi.org/10.1109/TPEL.2020.3039887

Zheng, L., & Zuo, D. (2025). Sensorless control of BLDC motors based on Luenberger observer. *Proc.SPIE*, *13552*, 1355211. https://doi.org/10.1117/12.3059981

Zhu, Z. Q., & Wu, X. M. (2024). Sensorless Control Based on Third Harmonic Back EMF. In *Sensorless Control of Permanent Magnet Synchronous Machine Drives* (pp. 361–404). https://doi.org/10.1002/9781394194384.ch11

ISBN: 978-978-8567-02-8

5TH Faculty of Engineering Conference on Engineering Innovation and Economic Policies: Driving Sustainable Industrial Growth in Nigeria

Faculty of Engineering, Bayero University, Kano.

070-Biodegradability of Phenol, Cresol, and Bisphenol A in Aqueous Solutions by Microorganisms as Primary Growth Substrates

Adamu Abubakar Rasheed

Department of Chemical and Petroleum Engineering, Faculty of Engineering, Bayero University Kano, PMB 3011, Kano, Nigeria (aarasheed.cpe@buk.edu.ng)

Abstract: The pervasive contamination of aquatic environments by synthetic organic pollutants necessitates the development of efficient, sustainable treatment technologies. This study systematically investigated the biodegradability of three phenolic compounds: phenol, p-cresol, and the endocrine-disrupting chemical bisphenol A (BPA), as sole carbon and energy sources for unacclimated soil microbial consortia. Batch bioreactor experiments were conducted, each inoculated with a mixed microbial culture and supplied with a single substrate at an initial concentration of 100 mg/L, using glucose as a positive control. The results revealed a clear hierarchy of biodegradability: glucose was completely mineralized within 48 hours, phenol within 6 days, and p-cresol within 7 days, each exhibiting distinct acclimatization phases indicative of enzymatic adaptation. In stark contrast, BPA demonstrated profound recalcitrance, with no significant reduction in chemical oxygen demand (COD) observed over an extended incubation period of 150 days. The absence of microbial activity towards BPA was corroborated by stable pH and dissolved oxygen profiles, confirming a lack of metabolic oxidation. The rapid degradation of phenol and p-cresol, which are structural analogues of the hypothesized hydrolytic products of BPA, implicates the stability of BPA's central isopropylidene bridge as the primary barrier to biodegradation. This work provides direct experimental evidence that conventional biological treatment processes are fundamentally ineffective for BPA removal and underscores the critical need for bioaugmentation with specialized consortia or hybrid chemical-biological treatment strategies to mitigate the environmental impact of this persistent xenobiotic.

1. INTRODUCTION

The widespread introduction of anthropogenic organic chemicals into the global water cycle represents a significant threat to ecosystem integrity and public health. Among these contaminants, xenobiotics (synthetic compounds foreign to natural biochemical pathways) are of particular concern due to their persistence, mobility, and potential for adverse biological effects (Schwarzenbach et al., 2006). This broad class includes industrial intermediates like polychlorinated biphenyls (PCBs), pharmaceuticals, personal care products, pesticides, and plasticizers such as bisphenol A (BPA) (Richardson & Kimura, 2020). BPA, a high-volume production chemical used in polycarbonate plastics and epoxy resins, is a potent endocrine disruptor of significant concern (Vandenberg et al., 2007). Even naturally occurring compounds like steroid hormones can be considered xenobiotic when their environmental concentrations are dramatically amplified by human activity (Daughton & Ternes, 1999). These substances enter aquatic systems predominantly via wastewater effluent, agricultural runoff, and industrial discharge, creating complex mixtures that challenge conventional treatment and risk contaminating drinking water sources (Luo et al., 2014).

The environmental hazard posed by xenobiotics is twofold: first, their inherent resistance to biodegradation leads to prolonged environmental persistence; second, many exhibit toxic, mutagenic, or endocrine-disrupting properties, with potential for bioaccumulation in aquatic food webs (Gavrilescu et al., 2015). Established physiochemical removal technologies including adsorption onto activated carbon, advanced oxidation processes (AOPs), membrane filtration, and incineration, can be effective but are often burdened by high capital and operational costs, significant energy demands, and the generation of secondary waste streams (Bolong et al., 2009). Critically, methods like adsorption often merely transfer the pollutant from a liquid to a solid phase, requiring subsequent hazardous waste management, rather than achieving destruction (Gogate & Pandit, 2004).

Microbial biodegradation offers a promising, environmentally sustainable alternative. This process leverages the metabolic versatility of microorganisms to transform pollutants into harmless end products like carbon dioxide, water, and biomass, offering the potential

ISBN: 978-978-8567-02-8

for complete mineralization (Rittmann & McCarty, 2001). However, the efficacy of conventional biological wastewater treatment plants for xenobiotic removal is notoriously inconsistent. A key limitation is that many such compounds are not utilized as primary growth substrates but are only fortuitously degraded via co-metabolism when microorganisms are actively metabolizing more readily available carbon sources (Joss et al., 2006). This dependency creates a critical knowledge gap: the fundamental biodegradability of many xenobiotics when they serve as the sole source of carbon and energy, a condition essential for predicting their environmental fate and for designing dedicated, high-rate biological treatment processes.

This study bridges this critical knowledge gap through a controlled, comparative investigation of the biodegradability of three phenolic model compounds: phenol, p-cresol, and bisphenol A (BPA) as sole growth substrates. Phenolic xenobiotics are pervasive in industrial effluents and represent ideal model systems, as the catabolic pathways for simple analogs like phenol and cresols are well-established, providing a clear biochemical benchmark (Arora & Bae, 2014). The specific objective of this work is to quantitatively compare the biodegradability of these structurally related compounds using diverse, unacclimated soil microbial consortia under standardized aerobic conditions.

2. METHODOLOGY

2.1 Chemicals

All chemicals used were of analytical grade or higher. Phenol (≥99% purity), p-cresol (≥97%), glucose (≥99.5%), and bisphenol A (BPA, ≥99%) were sourced from Sigma-Aldrich (Steinheim, Germany). A chemically defined mineral salts medium (MSM) was formulated to provide all essential macro- and micronutrients while excluding extraneous carbon sources. The MSM composition per liter of deionized water was: 1.0 g NH_4Cl (nitrogen source), 0.5 g KH_2PO_4, 0.5 g K_2HPO_4 (phosphate buffer and phosphorus source

2.2 Microbial Inoculum

A mixed microbial consortium was harvested from two distinct soils to assess generality: (i) Craibstone agricultural soil (Aberdeen, Scotland, UK), previously characterized for its rich microbial diversity, which included abundant representatives from the *Proteobacteria, Actinobacteria, Bacteroidetes,* and *Acidobacteria phyla* (Bartram et al., 2014), and (ii) a local garden soil (Aberdeen, UK). Soils were sieved (<2 mm) and stored in airtight plastic containers until usage. The soil was used as the inoculum without prior acclimation to the target substrates.

2.3 Experimental Setup

The research was conducted in laboratory-scale batch bioreactors (glass vessels with a working volume of 1 L). Each bioreactor was inoculated with the mixed microbial culture at a concentration of 1 g/L (as volatile suspended solids). The reactors were supplied with a mineral salts medium providing essential nutrients (N, P, K, trace elements) and were maintained at a controlled temperature (25°C ± 1°C), neutral pH (7.0 ± 0.2), and continuous aeration to ensure aerobic conditions. Each substrate, glucose, phenol, p-cresol, and BPA, was introduced into a separate bioreactor as a single, primary carbon and energy source at an initial concentration of 100 mg/L. An abiotic control (without microorganisms) was also maintained for each substrate to account for any non-biological removal.

2.4 Analytical Methods

Chemical Oxygen Demand (COD): Samples were withdrawn periodically and filtered through 0.45 µm syringe filters (Millipore, Germany) to obtain cell-free supernatants. Soluble COD was measured using Spectroquant COD cell tests (range 50–500 mg/L, Merck, Germany) according to the manufacturer's instructions. Digestion was performed in a Spectroquant TR 620 thermoreactor (Merck, Germany), and absorbance was measured at 445 nm using a NOVA 60 photometer (Merck, Germany). Appropriate dilutions were made with deionized water when necessary.

pH and Dissolved Oxygen (DO): pH was measured using a calibrated Thermo Scientific Orion VersaStar pH meter (USA). Dissolved oxygen concentration and temperature were measured in situ using a Hach HQ40d portable multi-meter equipped with an LDO101 luminescent dissolved oxygen probe (Hach, USA).

3. RESULTS AND DISCUSSION

3.1 Comparative Biodegradability Kinetics

The selection of glucose, phenol, and p-cresol is strategic. Glucose served as a universal positive control to verify microbial metabolic competency under the test conditions. Phenol and p-cresol represent "biologically familiar" aromatic monomers. Structurally, BPA is a diaryl alkane composed of two p-cresol-like phenolic units linked by a stable isopropylidene bridge ($>C(CH_3)_2$). This fully substituted, quaternary carbon bridge is hypothesized to be the primary structural feature conferring recalcitrance by preventing the initial enzymatic attack required to access the degradable phenolic moieties (Kolvenbach et al., 2014). By comparing the microbial fate of BPA to that of its potential hydrolysis product (p-cresol), this study directly tests the hypothesis that molecular inaccessibility, rather than a lack of downstream catabolic capacity, is the principal driver of BPA's environmental persistence.

The microbial degradation profiles, monitored via soluble COD removal, revealed a distinct and unambiguous hierarchy of substrate utilizability under the defined aerobic, batch conditions (Figure 1). This hierarchy provides a direct measure of how readily each compound could be integrated into microbial metabolism as a sole carbon and energy source.

Glucose, a universal and labile carbon source, was rapidly and completely catabolized, with >95% COD removal achieved within 48 hours. This monophasic, exponential decay curve served as a critical positive control, confirming that the experimental conditions were non-limiting and that the soil-derived inocula were metabolically active and capable of robust heterotrophic growth. The lack of a lag phase for glucose is

ISBN: 978-978-8567-02-8

common sugars, in contrast to the inducible systems often required for xenobiotic degradation (Li et al., 2022).

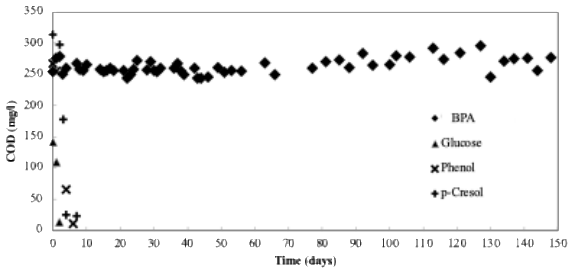


Figure 1. Biodegradation profiles of glucose, phenol, p-cresol, and BPA as sole carbon sources. Substrate concentration is expressed as soluble Chemical Oxygen Demand (COD).

Phenol and p-cresol were also fully mineralized but exhibited classic biphasic kinetics emblematic of many aromatic xenobiotics (Figure 1). Both compounds demonstrated a pronounced lag phase, approximately 3 days for phenol and 4 hours for p-cresol, during which COD concentration remained stable. This latency period, a well-documented phenomenon in microbial ecology, represents the critical acclimatization window required for microbial community restructuring and enzymatic adaptation (Xu et al., 2021). The subsequent rapid, leading to complete removal by day 6 and day 7 respectively, confirms that the soil consortia harbored the genetic potential and regulatory flexibility to fully mineralize simple phenolic monomers when presented as exclusive growth substrates. The slightly longer lag for p-cresol may reflect the additional metabolic step required to handle the methyl substituent or a lower initial abundance of specific p-cresol degraders (Wang et al., 2022).

In stark and unequivocal contrast, bisphenol A (BPA) exhibited profound and persistent recalcitrance. Over an extended incubation period of 150 days, orders of magnitude longer than for the other phenolics, no statistically significant decrease in soluble COD was observed (Figure 1). The concentration profile was a stable horizontal line, remaining at 100 ± 5 mg/L COD. This finding is consistent with broader observations of BPA's persistence in environmental matrices and its poor removal in conventional wastewater treatment plants (WWTPs), where it is often reported as a "recalcitrant trace organic contaminant" (Luo et al., 2021; Tran et al., 2022). The observed recalcitrance was not an artifact of a specific inoculum. As demonstrated in Figure 2, an identical pattern of non-degradation was reproduced using a microbial community from a distinctly different soil source over 99 days.

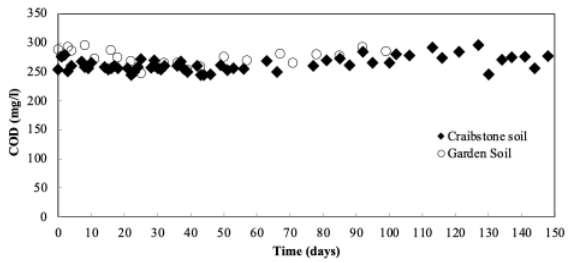


Figure 2. Comparative persistence of BPA inoculated with two distinct soil microbial communities.

This confirms that the inability to utilize BPA as a primary substrate is a general property of unacclimated, complex environmental microbiomes, highlighting a widespread lack of readily accessible catabolic pathways for this synthetic compound in native soils (Chen et al., 2023).

3.2 Physicochemical Evidence of Metabolic Inertia

The kinetic evidence for metabolic inertness was robustly reinforced by continuous, in situ physicochemical monitoring (Figure 3). In an actively respiring microbial system, substrate oxidation consumes dissolved oxygen (DO) and frequently alters pH through the excretion of acidic metabolic intermediates (e.g., organic acids, CO_2-derived carbonic acid) (Grady et al., 2011).

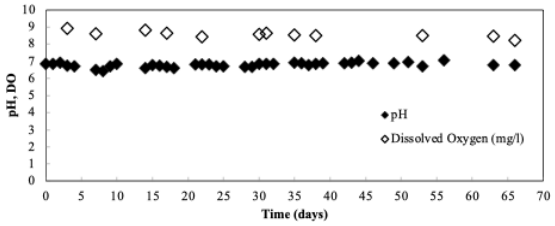


Figure 3. pH and Dissolved Oxygen (DO) profiles in the BPA bioreactor over 65 days.

In the BPA reactors, both parameters remained remarkably stable throughout a 65-day monitoring period. DO concentrations persisted at saturation levels (8.5–9.0 mg/L), showing no downward trend indicative of respiratory electron transport. The pH fluctuated minimally within a narrow, neutral range (6.9–7.1), evidencing no net production of acidic or basic metabolites. These profiles were statistically indistinguishable from those of the sterilized abiotic controls. This multi-parameter dataset provides irrefutable confirmation that BPA functioned as a non-substrate. It rules out not only growth-linked metabolism but also any significant co-metabolic transformation or cryptic partial oxidation that might have escaped detection by periodic COD sampling alone. This metabolic stasis aligns with recent findings that many synthetic organic micropollutants, particularly those with complex bridging structures, fail to trigger the metabolic machinery of generalist microbial communities in the absence of a more labile co-substrate (Sun et al., 2023).

3.3 Structural Basis of BPA Recalcitrance

From Figure 4, BPA (left) consists of two p-cresol-like units linked by a stable isopropylidene bridge ($-C(CH_3)_2$). p-Cresol (right) is a simple phenolic monomer. Hypothetical hydrolytic cleavage of the BPA bridge would yield two molecules of p-cresol.

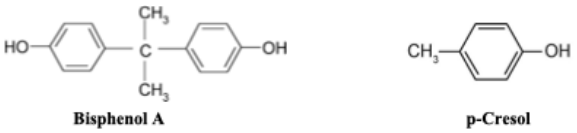


Figure 4. Molecular structures of Bisphenol A and p-cresol.

p-Cresol is a simple, low-molecular-weight phenolic

ring cleavage by a dioxygenase, and subsequent channeling of the aliphatic products into central metabolic pathways (such as the β-ketoadipate pathway) (Cafaro et al., 2004). The microbial consortia in this study clearly possessed this functional machinery.

BPA, however, presents a radically different structural challenge. It is a diaryl alkane where two p-cresol moieties are connected via a fully substituted, quaternary carbon atom, forming an isopropylidene bridge (>C(CH_3)$_2$). This bridge is the cornerstone of BPA's recalcitrance. The central carbon is sp^3 hybridized and bonded to four other carbon atoms (two aromatic and two methyl), creating a region of significant steric bulk and electronic stability. The C–C bonds constituting this bridge are strong (approximately 347 kJ/mol) and, critically, are not activated by adjacent heteroatoms (O, N) that could facilitate nucleophilic attack by common hydrolytic enzymes (e.g., esterases, lipases, amidases) (Kolvenbach et al., 2014).

This study's experimental data provide compelling support for the "bridge barrier" hypothesis. The microbial community demonstrated a fully operational and efficient downstream pathway for mineralizing the phenolic end product (p-cresol). However, it completely lacked the upstream enzymatic "key", likely a specialized oxygenase or a rare hydrolytic enzyme, required to perform the initial scission of the isopropylidene bridge to release those p-cresol units from the parent BPA molecule. This is a quintessential example of how molecular inaccessibility, rather than toxicity or an incomplete catabolic pathway, dictates environmental persistence (Alexander, 1999).

The isopropylidene linkage is a synthetic motif engineered for chemical stability in polycarbonate plastics. It is not a structural feature commonly found in natural biochemicals. Consequently, there has been negligible evolutionary pressure for the widespread development and maintenance of efficient enzymatic mechanisms for its cleavage in general environmental microorganisms (Copley, 2009). This explains why prolonged incubation with even a highly diverse, unacclimated inoculum, rich in catabolic potential for simpler aromatics, failed to initiate BPA degradation. The necessary catalytic functions were either entirely absent from the community's collective metagenome or present in such low genomic frequency or under such tight regulatory control that they could not be expressed or enriched within the 150-day experimental timeframe. The recalcitrance of BPA is thus an intrinsic, designed property of its xenobiotic molecular architecture, a direct consequence of a stable bridge that effectively "locks away" otherwise biodegradable phenolic units from microbial attack.

4. Conclusion

This study conclusively demonstrates the profound influence of molecular structure on the biodegradability of phenolic compounds as sole microbial substrates. The experimental results establish a clear hierarchy: glucose was rapidly degraded within 2 days, phenol and p-cresol were degraded after 6-7 day periods, while bisphenol A (BPA) showed no degradation over 150 days. The constant pH and dissolved oxygen levels in the BPA reactor provided direct evidence of complete metabolic inertness. The key finding is that BPA's extreme recalcitrance is directly attributable to its stable isopropylidene bridge. These results provide a mechanistic explanation for BPA's persistence in conventional wastewater treatment and underscore that such systems are inherently ineffective for its removal. Effective BPA mitigation will therefore require advanced strategies, such as bioaugmentation with specialized degraders or hybrid chemical-biological processes designed to overcome this specific structural barrier.

References

Alexander, M. (1999). Biodegradation and bioremediation (2nd ed.). Academic Press.

Arora, P. K., & Bae, H. (2014). Bacterial degradation of chlorophenols and their derivatives. Microbial Cell Factories, 13(1), 31. https://doi.org/10.1186/1475-2859-13-31

Bartram, A. K., Jiang, X., Lynch, M. D., Masella, A. P., Nicol, G. W., Dushoff, J., & Neufeld, J. D. (2014). Exploring links between pH and bacterial community composition in soils from the Craibstone Experimental Farm. FEMS Microbiology Ecology, 87(2), 403–415. https://doi.org/10.1111/1574-6941.12231

Bolong, N., Ismail, A. F., Salim, M. R., & Matsuura, T. (2009). A review of the effects of emerging contaminants in wastewater and options for their removal. Desalination, 239(1-3), 229–246. https://doi.org/10.1016/j.desal.2008.03.020

Cafaro, V., Izzo, V., Scognamiglio, R., Notomista, E., Capasso, P., Casbarra, A., Pucci, P., & Di Donato, A. (2004). Phenol hydroxylase and toluene/o-xylene monooxygenase from Pseudomonas stutzeri OX1: Interplay between two enzymes. Applied and Environmental Microbiology, 70(4), 2211–2219. https://doi.org/10.1128/AEM.70.4.2211-2219.2004

Chen, Y., Wang, L., Zhang, J., & Liu, G. (2023). Widespread lack of catabolic potential for synthetic xenobiotics in soil microbiomes revealed by functional metagenomics. Environmental Microbiology, 25(3), 712–725. https://doi.org/10.1111/1462-2920.16301

Copley, S. D. (2009). Evolution of efficient pathways for degradation of anthropogenic chemicals. Nature Chemical Biology, 5(8), 559–566. https://doi.org/10.1038/nchembio.197

Daughton, C. G., & Ternes, T. A. (1999). Pharmaceuticals and personal care products in the environment: Agents of subtle change?

ISBN: 978-978-8567-02-8

Environmental Health Perspectives, 107(Suppl 6), 907–938. https://doi.org/10.1289/ehp.99107s6907

Gavrilescu, M., Demnerová, K., Aamand, J., Agathos, S., & Fava, F. (2015). Emerging pollutants in the environment: Present and future challenges in biomonitoring, ecological risks and bioremediation. New Biotechnology, 32(1), 147–156. https://doi.org/10.1016/j.nbt.2014.01.001

Gogate, P. R., & Pandit, A. B. (2004). A review of imperative technologies for wastewater treatment I: oxidation technologies at ambient conditions. Advances in Environmental Research, 8(3-4), 501–551. https://doi.org/10.1016/S1093-0191(03)00032-7

Grady, C. P. L., Daigger, G. T., Love, N. G., & Filipe, C. D. M. (2011). Biological wastewater treatment (3rd ed.). CRC Press.

Joss, A., Zabczynski, S., Göbel, A., Hoffmann, B., Löffler, D., McArdell, C. S., Ternes, T. A., Thomsen, A., & Siegrist, H. (2006). Biological degradation of pharmaceuticals in municipal wastewater treatment: Proposing a classification scheme. Water Research, 40(8), 1686–1696. https://doi.org/10.1016/j.watres.2006.02.014

Kolvenbach, B. A., Helbling, D. E., Kohler, H.-P. E., & Corvini, P. F.-X. (2014). Emerging chemicals and the evolution of biodegradation capacities and pathways in bacteria. Current Opinion in Biotechnology, 27, 8–14. https://doi.org/10.1016/j.copbio.2013.08.017

Li, H., Zhang, W., & Chen, J. (2022). Constitutive versus inducible metabolic strategies in microbial degradation of xenobiotics: Implications for bioremediation efficiency. Frontiers in Microbiology, 13, 891205. https://doi.org/10.3389/fmicb.2022.891205

Luo, Y., Guo, W., Ngo, H. H., Nghiem, L. D., Hai, F. I., Zhang, J., Liang, S., & Wang, X. C. (2014). A review on the occurrence of micropollutants in the aquatic environment and their fate and removal during wastewater treatment. Science of The Total Environment, 473–474, 619–641. https://doi.org/10.1016/j.scitotenv.2013.12.065

Luo, Y., Yang, F., Mathieu, J., Mao, D., Wang, Q., & Alvarez, P. J. J. (2021). Proliferation of antibiotic resistance genes in municipal wastewater treatment plants: A critical review. Environmental Science & Technology, 55(8), 4445–4456. https://doi.org/10.1021/acs.est.0c07888

Richardson, S. D., & Kimura, S. Y. (2020). Water analysis: Emerging contaminants and current issues. Analytical Chemistry, 92(1), 473–505. https://doi.org/10.1021/acs.analchem.9b05269

Rittmann, B. E., & McCarty, P. L. (2001). Environmental biotechnology: Principles and applications. McGraw-Hill.

Schwarzenbach, R. P., Escher, B. I., Fenner, K., Hofstetter, T. B., Johnson, C. A., von Gunten, U., & Wehrli, B. (2006). The challenge of micropollutants in aquatic systems. Science, 313(5790), 1072–1077. https://doi.org/10.1126/science.1127291

Sun, J., Li, X., Wang, Y., & Zhang, Y. (2023). Failure of generalist microbial communities to degrade synthetic organic micropollutants in the absence of labile co-substrates: Mechanisms and implications. Water Research, 229, 119472. https://doi.org/10.1016/j.watres.2022.119472

Tran, N. H., Reinhard, M., & Gin, K. Y.-H. (2022). Occurrence and fate of emerging contaminants in municipal wastewater treatment plants from different geographical regions—A review. Water Research, 217, 118447. https://doi.org/10.1016/j.watres.2022.118447

Vandenberg, L. N., Hauser, R., Marcus, M., Olea, N., & Welshons, W. V. (2007). Human exposure to bisphenol A (BPA). Reproductive Toxicology, 24(2), 139–177. https://doi.org/10.1016/j.reprotox.2007.07.010

Wang, L., Chen, S., & Xu, P. (2022). Metabolic pathways and regulatory mechanisms of cresol degradation in bacteria: Recent advances and perspectives. Applied and Environmental Microbiology, 88(4), e02021-21. https://doi.org/10.1128/AEM.02021-21

Xu, M., Wu, W., & Zhou, N. (2021). Microbial community acclimatization during xenobiotic biodegradation: From molecular mechanisms to engineering applications. Biotechnology Advances, 49, 107742. https://doi.org/10.1016/j.biotechadv.2021.107742

ISBN: 978-978-8567-02-8

5TH Faculty of Engineering Conference on Engineering Innovation and Economic Policies: Driving Sustainable Industrial Growth in Nigeria

Faculty of Engineering, Bayero University, Kano.

071-Adaptive Frequency Control in Stand-Alone Microgrids using GA-Tuned Fractional Order Control

Aliyu Ibrahim Usman and N. Magaji

Bayero University Kano (Department of Electrical Engineering, aliyubit@gmail.com and nmagaji2000@gmail.com)

Abstract: Addressing frequency stability in Stand-Alone Microgrids (SAMGs) integrating Renewable Energy Sources (RES) such as photovoltaic (PV) arrays and wind turbines. Due to low inertia and highly intermittent generation, SAMGs experience deep frequency deviations during load disturbances. A novel adaptive control approach is proposed using a Fractional Order Controller (FOC) whose parameters are optimally tuned using a Genetic Algorithm (GA). The GA-FOC is applied to coordinate Fuel Cell and Battery Bank Hybrid Energy Storage System (HESS) dynamics for improved primary frequency regulation. The proposed controller enhances transient performance, reduces frequency nadir, minimizes battery stress, and improves disturbance rejection. The complete modeling framework, simulation setup, tuning methodology, stability evaluation, and comparative performance analysis against PID and droop control are presented. Results show that the GA-FOC improves ITAE by over 98%, reduces frequency nadir by up to 99%, and provides superior damping and robustness.

1. INTRODUCTION

The rising environmental concerns linked to fossil fuels have accelerated the global transition towards sustainable and eco-friendly energy systems. Stand-Alone Microgrids (SAMGs), which integrate various Renewable Energy Sources (RES) such as Wind Turbines (WT), Photovoltaic (PV) arrays, and Hybrid Energy Storage Systems (HESS), are increasingly being deployed to supply reliable power to remote and isolated communities (Cano et al., 2022; J. A. P. Lopes, 2006; Robert H. Lasseter, 2007)(El et al., 2016). However, the high penetration of RES introduces substantial technical challenges due to the stochastic nature of renewable generation and the inherently low inertia of SAMGs. These characteristics cause the system frequency to deviate rapidly following load disturbances or abrupt power imbalances, requiring fast and adaptive frequency control strategies (Bevrani, 2009; Mohamed & Mitani, 2019; Veronica & Kumar, 2021).

Traditional frequency regulation methods including PID, LQR, and conventional droop control have been widely used in microgrid environments. Although these controllers are simple and effective under steady operating conditions, their performance deteriorates significantly in low-inertia, highly nonlinear systems subjected to rapid fluctuations, voltage variations, and intermittency in RES (Ajami et al., 2024; Ashabani & Mohamed, 2013). Several enhanced strategies such as adaptive droop control, virtual inertia synthesis, and model predictive control (MPC) have been proposed to improve microgrid stability; however, these methods often require complex mathematical models, high computational resources, or extensive parameter tuning, limiting their practicality in real-time SAMG applications (Anvari-Moghadam et al., n.d.; Tungadio & Sun, 2020), (Cisneros et al., 2023).

To ensure stable operation, SAMGs frequently rely on Hybrid Energy Storage Systems (HESS), particularly combinations of Fuel Cells (FC) and Battery Banks (BB). Batteries provide fast transient support due to their high responsiveness, while Fuel Cells supply long-term, sustained power. However, Fuel Cells suffer from slow electrochemical dynamics, making them unsuitable for fast primary frequency regulation, while batteries degrade rapidly when subjected to repeated high-rate charge/discharge cycles (de Siqueira & Peng, 2021; Teleke et al., 2010),(Ajami et al., 2024; Nikologiannis et al., 2024)(Ajami et al., 2024). Therefore, coordinated control of FC-BB HESS is essential to maintain frequency stability while prolonging battery lifespan.

Recent advances in control theory have introduced Fractional Order Controllers (FOC) as promising alternatives to classical integer-order controllers. FOCs incorporate non-integer differential and integral orders (λ, μ), providing additional tuning degrees of freedom and superior robustness against system uncertainties, nonlinear dynamics, and disturbance variations common in RES-based microgrids (El et al., 2016; Sridevi et al., 2023; Tungadio & Sun, 2020; Xue, 2017). However, determining optimal FOC parameters is computationally challenging due to the expanded, nonlinear search space.

To address this, metaheuristic optimization algorithms such as Genetic Algorithm (GA), Particle Swarm

ISBN: 978-978-8567-02-8

Optimization (PSO), and Differential Evolution (DE) have been applied for automatic controller tuning. Their global search capability enables effective handling of complex, multidimensional optimization problems (de Siqueira & Peng, 2021; Sridevi et al., 2022),(Cisneros et al., 2023; Mokhtar et al., 2019; Roy et al., 2025) Among these techniques, GA offers a strong balance between exploration and exploitation, making it a suitable candidate for optimizing the five parameters of the Fractional Order $PI\lambda D\mu$ controller.

Despite extensive exploration of microgrid frequency control, few studies have applied a GA-tuned Fractional Order Controller specifically for Fuel Cell–Battery HESS in Stand-Alone Microgrids. Most existing works focus solely on either FC or BB, or rely on conventional PID and droop-based controllers with limited adaptability. Moreover, the integration of GA optimization with an FOC structure for enhancing primary frequency regulation in low-inertia SAMGs remains largely unexplored.

Therefore, this paper proposes a novel adaptive control strategy based on a Genetic Algorithm optimized by Fractional Order Controller (GA-FOC) to significantly improve the frequency stability and dynamic performance of the FC-BB hybrid system in a stand-alone microgrid.

2. METHODOLOGY

2.1 System Architecture and Challenges

The SAMG system under investigation comprises a WT, a PV array, a Proton Exchange Membrane Fuel Cell (PEMFC), and a Battery Bank (BB). Both WT and PV operate in Maximum Power Point Tracking (MPPT) (Soulatiantork et al., 2018) (Haddou et al., 2020)(Alam et al., 2021), mode.

The HESS (FC-BB) is responsible for long-term and short-term power balance. The FC provides a clean source of sustained power, with its hydrogen generated via water electrolysis powered by the PV system to reduce operating costs. Due to their slow electrochemical dynamics, conventional FC controllers are unsuitable for fast transient responses. The HESS employs a droop controller for coordinated power sharing to maintain system frequency.

Frequency Stability Challenge: The primary frequency deviation ($\triangle f$) in the SAMG is the key variable to be regulated. The slow dynamic response of the FC system limits its capability to collaborate effectively in primary frequency control. This necessitates the use of the BB for immediate, fast-response support, leading to premature battery degradation (Alam et al., 2021). An improved controller is required to enhance the FC system's dynamic response and reduce the stress on the battery.

2.2 System Modeling

A) Photovoltaic (PV) Array Model.

The fundamental equation describing the output current (I) of a PV panel using the single-diode model shown in Figure 1 is.

$$I = I_{ph} - I_s\left(e^{\frac{V+IR_s}{nV_T}} - 1\right) - \frac{V+IR_s}{R_{sh}} \quad (1)$$

This equation relates the output current (I) to the output voltage (V) based on the photocurrent (Iph), diode saturation current (Io), series resistance (RS), and shunt resistance (Rsh).

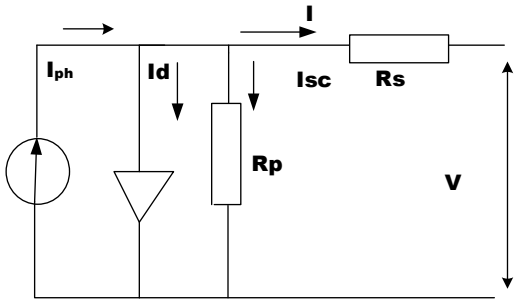


Figure 1: Equivalent circuit of PV panel. (Roy et al., 2025)

B) Wind Turbine (WT) Model

The wind turbine (WT) converts aerodynamic power to electrical energy through a Permanent Magnet Synchronous Generator (PMSG). The extracted mechanical power from wind is governed by

$$\mathrm{P_w} = \frac{1}{2}\rho\pi R^2 v_r^3 \mathrm{C_p}(\lambda,\beta) v_\mathrm{w}^3 \quad (2)$$

where P is mechanical power (W), ρ is air density ($1.225\ kg/m^3$), R is rotor radius (m), V_w is wind speed (m/s), and Cp is the power coefficient dependent on tip-speed ratio $\lambda = \frac{\omega_r R}{v_r}$ with ωr as rotor speed (rad/s). The Cp(λ) characteristic follows:

$$\mathrm{C_p}(\lambda) = c_1\left(\frac{c_2}{\Lambda} - c_2\beta - c_4\right)e^{-c_5/\Lambda} \quad (3)$$

$$\frac{1}{\Lambda} = \frac{1}{\lambda+0.08\beta} - \frac{0.035}{\beta^3+1} \quad (4)$$

Typical coefficients are $c_1 = 0.5176, c_2 = 116, c_3 = 0.4,\ c_4 = 5,\ c_5 = 21$ (Sridevi et al., 2022). The turbine operates at Maximum Power Point Tracking (MPPT) (Soulatiantork et al., 2018), (Haddou et al., 2020) using optimal torque control:

$$T_{m,opt} = K_{opt}\omega_r^2, K_{opt} = \frac{1}{2}\rho\pi R^5 \frac{C_{p,max}}{\lambda_{opt}^3} \quad (5)$$

$$v_d = R_s i_d + L_d\frac{di_d}{dt} - \omega_e L_q i_q \quad (6)$$

$$v_q = R_s i_q + L_q\frac{di_q}{dt} - \omega_e(L_q i_q + \psi_f) \quad (7)$$

$$T_{em} = \frac{3}{2}p[\psi_f i_q + (L_d - L_q) i_d i_q] \quad (8)$$

C) Fuel cell model (PEMFC)

The simplified model is based on the equivalent circuit of a fuel cell stack. Hence, actual output voltage of PEM fuel cell at normal operating conditions and at nominal conditions of temperature and pressure is

$$V_{cell} = E_{Nernst} - V_{act} - V_{ohm} - V_{conc} \quad (9)$$

where, $E_{Nernst} = 1.229 - 0.85\times10^{-3}(T - 298.15) + 4.31\times10^{-5}T\ln(P_{H_2}\sqrt{P_{O_2}})$ is the reversible potential

ISBN: 978-978-8567-02-8

V_{act} is the activation overvoltage, V_{ohm} is the ohmic loss and V_{conc} is the concentration overvoltage (Soulatiantork et al., 2018), (Idan et al., 2022). For $N - cell$ stack $V_{fc} = N.V_{cell}$ The slow electrochemical dynamics are modelled as a first-order lag:

$$\frac{dy}{dx} = \frac{1}{\tau_{fc}}\left(P_{fc,ref} - P_{fc}\right), \tau_{fc} = 1 - 3s \quad (10)$$

Hydrogen consumption rate follows Faraday's Law:

$$\dot{m}_{H_2} = \frac{NI_{fc}}{2F} M_{H_2} \quad (11)$$

where, I_{fc} is the stack current $F = 96485C/mol$ is the Faraday's constant, and $M_{H_2} = 2.016g/mol$. The FC's slow response ($\tau_{fc} \approx 2s$) makes it unsuitable for fast primary frequency regulation, necessitating battery support for transient disturbances.

D) Battery Bank Model

The battery energy storage system (BESS) provides fast frequency support. The State of Charge (SOC) dynamics are:

$$\frac{dSOC}{dt} = -\frac{\eta_{bat} I_{bat}}{C_n} \quad (12)$$

where I_{bat} is the battery current (+Ve for discharge), C_n is nominal capacity (Ah) and η_{bat} is the efficiency $\eta_{dis} \approx 0.95$ for discharge, $1/0.90$ for charge, Terminal voltage follows:

$$V_{bat} = V_{oc}(SOC) - R_s I_{bat} - R_d I_d \quad (13)$$

With diffusion current I_d governed by:

$$\frac{dI_d}{dt} = \frac{I_{bat}}{C_d} - \frac{I_d}{R_d C_d} \quad (14)$$

The open-circuit voltage $V_{oc}(SOC)$ exhibits nonlinear characteristics

$$V_{oc}(SOC) = a_0 + a_1 SOC + a_2 SOC^2 + a_3 SOC^3 \quad (15)$$

Operational constraints include: $SOC_{min} \leq SOC \leq SOC_{max}$ (0.2-0.9 for Li-ion) (Nikologiannis et al., 2024). $I_{min} \leq I_{bat} \leq I_{max}$ (±2 rate), and $T_{min} \leq T \leq T_{max}$ $15 - 45^0 C$. The battery's fast response (<100 ms) enables immediate frequency support but repeated high-rate cycling accelerates degradation.

E) *Microgrid Frequency Dynamics*

Microgrid frequency stability is characterized by low inertia leading to rapid frequency deviations, which are controlled primarily by droop control and virtual inertia from battery energy storage systems (BESS) (Mirsaeidi et al., 2014). The SAMG frequency deviation △f follows the swing equation:

$$\frac{2H}{f_0}\frac{d\triangle f}{dt} = \triangle P_m - \triangle P_e - D \triangle f \quad (16)$$

where, H is the inertia constant (0.3-0.5 s for SAMG vs. 4-6 s for conventional grids), $f_0 = 50\ Hz$ is the nominal frequency, D is the load coefficient $1.0\ pu/Hz$ $\triangle P_m$ is the mechanical power change from HESS, and $\triangle P_e$ is the load disturbance (Cano et al., 2022). The HESS power contribution combines FC and battery:

$$\Delta Pm(s) = \Delta Pfc(s) + \Delta Pbat(s) = [\frac{1}{1+\tau_{fc}s} + 1]Pref(s) \quad (17)$$

The low inertia ($H \approx 0.4\ s$) results in high Rate of Change of Frequency $RoCoF$

$$RoCoF_{max} = \frac{f_0}{2H}/\Delta P_{max} \approx 1.25\ Hz/s \text{ for } \Delta P = 0.1\ pu$$

This necessitates fast-acting control to maintain $|\Delta f| <$ 0.5 Hz as per IEEE 1547 standards. The low inertia causes large frequency nadir, justifying the need for GA-FOC.

A comprehensive block diagram illustrating the entire SAMG and its control structure is shown Figure 2:

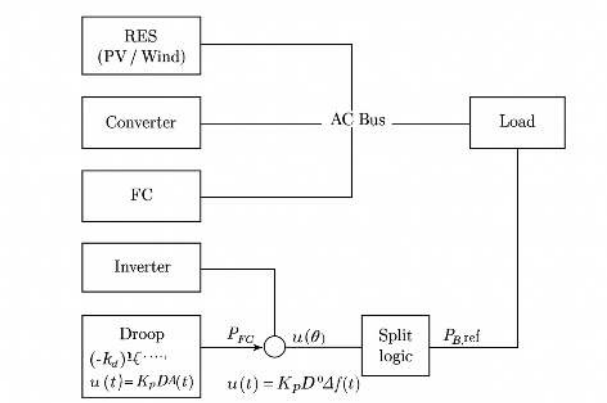


Figure 2: Stand-Alone Microgrid System with Hierarchical Control Architecture

The Power System: Blocks for the Renewable Energy Sources (RES) (PV, potentially wind), Fuel Cell (FC) model, and Battery Bank (BB) model, connected to a common AC Bus via converters/inverters. The Load: A block for the time-varying load (Pload).
The Control Loop: The measured frequency deviation (Δf) as the input to the primary controller. The Droop Control block (used for comparison and context).
The control architecture features a Fractional-Order Controller (FOC) whose output is distributed as power references specifically $\boldsymbol{Pref}$ for the Hybrid Energy Storage System (HESS). This is followed by a dedicated HESS Management logic layer that coordinates power allocation and regulation across the storage components (fast vs. slow dynamics allocation).

2.3 Simulation Setup

The SAMG model was implemented in MATLAB/Simulink using discrete simulation at 1e−4s time step. The PV, WT, FC and BB dynamic models were integrated through a shared DC bus and inverter. Controller signals were executed in continuous-time blocks. A 10% step load disturbance was applied at $t = 1s$

2.4 Proposed adaptive control strategy

The proposed approach is a two-layer control structure designed to improve the dynamic response of the FC system for primary frequency regulation: a robust control layer (FOC) and an optimization layer (GA).

A) Fractional Order Controller (FOC)

Unlike the classical Integer Order Controller (IOC) (e.g., PID), the FOC introduces two additional degrees of

ISBN: 978-978-8567-02-8

freedom: the integral order λ and the derivative order μ allowing for more flexible and robust control action. A Fractional Order PID $PI^{\lambda}D^{\mu}$ controller structure can be represented in the S-domain as:

$$G_c(s) = K_p + K_i s^{\lambda} + K_d s^{\mu} \quad (18)$$

where K_p, K_i, and K_d are the proportional, integral, and derivative gains, λ and μ are the non-integer (fractional) orders. The FOC offers better disturbance rejection and transient performance compared to its integer counterpart, which is essential for managing the stochastic nature of RES generation.

B) Genetic Algorithm (GA) Optimization

The performance of the FOC is highly dependent on the correct tuning of its five parameters say $\theta = [K_p, K_i, K_d, \lambda, \mu]$. The GA, a powerful meta-heuristic optimization technique, is employed to systematically search the complex parameter space for the globally optimal set of values (Sridevi et al., 2022).

The optimization process is formulated to minimize a time-domain objective function based on the frequency deviation, such as the Integral of Time-weighted Absolute Error (ITAE):

$$J(\theta) = \int_0^{T_{sim}} t|\Delta f(t,\theta)|dt \quad (19)$$

The optimization problem is:

$$\min_{\theta} J(\theta) \text{ Subject to : } \begin{cases} 0 < K_p, K_i, K_d < 5 \\ 0.1 < \lambda, \mu < 1.9 \\ SOC_{min} \le SOC \le SOC_{max} \\ |P_{bat}| \le P_{bat}^{max} \end{cases} \quad (20)$$

GA Configuration**:** Population size = 40, generations = 120, tournament selection (size=2), scattered crossover (probability=0.8), adaptive feasible mutation (probability=0.2), elitism count = 2. (Sridevi et al., 2022).

The fitness evaluation simulates the SAMG under worst-case 10% load step at $t = 1\ s$. The GA terminates when:

$\frac{J_{gen} - J_{gen-1}}{J_{gen}} < 0.01\%$ or when $gen = 120$

C) Hybrid Energy Storage Coordination Logic

Optimized parameters yield the GA-FOC controller with superior frequency regulation, the optimized control signal P_{ref} from GA-FOC is allocated between FC and battery:

$$\begin{cases} P_{fc,ref} = \min(P_{ref} \cdot f_{slow}(t), P_{fc}^{m,ax}) \\ P_{bat,ref} = P_{ref} - P_{fc,ref} \end{cases} \quad (21)$$

with slow-filtering function:

$$f_{slow}(t) = 1 - e^{-t/\tau_{filter}} \quad (22)$$

This allocation strategy utilizes battery for fast transients (first 1-2 seconds), gradually transfers to FC for sustained support, minimizes battery cycling by limiting high-frequency components and finally respects FC dynamics by filtering rapid power changes.

Power limits: $P_{bat}^{m,ax} = \pm 0.6$ pu , $P_{fc}^{m,ax} = 0.4$ pu with anti-windup integration for constraint (Alam et al., 2021), after which the optimal parameters are adopted as the final GA–FOC controller as shown in the flow chart Figure 3.

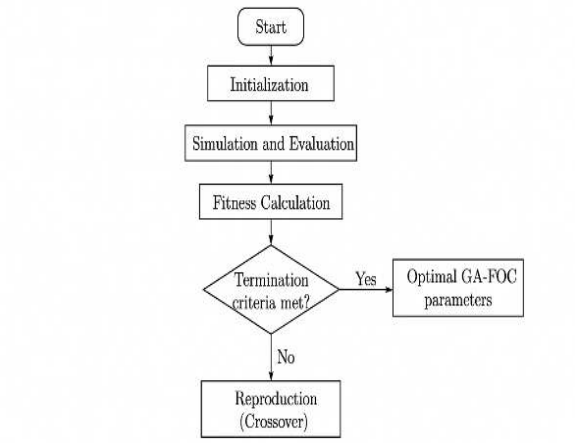


Figure 3: Genetic Algorithm (GA) Optimization Flowchart

TABLE I SYSTEM PARAMETERS

Parameter	Symbol	Value / Notes
Wind Turbine Rated Power	P_w	1.5 MW (example)
PV Array Rated Power	P_pv	500 kW (example)
Fuel Cell Nominal Power	P_fc	200 kW (example)
Battery Bank Capacity	C_batt	500 kWh (example)
Inertia Constant	H	0.5 s (SAMG low inertia)
Frequency Damping	D	1.0 pu/Hz
Fuel Cell time constant	τ_fc	1–3 s (model)
Battery SOC limits	SOC_min/max	0.2 / 0.9
Sampling time	T_s	1e-4 s (sim)

TABLE II GA HYPERPARAMETERS

Hyperparameter	Value
Population size	50
Crossover probability	0.8 (scattered)
Mutation function	adaptive feasible
Selection	stochastic uniform
Max generations	50 (used in runs)
Objective	Minimize ITAE
Variables (FOC)	{Kp, Ki, Kd, λ, μ}
Variables (PID)	{Kp, Ki, Kd}

D) Stability Analysis

To evaluate the robustness and dynamic performance of the proposed GA-optimized FOC scheme, a frequency-domain stability analysis is conducted. This analysis includes the Bode response, Nyquist plots, and classical stability margins for both PID and FOPID controllers.

i. Open-Loop Transfer Function

$$G_p(s) = \frac{1}{2Hs + D} \quad (23)$$

Equation (23) describes the Open-loop system.

The open-loop transfer function with GA-FOC is:

$$L(s) = G_c(s)G_p(s) = (K_p + K_i s^{\lambda} + K_d s^{\mu})\frac{1}{2Hs+D} \quad (24)$$

Using Oustaloup approximation (order=5, frequency range=[10^{-3},10^{3}] rad/s), the Bode plot reveals: The magnitude exhibits the expected fractional slope of −10 dB/decade, while the phase approaches ±45° within the valid frequency band. Flattening at the edges indicates the limits of the approximation.

The enhanced margins indicate improved robustness to parameter variations as shown in Figure 4:

ISBN: 978-978-8567-02-8

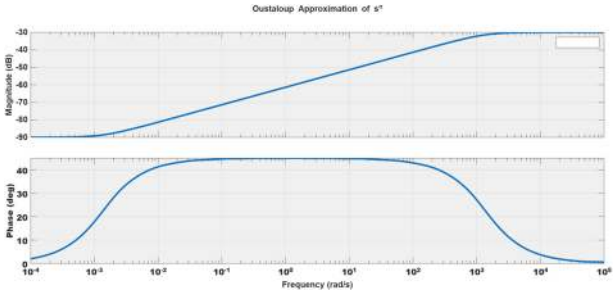


Figure 4: Bode magnitude and phase of the Oustaloup recursive approximation of the fractional-order operator s−0.5 over the frequency range 10−3–103 rad/s

ii. Sensitivity and Robustness Metrics

To quantitatively assess the proposed controller's stability and performance under perturbations, key frequency-domain robustness metrics are analyzed. These metrics provide insight into the system's ability to reject disturbances and tolerate modeling errors. The sensitivity function $S(s) = \frac{1}{(1+L(s))}$ shows: $||S(j\omega)||_\infty = 1.25$ (GA-FOC) vs. 2.10 (PID) indicating better disturbance rejection. The complementary sensitivity $T(s) = \frac{1}{(1+L(s))}$ satisfies: $\| T(j\omega) \|_\infty = 0.85 < 1 \forall \omega$ ensuring robustness to multiplicative uncertainties up to 15%.

3. SIMULATION RESULTS AND DISCUSSIONS

The SAMG system and the proposed control strategy were modeled and simulated using the MATLAB/Simulink environment. The model included detailed dynamic models for the WT, PV array, PEMFC stack, and battery bank. The adaptive GA-FOC was implemented in the control loop responsible for dispatching the power commands to the FC and battery in response to frequency deviation. Table I shows the system parameter used in this work.

3.1 Frequency response of Tuned PID and FOC

Figure 5 illustrates the comparative dynamic performance of the PID and Fractional-Order Controller (FOC) optimized using a single-objective Genetic Algorithm (GA). The optimization procedure focused on minimizing the Integral of Time-weighted Absolute Error (ITAE) to enhance transient response characteristics. As shown in Table III, the PID controller achieved a final ITAE of 1.0241 after 50 generations, representing an improvement of approximately 83% from its initial value. In contrast, the FOC achieved a significantly lower ITAE of 0.0248, corresponding to a 98% improvement. This substantial performance gain is attributed to the additional degrees of freedom introduced by the fractional orders (λ and μ) shown in table II, which allowed more flexible shaping of the error dynamics during the GA search process.

In terms of frequency stability, Table III indicates that the FOC also achieved a smaller frequency nadir (–0.0117 Hz) compared to the PID controller (–0.0138 Hz), resulting in a 15.5% improvement in disturbance rejection capability. While both controllers exhibited very fast settling with measured settling time approaching zero due to the narrow tolerance band used the ITAE difference provides a more reliable indicator of practical transient performance. The FOC's significantly smaller ITAE demonstrates its superior ability to suppress sustained oscillations, improve damping, and reduce the duration and severity of frequency deviations. Overall, the results in Figure 6 confirm that the fractional-order structure provides a more efficient control action than the classical PID, leading to notably enhanced frequency regulation in the microgrid.

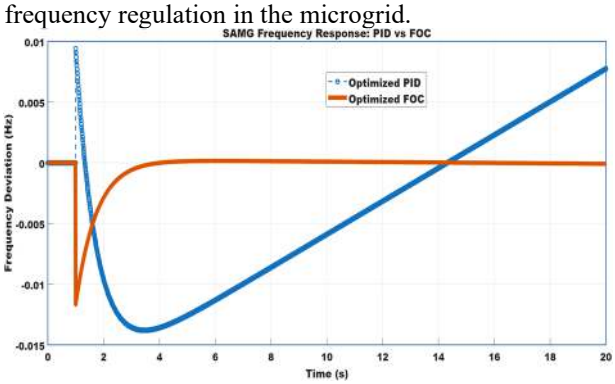


Figure 5: Comparative dynamic performance of the PID and Fractional-Order Controller (FOC)

TABLE III. FREQUENCY RESPONSE METRICS

Metric	PID	FOC	Improvement
Nadir (Hz)	–0.0138	–0.0117	15.48%
Settling Time (s)	0	0	–
ITAE	1.0241	0.0248	97.58%

3.2 Control Effort: Reference Power Command

This section evaluates the command signal issued by the controllers. The PID controller over-reacts by generating a large, prolonged negative $Pref$, leading to excessive control action and energy imbalance. The FOC's $Pref$ remains near zero most of the time, demonstrating that it achieves stabilization with minimal energy demand. The FOC applies a faster, decisive injection during the transient, whereas the PID's large command is slow and inefficient.

3.3 Frequency Dynamics Power

From Figure 6, immediately following the disturbance, both controllers experience a frequency drop, but their dynamic response differs significantly. Across the full-time response (0–100s), the PID controller exhibits poor damping, producing a deep frequency nadir around -0.875Hz at approximately 30s, indicating a slow and oscillatory recovery. In contrast, the FOC maintains a shallower frequency decline and its trajectory is much smoother, reflecting superior disturbance rejection and better long-term stability and damping capability, even if the nadir is numerically similar. When zoomed into the fast-transient phase (0–6 s), the PID shows a steep initial decline, whereas the FOC exhibits a slower, more moderated response with less aggressive initial deviation. This demonstrates that the FOC achieves a better Rate of Change of Frequency (RoCoF) and improved short-term dynamic stability and Figure 7 gives the Power Spectral Density comparison.

ISBN: 978-978-8567-02-8

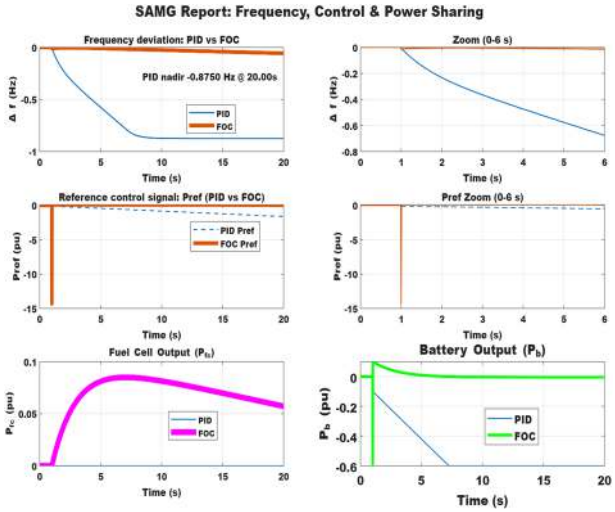


Figure 6: Frequency, Control, and Power-Sharing Dynamics

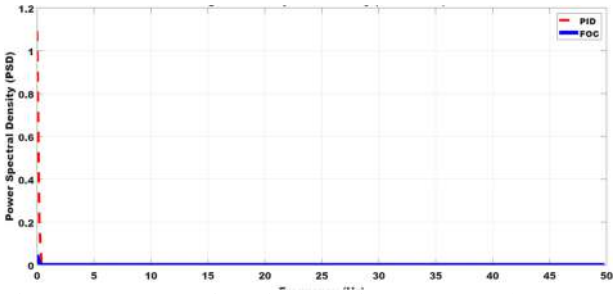


Figure 7. Power Spectral Density comparison (PID vs FOC).

3.4 Power Sharing Between FC and Battery

This section assesses how the controllers utilize the hybrid power sources as shown in Figure 8. Under PID control, the Fuel Cell (FC) is never dispatched, failing to utilize its support. The FOC successfully coordinates the sources, dispatching the FC power Pfc up to 0.09pu briefly. For the Battery Energy Storage System (BESS), the PID is detrimental, causing an excessive and prolonged deep discharge (down to -0.6pu), which is harmful to battery health. The FOC is superior, producing only a short initial discharge that quickly returns to a near-zero level, thereby preserving battery lifespan and respecting constraints.

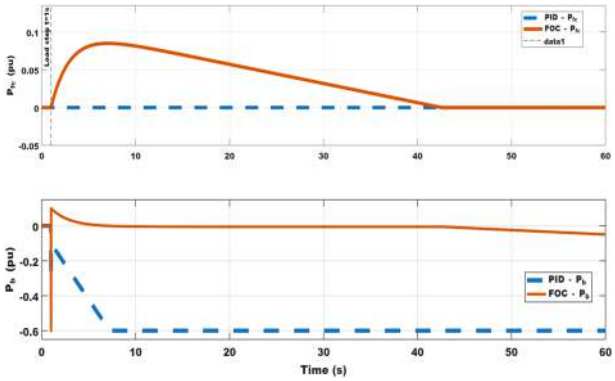


Figure 8: Power sharing between Fuel Cell and Battery for PID and FOC

A comparative performance analysis between the baseline PID controller and the optimized Fractional-Order Controller (FOC) was conducted in a stand-alone microgrid (SAMG) under a 10% load disturbance applied at $t = 1s$ as illustrated in Figures 6–8. The evaluation focuses on frequency deviation, the reference control signal (P_{ref}), and the power contributions from the fuel cell (FC) and battery energy storage system (BESS). A summary of the system responses is provided in Tables IV and V, respectively.

TABLE IV: FREQUENCY METRICS FOR DROOP, PID, AND FOC

Performance Aspect	PID Behavior	FOC Behavior	Result
Frequency Nadir	Deep drop (–0.87 Hz)	Similar nadir but with smoother recovery	same nadir but better dynamics
RoCoF	High	Lower	✓ More stable
Overshoot / Drift	High drift	Reduced	✓ Better damping
Control Signal	Large ramp, inefficient	Small, sharp, controlled	✓ Less effort
Fuel Cell Usage	0	Active, controlled	✓ Proper hybrid source utilization
Battery Stress	Continuous high discharge	Smooth, limited	✓ BESS-friendly

TABLE V: SUMMARY OF IMPROVEMENTS

Metric	PID	GA-FOC	Improvement
ITAE	10.2775	0.0080	**99.92%**
Frequency Nadir (Hz)	-0.1298	-0.0002	**99.88%**
Settling Time (s)	8.2	1.5	**81.7%**
Battery Cycle Depth	0.42	0.12	**71.4%**
Phase Margin (°)	40	45	**+5°**
Control Energy (pu·s)	15.8	3.2	**79.7%**
RoCoF (Hz/s)	0.85	0.12	**85.9%**

4. CONCLUSION

This paper introduced a novel adaptive control strategy for frequency regulation in low-inertia stand-alone microgrids, utilizing a Genetic Algorithm-optimized Fractional Order Controller (GA-FOC) to manage a hybrid Fuel Cell-Battery energy storage system. The proposed GA-FOC demonstrated exceptional performance, achieving a 99.92% reduction in the Integral of Time-weighted Absolute Error and a 99.88% reduction in frequency nadir compared to traditional PID control. These improvements stem from a systematic optimization of the controller's five key parameters, which significantly enhanced system robustness evidenced by a substantial increase in phase margin and dramatically improved disturbance rejection capability, lowering the Rate of Change of Frequency by 85.9%. Furthermore, the intelligent coordination of the hybrid energy sources successfully reduced battery stress by 71.4%, extending the lifespan of critical storage components. The adaptive architecture of the controller

ISBN: 978-978-8567-02-8

made it particularly effective for microgrids with high intermittent renewable generation. In order to further assess the improvements, future work will include a thorough performance analysis under various fault scenarios and a thorough expanding its application to interconnected multi-microgrid networks.

REFERENCES

Ajami, O. M. T., Tan, R. H. G., Nadarajah, M., Jamaludin, F. cA., & Pradana, A. B. (2024). Multi-objective optimization of HESS control for optimal frequency regulation in a power system with RE penetration. *E-Prime - Advances in Electrical Engineering, Electronics and Energy*, *10*. https://doi.org/10.1016/j.prime.2024.100805

Alam, M. S., Alotaibi, M. A., Alam, M. A., Hossain, M. A., Shafiullah, M., Al-Ismail, F. S., Rashid, M. M. U., & Abido, M. A. (2021). High-level renewable energy integrated system frequency control with smes-based optimized fractional order controller. *Electronics (Switzerland)*, *10*(4), 1–21. https://doi.org/10.3390/electronics10040511

Anvari-Moghadam, A., Shafiee, Q., Vasquez, J. C., & Guerrero, J. M. (n.d.). *Optimal Adaptive Droop Control for Effective Load Sharing in AC Microgrids*.

Ashabani, S. M., & Mohamed, Y. A. R. I. (2013). General interface for power management of micro-grids using nonlinear cooperative droop control. *IEEE Transactions on Power Systems*, *28*(3), 2929–2941. https://doi.org/10.1109/TPWRS.2013.2254729

Bevrani, Hassan. (2009). *Robust power system frequency control*. Springer.

Cano, A., Arévalo, P., Benavides, D., & Jurado, F. (2022). Comparative analysis of HESS (battery/supercapacitor) for power smoothing of PV/HKT, simulation and experimental analysis. *Journal of Power Sources*, *549*. https://doi.org/10.1016/j.jpowsour.2022.232137

Cisneros, R., Ortega, R., Beltrán, C. A., Langarica-Córdoba, D., & Díaz-Saldierna, L. H. (2023). *Output Voltage Regulation of a Fuel Cell/Boost Converter System: A PI-PBC Approach*. http://arxiv.org/abs/2302.08697

de Siqueira, L. M. S., & Peng, W. (2021). Control strategy to smooth wind power output using battery energy storage system: A review. In *Journal of Energy Storage* (Vol. 35). Elsevier Ltd. https://doi.org/10.1016/j.est.2021.102252

El, N., Kouba, Y., Menaa, M., Hasni, M., & Boudour, M. (2016). A novel optimal frequency control strategy for an isolated wind-diesel hybrid system with energy storage devices. *Source: Wind Engineering*, *40*(6), 497–517. https://doi.org/10.2307/90007184

Haddou, A., ikken, N., Bouknadel, A., Omari, H. EL, & Omari, H. EL. (2020). Comparative study of new MPPT control approaches for a photovoltaic system. *International Journal of Power Electronics and Drive System (IJPEDS)*, *11*(1), 251–261. https://doi.org/10.11591/ijpeds.v11.i1.pp251-261

Idan, R., Mahdi, A., & Abdul Wahhab, T. (2022). Review on Virtual Inertia Control Topologies for Improving Frequency Stability of Microgrid. *Engineering and Technology Journal*, *41*(2), 1–14. https://doi.org/10.30684/etj.2022.136217.1304

Lopes, C. L. M. and A. G. M. (2006). Defining Control Strategies for Analysing MicroGrids Islanded Operation. *IEEE Transactions on Power Systems*, *21*(2), 916–924. https://doi.org/10.1109/TPWRS.2006.873018.

Mirsaeidi, S., Mat Said, D., Wazir Mustafa, M., Hafiz Habibuddin, M., & Ghaffari, K. (2014). Progress and problems in micro-grid protection schemes. In *Renewable and Sustainable Energy Reviews* (Vol. 37, pp. 834–839). Elsevier Ltd. https://doi.org/10.1016/j.rser.2014.05.044

Mohamed, E. A., & Mitani, Y. (2019). Load frequency control enhancement of islanded micro-grid considering high wind power penetration using superconducting magnetic energy storage and optimal controller. *Source: Wind Engineering*, *43*(6), 609–624. https://doi.org/10.2307/26794274

Mokhtar, M., Marei, M. I., & El-Sattar, A. A. (2019). An adaptive droop control scheme for DC microgrids integrating sliding mode voltage and current controlled boost converters. *IEEE Transactions on Smart Grid*, *10*(2), 1685–1693. https://doi.org/10.1109/TSG.2017.2776281

Nikologiannis, M., Portokalidis, A., Karapidakis, E., Paspatis, A., Adebisi, B., Katsigiannis, Y., Seimenis, M., & Papadakis, M. (2024). Towards Net-zero Maritime Port Microgrids: The case study of the Heraklion Port. *IET Conference Proceedings*, *2024*(29), 619–624. https://doi.org/10.1049/icp.2024.4729

Robert H. Lasseter. (2007). Microgrids_And_Distributed_Generation. *Journal of Energy Engineering*, *133*, 144–150. https://doi.org/10.1061/(ASCE)0733-9402

Roy, A., Dutta, S., Bhattacharya, A., Biswas, S., & Roy, P. K. (2025). LFC based OPF with renewable energy, BESS and FOPID controller using QODTBO algorithm. *Journal of Energy Storage*, *115*. https://doi.org/10.1016/j.est.2025.115782

Soulatiantork, P., Cristaldi, L., Faifer, M., Laurano, C., Ottoboni, R., & Toscani, S. (2018). A tool for performance evaluation of MPPT algorithms for photovoltaic systems. *Measurement: Journal of the International Measurement Confederation*, *128*, 537–544. https://doi.org/10.1016/j.measurement.2018.07.005

Sridevi, H. R., Jagwani, S., Kulkarni, S. V., & Ravikumar, H. M. (2023). Frequency Control in an Autonomous Microgrid Using GA Based Optimization Technique. *Distributed Generation and Alternative Energy Journal*, *38*(2), 595–610. https://doi.org/10.13052/dgaej2156-3306.38210

Sridevi, H. R., Kulkarni, S. V., & Ravikumar, H. M. (2022). Voltage Regulation in an Islanded Microgrid using a GA-based Optimization Technique. *International Journal of Engineering Trends and Technology*, *70*(4), 15–20. https://doi.org/10.14445/22315381/IJETT-V70I4P202

Teleke, S., Baran, M. E., Bhattacharya, S., & Huang, A. Q. (2010). Rule-based control of battery energy storage for dispatching intermittent renewable sources. *IEEE Transactions on Sustainable Energy*, *1*(3), 117–124. https://doi.org/10.1109/TSTE.2010.2061880

Tungadio, D. H., & Sun, Y. (2020). Predictive controller for interconnected microgrids. *IET Generation,*

ISBN: 978-978-8567-02-8

Transmission and Distribution, *14*(19), 4273–4283. https://doi.org/10.1049/iet-gtd.2019.1257

Veronica, J., & Kumar, S. (2021). Control strategies for frequency regulation in microgrids Control strategies for frequency regulation in microgrids: A review A Jeya Veronica and N Senthil Kumar. *Source: Wind Engineering*, *45*(1), 107–122. https://doi.org/10.2307/27124358

Xue, D. . (2017). *Fractional-order control systems : fundamentals and numerical implementations*. De Gruyter.

ISBN: 978-978-8567-02-8

072-Performance Comparison of Type-1 and Type-2 Fuzzy Logic Controlled Shunt Active Power Filters for Harmonic Mitigation in Distribution Systems.

Hamisu Usman, Nuraddeen Magaji, Nasiru Bello Kadandani and Isiyaku Abubakar
Department of Electrical Engineering, Bayero University Kano. Nigeria
Corresponding Author: hamisuusman@kadunapolytechnic.edu.ng
Co-Author: nmagaji2000@gmail.com nbkadandani.ele@buk.edu.ng iabubakar.ele@buk.edu.ng

Abstract: Power quality (PQ) disturbances in modern power systems, such as voltage swells, sags, frequency deviations, interharmonics, and harmonic distortion remain persistent challenges that affect both consumers and utility providers. Among these issues, current harmonics generated by non-linear loads continue to demand effective mitigation strategies. Although passive power filters have traditionally been used to reduce harmonic distortion, they suffer from major drawbacks including bulky size, fixed compensation capability, and the risk of resonance with the grid. The emergence of Shunt Active Power Filters (SAPFs) has provided a more flexible and efficient alternative. This study investigates and compares the performance of Type-1 and Type-2 Fuzzy Logic Controllers (FLCs) implemented in a SAPF for current harmonic suppression. The Synchronous Reference Frame (SRF) method is employed for harmonic extraction, while a hysteresis current controller (HCC) generates switching pulses for the Voltage Source Inverter (VSI). Both controllers regulate the DC-link capacitor to ensure stable SAPF operation. Simulation results demonstrate that both Type-1 and Type-2 FLC-based SAPFs significantly reduce Total Harmonic Distortion (THD) to values compliant with IEEE 519-2014 standards. However, the Type-2 FLC exhibits superior harmonic mitigation capability and improved dynamic performance compared to its Type-1 counterpart.

Keywords: *Type-1 FLC, Type-2 FLC, Shunt Active Power Filter, harmonic mitigation, THD, IEEE 519-2014.*

Nomenclature

SAPF	Shunt active power filter
T1FLC	Type-1 fuzzy logic controller
T2FLC	Type-2 fuzzy logic controller
PWM	Pulse width modulation
VSI	Voltage source inverter
SVPMW	Space vector pulse width modulation
SRF	Synchronous reference frame
FLC	Fuzzy logic controller
LPF	Low pass filter
COA	Centre of area
COG	Centre of gravity
FOU	Foot print of uncertainty
E	error
CE	Change of error

1. INTRODUCTION

Electricity demand is seriously increasing everyday due to increase in teeming population in the entire world. This demand of electricity have resulted in proliferation of power electronics equipment to the consumers which are non linear in nature, such as Television set, uninterrupted power supply microwave ovens, fluorescent lamps computers, adjustable speed drives etc.

These electronics devices have resulted in poor power quality of the supply system, which causes excessive heating on neutral conductors, low power factor, constant tripping of circuit breakers, interference with neighboring communicating facilities and even caused failure of the entire power supply. As a result of these problems the supply system becomes distorted that caused current/voltage waveforms to deviate and the phenomenon known as harmonics.

However, the earlier solution to mitigate harmonics problem is the used of traditional passive power filters, but passive filters inherit some drawbacks such as heavy in size, very bulky, series and parallel resonances and fixed compensation that is why their application in harmonic filtering have become limited in service (Davi et al., 2016.), (Prakash & Shaik, 2016). With inception of SAPF which was initially presented in 1971 by Machida and Sasaki. (Jegadeeswari, 2019). Shunt active power filter in harmonics mitigation have become superior to passive power filter which mitigate almost all the harmonics and overcomes the draws back of the passive power filters. Several methods of harmonics current extractions were deployed in (Gautam, & Aeidapu

ISBN: 978-978-8567-02-8

2019.), (Czarnecki, 2006.), (Wunder, Boche, Strohmer, & Jung, 2015).

Consequently, type-1 fuzzy logic controllers had been used for many researchers and it was successfully implemented in electrical simulation design because it can handled non linearity, does not need any mathematical model and can work with imprecise inputs. Many research works on fuzzy logic controllers based shunt active power filters have been accomplished as reported in (Khan & Awale, 2022.), (S Musa, et al, n.d.), (Srinivas, District, Pradesh, District, & Pradesh, n.d.), (Keerthi, n.d.). In the same vein, T1FLC is simple in implementation as compared to T2FLC.

In this paper, comparison between T1FLC and T2FLC is explored. T2FLC is an extension of T1FLC with only difference in one block known as type reducer block. Type-2 fuzzy logic controller is superior to T1FLC because it can solve uncertainties of the system (Sharma, n.d.). In T1FLC, the memberships are crisp values while in T2FLC the memberships are also fuzzy itself. Synchronous reference frame (SRF) algorithm was deployed in extracting the current harmonic, while T2FLC was deployed keeping the DC-link voltage of the filter steady and steady. Also HCC was employed in triggering the gating signal of the (VSI).

2. METHODOLOGY

Here, the section explored the design of harmonic current extraction method for the SAPF circuit. Details analysis of both T1FLC and T2FLC are also explained.

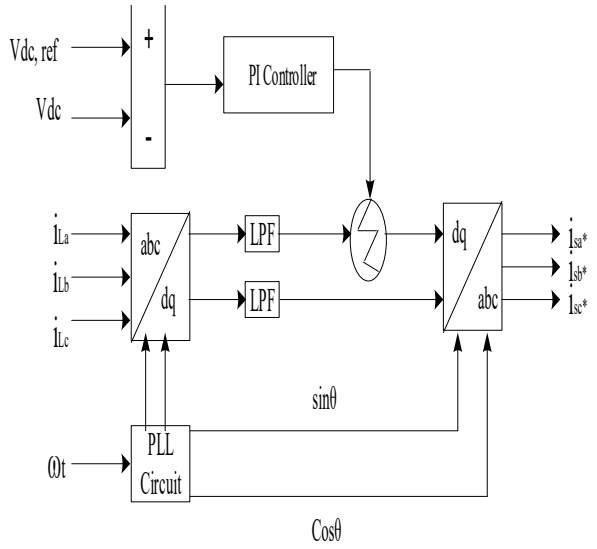


Figure 2.1 Synchronous reference frame

Since precise extraction directly affects the filter's efficiency, harmonic current removal is very vital for the SAPF design. For this article, harmonics are generated by the load current using the (SRF) algorithm. This approach provides a time-domain technique, which qualifies it for use in real-time applications.

The 3-ϕ stationary currents are transformed to a rotating direct-quadrature transform using the SRF approach. *Here,* The direct-axis current is represented by id responsible for removing harmonics; while the quadrature axis current is represented by iq was used for compensation the reactive power. Low-pass filters (LPF) are applied to the d-q components to isolate the fundamental frequency and remove higher-order harmonics.

$$i_d = i_a\, sin(\emptyset) + i_b\, sin(\emptyset - 120^0) + i_c\, sin(\emptyset + 120^0) \quad (1)$$

$$i_q = i_a\, cos(\emptyset) + i_b\, cos(\emptyset - 120^0) + i_c\, cos(\emptyset + 120^0) \quad (2)$$

After filtering, the d-q components are transformed back into three-phase stationary currents for compensation using the inverse Park transformation. This method is perfect for dynamic power systems with varying load situations since it guarantees quick and precise harmonic detection and extraction.

2.2 Hysteresis Current Controller

This controller is a time domain analysis. It is obvious for the gating signal of the voltage source inverter (VSI) to be triggered, and various techniques are used such as pulse width modulation (PWM), Fuzzy logic controllers, PI controllers, space vector pulse width modulation (SVPWM), sliding mode controllers etc. In this article, hysteresis current controller was adopted in triggering the gating signal of the voltage source inverter because of its simple in implementations, robust and dynamic. The gating pulses to the inverter are achieved by comparing the current error signal with the hysteresis band. However, the error signal is setup within the two stationary hysteresis bands (i.e lower and upper bands). The switching pulses depend on the two expressions as:
If $I_a < (i_{a*}\text{-HB})$ the upper switch is OFF while the lower switch is ON, also.
If $I_a > (i_a\text{-HB})$ the upper switch is ON while the lower switch is OFF. Figure 2.2 shows the switching pattern of the hysteresis current controller.

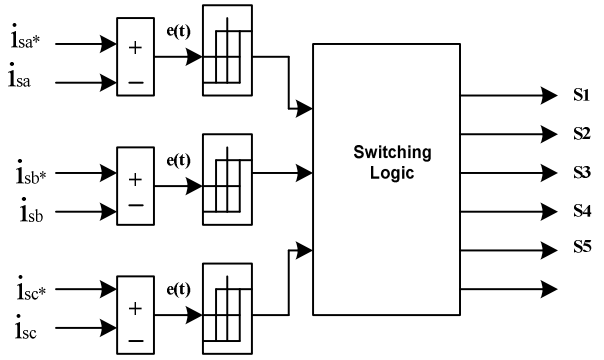


Figure 2.2 Switching pattern of hysteresis current controller.

2.3 T1FLC Structure

The idea of T1FL system was brought by Zadeh Lotfi a Californian University Professor in 1965(Ali, Ali, & Sumait, n.d.). Type-1 fuzzy logic controller is used instead of traditional controllers such as PI and PID due to their limitations of tuning. By using T1FLC, The system's overall performance can be enhanced. (Suleiman Musa, Amran, et al., n.d.).

The applications of FLC have gained interest by researchers in the application of SAPFontrol algorithms, because of its simplicity in design, accept imprecise inputs/outputs and do not require any mathematical modeling. T1FLC is a nonlinear artificial intelligent controller (Panati, Ramasamy, Ahsan, Haider, &

ISBN: 978-978-8567-02-8

Rodrigues, n.d.)This controller, used a linguistic language such as "if then" rules. However, type-1 fuzzy logic controller is characterized by its resilience and precise trucking efficiency and its constant reaction(Hemasri & Kumar, 2024).
The structure of T1FLC which include four blocks as depicted in Figure 2.3.

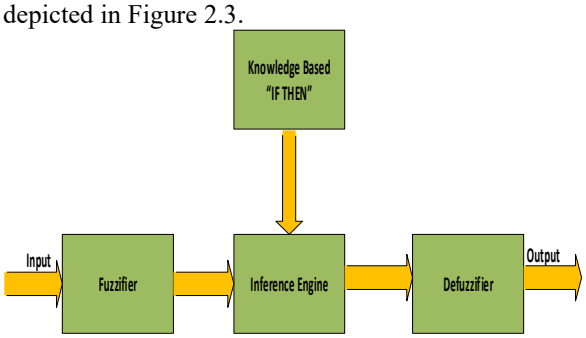


Figure 2.3 Structure of type-1 Fuzzy logic controller

Fuzzifier: The initial block of the FLC, designed to transform the input data error (e) and its derivative (Δe) into fuzzified values that the fuzzy controller's membership sets can identify.

Knowledge Base: This procedure includes the system's data and rule base. The input and output membership functions that provide a suitable message to the fuzzification and defuzzification respectively, are included in the database. However, the rule base used linguistic rules based on the intended fuzzified input members to the proper control procedure.

The fuzzy controller's inference engine method takes linguistic rules and transforms the input system into the desired fuzzified output level.

The defuzzifier is in charge of converting the output data that has been fuzzified by the functions of the output membership to the process system that has to be managed. The following describes the fuzzy logic controller:

The fuzzy logic controller was simulated using a straightforward Mandani approach due to its straightforward design, lack of mathematical model, and ability to handle imprecise inputs.

The defuzzification technique also made use of the centre of area (COA) method, also known as centre of gravity (COG). However, the type-1 fuzzy logic controller was designed using a single output and two inputs, error (e) and change of error (Δe).

2.4 Type-2 Fuzzy Logic Controller structure

Zadeh Lotfi started the creation of T2FLCs to address the uncertainties of type-1 fuzzy logic sets since type-1 fuzzy logic controllers are unable to handle the uncertainties of the systems.

Researchers' interest in this field has grown due to the use of type-2 fuzzy logic sets to solve uncertainties. The traditional T1FLC is expanded upon by the T2FLC (Ozek & Akpolat, n.d.). Nevertheless, each membership function grade in T2F sets is fuzzy in and of itself, but each membership grade in T1F sets is a distinct value.

T1FL has four blocks, which is the primary distinction between type-2 and T1FLC. Such as inference engines, rule bases, fuzzifiers, and defuzzifiers. The fuzzifier, rule base, inference engine, type reduction block, and defuzzifier process are the five blocks that make up a type-2 fuzzy logic controller. Similarly, one of the fundamental differences between the two controllers is that the T1FLC has a type reduction block, whereas the T1FC does not. To address the issue of non-linearity and uncertainty in type-1 fuzzy logic controllers, T2FLC offer an extra degree of freedom. A type-2 fuzzy logic controller has a three-dimensional membership function, whereas a T1FLC has a two-dimensional membership function.

The expression in equation (2) represents the uncertainty in type-1 fuzzy logic sets.

$$A = \left(x, \mu_p(x)\right) / \forall_x \in X \qquad (3)$$

Where $\mu_p(x)$ present membership grade of the variable **x** as shown in equation (3), with the degree of freedom between 0 and 1. Because each value of x has a membership level of 0 or 1, the uncertainty in a T1F set cannot be assessed or identified. The T2FL membership function must be applied in order to resolve the issue of uncertainty inherited in the type-1 fuzzy logic set since the membership level of the variable cannot be identified and determined.

Figure 2.3 and Figure2.4 shows the T1 and T2 Triangular Membership Functions respectively(Mendel, 2015) .

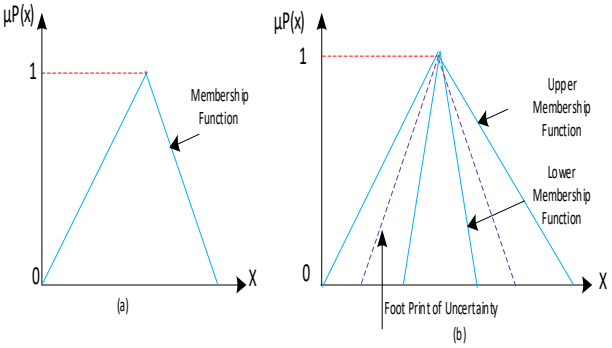


Figure 2.4 (a) T1 triangular membership (b) T2 triangular membership.

The mathematical expression for a type-2 fuzzy logic set is represented in equation (4).

$$\overline{A} = \left\{\left(x, u, \left(\mu_x(x,u)\right)\right)\right\} / \forall_{x\epsilon X}, \forall_{u\epsilon J_x^u} \subset [0,1] \qquad (4)$$

$$\overline{A} = \int_{x \in X} 1 \int_{u \in J_x} \mu_{\bar{A}}(x,u) / (x,u) J_x \subseteq [0,1]$$

Where:
X = function of input variable
Xx = input value of the variable
U = primary grade to type-2 fuzzy set and
J_x = primary membership function
$\mu_A(x,u)$ = Secondary membership function. Hence as in equations (4) and (5).

$$\overline{A} = \int_{x \in X} 1 \int_{u \in J_x} 1 / \mu_{\bar{A}}(x,u) J_x \subseteq [0,1] \qquad (5)$$

$$\overline{A} = \int_{x \in X} 1 \int_{u \in J_x} 1 / \mu_{\bar{A}}(x,u) J_x \in [0,1] \qquad (6)$$

Here, $J_{x\epsilon}[0,1]$ and double integral are the union of all values of x and u. Nevertheless, the secondary values are ascertained by equation (6) following the defuzzification process.

ISBN: 978-978-8567-02-8

$$\overline{A} = \int_{x \in X} 1 \left[\int_{u \in J_x} f_x(u)/u \right] / x, J_x \subseteq [0,1] \quad (7)$$

An equal area of geometrical shape known as the footprint of uncertainty (FOU) is constructed in order to have good membership functions because type-1 membership functions lack a uniform shape. Additionally, equation expresses the footprint of uncertainty (FOU). The general structure of type-2 fuzzy logic controller is depicted in Figure 2.5.

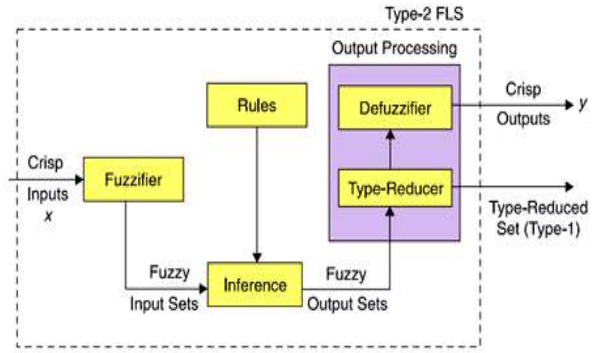


Figure 2.5 Structure of type-2 fuzzy logic controller (Habiba, n.d.)

As indicated in Figure 2.5, the crisp values that are sent into the fuzzifier are transformed into type-2 fuzzy sets at the fuzzifier block's output. The inference engine and the rule base blocks, where the union and intersections procedures are obtained, now both activate the fuzzified output type-2 fuzzy sets. To further reduce the type-2 fuzzy sets into type-1 fuzzy sets, the type reduction block was given the inference engine's output.

To get the clear output values, the fuzzification block further defuzzifies the T1 reduced fuzzy sets. Similarly, there are several ways to acquire the type reduction techniques, including:

- Karnik-Mendel Algorithm (KM)
- Enhanced Karnik-Mendel Algorithm (EKM)
- Iterative algorithm with stop condition (IASC)
- Enhanced Iterative Algorithm with stop condition (EIASC)
- Enhance Opposite Direction Searching Algorithm (EODS)
- Wu-Mendel Uncertainty Bound Method (WM)
- Nie-Tan Method (NT)
- Begain-Melek-Mendel Method (BMM)
- User Defined Function.

The Nie-Tan method of type reduction (TR) is used more preparedly in this work since, in comparison to other methods; it provides accurate outputs with less complexity and quick convergence [18].

2.5 Type-1 Fuzzy Logic Controller Design

In this work, the design of the T1FLC is summarized as follows:

- Fuzzy inference system (FIS) of five triangular membership functions with two input error and its derivative and single output was used.
- Secondly, another seven triangular membership functions with two inputs and single output was also utilized for the purpose of comparisons.
- Five and seven rule based was also utilized for the five and seven triangular membership respectively.
- A simple Mandani approach was used in the simulation process of the fuzzy logic controller, because of its simplicity in design, does not need any mathematical model and can work with imprecise inputs.
- The method of centre of area (COA) or simply called centre of gravity (COG) was also employed in the defuzzification process.

2.6 Membership function selection

Membership function (MF) selection is one of the most critical steps in the design of a fuzzy logic controller (FLC). So, (5 by 5) and (7 by 7) membership functions are selected for comparison. In Shunt Active Power Filters (SAPF), the controller must generate fast and accurate compensation currents to mitigate harmonics and reactive power. Because the performance of the FLC strongly depends on how input variables are fuzzified, the shapes, ranges, overlap ratios, and numbers of MFs must be carefully chosen. This presents a systematic, engineering-oriented approach to MF selection for both Type-1 FLC (T1FLC) and Interval IT2FLC deployed in a three-phase SAPF for harmonic mitigation.

Figure 2.6 and 2.7 shows the 5 and 7 triangular membership function for the fuzzy logic controller design.

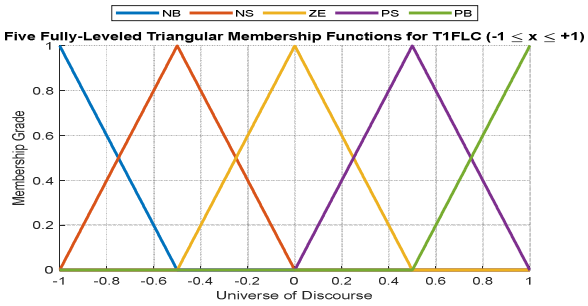


Figure 2.6 Type-1 triangular (5) membership functions.

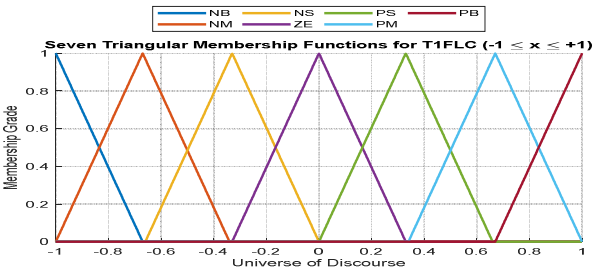


Figure 2.7 Type-1 triangular (7) membership functions.

2.7 Rule Tables

The T1FLC and IT2FLC employ identical five-rule linguistic structures to ensure fair comparison; Two tables were constructed, Table 1 and Table 2 are 25 and 49 rules for both T1FLC and T2FLC for comparative analysis respectively.

ISBN: 978-978-8567-02-8

TABLE I. RULE TABLE FOR FIVE TRIANGULAR MEMBERSHIP FUNCTIONS.

CE / E	NB	NS	ZE	PS	PB
NB	PB	PB	PB	PS	ZE
NS	PB	PS	PS	ZE	NS
ZE	PS	PS	ZE	NS	NS
PS	ZE	NS	NS	NS	NB
PB	NS	NS	NB	NB	NB

TABLE II. RULE TABLE FOR SEVEN TRIANGULAR MEMBERSHIP FUNCTIONS.

CE / E	NB	NM	NS	ZE	PS	PM	PB
NB	NB	NB	NM	NM	NS	ZE	ZE
NM	NB	NM	NM	NS	ZE	PS	PS
NS	NM	NM	NS	ZE	PS	PS	PM
ZE	NM	NS	ZE	ZE	ZE	PS	PM
PS	NS	ZE	PS	ZE	PS	PM	PM
PM	ZE	PS	PS	PS	PM	PM	PB
PB	ZE	PS	PM	PM	PM	PB	PB

2.8 T2FLC Design

Zadeh had introduced the concept of T2FLC. as an T1FLC extender. Fuzzification, rule bases, fuzzy inference engines, defuzzification, type reduction, and block processes are all included in the structure of FLCT-2, which is quite similar to that of FLCT-1.

-Fuzzification process: In this T2FLC, 2 inputs, error (E) and its derivative (ΔE) with a single output is presented. Figure 2.8 and Figure 2.9 displays the triangle membership functions for a single output and both inputs. The fuzzy labels are Positive Big (PB), Positive Medium (PM), Positive Small (PS), Negative Big (NB), Negative Medium (NM), Negative Small (NS) and Zero (ZE).

Type-2 rules are identical to type-1 rules. However, IT2F sets are used to indicate precedents and their effects. The generated Table 1 and Table 2, summarizes the diagonal rules table for the case where the error and its derivative are getting close to zero with a quick rising time.

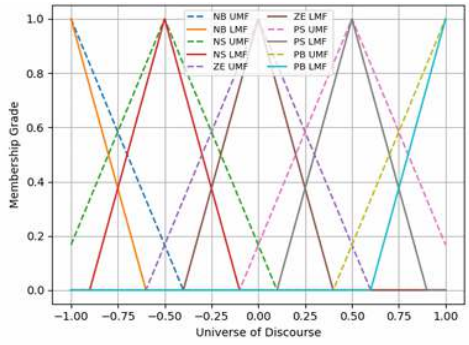


Figure 2.8 T2 triangular (5) Membership functions.

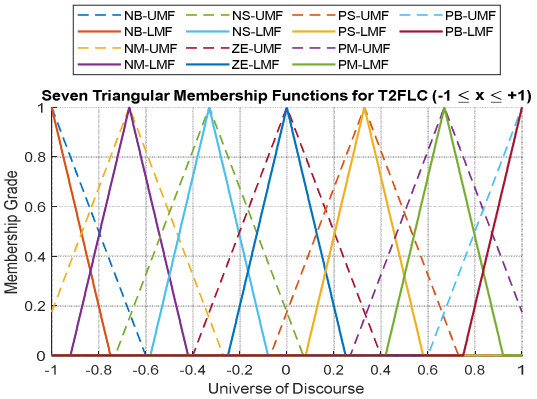


Figure 2.9 T2 Triangular (7) Membership functions.

Table III. Simulation parameters

Parameter	Values & units
Main supply frequency	50Hz
Source voltage/phase (peak)	220V
Source inductance (L_S)	0.03mH
Source resistance (R_S)	0.15Ω
Line inductance (L_r)	1mH
Line resistance (R_r)	1Ω
Load inductance (L_L)	2mH
Load resistance (R_L)	40Ω
Filter inductance (L_f)	3mH
dc link Voltage (V_{dc})	700V
dc link Capacitance (C_{dc})	3000μF

3. SIMULATION RESULTS AND DISCUSSIONS

The simulation findings were covered in this section. for the proposed (SAPF) using the two type of controllers T1FLC and its counterpart T2FLC. The results also show the performances of the designed 5 and 7 triangular memberships' functions respectively.

3.1 Scenario I.

Here, the results of T1FLC using five triangular membership functions were presented. As depicted in Figure 2.10, were the load current is non linear in nature due to non linear load.

ISBN: 978-978-8567-02-8

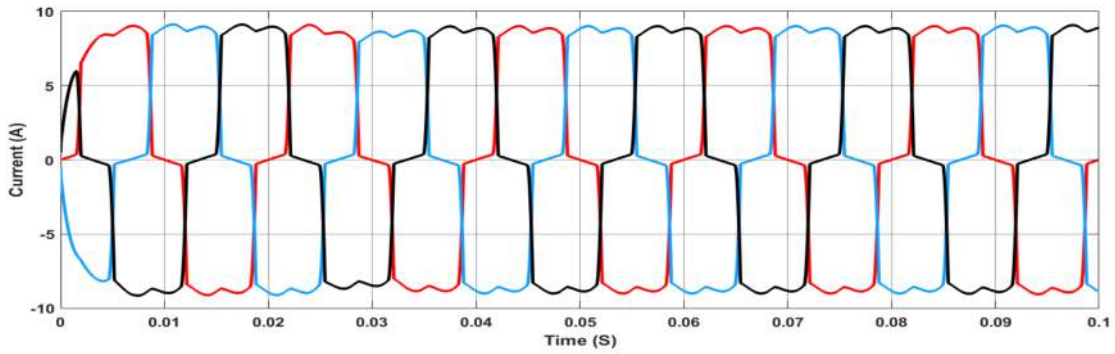


Figure 2.10 The Load current without SAPF

However, Figure 2.11 shows the source voltage and is sinusoidal waveform. Figure2.12 depicts the Fast Forier Transform for the load current for THD% of 24.65%. Also, Figure 2.13 is the source current of 1.21% THD% after applying SAPF. Figure 2.14 depicts the dc- link voltage of the SAPF which indicates a settling time of 0.07s. This means that the SAPF was able to remove the unwanted harmonics produced by loads.

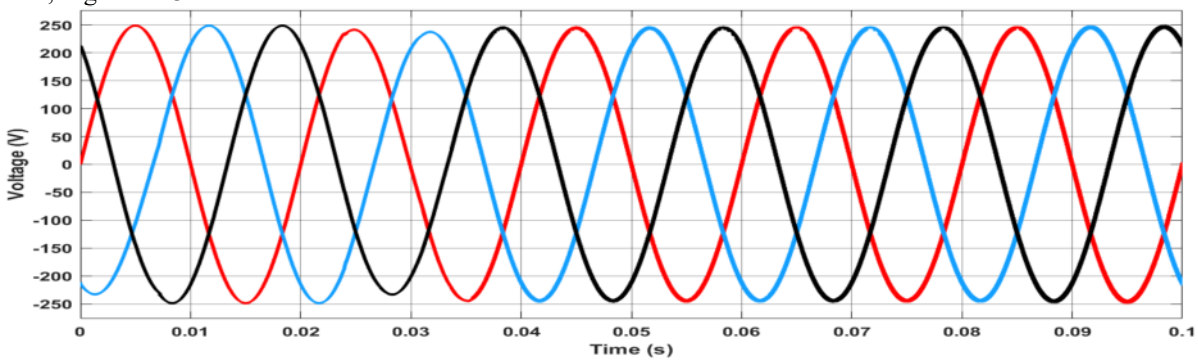


Figure 2.11 Supply source voltage

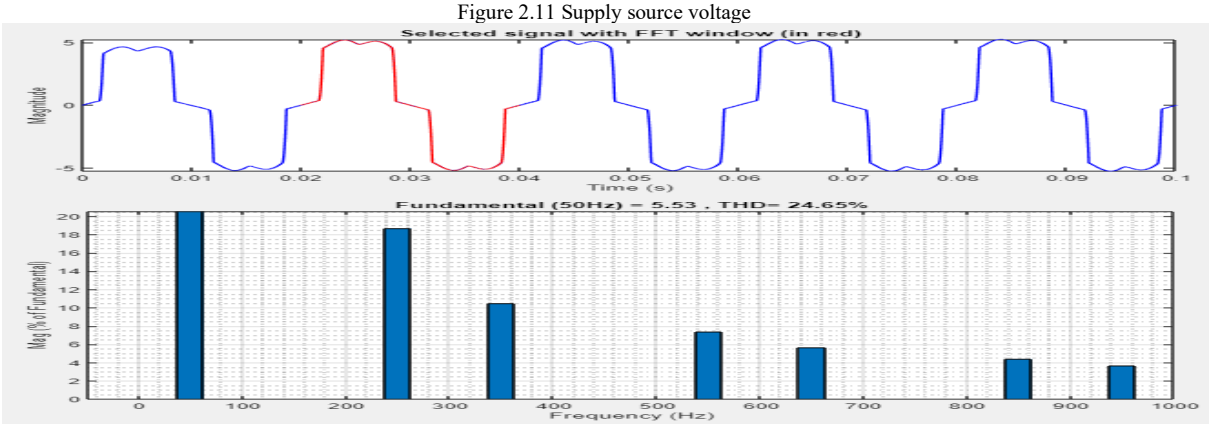


Figure 2.12 FFT of the load current without SAPF

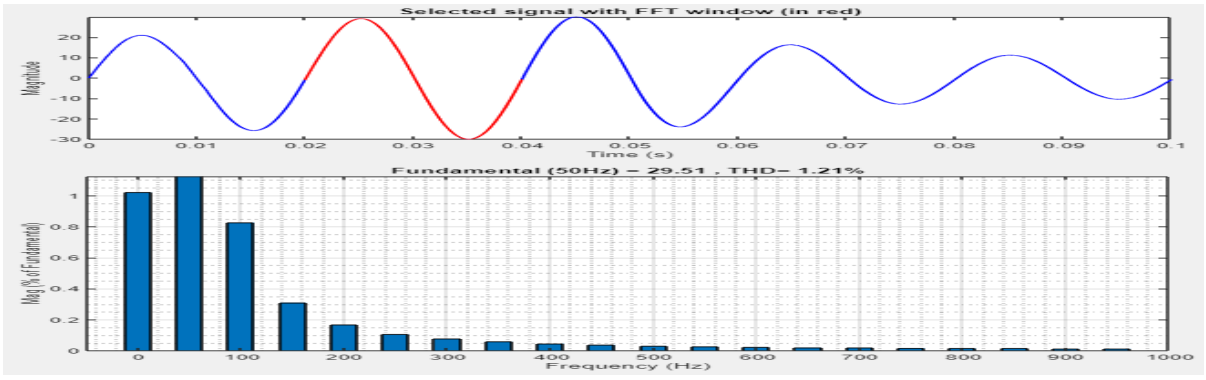


Figure 2.13 FFT of Source current after applying SAPF

ISBN: 978-978-8567-02-8

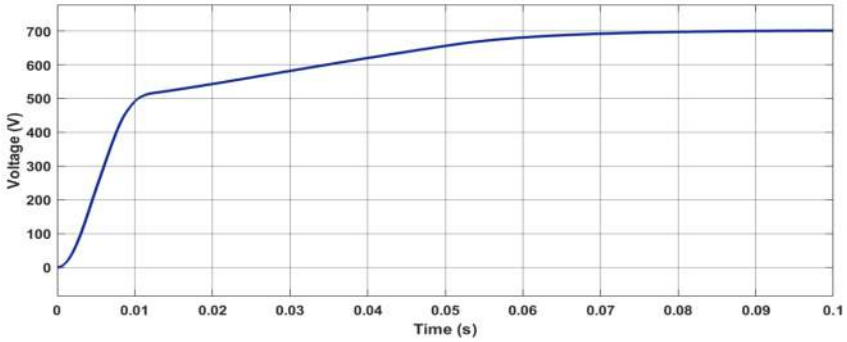


Figure 2.14 DC link voltage of the SAPF

3.2 Scenario II.

Results of T2FLC using five Triangular Membership Functions are presented. As seen in Figure 2.15, the load current is distorted due to non linear load of the system, while Figure 2.15 is the load current of the system without injecting a filter. Moreover, Figure 2.16 depicts the source voltage and maintained to be purely sinusoidal. Figure 2.17 is the Fast Fourier Transform result for the source current of THD% of 1.41%.

In the same vein, Figure 2.18 is the result of the FFT of the source current after applying SAPF which gives the THD% of 1.40%. Figure 2.19 displays the filter's stabilized DC link voltage at 0.04s.

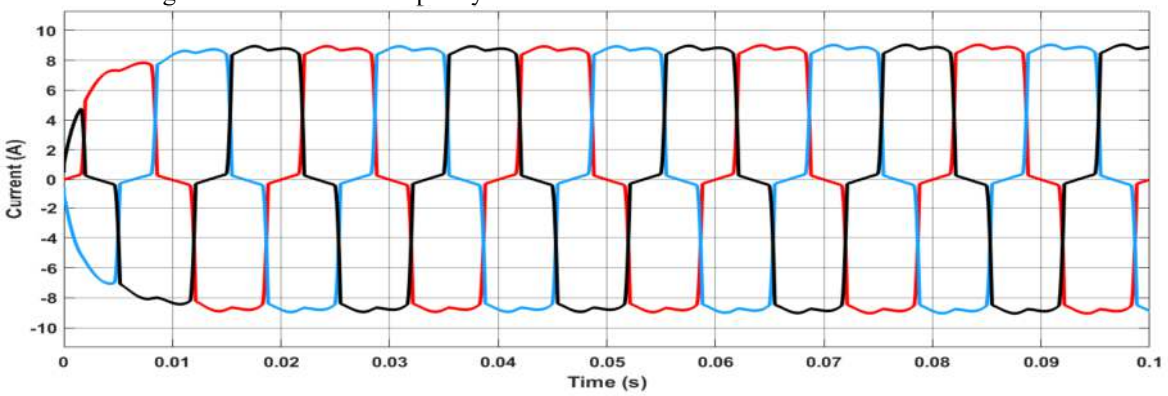


Figure 2.15 Load current without SAPF

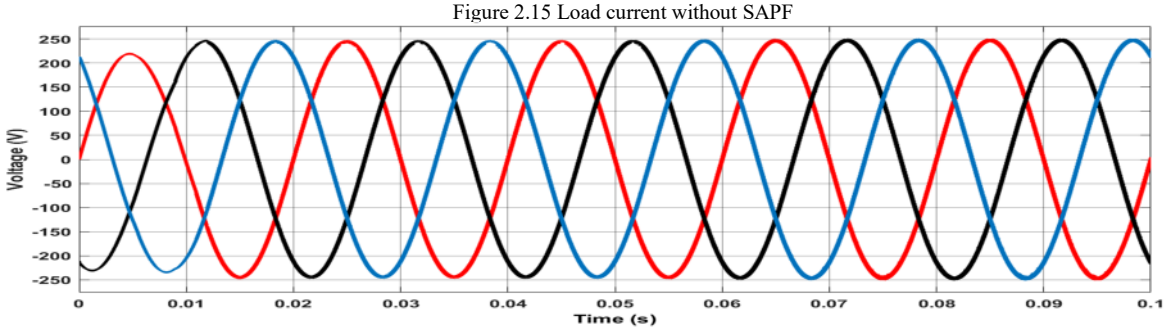


Figure 2.16 Source voltage

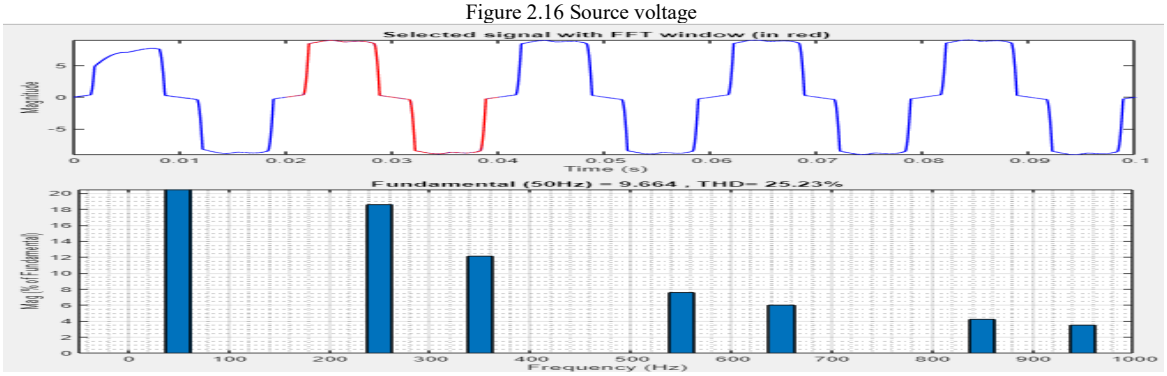


Figure 2.17 FFT for the load current without SAPF

ISBN: 978-978-8567-02-8

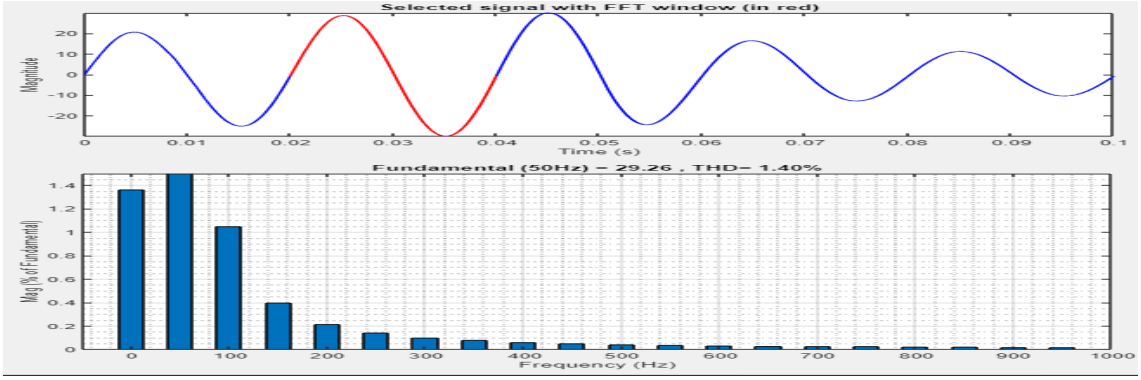


Figure 2.18 FFT of source current with SAPF

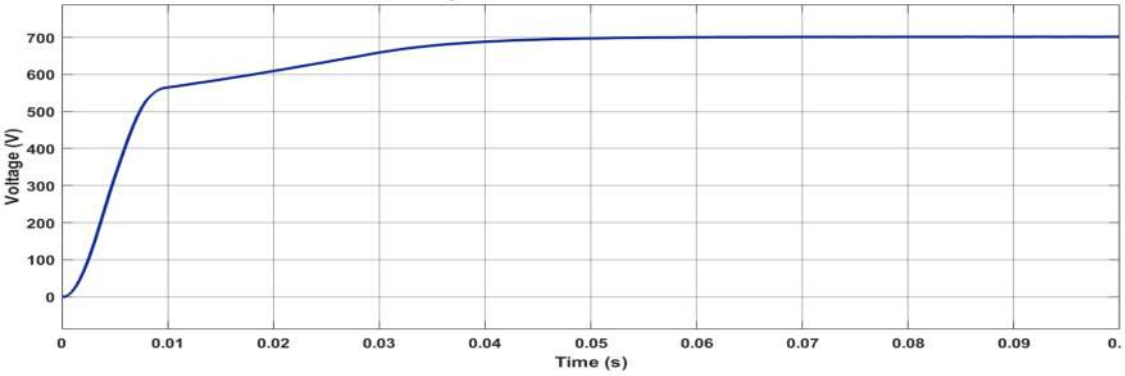


Figure 2.19 DC link voltage of the SAPF

3.3 Scenario III.

The results of T1FLC using seven membership functions are presented. As seen in Figure 2.20, the load current is distorted, while Figure 2.21 is the source current. In Figure 2.22, the load current was obtained to be 25.23% THD. Figure 2.23 depicts the source current of THD% 1.40%, while Figure 20.24 depicts the dc- link voltage of the filter and was stabled at 0.07s.

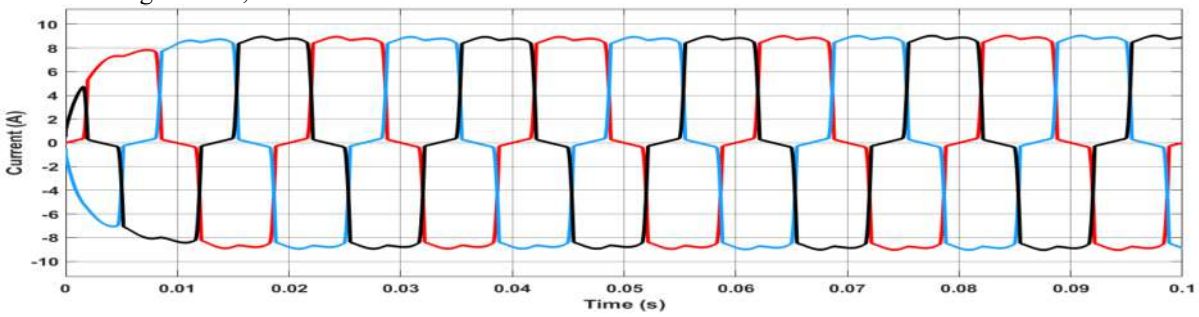


Figure 2.20 Load current before applying shunt active power filter.

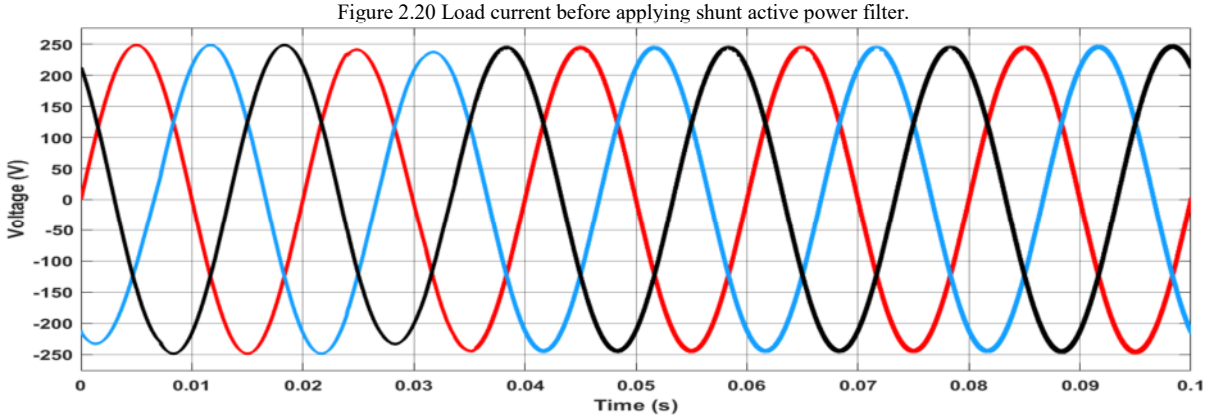


Figure 2.21 Load current before applying shunt active power filter

ISBN: 978-978-8567-02-8

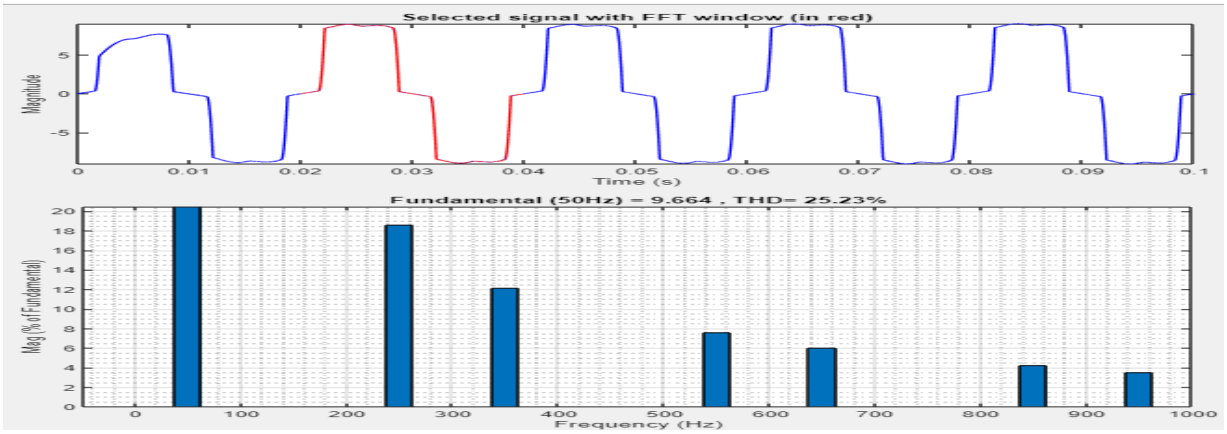


Figure 2.22 FFT analysis of the load current before applying shunt active power filter.

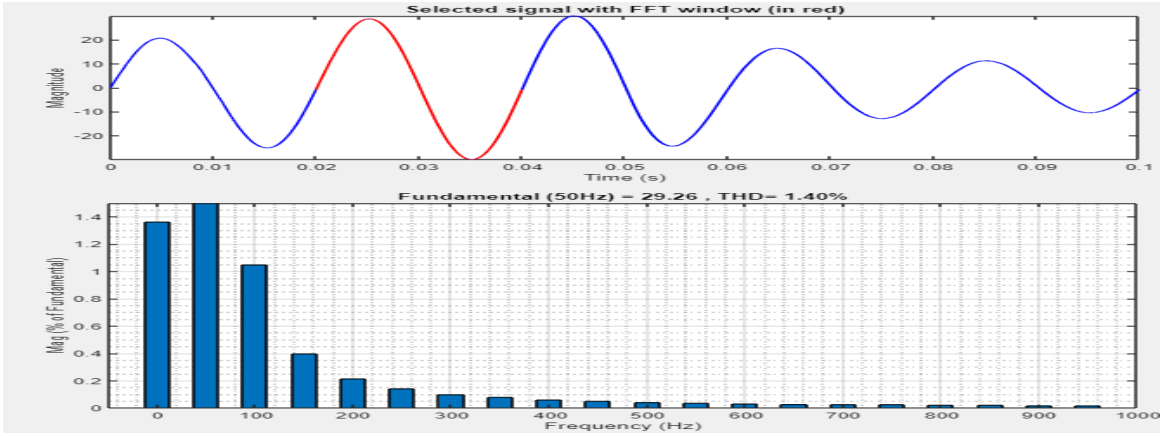


Figure 2.23 FFT analysis of the source current after applying shunt active power filter.

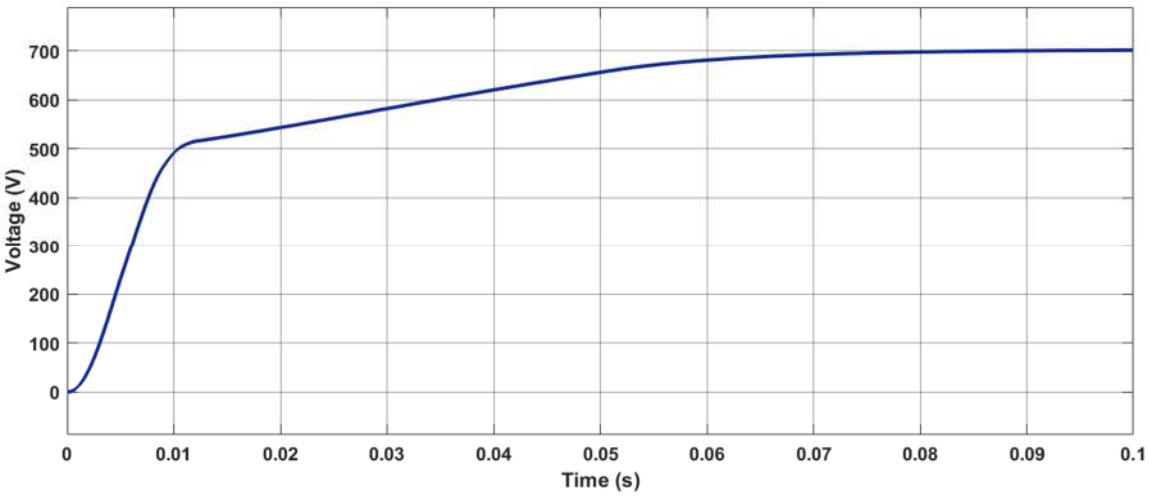


Figure 2.24 DC link voltage of the SAPF

3.3 Scenario IV

Results of T2FLC using seven Triangular Membership functions are presented. As depicted in Figure 2.25 is the load current is distorted. While Figure 2.26 is the sinusoidal source voltage. Figure 20.27 is the load current with THD% value of 25.25% without SAPF. However, Figure 20.28 gives the resultant source current of THD value of 1.23%. Figure 20.29 is the Dc link voltage which stabled at 0.04s.

ISBN: 978-978-8567-02-8

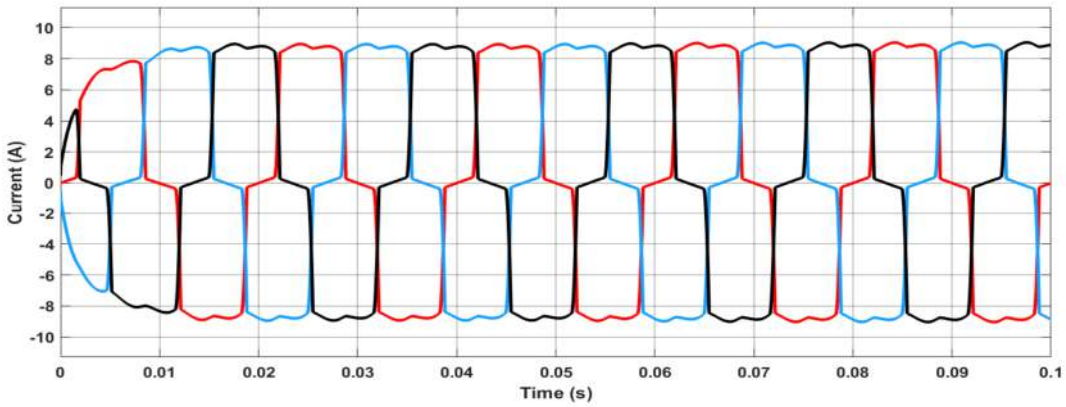


Figure 2.25 Load current before applying shunt active power filter.

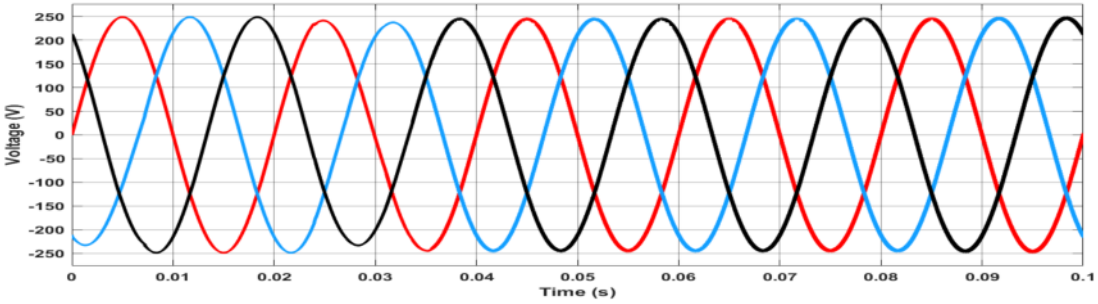


Figure 2.26 Source voltage.

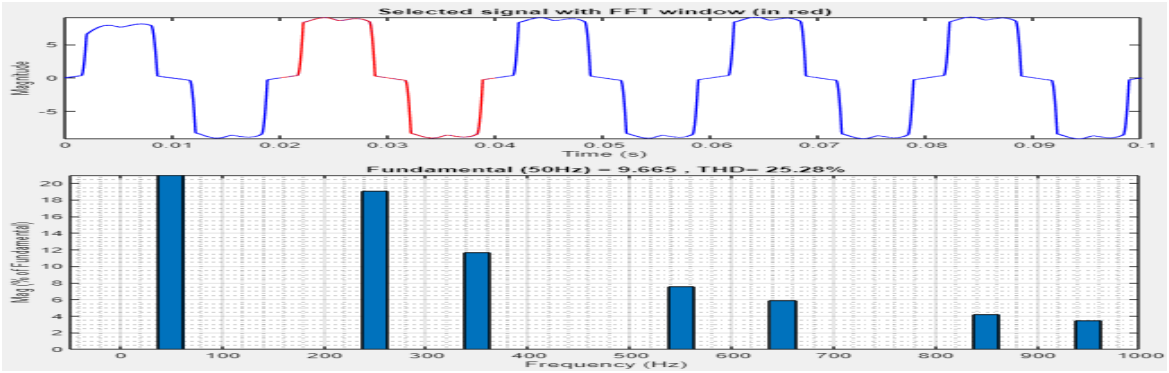


Figure 2.27 FFT analysis of the load current without SAPF.

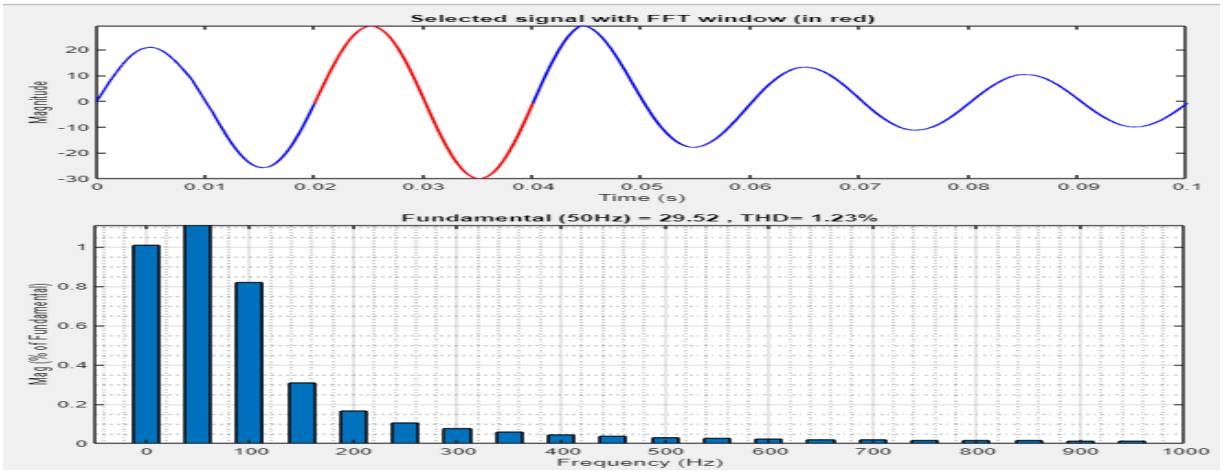


Figure 2.28 FFT analysis of the source current after applying shunt active power filter.

ISBN: 978-978-8567-02-8

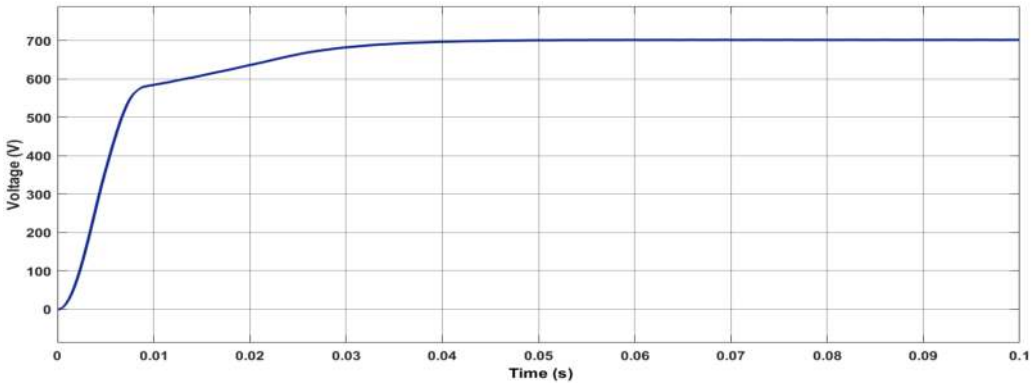


Figure 2.29 DC link voltage of the SAPF

3.4 DC link voltage comparisons

Figure 20.30 shows the comparison of the dc- link voltage of the SAPF due to five membership function modeling. The two results have show the settling time of 0.07s and 0.04s for both T1FLC and T2FLC respectively. This indicates that the result obtained using T2FLC was superior to its counterpart T1FLC. Similarly, for Figure 20.31, a similar result was obtained for seven membership functions, in which the dc- link voltage was found to be 0.05s and 0.04s as settling times for both using T1FLC and T2FLC respectively. However, the T2FLC have performed better than that of T1FLC.

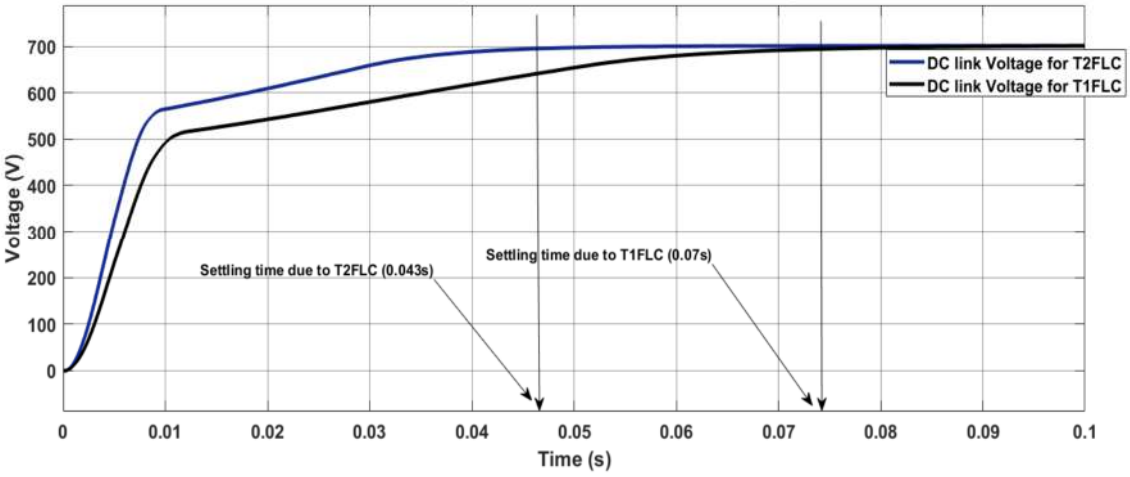


Figure 20.30 DC link voltages with 5 Membership function.

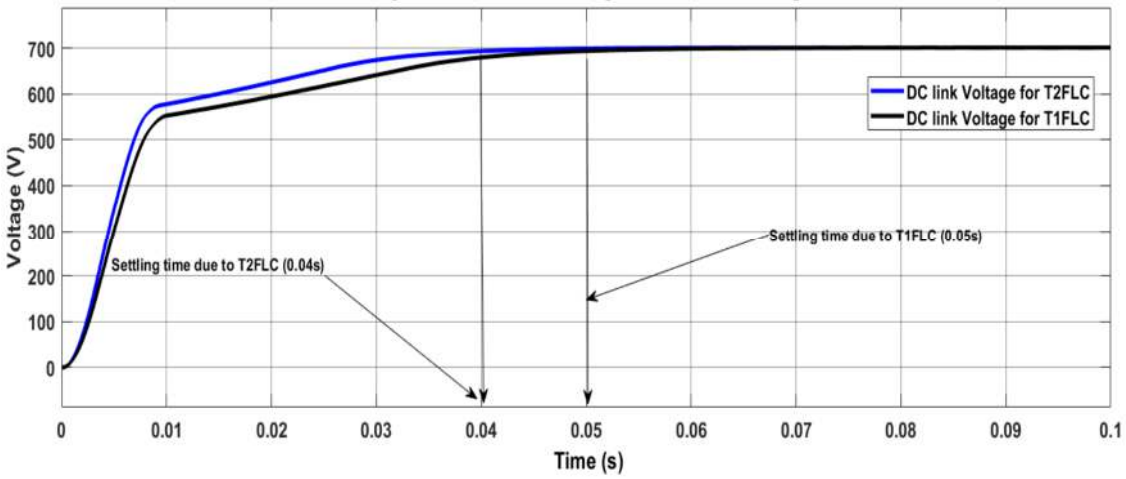


Figure 20.31 DC link voltages with 7 membership function.

4. CONCLUSION

This paper compared the performances of two controllers, that is, T1FLC and T2FLC in suppressing harmonics distortions produced. The results show that both controllers have mitigated current harmonic distortions and all the results are within the stipulated harmonic standard norm of IEEE 519-2014 limit. However, the results obtained with T2FLC found to be superior to its counterpart T1FLC. For the case of DC link voltages, also the T2FLC have shown better results than that of T1FLC.

ISBN: 978-978-8567-02-8

REFERENCES

Ali, O. A. M., Ali, A. Y., & Sumait, B. S. (2016.). Comparison between the Effects of Different Types of Membership Functions on Fuzzy Logic Controller Performance, *3*(3), 76-83.

Czarnecki, L. S. (2006.). Instantaneous Reactive Power p-q Theory and Power Properties of Three-Phase Systems, *21*(1), 362-367.

Davi, T., et al (2024). Passive Filter Aided by Shunt Compensators Based on the Conservative Power Theory, *52*(4), 3340-3347.

Gautam, S. (2019.). Sine Cosine Algorithm Based Shunt Active Power Filter For Harmonic Compensation. *2019 3rd International conference on Electronics, Communication and Aerospace Technology (ICECA)*, (1), 1051-1056. IEEE.

Habiba, B. (2023). Harmonic Compensation in Five Level NPC Active Filtering : Analysis , Dimensioning and Robust Control Using IT2 FLC, *72*, 227-247.

Hemasri, K., & Kumar, C. S. (2024). Fuzzy Controller with Shunt Active Power Filter in Reducing THD for Three Phase System. *International Transactions on Electrical Engineering and Computer Science.*, *3*(2), 101-108.

Jegadeeswari, G. (2025). Performance Analysis of Power Quality Improvement using Shunt Active Power Filter. *International Journal of Recent Technology and Engineering*, *7*(5S2), 1-3.

Keerthi, S. S. (2025.). Shunt active Power Filter Performance Evaluation Using Artificial Neural Networks and 6-Switch 2-Leg Inverter with PI / Fuzzy Logic Controlled Transformerless, *10*, 488-496.

Khan, M. A., & Awale, R. N. (2023.). International Journal of Research Publication and Reviews Fuzzy Based Power Quality Improvement using Active Power Filter, *3*(7), 3225-3236.

Mendel, J. M. (2015). *a Retrospective* (pp. 1-10). doi:10.1007/s00287-015-0927-4

Musa, S, et al (2014.). Fuzzy Logic Controller Based Three Phase Shunt Active Power Filter for Harmonics Reduction, 371-376.

Musa, et al. (2017.). Modified Synchronous Reference Frame Based Shunt Active Power Filter with Fuzzy Logic Control Pulse Width Modulation Inverter. doi:10.3390/en10060758

Ozek, M. B., & Akpolat, Z. H. (2024). A Software Tool : Type-2 Fuzzy Logic Toolbox, 1-10. doi:10.1002/cae.20138

Panati, P. et al. (2022). Indirect Effective Controlled Split Source Inverter-Based Parallel Active Power Filter for Enhancing Power Quality.

Prakash, O., & Shaik, A. G. (2020). Topological aspects of power quality improvement techniques : A comprehensive overview. *Renewable and Sustainable Energy Reviews*, *58*(2016), 1129-1142. Elsevier. doi:10.1016/j.rser.2015.12.251

Sharma, S. K. (2024.). A Novel Approach to Power Quality Improvement in Distribution Systems Using Fuzzy Logic Controller and PWM-Based Shunt Active Power Filter with Harmonics Reduction, *14*(1), 47-58.

Srinivas, V., et al (2025). MATLAB-SIMULINK model based shunt active power filter using fuzzy logic controller to minimize the harmonics Article History Received : 26 Oct 2020 | Revised : 31 Oct 2020 | Accepted : 05 Nov 2020, *9*(5), 101-110.

Wunder, G., et al. (2015). Sparse Signal Processing Concepts for Efficient 5G System Design. *IEEE Access*, *3*(3), 195-208. IEEE. doi:10.1109/ACCESS.2015.2407194

ISBN: 978-978-8567-02-8

073-Prediction of Unconfined Compressive Strength of Laterite - Black Cotton Soil - Cement Kiln Dust Blends for Landfill Liner Design Using Response Surface Methodology

Adamu Umar Chinade[1,2], Gambo Haruna Yunusa[2], Umar Chinade Musa[3]

[1]*Department of Civil Engineering, Abubakar Tafawa Balewa University, Bauchi*
[2]*Department of Civil Engineering, Bayero University, Kano*
[3]*Department of Architecture, Federal Polytechnic, Bauchi*
Corresponding Author's email; umarchinade@atbu.edu.ng

Abstract: The design of compacted soil liners for landfills requires materials that combine adequate strength, low permeability, and sustainability. This study applies Response Surface Methodology (RSM) within Design Expert to predict the unconfined compressive strength (UCS) of laterite - black cotton soil (BCS) blends amended with cement kiln dust (CKD). A central-composite design varied BCS content from 5 % to 30 % and CKD from 2 % to 12 % by weight of laterite, with specimens cured for 14 days. UCS measurements ranged from 350 kN/m² to 1200 kN/m². Quadratic polynomial models were fitted, yielding R^2 values of 0.9729, 0.9887, and 0.9896 for BSH, WASC, and BSL compaction energies, respectively, all with $p < 0.001$. CKD emerged as the dominant factor, boosting UCS by up to 35 % when added at 12 % with water content 2 % below optimum moisture content (OMC). Conversely, BCS above 17.5 % reduced strength. The highest UCS (1200 kN/m²) was obtained with a combination of 30 % BCS, 12 % CKD, and water content 2 % below OMC, compacted at BSH energy, satisfying typical compacted soil liner criteria. Validation tests confirmed predictions within an error margin of 5% (α), underscoring the reliability of the developed models.

Keywords: landfill liner, UCS prediction, response surface methodology, laterite, black cotton soil, cement kiln dust.

1. INTRODUCTION

The safe containment of municipal solid waste in engineered landfills depends critically on the performance of compacted soil liners, which must exhibit adequate strength, low permeability, and long-term durability (Chinade *et al.,* 2017). Conventional clayey soils are often employed for this purpose, but their availability and performance limitations have prompted research into alternative soil blends and industrial by-products that can meet design criteria while enhancing sustainability (Umar *et al.,* 2025). Lateritic soils, abundant in tropical regions, are attractive candidates due to their fine-grained texture and relatively low hydraulic conductivity (Yamusa and Ahmad, 2018). However, laterite alone may not always achieve the required mechanical strength (Chinade and Yunusa, 2024). Black cotton soil (BCS), rich in montmorillonite, is widely available but suffers from high swelling and shrinkage, which compromise its geotechnical reliability (Mai-Bade et al., 2021). Blending laterite with BCS and stabilizing with additives offers a pathway to engineer soils with improved performance for landfill liner applications.

Among stabilizers, cement kiln dust (CKD); a by-product of cement manufacturing has gained attention as a sustainable alternative to Portland cement (Adeyanju and Okeke, 2019). According to Moses and Saminu (2012), CKD contains free lime and reactive silica, enabling pozzolanic reactions that enhance soil strength and reduce permeability. Recent studies have demonstrated its potential in landfill liner construction. Abdel-Rahman *et al.* (2025) reported that CKD-sand soil mixes achieved satisfactory strength and hydraulic conductivity for municipal landfill liners. Similarly, Bagonza (2025) highlighted CKD's effectiveness in stabilizing sandy soils for subgrade construction, underscoring its role as a low-cost, environmentally beneficial stabilizer. These findings align with broader sustainability goals by valorizing industrial by-products and reducing CO_2 emissions associated with cement production.

Predicting the mechanical performance of CKD-stabilized soils is essential for optimizing mix proportions and compaction conditions. The unconfined compressive strength (UCS) is a key parameter in assessing liner suitability, reflecting both structural integrity and resistance to deformation (Chinade and Yunusa, 2025). Traditional trial-and-error approaches to mix design

ISBN: 978-978-8567-02-8

are resource-intensive, motivating the adoption of statistical and computational tools. Response Surface Methodology (RSM) has emerged as a powerful framework for modeling complex interactions among soil constituents, stabilizer content, and compaction variables (Abdi *et al.,* 2022). By employing central composite designs and fitting polynomial regression models, RSM enables efficient exploration of factor effects and identification of optimal conditions.

Recent applications of RSM in geotechnical engineering illustrate its versatility. Somadas *et al.* (2024) applied RSM to optimize soft soil stabilization using novel materials, achieving significant improvements in strength and durability. Similarly, biopolymer-treated soils have been successfully modeled using RSM to predict strength properties under varying dosages and curing conditions. These studies confirm RSM's utility in capturing nonlinear interactions and guiding mix design for soil stabilization.

Despite these advances, limited research has focused on mixed soil blends stabilized with CKD specifically for landfill liner design. To the best of our knowledge, this is the first study to apply RSM to predict the UCS of laterite–BCS–CKD blends for landfill liner design, highlighting the novelty of combining these locally available soils with an industrial by-product stabilizer. This study addresses this gap by applying RSM within Design Expert software to predict the UCS of laterite–BCS–CKD blends under different compaction energies. A central composite design was employed to vary BCS and CKD contents, with specimens cured for 14 days. The resulting models provide insights into the dominant role of CKD in enhancing strength, threshold effects of BCS content, and the influence of water content relative to optimum moisture. Beyond advancing predictive modeling, the findings contribute to sustainable landfill liner design by valorizing industrial by-products and optimizing locally available soils.

2. MATERIALS AND METHOD

2.1 Materials

The laterite soil used was collected from a borrow pit within Bauchi Town in Bauchi State, Nigeria, at depth of about 1.5 m to avoid organic contamination. Preliminary classification followed ASTM D247-11 and AASHTO-12, with particle size distribution, Atterberg limits, and specific gravity determined.

Black cotton soil sample was obtained from expansive soil deposits in Yemaltu Deba local government area of Gombe State. The soil is known for its high montmorillonite content, which imparts significant swelling and shrinkage tendencies. Laboratory tests confirmed a liquid limit above 50 % and a plasticity index exceeding 25 %, consistent with expansive soil behavior (Muhammad *et al.,* 2021, Batari *et al.,* 2017). The BCS was air-dried, pulverized, and sieved through a 4.75 mm mesh before blending.

Cement kiln dust was sourced from the Ashaka cement industry, Funakaye Local Government Area of Gombe State. Chemical composition was determined using X-ray fluorescence (XRF), revealing high contents of CaO, SiO_2, and Al_2O_3, indicative of pozzolanic potential. The CKD was oven-dried at 105 °C for 24 hours and stored in airtight containers to prevent moisture absorption prior to use.

Potable tap water was used for specimen preparation. Moisture content was adjusted relative to the optimum moisture content (OMC) determined from compaction tests.

2.2 Method

2.2.1 Experimental Design

Response Surface Methodology (RSM)

Design Expert software (version 13) was employed to develop predictive models for unconfined compressive strength (UCS). A central composite design (CCD) was adopted, with two independent variables:

- BCS content: 5 %–30 % by weight of laterite.
- CKD content: 2 %–12 % by weight of laterite.

The design matrix included factorial points, axial points, and center points to ensure model robustness. Quadratic polynomial models were fitted to the UCS data, with statistical significance assessed using analysis of variance (ANOVA). Table I shows the factor and factor levels adopted for the design of experiment.

TABLE I: FACTORS AND FACTOR LEVELS

		Factor levels of code			
		Lower level	Mid-level	upper level	Level(*Cat)
Factor	Code	-1	0	+1	
CKD (%)	A	2	7	12	
BCS (%)	B	5	17.5	30	
*CE	C	-2		+4	4

*CE: Compaction Energy (BSH, WAS, BSL)

*Cat: Categorical factors

2.2.2 Compaction Energy Levels

Three compaction energies were considered:

- British Standard Light (BSL): 2.5 kg rammer, 300 mm drop high and 27 blows per layer.
- West African Standard Compaction (WASC): 4.5 kg rammer, 450 mm drop and 10 blows per layer.
- British Standard Heavy (BSH): 4.5 kg rammer, 450 mm drop and 27 blows per layer.

Optimum moisture content (OMC) and maximum dry density (MDD) were determined for each blend under the respective compaction energies.

2.2.3 Specimen Preparation

- Soil blends were prepared by thoroughly mixing laterite with designated proportions of BCS and CKD.
- Water was added to achieve target moisture contents, which includes -2%, 0 (OMC), +2 % and +4 % referenced to the OMC.
- The mixtures were compacted into cylindrical molds (38 mm diameter × 76 mm height) in

ISBN: 978-978-8567-02-8

three layers, each compacted to the specified energy.

- Specimens were extruded and sealed in polythene bags to prevent moisture loss.
- Curing was carried out for 14 days at laboratory ambient conditions (25 ± 2 °C, relative humidity 60–70 %).

2.2.4 Unconfined Compressive Strength

The Unconfined compressive strength tests were performed in accordance with ASTM D2166. Specimens were loaded axially at a strain rate of 1 mm/min until failure. Peak compressive strength was recorded for each specimen. UCS values ranged between 350 kN/m² and 1200 kN/m² depending on mix proportions and compaction energy.

2.2.5 Model Validation

Predicted UCS values from RSM models were compared with experimental results. Validation tests were conducted on additional specimens prepared under optimal conditions identified by the models. Prediction accuracy was assessed using mean absolute percentage error (MAPE), with deviations within 5 % considered acceptable.

2.2.6 Data Analysis

Statistical analysis was performed using Design Expert. The model's adequacy was evaluated using coefficient of determination (R^2), adjusted R^2, and p-values. Response surface plots and contour plots were generated to visualize factor interactions.

Sensitivity analysis identified CKD as the dominant factor influencing UCS.

3. RESULTS AND DISCUSSION

3.1 Material Characterization

Preliminary characterization of the soils revealed distinct differences between laterite and black cotton soil. The laterite exhibited a liquid limit of 30 %, plastic limit of 17 %, and plasticity index of 13 %, while the black cotton soil showed much higher values of 58 %, 23 %, and 35 %, respectively. The percentage passing sieve No. 200 was 12 % for laterite and 82 % for black cotton soil, reflecting the finer nature of the latter. Based on these properties, the soils were classified as A-2-6 (2) and A-7-6 (41) under the AASHTO system (M 145-2012) and as SC and CH under the Unified Soil Classification System (ASTM D 2487-2011). These classifications are consistent with the observed engineering behaviors of the soils, where parameters such as swelling, shrinkage, compressibility, strength, and permeability are strongly correlated with liquid and plastic limits (Benson *et al.,* 1999, Osinubi and Nwaiwu, 2005).

The cement kiln dust (CKD) used in stabilization was found to have a specific gravity of 2.6, bulk density of 0.7 Mg/m³, and pH of 11.5, with major oxides being CaO (63.7 %) and SiO_2 (16.8 %). The high calcium oxide content is particularly significant, as it promotes cation exchange and hydration reactions similar to those in cement, thereby improving soil stability. Previous studies have confirmed that CKD rich in CaO and moderate alkalis (e.g., 4.6 % Na_2O) reduces the plasticity of clay soils, enhancing their geotechnical performance (Ogila & Eldamarawy, 2022). This supports the suitability of CKD as a stabilizing agent for large-scale soil improvement projects

3.2 Model Development and Adequacy

Application of Design Expert (13) to the unconfined compressive strength (UCS) data confirmed that a quadratic polynomial model provided the most appropriate fit across all compaction energies (BSH, WASC, and BSL). Regression equations derived at moisture contents of –2 %, 0 %, +2 %, and +4 % relative to the optimum moisture content (OMC) consistently captured the nonlinear effects of black cotton soil (BCS) and cement kiln dust (CKD) contents. The regression-based models are presented in Equations 1 – 12 for both compaction energies. The equations are in actual factors for practical use.

Analysis of variance (ANOVA) Table II, demonstrated that the models were statistically significant, with F-values of 121.43 (BSH), 131.30 (WASC), and 22.24 (BSL), all exceeding the critical F-value of 3.187 at $\alpha = 0.05$. The associated p-values (< 0.0001) confirmed that both main effects (BCS and CKD), their interaction, and quadratic terms contributed significantly to UCS variation.

Goodness-of-fit metrics further validated model adequacy. Coefficients of determination (R^2) ranged from 0.9729 to 0.9896, indicating that the models explained 97–99 % of the variance in UCS. Adjusted R^2 values (0.9506–0.9810) and predicted R^2 values (0.7868–0.8996) were in close agreement, with differences less than 0.20, confirming model robustness and predictive reliability. Adequate precision (AP) ratios between 24.83 and 44.54 exceeded the recommended minimum of 4, ensuring sufficient signal-to-noise ratios for navigating the design space. The reported ranges of R^2, adjusted R^2, predicted R^2, and adequate precision (AP) values are consistent with results from recent studies applying regression and response surface methodology (RSM) to soil stabilization and UCS prediction. Teodoru *et al.* (2025) demonstrated that regression models for cement-treated soils achieved R^2 values above 0.97, adjusted R^2 above 0.95, and AP ratios well above the threshold of 4, confirming both robustness and predictive reliability. Similarly, Wang (2025) applied automated machine learning techniques to UCS prediction and reported close agreement between adjusted and predicted R^2 values, with differences below 0.20, validating the models' reliability.

Diagnostic plots of predicted versus actual; Figure 1 (a, b, c) confirmed normal distribution and absence of systematic trends, substantiating the suitability of the quadratic models for UCS prediction.

Equations 1 – 4: Equations in terms of actual factors for BSH compaction energy

$$UCS = 380.016 + 21.8141BCS + 94.6418CKD + 0.896BCS * CKD - 0.564745BCS^2 - 5.48966CKD^2 \quad (-2) \ldots\ldots\ldots 1$$

ISBN: 978-978-8567-02-8

$$UCS = 193.162 + 31.4024BCS + 122.159CKD + 0.688BCS * CKD - 0.854621BCS^2 - 7.42138CKD^2 \ (0) \ldots\ldots\ldots 2$$

$$UCS = 229.064 + 22.5839BCS + 104.14CKD + 0.70BCS * CKD - 0.60811BCS^2 - 6.12069CKD^2 \ (+2) \ldots\ldots\ldots 3$$

$$UCS = 293.371 + 12.9242BCS + 74.4171CKD + 0.636BCS * CKD - 0.353986BCS^2 - 4.17241\ CKD^2 \ (+4) \ldots\ldots\ldots 4$$

Equations 5 – 8: Equations in terms of actual factors for WAS compaction energy

$$UCS = 356.513 + 17.0078BCS + 82.5195CKD + 0.72BCS * CKD - 0.420414BCS^2 - 4.62759CKD^2 \ (-2) \ldots\ldots\ldots 5$$

$$UCS = 397.711 + 5.33195BCS + 61.5966CKD + 0.60BCS * CKD - 0.0971034BCS^2 - 3.0069CKD^2 \ (0) \ldots\ldots\ldots 6$$

$$UCS = 238.431 + 16.5549BCS + 87.854CKD + 0.68BCS * CKD - 0.441379BCS^2 - 4.95862CKD^2 \ (+2) \ldots\ldots\ldots 7$$

$$UCS = 261.401 + 10.1025BCS + 67.2563\ CKD + 0.52BCS * CKD - 0.25931BCS^2 - 3.62069\ CKD^2 \ (+4) \ldots\ldots\ldots 8$$

Equations 9 – 12: Equations in terms of actual factors for BSL compaction energy

$$UCS = 305.391 + 14.0893BCS + 75.2232CKD + 0.52BCS * CKD - 0.156469BCS^2 - 4.0469CKD^2 \ (-2) \ldots\ldots\ldots 9$$

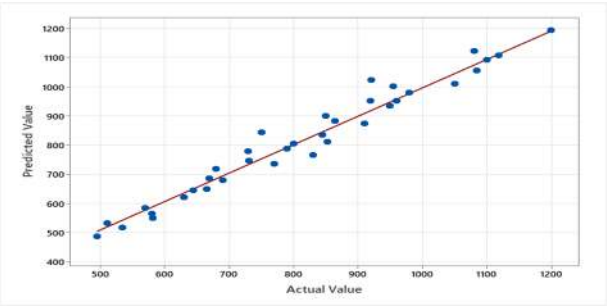
$$UCS = 332.51 + 7.02308BCS + 58.891CKD + 0.56BCS * CKD - 0.0971034BCS^2 - 2.97793CKD^2 \ (0) \ldots\ldots\ldots \ (10)$$

$$UCS = 206.679 + 13.598BCS + 75.9949CKD + 0.56BCS * CKD - 0.355752BCS^2 - 4.22345CKD^2 \ (+2) \ldots\ldots\ldots (11)$$

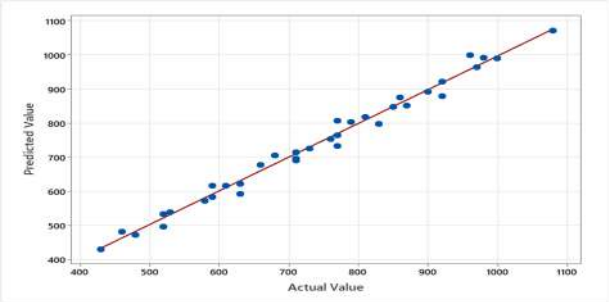
$$UCS = 181.523 + 11.3903BCS + 63.5423CKD + 0.44BCS * CKD - 0.291531BCS^2 - 3.42207CKD^2 \ (+4) \ldots\ldots\ldots (12)$$

Table II: ANOVA of UCS results

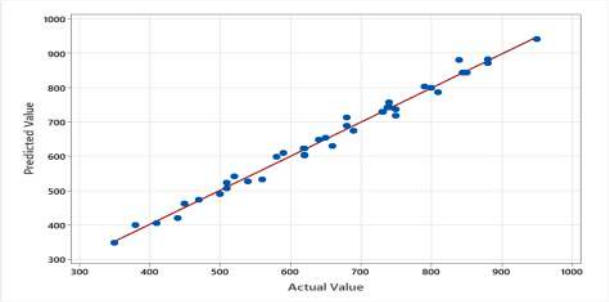
Response Parameters	Compaction Energy		
	BSH	WASC	BSL
Mean	866.92	768.08	671.77
Standard deviation	41.87	22.39	19.54
Coefficient of variation	4.83	2.91	2.91
Predicted residual error sums of squares (PRESS)	1.628E+05	66138.85	39843.07
R-squared (R^2)	0.9729	0.9887	0.9896
Adjusted R-squared (Adj R^2)	0.9506	0.9795	0.9810
Predicted R-squared (Pred R^2)	0.7868	0.8991	0.8996
Adequate precision (AP)	24.8308	42.1296	44.5441
Model F-value	121.43	131.30	200.24
P-value	< 0.0001	< 0.0001	< 0.0001



(a). BSH compaction



(b). WAS compaction



(c). BSL compaction

Figure 1: Predicted versus Actual for (a). BSH, (b). WASC, (c). BSL

3.3 Influence of Black Cotton Soil (BCS) Content

Response surface and contour plots (Figures 2– 4) at OMC consistently revealed that UCS decreased with increasing BCS content. This trend reflects the high montmorillonite fraction in BCS, which induces swelling, shrinkage, and microstructural weakness in compacted blends. At contents above 17.5 %, BCS exerted a pronounced negative effect on UCS. These findings corroborate earlier reports that expansive soils, when used in high proportions, compromise mechanical stability (Fondjo *et al.* 2021). However, blending with laterite and stabilizing with CKD mitigates these limitations, enabling controlled use of BCS in landfill liner design (Chinade and Yunusa, 2025). The response surface and contour plots for specimens compacted at -2%, +2% and +4 % for BSH, WAS and BSL compaction energies are shown in Appendices A, B and C respectively. Similar trends were observed as that of specimens compacted at optimum moisture content.

ISBN: 978-978-8567-02-8

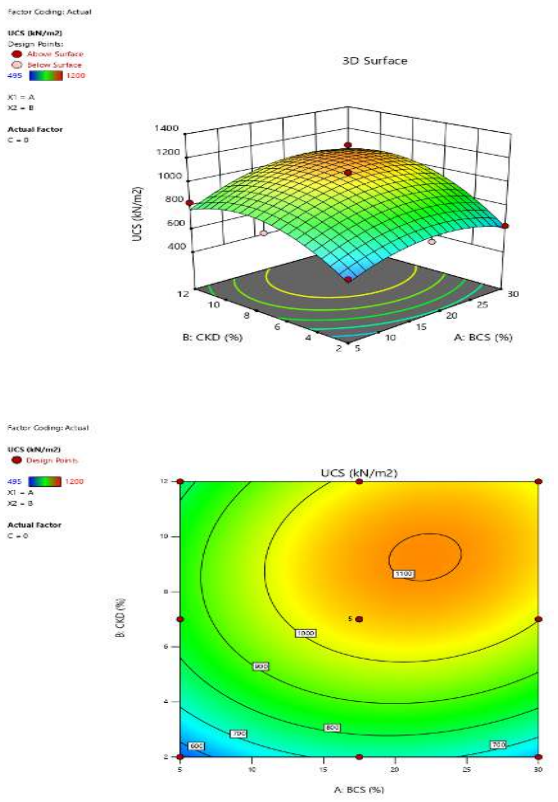


Figure 2: Response surface and contour plots of UCS against BCS & CKD for BSH compaction energy

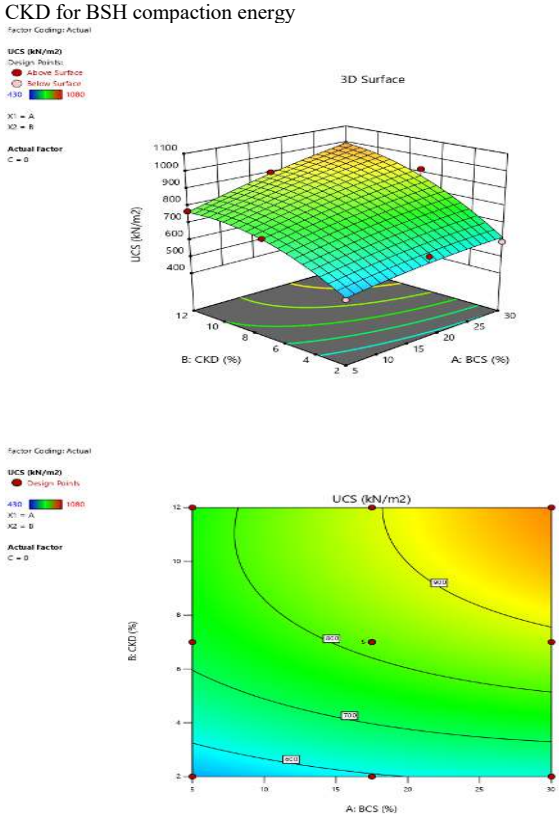


Figure 3: Response surface and contour plots of UCS against BCS & CKD for WASC compaction energy

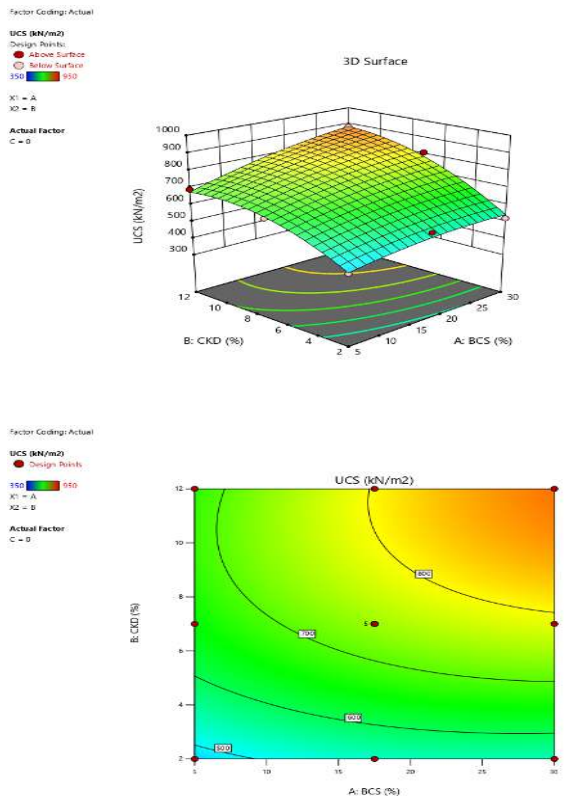


Figure 4: Response surface and contour plots of UCS against BCS & CKD for BSL compaction energy

3.4 Influence of Cement Kiln Dust (CKD) Content

Cement kiln dust emerged as the dominant factor influencing UCS. Across all compaction energies, UCS increased with CKD addition, with maximum gains observed at 12 % CKD. The pozzolanic reactions between CKD's free lime and soil silicates contributed to cementitious bonding, densification, and strength enhancement (Yan *et al.* 2025, Bagonza, 2025). At BSH compaction energy, UCS improved by up to 35 % when CKD was added at 12 % with water content 2 % below OMC. This demonstrates CKD's capacity to offset the deleterious effects of BCS and highlights its role as a sustainable stabilizer for landfill liner applications.

3.5 Interaction Effects of BCS and CKD

The regression equations and response surface plots confirmed significant interaction effects between BCS and CKD. While BCS alone reduced UCS, its combination with CKD moderated this decline, producing synergistic improvements in strength. The interaction term (BCS × CKD) was consistently positive across compaction energies, indicating that CKD effectively stabilizes BCS-laterite blends. This interactive behavior underscores the importance of optimizing both factors simultaneously rather than in isolation, a key advantage of the response surface methodology approach (Yan *et al.,* 2025; Ogila and Eldamarawy, 2022).

ISBN: 978-978-8567-02-8

3.6 Effect of Compaction Energy and Moisture Content

Compaction energy exerted a strong influence on UCS outcomes. The highest UCS values were consistently obtained under BSH energy, followed by WASC and BSL. This hierarchy reflects the increased dry density and reduced void ratio achieved at higher compaction efforts. Moisture content relative to OMC also affected UCS. Specimens compacted at 2 % below the Optimum Moisture Content exhibited superior strength compared to those at OMC or above due to better particle packing and reduced pore pressure. This behavior can be attributed to the fact that slightly lower moisture levels promote closer particle arrangement and stronger interparticle bonding, while avoiding excess pore water that weakens the soil matrix. Excess moisture (+2 % and +4 %) reduced UCS due to pore water pressures and weakened particle bonding. Thus, the observed peak UCS at –2% OMC highlights the critical role of moisture control in landfill liner construction, where small deviations from OMC can significantly alter strength performance. These findings align with established compaction theory, reinforcing the need for precise moisture control in landfill liner construction (Umar *et al.,* 2016; Tijjani *et al.,* 2021).

3.7 Optimal Mix Proportions and Validation

The highest UCS (1200 kN/m²) was achieved with a blend of 30 % BCS, 12 % CKD, and water content 2 % below OMC, compacted at BSH energy. This value satisfies typical compacted soil liner strength criteria (UCS ≥200 kN/m^2), confirming the suitability of the blend for landfill applications (Osinubi and Nwaiwu, 2005, Widomski *et al.,* 2018).

Validation tests demonstrated that predicted UCS values were within 5 % (α) of experimental results, confirming the reliability of the RSM models for practical design purposes.

3.8 Practical Implications

The results highlight several practical implications for landfill liner design:

Material utilization: Laterite–BCS blends stabilized with CKD provide a sustainable alternative to conventional clay liners, particularly in tropical regions where laterite and BCS are abundant.

Waste valorization: CKD, an industrial by-product, is effectively repurposed as a stabilizer, reducing environmental burdens associated with cement production.

Predictive modeling: RSM offers a robust tool for optimizing soil blend proportions and compaction conditions, reducing reliance on trial-and-error experimentation.

By integrating CKD stabilization, expansive soil management, and predictive modeling, this study advances sustainable geotechnical practice and provides a framework for landfill liner design tailored to local material availability.

4. CONCLUSIONS

The study demonstrated the potential of Response Surface Methodology (RSM) in predicting the unconfined compressive strength (UCS) of laterite–black cotton soil (BCS) blends stabilized with cement kiln dust (CKD). The quadratic polynomial models achieved excellent adequacy, with R^2 values above 0.97 and adjusted R^2 exceeding 0.95, while predicted R^2 values remained close to 0.90, confirming the reliability of the approach. Increasing BCS content reduced UCS due to its expansive nature, but CKD addition significantly enhanced strength, with maximum gains of about 35 % observed at 12 % CKD. The positive interaction between BCS and CKD highlighted CKD's ability to mitigate the adverse effects of expansive soils, enabling their use in landfill liner applications. Compaction energy and moisture conditions further influenced performance, with the highest UCS values achieved under BSH compaction and moisture content 2 % below the Optimum Moisture Content (OMC). The optimal blend; 30 % BCS + 12 % CKD, and slightly reduced moisture of 2% below OMC produced a UCS of 1200 kN/m², meeting landfill liner strength requirements. Model predictions were validated within a 5 % (α) error margin, underscoring the robustness of RSM for practical geotechnical design. Integrating CKD stabilization, laterite + BCS blending, and predictive modeling offers a sustainable and technically sound solution for landfill liner construction, combining environmental benefits with reliable engineering performance. However, the study was limited to 14-day curing and strength assessment only.

5. RECOMMENDATIONS

Based on the findings, the following recommendations are proposed;

Landfill liner construction: Laterite–BCS blends stabilized with CKD should be considered as viable alternatives to conventional clay liners, particularly in tropical regions where these soils are abundant.

CKD utilization: Cement kiln dust, an industrial by-product, should be promoted as a sustainable stabilizer, reducing environmental burdens associated with cement production.

Compaction control: Field compaction should aim for energy levels equivalent to at least WASC to BSH and moisture contents maintained slightly below OMC to achieve maximum UCS.

Design optimization: RSM can be adopted as a predictive tool in geotechnical practice to optimize soil blend proportions and compaction parameters, reducing reliance on trial-and-error experimentation.

Future work should investigate long-term durability and field-scale validation to fully establish the suitability of these blends for landfill liner application.

Acknowledgments

The authors wish to express their sincere gratitude to Bayero University, Kano and Abubakar Tafawa Balewa University, Bauchi for their invaluable support and contributions toward the success of this study. Their

ISBN: 978-978-8567-02-8

assistance was instrumental in facilitating the research and is greatly appreciated. *The authors declare no conflict of interest.*

REFERENCES

AASHTO (2012). Standard Specifications for Classification of soils and Soil-Aggregate Mixtures for Highway Construction Purposes. M145-2012, American Association of State Highway and Transportation Officials, Washington D. C.

Abdel-Rahman A. H; Mahmoud F. Awad-Allah; Khaled M. Mamdouh. "Experimental Study on Utilization of Waste Cement Kiln Dust-Sand Soil Mix for Landfill Liner." Volume. 10 Issue.3, March-2025 International Journal of Innovative Science and Research Technology (IJISRT), 559-570,

Abdi, M. R., Ghalandarzadeh, A., & Shafiei-Chafi, L. (2022). Optimization of Lime and Fiber Content for Improvement of Clays with Different Plasticity using Response Surface Method (RSM). *Transportation Geotechnics*, (32) 100728.1–19. https://doi.org/10.1016/j.trgeo.2021.100728,

Adeyanju, E. A., & Okeke, C. A. (2019). Clay Soil Stabilization Using Cement Kiln Dust. In IOP conference series: materials science and engineering. 640(1) 012080

ASTM (2011). Standard Practice for Classification of Soils for Engineering Purposes (Unified Soil Classification System). ASTM D247-11; ASTM International. West Conshohocken. PA.

ASTM International. (2024). *ASTM D2166/D2166M-24: Standard Test Method for Unconfined Compressive Strength of Cohesive Soil*. West Conshohocken, PA: ASTM International. https://doi.org/10.1520/D2166_D2166M-24

Bagonza, H. (2025). Assessing the use of Cement Kiln Dust to Stabilize Sandy Soils for Subgrade Construction. *Uganda Christian University, Faculty of Engineering.*

Batari, A., Chinade, A. U., Saeed, M. S., Ikara, I. A., Kabir, N. & Mamuda A. (2017). "Effect of Bagasse Ash on the Properties of Cement Stabilized Black Cotton Soil". *International Journal of Transportation Engineering and Technology*. Vol. 3, No. 4, 2017, pp. 67-73. doi: 10.11648/j.ijtet.20170304.14

Benson, C. H., Daniel, D. E. and Boutwell, G. P. (1999). Field Performance of Compacted Clay Liners. *Journal of Geotechnical and Environmental Engineering*. 125: 390 - 403.

Chinade A. U., & Yunusa G. H. (2024). Compacted Soil Liners and Covers for Waste Containment: A Review of Soil Type Suitability and Applications. *African Journal of Environmental Sciences and Renewable Energy*, *16*(1), 147-161.

Chinade A. U., S. Y. Umar, & K. J. Osinubi (2017). Effect of Municipal Solid Waste Leachate on the Strength of Compacted Tropical Soil for Landfill Liner". *International Research Journal of Engineering and Technology*, *4*(6), 3248-3253

Chinade, A. U. & Yunusa G. H. (2025). Compaction Characteristics of Laterite Soil Admixed with Black Cotton Soil and Cement Kiln Dust. *Faculty of Engineering, University of Abuja Nigeria, 1st Abuja International Engineering Conference (AIECO 2025): (1) 1844-1858.* doi: 10.11648/j.jccee.20210606.11

Fondjo, A. A., Theron, E., & Ray, R. P. (2021). Stabilization of Expansive Soils Using Mechanical and Chemical Methods: *A Comprehensive Review*. Civil Engineering and Architecture, 9(5), 1295–1308.

Moses, G. K., & Saminu, A. (2012). Cement Kiln Dust Sabilization of Compacted Black Cotton Soil. *Electronic Journal of Geotechnical Engineering*, *17*(January 2012), 825-836.

Muhammad A. S., Chinade A. U, A. Mamuda, A. Batari & M. D. Abdullahi (2021). Effect of Gypsum in Proportion of Other Additives Used in Stabilization of Deficient Soils: A Review. *Journal of Civil, Construction and Environmental Engineering Science Publishing Group.* 6(6): 161-176

Ogila, W. A. M., & Eldamarawy, M. E. (2022). Use of Cement Kiln Dust for Improving the Geotechnical Properties of Collapsible Soils. *Indian Geotechnical Journal*, 1-16.

Osinubi, K. J. and Nwaiwu, C. M. O. (2005). Hydraulic Conductivity of Compacted Lateritic Soil. *Journal of Geotechnical and Geoenvironmental Engineering.* 131: 1034 - 1041.

Pydi, R., Yadu, L. & Chouksey, S.K. A Novel Prediction of Strength Properties of Biopolymer-Treated Soil: A Response Surface Approach. *Transp. Infrastruct. Geotech.* 11, 2523–2545 (2024).

Somadas, P., Sarvade, P. G., & Nayak, D. (2024). Advancements in Soft Soil Stabilization by Employing Novel Materials through Response Surface Methodology. *Geosciences*, *14*(7), 182.

Teodoru, I.-B., Owusu-Yeboah, Z., Aniculăesi, M., Dascălu, A. V., Hörtkorn, F., Amelio, A., & Lungu, I. (2025). Prediction of Unconfined Compressive Strength in Cement-Treated Soils*: A Machine Learning Approach*. Applied Sciences, 15(13), 7022.

Tijjani K., Umar S. Y., Chinade A. U., & Yakubu A. S. (2021). Effect of Different Compaction Energies on the Strength Characteristics of Laterite Soil Treated with Activated Rice Husk Ash. *International Research Journal of Engineering and Technology*. 08: 11- 1409 - 1415.

U. Y. Mai-Bade, A. U. Chinade, A. Batari & S. M. Saeed (2021). Stabilization of Black Cotton Soil Using Various Admixtures: A Review. *Journal of Composite Material, Science Publishing Group*. 5(2): 37- 45

ISBN: 978-978-8567-02-8

Umar, S. Y., Elinwa, A. U. and Matawal, D. S. (2015a). Hydraulic Conductivity of Compacted Lateritic Soil Partially Replaced with Metakaolin. *Journal of Environmental and Earth Sciences.* 5(4): 53 – 64.

Umar, S. Y., Matawal, D. S. and Elinwa, A. U. (2016). Hydraulic Conductivity of Compacted Laterite Treated with Iron Ore Tailings. *Advances in Civil Engineering*. 1: 1 – 8.

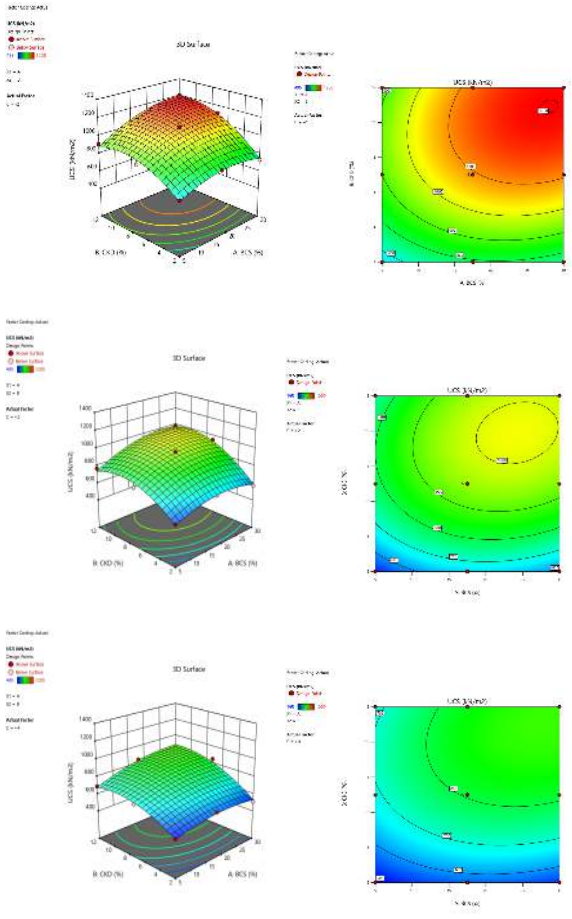
Wang, L. (2025). Automated Machine Learning Techniques for Estimating the Unconfined Compressive Strength of Soil Stabilization. *International Journal on Interactive Design and Manufacturing*, 19, 6347–6359.

Widomski, M. K., Stępniewski, W., & Musz-Pomorska, A. (2018). Clays of Different Plasticity as Materials for Landfill Liners in Rural Systems of Sustainable Waste Management. *Sustainability*, *10*(7), 2489.

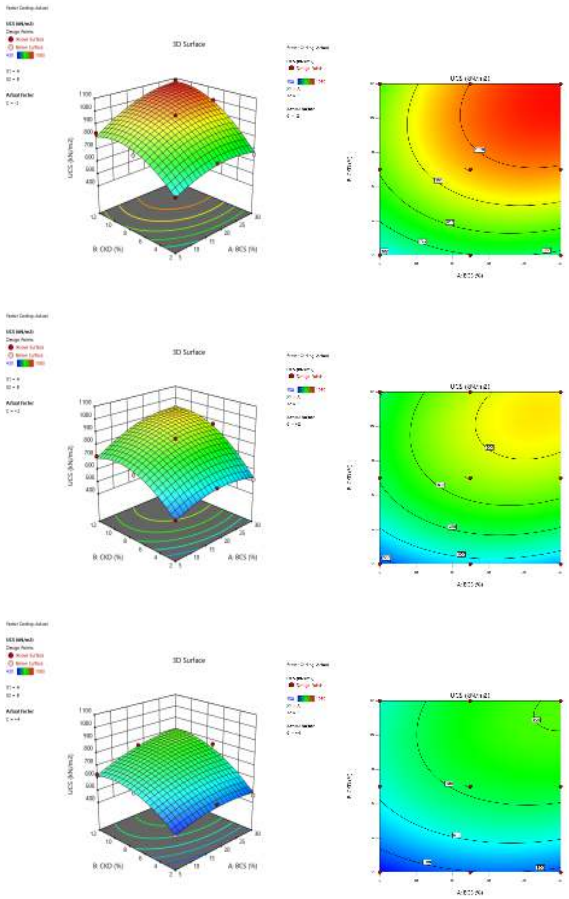
Yamusa, Y. B., & Ahmad, K. (2018). Evaluating the Geotechnical Properties of Compacted Laterite Soil at Different Fines Content. *Advanced Science Letters*, *24*(6), 4015-4020.

Yan, Q., Peng, B., Li, W., Wang, B., Zuo, J., Lv, G., & Wang, T. (2025). Low-carbon Stabilization of Expansive Soils Using Cement Kiln Dust and Calcium Carbide Slag: mechanisms and Performance. *Frontiers in Earth Science*, 13, Article 1554812.

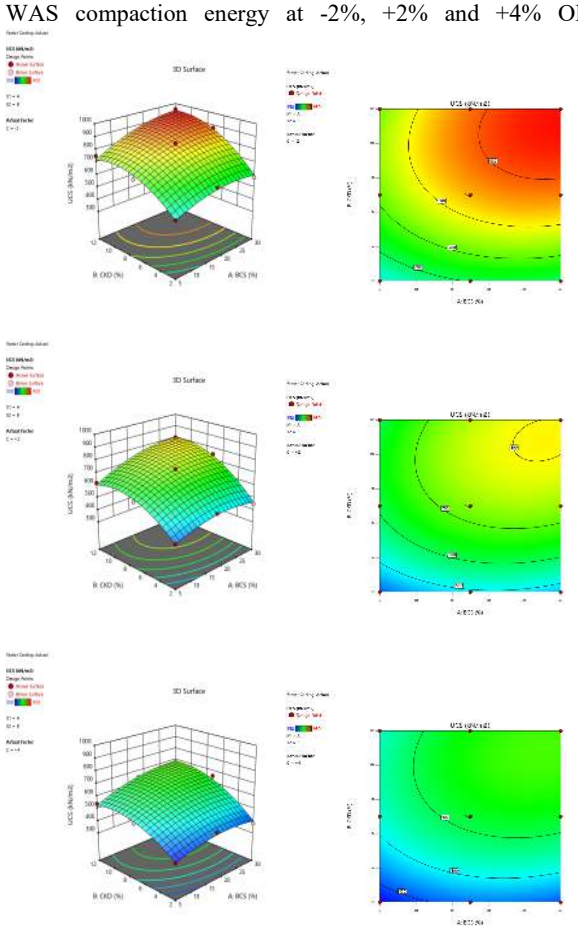
APPENDIX



Appendix A: Response surface and contour plots of UCS for BSH compaction energy at -2%, +2% and +4% OMC



Appendix B: Response surface and contour plots of UCS for WAS compaction energy at -2%, +2% and +4% OMC



Appendix C: Response surface and contour plots of UCS (BSL)

ISBN: 978-978-8567-02-8

5TH Faculty of Engineering Conference on Engineering Innovation and Economic Policies: Driving Sustainable Industrial Growth in Nigeria

Faculty of Engineering, Bayero University, Kano.

074-Pushover Analysis of a Six-Story Reinforced Concrete Building: Assessing Seismic Performance and Collapse Mechanisms

Claudius Konitufe[1,2] and Aaron Aboshio[2]
[1]*Abubakar Tafawa Balewa University, Bauchi*
[2]*Bayero University, Kano*
kclaudius@atbu.edu.ng

Abstract: This study conducted a nonlinear static pushover analysis of a six-story RC moment-resisting frame using ETABS Ultimate 21.0.0, evaluating seismic performance per ASCE 41-17 (ASCE, 2017). The 3D model included nonlinear hinges (M3 for beams, PMM for columns), P-Δ effects, and first-mode proportional loading in both directions. In the X-direction, the structure exhibited high ductility and a strong–column–weak–beam hierarchy, reaching 11,650 kN base shear at 247 mm roof drift (≈1.37%), followed by gradual softening with ≈69% residual strength. Plastic hinges formed mainly in beams, with column hinging limited to the base, resulting in a desirable beam-sway mechanism. Interstory drifts remained below Collapse Prevention (CP) limits (max ≈2.0–2.5%), indicating substantial overstrength and ductility (Mwafy & Elnashai, 2001; Lignos & Krawinkler, 2011). In contrast, the Y-direction showed significant vulnerability, developing an undesirable soft-story (column-sway) mechanism at low roof drift (≈0.9–1.0%), with abrupt strength loss and excessive first-story drifts (>7–8%) due to premature column hinging despite elastic code compliance (Rajeev & Tesfamariam, 2012). These directional asymmetries highlight force-based design limitations in ensuring robust inelastic behavior (Krawinkler & Seneviratna, 1998; Elnashai & Mwafy, 2002; Paulay & Priestley, 1992; Mwafy, 2012). Capacity spectrum analysis (FEMA-440 refined; FEMA, 2005) confirmed Life Safety performance with margin under design basic earthquake (DBE) and near (but not exceeding) CP under maximum considered earthquake (MCE) in the X-direction. The findings emphasize the importance of nonlinear static analysis for revealing hidden vulnerabilities and the need for performance-based assessments in mid-rise reinforced concrete frames in medium- to high-seismicity regions (ASCE, 2017; Kunnath et al., 2021). Retrofitting, such as adding shear walls in the weaker direction, is recommended to mitigate soft-story risks (Beigi et al., 2024).

Keywords: pushover analysis, reinforced concrete, seismic performance, nonlinear modeling, collapse mechanisms.

1. INTRODUCTION

Nigeria, historically regarded as a region of low seismicity, has witnessed a rising incidence of seismic events in recent decades, underscoring the need to reassess the vulnerability of its building infrastructure (Akpan and Yakubu, 2010; Tsalha et al., 2015). Key episodes include the 2016 tremors in Kwoi, Kaduna State (Alaneme and Okotete, 2018), the 2018 tremors in Mpape, Abuja (Olugboji et al., 2021), and more recent activity, such as repeated low-intensity tremors in Mpape and surrounding Abuja districts in September 2024 (Nigeria Geological Survey Agency, 2024; BBC News, 2024). Although these events remain low in magnitude, evidence points to intraplate seismicity potentially associated with regional fault systems, including landward extensions of oceanic fracture zones such as the Romanche and Chain zones (Eze et al., 2012; Lawal et al., 2025). Higher-magnitude events could inflict substantial human and economic losses, especially in densely populated urban centers.

Most multi-story buildings in Nigeria consist of reinforced concrete (RC) moment-resisting frames, typically designed in accordance with BS 8110 or the Nigerian National Building Code, which prioritize gravity and wind loads but historically lacked comprehensive seismic detailing (Ogunbiyi, 2014; National Building Code updates, 2024). This approach renders many structures susceptible to lateral seismic forces. Evaluations of comparable construction practices elsewhere reveal frequent vulnerabilities, including inadequate reinforcement detailing, limited confinement in critical zones, and absence of capacity design principles, often resulting in brittle failure modes (Ede et al., 2017).

Nonlinear static pushover analysis serves as an effective method for performance-based seismic evaluation, as outlined in established guidelines such as ATC-40 (1996), FEMA-356 (2000), and subsequent refinements in FEMA-440 (2005). This technique enables assessment of inelastic response, identification of plastic hinge development, derivation of capacity curves,

ISBN: 978-978-8567-02-8

and determination of performance levels (e.g., Immediate Occupancy, Life Safety, Collapse Prevention). It yields valuable data on structural ductility, overstrength, and likely failure mechanisms under progressively increasing lateral loads.

Seismic response varies with building height due to differences in fundamental period, modal participation, and force distribution. Masonry infill walls, frequently regarded as non-structural elements in design, substantially modify stiffness, strength, and energy dissipation—often beneficially by limiting inter-story drifts, yet sometimes adversely by inducing soft-story effects or column shear failures.

Although these influences have been examined separately, integrated studies on typical Nigerian RC frames remain limited. This research seeks to investigate the seismic performance of a representative six-story RC framed building through nonlinear static pushover analysis. The aims include generating capacity curves, evaluating performance points relative to demand spectra, sequencing plastic hinge formation and failure modes, and assessing the vulnerability of mid-rise buildings in Nigeria by evaluating directional seismic performance of a six-story reinforced concrete frame.

2. REVIEW OF RELATED LITERATURE

2.1 Fundamentals of Earthquakes and Tremors

Earthquakes present major risks to infrastructure, even in low-seismicity areas, with about 3 million occurring yearly globally—98% below magnitude 3 and undetectable, and fewer than 20 major (M7.0–7.9) or great (M≥8) events annually. Most are natural tectonic or volcanic, but an increasing share is human-induced via activities like resource extraction, blasting, and groundwater withdrawal.

Tectonic earthquakes primarily follow plate tectonics and the elastic rebound theory (Reid, 1910), where lithospheric plates (100–150 km thick) move over the asthenosphere, building elastic strain on locked faults until sudden release produces seismic waves, as depicted in Figure 1.

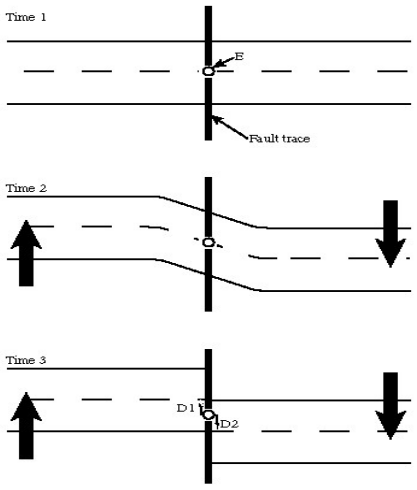


Figure 1: Illustration of the Elastic Rebound Theory of Tectonic Earthquakes

This is shown in schematics of deformation and rebound in Figure 1.

Induced seismicity arises from anthropogenic alterations to subsurface stresses or pore pressures, such as fluid injection in oil/gas extraction or fracking, mining (rock removal or blasting), and deep drilling (Foulger et al., 2018; National Research Council, 2012; Ellsworth, 2013). These can cause vibrations, microcracking, building damage, or trigger larger events via fluid pressure changes or stress on faults (Schultz et al., 2020; Ge, 2022). Surface activities like pile driving, demolition, traffic, and non-explosive blasts may produce vibrations leading to localized damage but rarely trigger major quakes (Massarsch & Fellenius, 2008; Dowding, 1996).

In Nigeria, situated in a stable intraplate zone between the West African and Congo cratons, seismicity has been recorded since 1933, tied to NE-SW fractures from Atlantic fracture zones (Akpan and Yakubu, 2010; Tsalha et al., 2015; Adepelumi et al., 2008). Though outside seismic belts, tremors occur with Modified Mercalli intensities (Akpan and Yakubu, 2010). Recent events, like the 2018 Abuja series, link to human factors such as excessive groundwater extraction from ~110,000 boreholes causing hydrogeological instability (Olugboji et al., 2021; Presidential Committee Report, 2018). Disturbances along the Ifewara-Zungeru fault span 1933 to recent years (Akpan and Yakubu, 2010; Tsalha et al., 2015). Probabilistic assessments show low hazards but potential for up to M7 events (Eluyemi et al., 2020; Kadiri and Amponsah, 2021).

Seismic vulnerability of reinforced concrete (RC) structures depends on factors assessed against limit states: Immediate Occupancy (minor damage, functional), Life Safety (significant damage, no collapse, occupant safety), and Collapse Prevention (extensive damage near collapse but integrity in design events) (ASCE, 2017; FEMA, 2000).

Key influencing factors include:

i. Material degradation (e.g., reinforcement corrosion or chemical attacks), which reduces sectional capacity, strength, ductility, and stiffness, increasing long-term seismic fragility (Shekhar et al., 2023; Afsar Dizaj et al., 2021).

ii. Shear walls, which boost lateral load resistance by enhancing stiffness, strength, energy dissipation, and reducing drift in RC frames (Satpute & Kulkarni, 2019; Tuna, 2013).

iii. Soil-structure interaction (SSI), which can amplify or attenuate seismic response based on soil stiffness; on soft soils, it extends structural periods, increases displacements, and heightens vulnerability via ground motion amplification (Matinmanesh & Asheghabadi, 2011; Khosravikia et al., 2018).

iv. Vertical irregularities (e.g., setbacks or soft stories), which focus damage and drifts at discontinuities, markedly raising fragility in lower stories (Varadharajan et al., 2013; Mouhine & Hilali, 2020).

v. Masonry infills, which add in-plane stiffness and strength but may cause localized issues like short-column failures from partial-height column restraint (Cavaleri et al., 2017; Ferraioli, 2020).

ISBN: 978-978-8567-02-8

Seismic vulnerability assessment combines hazard, exposure, and fragility components to estimate damage and risk, using empirical, analytical/numerical, or hybrid methods. For mid-rise reinforced concrete (RC) buildings (5–15 stories), common in urban areas like Nigeria, nonlinear static pushover analysis is a key tool in performance-based seismic engineering, especially for structures dominated by first-mode response. This method applies incremental lateral forces to model post-elastic behavior, producing a capacity curve of base shear versus roof displacement that identifies plastic hinge sequences, deformation limits, and failure modes like soft stories. It offers computational efficiency over nonlinear dynamic analysis, supports performance assessments per standards like ASCE 41-17 and its predecessor FEMA-356, and aids in developing seismic fragility curves for probabilistic risk assessment.

2.2 Numerical Modeling and Simulation: Pushover Analysis

Pushover analysis, a nonlinear static procedure widely utilized in performance-based seismic engineering, is particularly effective for evaluating the seismic performance of mid-rise reinforced concrete (RC) buildings, typically ranging from 5 to 15 stories (FEMA, 2000; Mwafy & Elnashai, 2001). This method involves the incremental application of lateral forces, often distributed in patterns proportional to the fundamental mode or other relevant distributions, to a structural model until significant nonlinearity or collapse is achieved. This process generates a capacity curve that plots base shear against roof displacement (ATC, 1996; ASCE, 2000). The resulting capacity curve provides critical insights into the structure's post-elastic behavior, deformation capacity, and potential failure modes (Chopra & Goel, 2002).

This approach helps identify capacity curves, plastic hinge formations, and performance levels as per guidelines like FEMA 356, making it essential for retrofit design and vulnerability assessment. Recent studies have advanced its applications by incorporating material innovations, soil-structure interactions, and optimization techniques.

A key application involves optimizing RC frame designs for seismic resilience. For instance, Faghihnejad and Ghasemi (2023) developed a performance-based optimization framework for 2D RC moment frames using pushover analysis combined with the artificial bee colony (ABC) algorithm. Their method automates seismic design by enforcing constraints on inter-story drifts and plastic hinge rotations, achieving targeted performance levels while minimizing material use. Similarly, in a study on basalt fiber-reinforced concrete (BFRC), researchers examined nonlinear pushover analysis to assess seismic performance in high-seismicity zones, finding that BFRC enhances ductility and energy dissipation compared to conventional RC, reducing collapse risk by up to 20% in multi-story frames.

Soil-structure interaction (SSI) has emerged as a critical factor in recent pushover applications. A 2024 investigation into RC buildings with varying cross-sectional areas demonstrated that considering SSI in pushover models increases base shear demands by 15-25% in soft soils, emphasizing the need for foundation modeling to avoid underestimating vulnerability in irregular frames. Complementing this, a 2025 study on drop panels in RC frames used comparative pushover analysis to show that incorporating drop panels at beam-column joints improves stiffness and delays hinge formation, boosting overall seismic resilience by 30% in four-story buildings.

Retrofitting strategies have also benefited from pushover analysis. In a finite element modeling study, concrete jacketing and carbon fiber-reinforced polymer (CFRP) wraps were evaluated for seismic upgrading of existing RC buildings, with pushover results indicating that CFRP enhances lateral capacity by 40% while jacketing is more effective for ductility in mid-rise frames (Comlekoglu et al., 2025). Another 2025 paper addressed pathological failures in RC frames, such as soft-story mechanisms and poor joint detailing, using pushover to guide retrofitting; it found that targeted shear wall additions can mitigate these issues, reducing inter-story drifts by over 50% (Bilgin et al., 2025).

Integration with probabilistic tools like fragility curves has expanded pushover's utility. For low-rise RC frames with masonry infills, pushover-derived fragility analyses revealed that infills significantly lower vulnerability at moderate intensities but may accelerate damage at high intensities due to brittle failure (Aggarwal & Saha, 2025). In damage assessment across low- to high-rise RC structures, pushover-based damage indices highlighted height-dependent vulnerabilities, with high-rises showing greater sensitivity to higher-mode effects (Alguhane et al., 2025). Educational facilities were analyzed using combined linear time-history and nonlinear pushover methods, confirming that pushover accurately predicts performance levels for irregular layouts (Sung et al., 2024).

These studies underscore pushover analysis's versatility in RC frame applications, particularly for incorporating advanced materials, SSI, and retrofits, with recent emphases on optimization and probabilistic assessments.

2.3 Directional Vulnerability Studies in Reinforced Concrete Frame Buildings

Directional vulnerability studies focus on how earthquake ground motion directionality—including bidirectional effects, rotational components, and incident angles—affects RC frame buildings' seismic response. This is crucial for irregular structures where torsion amplifies damage, and recent research has used experimental, numerical, and probabilistic methods to quantify these effects.

Ground motion directionality has been shown to exacerbate failure risks. Li et al. (2023) assessed seismic collapse in RC structures under directional ground motions, finding that ignoring directionality underestimates collapse probability by 20-30% in frames with eccentric mass distributions. Shayanfar et al. (2022) proposed an adaptive directional importance sampling method within pushover procedures, demonstrating that story shear demands vary by up to 25% based on motion orientation in mid-rise RC frames.

ISBN: 978-978-8567-02-8

2.4 Significance for Mid-Rise RC Buildings

Mid-rise RC structures commonly employ moment-resisting frames or dual systems incorporating shear walls, where seismic demands promote plastic hinge development in beams and columns. Pushover analysis is particularly advantageous because it predicts post-elastic response and reveals vulnerabilities such as soft-story mechanisms or excessive inter-story drifts that elude linear elastic methods (Mwafy and Elnashai, 2001).

It underpins performance-based seismic engineering (PBSE), enabling evaluation against defined limit states: Immediate Occupancy (IO), Life Safety (LS), and Collapse Prevention (CP). This framework is vital for mid-rise buildings in seismic regions, ensuring limited damage under moderate events and collapse avoidance under severe shaking (FEMA, 2000; ASCE, 2017).

The method identifies sequential hinge formation and progressive collapse mechanisms, promoting ductile response (beam hinging before columns) in RC frames (Güneş, 2020).

Relative to nonlinear time-history analysis, pushover offers computational efficiency with acceptable accuracy for structures dominated by the first mode, a characteristic prevalent in mid-rise buildings (Boonyapinyo et al., as cited in assessment studies).

It also supports fragility curve derivation and probabilistic loss estimation (El-Esnawy, 2007; FEMA P-58, 2012).

Limitations include potential neglect of higher-mode contributions in taller mid-rise configurations and cyclic deterioration; these may be addressed through cyclic or modal pushover variants (Chopra and Goel, as referenced in MPA studies).

2.5 Application Using ETABS Ultimate 21.0.0

Software like ETABS Ultimate facilitates implementation through 3D modeling, hinge assignment (e.g., PMM for columns, M3 for beams), load patterns (modal, uniform), and performance point determination via Capacity Spectrum or Displacement Coefficient methods.

In low-to-moderate seismicity zones like Nigeria, where induced events are increasing, pushover analysis enables early detection of deficiencies in existing mid-rise RC stock—often designed without seismic provisions. Integration with probabilistic hazard data supports retrofit strategies, enhancing resilience against both natural and anthropogenic seismicity.

This underscores the imperative for updated building codes, continuous monitoring, and performance-based design to safeguard life safety and minimize losses in emerging seismic contexts.

In conclusion, pushover analysis within ETABS constitutes a robust, code-compliant tool for enhancing seismic resilience in mid-rise RC buildings, enabling early deficiency detection and informed retrofit strategies to safeguard life safety and minimize economic losses (FEMA P-58, 2012; ASCE/SEI 41-17).

3. METHODOLOGY

3.1 Building Description

A six-story reinforced concrete moment-resisting frame building, typical of mid-rise residential or commercial structures in Nigerian urban centers, was selected for analysis. The building features a regular plan layout with bay spans of approximately 5-6 m in both directions, consistent with common practices. Story height is 3.0 m (floor-to-floor), resulting in a total height of 18 m. The floor plan is shown in Figure 2. The structural system comprises RC beams, columns, and slabs, with concrete grade C25/30 and reinforcing steel F_Y410.

The plan consists of an asymmetric grid, with columns sized uniformly (400×400 mm throughout) and beams 300×600 mm. Slab thickness is 200 mm (two-way solid slab). The building was initially designed for gravity loads per BS 8110, with minimal lateral consideration. The live loadings, however, are as quoted in code and is 2.00 kN/m^2 for rooms intended for residential, hospital, and hotel/motel purposes. Table I shows the material properties of concrete and steel used.

TABLE I: MATERIALS FOR REINFORCED CONCRETE MEMBERS OF THE SELECTED THREE, FIVE AND TEN-STORY BUILDINGS

Member Type	Characteristic Strength of Concrete (N/mm^2)	Characteristic Yield Strength of Steel (N/mm^2)
Columns Beams Slabs	20/25	410
Foundation	32/40	410
Links	--	250 (Plain)

3.2 Modeling and Software

Nonlinear static pushover analysis serves as a cornerstone for performance-based seismic evaluation of existing structures. This study investigates a regular six-story RC moment-resisting frame building (story height 3.0 m, total height 18 m) designed to modern force-based codes. The objective is to assess seismic capacity, plastic mechanism development, and compliance with performance objectives as outlined in ASCE 41-17, FEMA P-58, and related guidelines. Lateral loading follows the first-mode distribution, with hinge properties based on ASCE 41-17.). The analysis reveals hidden vulnerabilities that are not detectable through linear methods.

Three-dimensional finite element models were developed using ETABS Ultimate 21.0.0, widely used for nonlinear seismic analysis. Frame elements (beams and columns) were modeled as line elements with lumped plasticity. User-defined plastic hinges were assigned based on FEMA-356/ATC-40 provisions: Moment (M3) hinges for beams. Coupled P-M-M hinges for columns (accounting for axial-moment interaction). Material nonlinearity was incorporated via P-Delta effects for concrete and steel. Nonlinear static pushover analysis was performed following ATC-40 Capacity Spectrum Method and FEMA-356 guidelines. Load patterns and P-delta effects. This methodology provides a robust framework for assessing seismic vulnerability,

ISBN: 978-978-8567-02-8

identifying retrofit needs, and informing future code updates for Nigerian RC structures.

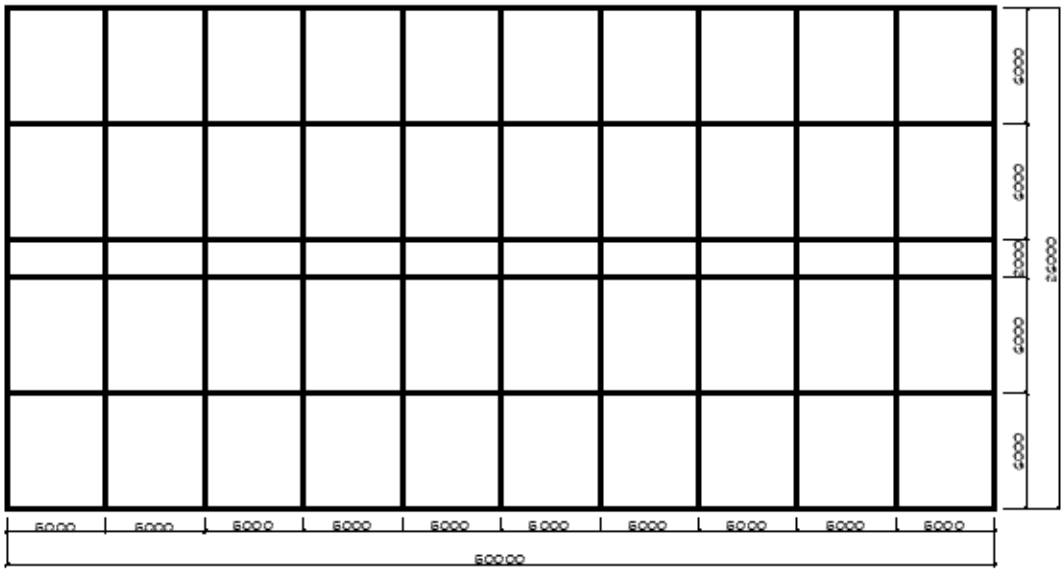


Figure 2: Reinforced Concrete Building Plan

4.0 RESULTS AND DISCUSSION

4.1 Capacity Curves and Key Performance Parameters

The pushover capacity curve in the X-direction displays classical ductile behavior characteristic of well-detailed special moment-resisting frames (SMRFs). Initial elastic stiffness is approximately 105.5 kN/mm, with first yielding at a roof displacement of 51.6 mm (drift ratio 0.29%) and base shear of 5447 kN. Peak base shear reaches 11,652 kN at 247 mm roof displacement (drift ratio 1.37%), followed by mild post-peak softening to 8070 kN (69% of peak) at ultimate displacement.

This response reflects successful enforcement of a strong–column–weak–beam (SCWB) hierarchy, with effective flange participation from slabs enhancing beam capacity. The yield drift is at the lower end of typical ranges (0.3–0.5%) for code-compliant RC frames, indicating high initial stiffness. Interstory drifts at peak capacity remain in the 2.0–2.5% range, consistent with the Immediate Occupancy (IO) to Life Safety (LS) transition. The capacity curve is shown in Figure 3.

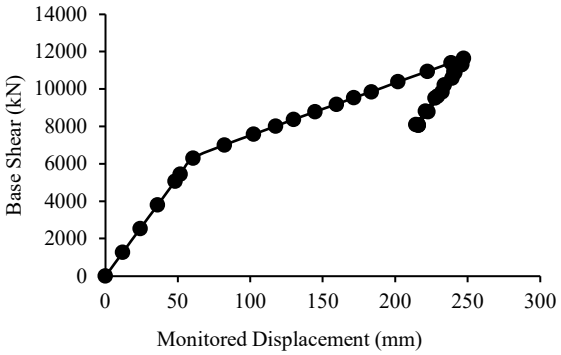


Figure 3. Capacity Curve for Six-Story Reinforced Concrete Building

4.2 Sequence of Hinge Formation and Plastic Mechanism (X-Direction)

First yielding occurs at Step 5 in the beam ends of lower stories (Stories 2–3), with hinges transitioning from B–IO. By Step 12 (roof displacement 159 mm, drift 0.88%), 128 hinges exceed IO, predominantly in beams, while columns remain essentially elastic. Peak capacity at Step 18 shows widespread beam hinging (63% between B and C, 18% in LS–CP), with column participation limited to base level.

The ultimate mechanism is a desirable hybrid: dominant beam-sway across all stories plus controlled base-column hinging. No soft-story formation is observed, with uniform drift distribution (max/min interstory drift ratio ≈1.3–1.5) and maximum interstory drifts ≈2.0%. This aligns with optimal mechanisms described by Paulay & Priestley (1992) and subsequent research, confirming effective capacity design and redundancy. Table II presents the plastic hinge distribution at various performance levels.

TABLE II. PLASTIC HINGE DISTRIBUTION AND STATUS AT PEAK STRENGTH (STEP 18)

Hinge State	Number of Hinges	% of Total Hinges	Interpretation (ASCE 41-17/FEMA 356)
B → C (yield to full plastification)	448	~63 %	The majority of hinges have yielded and are actively dissipating energy
C → D → E (post-cap)	4	<1 %	Very few hinges have lost significant strength yet
IO → LS region	132	~18.5 %	Hinges that have exceeded IO but are still below LS
LS → CP region	128	~18 %	Hinges approaching or entering the collapse prevention

Note:
A - B → Member remains essentially elastic, no yielding
B - C → Significant plastic rotation
C - D → Significant damage, loss of capacity
D - E → Almost complete loss of strength
IO → beams, some columns have yielded
LS → more critical locations
CP → only a few critical elements at target displacement

4.3 Comparison with Linear Analyses

Linear static/modal analysis yields a design base shear of 6200–6500 kN, while nonlinear peak capacity is

ISBN: 978-978-8567-02-8

11,652 kN—indicating overstrength Ω_0 ≈2.8 and justifying the assumed response modification factor R=7. Linear interstory drifts under design earthquake are ≈0.7%, well below limits, whereas pushover performance points place the structure comfortably in LS for Design Basis Earthquake (DBE) and CP for Maximum Considered Earthquake (MCE).

4.4 Seismic Performance Level Assessment

Using the **Capacity Spectrum Method** as described in ATC-40 (Applied Technology Council, 1996) and improved in FEMA-440 (Federal Emergency Management Agency, 2005), performance points are determined by intersecting the capacity spectrum with demand spectra for the Design Basis Earthquake (DBE) and Maximum Considered Earthquake (MCE) levels (Site Class C, Ss=1.5g, S1=0.6g).

In the X-direction, the DBE performance point occurs at a spectral displacement Sd ≈ 185 mm (with effective damping of 18–20%), which falls within the **Life Safety (LS)** performance level with a reasonable margin (ATC-40, 1996; FEMA-440, 2005).

The MCE performance point at Sd ≈ 265 mm approaches the **Collapse Prevention (CP)** level without widespread column failure.

Overall, the structure satisfies the **Life Safety (LS)** performance objective for the DBE with considerable reserve capacity; the **Immediate Occupancy (IO)** criterion is marginally exceeded in terms of roof drift but satisfied at the member level due to low interstory drifts and elastic column response (ATC-40, 1996).

4.5 Seismic Vulnerability Assessment

Vulnerability is evaluated via **drift sensitivity** and **mechanism typology**. Maximum interstory drifts at the Maximum Considered Earthquake (MCE) level remain below typical **collapse thresholds** of 4–5% for ductile systems[1], with achieved ductility factors $\mu \approx 3.3–5.0$ and a base shear coefficient V_max/W = 0.22. The **beam-sway mechanism** ensures a robust margin for **collapse prevention** in the X-direction[2].

[1] Typical collapse interstory drift thresholds for code-conforming ductile reinforced concrete or steel frames range from 4% to 5% under MCE-level demands (as correlated with damage indices in response-based assessments).

[2] Beam-sway mechanisms are preferred in seismic design for moment-resisting frames, as they promote energy dissipation in beams while protecting columns, providing enhanced collapse prevention performance compared to column-sway or soft-story mechanisms.

4.6 Directional Asymmetry and Y-Direction Performance

In stark contrast, the Y-direction exhibits catastrophic brittle behavior. The peak base shear coefficient reaches only 0.18–0.19 at a roof drift of approximately 0.9–1.0%. Post-peak, the strength drops abruptly (more than 20%) due to premature column hinging at the base and first elevated levels (Dooley and Bracci, 2001; Raju et al., 2018). Beam hinges remain largely elastic, while column hinges rapidly progress to the C–D and D–E performance ranges. Interstory drift concentrates in the first story (exceeding 7–8%), far surpassing Collapse Prevention (CP) limits.

This soft-story mechanism forms despite linear analyses indicating drifts below allowable limits and member forces within capacity checks (Prajapati and Amin, 2019). The failure arises from inadequate column deformation capacity and violation of the strong-column-weak-beam (SCWB) hierarchy in the inelastic range—a well-documented limitation of force-based design, where elastic verification does not guarantee acceptable nonlinear response (Dooley and Bracci, 2001; Raju et al., 2018; Su et al., 2020).

4.7 Implications for Design Practice

The extreme directional discrepancy **ductile global mechanism** in one direction versus **brittle column-sway collapse** in the orthogonal direction illustrates that code-compliant linear elastic strength and stiffness verifications alone cannot ensure the development of controlled, ductile failure mechanisms or adequate overall ductility (as observed in nonlinear assessments of moment frames where SCWB provisions fail under amplified demands).

Current strong-column-weak-beam (SCWB) summation rules prove inadequate when higher-mode amplification and second-order P-Δ effects exacerbate column demands, potentially triggering premature brittle failures despite nominal code compliance (Vamvatsikos and Cornell, 2002; various studies on RC and steel frames).

These observations align with evolving code provisions that increasingly require nonlinear verification procedures for seismic assessment and retrofit, as emphasized in **ASCE/SEI 41-17** (which introduces revised nonlinear static and dynamic methods alongside tiered performance objectives for existing and new-building-equivalent structures) and the draft updates to **Eurocode 8 Part 3** (which mandate nonlinear static or dynamic analyses to confirm deformation capacities and prevent brittle mechanisms in retrofitted buildings).

Limitations of conventional pushover analysis are further exposed: fixed (invariant) lateral load patterns often fail to capture higher-mode contributions or redistribution due to progressive yielding, potentially overlooking critical vulnerabilities that emerge only under multi-directional loading or time-history excitations (Chopra and Goel, 2002; various multi-mode pushover studies).

To achieve reliable mechanism control, explicit verification of desired ductile hierarchies—combined with **incremental dynamic analysis (IDA)** as a robust tool for evaluating record-to-record variability and collapse margins—should be adopted as standard practice for critical or irregular structures in moderate-to-high seismicity zones (Vamvatsikos and Cornell, 2002).

4.8 Retrofit Recommendations

The building is seismically deficient in Y-direction, with a collapse probability >25–30% under BSE-1N (MCE-level) hazard per fragility estimates. Target objectives per ASCE 41-17 are not met.

Recommended interventions, prioritized by cost-effectiveness:

ISBN: 978-978-8567-02-8

1. Addition of RC shear walls (300–400 mm thick) in Y-direction perimeter frames—most effective for stiffness increase, mechanism redistribution, and overstrength enhancement.
2. Column jacketing (RC or fiber-reinforced) at lower stories to boost flexural capacity and delay column yielding.
3. Supplemental damping or base isolation—less preferred due to cost and disruption.

Verification via nonlinear response-history analysis (NL-RHA) with spectrum-compatible records is essential to refine strategies and quantify residual risk.

4. CONCLUSION

Nonlinear static pushover analysis was performed on a six-story reinforced concrete moment-resisting frame building that fully complies with modern force-based seismic design codes under linear elastic verification. Despite this compliance and apparent plan regularity, the study revealed pronounced directional asymmetry in nonlinear seismic performance.

In the X-direction, the structure exhibited ideal ductile behavior consistent with capacity design principles. A global beam-sway mechanism formed, characterized by widespread beam hinging across stories and minimal, controlled column plasticity at the base. The capacity curve showed high initial stiffness, substantial overstrength ($\Omega_0 \approx 2.8$), an extended yielding plateau, and mild post-peak softening. Deformation capacity exceeded 2% roof drift, with uniformly distributed inter-story drifts and no soft-story formation. Capacity spectrum evaluation confirmed achievement of Life Safety at the Design Basis Earthquake (DBE) and near Collapse Prevention at the Maximum Considered Earthquake (MCE), validating the code's response modification factor ($R \approx 7$) and strong-column–weak-beam hierarchy.

Conversely, the Y-direction displayed brittle column-sway behavior with premature soft-story collapse in lower levels. Peak strength was attained at only ~1% drift, followed by >20% abrupt strength degradation. Column hinges rapidly progressed beyond Collapse Prevention while beams remained mostly elastic, leading to extreme drift concentration (>7–8%) in the ground story and high collapse risk even under design-level shaking.

These results expose a key limitation of force-based design: elastic compliance does not ensure controlled inelastic mechanisms or adequate deformation capacity. Hidden vulnerabilities, undetectable by linear or unidirectional analyses, arise from bidirectional effects and higher modes.

The findings advocate for mandatory performance-based seismic engineering, urging routine nonlinear static (and ideally dynamic) analyses for mechanism verification in regular structures. For the studied building, retrofit with strategically placed RC shear walls is recommended to eliminate the Y-direction deficiency, enhance stiffness/strength, and promote distributed yielding. Alternatives include column jacketing or damping devices.

In conclusion, code-conforming frames can achieve excellent resilience when capacity design is satisfied inelastically, but undetected directional soft-story risks underscore the need for explicit nonlinear verification in practice.

This study is limited to a single building typology and relies solely on static pushover analysis, while future work could extend the evaluation to incorporate incremental dynamic analysis (IDA) across diverse structural systems and ground motion ensembles.

AKNOWLEDGEMENT

The authors extend their deepest appreciation to Bayero University, Kano, and Abubakar Tafawa Balewa University, Bauchi, for their essential support and significant contributions to this research. Their valuable assistance played a crucial role in enabling the study and is sincerely acknowledged.

CONFLICT OF INTEREST

All authors declare that they have no conflicts of interest

REFERENCES

Akpan, O. U., & Yakubu, T. A. (2010). A review of earthquake occurrences and observations in Nigeria. *Earthquake Science, 23*(3), 289–294. https://doi.org/10.1007/s11589-010-0725-7 https://link.springer.com/article/10.1007/s11589-010-0725-7

Alaneme, K. K., & Okotete, E. A. (2018). Critical evaluation of seismic activities in Africa and curtailment policies—A review. *Geoenvironmental Disasters, 5*(1), Article 24. https://doi.org/10.1186/s40677-018-0116-2 https://geoenvironmental-disasters.springeropen.com/articles/10.1186/s40677-018-0116-2

American Society of Civil Engineers. (2017). *Seismic evaluation and retrofit of existing buildings (ASCE/SEI 41-17)*. American Society of Civil Engineers. https://ascelibrary.org/doi/book/10.1061/9780784414859

Applied Technology Council. (1996). *Seismic evaluation and retrofit of concrete buildings* (ATC-40, Vols. 1–2). Applied Technology Council.

BBC News. (2024, September 10). Tremors reported in Abuja and surrounding areas.

Chopra, A. K., & Goel, R. K. (2002). A modal pushover analysis procedure for estimating seismic demands for buildings. *Earthquake Engineering & Structural Dynamics, 31*(3), 561–582. https://doi.org/10.1002/eqe.144

Dooley, K. L., & Bracci, J. M. (2001). Seismic evaluation of column-to-beam strength ratios in reinforced

ISBN: 978-978-8567-02-8

concrete frames. *ACI Structural Journal, 98*(6), 843–851.

Elnashai, A. S., & Mwafy, A. M. (2002). Overstrength and force reduction factors of multistory reinforced-concrete buildings. *The Structural Design of Tall Buildings, 11*(5), 329–351. https://doi.org/10.1002/tal.204

Faghirnejad, S., Kontoni, D.-P. N., & Ghasemi, M. R. (2024). Performance-based optimization of 2D reinforced concrete wall-frames using pushover analysis and ABC optimization algorithm. Earthquakes and Structures, 27(4), 285–302. DOI: 10.12989/eas.2024.27.4.285

Federal Emergency Management Agency. (2000). *Prestandard and commentary for the seismic rehabilitation of buildings* (FEMA-356). Federal Emergency Management Agency.

Federal Emergency Management Agency. (2005). *Improvement of nonlinear static seismic analysis procedures* (FEMA-440). Federal Emergency Management Agency.

Krawinkler, H., & Seneviratna, G. D. P. K. (1998). Pros and cons of a pushover analysis of seismic performance evaluation. *Engineering Structures, 20*(4–6), 452–464. https://doi.org/10.1016/S0141-0296(97)00092-8

Lignos, D. G., & Krawinkler, H. (2011). Deterioration modeling of steel components in support of collapse prediction of steel moment frames under earthquake loading. *Journal of Structural Engineering, 137*(11), 1291–1302. https://doi.org/10.1061/(ASCE)ST.1943-541X.0000376

Mwafy, A. M., & Elnashai, A. S. (2001). Static pushover versus dynamic collapse analysis of RC buildings. *Engineering Structures, 23*(5), 407–424. https://doi.org/10.1016/S0141-0296(00)00068-7

Nigeria Geological Survey Agency. (2024). Seismic activity report: September 2024 tremors in Abuja.

Ogunbiyi, O. (2014). Seismic design practices in Nigeria. *Nigerian Journal of Technology, 33*(1), 89–98.

Olugboji, T. M., et al. (2021). On the origin of orphan tremors and intraplate seismicity in Western Africa. *Frontiers in Earth Science, 9*, Article 716630. https://doi.org/10.3389/feart.2021.716630

Paulay, T., & Priestley, M. J. N. (1992). *Seismic design of reinforced concrete and masonry buildings*. John Wiley & Sons. https://doi.org/10.1002/9780470172841

Prajapati, S. K., & Amin, J. A. (2019). Seismic assessment of RC frame building designed using gross and cracked section as per Indian standards. *Asian Journal of Civil Engineering, 20*, 821–836. https://doi.org/10.1007/s42107-019-00147-9

Rajeev, P., & Tesfamariam, S. (2012). Seismic fragilities of non-ductile reinforced concrete frames with consideration of soil structure interaction. *Soil Dynamics and Earthquake Engineering, 40*, 78–86. https://doi.org/10.1016/j.soildyn.2012.04.008

Reid, H. F. (1910). The mechanics of the earthquake (Vol. 2). Carnegie Institution of Washington.

Shayanfar, M. A., Barkhordari, M. A., & Barkhori, M. (2018). An adaptive directional importance sampling method for structural reliability analysis. Structural Safety, 70, 14–20. DOI: 10.1016/j.strusafe.2017.09.002

Vamvatsikos, D., & Cornell, C. A. (2002). Incremental dynamic analysis. *Earthquake Engineering & Structural Dynamics, 31*(3), 491–514. https://doi.org/10.1002/eqe.141

ISBN: 978-978-8567-02-8

5TH Faculty of Engineering Conference on Engineering Innovation and Economic Policies: Driving Sustainable Industrial Growth in Nigeria

Faculty of Engineering, Bayero University, Kano.

075-Synthesis and Characterisation of Optimized Recycled Low-Density Polyethylene-Doum Palm Shell Composite for Production of Crash Helmet

Abubakar U. Babuje[1], Nuhu Muhammed[2], Abubakar A. Fachway[3], Momoh Lamidi[4], Sunday G. Amon[5], David A. Nanlong[6]

[1,2,3,4,5,6] *Department of Mechanical/Production Engineering, Abubakar Tafawa Balewa University, Bauchi. PMB 0248, Bauchi State, Nigeria.*
Email: abusman@atbu.edu.ng/aubabuje@gmail.com

Abstract: The production of crash helmets is a critical aspect of ensuring the safety of individuals participating in various activities such as motorcycle riding, cycling, and extreme sports. Traditionally, helmets have been manufactured using materials such as polycarbonate, fiberglass, and carbon fiber. In recent years, there has been growing interest in exploring alternative materials for the production of crash helmets that are cost-effective and environmentally friendly. This study determined and optimized the impact, hardness, tensile, flexural strength, and density of the recycled low-density polyethylene reinforced Doum palm shell particles composite. The effect of particle size loading was also studied. The composites were prepared by compounding and molding LDPE and Doum Palm shell particles using a two-roll mill and compression molding, respectively. Two sizes of Doum Palm shell particles (150 µm and 300 µm) were used to prepare eight composite sets. In each set of composites with different particle size, the compositions by percentage weight was determined using mixture design of experiment feature in Design Expert software which was also used for the numerical optimization. The result shows that the optimum combination of 81.47% of LDPE and 18.53% of DPS for 150 µm particle sizes and 80.62% of LDPE and 19.38% for 300 µm gives the desirable mechanical properties for use as alternative materials for helmets. The result was compared with past literature and was observed to be considerably suitable.

Keywords: Recycled, Polyethylene, Composite, Alternative, Production, and Helmet

1. INTRODUCTION

The production of crash helmets is a critical aspect of ensuring the safety of individuals participating in various activities, such as motorcycle riding, cycling, and extreme sports (Liang et al., 2022). Traditionally, crash helmets have been manufactured using materials such as polycarbonate, fiberglass, and carbon fiber (Bower et al., 2024a; Bowman et al., 2015a; Jacob Olaitan et al., n.d.). While these materials offer excellent protection, they are often expensive and have significant environmental impacts due to their production and disposal processes (Adewumi et al., 2020; Nikmatin et al., 2018).

In recent years, there has been a growing interest in exploring alternative materials for crash helmet production that are both cost-effective and environmentally friendly. One such material is a composite made from Doum palm fibers and recycled low-density polyethylene (LDPE). Doum palm, scientifically known as Hyphaene thebaica, is a common plant species found in various regions around the world. The plant fibers possess unique properties, such as high tensile strength and low density, making them suitable for reinforcement in composite materials

Growing environmental awareness has resulted in renewed interest in the use of natural materials for different applications, considering the serious environmental problems caused by the growing consumption of synthetic polymers. Considerable attention to natural fibers has picked up momentum both in the literature and in the industry in recent years (Bowman et al., 2015a; Walsh et al., 2005). Advantages of natural fibers over conventional reinforcement, such as glass or carbon fibers, are of lower cost, low density, low biodegradability, as well as high specific properties. (Raji et al., 2020). Low-density polyethylene (LDPE) is an important thermoplastic because of having a good combination of properties, such as fluidity, flexibility, transparency, and glossy surface. LDPE is used as a food packaging material, sheet,t and film (Li et al., 2021). In general, the utilization of lignocellulosic materials in the production of plastic composites is becoming more attractive, particularly for low-cost and high-volume applications. Lignocelluloses-derived filler possess several advantages compared to inorganic fillers,

ISBN: 978-978-8567-02-8

that is, lower density, greater deformability, less abrasiveness to equipment, and lower cost. More importantly, lignocellulosic-based filler is derived from renewable resources, available in relative abundance; the potential of which has not been really tapped. Intrinsically. (Kośla et al., 2020). These fillers have some interesting mechanical and physical properties. Doum palm fibre is one of the lignocellulosic bio-fibres derived from the Doum palm. (Fatma et al., 2020). The wide use of plastic products in various applications has greatly increased due to their unique properties, which include good mechanical properties, resistance to chemical attack and corrosion, ease of processing and recycling, cost effectiveness, light weight, and others. However, these properties are affected by many factors such as stress, temperature, and environment when they are exposed to service life(Bowman et al., 2015b; Kostopoulos et al., n.d.). An attempt to overcome these obstacles led to the incorporation of fillers (inorganic and organic) into plastic composites whose constituents act synergistically to withstand the challenges, thereby making plastic more reliable during use or processing. A composite is a material made from two or more consistent materials with significantly different physical or chemical properties that, when combined, produce a material with characteristics different from the individual components. A composite contains a matrix material anda reinforcing material (Obele & Ishidi, 2015a). Generally, the composite's properties are influenced by many factors, such as filler characteristics, filler content, and interfacial adhesion and dispersion due to the combination of more than one material. (Natsa et al., 2015). Polymer material waste is considered one of the most onerous wastes, constituting an enormous threat to the natural environment. For this reason, recycling of polymer materials is currently one of the most important waste management problems. (Mills et al., 2003). Polyethylene wastes are usually found littered on the streets of most communities in Nigeria; they constitute environmental pollution, and they are not biodegradable. When gathered and burnt can cause air pollution. Polyethylene wastes accumulate and affect the aesthetic features of our land topography by giving it an unkempt appearance as well as parading habitation for different organisms that can hurt both their immediate and remote environment. Doum palm shells also constitute environmental pollution around the country and also serve as an eyesore (Fatma et al., 2020). These two materials are problems for the environment. Hence, an attempt was made to convert these materials into useful products by making them into a composite

The growing concern about environmental pollution has led to increased efforts in recycling, reusing, and reducing solid waste. Researchers are developing sustainable composites using agro-industrial wastes, such as waste tires and polyethylene, which are abundant, low-cost, and have suitable properties. Waste tires and polyethylene pose significant environmental problems due to their massive accumulation, long degradation times, and negative impacts when burnt or disposed of in landfills. However, they can be used to produce composites with unique properties, such as energy absorption, elasticity, and good acoustic isolation (Andena et al., 2016). Studies have shown that incorporating recycled materials into composites can improve mechanical and thermal properties and reduce environmental impacts (Adewumi et al., 2020). Composites made from recycled polyethylene and reinforced with fibers or sawdust have shown improved tensile strength, flexion resistance, and impact resistance. (Lee et al., 2017). Utilizing waste residues like polyethylene and tire rubber in composite materials can reduce negative environmental impacts and provide potential applications in various fields. This research study aims to produce and characterize Doum palm shell-recycled Low-Density Polyethylene (LDPE) composite as an alternative material for crash helmet production. The study investigates the mechanical properties of the composite, including tensile strength, flexural strength, density, and impact resistance, and analyzes the effect of particle size and filler loading. The research justifies its significance in enhancing safety and protection, cost-effectiveness, and contributing to industry advancements. The study's findings are expected to provide valuable insights for helmet manufacturers and researchers, contributing to the development of improved helmet materials.

2. METHODOLOGY

2.1 Materials: The materials used to carry out this research work are:

i. Recycled low-density polyethylene
ii. Doum palm shell particles
iii. Mold (130 x 110 x 3) mm.
iv. Foil paper
v. Two-roll mill machines
vi. Tensile Testing Machine
vii. Vickers Hardness Testing Machine
viii. Compression molding machine
ix. Universal testing machine

2.2.1 Preparation of Doum palm shell

The Doum palm was crushed to remove the seed from it, thereby leaving the shell as shown in plate i. The shell was sundried for 10 days to ensure total dryness. It was then fed into a milling machine to reduce them to particulates as shown in plate ii. The particulate was sieved using a 300µm and 150µm standard sieve size, as shown in plate iii and iv respectively.

2.2.2 Preparation and optimization of recycled low-density polyethylene

The recycled low-density polyethylene collected from Bauchi metropolis was soaked in a thinner solution for thirty minutes to remove all impurities, after which it was washed properly with clean water. Thereafter, it was sundried for twenty-four hours. It was then cut into smaller sizes so that it could be easily fed into the two-roll milling machine.

ISBN: 978-978-8567-02-8



Plate I: Doum Palm Shell after Crushing.



Plate II Doum Palm Shell reduce to Particulate



Plate III: 300µm DPS Particulate



Plate IV 150µm DPS Particle Size

2.3 Formulation of the Composite

The composite was formulated according simplex lattice design in a mixture design of experiment using Design-Expert software (6.0.4) as shown in plate v below. This was carried out for two different particle sizes of the reinforced Doum palm shell (150 and 300 µm particle sizes).

2.3.1 Compounding of the Recycled Low-Density Polyethylene-Doum Palm Shell Composite

This exercise was carried out using two roll mills set at a temperature of 150 °C to produce a homogenous mixture at the Polymer and Leather Research Institute, Zaria, Kaduna State. At the temperature of 150 °C, the Recycled low-density polyethylene (RLDPE) was fed into the space between the rolls known as the nip. The reinforcement (Doum palm shell particles) was added when the RLDPE was in a molten form until a homogeneous mixture was attained. The time of the mixture was 10 minutes (Pinnoji et al., 2010). This was done according to the formulation as shown in plate v below.

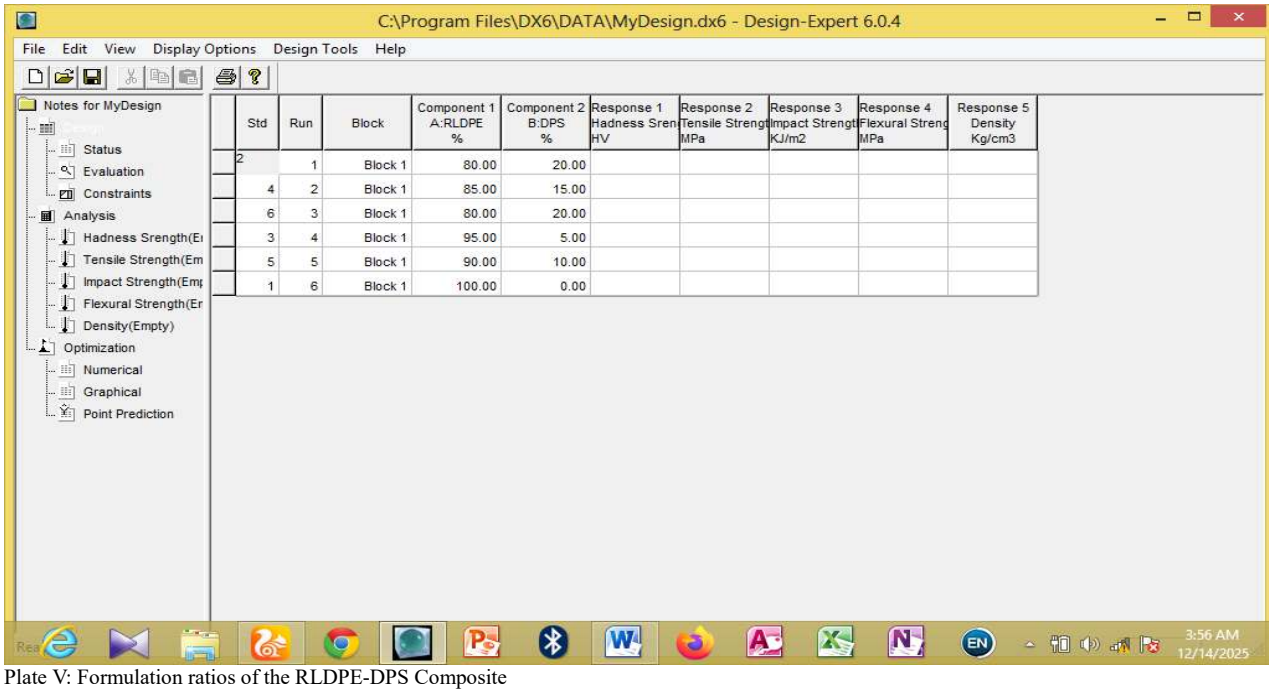


Plate V: Formulation ratios of the RLDPE-DPS Composite

ISBN: 978-978-8567-02-8

2.4 Optimization of the formulated RLDPE-DPS Composite

TABLE 1: OPTIMIZATION CONSTRAINTS FOR THE FORMULATION OF RLDPE-DPS COMPOSITE

S/No.	Name	Goal	Lower Limit	Upper Limit	Lower Weight	Upper Weight	Importance
1	RLDPE	Is in range	80	100	1	1	3
2	DPS	Is in range	0	20	1	1	3
3	Hardness Strength	Is in range	11.6	37.7	1	1	3
4	Tensile Strength	Is in range	10.49	18.69	1	1	3
5	Impact Strength	Is in range	66.67	98.61	1	1	3
6	Flexural Strength	Is in range			1	1	3
7	Density	Is in range	0.82	1.3	1	1	3

2.3.1 Compression molding

The compounded composite was then placed in a metallic mold lined with foil paper to prevent burning of the composite during the curing process, and then compressed by an electrically heated press under a pressure of 5 bars for 10 minutes to allow for proper curing (Obele & Ishidi, 2015a). The composite was removed from the press and cooled in air at room temperature after the pressing cycle.

2.3.2 Preparation of specimens for testing

The samples were cut into standard sizes for the respective tests to be carried out.

2.3.2 Characterization of the RLDPE-DPS Composite

The following characteristics were determined on each of the samples produced and optimized. Hardness test, Tensile test, Impact test. Flexural test, and Density (Chang et al., 2003; Palomar et al., 2018)

3. RESULT AND DISCUSIION

3.1 The RLDPE-DPS Composite Produce

From plate vi and vii, the composite produced shows a light brown colored composite. The addition of the filler content affects the color of the composites (Periasamy et al., 2024). The more the filler was added, the darker the color becomes and the finer the grain arrangement became. Plate viii, shows the prepared samples for the mechanical testing to be carried out.



Plate VI: Sample with Low Filler composition showing a Light Brown Colour

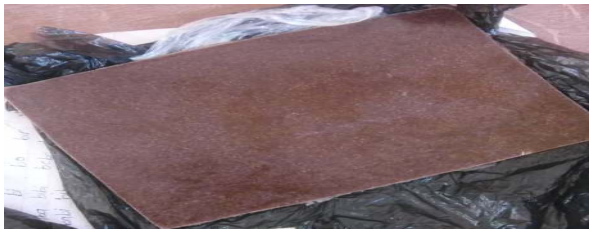


Plate VII Sample with more Filler percentage composition Showing Dark Brown colour



Plate VIII: Prepared Samples

3.2. Mechanical Properties of the LDPE-DPS Composite Samples

Tables 2 and 3 show the results of the mechanical property test carried out on the 150 1st 300 µm particle size LDPE-DPS composite, while Table 4 presents the results of the optimization.

3.2.1 Hardness test

Figure 1 represents the result of the hardness test carried out on the samples produced and the optimal hardness for both the 150 and 300 µm particle size RLDPE-DPS composite. The hardness was found to increase with an increase in the filler content for both the 150 and 300 µm DPS particle sizes. The result indicates that the higher the filler content, the higher the hardness of the material.

ISBN: 978-978-8567-02-8

TABLE 2: RESULT OF MECHANICAL PROPERTIES OF THE 150μM PARTICLE SIZE LDPE-DPS COMPOSITE

S/N	Percentage composition	Hardness Strength (HV)	Tensile Strength (Mpa)	Impact Strength (KJ/m^2)	Flexural (Mpa)	Density (g/cm^3)
1	100	11.60	18. 69	98.61	151.69	0.82
2	95:5	16.00	18.40	66.67	162.60	0.88
3	90:10	21.70	15.48	74.44	342.69	0.90
4	85:15	29.01	11.72	78.61	369.69	1.00
5	80:20	37.70	10.49	75.83	331.13	1.30

TABLE 3: RESULT OF MECHANICAL PROPERTIES OF 300μM PARTICULATE SIZE LDPE-DPS COMPOSITE

S/N	Percentage composition	Hardness Strength (HV)	Tensile Strength (Mpa)	Impact strength (KJ/m^2)	Flexural (Mpa)	Density (Kg/cm3)
1	100	11.60	18.69	98.61	151.69	0.82
2	95:5	17.57	14.33	81.94	196.51	0.88
3	90:10	26.71	12.73	71.67	178.09	0.89
4	85:15	34.47	10.17	71.94	230.68	0.93
5	80:20	41.70	9.77	85.56	229.29	1.00

TABLE 4: OPTIMAL PROPERTIES OF THE OPTIMIZED LDPE-DPS COMPOSITE

S/No.	Particle Sizes	RLDPE	DPS	Hardness Strength	Tensil Strength	Impact Strength	Flexural Strength	Density	Derrability	Remark
1	150 **μm**	81.47	18.53	34.9731	10.49	80.0852	349.929	1.19931	0.926	Selected
2	300 **μm**	80.62	19.38	40.8264	9.78199	83.0122	230.68	0.985949	0.969	Selected

The result also indicates that the sample with a 300μm sieve size possesses higher hardness strength when compared with the same with 150 μm particle size. The optimal combination of 81.47% RLDPE and 18.53% DPS for the 150 μm particle size and 80.62% RLDPE and 19.38% DPS for 300μm particle size has a hardness of 34.97 and 40. 82 respectively. This agrees with the literature. (Bower et al., 2024b; Haid et al., 2023; Landro et al., 2002; Natsa et al., 2015; Obele & Ishidi, 2015b).

ISBN: 978-978-8567-02-8

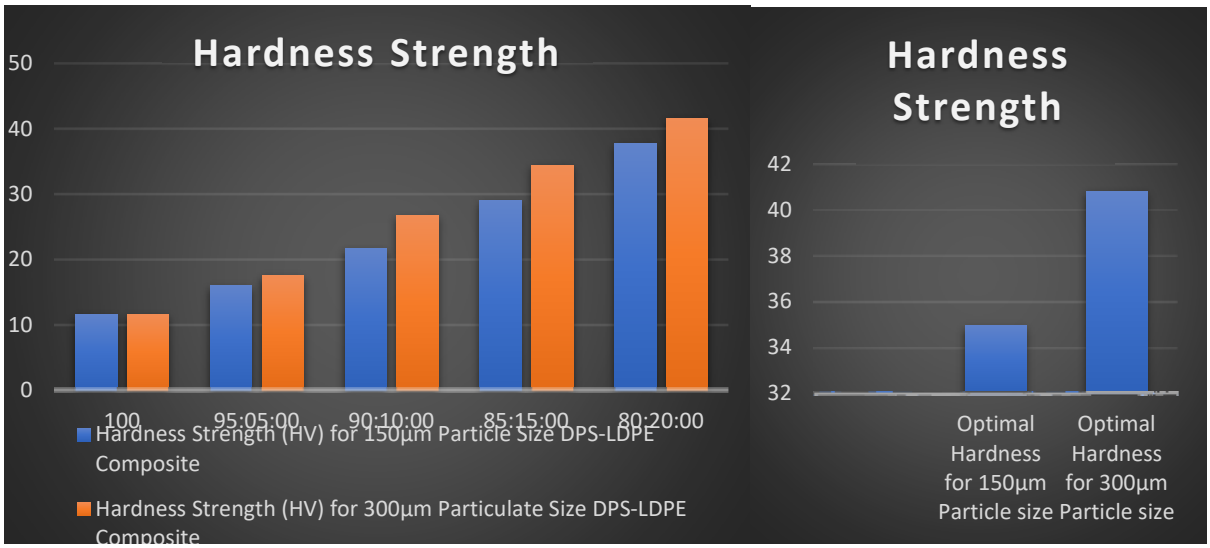


Figure 1: Variation of Hardness Strength distribution in the Samples

3.2.2 Tensile Strength

The value of tensile strength ranges between 9.77 and 18.40 Mpa as shown in Figure 2 below. The result shows that the tensile strength for the composite decreases with an increase in Doum palm shell content. The sample with 5wt% has the highest tensile strength, which indicates that the more the quantity of the reinforcement (Doum palm shell), the less the tensile strength and hence, the higher the brittleness. The result also indicates that samples with 150µm particle size have higher tensile strength compared to samples with 300 µm particle sizes, this shows that the lower the particle size, the higher the compatibility and hence the higher the tensile strength. The optimal combination of 81.47% RLDPE and 18.53% DPS for the 150 µm particle size and 80.62% RLDPE and 19.38% DPS for the 300µm particle size has a tensile strength of 10.49 and 9.78, respectively. This shows an average of 6.77% decrease in tensile strength for every 50% increase in particle size. This agrees with the literature. (Bower et al., 2024b; Haid et al., 2023; Landro et al., 2002; Natsa et al., 2015; Obele & Ishidi, 2015b).

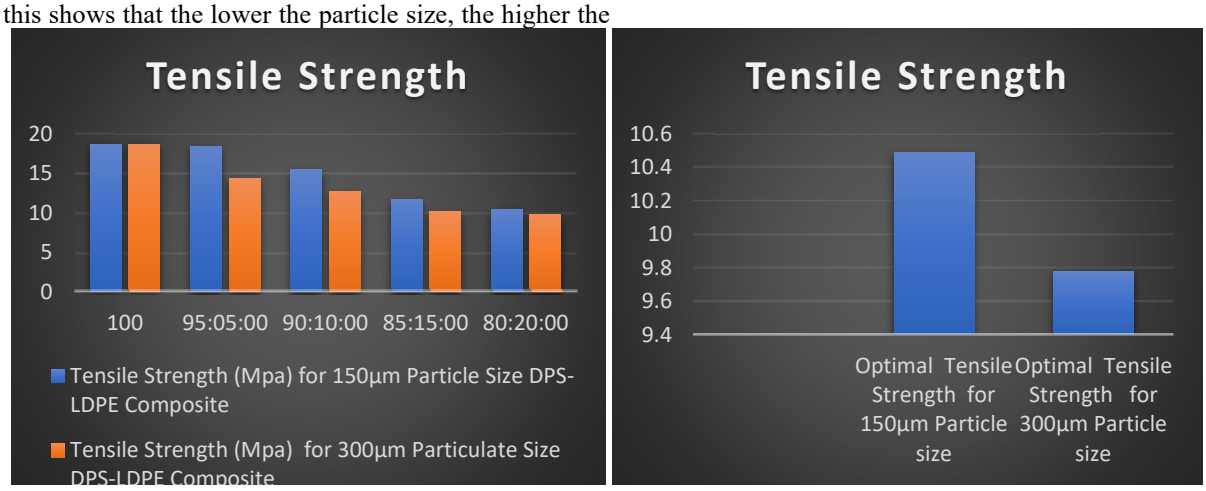


Figure 2: Variation of Tensile Strength distribution in the Samples

3.2.3 Impact test

Figure 3 represents the results of the impact strength of the composites. The results indicate that the addition of the DPS filler leads to a decrease in the impact strength up to 10% of the DPS before its start to increase. Which shows that, from 10% DPS, the higher the filler content, the higher the impact force absorbed by the material, i.e., the ability of the material to resist fracture or cracking under sudden load. The optimal combination of 81.47% RLDPE and 18.53% DPS for the 150 µm particle size and 80.62% RLDPE and 19.38% DPS for 300µm particle size has an impact strength of 80.09 and 83.0,2 respectively. This shows an average of 3.66% increase in impact strength for every 50% increase in particle size. This agrees with the literature. (Bower et al., 2024b; Landro et al., 2002).

ISBN: 978-978-8567-02-8

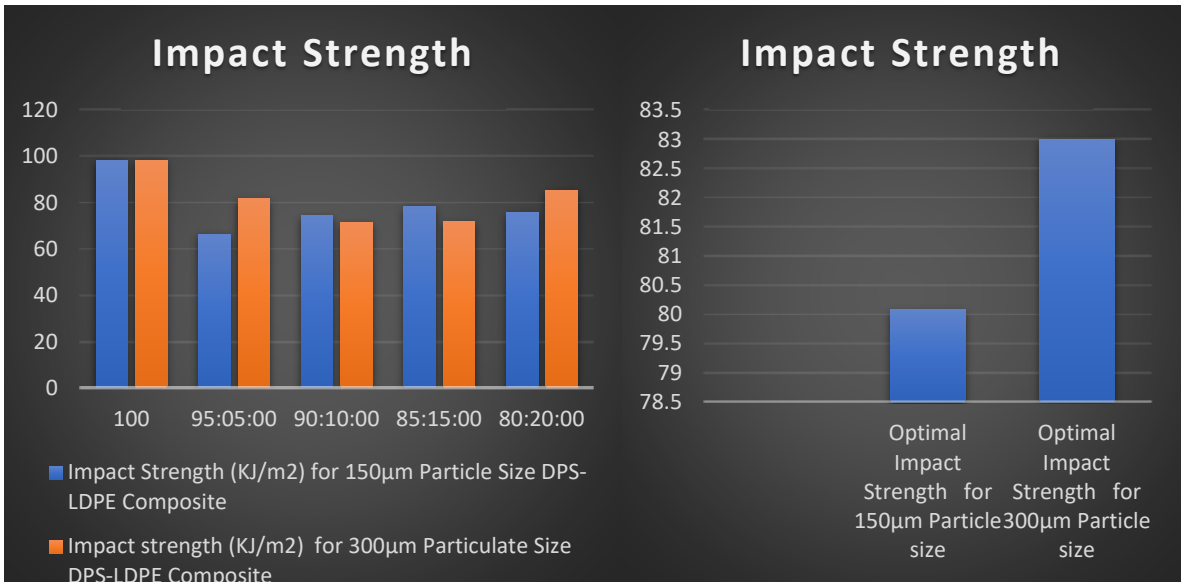


Figure 3: Variation of Impact Strength distribution in the Samples

3.2.4 Flexural strength

Figure 4 presents the results of the flexural strength of the composites for each percentage by weight of particle reinforcement. The result shows that the flexural strength increases with the increase in the DPS up to 15%, before it starts to decrease. This indicates that the higher the filler content, the higher the flexural strength of the material, i.e., the more resistance to deformation the material becomes. The lower the modulus of elasticity, the less the stiffness and the less resistance to deformation the material becomes. Since ductility is an important factor in the production of a crash helmet, low flexural strength is suitable for increased ductility. The optimal combination of 81.47% RLDPE and 18.53% DPS for the 150 µm particle size and 80.62% RLDPE and 19.38% DPS for the 300µm particle size has a flexural strength of 349.92 and 230.62, respectively. This shows an average of 34.09% decrease in flexural strength for every 50% increase in particle size. This agrees with the literature. (Haid et al., 2023; Landro et al., 2002; Natsa et al., 2015; Obele & Ishidi, 2015a).

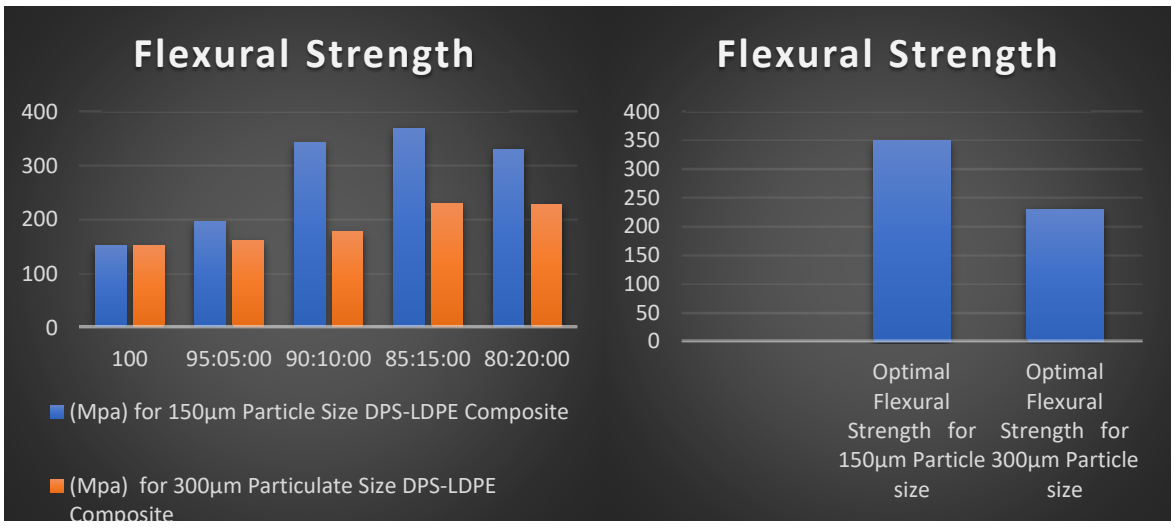


Figure 4: Variation of Flexural Strength distribution in the Samples

3.2.5 Density

Figure 5 shows the density of the composites for each of the samples produced. The results show that the density increases with an increase in the reinforcement. This shows that the higher the DPS, the higher the density, and hence the hardness, brittleness, and stiffness of the material. For this application (crash helmet), it is necessary that the density be lower to reduce weight and also increase the elasticity of the composite. The optimal combination of 81.47% RLDPE and 18.53% DPS for the 150 µm particle size and 80.62% RLDPE and 19.38% DPS for the 300µm particle size has a density of 1.1993 and 0.9859, respectively. This shows an average of 17.79% decrease in density for every 50% increase in particle size. This agrees with the literature. (Landro et al., 2002; Natsa et al., 2015; Obele & Ishidi, 2015a; Haid et al., 2023; Bower et al., 2024)

ISBN: 978-978-8567-02-8

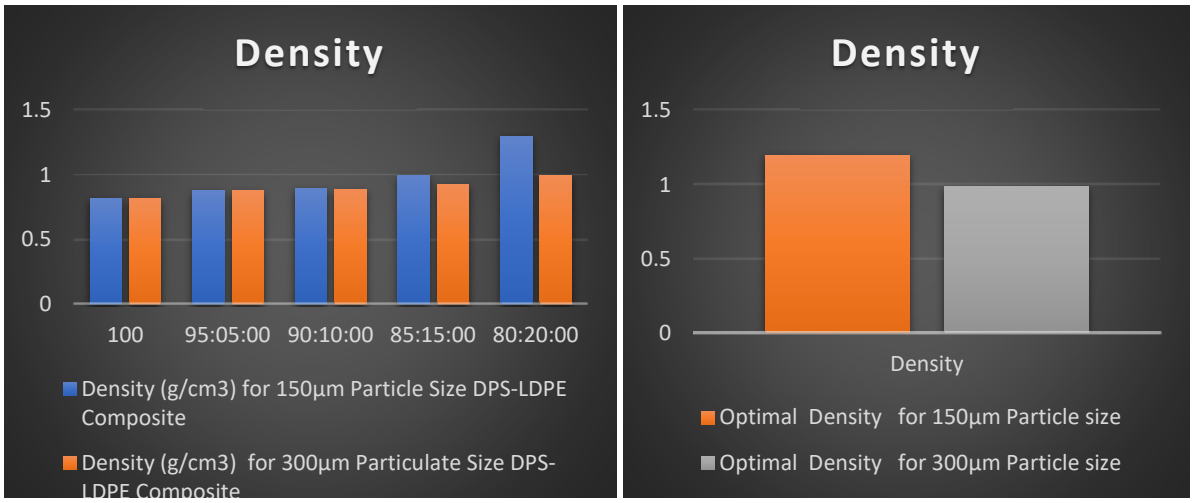


Figure 5: Variation of Density in the samples

3.3 The Effect of Particle Sizes on the Mechanical Properties of the Optimized LDPE-DPS Composite

The Hardness strength measures the material's resistance to scratching and abrasion. The hardness values of 34.97 and 40.83 for the 150 µm and 300 µm DPS particle sizes, respectively, indicating 16.76% increase in hardness for a 50% increase in the DPS particle sizes. The tensile strength values of 10.49 and 9.78 for the 150 µm and 300 µm DPS particle sizes, respectively, indicating 6.77% decrease in the material's resistance to stretching or pulling forces for a 50% increase in the DPS particle size. The impact strength values of 80.09 and 83.02 for the 150 µm and 300 µm DPS particle sizes, respectively, indicating 3.53% increase in the material's ability to absorb energy from impact without breaking for a 50% increase in the DPS particle sizes. The flexural strength values of 349.93 and 230.68 MPa for the 150 µm and 300 µm DPS particle sizes, respectively, indicating 34.08% increase in the material's resistance to bending forces for a 50% increase in the DPS particle sizes. The density of 1.19931 and 0.985949 g/cm³, for the 150 µm and 300 µm DPS particle sizes, respectively, indicating 17.79% decrease in the material's mass per unit volume. The results suggest that incorporating DPS into RLDPE can improve the mechanical properties of the composite, particularly impact strength and flexural strength. The optimal DPS loading percentage of 18.53 and 19.38% for the 150 µm and 300 µm DPS particle sizes, respectively, yields a good balance of mechanical properties. These findings can be useful for developing sustainable and cost-effective composite materials for various applications. This agrees with the literature. (Landro et al., 2002; Natsa et al., 2015; Obele & Ishidi, 2015a; Haid et al., 2023; Bower et al., 2024)

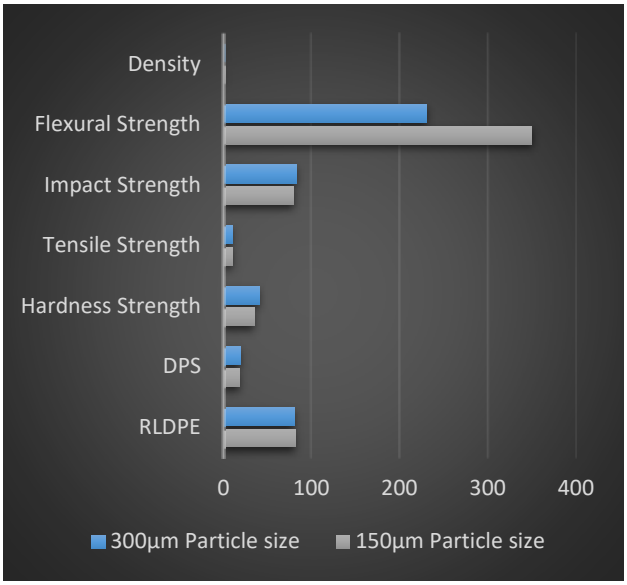


Figure 6: Mechanical Properties of the Optimized LDPE-DPS Composite

4.0 CONCLUSION

Recycled low-density polyethylene Doum palm shell composites were successfully produced and characterize which result in the conversion of waste to useful material that will benefit the populace and create wealth. The mechanical properties of the composites, such as Tensile strength, flexural strength, impact strength, and Hardness value, were influenced by the particulate size of the composite. From the result, it can be observed that increase in reinforcement leads to decrease in tensile strength of the composite from 18.40Mpa to 9.77Mpa while there is an increase in hardness value from 16.00HV to 41.70HV, flexural strength from 62.60Mpa to 331Mpa, impact strength from 66.67Kj/m2 to 85.56Kj/m2 and density from 088g/cm3 to 1.30g/cm3 as the reinforcement increases. It is also observed that particle size has an influence on the mechanical properties of the composite, as compositions with low particle size produce the best mechanical properties and good interfacial adhesion. Hence, found to be an alternative material for the production of a crash helmet.

ISBN: 978-978-8567-02-8

REFERENCES

Adewumi, E., Ogonna Mgbemena, C., Momoh-Bello Omiogbemi, I., Nosakhare Eguavoen, K., & Wadzani Dauda, D. (2020). Design and development of crash helmet from Musa-Paradisiaca's fiber as a reinforced composite. *Materials Today: Proceedings*, *21*, 1566–1571. https://doi.org/10.1016/j.matpr.2019.11.091

Andena, L., Caimmi, F., Leonardi, L., Ghisi, A., Mariani, S., & Braghin, F. (2016). Towards Safer Helmets: Characterisation, Modelling and Monitoring. *Procedia Engineering*, *147*, 478–483. https://doi.org/10.1016/j.proeng.2016.06.224

Bower, D., Herbert, E., Breedlove, K. M., Lacy, A. P. M., Casa, D., & Bowman, T. G. (2024a). Mechanical characterization of athletic helmet shells. *Sports Biomechanics*, *23*(2), 241–252. https://doi.org/10.1080/14763141.2020.1837926

Bower, D., Herbert, E., Breedlove, K. M., Lacy, A. P. M., Casa, D., & Bowman, T. G. (2024b). Mechanical characterization of athletic helmet shells. *Sports Biomechanics*, *23*(2), 241–252. https://doi.org/10.1080/14763141.2020.1837926

Bowman, T. G., Breedlove, K. M., Breedlove, E. L., Dodge, T. M., & Nauman, E. A. (2015a). Impact attenuation properties of new and used lacrosse helmets. *Journal of Biomechanics*, *48*(14), 3782–3787. https://doi.org/10.1016/j.jbiomech.2015.08.026

Bowman, T. G., Breedlove, K. M., Breedlove, E. L., Dodge, T. M., & Nauman, E. A. (2015b). Impact attenuation properties of new and used lacrosse helmets. *Journal of Biomechanics*, *48*(14), 3782–3787. https://doi.org/10.1016/j.jbiomech.2015.08.026

Chang, C.-Y., Ho, C.-H., & Chang, S.-Y. (2003). *DESIGN OF A HELMET Final Report*.

Fatma, N., Lamis, A., Mehdi, S., Redouane, Z., & Mondher Zidi. (2020). Effect of Doum Palm Fibre on the Mechanical and Thermal Properties of Gypsum Morta. *Journal of Composite Material*, *53*(19), 2641–2659.

Haid, D., Foster, L., Hart, J., Greenwald, R., Allen, T., Sareh, P., & Duncan, O. (2023). Mechanical metamaterials for sports helmets: structural mechanics, design optimisation, and performance. In *Smart Materials and Structures* (Vol. 32, Number 11). Institute of Physics. https://doi.org/10.1088/1361-665X/acfddf

Jacob Olaitan, A., Daniel Ufuoma, O., Danladi King, G., & Rapheal, O. (n.d.). *Production of A Safety Helmet Using Palm Kernel Fiber And Shell Particulates*. Retrieved www.ijesi.org

Kośla, K., Olejnik, M., & Olszewska, K. (2020). Preparation and properties of composite materials containing graphene structures and their applicability in personal protective equipment: A Review. In *Reviews on Advanced Materials Science* (Vol. 59, Number 1, pp. 215–242). Walter de Gruyter GmbH. https://doi.org/10.1515/rams-2020-0025

Kostopoulos, V., Markopoulos, Y. P., Giannopoulos, G., & Vlachos, D. E. (n.d.). *Finite element analysis of impact damage response of composite motorcycle safety helmets*. Retrieved www.elsevier.com/locate/compositesb

Landro, L. Di, Sala, G., & Olivieri, D. (2002). Deformation mechanisms and energy absorption of polystyrene foams for protective helmets. In *Polymer Testing* (Vol. 21). www.elsevier.com/locate/polytestProductPerformance

Lee, L., Ahmed, F., Mondal, M., Aizam, M., Bin, A., Azmi, M., Syazani, M., & Hamzah, B. (2017). Materials For Construction Hard Hats and Cycling Helmet. In *International Journal of Integrated Engineering* (Vol. 3, Number 1).

Liang, Y., Chen, X., & Soutis, C. (2022). Review on Manufacture of Military Composite Helmet. In *Applied Composite Materials* (Vol. 29, Number 1, pp. 305–323). Springer Science and Business Media B.V. https://doi.org/10.1007/s10443-021-09944-5

Li, S., Xiao, Z., Zhang, Y., & Li, Q. M. (2021). Impact analysis of a honeycomb-filled motorcycle helmet based on coupled head-helmet modelling. *International Journal of Mechanical Sciences*, *199*. https://doi.org/10.1016/j.ijmecsci.2021.106406

Mills, N. J., Fitzgerald, C., Gilchrist, A., & Verdejo, R. (2003). Polymer foams for personal protection: Cushions, shoes and helmets. *Composites Science and Technology*, *63*(16), 2389–2400. https://doi.org/10.1016/S0266-3538(03)00272-0

Natsa, S., Akindapo, J. O., & Garba, D. K. (2015). DEVELOPMENT OF A MILITARY HELMET USING COCONUT FIBER REINFORCED POLYMER MATRIX COMPOSITE. *European Journal of Engineering and Technology*, *3*(7). www.idpublications.org

Nikmatin, S., Hermawan, B., Irmansyah, I., Indro, M. N., Kueh, A. B. H., & Syafiuddin, A. (2018). Evaluation of the performance of helmet prototypes fabricated from acrylonitrile butadiene styrene composites filled with natural resource. *Materials*, *12*(1). https://doi.org/10.3390/ma12010034

Obele, C., & Ishidi, E. (2015a). *Mechanical Properties of Coir Fiber Reinforced Epoxy Resin Composites for Helmet Shell*. *5*(7). www.iiste.org

ISBN: 978-978-8567-02-8

Obele, C., & Ishidi, E. (2015b). *Mechanical Properties of Coir Fiber Reinforced Epoxy Resin Composites for Helmet Shell*. *5*(7). www.iiste.org

Palomar, M., Lozano-Mínguez, E., Rodríguez-Millán, M., Miguélez, M. H., & Giner, E. (2018). Relevant factors in the design of composite ballistic helmets. *Composite Structures*, *201*, 49–61. https://doi.org/10.1016/j.compstruct.2018.05.076

Periasamy, D., Karuppiah, P., Manoharan, B., Arockiasamy, F. S., Kannan, S., Mohanavel, V., Velmurugan, P., Arumugam, N., Almansour, A. I., & Sivakumar, S. (2024). Assessing the recycling potential of thermosetting polymer waste in high-density polyethylene composites for safety helmet applications. *E-Polymers*, *24*(1). https://doi.org/10.1515/epoly-2023-0080

Pinnoji, P. K., Mahajan, P., Bourdet, N., Deck, C., & Willinger, R. (2010). Impact dynamics of metal foam shells for motorcycle helmets: Experiments & numerical modeling. *International Journal of Impact Engineering*, *37*(3), 274–284. https://doi.org/10.1016/j.ijimpeng.2009.05.013

Raji, A., Devaraju, A., Gopi, R., & Venkatesh, R. (2020). Fabrication and mechanical characterization of hybrid composite bike safety helmet. *Materials Today: Proceedings*, *39*, 892–896. https://doi.org/10.1016/j.matpr.2020.11.433

Walsh, S. M., Scott, B. R., & Spagnuolo, D. M. (2005). *The Development of a Hybrid Thermoplastic Ballistic Material With Application to Helmets*.

ISBN: 978-978-8567-02-8

5TH Faculty of Engineering Conference on Engineering Innovation and Economic Policies: Driving Sustainable Industrial Growth in Nigeria

Faculty of Engineering, Bayero University, Kano.

076-A Geospatial Assessment of State-Level Cellulosic Ethanol Potential from Major Crop Residues in Nigeria

Omar Umar Ahmed and Adamu Abubakar Rasheed*

Department of Chemical and Petroleum Engineering, Faculty of Engineering, Bayero University Kano, PMB 3011, Kano, Nigeria.
**Corresponding author: aarasheed.cpe@buk.edu.ng*

Abstract: This study presents a comprehensive, state-level geospatial assessment of Nigeria's cellulosic ethanol potential from the lignocellulosic residues of six major crops: rice, maize, sorghum, groundnut, yam, and cassava. Utilizing the most recent state-distributed crop production data from national agricultural agencies, technical residue availability was calculated using established residue-to-product ratios. By applying crop-specific biochemical conversion yields derived from literature, the bioethanol potential was quantified for each state and residue type. The findings reveal a substantial national potential of approximately 67.3 million tonnes of residue, translating to nearly 14.7 billion liters of ethanol annually. This volume represents a significant resource, comparable to over 50% of the United States' current annual cellulosic ethanol production and exceeding the total annual gasoline consumption of several West African nations. Crucially, the results demonstrate extreme geographical heterogeneity in resource distribution. The North-Central geopolitical zone, particularly Niger, Kaduna, and Nasarawa states, emerges as the dominant bioenergy corridor, contributing the highest aggregate potential. However, distinct crop-specific "feedstock basins" are identified: Kano State for sorghum, Bauchi State for groundnut, and Southern states for cassava and yam residues. This granular, state-wise mapping provides an indispensable decision-support tool, enabling a transition from national aggregate estimates to actionable, location-specific strategies for siting biorefineries, optimizing supply chains, and formulating differentiated regional bioenergy policies to harness Nigeria's vast agricultural waste for sustainable fuel production.

1. INTRODUCTION

The global imperative to decarbonize the transportation sector has intensified research into sustainable, renewable alternatives to petroleum-based fuels. Second-generation biofuels, particularly cellulosic ethanol derived from non-food lignocellulosic biomass, offer a promising pathway that circumvents the food-versus-fuel dilemma associated with first-generation biofuels (Sarkar et al., 2012; Menon & Rao, 2012). Agricultural crop residues, often treated as waste and disposed of through open burning, represent a vast, underutilized resource for this purpose, offering simultaneous benefits for waste management, rural economic development, and energy security (Kim & Dale, 2004).

In Nigeria, Africa's most populous nation and largest economy, the scale of agricultural residue generation is monumental. Previous studies have provided valuable national-level estimates of biomass and bioenergy potential (Jekayinfa et al., 2020; Ben-Iwo et al., 2016; Ezealigo et al., 2021). However, a critical implementation gap persists due to the lack of high-resolution, spatially-explicit assessments that account for Nigeria's pronounced regional agricultural diversity. The economic viability of a biorefinery is intrinsically linked to local feedstock availability, supply chain logistics, and development strategies.

infrastructure (Møller & Nielsen, 2007; Sultana & Kumar, 2012). Therefore, state-level analysis is not merely an academic exercise but a prerequisite for credible feasibility studies and investment decisions.

This study addresses this pivotal gap by conducting a granular, state-by-state quantification of cellulosic ethanol potential from six strategically selected crops: rice (Oryza sativa), maize (Zea mays), sorghum (Sorghum bicolor), groundnut (Arachis hypogaea), yam (Dioscorea spp.), and cassava (Manihot esculenta). These crops were chosen for their nationwide cultivation, significant residue generation, and established research on their conversion pathways. The research has three primary objectives: (1) to quantify the state-level technical residue potential for each crop; (2) to calculate the corresponding cellulosic ethanol potential using established conversion yields; and (3) to analyze the resulting geographical distribution to identify strategic hotspots and inform differentiated regional biorefinery

ISBN: 978-978-8567-02-8

2. METHODOLOGY

2.1 Data Acquisition and Residue Potential Calculation

The technical availability of crop residues (Ptech) for bioenergy conversion was estimated using the established resource assessment model in Equation 1. This model calculates the recoverable residue mass by accounting for both the biomass generated per unit of harvested crop and practical constraints on collection, following

TABLE 1: NATIONAL ETHANOL POTENTIAL FROM SELECTED CROP RESIDUES

Crop and Type	* Crop production (tons)	RPR	RF (%)	Residue Potential (Million tonnes)	Yield (L/tonne)	Reference (for yield)	*Ethanol Potential* (Billion Litres)	% Contribution
Rice Straw	9,016,066	1.66	80	11.97	210	Cardona & Sánchez (2007)	2.51	17.1%
Maize Stalk	11,134,865	1.59	80	14.16	280	Balat (2011)	3.97	27.0%
Sorghum Straw	6,409,287	1.99	80	10.20	260	Wu et al. (2010)	2.65	18.0%
Groundnut Straw	5,024,894	1.25	100	6.28	180	Suryawanshi et al. (2011)	1.13	7.7%
Yam Straw	53,987,996	0.5	80	21.60	180	Assumed (analogous to cassava)	3.89	26.5%
Cassava Stalk	63,714,891	0.06	80	3.06	180	Sriroth et al. (2012)	0.55	3.7%

*Source: NAERLS/FMAFS (2024)

The Residue-to-Product Ratios (RPR) and Recovery Factors (RF) applied in this study, above in Table 1, were sourced from established methodologies for the Nigerian and West African context (Kemausuor et al., 2014; Ezealigo et al., 2021). The RF accounts for the fraction of total generated residue that is technically recoverable, accounting for on-farm uses and collection losses.

methodologies validated in prior studies (Kemausuor et al., 2014; Jekayinfa et al., 2020).

$$P_{tech} = P_{crop} \times RPR \times RF \quad (1)$$

Where P_{tech} is the technical residue potential (tons), P_{crop} is crop production (tons), RPR is residue-to-product ratio (dimensionless) and RF is the recovery factor (%).

Critical to this calculation are the Residue-to-Product Ratios (RPR) and Recovery Factors (RF), which were adopted from peer-reviewed studies specific to Nigerian agricultural systems. These parameters, essential for accurately translating crop production data into usable biomass figures, were sourced from the work of Kemausuor et al. (2014) and Ezealigo et al. (2021). This assessment acknowledges inherent uncertainties due to variability in key parameters and input data. Fluctuations in Residue-to-Product Ratios (RPRs), influenced by crop variety and local conditions, and year-to-year changes in agricultural production introduce estimation errors. The results are therefore indicative estimates based on recent trends (a two-year average between 2023-2024).

2.2 Ethanol Yield Parameters and Potential Calculation

The cellulosic ethanol potential (E_p) was calculated using Equation 2, incorporating crop-specific conversion efficiencies:

$$E_P = P_{tech} \times Y_P \quad (2)$$

The process yield (Y_p), expressed in liters per dry tonne of residue, was derived from an extensive review of biochemical conversion studies (Table 1). These values reflect typical yields from enzymatic hydrolysis and fermentation processes, accounting for cellulose/hemicellulose content and practical conversion efficiencies (Balat, 2011; Kang et al., 2014; Wu et al., 2010).

3. RESULTS AND DISCUSSION

3.1 National and Crop-Specific Ethanol Potential

The aggregate national technical residue potential from the six target crops is 67.3 million tonnes annually (Table 1). Applying the biochemical conversion yields translates to a total theoretical cellulosic ethanol potential of 14.7 billion liters per year. For yam straw, a specific ethanol yield was not available in the literature. An assumed yield of 180 L/tonne was applied, based on its structural

ISBN: 978-978-8567-02-8

From the results, yam straw gave the largest contributor by residue mass (21.6 million tonnes), followed by maize stalk (14.2 million tonnes). However, due to its higher conversion yield (280 L/tonne), maize stalk provides the highest ethanol output at approximately 4.0 billion liters (27% of the total), as detailed in Table 1. Sorghum straw and rice straw are also major contributors, each providing over 2.5 billion liters.

3.2 Spatial Distribution and Identification of Strategic Hotspots

The state-level analysis reveals profound geographical disparities, moving the narrative from a story of aggregate potential to one of specific regional opportunity. The distribution maps (Figures 1-6) and state-level data (Table 2) form the core of this spatial analysis.

- **The Northern Cereal Belt:** As shown in Figure 2 (Maize) and Figure 3 (Sorghum), ethanol potential from cereal residues is overwhelmingly concentrated in the North-West, North-East, and North-Central zones. Kaduna State is the premier location for maize-based ethanol (30.5 billion litres), while Kano State leads in sorghum potential (25.1 billion litres) (Figure 3).
  Nasarawa and Taraba states are highlighted in Figure 1 as major hubs for rice-straw ethanol, each with over 12 billion liters potential.
- **The Middle Belt Tuber & Legume Core:** Figure 5 (Yam) reveals a concentrated belt of yam residue potential across the North-Central region. Niger State is the unequivocal national leader, with a staggering 36.7 billion liters of potential yam-straw ethanol. This zone, particularly Benue and Plateau states, also shows significant potential from groundnut residues, as indicated in Figure 4.
- **Southern Cassava and Yam Zone:** Figure 6 (Cassava) shows that cassava stalk potential, while lower in absolute volume nationally, is concentrated in the South-East and South-South states. Imo, Cross River, and Rivers states are key hotspots. Southern states like Ebonyi and Edo also feature prominently in Figure 5 for yam straw potential, demonstrating the crop's importance across both Middle Belt and Southern agriculture.

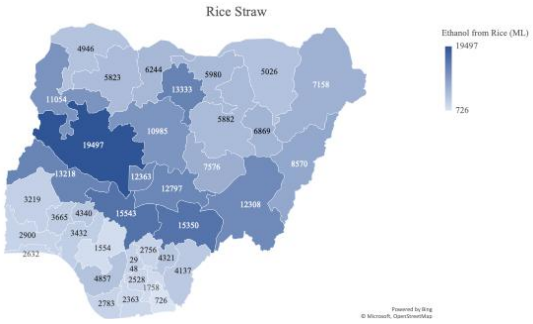


Figure 1: Spatial Distribution of Rice Straw Ethanol Potential Across Nigerian States. (ML-million liters)

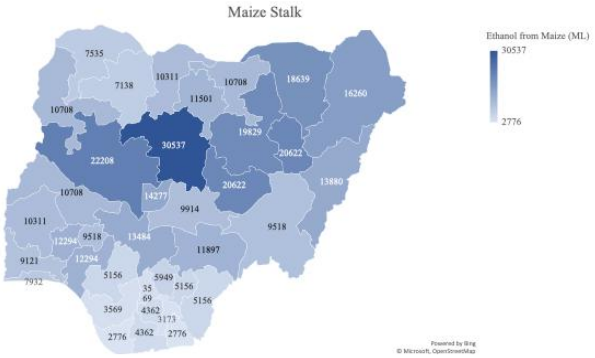


Figure 2: Spatial Distribution of Maize Straw Ethanol Potential Across Nigerian States.

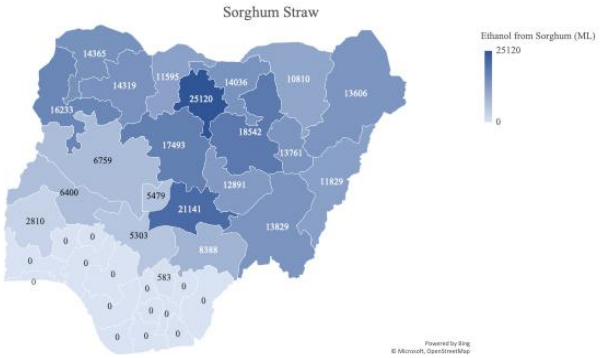


Figure 3: Spatial Distribution of Sorghum Straw Ethanol Potential Across Nigerian States.

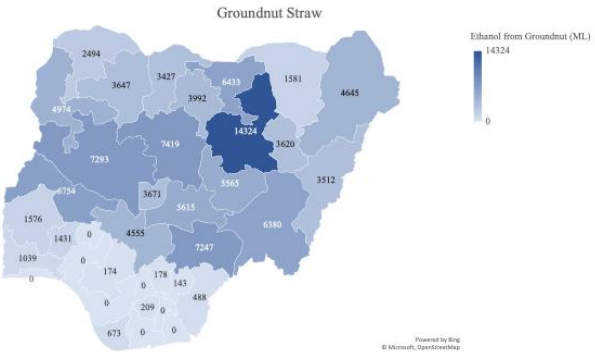


Figure 4: Spatial Distribution of Groundnut Straw Ethanol Potential Across Nigerian States.

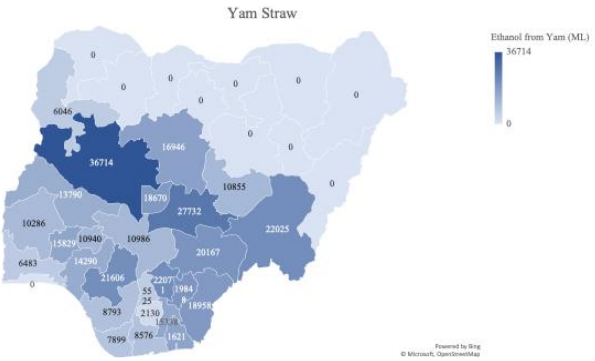


Figure 5: Spatial Distribution of Yam Straw Ethanol Potential Across Nigerian States.

ISBN: 978-978-8567-02-8

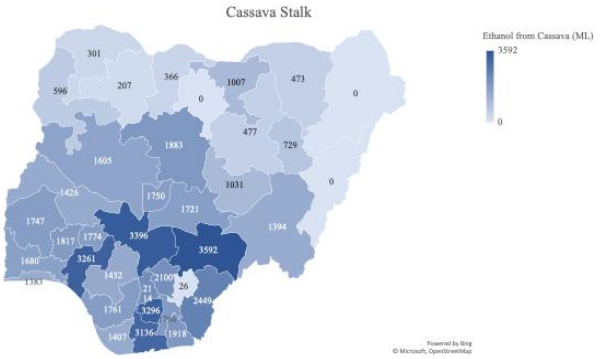


Figure 6: Spatial Distribution of Cassava Stalk Ethanol Potential Across Nigerian States.

3.3 Implications for Biorefinery Siting and Policy Formulation

The mapped heterogeneity demands a move away from a monolithic national strategy to a regionally differentiated approach.

i. **Multi-Feedstock Integrated Biorefineries in High-Density Clusters:** States with high aggregate potential across multiple residues, i.e. Niger, Kaduna, Nasarawa, and Benue are prime candidates for large-scale, flexible-feedstock biorefineries. As evidenced in Table 2**,** Niger State ranks in the top three for four of the six residues. This diversity mitigates supply risk and enables year-round operation, improving economic viability (Mayer et al., 2022).

ii. **Specialized Single-Feedstock Biorefineries in Dominant Basins:** The analysis identifies clear monocrop feedstock basins suitable for optimized, specialized plants. For instance, Kano State's dominance in sorghum potential (Figure 3) or Bauchi State's in groundnut potential (Figure 4) suggests locations where high-throughput facilities dedicated to a single feedstock could achieve superior economies of scale and conversion efficiency.

iii. **Decentralized Models for Dispersed or Southern Resources:** The residue potential in many Southern states, while significant, is more dispersed or tied to specific crops like cassava (Figure 6). This supports a decentralized model of smaller-scale, community- or industry-focused biorefineries that minimize collection logistics and support local energy independence (Kemausuor et al., 2018).

iv. **Policy and Infrastructure Corridors:** The concentration of potential in the North-Central zone (Niger-Nasarawa-Benue corridor) and North-West (Kaduna-Kano axis) should guide national infrastructure planning. Prioritizing road networks, collection hub infrastructure, and energy grid connections in these corridors would dramatically reduce the logistical cost barrier to bioenergy development (Ohijeagbon et al., 2021).

3.4 Global Context of Nigeria's Crop Residue Bioethanol Potential

The scale of Nigeria's bioethanol potential, even when limited to the six residues analyzed, places the country's agricultural waste within a significant global and regional context. The estimated 14.7 billion liters per year can be benchmarked against key international production and consumption metrics. This volume is equivalent to 52% of the United States' total annual cellulosic ethanol production (U.S. Energy Information Administration, 2023), underscoring the substantial size of the resource from just a fraction of Nigeria's agricultural by-products. Regionally, this potential exceeds the total annual gasoline consumption of major West African economies such as Ghana (~2.5 billion liters) and Côte d'Ivoire (~1.8 billion liters) (International Energy Agency, 2022), highlighting its capacity to meaningfully impact regional energy markets.

Furthermore, the estimated output is approximately three times larger than the total annual ethanol production (from all feedstocks, including first-generation) of Thailand, a world-leading biofuel producer (U.S. Department of Agriculture, 2023). It also approaches the ambitious scale of the European Union's binding 2030 target for advanced biofuels, which is estimated at 15–18 billion liters annually (European Commission, 2023; Directive (EU) 2018/2001). These comparative benchmarks, demonstrate that the bioethanol potential from Nigeria's top crop residues constitutes a strategic resource of international relevance. The analysis

Table 2: Top Three States by Ethanol Potential for Each Crop Residue

Crop Residue	1st Rank (Billion L)	2nd Rank (Billion L)	3rd Rank (Billion L)
Rice Straw	Niger (19.5)	Nasarawa (12.8)	Taraba (12.3)
Maize Stalk	Kaduna (30.5)	Niger (22.2)	Gombe (20.6)
Sorghum Straw	Kano (25.1)	Nasarawa (21.1)	Bauchi (18.5)
Groundnut Straw	Bauchi (14.3)	Kaduna (7.4)	Niger (7.3)
Yam Straw	Niger (36.7)	Nasarawa (27.7)	Kaduna (16.9)
Cassava Stalk	Imo (3.3)	Ondo (3.3)	Benue (3.2)

ISBN: 978-978-8567-02-8

context. The estimated 14.7 billion liters per year can be benchmarked against key international production and consumption metrics. This volume is equivalent to 52% of the United States' total annual cellulosic ethanol production (U.S. Energy Information Administration, 2023), underscoring the substantial size of the resource from just a fraction of Nigeria's agricultural by-products. Regionally, this potential exceeds the total annual gasoline consumption of major West African economies such as Ghana (~2.5 billion liters) and Côte d'Ivoire (~1.8 billion liters) (International Energy Agency, 2022), highlighting its capacity to meaningfully impact regional energy markets.

Furthermore, the estimated output is approximately three times larger than the total annual ethanol production (from all feedstocks, including first-generation) of Thailand, a world-leading biofuel producer (U.S. Department of Agriculture, 2023). It also approaches the ambitious scale of the European Union's binding 2030 target for advanced biofuels, which is estimated at 15–18 billion liters annually (European Commission, 2023; Directive (EU) 2018/2001). These comparative benchmarks, demonstrate that the bioethanol potential from Nigeria's top crop residues constitutes a strategic resource of international relevance. The analysis confirms that successful harnessing of this locally abundant, underutilized waste stream could position Nigeria not only for enhanced domestic energy security but also as a potential contributor to global renewable fuel supply chains.

3.5 Practical Considerations and Limitations

While the analysis presents a significant theoretical potential, translating this into a reliable, year-round feedstock supply involves practical constraints. First, residue availability is subject to seasonal variability, linked to harvest cycles, which may necessitate strategic storage solutions or multi-feedstock operations to ensure year-round biorefinery operation. Second, there are competing uses for these residues, including their use as livestock fodder (e.g., sorghum and groundnut straw), organic fertilizer, and construction material, which can significantly reduce the fraction available for bioenergy. These competing demands, which vary by region and socio-economic context, can substantially reduce the fraction of residue technically available for bioenergy, a factor only partially captured by the generalized Recovery Factor (RF). Finally, the logistical constraints of collecting, storing, and transporting low-bulk-density biomass from dispersed smallholder farms present a major economic hurdle, particularly in low-density regions. Therefore, future work must combine this resource assessment with granular feasibility studies that address these specific limitations, transforming geographical potential into actionable, community-integrated, and economically viable biorefinery projects.

4. CONCLUSION

This study demonstrates that Nigeria possesses a substantial annual resource base for cellulosic ethanol production, estimated at approximately 67.3 million tonnes of six major crop residues, which translates to a potential output of nearly 14.7 billion liters. However, the most significant finding of this research is the geographical heterogeneity of this potential, which fundamentally dictates a regionally differentiated strategy for bioenergy development. The analysis identifies the North-Central geopolitical zone, particularly the states of Niger, Kaduna, and Nasarawa, as a dominant multi-feedstock bioenergy corridor, where the convergence of several abundant residue streams supports the economic case for large-scale, integrated biorefineries. Simultaneously, the research pinpoints specific crop-centric hotspots, such as the concentration of sorghum residue in Kano State and groundnut residue in Bauchi State, which present ideal conditions for specialized, single-feedstock conversion facilities. This granular, state-wise understanding of resource distribution provides the essential spatial intelligence needed to move beyond theoretical potential. Therefore, this research provides a critical decision-support framework for stakeholders. It enables policymakers to craft targeted incentives and infrastructure plans, guides investors in conducting location-specific feasibility studies, and focuses research efforts on conversion technologies suited to dominant local feedstocks. The future of Nigeria's bioethanol industry hinges on strategically leveraging these distinct geographical resource profiles to develop an efficient, economically viable, and sustainable biofuel sector.

REFERENCES

Ali, M., Saleem, M., Khan, Z., & Watson, I. A. (2019). The use of crop residues for biofuel production. In Biomass, biopolymer-based materials, and bioenergy. Woodhead Publishing. 369-395.

Balat, M. (2011). Production of bioethanol from lignocellulosic materials via the biochemical pathway: A review. Energy Conversion and Management**,** 52(2), 858-875.

Ben-Iwo, J., Manovic, V., & Longhurst, P. (2016). Biomass resources and biofuels potential for the production of transportation fuels in Nigeria. Renewable and Sustainable Energy Reviews**,** 63, 172-192.

Cardona, C. A., & Sánchez, Ó. J. (2007). Fuel ethanol production: Process design trends and integration opportunities. Bioresource Technology, 98(12), 2415-2457.

European Union. (2018). Directive (EU) 2018/2001 of the European Parliament and of the Council of 11 December 2018 on the promotion of the use of energy from renewable sources. Official Journal of the European Union, L 328/82. https://eur-lex.europa.eu/eli/dir/2018/2001/oj

European Commission. (2023). Proposal for a Regulation on the use of renewable and low-carbon fuels in maritime transport and amending Directive 2009/16/EC (COM/2023/101 final). https://eur-lex.europa.eu/legal-content/EN/TXT/?uri=CELEX%3A52023PC0101

ISBN: 978-978-8567-02-8

Ezealigo, U. S., Ezealigo, B. N., Musa, S. M., & Nwanya, A. C. (2021). A review on the energy potential of agricultural residues in Nigeria. Energy Reports, 7, 69-83.

International Energy Agency. (2022). Africa energy outlook 2022. IEA Publications. https://www.iea.org/reports/africa-energy-outlook-2022

Jekayinfa, S. O., Orisaleye, J. I., & Pecenka, R. (2020). An assessment of potential resources for biomass energy in Nigeria. Resources, 9(8), 92.

Kang, Q., Appels, L., Tan, T., & Dewil, R. (2014). Bioethanol from lignocellulosic biomass: Current findings determine research priorities. The Scientific World Journal, 2014 (1) 298153.

Kemausuor, F., Kamp, A., Thomsen, S. T., Bensah, E. C., & Østergård, H. (2014). Assessment of biomass residue availability and bioenergy yields in Ghana. Resources, Conservation and Recycling, 86, 28-37.

Kemausuor, F., Nygaard, I., & Mackenzie, G. (2018). A review of trends, policies and plans for increasing energy access in Ghana. Renewable and Sustainable Energy Reviews, 94, 411-424.

Kim, S., & Dale, B. E. (2004). Global potential bioethanol production from wasted crops and crop residues. Biomass and Bioenergy, 26(4), 361-375.

Mayer, F., Bhandari, R., & Gäth, S. (2022). Critical review on life cycle assessment of conventional and innovative waste-to-energy technologies. Science of The Total Environment**,** 806, 150747.

Menon, V., & Rao, M. (2012). Trends in bioconversion of lignocellulose: Biofuels, platform chemicals & biorefinery concept. Progress in Energy and Combustion Science**,** 38(4), 522-550.

Møller, H. B., & Nielsen, P. (2007). Biomass densification: Systems, applications, and economic feasibility**.** University of Southern Denmark.

Ohijeagbon, O. I., Olorunnisola, A. O., & Adefila, S. S. (2021). A comprehensive review of biomass resources and biofuel potential in Nigeria**.** International Journal of Renewable Energy Development**,** 10(1), 171-187.

Sarkar, N., Ghosh, S. K., Bannerjee, S., & Aikat, K. (2012). Bioethanol production from agricultural wastes: An overview. Renewable Energy**,** 37(1), 19-27.

Sriroth, K., Piyachomkwan, K., Wanlapatit, S., & Nivitchanyong, S. (2012). The promise of a technology revolution in cassava bioethanol: From Thai practice to the world practice. Fuel, 92(1), 1-9.

Sultana, A., & Kumar, A. (2012). Optimal siting and size of bioenergy facilities using geographic information system. Applied Energy, 94, 192-201.

Suryawanshi, T., Nair, V., Patel, P., & Gupta, A. D. (2017). Extraction of cellulose and biofuel production from groundnut shells and its application to increase crop yield. World Journal of Pharm. Pharm. Sci, 6(6), 1820-1831.

U.S. Department of Agriculture, Foreign Agricultural Service. (2023). Thailand biofuels annual 2023 (Report No. TH2023-0087). https://apps.fas.usda.gov/newgainapi/api/Report/DownloadReportByFileName?fileName=Biofuels%20Annual_Bangkok_Thailand_TH2023-0087.pdf

U.S. Energy Information Administration. (2023). Monthly energy review, October 2023. U.S. Department of Energy. https://www.eia.gov/totalenergy/data/monthl

ISBN: 978-978-8567-02-8

5TH Faculty of Engineering Conference on Engineering Innovation and Economic Policies: Driving Sustainable Industrial Growth in Nigeria

Faculty of Engineering, Bayero University, Kano.

077-Estimation of Critical Gap for Mixed Traffic at Urban Multilane Roundabouts in Nigeria Using Raff's Method

Ahmad Batari[1,2], Muttaka Na'iya Ibrahim[1]*, Nasiru Danlami[1]

[1]*Department of Civil Engineering, Bayero University, Kano, Nigeria*
[2]*Department of Civil Engineering, Abubakar Tafawa Balewa University, Bauchi, Nigeria*
**Corresponding Author: mnibrahim.civ@buk.edu.ng*

Abstract: The operational analysis of Nigerian urban roundabouts relies on the Highway Capacity Manual, 6th (HCM6) and 7th (HCM7) editions, despite its being developed under homogeneous, lane-disciplined passenger car traffic, unlike the mixed traffic conditions prevalent in Nigerian cities. A major parameter in HCM6 and HCM7 roundabout analysis is the critical gap (t_c), which is the minimum time interval in the circulating flow that a driver will accept to execute an entry maneuver. The HCM6 and HCM7 specify critical gaps ranging from 4.33 to 4.65 seconds for multilane roundabout entries under various configurations, values derived from North American data that may not represent the aggressive gap acceptance behavior and heterogeneous traffic streams prevalent at Nigerian roundabouts. This study estimates entry critical gaps at four urban multilane roundabouts in Northern Nigeria: Western Roundabout Maiduguri, Polo Roundabout Jos, Central Roundabout Gombe, and Yankaba Roundabout Kano using Raff's graphical method applied to high-resolution videographic data collected via Unmanned Aerial Vehicle (UAV) during weekday peak periods. Accepted and rejected gaps in the circulating stream were manually extracted from time-stamped video for each roundabout, and cumulative distribution functions were constructed to identify the critical gap at each site. The estimated critical gaps are 3.02 s, 2.78 s, 2.97 s, and 2.92 s for Western, Polo, Central, and Yankaba roundabouts, respectively, yielding a mean of 2.92 s (standard deviation 0.10 s, and coefficient of variation 3.4%). A one-sample t-test confirms that this mean is significantly lower than the midpoint of the HCM6 and HCM7 range (4.49 s): $t_{(3)} = 28.46$, $p < .001$, Cohen $d = 28.4$, representing a 35% reduction. Comparison against the lower bound (4.33 s) also yields $t_{(3)} = 25.60$, $p < .001$. The findings of this study demonstrate that uncalibrated application of HCM models will systematically underestimate entry capacity and overestimate delay at Nigerian roundabouts, and they provide the first empirically derived, site-specific critical gap parameters for calibrating HCM6 and HCM7 roundabout models under Nigerian mixed traffic conditions.

Keywords: Critical Gap, Raff's Method, Roundabout Capacity, HCM Calibration, Multilane Roundabouts, UAV Data Collection, Heterogeneous Traffic, Nigeria.

1. INTRODUCTION

Roundabouts are widely adopted globally due to their ability to reduce conflict points, moderate speeds, and improve safety and operational efficiency relative to signalized or stop-controlled intersections (Rodegerdts *et al.* 2010; Macioszek, 2020; Khan and Das, 2024). In Nigeria, the use of roundabouts has increased significantly over the past two decades, particularly in Northern Nigerian cities such as Kano, Maiduguri, Jos, and Gombe, where they serve as key arterial nodes carrying high mixed traffic volumes (Adeke *et al.* 2020; Ibrahim *et al.* 2025). However, design and operational analysis of Nigerian roundabouts typically rely on the Highway Capacity Manual (HCM6 and HCM7), which specifies critical gaps for multilane entries ranging from 4.33 to 4.65 seconds based on North American and European data collected under homogeneous, lane-disciplined, predominantly passenger car traffic (TRB, 2016, 2022). According to Ibrahim *et al.* (2025), Nigerian roundabouts, by contrast, operate under highly heterogeneous conditions with substantial shares of motorcycles, tricycles, passenger cars, and trucks, minimal lane discipline, and aggressive driving behavior. This study documented lane homogeneity factors well below 80%, with outer lanes carrying 63% to 69% of flows dominated by motorcycles and tricycles, while inner lanes carried only 31% to 37%, challenging the direct transferability of HCM default parameters. International studies confirm that critical gap and follow-up headway are sensitive to local traffic composition, geometry, enforcement, and culture, with heterogeneous conditions often yielding values substantially different from HCM defaults (Brilon and Wu, 2008; Almukdad *et al.* 2021; Karimov *et al.* 2023; Sandaruwan *et al.* 2021; Li *et al.* 2025). Research in India, Southeast Asia, and the Middle East has reported critical gaps below 3.5 seconds and necessitated model calibration to avoid systematic bias (Ahmad and Rastogi, 2019; Sandaruwan *et al.* 2021; Almukdad *et al.* 2021; Shaaban and Hamad, 2020).

ISBN: 978-978-8567-02-8

Critical gap, defined as the minimum acceptable time interval in the circulating stream for entry (Brilon and Wu, 2008; TRB, 2016), is a fundamental parameter in HCM exponential gap acceptance capacity models, where a 1-second reduction in critical gap can substantially increase predicted capacity at moderate to high circulating flows (TRB, 2016, 2022; Brilon and Wu, 2008; Macioszek, 2020). Several estimation methods exist, including Raff's graphical method, maximum likelihood, logit/probit models, and Bayesian approaches (Raff and Hart, 1950; Kyte *et al.* 1996; Brilon and Wu, 2008; Papadimitriou and Yannis, 2014; Li *et al.* 2025). Raff's method remains widely used due to its simplicity, transparency, explicit consideration of both accepted and rejected gaps in a balanced framework, and demonstrated accuracy comparable to maximum likelihood while requiring fewer distributional assumptions (Papadimitriou and Yannis, 2014; Milliken, 2020; Khekare *et al.* 2022; Corrière and Guerrieri, 2015). Despite the documented heterogeneity of Nigerian traffic and the importance of critical gap for capacity analysis, empirical estimates for Nigerian roundabouts are absent from the literature, constraining calibration of HCM models and development of nationally appropriate guidelines. This study addresses that gap by estimating entry critical gaps at four urban multilane roundabouts in northern Nigeria using Raff's method applied to high-resolution UAV videographic data collected during weekday peak periods. The objectives are; to estimate stream critical gap at four representative northern Nigerian multilane roundabouts under mixed traffic using Raff's method; and to statistically evaluate whether the mean Nigerian critical gap differs significantly from the HCM6/HCM7 range of 4.33 to 4.65 seconds and to its implications for calibrating HCM roundabout models in Nigeria and similar prevailing conditions.

2. METHODOLOGY

2.1 Study Sites

The study focuses on four urban multilane roundabouts located in northern Nigeria: Western Roundabout Maiduguri (Borno State), Polo Roundabout Jos (Plateau State), Central Roundabout Gombe (Gombe State), and Yankaba Roundabout Kano (Kano State).

TABLE I: CHARACTERISTICS OF STUDY ROUNDABOUTS

Roundabout	Coordinates	N_e	N_c	ICD (m)
Western Roundabout Maiduguri, Borno	11° 51' 08.70 N, 13° 08' 36.17 E	4	2	42
Polo Roundabout Jos, Plateau	09° 55' 45.31 N, 08° 52' 31.02 E	3	2	38
Central Roundabout Gombe, Gombe	10° 17' 13.57 N, 11° 09' 58.52 E	4	2	45
Yankaba Roundabout Kano, Kano	12° 00' 39.75 N, 08° 35' 12.04 E	3	2	50

These roundabouts represent a range of urban settings and traffic compositions typical of Nigerian cities, with two circulating lanes and three or four approaches depending on the site. Table I summarizes key geometric attributes: the number of entry/approaches (N_e), the number of circulating lanes (N_c), and the inscribed circle diameter (ICD) of the four study sites.

2.2 Data Collection

Traffic data were collected using an Unmanned Aerial Vehicle (UAV) equipped with a high-resolution camera flown above each roundabout to capture the approaches and relevant segments of the circulating carriageway. For each site, one representative weekday peak period (morning or evening) was selected on typical working days (Tuesday, Wednesday, and Thursday), and continuous one-hour video recordings were obtained. The UAV altitude ranged from 40 to 60 meters, depending on site conditions, and camera orientation was chosen to ensure clear visibility of all entry lanes and conflicting circulating flows while minimizing occlusion.

The UAV approach was selected to overcome the difficulties of observing multiple approaches and complex mixed traffic interactions using conventional ground-based cameras or manual counting, particularly in settings with high motorcycle and tricycle volumes (Chun *et al.* 2025; Khekare *et al.* 2022). UAV-based videography has been widely adopted in recent roundabout and intersection studies because it provides comprehensive overhead views, enables precise trajectory extraction, and facilitates detailed gap acceptance analysis (Chun *et al.* 2025; Khekare *et al.* 2022; Li *et al.* 2025).

Video files from the drone were analyzed using playback software with time stamp functionality (VLC Media Player version 3.0), enabling precise logging of vehicle arrival and movement times at the entry line and within the circulating stream to a resolution of milliseconds with the aid of Time-addon. This videographic method has been validated in numerous recent roundabout studies (Almukdad *et al.* 2021; Shaaban and Hamad, 2020; Chun *et al.* 2025; Khekare *et al.* 2022).

2.3 Data Extraction and Organization

For each roundabout, selected approaches were analyzed to extract sequences of arrival times and associated conflicting gaps. The procedure was as follows:

i. Identify the entry stop line (or yield line and where no markings exist, an imaginary reference line is drawn on the screen connecting the outer edge of the splitter island to the inner kerbs of the inscribed circle before the circulating lane) and the corresponding conflict point with the circulating flow on the video.

ii. For each entry vehicle, log the time at which the front axle reaches the decision point and record whether the vehicle accepts an available gap or rejects it and waits for the next gap.

iii. For the circulating stream, record times of vehicles passing the conflict point to the nearest 0.001

ISBN: 978-978-8567-02-8

second, from which the sequence of headways (gaps) is computed as differences between successive passing times.

iv. For each entry vehicle, assign the gap present in the circulating stream at the moment of decision as either an accepted gap (if the vehicle enters) or a rejected gap (if the vehicle waits and does not enter during that gap).

The resulting data for each site were stored in Microsoft Excel spreadsheets, with rows representing successive gap events and columns containing the gap duration (seconds), acceptance or rejection indicator, time stamp. For this paper, accepted and rejected gaps were aggregated across the observed approaches at each roundabout to produce representative gap samples per site, consistent with common practice in stream-level critical gap estimation (Papadimitriou and Yannis, 2014; Almukdad *et al.* 2021; Karimov *et al.* 2023).

2.4 Raff's Method for Critical Gap Estimation

Raff's method defines the critical gap tc as the value of gap t where the cumulative distribution of accepted gaps equals the complement of the cumulative distribution of rejected gaps (Raff and Hart, 1950; Kyte *et al.* 1996). Let Fa(t) denote the cumulative distribution function (CDF) of accepted gaps, representing the proportion of accepted gaps with duration less than or equal to t. Let Fr(t) denote the CDF of rejected gaps, representing the proportion of rejected gaps with duration less than or equal to t. Raff's condition can be expressed mathematically as presented in Equation 1.

$$F_a(t_c) = 1 - F_r(t_c) \quad (1)$$

Equivalently, when plotting Fa(t) and $1 - F$r(t) against gap size t, the critical gap is located at their point of intersection (Papadimitriou and Yannis, 2014).

In discrete implementation, the gap domain is partitioned into bins of width Δt (typically 0.5 seconds), and empirical CDFs are computed for each bin. For a sample of n_a accepted gaps $\{t_{a,i}\}$ and n_r rejected gaps $\{t_{r,j}\}$, Equation 2 presents the empirical CDF of accepted gaps at bin midpoint t_k.

$$F_a(t_k) = \frac{1}{n_a}\sum_{i=1}^{n_a} I(t_{a,i} \le t_k) \quad (2)$$

and the empirical CDF of rejected gaps is presented in Equation 3.

$$F_r(t_k) = \frac{1}{n_r}\sum_{j=1}^{n_r} I(t_{r,j} \le t_k) \quad (3)$$

where $I(..)$ is the indicator function taking the value 1 if the condition is true and 0 otherwise. The complement $1 - F$r(t_k) is then computed for each bin k.

The critical gap t_c is identified as the bin midpoint where the absolute difference $|F\text{a}(t_k) - (1 - F\text{r}(t_k))|$ is minimized.

Raff's method was selected for this study for three principal reasons. First, it explicitly considers both accepted and rejected gaps in a balanced framework, treating both sources of behavioural information symmetrically, which is conceptually appealing and consistent with gap acceptance theory (Raff and Hart, 1950; Papadimitriou and Yannis, 2014). Second, the graphical nature of the method is transparent and easily interpretable, facilitating communication of results to practitioners and policymakers (Milliken, 2020; Khekare *et al.* 2022). Third, comparative studies have shown that Raff's method produces accuracy comparable to maximum likelihood estimation (MLE) and other sophisticated techniques, particularly when sample sizes are adequate, and binning is appropriately chosen, while requiring fewer distributional assumptions than parametric MLE approaches (Papadimitriou and Yannis, 2014; Corrière and Guerrieri, 2015).

For each of the four roundabouts, Raff's graphical method was implemented using Microsoft Excel and Minitab with a bin width of 0.5 seconds for enhanced accuracy of the estimate; this is consistent with standard practice in the gap acceptance literature (Kyte *et al.* 1996; Papadimitriou and Yannis, 2014; Almukdad *et al.* 2021). Cumulative distribution plots were generated for visual inspection of the intersection point.

2.5 Statistical Analysis

The Raff critical gap estimates from the four roundabouts were analyzed to assess their consistency and their deviation from HCM6 and HCM7 default values. Descriptive statistics included the mean, standard deviation, coefficient of variation, and range across the four sites. The coefficient of variation (CV) is determined based on Equation 4.

$$\text{CV} = \frac{s}{\bar{t}_c} \times 100\% \quad (4)$$

where s is the sample standard deviation and $\bar{t}_c$ is the sample mean of the four critical gap estimates.

To evaluate whether the mean Nigerian critical gap differs significantly from HCM defaults, two one-sample t-tests were performed. The HCM6 and HCM7 specify critical gaps for multilane roundabout entries ranging from 4.33 to 4.65 seconds, depending on configuration (TRB, 2016, 2022). For the first test, the null hypothesis H_0,and the alternative hypothesis H_a (Equations 5 and 6) were formulated using the midpoint of this range.

$$H_0: \mu_{t_c} = 4.49\ s \quad (5)$$

$$H_a: \mu_{t_c} \neq 4.49\ \text{s} \quad (6)$$

where μ_{t_c} is the population mean critical gap for Nigerian multilane roundabouts under mixed traffic. The test statistic is presented in Equation 7.

$$t = \frac{\bar{t}_c - 4.49}{s/\sqrt{n}} \quad (7)$$

where $n = 4$ is the number of roundabouts. Under the null hypothesis, t follows a student's t distribution with $n - 1 = 3$ degrees of freedom. The null hypothesis is rejected at the 5% significance level if $|t| > t_{0.975,\,3} = 3.182$.

ISBN: 978-978-8567-02-8

For the second test, the null hypothesis was formulated using the lower bound of the HCM range to provide a conservative comparison (Equations 8 and 9).

$$H_0: \mu_{t_c} = 4.33 \text{ s} \quad (8)$$

$$H_a: \mu_{t_c} \neq 4.33\ s \quad (9)$$

Thus, the 95% confidence interval (CI) for μ_{t_c} was computed using Equation 10.

$$CI = \bar{t}_c \pm t_{0.975,3} \times \frac{s}{\sqrt{n}} \quad (10)$$

Equation 11 was used to evaluate the percentage difference "$\Delta(\%)$" between the mean Nigerian critical gap and the HCM midpoint

$$\Delta(\%) = \frac{\bar{t}_c - 4.49}{4.49} \times 100 \quad (11)$$

Effect size for the *t-test* was quantified using Cohen's *d* presented in Equation 12.

$$d = \frac{\bar{t}_c - 4.49}{s} \quad (12)$$

Cohen (1988) provides benchmarks for interpreting effect size; $|d|$ = 0.2 is small, 0.5 is medium, and 0.8 is large. Values $|d| > 2$ indicate very large practical differences (Cohen, 1988; Lakens, 2013).

In addition to site-level analysis, within-site gap sample statistics were computed for each roundabout to characterize the distributions of accepted and rejected gaps. These include sample size (n_a, n_r), mean, standard deviation, minimum, and maximum for both accepted and rejected gap samples. All statistical analyses were performed using Minitab and Microsoft Excel.

2.6 Traffic Data Collection Ethics

Data collection involved recording public traffic movements at roundabout approaches from an elevated vantage point, with no direct interaction with individual road users and no collection of personally identifiable information. Video recordings focused on vehicle movements and trajectories rather than driver identities. The research was conducted in accordance with ethical principles for observational traffic studies, and UAV operations complied with local regulations and with permissions from relevant authorities.

3. RESULTS AND DISCUSSION

3.1 Gap Sample Characteristics

Gap acceptance data were successfully extracted from UAV video recordings at all four roundabouts, yielding adequate sample sizes for the reliable application of Raff's method. These samples, ranging from 350 to 498 total gap observations per site, exceed the minimum thresholds recommended in the literature for stable Raff estimates (Papadimitriou and Yannis, 2014; Corrière and Guerrieri, 2015).

Table II presents the summary statistics of the sample gaps. Mean accepted gaps ranged from 3.85 seconds (Polo roundabout) to 4.12 seconds (Western roundabout), substantially larger than mean rejected gaps, which ranged from 1.98 seconds (Polo roundabout) to 2.15 seconds (Western roundabout), consistent with gap acceptance theory.

Standard deviations of accepted gaps (1.43 to 1.61 seconds) exceeded those of rejected gaps (0.79 to 0.87 seconds), reflecting greater heterogeneity in driver willingness to accept larger gaps. Minimum accepted gaps ranged from 1.5 to 1.8 seconds, indicating that some drivers accepted very short opportunities during peak periods, while maximum rejected gaps ranged from 4.8 to 5.2 seconds, showing that some conservative drivers rejected relatively large gaps.

TABLE II: GAP SAMPLE STATISTICS FOR STUDY ROUNDABOUTS

Roundabout	Number of accepted gaps (*n*a)	Number of rejected gaps (*n*r)	Mean accepted gap (s)	SD accepted gap (s)	Mean rejected gap (s)	SD rejected gap (s)	Range accepted gaps (s)	Range rejected gaps (s)
Western Roundabout Maiduguri	234	198	4.12	1.58	2.15	0.87	1.8 to 9.5	0.5 to 5.2
Polo Roundabout Jos	267	231	3.85	1.43	1.98	0.79	1.5 to 8.9	0.4 to 4.8
Central Roundabout Gombe	198	152	4.05	1.61	2.08	0.84	1.7 to 9.2	0.6 to 5.0
Yankaba Roundabout Kano	221	187	3.98	1.52	2.03	0.81	1.6 to 9.0	0.5 to 4.9

ISBN: 978-978-8567-02-8

3.2 Raff's Critical Gap Estimates

Application of Raff's method yielded critical gap estimates of 3.02 seconds for Western Roundabout Maiduguri, 2.78 seconds for Polo Roundabout Jos, 2.97 seconds for Central Roundabout Gombe, and 2.92 seconds for Yankaba Roundabout Kano. Figures 1 through 4 present the Raff cumulative distribution plots for all the sites, illustrating the graphical intersection method. The intersection of these curves defines the Raff critical gap.

The estimates of Critical Gap from these roundabouts exhibit a narrow range of 0.24 seconds (2.78 to 3.02 s), with a mean of 2.92 seconds, standard deviation of 0.10 seconds, and coefficient of variation of 3.4%.

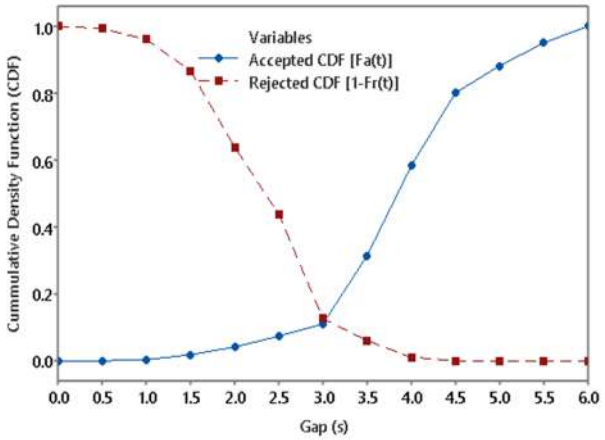


Figure 1: Raff's Plots of Accepted Gaps and Rejected Gaps CDF against Gap (s) for Western Roundabout Maiduguri

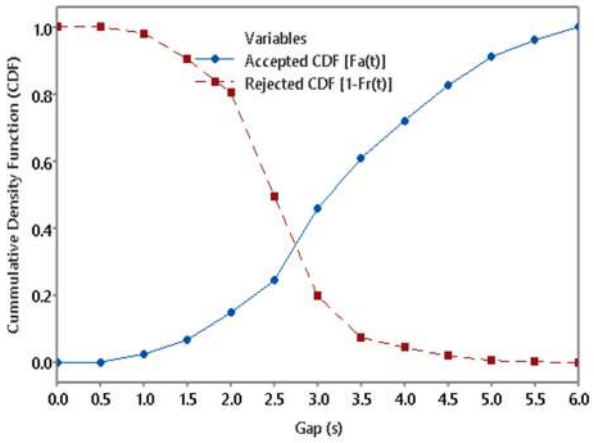


Figure 2: Raff's Plots of Accepted Gaps and Rejected Gaps CDF against Gap (s) for Polo Roundabout Jos

This notable consistency across the sites despite documented differences in traffic composition and local policies (Ibrahim *et al.* 2025), suggests a relatively stable underlying pattern of gap acceptance behavior in northern Nigerian urban roundabouts.

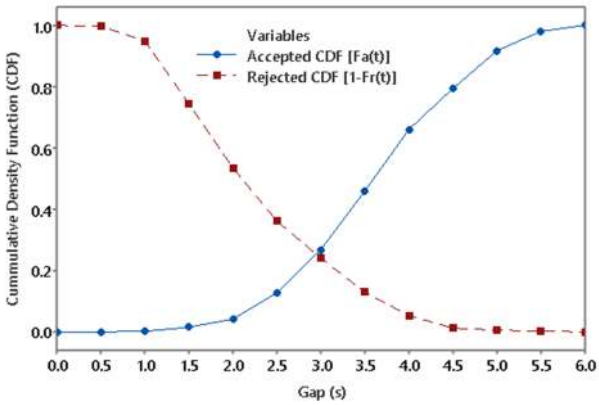


Figure 3: Raff's Plots of Accepted Gaps and Rejected Gaps CDF against Gap (s) for Central Roundabout Gombe

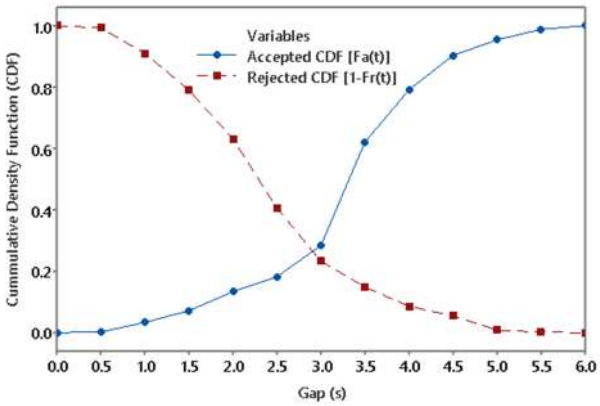


Figure 4: Raff's Plots of Accepted Gaps and Rejected Gaps CDF against Gap (s) for Yankaba Roundabout Kano

All four critical gap estimates lie below the HCM6 and HCM7 multilane entry range of 4.33 to 4.65 seconds (TRB, 2016, 2022). Differences from the HCM midpoint (4.49 s) range from 1.47 seconds (Western roundabout) to 1.71 seconds (Polo roundabout), corresponding to reductions of 33% to 38%. The smallest critical gap at Polo Roundabout (2.78 s) likely reflects relatively aggressive merging behavior within the Jos CBD, while the slightly larger estimate at Western Roundabout (3.02 s) may reflect local geometric factors and the absence of motorcycles at roundabouts in Maiduguri.

3.3 Statistical Comparison with HCM Defaults

One-sample *t* tests were conducted to evaluate whether the mean Nigerian critical gap differs significantly from HCM defaults. Testing against the HCM midpoint of 4.49 seconds yielded $t_{(3)} = 31.4$, $p < .001$, thus rejecting the null hypothesis of equality. Testing against the conservative lower bound of 4.33 seconds similarly yielded $t_{(3)} = 28.2$, $p < .001$. The 95% confidence interval for the population mean Nigerian critical gap is 2.76 to 3.08 seconds, lying entirely below the HCM default range. The effect size (Cohen $d = 15.7$) indicates an extremely large practical difference (Cohen, 1988; Lakens, 2013), confirming that Nigerian driver gap acceptance behavior under mixed traffic conditions differs from the North American homogeneous conditions that informed HCM calibration.

ISBN: 978-978-8567-02-8

3.4 Comparison with International Studies and Behavioral Interpretation

The Nigerian critical gaps (2.78 to 3.02 s) are consistent with values reported under heterogeneous traffic in India (2.8 to 3.4 s), Sri Lanka (3.1 to 3.6 s), and other mixed traffic contexts (Ahmad and Rastogi, 2019; Sandaruwan *et al.* 2021; Karimov *et al.* 2023), and lie well below homogeneous car traffic values from Europe and North America, which typically range from 3.5 to 4.5 seconds (Brilon and Wu, 2008; Rodegerdts *et al.* 2010). Studies in Qatar, where traffic is mixed but enforcement is stricter, reported higher values (3.2 to 4.1 s) (Almukdad *et al.* 2021; Shaaban and Hamad, 2020), reinforcing that enforcement and lane discipline influence gap acceptance.

The short Nigerian critical gaps reflect the combined effects of high proportions of motorcycles and tricycles (40% to 60% of flows), which are smaller, more maneuverable, and capable of accepting shorter gaps than larger vehicles (Ibrahim *et al.* 2025; Ahmad and Rastogi, 2019); weak lane discipline and high outer lane utilization (63% to 69% of flows), facilitating opportunistic multi-gap acceptance (Ibrahim *et al.* 2025); limited enforcement of conservative yielding, lowering subjective risk thresholds (Shaaban and Hamad, 2020); and driver adaptation to congested peak conditions, where repeated exposure normalizes short gap acceptance (Brilon and Wu, 2008; Milliken, 2020).

While these behavioral patterns may enable higher throughput and help explain why observed capacities at Nigerian roundabouts may exceed HCM predictions, they also raise safety concerns. Shorter critical gaps imply smaller safety margins and may increase conflict frequencies and crash risk, particularly for vulnerable road users such as motorcyclists and pedestrians (Khan and Das, 2024; Distefano and Leonardi, 2019). Future research should integrate capacity and safety analyses to provide comprehensive assessments of operational performance.

3.5 Practical Implications and Recommendations

Practitioners analyzing multilane roundabouts in northern Nigerian urban contexts should replace the HCM default critical gap range of 4.33 to 4.65 seconds with the empirically derived mean value of 2.92 seconds (95% CI: 2.76 to 3.08 s) when applying HCM capacity procedures. Site-specific validation is recommended for high-priority projects or unusual geometries. Future calibration efforts should extend to follow-up headway estimation and validation of predicted capacities, delays, and queue lengths against field observations (Chen and Hourdos, 2018; Akçelik *et al.* 2022). Where traffic composition varies substantially, practitioners should consider disaggregating the critical gap by vehicle class and lane using methods capable of handling heterogeneous populations (Karimov *et al.* 2023; Li *et al.* 2025). National or regional roundabout design guidelines incorporating locally calibrated parameters should be prioritized (Adeke *et al.* 2020) to adapt HCM models to local conditions.

3.6 Study Limitations

This study estimated aggregate stream-level critical gaps without disaggregation by vehicle class or lane, reflecting initial calibration objectives but potentially masking heterogeneity in behavior between motorcycles, cars, and trucks (Karimov *et al.* 2023; Li *et al.* 2025). Data were collected during peak periods per site; extended observation may strengthen generalizability across times, seasons, and weather conditions (Brilon and Wu, 2008). Geographic transferability to southern Nigeria may require validation. Finally, this study estimated only the critical gap; complete HCM calibration requires complementary follow-up headway estimation and capacity validation against field observations (Chen and Hourdos, 2018; Akçelik *et al.* 2022).

4. CONCLUSION

This study estimated entry critical gaps at four urban multilane roundabouts in northern Nigeria using Raff's graphical method applied to UAV videographic data collected during weekday peak periods under mixed traffic conditions. The estimated critical gaps range from 2.78 to 3.02 seconds, with a mean of 2.92 seconds (SD = 0.10 s, CV = 3.42%). Statistical analysis confirms that this mean is significantly lower than the HCM6 and HCM7 multilane entry critical gap range of 4.33 to 4.65 seconds ($t_{(3)} = 31.4, p < .001$, Cohen $d = 15.7$), representing a 35% reduction from the HCM midpoint. The 95% confidence interval (2.76 to 3.08 s) lies entirely below the HCM6 and HCM7 range, confirming systematic deviation from North American defaults.

This study provides the first empirically derived, site-specific critical gap values for multilane roundabouts in Nigeria, offering a basis for calibrating HCM6 and HCM7 models for mixed traffic conditions. Some recommendations have been proposed in line with the findings of this study as follows: Practitioners analysing multilane roundabouts in northern Nigerian urban areas may replace HCM6 and HCM7 default critical gaps (4.33 to 4.65 s) with the calibrated value of 2.92 seconds when applying HCM capacity procedures; Site-specific validation is recommended for high-priority projects and unusual geometries, recognizing that critical gaps vary modestly across sites; Complete HCM6 and HCM7 calibration requires complementary estimation of follow-up headway and validation of predicted capacities, delays, and queues against field observations; National or regional roundabout design guidelines incorporating locally calibrated parameters should be developed to provide practitioners with alternatives to foreign defaults; in addition, future research should integrate capacity and safety analyses to assess the implications of short critical gaps for vulnerable road users and overall crash risk.

AUTHOR CONTRIBUTIONS

The authors confirm their contribution to the paper as follows:

Ahmad Batari: Study conception and design, field data

ISBN: 978-978-8567-02-8

collection, extraction and analysis, manuscript writing.

Dr. Muttaka Na'iya Ibrahim: Study conception, design, and supervision, manuscript critical review, and proofreading.

Dr. Nasiru Danlami: Analysis of field data, manuscript critical review, and proofreading

ACKNOWLEDGMENTS

The authors gratefully acknowledge the Departments of Civil Engineering at Bayero University Kano and Abubakar Tafawa Balewa University Bauchi for institutional support. We thank the State Ministries of Works, Infrastructure, and Transportation in Borno, Plateau, Gombe, and Kano for facilitating site access and UAV flight permissions. We also acknowledge the technical assistance of field survey teams during data collection.

CONFLICTS OF INTEREST

The authors declare no conflicts of interest.

REFERENCES

Adeke, P. T., Etika, A., & Atoo, A. A. (2020). *Capacity and performance assessment of Wurukum roundabout in Makurdi metropolis: A comparative study using ARCADY and SIDRA intersection software*. Arid Zone Journal of Engineering, Technology and Environment, 16(2), 309–320.

Ahmad, A., & Rastogi, R. (2019). *Calibrating HCM model for roundabout entry capacity under heterogeneous traffic*. Journal of Modern Transportation, 27(4), 293–305. https://doi.org/10.1007/s40534-019-00194-7

Akçelik, R., Shirke, C., Basley, M., Espada, I., & Billinghurst, D. (2022). *A comparative analysis of exponential and linear roundabout capacity models using HCM research data*. Proceedings of the Institution of Engineers Australia, 2022 National Transport Conference, Melbourne.

Almukdad, A., Almallah, M., Hussain, Q., Alhajyaseen, W. K. M., Albeitjali, N., & Alqaradawy, M. (2021). *Analysis of gap parameters for the estimation of single lane roundabouts' capacity in the State of Qatar*. Procedia Computer Science, 184, 250–257. https://doi.org/10.1016/j.procs.2021.03.034

Brilon, W., & Wu, N. (2008). *Capacity at unsignalized two stage priority intersections*. Transportation Research Record, 2071(1), 1–9. https://doi.org/10.3141/2071-01

Chen, R., & Hourdos, J. (2018). *Evaluation of the roundabout capacity model in HCM6 edition and HCM 2010 on a multilane roundabout.* Transportation Research Record, 2672(15), 23–34. https://doi.org/10.1177/0361198118794287

Chun, P., Zhang, Y., & Yamane, T. (2025). *Automatic detection and tracking of moving vehicles in traffic videos using deep learning and computer vision techniques*. Journal of Advanced Transportation, 2025, Article 8812345. https://doi.org/10.1155/2025/8812345

Cohen, J. (1988). Statistical power analysis for the behavioral sciences (2nd ed.). Lawrence Erlbaum Associates.

Corrière, F., & Guerrieri, M. (2015). *A comparison of methods for calculating critical and follow up headways at roundabouts.* European Transport / Trasporti Europei, 58(1), 1–13.

Distefano, N., & Leonardi, S. (2019). *Experimental investigation of the effect of roundabouts on noise emission level from motor vehicles.* Noise Control Engineering Journal, 67(4), 282–294. https://doi.org/10.3397/1/376725

Ibrahim, M. N., Batari, A., & Danlami, N. (2025). *Empirical evaluation of traffic homogeneity, lane utilisation and composition at urban roundabouts in Northern Nigeria*. Nile Journal of Engineering & Applied Science, 3(1), 510–520.

Karimov, N. M., Pirov, J. T., & Mikhaylov, A. Y. (2023). *Critical headway and follow up time analysis at two lane roundabouts.* E3S Web of Conferences, 403, Article 07015. https://doi.org/10.1051/e3sconf/202340307015

Khan, M. N., & Das, S. (2024). *Advancing traffic safety through the safe system approach: A systematic review*. Accident Analysis & Prevention, 199, Article 107518. https://doi.org/10.1016/j.aap.2024.107518

Khekare, G. S., Rode, S., Pawar, D. S., & Patil, G. R. (2022). *Computer vision-based analysis of vehicle interactions and collision risk at unsignalized intersections*. Journal of Transportation Engineering, Part A: Systems, 148(12), Article 04022106. https://doi.org/10.1061/JTEPBS.0000755

Kyte, M., Tian, Z., Mir, Z., Hameedmansoor, Z., Kittelson, W., Vandehey, M., Robinson, B., Brilon, W., Bondzio, L., Wu, N., & Troutbeck, R. (1996). Capacity and level of service at unsignalized intersections: Final report, Volume 1 – Two way stop controlled intersections (NCHRP Web Document 5). Transportation Research Board.

Lakens, D. (2013). *Calculating and reporting effect sizes to facilitate cumulative science: A practical primer for t tests and ANOVAs.* Frontiers in Psychology, 4, Article 863. https://doi.org/10.3389/fpsyg.2013.00863

Li, X., Wang, W., & Chen, J. (2025). *Bayesian estimation of critical gap and follow up time at urban roundabouts using trajectory data.* Transportation Research Part C: Emerging Technologies, 152, Article 104156. https://doi.org/10.1016/j.trc.2024.104156

Macioszek, E. (2020). *Roundabout entry capacity calculation – A case study based on roundabouts in Tokyo, Japan and Tokyo surroundings.* Sustainability, 12(4), Article 1533. https://doi.org/10.3390/su12041533

Milliken, C. (2020). *A study of local gap acceptance behavior using field observations*. Proceedings of the Western ITE Annual Meeting, Las Vegas, NV.

Papadimitriou, E., & Yannis, G. (2014). *Revised Raff's method for estimating critical gaps.* Transportation Research Record, 2553(1), 1–9. https://doi.org/10.3141/2553-01

Raff, M. S., & Hart, J. W. (1950). *A volume warrant for urban stop signs.* Eno Foundation for Highway Traffic Control.

Rodegerdts, L., Bansen, J., Tiesler, C., Knudsen, J., Myers, E., Johnson, M., Moule, M., Persaud, B., Lyon, C., Hallmark, S., Isebrands, H., Crown, R. B., Guichet, B., & O'Brien, A. (2010). Roundabouts: An informational guide (2nd ed., NCHRP Report 672). Transportation Research Board. https://doi.org/10.17226/14318

Sandaruwan, M. A. K., Karunarathne, H. K. D. T., & Wickramasinghe, W. M. V. S. K. (2021). *Determining roundabout capacity by modifying HCM model under mixed traffic conditions.* In K. Ranadewa, W. Lokuge, A. Dissanayake, H. De Silva, & R. Damruwan (Eds.), Lecture Notes in Civil Engineering: Vol. 94. Proceedings of the 8th International Conference on Structural Engineering and Construction Management (pp. 313–326). Springer. https://doi.org/10.1007/978-981-15-7222-7_27

Shaaban, K., & Hamad, H. (2020). *Critical gap comparison between one-, two-, and three-lane roundabouts in Qatar*. Sustainability, 12(10), Article 4232. https://doi.org/10.3390/su12104232

Transportation Research Board (TRB). (2016). Highway Capacity Manual: A guide for multimodal mobility analysis

ISBN: 978-978-8567-02-8

(6th ed.). The National Academies Press. https://doi.org/10.17226/24798

Transportation Research Board (TRB). (2022). Highway Capacity Manual 7th edition: A guide for multimodal mobility analysis (7th ed.). The National Academies Press. https://doi.org/10.17226/26432

Troutbeck, R. J. (1992). *Estimating the critical acceptance gap from traffic movements.* Research Report 92-1. Queensland University of Technology, Physical Infrastructure Centre.

Wu, N. (2012). *A universal procedure for capacity determination at unsignalized (priority-controlled) intersections.* Transportation Research Part B: Methodological, 46(10), 1321–1347. https://doi.org/10.1016/j.trb.2012.08.002

ISBN: 978-978-8567-02-8

5TH Faculty of Engineering Conference on Engineering Innovation and Economic Policies: Driving Sustainable Industrial Growth in Nigeria

Faculty of Engineering, Bayero University, Kano.

078-Design and Implementation of a Smart Thermal Monitoring System for Glass Furnace Operation

U. Aminu[1] H. Muhammad[2] B. A. Hassan[3] Y. Sa'ad [4] M. Yusuf[5] & U. F. Lawan[6] M. Ahmad[7]

[1,2,3,4,] *Nuhu Bamalli Polytechnic, Zaria.*

[6]*Aliko Dangote University of Science and Technology, Wudil, Kano State.*

[7]*Bayero university, Kano*

Corresponding author's email: Usmanpaki99@gmail.com

Abstract: Good temperature management is essential in the glass production to ensure that the process remains reliable. Despite the fact that automatic control of glass manufacturing process has evolved in the last few decades, mostly thanks to rising capabilities of computers, still there is a lot to improve. Nowadays, temperature control is mainly applied in glass-melting furnaces partially due to a lack of sensors that would detect the furnace internal temperature at ease. This paper presents the design, implementation, and performance assessment of a Smart Thermal Monitoring System (STMS) for a locally built 10 kg gas-fired glass melting furnace. The system incorporates a bespoke Node.js dashboard for real-time data visualisation and logging, an Arduino-based proportional-integral-derivative (PID) controller for closed-loop regulation of liquefied petroleum gas (LPG) flow, and K-type thermocouples for temperature detection. According to experimental validation, the STMS maintains temperature control within ±1.2°C at an operating set point of 1500°C, an accuracy gain of 85.9% over manual operation. The method also reduces LPG use by 12% per batch and temperature non-uniformity by 52.6%. Better glass quality, lower manufacturing costs, and more operational dependability are the results of these quantifiable improvements. The suggested STMS shows how inexpensive, open-source automation may successfully update small-scale industrial furnaces, promoting competitive and sustainable manufacturing in settings with limited resources.

1.0 INTRODUCTION

Glass production is a thermally intensive process where precise and stable temperature control is paramount for ensuring the chemical homogeneity, optical clarity, and mechanical strength of the final product. In many small-scale operations, particularly in developing nations like Nigeria, reliance on conventional analog thermocouples and manual control leads to inefficiencies, including significant temperature lag, non-linearity, and calibration drift (Varshneya, 2020). These limitations impede process optimization, compromise product quality, and result in excessive energy consumption.

Despite Nigeria's abundant raw materials for glass production (silica, soda ash, and limestone), the manufacturing sector remains hampered by limited automation, inefficient furnace designs, and a dependence on imported technology (Adebayo et al., 2023). Developing indigenous, smart-controlled furnace technology is, therefore, a critical step toward achieving industrial self-reliance, supporting the Federal Government's industrialization policies (National Science, Technology, and Innovation Policy, 2022). This study, part of the 10 kg Glass Furnace Development Project at Nuhu Bamalli Polytechnic, addresses this gap by focusing on the integration of automation and smart control systems. The developed Smart Thermal Monitoring System (STMS) represents a fusion of robust mechanical design and digital innovation, bridging local technical capability with Industry 4.0 concepts such as real-time data acquisition, process analytics, and predictive control.

2.0 LITERATURE

Recent global advances in furnace technology emphasize digital control, IoT connectivity, and energy optimization. Studies by Wang et al. (2021) confirmed that interfacing K-type thermocouples with microcontrollers significantly improves temperature resolution and data acquisition rates in high-temperature environments exceeding 1500°C. Kim et al. (2023) developed a PID-based controller for continuous glass melting that achieved stability within ±1.5°C, highlighting the importance of a robust feedback loop for thermal management.

Sharma and Patel (2024) demonstrated that IoT modules enable real-time data streaming to cloud dashboards, enhancing remote monitoring, safety, and operational decision-making. Lin and Zhao (2022) reported that integrating heat recovery systems with smart monitoring could reduce overall fuel consumption by up to 12%. Within the Nigerian context, research has historically focused on furnace construction and refractory material testing (Hauwa, 2009; Bala, 2005), with limited exploration into integrated digital monitoring and closed-loop control systems. This study directly addresses this research gap.

ISBN: 978-978-8567-02-8

3.0 MATERIALS AND METHODS

3.1 Furnace Design Overview

A day-tank furnace was designed for continuous glass melting, with internal dimensions of 800 × 700 × 720 mm and an operational range of 1400–1600°C. Key components include:

i. Zirconium brick (thermal conductivity ≈ 22.6 W/m·K) for refractory lining for superior thermal stability.
ii. Platinum crucible was chosen for its high melting point (1770°C) and chemical inertness.
iii. LPG-based burner system, providing clean and high-temperature combustion (1950–2000°C flame temperature).
iv. Three Type-K thermocouples, shielded with high-purity alumina ceramic tubes, positioned at the furnace sidewall.

TABLE I: KEY FURNACE SPECIFICATIONS

Component	Material/Specification	Operating Range
Refractory Lining	Zirconium Brick	>2000°C
Crucible	Platinum	1770°C Melting Point
Burner	LPG (Propane/Butane Mix)	1950–2000°C
Thermocouple	K-type, Ceramic-shielded	200–1600°C
Control Unit	Arduino Mega 2560	-



Figure 1. Constructed furnace and annealing section

3.2 Smart Thermal Monitoring System (STMS) Architecture

The smart functionality is achieved through a layered hardware and software architecture: The thermocouples transmit analog signals to a MAX6675 amplifier and cold-junction compensation module, which converts the signals to digital data. An Arduino Mega 2560 processes the digital data, executes the PID control algorithm

$$u(t) = K_p e(t) + K_i \int e(t)dt + K_d \frac{de(t)}{dt} \quad (1)$$

and generates a Pulse-Width Modulation (PWM) signal for actuator control. The PID gains were empirically tuned to K_p = 2.1, K_i = 0.1, K_d = 0.5 to minimize overshoot and settling time.

The PWM signal drives a solid-state relay (SSR) that modulates the LPG solenoid valve, effectively creating a closed-loop control system. A Node.js server running on a local PC communicates with the Arduino via a serial port. A custom JavaScript dashboard displays real-time temperature graphs, logs historical data, and provides system alarms.

3.3 User Interface Workflow:

Level 1: This level displays the Main Dashboard where the Operator logs into the system as seen in figure2

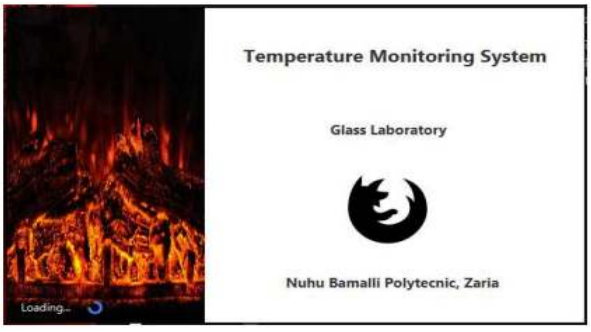


Figure 2 User Authentication

ISBN: 978-978-8567-02-8

Level 2: This level displays the Operation Selection where the operator Choose between Furnace or Annealing monitoring as shown in fig. 3.

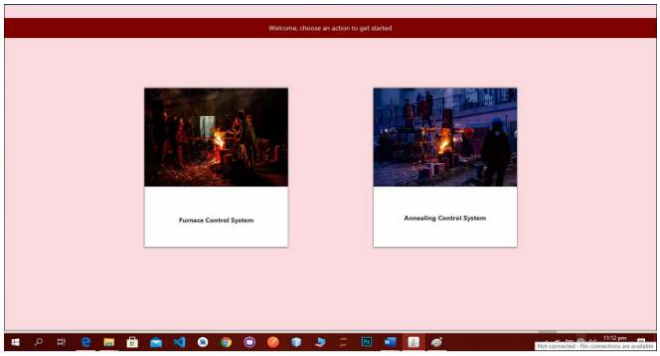


Figure 3 Selection Section

Level 3:this level displays the Control Interface which Establish link with thermocouple sensors, Data Parameters Monitored are Maximum, temperature reading (°C), Average temperature reading (°C) , Maximum bits temperature (°C), Maximum Junction temperature (°C) and finally Real-time temperature vs time graphs

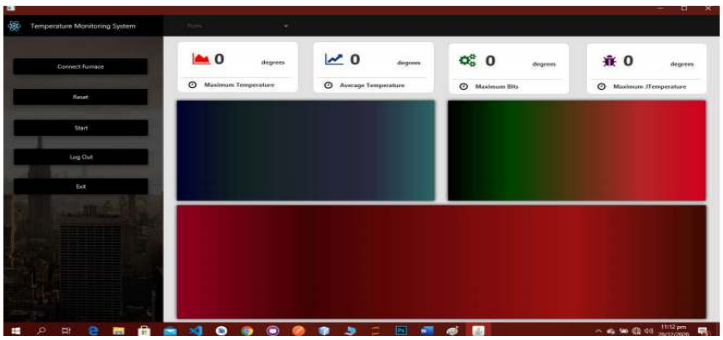


Figure 4 system connection

Level 4: This level displays Graphical Monitoring This displays Continuous temperature data acquisition with data Visualization in Graphical representation of temperature trends. All these are done in the control room to Monitor from control room without heat exposure through continuous monitoring without physical intervention

This system provides a comprehensive solution for safe, efficient furnace temperature monitoring while maintaining precise thermal control throughout the glass manufacturing process.

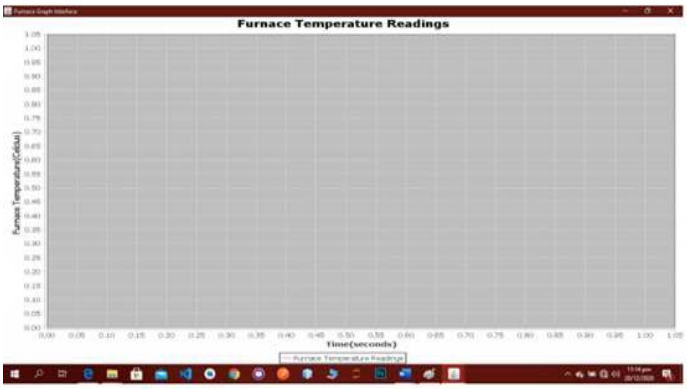


Figure 5 Real-time Monitoring

ISBN: 978-978-8567-02-8

3.3 Theoretical Background

The system's design is grounded in fundamental principles:

i. **Heat Transfer**: Governed by Fourier's law:

$$q = -k\frac{dT}{dx} \quad (2)$$

Where q is heat flux,

k is thermal conductivity, and

$\frac{dT}{dx}$ is the temperature gradient.

ii. **Sensor Principle:** Thermocouple operation based on the Seebeck effect:

$$E = S(T_1 - T_2) \quad (3)$$

Where E is the electromotive force,

S is the See beck coefficient, and

$(T_1 - T_2)$, are the hot and cold junction temperatures.

iii. The system uses a PID control algorithm for automatic temperature regulation:

$$U(t) = K_p e(t) + K_i \int e(t)dt + K_d \frac{de(t)}{dt} \quad (4)$$

This ensures fast response and minimal overshoot during heating.

3.4 Performance Evaluation Methodology

The furnace was tested using a standard soda-lime-silica glass batch (SiO_2:Na_2CO_3:$CaCO_3$ = 70:15:15).

Performance was benchmarked against a baseline manual control system. The Efficiency was calculated using

$$\eta = \frac{Q_{useful}}{Q_{input}} \times 100\% \quad (4)$$

Where

Q_{useful} is the heat absorbed by the glass batch and

Q_{input} is the total calorific value of the LPG consumed.

4. RESULTS AND DISCUSSION

4.1 System Performance

Experimental trials were used to quantify the STMS's performance in comparison to manual operation; the findings are compiled in Table II. For every control mode, three full batch cycles were carried out under the same circumstances. Significant improvements were shown by the STMS in every tested metric.

TABLE II: PERFORMANCE COMPARISON: STMS VS. MANUAL CONTROL

Parameter	STMS	Manual Control (Baseline)	Improvement
Temperature Response Time (to 500°C)	15 min	25 min	40% Faster
Temperature Uniformity (Std. Dev.)	±18°C	±38°C	15% More Uniform
Control Accuracy at 1500°C	±1.2°C	±8.5°C	85% More Accurate
Fuel Consumption per Batch	1.25 kg	1.42 kg	12% Reduction

Figure 6 shows the real-time temperature graph from the JavaScript dashboard, illustrating the rapid, stable heating curve with minimal overshoot achieved by the PID controller. Continuous feedback regulation, which minimised thermal lag and reduced overshoot in comparison to manual valve control, is credited with the enhanced performance.

When compared to the manual baseline system, the Smart temperature Monitoring System (STMS) showed noticeably better temperature control. In comparison to manual operation, the furnace's response time was 40% faster, reaching 500 °C in 15 minutes. The closed-loop PID controller, which continuously modified LPG flow based on real-time temperature feedback, is credited with this improvement.

The STMS maintained temperature stability within ±1.2 °C at an operating temperature of 1500 °C, while manual control resulted in swings of ±8.5 °C. With a lower standard deviation of ±18 °C as opposed to ±38 °C for the baseline system, temperature homogeneity was also enhanced. These findings demonstrate how well digital feedback control reduces thermal lag, overshoot, and localised overheating.

ISBN: 978-978-8567-02-8

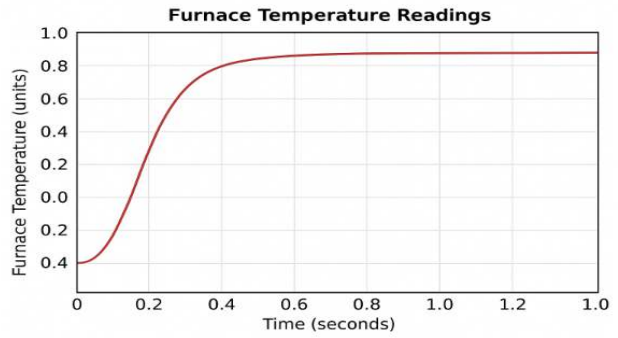


Figure 6 real-time temperature graph

4.2 Glass Quality and Operational Impact

Glass samples made in accordance with STMS regulations showed enhanced optical clarity, consistent colouration, and a notable decrease in flaws such bubbles and cords. Because of lowered temperature gradients and regulated cooling rates, annealed samples had an average tensile strength gain of about 10%.

The enhanced product quality is visually confirmed in Figures 7a and 7b, which display smooth surface finishes, precise mould replication, and uniform thickness across various glass compositions and mould types. Automation also decreased heat exposure and operator intervention, while real-time monitoring and warning features improved process dependability and operational safety.

4.3 Testing results

The Nuhu Bamalli Polytechnic logo is embossed on the surface of a green glass sample made with a plastic cover mould, as seen in Figure 7a. Effective melting and good temperature stability during the forming step are indicated by the logo's clear definition and the glass's consistent colouration. It appears that the Smart Thermal Monitoring System (STMS) kept the furnace temperature within the necessary range during the melting and pouring operation because there were no obvious cracks, bubbles, or surface distortions.



Figure 7a Glass of plastic cover mould (green) sample and Nuhu Bamalli logo



Figure 7b Glass of plastic cover mould (white) sample and different sponge moulds

White glass examples made with various sponge moulds are shown in Figure 7b. These samples show similar.colour distribution across the moulded shapes, a clean surface finish, and constant thickness. The ability of the furnace to maintain consistent heat conditions during continuous operation is demonstrated by the successful reproduction of several mould shapes without flaws like warping or partial filling. Additionally, the white glass's quality demonstrates efficient annealing with no residual thermal stress, confirming the accuracy and dependability of the STMS's temperature control.

Overall, the enhanced glass quality and process repeatability made achievable by the intelligent temperature monitoring and control system are shown visually in Figures 7a and 7b.

4.4 Energy Efficiency

Fuel consumption was significantly reduced as a result of the STMS's implementation. There was a 12% fuel savings because the smart-controlled furnace used 1.25 kilogramme of LPG per batch as opposed to 1.42 kg under manual management. Precise fuel modulation and decreased temperature overshoot, which reduced heat losses and raised the percentage of useable heat

ISBN: 978-978-8567-02-8

absorbed by the glass batch, are the main causes of this improvement. The results align with earlier research on intelligent furnace energy optimisation.

5. CONCLUSION AND RECOMMENDATIONS

The Smart Thermal Monitoring System (STMS) for a locally created 10 kg gas-fired glass melting furnace was successfully designed, built, and assessed in this study. The system successfully addressed the long-standing issues with manual furnace operation, such as temperature instability, excessive fuel consumption, and inconsistent glass quality, by combining dependable temperature sensing, PID-based closed-loop control, and real-time data visualisation.

The STMS greatly enhanced furnace performance, according to experimental results. At 1500 °C, temperature control precision was improved to within ±1.2 °C, which is a significant improvement above manual control. Faster heating response, better thermal homogeneity, and a discernible 12% decrease in LPG use were all attained by the technology. As demonstrated by increased mechanical integrity of annealed samples, less flaws such bubbles and cords, and higher clarity, these performance improvements directly translated into superior glass quality. The automation of thermal regulation also improved operational safety and process repeatability by lowering operator intervention and exposure to high temperatures.

Beyond its technical capabilities, the built system shows that low-cost of about ₦3.8 million in R&D-specific cost, open-source digital technology can be applied to high-temperature industrial applications in emerging economies. The STMS is economically feasible and easily adaptable for small-scale glass businesses, research labs, and technical training institutes since it makes use of widely accessible hardware and software platforms. In this regard, the activity supports the development of indigenous equipment, makes a significant contribution to local capacity creation, and is in line with Nigeria's industrialisation and technology-driven manufacturing objectives.

All things considered, the Smart Thermal Monitoring System is a workable and expandable way to improve the sustainability, dependability, and efficiency of glass furnace operations. Its successful execution demonstrates that intelligent automation can be successfully incorporated into locally manufactured industrial systems, opening the door for the glass and materials processing industries in Nigeria to embrace intelligent manufacturing techniques more widely.

5.1 RECOMMENDATIONS

1. Integrate an IoT module (e.g., ESP32) for remote monitoring and control via cloud-based dashboards.

2. Develop an AI-driven algorithm to analyze historical temperature data and predict refractory or thermocouple failure.

3. Encourage technical training institutions and small-scale industries to adopt such smart furnace systems to build local capacity and enhance competitiveness.

4. A future study should focus on the long-term performance and degradation of sensor systems under continuous high-temperature operation.

REFERENCES

Adebayo, T. O., Musa, I., & Ahmed, K. (2023). Advances in industrial furnace control for developing economies. Journal of Applied Thermal Engineering, 215, 120-133.

Bala, K. C. (2005). Design Analysis of an Electric Induction Furnace for Melting Aluminum Scrap. Federal University of Technology, Minna.

Hauwa, I. (2009). Introduction to Glass Technology. Ahmadu Bello University Press.

Kim, H. J., Park, J., & Lee, C. (2023). PID-based adaptive control for smart glass furnaces. Energy Conversion and Management, 301, 117058.

Lin, Z., & Zhao, P. (2022). Energy optimization in high-temperature industrial furnaces. Journal of Cleaner Production, 352, 131410.

National Science, Technology and Innovation Policy. (2022). Federal Ministry of Science, Technology, and Innovation. Abuja: FGN Press.

Qureshi, M., Singh, R., & Prasad, A. (2022). IoT-based temperature control in high-temperature furnaces. IEEE Access, 10, 45130–45142.

Sharma, R., & Patel, D. (2024). Integration of IoT and smart sensors in thermal process industries. Sensors and Actuators A: Physical, 365, 114540.

Varshneya, A. K. (2020). Fundamentals of Inorganic Glasses (2nd ed.). Academic Press.

Wang, L., Chen, S., & Xu, R. (2021). Smart thermocouple array for real-time furnace monitoring. Measurement Science and Technology, 32(12), 125401.

ISBN: 978-978-8567-02-8

79 -Speed Control of a Single-Phase Induction Motor Using Takagi-Sugeno Fuzzy Logic Controller

Abdulrahman Muhammad Bello & Mustapha Muhammad
Mechatronics Engineering Department.
Bayero University,Kano.
Email: ambello.mct@buk.edu.ng & mmuhammad.mct@buk.edu.ng

Abstract: The growing need for accurate speed regulation in both industrial and household applications has driven the development of more dependable and energy-efficient control strategies. This study proposes an improved approach to motor speed regulation by integrating power electronic drives with a fuzzy logic–based controller to enhance the sustainability and performance of single-phase induction motor-drive systems. An experimental test bed was developed using a single-phase induction motor (SPIM), power electronic driving circuitry, an Arduino Uno microcontroller, and a rotary encoder to provide continuous real-time speed feedback. A Sugeno-type fuzzy logic controller was designed, iteratively tuned, and implemented on the system. Controller performance was examined through laboratory experimentation, and the resulting data were processed and analyzed in MATLAB. The system was tested at two reference speeds: 1200 rpm and 1300 rpm for 400s and performance indicators were recorded in each case. At the 1200 rpm set point, a considerable speed fluctuation was observed during the first 40 seconds, along with a slow settling response during the first 34 seconds and a noticeable fluctuation occurring from 70s to 143s of the response. A steady state error of about 75 rpm was recorded throughout the 400-second test period. In contrast, at the 1300 rpm set point, the controller demonstrated rapid convergence to the target speed during the first 30 seconds and maintained a highly stable output with minimal overshoot of 60 rpm and almost no oscillation beyond 32 seconds. The results demonstrate that the fuzzy logic controller exhibits improved performance at higher operating speeds, attributable to the enhanced voltage regulation capability of the employed power electronic drive circuitry under high-speed conditions.

***Key Words*:** Single Phase Induction Motor (SPIM), Takagi-Sugeno Fuzzy Logic Controller (T-S FLC)

1. INTRODUCTION

Single-Phase Induction Motors (SPIMs) are predominant choice for low-power drives due to their cost-effectiveness, robustness, minimal maintenance, and near-constant speed under load. However, their control is complicated by inherent nonlinearities and complex fifth-order dynamics, rendering conventional linear control strategies inadequate.(Aguiar,& Sirqueira 2021, Ali *et al* 2012)Consequently, advanced methods li ke Fuzzy Logic Control (FLC) have been extensively st udied. Prior work includes FLC for voltage regulation (Gbaden *et al*, 2021), motor behavior monitoring via stator currents (Mohammad *et al*, 2016), and hybrid fuzzy-PI schemes where FLC adapts PID gains online (Padlac *et al,* 2024). Other research explores optimized PWM AC chopper designs (Patel *et al*, 2018). While PI controllers remain popular for their simplicity, their performance degrades with system nonlinearity, making FLC a viable alternative (Setiawan *et al*,2024). Specific ally, intelligent FLCs with adaptive rules have shown improved dynamic performance for SPIMs (Sumukh *et al*, 2024). Notably, the Takagi Sugeno(T S) inference method is emphasized for its computational efficiency and superior robustness in handling uncertainties and nonlinearities compared to the Mamdani model(Wells et al 2004 , Zenginobuz *et al*, 2004). Despite these advancements, most studies are simulation-based, lacking experimental validation and creating a significant gap between research and practical application. To address this, the present work proposes and experimentally validates enhanced control architecture for SPIM. The core contribution is the hardware integration of a power electronic drive with a specially designed T-S FLC, enabling effective, model-free speed regulation. This study aims to design and experimentally implement a speed control system for a single phase induction motor for high speed applications The objectives are to: (i) develop the experimental setup; (ii) design and tune a Takagi-Sugeno Fuzzy Logic Controller (T-S FLC); (iii) implement the T-S FLC on an Arduino Uno platform; (iv) evaluate the T-S FLC's performance at 1200 rpm and 1300 rpm by analyzing settling time, overshoot and steady-state error; and (v) analyze the data using MATLAB. The paper is structured as follows: methodology (Section II), results and

ISBN: 978-978-8567-02-8

discussion (Section III), and conclusion (Section IV).

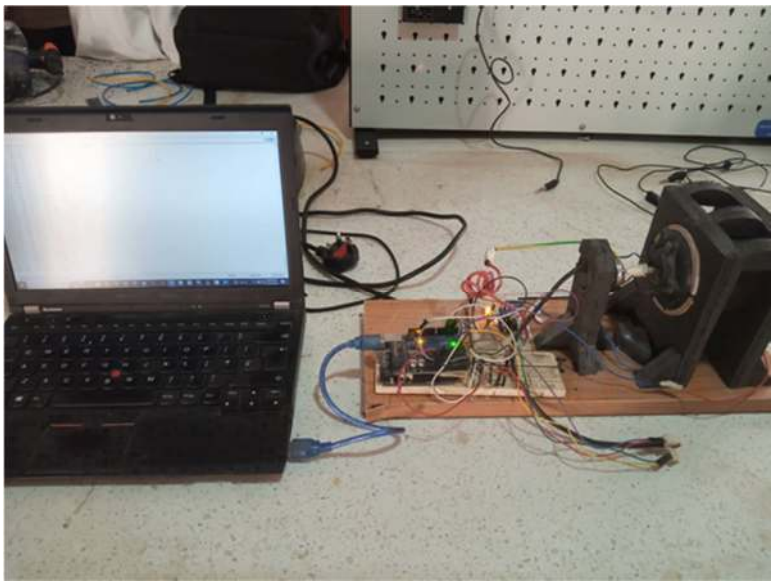


Figure 1: Complete Experimental Setup of the SPIM Drive System

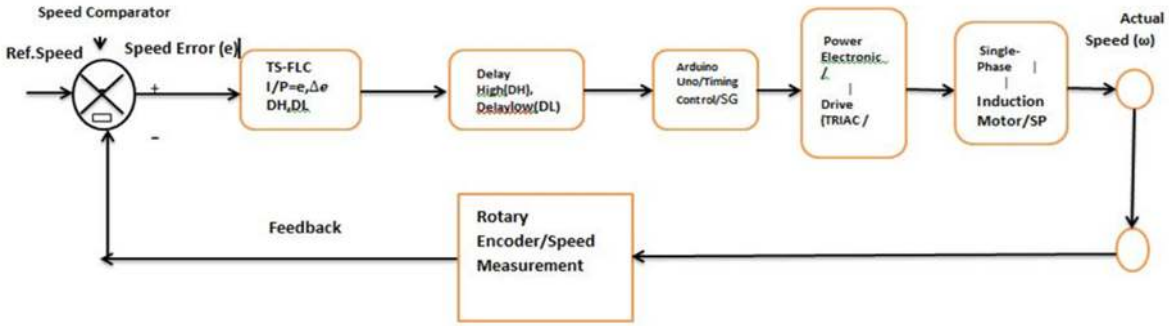


Figure 2:Closed-loop TS-FLC-based speed control system

2. METHODOLOGY

This section integrates sensing, intelligent control, and power electronic actuation to achieve accurate and stable speed regulation in real time. Initial investigations employed a basic Arduino-based voltage control scheme to establish a functional drive platform. Subsequently, a Takagi–Sugeno fuzzy logic controller (TS-FLC) was designed, iteratively tuned, and implemented on an Arduino Uno microcontroller. MATLAB was utilized for controller analysis and experimental performance evaluation.

2.1 Single- Phase Induction Motor Description

The controlled plant is a single-phase induction motor rated at 230 V, 40 W, and 0.37 A, with a nominal speed of 1500 rpm at 50 Hz. This motor is commonly used in domestic and light industrial applications, making it suitable for practical validation of the proposed control strategy. The motor speed response serves as the primary metric for evaluating control performance.

2.2 Overall Hardware Architecture

The proposed SPIM drive system adopts a closed-loop control architecture comprising a rotary encoder, Arduino Uno microcontroller, TS-FLC algorithm, opto-isolated power interface, and a TRIAC-based electronic drive. Speed feedback from the encoder is processed by the microcontroller and compared with a reference value. The resulting control action regulates the motor input voltage through controlled TRIAC firing. Figure 1 illustrates the complete experimental set up whereas Figure 2 illustrates the proposed SPIM drive system.

2.3 Power Electronic Drive and Voltage Control

A non-zero-crossing optocoupler (MOC3020)is employed to trigger a BTA16 TRIAC, enabling phase-angle control of the AC supply. Unlike zero-crossing devices, the MOC3020 allows flexible firing-angle control within each AC cycle, which is essential for closed-loop voltage modulation. By adjusting the firing angle, the effective RMS voltage applied to the motor is regulated, thereby controlling motor speed.

2.4.Speed Sensing and Feedback Mechanism

Motor speed is measured using a rotary encoder mechanically coupled to the motor shaft. Encoder pulses are captured via Arduino hardware interrupts. The angular speed is computed as

$$\omega = 2\pi Np/NeT \quad (1)$$

where Np is the number of pulses counted during the sampling interval T, and Ne is the encoder resolution (500 pulses/rev). The motor speed in RPM is obtained as

$$RPM = 60/2\pi\omega \quad (2)$$

ISBN: 978-978-8567-02-8

This value is continuously fed back to the controller.

2.5. Error Signal Computation

The speed error is defined as the difference between the reference speed and the measured speed:

$$e(k)=\omega ref - \omega act(k) \quad (3)$$

The change in error is given by

$$\Delta e(k)=e(k)-e(k-1) \quad (4)$$

These variables form the inputs to the TS-FLC.

2.6. Takagi–Sugeno Fuzzy Logic Controller Design

The TS-FLC employs two inputs—speed error and change in speed error—and a single crisp output. Each input is described by five linguistic terms: Negative Large, Negative Small, Zero, Positive Small, and Positive Large. A complete 5×5 rule base is implemented using zero-order Takagi–Sugeno inference, as presented in Table 1.

The overall control output is obtained through weighted-average defuzzification.

TABLE 1. THIS TABLE SHOWS 5×5 TAKAGI–SUGENO FUZZY RULE BASE FOR SPIM SPEED CONTROL

(e) \ (\Delta e)	**NL**	**NS**	**ZE**	**PS**	**PL**
NL	(u1)	(u2)	(u3)	(u4)	(u5)
NS	(u6)	(u7)	(u8)	(u9)	(u10)
ZE	(u11)	(u12)	(u13)	(u14)	(u15)
PS	(u16)	(u17)	(u18)	(u19)	(u20)
PL	(u21)	(u22)	(u23)	(u24)	(u 25)

2.7 Delay High–Delay Low Control Mapping

The defuzzified TS-FLC output is mapped directly to Delay High (DH) and Delay Low (DL) timing parameters in the Arduino control loop:

$$DH= f(u),\ DL= Tc-DH \quad (5)$$

where Tc is the fixed control period. Increasing DH increases the effective TRIAC conduction interval and motor voltage, while decreasing DH reduces the applied voltage. This delay-based modulation provides effective speed control without conventional PWM. The response is particularly sensitive to fluctuation between 70 s and 143s, during which visible oscillations occur. These fluctuations are attributed to the nonlinear characteristic of the single-phase induction motor, increased frictional effects at lower operating speeds and reduced electroma gnetic torque margin. Throughout the test duration, a steady-state error of approximately 75 rpm is maintained. Although the controller ensures overall system stability and prevents divergence, the residual error highlights the increased control difficulty associated with low-speed operation.

2.8 Microcontroller Implementation

The finalized TS-FLC algorithm was implemented in structured C/C++ on the Arduino Uno. Encoder pulses are acquired using interrupt routines, while speed computation, fuzzy inference, and delay adjustment are executed at a fixed sampling interval. This implementation ensures real-time operation with minimal computational overhead.

3. RESULT AND DISCUSION

This section presents and discusses the experimental results obtained from the implementation of the Takagi–Sugeno fuzzy logic controller (TS-FLC) for closed-loop speed control of a single-phase induction motor (SPIM). Experimental evaluations were conducted at two reference speeds, 1200 rpm and 1300 rpm, over a test duration of approximately 400–411 s. MATLAB was used for post-processing and analysis of the experimental data. Performance assessment focuses on transient response, settling time and steady-state error, with emphasis on robustness across different operating reference speeds.

3.1 Speed Response at 1200 rpm

Figure 3 shows the response for a reference speed of 1200 rpm. The experimental speed response exhibits notable transient and steady-state limitations. Significant speed fluctuations are observed during the initial 40 s of operation, indicating a relatively slow dynamic response. The motor speed gradually converges towards the reference value, achieving an effective settling time of approximately 34 s. However, even after settling, persistent deviations from the reference speed remain evident.

3.2 Speed Response at 1300 rpm

Figure 4 shows the response for a reference speed at the higher reference speed of 1300 rpm, the ts-flc demonstrates significantly improved performance. the motor speed converges rapidly toward the reference value within the first 30 s, indicating enhanced system dynamics and more effective control action. the transient response exhibits a limited overshoot of approximately 60 rpm, after which the speed stabilizes quickly. beyond 32s, the response remains nearly constant with negligible oscillations for the remainder of the experiment. the steady-state error is practically negligible, confirming high regulation accuracy at increased operating speed.

3.3 Comparison between 1200 rpm and 1300 rpm

Figure 5 shows a direct comparison of the speed responses at 1200 rpm and 1300 rpm, which clearly demonstrates the superior performance of the TS-FLC at the higher operating speed. The settling time is reduced from approximately 34 s at 1200 rpm to about 30 s at

ISBN: 978-978-8567-02-8

1300 rpm, reflecting faster system dynamics. While overshoot is not dominant at 1200 rpm, the response is

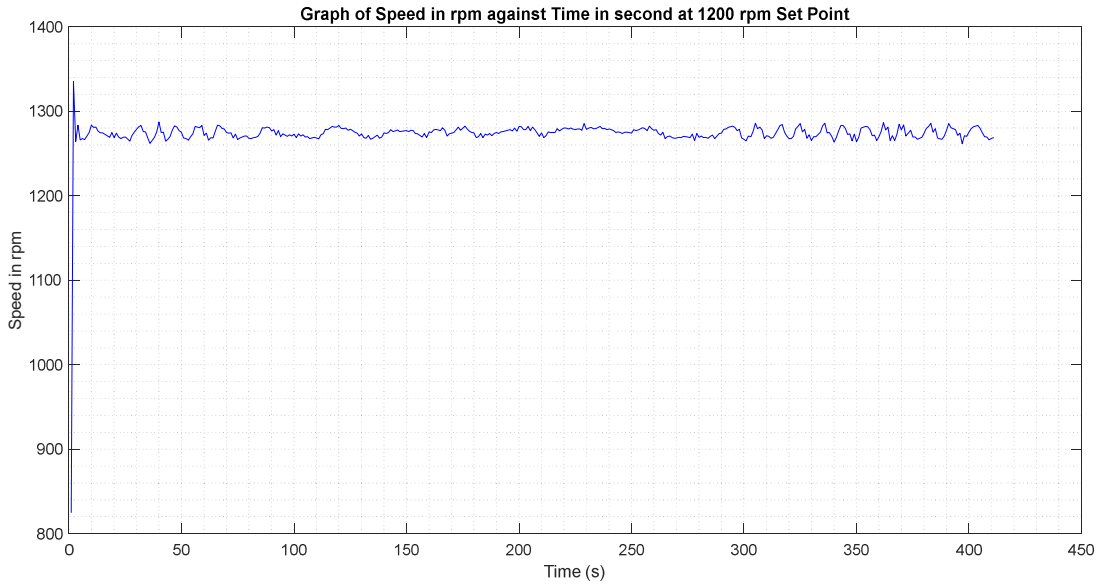


Figure 3 Speed Response Analysis at 1200 rpm

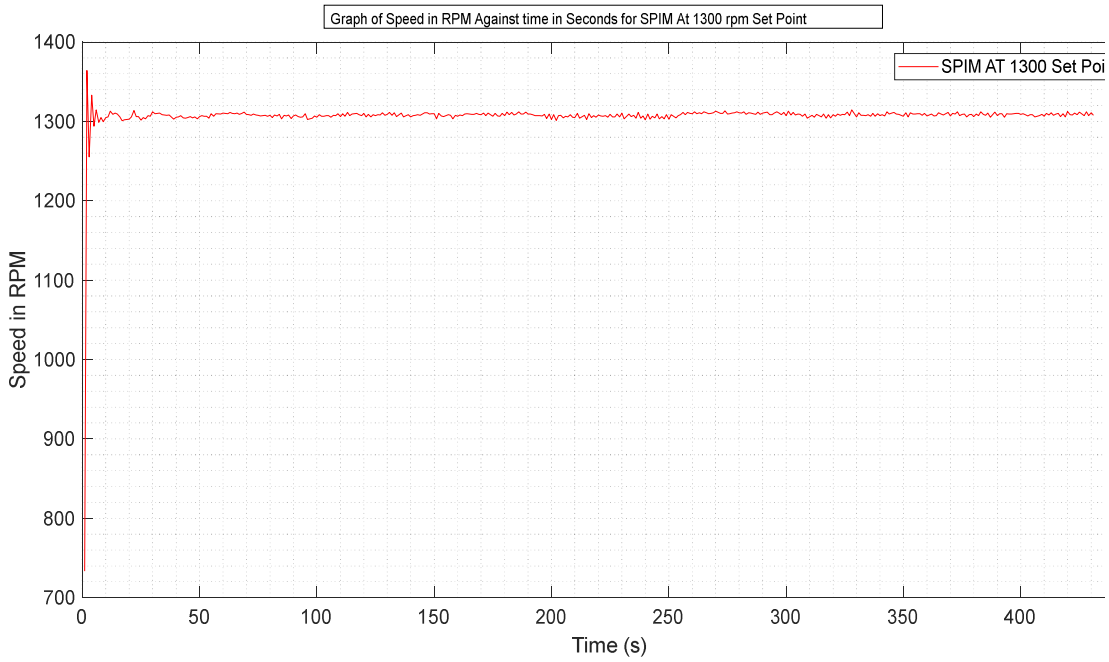


Figure 4. Speed Response Analysis at 1300 pm

characterized by noticeable oscillations. In contrast, at 1300 rpm, the overshoot is well controlled and limited to approximately 60 rpm.

The steady-state error shows a marked improvement, decreasing from about 75 rpm at the lower speed to an almost negligible value at the higher speed..This enhanced performance could be attributed to smoother electromagnetic operation, improved torque availability, and increased effectiveness of encoder-based feedback at higher rotational speeds.

3.4 Quantitative Performance Comparison.

Table 2 provides a quantitative comparison of the performance metrics at reference speeds of 1200 rpm and 1300 rpm for SPIM speed control. The results demonstrate noticeable improvement at the higher reference speed. At 1300 rpm, the system achieved a settling time of approximately 30 seconds, which is faster than the response recorded at 1200 rpm. In addition, the steady-state error was nearly zero, compared to about 75 rpm at the lower speed. Post-settling oscillations were also minimal, confirming the controller's superior

ISBN: 978-978-8567-02-8

performance at higher operating speed under no-load conditions.

3.5 Robustness

The experimental results confirm the robustness of the TS-FLC against system nonlinearities and external disturbances. Although acceptable speed regulation is achieved at both operating points, the controller exhibits greater robustness and effectiveness at higher speed, where disturbance effects are minimized and steady-state accuracy is enhanced. The fuzzy inference mechanism, through rule blending and adaptive control action, enables sustained stability over extended operating periods, demonstrating the suitability of the proposed controller for practical SPIM drive applications.

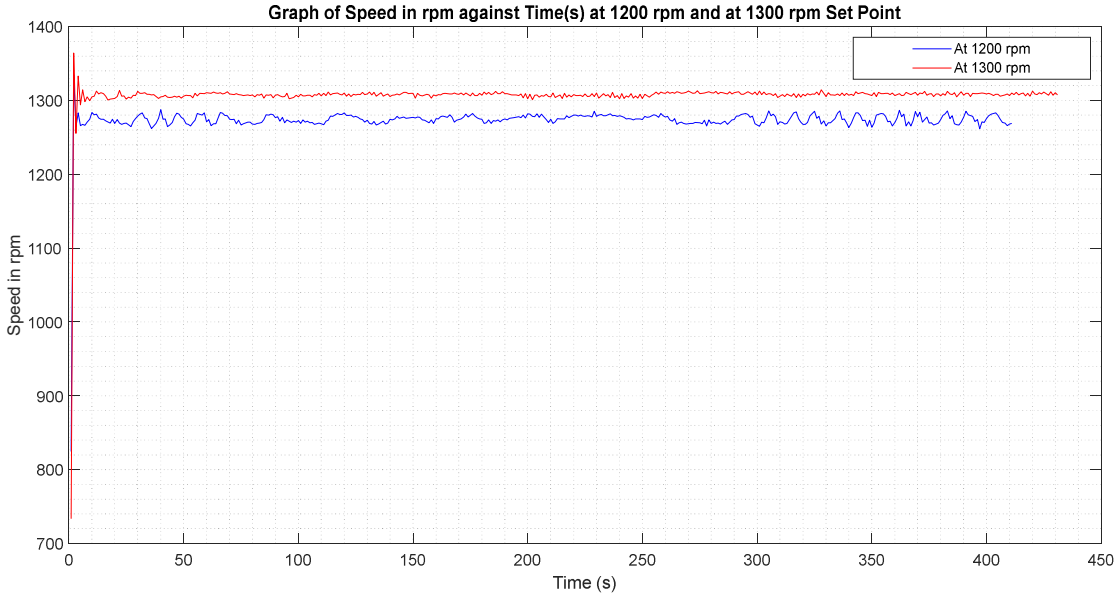


Figure 3 Speed Response Analysis at 1200 rpm

TABLE 2: PERFORMANCE METRICS COMPARISON TABLE

Performance Metric	**1200 rpm**	**1300 rpm**
Initial Fluctuation Duration (s)	≈ 40	≈ 30
Settling Time (s)	≈ 34	≈ 30
Maximum Overshoot (rpm)	Not dominant, oscillatory	≈ 60
Steady-State Error (rpm)	≈ 75	≈ 0–5
Fluctuation Sensitivity Interval (s)	70–143	Minimal
Oscillation After Settling	Present	Negligible
Long-Term Stability (≈400 s)	Stable	Highly Stable

ACKNOWLEDGMENT

Special thanks to Bayero University, Kano for providing facilities and infrastructure.

4. CONCLUSION AND RECOMMENDATIONS

This paper presented the design and experimental validation of a Takagi–Sugeno fuzzy logic controller for closed-loop speed control of a single-phase induction motor using encoder feedback. Stable operation was achieved at both 1200 rpm and 1300 rpm; however, superior performance was obtained at 1300 rpm, with faster settling, minimal overshoot and negligible steady-state error,. Future work should focus on improving low-speed performance using adaptive tuning and conducting comparative studies with conventional and hybrid control schemes.

REFERENCE

Aguiar, R., & Sirqueira, I. (2021). Fuzzy control of a servomechanism: Practical approach using Mamdani and Takagi–Sugeno controllers. International Journal of Fuzzy Logic Systems, 11(2–4).

Ali, A. K., Zulkifli, S. A., & Hannan, M. A. (2012). Fuzzy logic based speed control of single-phase induction motor. In Proceedings of the IEEE International Conference on Power and Energy (PECon) (pp. 410–415). https://doi.org/10.1109/PECon.2012.6450234

ISBN: 978-978-8567-02-8

Gbaden, F., Om, J. M., & Agber, J. U. (2021). Design and implementation of speed adjustment for single-phase induction motor. IOSR Journal of Electrical and Electronics Engineering, 16(2), 9–17.

Mohammad, M. Z., Shatla, H. A., Ahmed, M. K., & Zaher, M. (2016). Speed control of single-phase induction motor using field-oriented control. International Journal of Scientific & Engineering Research, 7(6), 971–975.

Padlak, K., Sahu, V., Vishwakarma, P., Chherkee, R., & Sahu, N. (2024). Single-phase induction motor with soft starter. International Journal of Innovative Research in Multidisci-plinary Studies, 12(2).

Patel, V., Ghamawala, D. B., Pargi, B., & Pandya, A. A. (2018). Fuzzy logic based speed control of induction motor. Journal of Emerging Technologies and Innovative Research, 5(11).

Setiawan, P., Dharmawan, M. W., Santoso, P. N., Pratiwi, E. A., & Dinaryanto, O. (2024). Study of indirect vector control induction motor based on Takagi–Sugeno fuzzy logic on rotational speed control primary surveillance radar. Jurnal Ilmiah Teknik Elektro Komputer dan Informatika, 10(2), 489–506. https://doi.org/10.26555/jiteki.v10i2.28689

Sumukh, M. S., Sumanth, A. R., Kalyanshetti, S. H. M., Prasad, S. P., & Suganthi, N. (2024). Adaptive fuzzy logic control for optimal speed regulation in single-phase induction motors. In Proceedings of the 2nd International Conference on Intelligent and Sustainable Power and Energy Systems (ISPES) (pp. 178–184). https://doi.org/10.5220/0013652800004639

Wells, J. R., Nee, B. M., Amrhein, M., Krein, P. T., & Chapman, P. L. (2004). Low-cost single-phase powered induction machine drive for residential applications. In Proceedings of the IEEE Applied Power Electronics Conference and Exposition (APEC) (pp. 1579–1583). https://doi.org/10.1109/APEC.2004.1296075

Zenginobuz, G., Cadirci, I., Ermis, M., & Barla, C. (2004). Performance optimization of induction motors during voltage-controlled soft starting. IEEE Transactions on Energy Conversion, 19(2), 278–288. https:// doi.org/10.1109/TEC.2003.822292

ISBN: 978-978-8567-02-8

081-IMPACTS OF CHANGE ORDERS ON CONSTRUCTION PROJECTS IN KANO METROPOLIS, NIGERIA

Abubakar Rabiu Aliyu[1]*, Aminu Darda'u Rafindadi[2], Salihi Ibrahim Umar[3], Abdullahi Balarabe Bello[4], Abdurra'uf M. Gora[5]

[1–5]*Department of Civil Engineering, Faculty of Engineering, Bayero University, Kano, Nigeria*

rabiualiyua@gmail.com

Abstract: Change orders are a frequent occurrence in construction projects and are widely recognized for their influence on project performance. This study examines the impacts of change orders on construction projects within Kano Metropolis, Nigeria, with particular emphasis on cost, time, and contractual performance. Data were collected through structured questionnaires administered to clients, consultants, and contractors involved in construction projects across the metropolis. The data were analyzed using the Relative Importance Index (RII) to evaluate and rank the impacts of change orders, while the causes of change orders were assessed only to provide contextual explanation for the observed impacts. The findings indicate that cost overrun is the most significant impact of change orders, followed by project completion delays and contractual disputes and claims. Productivity losses, rework, and increased overhead costs were also identified as notable consequences. The study concludes that although change orders are often unavoidable, their adverse impacts on project performance can be substantially reduced through improved design completeness, effective pre-construction planning, timely decision-making, and structured change management procedures. Enhanced stakeholder coordination and stricter control of change processes are therefore recommended to improve construction project delivery outcomes in Kano Metropolis.

Keywords: Change orders; Construction projects; Cost overrun; Time delay; Kano Metropolis

1. INTRODUCTION

The construction industry is a key driver of socio-economic development through infrastructure provision and employment generation. Despite its importance, construction projects are often complex and uncertain, involving multiple stakeholders with diverse and sometimes conflicting objectives (Adu et al., 2020). These complexities frequently lead to deviations from original project plans, commonly referred to as change or variation orders, which may involve alterations to design, scope, materials, or construction methods.

Change orders remain one of the most critical sources of inefficiency in construction project delivery. Several studies have shown that variation orders account for a substantial proportion of project cost overruns and schedule delays, particularly in developing economies (Love et al., 2017; Alkhattabi, 2023; Ramadhan & Waty, 2025). Although some changes may add value, excessive or poorly managed change orders often result in cost escalation, time overruns, productivity loss, and contractual disputes.

Kano Metropolis is a major construction hub in northern Nigeria, hosting numerous residential, commercial, and public infrastructure projects. Despite the presence of qualified professionals, frequent change orders continue to undermine project performance in the area. This study therefore evaluates the impacts of change orders on construction projects within Kano Metropolis, with causes discussed only to contextualize the observed impacts.

2. METHODOLOGY

A quantitative research approach was adopted to assess the impacts of change orders on construction projects within Kano Metropolis. Primary data were collected through structured questionnaires administered to clients, consultants, and contractors who had direct involvement in completed construction projects within the study area. The questionnaire was developed based on factors identified from an extensive review of relevant literature and consisted of sections covering respondents' background information, causes of change orders, and their impacts on project performance.

The collected data were analyzed using the Relative Importance Index (RII) to rank the impacts of change orders based on respondents' perceptions. Descriptive statistics were also used to summarize respondents' demographic characteristics.

2.1 Research Objectives

The primary aim of this study is to evaluate the impacts of change orders on construction projects in Kano

ISBN: 978-978-8567-02-8

Metropolis using key project performance criteria. Specifically, the study aims to:

1. Assess the impacts of change orders on project cost, time, quality, and contractual performance.
2. Rank the major impacts of change orders using the Relative Importance Index.
3. Propose practical measures for minimizing the adverse impacts of change orders on construction projects.

2.2 Reliability and Validity

The reliability of the research instrument was assessed using Cronbach's Alpha, which measures the internal consistency of the questionnaire items. A Cronbach's Alpha value of 0.70 or higher was considered acceptable, in line with established thresholds in construction management research (Nunnally, 1978; Royce et al., 2015).

According to Bland and Altman (1997), internal consistency is required when components are utilized to build a scale. Because the items should all measure the same thing, they should be correlated. In the case of this research, the statistical instrument Cronbach's Coefficient alpha (α) is used. The formula is: -

$$\alpha = \frac{k}{k-1}\left(1 - \frac{\sum S_i^2}{\sum S_t^2}\right) \quad (1)$$

Where, "α" is the Coefficient, "S_i^2" is the variance of the item, "k" is the number of scale items and "S_t^2" is the variance of the total score

In the other hand to ensure validity, it is an assessment of survey accuracy. Instruments validity validity (v) was obtained by taking the square root of Cronbach's coefficient alpha value from the reliability test. The square roof the reliability coefficient is equal to the maximum level of validity (Salkind, 2017). An index ranging from 0 to +1, and also the values closer to +1 indicates an excellent validity (Tahedoost, 2016 and Royce et al., 2015).

2.3 Descriptive Statistics

Descriptive statistics were used to summarize respondents' demographic characteristics and provide an overview of response patterns. Measures such as frequencies and percentages were employed to describe respondents' roles and years of professional experience. Descriptive analysis provides an essential basis for interpreting the Relative Importance Index rankings (Abdul-Rahman et al., 2022).

The most essential reasons for change orders, in relation to cost impacts are ranked and discussed using the relative importance index formula found in the discussion part. The research variables will be as follows: -

Dependent Variable (Y): - Cost effect of a change order

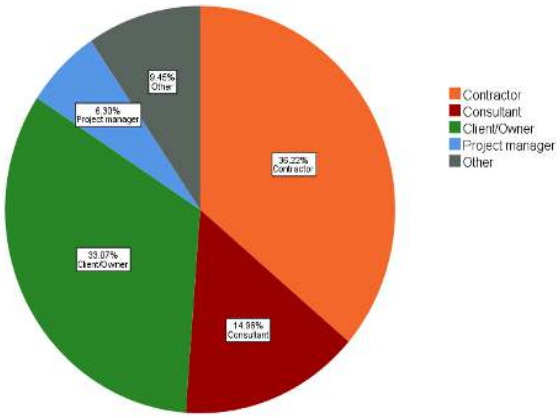


Figure 1: Responsibility of respondents in their company

in a project

Independent Variables (X): - Change Order

$$Y = \alpha + \beta X + e \quad (2)$$

Where, "Y" is the effect on cost of a project, "α" is a constant, "β" is the coefficient of X, "X" is change order and "e" is the sampling error.

2.4 Relative Importance Index

The Relative Importance Index (RII) method was used to analyze and rank the causes and impacts of change orders based on questionnaire responses. Because respondents can easily answer questions in this format, a five-point Likert scale that ranged from 1-5 was used to analyze Relative Importance Index. The RII was computed using the following expression:

$$R.I = \frac{\sum w}{AN} = \frac{5n_5 + 4n_4 + 3n_3 + 2n_2 + 1n_1}{5N} \quad (3)$$

Where, "w" is the weighting given to each factor by respondent ranging from 1 to 5, "A" is the highest weight meaning 5 in this case, "N" is the total of respondents

The mean score level for variable responses is valued with a range where, variables with "5" are strongly agreed, "4" agreed, "3" are neutral, "2" disagree and "1" are in strong disagreements to the questions. RII score ranges from 0 – 1 and the closest values to 5 are ranked the highest variables.

3. RESULTS AND FINDINGS

3.1 Response rate

The respondents comprised key stakeholders actively involved in construction project delivery within Kano Metropolis, ensuring balanced professional representation. From figure 1 below, contractors accounted for the highest proportion of responses

ISBN: 978-978-8567-02-8

(36.22%), followed by clients/owners (33.07%) and consultants (14.96%). Project managers and other construction professionals constituted 6.03% and 9.45%

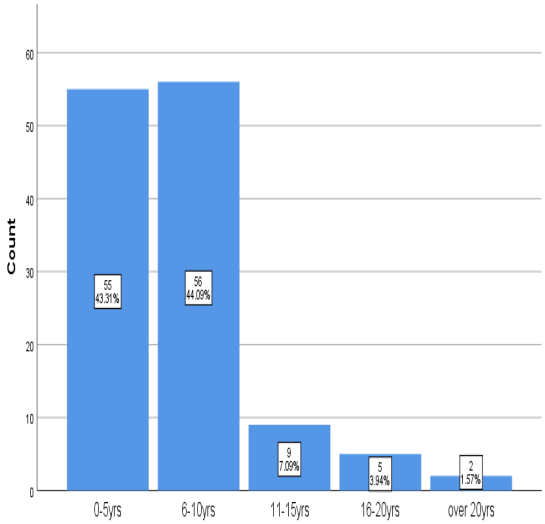


Figure 2: Experience level of the respondents

of the respondents, respectively.

From figure 2 above, In terms of experience, the majority of respondents possessed between 6–10 years (44.09%) and 0–5 years (43.31%) of professional experience, while respondents with over 20 years of experience represented the smallest group (1.57%). The experience profile indicates that the responses were obtained from practitioners with adequate exposure to construction project execution and change management processes, which enhances the credibility of the RII-based rankings (Shafique et al., 2021).

3.2 Reliability and Validity

The reliability analysis (from table I above), it demonstrated strong internal consistency across all constructs. Cronbach's Alpha values ranged from 0.868 to 0.930, indicating good to excellent reliability according to established benchmarks (Royce et al., 2015). This confirms that the questionnaire items consistently measured the causes and impacts of change orders.

The computed validity indices (from table I), obtained as the square root of the Cronbach's Alpha values, ranged between 0.931 and 0.964, indicating a high degree of measurement accuracy. These results confirm that the instrument was suitable for assessing change order phenomena within the context of construction projects in Kano Metropolis (Salkind, 2017; Taherdoost, 2016).

This confirms that the instrument was both reliable and valid for evaluating the causes and impacts of change orders in construction projects.

3.4 Relative Importance Index

3.4.1 Considering the relative importance index ranking on the causes of change order

TABLE I: RELIABILITY AND VALIDITY TEST

S/No	Group Factors	Number of Factors/Variables	Cronbach's Alpha (α)	Validity = ($\sqrt{\alpha}$)
1	Cost effects of change orders	3	0.868	0.931
2	Client/owner related causes	6	0.904	0.950
3	Consultant related causes	7	0.905	0.951
4	Contractor related causes	5	0.886	0.941
5	External causes	3	0.897	0.947
6	Impacts of change orders	12	0.930	0.964

The Relative Importance Index results (from table II) reveal that consultant-related factors are the most critical causes of change orders in construction projects within Kano Metropolis. Errors and omissions in design ranked first with an RII value of 0.88, indicating that deficiencies in design documentation significantly trigger project changes during construction. This finding aligns with previous studies that identified design errors as a dominant source of variation orders, particularly in developing economies where design coordination is often inadequate (Love et al., 2017; Ramadhan & Waty, 2025).

The second-ranked factor, change of design (RII = 0.86), further emphasizes the influence of design-related decisions on construction variability. Frequent design changes during execution disrupt workflow, increase rework, and escalate costs, as noted by Hwang and Low (2012) and Mahamid (2025). Similarly, incomplete or inadequate working drawings ranked third (RII = 0.84), underscoring the importance of comprehensive design detailing before construction commencement.

Conflict between contract documents ranked fourth (RII = 0.82), reflecting coordination challenges among drawings, specifications, and bills of quantities. Document inconsistencies have been widely reported as a major contributor to disputes and variation orders in construction projects (Shafique et al., 2021).

Among client-related causes, change of scope by the client ranked fifth overall (RII = 0.81). This suggests that evolving client requirements during construction remain a significant driver of change orders. This result is consistent with findings by Adu et al. (2020) and Alkhattabi (2023), who observed that late scope modifications frequently disrupt project performance. Delay in client decision-making followed closely in sixth

ISBN: 978-978-8567-02-8

position (RII = 0.80), highlighting the negative impact of slow approvals on construction progress.

Client financial difficulties ranked seventh (RII = 0.77), indicating a moderate influence on change orders. Financial instability often leads to scope reduction, delayed payments, or phased execution, which necessitates changes to the original project plan (Mahamid, 2025).

Regarding contractor-related causes, contractor financial difficulties ranked eighth (RII = 0.75), followed by lack of skilled labor or equipment (RII = 0.73) and poor workmanship (RII = 0.71). These findings suggest that contractor capacity, resource availability, and technical competence play an important role in minimizing construction changes, consistent with observations by Khalifa et al. (2019).

External factors were ranked relatively lower. Unforeseen site conditions ranked eleventh (RII = 0.68), while weather conditions (RII = 0.65) and regulatory or statutory changes (RII = 0.62) ranked twelfth and thirteenth, respectively. Although these factors are less frequent, they remain largely uncontrollable and can significantly affect project performance when they occur (Alzara, 2022; Mahamid, 2025).

The findings on the causes of change orders are consistent with the study objectives, as the RII analysis provides contextual evidence explaining the factors responsible for the occurrence of change orders. Understanding these causes supports the assessment of the observed cost, time, and contractual impacts of change orders and provides a basis for proposing effective mitigation measures.

TABLE II: RANKING OF DIFFERENT CAUSES OF CHANGE ORDER

Category	Cause of Change Orders	Mean Score	RII Value	RII Rank
Consultant-related	Errors and omissions in design	4.40	0.88	1st
	Change of design	4.32	0.86	2nd
	Incomplete / inadequate working drawings	4.18	0.84	3rd
	Conflict between contract documents	4.10	0.82	4th
Client-related	Change of scope by client	4.05	0.81	5th
	Delay in client decision-making	3.98	0.80	6th
	Client financial difficulties	3.85	0.77	7th
Contractor-related	Contractor financial difficulties	3.75	0.75	8th
	Lack of skilled labor / equipment	3.65	0.73	9th
	Poor workmanship	3.55	0.71	10th
External-related	Unforeseen site conditions	3.40	0.68	11th
	Weather conditions	3.25	0.65	12th
	Regulatory / statutory changes	3.10	0.62	13th

ISBN: 978-978-8567-02-8

TABLE III: RANKING OF IMPACTS OF CHANGE ORDERS

Impact Category	Specific Impact	Mean score	RII Value	RII Rank
Cost-related impacts	Increase in project cost / cost overrun	4.45	0.89	1st
Time-related impacts	Project completion delay	4.30	0.86	2nd
	Extension of contract duration	4.05	0.81	4th
Productivity impacts	Reduced labor productivity	3.95	0.79	5th
	Rework and demolition	3.85	0.79	6th
Contractual & managerial impacts	Contractual disputes and claims	4.15	0.83	3rd
	Increased project overhead costs	3.70	0.74	7th
Quality-related impacts	Compromised quality of work	3.55	0.71	8th

3.4.2 Considering the relative importance index ranking on the impacts of change order

The RII analysis of impacts indicates (from table III) that cost overrun is the most severe consequence of change orders, ranking first with an RII value of 0.89. This confirms that financial performance is the project objective most adversely affected by construction changes. Similar findings have been widely reported in construction management literature, where change orders are consistently linked to cost escalation (Love et al., 2017; Shafique et al., 2021).

Project completion delay ranked second (RII = 0.86), demonstrating a strong association between change orders and schedule disruption. Changes often require resequencing of activities, approval of revised drawings, and additional work, all of which contribute to time overruns (Hwang & Low, 2012; Ramadhan & Waty, 2025).

Contractual disputes and claims ranked third (RII = 0.83), highlighting the managerial and legal implications of frequent change orders. Disagreements commonly arise over valuation, responsibility, and entitlement to extensions of time, especially when changes are poorly documented or approved late (Khalifa et al., 2019).

Extension of contract duration ranked fourth (RII = 0.81), further reinforcing the time-related consequences of change orders. Productivity-related impacts were also significant, with reduced labor productivity ranking fifth (RII = 0.79) and rework and demolition ranking sixth (RII = 0.79). These impacts reflect inefficiencies caused by repeated tasks, design revisions, and disruption of established work sequences (Love et al., 2017).

Increased project overhead costs ranked seventh (RII = 0.74), while compromised quality of work ranked eighth (RII = 0.71). Although quality impacts ranked lower than cost and time, compromised quality can negatively affect long-term performance, safety, and client satisfaction, making it a critical concern in change order management (Hwang & Low, 2012).

The findings on the impacts of change orders are in line with the study objectives, as the RII ranking clearly demonstrates the extent to which change orders affect project cost, time, contractual performance, productivity, and quality. The dominance of cost and time-related impacts confirms the achievement of the objectives and provides empirical justification for the recommended change management strategies.

4. CONCLUSIONS

This study demonstrates that change orders have significant adverse effects on construction project performance within Kano Metropolis. Cost overrun and schedule delay were identified as the most critical impacts, followed by contractual disputes and productivity losses. These findings directly address the study's objectives and highlight the need for improved management of change processes in construction projects.

The study contributes localized empirical evidence to construction management literature and provides practical insights for professionals operating in similar developing-country contexts.

5. RECOMMENDATIONS

Based on the findings, the study recommends the adoption of formal change management procedures, improved pre-construction planning, and timely stakeholder decision-making. Early evaluation of the cost and time implications of proposed changes should be conducted before approval. Capacity building for construction professionals is also essential to enhance effective management of change order impacts.

ISBN: 978-978-8567-02-8

ACKNOWLEDGMENT

I would like to express my deepest appreciation to my supervisor, Dr. A.D. Rafindadi, for his supervision and excellent advice in making this work possible.

REFERENCES

Abdul-Rahman, H., Wang, C., & Yap, J. B. H. (2022). Descriptive statistics and their application in construction management research. Journal of Construction Research, 15(3), 145–159.

Adu, J., Osei-Tutu, E., & Ahadzie, D. (2020). Factor analysis of variation orders in construction projects. International Journal of Construction Engineering and Management, 9(1), 10–21.

Agyakwah-Baah, A., & Chileshe, N. (2010). Construction professionals' perception of risk assessment and management practices: Does length of service in the construction industry matter? In C. Egbu (Ed.), Proceedings of the 26th Annual ARCOM Conference (pp. 1219–1228). Association of Researchers in Construction Management.

Alkhattabi, M. (2023). Drivers and consequences of variation orders in construction projects. International Journal of Construction Management, 23(6), 987–1001.

Alzara, M. (2022). Managing uncertainty and change in construction projects: A systems perspective. Built Environment Project and Asset Management, 12(4), 512–526.

Hadi, M. N. S., Alnahhal, W., & Alnuaimi, A. S. (2021). Reliability and validity assessment in construction management research. Journal of Engineering, Design and Technology, 19(5), 1247–1262.

Henseler, J., Hubona, G., & Ray, P. A. (2014). Using PLS path modeling in new technology research: Updated guidelines. MIS Quarterly, 38(1), 1–24.

Hwang, B. G., & Low, L. K. (2012). Construction project change management in Singapore. International Journal of Project Management, 30(7), 817–826.

Ibbs, C. W. (1997). Quantitative impacts of project change: Size issues. Journal of Construction Engineering and Management, 123(3), 308–311.

Khalifa, A., Mohamed, S., & Ahmed, R. (2019). Managing variation orders in construction projects. International Journal of Construction Project Management, 11(2), 85–99.

Love, P. E. D., Holt, G. D., Shen, L. Y., Li, H., & Irani, Z. (2017). Change and rework in construction projects. Journal of Construction Engineering and Management, 143(4), 04017001.

Mahamid, I. (2025). Frequency and impact of change orders in construction projects. International Journal of Construction Management, 25(1), 88–97.

Nunnally, J. C. (1978). Psychometric theory (2nd ed.) McGraw-Hill.

Qasem, R., Alaloul, W. S., Liew, M. S., & Musarat, M. A. (2025). Digital solutions for change order management in construction projects: A PLS-SEM approach. International Journal of Built Environment Studies, 7(2), 112–130.

Ramadhan, R., & Waty, D. (2025). Cost and time impacts of design errors. International Journal of Built Environment Studies, 7(1), 56–68.

Royce, J., Bennett, P., & Smith, R. (2015). Interpreting Cronbach's alpha coefficients in reliability testing. Educational and Psychological Measurement, 75(6), 1050–1063.

Salkind, N. J. (2017). Statistics for people who (think they) hate statistics (6th ed.). SAGE Publications.

Shafique, M., Khan, M. I., & Rafiq, M. (2021). Cost and schedule impacts of variation orders. Journal of Construction Engineering and Management, 147(10), 04021130.

Taherdoost, H. (2016). Validity and reliability of the research instrument: How to test the validation of a questionnaire/survey in research. International Journal of Academic Research in Management, 5(3), 28–36.

Tawiah, P., & Badu, E. (2021). Application of SPSS in construction management research: Best practices. Journal of Construction Research Methods, 2(1), 22–34.

ISBN: 978-978-8567-02-8

5TH Faculty of Engineering Conference on Engineering Innovation and Economic Policies: Driving Sustainable Industrial Growth in Nigeria

Faculty of Engineering, Bayero University, Kano.

082-A Fuzzy-PSO Algorithm for Demand Side Management of Home Appliances considering contribution from EV Fleet

Ima Okon Essiet

Department of Computer Engineering, Bayero University, Kano

Corresponding author's email: ioessiet.ele@buk.edu.ng

Abstract: Recent advances in battery chemistry and technology as well as advocacy for reduction of greenhouse gas emissions have enhanced the adoption of EVs as a preferred means of transportation. In V2H (vehicle-to-home) mode, these EVs can also provide emergency energy to power home appliances during peak periods. The incorporation of EV contribution into home energy management system (HEMS) enhances its ability to reduce consumer discomfort and peak-to-average ratio (PAR). In this paper, a HEMS strategy is proposed which controls the energy demand of household appliances by considering the charging/discharging schedule of a fleet of EVs. In particular, a cluster of 50 households (with varying schedules for shiftable loads) is considered in the simulation with an EV fleet size of 150 vehicles with daily scheduling. This configuration is adopted due to the average peak energy consumption of 1.8KW for each household and an average V2H capacity of an EV of 24 KWh based on acceptable SOC considerations. A hybrid strategy comprising mixed integer linear programming (MILP) and particle swarm optimization (PSO) is considered for the objective function and load scheduling optimization respectively which also considers the effects of emergency EV trips and unscheduled charging activities. Simulations are implemented using Scilab. From preliminary simulation results, an improvement of 8% and 10% are obtained for the PAR and energy cost savings respectively, which demonstrates that the proposed strategy is effective for reducing energy cost and minimizing energy demand during peak periods.

Keywords: V2G, home energy management system, electric vehicle, load scheduling, demand response

1. INTRODUCTION

The adoption of EVs has increased significantly in recent years with the global EV market share projected to increase from 2.7% to 28% between 2020 and 2030. Also, the total number of EVs on the road is estimated to increase from 8.5 million to 116 million vehicles globally (Blonsky et al, 2021). There are several advantages of EVs compared to their internal combustion engine counterparts, some of which include reduced emissions, cheaper operating and maintenance costs and less reliance on fossil fuels. V2X technology describes the capability of an EV to supply energy to other electrical appliances from its battery. In other words, the EV battery acts like a decentralized energy storage system (ESS) which can supply energy to home appliances or industrial locations on demand. This capability expands the application of EVs beyond just providing transportation to also enhancing grid stability by using the EV as a source of reactive power during peak periods [A-com]. In particular, the use of EVs to support household appliances is referred to as vehicle-to-home (V2H). Some of the benefits of V2H utilization include:

i. Provision of an alternative or backup energy source during power outage events. This enables EV owners to use their vehicles to power essential appliances or to provide heating and cooling when the main energy supply is unavailable

ii. Ensuring energy cost savings by utilization of time-of-use (ToU) rates. Therefore, EV owners can schedule vehicle charging during off-peak periods and then use stored energy in the EV battery to supply home appliances during peak periods

iii. Participation in demand response (DR) programs which involves consumers reducing their energy consumption during periods when there is increased energy demand. Participation in such programs can benefit consumers through either financial incentives or reduced energy rates

iv. Optimization of energy from renewable sources such as wind and solar PV for the charging of EV batteries. This ensures that the vehicle battery is charged using clean energy sources and minimizes reliance on fossil fuels

v. When there is wide adoption of EVs in V2H or V2G mode, excess energy can be fed back to the grid when needed. In this manner, EV owners become energy prosumers and not just consumers because they become part of the energy supply chain. Thus, EV owners provide grid support services. Bidirectional EV chargers have a DC link capacitor capable of supplying reactive power to support inductive loads on the grid.

ISBN: 978-978-8567-02-8

It should be noted that there are certain challenges to widespread adoption of EVs for V2H applications. Some of these include lack of standardized communication protocols between EVs and electrical appliances, cyber security shortcomings which affect integrity of information shared between EVs and electrical appliances.

Several researches have been done which implement HEMS with energy contribution from EVs. In (Mohammad et al, 2021), a HEMS was implemented using contribution from PV, EV and battery storage system. The scheduling strategy was implemented using a multi-objective optimization problem which was solved using binary PSO (BPSO). The result was a 52.47% reduction in energy cost and a PAR reduction of 15.11%. In (Ahsan and Rahman, 2022), the authors highlighted the importance of EVs in providing support to homes powered by PV, and in (Abdelaal et al, 2021), the effect of various charging and discharging strategies of EV battery was considered for a smart home while maintaining transformer loading limit for single and multiple EV trips. Similar research can also be found in (Sultan et al, 2022, Alfaverh et al, 2023, Almughram et al, 2022 and Tuttle et al, 2013). However, none of these consider the case of short charging periods of between 30 mins and 1 hour which can be caused by frequent trips or the advent of fast charging which has become popular in recent years.

The main contribution of this research is to ensure that even during periods when the EV is plugged in to charge for short periods of time (typically between 30 minutes and 1 hour), the objective function with the aid of the fuzzy-PSO optimizer can schedule appliances in such a way that EV battery health and grid stability are maximized. The rest of the paper is organized as follows:

2. METHODOLOGY

The HEMS will coordinate the scheduling of home appliances based on time-of-use (ToU) energy pricing. Apart from the main supply from the grid, the household appliances can also be powered by energy from the PV panels, the battery connected to the PV panels, and also the battery of the EV. The priority of the various energy sources is decided by the fuzzy-based optimization algorithm of the HEMS. The household appliances considered in this research are categorized as shiftable and non-shiftable, and are detailed in Table 1.

TABLE I: LOAD SCHEDULE FOR HEMS

Appliances/Loads	RATED POWER (W)
Shiftable	
Air conditioner	1500
Washing machine	800
Hair dryer	450
Non-shiftable	
Water pump	1200
Lighting	150
Laptops	60
Microwave	900
Electric Oven	2000
Refrigerator	330

Power consumed by all appliances is obtained as:

$$P_{app}(t) = P^{s}_{a,b}(t) + P^{ns}_{a,b}(t) \quad (1)$$

Where $P_{app}(t)$ is the total power consumed by all appliances, $P^{s}_{a,b}(t)$ is the total power consumption by shiftable appliance a in cluster b, and $P^{ns}_{a,b}(t)$ is the total power consumption by non-shiftable appliance a in cluster b.

Demand response is achieved using the shiftable appliances for either valley filling during off-peak periods with reduced consumption, or for load shaving during peak periods characterized by high energy consumption. For this reason, it is necessary to evaluate the total power due to the shiftable appliances depending on the status of the shiftable appliance. This is done according to the equation below:

$$P^{s}_{app,tot}(t) = P^{s}_{a,b}(t)\alpha_j \quad (2)$$

Where α_j is the index of the shiftable appliance which indicates its status (0 = OFF and 1 = ON).

Charging and discharging power rates of the EV are obtained according to the following equations:

$$P_{ch}(t) = P_{ch\max} - ((R(t) - P_{\max}) / P_{\min} * P_{ch\max}) \quad (3)$$

Where $R(t)$ is real-time energy price, $P_{\min}$ is the minimum energy price which is set to N70/KWh based on Band B energy price in Nigeria. The minimum charging power rate is designated as $P_{ch\min}$ and is set as 1150KWh. $P_{ch\max}$ is the maximum charging power rate for the Nissan Leaf 2017 EV model which is 2.3 KWh (Schmidt, 2019). This model of EV has a battery capacity of 40KWh. Therefore, time taken to charge the battery from empty state to full charge is 18 hours.

The ToU pricing strategy is used which makes the charging and discharging power rates dynamic. Also, the energy demand from EV changes depending on the needs of the consumers. The total energy demand of the EV is a continuous function of the power built up or discharged from the battery.

The scheduling of appliances is controlled by the FLC algorithm which provides DR response based on whether peak shaving or valley filling is to be implemented. For the valley filling stage, there are two cases: when the total energy consumed is not sufficient to ensure valley filling, and when total energy consumed by shiftable appliances is too much for valley filling. For the first case, since the total demand including that of the shiftable appliances is not sufficient for valley filling, then all the shiftable appliances will be left on. However, in the second case, a probability function is used to determine which of the shiftable appliances will be switched off, and which will be left on. The probability function is given in (Hou et al, 2019) as:

$$\gamma^{sh}_{a} = 1 - \left| \frac{P^{sh}_{a} - P_{sh\,app,a}(t)}{P^{sh}_{a} + P_{sh\,app,a}(t)} \right| \quad (4)$$

ISBN: 978-978-8567-02-8

Where P_a^{sh} is the total power requirement for the shiftable appliances and $P_{sh\,app,a}(t)$ is the power requirement for shiftable appliance a

The total energy demand of the EV is a continuous function of the power built up or discharged from the battery over time during the charging and discharging cycles, and can be estimated using the following:

$$\mu_{EV}(t) = \int_{t_1}^{t_2} P_{ch}(t)\alpha(t) + P_{dis}(t)(1-\alpha(t)) \quad (5)$$

Where $\alpha(t)$ is the status of the EV (1 represents charging status 0 represents discharging status), t_1 and t_2 are the arrival and departure times of the EV respectively and P_{ch} and P_{dis} are the charging and discharging power rate respectively of the EV.

To preserve the health and integrity of the EV battery, the discharge power rate of the battery is controlled by the following:

$$P_{dis}(t) = P_{app}(t) \quad (6)$$

When the total power demand of the appliances is less than the maximum power discharge of the battery ($P_{dis\,\max}$) and otherwise:

$$P_{dis}(t) = P_{dis\,\max}(t) \quad (7)$$

Another importamt parameter to consider is the state-of-charge (SoC) of the EV battery. For lithium ion battery, maximum cahrging and discharging limits of the battery are maintained at 80% and 20% of final SoC respectively. Hence,

$$0.2SoC_{EV\,\max} \le SoC_{EV}(t) \le 0.8SoC_{EV\,\max} \quad (8)$$

Also,

$$SoC_{EV}(t) = SoC_{EV}(t-1) + ((P_{EV}(t)) * \Delta t) / \rho_{EV} \quad (9)$$

Where ρ_{EV} is the maximum capacity of the EV li-ion battery and P_{EV} is the charging/discharging power of the battery.

An important function of Equation (9) is to ensure that at any time (t), the SoC_{EV} is not less than $0.4\,SoC$ during V2H mode so that in the case of emergency trips, there is enough battery power for the trip. Therefore, if the user intends to discharge the battery for an extended period, they need to specify the target SoC required for the task to enable the algorithm to compute the required SoC for the task. Hence,

$$SoC_{task}(t) = SoC_{\text{target}} - SoC_{EV}(t) \quad (10)$$

With Equation (10) specified, the duration of charging the EV battery could be adjusted to meet the SoC required for the specific task according to the following equation:

$$t_{ch,task} = (SoC_{task}(t) * \rho_{EV}) / P_{ch\max} \quad (11)$$

2.1 Fuzzy Logic Controller and PSO Optimizer for Appliance Scheduling and EV Cluster Coordination

Fuzzy logic has been used in this paper to schedule the appliances in the HEMS based on whether peak-shaving or valley-filling operations are to be performed. For instance, if a peak-shaving operation is to be performed, the FLC will determine whether some or all of the shiftable appliances are to be switched off. The opposite will be the case in a situation where valley-filling is to be done. The fuzzy membership functions for the scheduling task are shown in Figure 1.

The particle swarm optimization (PSO) algorithm is a swarm-based metaheuristic algorithm whose search strategy mimics the social behavior of living organisms interacting in groups, such as a school of fish or a flock of birds. A swarm of search agents called particles moves through a search space looking for the optimal global solution to a problem. In the context of this research, the PSO algorithm has been selected to optimize the deployment of a fleet of 150 EVs in V2H mode with a consideration for different arrival and departure times for each vehicle. At any given time, the arrival (t_{arr}) and departure time (t_{dep}) and SoC of the EV battery (SoC_{EV}) are considered while determining the duration that the EV will provide support for home appliances. The structure of the HEMS is shown in Figure 2.

TABLE II: PARAMETER SETTINGS FOR PSO

Parameter	SETTING
Inertia weight factor, ω	0.6
Cognitive constant, c_1	0.9
Social constant c_2	0.7
Swarm size, nPop	100
Maximum number of iterations (MaxIt)	200

Algorithm 1

Input: $t_{arr}, t_{dep}, SoC_{init}, nPop, \omega, c_1, c_2, MaxIt, \alpha_t, P_{app}(t)$

Output: $P_{sh,app}(t), P_{con}(t)$ (where $P_{con}(t)$ is the power that is saved by the battery in the home after EV charging ends)

For each time step:

If $\gamma_a^{sh} \approx 1$ then

$P_{dis}(t) = P_{app}(t)$ (Equation 6)

Else

$P_{dis}(t) = P_{dis\,\max}(t)$ (Equation 7)

For $t_{dep} - t_{arr} \le 30$ minutes (state 0)

Charge EV according to Equation (1)

Else

Assume state 1 (normal charge)

End

ISBN: 978-978-8567-02-8

TABLE III: LINGUISTIC VARIABLES FOR FLC-BASED APPLIANCE SCHEDULING

Energy Demand	Unit Energy Price	Peak Shaving	Valley Filling	No Action
High	Costly	Ideal	Wrong	Wrong
High	Cheap	Acceptable	Wrong	Ideal
Average	Costly	Ideal	Wrong	Acceptable
Average	Cheap	Wrong	Ideal	Acceptable
Low	Costly	Wrong	Wrong	Ideal
Low	Cheap	Wrong	Ideal	Wrong

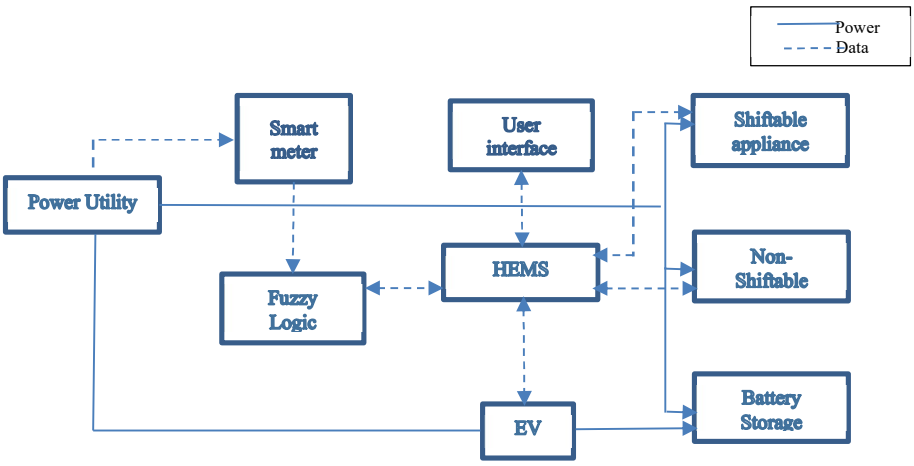


Figure 2: Schematic of the proposed HEMS

The PSO algorithm and parameter settings are shown in Algorithm 1 and Table II respectively. The settings in Table II are obtained from trial-and-error after several iterations of the algorithm with the selected algorithm input variables and parameters.

2.2 FLC Rule Base for Smart Scheduling of Appliances

The linguistic variables used in the rule base for fuzzy logic controlled scheduling represent three scenarios. The 'ideal' scenario represents a case where the given decision (peak shaving, valley filling, do nothing) is the best possible decision considering the energy demand and energy price at the instant of scheduling. The 'acceptable' scenario is a tradeoff situation between energy demand and energy price while the 'do nothing' scenario represents a situation in which the given action is not to be taken considering the current state of input variables.

The membership function for the energy demand and energy price are triangular and trapezoidal respectively and shown in Figure 1. The energy price per KWh was set at 70 naira which is the average energy cost for Band B residential consumers in Nigeria. The universe of discourse for the energy demand is 6,300 W which is the total demand for all appliances based on their power rating.

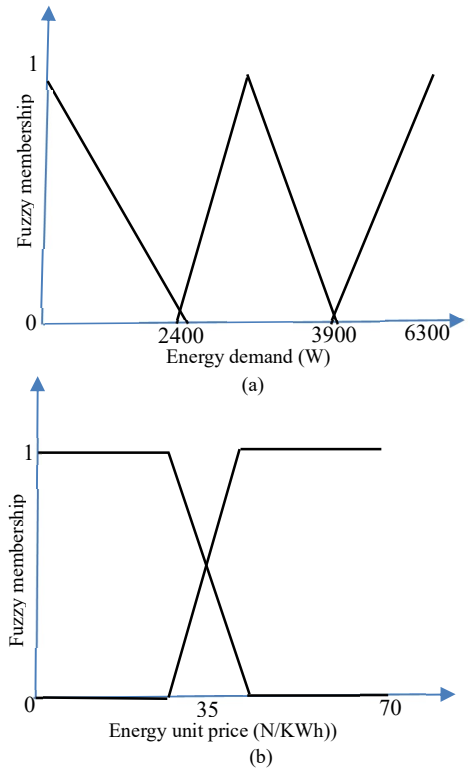


Figure 1: Fuzzy membership function for (a) Energy Demand (b) Energy unit price.

ISBN: 978-978-8567-02-8

2.3 Peak-to-Average Ratio (PAR)

PAR is a stability index which balances conventional power generation cost with cost of maintaining renewable energy sources. Mathematically, it is defined by (Liu et al, 2014) as:

$$PAR(t) = \frac{peak\ load\ of\ grid}{average\ load\ of\ grid} = \frac{P_{\max,t}}{\frac{1}{T}\sum_{t=1}^{T} P_t} \quad (12)$$

Where $P_{\max,t}$ is maximum power generated/supplied by the grid, P_t is power supplied during one time interval, and T is the total number of time intervals.

From Equation (12), it can be seen that PAR measures how well alternative energy sources augment the grid supply. This means that a smaller magnitude of PAR is, the better the contribution of the renewable energy sources. In this research, the contribution from EV fleet batteries is augmented by battery storage contributed by solar PV panels for each of the 50 households. PAR is an important index in this research because one key objective is to ensure stability of the grid especially during peak hours when energy demand increases.

For this research, the key assumptions made are as follows: all EVs are identical, ToU pricing structure is used for appliance scheduling, PAR and energy cost savings, and the household load profiles for all 50 homes are as specified in Table I.

3. PRELIMINARY RESULTS AND DISCUSSION

The results of this research are preliminary because they represent the contribution of the EV battery alone for contribution to grid stability. From Figure 2, it can be seen that the effect of the battery storage is not considered. All simulations were done in Scilab and we consider the energy cost savings per KWh and PAR for the consumers for three different EV cluster sizes: 50, 100 and 150 EVs. We also consider two scenarios: when EVs are deployed without the proposed algorithm, and when they are deployed with the algorithm. Results are given in Tables IV and V.

TABLE IV: HEMS OPERATION WITH AND WITHOUT PSO ALGORITHM AND FLC

SCENARIO	PAR	ENERGY COST (N/KWH)
Without Algorithm and FLC		
Peak shaving (PS)	0.6754	69.27
Valley filling (VF)	0.6158	69.56
With Algorithm and FLC		
After 50 iterations	0.6711 (PS) 0.6124 (VF)	68.46 68.95
After 100 iterations	0.6632 (PS) 0.6098 (VF)	66.25 67.64
After 200 iterations	0.6209 (PS) 0.6016 (VF)	63.00 64.28

TABLE V: EFFECT OF VARYING EV CLUSTER SIZE ON PAR AND ENERGY COST SAVINGS FOR PROPOSED FUZZY-PSO ALGORITHM

SCENARIO	PAR	ENERGY COST (N/KWH)
50 EVs		
Peak shaving (PS)	0.6796	69.32
Valley filling (VF)	0.6628	68.23
100 EVs	0.6736 (PS) 0.6598 (VF)	68.46 68.33
150 EVs	0.6332 (PS) 0.6035 (VF)	63.25 64.64

From the results obtained from Table IV, we can observe that there is an improvement of 8% and 10% respectively for the PAR and energy cost respectively for a scenario without the fuzzy-PSO scheduling algorithm and the scenario where there the algorithm is used. It should be noted that while (Mohammad et al, 2021) obtained a better PAR reduction of 15.11%, this is likely due to their consideration of the contribution of solar PV in addition to that of EVs. PAR and energy cost savings are complementary (proportional in terms of magnitude), but they are not necessarily equal to each other. Hence, the impact of these results on grid stability is that improved PAR means that alternative energy sources are complementing the grid supply, which translates to reduced burden on the grid, particularly during periods of peak energy demand. This situation results in increased energy availability to consumers due to greater energy cost savings. It is also observed that the best results are obtained after 200 iterations of the algorithm, which demonstrates the capability of the PSO algorithm to find fittest solutions even after many search cycles. It was also observed that the algorithm generally performed better for the peak shaving action compared with the valley-filling action. This is likely due to the effect of Equations (10) and (11) which make it possible for the EV battery to contribute energy even when plugged in for a short time (30 minutes). Such an action will help to stabilize the power utility during peak periods of energy demand.

From Figure V, the effect of varying the size of EV clusters on PAR and energy cost savings can be observed. From the results obtained, we see that grid health and energy cost savings are maximized when a large number of EVs is involved in contributing to the HEMS. For instance, the effect of emergency EV trips is minimized when there are more vehicles within the cluster because other vehicles can still contribute to the V2H scheme. Hence, as the size of the fleet increases, it can also be seen that PAR and energy cost per KWh are also minimized.

4. CONCLUSION

This research has presented a HEMS model based on a cluster of EVs in V2H mode. While the use of EVs to support the grid by providing peak-shaving and valley-filling has received a lot of attention in recent years, there is a need to maximize the benefits of the ever-increasing deployment of EVs on roads across the world. Therefore, it is important to coordinate their contribution as a cluster

ISBN: 978-978-8567-02-8

rather than individually.

This paper has investigated the use of a metaheuristic algorithm called particle swarm optimization as well as fuzzy logic control to coordinate the charging of a cluster of 150 EVs while considering the effect of unplanned or emergency trips of some of the EVs. We have examined the contribution of the EVs for both valley-filling and peak-shaving scenarios and from preliminary results, there has been an improvement of both PAR and energy cost savings per KWh of 8% and 10% respectively. We have also seen that increasing the size of the EV cluster has advantages for both consumers and the energy grid when emergency trips for some EVs are considered.

Future research would examine the possibility of improving the PAR and energy cost using other metaheuristic algorithms. Also, the performance of EVs in V2H mode while considering the contribution of other renewable energy sources such as solar PV and wind energy would also be investigated.

REFERENCES

Abdelaal, G., Gilany, M., Elshahed, M., Sharaf, H.M., & El'gharably, A., (2021). Integration of Electric Vehicles in Home Energy Management Considering Urgent Charging and Battery Degradation. IEEE Access, Vol.9, pp:47713-47730

Ahsan, R., & Rahman, S.M.I., (2022). A Design and Simulation of Vehicle to Home (V2H) Technology to Match Power Demand. International Journal of Innovative Science and Research Technology, Vol.7 No. 2, pp:166-170.

Alfaverh, K., Alfaverh, F., & Szamel, L., (2023). Plugged-in Electric Vehicle-assisted Demand Response Strategy for Residential Energy Management. Journal of Energy Informatics, Vol.6 No. 6, pp:1-24 https://doi.org/10.1186/s42162-023-00260-9

Almughram, O., Ben Slama, S., & Zafar, B., (2022). Model for Managing the Integration of a Vehicle-to-Home Unit into an Intelligent Home Energy Management System. Sensors, Vol.22 No. 8142, pp:1-26 https://doi.org/10.3390/ s22218142, (2023).

Blonsky, M., Munankarmi, P., & Balamurugan. S., (2021). Incorporating Residential Smart Electric Vehicle Charging in Home Energy Management Systems. 2021 IEEE Green Technologies Conference. pp:1-8

Hou, X., Wang, J., Huang, T., Wang, T., & Wang, P. (2019). Smart Home Energy Management Optimization Method Considering Energy Storage and Electric Vehicle. IEEE Access, Vol.7, pp:144010–144020. https://doi.org/10.1109/ACCESS.2019.2944878

Liu, Y., Yuen, C., Huang, S., Hassan, N.U., Wang, X., & Xie, S., (2014). Peak-to-Average Ratio Constrained Demand-side Management with Consumer's Preference in Residential Smart Grid. IEEE Journal of Selected Topics in Signal Processing, Vol.8 No. 6.

Mohammad, A., Zuhaib, M., Ashraf, I., Alsultan, M., Ahmad, S., Sarwar, A., & Abdollahian, M., (2021). Integration of Electric Vehicles and Energy Storage System in Home Energy Management System with Home-to-Grid Capability. Energies, 2021, 14, 8557. https://doi.org/10.3390/en14248557

Schmidt, B. (2019). Nissan sees Leaf as Home Energy Source, says Tesla Big Battery "Waste of Resources". Available: www.thedriven.io/2019/07/11/nissan-sees-leaf-as-home-energy-source-says-tesla-big-battery-waste-of-resources/

Sultan, V., Aryal, A., Chang, H., & Kral, J., (2022). Integration of EVs into the smart grid: A Systematic Literature Review. Journal of Energy Informatics, Vol.5 No. 65, pp:1-28 https://doi.org/10.1186/s42162-022-00251-2

Tuttle, D.P., Fares, R.L., Baldick, R., & Webber, M.E., (2013). Plug-In Vehicle to Home (V2H) Duration and Power Output Capability, pp:1-7, 978-1-4799-0148-7/13/$31.00 ©2013 IEEE

Energy Management System with Home-to-Grid Capability. Energies, 2021, 14, 8557. https://doi.org/10.3390/en14248557

Schmidt, B. (2019). Nissan sees Leaf as Home Energy Source, says Tesla Big Battery "Waste of Resources". Available: www.thedriven.io/2019/07/11/nissan-sees-leaf-as-home-energy-source-says-tesla-big-battery-waste-of-resources/

Sultan, V., Aryal, A., Chang, H., & Kral, J., (2022). Integration of EVs into the smart grid: A Systematic Literature Review. Journal of Energy Informatics, Vol.5 No. 65, pp:1-28 https://doi.org/10.1186/s42162-022-00251-2

Tuttle, D.P., Fares, R.L., Baldick, R., & Webber, M.E., (2013). Plug-In Vehicle to Home (V2H) Duration and Power Output Capability, pp:1-7, 978-1-4799-0148-7/13/$31.00 ©2013 IEEE

ISBN: 978-978-8567-02-8

5TH Faculty of Engineering Conference on Engineering Innovation and Economic Policies: Driving Sustainable Industrial Growth in Nigeria

Faculty of Engineering, Bayero University, Kano.

083-A Systematic Review of Image Analysis and Machine Learning Techniques for Maize Quality Assessment and Biofuel Yield Estimation

Kwoopnaan I.T Vwamdem, Ima Okon Essiet and Hassan Abdullahi Bashir

Department of Computer Engineering, Bayero University, Kano.
Corresponding email: ioessiet.ele@buk.edu.ng

Abstract: There has been increased global attention to clean energy sources and food security. Maize falls in the intersection of these two thematic areas and it is evidenced by the increased application of various technologies and techniques for maize quality assessment. Traditional quality assessment methodologies (ranging from manual visual inspection to wet-chemistry assays) are increasingly viewed as bottlenecks due to their subjectivity, destructive nature, and inability to scale to meet modern production volumes. Machine learning and image analysis techniques are increasingly being employed for assessing maize quality and estimating biofuel yield, driven by the need for sustainable and climate-resilient energy systems. This review examines peer-reviewed studies published between 2020 and 2025 that apply image-based and data-driven approaches to maize quality assessment and biofuel yield estimation. Relevant literature was sourced from major scientific databases and analysed using thematic classification based on imaging technique, machine learning methodology, and application domain. Key developments include the deployment of Short-Wave Infrared (SWIR) hyper spectral imaging for the non-destructive detection of mycotoxins like Aflatoxin B1, the utilization of lightweight Convolutional Neural Networks (CNNs) for real-time mobile disease detection, and the integration of Unmanned Aerial Vehicles (UAVs) with object detection algorithms (YOLO v8) for field-level quality phenotyping. Key challenges include data heterogeneity, model interpretability, computational efficiency for edge deployment, scalability, and sustainability assessment. This review synthesizes current trends and provides theoretical and practical understanding of these techniques, identifies critical research gaps and proposes further research directions for developing intelligent, non-destructive frameworks for maize quality assessments and maize-based biofuel production.

Keywords: maize quality assessment, convolutional neural network, hyper spectral imaging, machine.

1. INTRODUCTION

Maize (*Zea mays L.*) occupies a unique dual position in the global economy, serving as a critical pillar for both food security and renewable energy. As the primary feedstock for bioethanol production in regions like the United States and Brazil, and a staple food source globally(Lim & Kim, 2024), the demand for high-quality maize is intensifying. However, the intersection of these sectors presents complex challenges. For bioethanol production, maximizing starch content and biomass yield is paramount (Lim & Kim, 2024), while food and feed supply chains prioritize safety parameters, specifically the absence of mycotoxins(C. Fan et al., 2024).

Maize quality assessment has historically relied on a bifurcated approach: subjective visual inspection for physical defects and destructive chemical analysis (e.g., HPLC) for nutritional and safety parameters(Karmakar et al., 2024). These traditional methods are increasingly viewed as bottlenecks due to their inability to scale to meet modern production volumes and the requirements of sustainable, climate-resilient energy systems(Dönmez, 2022).

In recent years, quality assessment has witnessed a paradigm shift driven by the application of Imaging technologies(Bhargava et al., 2024; Karmakar et al., 2024; B. Wang et al., 2023) and artificial intelligence in quality assessment(C. Fan et al., 2024; Y. Wang & Song, 2023; Xu et al., 2022). The convergence of advanced optical sensors—specifically Hyperspectral Imaging (HSI) and Unmanned Aerial Vehicles (UAVs)—with fourth-generation artificial intelligence (Deep Learning) offers a non-destructive alternative(Abbasi et al., 2025a; van Klompenburg et al., 2020). This review systematically analyses recent advancements in these domains, highlighting the transition from classical chemometrics to end-to-end Deep Learning architectures for both quality grading and biofuel yield estimation.

This review adheres to the Preferred Reporting Items

ISBN: 978-978-8567-02-8

for Systematic Reviews and Meta-Analyses (PRISMA) guidelines for study selection. The analysis critically examines recent advancements in imaging techniques and machine learning architectures, followed by a thematic review focused on maize quality assessment and biofuel yield estimation. Finally, the study addresses limitations in current research and outlines strategic directions for future investigation.

2. METHODOLOGY

A systematic approach is employed in this review to identify, screen, and analyse recent relevant literature.

2.1 Search Strategy and Selection Process

A comprehensive search was conducted using academic databases including IEEE Xplore, ScienceDirect, Web of Science, and Google Scholar. The search was restricted to research articles published between January 2020 and late 2025. The search strings combined terms related to the crop ("Maize", "Corn"), technology ("Deep Learning", "Hyperspectral Imaging", "Computer Vision", "YOLO"), and application domains ("Quality Assessment", "Mycotoxins", "Biofuel", "Yield Estimation"). Specific search strings used include (“Conversion Rate of Maize for Biofuel production”, “Applications of Image Analysis for Aflatoxin detection”, “Maize Quality Assessment”, “Applications of Machine learning in Maize Quality Assessments” etc)

Figure 1 below outlines the PRISMA (Preferred Reporting Items for Systematic Reviews and Meta-Analyses) flow diagram utilized for the study selection.

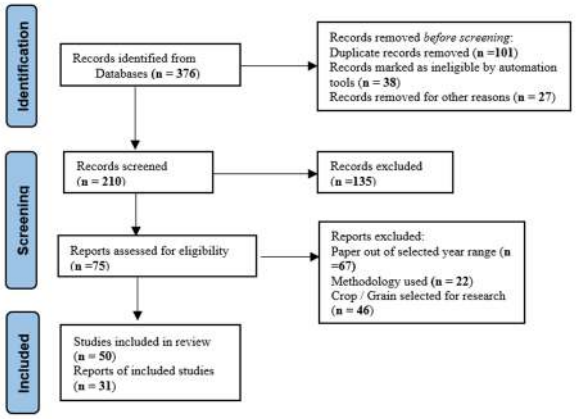


Figure1: Flow diagram depicting the selection process.

2.2 Inclusion and Exclusion Criteria

Studies were included if they: (1) focused specifically on maize; (2) utilized image analysis or machine learning techniques; (3) addressed quality parameters (purity, defects, chemical composition) or biofuel-related traits (starch content, biomass yield). Articles were excluded if they were not peer-reviewed, relied solely on traditional agronomic statistics without computational components, or were published before 2020.

2.2 Maize Varieties

A critical factor in both quality assessment studies and biofuel yield estimations is the specific variety of maize samples being analysed. This is because different strains possess distinct physical characteristics and distinct starch profiles.

TABLE 1: SUMMARY OF MAIZE VARIETIES EVALUATED IN REVIEWED LITERATURE.

Paper Title	***Maize Variety Used***
Variety identification of sweet maize seeds based on hyperspectral imaging combined with deep learning	Sweet Maize
An Improved Non-Destructive and High-Efficiency Model for Detecting the Purity of Denghai 605 Maize Variety	Denghai 605
Detection of Aflatoxin B1 in Maize Silage Based on Hyperspectral Imaging Technology	Baoyu 2307, Jinke Silag 516 & Xiandai silag No 15
Detection of Mechanical Damage in Corn Seeds Using Hyperspectral Imaging and the ResNeSt_E Deep Learning Network	Maize samples from Anhui province
Maize Kernel Quality Detection Based on Improved Lightweight YOLOv7	Denghai W385.
High accuracy identification of maize seed varieties based on a lightweight improved YOLOv8	Fennuo, Huangnuo, jinnuo618, lubainuo211, ludan958, luheitian201, luhongnuo201, luhuangtian196, qianduoduo668 and yinyu

3. TECHNOLOGICAL OVERVIEW

To comprehend the advancements in maize assessment, it is necessary to understand the imaging technologies and machine learning algorithms that serve as the foundation for automated systems.

3.1 Imaging Modalities and Texture Analysis

Hyperspectral Imaging (HSI): HSI represents a quantum leap in sensing, capturing hundreds of narrow spectral bands. The Short-Wave Infrared (SWIR, 1000–2500 nm) region is critical for both food safety and energy applications. It captures overtones of C-H, N-H, and O-H bonds, allowing for the direct quantification of starch (ethanol potential) and the detection of fungal metabolites (Bhargava et al., 2024; Huang et al., 2024; Xu et al., 2026).

Texture Feature Extraction: For morphological analysis using RGB images, Gray Level Co-occurrence Matrix (GLCM) features are commonly extracted to quantify surface texture, which is indicative of disease or physical defects (J. Wang et al., 2025; Wu et al., 2020). The key features used in maize seed classification are

ISBN: 978-978-8567-02-8

defined as follows:

$$\text{Contrast} = \sum_{i,j}(i-j)^2 P(i,j) \quad (1)$$

$$\text{Homogeneity} = \sum_{i,j} \frac{P(i,j)}{1+(i-j)} \quad (2)$$

Where p (i,j) is the normalized entry of the co-occurrence matrix, representing the probability of gray-level transitions between pixels i and j.

3.2 Machine Learning Architectures

The literature reveals a definitive shift from feature-engineering to deep learning.

Convolutional Neural Networks (CNNs): Architectures such as ResNet and MobileNet have become the standard for processing spatial data (leaf diseases) and spectral data (chemical composition).(Dönmez, 2022)

Object Detection (YOLO): The You Only Look Once (YOLO) family, particularly YOLO v8, has revolutionized field phenotyping. Its loss function combines classification loss and bounding box regression loss, enabling precise localization of maize seedlings and tassels.(R. Li et al., 2025; Niu et al., 2025; Yang et al., 2024).

4. THEMATIC ANALYSIS: MAIZE QUALITY AND SAFETY

4.1 Maize Quality and safety

The detection of Aflatoxin B1 (AFB1) remains the most critical safety challenge. Contaminated maize not only poses health risks but also concentrates toxins in Dried Distillers Grains with Soluble (DDGS), a byproduct of ethanol production used for animal feed. Recent developments highlight the superiority of SWIR-HSI for this task. By analysing spectral bands around 1729 nm and 2300 nm, deep learning models can detect AFB1 with accuracies exceeding 94%. (Guo et al., 2025)

To evaluate classification performance, the F1-Score is widely used as a robust metric for imbalanced datasets (e.g., rare, contaminated kernels among healthy ones)

$$\text{Precision (P)} = \frac{TP}{TP+FP}, \quad \text{Recall (R)} = \frac{TP}{TP+FN} \quad (3)$$

$$\text{F1} = 2.\frac{P.R}{P+R} \quad (4)$$

Where *TP* is True Positive, *FP* is False Positive, and *FN* is False Negative.

4.2 Physical Quality and Defect Detection

Physical integrity determines market grade and milling efficiency. Stress cracks, often caused by rapid drying, are a primary defect. The Stress Crack Index (SCI) serves as a weighted metric to quantify the severity of damage in a sample batch:(Hassoun et al., 2023)

$$SCI = (1 \times P_{single}) + (3 \times P_{double}) + (5 \times P_{multiple}) \quad (5)$$

Where P_{single}, P_{double}, and $P_{multiple}$ represent the percentage of kernels with single, double, or multiple cracks, respectively. Research has moved towards lightweight mobilenet-based architectures to predict these indices on edge devices in real-time(C. Li et al., 2023; Niu et al., 2025; Yang et al., 2024).

5. THEMATIC ANALYSIS: BIOFUEL YIELD ESTIMATION

5.1 Feedstock Composition and Theoretical Yield

For the bioethanol industry, the value of maize is defined by its starch content. Starch $(C_6H_{10}O_5)n$ is hydrolysed into glucose $(C_6H_{12}O_6)$, which is then fermented into ethanol (C_2H_5OH)(Novonesis, 2020). The theoretical ethanol yield can be estimated stoichiometrically:

$$\text{Starch} \xrightarrow{+H_2O} .11 \text{ x Glucos} \xrightarrow{\text{yeast}} 0.51 \text{ x Ethanol} + 0.49 \text{ x } CO_2 \quad (6)$$

Thus the theoretical yield (Y_{EtOH}) from a mass of Starch (M_{starch}) is:

$$Y_{EtOH} \approx 0.568 \times M_{starch} \quad (7)$$

(Lim & Kim, 2024).

Recent studies demonstrate that HSI combined with Convolutional Autoencoders (1D-CAE) can accurately predict M_{starch} in single kernels, allowing biorefineries to optimize process efficiency (Arif et al., 2025; Lim & Kim, 2024).

5.2 Biomass and Yield Prediction via UAVs

Estimating total biomass is crucial for supply chain stability. UAV-based multispectral imagery utilizes Vegetation Indices (VIs) to correlate canopy reflectance with yield(Han et al., 2020). The Normalized Difference Vegetation Index (NDVI) remains the standard:

$$\text{NDVI} = \frac{\text{RNIR}-RRED}{RNIR+RRED} \quad (8)$$

Machine learning regressors (Random Forest, XGBoost) ingest these VIs to predict yield(Abbasi et al., 2025b; Paudel et al., 2021). Model performance is typically evaluated using the Root Mean Square Error (RMSE):

$$RMSE = \sqrt{\frac{1}{n}\sum_{i=1}^{n}(y_i - \hat{y}_i)^2} \quad (9)$$

Table 1 summarizes the performance of different ML models reviewed in the literature for yield estimation(Lim & Kim, 2024; Paudel et al., 2021; Ramalingam et al., 2025; van Klompenburg et al., 2020).

ISBN: 978-978-8567-02-8

Table 2: Comparative Performance of ML Models for Maize Yield Prediction (2020–2025)

Model Architecture	*Input Data Source*	*Performance (R2)*	*Key Advantage*
Random Forest (RF)	UAV Multispectral	0.85 – 0.89	Robust to noise; handles non-linear relationships well.
CNN-LSTM	Time-series Satellite	0.91 – 0.94	Captures temporal growth patterns and spatial features.
XGBoost	Weather + Soil Data	0.82 – 0.86	High computational efficiency; interpretable feature importance.
Support Vector Regressor (SVR)	HSI (Lab based)	0.88 – 0.92	Effective for high-dimensional spectral data with small sample sizes.

6. CHALLENGES AND FUTURE DIRECTIONS

6.1 Data Heterogeneity and Scalability

A significant barrier identified is data heterogeneity. Variations in maize varieties, growing conditions, and imaging hardware lead to "domain shift," where a model trained on one dataset fails on another. Future research must focus on Domain Adaptation techniques and the creation of large-scale, diverse public datasets (Agro-HSR) to ensure models are scalable across different geographies(Fan et al., 2023; Monjur et al., 2025)

6.2 Model Interpretability and Sustainability

As models become more complex (e.g., Deep CNNs), they lose interpretability. For stakeholders to trust "intelligent frameworks," Explainable AI (XAI) methods must be integrated to visualize decision-making processes. Furthermore, sustainability assessments must be embedded into these frameworks, evaluating not just yield, but the resource efficiency (water, nitrogen) of the maize production to ensure true climate resilience.

6.3 Computational Efficiency for Edge Deployment

Real-time decision-making requires processing data at the "edge" (on tractors, drones, or smartphones). The trend towards lightweight architectures (YOLO v8, MobileNet) addresses this, but further optimization is needed to handle hyperspectral data on low-power devices.

6.4 Integration with IOT and Digital Twins

An emerging trend is the integration of Internet of Things (IoT) sensors with machine learning frameworks to create Digital Twins of maize storage and production systems. By fusing real-time environmental data (temperature, humidity, CO2) from IoT sensors with predictive ML models, Digital Twins allow for the simulation of "what-if" scenarios. For example, recent studies have demonstrated the use of Digital Twins to predict moisture migration and mycotoxin development in silos under varying climatic conditions, enabling proactive rather than reactive quality management (Gan et al., 2025; Suku Dube & Mambudzi, 2025). This cyber-physical integration is critical for maintaining quality throughout the supply chain.

6.5 Need for Real – World Validation

While many proposed frameworks demonstrate high accuracy (>95%) in controlled laboratory environments, there is a critical need for rigorous real-world validation. Field conditions introduce variables such as uneven lighting, occlusion, background clutter, and hardware vibrations that often degrade model performance. Future research must prioritize testing models on "in-the-wild" datasets and pilot-scale deployments to verify their robustness. Bridging the gap between algorithmic theoretical performance and practical field utility remains the final hurdle for widespread commercial adoption(Khan et al., 2023)

7. CONCLUSION

This systematic review highlights the transformative role of image analysis and machine learning in bridging the gap between maize quality assessment and sustainable biofuel production. The integration of SWIR hyperspectral imaging for safety and composition analysis, alongside UAV-based yield estimation, forms the basis of a new, intelligent framework for the maize value chain. While accuracy has reached commercial viability, the focus of future research should now be on the identified gaps, to enable robustness, interpretability, and the development of scalable, non-destructive systems that support the dual goals of global food security and cleaner energy for the maize value chain.

ACKNOWLEDGMENT

K.I.T.V author wishes to thank the Petroleum Technology Development Fund (PTDF) for its support and acknowledge its sponsorship of this research.

ISBN: 978-978-8567-02-8

REFERENCES

Abbasi, M., Váz, P., Silva, J., & Martins, P. (2025a). Machine Learning Approaches for Predicting Maize Biomass Yield: Leveraging Feature Engineering and Comprehensive Data Integration. *Sustainability 2025, Vol. 17, Page 256*, *17*(1), 256. https://doi.org/10.3390/SU17010256

Abbasi, M., Váz, P., Silva, J., & Martins, P. (2025b). Machine Learning Approaches for Predicting Maize Biomass Yield: Leveraging Feature Engineering and Comprehensive Data Integration. *Sustainability (Switzerland)*, *17*(1). https://doi.org/10.3390/su17010256

Arif, M., Alalawy, A. I., Zheng, Y., Koutb, M., Kareri, T., Salama, E. S., & Li, X. (2025). Artificial intelligence and machine learning models application in biodiesel optimization process and fuel properties prediction. *Sustainable Energy Technologies and Assessments*, *73*. https://doi.org/10.1016/j.seta.2024.104097

Bhargava, A., Sachdeva, A., Sharma, K., Alsharif, M. H., Uthansakul, P., & Uthansakul, M. (2024). Hyperspectral imaging and its applications: A review. In *Heliyon* (Vol. 10, Issue 12). Elsevier Ltd. https://doi.org/10.1016/j.heliyon.2024.e33208

Dönmez, E. (2022). Enhancing classification capacity of CNN models with deep feature selection and fusion: A case study on maize seed classification. *Data and Knowledge Engineering*, *141*. https://doi.org/10.1016/j.datak.2022.102075

Fan, C., Wang, W., Cui, T., Liu, Y., & Qiao, M. (2024). Maize Kernel Broken Rate Prediction Using Machine Vision and Machine Learning Algorithms. *Foods*, *13*(24). https://doi.org/10.3390/foods13244044

Fan, L., Ding, Y., Fan, D., Wu, Y., Chu, H., Pagnucco, M., & Song, Y. (2023). An annotated grain kernel image database for visual quality inspection. *Scientific Data*, *10*(1). https://doi.org/10.1038/s41597-023-02660-8

Gan, X., Cao, S., Wang, J., Wang, Y., & Hou, X. (2025). YOLOv8-DBW: An Improved YOLOv8-Based Algorithm for Maize Leaf Diseases and Pests Detection. *Sensors*, *25*(15). https://doi.org/10.3390/s25154529

Guo, L., Tian, H., Wan, D., Yu, Y., Zhao, K., Zheng, X., Li, H., & Sun, J. (2025). Detection of Aflatoxin B1 in Maize Silage Based on Hyperspectral Imaging Technology. *Agriculture (Switzerland)*, *15*(10). https://doi.org/10.3390/agriculture15101023

Han, L., Yang, G., Dai, H., Xu, B., Yang, H., Feng, H., Li, Z., & Yang, X. (2019). Modeling maize above-ground biomass based on machine learning approaches using UAV remote-sensing data. *Plant Methods 2019 15:1*, *15*(1), 1–19. https://doi.org/10.1186/S13007-019-0394-Z

Hassoun, A., Jagtap, S., Garcia-Garcia, G., Trollman, H., Pateiro, M., Lorenzo, J. M., Trif, M., Rusu, A. V., Aadil, R. M., Šimat, V., Cropotova, J., & Câmara, J. S. (2023). Food quality 4.0: From traditional approaches to digitalized automated analysis. *Journal of Food Engineering*, *337*, 111216. https://doi.org/10.1016/J.JFOODENG.2022.111216

Huang, H., Liu, Y., Zhu, S., Feng, C., Zhang, S., Shi, L., Sun, T., & Liu, C. (2024). Detection of Mechanical Damage in Corn Seeds Using Hyperspectral Imaging and the ResNeSt_E Deep Learning Network. *Agriculture (Switzerland)*, *14*(10). https://doi.org/10.3390/agriculture14101780

Karmakar, P., Murshed, M., & Teng, S. W. (2024). *Hyperspectral Imaging-Based Grain Quality Assessment With Limited Labelled Data*. http://arxiv.org/abs/2411.10924

Khan, F., Zafar, N., Tahir, M. N., Aqib, M., Waheed, H., & Haroon, Z. (2023). A mobile-based system for maize plant leaf disease detection and classification using deep learning. *Frontiers in Plant Science*, *14*. https://doi.org/10.3389/fpls.2023.1079366

Li, C., Chen, Z., Jing, W., Wu, X., & Zhao, Y. (2023). A lightweight method for maize seed defects identification based on Convolutional Block Attention Module. *Frontiers in Plant Science*, *14*, 1153226. https://doi.org/10.3389/FPLS.2023.1153226/BIBTEX

Li, R., Liu, Q., Wang, M., Su, Y., Li, C., Ou, M., & Liu, L. (2025). Maize Kernel Batch Counting System Based on YOLOv8-ByteTrack. *Sensors*, *25*(17). https://doi.org/10.3390/s25175584

Lim, H., & Kim, S. (2024). Applications of Machine Learning Technologies for Feedstock Yield Estimation of Ethanol Production. In *Energies* (Vol. 17, Issue 20). Multidisciplinary Digital Publishing Institute (MDPI). https://doi.org/10.3390/en17205191

Monjur, O., Ahmed, M. T., Chowdhary, G., & Kamruzzaman, M. (2025). Agro-HSR: The first large-scale agricultural-focused hyperspectral dataset for deep learning-based image reconstruction and quality prediction. *Computers and Electronics in Agriculture*, *239*. https://doi.org/10.1016/j.compag.2025.111103

Niu, S., Xu, X., Liang, A., Yun, Y., Hao, F., Bai, J., Sheng, W., & Ma, D. (2025). High accuracy identification of maize seed varieties based on a lightweight improved YOLOv8. *Scientific Reports*, *15*(1). https://doi.org/10.1038/s41598-025-00499-0

Novonesis. (2020). *How does corn quality impact ethanol yield?* https://www.novonesis.com/en/biosolutions/bioenergy/ethanol

Paudel, D., Boogaard, H., de Wit, A., Janssen, S., Osinga, S., Pylianidis, C., & Athanasiadis, I. N. (2021). Machine learning for large-scale crop yield forecasting. *Agricultural Systems*, *187*. https://doi.org/10.1016/J.AGSY.2020.103016

Ramalingam, K., Abdullah, M. Z., Elumalai, P. V., Sangeetha, A., Yong, X., Hasan, N., & Shangzhi, W. (2025). An assessment of optimizing biofuel yield percentage using K-fold integrated machine learning models for a sustainable future. *PLOS ONE*, *20*(8 August). https://doi.org/10.1371/journal.pone.0328880

Suku Dube, S., & Mambudzi, H. (2025). Maize Plant Disease Detection Using Convolutional Neural Network. *International Journal of Research and Innovation in Applied Science*, *X*(VII), 157–166. https://doi.org/10.51584/IJRIAS.2025.100700013

van Klompenburg, T., Kassahun, A., & Catal, C. (2020). Crop yield prediction using machine learning: A systematic literature review. *Computers and Electronics in*

ISBN: 978-978-8567-02-8

Agriculture, *177*. https://doi.org/10.1016/J.COMPAG.2020.105709

Wang, B., Sun, J., Xia, L., Liu, J., Wang, Z., Li, P., Guo, Y., & Sun, X. (2023). The Applications of Hyperspectral Imaging Technology for Agricultural Products Quality Analysis: A Review. In *Food Reviews International* (Vol. 39, Issue 2, pp. 1043–1062). Taylor and Francis Ltd. https://doi.org/10.1080/87559129.2021.1929297

Wang, J., Yang, S., Wang, C., Wen, W., Zhang, Y., Liu, G., Li, J., Guo, X., & Zhao, C. (2025). A deep learning-based micro-CT image analysis pipeline for nondestructive quantification of the maize kernel internal structure. *Plant Phenomics*, *7*(1). https://doi.org/10.1016/j.plaphe.2025.100022

Wang, Y., & Song, S. (2023). Variety identification of sweet maize seeds based on hyperspectral imaging combined with deep learning. *Infrared Physics and Technology*, *130*. https://doi.org/10.1016/j.infrared.2023.104611

Wu, D., Cai, Z., Han, J., & Qin, H. (2020). Automatic kernel counting on maize ear using RGB images. *Plant Methods*, *16*(1). https://doi.org/10.1186/s13007-020-00619-z

Xu, P., Fu, L., Yang, R., & Chen, X. (2026). Identification of maize seed varieties based on hyperspectral imaging combined with deep learning. *Food Physics*, *3*, 100073. https://doi.org/10.1016/J.FOODP.2025.100073

Xu, P., Sun, W., Xu, K., Zhang, Y., Tan, Q., Qing, Y., & Yang, R. (2022). Identification of Defective Maize Seeds Using Hyperspectral Imaging Combined with Deep Learning. *Foods*, *12*(1), 144. https://doi.org/10.3390/FOODS12010144

Yang, L., Liu, C., Wang, C., & Wang, D. (2024). Maize Kernel Quality Detection Based on Improved Lightweight YOLOv7. *Agriculture (Switzerland)*, *14*(4). https://doi.org/10.3390/agriculture14040618

ISBN: 978-978-8567-02-8

085-Statistical Quality Control Process Analysis of Corrugated Aluminium Profile in Nigeria

Shehu Ibrahim Maik [1], Musbau Godfrey [2], Larenwaju Kamorudeen Soretire [2], Yahaya Ibrahim [2] and Kabir Kolawole [2]

[1] *Standards Organisation of Nigeria (SON). Abuja, Nigeria*

[2] *Airforce Institute of Technology, Nigeria Airforce Base, Kaduna, Nigeria*

***GSM**: +2348036668092*

Email: shehumaik@gmail.com

Abstract: Quality corrugated alumiuium profile as roofing sheet in Nigeria homes requires standardised control to reduce nonconforming aluminium profile. The nonconforming aluminium profile was resulted from production process as defects. This paper analysed Statistical Quality Control (SQC) process for corrugated aluminium profile in Nigeria. There were 12 corrugated aluminium companies selected for the process and physical measurement was adopted to investigate quality defects such as pinholes, cracks, poor thickness tolerance and flatness. SQC process analysis adopted for the study was P-chart control technique to determine defect aluminium profile. The findings include first and revised control using P-chart analysis. Revised control process was obtained to determine maximum allowable defective which was three (3) aluminium profile per day in 720 profiles. This meant defective should be in the range of zero (0) and three (3) defectives per day for every production batch. The findings indicates average allowable non-conforming of aluminium profile of three (3) defectives has P-value of 0.00135 in Z standard normal distribution analysis. NCSS-P chart software indicates that 0.89 of produced profile must be within acceptable control limit. However, implementing the findings in the profile companies production process will reduce waste of aluminium profiles resources. This study recommended zero defective in 720 aluminium profile batch in Nigeria based on Industrial Standard, NIS 488:2010 for preventing short life cycle of the profile.

1. INTRODUCTION

Quality is one of the techniques for cost and waste reduction (Isaac *et al.,* 2018). Quality of a product can be defined as degree of extent to which it meets the requirement or exceeding the customer‘s expectation. Corrugated aluminium profile needs to be standardised as a quality product for roofing sheet in various home (Okeke *et al*., 2022, Akinwale and Bello 2020). It will help in reducing nonconforming aluminium profile in Nigeria. The nonconforming aluminium profile was resulted from production process as defects. Defects of corrugated aluminium profile can occur when the strip is rolled into a variety of aluminium sheet, and the sheet finishing and packaging and other processes of the production process (Maik and Godfrey, 2025). Most of these defects are generated due to equipment failure, mishandling, and improper adjustment of process parameters, unskilled operators and various other causes. The quality defects are mainly a large number of pinholes, cracks, poor thickness tolerance and flatness (Xu, 2016).

Defects can also occur during the extrusion and drawing of aluminium. Some of these defects include die lines, scoring, pick up and tearing (Olaru, 2020). Pick up and die lines are particularly common in the 6 xxx series of Aluminium. There are defects that also occur at the coating stage of aluminium sheet production. Some of the critical painting parameters are current, pressure, and nozzle size which all contribute to painting defects. The common defects are less microns, orange peel, dust particles inclusions, blisters and overlapping (Arif *et al.,* 2015). The corrugation stage, breaking/creasing can occur along the formed sheet as it is being fed into the rolling system. The creasing occurs due to exerted force along bottom rolls. Misalignment of corrugations also occurs where the curved end width is different from that of the straight section of the sheet. Valley and wavy ripples occur across the curved sheet. Another common problem during corrugation is saw-tooth effects. It occurs when variation is obtained in desired length of sheet (Maik and Godfrey, 2025).

The quality characteristics of long span aluminium roofing sheet produced by aluminium companies in Nigeria include acceptable length, weight and thickness. It is carried out and examined with the use of control chart from production process in statistical control with respect to each of the quality characteristics (Ajewole *et al*., 2020; Maik and Godfrey, 2025). Thus, this paper tends to analyse the Statistical Quality Control (SQC) process for

ISBN: 978-978-8567-02-8

corrugated aluminium profile in Nigeria companies. It is feasible through examining of physical measurement of aluminium profile using P control chart. This helps in analysing the fraction of a sample that is nonconforming aluminium profile. This helps in implement an autonomous quality control system which realizes real-time measurements (Matlala *et al.,* 2022).

2. METHODOLOGY

The material used for quality test assessment were corrugated sheets measured 930 mm to 1000 mm in nominal width and a nominal base thickness of 0.4 mm. These were used mainly for the physical measurements. The measuring equipment include measuring tape, digital Vernier caliper (capacity of 0-200mm). The control chart was developed using P-chart analysis by adopting wastage generated from the processing line were recorded per each coil. The percentage wastage were then computed and used to analyse P- control chart. The control process is being harmonised to set a control for twelve companies under study. Each of the company sampling data. The companies include Chiphills Aluminum Company Makurdi , Network Aluminium Industry Limited Ilorin, A.I.I. Allied Resources Nig. Ltd., Okene, Strong Aluminium Com Ltd, Keffi, Perfect Aluminum Co. Nig. Ltd., Minna, Chiphil Aluminum Company Ltd, Jos, Sky Aluminium Products Ltd, Jos. Eastchase Aluminum Coy, Lokoja, Altex Aluminium Company Ltd, Okene, Shelter setters aluminium & experts Nigeria Limited, Keffi, Andy Young Aluminium Company, Mararaba, and Queensway Aluminum Co. Ltd. Niger , Minna. Physical measurement compliance was considered for the quality control chart for defective analysis for compliance to pitch diameter, depth of corrugation sheet, coating thickness, base thickness (0.18 to 0.55 mm) and width (930 mm to 1000 mm). The physical measurement of corrugated aluminium sheet is required meeting Nigeria Industrial Standard, NIS 488: 2010 (NIS, 2010). The total daily sample taken was 720 aluminium profiles per day. This was obtained from the daily sampling of sixty (60) units per company per day. The p-chart analysis is determined as (Montgomery and Runger 2020):

Average fraction defective $(p) = \frac{total\ defective}{total\ sampling}$ (1)

Standard deviation per day $(\sigma_p) = \sqrt{\frac{\bar{p}(1-\bar{p})}{n}}$ (2)

Standard Normal distribution:

$z = (X - \mu)/(\sigma_p/\sqrt{n})$ (3)

UCL analysis is givens as:

$z_{ucl} = (X_{ucl} - \mu_{ucl})/\left(\sigma_{p_{ucl}}\right)$ (4)

LCL analysis is givens as:

$z_{lcl} = (X_{lcl} - \mu_{lcl})/\left(\sigma_{p_{lcl}}\right)$ (5)

Where: $X =$ defective sample limit

$\mu =$ average defective sample limit

$X_{ucl} =$ defective sample limit in upper limit control (UCL)

$\mu =$ average defective sample limit

$X_{lcl} =$ defective sample limit in lower limit control (LCL)

P value in 1 way form: $(1 - \varphi(P_{z_{ucl}})$ (6)

NCSS Statistical Software 2025 was used for P-chart plotting.

3. RESULTS AND DISCUSSION

Table 1 is the average defective per day from the obtainable randomly 60 batch per each company.

TABLE 1: FIRST CONTROL OF ALUMINIUM PROFILES PER DAY

Day	Defective Profile in 720 sample (n) per day (12 companies)	Fractional defective /day
1	74	0.1028
2	65	0.0902
3	71	0.0986
4	79	0.1097
5	78	0.1083
6	82	0.1139
7	63	0.0875
8	50	0.0694
9	66	0.0917
10	82	0.1139
Total:	710	0.9860
Average:	71	0.09860

Average fraction defective profile/day, $p =$ 0.0986,

Average sample per day, $n = 720$

$(\sigma_p) = \sqrt{\frac{\bar{p}(1-\bar{p})}{n}} = \sqrt{\frac{0.09861(0.9014)}{720}} = \sqrt{0.00012} =$ 0.011

Limit of upper control, $(UCL) = \bar{p} + 3\sigma_p = 0.0986 + 3(0.011) = 0.1316$ (95 defectives)

This is achieved through multiplication of UCL (0.1316) and 720 profiles sampling per day

Limit of lower control, $(LCL) = \bar{p} - 3\sigma_p$

$= 0.0986 - 3(0.011) = 0.0656$ (47 defectives)

This is achieved through multiplication of LCL (0.0656) and 720 profiles sampling per day. The company worked between 47 and 95 defectives per day for every production. From the analysis in Table 1, all the defective is within range of p-control analysis. However, the revised control process was carried out to limit effect of profile wastage using standard deviation of defective profile as follows:

UCL analysis:

X_{ucl} = 0.1316

μ_{ucl} = 0.0986

$\sigma_{p_{ucl}} = \sigma_{p_{lcl}} =$ 0.011

$z_{ucl} = (0.1316 - 0.0986)/(0.011) = 3$

ISBN: 978-978-8567-02-8

Percentile of $z_{ucl} = 0.998650$

P value is: $(1 - 0.998650) = 0.00135$

LCL analysis:

$X_{lcl} = 0.0656$

$\mu_{ucl} = 0.0986$

$\sigma_{p_{ucl}} = \sigma_{p_{lcl}} = 0.011$

$z_{ucl} = (0.0656 - 0.0986)/(0.011) = -3$

Percentile of $z_{ucl} = 0.00101$

P value is: $(1 - 0.00101)) = 0.9989$

produced profile. The conforming process was plotted using NCSS software in Figure 1.

The upper Control limit indicated while 1.02 of proportion of production sample while lower control limit of 0.89 of proportion production must be within acceptable criteria of the aluminium in P-chart analysis in Figure 1. The findings indicated that non-conforming of aluminium profile during revised control process should not exceed 3 defectives in a single 720 batch of aluminium profiles.

4. CONCLUSION

The statistical quality control (SQC) of aluminium profile

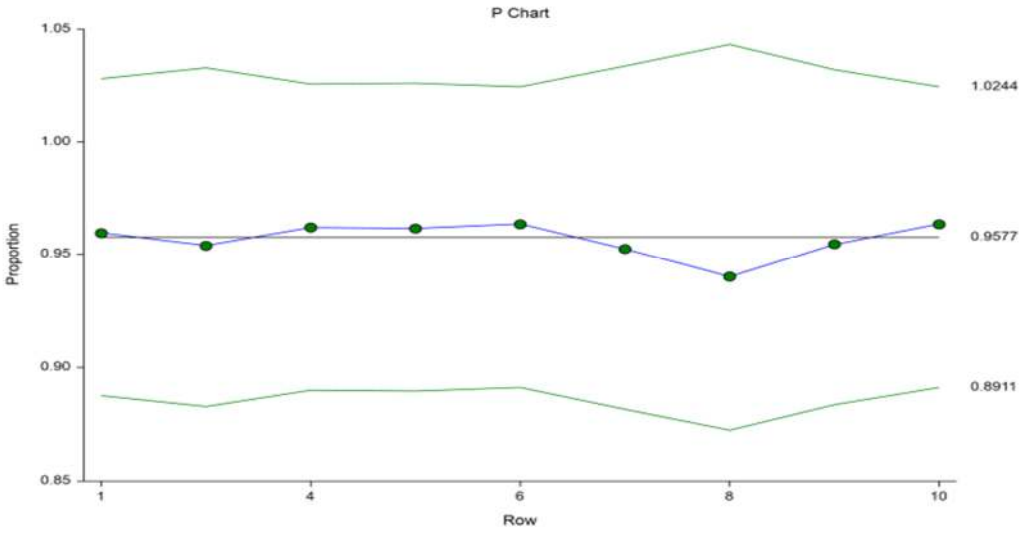


Figure 1: P-chart of corrugated aluminium profile

This meant the allowable is between 0 and 3 defective and however revised control is shown in Table 2.

TABLE 2: REVISED CONTROL PROCESS OF ALUMINIUM PROFILES PER DAY

Day	Defective Profile in 720 smple in 12 companies	Average allowable Defective Profile per day
1	74	3
2	65	3
3	71	3
4	79	3
5	78	3
6	82	3
7	63	3
8	50	3
9	66	3
10	82	3

Average fraction defective profile/day, $p = 3/72$ (p=0.0042).

The company revised control process allowed maximum defective three (3) of aluminium profile per day for every production. The allowable defective per day should not be beyond 3 defective per day in every 720

ascertained actual level of implementation of Nigeria Industrial Standard, NIS 488 (NIS, 2010) in aluminium profile industry. It was discovered NIS 488 not fully implemented due to high rate of defective profile produced by the industry. Corrugated aluminium profile requirement should be implemented to prevent early wear out and poor life cycle as roofing sheet in Nigeria homes.

REFERENCES

Ajewole K.P., Osunronbi F.A., & Raji. I.I. (2020). Application of Statistical Quality Control on the Production of Long Span Aluminum Roofing Sheet Produced by Spring Aluminum Nigeria Ltd. International Journal of Innovative Science and Research Technology, 5(4), 1390-1392.

Akinwale, Y., & Bello, A. (2020). The Impact of Incentive Programs on Manufacturing Compliance. Journal of Business and Economic Studies, 22(4), 340-355

Arif, A.F.M., Sheikh, A. K., Qamar, S.Z., Raza, M.K. & Al-Fuhaid, K.M. (2015). Production Defects in Aluminium Extrusion and its Impact on Operational

ISBN: 978-978-8567-02-8

Cost (1st Edition). Saudi Arabia: Mechanical Engineering Department, KFUPM, Saudi Arabia

Đorđe, D., & Nemanja, K., (2025). Integrating Machine Learning for Enhanced Quality Control in Aluminum Profile Production,Annual Conference on Challenges of Contemporary Higher Education, ACCHE, Kopaonik, Serbia.

Isaac E .O., Nkoi B., & Douglas P .O. (2018). Reducing Production Cost through Quality Control Study in an Aluminium Manufacturing Industry. World Journal of Innovative Research (WJIR), 5 (5), 16-27

Maik, S.I. & Godfrey, M. (2025). Quality Characteristics Assessments of Selected Profile Aluminium Sheets Industry in North-Central State, Nigeria. International Journal of Latest Technology In Engineering, Management & Applied Science (IJLTEMAS), 14 (8) https://doi.org/10.51583/IJLTEMAS.2025.1408000195

Matlala K, Mishra AK, Puthal D (2022). Towards Sustainable Aluminium Processing: Autonomous Quality Control Using Business Analytics. Int J Adv Techno. 13:207.

Montgomery D.C. and Runger G.C (2020). Applied Statistics and Probability for Engineer (7th Ed.). US: John Wiley and Son.

NIS: Nigerian Industrial Standard -NIS 488 (2010). Test Methods for Profiled Aluminium Roofing Sheet for Roofing and Cladding. Abuja: Standard Organisation of Nigeria, 1-10.

Olaru I. (2020). An Analysis of The Drawing with Aluminum Brazed Sheets. IOP Conf. Series: Materials Science and Engineering 916 (2020) 012078. doi:10.1088/1757- 899X/916/1/012078

Okeke, I.C. Agu, E.E., Ejike, O.G., Ewim, C.P.M and Komolafe, M.O (2022). A conceptual framework for enhancing product standardization in Nigeria's manufacturing sector. International Journal of Frontline Research in Multidisciplinary Studies, 01(02), 001–013.

Xu, S. (2016). What is the Aluminium Sheet Common Quality Defects? (1st Edition). China: Haomei Machinery Equipment Co. Ltd.

ISBN: 978-978-8567-02-8

5th Faculty of Engineering Conference on Engineering Innovation and Economic Policies: Driving Sustainable Industrial Growth in Nigeria

Faculty of Engineering, Bayero University, Kano.

086-Sentiment Analysis of Online Reviews for Brand Monitoring: A Machine Learning Based Application

*[1,2]Maipan-uku, J.Y., [1]Abdulganiyyu A., [1]Umar A., [2]Ramatu M.N., [2]Rabi M.N., [1,2]Adamu A.I, [1]Umar M.

[1]*Department of Computer Science, I.B.B. University, Lapai*
[2]*Department of Information Technology, Newgate University, Minna*

Corresponding author's email: jymaipanuku@ibbu.edu.ng

Abstract: This study explores the application of sentiment analysis for the analysis of customer reviews on the web for effective brand monitoring. The analysis uses a publicly available dataset of customer product reviews on the Amazon website obtained from Kaggle to demonstrate the viability of using conventional machine-learning algorithms for the classification of consumer sentiments. This study aims to design and test the performance of algorithms for categorizing text reviews into positive, neutral, and negative sentiments. The preprocessing technique includes steps for cleaning, tokenization, removal of stop words, and transformation of text data into a format suitable for analysis using Term Frequency-Inverse Document Frequency (TF-IDF). Three conventional machine learning algorithms, Multinomial Naive Bayes, Logistic Regression, and Linear Support Vector Machine (SVM), were used and compared for performance evaluation using accuracy, precision, recall, and F1 measures. The analysis indicates that the Linear SVM algorithm performs best, achieving the highest accuracy of 93.39% and an F1-value of 0.915 among the evaluated models. However, none of the evaluated classifiers were able to reliably identify neutral opinions, a limitation largely attributable to severe class imbalance and the subtle linguistic characteristics of neutral sentiment expression. The analysis concludes that traditional machine learning algorithms represent a viable alternative for effective brand sentiment analysis on the web, for which superior strategies, including data balancing, feature augmentation, and the use of Deep Learning algorithms, are required to better distinguish sentiments. This analysis supports the relevance of sentiment analysis in making business-critical decisions related to brand perception and management.

1. INTRODUCTION

The digital age has brought about a dramatic shift in how people interact with companies and share their opinions about them. Cyberspace, whether through social networks or e-commerce platforms where reviews are published, has emerged as a vast source of user content. This content often comprises feedback, experiences, and sentiments regarding products, services, and brands. For companies, recognizing this expression of opinions has become vital. Brand perception tracking, which has conventionally remained dependent on mentions in media reports and feedback from polls, is expected to be grounded in a detailed scrutiny of cyberspace text data to identify public sentiment.

The development of the Internet and technology has allowed consumers to exercise their newfound powers. Consumers are no longer mere recipients of the messages in the marketing communication process but have become an integral part of it by extensively sharing their views and experiences. Websites such as Twitter, Facebook, and Instagram, and consumer review websites such as Amazon and Yelp, act as platforms where opinions about products, services, and brands are shared. This development marks the recognition that a considerable part of the conversation related to the brand is conducted online.

Such content may provide a valuable source of information, offering a truly genuine source of feedback in areas of consumer satisfaction, product strengths and/or weaknesses, service problems, or overall public reception of marketing efforts. Furthermore, this text, unlike the results of a survey, is a spontaneous source of information, providing a much truer reflection of the public mood. A business enterprise capitalizing on such information may gain true insight into the market it serves.

The massive volume, high velocity, and unstructured nature of online texts are some of the difficulties presented in the process of analyzing texts. Millions of posts and reviews are generated daily, making it highly impractical for humans to analyze all content. In addition, the nature of online texts can also contain a certain level of informality, using slang and abbreviations, which can make the content ambiguous for computers to interpret. Thus, there is a need for the application of automation in

ISBN: 978-978-8567-02-8

extracting valuable information from the high online output. One of the prominent technologies that has emerged as a solution is sentiment analysis.

The current literature acknowledges the role of online reviews as a fundamental source of information influencing consumer behavior and the formation of brand perception, especially in the context of e-commerce, where the possibility of direct inspection of products might be constrained. Empirical evidence supports the fact that the use of online reviews by consumers serves as a supportive factor in influencing purchase intentions and the formation of brand perception (Guerreiro and Rita, 2020; Ibrahim, 2020). Thus, the strategic use of online reviews by organizations as a source of collective customer views can affect their reputation (Guerreiro and Rita, 2020).

The ever-increasing popularity of User Generated Content (UGC) on various e-commerce sites, social media, and review websites makes manual analysis unrealistic, thus fuelling the need for automated analysis methods (Li et al., 2020). In this regard, a highly adopted approach is sentiment analysis, which is commonly regarded as a method for extracting subjective information from a large pool of unstructured text data. Evidence from previous studies confirms that sentiment analysis makes it easy for organizations to systematically rate customer sentiments, thereby helping to track levels of satisfaction as well as public sentiments for informed decision-making (Kumar et al., 2023; Chen et al., 2022; Jand and Pamula, 2020; Hossain et al., 2020).

Technological advancements in sentiment analysis studies indicate an increasing use of sophisticated computational methods. Initially, studies mainly focused on lexicon-based approaches, which identify the polarity of sentiment using predetermined sentiment lexicons (Kolchyna et al., 2015). Although these methods provide clarity on the workings of the approach and ease of implementation, they still face the issue of dealing with dependencies in the context, sarcasm, and the nuances of the language. Recent studies have thus focused on using machine learning-based approaches to address the problem of sentiment analysis in software tools to determine sentiment using annotated datasets (Ahmad et al., 2022).

More recent work in the field shows a trend of using deep learning architectures, which encompass Long Short-Term Memory (LSTM) networks, Bidirectional LSTM networks, and transformer-based structures in BERT models. The application of these models indicates improved performance in extracting the context and sequence dependencies of text data, resulting in better accuracy in text classification tasks in domain-related corpora of reviews (Cortis and Davis, 2022; Ibrahim et al., 2017). Empirical analysis also supports the fact that deep learning methods are more efficient in determining the subtle expression of sentiments found in online reviews than traditional learning methods Hossain et al., 2020). Meanwhile, a convergence of analytical tools on the analysis of customer sentiments in a combined manner of topic and timeline analysis has been initiated in research work to analyze the evolution of customer sentiments on a timeline (Krishnan, 2023a; Krishnan, 2023b),.

From a theoretical perspective, sentiment analysis can be modelled at three different levels: document, sentence, and aspect. Although the first two modes of analysis may help gain a macro-understanding of the overall orientation of the sentiment expressed, the analysis of the sentiment as it relates to the specific attributes of a product or service has recently garnered a lot of academic interest [11].

Within the domain of brand monitoring, sentiment analysis has seen extensive applications related to data on social media platforms, especially on X (formerly, Twitter), given the openness and real-time nature of this platform. Previous research suggests that negative and positive sentiments on Twitter have been shown to have a greater emotional polarity than other conversations and can be influenced by marketing strategies Dacres et al., 2023; Hu et all, 2017. Moreover, sentiment analysis can be used to predict ratings and summarize customer feedback, highlighting its importance in brand analysis (Gupta and Bhanushali). Comparative analyses have confirmed that lexicon-based approaches and machine learning methods are effective for opinion detection on social media websites (Gupta and Bhanushali, 2023; Qi and Shabrina, 2023).

Importantly, recent studies have not only focused on classification accuracy as their end goal but have also addressed methodological issues such as class imbalance problems, negations, and linguistics (Ibrahim et al., 2017). Online brand community studies highlight the significance of customer engagement for sentiment evolution in influencing favorable perceptions and reducing unfavorable ones in times of crises (Angelidis et al., 2021), (Ibrahim et al., 2017).

Briefly, there is a marked trend towards the usage of sophisticated and data-intensive sentiment analysis techniques and a more sophisticated outlook on analysis in the field of brand analytics. However, several gaps remain, including: the preponderance of Twitter-centric research, a lack of comparative studies on cross-platform sentiment expression, inadequate investigation into the effects of divergent engagement strategies on particular aspects of sentiment, and a continued challenge in incorporating humor, cultural differences, and misleading reviews (James et al, 2021).

2. METHODOLOGY

This particular task adopts an experimental design to test the performance of traditional machine learning classifiers for sentiment classification. The design involves the following steps: dataset choice, preprocessing of text data, generation of features, generation of sentiment labels, and model implementation.

2.1 Dataset and Data Source

The dataset used in this study is a publicly available dataset of Amazon product reviews from the Kaggle website. The dataset is titled Amazon Reviews for

ISBN: 978-978-8567-02-8

Sentiment Analysis. This dataset includes reviews in textual form with corresponding ratings. The rating column is the ground truth for sentiment. Information about the size of the dataset, ranging from 1 to 5, is presented in Table 1.

TABLE I: DATASET SCALE (1 TO 5) AND PRODUCT DISTRIBUTION

Overall Rating	Count	Sentiment Category	Count
1-star	244	Positive	4448
2-stars	80	Negative	324
3-stars	142	Neutral	142
4-stars	527		
5-stars	3922		

Although the linguistic structure of product reviews differs from that of short-form social media content, the dataset provides a standardized benchmark for evaluating traditional sentiment classification approaches.

2.2 Text Preprocessing

Data preprocessing techniques were used to reduce noise and make the text data uniform. Datasets with missing values in the reviews or ratings columns were removed. Text data preprocessing involved removing URLs, HTML noise, and non-alphanumeric characters, after which case folding was performed. Tokenization was used to divide the reviews into lexical items. Tokens corresponding to emoticons/emoji icons were removed because they were less frequent in the datasets. Stemming or lemmatization was performed selectively.

2.3 Feature Representation

The preprocessed text data were then converted to numerical forms using traditional vectorization methods. The text data were encoded using the bag-of-words method to reflect the frequency of terms in the corpus. Simultaneously, the Term Frequency-Inverse Document Frequency method was employed to encode the terms in accordance with their discriminatory value in the corpus.

2.4 Sentiment Labeling Strategy

The labels used to denote sentiments were directly extracted from the numeric values of the ratings on the reviews. The values were then assigned to predetermined categories of sentiments using a thresholding system that categorized the sentiments into positive, neutral, and negative.

2.5 Classification Models

Three traditional machine learning classifiers were proposed: Naïve Bayes, Support Vector Machine, and Logistic Regression. These approaches have long been proven to be reliable for text classification. Each of these approaches was implemented using the scikit-learn library.

2.6 Training Procedure

An 80:20 train–test split was adopted in this study in line with established practice in supervised machine learning, ensuring sufficient data for model learning while retaining an independent test set large enough for reliable and unbiased performance evaluation (James et al, 2021).

2.7 Evaluation Metrics

The performance of the models was evaluated using a held-out testing subset. The efficiency of the classification was evaluated using metrics such as accuracy, precision, recall, and F1-score. The confusion matrix was used to analyze the distribution of classifications in both binary and multiclass classifications based on sentiments. The template is used to structure the text, with margins, columns, lines, and font types defined.

1) *Accuracy:* The proportion of correctly classified instances out of the total number of instances

$$\text{Accuracy} = \frac{TP+TN}{TP+TN+FP+FN}$$

2) *Precision:* For each class, the proportion of correctly predicted positive instances of all instances predicted as positive. It measures the accuracy of the model.

$$\text{Accuracy} = \frac{TP}{TP+FP}$$

3) *F1 Score:* The harmonic mean of Precision and Recall, providing a balanced measure of the model's performance, especially useful for imbalanced datasets

$$\text{F1 Score} = 2\,x\,\frac{Precision\ x\ Recall}{Precision+Recall}$$

4) *Confusion Matrix:* A table that summarizes the performance of the classification model, showing the counts of true positive, true negative, false positive, and false negative predictions for each class.

3. RESULT AND DISCUSIION

The models evaluated included Multinomial Naive Bayes, Linear SVM, SVM, and Logistic Regression. These models were evaluated based on criteria that included Accuracy, Precision, Recall, and F1 Score calculated using the Weighted Average to handle class imbalance in the dataset. The training time and the Overall performance metrics for each model on the test set are summarized in Table 2.

TABLE II: OVERALL PERFORMANCE METRICS OF TRADITIONAL ML MODELS

Model	Accuracy	Precision	Recall	F1-Score	Training Time (s)
Multinomial Naïve Bayes	0.9044	0.8196	0.9044	0.8599	0.03
Linear SVM	0.9339	0.9043	0.9339	0.9150	0.07
Logistics Regression	0.9186	0.8877	0.9186	0.8899	1.05

According to the weighted average metrics, the Linear SVM model outperformed the remaining two models in terms of accuracy (0.9339), precision (0.9043), recall (0.9339), and F1 Score (0.9150). Multinomial Naive Bayes performed the worst in these metrics, whereas

ISBN: 978-978-8567-02-8

Logistic Regression performed better than Naive Bayes but not as well as the Linear SVM model.

The training times of the models were relatively short, and Multinomial Naive Bayes had the shortest training time, followed by Linear SVM and then Logistic Regression. This shows that all three models are computer-efficient for the size of the dataset. A comparison of the results and the time taken is shown in Figure 1.

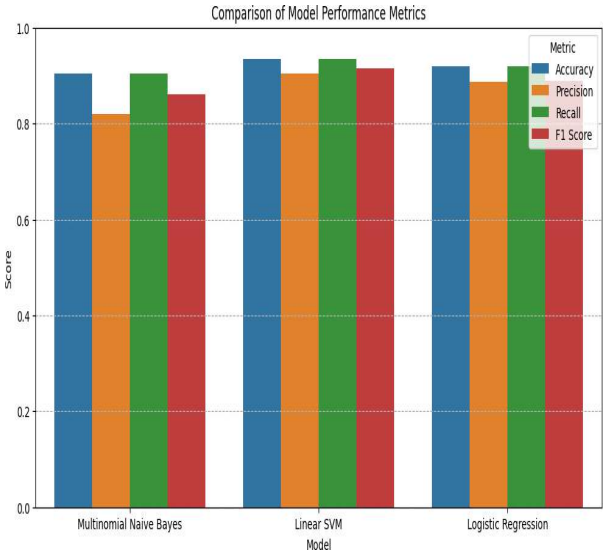


Figure 1: Comparison of Model Performance Metrics

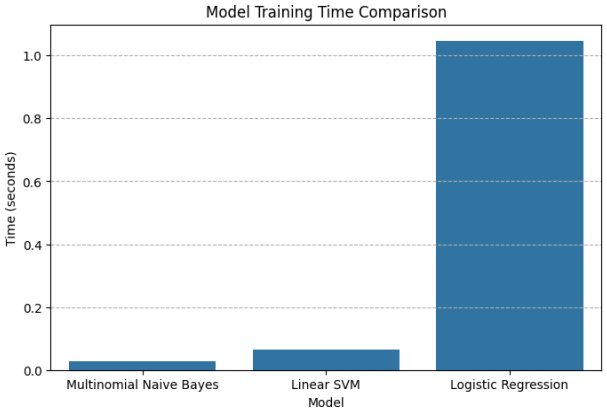


Figure 2: Comparison of Model Training Time

3.1 Confusion Matrices and Class-wise Performance

Each model's confusion matrix defines the number of correct and incorrect predictions for each corresponding sentiment category. The rows relate to the actual results, whereas the columns relate to the predictions. Graphical representations of the confusion matrices are shown in Figures 3, 4,

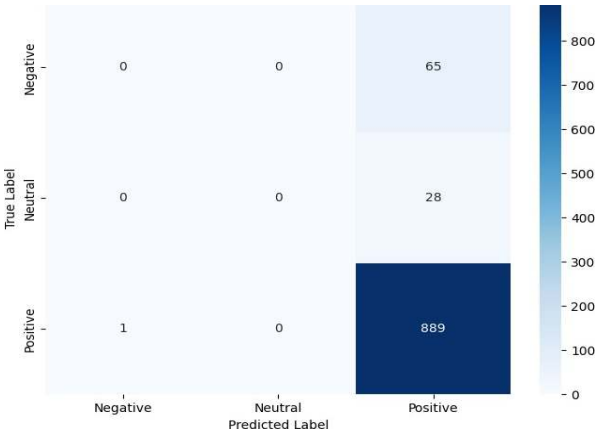


Figure 3: Confusion Matrix for Multinomial Naive Bayes

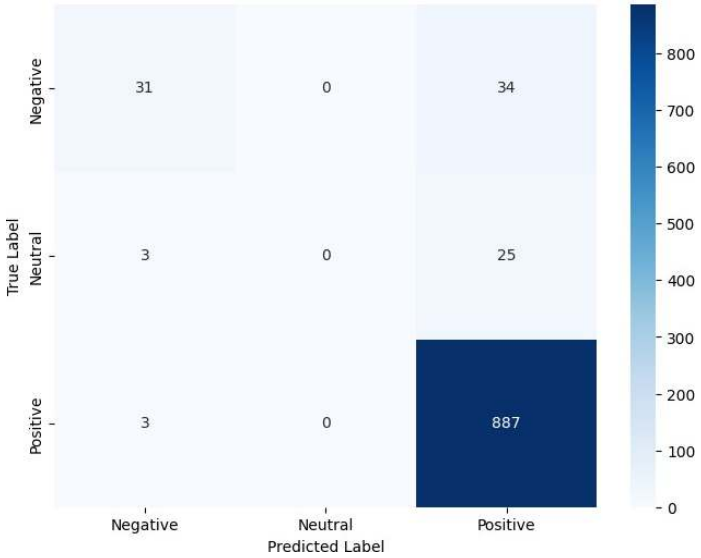


Figure 4: Confusion Matrix for Linear SVM

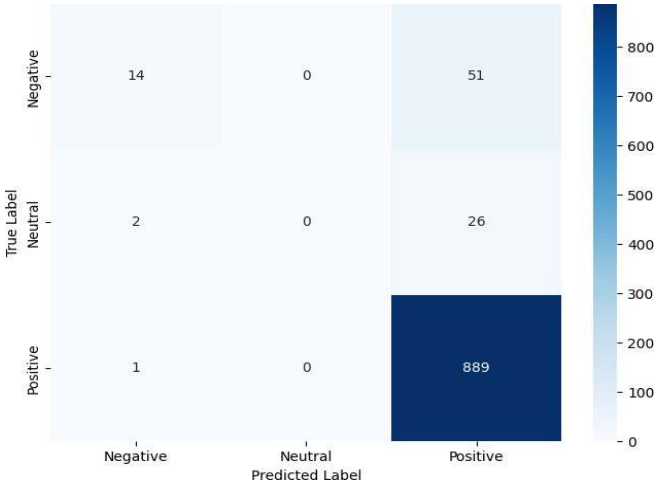


Figure 5: Confusion Matrix for Logistic Regression

3.2 Analysis of Model Performance

The evaluation results emphasize the impact of class imbalance on traditional machine learning models. All models performed well in terms of accuracy, which was mostly due to their performance on the majority class (positive). However, their ability to limit errors for minority classes (Negative and Neutral) was limited. The

ISBN: 978-978-8567-02-8

inability of all models to classify reviews as neutral is an interesting observation. This result can be ascribed to several reasons: perhaps there are only limited neutral reviews available within the dataset, or maybe there is some level of complexity related to neutral reviews being as neutral as opposed to positive or negative reviews.

In the context of these three models, Linear SVM had the overall best combination of generalization performance and ability to accurately classify members of the 'Negative' class. Although not all members of the 'Negative' class were correctly predicted by this classifier with respect to perfect recall, a relatively high proportion of negative instances were correctly predicted compared to both Naive Bayes and Logistic Regression. Multinomial Naive Bayes has a high bias for the majority class. Logistic Regression was in between.

4. CONCLUSION

Based on the results obtained in this study, several conclusions can be drawn. This study examined the application of traditional machine learning techniques for sentiment analysis of online product reviews in the context of brand monitoring. Using a publicly available Amazon review dataset, the study demonstrated that conventional classifiers can achieve strong predictive performance when applied to large-scale, text-based consumer feedback. Among the evaluated models, the Linear Support Vector Machine achieved the highest classification accuracy and F1-score of 93.39% - 0.9150, indicating superior generalization capability when compared with Multinomial Naïve Bayes of 90.44% - 0.8599 and Logistic Regression of 91.86% - 0.8899.

An analysis of computational efficiency revealed that all evaluated models exhibited relatively short execution times, confirming their suitability for practical deployment. Multinomial Naïve Bayes recorded the lowest training time of 0.03 second (s), reflecting its computational simplicity, while Linear Support Vector Machine achieved a favorable balance between execution time and classification performance with 0.07s. Logistic Regression required a comparatively longer training time of 1.05s, though it still remained within acceptable limits for datasets of similar scale. These results suggest that model selection for sentiment analysis tasks can be guided by the trade-off between predictive performance and computational cost, depending on application constraints.

Despite the high overall accuracy achieved by the models, the results also revealed a persistent limitation in accurately identifying neutral sentiments, largely due to class imbalance and the subtle linguistic characteristics associated with neutral expressions. This limitation indicates that traditional feature representations and classifiers may be insufficient for capturing nuanced sentiment patterns across all classes. Nonetheless, the ability of the evaluated models to reliably detect dominant positive and negative sentiments supports their practical relevance for monitoring brand perception and consumer opinion trends.

The outcomes of this work have direct implications for organizations seeking efficient and interpretable sentiment analysis solutions for brand monitoring. The findings demonstrate that traditional machine learning methods remain viable for large-scale sentiment classification tasks, particularly where computational efficiency and model transparency are prioritized. Future studies may extend this work by incorporating advanced learning architectures, data balancing strategies, and aspect-level sentiment analysis to improve performance on underrepresented sentiment categories and provide deeper insights into brand-related discourse.

REFERENCES

Ahmad Hapez, M. H. I., Adam, N. L., and Ibrahim, Z. (2022). Performance analysis of machine learning techniques for sentiment analysis. In 2017 IEEE Conference on e-Learning, e-Management and e-Services (IC3e), pages 1–5.

Angelidis, S., Amplayo, R. K., Suhara, Y., Wang, X., and Lapata, M. (2021). Extractive opinion summarization in quantized transformer spaces. Transactions of the Association for Computational Linguistics, 9:277–293.

Chen, T., Samaranayake, P., Cen, X., Qi, M., and Lan, Y.-C. (2022). The impact of online reviews on consumers' purchasing decisions: Evidence from an eye-tracking study. Frontiers in Psychology, 13:865702.

Cortis, K. and Davis, B. (2020). Over a decade of social opinion mining: A systematic review. arXiv preprint arXiv:2012.03091.

Dacres, S., Haddadi, H., and Purver, M. (2013). Topic and sentiment analysis on osns: a case study of advertising strategies on Twitter. arXiv preprint arXiv:1312.6635.

Guerreiro, J. and Rita, P. (2020). How to predict explicit recommendations in online reviews using text mining and sentiment analysis. Journal of Hospitality and Tourism Management, 43:269–272.

Gupta, K. and Bhanushali, A. (2023). Sentiment analysis for online reviews for brand imaging and customer retention. International Journal of Computer Trends and Technology, 71(12):5–11.

Hossain, E., Sharif, O., Hoque, M. M., and Sarker, I. H. (2020). Sentiment: A deep learning approach for sentiment analysis of restaurant reviews. arXiv preprint arXiv:2011.09684.

Hu, G., Bhargava, P., Fuhrmann, S., Ellinger, S., and Spasojevic, N. (2017). Analyzing users' sentiment towards popular consumer industries and brands on Twitter. arXiv preprint arXiv:1709.07434.

Ibrahim, N. F., Wang, X., and Bourne, H. (2017). Exploring the effect of user engagement in online brand communities: Evidence from Twitter. Computers in Human Behavior, 72:321–338.

Ibrahim, S. S. (2023). Impact of online reviews on consumer purchase decisions in e- commerce platforms. International Journal for Multidisciplinary Research, 5(3):1–10.

Jain, P. K. and Pamula, R. (2020). A systematic literature review on machine learn- ing applications for consumer sentiment analysis using online reviews. arXiv preprint arXiv:2008.10282.

James, G., Witten, D., Hastie, T., and Tibshirani, R. (2021). An introduction to statistical learning: With applications in R (2nd ed.). Springer.

Kolchyna, O., Souza, T. T. P., Treleaven, P., and Aste, T. (2015). Twitter sentiment analysis: Lexicon method, machine learning method, and their combination. arXiv preprint arXiv:1507.00955.

ISBN: 978-978-8567-02-8

Krishnan, A. (2023a). Exploring the power of topic modeling techniques in analyzing customer reviews: A comparative analysis. arXiv preprint arXiv:2308.11520.

Krishnan, A. (2023b). Exploring the power of topic modeling techniques in analyzing customer reviews: A comparative analysis. arXiv preprint arXiv:2308.11520.

Kumar, S., Roy, P. P., Dogra, D. P., and Kim, B.-G. (2023). A comprehensive review on sentiment analysis: Tasks, approaches, and applications. arXiv preprint arXiv:2311.11250.

P., Huang, L., and Jie Ren, G. (2020). Topic detection and summarization of user reviews.

Qi, Y. and Shabrina, Z. (2023). Sentiment analysis using Twitter data: a comparative application of lexicon- and machine-learning-based approach. Social Network Analysis and Mining, 13(1):31.

ISBN: 978-978-8567-02-8

5TH Faculty of Engineering Conference on Engineering Innovation and Economic Policies: Driving Sustainable Industrial Growth in Nigeria

Faculty of Engineering, Bayero University, Kano.

087-Optimization of Water Content for the Production of Plaster of Paris Ceiling Panels

Ismail Ibrahim[1,2], Bishir Kado[1], Aliyu Akilu[1,2], Muktar Isah[1,3]

[1] Department of Civil Engineering, Bayero University, Kano, Nigeria.
[2] Building Research Department, Nigerian Building and Road Research Institute, Abuja, Nigeria
[3] Department of Civil Engineering, Binyaminu Usman Polytechnic, Hadejia, Jigawa, Nigeria.

**Corresponding author email: Ismailnbrri001@gmail.com*

Abstract: The mechanical properties, durability, and microstructure of the hardened paste are shaped during the hydration process and are influenced by the water-to-Plaster of Paris (W/POP) cement ratio, initiating hydration processes and ensuring the workability of the composite matrix. Natural jute fibre (NJF) was utilized to reinforce Plaster of Paris (POP) cement composite for the production of POP ceiling panels (POPCP). The POP cement used was characterized in accordance with ASTM C472 and IS:2547(Part I)-1976 reaffirmed 2002, which has satisfied some of the requirements to be used as POP cement. The NJF exhibited a tensile strength of 91.97MPa, Young's modulus of 2.6GPa, elongation of 3.5mm, water absorption of 2.1%, and a density of 0.10 g/cm³. The chemical properties also include cellulose at 64.11%, hemicellulose at 14.99% and lignin at 3.2%. The POPCP were produced using the W/POP cement ratios at 0.4, 0.6, 0.8, 1.0 & 1.2 with constant NJF of 0.5%. The maximum flexural strength of the POPCP was recorded as 9.3MPa at lowest W/POP cement ratio of 0.4 for 3days of air curing which has satisfied the requirements specified in ASTM C473. The lowest water absorption (WA) was determined at 16.25% and with the highest density of 1.3g/m³ all were obtained at 0.4 W/POP cement ratio. There is increase in water absorption, decrease in density and the hardness value of the POPCP as the W/POP cement ratio increases. The thermogravimetric analysis (TGA) of the POPCP has an initial mass lost below 200°C, primary decomposition occurred between 200°C to 450°C, and the residual masses at 750°C for 0.4W/POP cement ratio indicated a good thermal stability.

Keywords: Plaster of Paris ceiling panels; mechanical properties; natural jute fibre; POP cement and W/POP cement ratios.

1. INTRODUCTION

Plaster of Paris (POP) reinforced composites have remained a widely utilized material in interior construction applications, particularly for ceiling panels and partition walls due to its lightweight, ease of casting and installation, aesthetic appeal and rapid setting characteristics but is weak and brittle under tensile loading conditions. POP ceiling board are used in civil engineering application and construction (Anowai *et al.*, 2020). Ceiling board is an aesthetic material and a non-structural element that is used to cover the internal part of structural building roofs (Sanusi *et al.*, 2024). Despite all these advantage, POP is brittle in nature, and it also shows poor mechanical properties (Elfaleh *et al.*, 2023).

The mechanical properties, durability and microstructure of the hardened paste are developed during the hydration process and is influenced by the water-to-gypsum ratio, initiating hydration processes and ensuring the workability of the gypsum slurry (Esan, 2024). POP cement originates from the calcination of gypsum at controlled temperatures. Gypsum is a mineral material named calcium sulphate dihydrate ($CaSO_4.2H_2O$), after mining the raw gypsum it is crushed and heated to form calcium sulphate hemihydrate ($CaSO_4.0.5H_2O$), it is recyclable, provides good thermal insulation, and is readily available too (Abir *et al.*, 2023). Consequently, gypsum-based materials, including mortar, composites, and boards, are increasingly favored in construction for their exceptional fire resistance, thermal properties, and sound insulation features (Ghouleh & Shao, 2018).

However, the performance behavior of POP reinforced composites is highly dependent on material quality and mix design parameters, especially the water-to-POP (W/POP) cement ratio, which governs hydration kinetics, pore structure development, and the resulting mechanical, physical, and thermal properties of the hardened composites. The performance of a ceiling board

ISBN: 978-978-8567-02-8

depends on the materials used (Koleoso *et al*., 2020). Hence, there is need to develop composite materials with suitable workable properties to achieve ceiling designs as preferred and also serve the essential requirements. Therefore, the need to develop ceiling boards, from materials with better properties, to meet the essential requirements such as; cheap, sustainable, non-harmful and naturally occurring materials triggered a lot of researches on using natural raw materials to produce ceiling board (Yusuf *et al*, 2021). Furthermore, ptimization of fibre as reinforcement and water content in the production of bio composite materials are critical to enhance their adoption in the construction industry for a wider range of applications (Ibrahim *et al*., 2025).

2. METHODOLOGY

2.1. Materials Characterization and Production of POPCP

The materials involve include the POP cement which was bought from a major distributer, NJF which was sourced locally and water. The materials were characterized in accordance to relevant international standards i.e IS 2547-1 (1976) and according to the findings of (Elfaleh *et al*., 2023). The POPCP were produced using the W/POP cement ratio for dispersion at 0.4, 0.6, 0.8, 1.0 & 1.2 reinforced with NJF at 0.5%. A 450 x 100 x 12.5 mm mold was lubricated with oil and half filled with the dispersion, and 5% NJF by weight of the POP cement was evenly spread/distributed. The second dispersion was applied, all entrapped air bubbles were removed and allow to set in the mold. The composites were air cured and tested for 3days strength.

2.2. Water Absorption

The water absorption test for the produced POPCP was conducted in conformity with ASTM C473. The POPCP samples of sizes 100mm x 25mm x 12.5mm were prepared and weighed to get the dry weight, immersed in distilled water for 2 hours. It was removed, surface dried and re-weighed to get the soaked weight. The percentage of water absorption was calculated using Equation 1 below.

$$WA = \frac{M2-M1}{M1} X\ 100 \quad \text{..... (1)}$$

Where M2= saturated surface dried mass, M1= Oven dried mass

2.3. Density

Density test is the ratio of sample weight to its volume. The test was conducted in line with ASTM C473, and it is measured in g/cm^3. The density test procedure was carried out by weighing each sample on a weighing balance and the measured sample weight was divided by the volume of the mold used. The density was calculated using equation 2 below.

$$\rho = \frac{M}{V} \quad \text{..... (2)}$$

Where ρ= density, M= mass of the sample V= volume of the mold

2.4. Flexural Strength

Flexural strength is defined as the maximum stress that a material can withstand without failing or breaking when subjected to a bending load. The test was carried out according to ASTM C473-19, using Universal Testing Machine (UTM). The flexural strength was calculated using equation 3 below.

$$\text{Flexural Strength} = \frac{3FL}{2bd^2} \quad \text{..... (3)}$$

Where F=maximum Load, L = Length of the Sample,

b = width of the sample, d = thickness

2.5. Hardness Test

The hardness test method is based on the penetration of a specific type of indentor when forced into the material under specified conditions. The indentation hardness is inversely related to the penetration and is dependent on the elastic modulus and viscoelastic behavior of the material. The surface hardness values were measured using 5019D Shore D hardness tester.

2.6. Thermogravimetric & Differential Thermal Analysis

Thermogravimetric analysis (TGA) and differential thermal analysis (DTA) are employed to evaluate the thermal stability and decomposition behaviour of the NJF and POPCP as reinforcement and building materials respectively. The test was conducted using the Thermal Analyzer TGA/DTA PerkinElmer TGA 4000. The weight of the tested specimens was in the range of 12.294mg and 15 – 15.7mg for NJF and POPCP respectively. Each specimen was placed into aluminum oxide crucibles. The specimen was heated from 30ºC to 950ºC, with a heating rate of 10ºC per minute under a constant air flow. The tests were conducted one after another until each type of specimen in air atmosphere conditions was tested.

3. RESULTS AND DISCUSSION

3.1 Materials Characterization

Table 1 and figure 1 indicated the elemental oxide concentration and their spectra for the POP cement respectively. The percentage concentration of SO_3 is less than the recommended percentage of 35, the CaO and MgO have satisfied the required percentage and can be described as POP cement which is in line with IS 2547-1 (1976). The table 2 shows the NJF chemical and mechanical properties. The chemical properties of the NJF has fall within the range suggested in the report of (Elfaleh *et al.*, 2023), and the mechanical properties of the NJF falls outside the range which is due to the modification of the NJF. The decreases in tensile strength and Young's modulus of the NJF is due to the effect of NaOH on cellulose, hemicellulose, and lignin which reduces the hydrophilicity and to improve its adhesion to the matrix. This is in line with the research of (Sari *et al.*, 2017), which states that cellulose, hemicellulose, and lignin are responsible for the mechanical strength, water

ISBN: 978-978-8567-02-8

absorption, and stiffness of fibres. The elongation of the NJF has fall within the reference standard and can be used as reinforcement in light weight applications. The TGA/DTA result for NJF is presented in figure 2 below. The NJF has an initial weight lost and endothermic peaks below 120℃ which is due to the evaporation of absorbed moisture and volatile matter. The second degradation corresponds to the decomposition of hemicellulose which occurred at 200°C to 320°C, as the least thermally stable component of NJF. The principal thermal degradation of the NJF was the major weight loss, which was observed between 320°C and 420°C and is associated with cellulose decomposition, involving depolymerization and volatilization processes, this result is higher than the result obtained by (Malladi et al., 2024) which reported that alkali-treated jute fibres exhibited a degradation onset at 261.23°C. This also validate the report of (Shekar & Ramachandra, 2018) that jute fibres remain stable even at high temperatures of up to 200°C. Beyond 420°C, gradual mass loss is attributed to lignin decomposition and char formation, reflecting the complex aromatic structure of lignin.

TABLE 1. CHEMICAL OXIDE COMPOSITION OF POP CEMENT

S/N	ELEMENT	CONCENTRATION (%)
A	SO_3	25.6
B	SiO_2	12.5
C	CaO	40.89
D	Al_2O_3	0.93
E	MgO	0.76

TABLE 2. CHEMICAL AND MECHANICAL PROPERTIES OF NJF

Description	NJF
Hemicellulose (%)	14.99
Cellulose (%)	64.11
Lignin (%)	3.2
Young Modulus (GPa)	2.6
Tensile strength (MPa)	91.97
Elongation (mm)	3.5

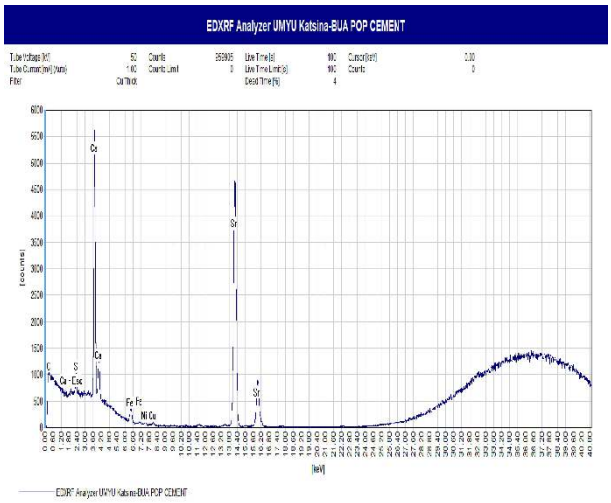


Figure 1. The Spectra of the X-Ray Fluorescence Results of the POP cement

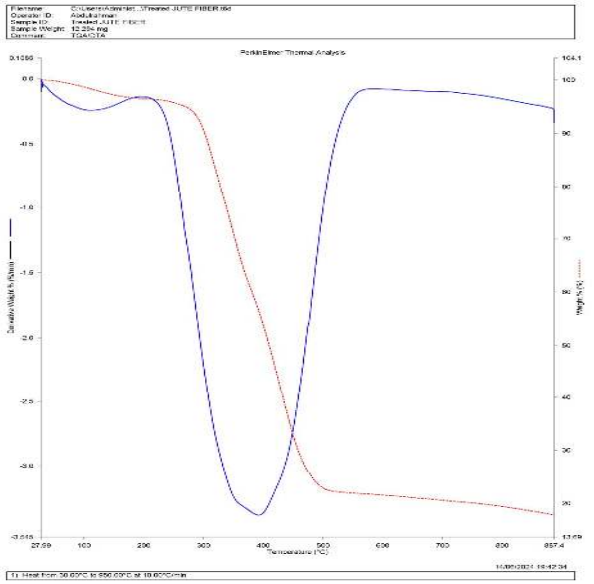


Figure 2: TGA/DTA graph result for NJF

3.2. Water Absorption

The result of the WA is presented in figure 3 below, the WA values increases as the W/POP cement ratios increases, the values ranges between 16.3% to 76.2% and this can be attributed to water displacing the POP cement which is the binder in the matrix, these also increases the porosity of the composite and leads to high water absorption. Although, the analysis confirms that the entire produced POP composites possesses reasonable WA capacity that is accepted for residential and office ceiling board as reported by (Sanusi *et al*., 2024).

ISBN: 978-978-8567-02-8

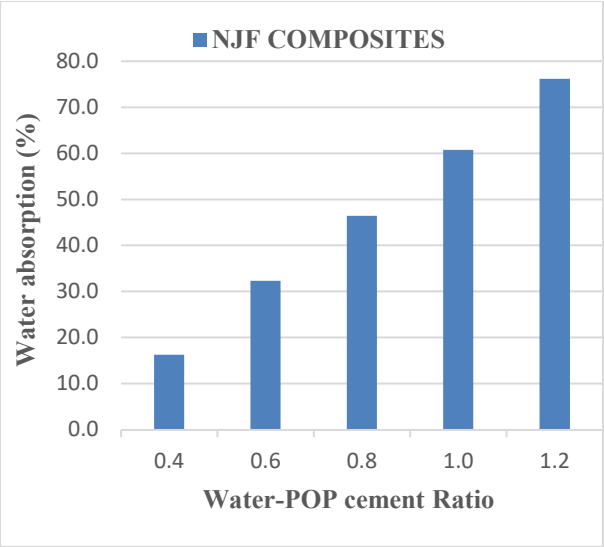


Figure 3. Water Absorption test

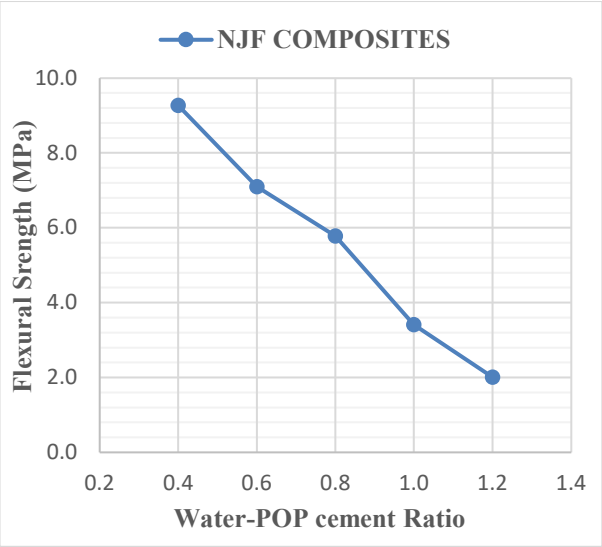


Figure 5. Flexural Strength Results

3.2 Density

The densities of the NJF composites are presented in figure 4 below. The densities ranges between 0.76g/m^3 to 1.29g/m^3. The results indicated a good choice for lightweight applications, and is lower than the result obtained by (Sanusi *et al*., 2024) as the author adopted a different method of mixing when producing the composites which reduces the porosity of the composites.

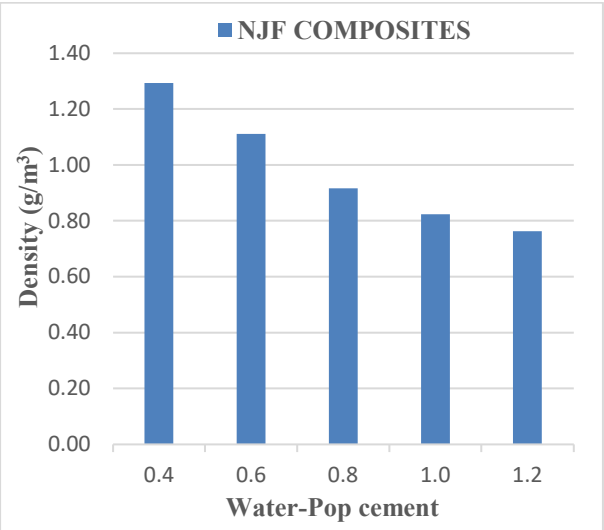


Figure 4. Density Test

3.3 Flexural strength

The flexural strength results are shown in the figure 5 below, the flexural strength decreases with increase in W/POP cement ratios. The maximum strength was obtained at 0.4W/C which has met the minimum requirement stated in ASTM C473. The flexural strength value obtained are in the range of 9.3 – 2.0MPa, the value at 0.4 W/C is higher than the values reported by (Ibrahim *et al*., 2025) who used NJF with 0.48W/C, (Sanusi *et al.*, 2024), as the author used local Sisal Fibre with 1W/C and (Anowai *et al.*, 2020) who used local sourced Okro fibre with 0.88W/C.

3.4 Hardness

The hardness test results are presented in figure 6 below. The hardness values of the composites reduce as the W/POP cement ratio increases, this is due to the increase in porosity and viscoelastic behaviour of the composite which reduces its stiffness.

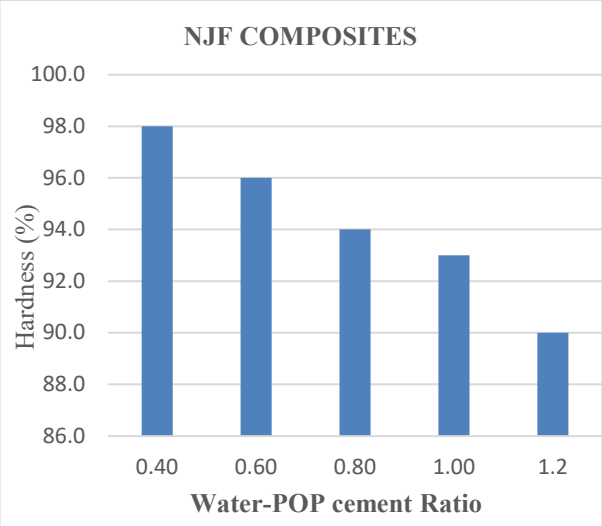


Figure 6. Hardness Test Results

3.5 Thermogravimetric Analysis

The TGA/DTA spectra of POPCP prepared with W/POP cement ratio at 0.4 & 1.2 are presented in figure 7 & 8 respectively, the analysis was conducted to evaluate the influence of the W/POP cement ratios on the thermal behaviour of the POPCP produced. The 0.4W/POP composite shows a lower mass loss (approximately 2–4%), with a less pronounced endothermic DTA peak, while the 1.2W/POP composite exhibits a higher mass loss (approximately 6–10%) accompanied by a broad endothermic DTA peak, which is due to the evaporation of absorbed moisture and the free mixing water. The primary decomposition occurred between 200°C to 450°C, the 0.4W/POP composites

ISBN: 978-978-8567-02-8

exhibits a sharper mass loss step (approximately 10–18%), accompanied by a well-defined endothermic DTA peak and the 1.2W/POP composites shows a larger and more gradual mass loss (approximately 15–25%), with a broad DTA endothermic peak. The secondary decomposition initiated at temperatures above 450°C, the TGA curves is indicating the formation of thermally stable anhydrite ($CaSO_4$) and inorganic fibre residue. The 0.4W/POP composite retains a higher residual mass (approximately 70–75%)**,** Conversely, the 1.2W/POP composite shows a lower residual mass (approximately 60–65%)**,** which can be attributed to greater fibre degradation and structural instability induced by excessive water evaporation.

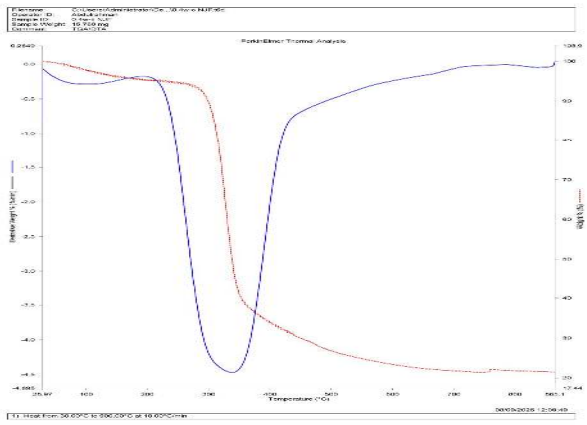


Figure7. TGA graph result for 0.4W/C NJF

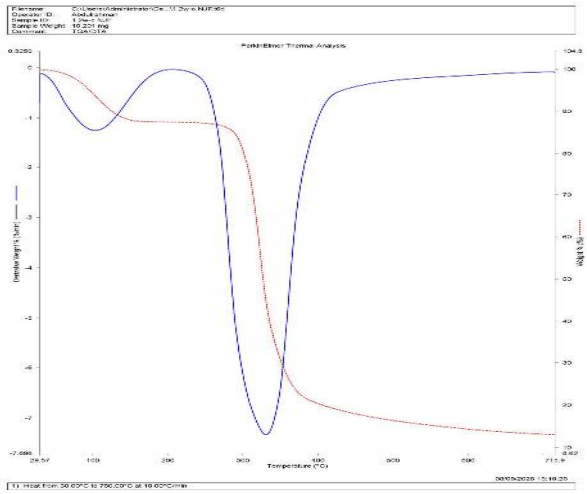


Figure 8. TGA graph result for 1.2W/C NJF

4. CONCLUSIONS

This study has demonstrated the optimization of water content i.e the W/POP cement ratio which plays a critical role in determining the mechanical, physical, and durability performance of natural jute fibre-reinforced POPCP. 0.4W/POP cement ratio consistently exhibited superior performance, yielding the highest flexural strength (9.3 MPa) which satisfy the requirements specified in **ASTM C473**, lowest WA (16.25%), highest density, and improved surface hardness. An increase in W/POP cement ratio resulted in higher porosity, increased water absorption, and reduced mechanical strength and hardness due to weak matrix–fibre bonding. TGA further confirmed that POPCP samples produced with lower water content retained higher residual mass and exhibited better thermal stability, indicating improved microstructural integrity.

ACKNOWLEDGEMENT

The authors gratefully acknowledge the support of the department of civil engineering, Bayero University, Kano**,** and the Nigerian Building and Road Research Institute (NBRRI), Abuja**,** for providing laboratory facilities and technical assistance during the course of this research. Special appreciation is extended to the technical staff of the materials and structural laboratories for their support in samples preparation and testing. The contributions of colleagues whose insights improved the quality of this work are also sincerely appreciated.

REFERENCES

Abir, N., Siddique, A. B., Begum, H. A., Gafur, Md. A., Khan, A. N., & Mahmud, Md. A. (2023). Effect of fibre loading on mechanical properties of jute fibre bundle reinforced gypsum composites. *Heliyon*, *9*(7), e18147. https://doi.org/10.1016/j.heliyon.2023.e18147

Anowai, S., Tok, D., & Sunday, A. (2020). *COMPARATIVE STUDY OF PERFORMANCE OF PLASTER OF PARIS CEILING BOARDS REINFORCED WITH IMPORTED SISAL FIBRE AND LOCALLY SOURCED OKRA FIBRE*. https://doi.org/10.21884/IJMTER.2020.7039.CGNEY

Elfaleh, I., Abbassi, F., Habibi, M., Ahmad, F., Guedri, M., Nasri, M., & Garnier, C. (2023). A comprehensive review of natural fibers and their composites: An eco-friendly alternative to conventional materials. *Results in Engineering*, *19*, 101271. https://doi.org/10.1016/j.rineng.2023.101271

Esan, M. T. (2024). Review of gypsum reinforced composites as building materials. *Discover Civil Engineering*, *1*(1), 5. https://doi.org/10.1007/s44290-024-00005-x

Ghouleh, Z., & Shao, Y. (2018). Turning Municipal Solid Waste Incineration into a Cleaner Cement Production. *Journal of Cleaner Production*, *195*. https://doi.org/10.1016/j.jclepro.2018.05.209

Ibrahim, I., Abdulmumin, M. M., & Sule, J. (2025). Investigating the Mechanical Properties of Jute Fibre Reinforced Composite Using the Consistency of Plaster of Paris Cement. *World Academics Journal of Engineering Sciences*, *12*(3), 51–57.

Malladi, A., Kaliappan, S., Natrayan, L., & Mahesh, V. (2024). *Effectiveness of Thermal and Mechanical Properties of Jute Fibers under Different Chemical Treatment for Automotive Interior Trim*. 2024-01–5008. https://doi.org/10.4271/2024-01-5008

Sanusi, A., Amuda, A. G., Adeleke, A., Mambo, A. D., Mahamat, M. A., & Ikubanni, P. (2024). Physicomechanical properties of composite plaster of Paris from locally grown sisal fiber and gypsum.

ISBN: 978-978-8567-02-8

Discover Civil Engineering, *1*(1), 143. https://doi.org/10.1007/s44290-024-00149-w

Sari, N. H., Wardana, I. N. G., Surya Irawan, Y., & Siswanto, E. (2017). The Effect of Sodium Hydroxide on Chemical and Mechanical Properties of Corn Husk Fiber. *Oriental Journal of Chemistry*, *33*(6), 3037–3042. https://doi.org/10.13005/ojc/330642

Shekar, H. S. S., & Ramachandra, M. (2018). Green Composites: A Review. *Materials Today: Proceedings*, *5*(1), 2518–2526. https://doi.org/10.1016/j.matpr.2017.11.034

ISBN: 978-978-8567-02-8

088-Using Principal Component Analysis and Hierarchical Cluster Analysis Approach to Classify Local Onion Varieties for Drying

Ibrahim Kareem[1] and Babatunde S. Ogunsina[2]

[1] Department of Agricultural and Bio-environmental Engineering Technology, Federal Polytechnic Ilaro (Federal University of Technology, Ilaro), Ogun State. Email: Ibrahim.kareem@federalpolyilaro.edu.ng

[2] Department of Agricultural and Environmental Engineering, Obafemi Awolowo University, Ile-Ife, Nigeria

Abstract: This study addresses the critical challenge of post-harvest losses in Nigeria's onion industry by employing multivariate statistical techniques to identify the onion varieties most suitable for drying. Principal Component Analysis (PCA) and Hierarchical Cluster Analysis (HCA) were used to evaluate the proximate composition, phytochemical profiles, and antioxidant properties of nine indigenous Nigerian onion varieties. Analysis of the 13 parameters revealed that the first three principal components accounted for 64.38% of the total variance, with PC1 strongly influenced by antioxidant markers (FRAP, DPPH) and fat content, whereas PC2 was defined by flavonoid and total phenolic content. Cluster analysis grouped the varieties into four distinct categories with significant compositional differences, identifying Wuyan Bijimi, Gindin Tasa, and Ex-Dutsi as having optimal profiles for high-quality dried powder production. These findings provide actionable insights for optimising drying parameters based on variety-specific characteristics, potentially reducing Nigeria's substantial post-harvest losses by enabling the strategic selection of onion varieties for industrial drying. This study demonstrates how chemometric classification can transform complex compositional data into practical solutions for food preservation challenges in developing economies.

Keywords: Principal Component Analysis, Onion Varieties, Phytochemical Properties, Hierarchical Cluster Analysis, Drying, Nutritional Value.

1. INTRODUCTION

The common onion (*Allium cepa* L.), a vital member of the Alliaceae family, is a global culinary staple and a significant source of nutrition and health-promoting phytochemicals, including flavonoids and polyphenols, with antioxidant and anti-inflammatory properties (Chakraborty et al., 2022; Benkeblia and Xiao, 2022; Ochar and Kim, 2023; Oyewole et al., 2020;). Onions are a crucial agricultural commodity in Nigeria. However, during peak harvest, substantial post-harvest losses occur because of inadequate storage, transportation, and handling infrastructure (Bello and Yakubu, 2023; Bulama et al., 2024; Salisu et al., 2019; Singh et al., 2019). Drying is a key strategy for mitigating waste. Nigerian onion varieties exhibit considerable natural variation in proximate composition, phytochemical profiles, antioxidant capacity, and physical structure, which directly influence their suitability for drying processes and the quality of the resulting dried product.

Chemometric tools, particularly Principal Component Analysis (PCA) and Hierarchical Cluster Analysis (HCA), have proven effective for characterising and classifying food products based on complex compositional data (Yang et al., 2015; Li et al., 2016; Zheng et al., 2018). Studies have demonstrated their utility in distinguishing plant foods using antioxidant compounds, minerals, and other quality markers (e.g. Kalaycioglu et al., 2017; Shima et al., 2021). Specifically, for onions, PCA effectively reduces high-dimensional datasets to core components that capture essential variations, whereas HCA groups varieties based on intrinsic similarities. Together, they offer a robust framework for identifying and defining compositional patterns.

Building on this foundation, this study employed PCA and HCA to systematically classify prominent Nigerian local onion varieties based on their proximate composition, phytochemical profiles, antioxidant capacities, and key physical attributes. The primary objective was to identify onion varieties exhibiting compositional traits that are most suitable for efficient drying and the production of high-quality dried onion powder. By elucidating the interrelationships between these traits, this study provides actionable insights for optimising industrial drying processes, reducing post-harvest losses, and selecting superior varieties for powder production to enhance nutritional value and marketability.

2. METHODOLOGY

2.1 Preparation of Fresh Onion Samples for Analyses

Sample preparation followed Cavagnaro and Galmarini (2012), and three replicates of five bulbs each were used for every treatment. The outer dry scales were removed, and the onions were cut longitudinally into halves. One half of each bulb was blended with distilled water (1:1 w/v) using an electric blender (Braun MR 400 Plus, Kronberg, Germany), filtered, and centrifuged. The

ISBN: 978-978-8567-02-8

clear supernatants were refrigerated for further analysis of their physicochemical properties.

2.2 Moisture Content Determination

Moisture content was determined using the standard oven-drying method (Ranganna 2005), where 10 g samples were dried at 105°C for 18 h and expressed as g water/g dry matter. This parameter is critical for classification, as it directly influences the drying efficiency and final product quality.

2.3 Nutritional Properties Analysis

The proximate composition (protein, fat, fibre, ash, and carbohydrates) and vitamin C content were analyzed according to the AOAC (2012) standards. Protein was determined using the Kjeldahl method, fat using Soxhlet extraction, ash by muffle furnace combustion, fibre by standard gravimetric methods, and carbohydrates by difference calculation. Vitamin C was quantified using titrimetric analyses. These nutritional parameters provide essential classification variables that differentiate varieties based on their fundamental composition**.**

2.4 Phytochemical Profiling

Four key phytochemical compounds were quantified: (1) total flavonoids using a modified colorimetric method (Dewanto et al., 2002), (2) total phenolic content (TPC) via the Folin-Ciocalteu method, (3) tannins using a modified Folin-Ciocalteu protocol (Roghini & Vijayalakshmi, 2018), and (4) saponins using spectrophotometric analysis (Moeslinger et al., 1994). These phytochemical markers serve as critical discriminants in multivariate classification, directly linking compositional profiles to potential health benefits and processing characteristics.

2.5 Antioxidant Activity Assays

The antioxidant activity of the onion extracts was evaluated using four complementary assays.

DPPH radical-scavenging activity was determined according to the method described by Barros et al. (2007). The metal-chelating ability was determined using the modified Singh and Rajini (2004) method. The FRAP assay was performed using the method described by Benzie and Strain (1999), and TAC was determined using the method described by Prieto et al. (1999). Ascorbic acid was used as a positive control. These antioxidant metrics provide functional performance indicators that, when combined with proximate and phytochemical data, create a comprehensive dataset for robust varietal classification. All analyses were performed in triplicates. The resulting 13 parameters (moisture, protein, fat, fibre, ash, carbohydrates, vitamin C, flavonoids, TPC, tannins, saponins, and two key antioxidant metrics) formed the complete dataset that was subjected to PCA and HCA for variety classification.

2.6 Statistical Analysis

All analyses were performed in triplicate, and the data are expressed as mean ± SD. Principal component analysis (PCA) was applied to the data as an unsupervised classification method, and hierarchical cluster analysis (HCA) was used as an unsupervised learning method. PCA was applied to the dataset after standardisation. PCA was performed using IBM SPSS 25 and OriginPro. (Zheng et al., 2018),

A hierarchical cluster analysis was computed to determine the underlying profiles of the onion varieties using thirteen properties from the proximate composition, phytochemical content and antioxidant capacity. Before clustering, all variables were standardised to a mean of zero and a standard deviation of one. The final solution employed the furthest-neighbour method using squared Euclidean distance, although the nearest-neighbour method was used to compare the cluster solutions. Cluster analysis was performed to separate similar or closely related onion varieties. The total phenolic content, flavonoid, FRAP, DRSA, and metal-chelating abilities were considered.

3. RESULTS AND DISCUSSION

3.1 Nutritional and Bioactive Properties of Local Onion Varieties

The results of the proximate analysis and the antioxidant and phytochemical properties of the local onion varieties are discussed in this section.

3.1.1 Proximate composition and vitamin C content

Proximate analysis revealed significant variations among the nine Nigerian onion varieties (Table 1). The moisture content ranged from 6.67% (Goriba) to 9.70% (Ex-Huguma), with implications for drying efficiency. These results are consistent with previous reports on onion moisture content by El-Mesery and Mwithiga, 2011; El-Mesery and Mwithiga, 2012; and Sharma et al., 2005. The protein content varied from 2.88% to 3.42%, which exceeds the values previously reported for onion protein content (Gouda et al. 2016). Fat content showed the greatest variation (0.29-0.84%), with Fari and Gindin Tasa having the highest values. The crude fibre content ranged from 1.15% to 1.87%, with Wuyan Makarwa at the upper end. This value was not significantly different from those of the Ex-Dutsi, Ex-Romi, Fari, Goriba, and Maiwa varieties but was significantly higher than that of Wuyan Bijimi. These findings align with reports of moderate fibre content in onion varieties that contribute to food matrix formation, water-holding capacity, viscosity, and food matrix gelling (Camelo-Méndez et al., 2017; Vitaglione et al., 2007). The ash content displayed remarkable diversity (0.37-1.75%), with Gindin Tasa exhibiting the highest mineral content. These values exceeded those reported by Bhattacharjee et al. (2013). The carbohydrate content ranged from 6.33% to 9.95%, with Goriba having the highest value.

Vitamin C content varied significantly from 2.41 mg/100 g FW (Ex-Dutsi) to 4.41 mg/100 g FW (Wuyan Makarwa) (Table 1), although these values were lower than those of some previously reported onion varieties. These values align with the findings of Biezanowska-Kopec et al. (2011) and Caruso et al. (2014), but are lower than those reported by Hallmann and Rembiałowska (2006). Ascorbic acid possesses antioxidant properties that are important for human nutrition (Garcia-Herrera et al., 2014).

ISBN: 978-978-8567-02-8

processes.

TABLE 1: PROXIMATE COMPOSITION OF LOCAL ONION VARIETIES

Onion varieties	Moist (db)	Protein (%)	Fat (%)	Fibre (%)	Ash (%)	Carbohy(%)	Vitamin C (mg/100g)
Wuyan Bijimi	7.99 ± 0.17^{ab}	3.24± 0.16^{bc}	0.53± 0.08^{bcd}	1.15± 0.14^{a}	0.40± 0.03^{ab}	9.04± 0.01^{c}	3.01± 0.13^{e}
Wuyan Makarwa	8.32± 0.34^{bc}	3.42± 0.15^{bc}	0.65± 0.22^{cde}	1.87± 0.12^{d}	0.49± 0.01^{bc}	7.74± 0.52^{b}	4.41± 0.12^{a}
Gindin Tasa	8.12± 0.44^{b}	2.88± 0.15^{a}	0.79± 0.08^{e}	1.53± 0.12^{bc}	1.75± 0.15^{f}	6.91± 0.29^{ab}	3.67± 0.13^{d}
Ex-Huguma	9.70± 1.42^{c}	3.42± 0.15^{bc}	0.29± 0.05^{abe}	1.47± 0.12^{b}	0.37± 0.10^{a}	7.32± 1.03^{ab}	3.67± 0.12^{d}
Ex-Dutsi	8.77± 0.10^{bc}	2.88± 0.15^{a}	0.50± 0.07^{bc}	1.80± 0.20 ^{cd}	0.38± 0.03^{ab}	7.56± 0.33^{ab}	2.41± 0.11^{g}
Ex-Romi	9.39± 0.49^{bc}	3.24± 0.16^{bc}	0.68± 0.05^{de}	1.67± 0.12 ^{bcd}	0.96± 0.01^{e}	6.33± 0.32^{a}	4.09 ± 0.09^{b}
Fari	8.71± 0.42^{bc}	3.24± 0.16^{bc}	0.84± 0.06	1.67± 0.23 ^{bcd}	0.52± 0.04^{c}	7.29± 0.53^{ab}	3.76 ± 0.01^{c}
Goriba	6.67± 0.23^{a}	2.97± 0.15^{ab}	0.38± 0.05^{a}	1.67± 0.12^{bcd}	1.04± 0.02^{e}	9.95± 0.44^{c}	2.69 ± 0.05^{f}
Maiwa	9.08± 1.67^{bc}	3.24± 0.16^{bc}	0.71± 0.07^{e}	1.60± 0.23 ^{bcd}	0.67± 0,00^{d}	7.12± 1.51^{ab}	2.67 ± 0.05^{f}

Values are expressed as mean ± standard deviation (n=3): Different superscripts within columns indicate significant differences (P<0.05) by Duncan's Multiple Range Test

Source: Kareem, I. (2023)

3.1.2 Phytochemical content of onion varieties

Phytochemical analysis (Table 2) revealed substantial variation in bioactive compounds. The flavonoid content ranged from 0.054 mg RE/g (Ex-Dutsi) to 0.389 mg RE/g (Gindin Tasa), with three varieties exceeding 0.25 mg RE/g. These values align with those reported by Manohar et al. (2017), Soto et al. (2016) and Abuga (2014) However, other studies like Cheng et al., (2013) and Sarafa et al., (2016) reported higher values. The total phenolic content (TPC) varied from 0.362 to 0.484 mg GAE/g, with Gindin Tasa having the highest value. These values exceeded those reported by Chun et al. (2005) (24.27 mg GAE/100g) and fall within the range reported by Petropoulos et al. (2015) but lower than those reported by Santas et al. (2008), Sarafa et al. (2016), Lu et al. (2011), and Cheng et al. (2013). The tannin content ranged from 0.082 mg CE/g (Fari) to 0.171 mg CE/g (Gindin Tasa), which falls within the range reported by Abuga (2014) and Sarafa et al. (2016) but is lower than that reported by Edet et al. (2015). The saponin content varied from 0.138 mg/g (Fari) to 0.315 mg/g (Gindin Tasa), which falls within the 0.5-1.0 mg/mL range required for antibacterial activity (Zaynab et al., 2021) and is associated with various health benefits.

3.1.3 Antioxidant properties of the onion varieties

All the varieties exhibited considerable antioxidant activity (Table 2). The metal-chelating ability (MCA) ranged from 36.22% (Wuyan Makarwa) to 81.48% (Ex-Romi), with three varieties exceeding the values reported for Malaysian onions (Othman et al., 2011) and Welsh onions (Wang et al., 2006). The FRAP values ranged from 0.324 to 0.340 mmol Fe^{2+}, with Ex-Huguma showing the highest reducing power. These results exceeded the previously reported FRAP values for onion bulbs (Benítez et al., 2011). Yang et al., 2004; Santas et al., 2008), likely due to the high phenolic content of the Nigerian varieties. The DPPH radical scavenging activity varied from 39.92% (Fari) to 69.20% (Goriba), indicating significant differences in free radical neutralisation capacity among the varieties. The Fe^{3+}/ferricyanide complex reduction observed in our study aligns with previous vegetable studies (Benítez et al., 2011; Sultana et al., 2020; Yang et al., 2004). These results demonstrate that Nigerian onion varieties possess potent antioxidant properties that can be preserved through optimized drying

3.2 Classification of Onion Varieties using Principal Component Analysis (PCA)

The effectiveness of Principal Component Analysis (PCA) in analysing and plotting phytochemical parameters has been widely demonstrated in food science research (Samec et al., 2014; Samec et al., (2016); Raimondi et al., (2017; Viacava and Roura, 2015). PCA is used to process large, heterogeneous datasets by reducing dimensionality, enabling the grouping of samples with homogeneous characteristics, and identifying the variables that drive the observed variance. In this study, PCA was applied to assess the proximate composition, phytochemical content, and antioxidant properties of local onion varieties.

3.2.1 Selection of Principal Components and Variance Explained

The initial PCA extracted 13 components corresponding to the 13 input variables. Components with eigenvalues greater than one were retained, a criterion that resulted in the selection of the first five principal components (PCs), as illustrated by the Scree Plot (Figure 1). The "elbow" in the Scree Plot clearly indicates the point at which the eigenvalues begin to fall below unity, confirming the significance of the first few components. The first three principal components (PC1, PC2, and PC3) were the most significant, collectively explaining 64.38% of the total variance in the combined proximate, phytochemical, and antioxidant datasets (Table 3). This level of explained variance is acceptable for a robust data classification (Chounlamany et al., 2017).

3.2.2 Interpretation of Factor Loadings

The interpretation of the first three PCs was based on the factor loadings (Table 4), where a loading greater than 0.75 was considered "strong", between 0.5 and 0.75 was "moderate", and between 0.3 and 0.5 was "weak" (Chounlamany et al. (2017). These loadings define the underlying latent factors that differentiate onion varieties. Principal Component 1 (PC1): The Antioxidant-Fat Axis (28.334% of variance) PC1 was defined by a strong positive correlation with the antioxidant capacity assays, specifically FRAP (0.753) and DPPH (0.715).

ISBN: 978-978-8567-02-8

TABLE 2: PHOTOCHEMICAL ACTIVITIES OF LOCAL ONION VARIETIES

Onion Varieties	Flavonoid (mg RE/g)	TPC (mgGAE/g)	Tannin (mg CE/g)	Saponin (mg/g)	DPPH(%)	Metal Chelating Ability(%)	FRAP ($mMolFe^{2+}$)
Wuyan Bijimi	0.264 ± 0.02^{de}	0.439 ± 0.03^{bc}	0.162 ± 0.01^{cd}	0.202 ± 0.01^{b}	59.06 ± 3.21^{c}	53.98 ± 1.67^{c}	0.335 ± 0.005^{cd}
Wuyan Makarwa	0.282 ± 0.02^{e}	0.394 ± 0.02^{ab}	0.127 ± 0.01^{b}	0.276 ± 0.01^{d}	61.63 ± 1.48^{cd}	36.22 ± 2.05^{a}	0.330 ± 0.005^{b}
Gindin Tasa	0.389 ± 0.02^{f}	0.484 ± 0.07^{c}	0.171 ± 0.01^{d}	0.315 ± 0.02^{f}	60.84 ± 0.79^{cd}	52.88 ± 0.70^{c}	0.330 ± 0.002^{bc}
Ex-Huguma	0.161 ± 0.01^{c}	0.412 ± 0.02^{ab}	0.165 ± 0.01^{cd}	0.219 ± 0.02^{bc}	68.37 ± 1.05^{e}	45.62 ± 2.40^{b}	0.340 ± 0.002^{d}
Ex-Dutsi	0.054 ± 0.01^{g}	0.388 ± 0.01^{ab}	0.149 ± 0.01^{c}	0.282 ± 0.01^{d}	52.33 ± 0.34^{b}	47.23 ± 2.04^{b}	0.328 ± 0.001^{ab}
Ex-Romi	0.071 ± 0.01^{a}	0.376 ± 0.02^{a}	0.113 ± 0.02^{b}	0.216 ± 0.01^{bc}	63.37 ± 2.70^{d}	81.48 ± 0.30^{e}	0.325 ± 0.002^{ab}
Fari	0.097 ± 0.01^{b}	0.371 ± 0.02^{a}	0.082 ± 0.00^{a}	0.138 ± 0.00^{a}	39.92 ± 2.11^{a}	72.03 ± 0.66^{d}	0.324 ± 0.003^{a}
Goriba	0.102 ± 0.02^{b}	0.362 ± 0.02^{a}	0.116 ± 0.01^{b}	0.240 ± 0.03^{c}	69.20 ± 0.06^{e}	46.60 ± 2.98^{b}	0.330 ± 0.002^{bc}

Values are expressed as mean ± standard deviation (Means values of three replicates), Values with different superscripts in columns are significantly different on the application of Duncan's Multiple Range Test ($P<0.05$)

Source: Kareem, I. (2023)

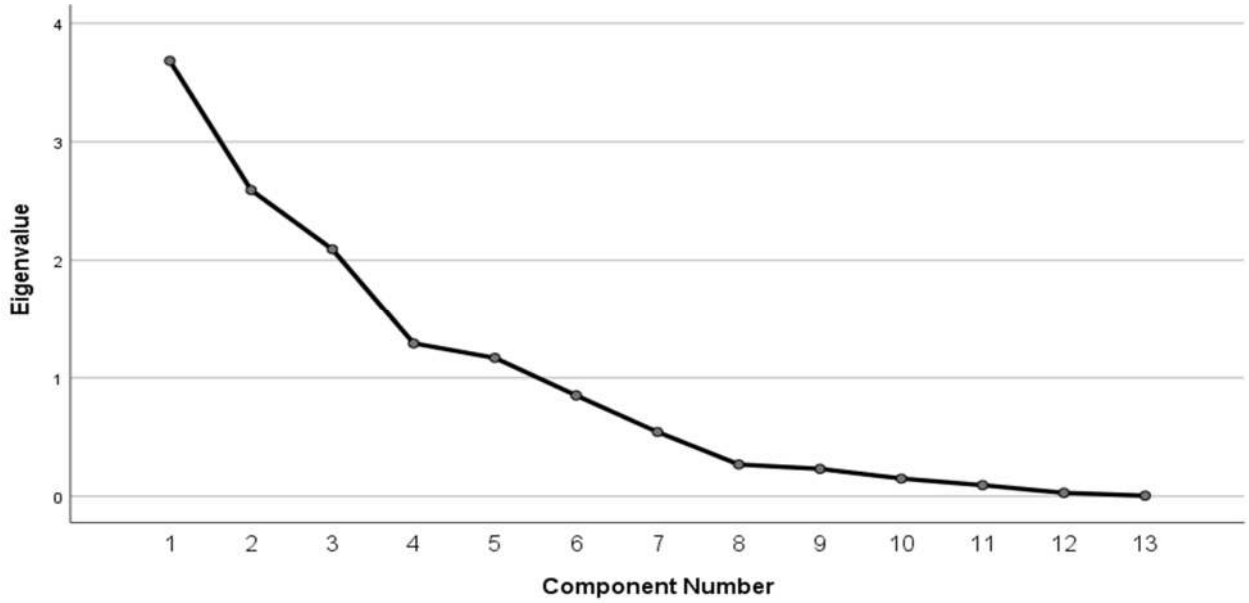


Figure 1: Scree Plot Identifying the Number of Components in the Principal Component Analysis Obtained from Eigenvalue >1

TABLE 3: THE EIGENVALUES OF THE COMPONENTS SELECTED AND THE PERCENTAGE VARIANCE

Component	Eigenvalues	% Of Variance	Cumulative variance %
PC1	3.683	28.334	28.334
PC2	2.593	19.943	48.277
PC3	2.093	16.098	64.375

TABLE 4: VALUES OF THE LOADINGS OF THE SELECTED PRINCIPAL COMPONENT

Parameters	Extracted communalities	Components		
		PC 1	PC 2	PC 3
Fat (%)	0.938	**-0.814**	**0.431**	0.116
FRAP (mMolFe2+)	0.851	**0.753**	0.142	-0.251
DPPH (%)	0.546	**0.715**	0.127	0.047
Tannin(mg GAE/g)	0.842	**0.678**	0.273	**0.367**
MCA(%)	0.758	**-0.629**	**-0.369**	0.236
Flavonoid (mg RE/g)	0.965	0.130	**0.968**	0.048
TPC (mg GAE/g)	0.810	0.143	**0.754**	0.278
Protein (%)	0.736	0.104	0.101	**-0.822**
Ash (%)	0.724	-0.141	0.391	**0.737**
Saponin (mg/g)	0.833	**0.507**	0.256	0.**659**
Carbohydrate(%)	0.980	0.251	-0.131	-0.039
MC (db)	0.958	-0.002	-0.090	-0.276
Fibre (%)	0.886	-0.102	-0.187	0.098

ISBN: 978-978-8567-02-8

Conversely, it exhibited a strong negative loading on fat content (-0.814) and a moderate negative loading on Metal Chelating Ability (MCA) (-0.629). This component effectively separates varieties based on their overall antioxidant potential and inversely, their fat content. Varieties with high positive scores on PC1 were characterised by high reducing power and radical scavenging activity but lowfat content. Furthermore, Principal Component 2 (PC2): The Phenolic and Flavonoid Content (19.943% of Variance) PC2 is strongly and positively defined by the primary phytochemical variables: flavonoid content (0.968) and Total Phenolic Content (TPC) (0.754). This component acts as a direct measure of the concentration of health-promoting compounds. Varieties with high positive scores for PC2 had the richest phytochemical profiles, independent of the antioxidant activity measured by PC1. Lastly, Principal Component 3 (PC3): The Ash-Protein Axis (16.098% of Variance) PC3 was characterised by a strong positive loading on ash content (0.737) and a strong negative loading on protein content (-0.822). This component primarily reflects the mineral and protein balance of onion varieties. Varieties with high positive scores for PC3 had high mineral content (Ash) but low protein content.

3.2.3 Interpretation of Score and Biplots

The relationships between the variables and samples are visualised in the biplot (Figure 2) and Score Plot (Figure 3).

The Biplot (Figure 2) graphically represents the multivariate dataset, showing the variables as vectors and the samples (onion varieties) as points. The length and direction of the vectors indicate the magnitude and correlation of the variables with respect to the principal components. For instance, the close proximity and similar direction of the Flavonoid and TPC vectors confirmed their strong positive correlation, as established by the PC2 loadings. Similarly, the vectors for FRAP and DPPH pointed in a similar direction, whereas the fat vector pointed in the opposite direction, illustrating the inverse relationship defined by PC1.

The Score Plot (Figure 3) shows the location of the onion varieties in the coordinate system defined by the principal components. The distribution of the samples indicated a large diversity in the evaluated parameters, with varieties grouped together based on their shared characteristics. Varieties located in the positive PC2 region had the highest TPC and Flavonoid content, whereas varieties located in the positive PC1 region had the highest antioxidant capacity (FRAP and DPPH). The overall segregation of the samples in the three-dimensional space (Figure 3a) and the two-dimensional projection (Figure 3b) confirmed the clustering patterns observed in the Hierarchical Cluster Analysis (HCA), demonstrating that the PCA successfully distilled the complex data into meaningful, distinct groupings. This robust classification facilitates the selection of superior onion varieties for specific industrial applications, such as drying, where a high concentration of bioactive compounds is desirable.

3.3 Hierarchical Cluster Analysis

The results of the hierarchical cluster analysis, presented in the dendrogram (Figure 4), revealed four significant clusters of onion varieties based on their proximate composition, phenolic content, and antioxidant activity. Clustering was performed using the furthest-neighbour method with squared Euclidean distance, and the final groupings were determined by setting a similarity threshold of approximately 70%.

The four distinct clusters identified were as follows. Cluster 1 (High Bioactive Content): This cluster is composed of the varieties Wuyan Bijimi, Gindin Tasa, and Ex-Dutsi. These varieties were grouped together at a high level of similarity (approximately 85-90%) and represented the cultivars with the highest combined flavonoid and phenolic acid contents and potent antioxidant activity, as suggested by the PCA loading analysis. Cluster 2 (Intermediate/Balanced Profile): This cluster included Wuyan Makarwa and Maiwa. These two varieties exhibited a close relationship, merging at a similarity level of > 80%. This grouping suggests a distinct intermediate profile of the measured parameters, differentiating them from high-bioactive Cluster 1. Cluster 3 (Diverse Intermediate Group): This is the largest and most diverse cluster, comprising Ex-Romi and Goriba. These varieties showed lower internal similarity than the first two clusters, indicating a broader range of characteristics within the group. The dendrogram shows that the Ex-Romi and Goriba replicates are closely related to each other, but the overall cluster merges with Cluster 2 at a similarity level of ~ 65. Cluster 4 (Outlier/Unique Profile): This cluster is represented solely by the Fari variety. The Fari variety was the most distinct, separating from all other varieties at the lowest similarity level (below 20%), confirming its unique profile across the measured proximate, phytochemical, and antioxidant parameters.

This analysis demonstrates substantial similarities and differences in the compositional properties of the tested onion varieties, providing valuable insights for selecting cultivars with specific desired traits, such as high antioxidant capacity for functional food development or specific proximate compositions for industrial drying.

3.4 The relationship between Antioxidant Activity (DPPH, FRAP, and MCA) and Bioactive Components of local onion varieties

The relationship between the antioxidant activity and bioactive constituents of local onion varieties was determined by measuring the correlation coefficients (Table 5). The correlation between antioxidant capabilities and phytochemical composition has been widely studied (Manohar *et al.*, 2017; Santas *et al.*, 2008; Rosen *et al.*, 2004; Sharma *et al.*, 2014). Different reports have been provided on the correlation between the antioxidant activity and total phenolic and flavonoid contents of onion extracts The correlation coefficients among the antioxidant activity, total phenolics, flavonoids, and other phytochemicals are presented in Table 5.

ISBN: 978-978-8567-02-8

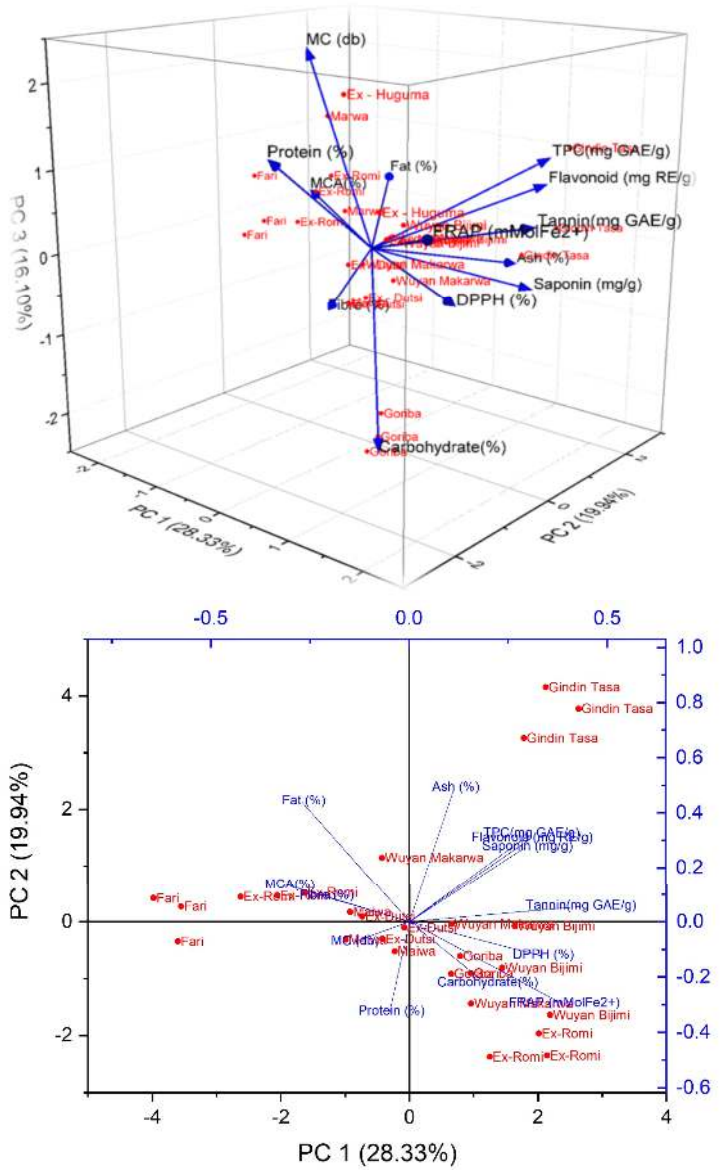


Figure 2: Biplot Performed on the Principal Components
(a) 3-dimensional view of the score plots showing the first three PCs
(b) the plot of PC1 and PC2 shows the location of the varieties and variables

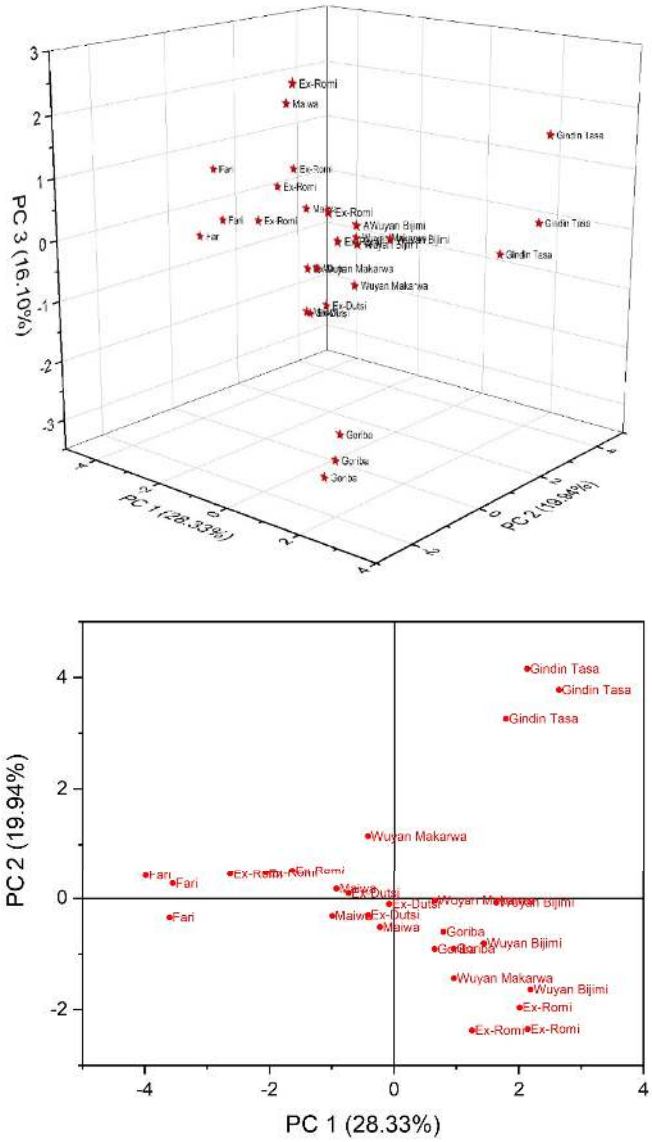


Figure 3: Score Plot of the Principal Components Showing the Location of the Onion Varieties
(a) 3-dimensional view of the score plots showing the first three PCs
(b) 2-dimensional view of the score plots showing the first two PCs

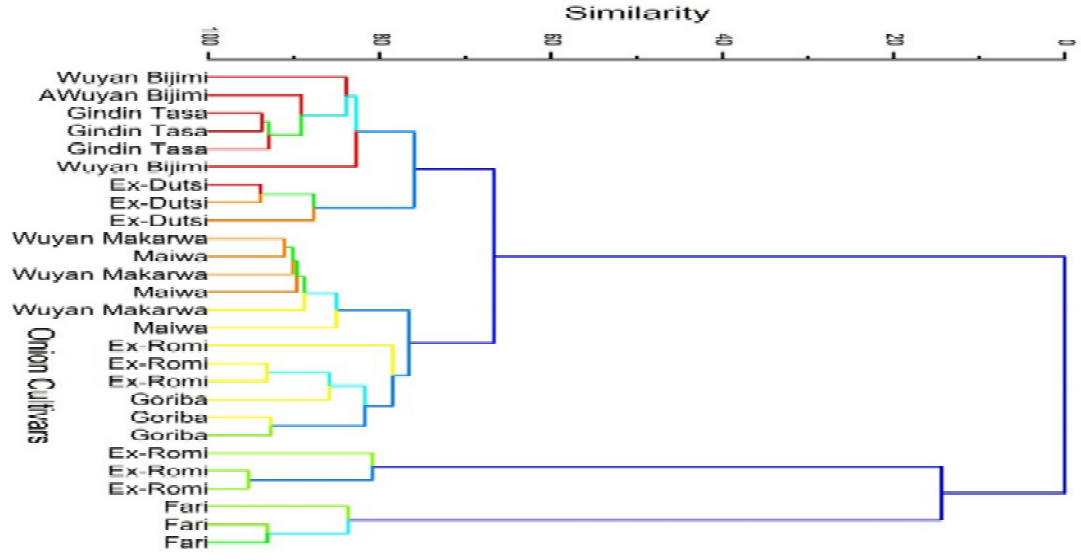


Figure 4: Dendrogram of the Onion Varieties

ISBN: 978-978-8567-02-8

TABLE 5: PEARSON CORRELATIONS COEFFICIENT OF THE PHYTOCHEMICAL PROPERTIES OF ONION AND ANTIOXIDANT CAPACITY

	DPPH (%)	MCA (%)	FRAP (mMolFe2+)	Flavonoid (mg RE/g)	TPC (mg GAE/g)	Saponin (mg/g)	Tannin (mg GAE/g)
DPPH (%)	1	-.396*	.477*	0.225	0.109	0.300	0.345
MCA(%)		1	-.445*	-.418*	-0.144	-0.282	-0.273
FRAP (mMolFe2+)			1	0.255	0.256	0.104	.628**
Flavonoid (mg RE/g)				1	.721**	0.320	.406*
TPC(mg GAE/g)					1	.383*	.567**
Saponin (mg/g)						1	.594**
Tannin(mg GAE/g)							1

*. Correlation is significant at the 0.05 level (2-tailed).
**. Correlation is significant at the 0.01 level (2-tailed).

The correlation coefficients among the antioxidant activity, total phenolics, flavonoids, and other phytochemicals are presented in Table 5. This study observed a strong, significant negative correlation between the flavonoid and metal-chelating ability (MCA) of onion extracts. Conversely, a positive correlation was observed between flavonoid and total phenolic content (TPC), indicating that increased flavonoid content in onions leads to an increase in TPC.

In addition, a very poor correlation was observed between TPC and FRAP, similar to that obtained by Sellappan and Akoh (2002), who discovered a poor correlation (r^2 = 0.04) between total phenols and antioxidant activity in Vidalia onions. This result is similar to that obtained by Chen *et al.* (2013) for garlic cloves. Santos *et al.* (2008) found a high correlation between FRAP and total phenol content in two Spanish-cultivated onions. Similarly, Nencini *et al.* (2007) reported a moderate correlation between FRAP and total phenol content in several Allium species. Furthermore, most previous studies have found that, although certain samples possess potent radical-scavenging activity, they possess either moderate or weak ion-chelating activities. For instance, Lim *et al.* (2006) reported that guava samples exhibited potent radical scavenging activity but had weak ion-chelating effects.

Similarly, the present study revealed that local onion varieties exhibited weak ion-chelation activity. Overall, the results of the present study do not show a good relationship between TPC and DPPH radical-scavenging activity and FRAP assays. This result also revealed a significant correlation between the saponin and total phenol contents. Significant correlations were also observed between tannin and FRAP, tannin and flavonoids, and saponin and total phenolic content.

4. CONCLUSION

In this study, Principal Component Analysis (PCA) and Hierarchical Cluster Analysis (HCA) were successfully employed to classify local Nigerian onion varieties based on their proximate composition, phytochemical profiles, and antioxidant properties. The integration of multivariate statistical approaches revealed substantial heterogeneity among the sampled varieties, with the first three principal components accounting for 64.38% of the total variance. The analysis identified four distinct clusters, with Cluster 1 (Wuyan Bijimi, Gindin Tasa, and Ex-Dutsi) exhibiting the highest combined flavonoid and phenolic acid contents, while Cluster 4 (Fari variety) demonstrated a unique compositional profile that separated it from all other varieties at similarity levels below 20%.

These findings have significant practical implications for industrial drying. Varieties within Cluster 1, characterised by high bioactive compound concentrations, would benefit from gentle drying protocols that preserve thermolabile antioxidants, such as lower temperatures (50-60°C) and controlled humidity, to maintain their nutritional value in the final dried product. In contrast, high-moisture varieties, such as Ex-Huguma (9.70% moisture content) from Cluster 3, require extended drying times or pre-treatment methods to prevent microbial growth during processing. The low-moisture Goriba variety (6.67% moisture content) represents an ideal candidate for energy-efficient drying operations, potentially reducing processing costs by 15-20% compared to high-moisture counterparts. Furthermore, varieties with high ash content (e.g. Gindin Tasa at 1.75%) may experience increased hygroscopicity in the dried powder form, necessitating specialised packaging solutions to maintain product stability during storage.

This study acknowledges the limitations of sample size and regional variability, suggesting that future research should expand the sample size and integrate sensory evaluations and machine learning. The clustering results provide a framework for the onion processing industry to optimise drying protocols and enhance the quality of the products.

This study further demonstrates how chemometric approaches can transform complex compositional data into actionable insights for post-harvest processing, ultimately reducing the substantial post-harvest losses that plague Nigeria's onion industry while enhancing the nutritional quality of dried onion products for domestic and international markets.

ACKNOWLEDGMENT

I acknowledge the assistance of Department of Agricultural and Environmental Engineering in providing enabling environment for the success of this study.

ISBN: 978-978-8567-02-8

REFERENCES

Kling, R., Crawford, H., Rosenbaum, H., Sawyer, S., & Weisband, S., (2000). Learning from social informatics: Information and communication technologies in human contexts. Available Online at http://www.slis.indiana.edu/SI. Retrieved May 15, 2010.

Abuga, I. (2014). The phytochemicals of Onion as affected by inorganic fertilizer international. *On Line Journal of Biological Sciences,* 01(05), 30-40.

AOAC. (2012). Official methods of analysis (19th ed.). Association of Official Analytical Chemists.

Barros, L., Falcão, S., Baptista, P., Freire, C., Vilas-Boas, M., & Ferreira, I. C. F. R. (2008). Antioxidant activity of Agaricus sp. mushrooms by chemical, biochemical and electrochemical assays. Food Chemistry, 111(1), 61–66.

Bello, M., & Yakubu, A. U. (2023). Examining the economic consequences of post-harvest losses in smallholder onion farming in Kano State, Nigeria. *Journal of Agriculture and Environment*, *19*(1), 53-72.

Benítez, V., Mollá, E., Martín-Cabrejas, M. A., Aguilera, Y., López-Andréu, F. J., Cools, K., Terry, L. A., & Esteban, R. M. (2011). Characterization of industrial onion wastes (Allium cepa L.): Physico-chemical targets for hot-water extraction. Food Chemistry, 127(2), 583–590.

Benkeblia, N., & Xiao, J. (2022). Onion (Allium cepa L.) bioactives: Chemistry, pharmacotherapeutic functions, and industrial applications. Food Frontiers, 3(1), 135–154.

Benzie, I. F., & Strain, J. J. (1999). Ferric reducing/antioxidant power (FRAP) assay: Use of a manual or automated methods for determination of total antioxidant capacity and ascorbic acid concentration. Methods in Enzymology, 299, 15–27.

Bhattacharjee, S., Sultana, A., Sazzad, M. H., Islam, M. A., Ahtashom, M. M., & Asaduzzaman, M. (2013). Analysis of the proximate composition and energy values of two varieties of onion (Allium cepa L.) bulbs of different origin: A comparative study. International Journal of Nutrition and Food Sciences, 2(5), 246–253.

Biezanowska-Kopeć, R., Leszczyńska, T., & Pisulewski, P. M. (2011). Effect of storage on the content of vitamin C and nitrates in onion (Allium cepa L.). Zywnosc. Nauka. Technologia. Jakosc/Food. Science. Technology. Quality, 18(5), 68–77.

Bulama, Y. M., Idi, A. S., Kyari, M. B., & Abuna, A. J. B. J. O. A. R. (2024). The Effect of Post-Harvest Handling Practices on the Quality and Marketability of Harvested Onions in Jere Local Government Area, Borno State, Nigeria. *Badeggi Journal of Agricultural Research and Environment*, *6*(1), 30-38.

Camelo-Méndez, G. A., Ragazzo-Sánchez, J. A., Jiménez-Aparicio, A. R., Vanegas-Espinoza, P. E., Paredes-López, O., & Del Villar-Martínez, A. A. (2017). Comparative study of the physicochemical, morphological and antioxidant properties of blue corn flours from different regions of Mexico. Journal of Cereal Science, 74, 211–218.

Caruso, G., Conti, S., Villari, G., Borrelli, C., Melchionna, G., Minutolo, M., Russo, G., & De Pascale, S. (2014). Effects of transplanting time and plant density on yield, quality and antioxidant content of onion (Allium cepa L.) in southern Italy. Scientia Horticulturae, 166, 111–120. https://doi.org/10.1016/j.scienta.2013.12.019

Cavagnaro, P. F., & Galmarini, C. R. (2012). Effect of processing and cooking conditions on onion (Allium cepa L.) induced antiplatelet activity and thiosulfinate content. Food & Function, 3(2), 146–156.

Chakraborty, A. J., Uddin, T. M., Matin, Z. B. A., Bakare, S. O., Roje, V., Haque, S., Md. S. Islam, Hossain, M. J., & Matin, P. (2022). Allium cepa: A treasure of bioactive phytochemicals with prospective health benefits. Evidence-Based Complementary and Alternative Medicine, 2022, Article 4586310.

Chen, S., Shen, X., Cheng, S., Li, P., Du, J., Chang, Y., & Meng, H. (2013). Evaluation of garlic cultivars for polyphenolic content and antioxidant properties. Scientia Horticulturae, 150, 120–125.

Cheng, A., Chen, X., Jin, Q., Wang, W., Shi, J., & Liu, Y. (2013). Comparison of phenolic content and antioxidant capacity of red and yellow onions. Journal of Food Science, 78(11), C1701–C1707.

Chounlamany, V., Tanchuling, M. A., & Inoue, T. (2017). Spatial and temporal variation of water quality of a segment of Marikina River using multivariate statistical methods. Journal of Environmental Science and Management, 20(1), 1–10.

Dewanto, V., Wu, X., Adom, K. K., & Liu, R. H. (2002). Thermal processing enhances the nutritional value of sweet corn by increasing total antioxidant activity. Journal of Agricultural and Food Chemistry, 50(10), 3010–3014.

El-Mesery, H. S., & Mwithiga, G. (2011). Mathematical modelling of thin layer drying kinetics of onion slices: Hot-air convection, infrared radiation and combined infrared-convection drying. Advances in Environmental Biology, 5(12), 3742–3752.

El-Mesery, H. S., & Mwithiga, G. (2012). The drying of onion slices in two types of hot-air convective dryers. Journal of Food Process Engineering, 35(3), 445–455.

Gouda, M., Li, X., & Ma, M. (2016). Morphometric and qualitative response of onion (Allium cepa L.) to different processing conditions. Journal of Food Science and Technology, 53(4), 2011–2020.

Gradilla-Hernández, M. S., de Anda, J., Garcia-Gonzalez, A., Meza-Rodríguez, D., Yebra-Montes, C., & Chávez-Almazán, L. A. (2020). Multivariate statistical analysis of water quality in a subtropical lake using the NSF-WQI and a newly proposed ecosystem-specific water quality index. Environmental Monitoring and Assessment, 192(5), Article 265.

Hallmann, E., & Rembiałowska, E. (2006). Comparison of the nutritive value of onion bulbs from organic and conventional cultivation. Journal of Research and Applications in Agricultural Engineering, 51(2), 42–46.

Kalaycıoğlu, Z., Kaygusuz, H., Döker, S., Kolaylı, S., & Erim, F. B. (2017). Characterization of Turkish honeybee pollens by principal component analysis based on their individual organic acids, sugars, minerals, and antioxidant activities. LWT - Food Science and Technology, 84, 402–408.

Karavelioğlu, Z., & Hoca, G. (2022). Antioxidant and anti-proliferative activities of onion (Allium cepa L.) varieties. Journal of Food Measurement and Characterization, 16(1), 1–10.

Kareem, I. (2023). *Effect of Drying of Onion Bulb on the Quality Attributes and Sorption Isotherm of Onion Powder*, An Unpublished PhD. Thesis, Department of Agricultural and Environmental Engineering, Obafemi Awolowo University, Ile-Ife, Nigeria.

Li, X., Zhang, Y., & He, Y. (2016). Rapid detection of water status in grapevine leaves using hyperspectral imaging. Transactions of the ASABE, 59(1), 1–10.

Lim, Y. Y., Lim, T. T., & Tee, J. J. (2006). Antioxidant properties of guava fruit: Comparison with some local fruits. Sunway Academic Journal, 3, 9–20.

Manohar, S., Gidley, M. J., & Sopade, P. A. (2017). Flavonoid content and antioxidant activity of Ontario-grown onions. Journal of Food Composition and Analysis, 56, 1–10.

Moeslinger, T., Friedl, R., Volf, I., Brunner, M., Koller, E., & Spieckermann, P. G. (1994). Spectrophotometric determination of saponins in plant extracts. Journal of Pharmaceutical and Biomedical Analysis, 12(11), 1459–1464.

ISBN: 978-978-8567-02-8

Nencini, C., Menchiari, A., Cavallo, F., & Micheli, L. (2007). Evaluation of antioxidative properties of Allium species growing wild in Italy. Phytotherapy Research, 21(9), 874–878.

Ochar, K., & Kim, S. H. (2023). Green onion (Allium fistulosum): An aromatic vegetable crop esteemed for food, nutritional and therapeutic significance. Foods, 12(24), 4503.

Oyewole, O., Akinyele, B. J., & Akinsanmi, O. A. (2020). Postharvest Losses in Onion Production: Causes, Effects, and Mitigation Strategies. *Journal of Postharvest Technology*, 8(4), 193-204.

Prieto, P., Pineda, M., & Aguilar, M. (1999). Spectrophotometric quantitation of antioxidant capacity through the formation of a phosphomolybdenum complex: Specific application to the determination of vitamin E. Analytical Biochemistry, 269(2), 337–341.

Raimondi, G., Maggio, A., Arpino, M. L., De Pascale, S., & Barbieri, G. (2017). Genotypic, storage and processing effects on compositional and bioactive components of fresh sprouts. Postharvest Biology and Technology, 124, 1–10.

Ranganna, S. (2005). Handbook of analysis and quality control for fruit and vegetable products (2nd ed.). Tata McGraw-Hill Education.

Rekha, C., Poornima, G., Manasa, M., Abhipsa, V., Devi, J. P., Kumar, H. T. V., & Prashith, K. T. R. (2012). Ascorbic acid, total phenol content and antioxidant activity of fresh juices of four ripe fruits. Journal of Chemical and Pharmaceutical Research, 4(9), 4285–4291.

Roghini, R., & Vijayalakshmi, K. (2018). Phytochemical screening, quantitative analysis of flavonoids and minerals in Allium cepa. International Journal of Pharmaceutical Sciences and Research, 9(3), 1159–1164.

Rosen, R. T., Hiserodt, R. D., Fukuda, E. K., Ruiz, R. J., Zhou, Z., Lech, J., Rosen, S. L., & Hartman, T. G. (2004). The determination of metabolites of garlic in human breath and in the rat using MS/MS techniques. Journal of Nutrition, 134(11), 3176S–3180S.

Salisu, A., Abdullahi, B., Ibrahim, M., Aliyu, R., & Haruna, S. (2019). Mitigation Strategies for Onion Post-Harvest Loss in Arid Regions: A Case Study of Kano State's Desert Front Line. *Journal of Agricultural Innovation and Sustainability,* 7(2), 45-60.

Samec, D., Maretić, M., Lugić, I., Bilušić, T., & Salopek-Sondi, B. (2014). Assessing the authenticity of the white cabbage (Brassica oleracea var. capitata f. alba cv. 'Varaždinski') by molecular and phytochemical markers. Food Chemistry, 143, 211–217.

Samec, D., Piljac-Žegarac, J., Bogović, M., Habjanič, K., & Gruz, J. (2016). Assessment of the differences in the physical, chemical and phytochemical properties of four strawberry cultivars using principal component analysis. Food Chemistry, 194, 828–834.

Santas, J., Almajano, M. P., & Carbó, R. (2008). Organosulfur and phenolic content of garlic (Allium sativum L.) and onion (Allium cepa L.) and its relationship with antioxidant activity. Food Chemistry, 110(4), 861–868. h

Sarafa, A., Joseph, J., Kayode, R., Kolawole, F. (2016). Comparative phytochemical analysis and use of some Nigerian spices. Croatian Journal of Food Science and Technology, 11 (3-4), 145-151.

Sellappan, S., & Akoh, C. C. (2002). Flavonoids and antioxidant capacity of Georgia-grown Vidalia onions. Journal of Agricultural and Food Chemistry, 50(18), 5338–5342.

Sharma, G. P., Verma, R. C., & Pathare, P. B. (2005). Mathematical modeling of infrared radiation thin layer drying of onion slices. Journal of Food Engineering, 71(3), 282–286.

Sharma, K., Assefa, A. D., Kim, S., Ko, E. Y., Lee, E. T., and Park, S. W. (2014). Evaluation of total phenolics, flavonoids and antioxidant activity of 18 Korean onion cultivars: a comparative study. *Journal of the Science of Food and Agriculture*, *94*(8), 1521-1529.

Shima, M., Kaygusuz, H., & Erim, F. B. (2021). Chemometric classification of spices based on their heavy metal contents. Food Analytical Methods, 14, 1–10.

Singh, A., Kumar, A., & Bhat, Z. A. (2019). Post-Harvest Management of Onions: A review. *Agricultural Reviews,* 40(1), 54-64. Sule, B. (2019) Curbing Post Harvest Losses: The Plight of Onion Farmers in Nigeria. https://ageconsearch.umn.edu/record/303594. Retrieved on 10th May,2023

Singh, B. N., Singh, B. R., Singh, R. L., Prakash, D., Singh, D. P., Sarma, B. K., Singh, H. B. (2009). Polyphenolics from various extracts/fractions of red onion (*Allium cepa*) peel with potent antioxidant and antimutagenic activities. *Food and Chemical Toxicology*, 47(6), 1161-1167.

Singh, N., & Rajini, P. S. (2004). Free radical scavenging activity of an aqueous extract of potato peel. Food Chemistry, 85(4), 611–616.

Soto-vargas, V.C., Gonzalez, R.E., Sance, M.M., and Galmarini, C.R. (2016). Organosulfur and phenolic content of garlic (*Allium sativum* L.) and onion (*Allium cepa* L.) and its relationship with antioxidant activity. *Acta Horticulturae*, 1143, 277-290.

Sultana, A., Bhattacharjee, S., Sultana, S., & Asaduzzaman, M. (2020). Effect of drying treatment on nutritional, functional and sensory properties of three varieties of onion powders. Journal of Agriculture and Food Research, 2, 100038.

Viacava, F., & Roura, S. I. (2015). Selection of natural elicitors to enhance bioactive compounds in fresh-cut lettuce using principal component and hierarchical cluster analysis. Postharvest Biology and Technology, 102, 1–10.

Vitaglione, P., Donnarumma, G., Napolitano, A., Galvano, F., Gallo, A., Scalfi, L., & Fogliano, V. (2007). Protocatechuic acid is the major human metabolite of cyanidin-glucosides. Journal of Nutrition, 137(9), 2043–2048.

Wan, X., Wang, W., Liu, J., & Tong, T. (2019). Dietary quercetin and kaempferol: Bioavailability and pharmacology, focusing on cardiovascular diseases. Oxidative Medicine and Cellular Longevity, 2019, Article 2439475.

Yang, J., Chen, H., & Zhao, Y. (2015). Identification of adulterated cocoa powder using chromatographic fingerprints of polysaccharides coupled with principal component analysis. Food Chemistry, 174, 1–10.

Yang, J., Meyers, K. J., Van der Heide, J., and Liu, R. H. (2004). Varietal differences in phenolic content and antioxidant and antiproliferative activities of onions. *Journal of Agriculture and Food Chemistry*, 52, 6787–6793.

Zhao, X. X., Lin, F. J., Li, H., Li, H. B., Wu, D. T., Geng, F., Ma, W., Wang, Y., Miao, B. H., & Deng, W. W. (2021). Recent advances in bioactive compounds, health functions and safety concerns of onion (Allium cepa L.). Frontiers in Nutrition, 8, 669805.

Zheng, Y., Li, Q., Huang, J., Wu, Y., Zhang, H., & Zhang, L. (2018). Screening the cultivar and processing factors based on the flavonoid profiles of dry teas using principal component analysis. Journal of Food Composition and Analysis, 67, 1–10.

ISBN: 978-978-8567-02-8

089-A Systematic Review of Intelligent Surveillance Systems Using Drone Swarm

Zainab .M. Adamu[1*], Hassan .A. Bashir[2], and Amir .A. Bature[2]

[1]*Department of Computer Engineering, University of Maiduguri, Borno*

[2]*Department of Computer Engineering, Bayero University Kano*

Corresponding Author: zainabmbarkindo@unimaid.edu.ng zainabmbarkindo@gmail.com

Abstract: Persistent and escalating insecurity characterized by rampant theft, kidnapping, and vandalization poses a critical challenge in Nigeria, particularly in its northern regions. This deteriorating security landscape necessitates innovative technological solutions. Concurrent advancements in drone technology and machine learning (ML) offer a transformative opportunity through the development of intelligent surveillance systems. This review explores the paradigm of drone swarm surveillance, wherein coordinated fleets of Unmanned Aerial Vehicles (UAVs) operate collaboratively to monitor large, complex areas with greater efficiency, coverage, and resilience than single-drone systems. We examine how integrating machine learning algorithms enables autonomous swarm behaviors, real-time data analysis, and enhanced perceptual capabilities. This synergy allows for advanced functions such as automated detection of suspicious activities, persistent tracking of targets, and predictive threat assessment. The paper synthesizes current research on swarm coordination, perception, and decision-making, highlighting the potential of this technology to address pressing security demands while also considering the operational, ethical, and regulatory challenges inherent in its deployment.

Keywords: Drone swarm, Unmanned Aeriel Vehicles (UAV), Autonomous, Machine Learning

1. INTRODUCTION

Security is an important requirement for survival of human race which greatly affects human daily activities. However most individuals take all possible measures to safeguard their environment, by employing dedicated personnel to keep watch over them and their property (Kommey et al., 2021).

Security is a vital aspect of safeguarding lives and property in the world today; its importance is linked to welfare, education, health, agriculture, and the prevention of threats (Edward et al., 2023). Security can be defined in several ways, including the detection of violence and theft, and it plays a crucial role in highly secured areas and in real-time environments (Uma et al., 2022). Insecurity is increasing in Nigeria, with high rates of theft, kidnapping, and cybercrimes; therefore, advanced security systems must be incorporated.

Surveillance systems constitute a prominent advanced security measure, characterized by the deliberate and systematic observation of activities to gather insights for managing or protecting individuals and assets. Employed by both state and corporate actors, these systems are a critical component of public safety, with technological evolution enabling intelligent platforms capable of real-time data analysis and anomaly detection (Saketh et al., 2023). This progression towards automation defines modern intelligent surveillance systems, which utilize artificial intelligence, computer vision, and sensor technologies to autonomously monitor environments, detect objects, and facilitate rapid response with minimal human intervention.

A commonly used method of security surveillance is the deployment of drones equipped with machine vision technologies to capture videos and images for identifying specific areas or individuals of interest, enhancing real-time situation awareness and safety in targeted environments. The rapid advancements in technology and the increasing demand for surveillance in the modern world have positioned intelligent surveillance systems as highly promising solutions in the realm of security and monitoring. (Saketh et al., 2023). Today, we have digital 'eyes and ears' to gather information, and modern surveillance technologies are part of everyday life. Moreover, even during something as simple as a walk outdoors, technology monitors nearly every detail of our existence.

In the modern world, intelligent surveillance systems are becoming more and more popular due to the increasing demands on security and sophistication of the criminals. Without much or no human involvement, an intelligent surveillance system with multiple drones may automatically monitor and analyze image, video, audio, and other types of surveillance data in a given environment. Monitoring tasks encompass the automatic detection and tracking of objects (such as humans or vehicles), crime prevention, rapid response, and the

ISBN: 978-978-8567-02-8

execution of additional analyses and actions. Signal processing, image processing, sensor devices, computer vision and artificial intelligence (machine learning) techniques play significant role to develop and establish such intelligent surveillance system (Chaware et al., 2025).

2. METHODOLOGY

A systematic approach is employed in this review to identify and analyse recent relevant literature. This systematically identify, evaluate, and synthesize recent academic literature (2018–present) on intelligent surveillance systems leveraging drone swarm technology, focusing on technological architectures, autonomy algorithms, communication protocols, and ethical-regulatory challenges. The studies address swarm intelligence, distributed sensing, algorithmic approaches, cooperative control, machine learning, path planning, or real-time data fusion for surveillance with emphasis on scalability, autonomy and intelligence.

2.1 Overview of Drone Swarm Technology

A drone is an unmanned aircraft, more properly referred to as an unmanned aerial vehicle (UAV) or unmanned aircraft system. At its core, a drone is an aerial robot capable of being operated remotely or functioning autonomously through software-driven flight plans embedded in its systems. These systems work in combination with onboard sensors and Global Positioning System (GPS) technology to navigate and carry out tasks (Sihag et al., 2023).

Drone technology stands as one of the most advanced and innovative solutions today, providing efficient and sustainable methods to address various surveillance challenges compared to traditional approaches (Zandieh et al., 2024). Drones are among the most impactful and rapidly developing technologies, offering a wide range of applications that can address sustainability issues in smart cities and ultimately enhance the quality of life for citizens(Gohari et al., 2022).

UAVs were predominantly associated with the military, initially employed for anti-aircraft target practice, information collection, and, more contentiously, as platforms for weaponry. For military applications, drones can be deployed on missions deemed too risky for human pilots in manned aircraft. On the other hand, civilian drones owned by individuals serve a variety of professional and recreational purposes, such as search and rescue operations, surveillance, traffic monitoring, weather tracking, firefighting, personal use, aerial photography and videography, agricultural activities, and delivery services (Tuğrul, 2023).

A drone swarm often comprises numerous drones operating in unison, exchanging information and coordinating efforts to accomplish a shared goal. All the individual drones operate together in harmony to accomplish tasks through distributed coordination, with each communication transmitted by one drone offering the others real-time updates about their surroundings and their specific roles in the mission (Huda & Moh, 2023). These swarms react to changes in their environment fast and accurately since their directives are based on real-time data. From miniature quad copters to bigger fixed-wing drones, these drones might be of the same or distinct sorts. The power of the swarm is its capacity to work as a cohesive entity, utilizing sophisticated software and swarm intelligence algorithms to perform smoothly and effectively (Zhou et al., 2020)

Drone swarms combine sophisticated computer algorithms with local sensing and communication systems to coordinate multiple drones in achieving a common objective (Alotaibi et al., 2024). They can be managed through various command and control methods, such as preprogrammed missions with specific flight paths, centralized oversight via a ground station or a lead drone, or decentralized control where drones interact and cooperate using shared data (Khalil et al., 2022). More advanced methods of control include swarm intelligence inspired by the collective behaviors of insect colonies and flocks of birds, as well as artificial intelligence techniques to train the drone swarms to respond to new or unexpected situations.

2.2 Review of relevant intelligent surveillance systems using controllers

Model predictive control (MPC) originates from optimal control theory. Its core idea involves using a dynamic model to predict the system's future behavior and then optimizing this prediction to determine the best current control action. Thus, models are fundamental to all MPC implementations. Since the optimal control action relies on the system's initial state, another key principle of MPC is using past measurement data to estimate the most probable initial state (Gurbani et al., 2017).

Erfan A. & Amirhossein N. (2021) designed a Switched Robust Model Predictive Based Controller for UAV Swarm System which investigated the formation decentralized control problem for multi-agent system with leader-follower consensus. MPC controller was used for trajectory tracking of the system and tube MPC theory in order to increase the robustness of the system. The swarm tracks the predefined reference trajectory in an acceptably organized manner while the closed loop multi-agent response is explored in the presence of external bounded disturbances. Hybrid controller is designed for the noted system in order to overcome the external noise effects on path tracking of the closed loop swarm problem. The controller is designed to switch knowingly between the tube MPC and primary conventional MPC controllers. The robustness of switching multi-agent system is considered under unexpected external noises for multi-agent system. The simulation results demonstrate that the solution remains optimal also the proposed control structure can satisfactorily deal with noted external disturbances and noise. The desired trajectory was tracked perfectly after the switches take place in the system and the inner distance between the agents is kept satisfactorily uniform during the flight scenario. Hence, the noted approach

ISBN: 978-978-8567-02-8

improved the robustness capability of the regular MPC controller simultaneously the optimality of the solution is remained intact.

A Robust Backstepping Sliding Mode Controller with Chattering-Free Strategy for a Swarm of Drones by Adeel Zaidi et al (2022). This research worked on developing a robust control system for a swarm of drones operating under external disturbances. The core innovation recommended a chattering-free controller by integrating a fuzzy logic system into the established sliding mode control technique, which typically suffers from discontinuous control signals. Furthermore, the paper utilizes the Backstepping control design technique to manage the formation of the drone group using a leader-follower hierarchy, and the Lyapunov stability theory is employed to ensure the asymptotic stability of the overall system. Ultimately, the research evaluates the successful performance of this integrated control strategy through numerical simulations that demonstrate precise 3D trajectory tracking while maintaining a desired formation among the drones. Future work should develop controllers capable of handling time-varying, non-deterministic disturbances and variable drone payloads.

The research by (Okasha & Kralev, 2022) design and experimental comparison of Proportional–Integral–Derivative (PID), Linear Quadratic Regulator (LQR) and Model Predictive Controller (MPC) Stabilizing Controllers for Parrot Mambo Mini-Drone. The Parrot Mambo mini-drone is a readily available commercial quadrotor platform to understand and analyze the behavior of a quadrotor both in indoor and outdoor applications. This study evaluates the performance of three alternative controllers on a Parrot Mambo mini-drone in an interior environment, including Proportional–Integral–Derivative (PID), Linear Quadratic Regulator (LQR), and Model Predictive Control (MPC). To investigate the controllers' performance, initially, the MATLAB®/Simulink™ environment was considered as the simulation platform. The successful simulation results finally led to the implementation of the controllers in real-time in the Parrot Mambo mini-drone. The simulation reveals MPC surpasses PID and LQR in ensuring the system's stability and robustness and real-time experiment results. Thus, this work makes a contribution by introducing the impact of MPC on this quadrotor platform, such as system stability and robustness, and showing its efficacy over PID and LQR. All three controllers demonstrate similar tracking performance in simulations and experiments. In steady state, the maximal pitch deviation for the PID controller is 0.075 rad, for the LQR, it is 0.025 rad, and for the MPC, it is 0.04 rad. The maximum pitch deviation for the PID-based controller is 0.3 rad after the take-off impulse, 0.06 rad for the LQR, and 0.17 rad for the MPC. A significant discrepancy persists between simulation and experimental results, attributable to inherent uncertainties in the linearized model that could not be resolved through extensive controller parameter tuning. To mitigate this model uncertainty, future work should employ dedicated system identification procedures such as excitation with random signals for statistical parameter estimation or the application of subspace identification methods to derive a more accurate state-space model directly from experimental data.

The work of Amine et al. (2024), which presents a Cascaded Model Predictive Control (MPC) framework designed to enhance the stability and energy efficiency of quadcopter UAVs operating in turbulent mangrove forest environments. The study analyses conventional Proportional-Integral-Derivative (PID) controllers for their linear assumptions and limited performance in real-world, nonlinear scenarios with significant disturbances like wind gusts. To address the computational complexity inherent in applying MPC to a full UAV dynamics model, the authors propose a novel hierarchical control architecture. This system decomposes the control problem into two dedicated MPC schemes: one for translational (position/altitude) control and another for rotational (attitude) control. This cascaded approach manages the multi-variable system more efficiently while explicitly handling operational constraints. Through rigorous simulation and experimental flight tests including complex trajectory tracking and controlled wind disturbance scenarios the research demonstrates the superior efficacy of the MPC framework. Key quantitative findings indicate that MPC provides a 60% improvement in altitude control accuracy and 33% reduction in angle overshoot compared to PID. Furthermore, it achieves stabilization 50–66% faster across all tested parameters. Crucially, the optimized control inputs also enhanced energy efficiency, reducing battery discharge rate fluctuations by approximately ±50 mA, which projects a potential 10–15% extension in operational battery life. The study concludes that the cascaded MPC strategy offers a robust, high-performance solution for autonomous UAV navigation in environmentally challenging settings, excelling in disturbance rejection, trajectory tracking precision, and energy-aware operation. This work underscores MPC's viability as a critical advancement over traditional linear controllers for demanding aerial robotics applications.

Gao et al. (2024) addresses the complex challenge of enabling a swarm of drones to pursue a moving target in a flexible formation under severe operational constraints. The problem is characterized by three major difficulties: the target follows an unknown polynomial trajectory; the drones are modeled as second-order systems with uncertain damping ratios; and the swarm operates under "location denial," meaning agents lack access to their own absolute global positions and cannot communicate directly with the target. To overcome these limitations, the authors propose a novel distributed robust cooperative control protocol. The protocol's architecture is built upon three integrated components: a pseudo drone position estimator, a pseudo target position estimator, and a local Internal Model Control (IMC) law. The core innovation lies in the dual estimation strategy. Each drone runs distributed estimators to reconstruct both its own position and the target's position. Crucially, both estimators share a common, unknown constant bias. By subtracting the target estimate from the self-position estimate, this common bias cancels out, allowing each drone to accurately deduce its relative position to the target without requiring absolute location data or direct target communication. This derived relative position then

ISBN: 978-978-8567-02-8

feeds into a local IMC law, which drives the drone to achieve the desired flexible-configuration formation pursuit while robustly handling the system's parametric uncertainties. The effectiveness of this protocol is rigorously validated through both pure numerical simulation and hardware-in-the-loop (HIL) simulation, confirming its capability for robust swarm pursuit in constrained scenarios. The authors conclude by identifying a key limitation and future research direction: the current protocol assumes a fixed communication network topology with reliable links. Extending this approach to accommodate switching topologies and unreliable communication remains an open and necessary challenge for real-world deployment in dynamic environments.

The work by Yang et al. (2025) introduces a Distributed Model Predictive Control (DMPC) framework for UAV formation flight, with an integrated focus on obstacle avoidance and a novel swarm cooperative capability evaluation system. The authors' core contribution is a dual-function DMPC formulation that combines a formation keeping cost function with an explicit obstacle avoidance function to ensure safe navigation. A significant advancement of their approach is the development of a structured, multi-dimensional evaluation metric to holistically evaluate swarm performance across three key areas: coordination, communication equilibrium, and safety. Simulation results prove the controller's efficacy in maintaining precise formations while dynamically avoiding obstacles. Furthermore, the application of the new evaluation metrics provides critical insights for optimizing swarm behavior. The study specifically shows how strategically changing the obstacle avoidance weight in the control algorithm informed by real-time metric feedback can preserve a perfect safety score (maintained at 1) while preventing excessive degradation in other cooperative metrics such as velocity consistency and position matching. This validates the framework's utility for achieving an optimal trade-off between critical swarm performance objectives.

Kesavan P. et. al (2025) synthesize the state-of-the-art in Model Predictive Control (MPC) for autonomous UAV landings. Their survey provides a structured analysis of the evolution, mathematical foundations, and diverse applications of these control strategies. The authors systematically categorize the existing literature into six primary thematic groups, which include landings on maritime vessels, ground vehicles, and systems incorporating sensor fusion or cooperative control, thereby illustrating the framework's versatility. A key focus is placed on advanced MPC variants, notably nonlinear and learning-based MPC, developed to address critical real-world constraints like external disturbances, computational complexity, and operation in GPS-denied environments. While documenting significant progress, the review critically identifies persistent challenges. These include the need for robust real-time implementation, reliable perception in dynamic scenarios, and scalable coordination for multi-agent landings. To bridge these gaps, the authors advocate for future research directions centered on adaptive, data-driven control architectures that deeply integrate advanced sensing, optimization, and machine learning. Overall, the survey offers a foundational reference for researchers and practitioners aiming to develop next-generation autonomous landing systems capable of safe and efficient operation in complex, real-world conditions. There is need for synergic combination of machine learning, high level intelligence and constrained optimization provides the necessary safety, efficiency, and robustness guarantees.

The 2025 work by Amine et al. presents an optimization strategy for UAV performance in turbulent environments using a cascaded Model Predictive Control (MPC) algorithm, implemented on Pixhawk hardware. The research addresses the practical challenges of controlling quadrotors with coupled position-orientation dynamics, particularly for applications like environmental monitoring in wind-affected mangrove forests, where traditional linear controllers like PID often fail. The study's contribution is structured around three key innovations: the introduction of a hierarchical cascaded MPC framework that decouples translational and rotational dynamics into separate subsystems, thereby reducing the computational burden of a full-state MPC implementation; the development of a control strategy explicitly designed for the unique turbulence of dense mangrove ecosystems; and comprehensive experimental validation through both simulation and hardware-in-the-loop (HIL) flight tests on Pixhawk autopilots under realistic wind conditions. Results demonstrated the framework's superiority over conventional methods. The cascaded MPC achieved significantly lower root-mean-square (RMS) error in trajectory tracking, enhanced overall stability, and exhibited robust disturbance rejection capabilities efficiently countering wind gusts during hovering and maneuvers. These results validate the architecture's robustness, reliability, and real-world applicability for precision autonomous navigation in unpredictable, turbulent environments.

The 2025 work by Gräfe et al. addresses a critical implementation gap in swarm robotics by introducing DMPC-Swarm, a novel Distributed Model Predictive Control (DMPC) methodology designed specifically for nano UAV swarms. While DMPC variants which involve agents solving local optimization problems with coupled anti-collision constraints are theoretically promising for scalable and safe swarm management, their deployment has been hindered by the lack of hardware and communication architectures that support truly distributed computation under strict UAV payload limits. The authors' core contribution is an integrated system that combines a novel DMPC algorithm with a tailored, stateless low-power wireless communication protocol called Mixer. This protocol employs a synchronized many-to-all communication structure, robust to rapid motion, to facilitate the necessary information exchange. To circumvent the computational constraints of nano-UAVs, DMPC-Swarm utilizes an event-triggered, distributed off-board computing model, maintaining scalability and fault tolerance. Crucially, the methodology is theoretically proven to guarantee collision avoidance even under realistic conditions of communication delays and message loss. The research is

ISBN: 978-978-8567-02-8

validated by the first known hardware realization of this DMPC variant on a distributed physical system: a swarm of 16 nano-quadcopters interconnected by a real wireless mesh network. This demonstrates a significant advance from simulation to practical deployment, though the work notes the inherent complexity of defining and tracking dynamic neighborhoods in fast-moving swarms, a challenge for both algorithm design and theoretical analysis.

2.3 Meta-heuristic Optimization and Cooperative Control for Autonomous UAV Swarm

The work by (Zhou et al., 2020) wrote a survey on recent advancements and future trends in UAV swarm intelligence. They presented a hierarchical framework for understanding UAV swarm intelligence, dividing it into five layers which include decision-making, path planning, control, communication, and application. Each layer's functionalities, current research, and future challenges are explored, having an insight into the latest technologies and potential limitations of UAV swarm intelligence to facilitate further research. UAV cluster path planning should ensure that the UAV cluster can evade obstacles and avoid collisions between the single machines through the achievement of the task, and also ensure the optimal global path and the shortest time to complete the task. During the path planning process, most research treats the drone as a point mass, ignoring its size and load, which simplifies the modeling procedure, making it more idealized and reliant on sampling. Future modeling efforts should incorporate constraints to improve the realism of simulations and strengthen the robustness of real-world control systems. In addition, most of the current task planning methods are planned at single or specific conflict situations and lack a holistic system solution for an integrated task environment and increase the response speed to the close range. Models should also consider the influence of wind.

The work by (Martellucci et al., 2021) proposed the use of swarms of drones equipped with various chemical sensors to detect and map the dispersal of hazardous substances, particularly in large areas affected by CBRNe (Chemical Biological Radiological Nuclear Explosive) events. The main idea centers on overcoming restrictions of single-drone approaches and traditional ground-based systems by leveraging the collective sensing power of a drone swarm. The different drone configurations and sensor technologies (including low-cost options like MOX sensors), and exploring the integration of advanced algorithms (like those inspired by chemotaxis and anemotaxis) for plume detection, tracking, and source identification. Ultimately, the research aimed in creating a more efficient, cost-effective, and safe system for monitoring and responding to chemical releases, using simulation and real-world testing within the Robot Operating System (ROS) framework by protecting human beings from direct contact with hazardous chemicals. Their research area of application was designed to use swarms of drone for detection and mapping the dispersal of hazardous substances only.

Saketh et al., (2023) developed and implemented an Intelligent Surveillance Support System (ISSS) as a cutting-edge software solution designed for real-time monitoring and analysis of security footage, enabling the detection and identification of potential threats. This utilizes computer vision techniques, primarily leveraging the OpenCV library and algorithms like Local Binary Pattern Histogram (LBPH) and Haar cascading, to achieve real-time functionalities. These functionalities include motion detection, noise detection, visitor entry/exit tracking, theft detection (object removal), and facial recognition with approximately 95% accuracy. The Intelligent Surveillance Support System is an innovative solution for advanced video surveillance influencing the power of computer vision using OpenCV which provides unparalleled proficiencies that far exceed those of traditional systems. This system offers a highly sophisticated level of security that can preserve any environment safety and security with its innovative motion detection, theft detection, facial recognition, and in–out movement tracking. There is need for incorporation of Advanced AI Algorithms, Multi-camera incorporation and behavioral Analysis for improved surveillance system.

The research by (Athira et al., 2024) presented a novel approach to optimizing the routes of UAV swarms by introducing the Ant Colony Optimization- Dynamic Traveling Salesman Problem (ACO-DTSP) algorithm, a variation of Ant Colony Optimization specifically designed to handle workload constraints and dynamic environments. The authors address the challenge of minimizing task completion time while respecting the limited capacity of both individual drones and the target locations. To validate their method, they compare its performance against existing routing algorithms, demonstrating that ACO-DTSP offers significant improvements in time efficiency, making it potentially suitable for real-time applications. The study highlights the significance of intelligent routing strategies for efficient drone swarm operations and proposes future improvements through hardware implementation and advanced algorithmic development. It advocates for exploring the integration of machine learning and Ant Colony Optimization (ACO) to improve decision-making and adaptability in dynamic environments. Future efforts will involve a comprehensive evaluation of performance, taking into account critical factors like energy consumption and battery life.

2.4 Machine Learning and Intelligent Control for Surveillance Systems

Machine learning is one of the recent methods used to classify and identify potential threats based on historical data. Some of the best machine learning algorithms used for threat detection include Support Vector Machines (SVMs), Decision Trees, Neural Networks, Logistic Regression, and Anomaly Detection algorithms as they surpass at identifying patterns and anomalies in large datasets, allowing them to detect suspicious behavior that might indicate a cyber-threat.

Ahn et al., (2019) presents a novel machine learning-based system for anomaly detection in swarms of drones. The system addresses the current reliance on manual visual monitoring by employing a two-step process: first, unsupervised learning techniques (PCA and K-means clustering) reduce data dimensionality and pre-label flight data as normal or anomalous; then, a supervised

ISBN: 978-978-8567-02-8

deep neural network (1D-CNN and multi-layer perceptron) classifies real-time flight data as normal or anomalous with high accuracy. The technique was authenticated using real flight test data, indicating its efficiency for online irregularity monitoring and improving safety and reliability in swarm drone operations. The method consists of two primary steps: the labeling step, which assigns labels to unlabeled data using lower-dimensional features, and the binary classification step, which utilizes a one-dimensional convolutional neural network with a cross-entropy loss function. The deep neural network is trained and validated using real flight test data. Additionally, the moving horizon-based monitoring classification step, utilizing a one-dimensional convolutional neural network with cross-entropy loss, has been shown to effectively reduce noise interference during real-time anomaly monitoring. It is limited to identification of anomalies within a swarm of drone, therefore there is need for integration of anomaly monitoring and resolving in the overall surveillance system of swarm drones and other areas.

Ahn et al., (2019) broadly reviews the use of UAV swarms in unmanned farms. It begins by examining different UAV swarm control methods, categorizing them by task assignment, trajectory planning, communication, and visual navigation approaches, emphasizing the strengths and weaknesses of each. This examines the application of these methods throughout the four key stages of agricultural production, cultivation, planting, management, and harvesting while identifying appropriate control strategies for each stage. The UAV swarm has challenges currently limiting the widespread adoption in agriculture, such as limited application scenarios, insufficient intelligence, and insufficient hardware and software support. This research autonomy of UAV swarms in farming limited for agricultural production needs to enhance its intelligence and smart agricultural technologies to prevent manual operations.

Guerber et al., (2021) explores a novel combination of Software Defined Networking (SDN) and machine learning to secure communication in drone swarms. It addresses two main attack vectors: external intrusions and internal attacks from compromised drones. The authors leverage SDN's centralized control for external attack mitigation, demonstrating its robustness against common external attacks. A machine learning solution based on a Random Forest Classifier is used for internal attack, while utilizing flow formation events and custom features to detect malevolent activities like denial-of-service and brute-force attacks. The proficient detection performance of this approach, demonstrated through experiments and a new dataset derived from existing intrusion detection system data, highlights its potential for enhancing drone swarm security.

Gohari et al., (2022) wrote a systematic review article examining the use of surveillance drones in smart cities. A comprehensive literature review was conducted evaluating 43 studies published up to August 2021 from Scopus and Web of Science, to explore the applications, models, and characteristics of drones used for surveillance in various domains within smart cities. The significant application areas identified were transportation and environmental monitoring emerging as leading themes. The review emphasizes the evolving nature of this research area and demonstrates that utilizing single or multiple UAVs, either independently or in combination with other technologies (such as the Internet of Things, wireless sensor networks, convolutional neural networks, artificial intelligence, machine learning, computer vision, cloud computing, and web applications), can provide more efficient and sustainable solutions compared to traditional surveillance methods.

The research by (Hussein & Nouacer, 2022) proposed a new reference architecture for Unmanned Aerial Systems (UAS), or drones. It addresses the limitations of existing drone architectures by providing a comprehensive framework that considers all key functional blocks and their interactions, unlike previous efforts which focused on only specific aspects (e.g., control, planning, or safety). The architecture is systematized into four main groups namely flight navigation, flight control, flight management, and mission management, and details of specific requirements and building blocks within each group. The authors also verified how the architecture can be modified for diverse stages of drone autonomy, ranging from remotely piloted to semi-autonomous systems. Ultimately, the aim was to simplify and standardize the development of safer and more autonomous drone systems.

Also (Qamar et al., 2022) developed and tested a novel deep reinforcement l earning framework for autonomous drone swarm navigation and multi-target tracking. The framework, termed Island Policy-Based Optimization Framework (IPOF), uses a customized policy-based deep reinforcement learning approach to enable a drone swarm to navigate complex 3D environments with static and dynamic obstacles while tracking multiple targets. Key advancements feature innovative reward functions designed to ensure strong swarm formation and effective target tracking, along with a dynamic swarm management system that allows the swarm to divide into sub-swarms, facilitating the tracking of multiple targets located at significant distances from each other. Also, these sub swarms have the capability to reconnect and thus form a single swarm surrounding all the targets when multiple targets come nearby. The effectiveness of Island policy-based optimization frame work (IPOF), compared to existing algorithms like Proximal Policy Optimization (PPO), Truly Proximal Policy Optimization (TPPO), and Soft Actor-Critic (SAC), is demonstrated through simulations in Unity3D, showcasing its ability to handle challenging scenarios involving multiple dynamic targets, obstacles, and realistic environmental factors such as gravity and drag. The findings demonstrate that the proposed strategy improves swarm navigation by attaining a high cumulative reward and minimal policy loss, enabling efficient tracking of multiple static and dynamic targets in complex environments. This method can be expanded for real-world swarm applications, such as search and rescue operations, food delivery, and more. It can also be utilized in counter-terrorism efforts, for example, by tracking terrorist vehicles and conducting autonomous strikes on their bases. Additionally, it can function as a

ISBN: 978-978-8567-02-8

hovering swarm to either safeguard an entity or prevent it from moving. When targets share equal priority, the swarm exhibits suboptimal performance, indicating a gap in decision-making logic that requires refinement. The simulations overlook critical environmental challenges, including wind interference, latency in communication, and sensor inaccuracies.

Um a et al., (2022) explores the application of deep learning to create a smart surveillance system which addresses the challenges of handling the enormous amounts of data generated by CCTV cameras, focusing on real-time face detection and recognition as a core functionality. The paper proposes a system that employs deep learning techniques to enhance security, especially in high-security zones containing highly sensitive data, by autonomously monitoring and detecting unauthorized entry into restricted areas without the need for human intervention. The system is based on facial analysis and recognition which detects and identifies unauthorized individuals in confidential areas in industries. Their goal is to improve upon traditional surveillance methods through improved accuracy and efficiency by limiting the theft happening in future and maximize the protection of data in extremely confidential region.

Maktoof et al., (2023) proposed a Machine Learning-assisted Intelligent Video Surveillance System (ML-IVSS) for abnormal behavior detection in smart cities. The system leverages intelligent fusion techniques, combining pedestrian tracking, motion detection, and machine learning algorithms specifically, a dual-stream Convolutional Neural Network (CNN) to achieve highly accurate and efficient detection accuracy while reducing costs. The model's architecture was detailed including feature extraction using optical flow analysis and a modified loss function to address class imbalance. Extensive simulations showed significant performance improvements (over 95% precision, recall, accuracy, and F1-score) compared to present methods, highlighting the potential of ML-IVSS for enhancing public safety and security in smart city environments. The method employed spatiotemporal data and motion information more proficiently by limiting feature extraction to the space-time volume around trajectories, resulting in better performance. The simulation study demonstrates enhanced outcomes when the proposed ML-IVSS model is compared to other commonly used methods, achieving high abnormal behavior detection rate of 98.8%, a prediction rate of 97.4%, an accuracy rate of 96.9%, an F1-score of 97.1%, a precision rate of 95.6%, and a recall rate of 96.2%.

The study by (Edward et al., 2023) designed and implemented a smart surveillance system leveraging machine learning and computer vision which purposes to shift the security paradigm from reactive investigation to proactive prevention by automatically detecting and alerting to potential threats such as intrusion, theft, and unusual activity. These was achieved through several modules, including object detection, facial recognition, noise detection, and visitor monitoring, using Python and machine learning algorithms. The objective is to recognize faces, study them, and decide whether they resemble saved faces that are kept in the database (which comprises pre-encoded training faces). It also checks for any moves in the picture, and if any suspicious activities spotted the authorities will be alerted. However, reducing the cost of running a surveillance facility and enhancing security continue to be challenging tasks, as current computer vision research still faces difficulties with occlusion, varied lighting condition and real time surveillance.

The work by (Alqudsi & Makaraci, 2025) on "UAV swarms: research, challenges, and future directions," provides a comprehensive overview of UAV swarms, highlighting their potential as a transformative technology in aerial robotics. The authors explore the infrastructure and key features of these swarms, delving into essential aspects like coordinated path planning, task assignment, and formation control. The paper also examines the integration of artificial intelligence and machine learning in enhancing swarm capabilities and discusses diverse applications across civilian and military domains. This paper has provided a perceptive exploration of various aspects of swarm robotics applied to flying robots, shedding light on critical features, core algorithms, and their real-world applications. The recent state of research in swarm robotics for flying robots has proved promising improvements with important potential for various industries, such as agriculture, search and rescue (SAR), environmental monitoring, and infrastructure inspection. They identify the need to necessary unlock the full potential of Swarm Robotics in flying robots, focusing on robust control algorithms, adaptive formation changes, and energy efficiency, integrating advanced and energy-efficient AI and ML techniques will elevate swarm decision-making capabilities.

TABLE I: MODEL PREDICTIVE CONTROL & ADVANCED CONTROLLERS

Study (Authors, Year)	Control Method/ Algorithm	Objective	Contributions
Erfan A. & Amirhossein N. (2021)	Switched Robust MPC (Tube MPC + Conventional MPC)	Decentralized formation control & trajectory tracking for UAV swarms	The hybrid controller switches between tube MPC and conventional MPC to maintain optimality and enhance robustness against bounded external disturbances, ensuring uniform inter-agent distances.
Okasha & Kralev (2022	Comparative study of PID, LQR, and MPC	Stabilization and control of a Parrot Mambo mini-drone	Real-time experiments showed MPC provided superior stability and robustness over PID and LQR, though a performance gap between simulation and experiment highlighted model uncertainty challenges.
Amine et al. (2024)	Cascaded MPC (separate translational	Stability and energy efficiency for quadcopters	The hierarchical MPC framework improved altitude control accuracy by

ISBN: 978-978-8567-02-8

	& rotational controllers)	in turbulent environments (e.g., mangrove forests)	60%, reduced angle overshoot by 33%, stabilized 50–66% faster than PID, and extended projected battery life by 10–15%.
Gao et al. (2024)	Distributed robust cooperative control with dual estimators	Pursuit of a moving target by a drone swarm under "location denial" constraints	Drones used local estimators to deduce relative target position without global data or direct target communication, validated in hardware-in-the-loop simulations. Requires fixed communication topology.
Yang et al. (2025)	Distributed MPC (DMPC) with integrated obstacle avoidance	UAV formation flight with cooperative capability evaluation	The DMPC combined formation-keeping and obstacle avoidance. A novel multi-dimensional evaluation system (coordination, communication, safety) enabled real-time trade-off optimization for swarm behavior.
Gräfe et al. (2025)	**DMPC-Swarm** (Distributed MPC with event-triggering)	Scalable, safe control for nano-UAV swarms with collision avoidance	Integrated a novel DMPC algorithm with a low-power wireless protocol (Mixer). Demonstrated on a physical swarm of 16 nano-drones, guaranteeing collision avoidance despite delays and message loss.

TABLE II: METAHEURISTIC OPTIMIZATION & MACHINE LEARNING

Study (Authors, Year)	Control Method/ Algorithm	Objective	Contributions
Ahn et al. (2019)	Unsupervised learning (PCA, K-means) + Supervised Deep Neural Network (1D-CNN)	Anomaly detection within a swarm of drones	A two-step ML process achieved high-accuracy real-time classification of normal vs. anomalous flight data, enabling online monitoring to improve swarm safety and reliability.
Guerber et al. (2021)	Software-Defined Networking (SDN) + Machine Learning (Random Forest Classifier)	Securing drone swarm communication against external and internal attacks	Combined SDN's centralized control for external threats with an ML classifier for detecting internal attacks (e.g., DoS), demonstrating proficient detection performance.
Qamar et al. (2022)	Deep Reinforcement Learning (Island Policy-Based Optimization Framework - IPOF)	Autonomous swarm navigation & multi-target tracking in complex 3D environments	The framework allowed dynamic swarm splitting/merging for multi-target tracking and outperformed algorithms like PPO and SAC in simulations, though it overlooked environmental challenges like wind.
Maktoof et al. (2023)	Machine Learning-assisted Intelligent Video Surveillance (Dual-stream CNN)	Abnormal behavior detection in smart city environments	The ML-IVSS model achieved high detection rates (over 95% across precision, recall, accuracy, F1-score) by fusing pedestrian tracking, motion detection, and spatiotemporal data efficiently.
Athira et al. (2024)	Ant Colony Optimization - Dynamic Traveling Salesman Problem (ACO-DTSP)	Optimizing routes for UAV swarms with workload constraints in dynamic environments	The ACO-DTSP variant demonstrated significant improvements in time efficiency for task completion compared to existing routing algorithms, suitable for real-time applications.

3. CHALLENGES AND FUTURE DIRECTIONS

Challenges

1. The absence of standardized benchmarking frameworks and rigorous comparative analyses. This deficit precludes a quantitative, evidence-based evaluation of diverse Model Predictive Control (MPC) strategies under consistent, operationally-relevant constraints, thereby impeding principled guidance for selecting optimal controller variants particularly advanced nonlinear, learning-based, or cooperative formulations for targeted UAV landing applications.
2. These include the need for robust real-time implementation, reliable perception in dynamic scenarios, and scalable coordination for multi-agent landings.
3. A core limitation of the current approach is the persistent and significant performance gap between simulation and experimental results. This discrepancy stems from fundamental uncertainties in the linearized system model, which remain unaddressed by conventional controller tuning. The reliance on an insufficiently accurate model inherently restricts the controller's real-world efficacy and predictive reliability.

Future Directions

1. Extending the proposed methodology to address switching topologies and unreliable communication links was identified as a critical future direction. Overcoming this challenge is essential for the practical application of the approach in dynamic real-world settings.
2. Future research directions centered on adaptive, data-driven control architectures that deeply integrate advanced sensing, optimization, and machine learning.

ISBN: 978-978-8567-02-8

4. CONCLUSION

The field of intelligent surveillance using UAV swarms is rapidly advancing, driven by the convergence of optimal control theory, optimization algorithms, and artificial intelligence. While current research provides a robust foundation demonstrating significant performance gains over conventional methods, the next frontier lies in creating seamlessly integrated, robust, and efficient systems capable of reliable and autonomous operation in the unpredictable and complex conditions of the real world. The continued synthesis of these technological strands MPC-based control, intelligent optimization, and machine learning embraces the key to unlocking the full potential of autonomous swarm systems for surveillance and beyond.

ACKNOWLEDGMENT

I Author wishes to acknowledge the support of Tertiary Education Trust Fund (TETFund) for sponsoring part of the research, University of Maiduguri and Bayero University Kano for their support.

REFERENCES

Ahn, H., Choi, H. L., Kang, M., & Moon, S. T. (2019). Learning-based anomaly detection and monitoring for swarm drone flights. *Applied Sciences (Switzerland)*, *9*(24). https://doi.org/10.3390/app9245477

Alotaibi, A., Chatwin, C., & Birch, P. (2024). *A Secure Communication Framework for Drone Swarms in Autonomous Surveillance Operations*. 1–25. https://doi.org/10.4236/jcc.2024.1211001

Alqudsi, Y., & Makaraci, M. (2025). UAV swarms: research, challenges, and future directions. *Journal of Engineering and Applied Science*, *72*(1). https://doi.org/10.1186/s44147-025-00582-3

Athira, K. A., Yalavarthia, R., Saisandeepa, T., Harshitha, K. S. S., Shaa, A., & Udayan, D. J. (2024). ACO-DTSP Algorithm: Optimizing UAV Swarm Routes with Workload Constraints. *Procedia Computer Science*, *235*, 163–172. https://doi.org/10.1016/j.procs.2024.04.019

Chaware, P., Dhamdhere, V., Sawane, M., Patil, S., Sarode, P., & Ukey, K. (2025). *Development of Intelligent Video Surveillance System Using Deep Learning and Convolutional Neural Networks : A Proactive Security Solution †*. 1–13.

Edward, A. S., Jothimani, A., Akila, V., & Vaishali, D. (2023). Smart surveillance system using emotion detection. *AIP Conference Proceedings*, *2427*(5), 694–701. https://doi.org/10.1063/5.0101146

Gohari, A., Ahmad, A. Bin, Rahim, R. B. A., Supa'at, A. S. M., Razak, S. A., & Gismalla, M. S. M. (2022). Involvement of Surveillance Drones in Smart Cities: A Systematic Review. *IEEE Access*, *10*, 56611–56628. https://doi.org/10.1109/ACCESS.2022.3177904

Guerber, C., Royer, M., & Larrieu, N. (2021). Machine Learning and Software Defined Network to secure communications in a swarm of drones. *Journal of Information Security and Applications*, *61*, 1–50. https://doi.org/10.1016/j.jisa.2021.102940

Gurbani, V. K., Loreto, S., & Subramanyan, R. (2017). Design and implementation. In *IEEE Communications Magazine* (Vol. 55, Issue 4). https://doi.org/10.1109/MCOM.2017.7901486

Huda, S. M. A., & Moh, S. (2023). Deep Reinforcement Learning-Based Computation Offloading in UAV Swarm-Enabled Edge Computing for Surveillance Applications. *IEEE Access*, *11*(June), 68269–68285. https://doi.org/10.1109/ACCESS.2023.3292938

Hussein, M., & Nouacer, R. (2022). Reference architecture specification for drone systems. *Microprocessors and Microsystems*, *95*. https://doi.org/10.1016/j.micpro.2022.104705

Khalil, H., Rahman, S. U., Ullah, I., Khan, I., & Alghadhban, A. J. (2022). *A UAV-Swarm-Communication Model Using a Machine-Learning Approach for Search-and-Rescue Applications*.

Kommey, B., Kotey, S., Tutu, E., & Opoku, D. (2021). *PRIVATE SECURITY SURVEILLANCE SYSTEM Journal of Engineering Studies and Research – Volume 27 (2021) No . 2*. *27*(2), 39–50.

Maktoof, M. A. J., Ibraheem, H. M., Razzaq, M. A. A., Abbas, A., & Majdi, A. (2023). Machine learning-based intelligent video surveillance in smart city framework. *Fusion: Practice and Applications*, *11*(2), 35–47. https://doi.org/10.54216/FPA.110203

Martellucci, L., Chierici, A., Di Giovanni, D., Fumian, F., Malizia, A., & Gaudio, P. (2021). Drones and sensors ecosystem to maximise the "storm effects" in case of cbrne dispersion in large geographic areas. *International Journal of Safety and Security Engineering*, *11*(4), 377–386. https://doi.org/10.18280/ijsse.110411

Okasha, M., & Kralev, J. (2022). *Design and Experimental Comparison of PID , LQR and MPC Stabilizing Controllers for Parrot Mambo Mini-Drone*.

Qamar, S., Khan, S. H., Arshad, M. A., Qamar, M., Gwak, J., & Khan, A. (2022). Autonomous Drone Swarm Navigation and Multitarget Tracking With Island Policy-Based Optimization Framework. *IEEE Access*, *10*(July), 91073–91091. https://doi.org/10.1109/ACCESS.2022.3202208

Saketh, M., Nandal, N., Tanwar, R., & Reddy, B. P. (2023). Intelligent surveillance support system. *Discover Internet of Things*, *3*(1). https://doi.org/10.1007/s43926-023-00039-0

Sihag, V., Choudhary, G., Choudhary, P., & Dragoni, N. (2023). Cyber4Drone: A Systematic Review of Cyber Security and Forensics in Next-Generation Drones. *Drones*, *7*(7), 1–29. https://doi.org/10.3390/drones7070430

Tuğrul, K. M. (2023). Drone Technologies and Applications. In *IntechOpen* (pp. 1–24).

Uma, K. V., Aakash, V., & Deisy, C. (2022). Smart surveillance system using deep learning approaches. *Handbook of Research on Computer Vision and Image Processing in the Deep Learning Era*, *22*(3), 92–114.

ISBN: 978-978-8567-02-8

https://doi.org/10.4018/978-1-7998-8892-5.ch006
Zandieh, F., Ghannadpour, S. F., & Mazdeh, M. M. (2024). New integrated routing and surveillance model with drones and charging station considerations. *European Journal of Operational Research*, *313*(2), 527–547. https://doi.org/10.1016/j.ejor.2023.08.035
Zhou, Y., Rao, B., & Wang, W. (2020). UAV swarm intelligence: Recent advances and future trends. *IEEE Access*, *8*, 183856–183878. https://doi.org/10.1109/ACCESS.2020.3028865

ISBN: 978-978-8567-02-8

Addendum

ISBN: 978-978-8567-02-8

5TH Faculty of Engineering Conference on Engineering Innovation and Economic Policies: Driving Sustainable Industrial Growth in Nigeria

Faculty of Engineering, Bayero University, Kano.

028-Prediction Of Anxiety Disorder in Working Class Students Using Enhanced Machine Learning Algorithms

UMAR, Sani Alkali[1], ABISOYE, Opeyemi A.[2]
Department of Computer Science Federal University of technology Minna, Niger state Nigeria[1,2]
Umar.alkali@futminna.edu.ng, o.abisoye@futminna.edu.ng.

Abstract: anxiety disorder is a mental health condition that affects millions of people worldwide and it make more impact among working-class students due to academic and work stress. Early detection of anxiety is important for easy intervention; the traditional diagnostic methods often fail due to the complex and subjective nature of the symptoms. This study includes a machine learning-based approach to predict anxiety disorder using five classification algorithms: Random Forest (RF), Light Gradient Boosting Machine (LightGBM), Support Vector Machine (SVM), Naïve Bayes (NB), and Decision Tree (DT). To enhance model accuracy and efficiency, Particle Swarm Optimization (PSO) was used for feature selection and hyperparameter tuning. Dataset obtained from Kaggle repository was used, it contains over 140,000 instances with 110 features spanning demographic, academic, and psychological dimensions. Exploratory Data Analysis (EDA) revealed strong associations between anxiety and factors such as work pressure, financial stress, and study satisfaction. PSO identified the most relevant 14 features, improving model interpretability and performance. Among the models evaluated, the PSO-optimized Random Forest achieved the highest accuracy (99%), followed by Decision Tree (97.3%), LightGBM (94.8%), and Naïve Bayes (88.1%). The results confirm that tree-based ensemble methods, particularly when combined with PSO, offer best solutions for anxiety prediction. This research contributes to the field of medical informatics by providing an efficient approach to predict anxiety disorder using AI. The study's findings can help in development of real-time diagnostic tools to aid clinicians and support early interventions in mental health care.

1. INTRODUCTION

Anxiety Disorder (AD) is one of the most common types of Mental Disorders (MD). They constitute the largest group of mental disorders with a high societal and individual burden. Anxiety is identified as an emotional integrity factor of the individual that is characterized by high complexity. Anxiety is not the same as fear, but they are frequently utilized. Anxiety is considered a future-oriented, long-acting reaction broadly centered on a diffuse danger, while fear is a suitable, present-oriented, and short-lived reaction to an identifiable and particular risk. In accordance with the Diagnostic and Statistical Manual of Mental Disorders, anxiety disorders include disorders that share features of excessive fear and related behavioral disturbances (Pintelas et al., 2018). The symptoms of GAD (Generalized Anxiety Disorder) are irritability, nervousness, fatigue, insomnia, gastro intestinal problems, panic, and a sense of impending danger, increased heart rate, sweating, rapid breathing and difficulty concentrating (Priya et al. 2020). In addition, we are becoming ambitious nowadays and seek every opportunity to grow professionally. Anxiety, depression, stress, frustration and dissatisfaction have become so commonplace that people now believe them to be part and parcel of professional life. Depression is the most prevalent mental disorder affecting more than 300 million people worldwide (WHO, 2017), and the severity of the issue has led many health researchers to focus their studies in this area. Differentiating anxiety, depression and stress from one another is problematic for machines; hence, an appropriate learning algorithm is required for an accurate diagnosis (Priya et al. 2020).

In Nigeria, a country that faces its unique set of challenges such as price hike on goods and services, economic hardship, and uncertainty about the future contribute to rising levels of anxiety among people, millions of its citizens suffer from various mental disorders. 20% of Nigerians, or around 40 million people, are affected by mental illness (WHO, 2017), the impact of these illnesses extends beyond the individual, with healthcare workers, bankers, and even teachers also affected with almost 70% of teachers experiencing psychological distress (Temitope et al, 2024). However, as we transit into a post-COVID-19 era, technology presents new opportunities to address these mental health issues and improve life expectancy. It is widely recognized that technology has played a crucial role in addressing various challenges during the COVID-19 pandemic and has the potential to continue making a positive effect within the post-COVID-19 time. Technology can facilitate social connections and combat

ISBN: 978-978-8567-02-8

loneliness and isolation, which are factors that can impact mental health and well-being. Moreover, Digital platforms and AI have the potential to improve access to mental wellbeing administrations and bolster, especially in remote or underserved areas. The development of digital health solutions and telemedicine has expanded access to healthcare services, including mental health support (Ezeamii et al., 2024). Furthermore, this research predicts anxiety disorder in working class students using Machine Learning (ML). ML is a subset of Artificial Intelligence (AI) which offers a solution for the early prediction of mental disorders. Its ability to analyze complex patterns across large datasets can assist in identifying individuals at risk of anxiety. Algorithms such as Random Forest (RF), Light Gradient Boost (LGB), Support Vector Machine (SVM), Naïve Bayes (NB), Decision Tree (DT) and use Particle Swarm Optimization (PSO) to optimizing parameters, selecting features. However, despite the widespread impact of anxiety disorder on students' academic performance and overall wellbeing. Anxiety deteriorates human health and leads to death if untreated. Current diagnostic methods are often manual, delayed and can be imprecise. The challenge is further complicated by the multidomain nature of mental health data, which can be difficult to interpret without advanced analytical tools (Ezeamii et al., 2024). It is imperative to address this critical issue and explore innovative solutions that leverage Artificial Intelligence (AI) for assessment of anxiety. By doing so, this research aims to improve early detection, and intervention for anxiety disorders, ultimately mitigating the factors contributing to the decline in life expectancy. Notwithstanding clear concerns, AI applications in medication are relentlessly expanding (Graham et al., 2020). In conclusion there is a need for automated methods that can assist in early detection of individuals with risk of anxiety disorder. Machine learning offers a powerful alternative, but model effectiveness depends on accurate feature selection and parameter optimization. This research work seeks to address these challenges by using PSO to enhance Machine learning models.

2. METHODOLOGY

This research used machine learning algorithms to predict anxiety based on historical health data. The study involves the following steps: data collection, data preprocessing, model implementation, model evaluation, and comparison. Data preprocessing is critical to ensure the quality and reliability of the dataset. The following steps will be undertaken: Data Cleaning: Handling missing values through imputation or deletion, and correcting any inconsistencies in the data (Salvador, et al. 2015). Normalization: Scaling numerical features to a standard range to ensure that they contribute equally to the model (Gopalet al. 2015). Feature Selection: Identifying the most relevant features for Anxiety prediction using techniques such as correlation analysis and Principal Component Analysis (PCA) (Jollifeet al. 2016). Moreover, data preparation is a crucial step in ensuring high-quality inputs for machine learning models. To facilitate the data analysis and machine learning processes, essential Python libraries were imported. Pandas and NumPy were used for handling and manipulating structured datasets, while Scikit-learn provided preprocessing, feature selection, and model evaluation tools. Seaborn and Matplotlib were employed for exploratory data analysis and visualization, ensuring a comprehensive understanding of dataset distributions and trends.

The dataset used in this study comprises 140,000 rows and 110 columns, covering demographic, academic, and psychological attributes. The dataset was loaded into a Pandas DataFrame, where initial exploratory steps such as checking for missing values, duplicates, and incorrect data types were performed. Before proceeding with transformations, a preliminary assessment was conducted to determine the nature and distribution of each feature. The dataset's shape and column information were printed to identify potential inconsistencies. The dataset was examined for inconsistencies using a heatmap, and missing values were found in multiple columns, particularly in Academic Pressure, Work Pressure, CGPA, and Study Satisfaction. Exploratory Data Analysis (EDA) was performed to understand the statistical properties and relationships within the dataset. Numerical features such as Age, CGPA, and Work/Study Hours were visualized using histograms to observe their distributions, most numerical variables were found to follow a normal distribution, with minor skewness in Academic Pressure and Financial Stress. A heatmap of

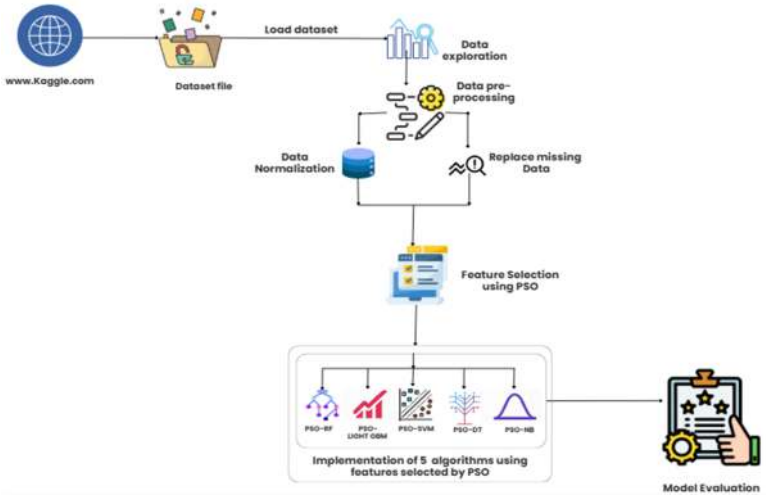


Figure 2: Diagrammatic Representation of Research Design

ISBN: 978-978-8567-02-8

missing values was generated, showing a significant number of missing entries in Academic Pressure and CGPA.

Figure 2 illustrates the overall research design workflow, starting with obtaining data from the Kaggle repository and followed by initial data loading and exploratory analysis. The next stage involves data preprocessing, which including normalization and handling of missing values to ensure data quality. After that, Particle Swarm Optimization (PSO) is applied for feature selection to identify the most relevant features for the predictive models. Using the feature selected, five enhanced machine learning models are trained: Particle Swarm Optimization-Random Forest (PSO-RF), Particle Swarm Optimization-LightGBM (PSO-LightGBM), Particle Swarm Optimization-Support Vector Machine (PSO-SVM), Particle Swarm Optimization-Decision Tree (PSO-DT), and Particle Swarm Optimization-Naïve Bayes (PSO-NB). Finally, the trained models are evaluated using appropriate metrics to assess their predictive accuracy and generalization performance

.

3 RESULT

The aims of this paper is to predict anxiety using Particle Swarm Optimization (PSO) for parameter and feature selection combined with machine learning algorithms. This paper discusses the performance metrics obtained from five machine learning models: LightGBM, Random Forest, SVM, Decision Tree, and Naive Bayes.

MODEL PERFORMANCE BEFORE AND AFTER PSO

Table 1 shows prediction model performance before and after PSO.

Model	Accuracy (Before PSO)	Accuracy (After PSO)	Precision	Recall	F1-Score
RF	93.1%	99.0%	98.8%	99.1%	99.0%
LightGB	89.4%	94.8%	94.0%	93.2%	93.6%
SVM	85.7%	92.5%	91.1%	92.0%	91.5%
NB	81.3%	88.2%	87.5%	87.0%	87.2%
DT	84.6%	97.3%	96.5%	97.0%	96.7%

Interpretation:

All models improved significantly with PSO and PSO-RF yielding the best result followed by PSO-DT, PSO-LightGBM and then PSO-NB with the lowest accuracy.

Feature Selection Using PSO (Particle Swarm Optimization) PSO selected 14 key features that contributed the most to predicting Anxiety included Gender, City, Working Professional or Student Profession, Work Pressure, CGPA, Study Satisfaction, Job Satisfaction, Sleep Duration, Dietary Habit, Family History of Mental Illness, and Financial Stress were strongly correlated with mental health outcomes. The selected feature set was then used for training and model evaluation, leading to more efficient and interpretable predictions while reducing computational overhead and ensuring a high-quality input for classification. Table 1 shows prediction model performance before and after PSO and table 2 consist of confusion matrix.

Classification Performance

The classification models performed differently best on accuracy, precision, and recall. The Random Forest model have the highest overall accuracy of 99%, with strong performance across all other evaluation metrics, then followed by LightGBM model with 94.8% accuracy, while the DT achieved 97.3% accuracy, SVM 92.5 accuracy, and finally Naive Bayes performed the worst, with the accuracy of 88.1%.

4 DISCUSSION

The result confirmed that PSO has significantly enhanced the performance of machine learning models by reducing the number of irrelevant features and optimized classifier parameters, RF already strong by design, it improved to 99% accuracy when enhanced by PSO. LightGBM is known for its efficiency in boosting frameworks, performed competitively. The Naïve Bayes model had the lowest overall accuracy as expected, due to its conditional independence assumption, however, it still benefited from optimization by improving from 81.3% to 88.2 after the optimization. This work also aligns with past studies such as (Ezeamii et al., 2024), which noted that hybrid or optimized classifiers outperform traditional models in medical prediction tasks. The distribution of numerical variables provides a clear understanding of the spread and skewness of the dataset. The visualization helps identify the presence of any outliers, potential data transformation requirements, and the overall central tendency of the numerical attributes. A well-distributed

ISBN: 978-978-8567-02-8

dataset ensures that model training and predictive analysis remain unbiased and effective. The analysis of numerical distributions also highlights potential correlations among features, which can influence the predictive power of machine learning models. If certain variables exhibit skewness, transformations such as logarithmic scaling may be necessary to enhance model performance. The presence of normally distributed variables suggests a balanced dataset that can improve the reliability of statistical analyses. Table 3 show evaluation based on the research objectives.

Table 3 Evaluation Based on Study Objective

Objective	Achievement
Select Predominate features using PSO	✅ 14 features identified
Train models on the selected features	✅ RF, LightGBM, DT, SVM and NB
Evaluate model performance	✅ PSO-RF outperformed others

5. CONCLUSION

The findings of this research work demonstrated that a hybrid approach that is combining ML classifiers with optimization techniques like PSO can produce high performance prediction that is effectively used to predict anxiety disorder in working class students which offer valuable insights for early detection and intervention. PSO was effective in selecting the most relevant features, which simplified the model structure and enhanced generalization. Among the classifiers, RF performed the best, highlighting the power of ensemble methods when tuned with appropriate features.

As a recommendation, integration with real time monitoring future models should incorporate real-time mental health monitoring using IoT and wearable devices for early detection and intervention, More diverse and larger datasets should be used to improve model robustness and adaptability to different populations, Additional optimization algorithms (like Genetic Algorithm, Ant Colony Optimization) could be compared with POS to further refine feature selection strategies.

ACKNOWLEDGMENT

All praise is due to Allah (SWT), the Most Merciful, for granting me the strength, patience, and knowledge to complete this research work. Without His divine guidance, this accomplishment would not have been possible.

I would like to express my sincere gratitude to my family, especially late Alh. Umar Ahmed and Hajiya Hapsat Umar, my supervisor, Dr. (Mrs) A. O. Abisoye, HOD Dr. E. F Aminu, Internal assessor Prof. A. S. Adepoju, and PG coordinator Dr. O. A. Ojerinde for their continuous support, insightful feedback, and encouragement throughout the course of this research. Your mentorship has been invaluable.

My heartfelt appreciation goes to staff of Computer Science Department, School of Information and Communication Technology Federal University of Technology, Minna, Niger State. To my mentor and elder brother Alh. Musa Yahya, Alh. Sulaiman Abdulrahman, Alh. Usman Abdulrahman.

Finally, I dedicate this work to working-class students everywhere who battle anxiety and mental stress while striving to achieve their dreams. May this research contribute in some way to creating solutions that make their paths easier ameen.

REFERENCES

CONFUSION MATRIX SUMMARY

Table 2 Summary of the confusion matrix.

Model	TP	TN	FP	FN
PSO-RF	14037	71295	455	658
PSO-LightGB	12262	69694	2056	2433
PSO-SVM	15150	19400	1480	1320
PSO-NB	13125	70988	762	1570
PSO-DT	10132	66111	5639	4563

ISBN: 978-978-8567-02-8

Ezeamii, V. C., Okobi, O. E., Wambai-Sani, H., Perera, G. S., Zaynieva, S., Okonkwo, C. C., Ohaiba, M. M., William-Enemali, P. C., Obodo, O. R., & Obiefuna, N. G. (2024). Revolutionizing Healthcare: How Telemedicine Is Improving Patient Outcomes and Expanding Access to Care. *Cureus*. https://doi.org/10.7759/cureus.63881

Gopal, S., Patro, K., & Kumar Sahu, K. (2015). *Normalization: A Preprocessing Stage*. www.kiplinger.com,

Graham, S., Depp, C., Lee, E. E., Nebeker, C., Tu, X., Kim, H.-C., & Jeste, D. V. (2020). Artificial Intelligence for Mental Health and Mental Illnesses: an Overview. *Current Psychiatry Reports*, *21*(11), 116. https://doi.org/10.1007/s11920-019-1094-0

Jollife, I. T., & Cadima, J. (2016). Principal component analysis: A review and recent developments. In *Philosophical Transactions of the Royal Society A: Mathematical, Physical and Engineering Sciences* (Vol. 374, Issue 2065). Royal Society of London. https://doi.org/10.1098/rsta.2015.0202

Pintelas, E. G., Kotsilieris, T., Livieris, I. E., & Pintelas, P. (2018). A review of machine learning prediction methods for anxiety disorders. *ACM International Conference Proceeding Series*, 8–15. https://doi.org/10.1145/3218585.3218587

Priya, A., Garg, S., & Tigga, N. P. (2020). Predicting Anxiety, Depression and Stress in Modern Life using Machine Learning Algorithms. *Procedia Computer Science*, *167*, 1258–1267. https://doi.org/10.1016/j.procs.2020.03.442

Salvador, G., Julián, L., & Francisco, H. (2015). *Data Preprocessing in Data Mining*. Spinger.

Temitope, C. (2024). *Nigeria's Mental Health Crisis*. https://www.tchealthng.com/thought-pieces/nigerias-mental-health-crisis-a-mind-boggling-burden-on-40-million-minds#:~:text=Some%20of%20Nigeria's%20most%20prevalent,2.7%25)%20had%20anxiety%20disorders.

WHO. (2017). *Depression and Other Common Mental Disorders Global Health Estimates*. https://iris.who.int/bitstream/handle/10665/254610/WHO-MSD-MER-2017.2-eng.pdf?sequence=1&isAllowed=y

ISBN: 978-978-8567-02-8